A Heat Transfer Textbook

A Heat Transfer Textbook

Sixth Edition

by

John H. Lienhard V

and

John H. Lienhard IV

Professor John H. Lienhard V
Department of Mechanical Engineering
Massachusetts Institute of Technology
77 Massachusetts Avenue
Cambridge MA 02139-4307 U.S.A.

Professor John H. Lienhard IV
Department of Mechanical Engineering
University of Houston
4800 Calhoun Road
Houston TX 77204-4792 U.S.A.

For updates and information, visit:

This copy is:

Version 6.00 dated 19 April 2024

Preface

Heat transfer is the process by which energy moves from high temperature regions to low temperature regions. Mass transfer is the similar process by which molecules naturally migrate. This textbook describes those physical phenomena. The book's objective is to teach the analysis, modeling, and design of engineered systems that apply heat and mass transfer. Readers should have a background in elementary thermodynamics and fluid mechanics, as is typical for junior- and senior-level engineering students. This book is suitable for a one-semester course in heat and mass transfer, with some of the more advanced material excluded. The text is also well suited to self-study of some or all the material.

Organization of the book

The book consists of eleven chapters, divided into five parts. Part 1, *The General Problem of Heat Exchange*, contains three chapters that provide a broad introduction to heat transfer. The first chapter introduces the modes heat transfer, and the second develops the basic theory of heat conduction and the essential ideas of thermal resistance and the overall heat transfer coefficient. The third chapter uses the first law of thermodynamics and the overall heat transfer coefficient to derive the relationships for heat exchange between two fluids streams. Together, these three chapters form a "minicourse" in heat transfer. We use all this material in later chapters. Readers should understand these topics before they venture farther into the text.

Part 2, *Analysis of Heat Conduction*, contains two chapters. We begin Chapter 4 with further discussion of the heat conduction equation, including well-posed boundary and initial conditions and some general solutions. We then develop a simplified approach to dimensional analysis, which we use throughout all chapters that follow. Chapter 4 closes with a discussion of heat conducting fins. Such fins arise frequently, in forms both obvious and subtle, throughout the practice of heat transfer.

Chapter 5 explores unsteady heat conduction and heat conduction in more than one dimension. One-dimensional unsteady conduction is at the foundation of heat transfer, with wide-ranging applications. In fact, unsteady conduction in semi-infinite media provides a conceptual framework for our study of convective boundary layers in Chapter 6. The last two sections of this chapter introduce multidimensional steady and unsteady conduction.

Part 3 addresses *Convective Heat Transfer*. These four chapters make up the largest section of the book. Chapter 6 introduces laminar and turbulent boundary layers. We discuss the physical behavior of boundary layers in detail. We also derive formulae for the heat transfer coefficient in various idealized configurations. The last three sections dig into turbulent boundary layers, which are arguably more common than laminar boundary layers.

Chapter 7 shifts focus to convection inside tubes and in some more complex external flows. The first three sections—on pipe flows—are of vital importance throughout heat transfer engineering. The next sections connect pipe flows to heat exchangers and generalize to noncircular ducts. Flow across the outside of tubes is the final topic.

Chapter 8 treats convection in which fluid flow is driven by buoyancy, called natural convection. This chapter also treats condensation from pure vapors, which bears a substantial physical and analytical similarity to natural convection. Chapter 8 requires Chapter 6, but not Chapter 7.

Chapter 9 is an introduction to the physics and modeling of boiling processes. This chapter should offer little difficulty at any point beyond Chapter 6.

Part 4 of the book consists of Chapter 10, *Radiative Heat Transfer*. This stand-alone chapter is accessible at any point after Chapter 2. Radiation heat transfer is present at any temperature, but it becomes increasingly important as the temperature rises. Some processes involve both high and low temperature radiation, as when the sun's heat is absorbed by the Earth. And radiative transfer through gases ultimately determines the temperature and climate on our planet.

Part 5, *Mass Transfer*, is the single Chapter 11. Many important phase-change processes occur in mixtures, not pure vapors, as when water condenses out of or evaporates into air. Mass transfer processes usually involve both diffusive and convective transport, and we discuss that distinction in detail. When one species in a mixture is dilute (as for water vapor in room-temperature air), we can form a simple analogy between heat and mass transfer. This analogy enables us to adapt many formulae

from Chapters 6, 7, and 8. In more concentrated or multicomponent mixtures, however, the analogy breaks down. We discuss alternate formulations in the final sections of this book. Many of the homework problems in this chapter expand upon ideas mentioned only briefly in the text. Readers who wish to master the material should attempt all the problems. This chapter does not require Chapter 9 and 10, nor any prior study of chemical thermodynamics.

Finally, Appendix A includes the physical property data needed for solving the end-of-chapter problems and the examples in text.

Changes in this edition

This edition differs from the fifth edition as follows. We have substantially edited Chapters 1, 2, 3, and 6 for content and clarity. We have entirely reworked the material on heat transfer in turbulent boundary layers in Chapter 6. We have extensively revised and rearranged Chapter 11, on mass transfer: we give greater attention to distinguishing between convection and diffusion, especially as the mass transfer rate rises; we treat concentrated mixtures in more detail; we have added a new section on multicomponent diffusion, for which Fick's law is inadequate; we have added many new figures and examples; and we have reviewed, edited, and changed all of the end-of-chapter problems.

In total, we have redrawn or added more than 40 figures in this edition. We have also added, revised, or replaced dozens of end-of-chapter problems throughout the book. In parallel, we have edited and added to the solutions manual, which now includes more than 520 solved problems. We have updated the properties of many fluids in Appendix A to accommodate new data. We have also made edits throughout the entire text to improve clarity or to eliminate typos or errors. And, we have reviewed the references cited, providing links for online access where available.

⸺◦◦◦⸺

A Heat Transfer Textbook has now existed for almost half a century. JHL IV wrote the first edition (1981) during the 1970s at the University of Kentucky. He based it on many years of teaching heat transfer to junior and senior level students in mechanical and chemical engineering. We added the material on mass transfer, by JHL V, to the second edition (1987). JHL V has led the third edition and all later editions. The third edition (2001) was primarily distributed as an e-book, and it was one of the very first engineering textbooks to be available in this format. Hundreds

of thousands of readers, from seven continents, accessed that e-book. The fourth (2011) and fifth (2019) editions incorporated many more updates, changes, and corrections within the existing framework of the text. We published those editions both as e-books and as low-cost paperbacks distributed by Dover Publications.

The present sixth edition continues the evolution of *A Heat Transfer Textbook*. We hope that readers will find the material to have lasting value.

JHL V, Massachusetts Institute of Technology
JHL IV, University of Houston
April 2024

Contents

THE GENERAL PROBLEM OF HEAT EXCHANGE

1.   Introduction

The radiation of the sun in which the planet is incessantly plunged, penetrates the air, the earth, and the waters; its elements are divided, change direction in every way, and, penetrating the mass of the globe, would raise its temperature more and more, if the heat acquired were not exactly balanced by that which escapes in rays from all points of the surface and expands through the sky.   **The Analytical Theory of Heat,** J. Fourier

1.1   Heat transfer

People have always understood that something flows from hot objects to cold ones. We call that flow *heat.* Scientists of the late eighteenth century finally decided that all bodies must contain an invisible fluid which they called *caloric.* Caloric was assigned a variety of properties, some of which proved to be inconsistent with nature—for example, caloric had weight and could not be created or eliminated. But the most important property was that caloric flowed from hot bodies into cold ones. Caloric provided a very useful way to think about heat. Later we shall explain the flow of heat in terms more satisfactory to the modern ear; however, it will seldom be wrong to imagine caloric flowing from a hot body to a cold one.

The flow of heat is all-pervasive. It is active to some degree or another in everything. Heat flows constantly from your bloodstream to the air around you. The warmed air buoys off your body to warm the room you are in. If you leave the room, some small buoyancy-driven (or *convective*) motion of the air will continue because the walls can never be perfectly isothermal. Such processes go on in all plant and animal life and in the air around us. They occur throughout the earth, which is hot at its core and cooled around its surface. The only conceivable domain free from heat flow would have to be isothermal and totally isolated from any other region. It would be "dead" in the fullest sense of the word — devoid of any process of any kind.

The overall driving force for these heat flow processes is the cooling (or leveling) of any temperature gradients. The heat flows that result from the cooling of the sun are the primary processes that we experience naturally. Earth's surface is also warmed by the cooling of its core, and even by radiation from the distant stars, however little those processes influence our lives.

The life forms on our planet have necessarily evolved to match the magnitude of these energy flows. But while most animals are in balance with these heat flows, we humans have used our minds, our backs, and our wills to harness and control energy flows that are far more intense than those we experience naturally.[1] To emphasize this point we suggest that the reader do the following experiment.

Experiment 1.1

Generate as much power as you can, in some way that permits you to measure your own work output. You might lift a weight, or run your own weight up a stairwell, against a stopwatch. Express the result in watts (W). Perhaps you might collect the results in your class. They should generally be less than 1 kW or even 1 horsepower (746 W). How much less might be surprising. ♦

Thus, when we do so small a thing as turning on a 150 W light bulb, we are manipulating a quantity of energy substantially greater than a human being could produce in sustained effort. The power consumed by an oven, toaster, or hot water heater is an order of magnitude beyond our capacity. The power consumed by an automobile can easily be three orders of magnitude greater. If all the people in the United States worked continuously like galley slaves, they could barely equal the output of even a single city power plant.

Our voracious appetite for energy has steadily driven the intensity of actual heat transfer processes upward until they are far greater than those normally involved with life forms on earth. Until the middle of the thirteenth century, the energy we use was drawn indirectly from the sun using comparatively gentle processes — animal power, wind and water power, and burning wood. Then population growth and deforestation drove the English to using coal. By the end of the seventeenth century,

---

[1]Some anthropologists think that the term *Homo technologicus* (those who use technology) serves to define human beings, as apart from animals, better than the older term *Homo sapiens* (those who are wise). We may not be as much wiser than the animals as we think we are, but only we do serious sustained tool making.

England had almost completely converted to coal in place of wood. At the turn of the eighteenth century, the first commercial steam engines were developed, and that set the stage for enormously increased consumption of coal. Europe and America followed England in these developments.

The development of fossil energy sources has been a bit like Jules Verne's description in *Around the World in Eighty Days* in which, to win a race, a crew burns the inside of a ship to power the steam engine. The combustion of nonrenewable fossil energy sources (and, more recently, the fission of uranium) has led to remarkably intense energy releases in power-generating equipment. The energy transferred as heat in a nuclear reactor is on the order of *one million watts per square meter.*

A complex system of heat and work transfer processes is invariably needed to bring these concentrations of energy back down to human proportions. We must understand and control the processes that divide and diffuse intense heat flows down to the level on which we can interact with them. To see how this works, consider a specific situation. Suppose we live in a town where coal is processed into fuel-gas and coke. (This domestic use of coked coal was once widespread. It has now almost vanished.) Let us list a few of the process heat transfer problems that must be solved before we can drink a glass of iced tea.

- A variety of high-intensity heat transfer processes are involved with combustion and chemical reaction in the gasifier unit itself.

- The gas goes through various cleanup and pipe-delivery processes to get to our stoves. The heat transfer processes involved in these stages are generally less intense.

- The gas is burned in the stove. Heat is transferred from the flame to the bottom of the teakettle. While this process is small, it is intense because boiling is a very efficient way to remove heat.

- The coke is burned in a steam power plant. The heat transfer rates from the combustion chamber to the boiler, and from the wall of the boiler to the water inside, are very intense.

- The steam passes through a turbine where it is involved with many heat transfer processes, possibly including some condensation in the last turbine stages. The spent steam is then condensed in any of a variety of heat transfer devices.

- Cooling must be provided in each stage of the electrical supply system: the winding and bearings of the generator, the transformers, the switches, the power lines, and the wiring in our houses.

- The ice cubes for our tea are made in an electrical refrigerator. It involves three major heat exchange processes and several lesser ones. The major ones are the condensation of refrigerant at room temperature to reject heat, the absorption of heat from within the refrigerator by evaporating the refrigerant, and the balancing heat leakage from the room to the inside.

- Let's drink our iced tea quickly because heat transfer from the room to the water and from the water to the ice will first dilute, and then warm, our tea if we linger.

A society based on power technology teems with heat transfer problems. Our aim is to learn the principles of heat transfer so we can solve these problems and design the equipment needed to transfer thermal energy from one substance to another. In a broad sense, all these problems resolve themselves into collecting and focusing large quantities of energy for the use of people, and then distributing and interfacing this energy with people in such a way that they can use it on their own puny level.

We begin our study by recollecting how heat transfer was treated in the study of thermodynamics and by seeing why thermodynamics is not adequate to the task of solving heat transfer problems.

1.2   Relation of heat transfer to thermodynamics

The First Law

The subject of thermodynamics, as taught in engineering programs, makes constant reference to the heat transfer between systems. The First Law of Thermodynamics for a closed system takes the following form on a rate basis:

$$\underbrace{Q}_{\substack{\text{positive toward}\\\text{the system}}} = \underbrace{Wk}_{\substack{\text{positive away}\\\text{from the system}}} + \underbrace{\frac{dU}{dt}}_{\substack{\text{positive when}\\\text{the system's}\\\text{energy increases}}} \tag{1.1}$$

where Q is the heat transfer rate and Wk is the work transfer rate. They may be expressed in joules per second (J/s) or watts (W). The derivative

a) The general case   b) No work transfer
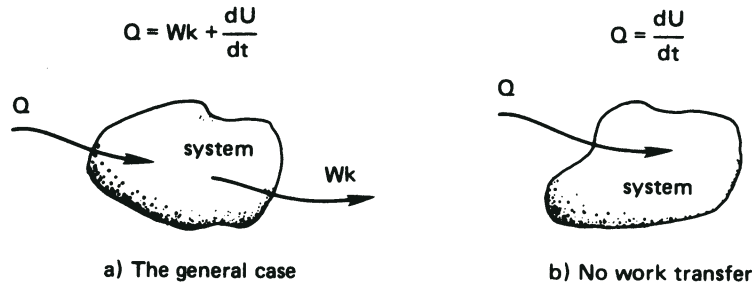
Figure 1.1 The First Law of Thermodynamics for a closed system.

dU/dt is the rate of change of internal thermal energy, U, with time, t. This interaction is sketched schematically in Fig. 1.1a.

The analysis of heat transfer processes can generally be done without reference to any work processes, although heat transfer might subsequently be combined with work in the analysis of real systems. If $p\,dV$ work is the only work that occurs, then eqn. (1.1) is

$$Q = p\,\frac{dV}{dt} + \frac{dU}{dt} \tag{1.2a}$$

This equation has two well-known special cases:

$$\text{Constant volume process:} \qquad Q = \frac{dU}{dt} = mc_v\,\frac{dT}{dt} \tag{1.2b}$$

$$\text{Constant pressure process:} \qquad Q = \frac{dH}{dt} = mc_p\,\frac{dT}{dt} \tag{1.2c}$$

where $H \equiv U + pV$ is the enthalpy, and c_v and c_p are the specific heat capacities at constant volume and constant pressure, respectively.

When the substance undergoing the process is incompressible (so that V is constant for any pressure variation), the two specific heats are equal: $c_v = c_p \equiv c$. The proper form of eqn. (1.2a) is then

$$\boxed{Q = \frac{dU}{dt} = mc\,\frac{dT}{dt}} \tag{1.3}$$

as in Fig. 1.1b. Since solids and liquids can frequently be approximated as being incompressible, we shall often make use of eqn. (1.3).

If the heat transfer were reversible, then eqn. (1.2a) would become[2]

$$\underbrace{T\,\frac{dS}{dt}}_{Q_{\text{rev}}} = \underbrace{p\,\frac{dV}{dt}}_{Wk_{\text{rev}}} + \frac{dU}{dt} \tag{1.4}$$

That might seem to suggest that Q can be evaluated independently for inclusion in either eqn. (1.1) or (1.3). However, it cannot be evaluated using $T\,dS$, because real heat transfer processes are all irreversible and S is not defined as a function of T in an irreversible process. The reader will recall that engineering thermodynamics might better be named thermo*statics*, because it only describes the equilibrium states on either side of irreversible processes.

Since the rate of heat transfer cannot be predicted using $T\,dS$, how can it be determined? If $U(t)$ were known, then (when $Wk = 0$) eqn. (1.3) would give Q, but $U(t)$ is seldom known *a priori*.

The answer is that a new set of physical principles must be introduced to predict Q. The principles are *transport laws*, which are not a part of the subject of thermodynamics. They include Fourier's law, Newton's law of cooling, and the Stefan-Boltzmann law. We introduce these laws later in the chapter. The important thing to remember is that a description of heat transfer requires that additional principles be combined with the First Law of Thermodynamics.

Reversible heat transfer as the temperature gradient vanishes

Consider a wall connecting two thermal reservoirs as shown in Fig. 1.2. As long as $T_1 > T_2$, heat will flow *spontaneously* and *irreversibly* from 1 to 2. In accordance with our understanding of the Second Law of Thermodynamics, we expect the entropy of the universe to increase as a consequence of this process. If $T_2 \longrightarrow T_1$, the process will approach being quasistatic and reversible. But the rate of heat transfer will also approach zero if there is no temperature difference to drive it. Thus all real heat transfer processes generate entropy.

Now we come to a dilemma: If the irreversible process occurs at steady state, the properties of the wall do not vary with time. We know that the entropy of the wall depends on its state and must therefore be constant. How, then, does the entropy of the universe increase? We turn to this question next.

---

[2] T = absolute temperature, S = entropy, V = volume, p = pressure, and "rev" denotes a reversible process.
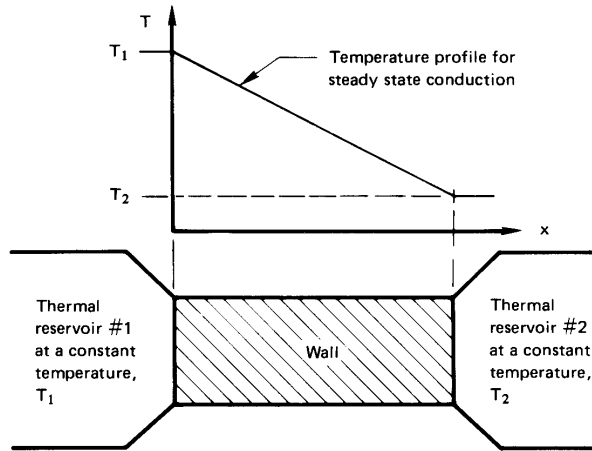
Figure 1.2 Irreversible heat flow between two thermal reservoirs through an intervening wall.

Entropy production

The entropy increase of the universe as the result of a process is the sum of the entropy changes of *all* elements that are involved in that process. The *rate of entropy production* of the universe, $\dot{S}_{\text{Un}}$, resulting from the preceding heat transfer process through a wall is

$$\dot{S}_{\text{Un}} = \dot{S}_{\text{res 1}} + \underbrace{\dot{S}_{\text{wall}}}_{\substack{= 0, \text{ since } S_{\text{wall}} \\ \text{must be constant}}} + \dot{S}_{\text{res 2}} \qquad (1.5)$$

where the dots denote time derivatives (e.g., $\dot{x} \equiv dx/dt$). Since the reservoir temperatures are constant,

$$\dot{S}_{\text{res}} = \frac{Q}{T_{\text{res}}} \qquad (1.6)$$

Now $Q_{\text{res 1}}$ is negative and equal in magnitude to $Q_{\text{res 2}}$, so eqn. (1.5) becomes

$$\dot{S}_{\text{Un}} = \left| Q_{\text{res 1}} \right| \left(\frac{1}{T_2} - \frac{1}{T_1} \right) \qquad (1.7)$$

The term in parentheses is positive, so $\dot{S}_{\text{Un}} > 0$. This agrees with Clausius's statement of the Second Law of Thermodynamics.

Notice an odd fact here: The rate of heat transfer, Q, and hence $\dot{S}_{\text{Un}}$, is determined by the wall's resistance to heat flow. Although the wall is the agent that causes the entropy of the universe to increase, its own entropy does not change. Only the entropies of the reservoirs change.

Help! The barn is on fire!
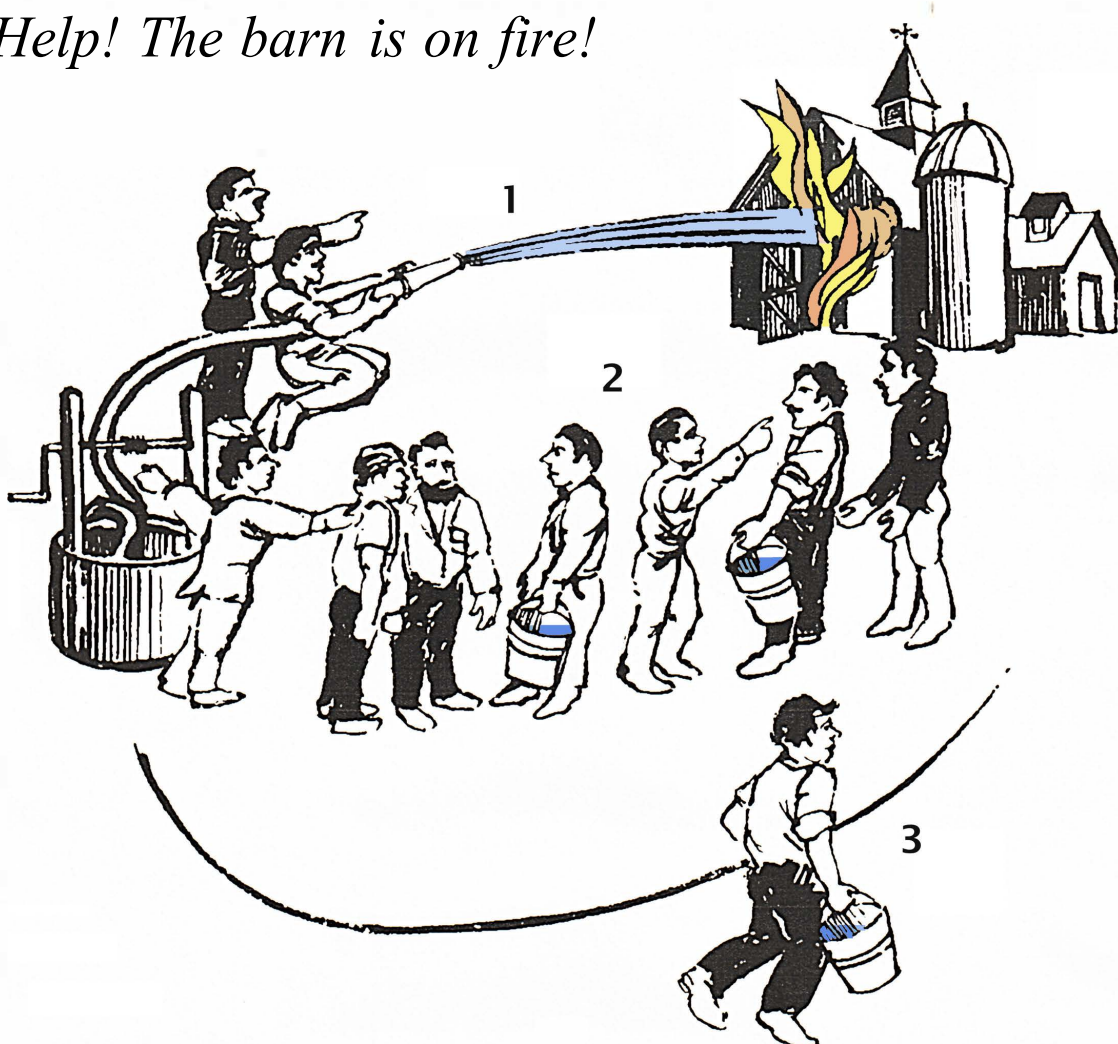
Let the water be analogous to heat. Let the people be analogous to the heat transfer medium. Then:

Case 1 The hose directs water from the well to the barn, independent of the medium. This is analogous to *thermal radiation* in a vacuum or in most gases.

Case 2 Water passes from the well to the barn through the bucket brigade medium. This is analogous to *heat conduction*.

Case 3 The medium is now a single runner carrying a bucket from the well to the barn. This is analogous to *heat convection*.

Figure 1.3 An analogy for the three modes of heat transfer.

1.3   Modes of heat transfer

Figure 1.3 shows an analogy that might be useful in fixing the concepts of heat conduction, convection, and radiation as we proceed to look at each in some detail.

Heat conduction

Fourier's law.   Joseph Fourier (see Fig. 1.4) published his remarkable book *Théorie Analytique de la Chaleur* in 1822 [1.1]. In it he formulated a very complete exposition of the theory of heat conduction. The heat flow rate per unit area, called the heat flux, q (W/m^2), has central importance in the theory.

Fourier began his treatise by stating the empirical law that bears his name: *the heat flux resulting from thermal conduction is proportional to the magnitude of the temperature gradient and opposite to it in sign.* If we denote the constant of proportionality as k, then

$$q = -k\frac{dT}{dx} \tag{1.8}$$

The constant, k, is called the *thermal conductivity.* It obviously must have the dimensions W/m·K, or J/m·s·K, or Btu/h·ft·°F if eqn. (1.8) is to be dimensionally correct.

The heat flux is a vector quantity. Equation (1.8) tells us that if temperature decreases with x, q will be positive—it will flow in the x-direction. If T increases with x, q will be negative—it will flow opposite the x-direction. In either case, q will flow from higher temperatures to lower temperatures. Equation (1.8) is the one-dimensional form of Fourier's law. We develop its three-dimensional form in Chapter 2, namely:

$$\vec{q} = -k\,\nabla T$$

Example 1.1

The front of a slab of lead ($k = 34$ W/m·K) is kept at 110°C and the back is kept at 50°C. If the area of the slab is $A = 0.4$ m^2 and it is 0.03 m thick, compute the heat flux, q, and the heat transfer rate, Q.

SOLUTION. Take $dT/dx \simeq (T_{\text{back}} - T_{\text{front}})/(x_{\text{back}} - x_{\text{front}})$ throughout the slab; we verify this in Example 2.2. Thus, eqn. (1.8) becomes

$$q = -34\left(\frac{50 - 110}{0.03}\right) = +68,000 \text{ W/m}^2 = 68 \text{ kW/m}^2$$

Figure 1.4 Baron Jean Baptiste Joseph Fourier (1768–1830). Joseph Fourier lived a remarkable double life. He served as a high government official in Napoleonic France and he was also an applied mathematician of great importance. He was with Napoleon in Egypt between 1798 and 1801, and he was subsequently prefect of the administrative area (or "Department") of Isère in France until Napoleon's first fall in 1814. During the latter period he worked on the theory of heat flow and in 1807 submitted a 234-page monograph on the subject. It was given to such luminaries as Lagrange and Laplace for review. They found fault with his adaptation of a series expansion suggested by Daniel Bernoulli in the eighteenth century. Fourier's theory of heat flow, his governing differential equation, and the now-famous "Fourier series" solution of that equation did not emerge in print from the ensuing controversy until 1822. (Etching from [1.2]).

and

$$Q = qA = 68(0.4) = 27 \text{ kW} \qquad \blacksquare$$

The direction of heat flow, from hotter to cooler, is always clear in one-dimensional heat conduction problems. Therefore, we can usually write Fourier's law in simple scalar form:

$$\boxed{q = k \frac{\Delta T}{L}} \qquad (1.9)$$

where L is the thickness in the direction of heat flow and q and ΔT are both written as positive quantities. When we use eqn. (1.9), we must remember that q always flows from high to low temperatures and that this equation is only for one-dimensional, steady state conduction.

Thermal conductivity values. Let us consider how conduction works, starting with conduction in gases. We know that molecular velocities depend on temperature. Consider conduction from a hot to a cold wall, in a situation where gravity can be ignored (see Fig. 1.5). The molecules near the hot wall collide with it and gain energy from the hot molecules in the wall. They leave with generally higher speeds and collide with their neighbors to the right, increasing the speed of those molecules. This process continues until the molecules on the far right pass their kinetic energy to molecules in the cold wall.[3]

Comparable processes occur within solids as the molecules vibrate within their lattice structures, and as the lattice vibrates as a whole. Similar processes are also at play within the "electron gas" that moves through a conductor. These processes are more efficient in most solids than they are in gases. Liquids conduct heat much better than gases, but not as well as most solids. Notice that

$$-\frac{dT}{dx} = \underbrace{\frac{q}{k}}_{\substack{\text{since, in steady} \\ \text{conduction, } q \text{ is} \\ \text{constant}}} \propto \frac{1}{k} \qquad (1.10)$$

Thus most solids, with their generally higher k values, yield smaller temperature gradients than gases or liquids for a given heat flux.

---

[3]In Section 6.4, we see that k is proportional to the molecular speed and the specific heat at constant volume. And in Section 11.10, we see that k is inversely proportional to the molecules' cross-sectional area.
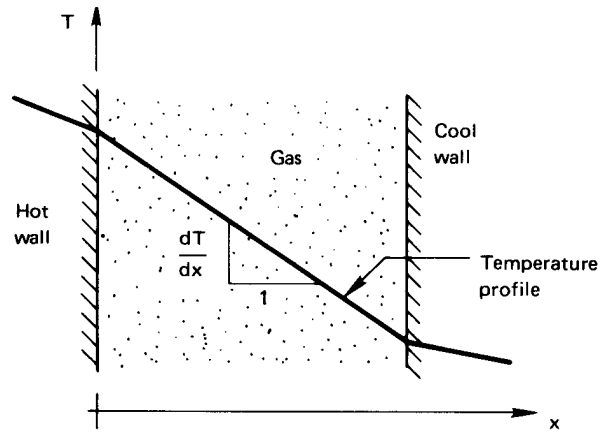
Figure 1.5   Heat conduction through gas separating two solid walls.

The range of thermal conductivities is enormous. As we see from Fig. 1.6, k varies by a factor of about 10^5 between gases and diamond at room temperature. This variation can be increased to about 10^7 if we include the effective conductivity of various cryogenic "superinsulations." (These involve powders, fibers, or multilayered materials that have been evacuated of all air.) The reader should study and remember the order of magnitude of the thermal conductivities of different types of materials. This will be a help in avoiding mistakes in future computations, and it will be a help in making approximations during problem solving. Actual numerical values of the thermal conductivity are given in Appendix A (which is a broad listing of many of the physical properties you might need in this course) and in Figs. 2.2 and 2.3.

This book deals almost exclusively with S.I. units, or *Système International d'Unités*. Since much reference material will continue to be available in English units, we should have at hand conversion factors. We shall present all of our conversion factors as a ratio of equal quantities in both systems. We can thus write for thermal conductivity:

$$1 = 1.731\,\frac{\text{W/m·K}}{\text{Btu/h·ft·°F}} \tag{1.11}$$

Let us apply this to copper, which has the highest conductivity (398 W/m·K) of any common substance at ordinary temperatures:

$$k_{\text{Cu at room temp}} = (398 \text{ W/m·K})\Big/1.731\frac{\text{W/m·K}}{\text{Btu/h·ft·°F}} = 230 \text{ Btu/h·ft·°F}$$

See Appendix B for more on handling units and conversion factors.
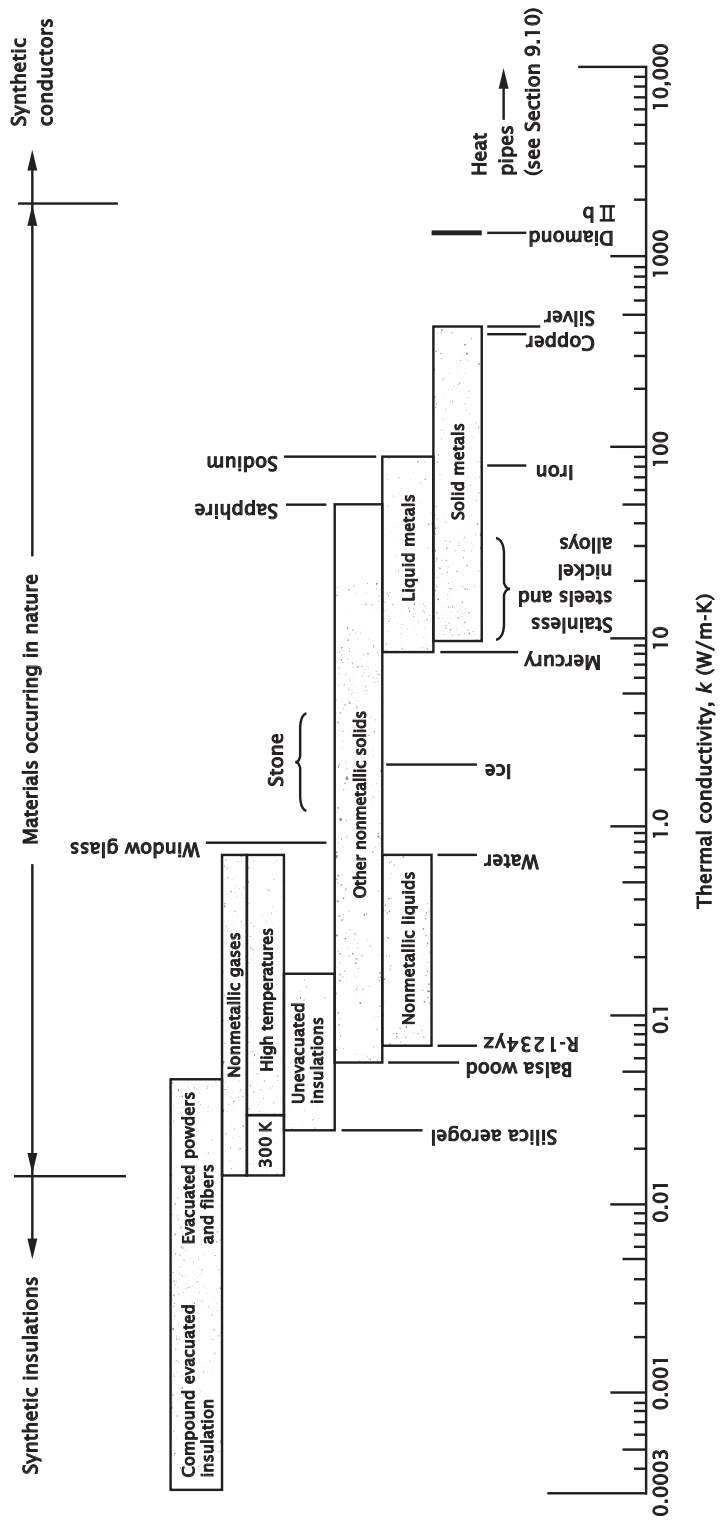
Figure 1.6: The approximate ranges of thermal conductivity of various substances. (All values are for the neighborhood of room temperature unless otherwise noted.)

15
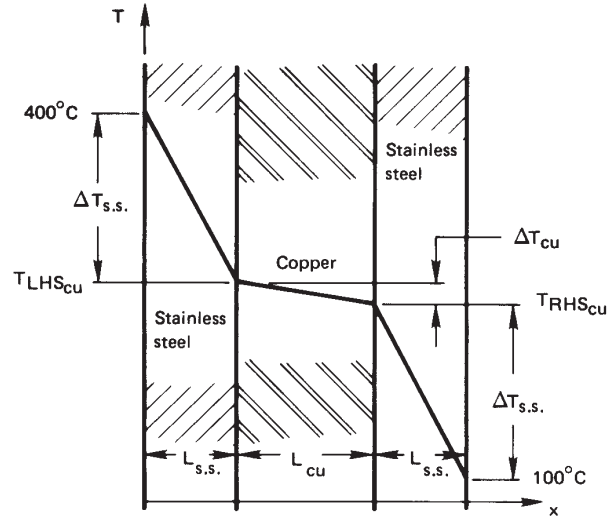
Figure 1.7   Temperature drop through a copper wall protected by stainless steel (Example 1.2).

Example 1.2

A copper slab (k = 387 W/m·K) is 3 mm thick. It is protected from corrosion on each side by a 2-mm-thick layer of stainless steel (k = 17 W/m·K). The temperature is 400°C on one side of this composite wall and 100°C on the other. Find the temperature distribution in the copper slab and the heat conducted through the wall (see Fig. 1.7).

SOLUTION. Conservation of energy requires that the steady heat flux through all three slabs must be the same. Therefore, $\Delta T_{\text{s.s.}}$ and ΔT_{Cu} are related by Fourier's law, eqn. (1.9), applied to either steel slab:

$$q = \left(k\frac{\Delta T}{L}\right)_{\text{s.s.}} = \left(k\frac{\Delta T}{L}\right)_{\text{Cu}}$$

The value of k copper is more than 20 times that for stainless steel, so the temperature difference in the copper is less than 1/20 that in the steel. Thus, the copper is nearly isothermal.

As a first estimate, we could treat the copper as exactly isothermal—as if it were not even there. Then, the two stainless steel slabs can be treated as a single 4 mm slab. Again using eqn. (1.9), we estimate

$$q = k\frac{\Delta T}{L} = (17 \text{ W/m·K}) \left(\frac{400 - 100}{0.004}\right) \text{K/m} = 1275 \text{ kW/m}^2$$

The accuracy of this rough calculation can be improved by account-ing for the temperature drop in the copper. Solving the first equation

for $\Delta T_{\text{s.s.}}$, we can evaluate the overall temperature drop in the wall:

$$
\begin{aligned}
(400 - 100)°\text{C} &= \Delta T_{\text{Cu}} + 2\Delta T_{\text{s.s.}} \\
&= \Delta T_{\text{Cu}} \left[1 + 2\frac{(k/L)_{\text{Cu}}}{(k/L)_{\text{s.s.}}} \right] \\
&= (31.35)\Delta T_{\text{Cu}}
\end{aligned}
$$

Solving this, we obtain $\Delta T_{\text{Cu}} = 9.57$ K. So $\Delta T_{\text{s.s.}} = (300 - 9.57)/2 = 145$ K. It follows that $T_{\text{Cu, left}} = 255°$C and $T_{\text{Cu, right}} = 245°$C.

The heat flux can be obtained by applying Fourier's law to any of the three layers. We consider either stainless steel layer and get

$$
q = 17\frac{\text{W}}{\text{m·K}}\frac{145\ \text{K}}{0.002\ \text{m}} = 1233\ \text{kW/m}^2
$$

Thus our initial approximation was accurate within a few percent. ∎

One-dimensional heat conduction equation. In Example 1.2 we had to deal with a major problem that arises in heat conduction problems. The problem is that Fourier's law involves two dependent variables, T and q. To eliminate q and first solve for T, we introduced the First Law of Thermodynamics implicitly: Conservation of energy required that q was the same in each metallic slab.

Now let us eliminate q in a more general way. Consider a one-dimensional element, as shown in Fig. 1.8. From Fourier's law applied at each side of the element, the net heat conduction out of the element during unsteady heat flow is

$$
Q_{\text{net}} = Aq\Big|_{x+\delta x} - Aq\Big|_x = -kA\left(\frac{\partial T}{\partial x}\Big|_{x+\delta x} - \frac{\partial T}{\partial x}\Big|_x\right) \simeq -kA\frac{\partial^2 T}{\partial x^2}\delta x \tag{1.12}
$$

To eliminate the heat loss Q_{net} in favor of T, we use the First Law statement, eqn. (1.3), for an incompressible mass $m = \rho A\delta x$:

$$
-Q_{\text{net}} = \frac{dU}{dt} = \rho cA\frac{\partial T}{\partial t}\delta x \tag{1.13}
$$

where ρ is the density of the slab and c is its specific heat capacity.[4] Combining eqns. (1.12) and (1.13) gives

$$
\boxed{\frac{\partial^2 T}{\partial x^2} = \frac{\rho c}{k}\frac{\partial T}{\partial t} \equiv \frac{1}{\alpha}\frac{\partial T}{\partial t}} \tag{1.14}
$$

---

[4]The reader may wonder how the equation differs for compressible systems. The compressible equation involves additional terms, and this particular terms emerges with c_p rather c under the conventional rearrangement of terms.

$Q_{net} = -kA \left\{ \dfrac{\left. \dfrac{\partial T}{\partial x}\right|_{x+\delta x} - \left.\dfrac{\partial T}{\partial x}\right|_{x}}{\delta x} \right\} \delta x$

$\equiv \left.\dfrac{\partial^2 T}{\partial x^2}\right|_{x}$ By the definition of a derivative
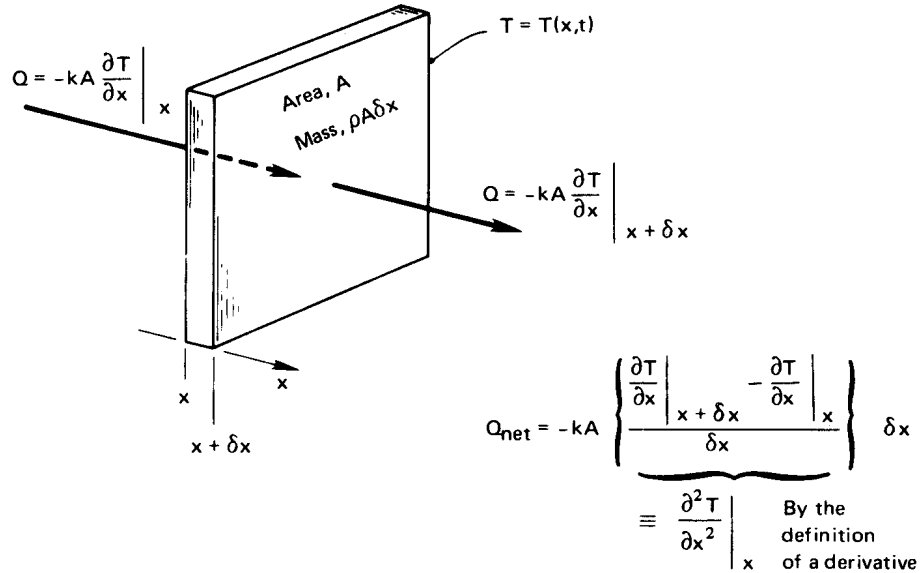
Figure 1.8 One-dimensional heat conduction through a differential element.

This result is the *one-dimensional heat conduction equation.*[5] Its importance is this: By combining the First Law with Fourier's law, we have eliminated the unknown heat transfer rate and obtained a differential equation that can be solved for the temperature distribution, $T(x, t)$. The heat conduction equation is the primary equation upon which all of heat conduction theory is based.

The heat conduction equation includes a new property which is as important to transient heat conduction as k is to steady-state conduction. This is the thermal diffusivity, α:

$$\alpha \equiv \frac{k}{\rho c} \frac{\text{J}}{\text{m·s·K}} \frac{\text{m}^3}{\text{kg}} \frac{\text{kg·K}}{\text{J}} = \alpha \;\; \text{m}^2/\text{s} \;\; (\text{or ft}^2/\text{hr})$$

The thermal diffusivity is a measure of how quickly a material can carry heat away from a hot source. Since material does not just transmit heat but must be warmed by it as well, α involves both the conductivity, k, and the volumetric heat capacity, ρc.

---

[5]This equation is sometimes called the *heat diffusion equation.*
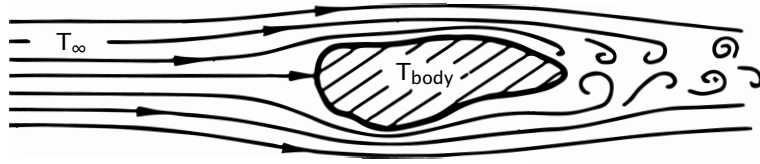
Figure 1.9 The convective cooling of a heated body.

Heat Convection

The physical process.   Consider a typical convective cooling situation. Cool gas flows past a warm body, as shown in Fig. 1.9. The fluid immediately adjacent to the body forms a thin slowed-down region called a *boundary layer*. Heat is conducted into this layer, which sweeps it away and, farther downstream, mixes it into the stream. We call such processes of carrying heat away by a moving fluid *convection*.

In 1701, Isaac Newton considered the convective process and suggested that the cooling would be such that

$$-\frac{dT_{\text{body}}}{dt} \propto T_{\text{body}} - T_{\infty} \tag{1.15}$$

where T_{∞} is the temperature of the oncoming fluid. Heat flows out of the body, so the time derivative is negative when $T_{\text{body}} > T_{\infty}$. By putting eqn. (1.15) into eqn. (1.3), we get (see Problem 1.2)

$$-Q \propto T_{\text{body}} - T_{\infty} \tag{1.16}$$

The sign is negative because heat leaves, rather than enters, the body. To use a positive value, let $-Q = Q_{\text{out}}$. Then eqn. (1.16) can be rephrased in terms of $q = Q_{\text{out}}/A$ and a constant of proportionality, $\overline{h}$, as

$$\boxed{q = \overline{h}\left(T_{\text{body}} - T_{\infty}\right)} \tag{1.17}$$

This result is usually called *Newton's law of cooling*, although Newton never wrote such an expression.

The constant h is the *film coefficient* or *heat transfer coefficient*. The bar over h indicates that it is an average over the surface of the body. Without the bar, h denotes the "local" value of the heat transfer coefficient at a point on the surface. The units of h and $\overline{h}$ are W/m²K or J/s·m²·K. The conversion factor for English units is:

$$1 = \frac{0.0009478 \text{ Btu}}{J} \cdot \frac{K}{1.8°F} \cdot \frac{3600 \text{ s}}{h} \cdot \frac{(0.3048 \text{ m})^2}{\text{ft}^2}$$

or

$$1 = 0.1761 \frac{\text{Btu/h·ft}^2 \cdot {}^\circ\text{F}}{\text{W/m}^2\text{K}} \tag{1.18}$$

Newton somewhat oversimplified convection when he suggested that the rate of cooling is proportional to the temperature difference. Actually, $\overline{h}$ can depend on the temperature difference $T_{\text{body}} - T_\infty \equiv \Delta T$. In Chapter 6, we find that h really *is* independent of ΔT in situations in which fluid is forced past a body and ΔT is not too large. This is called *forced convection*.

When fluid buoys up from a hot body or down from a cold one, h varies as some weak power of ΔT—typically as $\Delta T^{1/4}$ or $\Delta T^{1/3}$. This is called *free* or *natural convection*. If the body is hot enough to boil a liquid surrounding it, h will typically vary as ΔT^2.

For the moment, we restrict consideration to situations in which Newton's law is either true or at least a reasonable approximation to real behavior.

We should have some idea of how large h might be in a given situation. Table 1.1 provides some illustrative values of h that have been observed or calculated for different situations. They are only illustrative and should not be used in calculations because the situations for which they apply have not been fully described. Most of the values in the table could be changed a great deal by varying quantities that have not been specified, such as surface roughness or geometry.

The determination of h or $\overline{h}$ is a fairly complicated task and one that will receive a great deal of our attention in Part III. Notice, too, that $\overline{h}$ can change dramatically from one situation to the next. Reasonable values of h range over about six orders of magnitude.

Example 1.3

The heat flux, q, is 6000 W/m^2 at the surface of an electrical heater. The heater temperature is 120°C when it is cooled by air at 70°C. What is the average convective heat transfer coefficient, $\overline{h}$? What will the heater temperature be if the power is reduced so that q is 2000 W/m^2?

SOLUTION.
$$\overline{h} = \frac{q}{\Delta T} = \frac{6000}{120 - 70} = 120 \text{ W/m}^2\text{K}$$

If $\overline{h}$ stays fairly constant as the heat flux is reduced,

$$\Delta T = T_{\text{heater}} - 70°\text{C} = \frac{q}{\overline{h}} = \frac{2000 \text{ W/m}^2}{120 \text{ W/m}^2\text{K}} = 16.67 \text{ K}$$

so $T_{\text{heater}} = 70 + 16.67 = 86.67°\text{C}$.   ■

Table 1.1 Some approximate values of convective heat transfer coefficients

Situation (T_∞ near room temperature unless otherwise stated)	$\bar{h}$, $W/m^2 K$
Natural convection in gases	
• 0.3 m vertical wall in air, $\Delta T = 30°C$	4.2
• 1 mm diameter horizontal wire in air, $\Delta T = 100°C$	29
Natural convection in liquids	
• 40 mm O.D. horizontal pipe in water, $\Delta T = 30°C$	570
• 0.25 mm diameter wire in methanol, $\Delta T = 50°C$	4,000
Forced convection of gases	
• Air at 10 m/s inside 20 mm I.D. tube	45
• Air at 30 m/s over a 1 m flat plate	80
Forced convection of liquids	
• Water at 2 m/s over a 60 mm plate	590
• Aniline-alcohol mixture at 3 m/s in a 25 mm I.D. tube	2,600
• Water at 10 m/s inside 20 mm I.D. tube	34,500
• Liquid sodium at 5 m/s in a 13 mm I.D. tube at 370°C	75,000
Boiling water at 100 °C and 1 atm	
• During film boiling	300
• In a tea kettle	4,000
• At the highest pool-boiling heat flux	40,000
• During convective-boiling, range of highest values	10^5–10^6
Condensation	
• In a typical horizontal cold-water-tube steam condenser	15,000
• Same, but condensing benzene	1,700
• Dropwise condensation of water at 1 atm	160,000

Lumped-capacity solution.   We now wish to deal with a very simple but extremely important, kind of convective heat transfer problem. The problem is that of predicting the transient cooling of a convectively cooled object, such as we showed in Fig. 1.9, in the case when the body has an *almost uniform* internal temperature. When the internal temperature gradients are small, we can "lump" all of the heat capacitance at a single body temperature, $T = T(t)$.

With reference to Fig. 1.10, we apply our now-familiar First law statement, eqn. (1.3), to such a body:

$$\underbrace{Q}_{-\bar{h}A(T-T_\infty)} = \underbrace{\frac{dU}{dt}}_{\frac{d}{dt}[\rho c V(T-T_{\text{ref}})]} \qquad (1.19)$$

where A and V are the surface area and volume of the body, and T_{ref} is the arbitrary temperature at which U is taken to be zero. Thus[6]

$$\frac{d(T - T_\infty)}{dt} = -\frac{\overline{h}A}{\rho c V}(T - T_\infty) \tag{1.20}$$

The general solution to this equation is

$$\ln(T - T_\infty) = -\frac{t}{(\rho c V / \overline{h}A)} + C \tag{1.21}$$

If the initial temperature is $T(t = 0) \equiv T_i$, then $C = \ln(T_i - T_\infty)$. The group $\rho c V / \overline{h}A$ is the *time constant*, $\boldsymbol{T}$. The cooling of the body is then given by

$$\boxed{\frac{T - T_\infty}{T_i - T_\infty} = e^{-t/\boldsymbol{T}}} \tag{1.22}$$

All of the physical parameters in the problem are now contained in the time constant, $\boldsymbol{T}$. It represents the time required for a body to cool to $1/e$, or 37%, of the initial temperature difference above or below T_∞. The time constant can also be written as

$$\boldsymbol{T} = mc\left(\frac{1}{\overline{h}A}\right) \tag{1.23}$$

where $m = \rho V$ is the mass of the body. A body of greater mass or greater specific heat capacity will have a larger time constant and will take longer to cool. The quantity $1/\overline{h}A$ may be thought of as a "resistance" to heat loss by convection (see Section 2.3). In other words, a body with less surface area or lower $\overline{h}$ will also take longer to cool.

Notice that the thermal conductivity is missing from eqns. (1.22) and (1.23). The reason is that we have assumed that the temperature of the body is nearly uniform, and this means that internal conduction is not important. We see in Fig. 1.10 that, if $L/(k_b/\overline{h}) \ll 1$, the temperature of the body, T_b, is almost uniform within the body at any time. We name this group Bi, so

$$\text{Bi} \equiv \frac{\overline{h}L}{k_b} \ll 1 \text{ implies that } T_b(x,t) \simeq T(t) \simeq T_{\text{surface}}$$

---

[6]Is it clear why $(T - T_{\text{ref}})$ has been changed to $(T - T_\infty)$ under the derivative? Remember that the derivative of a constant (like T_{ref} or T_∞) is zero. We can therefore change T_{ref} to T_∞ without invalidating the equation, so as to get the same dependent variable on both sides of the equation.
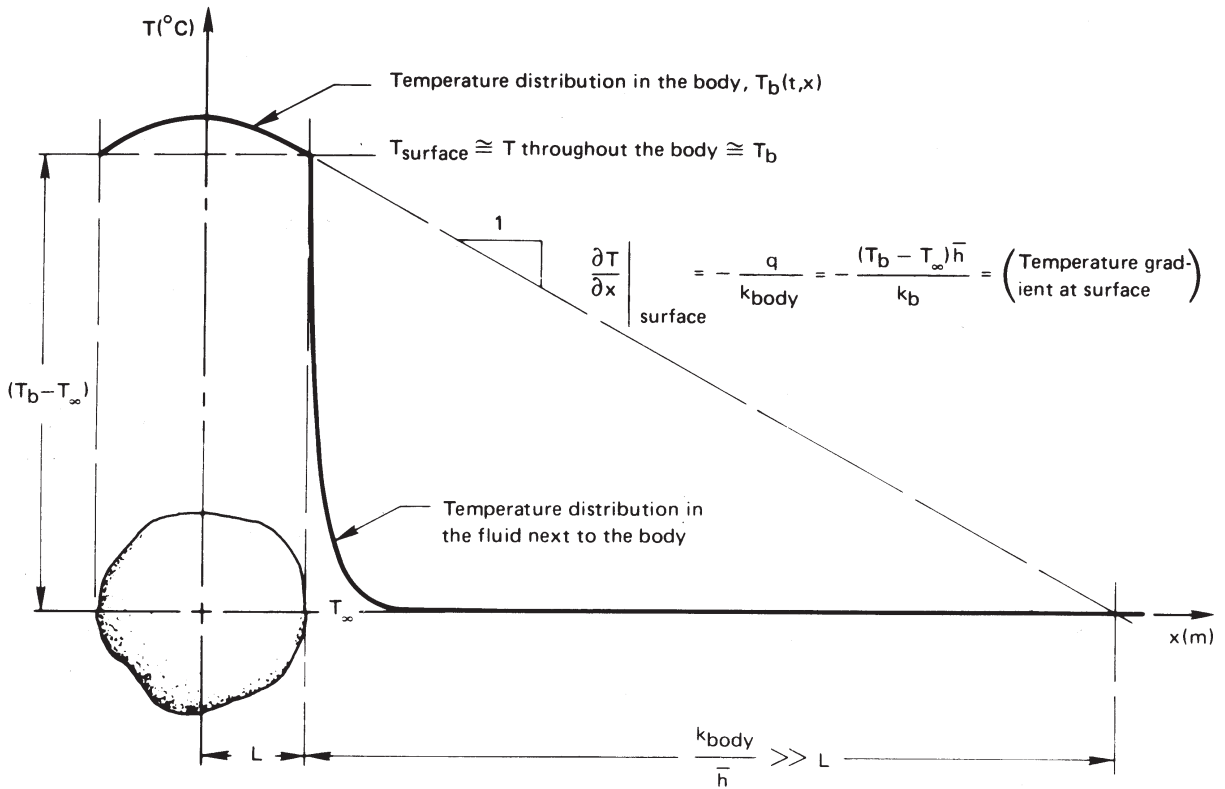
Figure 1.10   The cooling of a body for which the Biot number, $\mathrm{Bi} = \overline{h}L/k_b$, is small. The temperature variation within the body is less than $L\,dT/dx\big|_{\text{surface}} = (\overline{h}L/k_b)(T_b - T_\infty)$. Therefore, when $\mathrm{Bi} \ll 1$, the body temperature is nearly uniform.

and the thermal conductivity, k_b, becomes irrelevant to the cooling process. This condition must be satisfied or the lumped-capacity solution will not be accurate.

The group $\mathrm{Bi} = \overline{h}L/k_b$ is called the *Biot number*[7]. If Bi were large, of course, the situation would be reversed, as shown in Fig. 1.11. In this case $\mathrm{Bi} = hL/k_b \gg 1$ and the convection process offers little resistance

---

[7]Pronounced **Bee**-oh. J. B. Biot, although younger than Fourier, worked on the analysis of heat conduction even earlier—in 1802 or 1803. He grappled with the problem of including external convection in heat conduction analyses in 1804 but could not see how to do it. Fourier read Biot's work and by 1807 had determined how to analyze the problem. (Later we encounter a similar dimensionless group called the Nusselt number, $\mathrm{Nu} \equiv hL/k_{\text{fluid}}$. The latter relates only to the fluid flowing over a body and not to the body being cooled. We deal with it extensively in the study of convection.)
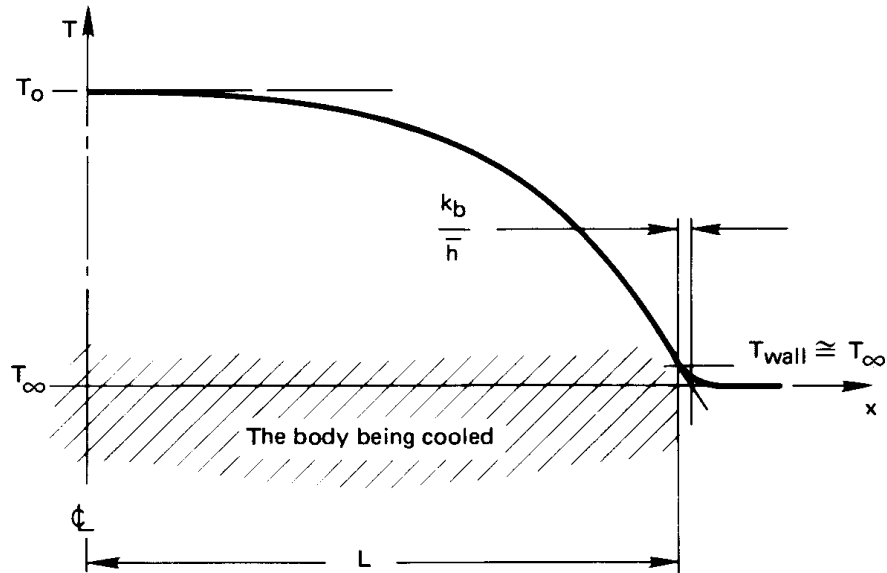
Figure 1.11 The cooling of a body for which the Biot number, $\overline{h}L/k_b$, is large.

to heat transfer. We could solve the heat conduction equation

$$\frac{\partial^2 T_b}{\partial x^2} = \frac{1}{\alpha}\frac{\partial T_b}{\partial t}$$

subject to the simple boundary condition $T_b(x,t) = T_\infty$ when $x = L$, to determine the temperature in the body and its rate of cooling in this case. The Biot number will therefore be the basis for determining what sort of problem we have to solve.

The lumped capacity solution will normally be accurate within about 3% if Bi $\lesssim 0.1$, and much more accurate for still smaller values of Bi [1.3].

Example 1.4

A thermocouple bead is largely solder, 1 mm in diameter. It is initially in a 20°C room and is then suddenly placed into a 200°C gas flow. The heat transfer coefficient $\overline{h}$ is 250 W/m²K, and the effective values of k, ρ, and c are 45 W/m·K, 9300 kg/m³, and 0.18 kJ/kg·K, respectively. Evaluate the response of the thermocouple.
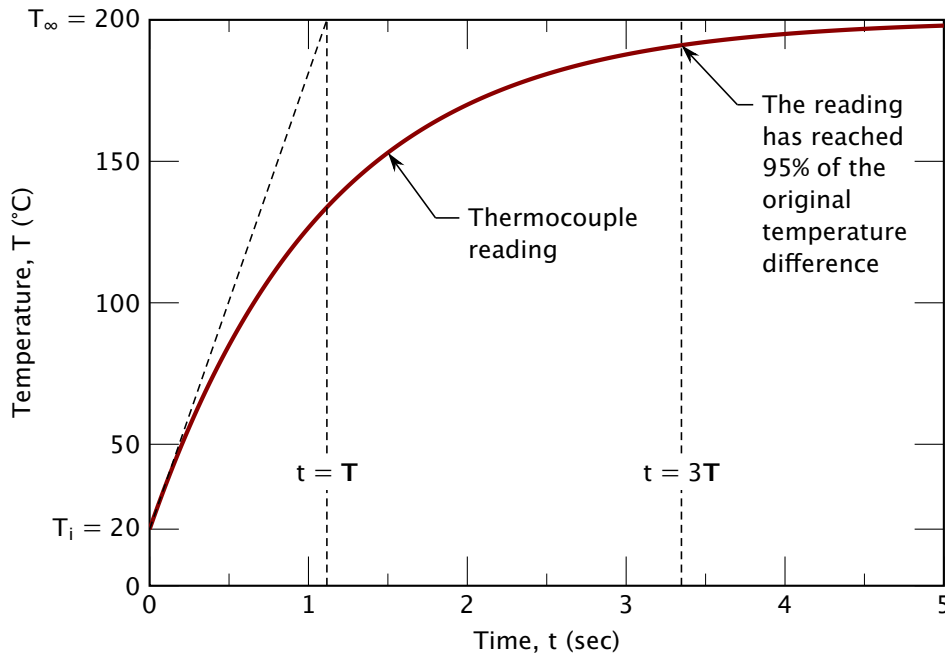
Figure 1.12 Thermocouple response to a hot gas flow.

SOLUTION. The time constant, T, is

$$
\begin{aligned}
T &= \frac{\rho c V}{\overline{h} A} = \frac{\rho c}{\overline{h}} \frac{\pi D^3/6}{\pi D^2} = \frac{\rho c D}{6 \overline{h}} \\
&= \frac{(9300)(0.18)(0.001)}{6(250)} \frac{\text{kg}}{\text{m}^3} \frac{\text{kJ}}{\text{kg·K}} \, \text{m} \, \frac{\text{m}^2\text{·K}}{\text{W}} \frac{1000 \text{ W}}{\text{kJ/s}} \\
&= 1.116 \text{ s}
\end{aligned}
$$

Therefore, with $T_i = 20°\text{C}$ and $T_\infty = 200°\text{C}$, eqn. (1.22) becomes

$$
\frac{T - 200°\text{C}}{(20 - 200)°\text{C}} = e^{-t/1.116} \ \text{ or } \ T = 200 - 180 \, e^{-t/1.116} \, °\text{C}
$$

This result is plotted in Fig. 1.12, where we see that, for all practical purposes, this thermocouple catches up with the gas stream in less than 5 s. Indeed, it should be apparent that any lumped system will come within 95% of the change in signal in three time constants, since $e^{-3} \simeq 0.050$.

This calculation is based entirely on the assumption that Bi $\ll 1$ for the thermocouple. We must check that assumption:

$$\text{Bi} \equiv \frac{\overline{h}L}{k} = \frac{(250 \text{ W/m}^2\text{K})(0.001 \text{ m})/2}{45 \text{ W/m·K}} = 0.00278$$

This is very small indeed, so the assumption is valid.   ■

To calculate the rate of entropy production in a lumped-capacity system, we note that the entropy change of the universe is the sum of the entropy decrease of the body and the more rapid entropy increase of the surroundings. The source of irreversibility is heat flow through the finite temperature difference in the boundary layer. Accordingly, we write the time rate of change of entropy of the universe, $dS_{\text{Un}}/dt \equiv \dot{S}_{\text{Un}}$, in terms of the entropy transfer out of the body and into the surroundings

$$\dot{S}_{\text{Un}} = \dot{S}_{\text{body}} + \dot{S}_{\text{surroundings}} = \frac{-Q}{T} + \frac{Q}{T_\infty}$$

where T is now the lumped temperature of the body. Then, with eqn. (1.19):

$$\dot{S}_{\text{Un}} = -\rho cV \frac{dT}{dt} \left(\frac{1}{T_\infty} - \frac{1}{T} \right)$$

We can multiply both sides of this equation by dt and integrate the right-hand side from $T(t = 0) \equiv T_0$ to T at the time of interest:

$$\Delta S = -\rho cV \int_{T_0}^{T} \left(\frac{1}{T_\infty} - \frac{1}{T} \right) dT \tag{1.24}$$

Equation 1.24 will give a positive ΔS whether $T > T_\infty$ or $T < T_\infty$ because the sign of dT will always oppose the sign of the integrand.

Experiment 1.2

Invent and carry out a simple procedure for evaluating the time constant of a fever thermometer in your mouth.   ♦

Radiation

Heat transfer by thermal radiation.   All bodies constantly emit energy by a process of electromagnetic radiation. The intensity of this radiant energy flux depends upon the temperature of the body and the nature of its surface. Most of the heat that reaches you when you sit in front of

a fire is radiant energy. Radiant energy browns your toast in an electric toaster, and it warms you when you walk in the sun.

Objects that are cooler than the fire, the toaster, or the sun emit much less energy because the emission varies as the fourth power of absolute temperature. Very often, the emission of energy, or *radiant heat transfer*, by cooler bodies can be neglected in comparison with forced convection and conduction. But heat transfer processes that occur at high temperature, or with conduction and convection suppressed by a vacuum, usually involve a significant fraction of radiation.

Experiment 1.3

Open the freezer door to your refrigerator. Put your face near it, but stay far enough away to avoid the downwash of cooled air. This way you cannot be cooled by convection; nor, because the air between you and the freezer is a fine insulator, can you be cooled by conduction. Still your face will feel cooler. The reason is that you radiate heat directly into the cold region, and it radiates very little heat to you. Consequently, your face cools perceptibly. ♦

The electromagnetic spectrum.   Thermal radiation is a form of electromagnetic energy. Accordingly, it exhibits the same wavelike properties as light or radio waves. Each quantum of radiant energy has a wavelength, λ, and a frequency, ν, associated with it.

The full electromagnetic spectrum includes an enormous variety of energy-bearing waves, of which heat is only a small part. Table 1.2 lists the various forms over a range of wavelengths that spans 17 orders of magnitude. Only the tiniest "window" of visible light exists in this spectrum, through which we see the world around us. Thermal radiation, whose main component is usually the spectrum of infrared radiation, passes through the much larger window—about three orders of magnitude in λ or ν.

Black bodies.   The model for the perfect thermal radiator is a so-called *black body*. This is a body which absorbs all energy that reaches it and reflects nothing. The term can be a little confusing, since such bodies *emit* energy. Thus, if we possessed infrared vision, a black body would glow with "color" appropriate to its temperature. Perfect radiators *are* "black" in the sense that they absorb all visible light (and all other radiation) that reaches them. Consequently, perfect radiators will look black unless they

Table 1.2 Forms of the electromagnetic wave spectrum

Characterization	Wavelength, λ	
Cosmic rays	< 0.3 pm	
Gamma rays	0.3–100 pm	
X rays	0.01–30 nm	
Ultraviolet light	3–400 nm	
Visible light	0.4-0.7 μm	**Thermal Radiation**
Near infrared radiation	0.7–30 μm	**0.1–1000 μm**
Far infrared radiation	30–1000 μm	
Millimeter waves	1–10 mm	
Microwaves	10–300 mm	
Shortwave radio & TV	300 mm–100 m	
Longwave radio	100 m–30 km	

are hot enough to radiate heat in the form of visible light, as do the sun and the orange flames of a fire.

We need to have an experimental method for making a perfectly black body. The conventional device for approaching this ideal is called by the German term *hohlraum*, which literally means "hollow space". Figure 1.13 shows how a hohlraum is arranged. It is simply a device that traps all the energy that reaches the aperture.

What are the important features of a thermally black body? Suppose that a radiant heat flux, q, falls upon a translucent plate that is not black, as shown in Fig. 1.14. A fraction, α, of the total incident energy, called the *absorptance*, is absorbed in the body; a fraction, ρ, called the *reflectance*, is reflected from it; and a fraction, τ, called the *transmittance*, passes through. Thus

$$1 = \alpha + \rho + \tau \tag{1.25}$$

This relation can also be written for the energy carried by each wavelength in the distribution of wavelengths that makes up *heat* from a source at any temperature:

$$1 = \alpha_\lambda + \rho_\lambda + \tau_\lambda \tag{1.26}$$

All radiant energy incident on a black body is absorbed, so that α_b or $\alpha_{\lambda_b} = 1$ and $\rho_b = \tau_b = 0$. Furthermore, the energy emitted from a
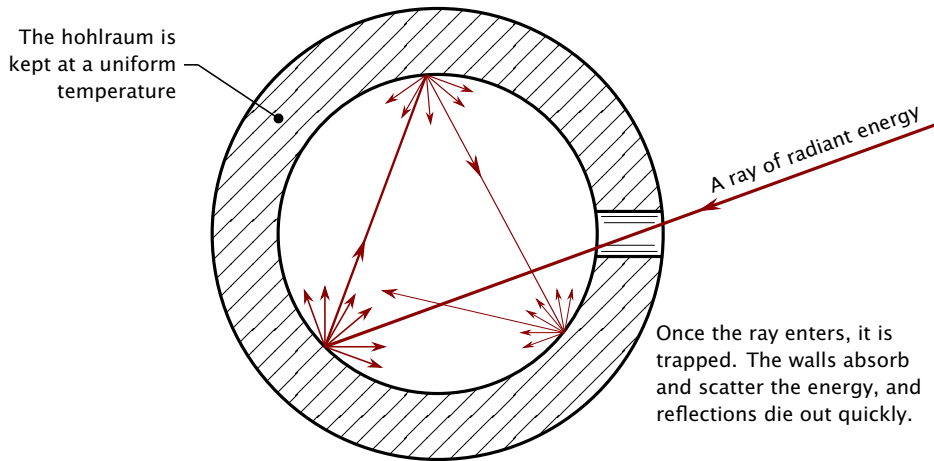
Figure 1.13 Cross section of a spherical hohlraum. The hole has the attributes of a nearly perfect thermal black body.

black body reaches a theoretical maximum, which is given by the Stefan-Boltzmann law. We look at this next.

The Stefan-Boltzmann law. We call the flux of energy radiating from a body the *emissive power*, $e(T)$ W/m^2. The radiative flux at any single wavelength is called the *monochromatic emissive power*, $e_\lambda(\lambda, T)$. ("Monochromatic" means "single color".) Thus, the emissive power is the integral of the monochromatic emissive power over all wavelengths

$$e(T) \equiv \int_0^\infty e_\lambda(\lambda, T)\, d\lambda \qquad (1.27)$$
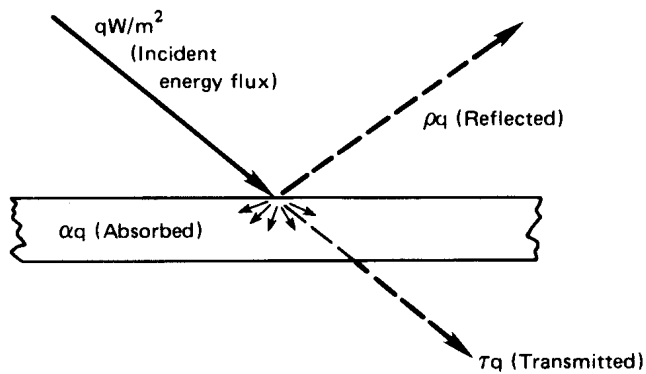
Figure 1.14 The distribution of energy incident on a translucent slab.

The dependence of $e(T)$ on T for a black body was established experimentally by Stefan in 1879 and explained by Boltzmann on the basis of thermodynamic arguments in 1884. The Stefan-Boltzmann law is

$$\boxed{e_b(T) = \sigma T^4}$$ (1.28)

where the Stefan-Boltzmann constant, σ, is 5.670374×10^{-8} W/m^2·K^4 or 1.714×10^{-9} Btu/hr·ft^2·°R^4, and T is the absolute temperature.

e_λ vs. λ.   Nature requires that, at a given temperature, a body will emit a unique distribution of energy in wavelength. Thus, when you heat a poker in the fire, it first glows a dull red—emitting most of its energy at long wavelengths and just a little bit in the visible regime. When it is white-hot, the energy distribution has been both greatly increased and shifted toward the shorter-wavelength visible range. At each temperature, a black body yields the highest value of e_λ that a body can attain.

The very careful measurements of the black-body energy spectrum made in 1899 by Lummer and Pringsheim [1.4] are shown in Fig. 1.15. The wavelength where the emissive power is maximum at any temperature is given by an exact relation called *Wien's displacement law:*

$$(\lambda T)_{e_\lambda=\max} = 2897.77 \text{ μm·K}$$ (1.29)

Notice that around three-fourths of the area under each curve — that is, three-fourths of the radiant energy — is carried by wavelengths greater than that at the maximum. Even as the peak moves toward the visible range at higher temperatures, the visible fraction of radiation remains very small.

How physical theory could predict the observed wavelength dependence of black body radiation became more and more perplexing toward the end of the 19th century. The answer to that question would be the keystone of the most profound scientific revolution the world has seen. In 1901, Max Planck developed a theoretical model to explain the dependence, although without yet understanding that he was setting the new quantum physics in motion. His precise result, *Planck's law*, was

$$e_{\lambda_b} = \frac{2\pi h c_o^2}{\lambda^5 \left[\exp(hc_o/k_B T\lambda) - 1\right]}$$ (1.30)

where c_o is the speed of light, equal to 2.99792458×10^8 m/s in vacuum; h is Planck's constant, $6.62607015 \times 10^{-34}$ J·s; and k_B is Boltzmann's constant, 1.380649×10^{-23} J/K.

Monochromatic emmissive power

Black Bodies

× × × Observed data
⊗ ⊗ ⊗ Calculated

1646°
(1653°)

1449°

1259°

1095°
998°
904°
723°

Wavelength (micrometers)

Approx. range of visible light
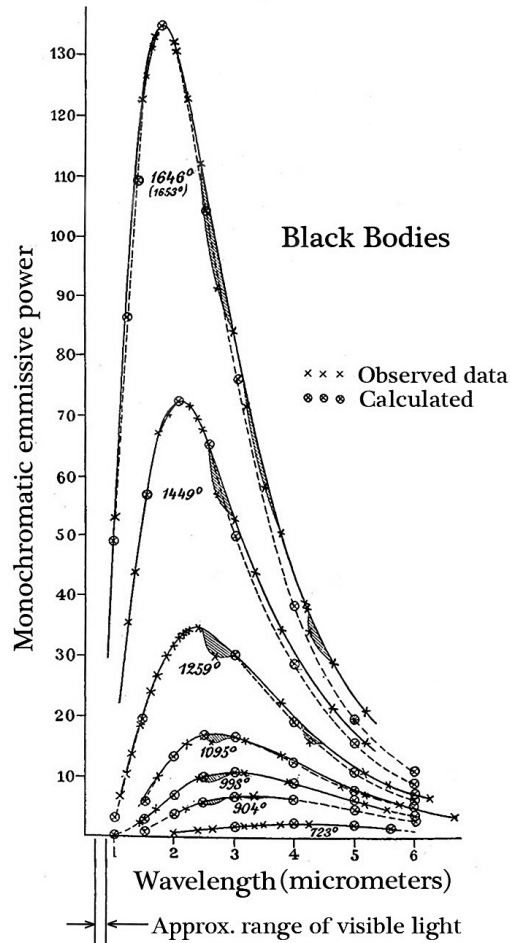
Figure 1.15 Black body data from Lummer and Pringsheim (1899). The curves show the monochromatic emissive power of black bodies at various temperatures (in K). The calculated values were based on a model due to Wien, which these data showed to run low at higher wavelengths. This comparison led Planck to a new model which matched the data for all wavelengths, using fitted values of h and k_B. (Today's e_{λ_b} data, and Planck's law with modern h and k_B, now in precise agreement, both lie a bit above these old curves.)

Radiant heat exchange. Suppose that a heated object (1 in Fig. 1.16a) radiates only to some other object (2) and that both objects are thermally black. All heat leaving object 1 arrives at object 2, and all heat arriving at object 1 comes from object 2. Thus, the net heat transferred from object 1 to object 2, Q_{net}, is the difference between $Q_{1 \text{ to } 2} = A_1 e_b(T_1)$ and $Q_{2 \text{ to } 1} = A_1 e_b(T_2)$

$$Q_{\text{net}} = A_1 e_b(T_1) - A_1 e_b(T_2) = A_1 \sigma \left(T_1^4 - T_2^4 \right) \qquad (1.31)$$

If the first object "sees" other objects in addition to object 2, as indicated in Fig. 1.16b, then a *view factor* (sometimes called a *configuration factor*

to ∞   to ∞

Q_{net}

T_1

T_2

a) Object 1 radiates
   only to object 2

T_2

$Q_{net} = Q_{1\text{-}2} - Q_{2\text{-}1}$

$Q_{other\ things\text{-}1}$

T_1

$Q_{1\text{-}other\ things}$

b) Object 1 radiates to object 2
   and to other things as well
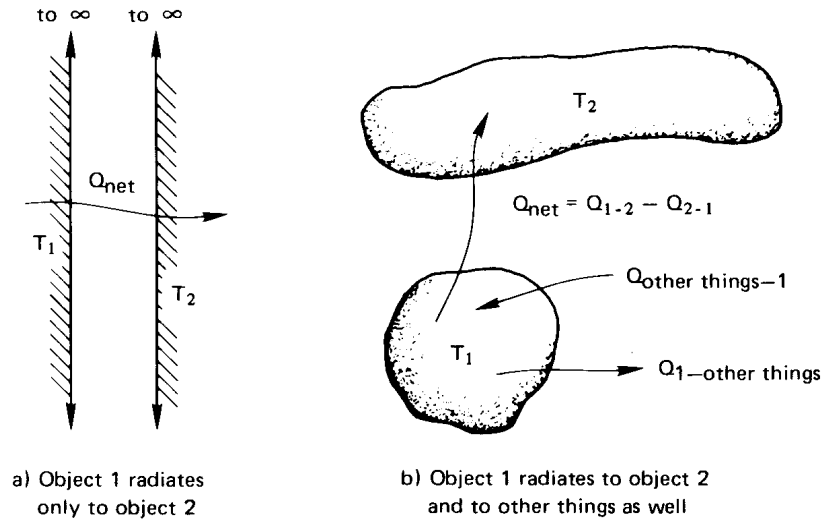
Figure 1.16 The net radiant heat transfer from one object to
another.

or a *shape factor*), $F_{1\text{-}2}$, must be included in eqn. (1.31):

$$Q_{net} = A_1 F_{1\text{-}2}\, \sigma \left(T_1^4 - T_2^4 \right) \tag{1.32}$$

We may regard $F_{1\text{-}2}$ as the fraction of energy leaving object 1 that is
intercepted by object 2.

Example 1.5

A black thermocouple is inside a chamber with black walls. If the air
around the thermocouple is at 20°C, the walls are at 100°C, and the
heat transfer coefficient between the thermocouple and the air is 75
W/m²K, what temperature will the thermocouple read?

SOLUTION. The heat convected away from the thermocouple by the air
must exactly balance that radiated to it by the hot walls if the system
is in steady state. Furthermore, $F_{1\text{-}2} = 1$ since the thermocouple (1)
radiates all its energy to the walls (2):

$$\overline{h} A_{tc} (T_{tc} - T_{air}) = -Q_{net} = -A_{tc} \sigma \left(T_{tc}^4 - T_{wall}^4 \right)$$

or, with T_{tc} in °C,

$$75(T_{tc} - 20)\ \text{W/m}^2 =$$
$$5.6704 \times 10^{-8} \left[(100 + 273)^4 - (T_{tc} + 273)^4 \right]\ \text{W/m}^2$$

since T for radiation must be in kelvin. Trial-and-error solution of this equation yields $T_{tc} = 28.4°C$. ■

We have seen that non-black bodies absorb less radiation than black bodies, which are perfect absorbers. Likewise, non-black bodies emit less radiation than black bodies, which also happen to be perfect emitters. We can characterize the emissive power of a non-black body using a property called *emittance, ε*:

$$e_{\text{non-black}} = \varepsilon e_b = \varepsilon \sigma T^4 \tag{1.33}$$

where $0 < \varepsilon \leqslant 1$ (emittance is sometimes called *emissivity*). When radiation is exchanged between two bodies that are not black, we have

$$Q_{\text{net}} = A_1 \mathcal{F}_{1\text{-}2}\, \sigma \left(T_1^4 - T_2^4\right) \tag{1.34}$$

where the *transfer factor*, $\mathcal{F}_{1\text{-}2}$, depends on the emittances of both bodies as well as the geometrical "view".

The expression for $\mathcal{F}_{1\text{-}2}$ is particularly simple in the important special case of a small object, 1, in a much larger isothermal environment, 2:

$$\mathcal{F}_{1\text{-}2} = \varepsilon_1 \quad \text{for} \quad A_1 \ll A_2 \tag{1.35}$$

We prove this result in Example 10.7, in the chapter on radiation.

Example 1.6

Suppose that the thermocouple in Example 1.5 were not black and had an emittance of $\varepsilon_{tc} = 0.4$. Further suppose that the walls were not black and had a much larger surface area than the thermocouple. What temperature would the thermocouple read?

SOLUTION. Q_{net} is now given by eqn. (1.34) and $\mathcal{F}_{1\text{-}2}$ is ε_{tc} according to eqn. (1.35):

$$\overline{h}A_{tc}\left(T_{tc} - T_{\text{air}}\right) = -A_{tc}\varepsilon_{tc}\sigma\left(T_{tc}^4 - T_{\text{wall}}^4\right)$$

or

$$75(T_{tc} - 20)\ \text{W/m}^2 =$$
$$(0.4)(5.6704 \times 10^{-8})\left[(100 + 273)^4 - (T_{tc} + 273)^4\right]\ \text{W/m}^2$$

Trial-and-error yields $T_{tc} = 23.5°C$. ■

Radiation shielding. The preceding examples point out an important practical problem than can be solved with radiation shielding. The idea is as follows: If we want to measure the true air temperature, we can place a thin foil casing, or shield, around the thermocouple. The casing is shaped to obstruct the thermocouple's "view" of the chamber but to permit the free flow of the air around the thermocouple. Then the shield, like the thermocouple in the two examples, will be cooler than the walls, and the thermocouple it surrounds will be influenced by this much cooler radiator. If the shield is highly reflecting on the outside, it will assume a temperature still closer to that of the air and the error will be still less. Multiple layers of shielding can further reduce the error.

Radiation shielding can take many forms and serve many purposes. It is an important element in superinsulations. A glass firescreen in a fireplace serves as a radiation shield because it is largely opaque to infrared radiation. It absorbs heat radiated by the fire and reradiates that energy (ineffectively) at a temperature much lower than that of the fire.

Experiment 1.4

Find a small open flame that produces a fair amount of soot. A candle, kerosene lamp, or a cutting torch with a fuel-rich mixture should work well. A clean blue flame will not work well because such gases do not radiate much heat. First, place your finger in a position about 1 to 2 cm to one side of the flame, where it becomes uncomfortably hot. Now take a piece of fine mesh screen and dip it in some soapy water, which will fill up the holes. Put it between your finger and the flame. You will see that your finger is protected from the heating until the water evaporates.   ♦

This experiment dramatizes that fact that water, while relatively transparent to light, is essentially opaque to infrared radiation. That fact is true of liquids in general. Air and other gases, on the other hand, let most infrared radiation pass. *We treat gases as transparent to thermal radiation*, until we reach Section 10.5. Radiation can be ignored in calculations for most liquids.

1.4   A look ahead

What we have done up to this point has been no more than to reveal the tip of the iceberg. The basic mechanisms of heat transfer have been

explained and some quantitative relations have been presented. However, this information will barely get you started when you are faced with a real heat transfer problem. Three tasks, in particular, must be completed to solve actual problems:

- We must solve the heat conduction equation subject to appropriate boundary conditions if the problem involves heat conduction of any complexity (Part II).

- We must determine the convective heat transfer coefficient, h, if convection is important in a problem (Part III).

- We must calculate F_{1-2} or $\mathcal{F}_{1-2}$ to evaluate the radiative heat transfer (Part IV).

Any of these determinations can involve a great deal of complication, and most of the chapters that lie ahead are devoted to these three basic problems.

Before becoming engrossed in these three questions, we shall first look at the archetypical applied problem of heat transfer–namely, the design of a heat exchanger. Chapter 2 sets up the elementary analytical apparatus that is needed, and Chapter 3 shows how to do such design if $\bar{h}$ is already known. This will make it easier to see the importance of the detailed study of the three basic problems later in the book.

1.5 About the end-of-chapter problems

We have noted that this book is set down almost exclusively in S.I. units. The only use of English units appears in some of the problems at the end of each chapter. A few such problems are included to provide experience in converting back into English units, since such units will undoubtedly persist in the U.S.A. for many more years. The student who has problems with dimensional conversion will find Appendix B helpful.

Partial numerical answers to some of the problems follow them in brackets. Tables of physical property data that we need to solve the problems are given in Appendix A.

Another matter often leads to some discussion between students and teachers in heat transfer courses. That is the question of whether a problem is "theoretical" or "practical". Quite often the student is inclined to view as "theoretical" a problem that does not involve numbers or that requires the development of algebraic results.

The problems assigned in this book are all intended to be useful in that they do one or more of five things:

1. They involve a calculation of a type that actually arises in practice (e.g., Problems 1.1, 1.3, 1.8 to 1.18, and 1.21 through 1.25).

2. They illustrate a physical principle (e.g., Problems 1.2, 1.4 to 1.7, 1.9, 1.20, 1.32, and 1.39). These are probably closest to having a real theoretical objective in that they clarify heat transfer's underlying principles.

3. They require using methods in the text to develop other results that are useful in certain applied problems (e.g., Problems 1.10, 1.16, 1.17, and 1.21). Such problems are usually the most difficult and the most instructive.

4. They anticipate development that will appear in subsequent chapters (e.g., Problems 1.16, 1.20, 1.40, and 1.41).

5. They require developing our ability to handle numerical and algebraic computation. (This is the case with most of the problems in Chapter 1, but it is especially true of Problems 1.6 to 1.9, 1.15, and 1.17).

Actually, we wish to look at the *theory*, *analysis*, and *practice* of heat transfer—all three—according to definitions in Webster's dictionary:

Theory: "a systematic statement of principles; a formulation of apparent relationships or underlying principles of certain observed phenomena."

Analysis: "the solving of problems by the means of equations; the breaking up of any whole into its parts so as to find out their nature, function, relationship, etc."

Practice: "the *doing* of something as an application of knowledge."

Problems

1.1 An unusual composite wall consists of successive layers of fir (5 cm thick), aluminum (1 cm thick), lead (1 cm thick), and corkboard (6 cm thick). The temperature is 60°C on the outside surface of the fir and 10°C on the outside surface of the corkboard. Plot

the temperature as a function of position going from one side of the wall to the other. Does the temperature profile suggest any simplifying assumptions that might be made in subsequent analysis of the wall? *Hint:* See Example 1.2 and Tables A.1 and A.2.

1.2 Verify that eqn. (1.16) is consistent with Newton's law of cooling, eqn. (1.15).

1.3 The heat flux in a 1 cm thick slab is $q = 5000$ W/m^2 and the temperature on the cold side is $T = -40°$C. Tabulate the temperature rise going to the opposite hot side of the slab if it is made of:

- Pure silver
- Pure aluminum
- Mild steel (0.5% carbon)
- Ice
- Spruce
- Insulation (85% magnesia)
- Silica aerogel

Indicate which situations would be unreasonable and why. [Silver: $\Delta T = 0.117°$C]

1.4 Explain in words why the heat conduction equation, eqn. (1.14), shows that in transient conduction the temperature depends on the thermal diffusivity, α, but we can solve steady conduction problems using just k (as in Example 1.1).

1.5 A 1 m rod of pure copper 1 cm^2 in cross section connects a 200°C thermal reservoir with a 0°C thermal reservoir. The system has already reached steady state. What are the resulting rates of change of entropy of: (a) the hot reservoir; (b) the cold reservoir; (c) the rod; and (d) the whole universe? Explain whether or not your answer satisfies the Second Law of Thermodynamics. [(d): +0.0121 W/K]

1.6 Two thermal energy reservoirs at temperatures of 27°C and $-43°$C, respectively, are separated by a slab of material 10 cm thick and 930 cm^2 in cross-sectional area. The slab has a thermal conductivity of 0.14 W/m·K. The system is operating at steady-state conditions. What are the rates of change of entropy of (a) the higher temperature reservoir, (b) the lower temperature reservoir, (c) the slab, and (d) the whole universe as a result of this process? (e) Does your answer satisfy the Second Law of Thermodynamics?

1.7 (a) If the thermal energy reservoirs in Problem 1.6 are suddenly replaced with adiabatic walls, determine the final equilibrium temperature of the slab. (b) What is the entropy change for the slab for this process? (c) Does your answer satisfy the Second Law of Thermodynamics in this instance? Explain. The density of the slab is 26 lb/ft^3 and the specific heat is 0.65 Btu/lb·°F. Recall from your thermodynamics course that the specific entropy of a solid is $s - s_{\text{ref}} = c \ln (T/T_{\text{ref}})$. [(b): 30.81 J/K]

1.8 A copper sphere 2.5 cm in diameter has a uniform initial temperature of 40°C. The sphere is suspended in a slow-moving air stream at 0°C. The air stream produces an average convection heat transfer coefficient of $\overline{h} = 15$ W/m^{2}K. Thermal radiation can be neglected. Since copper is highly conductive and the heat transfer coefficient is low, temperature gradients in the sphere will be small, and its temperature will be essentially uniform throughout the cooling process (i.e., Bi ≪ 1). Write the instantaneous energy balance between the sphere and the surrounding air. Solve this simple first-order differential equation and plot the resulting temperatures as a function of time between 40°C and 0°C. Also, confirm that Bi ≪ 1.

1.9 After working Problem 1.8, determine the total heat transfer (in J) in as the sphere cools from 40°C to 0°C. Also, plot the net entropy increase of the universe [eqn. (1.24)] resulting from the cooling process as a function of the sphere's temperature, ΔS vs. T (K). [Total heat transfer = 1125 J]

1.10 A truncated cone 30 cm high is constructed of Portland cement. The diameter at the top is 15 cm and at the bottom is 7.5 cm. The lower surface is maintained at 6°C and the top at 40°C. The side surface is insulated. Assume one-dimensional heat transfer and calculate the rate of heat transfer in watts from top to bottom. To do this, note that in steady state the rate of heat transfer, Q, must be the same at every cross section. Write Fourier's law locally, and integrate it from top to bottom to get a relation between this unknown Q and the known end temperatures. [$|Q| = 0.70$ W]

1.11 A hot water heater contains 100 kg of water at an initial temperature of 75°C in a 20°C room. Its surface area is 1.3 m^2. Select an insulating material and specify the minimum thickness of insulation to keep the water from cooling more than 3°C/h when the

heat is off. (Notice that this problem is greatly simplified if the temperature drop in the steel casing and the temperature drop in the convective boundary layers are neglected. Are these reasonable approximations? Explain why or why not.)
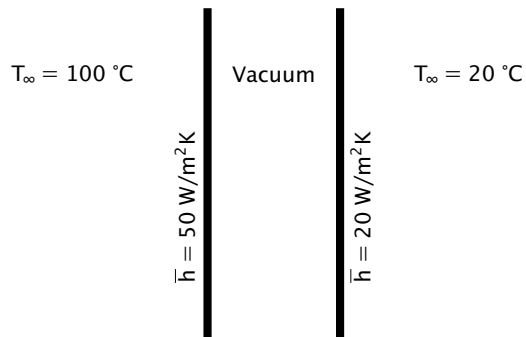
Figure 1.17 Configuration for Problem 1.12

1.12 Two walls facing each other are thin, very large in extent, highly conducting, and radiatively black on the facing surfaces (Fig. 1.17). They are separated by a vacuum. The outsides of the plates experience convection (without radiation) as shown. Set up an equation for the temperature of the left-hand plate and solve it by iteration. Then find the temperature of the right-hand plate. $[T_{right} = 42.5°C]$

1.13 Develop S.I. to English conversion factors for:

- The thermal diffusivity, α
- The heat flux, q
- The density, ρ
- The Stefan-Boltzmann constant, σ
- The view factor, F_{1-2}
- The molar entropy
- The specific heat per unit mass, c

In each case, begin with basic dimensions J, m, kg, s, °C. Check your answers against Appendix B if possible. $[1 \ m^2/s = 10.764 \ ft^2/s]$

1.14 Three infinite, parallel, black, opaque plates exchange heat by radiation, as shown in Fig. 1.18. Find T_2.

1.15 Four infinite, parallel, black, opaque plates transfer heat by radiation, as shown in Fig. 1.19. Find T_2 and T_3. $[T_2 = 75.53°C]$

Figure 1.18 Configuration for
Problem 1.14
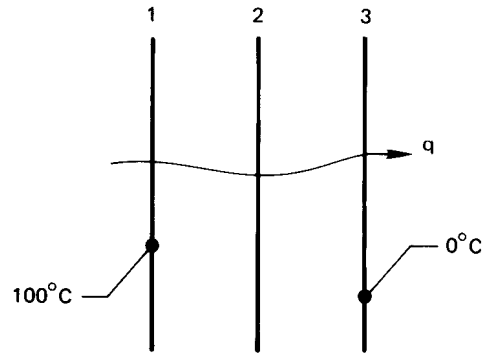
Figure 1.19 Configuration for
Problem 1.15
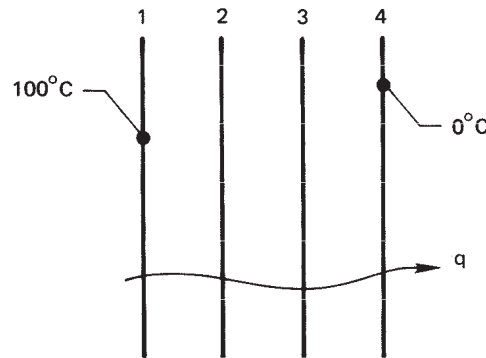
1.16 Two large, black, horizontal plates are spaced a distance L from
one another. The top one is warm at a controllable temperature,
T_h, and the bottom one is cool at a specified temperature, T_c. A
gas separates them. The gas is at rest because it is warm (less
dense) toward the top and cold (more dense) toward the bottom.
Let $\Theta \equiv T_h/T_c$, and write an equation for the ratio of radiation
to conduction heat flux through between the plates, $q_{rad}/q_{cond} =$
fn(N, Θ), where N is a dimensionless group containing σ, k, L, and
T_c, which you will identify.

    a. Plot N as a function of Θ for $q_{rad}/q_{cond} = 0.8$, 1, and 1.2 (and
    for other values if you wish).

    b. Suppose that you have a system in which $L = 10$ cm, $T_c =$
    100 K, and the gas is hydrogen with an average k of 0.1 W/m·K.
    Find the value of T_h for which the conduction and radiation
    heat fluxes are identical.

1.17 A blackened copper sphere 2 cm in diameter and uniformly at
200°C is introduced into a large evacuated black chamber that is

maintained at 20°C.

a. Write a differential equation that expresses $T(t)$ for the sphere, assuming the lumped thermal capacity.

b. Divide the radiation heat flux by temperature difference to find a "radiation heat transfer coefficient." Then identify a dimensionless group, analogous to the Biot number, than indicates whether the lumped-capacity solution is valid.

c. Show that the lumped-capacity solution is valid in this case.

d. Integrate your differential equation and plot the temperature response for the sphere.

1.18 A small instrumentation package is released from a space vehicle. It can be approximated as a solid aluminum sphere, 4 cm in diameter. The sphere is initially at 303 K and it contains a pressurized hydrogen component that will condense and malfunction at 30 K. If we approximate outer space to be at 0 K, how long will the instrumentation package function properly? Is it legitimate to use the lumped-capacity method for this problem? *Hint:* See the directions for Problem 1.17. [Time = 41 days]
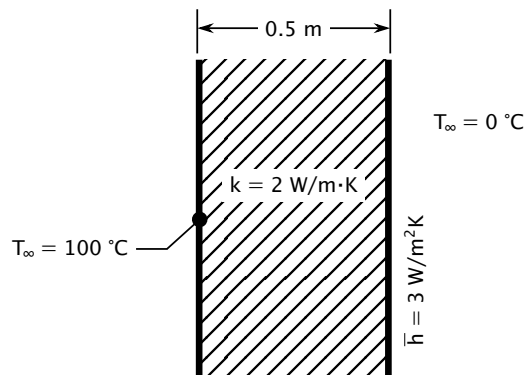
Figure 1.20 Configuration for Problem 1.19

1.19 Consider heat conduction through the wall as shown in Fig. 1.20. Calculate q and the temperature of the right-hand side of the wall.

1.20 Throughout Chapter 1 we have assumed that the steady temperature distribution in a uniform plane wall is a straight line. To prove this, simplify the heat conduction equation to the form appropriate for steady flow. Then integrate it twice and eliminate the two constants using the known outside temperatures T_{left} and T_{right} at $x = 0$ and $x = $ wall thickness, L.

1.21 The thermal conductivity in a particular plane wall depends as follows on the wall temperature, T (°C): $k = A + BT$, where A and B are constants. The temperatures are T_1 and T_2 on either side if the wall, and its thickness is L. By integration of Fourier's law, develop an expression for q. At what temperature should k be evaluated to avoid the need for integration?
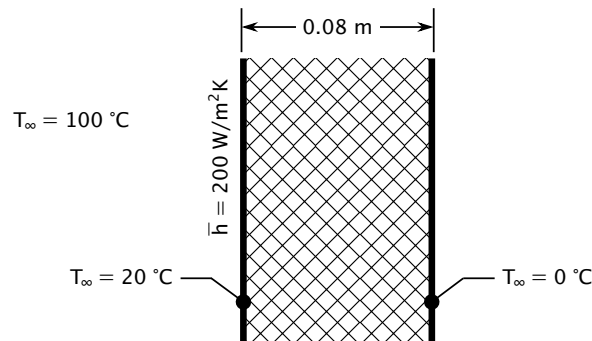
Figure 1.21   Configuration for
Problem 1.22

1.22 Find k for the wall shown in Fig. 1.21. Of what might it be made?

1.23 What are T_i, T_j, and T_r in the wall shown in Fig. 1.22? [$T_j = 16.44$°C]

1.24 An aluminum can of soda pop is removed from a refrigerator and set on a table. If $\overline{h}$ is 13.5 W/m^{2}K, estimate the time until the beverage will be at 15°C. Use reasonable values for the size of the can and for any other information that is not given. The liquid in the can circulates as a result of temperature-induced density changes, so that internal temperature gradients remain small. Assume thermal radiation is accounted for by an effective value of $\overline{h}$ (as will be discussed in Section 2.3) and that humidity is low.

1.25 One large, black wall at 27°C faces a second whose surface is at 127°C. The gap between the walls is evacuated. If the second wall is 0.1 m thick and has a thermal conductivity of 17.5 W/m·K, what is the temperature on the back side of that wall? Assume steady state.

1.26 A 1 cm diameter, 1% carbon steel sphere, initially at 200°C, is cooled by natural convection in air at 20°C. In this case, $\overline{h}$ is not independent of temperature. Instead, $\overline{h} = 3.51(\Delta T)^{1/4}$ W/m^{2}K for $\Delta T = (T_{\text{sphere}} - T_{\text{air}})$°C. Plot T_{sphere} as a function of t. Verify the lumped-capacity assumption.
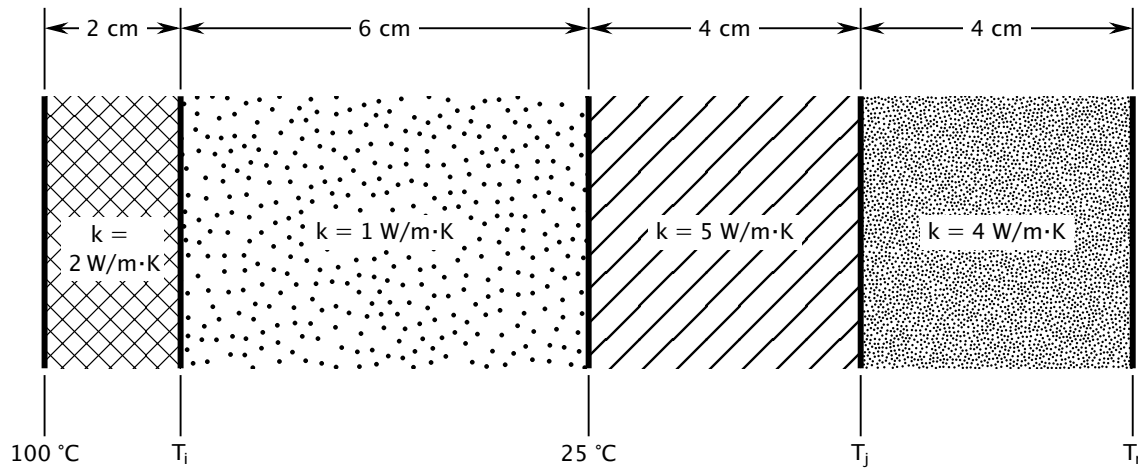
Figure 1.22 Configuration for Problem 1.23

1.27 A 3 cm diameter, black spherical heater is kept at 1100°C. It radiates through an evacuated space to a surrounding spherical shell of Nichrome V. The shell has a 9 cm inside diameter and is 0.3 cm thick. It is black on the inside and is held at 25°C on the outside. Find: (a) the temperature of the inner wall of the shell; and (b) the heat transfer rate, Q. Model conduction in the shell as if it were a plane wall. An iterative solution is needed. [Q = 568 W]

1.28 The sun radiates 650 W/m^2 on the surface of a particular lake. At what rate (in mm/hr) would the lake evaporate if all of this energy went to evaporating water (h_{fg} for water is 2,450,000 J/kg)? Discuss as many other ways as you can think of that the solar energy reaching the surface can be distributed. Do you suppose much of the 650 W/m^2 goes to evaporation?

1.29 It is proposed to make picnic cups, 0.005 m thick, of a new plastic for which $k = k_o(1 + aT^2)$, where T is expressed in °C, k_o = 0.15 W/m·K, and $a = 10^{-4}\,°\text{C}^{-2}$. We are concerned with thermal behavior in the extreme case in which $T = 100$°C inside the cup (as for boiling water) and $T = 0$°C outside. Find the heat flux, q, through the cup, and plot T against position in the cup wall. Assume that this thin wall has reached steady state quickly. *Hint:* To make the plot, find $x(T)$.

1.30 A disk-shaped wafer of diamond IIb is the target of a very high intensity laser. The disk is 5 mm in diameter and 1 mm deep. The flat side is pulsed intermittently with 10^{10} W/m^2 of energy for one microsecond. It then cools by natural convection from that same side until the next pulse. If $\overline{h} = 10$ W/m^{2}K and $T_\infty = 30°$C, plot T_{disk} as a function of time for pulses that are either 50 s apart or 100 s apart. Note that you must determine the temperature the disk reaches before it is pulsed each time, assuming that the process has been repeating over and over again.

1.31 An old-fashioned incandescent 60 W light bulb is roughly a 0.06 m diameter sphere. Its steady surface temperature is 115°C in a room at 25°C, and $\overline{h}$ on the outside is 8.2 W/m^{2}K.

    a. Show that the wavelength of peak radiation from the glass to the room is a near infrared wavelength.

    b. Calculate the heat loss from the glass surface (take $\varepsilon_{\mathrm{glass}} = 0.94$).

    c. How much heat transfer remains to occur by direct radiation from the filament through the glass? (Most of that energy is not in the visible spectrum. These bulbs were very inefficient.)

1.32 How much entropy does the light bulb in Problem 1.31 produce?

1.33 Air at 20°C flows over one side of a thin metal sheet ($\overline{h} = 10.6$ W/m^{2}K). Methanol at 87°C flows over the other side ($\overline{h} = 141$ W/m^{2}K). The metal functions as an electrical resistance heater, releasing 1000 W/m^2. Calculate: (a) the heater temperature; (b) the heat transfer from the methanol to the heater; and (c) the heat transfer from the heater to the air. [(b): -270 W/m^2]

1.34 One side of a planar black heater is simultaneously cooled by 20°C air ($\overline{h} = 14.6$ W/m^{2}K) and by radiation to a parallel black wall at 80°C. The other side of the heater is perfectly insulated. What is the temperature of the heater if it delivers 9000 W/m^2?

1.35 A 250 mL (8.3 oz.) aluminum beverage can is taken from a 3°C refrigerator and placed in a low humidity, 25°C room ($\overline{h} = 7.3$ W/m^{2}K). The 53.3 mm diameter by 112 mm high can is placed on an insulated surface. How long will it take to reach 12°C? Assume that emittance of this can is very low, so thermal radiation is negligible. Discuss your other approximations.

1.36 A resistance heater in the form of a thin sheet runs parallel with 3 cm slabs of cast iron on either side of an evacuated cavity. The heater, which releases 8000 W/m^2, and the cast iron are very nearly black. The outside surfaces of the cast iron slabs are kept at 10°C. Determine the heater temperature and the inside slab temperatures. [$T_{\text{heater}} = 254$°C]

1.37 A black wall at 1200°C radiates to the left side of a parallel slab of type 316 stainless steel, 5 mm thick. The right side of the slab is to be cooled convectively and is not to exceed 0°C. Find the heat flux. Can you suggest a convective process that will achieve the desired right-side temperature? Discuss several possibilities for the coolant and the configuration. (Obviously, you are not yet able do a detailed design!)

1.38 A cooler keeps the lower side of a 2 cm layer of ice at −10°C. The upper side is exposed to air at 15°C. What is $\overline{h}$ if the upper side is just on the edge of melting? Must $\overline{h}$ be raised or lowered if melting is to progress?

1.39 At what minimum temperature does a black radiator have its maximum monochromatic emissive power in the visible wavelength range? Look at Fig. 10.2; then describe the difference between what you might see looking at this object in comparison to looking at the sun. (Do *not* try to check your answer by looking directly at the sun, since doing so is harmful to your eyes.)

1.40 The local heat transfer coefficient for laminar flow of fluid over a flat plate of length L is $h(x) = F/x^{1/2}$, where x is the distance from the leading edge of the plate and F is a constant that depends on fluid properties and the flow velocity. How does $\overline{h}$ compare to $h(x = L)$?

1.41 An object is initially at a temperature above that of its surroundings. We have seen that many kinds of convective processes will bring the object into equilibrium with its surroundings. Describe the characteristics of a process that will do so with the least net increase of the entropy of the universe.

1.42 A 250°C cylindrical copper billet, 4 cm in diameter and 8 cm long, is cooled in air at 25°C. The heat transfer coefficient is 5 W/m^{2}K. Can this be treated as lumped-capacity cooling? What is the temperature of the billet after 10 minutes?

1.43 The diameter of the sun is roughly 1,391,000 km and it emits energy as if it were a black body at 5772 K. Determine the rate at which it emits energy. Compare this with the known value. How much energy does the sun emit per year? [1.21×10^{34} J/y]

1.44 Room temperature objects at 300 K and the sun at 5772 K each radiate thermal energy; but Planck's law, eqn. (1.30), shows that the wavelengths of importance are quite different.

    a. Find λ_{max} in micrometers for each of these temperatures from Wien's Law, eqn. (1.29).

    b. Using a spreadsheet or other software, plot eqn. (1.30) for $T = 300$ K as a function of wavelength from 0 to 50 µm and for $T = 5772$ K for wavelengths from 0 to 5 µm.

    c. By numerical integration, find the total area under each of these curves and compare the value to the Stefan-Boltzmann law, eqn. (1.28). Explain any differences.

    d. Show that about ¼ of the area under each curve is to the left of λ_{max} (in other words, ¾ of the energy radiated is on wavelengths greater than λ_{max}).

    e. What fraction of the energy radiated by the 300 K surface is carried on wavelengths less than 4 µm? What fraction of the energy radiated by the 5772 K surface is on wavelengths greater than 4 µm? [5772 K: 1%]

1.45 A crucible of molten metal at 1800°C is placed on a foundry floor. The foundryman covers it with a metal sheet to reduce heat loss to the room. If the transfer factor, $\mathcal{F}$, between the melt and the sheet is 0.4, and that between the top of the sheet and the room is 0.8, by what percentage will the heat loss to the room be reduced by the sheet if the transfer factor between the uncovered melt and the room had originally been 0.8? [66.7%]

1.46 Integration of Planck's law, eqn. (1.30) over all wavelengths leads to the Stefan-Boltzmann law, eqn. (1.28). Perform this integration and determine the Stefan-Boltzmann constant in terms of other fundamental physical constants. *Hint:* The integral can be written in terms of Riemann's zeta function, $\zeta(s)$, by using this beautiful relationship between the zeta and gamma functions

$$\zeta(s)\,\Gamma(s) = \int_0^\infty \frac{t^{s-1}}{e^t - 1}\,dt$$

for $s > 1$. When s is a positive integer, $\Gamma(s) = (s-1)!$ is just a factorial. Further, several values of $\zeta(s)$ are known in terms of powers of π and can be looked up.

Bibliography of Historical and Advanced Texts

Other than [1.1–1.4], we include no specific citations for the ideas introduced in Chapter 1 since these are common to introductory thermodynamics or physics books. References [1.1, 1.5–1.10] are some texts which have strongly influenced the field. The rest are relatively advanced texts or handbooks which go beyond the present textbook.

References

[1.1] J. Fourier. *The Analytical Theory of Heat.* Dover Publications, Inc., New York, 1955. Reprint of Fourier's 1822 monograph. https://archive.org/details/analyticaltheory00fourrich.

[1.2] Société Montyon et Franklin. *Portraits et Histoire des Hommes Utiles, Collection de Cinquante Portraits.* 1839-1840. Etching of Fourier may be downloaded here: http://web.mit.edu/lienhard/www/fourier.tif.

[1.3] A. G. Ostrogorsky. Simple explicit equations for transient heat conduction in finite solids. *Journal of Heat Transfer*, **131**(1):011303, January 2009. doi: 10.1115/1.2977540.

[1.4] O. Lummer and E. Pringsheim. 1. Die Vertheilung der Energie im Spectrum des schwarzen Körpers und des blanken Platins; 2. Temperaturbestimmung fester glühender Körper. *Verhandlungen der Deutschen Physikalischen Gesellschaft*, **1**:215–235, November 1899.

[1.5] L. M. K. Boelter, V. H. Cherry, H. A. Johnson, and R. C. Martinelli. *Heat Transfer Notes.* McGraw-Hill Book Company, New York, 1965. Originally issued as class notes at the University of California at Berkeley between 1932 and 1941. https://babel.hathitrust.org/cgi/pt?id=mdp.39015000967375.

[1.6] M. Jakob. *Heat Transfer.* John Wiley & Sons, New York, 1949.

[1.7] H. S. Carslaw and J. C. Jaeger. *Conduction of Heat in Solids.* Oxford University Press, New York, 2nd ed., 1959. Very comprehensive.

[1.8] H. Schlichting and K. Gersten. *Boundary-Layer Theory.* Springer-Verlag, Berlin, 9th ed., 2017. Comprehensive & modern update of Schlichting's 20th century classic.

[1.9] R. B. Bird, W. E. Stewart, and E. N. Lightfoot. *Transport Phenomena*. John Wiley & Sons, Inc., New York, 2nd ed., 2002.

[1.10] W. M. Kays and A. L. London. *Compact Heat Exchangers*. McGraw-Hill Book Company, New York, 3rd ed., 1984.

[1.11] W. M. Kays, M. E. Crawford, and B. Weigand. *Convective Heat and Mass Transfer*. McGraw-Hill Book Company, New York, 4th ed., 2005. Detailed coverage of boundary layers and internal flows.

[1.12] F. M. White. *Viscous Fluid Flow*. McGraw-Hill, Inc., New York, 3rd ed., 2005. Excellent development of fundamental results for boundary layers and internal flows.

[1.13] A. Bejan. *Convection Heat Transfer*. John Wiley & Sons, New York, 4th ed., 2013. This book makes good use of scaling arguments.

[1.14] J. R. Howell, M. P. Mengüç, and R. Siegel. *Thermal Radiation Heat Transfer*. CRC Press (Taylor and Francis), Boca Raton, FL, 6th ed., 2015.

[1.15] J. G. Collier and J. R. Thome. *Convective Boiling and Condensation*. Oxford University Press, Oxford, 3rd ed., 1996.

[1.16] J. R. Thome, editor. *Encyclopedia of Two-Phase Heat Transfer and Flow I: Fundamentals and Methods*. World Scientific, Singapore, 2015. doi: 10.1142/9310.

[1.17] R. K. Shah and D. P. Sekulić. *Fundamentals of Heat Exchanger Design*. John Wiley & Sons, Inc., Hoboken, NJ, 2003.

[1.18] A. F. Mills. *Mass Transfer*. Prentice-Hall, Inc., Upper Saddle River, 2001. Mass transfer from a mechanical engineer's perspective with strong coverage of convective mass transfer.

[1.19] D. S. Wilkinson. *Mass Transfer in Solids and Fluids*. Cambridge University Press, Cambridge, 2000. A systematic development of mass transfer with a materials science focus and an emphasis on modeling.

[1.20] G. Chen. *Nanoscale Energy Transport and Conversion*. Oxford University Press, New York, 2005.

[1.21] F. A. Kulacki, editor. *Handbook of Thermal Science and Engineering*. Springer, Cham, Switzerland, 2018.

[1.22] L. R. Glicksman and J. H. Lienhard V. *Modeling and Approximation in Heat Transfer*. Cambridge University Press, New York, 2016. Uses basic physical principles to develop simple models of complex processes. Follows the approach of MIT's doctoral qualifying exams in heat transfer.

2. Heat conduction concepts, thermal resistance, and the overall heat transfer coefficient

It is the fire that warms the cold, the cold that moderates the heat...the general coin that purchases all things...

Don Quixote, **M. de Cervantes, 1615**

2.1 The heat conduction equation

Objective

Now we must develop some basic tools for dealing with heat transfer. This means going farther in solving heat conduction problems in one dimension. Those solutions reveal the very helpful analogy of thermal and electrical resistance. With thermal resistance networks, we can describe heat transfer in many settings. For example, the combined resistances to convection and conduction in a heat exchanger form the *overall heat transfer coefficient*, which is central to Chapter 3.

We need values of $\overline{h}$ to treat convection. For now, we defer calculating $\overline{h}$ to Chapters 6, 7, and 8. Instead, we regard $\overline{h}$ as a number that we can look up. We likewise use only basic ideas about radiation, and leave the details for Chapter 10.

Let us begin with heat conduction analysis. The first step is to go beyond the planar treatments of Chapter 1 and derive the full heat conduction (or heat *diffusion*) equation.
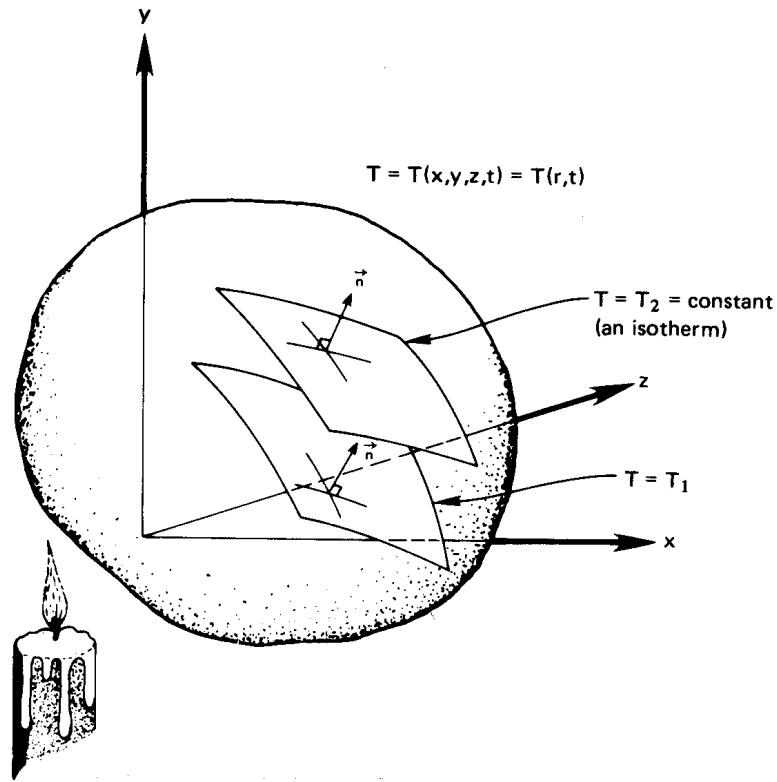
Figure 2.1 A three-dimensional, transient temperature field.

Fourier's law

Consider the general temperature distribution in a three-dimensional body as depicted in Fig. 2.1. For some reason, say heating from one side, the temperature of the body varies with time and space. This field $T = T(x, y, z, t)$ or $T(\vec{r}, t)$, defines instantaneous isothermal surfaces, T_1, T_2, and so on.

   We next consider a very important vector associated with the scalar, T. The vector that has both the magnitude and direction of the maximum increase of temperature at each point is called the *temperature gradient*, ∇T:

$$\nabla T \equiv \frac{\partial T}{\partial x}\vec{\imath} + \frac{\partial T}{\partial y}\vec{\jmath} + \frac{\partial T}{\partial z}\vec{k} \tag{2.1}$$

   "Experience"—that is, physical observation—suggests two things about the heat flow that results from temperature nonuniformities in a body.

These are:

$$|\vec{q}| \propto |\nabla T| \qquad \begin{cases} \text{This says that the magnitude of the heat flux is} \\ \text{directly proportional to the temperature gradient} \end{cases}$$

and

$$\frac{\vec{q}}{|\vec{q}|} = -\frac{\nabla T}{|\nabla T|} \qquad \begin{cases} \text{This says that } \vec{q} \text{ and } \nabla T \text{ are exactly opposite one} \\ \text{another in direction} \end{cases}$$

The heat flux is thus a quantity with a specified magnitude and a specified direction. Fourier's law summarizes this physical experience succinctly as

$$\boxed{\vec{q} = -k\nabla T} \tag{2.2}$$

which resolves itself into three components:

$$q_x = -k\frac{\partial T}{\partial x} \qquad q_y = -k\frac{\partial T}{\partial y} \qquad q_z = -k\frac{\partial T}{\partial z}$$

The coefficient k—the thermal conductivity—also depends on position and temperature in the most general case:

$$k = k[\vec{r}, T(\vec{r}, t)] \tag{2.3}$$

Fortunately, most materials (though not all of them) are very nearly homogeneous. Thus we can usually write $k = k(T)$. The most convenient assumption would be to take k as constant. Whether or not that is legitimate must be determined in each case. As is apparent from Fig. 2.2 and Fig. 2.3, k almost always varies with temperature. It always rises with T in gases at low pressures, but it may rise or fall in metals or liquids. The problem is that of assessing whether or not k is approximately constant in the range of interest. We could safely take k to be a constant for iron between 0° and 40°C (see Fig. 2.2), but we would incur error between $-100°$ and 800°C.

It is easy to prove (Problem 2.1) that if k varies as a straight line with T, and if heat transfer is plane and steady, then $q = k\Delta T/L$, with k evaluated at the average temperature in the plane. If heat transfer is not planar or if k is not simply $A + BT$, it can be much harder to specify a single accurate effective value of k. If ΔT is not large, one can still make a reasonably accurate approximation using a constant average value of k.
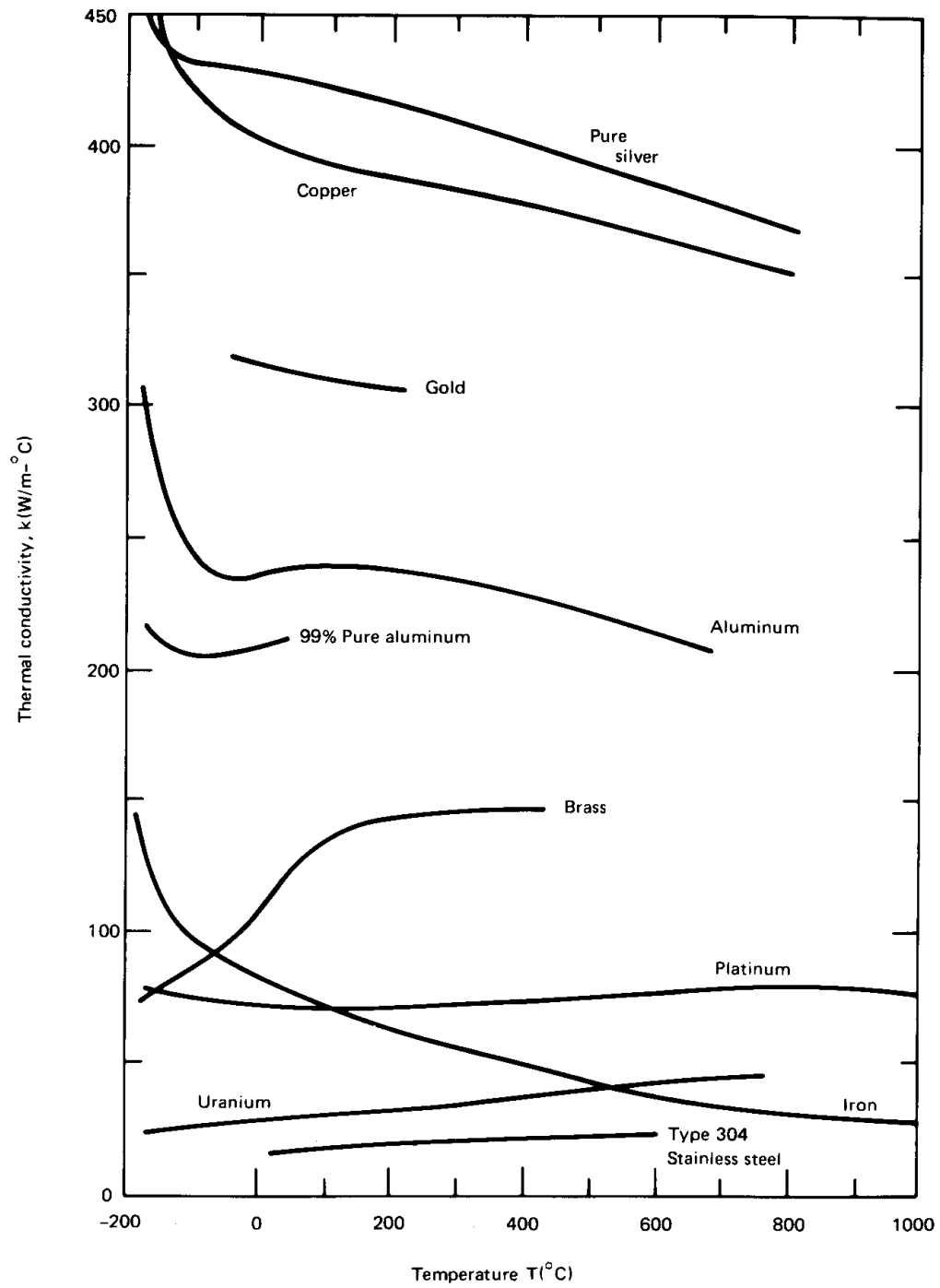
Figure 2.2 Variation of thermal conductivity of metallic solids with temperature
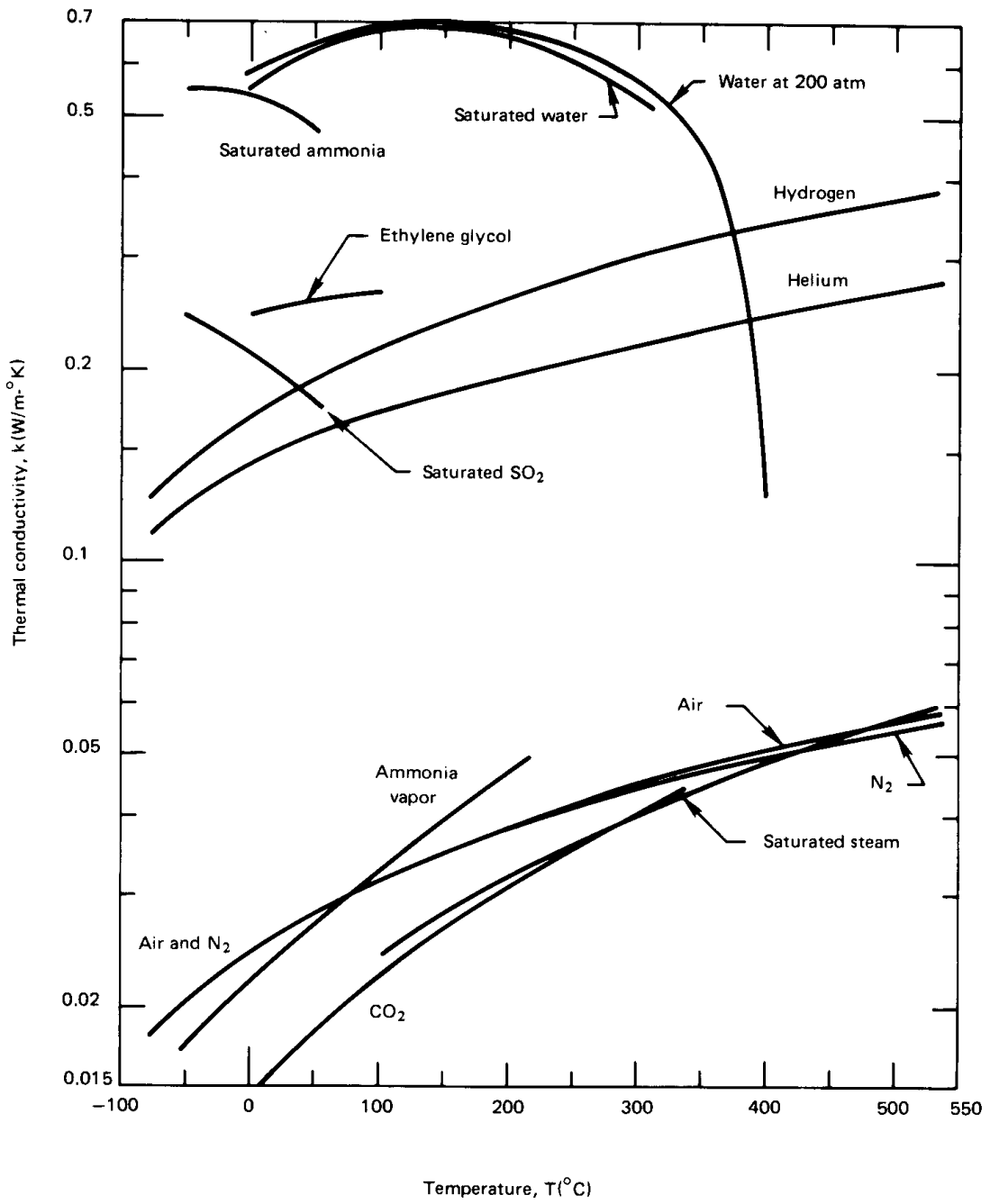
Figure 2.3 The temperature dependence of the thermal conductivity of liquids and gases that are either saturated or at 1 atm pressure.

53

Figure 2.4   Control volume in a
heat-flow field.
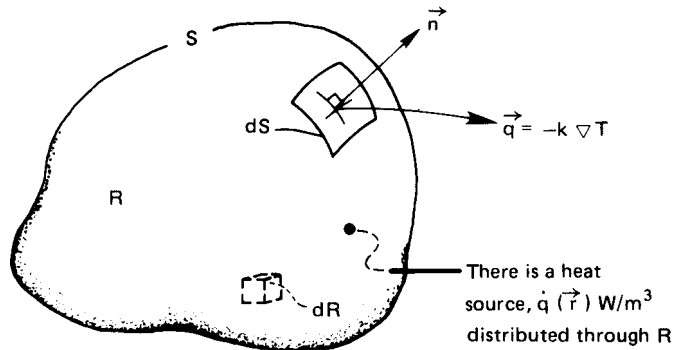
The three-dimensional heat conduction equation

Now that we have Fourier's law in three dimensions, we see that heat
conduction is more complex than it appeared to be in Chapter 1. We must
now write the heat conduction equation in three dimensions. We begin,
as we did in Chapter 1, with the First Law statement, eqn. (1.3):

$$Q = \frac{dU}{dt} \tag{1.3}$$

This time we apply eqn. (1.3) to a three-dimensional control volume, as
shown in Fig. 2.4.[1] The control volume is a finite region of a conducting
body, which we set aside for analysis. The surface is denoted as S and the
volume as R; both are at rest. An element of the surface, dS, is identified
and two vectors are shown on dS: one is the outward unit normal vector,
$\vec{n}$ (with $|\vec{n}| = 1$), and the other is the heat flux vector, $\vec{q} = -k\nabla T$, at that
point on the surface.

   We also allow the possibility that a volumetric heat release equal to
$\dot{q}(\vec{r})$ W/m^3 is distributed through the region. This might be the result
of electrical resistance heating, of chemical or nuclear reaction, of ex-
ternal radiation absorbed within the region, or of still other causes (see
Problem 2.47).

   With reference to Fig. 2.4, we can write the increment of heat conducted
out of dS, in watts, as

$$(-k\nabla T) \cdot (\vec{n}\, dS) \tag{2.4}$$

The heat released within the region R must be added to the total heat
flow *into* S to get the overall rate of heat addition to R:

$$Q = -\int_S (-k\nabla T) \cdot (\vec{n}\, dS) + \int_R \dot{q}\, dR \tag{2.5}$$

---

[1]Figure 2.4 is the three-dimensional version of the control volume shown in Fig. 1.8.

The rate of energy increase of the region R is

$$\frac{dU}{dt} = \int_R \left(\rho c \frac{\partial T}{\partial t} \right) dR \qquad (2.6)$$

where the derivative of T is in partial form because T is a function of both $\vec{r}$ and t.

Finally, we combine Q, as given by eqn. (2.5), and dU/dt, as given by eqn. (2.6), into eqn. (1.3). After rearranging the terms, we obtain

$$\int_S k\nabla T \cdot \vec{n}\, dS = \int_R \left[\rho c \frac{\partial T}{\partial t} - \dot{q} \right] dR \qquad (2.7)$$

To get the left-hand side into a convenient form, we introduce Gauss's theorem, which converts a surface integral into a volume integral. Gauss's theorem says that if $\vec{A}$ is any continuous function of position, then

$$\int_S \vec{A} \cdot \vec{n}\, dS = \int_R \nabla \cdot \vec{A}\, dR \qquad (2.8)$$

Therefore, if we identify $\vec{A}$ with $(k\nabla T)$, eqn. (2.7) reduces to

$$\int_R \left(\nabla \cdot k\nabla T - \rho c \frac{\partial T}{\partial t} + \dot{q} \right) dR = 0 \qquad (2.9)$$

Next, since the region R is arbitrary, the integrand must vanish identically.[2] We therefore get the *heat conduction equation* in three dimensions:

$$\boxed{\nabla \cdot k\nabla T + \dot{q} = \rho c \frac{\partial T}{\partial t}} \qquad (2.10)$$

The limitations on this equation are:

- Incompressible medium. (This was implied when no expansion work term was included.)

- The medium cannot undergo any relative motion. If it is liquid or gas, it must sit still. (Fluid motion is added in Section 6.3.)

---

[2]Consider $\int f(x)\, dx = 0$. If $f(x)$ were, say, $\sin x$, then this could only be true over intervals of $x = 2\pi$ or multiples of it. For eqn. (2.9) to be true for *any* range of integration one might choose, the terms in parentheses must sum to zero everywhere.

If the variation of k with T is small, k can be factored out of eqn. (2.10) to get

$$\nabla^2 T + \frac{\dot{q}}{k} = \frac{1}{\alpha}\frac{\partial T}{\partial t}$$

(2.11)

This is a three-dimensional version of the heat conduction equation derived in Chapter 1, eqn. (1.14). As before, the thermal diffusivity is $\alpha \equiv k/\rho c$. The term $\nabla^2 T \equiv \nabla \cdot \nabla T$ is called the *Laplacian*. It arises thus in a Cartesian coordinate system:

$$\nabla \cdot k\nabla T \simeq k\nabla \cdot \nabla T = k\left(\vec{i}\frac{\partial}{\partial x} + \vec{j}\frac{\partial}{\partial y} + \vec{k}\frac{\partial}{\partial x}\right) \cdot \left(\frac{\partial T}{\partial x}\vec{i} + \frac{\partial T}{\partial y}\vec{j} + \frac{\partial T}{\partial z}\vec{k}\right)$$

or

$$\nabla^2 T = \frac{\partial^2 T}{\partial x^2} + \frac{\partial^2 T}{\partial y^2} + \frac{\partial^2 T}{\partial z^2}$$

(2.12)

The Laplacian can also be expressed in cylindrical or spherical coordinates. The results are:

- Cylindrical:

$$\nabla^2 T = \frac{1}{r}\frac{\partial}{\partial r}\left(r\frac{\partial T}{\partial r}\right) + \frac{1}{r^2}\frac{\partial^2 T}{\partial \theta^2} + \frac{\partial^2 T}{\partial z^2}$$

(2.13)

- Spherical:

$$\nabla^2 T = \frac{1}{r}\frac{\partial^2 (rT)}{\partial r^2} + \frac{1}{r^2 \sin\theta}\frac{\partial}{\partial \theta}\left(\sin\theta\frac{\partial T}{\partial \theta}\right) + \frac{1}{r^2 \sin^2\theta}\frac{\partial^2 T}{\partial \phi^2}$$

(2.14a)

or

$$= \frac{1}{r^2}\frac{\partial}{\partial r}\left(r^2\frac{\partial T}{\partial r}\right) + \frac{1}{r^2 \sin\theta}\frac{\partial}{\partial \theta}\left(\sin\theta\frac{\partial T}{\partial \theta}\right) + \frac{1}{r^2 \sin^2\theta}\frac{\partial^2 T}{\partial \phi^2}$$

(2.14b)

where the coordinates are as displayed in Fig. 2.5.

2.2 Steady heat conduction in a slab: method

We are now in position to calculate the temperature distribution and/or heat flux in bodies with the help of the heat conduction equation. In every case, we first calculate $T(\vec{r}, t)$. Then, if we want the heat flux as well, we differentiate T to get q from Fourier's law.
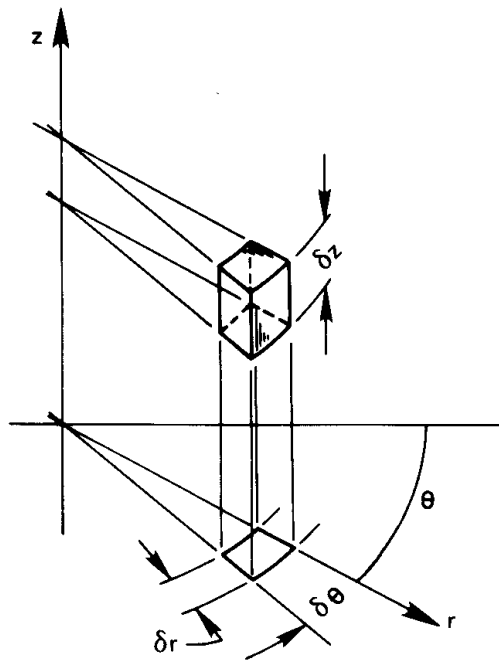
Polar coordinates
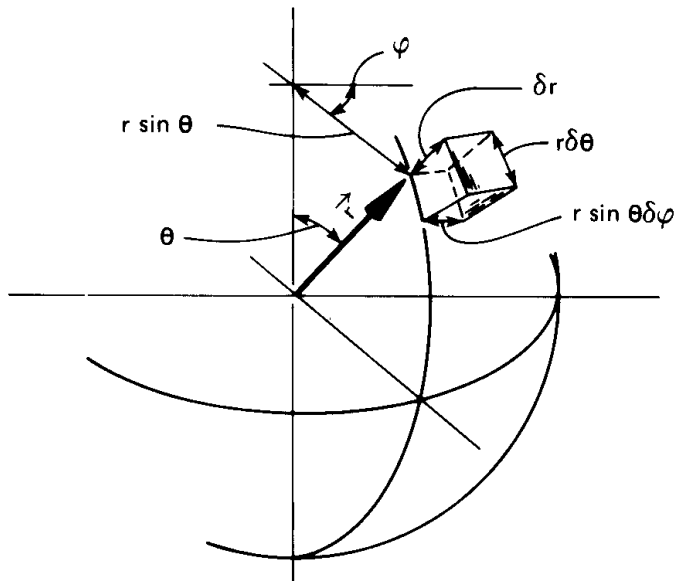
Spherical coordinates

Figure 2.5 Cylindrical and spherical coordinate systems.

The heat conduction equation is a partial differential equation (p.d.e.) and the task of solving it may seem difficult, but we can actually do a lot with fairly elementary mathematical tools. For one thing, in one-dimensional steady-state situations the heat conduction equation becomes an ordinary differential equation (o.d.e.); for another, the equation is linear, and therefore not too formidable, in any case.

We begin with a simple problem. But we use it to set forth a step-by-step procedure that will serve us well when we solve more complex heat conduction problems.

Example 2.1   Basic Method

A large, thin concrete slab of thickness L is "setting." Setting is an exothermic process that releases heat volumetrically, $\dot{q}$ (W/m^3). The outside surfaces are kept at the ambient temperature, so $T_w = T_\infty$. What is the maximum internal temperature?

SOLUTION.

Step 1. *Pick the coordinate scheme that best fits the problem and identify the independent variables that determine T.* In the example, T will probably vary only along the thin dimension, which we will call the x-direction. (If the edges are insulated and L is much smaller than the width or height, this approximation should be quite good.) Since the interior temperature will reach its maximum value when the process becomes steady, we will solve for the final steady-state case $T = T(x$ only).

Step 2. *Write the appropriate d.e., starting with one of the forms of eqn. (2.11).*

$$\frac{\partial^2 T}{\partial x^2} + \underbrace{\frac{\partial^2 T}{\partial y^2} + \frac{\partial^2 T}{\partial z^2}}_{\substack{= 0, \text{ since} \\ T \neq T(y \text{ or } z)}} + \frac{\dot{q}}{k} = \underbrace{\frac{1}{\alpha}\frac{\partial T}{\partial t}}_{\substack{= 0, \text{ since} \\ \text{steady}}}$$

Therefore, since $T = T(x$ only), the equation reduces to the o.d.e.

$$\frac{d^2 T}{dx^2} = -\frac{\dot{q}}{k}$$

Step 3. *Obtain the general solution of the d.e.*   (This is usually the easiest step.) We simply integrate the d.e. twice and get

$$T = -\frac{\dot{q}}{2k}x^2 + C_1 x + C_2$$

Step 4. *Write the "side conditions" on the d.e.—the initial and boundary conditions.* This is the trickiest part and the one that most seriously tests our physical or "practical" understanding any heat conduction problem.

Normally, we must specify the temperature at two different locations on each coordinate (for all times) and at one point in time (for all locations) to get rid of the constants of integration in the general solution. These matters are discussed at greater length in Chapter 4.

In this case we know two boundary conditions:

$$T(x = 0) = T_w \quad \text{and} \quad T(x = L) = T_w$$

Very Important Warning: Never, never introduce inaccessible information in a boundary or initial condition. Always stop and ask yourself, "Would I have access to a numerical value of the temperature (or other data) that I specify at a given position or time?" If the answer is no, then your result will be useless.

Step 5. *Substitute the general solution in the boundary and initial conditions and solve for the constants.* This process gets very complicated in the transient and multidimensional cases. Numerical methods are often needed to solve the problem. However, the steady one-dimensional problems are usually easy. In the example, by evaluating at $x = 0$ and $x = L$, we get:

$$T_w = -0 + 0 + C_2 \qquad \text{so} \qquad C_2 = T_w$$

$$T_w = -\frac{\dot{q}L^2}{2k} + C_1 L + \underbrace{C_2}_{=T_w} \qquad \text{so} \qquad C_1 = \frac{\dot{q}L}{2k}$$

Step 6. *Put the calculated constants back in the general solution to get the particular solution to the problem.* In the example problem we obtain:

$$T = -\frac{\dot{q}}{2k} x^2 + \frac{\dot{q}L}{2k} x + T_w$$

When we put this in neat dimensionless form, we can plot the result in Fig. 2.6 without having to know specific values of its parameters:

$$\frac{T - T_w}{\dot{q}L^2/k} = \frac{1}{2}\left[\frac{x}{L} - \left(\frac{x}{L}\right)^2\right] \qquad\qquad (2.15)$$
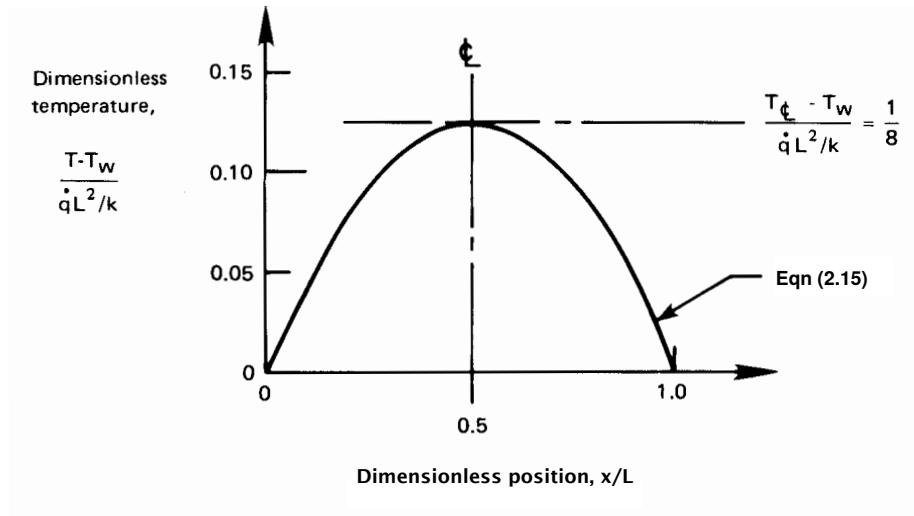
Figure 2.6 Temperature distribution in a setting concrete slab (Example 2.1).

Step 7. *Play with the solution—look it over—see what it has to tell you. Make any checks you can think of to be sure it is correct.* In this case, the resulting temperature distribution is parabolic and, as we would expect, symmetrical. It satisfies the boundary conditions at the wall and reaches a maximum in the center. By nondimensionalizing the result, we can represent all situations with a simple curve. That is highly desirable when the calculations are not simple, as they are here. (Even here T actually depends on *five* different things, but its nondimensional solution is a single curve on a two-coordinate graph.)

Finally, we check to see if the heat flux at the wall is correct:

$$q_{\text{wall}} = -k\frac{\partial T}{\partial x}\bigg|_{x=0} = k\left[\frac{\dot{q}}{k}x - \frac{\dot{q}L}{2k}\right]_{x=0} = -\frac{\dot{q}L}{2}$$

Thus, half of the total energy generated in the slab comes out of the front side, in the $-x$ direction, as we would expect. The solution appears to be correct.

Step 8. *If the temperature field is now correctly established, we can, if we wish, calculate the heat flux at any point in the body by substituting $T(\vec{r}, t)$ back into Fourier's law.* We did this already, in Step 7, to check our solution. ■

We offer additional examples in this section and the following one. In the process, we develop some important results for future use.

Example 2.2 The Simple Slab

A slab shown in Fig. 2.7 is at a steady state with dissimilar temperatures on either side and no internal heat generation. We want the temperature distribution and the heat flux through it.

SOLUTION. These can be found quickly by following the steps set down in Example 2.1:

Step 1. $T = T(x)$ for steady x-direction heat flow

Step 2. $\dfrac{d^2T}{dx^2} = 0$, the steady 1-D heat equation with $\dot{q} = 0$

Step 3. $T = C_1 x + C_2$ is the general solution of that equation

Step 4. $T(x = 0) = T_1$ and $T(x = L) = T_2$ are the b.c.s

Step 5. $T_1 = 0 + C_2$, so $C_2 = T_1$; and $T_2 = C_1 L + C_2$, so $C_1 = -\dfrac{T_1 - T_2}{L}$

Step 6. $T = T_1 - \dfrac{T_1 - T_2}{L}\, x$; or $\dfrac{T_1 - T}{T_1 - T_2} = \dfrac{x}{L}$
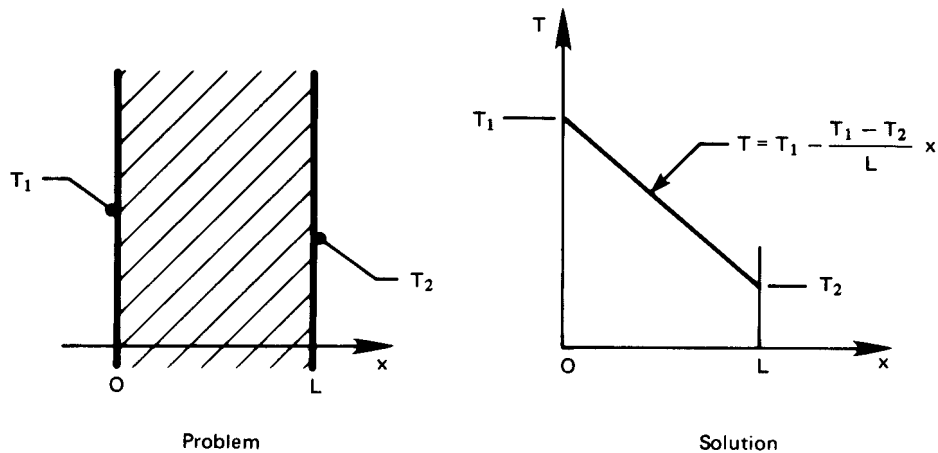
Figure 2.7 Heat conduction in a slab (Example 2.2).
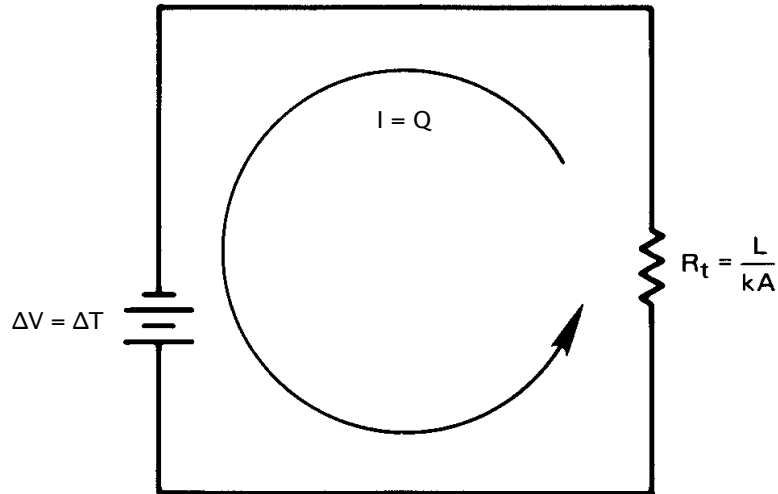
Figure 2.8 Ohm's law analogy to conduction through a slab.

Step 7. We note that the solution satisfies the boundary conditions and that the temperature profile is linear.

Step 8. $q = -k\dfrac{dT}{dx} = -k\dfrac{d}{dx}\left(T_1 - \dfrac{T_1 - T_2}{L}x\right) = k\dfrac{\Delta T}{L}$

which is the formula we obtained previously, as eqn. (1.9). ■

This result, which is the simplest heat conduction solution, calls to mind Ohm's law, if we think of the temperature difference as being a potential difference that drives a current. Thus, if we note that $Q = qA$,

$$Q = \frac{\Delta T}{L/kA} \equiv \frac{\Delta T}{R_{t_\text{slab}}} \qquad \text{is like} \qquad I = \frac{\Delta V}{R} \tag{2.16}$$

where L/kA assumes the role of a *thermal resistance* for the slab, to which we give the symbol R_{t_slab}. R_t has the dimensions of (K/W). Figure 2.8 shows how we can represent heat flow through the slab with a diagram that is perfectly analogous to an electric circuit.
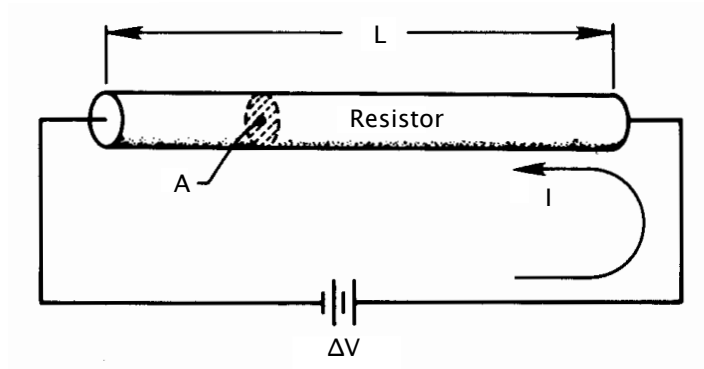
Figure 2.9 The one-dimensional flow of current.

2.3   Thermal resistance and the electrical analogy

Fourier's, Fick's, and Ohm's laws

Fourier's law has several extremely important analogs in other kinds of physical behavior, of which the electrical analogy is only one. These analogous processes provide us with a good deal of guidance in the solution of heat transfer problems. And, conversely, heat conduction analyses can often be adapted to describe those other processes.

Let us first consider *Ohm's law* in three dimensions:

$$\text{flux of electrical charge} = \frac{\vec{I}}{A} \equiv \vec{i} = -\gamma \nabla V \qquad (2.17a)$$

$\vec{I}$ is the vectorial electrical current in amperes, A is an area normal to the current vector, $\vec{i}$ is the flux of current or *current density*, γ is the electrical conductivity in $(\Omega \cdot m)^{-1}$, and V is the electric potential in volts. Like Fourier's law, eqn. (2.2), Ohm's law states that a flux is proportional to a gradient.

To apply eqn. (2.17a) to a one-dimensional current flow, as pictured in Fig. 2.9, we write eqn. (2.17a) as

$$i = -\gamma \frac{dV}{dx} = \gamma \frac{\Delta V}{L} \qquad (2.17b)$$

ΔV is the applied voltage difference, and the electrical resistance of the wire is $R \equiv L/\gamma A$. Then, since $I = iA$, eqn. (2.17b) becomes

$$I = \frac{\Delta V}{R} \qquad (2.18)$$

which is the familiar, but restrictive, one-dimensional form of Ohm's law.

Fick's law is another analogous relation. It states that during mass diffusion, the mass flux, $\vec{j}_1$, of a dilute component, 1, into a second substance, 2, is proportional to the gradient of its mass concentration, m_1. Thus

$$\vec{j}_1 = -\rho \mathcal{D}_{12} \nabla m_1 \tag{2.19}$$

where the constant $\mathcal{D}_{12}$ is the binary diffusion coefficient. We discuss Fick's law in detail in Chapter 11.

Example 2.3

Air fills a thin tube 1 m in length. A small water leak at one end causes the water vapor concentration in air to build to a mass fraction of $m_{\text{water}} = 0.01$ at that end. A desiccator maintains the concentration at zero at the other end. What is the steady flux of water vapor from one side to the other if $\mathcal{D}_{12} = 2.84 \times 10^{-5}$ m²/s and $\rho = 1.18$ kg/m³?

SOLUTION.

$$j_{\text{water}} = \left(1.18 \, \frac{\text{kg}}{\text{m}^3}\right)\left(2.84 \times 10^{-5} \, \frac{\text{m}^2}{\text{s}}\right)\left(0.01 \, \frac{\text{kg H}_2\text{O/kg mixture}}{1 \text{ m}}\right)$$

$$= 3.35 \times 10^{-7} \, \frac{\text{kg}}{\text{m}^2 \cdot \text{s}} = 0.335 \, \frac{\text{mg}}{\text{m}^2 \cdot \text{s}} \qquad \blacksquare$$

Resistances for cylinders and for convection

Many avenues of conduction can be reduced to thermal resistances. Here, we focus on cylindrical geometries and deal with convective boundary conditions. We begin with an example.

Example 2.4   Radial Heat Conduction in a Tube

Find the temperature distribution and the heat flux for the long hollow cylinder shown in Fig. 2.10.

SOLUTION.

Step 1. $T = T(r)$

Step 2.

$$\frac{1}{r}\frac{\partial}{\partial r}\left(r\frac{\partial T}{\partial r}\right) + \underbrace{\frac{1}{r^2}\frac{\partial^2 T}{\partial \phi^2} + \frac{\partial^2 T}{\partial z^2}}_{= \, 0, \text{ since } T \neq T(\phi, z)} + \underbrace{\frac{\dot{q}}{k}}_{= \, 0} = \underbrace{\frac{1}{\alpha}\frac{\partial T}{\partial t}}_{= \, 0, \text{ since steady}}$$

Configuration   Temperature profile
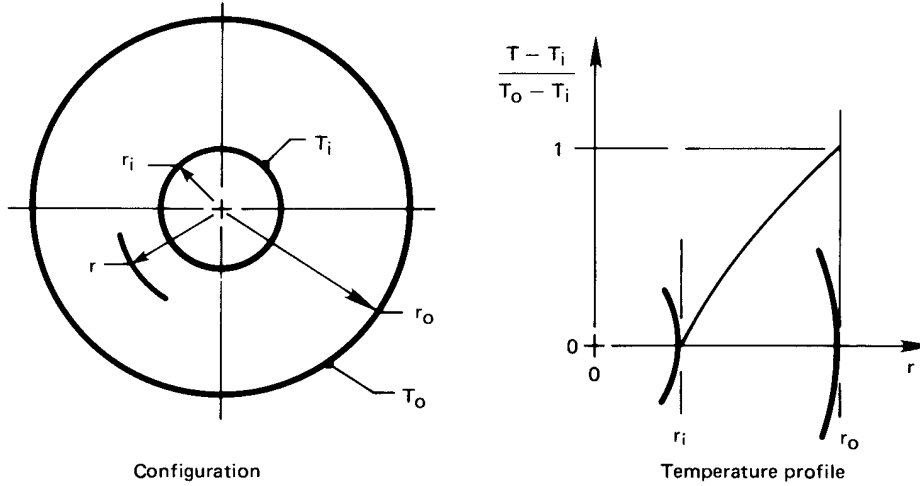
Figure 2.10 Heat transfer through a cylinder with a fixed wall temperature (Example 2.4).

Step 3. Integrate once: $r\dfrac{\partial T}{\partial r} = C_1$; integrate again: $T = C_1 \ln r + C_2$

Step 4. $T(r = r_i) = T_i$ and $T(r = r_o) = T_o$

Step 5.

$$
\begin{array}{l}
T_i = C_1 \ln r_i + C_2 \\[2mm]
T_o = C_1 \ln r_o + C_2
\end{array}
\Rightarrow
\left\{
\begin{array}{l}
C_1 = \dfrac{T_i - T_o}{\ln(r_i/r_o)} = -\dfrac{\Delta T}{\ln(r_o/r_i)} \\[4mm]
C_2 = T_i + \dfrac{\Delta T}{\ln(r_o/r_i)} \ln r_i
\end{array}
\right.
$$

Step 6. $T = T_i - \dfrac{\Delta T}{\ln(r_o/r_i)} (\ln r - \ln r_i)$ or

$$
\boxed{\dfrac{T - T_i}{T_o - T_i} = \dfrac{\ln(r/r_i)}{\ln(r_o/r_i)}}
\tag{2.20}
$$

Step 7. The solution is plotted in Fig. 2.10. We see that the temperature profile is logarithmic and that it satisfies both boundary conditions. Furthermore, it is instructive to see what happens when the wall of the cylinder is very thin, or when r_i/r_o is close to 1. In this case:

$$
\ln(r/r_i) \simeq \dfrac{r}{r_i} - 1 = \dfrac{r - r_i}{r_i}
$$

and

$$\ln(r_o/r_i) \simeq \frac{r_o - r_i}{r_i}$$

Thus eqn. (2.20) becomes

$$\frac{T - T_i}{T_o - T_i} = \frac{r - r_i}{r_o - r_i}$$

which is a simple linear profile. This is the same solution that we would get in a plane slab (see Problem 2.43).

Step 8. At any station, r, with $\Delta T = T_i - T_o$:

$$q_{\text{radial}} = -k\frac{\partial T}{\partial r} = +\frac{k\Delta T}{\ln(r_o/r_i)}\frac{1}{r}$$

So the heat *flux* falls off inversely with radius. That is reasonable, since the same heat flow must pass through an increasingly large cylindrical area as the radius increases. The total heat flow should be constant regardless of radial position, of course. Let us see if this is the case for a cylinder of length l:

$$Q \text{ (W)} = (2\pi r l)\, q = \frac{2\pi k l \Delta T}{\ln(r_o/r_i)} \neq \text{fn}(r) \tag{2.21}$$

Finally, we again recognize the similarity to Ohm's law and write the thermal resistance for a cylinder:

$$\boxed{R_{t_{\text{cyl}}} = \frac{\ln(r_o/r_i)}{2\pi l k}} \tag{2.22}$$

This resistance can be compared to that for a plane slab:

$$R_{t_{\text{slab}}} = \frac{L}{kA}$$

Both resistances are inversely proportional to k and have units of K/W, but each reflects a different geometry. When the cylinder has a thin wall, its resistance may be approximated using the slab formula because the cylindrical area does not vary much (see Problem 2.43). ∎

In the preceding examples, the boundary conditions were all the same—a temperature specified at an outer edge. Next let us suppose that the temperature is specified in the environment away from a body, with a heat transfer coefficient between the environment and the body.
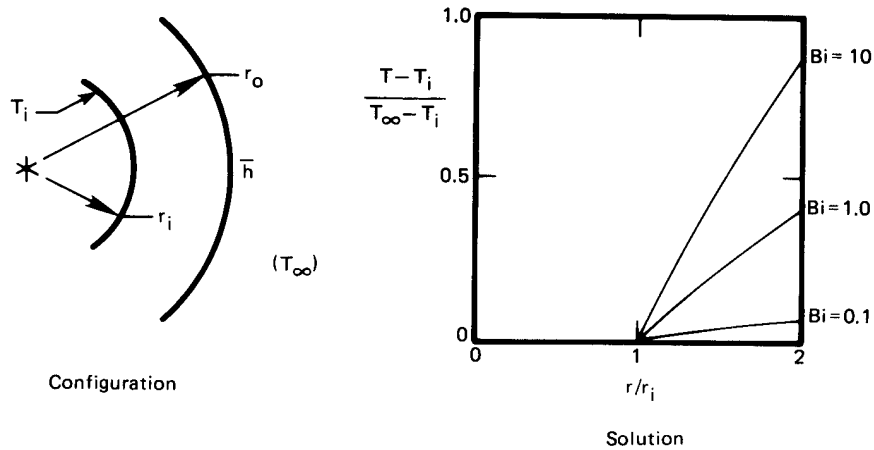
Figure 2.11 Heat transfer through a cylinder with a convective boundary condition (Example 2.5).

Example 2.5   A Convective Boundary Condition

A convective heat transfer coefficient around the outside of the cylinder in Example 2.4 provides thermal resistance between the cylinder and an environment at $T = T_\infty$, as shown in Fig. 2.11. Find the temperature distribution and heat flux in this case.

SOLUTION.

Step 1 through 3. These are the same as in Example 2.4.

Step 4. The first boundary condition is $T(r = r_i) = T_i$. The second boundary condition must be expressed as an energy balance at the outer wall (recall Section 1.3).

$$q_{\text{convection}} = q_{\substack{\text{conduction} \\ \text{at the wall}}}$$

or

$$\overline{h}(T - T_\infty)_{r=r_o} = -k \left.\frac{\partial T}{\partial r}\right|_{r=r_o}$$

Step 5. From the first boundary condition we obtain $T_i = C_1 \ln r_i + C_2$. It is easy to make mistakes when we substitute the general solution into the second boundary condition, so we will do it

in detail:

$$\overline{h}\left[(C_1 \ln r + C_2) - T_\infty\right]_{r=r_o}$$

$$= -k\left[\frac{\partial}{\partial r}(C_1 \ln r + C_2)\right]_{r=r_o} \quad (2.23)$$

A common error is to substitute $T = T_o$ on the lefthand side instead of substituting the entire general solution. That will do no good, because T_o is not an accessible piece of information. Equation (2.23) reduces to:

$$\overline{h}(T_\infty - C_1 \ln r_o - C_2) = -\frac{kC_1}{r_o}$$

When we combine this with the result of the first boundary condition to eliminate C_2:

$$C_1 = \frac{T_\infty - T_i}{k/(\overline{h}r_o) + \ln(r_o/r_i)} = \frac{T_\infty - T_i}{1/\mathrm{Bi} + \ln(r_o/r_i)}$$

Then

$$C_2 = T_i - \frac{T_\infty - T_i}{1/\mathrm{Bi} + \ln(r_o/r_i)} \ln r_i$$

Step 6. Substitute into $T = C_1 \ln r + C_2$:

$$T = \frac{T_\infty - T_i}{1/\mathrm{Bi} + \ln(r_o/r_i)} \ln(r/r_i) + T_i$$

This can be rearranged in fully dimensionless form:

$$\frac{T - T_i}{T_\infty - T_i} = \frac{\ln(r/r_i)}{1/\mathrm{Bi} + \ln(r_o/r_i)} \quad (2.24)$$

Step 7. Let us fix a value of r_o/r_i—say, 2—and plot eqn. (2.24) for several values of the Biot number. The results are included in Fig. 2.11. Some very important things show up in this plot. When $\mathrm{Bi} \gg 1$, the solution reduces to the solution given in Example 2.4, as if the convective resistance to heat flow were not there. That is exactly what we anticipated in Section 1.3 for $\mathrm{Bi} \gg 1$. When $\mathrm{Bi} \ll 1$, the opposite is true: $(T - T_i)/(T_\infty - T_i)$ remains on the order of Bi, and internal conduction can be neglected. How big is big and how small is small? We do not really have to specify exactly. But in this case $\mathrm{Bi} < 0.1$ signals constancy of temperature inside the cylinder with about ±3%. $\mathrm{Bi} > 20$ means that we can neglect convection with about 5% error.
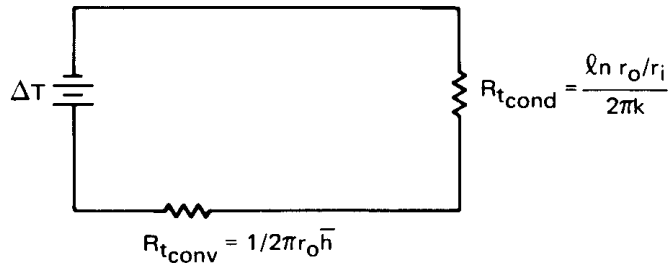
Figure 2.12   Thermal circuit with two resistances.

Step 8. $q_{\text{radial}} = -k\dfrac{\partial T}{\partial r} = k\dfrac{T_i - T_\infty}{1/\text{Bi} + \ln(r_o/r_i)}\dfrac{1}{r}$

This can be written in terms of Q (W) $= q_{\text{radial}}(2\pi r l)$ for a cylinder of length l:

$$Q = \frac{T_i - T_\infty}{\dfrac{1}{\overline{h}\,2\pi r_o l} + \dfrac{\ln(r_o/r_i)}{2\pi k l}} = \frac{T_i - T_\infty}{R_{t_{\text{conv}}} + R_{t_{\text{cond}}}} \qquad (2.25)$$

Equation (2.25) is once again analogous to Ohm's law. But this time the denominator is the sum of two thermal resistances, as would be the case in a series circuit. We accordingly present the analogous electrical circuit in Fig. 2.12. ∎

The presence of convection on the outside surface of the cylinder adds a new thermal resistance of the form

$$\boxed{R_{t_{\text{conv}}} = \frac{1}{\overline{h}A}} \qquad (2.26)$$

where A is the surface area over which convection occurs.

Example 2.6   Critical Radius of Insulation

An interesting consequence of the preceding result can be brought out with a specific example. Suppose that we insulate a 0.5 cm O.D. copper steam line with 85% magnesia ($k = 0.074$ W/m·K) to prevent the steam from condensing too rapidly. The steam is under pressure and stays at 150°C. The copper is thin and highly conductive—obviously a tiny resistance in series with the convective and insulation resistances, as we see in Fig. 2.13. The condensation of steam inside the tube also offers very little resistance.[3] But on the outside, a heat transfer

---

[3]Condensation heat transfer is discussed in Chapter 8. It turns out that $\overline{h}$ is generally enormous during condensation so that $R_{t_{\text{condensation}}}$ is tiny.
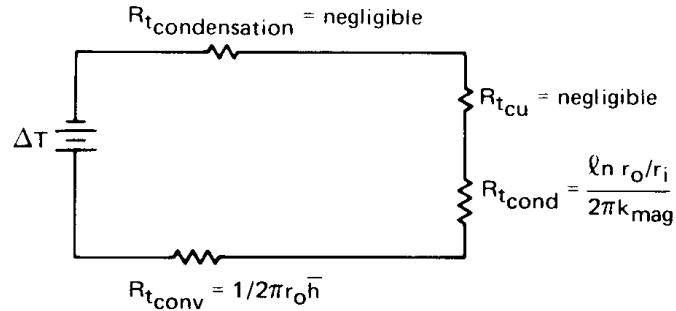
Figure 2.13 Thermal circuit for an insulated tube.

coefficient of $\overline{h} = 20$ W/m²K offers fairly high resistance. It turns out that insulation can actually *improve* heat transfer in this case.

The two significant resistances, for a cylinder of unit length ($l = 1$ m), are

$$R_{t_{\text{cond}}} = \frac{\ln(r_o/r_i)}{2\pi k l} = \frac{\ln(r_o/r_i)}{2\pi(0.074)} \quad \text{K/W}$$

$$R_{t_{\text{conv}}} = \frac{1}{2\pi r_o l \overline{h}} = \frac{1}{2\pi(20)r_o} \quad \text{K/W}$$

Figure 2.14 is a plot of these resistances and their sum. A very interesting thing occurs here. $R_{t_{\text{conv}}}$ falls off rapidly when r_o is increased, because the outside area is increasing. Accordingly, the total resistance passes through a minimum in this case. Will it always do so? To find out, we differentiate eqn. (2.25), again setting $l = 1$ m:

$$\frac{dQ}{dr_o} = \frac{(T_i - T_\infty)}{\left(\dfrac{1}{2\pi r_o \overline{h}} + \dfrac{\ln(r_o/r_i)}{2\pi k}\right)^2} \left(-\frac{1}{2\pi r_o^2 \overline{h}} + \frac{1}{2\pi k r_o}\right) = 0$$

When we solve this for the value of $r_o = r_{\text{crit}}$ at which Q is maximum and the total resistance is minimum, we obtain

$$\text{Bi} = 1 = \frac{\overline{h} r_{\text{crit}}}{k} \tag{2.27}$$

In the present example, adding insulation will *increase* heat loss instead of reducing it, until $r_{\text{crit}} = k/\overline{h} = 0.0037$ m or $r_{\text{crit}}/r_i = 1.48$. Indeed, insulation will not even start to do any good until $r_o/r_i = 2.32$ or $r_o = 0.0058$ m. We call r_{crit} the *critical radius* of insulation. ∎
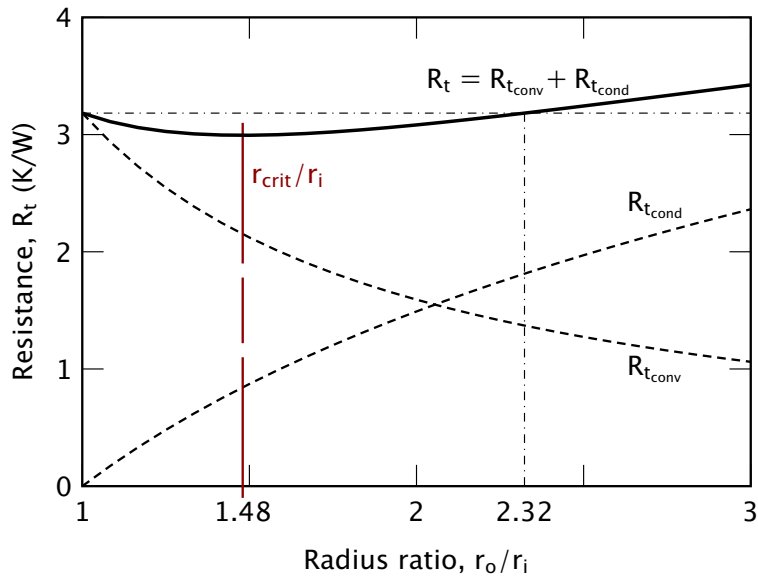
Figure 2.14 How the conductive and convective resistances combine to give a critical radius of insulation in the specific case of Example 2.6, written for a cylinder of unit length $l = 1$ m.

There is an interesting catch here. For most cylinders, $r_{\text{crit}} < r_i$ and the critical radius idiosyncrasy is of no concern. If our steam line had a 1 cm outside diameter, the critical radius difficulty would not have arisen. When we cool smaller cylinders, the critical radius can be important—in electrical wiring, for example. But critical radius is seldom a concern in large process equipment.

Resistance for thermal radiation

We saw in Chapter 1 that the net radiation exchanged by two objects separated by a gas or a vacuum is given by eqn. (1.34):

$$Q_{\text{net}} = A_1 \mathcal{F}_{1\text{-}2}\, \sigma \left(T_1^4 - T_2^4 \right) \tag{1.34}$$

When T_1 and T_2 are close, we can approximate this equation using a *radiation heat transfer coefficient*, h_{rad}. Specifically, suppose that the temperature difference, $\Delta T = T_1 - T_2$, is small compared to the mean temperature, $T_m = (T_1 + T_2)/2$. Then we can make the following expansion

and approximation:

$$
\begin{aligned}
Q_{\text{net}} &= A_1 \mathcal{F}_{1\text{-}2}\, \sigma \left(T_1^4 - T_2^4 \right) \\
&= A_1 \mathcal{F}_{1\text{-}2}\, \sigma (T_1^2 + T_2^2)(T_1^2 - T_2^2) \\
&= A_1 \mathcal{F}_{1\text{-}2}\, \sigma \underbrace{(T_1^2 + T_2^2)}_{=\,2T_m^2 + (\Delta T)^2/2}\, \underbrace{(T_1 + T_2)}_{=\,2T_m}\, \underbrace{(T_1 - T_2)}_{=\,\Delta T} \\
&\cong A_1 \underbrace{\left(4\sigma T_m^3\, \mathcal{F}_{1\text{-}2} \right)}_{\equiv\, h_{\text{rad}}} \Delta T \qquad\qquad\qquad (2.28)
\end{aligned}
$$

where the last step assumes that $(\Delta T)^2/2 \ll 2T_m^2$ or $(\Delta T/T_m)^2/4 \ll 1$. Thus, we have identified the radiation heat transfer coefficient

$$
\left.
\begin{aligned}
Q_{\text{net}} &= A_1 h_{\text{rad}}\Delta T \\
h_{\text{rad}} &= 4\sigma T_m^3 \mathcal{F}_{1\text{-}2}
\end{aligned}
\right\} \qquad \text{for} \quad \left(\Delta T/T_m \right)^2/4 \ll 1 \qquad (2.29)
$$

This leads us immediately to the introduction of a radiation thermal resistance, $R_{t_{\text{rad}}}$, analogous to that for convection, $R_{t_{\text{conv}}}$:

$$
R_{t_{\text{rad}}} = \frac{1}{A_1 h_{\text{rad}}} \qquad\qquad (2.30)
$$

For the special case of a small object (1) in a much larger environment (2), the transfer factor is given by eqn. (1.35) as $\mathcal{F}_{1\text{-}2} = \varepsilon_1$, so that

$$
\boxed{h_{\text{rad}} = 4\sigma T_m^3 \varepsilon_1} \qquad\qquad (2.31)
$$

If the small object is black, its emittance is $\varepsilon_1 = 1$ and h_{rad} is maximized. For a black object radiating near room temperature, say $T_m = 300$ K,

$$
h_{\text{rad}} = 4(5.67 \times 10^{-8})(300)^3 \cong 6 \text{ W/m}^2\text{K}
$$

This value is about the same size as $\overline{h}$ for natural convection in a gas. Thus, both effects must be taken into account near room temperature. In forced convection of a gas, however, $\overline{h}$ could be an order of magnitude larger than h_{rad}, making thermal radiation negligible.

Example 2.7

An electrical resistor dissipating 0.1 W has been mounted well away from other components in an electronics cabinet (Fig. 2.15). It is

$$T_{\text{resistor}}$$

$$R_{t_{\text{conv}}} = \frac{1}{\overline{h}\,A}$$

$$Q_{\text{conv}}$$

$$T_{\text{resistor}}$$ $$T_{\text{air}}$$

$$R_{t_{\text{rad}}} = \frac{1}{h_{\text{rad}}\,A}$$

$$Q_{\text{rad}}$$
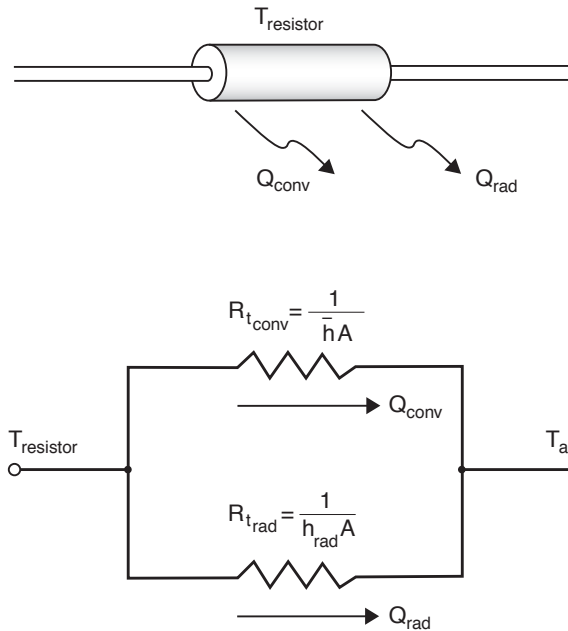
Figure 2.15   An electrical resistor cooled by convection and radiation.

cylindrical with a 3.6 mm O.D. and a length of 10 mm. If the air in the cabinet is at 35°C and at rest, and the resistor has $\overline{h} = 13$ W/m²K for natural convection and $\varepsilon = 0.9$, what is the resistor's temperature? Assume that the electrical leads are configured so that little heat is conducted into them.

SOLUTION. The resistor may be treated as a small object in a large isothermal environment. To compute h_{rad}, let us estimate the resistor's temperature as 50°C. Then

$$T_m = (35 + 50)/2 \cong 43°\text{C} = 316 \text{ K}$$

so

$$h_{\text{rad}} = 4\sigma T_m^3 \varepsilon = 4(5.67 \times 10^{-8})(316)^3(0.9) = 6.44 \text{ W/m}^2\text{K}$$

Heat is lost by natural convection and thermal radiation acting in parallel. To find the equivalent thermal resistance, we combine the two parallel resistances as follows:

$$\frac{1}{R_{t_{\text{equiv}}}} = \frac{1}{R_{t_{\text{rad}}}} + \frac{1}{R_{t_{\text{conv}}}} = A h_{\text{rad}} + A\overline{h} = A(h_{\text{rad}} + \overline{h})$$

Thus,

$$R_{t_{\text{equiv}}} = \frac{1}{A(h_{\text{rad}} + \overline{h})}$$

A calculation shows $A = 133 \text{ mm}^2 = 1.33 \times 10^{-4} \text{ m}^2$ for the resistor surface. Thus, the equivalent thermal resistance is

$$R_{t_{\text{equiv}}} = \frac{1}{(1.33 \times 10^{-4})(13 + 6.44)} = 386.8 \text{ K/W}$$

Since

$$Q = \frac{T_{\text{resistor}} - T_{\text{air}}}{R_{t_{\text{equiv}}}}$$

We find

$$T_{\text{resistor}} = T_{\text{air}} + Q \cdot R_{t_{\text{equiv}}} = 35 + (0.1)(386.8) = 73.68 \text{ °C}$$

We guessed a resistor temperature of 50°C in finding h_{rad}. Recomputing with this higher temperature, we have $T_m = 327$ K and $h_{\text{rad}} = 7.17 \text{ W/m}^2\text{K}$. If we repeat the rest of the calculation, we get a new value $T_{\text{resistor}} = 72.3$°C. Further iteration is not needed.

Since the use of h_{rad} is an approximation, we should check its applicability:

$$\frac{1}{4}\left(\frac{\Delta T}{T_m}\right)^2 = \frac{1}{4}\left(\frac{72.3 - 35.0}{327}\right)^2 = 0.00325 \ll 1$$

In this case, the approximation is a very good one.   ■

Example 2.8

Suppose that power to the resistor in Example 2.7 is turned off. How long does it take to cool? The resistor has $k \cong 10 \text{ W/m·K}$, $\rho \cong 2000 \text{ kg/m}^3$, and $c_p \cong 700 \text{ J/kg·K}$.

SOLUTION. The lumped capacity model, eqn. (1.22), may be applicable. To find out, we check the resistor's Biot number, noting that the parallel convection and radiation processes have an *effective* heat transfer coefficient $h_{\text{eff}} = \overline{h} + h_{\text{rad}} = 20.17 \text{ W/m}^2\text{K}$. Then,

$$\text{Bi} = \frac{h_{\text{eff}} r_o}{k} = \frac{(20.17)(0.0036/2)}{10} = 0.0036 \ll 1$$

so eqn. (1.22) can be used to describe the cooling process. The time constant is

$$T = \frac{\rho c_p V}{h_{\text{eff}} A} = \frac{(2000)(700)\pi(0.010)(0.0036)^2/4}{(20.17)(1.33 \times 10^{-4})} = 53.1 \text{ s}$$

From eqn. (1.22) with $T_0 = 72.3°\text{C}$

$$T_{\text{resistor}} = 35.0 + (72.3 - 35.0)e^{-t/53.1} \ °\text{C}$$

Ninety-five percent of the total temperature drop has occurred when $t = 3T = 159$ s. ∎

Contact resistance

The usefulness of the electrical resistance analogy is particularly apparent at the interface of two conducting media. No two solid surfaces ever form perfect thermal contact when they are pressed together, owing to tiny gaps that result from unavoidable roughness in the surfaces. A typical plane of contact between two surfaces is shown in Fig. 2.16 with an enormously exaggerated vertical scale.

Heat transfer follows two paths through such an interface. Conduction through points of solid-to-solid contact is very effective, but conduction through the gas-filled interstices is less efficient. These gaps are normally small, but gases have low thermal conductivities. If temperatures are modest, thermal radiation across the gap will be completely negligible.
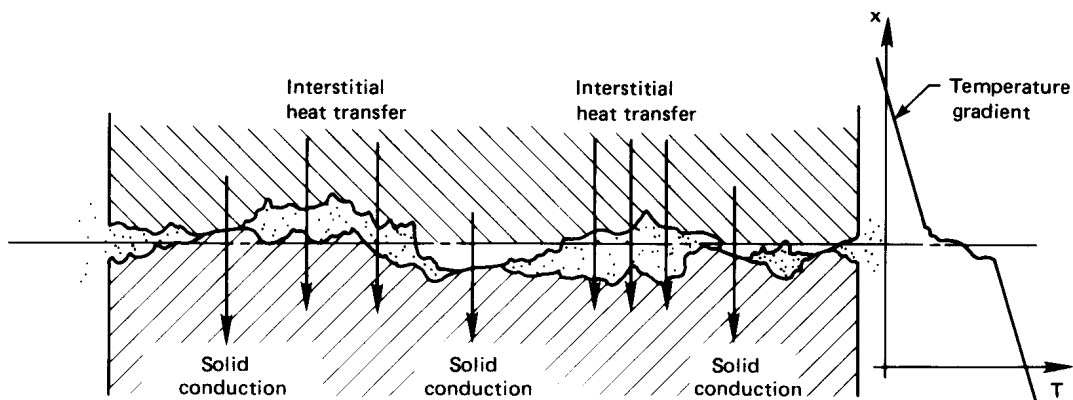
Figure 2.16 Heat transfer through the contact plane between two solid surfaces.

Table 2.1 Some typical interfacial conductances for normal surface finishes and moderate contact pressures (about 1 to 10 atm). Air gaps not evacuated unless so indicated.

Situation	h_c (W/m^{2}K)
Iron/aluminum (70 atm pressure)	45,000
Copper/copper	10,000–25,000
Aluminum/aluminum	2,200–12,000
Graphite/metals	3,000–6,000
Ceramic/metals	1,500–8,500
Stainless steel/stainless steel	2,000–3,700
Ceramic/ceramic	500–3,000
Stainless steel/stainless steel (evacuated interstices)	200–1,100
Aluminum/aluminum (low pressure and evacuated interstices)	100–400

These gaps create a resistance to heat transfer which results in additional temperature change across the interface, as shown in Fig. 2.16.

We model the temperature change using an interfacial conductance, h_c, in series with the solid materials on either side. The coefficient h_c is similar to a heat transfer coefficient and has the same units, W/m^{2}K. If ΔT is the additional temperature difference across an interface of area A, then $Q = Ah_c\Delta T$. It follows that $Q = \Delta T/R_t$ for a contact resistance $R_t \equiv 1/(h_c A)$ in K/W.

The interfacial conductance, h_c, depends on the following factors:

- The surface finish and cleanliness of the contacting solids.

- The materials that are in contact.

- The pressure with which the surfaces are forced together. This may vary over the surface, for example, in the vicinity of a bolt.

- The substance (or lack of it) in the interstitial spaces. Malleable shims or conductive filler pastes can raise the interfacial conductance.

The influence of contact pressure is usually a modest one up to around 10 atm in most metals. Beyond that, increasing plastic deformation of the local contact points causes h_c to increase more dramatically at high
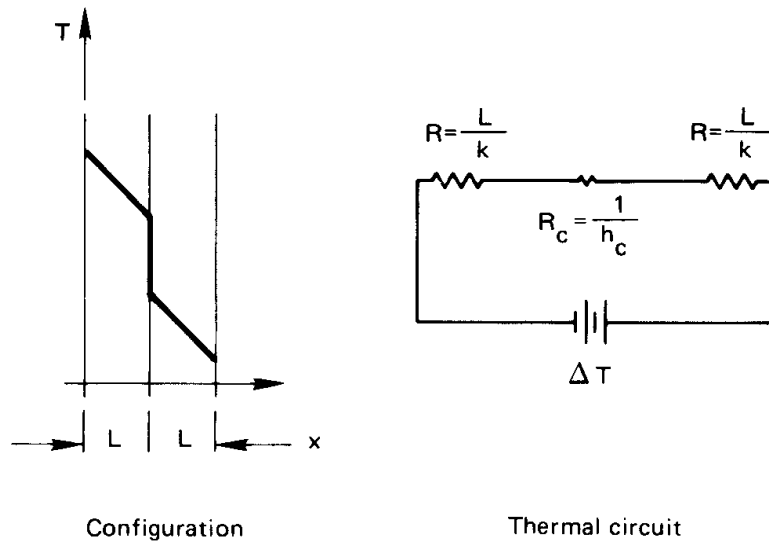
Figure 2.17 Conduction through two unit-area slabs with a contact resistance.

pressure. Table 2.1 gives typical values of contact resistances which bear out most of the preceding points. These values have been adapted from [2.1, Chpt. 3] and [2.2]. Theories of contact resistance are discussed in [2.3] and [2.4].

Example 2.9

Heat flows through two stainless steel slabs ($k = 18$ W/m·K) that are pressed together. The slab area is $A = 1$ m^2. How thick must the slabs be for contact resistance to be negligible?

SOLUTION. With reference to Fig. 2.17, the total or *equivalent* resistance is found by adding these resistances, which are in series:

$$R_{t_{\text{equiv}}} = \frac{L}{kA} + \frac{1}{h_c A} + \frac{L}{kA} = \frac{1}{A}\left(\frac{L}{18} + \frac{1}{h_c} + \frac{L}{18}\right)$$

Since h_c is about 3,000 W/m^{2}K,

$$\frac{2L}{18} \text{ must be } \gg \frac{1}{3000} = 0.00033$$

Thus, L must be large compared to $18(0.00033)/2 = 0.003$ m if contact resistance is to be ignored. If $L = 3$ cm, the error is about 10%. ∎

Figure 2.18 A thermal circuit with many resistances in series. The equivalent resistance is $R_{t_{\mathrm{equiv}}} = \sum_i R_i$.
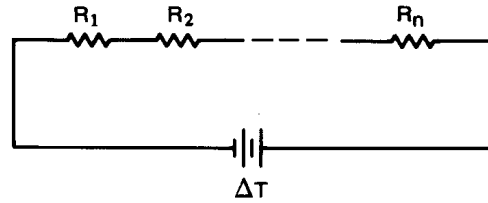
2.4 Overall heat transfer coefficient, U

Definition

We often want to transfer heat through composite resistances, such as the series of resistances shown in Fig. 2.18. Calculations can be greatly streamlined by combining the resistance into a single *overall heat transfer coefficient*[4], U, such that

$$\boxed{Q = UA\,\Delta T} \tag{2.32}$$

The value of U is determined by the details of the system. It is often nearly constant over a range of operating conditions.

In Example 2.5, for instance, two resistances are in series. We can use the value of Q given by eqn. (2.25) to get

$$U = \frac{Q\;(\mathrm{W})}{\left[2\pi r_o l\,(\mathrm{m}^2)\right]\,\Delta T\;(\mathrm{K})} = \frac{1}{\dfrac{1}{\overline{\overline{h}}} + \dfrac{r_o \ln(r_o/r_i)}{k}} \quad (\mathrm{W/m^2 K}) \tag{2.33}$$

We have based U on the outside area, $A_o = 2\pi r_o l$, in this case. We might instead have based it on inside area, $A_i = 2\pi r_i l$, and obtained

$$U = \frac{1}{\dfrac{r_i}{\overline{\overline{h}} r_o} + \dfrac{r_i \ln(r_o/r_i)}{k}} \tag{2.34}$$

It is therefore important to remember which area an overall heat transfer coefficient is based on. In particular, A and U must be consistent when we write $Q = UA\,\Delta T$.

In general, for any composite resistance, the overall heat transfer coefficient may be obtained from the equivalent resistance. The equivalent resistance is calculated taking account of series and parallel resistors, as in Examples 2.9 and 2.7. Then, because $Q = \Delta T/R_{t_{\mathrm{equiv}}} = UA\,\Delta T$, it follows that $UA = 1/R_{t_{\mathrm{equiv}}}$.

---

[4]This U must not be confused with internal energy. The two terms should always be distinct in context.

Physical configuration
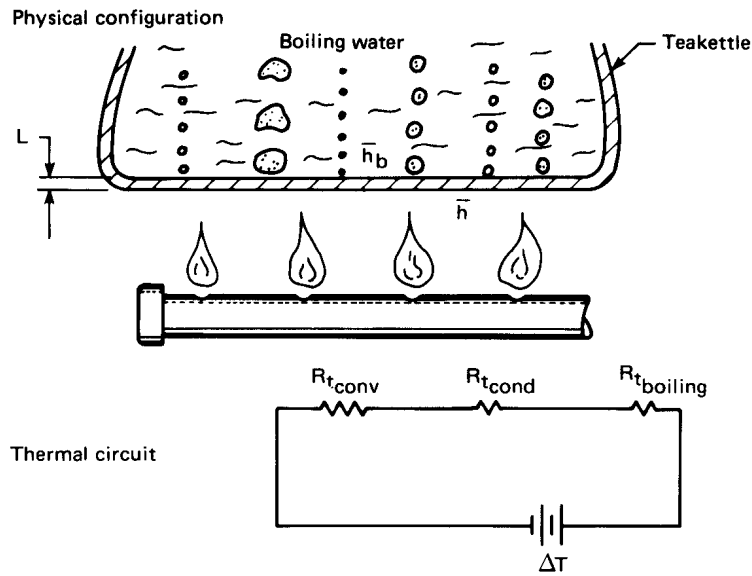
Figure 2.19 Heat transfer through the bottom of a tea kettle.

Example 2.10

Estimate the overall heat transfer coefficient for the tea kettle shown in Fig. 2.19. The hot gas of the flame convects heat to the thin aluminum. The heat is then conducted through the aluminum and finally convected by boiling into the water. Neglect radiation from the flame.

SOLUTION. We need not worry about deciding which area to base A on, in this case, because the area normal to the heat flux vector does not change. We simply write the heat flow

$$Q = \frac{\Delta T}{\sum R_t} = \frac{T_{\text{flame}} - T_{\text{boiling water}}}{\dfrac{1}{\overline{h}A} + \dfrac{L}{k_{\text{Al}}A} + \dfrac{1}{\overline{h}_b A}}$$

and apply the definition of U

$$U = \frac{Q}{A\Delta T} = \frac{1}{\dfrac{1}{\overline{h}} + \dfrac{L}{k_{\text{Al}}} + \dfrac{1}{\overline{h}_b}}$$

Let us see what typical numbers would look like in this example: $\overline{h}$ might be around 200 W/m^{2}K; L/k_{Al} might be 0.001 m/(160 W/m·K)

or $1/160{,}000$ W/m^{2}K; and $\overline{h}_b$ is quite large, perhaps about 5000 W/m^{2}K. Thus:

$$U \simeq \frac{1}{\dfrac{1}{200} + \dfrac{1}{160{,}000} + \dfrac{1}{5000}} = 192.1 \text{ W/m}^2\text{K} \qquad \blacksquare$$

The first resistance is clearly dominant. Notice that in such cases

$$UA \longrightarrow 1/R_{t_{\text{dominant}}} \tag{2.35}$$

where A is any area (inside or outside) in the thermal circuit.

Experiment 2.1

Boil water in a paper cup over an open flame and explain why you can do so. [Recall eqn. (2.35) and see Problem 2.12.]   ♦

Example 2.11

A wall consists of alternating layers of pine and sawdust, as shown in Fig. 2.20. The sheathes on the outside have negligible resistance and $\overline{h}$ is known on the sides. Compute Q and U for the wall.

Solution. So long as the wood and the sawdust do not differ dramatically from one another in thermal conductivity, we can approximate the wall as a parallel resistance circuit, as shown in the figure.[5] The equivalent thermal resistance of the circuit is

$$R_{t_{\text{equiv}}} = R_{t_{\text{conv}}} + \frac{1}{\left(\dfrac{1}{R_{t_{\text{pine}}}} + \dfrac{1}{R_{t_{\text{sawdust}}}} \right)} + R_{t_{\text{conv}}}$$

Thus

$$Q = \frac{\Delta T}{R_{t_{\text{equiv}}}} = \frac{T_{\infty_l} - T_{\infty_r}}{\dfrac{1}{\overline{h}A} + \dfrac{1}{\left(\dfrac{k_p A_p}{L} + \dfrac{k_s A_s}{L} \right)} + \dfrac{1}{\overline{h}A}}$$

and

$$U = \frac{Q}{A\Delta T} = \frac{1}{\dfrac{2}{\overline{h}} + \dfrac{1}{\left(\dfrac{k_p}{L}\dfrac{A_p}{A} + \dfrac{k_s}{L}\dfrac{A_s}{A} \right)}} \qquad \blacksquare$$

---

[5]For this approximation to be exact, the resistances must be equal. If they differ radically, the problem must be treated as two-dimensional.
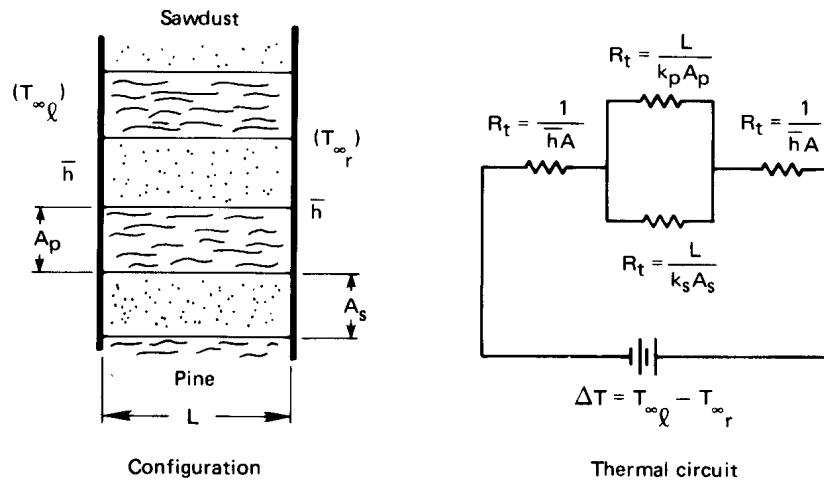
Figure 2.20 Heat transfer through a composite wall.

The approach illustrated in this example is very widely used in calculating U values for the walls and roofs houses and buildings. The thermal resistances of each structural element — insulation, studs, siding, doors, windows, etc. — are combined to calculate U or R_{t_equiv}, which is then used together with weather data to estimate heating and cooling loads [2.5].

Typical values of U

In a fairly general use of the word, a heat exchanger is anything that lies between two fluid masses at different temperatures. In this sense a heat exchanger might be designed either to impede or to enhance heat exchange. Consider some typical values of U shown in Table 2.2, which were assembled from a variety of technical sources. If the exchanger is intended to improve heat exchange, U will generally be much greater than 40 W/m^{2}K. If it is intended to impede heat flow, it will be less than 10 W/m^{2}K—anywhere down to almost perfect insulation. You should have some numerical concept of relative values of U, so we recommend that you scrutinize the numbers in Table 2.2. Some things worth bearing in mind are:

- The fluids with low thermal conductivities, such as tars, oils, or any of the gases, usually yield low values of $\overline{h}$. When such fluid flows on one side of an exchanger, U will generally be pulled down.

Table 2.2 Typical ranges or magnitudes of U

Heat Exchange Configuration	U (W/m²K)
Walls and roofs dwellings with a 24 km/h outdoor wind:	
• Insulated roofs	$0.3-2$
• Finished masonry walls	$0.5-6$
• Frame walls	$0.3-5$
• Uninsulated roofs	$1.2-4$
Single-pane windows	$\sim 6^{\dagger}$
Air to heavy tars and oils	As low as 45
Air to low-viscosity liquids	As high as 600
Air to various gases	$60-550$
Steam or water to oil	$60-340$
Liquids in coils immersed in liquids	$110-2,000$
Feedwater heaters	$110-8,500$
Steam-jacketed, agitated vessels	$500-1,900$
Shell-and-tube ammonia condensers	$800-1,400$
Steam condensers with 25°C water	$1,500-5,000$
Condensing steam to high-pressure boiling water	$1,500-10,000$

† Main heat loss is by infiltration.

- Condensing and boiling are very effective heat transfer processes. They greatly improve U but they cannot override one very small value of $\overline{h}$ on the other side of the exchange. (Recall Example 2.10.)

- For a high U, *all* resistances in the exchanger must be low.

- The highly conducting liquids, such as water and liquid metals, give high values of $\overline{h}$ and U.

Fouling resistance

Figure 2.21 shows one of the simplest forms of a heat exchanger—a pipe. The inside is new and clean on the left, but on the right it has built up a layer of scale. In conventional freshwater preheaters, for example, this scale is typically $MgSO_4$ (magnesium sulfate) or $CaSO_4$ (calcium sulfate) which precipitates onto the pipe wall after a time. To account for the resistance offered by these deposits, we must include an additional, highly
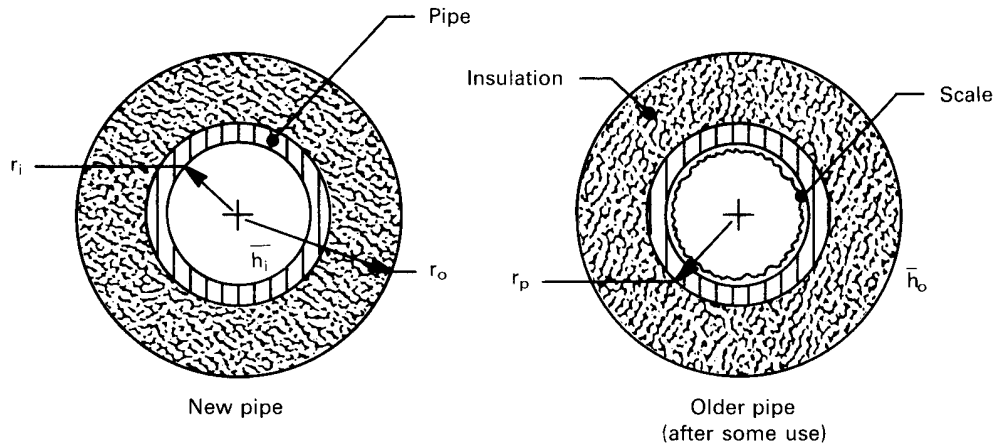
Figure 2.21 The fouling of a pipe.

empirical resistance when we calculate U. Thus, for the pipe shown in Fig. 2.21,

$$U\bigg|_{\substack{\text{older pipe}\\ \text{based on } A_i}} = \cfrac{1}{\cfrac{1}{h_i} + \cfrac{r_i \ln(r_o/r_p)}{k_{\text{insul}}} + \cfrac{r_i \ln(r_p/r_i)}{k_{\text{pipe}}} + \cfrac{r_i}{r_o h_o} + R_f}$$

where R_f is a fouling resistance for a unit area of pipe (in m^2K/W). And clearly

$$\boxed{R_f \equiv \frac{1}{U_{\text{old}}} - \frac{1}{U_{\text{new}}}} \tag{2.36}$$

Some typical values of R_f are given in Table 2.3. These values have been adapted from [2.6] and [2.7]. Notice that fouling has the effect of adding a resistance in series on the order of 10^{-4} m^2K/W. It is rather like another heat transfer coefficient, $\overline{h}_f$, on the order of 10,000 W/m^2K in series with the other resistances in the exchanger.

The tabulated values of R_f are given to only one significant figure because they are very approximate. Clearly, exact values would have to be referred to specific heat exchanger configurations, to particular fluids, to fluid velocities, to operating temperatures, and to age [2.8, 2.9]. The resistance generally drops with increased velocity and increases with temperature and age. The values given in the table are based on reasonable maintenance and the use of conventional shell-and-tube heat exchangers. With misuse, a given heat exchanger can yield much higher values of R_f.

Table 2.3 Some typical fouling resistances for a unit area.

Fluid and Situation	*Fouling Resistance* R_f (m^{2}K/W)
Distilled water	0.0001
Seawater	0.0001–0.0004
Treated boiler feedwater	0.0001–0.0002
Clean river or lake water	0.0002–0.0006
About the worst waters used in heat exchangers	< 0.0020
No. 6 fuel oil	0.0001
Transformer or lubricating oil	0.0002
Most industrial liquids	0.0002
Most refinery liquids	0.0002–0.0009
Steam, non-oil-bearing	0.0001
Steam, oil-bearing (e.g., turbine exhaust)	0.0003
Most stable gases	0.0002–0.0004
Flue gases	0.0010–0.0020
Refrigerant vapors (oil-bearing)	0.0040

Notice too, that if $U \lesssim 1,000$ W/m^{2}K, fouling will be unimportant because it will introduce a negligibly small resistance in series. Thus, in a water-to-water heat exchanger, for which U is on the order of 2000 W/m^{2}K, fouling might be important; but in a finned-tube heat exchanger with hot gas in the tubes and cold gas passing across the fins on them, U might be around 200 W/m^{2}K, and fouling will be usually be insignificant.

Example 2.12

You have unpainted aluminum siding on your house and the engineer has based a heat loss calculation on $U = 5$ W/m^{2}K. You discover that air pollution levels are such that R_f is 0.0005 m^{2}K/W on the siding. Should the engineer redesign the siding?

SOLUTION. From eqn. (2.36) we get

$$\frac{1}{U_{\text{corrected}}} = \frac{1}{U_{\text{uncorrected}}} + R_f = 0.2000 + 0.0005 \text{ m}^2\text{K/W}$$

Therefore, fouling is entirely irrelevant to domestic heat loads. ■

Example 2.13

Since the engineer did not fail you in the preceding calculation, you entrust him with the installation of a heat exchanger at your plant. He installs a water-cooled steam condenser with $U = 4000$ W/m²K. You discover that he used water-side fouling resistance for distilled water but that the water flowing in the tubes is not clear at all. How did he do this time?

SOLUTION. Equation (2.36) and Table 2.3 give

$$\frac{1}{U_{\text{corrected}}} = \frac{1}{4000} + (0.0006 \text{ to } 0.0020)$$
$$= 0.00085 \text{ to } 0.00225 \text{ m}^2\text{K/W}$$

Thus, U is reduced from 4,000 to between 444 and 1,176 W/m²K. Fouling is crucial here, and the engineer was in serious error. ■

2.5 Summary

We have done four things in this chapter:

- We have established the heat conduction equation. We have provided a method for solving it in simple problems. And we have presented some important results. (We say much more about solving the heat conduction equation in Part II of this book.)

- We have explored the electrical analogy to steady heat flow, paying special attention to the concept of thermal resistance. We exploited the analogy to solve heat transfer problems in the same way we solve electrical circuit problems.

- We have defined the overall heat transfer coefficient and seen how to build it up out of component resistances.

- We have treated some practical problems that arise in evaluating overall heat transfer coefficients.

We have put off three important issues until later chapters:

- In all evaluations of U that involve values of $\overline{h}$, we have taken these values as given information. In any real situation, we must determine correct values of $\overline{h}$ for the specific situation. Part III deals with such determinations.

- When fluids flow through heat exchangers, they give up or gain energy. Thus, the driving temperature difference varies along the exchanger. This variation complicates heat exchanger design, and we learn how to deal with it in Chapter 3. (Problem 2.14 asks you to consider this difficulty in its simplest form.)

- The heat transfer coefficients themselves vary with position inside many types of heat exchangers, causing U to be position-dependent.

Problems

2.1   Heat conduction in a slab is one dimensional and steady; and k varies linearly with T. Prove that q can then be evaluated precisely with eqn. (1.9) by taking k at the mean temperature in the slab.

2.2   For steady heat flow through a plane wall of thickness L, show that

$$qL = \int_{T_{\text{left}}}^{T_{\text{right}}} k(T) \, dT$$

for $k(T)$ an arbitrary function. Use a simple numerical integration to find q in a pure iron slab 1 cm thick if the temperature varies from $-100°C$ on the left to $400°C$ on the right. How far would you have erred if you had just taken $k_{\text{average}} = (k_{\text{left}} + k_{\text{right}})/2$ and used eqn. (1.9)? [Error: +6.5%]

2.3   The steady heat flux at one side of a slab has a known value q_o, and the thermal conductivity varies with temperature in the slab as $k(T)$. (a) Starting with eqn. (2.10), show that the heat flux is the same at every position x in the slab, and derive the integral given in Problem 2.2. (b) If the conductivity can be written as a power series in temperature

$$k = \sum_{i=0}^{i=n} A_i T^i$$

find the heat flux in terms of the temperature difference across the slab and a single effective conductivity. What is this conductivity when $n = 0$ or $n = 1$?

2.4   Combine Fick's law, eqn. (2.19), with the principle of conservation of mass (of the dilute species), similar to what was done for energy in developing eqn. (2.7). Note that the mass of species 1 per unit volume is the mass fraction, m_1, times the density of the mixture,

ρ. Eliminate j_1 to obtain a second-order differential equation in m_1. Discuss the importance and the use of the result. For this exercise, you may approximate ρ and $\mathcal{D}_{12}$ as constants.

2.5 Solve for the temperature distribution in a thick-walled pipe if the bulk interior temperature and the exterior air temperature, T_{∞_i}, and T_{∞_o}, are known. The interior and the exterior heat transfer coefficients are $\overline{h}_i$ and $\overline{h}_o$, respectively. Follow the method in Example 2.5 and put your result in the dimensionless form:

$$\frac{T - T_{\infty_i}}{T_{\infty_i} - T_{\infty_o}} = \text{fn}(\text{Bi}_i, \text{Bi}_o, r/r_i, r_o/r_i)$$

2.6 Put the boundary conditions from Problem 2.5 into dimensionless form so that the Biot numbers appear in them. Let the Biot numbers approach infinity. This should get you back to the boundary conditions for Example 2.4. Therefore, the solution that you obtain in Problem 2.5 should reduce to the solution of Example 2.4 when the Biot numbers approach infinity. Show that this is the case.

2.7 Write an accurate explanation of the idea of *critical radius of insulation* that your kid brother or sister, who is still in grade school, could understand. (If you do not have an available kid, borrow one to see if your explanation really works.)

2.8 The slab shown in Fig. 2.22 is embedded in insulating materials on five sides. The sixth side is exposed to an ambient temperature through a heat transfer coefficient. Heat is generated in the slab at the rate of 1.0 kW/m^3. The thermal conductivity of the slab is 0.2 W/m·K. (a) Solve for the temperature distribution in the slab, noting any assumptions you must make. Be careful to clearly identify the boundary conditions. (b) Evaluate T at the exposed front face and opposing back face of the slab. (c) Show that your solution gives the expected heat fluxes at the back and front faces. [(b): $T_{\text{back}} = 55°\text{C}$]

2.9 Consider the composite wall shown in Fig. 2.23. The concrete and brick sections are of equal thickness. Determine T_1, T_2, q, and the percentage of q that flows through the brick. To do this, approximate the heat flow as one-dimensional. Draw the thermal circuit for the wall and identify all four resistances before you begin. Neglect heat flow through the interface between the brick and the concrete. Was it valid to treat the problem as one dimensional? [47.6% through brick]
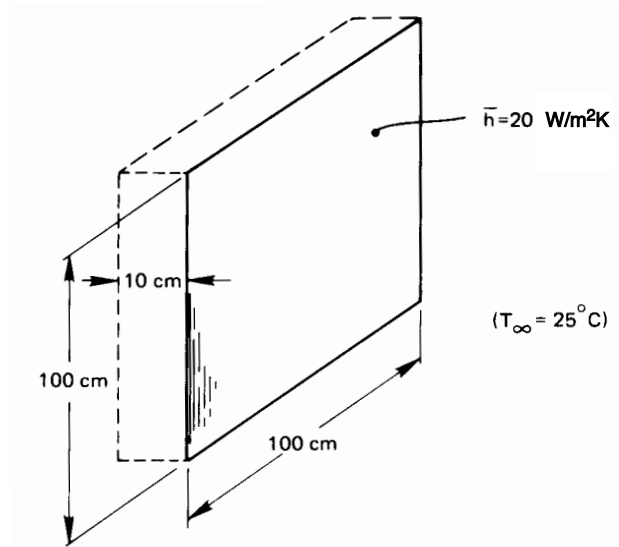
Figure 2.22   Configuration for
Problem 2.8.

2.10   Compute Q and U for Example 2.11 if the wall is 0.3 m thick. Five (each) pine and sawdust layers are 5 and 8 cm thick, respectively; and the heat transfer coefficients are 10 W/m²K on the left and 18 W/m²K on the right. $T_{\infty_l} = 30°$C and $T_{\infty_r} = 10°$C.

2.11   Compute U for the slab in Example 1.2.

2.12   Consider the tea kettle in Example 2.10. Suppose that the kettle holds 1 kg of water (about 1 liter) and that the flame impinges on 0.02 m² of the bottom. (a) Find out how fast the water temperature is increasing when it reaches its boiling point, and calculate the temperature of the bottom of the kettle immediately below the water if the gases from the flame are at 500°C when they touch the bottom of the kettle. Assume that the heat capacitance of the aluminum kettle is negligible. (b) There is an old parlor trick in which one puts a *paper* cup of water over an open flame and boils the water without burning the paper (see Experiment 2.1). Explain this *using an electrical analogy*. [(a): $dT/dt = 0.36°$C/s.]

2.13   Copper plates 2 mm and 3 mm thick are pressed rather lightly together. Non-oil-bearing steam condenses under pressure at $T_{sat} = 200°$C on one side ($\overline{h} = 12{,}000$ W/m²K) and methanol boils under pressure at 130°C on the other ($\overline{h} = 9{,}000$ W/m²K). Estimate U and q initially and after extended service. List the relevant thermal
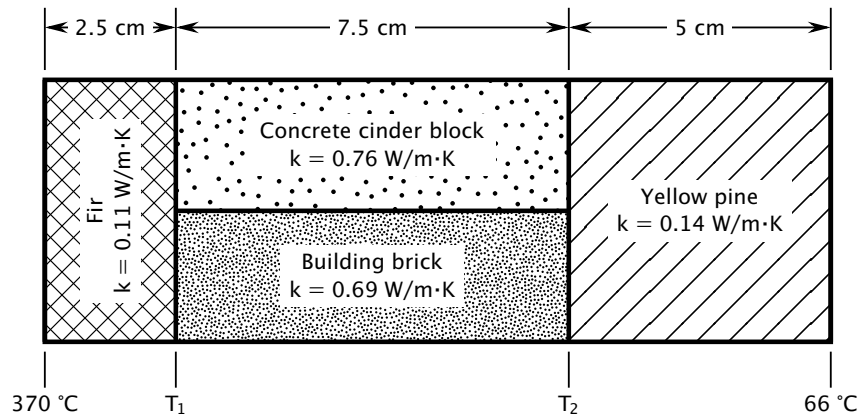
Figure 2.23 Configuration for Problem 2.9.

resistances in order of decreasing importance and suggest whether or not any of them can be ignored. Comment on the accuracy of this calculation.

2.14 0.5 kg/s of air at 20°C flows down a channel that is 1 m wide and of unspecified height. The bottom of the channel is a heat exchange surface ($U = 300$ W/m^{2}K) with steam condensing at 120°C on its exterior. Determine: (a) q at the entrance; (b) the rate of increase of the air temperature with x at the entrance; (c) the temperature and heat flux 2 m downstream. [(c): $T_{2\,m} = 89.7$°C.]

2.15 An isothermal sphere 3 cm in diameter at 80°C is embedded in a large clay region. The temperature of the clay far from the sphere is kept at 10°C. How much heat must be supplied to the sphere to maintain its temperature if $k_{clay} = 1.28$ W/m·K? *Hint:* You must solve the heat conduction equation not in the sphere but in the clay surrounding it. [$Q = 16.9$ W.]

2.16 Is it ever possible to increase the heat transfer from a convectively cooled isothermal sphere by adding insulation? Explain fully.

2.17 A wall consists of layers of metals and plastic with heat transfer coefficients on either side. U is 255 W/m^{2}K and the overall temperature difference is 200°C. One layer in the wall is 3 mm thick stainless steel ($k = 18$ W/m·K). What is ΔT across the stainless steel?

2.18 A 1% carbon-steel sphere 20 cm in diameter is kept at 250°C on the outside. It has an 8 cm diameter cavity containing boiling water ($\overline{h}_{\text{inside}}$ is very high) which is vented to the atmosphere. What is Q through the shell? *Hint:* Solve the heat conduction equation.

2.19 A slab is insulated on one side and exposed to a surrounding temperature, T_∞, through a heat transfer coefficient on the other. Heat is generated nonuniformly in the slab such that $\dot{q} = Ax$, where $x = 0$ at the insulated wall, $x = L$ at the cooled wall, and A is a constant. Derive the temperature distribution in the slab. [If you work this correctly, the temperature difference will vary as a cubic equation in position.]

2.20 800 W/m^3 of heat is generated within a 10 cm diameter nickel-steel sphere for which $k = 10$ W/m·K. The environment is at 20°C and there is a natural convection heat transfer coefficient of 10 W/m^{2}K around the outside of the sphere. Solve the heat conduction equation to find the center temperature at the steady state. [21.37°C.]

2.21 Derive an expression for the thermal resistance of a spherical shell of inner radius r_i and outer radius r_o.

2.22 Consider the hot water heater in Problem 1.11. Suppose that it is covered with 2 cm of insulation with $k = 0.12$ W/m·K, and suppose that $\overline{h} = 16$ W/m^{2}K. Find: (a) the time constant T for the tank, accounting for these two thermal resistances but neglecting the casing; (b) the initial rate of cooling in °C/h; (c) the time required for the water to cool from its initial temperature of 75°C to 40°C; (d) the percentage increase in heat loss that would result if an outer casing for the insulation were held on by eight segments of 1 cm diameter, 1% carbon steel rod between the inner and outer casings.

2.23 A slab of thickness L is subjected to a constant heat flux, q_1, on the left side. The right-hand side is cooled convectively by an environment at T_∞. (a) Develop a dimensionless equation for the temperature of the slab. (b) Present dimensionless equation for the left- and right-hand wall temperatures as well. (c) If the wall is made from facing brick, 10 cm thick, q_l is 400 W/m^2, $\overline{h} = 20$ W/m^{2}K, and $T_\infty = 20$°C, compute the lefthand and righthand temperatures. [(c): $T_l = 40$°C]

2.24 Heat flows steadily through a stainless steel wall of thickness $L_{ss} = 0.06$ m, with a variable thermal conductivity of $k_{ss} = 1.67 + 0.0143T$ for T in °C. The wall is partially insulated on the right side with glass wool of thickness $L_{gw} = 0.1$ m and conductivity $k_{gw} = 0.04$ W/m·K. The temperature on the left-hand side of the stainless steel is 400°C and on the right-hand side of the glass wool is 100°C. Evaluate q and T_i. *Hint:* See Problem 2.1

2.25 Rework Problem 1.29 with a heat transfer coefficient on the outside of the cup, $\overline{h}_o = 40$ W/m²K, keeping the air at 0°C. [$q = 2,200$ W/m²]

2.26 We must illuminate a Space Station experiment in a large tank of water at 20°C. What is the maximum wattage of a submerged 3 cm diameter spherical light bulb that will illuminate the tank without boiling the surrounding water. The bulb is an LED that converts 70% of the power to light. Bear in mind that this will occur in zero gravity.

2.27 A cylindrical shell is made of two concentric layers: an inner one with inner radius r_i and outer radius r_c and an outer one with inner radius r_c and outer radius r_o. There is a contact resistance, h_c, between two layers. The layers have different conductivities, and $T_1(r = r_i) = T_i$ and $T_2(r = r_o) = T_o$. Find the inner temperature of the outer shell, $T_2(r_c)$, in terms of T_o and T_i.

2.28 A 1 kW commercial electric heating rod, 8 mm in diameter and 0.3 m long, is to be used in a highly corrosive gaseous environment. Therefore, it must be covered by a cylindrical sheath of fireclay. The gas flows by at 120°C, and $\overline{h}$ is 230 W/m²K outside the sheath. The surface of the heating rod cannot exceed 800°C. Determine the maximum allowable sheath thickness and find the outer temperature of the fireclay. *Hint:* Use the heat flow and temperature boundary conditions with thermal resistances in series.

2.29 A very small diameter, electrically insulated heating wire runs down the center of a 7.5 mm diameter rod of type 304 stainless steel. The outside is cooled by natural convection ($\overline{h} = 6.7$ W/m²K) in room air at 22°C. The wire releases 12 W/m. Find the surface temperature of the rod, and plot T_{rod} vs. radial position, r, in the rod, for $r > 0$. Neglect any contact resistance. *Hint:* Is it clear why you cannot use a boundary condition at $r = 0$?

2.30 A contact resistance experiment involves pressing two slabs of different materials together, putting a known heat flux through them, and measuring the outside temperatures of each slab. Write the general expression for h_c in terms of known quantities. Then calculate h_c if the slabs are 2 cm thick copper and 1.5 cm thick aluminum, if q is 30,000 W/m², and if the two temperatures are 15°C and 22.1°C. [$h_c = 8,122$ W/m²K]

2.31 A student working heat transfer problems late at night needs a cup of hot cocoa to stay awake. She puts milk in a pan on an electric stove and seeks to heat it as rapidly as she can, without burning the milk, by turning the stove on high and stirring the milk continuously. Explain how this works using an analogous electric circuit. Is it possible to bring the entire bulk of the milk up to the burn temperature without burning part of it?

2.32 A small, spherical hot air balloon, 10 m in diameter, weighs 130 kg with a small gondola and one passenger. How much fuel must be consumed (in kJ/h) if it is to hover at low altitude in still 27°C air? Take $\overline{h}_{\text{outside}} = 215$ W/m²K and $\overline{h}_{\text{inside}} = 126$ W/m²K, as the result of natural convection. *Hint:* First determine the temperature inside the balloon that will keep it neutrally buoyant. [7.21×10^6 kJ/h]

2.33 A slab of 0.5% carbon steel, 4 cm thick, is held at 1,000°C on the back side. The front side is approximately black and radiates through a vacuum to black surroundings at 100°C. What is the temperature of the front side? [872°C]

2.34 Using the data in Fig. 2.3, develop an empirical equation for $k(T)$ for ammonia vapor. (The data form a nearly straight line on semilogarithmic coordinates, so the curve-fit must take an exponential form.) Then imagine a hot horizontal surface parallel to a cold surface a distance H below with ammonia vapor between them. Derive equations for $T(x)$ and q, with $x = 0$ at the cold surface and $x = H$ at the hot surface. Compute q if $T_{\text{hot}} = 150°C$, $T_{\text{cold}} = -5°C$, and $H = 0.15$ m.

2.35 A type 316 stainless steel pipe has a 6 cm inside diameter and an 8 cm outside diameter with a 2 mm layer of 85% magnesia insulation around it. Liquid at 112°C flows inside with $\overline{h}_i = 346$ W/m²K. The air around the pipe is at 20°C, and $\overline{h}_o = 6$ W/m²K. Calculate

U based on the inside area. Sketch the equivalent electrical circuit, showing all known temperatures. Discuss the results and suggest an improved design. [$T_o = 96.36°C$]

2.36 Two highly reflecting, horizontal plates are 5 mm apart. The upper one is kept at 1000°C and the lower one at 200°C. Air is between them. Neglect radiation and compute the heat flux and the mid-point temperature in the air. Use a fit of the form $k = aT^b$, for T in kelvin, to represent the air data in Table A.6.

2.37 A 0.1 m thick slab with $k = 3.4$ W/m·K is held at 100°C on the left side. The right side is cooled with air at 20°C through a heat transfer coefficient, and $\overline{h} = (5.1 \text{ W/m}^2\text{K}^{-5/4})(T_{\text{wall}} - T_\infty)^{1/4}$. Find q and T_{wall} on the right. *Hint:* Trial and error solution required.

2.38 Heat is generated at 54,000 W/m³ in a 0.16 m diameter sphere. The sphere is cooled by natural convection with fluid at 0°C, $\overline{h} = [2 + 6(T_{\text{surface}} - T_\infty)^{1/4}]$ W/m²K, and $k_{\text{sphere}} = 9$ W/m·K. Find the surface temperature and center temperature of the sphere.

2.39 Layers of equal thickness of spruce and pitch pine are laminated to make an insulating material. Does it matter how laminations are oriented relative to the temperature gradient?

2.40 The resistance of a thick cylindrical layer of insulation must be increased. Will Q be lowered more by a small increase of the outside diameter or by the same decrease in the inside diameter?

2.41 You are in charge of energy conservation at your plant. A 300 m run of 6 in. O.D. iron pipe carries steam at 125 psig. The pipe hangs in a room at 25°C, with a natural convection heat transfer coefficient $\overline{h} = 6$ W/m²K. The pipe has an emittance of $\varepsilon = 0.65$. The thermal resistances are such that the surface of the pipe will stay close to the saturation temperature of the steam. (a) Find the effective heat transfer coefficient between the pipe surface and the room, and the rate of heat loss from this pipe, in kWh/y. (b) It is proposed to add a 2 in. layer of glass fiber insulation with $k = 0.05$ W/m·K. The outside surface of the insulation has of $\varepsilon = 0.7$. What is the rate of heat loss with insulation? (c) If the installed insulation cost is $50/m including labor and the cost of thermal energy is $0.03/kWh, what is the payback time for adding insulation?

2.42   A large tank made of thin steel plate contains pork fat at 400°F, which is being rendered into oil. We consider applying a 3-inch layer of 85% magnesia insulation to the surface of the tank. The average heat transfer coefficient is 1.5 Btu/h·ft²·°F for natural convection on the outside. It is far larger on the inside. The outside temperature is 70°F. By what percentage would adding the insulation reduce the heat loss? [89%]

2.43   The thermal resistance of a cylinder is $R_{t_{cyl}} = (1/2\pi kl) \ln(r_o/r_i)$. If $r_o = r_i + \delta$, show that the thermal resistance of a thin-walled cylinder ($\delta \ll r_i$) can be approximated by that for a slab of thickness δ. Thus, $R_{t_{thin}} = \delta/(kA_i)$, where $A_i = 2\pi r_i l$ is the inside surface area. How much error is introduced by this approximation if $\delta/r_i = 0.2$? Plot $R_{t_{thin}}/R_{t_{cyl}}$ as a function of δ/r_i. *Hint:* Use a Taylor series.

2.44   A Gardon gage measures radiation heat flux by detecting a temperature difference [2.10]. The gage consists of a circular constantan membrane of radius R, thickness t, and thermal conductivity k_{ct} which is joined to a heavy copper heat sink at its edges. When a radiant heat flux q_{rad} is absorbed by the membrane, heat flows from the interior of the membrane to the copper heat sink at the edge, creating a radial temperature gradient. Copper leads are welded to the center of the membrane and to the copper heat sink, making two copper-constantan thermocouple junctions. These junctions measure the temperature difference ΔT between the center of the membrane, $T(r = 0)$, and the edge of the membrane, $T(r = R)$.

The following approximations can be made:

- The membrane surface has been blackened so that it absorbs all radiation that falls on it.

- The radiant heat flux is much larger than the heat lost from the membrane by convection or re-radiation. Thus, all absorbed radiation is conducted to the heat sink, and other loses can be neglected.

- The gage operates in steady state.

- The membrane is thin enough ($t \ll R$) that the temperature in it varies only with r, i.e., $T = T(r)$ only.

Solve the following problems.

a. For a fixed heat sink temperature, $T(R)$, qualitatively sketch the shape of the temperature distribution in the membrane, $T(r)$, for two heat radiant fluxes q_{rad1} and q_{rad2}, where $q_{rad1} > q_{rad2}$.

b. Derive the relationship between the radiant heat flux, q_{rad}, and the temperature difference obtained from the thermocouples, ΔT. *Hint:* Treat the absorbed radiant heat flux as if it were a volumetric heat source of magnitude q_{rad}/t W/m^3.

2.45 You have a 12 oz. (375 mL) can of soda at room temperature (70°F) that you would like to cool to 45°F before drinking. You rest the can on its side on the plastic rods of the refrigerator shelf. The can is 2.5 inches in diameter and 5 inches long. The can's emittance is $\varepsilon = 0.4$ and the natural convection heat transfer coefficient around it is a function of the temperature difference between the can and the air: $\overline{h} = 2\,\Delta T^{1/4}$ for ΔT in kelvin.

Assume that thermal interactions with the refrigerator shelf are negligible and that buoyancy currents inside the can will keep the soda well mixed.

a. Estimate how long it will take to cool the can in the refrigerator compartment, which is at 40°F.

b. Estimate how long it will take to cool the can in the freezer compartment, which is at 5°F. (*Continues on next page.*)

c. Are your answers for parts a and b the same? If not, what is the main reason that they are different?

2.46 An exterior wall of a wood-frame house is typically composed, from outside to inside, of a layer of wooden siding, a layer glass fiber insulation, and a layer of gypsum wall board. Standard glass fiber insulation has a thickness of 3.5 inch and a conductivity of 0.038 W/m·K. Gypsum wall board is normally 0.50 inch thick with a conductivity of 0.17 W/m·K, and the siding can be assumed to be 1.0 inch thick with a conductivity of 0.10 W/m·K.

a. Find the overall thermal resistance of such a wall (in K/W) if it has an area of 400 ft^2.

b. The effective heat transfer coefficient (accounting for both convection and radiation) on the outside of the wall is $\overline{h}_o = 20$ W/m^{2}K and that on the inside is $\overline{h}_i = 10$ W/m^{2}K. Determine the

total thermal resistance for heat loss from the indoor air to the outdoor air. Also obtain an overall heat transfer coefficient, U, in W/m²K.

c. If the interior temperature is 20°C and the outdoor temperature is -5°C, find the heat loss through the wall in watts and the heat flux in W/m².

d. Which of the five thermal resistances is dominant?

e. The wall is held together with vertical wooden studs between the siding and the gypsum. The studs are spruce, 3.5 in. by 1.5 in. on a 16 in. center-to-center spacing. If the wall is 8 ft high, by how much do the studs increase U?

2.47 The heat conduction equation in Section 2.1 includes a volumetric heat release rate, $\dot{q}$. We normally describe heat as a transfer of energy and entropy across a system boundary, so the notion of volumetric heat release needs some thought. Consider an electrical resistor carrying a current I with a voltage difference of ΔV in steady state. Electrical work is done on the resistor at the rate $\Delta V \cdot I$.

a. Use eqn. (1.1) to find the rate of heat and entropy flow out of the resistor. Assume that the resistor's surface temperature, T, is uniform. What is the rate of entropy generation, $\dot{S}_{\text{gen}}$?

b. Suppose that the resistor dissipates electrical work uniformly within its volume, $\mathcal{V}$, and that its thermal conductivity is high enough to provide a nearly uniform internal temperature. What is the volumetric entropy generation rate, $\dot{s}_{\text{gen}}$?

c. By considering the net heat leaving a differential volume $d\mathcal{V}$, use $\dot{s}_{\text{gen}}$ to define the volumetric heat release rate, $\dot{q}$.

d. If the resistor has a nonuniform internal temperature but a uniform rate of work dissipation, does the total entropy generation change? Why or why not?

e. If the resistor is insulated, so that no heat flows out, what is the entropy generation rate? Assume the resistor's temperature is nearly uniform, starting at T_0 at time $t = 0$.

2.48 If a temperature difference of ΔT is imposed across N thermal resistances in series, show that the temperature difference across the ith thermal resistance is

$$\Delta T_i = \frac{R_i}{\sum_{i=1}^{N} R_i} \Delta T$$

The electrical analogy to this result is called the *voltage divider*.
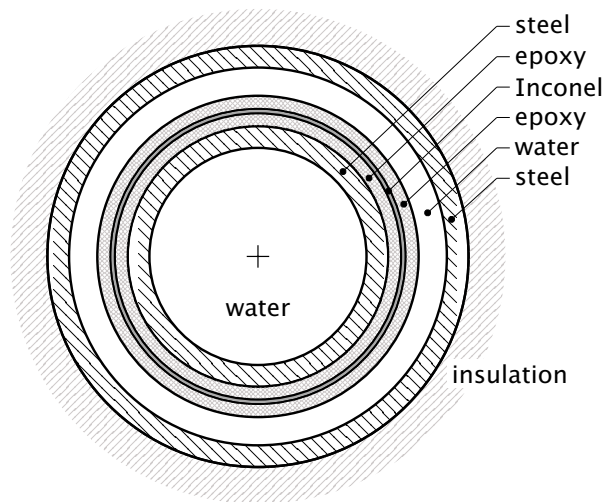
Figure 2.24 Configuration for Problem 2.49.

2.49 An electrical resistor is a 1 mm thick annulus of Inconel (Fig. 2.24). It dissipates 9.4 kW/m. The resistor is insulated on both sides by a 3 mm layer of epoxy (k_e = 0.5 W/m·K). A 316 stainless steel pipe inside the resistor is cooled internally by flowing water. The pipe is 5 cm I.D. and 6 cm O.D. A larger pipe forms an annular passage outside the resistor, through which water also flows; $\overline{h}_{\mathrm{inside}}$ = $\overline{h}_{\mathrm{outside}}$ = 1400 W/m^{2}K. The outer pipe has 8.7 cm I.D. and a 0.5 cm wall thickness and is wrapped with 2 cm thick glass-fiber pipe insulation, surrounded outside by ambient air. If the water temperature inside is 47°C and that outside is 53°C, find the resistor's temperature.

References

[2.1] W. M. Rohsenow and J. P. Hartnett, editors. *Handbook of Heat Transfer.* McGraw-Hill Book Company, New York, 1973.

[2.2] R. G. Wheeler. Thermal conductance of fuel element materials. Hanford Atomic Production Operations Report HW-60343, US Atomic Energy Commission, April 1959.

[2.3] M. M. Yovanovich. Recent developments in thermal contact, gap and joint conductance theories and experiment. In *Proc. Eight Int. Heat Transfer Conf.*, Vol. 1, pp. 35–45. San Francisco, 1986.

[2.4] C. V. Madhusudana. *Thermal Contact Conductance.* Springer-Verlag, New York, 1996.

[2.5] American Society of Heating, Refrigerating, and Air-Conditioning Engineers. *2017 ASHRAE Handbook—Fundamentals (SI Edition).* Atlanta, 2017.

[2.6] R. K. Shah and D. P. Sekulić. Heat exchangers. In W. M. Rohsenow, J. P. Hartnett, and Y. I. Cho, editors, *Handbook of Heat Transfer*, Chapter 17. McGraw-Hill, New York, 3rd ed., 1998.

[2.7] Tubular Exchanger Manufacturer's Association. *Standards of Tubular Exchanger Manufacturer's Association*. New York, 4th and 6th ed., 1959 and 1978.

[2.8] H. Müller-Steinhagen. Cooling-water fouling in heat exchangers. In T. F. Irvine, Jr., J. P. Hartnett, Y. I. Cho, and G. A. Greene, editors, *Advances in Heat Transfer*, Vol. 33, pp. 415–496. Academic Press, Inc., San Diego, 1999. doi: 10.1016/S0065-2717(08)70307-1.

[2.9] W. J. Marner and J. W. Suitor. Fouling with convective heat transfer. In S. Kakaç, R. K. Shah, and W. Aung, editors, *Handbook of Single-Phase Convective Heat Transfer*, Chapter 21. Wiley-Interscience, New York, 1987.

[2.10] R. Gardon. An instrument for the direct measurement of intense thermal radiation. *Rev. Sci. Instr.*, **24**(5):366–371, 1953. doi: 10.1063/1.1770712.

3. Heat exchanger design

The great object to be effected in the boilers of these engines is, to keep a small quantity of water at an excessive temperature, by means of a small amount of fuel kept in the most active state of combustion...No contrivance can be less adapted for the attainment of this end than one or two large tubes traversing the boiler, as in the earliest locomotive engines. **The Steam Engine Familiarly Explained and Illustrated,**
Dionysus Lardner, 1836

3.1 Function and configuration of heat exchangers

The archetypical function of any heat exchanger is getting energy from one fluid mass to another, as we see in Fig. 3.1. Some kind of wall separates the two flows and introduces some thermal resistance to heat exchange. We normally want to minimize this resistance. (In some cases, the separator resistance can be entirely eliminated, as in the direct steam condenser of Fig. 3.2.)

Heat exchangers come in a vast variety of configurations. However, most commercial exchangers reduce to one of three types. Figure 3.3 shows these types in schematic form. They are:

- *The simple parallel or counterflow configuration.* These arrangements are versatile. Figure 3.4 shows how the counterflow arrangement is bent around in a so-called Heliflow compact heat exchanger configuration.

- *The shell-and-tube configuration.* Figure 3.5 shows the U-tubes of a two-tube-pass, one-shell-pass exchanger being installed in the supporting baffles. The shell is yet to be added. Most of the really large heat exchangers are of the shell-and-tube form.
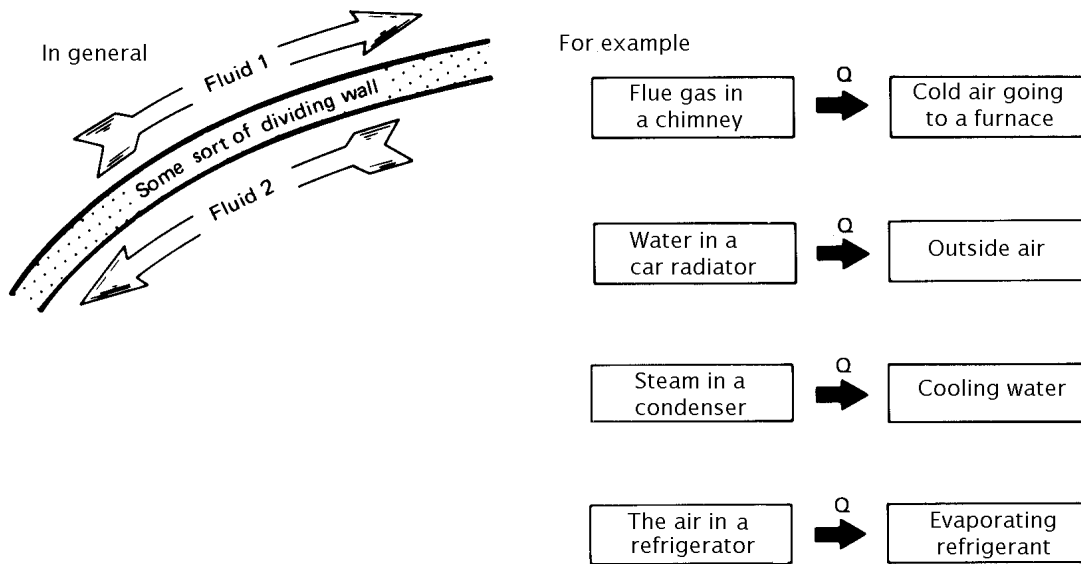
Figure 3.1 The basic concept of a heat exchanger and some common applications.

- *The cross-flow configuration.* Figure 3.6 shows typical cross-flow units. In Fig. 3.6a and c, both flows are *unmixed.* Each flow must stay in a prescribed path through the exchanger and is not allowed to "mix" to the right or left. Figure 3.6b shows a typical plate-fin cross-flow element. Here the flows are also unmixed.
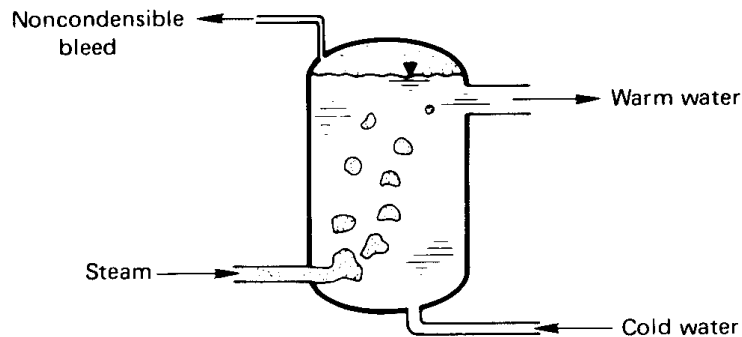
Figure 3.2 A direct-contact heat exchanger.
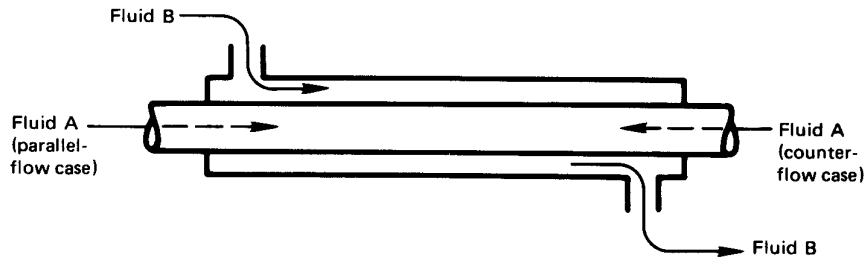
a) Parallel and counterflow heat exchangers
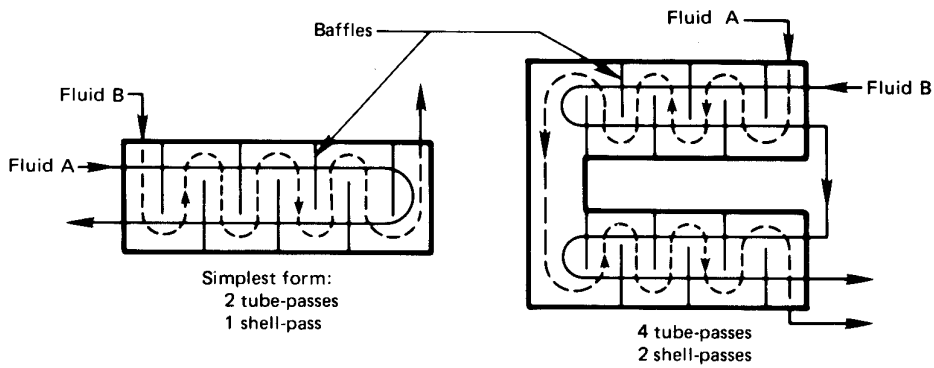
b) Two kinds of shell-and-tube heat exchangers
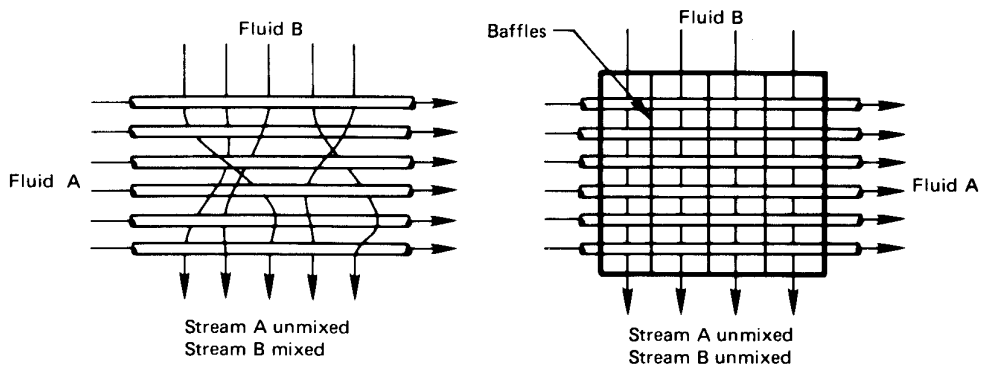
c) Two kinds of cross-flow exchangers

Figure 3.3 The three basic types of heat exchangers.

101
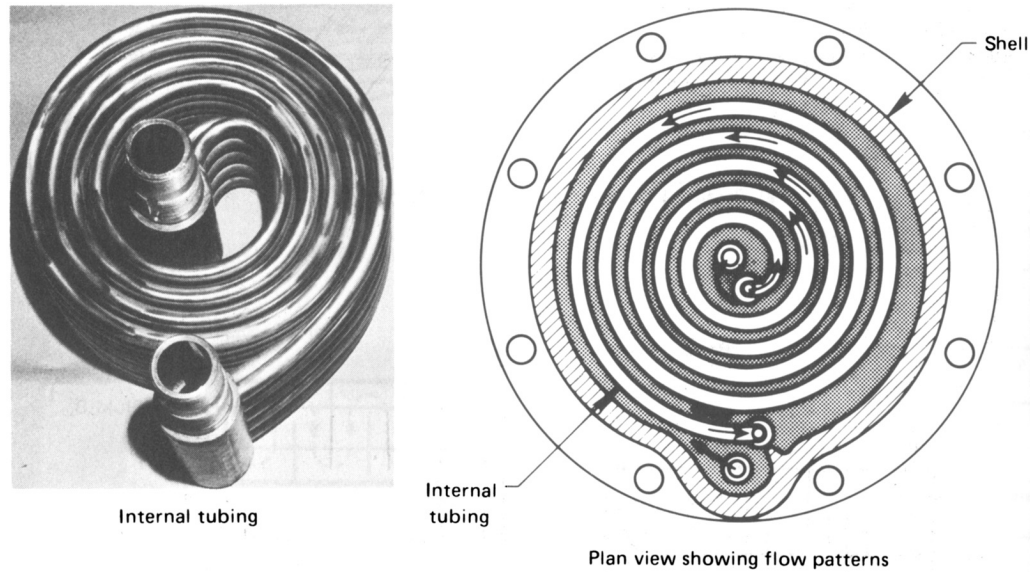
Figure 3.4 Heliflow compact counterflow heat exchanger. (Photograph courtesy of Graham Manufacturing Co., Batavia, NY.)

Figure 3.7, taken from the standards of the Tubular Exchanger Manufacturer's Association (TEMA) [3.1], shows four typical single-shell-pass heat exchangers and establishes nomenclature for such units.

These pictures also show some of the complications that arise in translating simple concepts into hardware. Figure 3.7a shows an exchanger with a single tube pass. Although the shell flow is baffled so that it crisscrosses the tubes, it still proceeds from the hot to cold (or cold to hot) end of the shell. Therefore, this exchanger is like a simple parallel (or counterflow) unit. The kettle reboiler in Fig. 3.7d involves a divided shell-pass flow configuration over two tube passes (from left to right and back to the "channel header"). The shell-side liquid is nearly isothermal at the saturation temperature, so its flow direction makes no difference. Therefore, this exchanger is also equivalent to either the simple parallel or counterflow configuration.

Notice that a salient feature of shell-and-tube exchangers is the presence of baffles. Baffles serve to direct the flow normal to the tubes. We find in Part III that heat transfer from a tube to a flowing fluid is usually better when the flow moves across the tube than when the flow moves along the tube. This augmentation of heat transfer gives the complicated shell-and-tube exchanger an advantage over the simpler single-pass parallel and counterflow exchangers.

However, baffles bring with them a variety of problems. The flow patterns are very complicated and almost defy analysis. A good deal of

the shell-side fluid might unpredictably leak through the baffle holes in the axial direction, or it might bypass the baffles near the wall. In certain shell-flow configurations, unanticipated vibrational modes of the tubes might be excited.

Heat exchangers between liquids and gases often include fins outside the tubes (Fig. 3.6a and b). Heat transfer coefficients for gases are much lower than for liquids. The fins offset this thermal resistance by increasing the surface area in contact with the gas. Fig. 3.6c shows a gas-to-gas exchanger with fins in both gas streams.

In all of these heat exchanger arrangements, vast human ingenuity has been directed towards the task of augmenting the heat transfer from one flow to another. The variations are endless, as you will quickly see if you try Experiment 3.1.

Experiment 3.1

Carry a notebook with you for a day and mark down every heat exchanger you encounter in home, university, or automobile. Classify each according to type and note any special augmentation features.♦

Many specialized and sophisticated software packages now aid the use and design of heat exchangers. Our task as engineers is to use those tools effectively—and to select and assess them critically before we rely on them. When a new heat exchange configurations arises, we must be able to "look under the hood" at the tools available to decide whether they are still applicable. We may need to modify existing analyses, or even create new analyses of our own.

This under-the-hood analysis of heat exchangers first becomes complicated when we account for the fact that two flow streams change one another's temperature. We turn next, in Section 3.2, to the problem of predicting an appropriate mean temperature difference. Then, in Section 3.3 we develop a strategy for use when this mean cannot be determined initially.

3.2 Evaluation of the mean temperature difference in a heat exchanger

Logarithmic mean temperature difference (LMTD)

To begin with, we take U to be a constant value. This is fairly reasonable in compact single-phase heat exchangers. In larger exchangers, particularly in shell-and-tube configurations and large condensers, U is apt to vary with position in the exchanger and/or with local temperature. But in
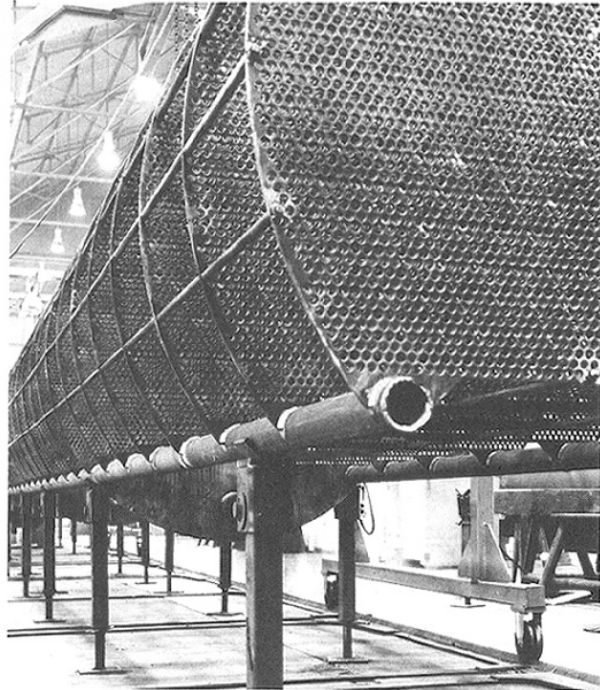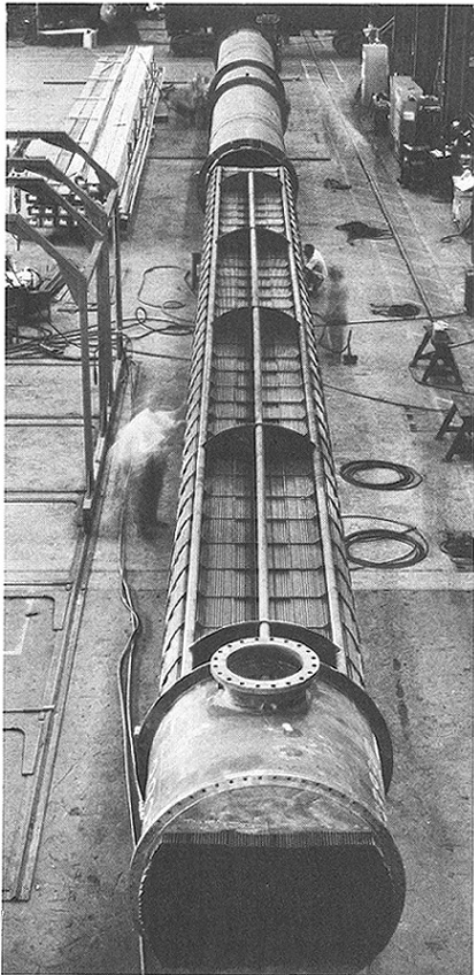
Above and left: A very large feed-water preheater. Tubes are shown withdrawn from the shell on the left. Inset above shows baffles before tubes are inserted. (Photos courtesy of Southwest Engineering Co., Subsidiary of Cronus Industries, Inc., Los Angeles, Calif.)

Below: Small "Swinglok" exchanger with tube-bundle removed from shell. (Photo courtesy of Graham Manufacturing Co. Inc., Batavia, New York.)

Figure 3.5 Typical commercial one-shell-pass, two-tube-pass heat exchangers.
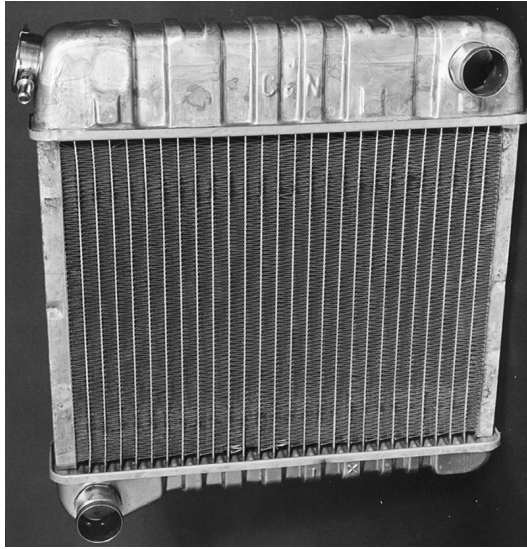
a. A 1980 Chevette radiator. Cross-flow exchanger with neither flow mixed. Edges of flat vertical tubes can be seen.
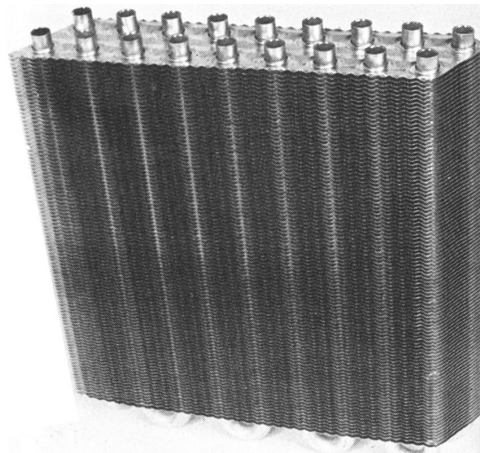
b. A section of an automotive air conditioning condenser. The flow through the horizontal wavy fins is allowed to mix with itself while the two-pass flow through the U-tubes remains unmixed.
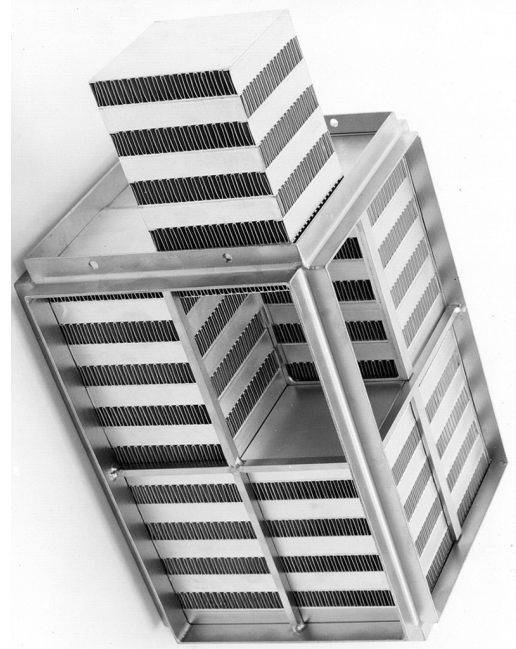
c. The basic 1 ft. $\times$ 1 ft.$\times$ 2 ft. module for a waste heat recuperator. It is a plate-fin, gas-to-air cross-flow heat exchanger with neither flow mixed.

Figure 3.6 Several commercial cross-flow heat exchangers. (Photographs courtesy of Harrison Radiator Division, General Motors Corporation.)
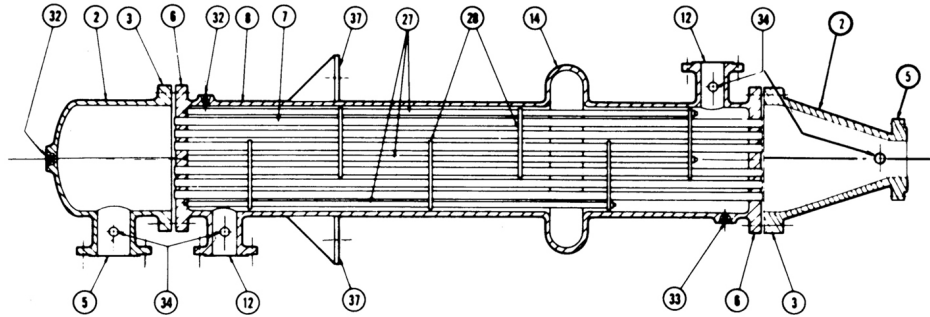
a) Single shell-pass, single tube-pass exchanger
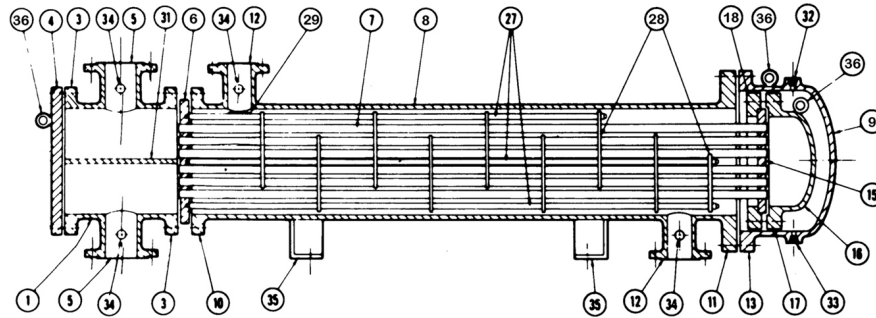
b) One shell-pass, two tube-pass exchanger

1. Stationary head-channel	14. Expansion joint	26. Lantern ring
2. Stationary head-bonnet	15. Floating tube sheet	27. Tie rods and spacers
3. Stationary head-flange- channel or bonnet	16. Floating head cover	28. Transverse baffles or support plates
4. Channel cover	17. Floating head flange	29. Impingement plate
5. Stationary head nozzle	18. Floating head backing device	30. Longitudinal baffle
6. Stationary tube sheet	19. Split shear ring	31. Pass partition
7. Tubes	20. Slip-on backing flange	32. Vent connection
8. Shell	21. Floating head cover- external	33. Drain connection
9. Shell cover	22. Floating tube sheet skirt	34. Instrument connection
10. Shell flange- stationary head end	23. Packing box	35. Support saddle
11. Shell flange- rear head end	24. Packing	36. Lifting lug
12. Shell nozzle	25. Packing gland	37. Support bracket
13. Shell cover flange		38. Weir
		39. Liquid level connection

Figure 3.7 Four typical heat exchanger configurations (continued on next page). (Drawings courtesy of the Tubular Exchanger Manufacturers' Association.)

106
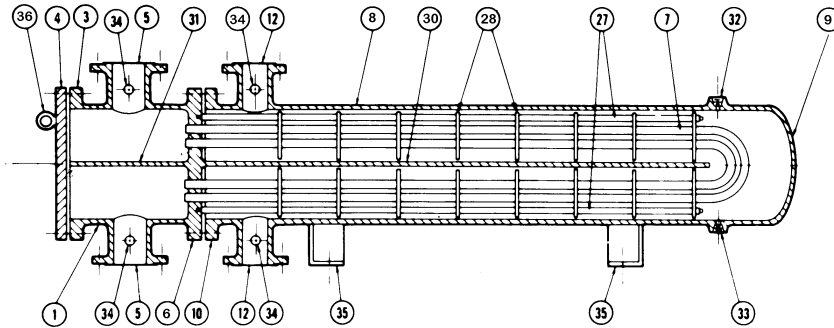
c) Two tube-pass, two shell-pass exchanger
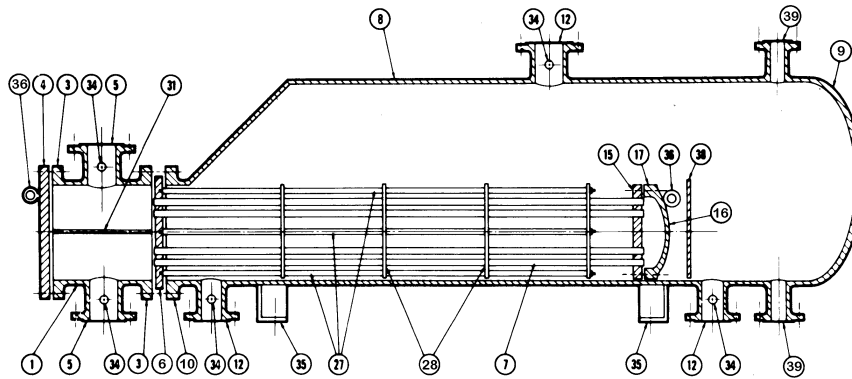
d) One split shell-pass, two tube-pass, kettle type of exchanger

Figure 3.7 *Continued*

situations in which U is fairly constant, we can deal with the varying temperatures of the fluid streams by writing the overall heat transfer in terms of a mean temperature difference between the two fluid streams:

$$Q = UA\,\Delta T_{\text{mean}} \qquad (3.1)$$

Our problem then reduces to finding the appropriate mean temperature difference that will make this equation true. Let us do this for the simple parallel and counterflow configurations, as sketched in Fig. 3.8.

The temperature of both streams is plotted in Fig. 3.8 for both single-pass arrangements—the parallel and counterflow configurations—as a function of the length of travel (or area passed over). Notice that, in the parallel-flow configuration, temperatures tend to change more rapidly
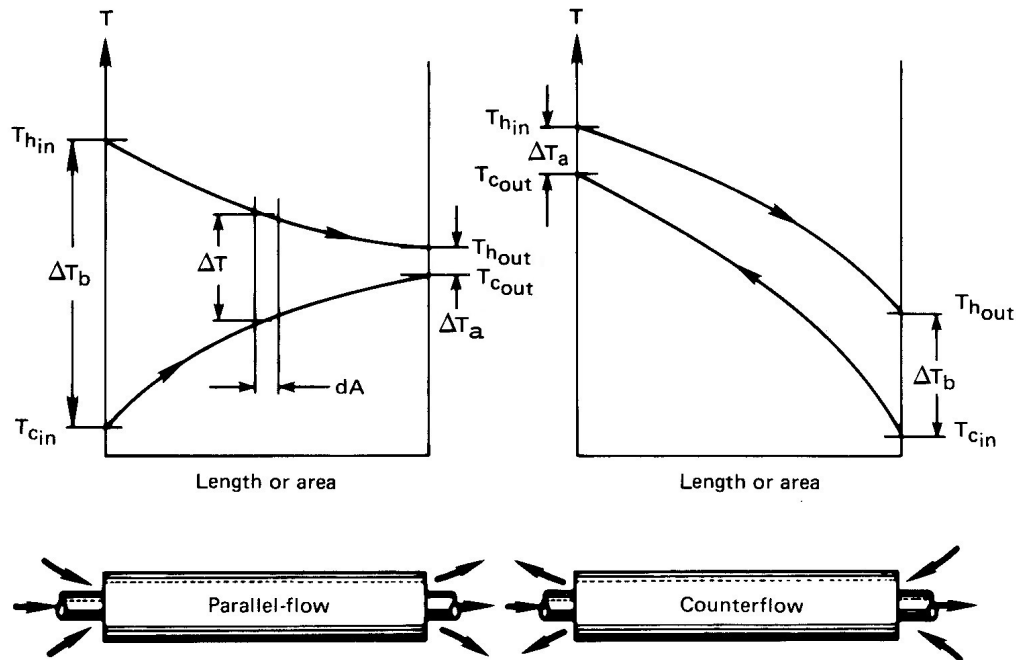
Figure 3.8 The temperature variation through single-pass heat exchangers.

with position and less length is required. But the counterflow arrangement generally achieves more complete heat exchange between the two streams.

Figure 3.9 shows another variation on the single-pass configuration. This is a condenser in which one stream flows through with its temperature changing, but the other simply condenses at uniform temperature. This arrangement has some special characteristics, which we point out in Example 3.3.

The determination of ΔT_{mean} for such arrangements goes thus: the differential heat transfer within either arrangement is (see Fig. 3.8)

$$dQ = U\Delta T\, dA = -(\dot{m}c_p)_h\, dT_h = \pm(\dot{m}c_p)_c\, dT_c \tag{3.2}$$

where the subscripts h and c denote the hot and cold streams, respectively; the upper and lower signs are for the parallel and counterflow cases, respectively; and dT denotes a change from left to right in the exchanger. We give symbols to the total heat capacities of the hot and cold streams:

$$C_h \equiv (\dot{m}c_p)_h\, \text{W/K} \qquad \text{and} \qquad C_c \equiv (\dot{m}c_p)_c\, \text{W/K} \tag{3.3}$$
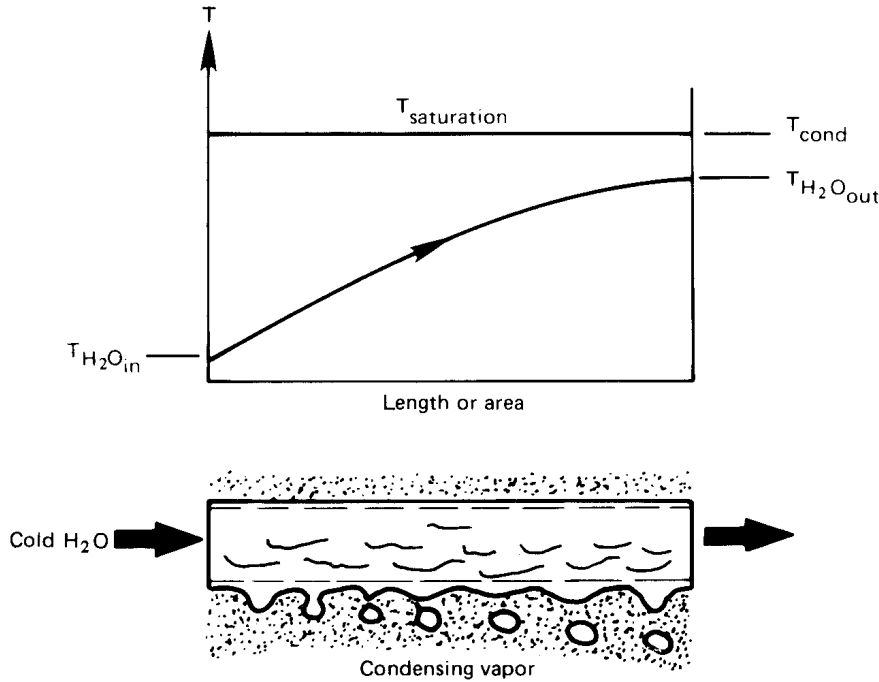
Figure 3.9 The temperature distribution through a condenser.

Thus, for either heat exchanger, $\mp C_h dT_h = C_c dT_c$. This equation can be integrated from the lefthand side, where $T_h = T_{h_{in}}$ and $T_c = T_{c_{in}}$ for parallel flow or $T_h = T_{h_{in}}$ and $T_c = T_{c_{out}}$ for counterflow, to some arbitrary point inside the exchanger. The temperatures inside are thus:

$$\text{parallel flow:} \quad T_h = T_{h_{in}} - \frac{C_c}{C_h}(T_c - T_{c_{in}}) \quad = T_{h_{in}} - \frac{Q}{C_h} \tag{3.4a}$$

$$\text{counterflow:} \quad T_h = T_{h_{in}} - \frac{C_c}{C_h}(T_{c_{out}} - T_c) = T_{h_{in}} - \frac{Q}{C_h} \tag{3.4b}$$

where Q is the total heat transfer from the entrance to the point of interest. Equations (3.4) can be solved for the local temperature differences:

$$\Delta T_{parallel} = T_h - T_c = T_{h_{in}} - \left(1 + \frac{C_c}{C_h}\right)T_c + \frac{C_c}{C_h}T_{c_{in}} \tag{3.5a}$$

$$\Delta T_{counter} = T_h - T_c = T_{h_{in}} - \left(1 - \frac{C_c}{C_h}\right)T_c - \frac{C_c}{C_h}T_{c_{out}} \tag{3.5b}$$

Substitution of these in $dQ = C_c dT_c = U \Delta T \, dA$ yields

$$\left. \frac{U \, dA}{C_c} \right|_{\text{parallel}} = \frac{dT_c}{\left[-\left(1 + \dfrac{C_c}{C_h} \right) T_c + \dfrac{C_c}{C_h} T_{c_{\text{in}}} + T_{h_{\text{in}}} \right]} \tag{3.6a}$$

$$\left. \frac{U \, dA}{C_c} \right|_{\text{counter}} = \frac{dT_c}{\left[-\left(1 - \dfrac{C_c}{C_h} \right) T_c - \dfrac{C_c}{C_h} T_{c_{\text{out}}} + T_{h_{\text{in}}} \right]} \tag{3.6b}$$

Equations (3.6) can be integrated across the exchanger:

$$\int_0^A \frac{U}{C_c} \, dA = \int_{T_{c_{\text{in}}}}^{T_{c_{\text{out}}}} \frac{dT_c}{[---]} \tag{3.7}$$

If U and C_c can be treated as constant, this integration gives

parallel: $\ln \left[\dfrac{-\left(1 + \dfrac{C_c}{C_h} \right) T_{c_{\text{out}}} + \dfrac{C_c}{C_h} T_{c_{\text{in}}} + T_{h_{\text{in}}}}{-\left(1 + \dfrac{C_c}{C_h} \right) T_{c_{\text{in}}} + \dfrac{C_c}{C_h} T_{c_{\text{in}}} + T_{h_{\text{in}}}} \right] = -\dfrac{UA}{C_c} \left(1 + \dfrac{C_c}{C_h} \right)$

$$\tag{3.8a}$$

counter: $\ln \left[\dfrac{-\left(1 - \dfrac{C_c}{C_h} \right) T_{c_{\text{out}}} - \dfrac{C_c}{C_h} T_{c_{\text{out}}} + T_{h_{\text{in}}}}{-\left(1 - \dfrac{C_c}{C_h} \right) T_{c_{\text{in}}} - \dfrac{C_c}{C_h} T_{c_{\text{out}}} + T_{h_{\text{in}}}} \right] = -\dfrac{UA}{C_c} \left(1 - \dfrac{C_c}{C_h} \right)$

$$\tag{3.8b}$$

If U were variable, the integration leading from eqn. (3.7) to eqns. (3.8) is where its variability would have to be considered. Any such variability of U can complicate eqns. (3.8) terribly.

We can simplify eqns. (3.8) with the help of the definitions of ΔT_a and ΔT_b, given in Fig. 3.8:

parallel: $\ln \left[\dfrac{(1 + C_c / C_h)(T_{c_{\text{in}}} - T_{c_{\text{out}}}) + \Delta T_b}{\Delta T_b} \right] = -UA \left(\dfrac{1}{C_c} + \dfrac{1}{C_h} \right)$ (3.9a)

counter: $\ln \dfrac{\Delta T_a}{(-1 + C_c / C_h)(T_{c_{\text{in}}} - T_{c_{\text{out}}}) + \Delta T_a} = -UA \left(\dfrac{1}{C_c} - \dfrac{1}{C_h} \right)$ (3.9b)

In every heat exchanger, $Q_c = Q_h$, by energy conservation. Therefore,

$$\boxed{\frac{C_c}{C_h} = -\frac{T_{h_{\text{out}}} - T_{h_{\text{in}}}}{T_{c_{\text{out}}} - T_{c_{\text{in}}}}} \tag{3.10}$$

Then eqns. (3.9) and eqn. (3.10) give

$$\text{parallel:}\quad \ln\left[\frac{\overbrace{(T_{c_{\text{in}}} - T_{c_{\text{out}}}) + (T_{h_{\text{out}}} - T_{h_{\text{in}}})}^{\Delta T_a - \Delta T_b} + \Delta T_b}{\Delta T_b}\right]$$

$$= \ln\left(\frac{\Delta T_a}{\Delta T_b}\right) = -UA\left(\frac{1}{C_c} + \frac{1}{C_h}\right) \tag{3.11a}$$

$$\text{counter:}\quad \ln\left(\frac{\Delta T_a}{\Delta T_b - \Delta T_a + \Delta T_a}\right) = \ln\left(\frac{\Delta T_a}{\Delta T_b}\right) = -UA\left(\frac{1}{C_c} - \frac{1}{C_h}\right) \tag{3.11b}$$

Finally, we write $1/C_c = (T_{c_{\text{out}}} - T_{c_{\text{in}}})/Q$ and $1/C_h = (T_{h_{\text{in}}} - T_{h_{\text{out}}})/Q$ on the right-hand side of either of eqns. (3.11) and get for either parallel or counterflow,

$$Q = UA\left(\frac{\Delta T_a - \Delta T_b}{\ln(\Delta T_a/\Delta T_b)}\right) \tag{3.12}$$

The appropriate ΔT_{mean} for use in eqn. (3.1) is the group on the right. We call it the *logarithmic mean temperature difference* (LMTD). It allows us to write $Q = UA(\text{LMTD})$:

$$\Delta T_{\text{mean}} = \text{LMTD} \equiv \frac{\Delta T_a - \Delta T_b}{\ln\left(\frac{\Delta T_a}{\Delta T_b}\right)} \tag{3.13}$$

Example 3.1

The idea of a logarithmic mean difference is not new to us. We have already encountered it in Chapter 2. Suppose that we had asked, "What mean radius of pipe would have allowed us to compute the conduction through the wall of a pipe as though it were a slab of thickness $L = r_o - r_i$?" (see Fig. 3.10). To answer this, we write

$$Q = kA\frac{\Delta T}{L} = k\,(2\pi r_{\text{mean}}l)\left(\frac{\Delta T}{r_o - r_i}\right)$$

and then compare it to eqn. (2.21):

$$Q = 2\pi kl\Delta T\,\frac{1}{\ln(r_o/r_i)}$$
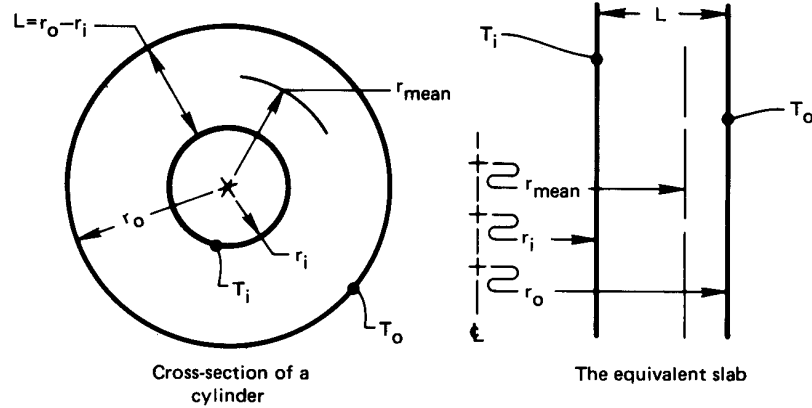
Figure 3.10 Calculation of the mean radius for heat conduction through a pipe.

It follows that

$$r_{\text{mean}} = \frac{r_o - r_i}{\ln(r_o/r_i)} = \text{logarithmic mean radius} \qquad \blacksquare$$

Example 3.2   Balanced Counterflow Heat Exchanger

Suppose that the heat capacity rates of a counterflow heat exchanger are equal, $C_h = C_c$. Such an exchanger is said to be *balanced*. From eqn. (3.5b), it follows the local temperature different in the exchanger is constant throughout, $\Delta T_{\text{counter}} = T_{h_{\text{in}}} - T_{c_{\text{out}}} = \Delta T_a = \Delta T_b$. Does the LMTD reduce to this value?

SOLUTION. If we substitute $\Delta T_a = \Delta T_b$ in eqn. (3.13), we get

$$\text{LMTD} = \frac{\Delta T_b - \Delta T_b}{\ln\left(\Delta T_b/\Delta T_b\right)} = \frac{0}{0} = \text{indeterminate}$$

Therefore it is necessary to use L'Hospital's rule:

$$\underset{\Delta T_a \to \Delta T_b}{\text{limit}} \frac{\Delta T_a - \Delta T_b}{\ln\left(\Delta T_a/\Delta T_b\right)} = \frac{\left.\dfrac{\partial}{\partial \Delta T_a}(\Delta T_a - \Delta T_b)\right|_{\Delta T_a = \Delta T_b}}{\left.\dfrac{\partial}{\partial \Delta T_a}\ln\left(\dfrac{\Delta T_a}{\Delta T_b}\right)\right|_{\Delta T_a = \Delta T_b}}$$

$$= \left.\left(\frac{1}{1/\Delta T_a}\right)\right|_{\Delta T_a = \Delta T_b} = \Delta T_a = \Delta T_b$$

So LMTD does indeed reduce to the intuitively obvious result when the capacity rates are balanced. ■

Example 3.3

Water enters the tubes of a small single-pass heat exchanger at 20°C and leaves at 40°C. On the shell side, 25 kg/min of steam condenses at 60°C. Calculate the overall heat transfer coefficient and the required flow rate of water if the area of the exchanger is 12 m². (The latent heat, h_{fg}, is 2358.7 kJ/kg at 60°C.)

SOLUTION.

$$Q = \dot{m}_{\text{condensate}} \cdot h_{fg}\Big|_{60°C} = \frac{25(2358.7)}{60} = 983 \text{ kJ/s}$$

and with reference to Fig. 3.9, we can calculate the LMTD without naming the exchanger "parallel" or "counterflow", since the condensate temperature is constant.

$$\text{LMTD} = \frac{(60 - 20) - (60 - 40)}{\ln\left(\dfrac{60 - 20}{60 - 40}\right)} = 28.85 \text{ K}$$

Then

$$U = \frac{Q}{A(\text{LMTD})}$$

$$= \frac{983(1000)}{12(28.85)} = 2839 \text{ W/m}^2\text{K}$$

and

$$\dot{m}_{H_2O} = \frac{Q}{c_p \Delta T} = \frac{983,000}{4180(20)} = 11.76 \text{ kg/s} \qquad ■$$

Extended use of the LMTD

Limitations. The use of an LMTD is limited in two basic ways. The first is that it is restricted to the single-pass parallel and counterflow configurations. This restriction can be overcome by adjusting the LMTD for other configurations—a matter that we take up in the following subsection.

The second limitation—our use of a constant value of U—is harder to deal with. The value of U must be negligibly dependent on T to
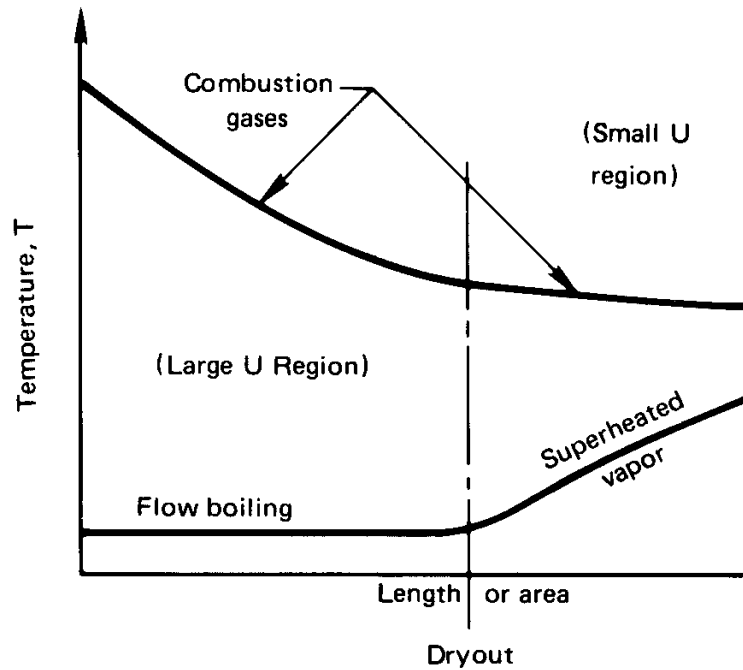
Figure 3.11   A typical case of a heat exchanger in which U varies dramatically: flow boiling in a tube followed by dry out.

complete the integration of eqn. (3.7). Even if $U \neq \text{fn}(T)$, the changing flow configuration and the variation of temperature can still give rise to large variations of U within a given heat exchanger. Figure 3.11 shows a typical situation in which U might vary greatly within a heat exchanger. Here, the mechanism of heat transfer completely changes as water boils into steam. If U were uniform in each portion of the heat exchanger, then we could treat it as two different exchangers in series.

However, the more common difficulty is that of designing heat exchangers in which U varies continuously with position within it. This problem is most severe in large industrial shell-and-tube configurations[1] (see, e.g., Fig. 3.5 or Fig. 3.12) and less serious in compact heat exchangers that have less surface area. If U depends on the location, analyses such as we have just completed [eqn. (3.1) to eqn. (3.13)] must be done using an average U defined as $\int_0^A U \, dA / A$.

_____

[1]Actual heat exchangers can have areas in excess of 10,000 m^2. Large power plant condensers and other large exchangers are often remarkably big pieces of equipment.
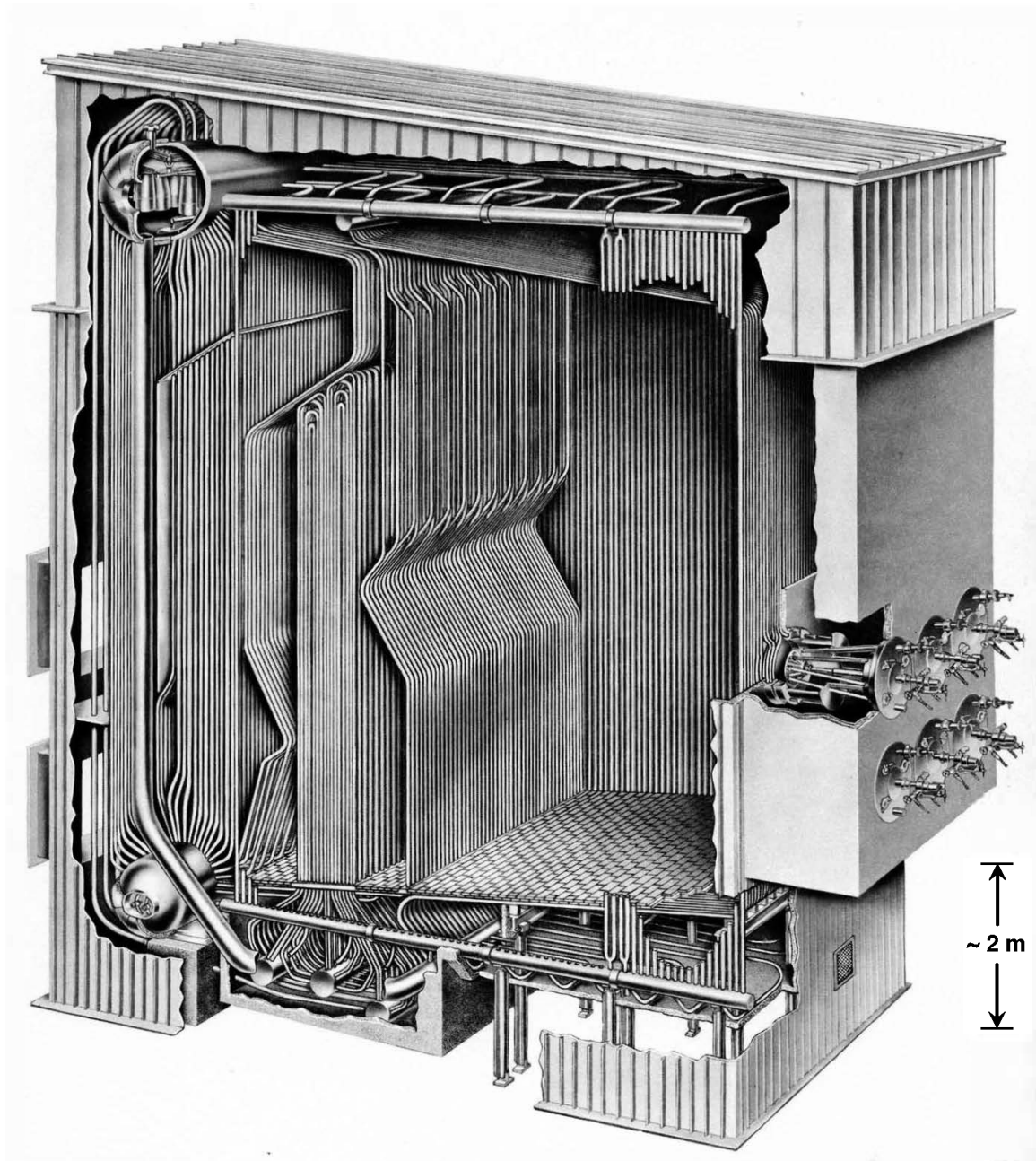
Figure 3.12 A package boiler with a heat transfer surface of 4560 m^2. The burners at right heat water within tubing in the furnace walls, boiler tubing (far left), and superheater tubing (middle left). The steam then drives a turbine. (These units actually come in much larger sizes. Image courtesy of Babcock & Wilcox Co.)

LMTD correction factor, *F*. Suppose we have a heat exchanger in which *U* can reasonably be taken constant, but one that involves such configurational complications as multiple passes and/or cross-flow. In these cases we must rederive the appropriate mean temperature difference in the same way as we derived the LMTD. Each configuration must be analyzed separately and the results are generally more complicated than eqn. (3.13).

This task was undertaken on an *ad hoc* basis during the early twentieth century. In 1940, Bowman, Mueller, and Nagle [3.2] organized such calculations for the common range of heat exchanger configurations. In each case they wrote

$$Q = UA(\text{LMTD}) \cdot F\left(\underbrace{\frac{T_{t_\text{out}} - T_{t_\text{in}}}{T_{s_\text{in}} - T_{t_\text{in}}}}_{P}, \underbrace{\frac{T_{s_\text{in}} - T_{s_\text{out}}}{T_{t_\text{out}} - T_{t_\text{in}}}}_{R}\right) \qquad (3.14)$$

where T_t and T_s are temperatures of tube and shell flows, respectively. The factor *F* is an LMTD correction that varies from one to zero, depending on conditions. The dimensionless groups *P* and *R* have the following physical significance:

- *P* is the relative influence of the overall temperature difference $(T_{s_\text{in}} - T_{t_\text{in}})$ on the tube flow temperature. It must obviously be less than one.

- *R*, according to eqn. (3.10), equals the heat capacity ratio C_t/C_s.

- If one flow remains at constant temperature (as, for example, in Fig. 3.9), then either *P* or *R* will equal zero. In this case the simple LMTD will be the correct ΔT_mean and *F* must go to one.

The factor *F* is defined in such a way that *the LMTD should always be calculated for the equivalent counterflow single-pass exchanger with the same hot and cold temperatures.* This is explained in Fig. 3.13.

Bowman et al. [3.2] summarized all the equations for *F*, in various configurations, that had been derived by 1940. They presented them in figures that were widely reproduced at the time, but which proved to be somewhat inaccurate. Accurate versions of these charts are shown in Fig. 3.14 for two shell-and-tube configuration and for the two simplest cross-flow configurations. Figures 3.14(a) and 3.14(d) are plotted from equations given by Shah and Sekulić [3.3], and Fig. 3.14(c) is plotted from an equation due to Roetzel and Nicole [3.4]. Figure 3.14(b) is plotted from
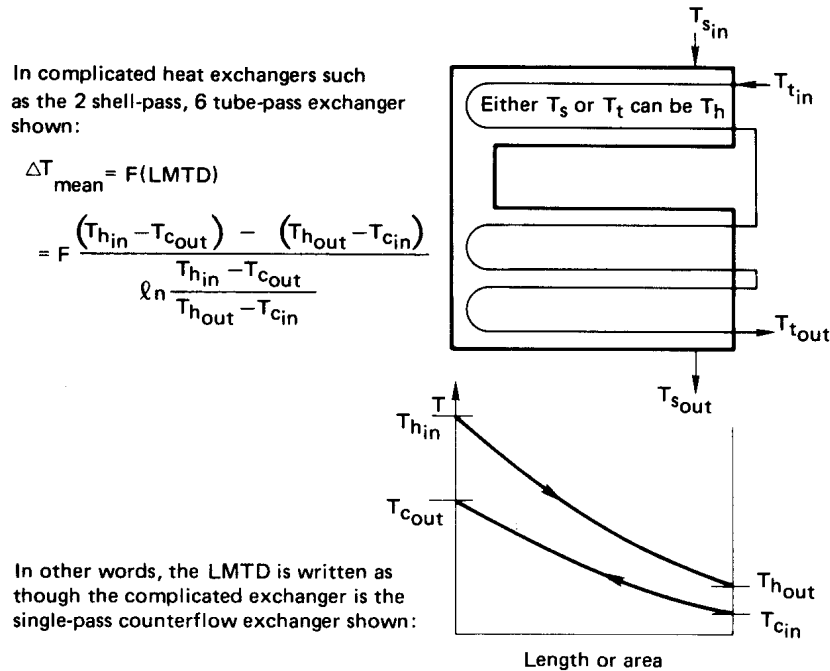
Figure 3.13 The basis of the LMTD in a multipass exchanger, prior to correction.

the equation given by Bowman et al. [3.2]. TEMA presents many additional curves for more complex shell-and-tube configurations.

Gardner and Taborek [3.5] examined the effect of the number of shell-and-tube baffles on F. A one-shell pass, one-tube pass counterflow heat exchanger [Fig. 3.7(a)] is more like a series of cross-flow exchangers than a counterflow device if fewer than 10 baffles are used, so F is less than the expected counterflow value of one. They also discussed the effect of flow by-passing the baffles, e.g., through the holes where tubes pass.

We have simplified Figs. 3.14(a) through 3.14(d) by including curves only for $R \leqslant 1$. Shamsundar [3.6] noted that for $R > 1$, one may obtain F using a simple reciprocal rule. He showed that so long as a heat exchanger has a uniform heat transfer coefficient and the fluid properties are constant,

$$F(P, R) = F(PR, 1/R) \tag{3.15}$$

Thus, if R is greater than one, we need only evaluate F using PR in place of P and $1/R$ in place of R.
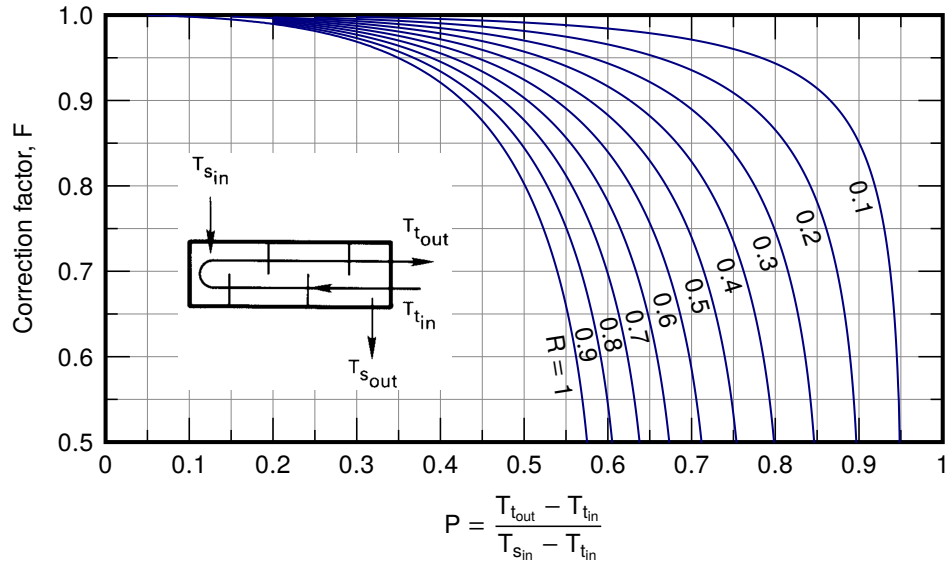
a. F for a one-shell-pass, two, four, six-,... tube-pass exchanger.
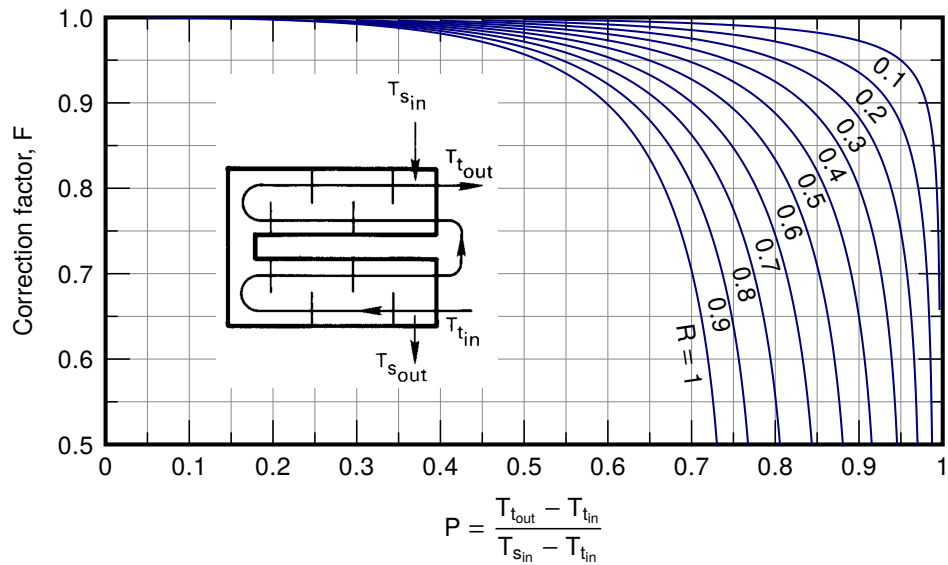
b. F for a two-shell-pass, four or more tube-pass exchanger.

Figure 3.14 LMTD correction factors, F, for multipass shell-and-tube heat exchangers and one-pass cross-flow exchangers. $R = (T_{s_{in}} - T_{s_{out}})/(T_{t_{out}} - T_{t_{in}}) = C_t/C_s$. For $R > 1$, use eqn. (3.15).
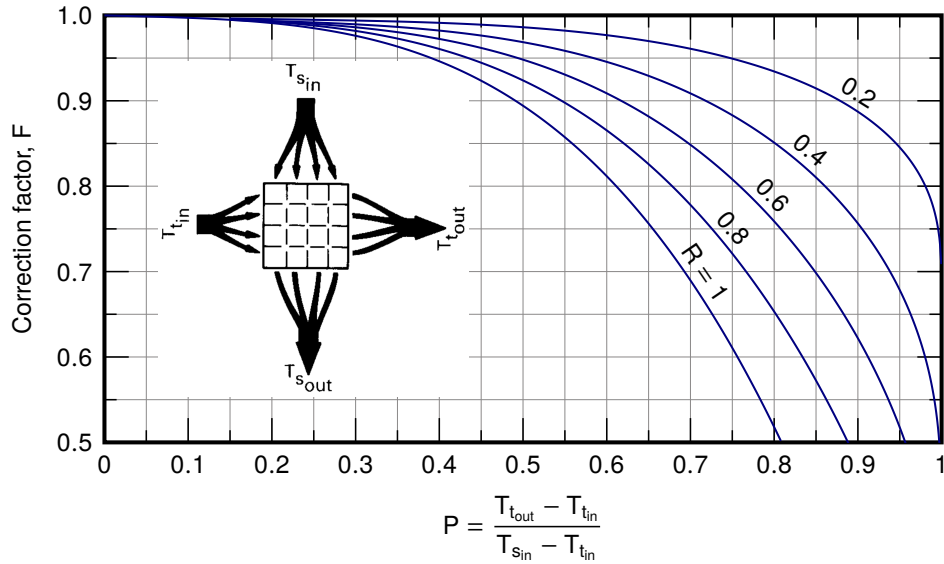
c. *F* for a one-pass cross-flow exchanger with both passes unmixed.
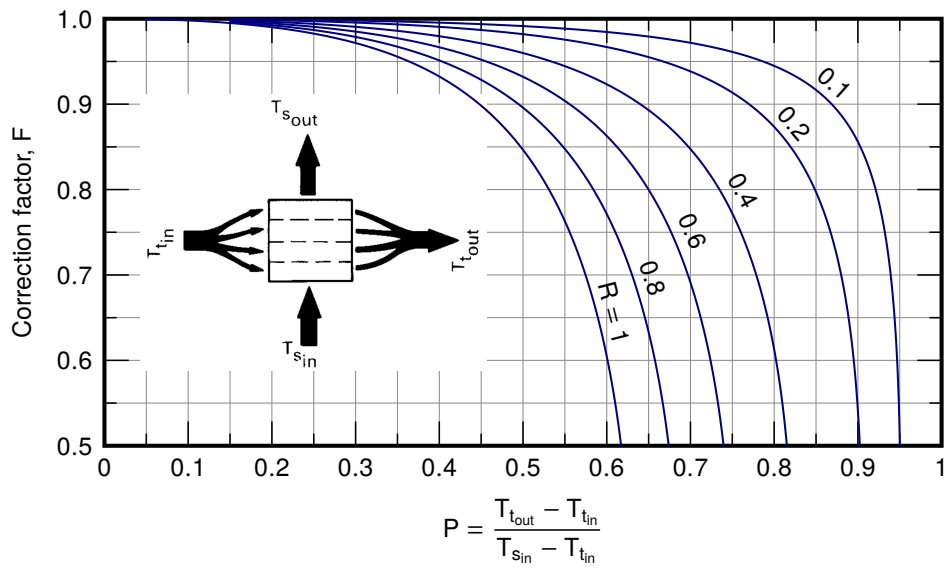
d. *F* for a one-pass cross-flow exchanger with one pass (T_s) mixed.

Figure 3.14 *Continued.* $R = (T_{s_{in}} - T_{s_{out}})/(T_{t_{out}} - T_{t_{in}}) = C_t/C_s$.

Example 3.4

5.795 kg/s of oil flows through the shell side of a two-shell pass, four-tube-pass oil cooler. The oil enters at 181°C and leaves at 38°C. Water flows in the tubes, entering at 32°C and leaving at 49°C. In addition, $c_{p,\text{oil}}$ = 2282 J/kg·K and U = 416 W/m²K. Find how much area the heat exchanger must have.

SOLUTION.

$$\text{LMTD} = \frac{(T_{h_{\text{in}}} - T_{c_{\text{out}}}) - (T_{h_{\text{out}}} - T_{c_{\text{in}}})}{\ln\left(\dfrac{T_{h_{\text{in}}} - T_{c_{\text{out}}}}{T_{h_{\text{out}}} - T_{c_{\text{in}}}}\right)}$$

$$= \frac{(181 - 49) - (38 - 32)}{\ln\left(\dfrac{181 - 49}{38 - 32}\right)} = 40.76 \text{ K}$$

$$R = \frac{181 - 38}{49 - 32} = 8.412 \qquad P = \frac{49 - 32}{181 - 32} = 0.114$$

Since $R > 1$, we use eqn. (3.15). For $P = 8.412(0.114) = 0.959$ and $R = 1/8.412 = 0.119$, Fig. 3.14(b) shows $F = 0.92$.[2] It follows that:

$$Q = \dot{m}_{\text{oil}}c_{p,\text{oil}}(T_{h_{\text{in}}} - T_{h_{\text{out}}}) = UAF(\text{LMTD})$$
$$5.795(2282)(181 - 38) = 416(A)(0.92)(40.76)$$
$$A = 121.2 \text{ m}^2 \qquad\qquad\blacksquare$$

3.3 Heat exchanger effectiveness

We are now able to use the LMTD to predict the performance of an exchanger once we know its configuration *and* the imposed temperature differences. Unfortunately, we do not often know that much about a system before the design is complete.

Often we begin with information such as is shown in Fig. 3.15. If we sought to calculate Q in such a case, we would have to do so by guessing an exit temperature such as to make $Q_h = Q_c = C_h\Delta T_h = C_c\Delta T_c$. Then we could calculate Q from UA(LMTD) or UAF(LMTD) and check it

---

[2]Notice that, for a 1 shell-pass exchanger, these R and P lines do not quite intersect [see Fig. 3.14(a)]. Therefore, no single-shell exchanger would give these values.
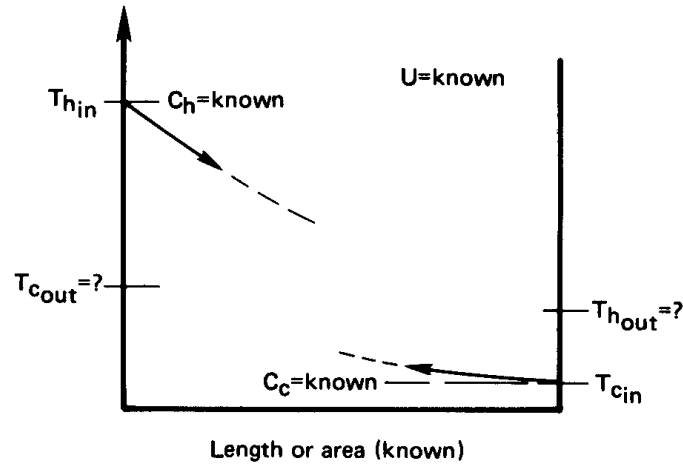
Figure 3.15 A design problem in which the LMTD cannot be calculated a priori.

against Q_h. The answers would differ, so we would have to guess new exit temperatures and try again.

Such problems can be greatly simplified with the help of the so-called *effectiveness-NTU method.* It was first developed in full detail in 1955 by Kays and London [3.7] in a book titled *Compact Heat Exchangers.* We should take particular note of the title. This method works if the overall heat transfer coefficient is fairly uniform, which is far more likely in a compact heat exchanger than in larger equipment.

The heat exchanger effectiveness is defined as

$$\varepsilon \equiv \frac{\text{actual heat transferred}}{\substack{\text{maximum heat that could possibly be} \\ \text{transferred from one stream to the other}}}$$

In mathematical terms, this is

$$\varepsilon = \frac{C_h(T_{h_{\text{in}}} - T_{h_{\text{out}}})}{C_{\min}(T_{h_{\text{in}}} - T_{c_{\text{in}}})} = \frac{C_c(T_{c_{\text{out}}} - T_{c_{\text{in}}})}{C_{\min}(T_{h_{\text{in}}} - T_{c_{\text{in}}})} \tag{3.16}$$

where $C_{\min}$ is the smaller of C_c and C_h. It follows that

$$Q = \varepsilon C_{\min}(T_{h_{\text{in}}} - T_{c_{\text{in}}}) \tag{3.17}$$

A second definition was originally made by E. K. W. Nusselt, whom we meet again in Part III. This is the *number of transfer units* (NTU):

$$\boxed{\text{NTU} \equiv \frac{UA}{C_{\min}}}$$
(3.18)

This dimensionless group compares the exchanger's capacity for transferring heat to the minimum capacity rate of the streams—both in W/K.

We can immediately reduce the parallel-flow result from eqn. (3.9) to the following equation, based on these definitions:

$$-\left(\frac{C_{\min}}{C_c} + \frac{C_{\min}}{C_h}\right)\text{NTU} = \ln\left[-\left(1 + \frac{C_c}{C_h}\right)\varepsilon\frac{C_{\min}}{C_c} + 1\right]$$
(3.19)

We solve this for ε and, regardless of whether $C_{\min}$ is associated with the hot or cold flow, obtain for the parallel single-pass heat exchanger:

$$\boxed{\varepsilon \equiv \frac{1 - \exp[-(1 + C_{\min}/C_{\max})\text{NTU}]}{1 + C_{\min}/C_{\max}} = \text{fn}\left(\frac{C_{\min}}{C_{\max}}, \text{NTU only}\right)}$$
(3.20)

The corresponding expression for the counterflow case is:

$$\boxed{\varepsilon = \frac{1 - \exp[-(1 - C_{\min}/C_{\max})\text{NTU}]}{1 - (C_{\min}/C_{\max})\exp[-(1 - C_{\min}/C_{\max})\text{NTU}]}}$$
(3.21)

Equations (3.20) and (3.21) are plotted in Fig. 3.16. Similar calculations can be made for other heat exchanger configurations (see [3.7] and Problem 3.38). We include some additional situations in Fig. 3.17 and Table 3.1. In every case, when NTU is small ε is also small: neither stream's temperature will change much (Problem 3.23).

We illustrate the use of effectiveness to *rate the performance* of an existing heat exchanger, and to *fix the size* of a new one, in the following two examples.

Example 3.5

Consider the following parallel-flow heat exchanger specification:

$$\text{cold flow enters at } 40°C: \quad C_c = 20,000 \text{ W/K}$$
$$\text{hot flow enters at } 150°C: \quad C_h = 10,000 \text{ W/K}$$
$$A = 30 \text{ m}^2 \qquad U = 500 \text{ W/m}^2\text{K}$$

Determine the heat transfer and the exit temperatures.
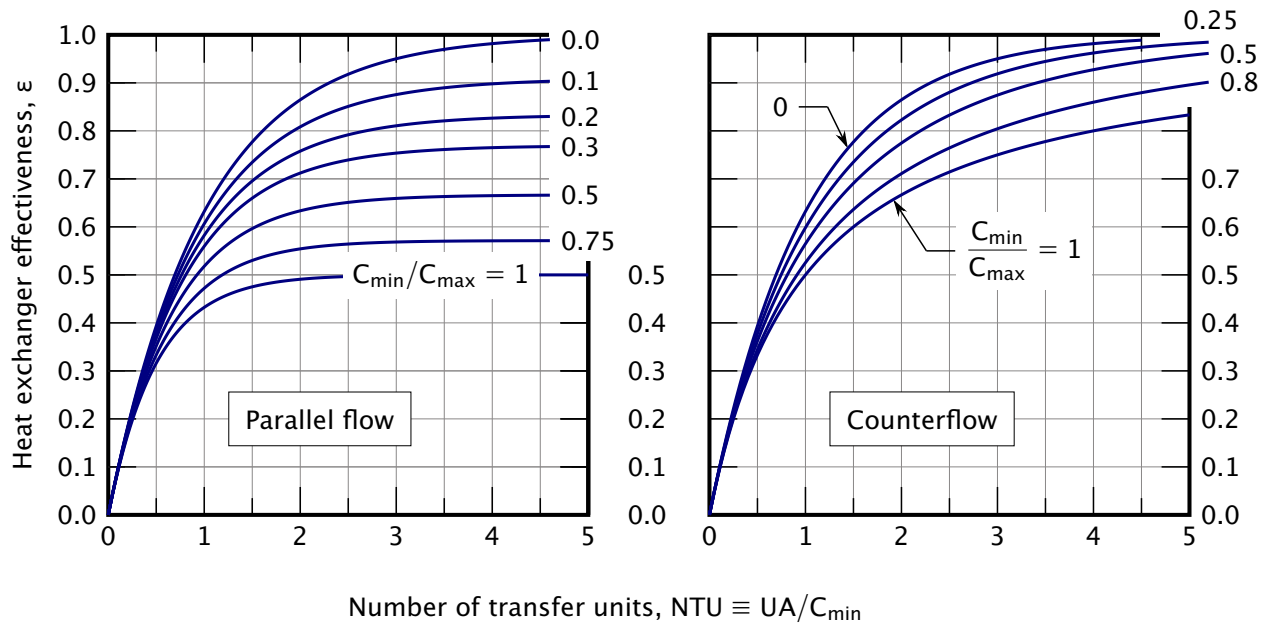
Figure 3.16 The effectiveness of parallel and counterflow heat exchangers, eqns. (3.20) and (3.21).

SOLUTION. In this case we do not know the exit temperatures, so it is not possible to calculate the LMTD. Instead, we can go either to the parallel-flow effectiveness chart in Fig. 3.16 or to eqn. (3.20), using

$$\text{NTU} = \frac{UA}{C_{min}} = \frac{500(30)}{10,000} = 1.5$$

$$\frac{C_{min}}{C_{max}} = 0.5$$

and we obtain $\varepsilon = 0.596$. Now from eqn. (3.17), we find that

$$Q = \varepsilon \, C_{min} \left(T_{h_{in}} - T_{c_{in}} \right) = 0.596(10,000)(150 - 40)$$
$$= 655,600 \text{ W} = 655.6 \text{ kW}$$

Finally, from energy balances, such as are expressed in eqn. (3.4), we get

$$T_{h_{out}} = T_{h_{in}} - \frac{Q}{C_h} = 150 - \frac{655,600}{10,000} = 84.44°\text{C}$$

$$T_{c_{out}} = T_{c_{in}} + \frac{Q}{C_c} = 40 + \frac{655,600}{20,000} = 72.78°\text{C} \qquad \blacksquare$$
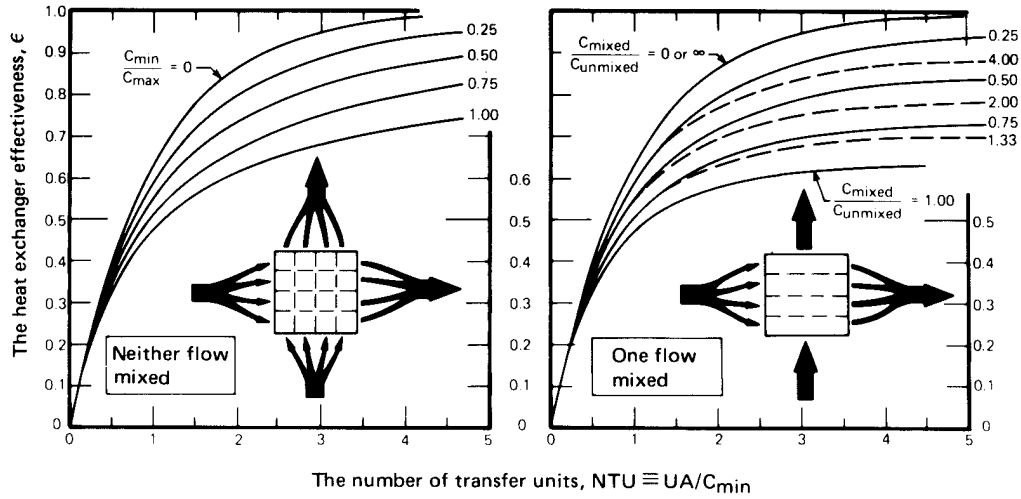
a.) Cross-flow exchanger, neither
   fluid mixed

b.) Cross-flow exchanger, one
   fluid mixed

The number of transfer units, $NTU \equiv UA/C_{min}$
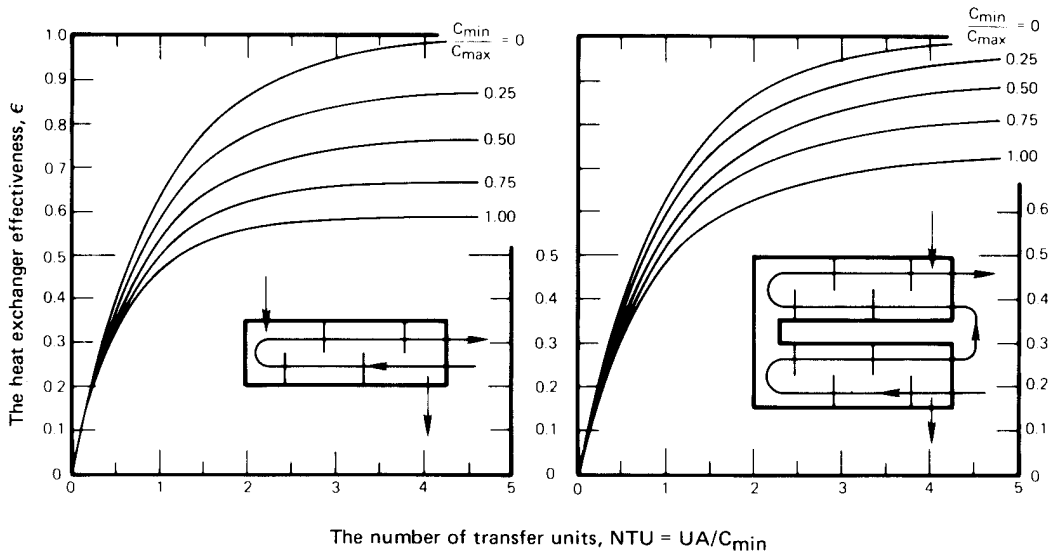
c.) One shell pass, two tube pass exchanger.
   (Can also be used for 4, 6, 8, 10, 12 tube
   passes with a maximum error in ϵ, of 0.040
   at $C_{min}/C_{max} = 1$ and large NTU.)

d.) Two shell pass 4 tube pass exchanger.
   (Can also be used for 4, 6, 8, ... tube
   passes with reasonable accuracy if
   there are equal numbers of tube
   passes in each shell pass.)

Figure 3.17 The effectiveness of some other heat exchanger
configurations.

Table 3.1 Effectiveness-NTU relationships for configurations in Fig. 3.17. $R = C_{\min}/C_{\max}$. Most of these equations can be rearranged to give NTU as a function of ε and R [3.7, 3.8].

Configuration	Effectiveness, ε
Crossflow, neither stream mixed	
$\quad R > 0.3$ and NTU > 1	$\varepsilon \simeq [1 + 0.44(1 - R)]\left\{1 - \left[0.92 + (\pi R^{0.15}\text{NTU})^{1.25}\right]^{-0.4}\right\}$
$\quad R \leqslant 0.3$ or NTU $\leqslant 1$	$\varepsilon \simeq 1 - \exp\left\{[\exp(-R^{1.15}\text{NTU}) - 1]/R^{1.15}\right\}$
Crossflow, one stream mixed	
$\quad C_{\min}$ mixed, $C_{\max}$ unmixed	$\varepsilon = 1 - \exp\left\{-[1 - \exp(-\text{NTU} \cdot R)]/R\right\}$
$\quad C_{\max}$ mixed, $C_{\min}$ unmixed	$\varepsilon = \dfrac{1}{R}\left(1 - \exp\left\{-R[1 - \exp(-\text{NTU})]\right\}\right)$
One shell pass, two tube pass	$\varepsilon = \dfrac{2}{(1 + R) + \sqrt{1 + R^2}\coth(\Gamma/2)}$
	where $\Gamma = \text{NTU}\sqrt{1 + R^2}$
N shell passes, $2N$ tube passes	$\varepsilon = \left[\left(\dfrac{1 - \varepsilon_p R}{1 - \varepsilon_p}\right)^N - 1\right]\left[\left(\dfrac{1 - \varepsilon_p R}{1 - \varepsilon_p}\right)^N - R\right]^{-1}$
	where ε_p is the effectiveness of each shell pass

Example 3.6

Suppose that we had the same kind of exchanger as we considered in Example 3.5, but that the area remained an unspecified design variable. Calculate the area that would bring the hot flow out at 90°C.

SOLUTION. Once the exit cold fluid temperature is known, the problem can be solved with equal ease by either the LMTD or the effectiveness approach. An energy balance [eqn. (3.4a)] gives

$$T_{c_{\text{out}}} = T_{c_{\text{in}}} + \frac{C_h}{C_c}(T_{h_{\text{in}}} - T_{h_{\text{out}}}) = 40 + \frac{1}{2}(150 - 90) = 70°\text{C}$$

Then, using the effectiveness method,

$$\varepsilon = \frac{C_h(T_{h_{\text{in}}} - T_{h_{\text{out}}})}{C_{\min}(T_{h_{\text{in}}} - T_{c_{\text{in}}})} = \frac{10,000(150 - 90)}{10,000(150 - 40)} = 0.5455$$

so from Fig. 3.16 we read NTU $\simeq 1.15 = UA/C_{\min}$. Thus

$$A = \frac{10,000(1.15)}{500} = 23.00 \text{ m}^2$$

We could also have calculated the LMTD:

$$\text{LMTD} = \frac{(150 - 40) - (90 - 70)}{\ln(110/20)} = 52.79 \text{ K}$$

so from $Q = UA(\text{LMTD})$, we obtain

$$A = \frac{10,000(150 - 90)}{500(52.79)} = 22.73 \text{ m}^2$$

The answers differ by 1%, which reflects graph-reading inaccuracy. ■

Single-stream heat exchangers.   When the temperature of either fluid in a heat exchanger is uniform, the problem of analyzing heat transfer is greatly simplified. We have already noted that no *F*-correction is needed to adjust the LMTD in this case. The reason is that when only one fluid changes in temperature, the configuration of the exchanger becomes irrelevant. Any such exchanger is equivalent to a single fluid stream flowing through an isothermal pipe.[3]

The single-stream limit, in which one stream's temperature is constant, occurs when heat capacity rate ratio $C_{\min}/C_{\max}$ goes to zero. The heat capacity rate ratio might *approach* zero because the flow rate or specific heat of one stream is very large compared to the other, as when a high mass flow rate of water cools a very low mass flow rate of air. Alternatively, it might effectively *be* infinite. That would be the case if one fluid were boiling or condensing and underwent phase change at a constant temperature, as in Fig. 3.9.

Since all heat exchangers are equivalent in this case, the equation for the effectiveness in any configuration must reduce to the same common expression. This limiting expression can be derived directly from energy-balance considerations (see Problem 3.11), but we obtain it here by letting $C_{\min}/C_{\max} \longrightarrow 0$ in either eqn. (3.20) or eqn. (3.21). The result is

$$\boxed{\varepsilon_{\text{single stream}} = 1 - e^{-\text{NTU}}} \qquad (3.22)$$

Equation (3.22) defines the curve for $C_{\min}/C_{\max} = 0$ in all six of the effectiveness graphs in Fig. 3.16 and Fig. 3.17.

---

[3]We make use of this notion in Section 7.4, when we analyze heat convection in pipes and tubes.

Balanced counterflow heat exchangers. In Example 3.2, we saw that when the heat capacity rates are balanced in a counterflow heat exchanger, so that $C_h = C_c$ (or $C_{max} = C_{min}$), the temperature difference between the hot and cold streams is constant. In this case, the effectiveness, eqn. (3.21), limits to

$$\varepsilon = \frac{NTU}{1 + NTU} \tag{3.23}$$

(see Problem 3.35). The balanced counterflow arrangement is used for heat recovery in power cycles and ventilation systems. For example, a warm exhaust air stream may be used to preheat an incoming cold air stream.

The P-NTU method. A more general NTU method is the *P*-NTU method, in which *P* is the "temperature effectiveness" defined in eqn. (3.14). In this approach, a separate value of *P* is given for each stream, P_t and P_s, by interchanging t and s in the definition. Then

$$Q = P_t C_t |T_{t_{in}} - T_{s_{in}}| = P_s C_s |T_{s_{in}} - T_{t_{in}}| \tag{3.24}$$

By comparison, we see that this approach is equivalent to eqn. (3.17) with *P* replacing ε when C_{min} is, respectively, the tube side or the shell side. The key difference is that $R_t = C_t/C_s$ can take any value from 0 to ∞ in the *P*-NTU method, whereas $C_{min} \leq C_{max}$ in the ε-NTU method. The *P*-NTU method thus has greater flexibility when the stream with C_{min} is unknown or varying. Formulas for $P_t = fn(R_t, NTU_t)$ are available for many heat exchanger configurations (see [3.3]).

3.4 Heat exchanger design

The methods of this chapter provide basic estimates of heat transfer and temperature change in a heat exchanger configuration for which U is known. Alternatively, these methods give the approximate size of an exchanger of a given type that can accomplish the required temperature changes in the process streams.

We use the term *rating* for the calculation of the heat transfer and outlet temperatures of a known heat exchanger. In a rating calculation, we find the performance of an already fully specified device. That will establish whether the exchanger meets the process requirements. We should also calculate the pressure drop of each fluid stream, to ensure that the head loss also meets requirements.

Very often, an engineer simply selects a heat exchanger from among off-the-shelf units. The selection is normally based on a rating calculation. We will choose a device that has at least the minimum heat transfer needed and no more than the maximum pressure drop allowed. Devices selected this way are not optimized for the application. But they may suffice for relatively small heat exchangers integrated into single projects. For larger exchangers (such as in chemical or LNG plants, for example) and for mass-produced heat exchangers (such as in automobiles or HVAC equipment) economics become a primary design consideration. Cost and performance must then be tailored for the specific application.

Tailored heat exchangers pose the more open-ended problem of *heat exchanger design*—the entire heat exchanger configuration must be determined. The designer must choose the layout, the tube sizes and lengths, the number of passes, the shell size and arrangement of baffles, and even the number of individual heat exchangers to be placed in parallel or in series. Such a problem clearly has multiple solutions. But further, the design must account for fouling conditions, material corrosion, maintenance access, mechanical stresses, tube vibration, assembly, and possibly other considerations. An engineer will seek the best alternative for performance, cost, and reliability while meeting any other constraints of the specific application, such as size, weight, material availability,…the list goes on. It might even include aesthetics.

To better understand the design process, faced with such an array of trade-offs between advantages and penalties, consider Taborek's list [3.9] of design considerations for a large shell-and-tube exchanger:

- Make a rough estimate of the size of the heat exchanger using, for example, U values from Table 2.2 and/or anything else that we might know from experience. This serves to circumscribe the subsequent work; it will help to size flow rates and to anticipate temperature variations; and it will help to avoid subsequent errors. Such a calculation should consider the range of possible U, given the uncertainties in estimating h and the progressive impact of fouling.

- Decide which fluid should flow on the shell side and which should flow in the tubes. The higher-pressure fluid should usually go inside the tubes. An especially corrosive fluid should go in the tubes, to minimize the use of expensive corrosion-resistant material. Generally, the more fouling-prone fluid should also go in the tubes because the insides of tubes in a tube bundle are easier to access for cleaning (by removing the headers) than the outsides of tubes. The more viscous fluid should go on the shell side, to help limit pressure drop.

- Early in the process, the designer should assess the cost of making calculations in comparison with:

    (a) The level of accuracy that is really needed.
    (b) The investment in the exchanger.
    (c) The cost of miscalculation.

- Evaluate the heat transfer, pressure drop, and cost of various exchanger configurations that appear reasonable for the application. We often do this with specialized software for heat exchanger design, which can account for a variety of configurations, complex flow patterns on the shell side, and engineering considerations beyond heat transfer and pressure drop. This process may be iterative, as options are evaluated and then discarded or refined.

Obviously, the selection of a specific heat configuration can benefit greatly from experience. The descriptions in this chapter provide a kind of first level of experience. References [3.3, 3.7, 3.11–3.13] provide a second level. Manufacturer's catalogues are also an excellent source of information for specific types of exchangers.

Once we have set the configuration and approximated U, the area becomes the basic design variable. The design can then proceed along the lines of Section 3.2 or 3.3. If it is possible to begin with a complete specification of inlet and outlet temperatures, we can write

$$\underbrace{Q}_{C\Delta T} = \underbrace{U}_{known} \; A \; \underbrace{F(\text{LMTD})}_{calculable}$$

and solve for A. A rough design can then be completed. We must then reevaluate U, check pressure loss, look for low velocity zones that promote fouling, high velocity zones that promote erosion or vibration, and then adjust the design as required by these and various other factors [3.9].

More often, we begin without full knowledge of the outlet temperatures. In such cases, we must apply trial-and-error to get the area, and then bring in a more complicated sequence of trials if we seek to optimize pressure drop and cost by varying the configuration as well. If the C's are design variables, U will change significantly because h's are generally velocity-dependent. More iteration will then be needed.

We conclude Part I of this book facing many incomplete issues. We need to be able to estimate the convective heat transfer coefficient in all kinds of heat transfer situations, of which designing heat exchanger is

only one. But before we undertake the calculation of h, we must turn, in Part II, to a far more thorough study of heat conduction. There, in addition to setting up the methods we will need to predict h's, we shall deal with many other issues of great practical importance in their own right.

Problems

3.1 Explain the meaning of "mixed" in a heat exchanger context. Can you have a cross-flow exchanger in which both flows are mixed? Discuss.

3.2 For one-dimensional heat conduction through a thick spherical shell, find the appropriate mean radius, $\overline{r}$, that will make $Q = k\Delta T \cdot A(\overline{r})/(r_o - r_i)$, where $A(\overline{r}) = 4\pi\overline{r}^2$ (cf. Example 3.1).

3.3 Rework Problem 2.14, using the LMTD. (*Hint:* Trial-and-error solution required.)

3.4 2.4 kg/s of a fluid having a specific heat of 0.80 kJ/kg·K enter a counterflow heat exchanger at 0°C and are heated to 400°C by 2 kg/s of a fluid having a specific heat of 0.96 kJ/kg·K entering the unit at 700°C. Show that heating the cooler fluid to 500°C would require the surface area for a heat transfer to be increased by 87.5%, if all other conditions remained unchanged.

3.5 A cross-flow heat exchanger with both fluids unmixed is used to heat water ($c_p = 4.18$ kJ/kg·K) flowing at 1.0 kg/s from 40°C to 80°C. Hot engine oil ($c_p = 1.9$ kJ/kg·K) flowing at 2.6 kg/s enters at 100°C. What is the overall heat transfer coefficient if the heat transfer area is 20 m^2? (Note that you can use either an effectiveness or an LMTD method. It would be wise to use both as a check on graphical accuracy.)

3.6 Saturated, non-oil-bearing steam at 1 atm enters the shell pass of a two-tube-pass shell condenser with thirty, 20 ft. tubes in each tube pass. The tubes are ¾ in., schedule 160 steel pipe (nominal diameter). Water at 60°F enters each tube at a volume flow rate of 0.01 ft^3/s (per tube). The condensation heat transfer coefficient is 2000 Btu/h·ft^2·°F, and $\overline{h} = 1380$ Btu/h·ft^2·°F for the water inside the tubes. Estimate the exit temperature of the water and the mass rate of condensation. [$\dot{m}_c \simeq 8393$ lb$_m$/h]

3.7 Consider a counterflow heat exchanger that must cool 3000 kg/h of mercury from 150°F to 128°F. The coolant is 100 kg/h of water, supplied at 70°F. If U is 300 W/m²K, complete the design by determining the necessary area and the exit temperature of water. [A = 0.147 m²]

3.8 An automobile air-conditioner condenses refrigerant by rejecting heat to the air outside the car. A particular condenser gives up 18 kW at 65 km/h when the outside temperature is 35°C. The refrigerant temperature is constant at 65°C while condensing, and the air rises 6°C in temperature as it flows across the heat exchanger tubes. The heat exchanger is of the finned-tube type shown in Fig. 3.6b, with $U \simeq 200$ W/m²K. If $U \sim$ (air velocity)$^{0.7}$ and the mass flow rate increases directly with the velocity, plot the percentage reduction of the heat transfer from the condenser as a function of air velocity between 15 and 65 km/h.

3.9 Derive eqn. (3.21).

3.10 Derive the infinite NTU limit of the effectiveness for both parallel and counterflow heat exchangers for arbitrary values of C_{min}/C_{max}. Use common sense, the definition of effectiveness, and the First Law of Thermodynamics. Refer to eqn. (3.20) and eqn. (3.21) only to check your results.

3.11 Derive the equation $\varepsilon = (NTU, C_{min}/C_{max})$ for the heat exchanger depicted in Fig. 3.9.

3.12 A single-pass heat exchanger condenses steam at 1 atm on the shell side and heats water from 10°C to 30°C on the tube side with U = 2500 W/m²K. The tubing is thin-walled, 5 cm in diameter, and 2 m in length. (a) How do you advise your boss, who wants to know whether the exchanger should be counterflow or parallel-flow? Evaluate: (b) the LMTD; (c) $\dot{m}_{H_2O}$; and (d) ε. [$\varepsilon \simeq 0.222$]

3.13 Air at 2 kg/s and 27°C and a stream of water at 1.5 kg/s and 60°C each enter a heat exchanger. Evaluate the exit temperatures if A = 12 m², U = 185 W/m²K, and:

   a. The exchanger is parallel flow;
   b. The exchanger is counterflow [$T_{h_{out}} \simeq 54.0$°C];
   c. The exchanger is cross flow, one stream mixed;

d. The exchanger is cross flow, neither stream mixed.
   [$T_{h_{out}} = 53.65°C$]

3.14   Air at 0.25 kg/s and 0°C enters a cross-flow heat exchanger. The air must be warmed to 20°C by 0.14 kg/s of air at 50°C. The streams are unmixed. As a first step in the design process, plot U against A and, with reference to Table 2.2, identify the approximate range of area for the exchanger.

3.15   A particular two shell-pass, four tube-pass heat exchanger uses 20 kg/s of river water at 10°C on the shell side to cool 8 kg/s of process water from 80°C to 25°C on the tube side. At what temperature will the coolant be returned to the river? If U is 800 W/m^{2}K, how large must the exchanger be?

3.16   A particular cross-flow heat exchanger operates with the fluid mixed on one side only. When it is new, $U = 2000$ W/m^{2}K, $T_{c_{in}} = 25°C$, $T_{c_{out}} = 80°C$, $T_{h_{in}} = 160°C$, and $T_{h_{out}} = 70°C$. After 6 months of operation, the plant manager reports that the hot fluid is only being cooled to 90°C and that he is suffering a 30% reduction in total heat transfer. What is the fouling resistance after 6 months of use? (Assume no reduction of cold-side flow rate by fouling.)

3.17   Water at 15°C is supplied to a one-shell-pass, two-tube-pass heat exchanger to cool 10 kg/s of liquid ammonia from 120°C to 40°C. You anticipate a U on the order of 1500 W/m^{2}K when the water flows in the tubes. If A is to be 90 m^2, choose the correct flow rate of water.

3.18   Suppose that the heat exchanger in Example 3.5 had been a two shell-pass, four tube-pass exchanger with the hot fluid moving in the tubes. (a) What would be the exit temperature in this case? (b) What would be the area if we wanted the hot fluid to leave at the same temperature as in the example? [(a) $T_{c_{out}} = 76.85°C$]

3.19   Plot the maximum tolerable fouling resistance as a function of U_{new} for a counterflow exchanger, with given inlet temperatures, if a 30% reduction in U is the maximum that can be tolerated.

3.20   Water at 0.8 kg/s enters the tubes of a two-shell-pass, four-tube-pass heat exchanger at 17°C and leaves at 37°C. It cools 0.5 kg/s of air entering the shell at 250°C with $U = 432$ W/m^{2}K. Determine:

(a) the exit air temperature; (b) the area of the heat exchanger; and (c) the exit temperature if, after some time, the tubes become fouled with $R_f = 0.0005 \text{ m}^2\text{K/W}$. [(c) $T_{\text{air}_{\text{out}}} = 135.7°\text{C}$]

3.21 You must cool 78 kg/min of a 60%-by-mass mixture of glycerin in water from 108°C to 50°C using cooling water available at 7°C. Design a one-shell-pass, two-tube-pass heat exchanger if $U = 637 \text{ W/m}^2\text{K}$. Which side should the water flow through? Explain any design decision you make and report the area, $T_{\text{H}_2\text{O}_{\text{out}}}$, and any other relevant features.

3.22 A mixture of 40%-by-weight glycerin, 60% water, enters a smooth 0.113 m I.D. tube at 30°C. The tube is kept at 50°C, and $\dot{m}_{\text{mixture}} = 8$ kg/s. The heat transfer coefficient inside the pipe is 1600 $\text{W/m}^2\text{K}$. Plot the liquid temperature as a function of position in the pipe.

3.23 Explain in physical terms why all effectiveness curves in Fig. 3.16 and Fig. 3.17 have the same slope as NTU $\longrightarrow$ 0. Obtain this slope from eqns. (3.20) and (3.21) and give an approximate equation for Q in this limit.

3.24 You want to cool air from 150°C to 60°C but you cannot afford a custom-built heat exchanger. You find a used cross-flow exchanger (both fluids unmixed) in storage. It was previously used to cool 136 kg/min of NH_3 vapor from 200°C to 100°C using 320 kg/min of water at 7°C; U was previously 480 $\text{W/m}^2\text{K}$. How much air can you cool with this exchanger, using the same water supply, if U is approximately unchanged? (Actually, you would have to modify U using the methods of Chapters 6 and 7 once you had the new air flow rate, but that is beyond our present scope.)

3.25 A one tube-pass, one shell-pass, parallel-flow, process heat exchanger cools 5 kg/s of gaseous ammonia entering the shell side at 250°C and boils 4.8 kg/s of water in the tubes. The water enters subcooled at 27°C and boils when it reaches 100°C. $U = 480 \text{ W/m}^2\text{K}$ before boiling begins and 964 $\text{W/m}^2\text{K}$ thereafter. The area of the exchanger is 45 m^2, and h_{fg} for water is 2.257×10^6 J/kg. Determine the quality, x (recall your thermodynamics), of the water at the exit.

3.26 0.72 kg/s of superheated steam enters a cross-flow heat exchanger at 240°C and leaves at 120°C. It heats 0.6 kg/s of water entering

at 17°C. $U = 612$ W/m^{2}K. By what percentage will the area differ if a both-fluids-unmixed exchanger is used instead of a one-fluid-unmixed exchanger? [-1.8%]

3.27 Compare values of F from Fig. 3.14(c) and Fig. 3.14(d) for the same conditions of inlet and outlet temperatures. Is the one with the higher F automatically the more desirable exchanger? Discuss.

3.28 Compare values of ε for the same NTU and C_{min}/C_{max} in parallel and counterflow heat exchangers. Is the one with the higher ε automatically the more desirable exchanger? Discuss and elaborate on your various criteria for desirability.

3.29 The *irreversibility rate* of a process is equal to the rate of entropy production times the lowest absolute sink temperature accessible to the process. Calculate the irreversibility rate (i.e., the lost work or exergy destruction rate) for the heat exchanger in Example 3.4. Could a different configuration would reduce the irreversibility, given the same end temperatures? [314 kW]

3.30 Plot T_{oil} and T_{H_2O} as a function of position in a very long counterflow heat exchanger where water enters at 0°C, with $C_{H_2O} = 460$ W/K, and oil enters at 90°C, with $C_{oil} = 920$ W/K, $U = 742$ W/m^{2}K, and $A = 10$ m^2. Criticize the design.

3.31 Liquid ammonia at 2 kg/s is cooled from 100°C to 30°C in the shell side of a two shell-pass, four tube-pass heat exchanger by 3 kg/s of water at 10°C. When the exchanger is new, $U = 750$ W/m^{2}K. Plot the exit ammonia temperature as a function of the increasing tube fouling factor.

3.32 Before Freon 12 was banned as a refrigerant, a one shell-pass, two tube-pass heat exchanger cooled 0.403 kg/s of methanol from 47°C to 7°C on the shell side. The coolant was 2.2 kg/s of Freon 12, entering the tubes at -33°C, with $U = 538$ W/m^{2}K. A colleague suggested that this arrangement wastes refrigerant. She thought you could do almost as well if you cut the refrigerant flow rate all the way down to 0.8 kg/s. Calculate the new methanol outlet temperature that would result from this flow rate, and evaluate her suggestion.

3.33 The factors dictating the heat transfer coefficients in a certain two shell-pass, four tube-pass heat exchanger are such that U increases

as $(\dot{m}_{shell})^{0.6}$. The exchanger cools 2 kg/s of air from 200°C to 40°C using 4.4 kg/s of water at 7°C, and U = 312 W/m²K under these circumstances. If we double the air flow rate, what will its temperature be leaving the exchanger? [$T_{air_{out}}$ = 61°C.]

3.34 A flow rate of 1.4 kg/s of water enters the tubes of a two-shell-pass, four-tube-pass heat exchanger at 7°C. A flow rate of 0.6 kg/s of liquid ammonia at 100°C is to be cooled to 30°C on the shell side; U = 573 W/m²K. (a) How large must the heat exchanger be? (b) How large must it be if, after some months, a fouling factor of 0.0015 m²K/W is expected to build up in the tubes but we still want to deliver ammonia at 30°C? (c) If we make it large enough to accommodate fouling, to what temperature will it cool the ammonia when it is new? (d) At what temperature does water leave the new, enlarged exchanger? [(d) T_{H_2O} = 49.9°C.]

3.35 Equation (3.21) is troublesome when $C_{min}/C_{max} \longrightarrow 1$. Show that ε is given by eqn. (3.23) in this limit. Compare it with Fig. 3.16.

3.36 Both C's in a parallel-flow heat exchanger are equal to 156 W/K, U = 327 W/m²K and A = 2 m². The hot fluid enters at 140°C and leaves at 90°C. The cold fluid enters at 40°C. If both C's are halved, what will be the exit temperature of the hot fluid?

3.37 A 1.68 ft² cross-flow heat exchanger with one fluid mixed condenses steam at atmospheric pressure ($\overline{h}$ = 2000 Btu/h·ft²·°F) and boils methanol (T_{sat} = 170°F and $\overline{h}$ = 1500 Btu/h·ft²·°F) on the other side. Evaluate U (neglecting resistance of the metal), F, LMTD, and Q. Can we evaluate NTU and ε? [Q = 60,470 Btu/h]

3.38 The effectiveness of a cross-flow exchanger with neither fluid mixed is approximated by the following formula due to R. M. Drake [3.8]

$$\varepsilon \simeq 1 - \exp\left\{\left[\exp(-NTU^{0.78}R) - 1\right](NTU^{0.22}/R)\right\}$$

where $R \equiv C_{min}/C_{max}$. How closely does this correspond to exact results known for limiting cases? Present your results graphically.

3.39 Calculate the area required in a two-tube-pass, one-shell-pass condenser that is to condense 10^6 kg/h of steam at 40°C using water at 17°C. Assume that U = 4700 W/m²K, the maximum allowable temperature rise of the water is 10°C, and h_{fg} = 2406 kJ/kg. [A = 8,112 m²]

3.40   An engineer wants to divert 1 gal/min of water at 180°F from his car radiator through a small cross-flow heat exchanger with neither flow mixed, to heat 40°F water to 140°F for shaving when he goes camping. If he produces a pint per minute of hot water, what will be the area of the exchanger and the temperature of the returning radiator coolant if $U = 720$ W/m^{2}K?

3.41   To make lead shot, molten droplets of lead are showered into the top of a tall tower. The droplets fall through air and solidify before they reach the bottom of the tower, where they are collected. Cool air is introduced at the bottom of the tower and warm air flows out the top. For a particular tower, 5,000 kg/hr of 2.8 mm diam. droplets are released at their melting temperature of 600 K. The latent heat of solidification is 23.1 kJ/kg. The droplets have a density of 6,700 droplets/m^3 in the tower. Air enters the bottom at 20°C with a mass flow rate of 2,400 kg/hr. The tower has an internal diameter of 0.6 m with adiabatic walls.

  a. Sketch, qualitatively, the temperature distributions of the shot and the air along the height of the tower.

  b. If it is desired to remove the shot at a temperature of 60°C, what will be the temperature of the air leaving the top of the tower?

  c. Determine the air temperature at the point where the lead has just finished solidifying.

  d. Determine the height that the tower must have in order to function as desired. The heat transfer coefficient between the air and the droplets is $\overline{h} = 170$ W/m^{2}K.

3.42   The entropy change per unit mass of a fluid taken from temperature T_i to temperature T_o at constant pressure is $s_o - s_i = c_p \ln(T_o/T_i)$ in J/K·kg. (a) Apply the Second Law of Thermodynamics to a control volume surrounding a counterflow heat exchanger to determine the rate of entropy generation, $\dot{S}_{gen}$, in W/K. (b) Write $\dot{S}_{gen}/C_{min}$ as a function of ε, the heat capacity rate ratio, and $T_{h,i}/T_{c,i}$. (c) Show that $\dot{S}_{gen}/C_{min}$ is minimized if $C_{min} = C_{max}$ (balanced counterflow) for fixed values of ε and $T_{h,i}/T_{c,i}$.

3.43   Entropy generation in a power cycle lowers efficiency relative to the Carnot efficiency. Heat exchangers contribute to this loss. As seen in Problem 3.42, balanced counterflow heat exchangers can help to

limit entropy generation. Let's look at the entropy generation of a balanced exchanger.

a. Let $\Delta T = T_h - T_c \ll T_{c, \text{in}}$ (in kelvin). Show that the entropy generation rate in a small area $dA = Pdx$ of the exchanger (with P the perimeter) is

$$d\dot{S}''_{\text{gen}} = dQ \left(\frac{1}{T_c} - \frac{1}{T_h} \right) \simeq \frac{UP\Delta T^2}{T_c^2} dx$$

b. Show that the total entropy generation rate is

$$\dot{S}_{\text{gen}} \simeq Q \left(\frac{\Delta T}{T_{\text{h,in}} T_{\text{c,in}}} \right)$$

c. If a fixed heat load, Q, needs to be transferred, how can entropy generation be reduced? Discuss how cost and fouling considerations affect your answer.

3.44 Water at 100°C flows into a bundle of 30 copper tubes. The tubes are 28.6 mm O.D. and 3 m long with a wall thickness of 0.9 mm. Air at 20°C flows into the bundle, perpendicular to the tubes. The mass flow rate of water is 17 kg/s and that of air is 25 kg/s. (a) Determine the outlet temperature of the water if $\overline{h}_{\text{water}} = 7200$ W/m²K and $\overline{h}_{\text{air}} = 110$ W/m²K. (b) To improve the heat removal, aluminum fins are placed on the outside of the tubes (see Fig. 3.6b). The surface area of the fins and tubes together is now 81 m². Explain in words why the fins improve heat removal. If the conduction resistance of the fins is small and $\overline{h}_{\text{air}}$ is unchanged, what is the new outlet temperature of the water? *Hint:* See Problem 3.38.

References

[3.1] Tubular Exchanger Manufacturer's Association. *Standards of Tubular Exchanger Manufacturer's Association.* New York, 4th and 6th ed., 1959 and 1978.

[3.2] R. A. Bowman, A. C. Mueller, and W. M. Nagle. Mean temperature difference in design. *Trans. ASME*, **62**(4):283–294, May 1940. doi: 10.1115/1.4021450.

[3.3] R. K. Shah and D. P. Sekulić. *Fundamentals of Heat Exchanger Design.* John Wiley & Sons, Inc., Hoboken, NJ, 2003.

[3.4] W. Roetzel and F. J. L. Nicole. Mean temperature difference for heat exchanger design—a general approximate explicit equation. *J. Heat Transfer*, **97**(1):5–8, February 1975. doi: 10.1115/1.3450288.

[3.5] K. Gardner and J. Taborek. Mean temperature difference: A reappraisal. *AIChE J.*, **23**(6):770–786, November 1977. doi: 10.1002/aic.690230602.

[3.6] N. Shamsundar. A property of the log-mean temperature-difference correction factor. *Mechanical Engineering News*, **19**(3):14–15, 1982.

[3.7] W. M. Kays and A. L. London. *Compact Heat Exchangers*. McGraw-Hill Book Company, New York, 3rd ed., 1984.

[3.8] A. Triboix. Exact and approximate formulas for cross flow heat exchangers with unmixed fluids. *Int. Comm. Heat Mass Transfer*, **36**(2):121–124, February 2009. doi: 10.1016/j.icheatmasstransfer.2008.10.012.

[3.9] J. Taborek. Evolution of heat exchanger design techniques. *Heat Transfer Engineering*, **1**(1):15–29, 1979. doi: 10.1080/01457637908939546.

[3.10] E. Fried and I. E. Idelchik. *Flow Resistance: A Design Guide for Engineers*. Hemisphere Publishing Corp., New York, 1989.

[3.11] A. P. Fraas. *Heat Exchanger Design*. John Wiley & Sons, Inc., New York, 2nd ed., 1989.

[3.12] G. F. Hewitt, editor. *Heat Exchanger Design Handbook 2008*. Begell House, New York, 2008.

[3.13] F. A. Kulacki, editor. *Handbook of Thermal Science and Engineering*. Springer, Cham, Switzerland, 2018.

Part II

Analysis of Heat Conduction

4. Conduction analysis, dimensional analysis, and fin design

The effects of heat are subject to constant laws which cannot be discovered without the aid of mathematical analysis. The object of the theory which we are about to explain is to demonstrate these laws; it reduces all physical researches on the propagation of heat to problems of the calculus whose elements are given by experiment.

The Analytical Theory of Heat, J. Fourier, 1822

4.1 The well-posed problem

This chapter has three aims. First, having derived the heat conduction equation in Chapter 2 and applied it to a few one-dimensional problems, we explore what is involved in treating multidimensional and transient conduction. Second, we introduce dimensional analysis, which can greatly simplify the process of solving conduction problems. Finally, as an example of one-dimensional conduction modeling, we consider the important matter of designing cooling fins.

To begin, a heat conduction problem must be posed in such a way that it can be solved. A *well-posed* heat conduction problem is one in which all the information required to obtain a unique solution is stated. It will always read as follows. Find $T(x, y, z, t)$ such that:

1. T satisfies the heat conduction equation

$$\nabla \cdot (k \nabla T) + \dot{q} = \rho c \frac{\partial T}{\partial t}$$

for $0 < t \leqslant t_{\max}$ (where $t_{\max}$ can $\longrightarrow \infty$), and for (x, y, z) belonging to some region, R, which might extend to infinity.[1]

---

[1] (x, y, z) might be any coordinates describing a position $\vec{r}$: $T(x, y, z, t) = T(\vec{r}, t)$.

2. $T = T_i(x, y, z)$ at $t = 0$. This is called an *initial condition*, or i.c.

   (a) Condition 1 above is not imposed at $t = 0$.

   (b) Only one i.c. is required. However,

   (c) The i.c. is not needed for:

      i. the steady-state case: $\nabla \cdot (k \nabla T) + \dot{q} = 0$.

      ii. the "periodic" case, where $\dot{q}$ or the boundary conditions vary periodically with time, and where we ignore the starting transient behavior.

3. T must also satisfy two *boundary conditions*, or b.c.'s, for each coordinate. The b.c.'s are very often of three common types.

   (a) *Dirichlet conditions*, or b.c.'s of the *first kind*:

      T is specified on the boundary of R for $t > 0$. We saw such b.c.'s in Examples 2.1, 2.2, and 2.4.

   (b) *Neumann conditions*, or b.c.'s of the *second kind*:

      The derivative of T normal to the boundary is specified on the boundary of R for $t > 0$. Such a condition arises when the heat flux, $-k(\partial T / \partial x)$, is specified on a boundary or when, with the help of insulation, we set $\partial T / \partial x$ equal to zero.[2]

   (c) b.c.'s of the *third kind*:

      A derivative of T in a direction normal to a boundary is proportional to the temperature on that boundary. Such a condition most commonly arises when convection occurs at a boundary, and it is typically expressed as

      $$-k \left. \frac{\partial T}{\partial x} \right|_{\text{bndry}} = \overline{h}(T - T_\infty)_{\text{bndry}}$$

      when the body lies to the left of the boundary on the x-coordinate. We have already used such a b.c. in Step 4 of Example 2.5, and we have discussed it in Section 1.3 as well.

This list of b.c.'s is not complete, by any means, but it includes a great number of important cases.

---

[2]Although we write $\partial T / \partial x$ here, we understand that this might be $\partial T / \partial z$, $\partial T / \partial r$, or any other derivative in a direction locally normal to the surface on which the b.c. is specified.
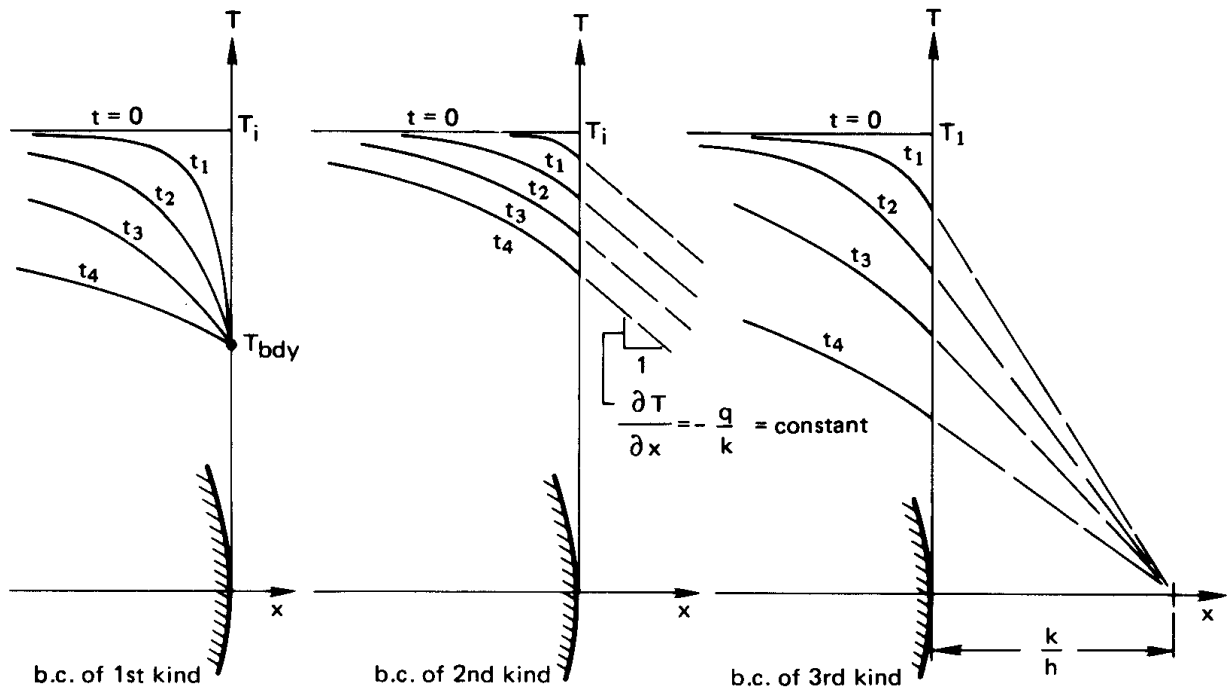
Figure 4.1 The transient cooling of a body as it might occur, subject to boundary conditions of the first, second, and third kinds.

Figure 4.1 shows the transient cooling of body from a constant initial temperature, subject to each of the three b.c.'s described above. Notice that the initial temperature distribution is not subject to the boundary condition, as pointed out previously under 2(a).

The eight-point procedure that was outlined in Section 2.2 for solving the heat conduction equation assures that a problem will meet the preceding requirements and will be well posed.

4.2   General solution of the heat conduction equation

Once the heat conduction problem has been posed properly, the first step in solving it is to find the general solution of the heat conduction equation. We have remarked that this is usually the easiest part of the problem. Let us consider some examples of general solutions.

One-dimensional steady heat conduction

Problem 4.1 emphasizes the simplicity of finding the general solutions of linear ordinary differential equations, by asking for a table of all general solutions of steady, one-dimensional heat conduction problems. We shall work out some of those results to show what is involved. We begin the heat conduction equation with constant k and $\dot{q}$:

$$\nabla^2 T + \frac{\dot{q}}{k} = \frac{1}{\alpha}\frac{\partial T}{\partial t} \tag{2.11}$$

Cartesian coordinates: Steady conduction in the y-direction.
Equation (2.11) reduces as follows:

$$\underbrace{\frac{\partial^2 T}{\partial x^2}}_{=0} + \frac{\partial^2 T}{\partial y^2} + \underbrace{\frac{\partial^2 T}{\partial z^2}}_{=0} + \frac{\dot{q}}{k} = \underbrace{\frac{1}{\alpha}\frac{\partial T}{\partial t}}_{= 0,\ \text{since steady}}$$

Therefore,

$$\frac{d^2 T}{dy^2} = -\frac{\dot{q}}{k}$$

which we integrate twice to get

$$T = -\frac{\dot{q}}{2k}y^2 + C_1 y + C_2$$

or, if $\dot{q} = 0$,

$$T = C_1 y + C_2$$

Cylindrical coordinates with a heat source: Tangential conduction.
This time, we look at the heat flow that results in a ring when two points are held at different temperatures. We now express eqn. (2.11) in cylindrical coordinates with the help of eqn. (2.13):

$$\underbrace{\frac{1}{r}\frac{\partial}{\partial r}\left(r\frac{\partial T}{\partial r}\right)}_{=0} + \underbrace{\frac{1}{r^2}\frac{\partial^2 T}{\partial \phi^2}}_{r=\text{constant}} + \underbrace{\frac{\partial^2 T}{\partial z^2}}_{=0} + \frac{\dot{q}}{k} = \underbrace{\frac{1}{\alpha}\frac{\partial T}{\partial t}}_{= 0,\ \text{since steady}}$$

Two integrations give

$$T = -\frac{r^2\dot{q}}{2k}\phi^2 + C_1\phi + C_2 \tag{4.1}$$

This would describe, for example, the temperature distribution in the thin ring shown in Fig. 4.2. Here the b.c.'s might consist of temperatures specified at two angular locations, as shown.
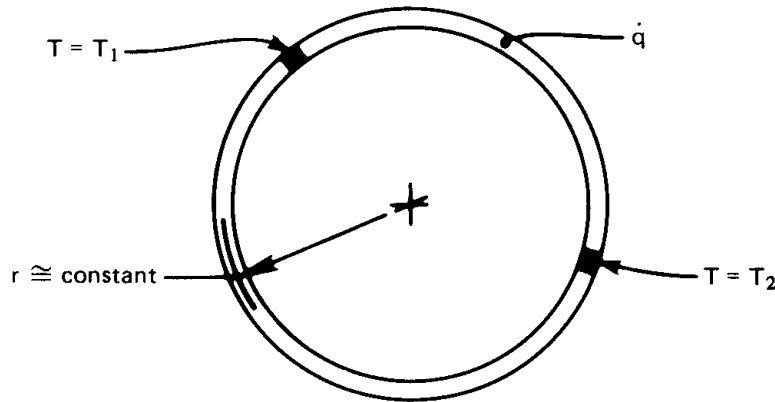
Figure 4.2 One-dimensional heat conduction in a ring.

Uniform time-varying temperature: $T = T(t$ only).
If T is spatially uniform, it can still vary with time. In such cases

$$\underbrace{\nabla^2 T}_{=0} + \frac{\dot{q}}{k} = \frac{1}{\alpha}\frac{\partial T}{\partial t}$$

and $\partial T/\partial t$ becomes an ordinary derivative. Then, since $\alpha = k/\rho c$,

$$\frac{dT}{dt} = \frac{\dot{q}}{\rho c} \tag{4.2}$$

This result is consistent with the lumped-capacity solution described in Section 1.3. If the Biot number is low and internal resistance is unimportant, the convective removal of heat from the boundary of a body can be *prorated* over the volume of the body and interpreted as

$$\dot{q}_{\text{effective}} = -\frac{\overline{h}(T_{\text{body}} - T_\infty)A}{\text{volume}} \text{ W/m}^3 \tag{4.3}$$

and the heat conduction equation for this case, eqn. (4.2), becomes

$$\frac{dT}{dt} = -\frac{\overline{h}A}{\rho c V}(T - T_\infty) \tag{4.4}$$

The general solution in this situation was given in eqn. (1.21). [A particular solution was also written in eqn. (1.22).]

Separation of variables: A general solution of multidimensional problems

Suppose that the physical situation permits us to throw out all but one of the spatial derivatives in a heat conduction equation. For example, we may wish to predict the transient cooling of a slab as a function of the location within it. If no heat is generated, the heat conduction equation is

$$\frac{\partial^2 T}{\partial x^2} = \frac{1}{\alpha}\frac{\partial T}{\partial t} \tag{4.5}$$

A common trick is to ask: "Can we find a solution in the form of a product of functions of t and x: $T = \mathcal{T}(t) \cdot X(x)$?" To find the answer, we substitute this form into eqn. (4.5) and get

$$X''\mathcal{T} = \frac{1}{\alpha}\mathcal{T}'X \tag{4.6}$$

where each prime denotes one differentiation of a function with respect to its argument. Thus $\mathcal{T}' = d\mathcal{T}/dt$ and $X'' = d^2X/dx^2$. Rearranging eqn. (4.6), we get

$$\frac{X''}{X} = \frac{1}{\alpha}\frac{\mathcal{T}'}{\mathcal{T}} \tag{4.7a}$$

This result is interesting in that the left-hand side depends only upon x and the right-hand side depends only upon t. Thus, we set *both* sides equal to the same constant, which we call $-\lambda^2$, instead of, say, λ, for reasons that will be clear in a moment:

$$\frac{X''}{X} = \frac{1}{\alpha}\frac{\mathcal{T}'}{\mathcal{T}} = -\lambda^2 \quad \text{a constant} \tag{4.7b}$$

It follows that the differential eqn. (4.7a) can be resolved into two ordinary differential equations:

$$X'' = -\lambda^2 X \quad \text{and} \quad \mathcal{T}' = -\alpha\lambda^2\mathcal{T} \tag{4.8}$$

The general solution of both of these equations are well known and are among the first ones dealt with in any study of differential equations. They are:

$$\begin{aligned} X(x) &= A\sin\lambda x + B\cos\lambda x \quad &\text{for} \quad \lambda \neq 0 \\ X(x) &= Ax + B \quad &\text{for} \quad \lambda = 0 \end{aligned} \tag{4.9}$$

and

$$
\begin{aligned}
\mathcal{T}(t) &= Ce^{-\alpha\lambda^2 t} \quad \text{for} \quad \lambda \neq 0 \\
\mathcal{T}(t) &= C \qquad\quad \text{for} \quad \lambda = 0
\end{aligned}
\tag{4.10}
$$

where we use capital letters to denote constants of integration. [In either case, these solutions can be verified by substituting them back into eqn. (4.8).] Thus the general solution of eqn. (4.5) can indeed be written in the form of a product, and that product is

$$
\begin{aligned}
T &= X\mathcal{T} = e^{-\alpha\lambda^2 t}(D\sin\lambda x + E\cos\lambda x) \quad \text{for} \quad \lambda \neq 0 \\
T &= X\mathcal{T} = Dx + E \qquad\qquad\qquad\qquad\quad \text{for} \quad \lambda = 0
\end{aligned}
\tag{4.11}
$$

The usefulness of this result depends on whether or not it can be fit to the b.c.'s and the i.c. In this case, we made the function $X(t)$ take the form of sines and cosines (instead of exponential functions) by placing a minus sign in front of λ^2. The sines and cosines make it possible to fit the b.c.'s using Fourier series methods. These general methods are not developed in this book; however, a complete Fourier series solution is presented for one problem in Section 5.3.

The preceding simple method for obtaining general solutions of linear partial d.e.'s is called *separation of variables*. The method can be applied to all kinds of linear d.e.'s. Consider, for example, two-dimensional steady heat conduction without heat sources:

$$
\frac{\partial^2 T}{\partial x^2} + \frac{\partial^2 T}{\partial y^2} = 0
\tag{4.12}
$$

Set $T = X(x) \cdot Y(y)$ and get

$$
\frac{X''}{X} = -\frac{Y''}{Y} = -\lambda^2
$$

where λ can be an imaginary number. Then

$$
\left.
\begin{aligned}
X &= A\sin\lambda x + B\cos\lambda x \\
Y &= Ce^{\lambda y} + De^{-\lambda y}
\end{aligned}
\right\} \text{for } \lambda \neq 0
$$

$$
\left.
\begin{aligned}
X &= Ax + B \\
Y &= Cy + D
\end{aligned}
\right\} \text{for } \lambda = 0
$$

The general solution is

$$
\begin{aligned}
T &= (E\sin\lambda x + F\cos\lambda x)(e^{-\lambda y} + Ge^{\lambda y}) \quad \text{for } \lambda \neq 0 \\
T &= (Ex + F)(y + G) \qquad\qquad\qquad\qquad\quad \text{for } \lambda = 0
\end{aligned}
\tag{4.13}
$$
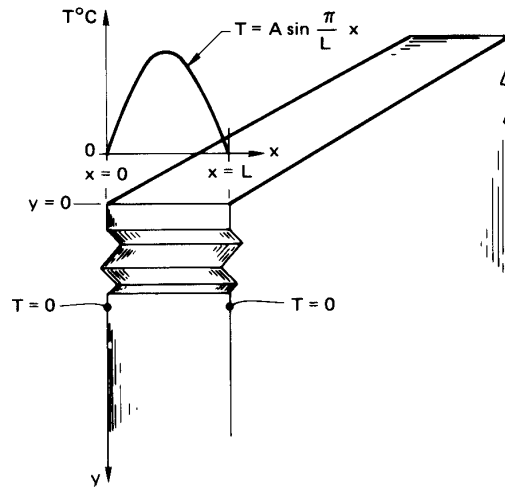
Figure 4.3 A two-dimensional slab maintained at a constant temperature on the sides and subjected to a sinusoidal variation of temperature on one face.

Example 4.1

A long slab is cooled to 0°C on both sides and a blowtorch is turned on the top edge, giving an approximately sinusoidal temperature distribution along the top, as shown in Fig. 4.3. Find the temperature distribution within the slab.

SOLUTION. The general solution is given by eqn. (4.13). We must therefore identify the appropriate b.c.'s and then fit the general solution to it. Those b.c.'s are:

$$\text{on the top surface}: \quad T(x,0) = A \sin \pi \frac{x}{L}$$

$$\text{on the sides}: \quad T(0 \text{ or } L, y) = 0$$

$$\text{as } y \longrightarrow \infty: \quad T(x, y \to \infty) = 0$$

Substitute eqn. (4.13) in the third b.c.:

$$(E \sin \lambda x + F \cos \lambda x)(0 + G \cdot \infty) = 0$$

The only way that this can be true for all x is if $G = 0$. Substitute eqn. (4.13), with $G = 0$, into the second b.c.:

$$(0 + F)e^{-\lambda y} = 0$$

so F also equals 0. Substitute eqn. (4.13) with $G = F = 0$, into the first b.c.:

$$E(\sin \lambda x) = A \sin \pi \frac{x}{L}$$

It follows that $A = E$ and $\lambda = \pi/L$. Then eqn. (4.13) becomes the particular solution that satisfies the b.c.'s:

$$T = A \left(\sin \pi \frac{x}{L} \right) e^{-\pi y/L}$$

Thus, the sinusoidal variation of temperature at the top of the slab is attenuated exponentially at lower positions in the slab. At a position of $y = 2L$ below the top, T will be $0.0019(A \sin \pi x/L)$. The temperature distribution in the x-direction will still be sinusoidal, but it will have less than $1/500$ of the amplitude at $y = 0$. ∎

Consider some important features of this and other solutions:

- The b.c. at $y = 0$ is a special one that works very well with this particular general solution. If we had tried to fit the equation to a general temperature distribution, $T(x, y = 0) = \text{fn}(x)$, it would not have been obvious how to proceed. Actually, this is the kind of problem that Fourier solved with the invention of his series method. We discuss this matter in more detail in Chapter 5.

- Not all forms of general solutions lend themselves to a particular set of boundary and/or initial conditions. In this example, we made the process look simple, but more often than not, *it is in fitting a general solution to a set of boundary conditions that we face difficulties.*

- Normally, on formulating a problem, we must *approximate* real behavior in stating the b.c.'s. It is advisable to consider what kind of assumption will put the b.c.'s in a form compatible with the general solution. The temperature distribution imposed on the slab by the blowtorch in Example 4.1 might just as well have been approximated as a parabola. But as small as the difference between a parabola and a sine function might be, the latter b.c. was far easier to accommodate.

- The twin issues of existence and uniqueness of solutions require a comment here: Mathematicians have established that solutions to all well-posed heat conduction problems are unique. Furthermore, we know from our experience that if we describe a physical process correctly, a unique outcome exists. Therefore, we are normally safe to ignore these issues in the sort of problems we discuss here.

- Given that a unique solution exists, we accept any solution as correct if we can carve it to fit the boundary conditions. In this sense, the solution of differential equations is often more of an inventive than a formal operation. The person who does it best is often the person who has done it before and so has a large assortment of tricks up his or her sleeve.

4.3 Dimensional analysis

Introduction

Most universities place the first course in heat transfer after an introduction to fluid mechanics, and most fluid mechanics courses include some dimensional analysis. This topic is normally treated using the *method of indices*, which is seemingly straightforward to teach but is cumbersome and sometimes misleading to use. That approach is presented well in [4.1].

The method we develop here is far simpler to use than the method of indices, and it does much to protect us from the common errors we might fall into. We refer to it as the *method of functional replacement* and strongly recommend this method in place of the method of indices.

The importance of dimensional analysis to heat transfer can be made clearer by recalling Example 2.5, which (like most problems in Part I) involved several variables. These variables included the dependent variable of temperature, $(T_\infty - T_i)$[3]; the independent variable, which was the radius, r; and five system parameters, $r_i, r_o, \overline{h}, k$, and $(T_\infty - T_i)$. By reorganizing the solution into dimensionless groups [eqn. (2.24)], we reduced the total number of variables to only four:

$$\underbrace{\frac{T - T_i}{T_\infty - T_i}}_{\text{dependent variable}} = \text{fn}\left[\underbrace{r/r_i,}_{\text{indep. var.}} \underbrace{r_o/r_i, \text{ Bi}}_{\text{two system parameters}} \right] \qquad (2.24\text{a})$$

This dimensionless solution offered a number of advantages over the dimensional solution. For one thing, we could plot *all* conceivable solutions for a particular shape of cylinder, (r_o/r_i), in a single figure, Fig. 2.11. For another, we could study the simultaneous roles of $\overline{h}$, k and r_o in defining the character of the solution. By combining them as a Biot number, we were able to say—even before we had solved the problem—whether or not external convection really had to be considered.

---

[3]Notice that we do not call T_i a variable. It is simply the reference temperature against which this problem calculates temperature changes. The absolute temperature level is not significant in this problem.

The nondimensionalization enabled us to consider, simultaneously, the behavior of all *similar* systems of heat conduction through cylinders. Thus a large, highly conducting cylinder might be *similar* in its behavior to a small cylinder with a lower thermal conductivity.

Finally, we shall discover that, by nondimensionalizing a problem *before* we solve it, we can often greatly simplify the process of solving it.

Our next aim is to map out a method for nondimensionalization problems before we have solved them, or, indeed, before we have even written the equations that must be solved. The key to the method is the *Buckingham pi-theorem*.

The Buckingham pi-theorem

The attention of scientific workers was drawn very strongly toward the question of similarity at about the beginning of World War I. Buckingham first organized previous thinking and developed his famous theorem in 1914 in the *Physical Review* [4.2], and he expanded upon the idea in the *Transactions of the ASME* one year later [4.3]. Lord Rayleigh almost simultaneously discussed the problem with great clarity in 1915 [4.4]. To understand Buckingham's theorem, we must first overcome one conceptual hurdle, which, if it is clear to the student, will make everything that follows extremely simple. Let us explain that hurdle first.

Suppose that y depends on r, x, z and so on:

$$y = \text{fn}(r, x, z, \dots)$$

We can take any one variable—say, x—and arbitrarily multiply it (or it raised to a power) by any other variables in the equation, without altering the truth of the functional equation. The equation above can thus just as well be written as:

$$\frac{y}{x} = \text{fn}\left(x^2 r, x, xz\right)$$

or an unlimited number of other rearrangements. Many people find such a rearrangement disturbing when they first see it. That is because these are not *algebraic* equations — they are *functional* equations. We have said only that if y depends upon r, x, and z that it will likewise depend upon $x^2 r$, x, and xz. Suppose, for example, that we gave the functional equation the following algebraic form:

$$y = \text{fn}(r, x, z) = r(\sin x)e^{-z}$$

This need only be rearranged to put it in terms of the desired modified variables and x itself ($y/x, x^2 r, x$, and xz):

$$\frac{y}{x} = \frac{x^2 r}{x^3}(\sin x)\exp\left[-\frac{xz}{x}\right]$$

We can do any such multiplying or dividing of powers of any variable we wish without invalidating any functional equation that we choose to write. This simple fact is at the heart of the important example that follows.

Example 4.2

Consider the heat exchanger problem described in Fig. 3.15. The "unknown", or dependent, variable in the problem is one or the other of the exit temperatures. Without any knowledge of heat exchanger analysis, we can write the functional equation on the basis of our physical understanding of the problem:

$$\underbrace{T_{c_{\text{out}}} - T_{c_{\text{in}}}}_{\text{K}} = \text{fn}\left[\underbrace{C_{\max}}_{\text{W/K}}, \underbrace{C_{\min}}_{\text{W/K}}, \underbrace{(T_{h_{\text{in}}} - T_{c_{\text{in}}})}_{\text{K}}, \underbrace{U}_{\text{W/m}^2\text{K}}, \underbrace{A}_{\text{m}^2} \right] \tag{4.14}$$

where the dimensions of each term are noted under the equation.

We want to know how many dimensionless groups the variables in eqn. (4.14) should reduce to. To determine this number, we use the idea explained above—that is, that we can arbitrarily pick one variable from the equation and divide or multiply it into other variables. Then— one at a time—we select a variable that has one of the dimensions. We divide or multiply it by the other variables in the equation that have that dimension in such a way as to eliminate the dimension from them.

We do this first with the variable $(T_{h_{\text{in}}} - T_{c_{\text{in}}})$, which has the dimension of K:

$$\underbrace{\frac{T_{c_{\text{out}}} - T_{c_{\text{in}}}}{T_{h_{\text{in}}} - T_{c_{\text{in}}}}}_{\text{dimensionless}} = \text{fn}\left[\underbrace{C_{\max}(T_{h_{\text{in}}} - T_{c_{\text{in}}})}_{\text{W}}, \underbrace{C_{\min}(T_{h_{\text{in}}} - T_{c_{\text{in}}})}_{\text{W}}, \right.$$

$$\left. \underbrace{(T_{h_{\text{in}}} - T_{c_{\text{in}}})}_{\text{K}}, \underbrace{U(T_{h_{\text{in}}} - T_{c_{\text{in}}})}_{\text{W/m}^2}, \underbrace{A}_{\text{m}^2} \right]$$

The interesting thing about the equation in this form is that the only remaining term in it with the units of K is $(T_{h_{\text{in}}} - T_{c_{\text{in}}})$. No such term *can* remain in the equation because it is impossible to achieve dimensional homogeneity without another term in K to balance it. Therefore,

we must remove it:

$$\underbrace{\frac{T_{c_{\text{out}}} - T_{c_{\text{in}}}}{T_{h_{\text{in}}} - T_{c_{\text{in}}}}}_{\text{dimensionless}} = \text{fn}\left[\underbrace{C_{\text{max}}(T_{h_{\text{in}}} - T_{c_{\text{in}}})}_{\text{W}}, \underbrace{C_{\text{min}}(T_{h_{\text{in}}} - T_{c_{\text{in}}})}_{\text{W}}, \right.$$
$$\left. \underbrace{U(T_{h_{\text{in}}} - T_{c_{\text{in}}})}_{\text{W/m}^2}, \underbrace{A}_{\text{m}^2} \right]$$

Now the equation has only two dimensions in it—W and m^2. Next, we multiply $U(T_{h_{\text{in}}} - T_{c_{\text{in}}})$ by A to get rid of m^2 in the second-to-last term. Accordingly, the term A (m^2) can no longer stay in the equation, and we have

$$\underbrace{\frac{T_{c_{\text{out}}} - T_{c_{\text{in}}}}{T_{h_{\text{in}}} - T_{c_{\text{in}}}}}_{\text{dimensionless}} = \text{fn}\left[\underbrace{C_{\text{max}}(T_{h_{\text{in}}} - T_{c_{\text{in}}})}_{\text{W}}, \underbrace{C_{\text{min}}(T_{h_{\text{in}}} - T_{c_{\text{in}}})}_{\text{W}}, \underbrace{UA(T_{h_{\text{in}}} - T_{c_{\text{in}}})}_{\text{W}} \right]$$

Finally, we divide the first and third terms on the right by the second. This leaves only $C_{\text{min}}(T_{h_{\text{in}}} - T_{c_{\text{in}}})$, with the dimensions of W. That term must then be removed, and we are left with the completely dimensionless result:

$$\frac{T_{c_{\text{out}}} - T_{c_{\text{in}}}}{T_{h_{\text{in}}} - T_{c_{\text{in}}}} = \text{fn}\left(\frac{C_{\text{max}}}{C_{\text{min}}}, \frac{UA}{C_{\text{min}}} \right) \qquad (4.15)$$

$\blacksquare$

Equation (4.15) has exactly the same functional form as eqn. (3.21), which we obtained by direct analysis.

Notice that we removed one variable from eqn. (4.14) for each dimension in which the variables are expressed. If there are n variables—including the dependent variable—expressed in m dimensions, we then expect to be able to express the equation in $(n - m)$ dimensionless groups, or *pi-groups*, as Buckingham called them.

This fact is expressed by the *Buckingham pi-theorem*, which we state formally in the following way:

A physical relationship among n variables, which can be expressed in *a minimum* of m dimensions, can be rearranged into a relationship among $(n - m)$ *independent* dimensionless groups of the original variables.

Two important qualifications have been italicized. They will be explained in detail in subsequent examples.

Buckingham identified the dimensionless pi-groups as $\Pi_1, \Pi_2, ..., \Pi_{n-m}$. Normally we call Π_1 the dependent variable and consider $\Pi_{2\rightarrow(n-m)}$ as the independent variables. Thus, the dimension*al* functional equation reduces to a dimension*less* functional equation of the form

$$\Pi_1 = \text{fn}(\Pi_2, \Pi_3, \ldots, \Pi_{n-m}) \tag{4.16}$$

Applications of the pi-theorem

Example 4.3

Is eqn. (2.24) consistent with the pi-theorem?

Solution. To find out, we first write the dimensional functional equation for Example 2.5:

$$\underbrace{T - T_i}_{K} = \text{fn}\left[\underbrace{r}_{m}, \underbrace{r_i}_{m}, \underbrace{r_o}_{m}, \underbrace{\overline{h}}_{W/m^2K}, \underbrace{k}_{W/m\cdot K}, \underbrace{(T_\infty - T_i)}_{K} \right]$$

There are seven variables ($n = 7$) in three dimensions, K, m, and W ($m = 3$). Therefore, we look for $7 - 3 = 4$ pi-groups. There *are* four pi-groups in eqn. (2.24):

$$\Pi_1 = \frac{T - T_i}{T_\infty - T_i}, \quad \Pi_2 = \frac{r}{r_i}, \quad \Pi_3 = \frac{r_o}{r_i}, \quad \Pi_4 = \frac{\overline{h} r_o}{k} \equiv \text{Bi.} \qquad \blacksquare$$

Consider two features of this result. First, the minimum number of dimensions was three. If we had written watts as J/s, we would have had four dimensions instead. But Joules never appear in that particular problem independently of seconds. They always appear as a ratio and should not be separated. (If we had worked in English units, the confusion would have been greater, since Btu/sec has no name unless we first convert it to horsepower.) The failure to identify dimensions that are consistently grouped together is one of the major errors that the beginner makes in using the pi-theorem.

The second feature is the *independence* of the groups. This means that we may pick any four dimensionless arrangements of variables, so long as no group or groups can be made into any other group by mathematical manipulation. For example, suppose that someone suggested that there

was a fifth pi-group in Example 4.3:

$$\Pi_5 = \sqrt{\frac{\overline{h}r}{k}}$$

It is easy to see that Π_5 can be written as

$$\Pi_5 = \sqrt{\frac{\overline{h}r_o}{k}}\sqrt{\frac{r}{r_i}}\sqrt{\frac{r_i}{r_o}} = \sqrt{\text{Bi}\,\frac{\Pi_2}{\Pi_3}}$$

Therefore Π_5 is not independent of the existing groups, nor will we ever find a fifth grouping that is.

Another matter that is frequently emphasized is that of identifying the pi-groups once the variables are identified for a given problem. In particular, the method of indices is a cumbersome arithmetic strategy for finding these groups. We shall instead find the groups by using either of two much simpler methods:

1. The groups can always be obtained formally by repeating the simple elimination-of-dimensions procedure that was used to derive the pi-theorem in Example 4.2.

2. One may often simply arrange the variables into the required number of independent dimensionless groups by inspection.

In any method, one must make judgments as one combines variables. These decisions can lead to different arrangements of the pi-groups. Therefore, if the problem can be solved by inspection, there is no advantage to be gained by the use of a more formal procedure.

The methods of dimensional analysis can be used to help find the solution of many physical problems. We offer the following example, not entirely with tongue in cheek:

Example 4.4

Einstein might well have noted that the energy equivalent, e, of a rest mass, m_o, depended on the velocity of light, c_o, before he developed the special relativity theory. He would then have had the following dimensional functional equation:

$$\left(e\ \text{N·m}\quad \text{or}\quad e\ \frac{\text{kg·m}^2}{\text{s}^2}\right) = \text{fn}(c_o\ \text{m/s},\ m_o\ \text{kg})$$

The minimum number of dimensions is only two: kg and m/s, so we look for $3 - 2 = 1$ pi-group. To find it formally, we eliminate the dimension of mass from e by dividing it by m_o (kg). Thus,

$$\frac{e}{m_o}\frac{\text{m}^2}{\text{s}^2} = \text{fn}\Big[\ c_o\ \text{m/s},\ \underbrace{m_o\ \text{kg}}\ \Big]$$

this must be removed because it is the only term with mass in it

Then we eliminate the dimension of velocity (m/s) by dividing e/m_o by c_o^2:

$$\frac{e}{m_o c_o^2} = \text{fn}(c_o\ \text{m/s})$$

This time c_o must be removed from the function on the right, since it is the only term with the dimensions m/s. This gives the result (which could have been written by inspection once it was known that there could only be one pi-group):

$$\Pi_1 = \frac{e}{m_o c_o^2} = \text{fn(no other groups)} = \text{constant}$$

or

$$e = \text{constant} \cdot \left(m_o c_o^2\right)$$

Of course, it required Einstein's special relativity theory to tell us that the constant is one. ∎

Example 4.5

What is the velocity of efflux of liquid from the tank shown in Fig. 4.4?

SOLUTION. In this case we can guess that the velocity, V, might depend on gravity, g, and the head, H. We might be tempted to include the density as well until we realize that g is already a *force per unit mass*. Then

$$\underbrace{V}_{\text{m/s}} = \text{fn}\Big[\ \underbrace{H}_{\text{m}}\ ,\ \underbrace{g}_{\text{m/s}^2}\ \Big]$$

so there are three variables in two dimensions, and we look for $3 - 2 = 1$ pi-group. It would have to be

$$\Pi_1 = \frac{V}{\sqrt{gH}} = \text{fn(no other pi-groups)} = \text{constant}$$
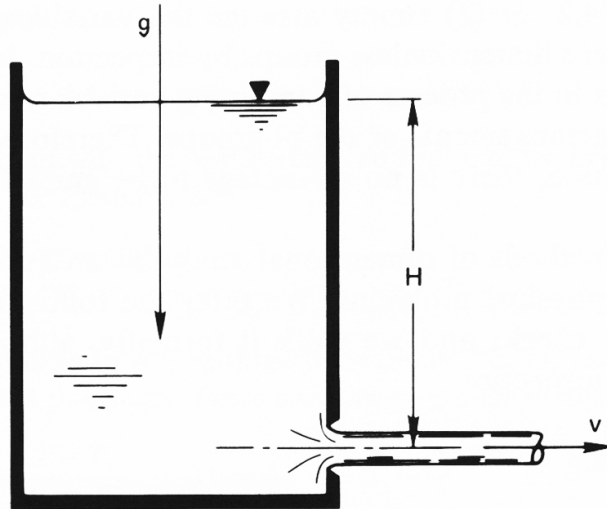
Figure 4.4   Efflux of liquid from a tank.

or

$$V = \text{constant} \cdot \sqrt{gH}$$

The analytical study of fluid mechanics tells us that this form is correct and that the constant is $\sqrt{2}$. The group V^2/gh, by the way, is called a *Froude number*, Fr (pronounced "Frood"). It compares inertial forces to gravitational forces. For all such jets Fr = 2, showing the strong role of gravity, whereas for a pitched baseball (which falls very little during its flight), Fr is about 1000. If Fr were based on the jet diameter, rather than H, it would correlate the shape of the jet—how quickly it bends over and flows downward.   ■

Example 4.6

Obtain the dimensionless functional equation for the temperature distribution during steady conduction in a slab with a heat source, $\dot{q}$.

SOLUTION. In such a case, there might be one or two specified temperatures in the problem: T_1 or T_2. Thus the dimensional functional equation is

$$\underbrace{T - T_1}_{\text{K}} = \text{fn}\left[\underbrace{(T_2 - T_1)}_{\text{K}}, \underbrace{x, L}_{\text{m}}, \underbrace{\dot{q}}_{\text{W/m}^3}, \underbrace{k}_{\text{W/m·K}}, \underbrace{\overline{h}}_{\text{W/m}^2\text{K}} \right]$$

where we presume that a convective b.c. is involved and we identify a characteristic length, L, in the x-direction. There are seven variables in three dimensions, or $7 - 3 = 4$ pi-groups. Three of these groups are ones we have dealt with in the past in one form or another:

$$\Pi_1 = \frac{T - T_1}{T_2 - T_1} \qquad \text{dimensionless temperature, to which we shall give the name } \Theta$$

$$\Pi_2 = \frac{x}{L} \qquad \text{dimensionless length, which we call } \xi$$

$$\Pi_3 = \frac{\overline{h}L}{k} \qquad \text{which we recognize as the Biot number, Bi}$$

The fourth group is new to us:

$$\Pi_4 = \frac{\dot{q}L^2}{k(T_2 - T_1)} \qquad \text{which compares the heat generation rate to the rate of heat loss; we call it } \Gamma$$

Thus, the solution is

$$\Theta = \text{fn}(\xi, \text{Bi}, \Gamma) \tag{4.17}$$

∎

In Example 2.1, we solved such a problem, but it differed in two respects. There was no convective boundary condition, and hence no $\overline{h}$, and only one temperature was specified. In that case, the dimensional functional equation was

$$(T - T_1) = \text{fn}(x, L, \dot{q}, k)$$

so there were only five variables in the same three dimensions. The resulting dimensionless functional equation therefore involved only two pi-groups. One was $\xi = x/L$ and the other is a new one equal to Θ/Γ. We call it Φ:

$$\Phi \equiv \frac{T - T_1}{\dot{q}L^2/k} = \text{fn}\left(\frac{x}{L}\right) \tag{4.18}$$

And this is exactly the form of the analytical result, eqn. (2.15).

Finally, we must deal with dimensions that convert into one another. For example, kg and N are defined in terms of one another through Newton's Second Law of Motion. Therefore, they cannot be identified as separate dimensions. The same would appear to be true of J and N·m, since both are dimensions of energy. However, we must discern whether or not a mechanism exists for interchanging them. If thermal energy

remains distinct from mechanical energy (or work) in a given problem, then J should not be interpreted as N·m.

This issue will prove important when we do the dimensional analysis of several heat transfer problems. See, for example, the analyses of laminar convection at the beginning of Section 6.4, of natural convection in Section 8.3, of film condensation in Section 8.5, and of pool boiling burnout in Section 9.3. In all of these cases, heat transfer normally occurs without any conversion of heat to work or work to heat and it would be misleading to break J into N·m.

Additional examples of dimensional analysis appear throughout this book. Dimensional analysis is, indeed, our court of first resort in solving most of the new problems that we undertake.

4.4   Illustrative use of dimensional analysis in a complex steady conduction problem

Heat conduction problems with convective b.c.s can rapidly grow difficult, even if they start out simple. So we look for ways to avoid making mistakes. For one thing, it is wise to take great care that dimensions are consistent at each stage of the solution. The best way to do this, and to eliminate a great deal of algebra at the same time, is to nondimensionalize the heat conduction problem before we apply the b.c.'s. This nondimensionalization should be consistent with the pi-theorem. The following example, although complex, illustrates several aspects of this idea.

Example 4.7

The slab shown in Fig. 4.5 has different temperatures and different heat transfer coefficients on either side, and heat is generated within it. Calculate the temperature distribution in the slab.

SOLUTION. The differential equation is

$$\frac{d^2 T}{dx^2} = -\frac{\dot{q}}{k}$$

and the general solution is

$$T = -\frac{\dot{q}x^2}{2k} + C_1 x + C_2 \tag{4.19}$$
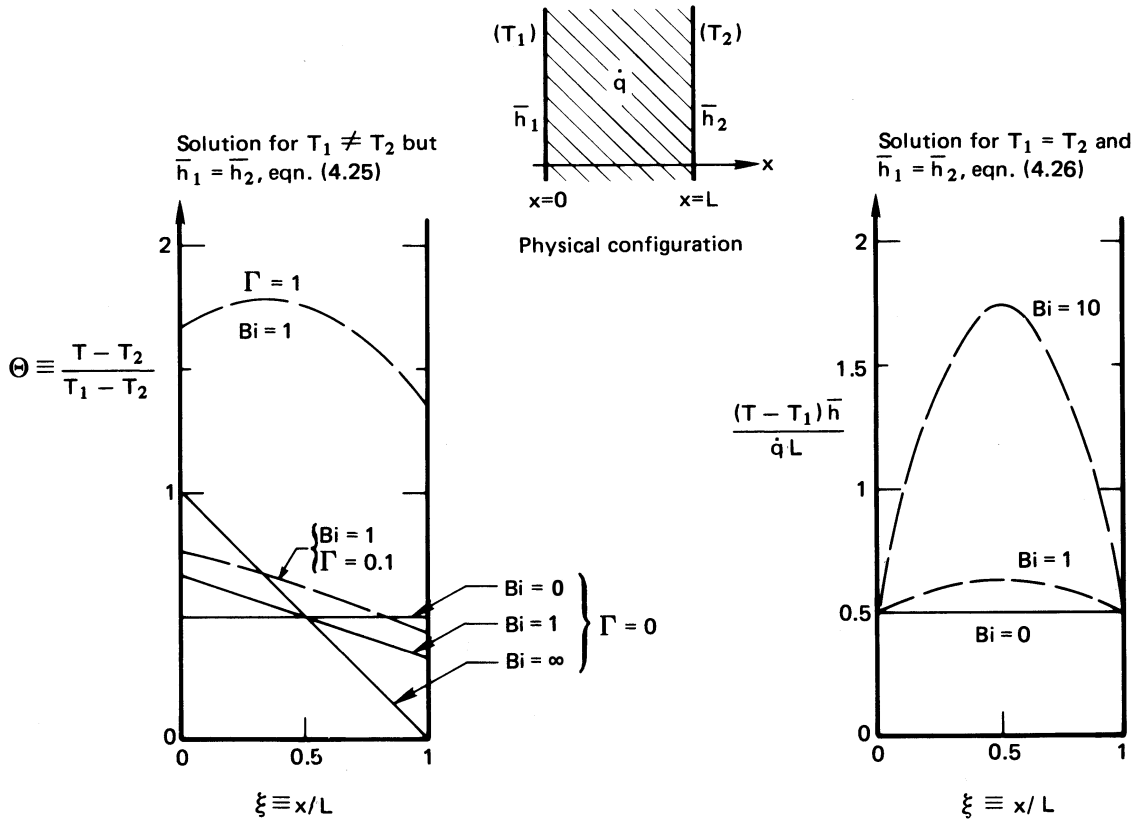
Figure 4.5 Heat conduction through a heat-generating slab with asymmetric boundary conditions.

with b.c.'s

$$\overline{h}_1(T_1 - T)_{x=0} = -k\left.\frac{dT}{dx}\right|_{x=0}, \qquad \overline{h}_2(T - T_2)_{x=L} = -k\left.\frac{dT}{dx}\right|_{x=L} \tag{4.20}$$

There are eight variables involved in the problem: $(T - T_2)$, $(T_1 - T_2)$, x, L, k, $\overline{h}_1$, $\overline{h}_2$, and $\dot{q}$; and there are three dimensions: K, W, and m. This results in $8 - 3 = 5$ pi-groups. For these we choose

$$\Pi_1 \equiv \Theta = \frac{T - T_2}{T_1 - T_2}, \qquad \Pi_2 \equiv \xi = \frac{x}{L}, \qquad \Pi_3 \equiv \text{Bi}_1 = \frac{\overline{h}_1 L}{k},$$

$$\Pi_4 \equiv \text{Bi}_2 = \frac{\overline{h}_2 L}{k}, \quad \text{and} \quad \Pi_5 \equiv \Gamma = \frac{\dot{q}L^2}{2k(T_1 - T_2)}$$

where Γ can be interpreted as a comparison of the heat generated in the slab to that which could flow through it.

Under this nondimensionalization, eqn. (4.19) becomes[4]

$$\Theta = -\Gamma\,\xi^2 + C_3\xi + C_4 \tag{4.21}$$

and b.c.'s become

$$\mathrm{Bi}_1(1 - \Theta_{\xi=0}) = -\Theta'_{\xi=0}, \qquad \mathrm{Bi}_2\Theta_{\xi=1} = -\Theta'_{\xi=1} \tag{4.22}$$

where the primes denote differentiation with respect to ξ. Substituting eqn. (4.21) in eqn. (4.22), we obtain

$$\mathrm{Bi}_1(1 - C_4) = -C_3, \qquad \mathrm{Bi}_2(-\Gamma + C_3 + C_4) = 2\Gamma - C_3 \tag{4.23}$$

Substituting the first of eqns. (4.23) in the second we get

$$C_4 = 1 + \frac{\Gamma\,[2(\mathrm{Bi}_1/\mathrm{Bi}_2) + \mathrm{Bi}_1] - \mathrm{Bi}_1}{\mathrm{Bi}_1(1 + \mathrm{Bi}_1/\mathrm{Bi}_2 + \mathrm{Bi}_1)}$$

and

$$C_3 = \mathrm{Bi}_1(C_4 - 1)$$

Thus, eqn. (4.21) becomes

$$\Theta = 1 + \Gamma\left[\frac{2(\mathrm{Bi}_1/\mathrm{Bi}_2) + \mathrm{Bi}_1}{\mathrm{Bi}_1(1 + \mathrm{Bi}_1/\mathrm{Bi}_2 + \mathrm{Bi}_1)} + \frac{2(\mathrm{Bi}_1/\mathrm{Bi}_2) + \mathrm{Bi}_1}{1 + \mathrm{Bi}_1/\mathrm{Bi}_2 + \mathrm{Bi}_1}\xi - \xi^2\right]$$
$$- \frac{\mathrm{Bi}_1}{1 + \mathrm{Bi}_1/\mathrm{Bi}_2 + \mathrm{Bi}_1}\xi - \frac{1}{1 + \mathrm{Bi}_1/\mathrm{Bi}_2 + \mathrm{Bi}_1} \quad\tag{4.24}$$
∎

This complicated result would have required enormous patience and accuracy to obtain without first simplifying the problem statement by nondimensionalization. If the heat transfer coefficients were the same on either side of the wall, then $\mathrm{Bi}_1 = \mathrm{Bi}_2 \equiv \mathrm{Bi}$, and eqn. (4.24) would reduce to

$$\Theta = 1 + \Gamma\left(1/\mathrm{Bi} + \xi - \xi^2\right) - \frac{1 + \mathrm{Bi}\,\xi}{2 + \mathrm{Bi}} \tag{4.25}$$

which is a very great simplification.

Equation (4.25) is plotted on the left-hand side of Fig. 4.5 for Bi equal to 0, 1, and ∞ and for Γ equal to 0, 0.1, and 1. The following features should be noted:

---

[4]The rearrangement of the dimensional equations into dimensionless form is straightforward algebra. If the results shown here are not immediately obvious, sketch the calculation on a piece of paper.

- When $\Gamma \ll 0.1$, the heat generation can be ignored.

- When $\Gamma \gg 1, \Theta \longrightarrow \Gamma/\text{Bi} + \Gamma(\xi - \xi^2)$. This is a simple parabolic temperature distribution displaced upward an amount that depends on the relative external resistance, as reflected in the Biot number.

- If both Γ and $1/\text{Bi}$ become large, $\Theta \to \Gamma/\text{Bi}$. This means that when internal resistance is low and the heat generation is great, the slab temperature is constant and quite high.

If T_2 were equal to T_1 in this problem, Γ would go to infinity. In such a situation, we should redo the dimensional analysis of the problem. The dimensional functional equation now shows $(T - T_1)$ to be a function of $x, L, k, \overline{h}$, and $\dot{q}$. There are six variables in three dimensions, so there are only three pi-groups

$$\frac{T - T_1}{\dot{q}L/\overline{h}} = \text{fn}(\xi, \text{Bi})$$

where the dependent variable is the product of Bi times Φ [recall eqn. (4.18)]. We can put eqn. (4.25) in this form by multiplying both sides of the equation by $\overline{h}(T_1 - T_2)/\dot{q}L$ and then letting $T_1 \longrightarrow T_2$. The result is

$$\frac{\overline{h}(T - T_1)}{\dot{q}L} = \frac{1}{2}\text{Bi}\left(\xi - \xi^2\right) + \frac{1}{2} \qquad (4.26)$$

which is plotted on the right-hand side of Fig. 4.5. The following features of the graph are of interest:

- Heat generation is the only "force" giving rise to temperature nonuniformity. Since it is symmetric, the graph is also symmetric.

- When $\text{Bi} \ll 1$, the slab temperature approaches a uniform value equal to $T_1 + \dot{q}L/2h$. (In this case, we would have solved the problem with far greater ease by using a simple lumped-capacity model, since the temperature gradients in the slab are negligible.)

- When $\text{Bi} > 10$, the temperature distribution is a very large parabola with ½ added to it. In this case, the problem could have been solved using boundary conditions of the first kind because the surface temperature stays very close to T_∞ (recall Fig. 1.11). In fact, since the lefthand side of eqn. (4.26) is just $\Phi \cdot \text{Bi}$, we could divide through by Bi, let $\text{Bi} \longrightarrow \infty$, and recover eqn. (2.15).

4.5 Fin design

The purpose of fins

We can substantially improve convective heat transfer to or from a surface by attaching extensions that increase the surface area. These extensions can take many forms. Figure 4.6, for example, shows just some of the ways in which the surface of commercial heat exchanger tubing can be extended with protrusions of a kind we call *fins*.

Figure 4.7 shows another intriguing appearance of fins for heat removal. This picture is taken from an issue of *Science* magazine in which Farlow et al. [4.5] present evidence suggesting that the strange rows of fins on the back of the *Stegosaurus* were used to shed excess body heat after strenuous activity.

These examples involve some rather complicated fins. But the analysis of a straight fin protruding from a wall displays the essential features of all fin behavior. This analysis has direct application to a host of problems.

Analysis of a one-dimensional fin

The equations.   Figure 4.8 shows a one-dimensional fin protruding from a wall. The wall—and the base, or *root*, of the fin—are at a temperature T_0, which is either greater or less than the ambient temperature, T_∞. The surface of the fin exchanges heat with the ambient fluid through a heat transfer coefficient, $\overline{h}$. The heat transfer coefficient will be assumed uniform, although (as we see in Part III) that approximation will not be strictly accurate even in forced convection and can introduce serious error in boiling, condensing, or some natural convection situations.

The tip of the fin may or may not exchange heat with the surroundings through a heat transfer coefficient, $\overline{h}_L$, which would generally differ from $\overline{h}$. The length of the fin is L, its uniform cross-sectional area is A, and its circumferential perimeter is P.

The characteristic dimension of the fin in the transverse direction (normal to the x-axis) may be taken to be A/P. Thus, for a circular cylindrical fin of radius R, $A/P = \pi R^2/(2\pi R) = R/2$. We define a Biot number for conduction in the transverse direction, based on this dimension, and require that it be small (so that radial or transverse conduction resistance is negligible):

$$\text{Bi}_{\text{fin}} = \frac{\overline{h}(A/P)}{k} \ll 1 \qquad (4.27)$$

This condition means that the transverse variation of T at any axial
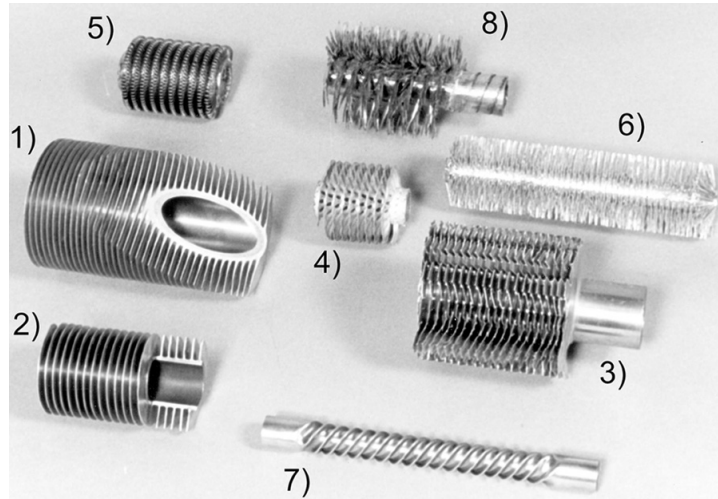
a. Eight examples of externally finned tubing: 1) and 2) typical commercial circular fins of constant thickness; 3) and 4) serrated circular fins and dimpled spirally-wound circular fins, both intended to increase $\overline{h}$; 5) spirally-wound copper coils outside and inside; 6) and 8) bristle fins, spirally wound and machined from base metal; 7) a spirally indented tube to improve convection and increase surface area.

b. An array of commercial internally finned tubing (photo courtesy of Noranda Metal Industries, Inc.)

Figure 4.6 Some of the many varieties of finned tubes.
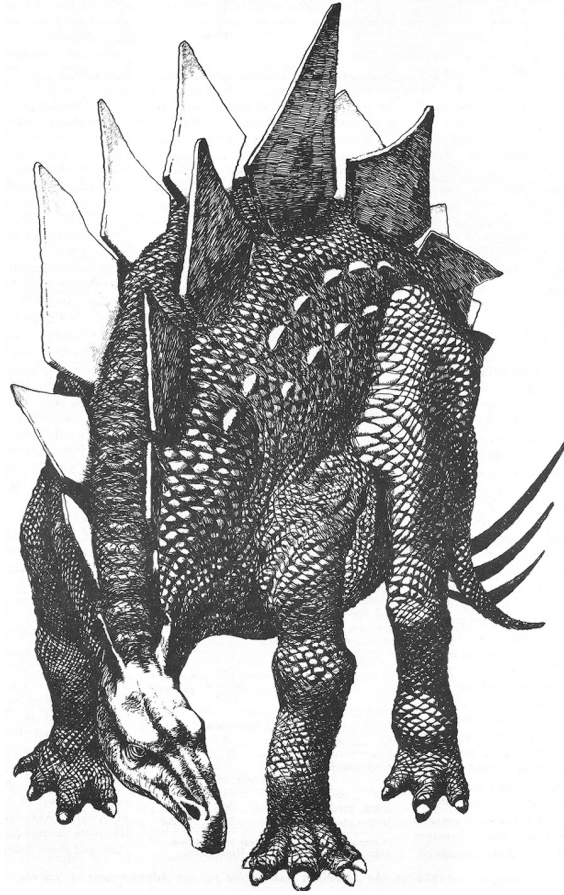
Figure 4.7   The Stegosaurus with what might have been cooling fins (etching by Daniel Rosner).

position, x, is much less than $(T_{\text{surface}} - T_\infty)$. Thus, $T \simeq T(x$ only) and the heat flow can be treated as one-dimensional. If this condition is not satisfied, the protrusion is not a fin as the term is used in heat transfer.

An energy balance on the thin slice of the fin shown in Fig. 4.8 gives

$$-kA \left.\frac{dT}{dx}\right|_{x+\delta x} + kA \left.\frac{dT}{dx}\right|_x + \overline{h}(P\delta x)(T - T_\infty)_x = 0 \qquad (4.28)$$

but, as $\delta x \longrightarrow 0$,

$$\frac{dT/dx|_{x+\delta x} - dT/dx|_x}{\delta x} \longrightarrow \frac{d^2 T}{dx^2} = \frac{d^2(T - T_\infty)}{dx^2} \qquad (4.29)$$

so

$$\frac{d^2(T - T_\infty)}{dx^2} = \frac{\overline{h}P}{kA}(T - T_\infty) \qquad (4.30)$$
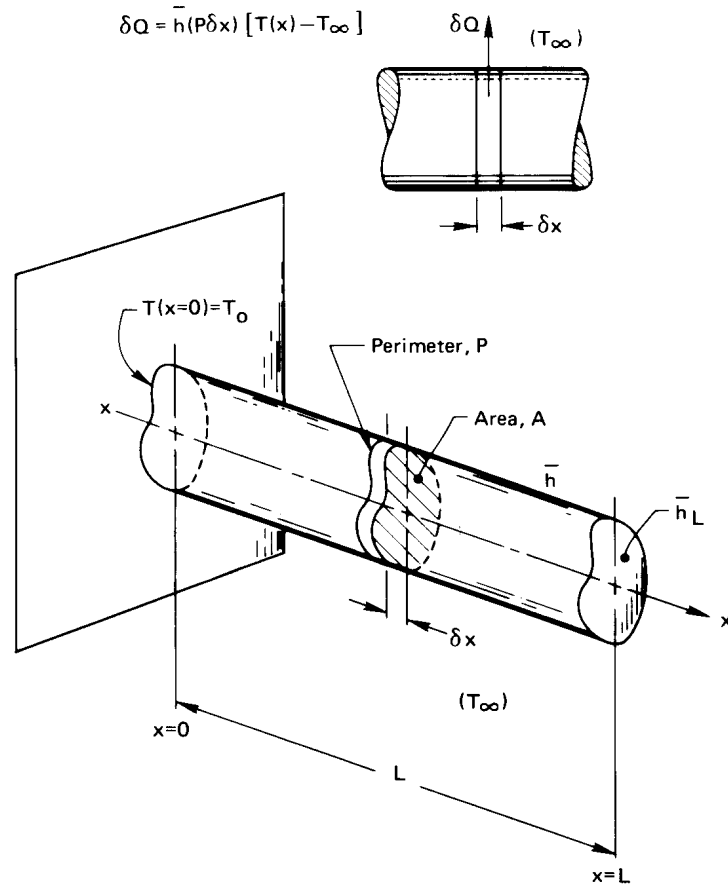
Figure 4.8 The analysis of a one-dimensional fin.

The b.c.'s for this equation are

$$(T - T_\infty)_{x=0} = T_0 - T_\infty$$

$$-kA \left.\frac{d(T - T_\infty)}{dx}\right|_{x=L} = \overline{h}_L A (T - T_\infty)_{x=L}$$

(4.31a)

Alternatively, if the tip is insulated, or if we can guess that $\overline{h}_L A$ is small enough to be unimportant, the b.c.'s are

$$(T - T_\infty)_{x=0} = T_0 - T_\infty \quad \text{and} \quad \left.\frac{d(T - T_\infty)}{dx}\right|_{x=L} = 0 \qquad (4.31b)$$

Before we solve this problem, it will pay to do a dimensional analysis. The

dimensional functional equation is

$$T - T_\infty = \text{fn}\left[(T_0 - T_\infty), x, L, kA, \overline{h}P, \overline{h}_L A\right] \qquad (4.32)$$

Notice that we have written kA, $\overline{h}P$, and $\overline{h}_L A$ as single variables. The reason for doing so is subtle but important. Setting $h(A/P)/k \ll 1$, erases any geometric detail of the cross section from the problem. The *only* place where P and A enter the problem is as product with k, $\overline{h}$, or $\overline{h}_L$. If they showed up elsewhere, they would have to do so in a physically incorrect way. Thus, we have just seven variables in W, K, and m. This gives four pi-groups if the tip is uninsulated:

$$\frac{T - T_\infty}{T_0 - T_\infty} = \text{fn}\left[\frac{x}{L}, \sqrt{\frac{\overline{h}P}{kA}L^2}, \underbrace{\frac{\overline{h}_L AL}{kA}}_{=\overline{h}_L L/k}\right]$$

or if we rename the groups,

$$\Theta = \text{fn}(\xi, mL, \text{Bi}_{\text{axial}}) \qquad (4.33\text{a})$$

where we set $m \equiv \sqrt{\overline{h}P/kA}$ because that terminology is common in the literature on fins, $\xi = x/L$, and $\text{Bi}_{\text{axial}} = \overline{h}_L L/k$.

If heat transfer from the tip of the fin is negligible, as if the tip were insulated or adiabatic, $\overline{h}_L$ will not appear in eqn. (4.32). One less variable is present but the same number of dimensions: hence, there will be only three pi-groups. The group that is removed is Bi_{axial}, which involves $\overline{h}_L$. Thus, for a fin with an adiabatic tip,

$$\Theta = \text{fn}(\xi, mL) \qquad (4.33\text{b})$$

We put eqn. (4.30) in these terms by multiplying it by $L^2/(T_0 - T_\infty)$. The result is

$$\boxed{\frac{d^2\Theta}{d\xi^2} = (mL)^2\Theta} \qquad (4.34)$$

This equation is satisfied by $\Theta = Ce^{\pm(mL)\xi}$. The sum of these two solutions forms the general solution of eqn. (4.34):

$$\boxed{\Theta = C_1 e^{mL\xi} + C_2 e^{-mL\xi}} \qquad (4.35)$$

Temperature distribution in a one-dimensional fin with the tip insulated.
When heat transfer at the tip is zero or negligible, the b.c.'s [eqn. (4.31b)]
can be written as

$$\Theta_{\xi=0} = 1 \quad \text{and} \quad \frac{d\Theta}{d\xi}\bigg|_{\xi=1} = 0 \tag{4.36}$$

Substituting eqn. (4.35) into both eqns. (4.36), we get

$$C_1 + C_2 = 1 \quad \text{and} \quad C_1 e^{mL} - C_2 e^{-mL} = 0 \tag{4.37}$$

Mathematical digression: Hyperbolic functions

To put the solution of eqn. (4.37) for C_1 and C_2 in the simplest form, we
need to recall a few properties of hyperbolic functions. The four basic
functions that we need are defined as

$$
\begin{aligned}
\sinh x &\equiv \frac{e^x - e^{-x}}{2} \\
\cosh x &\equiv \frac{e^x + e^{-x}}{2} \\
\tanh x &\equiv \frac{\sinh x}{\cosh x} = \frac{e^x - e^{-x}}{e^x + e^{-x}} \\
\coth x &\equiv \frac{\cosh x}{\sinh x} = \frac{e^x + e^{-x}}{e^x - e^{-x}}
\end{aligned}
\tag{4.38}
$$

where x is the independent variable. Additional functions are defined
by analogy to the trigonometric counterparts. The differential relations
can be written out formally, and they also resemble their trigonometric
counterparts.

$$
\begin{aligned}
\frac{d}{dx}\sinh x &= \frac{1}{2}\left[e^x - (-e^{-x})\right] = \cosh x \\
\frac{d}{dx}\cosh x &= \frac{1}{2}\left[e^x + (-e^{-x})\right] = \sinh x
\end{aligned}
\tag{4.39}
$$

These are analogous to the familiar results $d\sin x/dx = \cos x$ and
$d\cos x/dx = -\sin x$, but without the latter's minus sign.

The solution of eqns. (4.37) is then

$$C_1 = \frac{e^{-mL}}{2\cosh mL} \quad \text{and} \quad C_2 = 1 - \frac{e^{-mL}}{2\cosh mL} \tag{4.40}$$

Therefore, eqn. (4.35) becomes

$$\Theta = \frac{e^{-mL(1-\xi)} + (2\cosh mL)e^{-mL\xi} - e^{-mL(1+\xi)}}{2\cosh mL}$$

which simplifies to

$$\boxed{\Theta = \frac{\cosh mL(1-\xi)}{\cosh mL}} \tag{4.41}$$

for a one-dimensional fin with its tip insulated.

One of the most important design variables for a fin is the rate at which it removes (or delivers) heat the wall. To calculate this, we write Fourier's law for the heat flow into the base of the fin[5]:

$$Q_0 = -kA \left.\frac{d(T - T_\infty)}{dx}\right|_{x=0} \tag{4.42}$$

We multiply eqn. (4.42) by $L/kA(T_0 - T_\infty)$ and obtain, after substituting eqn. (4.41) on the right-hand side,

$$\frac{Q_0 L}{kA(T_0 - T_\infty)} = mL\frac{\sinh mL}{\cosh mL} = mL\tanh mL \tag{4.43}$$

which can be written

$$\boxed{\frac{Q_0}{\sqrt{kA\overline{h}P}\,(T_0 - T_\infty)} = \tanh mL} \tag{4.44}$$

Figure 4.9 includes two graphs showing the behavior of one-dimensional fin with no tip heat transfer. The top graph shows that the heat transfer increases with mL, hitting a maximum around $mL \simeq 3$. This means that the fin should not have a length in excess of $2/m$ or $3/m$ if it is being used to cool (or heat) a wall. Additional length would simply increase the cost without improving performance.

---

[5]We could also integrate $\overline{h}P(T - T_\infty)$ over the outside area of the fin to get Q_0. The answer would be the same, but the calculation would be a little more complicated.
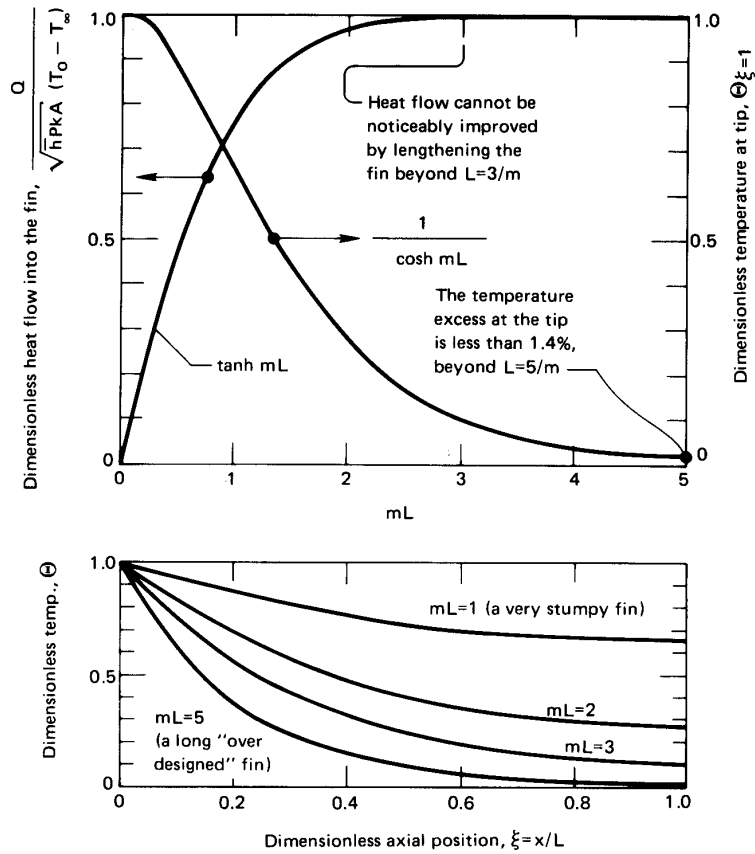
Figure 4.9 The temperature distribution, tip temperature, and heat flux in a straight one-dimensional fin with an adiabatic tip.

Also shown in the top graph is the temperature of the tip of the fin. Setting $\xi = 1$ in eqn. (4.41), we discover that

$$\Theta_{tip} = \frac{1}{\cosh mL} \tag{4.45}$$

This dimensionless tip temperature drops to about 0.014 when mL reaches 5. This means that the end is $0.014(T_0 - T_\infty)$ K above T_∞ at the end. Thus, if the fin is actually functioning as a holder for a thermometer or a thermocouple that is intended to read T_∞, the reading will be in error if mL is not significantly greater than five.

The lower graph in Fig. 4.9 shows how the temperature is distributed in insulated-tip fins for various values of mL.

Experiment 4.1

Clamp a 20 cm or so length of copper rod by one end in a horizontal position. Put a candle flame very near the other end and let the arrangement come to a steady state. Run your finger along the rod. How does what you feel correspond to Fig. 4.9? (The diameter of the copper rod should not exceed about 3 mm, although a larger rod of lower conductivity metal will also work.)   ♦

Exact temperature distribution in a fin with an uninsulated tip. The approximation of an adiabatic tip may be avoided using the b.c's given in eqn. (4.31a), which take the following dimensionless form:

$$\Theta_{\xi=0} = 1 \quad \text{and} \quad -\frac{d\Theta}{d\xi}\bigg|_{\xi=1} = \text{Bi}_{\text{ax}}\Theta_{\xi=1} \tag{4.46}$$

Substitution of the general solution, eqn. (4.35), in these b.c.'s yields

$$C_1 + C_2 = 1$$
$$-mL\left(C_1 e^{mL} - C_2 e^{-mL}\right) = \text{Bi}_{\text{ax}}\left(C_1 e^{mL} + C_2 e^{-mL}\right) \tag{4.47}$$

Some manipulation is required to solve eqn. (4.47) for C_1 and C_2 and to substitute the results in eqn. (4.35). We leave this as an exercise (Problem 4.11). The result is

$$\Theta = \frac{\cosh mL(1-\xi) + (\text{Bi}_{\text{ax}}/mL)\sinh mL(1-\xi)}{\cosh mL + (\text{Bi}_{\text{ax}}/mL)\sinh mL} \tag{4.48}$$

which has the form of eqn. (4.33a), as we anticipated. The corresponding heat flux equation is

$$\frac{Q_0}{\sqrt{kA\overline{h}P}\,(T_0 - T_\infty)} = \frac{(\text{Bi}_{\text{ax}}/mL) + \tanh mL}{1 + (\text{Bi}_{\text{ax}}/mL)\tanh mL} \tag{4.49}$$

We have seen that mL is not too much greater than one in a well-designed fin with an insulated tip. Furthermore, when $\overline{h}_L$ is small (as it might be in natural convection), Bi_{ax} is normally much less than one. Therefore, in such cases, we expect to be justified in neglecting terms multiplied by Bi_{ax}. Then eqn. (4.48) reduces to our previous equation, (4.41), for a fin with an adiabatic tip:

$$\Theta = \frac{\cosh mL(1-\xi)}{\cosh mL} \tag{4.41}$$

It is worth pointing out that we are in serious difficulty if $\overline{h}_L$ is so large that we cannot assume the tip to be insulated. The reason is that $\overline{h}_L$ is nearly impossible to predict in most practical cases.

Example 4.8

A 2.0 cm diameter aluminum rod with $k = 205$ W/m·K, 8.0 cm in length, protrudes from a 150°C wall. Air at 26°C flows by it, and $\overline{h} = 120$ W/m²K. Determine whether or not tip conduction is important in this problem. To do this, make the very crude assumption that $\overline{h} \simeq \overline{h}_L$. Then compare the tip temperatures as calculated with and without considering heat transfer from the tip.

SOLUTION.

$$mL = \sqrt{\frac{\overline{h}PL^2}{kA}} = \sqrt{\frac{120(0.08)^2}{205(0.01/2)}} = 0.8656$$

$$\text{Bi}_{\text{ax}} = \frac{\overline{h}L}{k} = \frac{120(0.08)}{205} = 0.0468$$

Therefore, eqn. (4.48) becomes

$$\Theta\,(\xi = 1) = \Theta_{\text{tip}} = \frac{\cosh 0 + (0.0468/0.8656)\sinh 0}{\cosh(0.8656) + (0.0468/0.8656)\sinh(0.8656)}$$

$$= \frac{1}{1.3986 + 0.0529} = 0.6886$$

so the exact tip temperature is

$$T_{\text{tip}} = T_\infty + 0.6886(T_0 - T_\infty)$$
$$= 26 + 0.6886(150 - 26) = 111.4°\text{C}$$

Equation (4.41) or Fig. 4.9, on the other hand, gives

$$\Theta_{\text{tip}} = \frac{1}{1.3986} = 0.7150$$

so the approximate tip temperature is

$$T_{\text{tip}} = 26 + 0.715(150 - 26) = 114.7°\text{C}$$

Thus the insulated-tip approximation is more than adequate in this case: the four percent difference in Θ_{tip} is within likely accuracy of the given information. ∎

Very long fin.   If a fin is so long that $mL \gg 1$, then eqn. (4.41) simplifies

$$\Theta = \frac{e^{mL(1-\xi)} + e^{-mL(1-\xi)}}{e^{mL} + e^{-mL}} \simeq e^{-mL} \left[e^{mL(1-\xi)} + e^{-mL(1-\xi)} \right] \simeq e^{-mL\xi}$$

or

$$\lim_{mL \to \text{large}} \Theta = e^{-mL\xi} = e^{-mx} \tag{4.50}$$

Substituting this result in eqn. (4.42), we obtain [cf. eqn. (4.44)]

$$Q_0 = \sqrt{kA\overline{h}P}\,(T_0 - T_\infty) \tag{4.51}$$

A heating or cooling fin would have to be terribly overdesigned for these results to apply—that is, mL would have been made much larger than necessary. Long extensions from surfaces often have importance beyond increasing heat removal. A thermometer well protruding into a pipe, for example, should very nearly reach the surrounding fluid temperature to be useful. In practice, a fin may be regarded as "infinitely long" in computing its temperature if $mL \gtrsim 5$; in computing Q_0, $mL \gtrsim 3$ is sufficient for the infinite fin approximation.

Physical significance of mL.   The group mL has thus far proved to be extremely useful in the analysis and design of fins. We should therefore say a brief word about its physical significance. Notice that

$$(mL)^2 = \frac{L/kA}{1/\overline{h}(PL)} = \frac{\text{internal resistance in } x\text{-direction}}{\text{gross external resistance}}$$

Thus $(mL)^2$ is a hybrid Biot number. When it is big, $\Theta|_{\xi=1} \to 0$ and we can neglect tip convection. When it is small, the temperature drop along the axis of the fin becomes small (see the lower graph in Fig. 4.9).

The group $(mL)^2$ also has a peculiar similarity to the NTU (Chapter 3) and the dimensionless time, t/T, that appears in the lumped-capacity solution (Chapter 1). Thus,

$$\frac{\overline{h}(PL)}{kA/L} \quad \text{is like} \quad \frac{UA}{C_{\min}} \quad \text{is like} \quad \frac{\overline{h}A}{\rho cV/t}$$

In each case a convective heat rate is compared with a heat rate that characterizes the system; and in each case the system temperature asymptotically approaches its limit as the numerator becomes large. This was true in eqn. (1.22), eqn. (3.21), eqn. (3.22), and eqn. (4.50).

Fin performance and design

Two measures of fin performance are particularly useful in fin design or selection. The first is called the *fin efficiency*, η_f,

$$\eta_f \equiv \frac{\text{actual heat transferred by a fin}}{\text{heat transfer if the entire fin were at } T = T_0} \tag{4.52}$$

To see how this works, we evaluate η_f for a one-dimensional fin with an insulated tip:

$$\eta_f = \frac{\sqrt{kA\overline{h}P}\,(T_0 - T_\infty)\tanh mL}{\overline{h}(PL)(T_0 - T_\infty)} = \frac{\tanh mL}{mL} \tag{4.53}$$

This says that, under the definition of efficiency, a very long fin will give $\tanh(mL)/mL \longrightarrow 1/\text{large number}$, so the fin will have low efficiency. On the other hand, the efficiency goes up to 100% as the length is reduced to zero, because $\tanh(mL)/mL \longrightarrow 1$ as $mL \longrightarrow 0$. While a fin of zero length would accomplish little, a fin of small m might be designed in order to keep the tip temperature near the root temperature; this, for example, is desirable if the fin is the tip of a soldering iron.

We note that while η_f provides some useful information to how a fin behaves, we have no basis for designing toward any particular value of η_f.

A second measure of fin performance is called the *fin effectiveness*, ε_f:

$$\varepsilon_f \equiv \frac{\text{heat flux from the wall with the fin}}{\text{heat flux from the wall without the fin}} \tag{4.54}$$

The value can easily be computed from the efficiency:

$$\varepsilon_f = \eta_f \frac{\text{surface area of the fin}}{\text{cross-sectional area of the fin}} \tag{4.55}$$

Normally, we want the effectiveness to be as high as possible. The effectiveness can always be raised by extending the length of the fin, but that—as we have seen—rapidly becomes a losing proposition.

The metrics η_f and ε_f probably attract the interest of designers not because their absolute values guide the designs, but because they are useful in characterizing fins with more complex shapes. In such cases the analytical solutions are often so complex that plots of η_f and ε_f serve as labor-saving graphical solutions. We deal with some of these curves later in this section.

The design of a fin is an open-ended matter of optimization, subject to many factors. Some of the factors that must be considered include:

- The weight of material added by the fin. This might be a cost factor or it might be an important consideration in its own right.

- The possible dependence of $\overline{h}$ on $(T - T_\infty)$, flow velocity past the fin, or other influences.

- The influence of the fin (or fins) on the heat transfer coefficient, $\overline{h}$, as the fluid moves around it (or them).

- The geometric configuration of the channel that the fin lies in.

- The cost and complexity of manufacturing fins.

- The pressure drop the fins create in the surrounding fluid flow.

Fin thermal resistance

When fins occur in combination with other thermal elements, calculations can be significantly simplified by treating them as a thermal resistance between the root and the surrounding fluid. Specifically, for a straight fin with an insulated tip, we can rearrange eqn. (4.44) as

$$Q = \frac{(T_0 - T_\infty)}{\left(\sqrt{kA\overline{h}P}\ \tanh mL\right)^{-1}} \equiv \frac{(T_0 - T_\infty)}{R_{t_\text{fin}}} \tag{4.56}$$

where

$$R_{t_\text{fin}} = \frac{1}{\sqrt{kA\overline{h}P}\ \tanh mL} \qquad \text{for a straight fin} \tag{4.57}$$

In general, for a fin of any shape, fin thermal resistance can be written in terms of fin efficiency and fin effectiveness. From eqns. (4.52) and (4.54), we obtain

$$R_{t_\text{fin}} = \frac{1}{\eta_\text{f} A_\text{surface} \overline{h}} = \frac{1}{\varepsilon_\text{f} A_\text{root} \overline{h}} \tag{4.58}$$

Example 4.9

Consider again the resistor described in Examples 2.7 and 2.8, starting on page 72. Suppose that the two electrical leads are long straight wires 0.62 mm in diameter with $k = 16$ W/m·K and $h_\text{eff} = 23$ W/m²K. Recalculate the resistor's temperature taking account of heat conducted into the leads.

SOLUTION. The wires act as very long fins connected to the resistor, so that $\tanh mL \cong 1$ (see Problem 4.44). Each has a fin resistance of

$$R_{t_{\mathrm{fin}}} = \frac{1}{\sqrt{kA\overline{h}P}} = \frac{1}{\sqrt{(16)(23)(\pi)^2(0.00062)^3/4}} = 2,150 \text{ K/W}$$

These two thermal resistances are in parallel to the thermal resistances for natural convection and thermal radiation from the resistor surface found in Example 2.7. The equivalent thermal resistance is now

$$
\begin{aligned}
R_{t_{\mathrm{equiv}}} &= \left(\frac{1}{R_{t_{\mathrm{fin}}}} + \frac{1}{R_{t_{\mathrm{fin}}}} + \frac{1}{R_{t_{\mathrm{rad}}}} + \frac{1}{R_{t_{\mathrm{conv}}}} \right)^{-1} \\
&= \left[\frac{2}{2,150} + (1.33 \times 10^{-4})(7.17) + (1.33 \times 10^{-4})(13) \right]^{-1} \\
&= 276.8 \text{ K/W}
\end{aligned}
$$

The leads reduce the equivalent resistance by about 30% from the value found before. The resistor temperature becomes

$$T_{\mathrm{resistor}} = T_{\mathrm{air}} + Q \cdot R_{t_{\mathrm{equiv}}} = 35 + (0.1)(276.8) = 62.68 \ {}^\circ\text{C}$$

or about 10°C lower than the value found without considering the electrical leads. ∎

Fin Arrays

Fins are often arrayed in banks that are machined, cast, or extruded from single pieces of metal, with a thick base that holds the fin array. The base is fixed to the device to be cooled—a power transistor, a microprocessor, a computer video card—anything that generates a lot of heat that must be removed. Figure 4.10 shows several typical arrays.

Manufacturers will sometimes simply specify a single thermal resistance for a fin array (or *heat sink*) as a function of the air velocity in the vicinity of the array. Or one might estimate the resistance of the array using the techniques introduced here, taking into account the airflow conditions between the fins and the heat loss from the exposed base between the fins. The detailed treatment of fin arrays becomes highly specialized. We recommend [4.6].
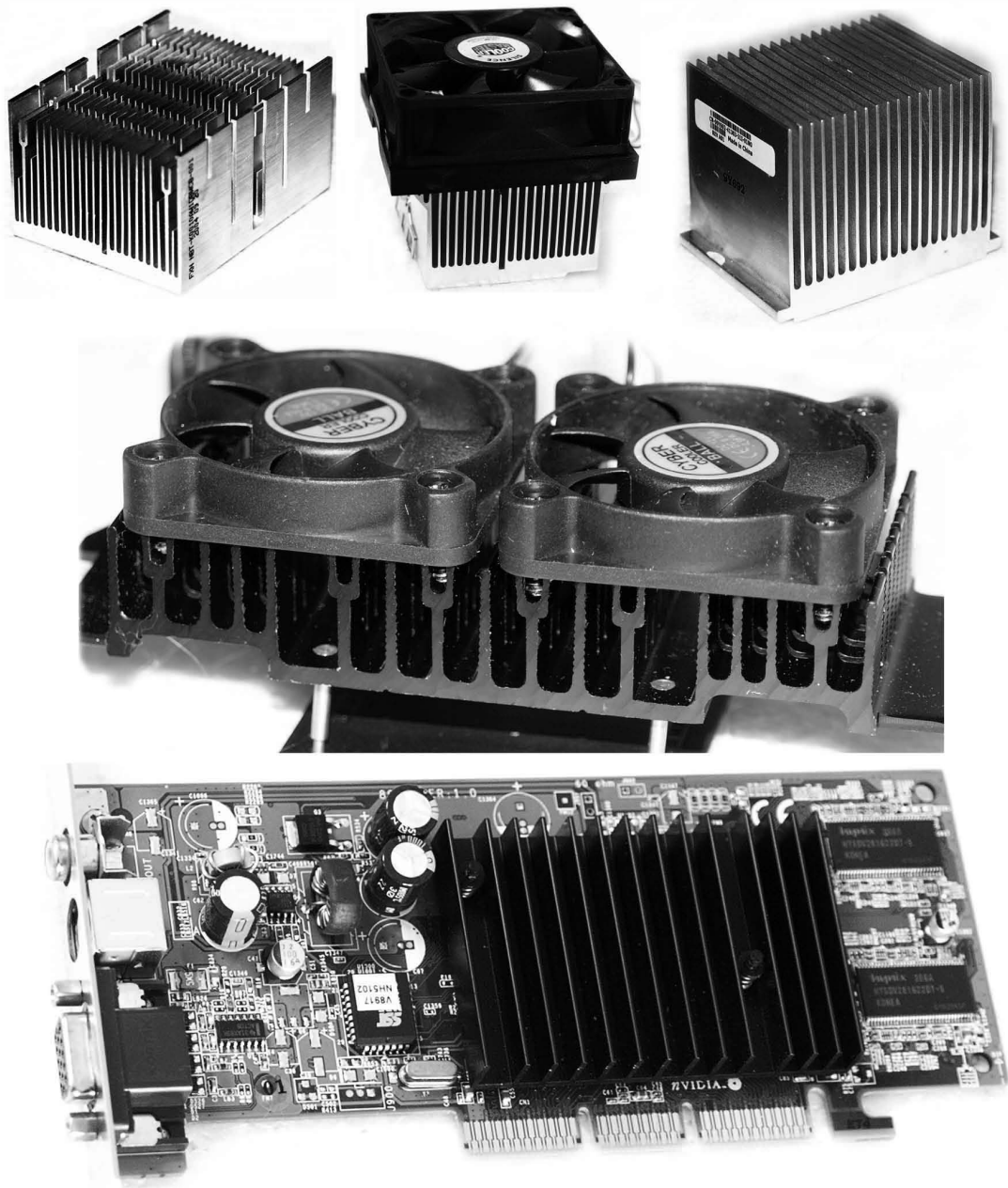
Figure 4.10 Several fin arrays of the kind used to cool computer elements. The top-center and middle arrays are fan-cooled. The other four are cooled by natural convection. Courtesy of Gene Quach, PC&C Computers, Houston, TX.
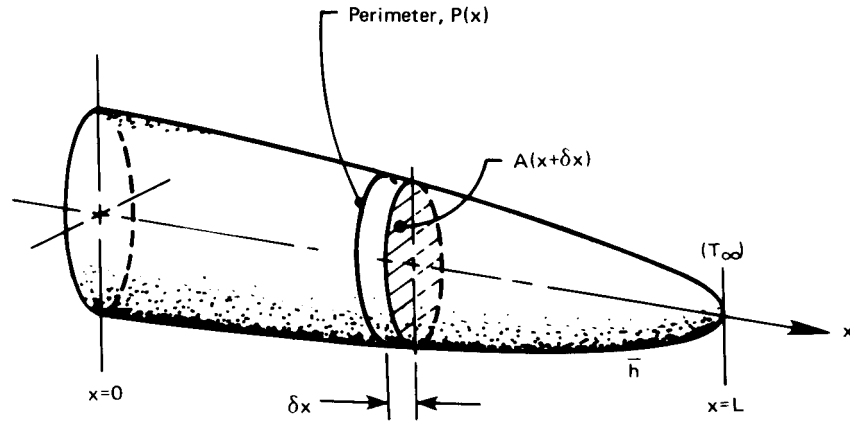
Figure 4.11 A general fin of variable cross section.

Fins of variable cross section

Let us consider what is involved is the design of a fin for which A and P are functions of x. Such a fin is shown in Fig. 4.11. We restrict our attention to fins for which

$$\frac{\overline{h}(A/P)}{k} \ll 1 \quad \text{and} \quad \frac{d(A/P)}{dx} \ll 1$$

so the heat flow will be approximately one-dimensional in x.

We begin by applying the First Law to a thin slice of thickness δx

$$Q_{\text{net}} = Q_{\text{cond}} - Q_{\text{conv}} = \frac{dU}{dt}$$

so that[6]

$$\underbrace{\left[kA(x + \delta x)\left.\frac{dT}{dx}\right|_{x+\delta x} - kA(x)\left.\frac{dT}{dx}\right|_{x} \right]}_{\simeq \frac{d}{dx}\left(kA(x)\frac{dT}{dx} \right)\delta x} - \overline{h}P\,\delta x\,(T - T_\infty)$$

$$= \underbrace{\rho c A(x)\delta x \frac{dT}{dt}}_{=0,\text{ since steady}}$$

---

[6]Note that we approximate the external area of the fin as horizontal when we write it as $P\,\delta x$. The actual area is larger by an amount that is negligible in most cases. An exception would be the tip of the fin in Fig. 4.11 where the cross-section changes rapidly.
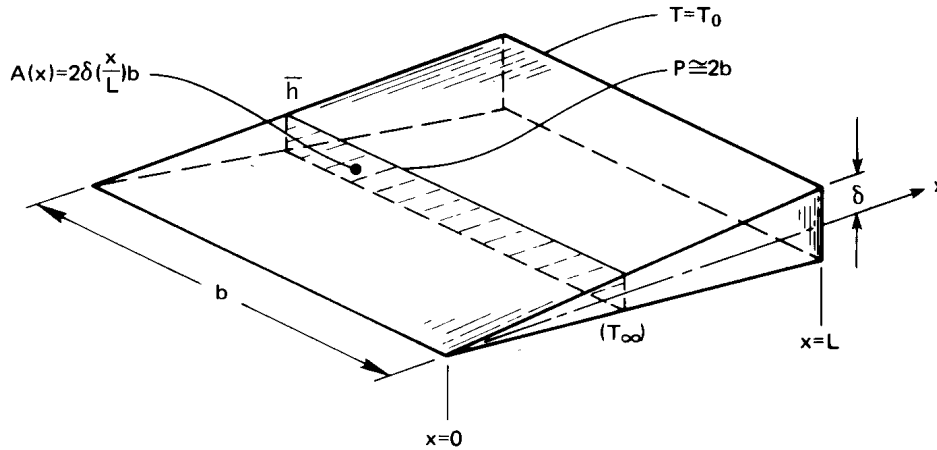
Figure 4.12 A two-dimensional wedge-shaped fin.

Therefore,

$$\frac{d}{dx}\left[A(x)\frac{d(T-T_\infty)}{dx}\right] - \frac{\overline{h}P}{k}(T-T_\infty) = 0 \tag{4.59}$$

If $A(x)$ = constant, this reduces to $\Theta'' - (mL)^2\Theta = 0$, which is the straight fin equation.

To see how eqn. (4.59) works, consider the triangular fin shown in Fig. 4.12. In this case eqn. (4.59) becomes

$$\frac{d}{dx}\left[2\delta\left(\frac{x}{L}\right)b\frac{d(T-T_\infty)}{dx}\right] - \frac{2\overline{h}b}{k}(T-T_\infty) = 0$$

or

$$\xi\frac{d^2\Theta}{d\xi^2} + \frac{d\Theta}{d\xi} - \underbrace{\frac{\overline{h}L^2}{k\delta}}_{\substack{\text{a kind} \\ \text{of } (mL)^2}}\Theta = 0 \tag{4.60}$$

This second-order linear differential equation is difficult to solve because it has a variable coefficient. Its solution is expressible in Bessel functions:

$$\Theta = \frac{I_0\left(2\sqrt{\overline{h}Lx/k\delta}\right)}{I_0\left(2\sqrt{\overline{h}L^2/k\delta}\right)} \tag{4.61}$$

where the modified Bessel function of the first kind and order zero, I_0, can be found in tables or in online calculators.

Rather than explore the mathematics of solving eqn. (4.59), we simply show the result for several geometries in terms of the fin efficiency, η_f, in Fig. 4.13. These curves were given by Schneider [4.7]. Kraus, Aziz, and Welty [4.6] provide a very complete discussion of fins and show a great many additional efficiency curves.

Example 4.10

A thin brass pipe, 3 cm in outside diameter, carries hot water at 85°C. It is proposed to place 0.8 mm thick straight circular fins on the pipe to cool it. The fins are 8 cm in diameter and are spaced 2 cm apart. Estimates suggest that $\overline{h}$ will equal 20 W/m²K on the pipe and 15 W/m²K on the fins, when they have been added. If $T_\infty = 22$°C, compute the heat loss per meter of pipe before and after the fins are added.

SOLUTION. Before the fins are added,

$$Q = \pi(0.03 \text{ m})(20 \text{ W/m}^2\text{K})[(85 - 22) \text{ K}] = 119 \text{ W/m}$$

where we set $T_{\text{wall}} = T_{\text{water}}$ since the pipe wall is thin. Then we can enter Fig. 4.13a with

$$\frac{r_2}{r_1} = 2.67 \quad \text{and} \quad mL\sqrt{\frac{L}{P}} = \sqrt{\frac{\overline{h}L^3}{kA}} = \sqrt{\frac{15(0.04 - 0.015)^3}{125(0.025)(0.0008)}} = 0.306$$

and we obtain $\eta_f = 89\%$. Thus, the actual heat transfer is given by

$$\underbrace{Q_{\text{without fin}}}_{119 \text{ W/m}} \underbrace{\left(\frac{0.02 - 0.0008}{0.02}\right)}_{\text{fraction of unfinned area}}$$

$$+ 0.89 \underbrace{[2\pi(0.04^2 - 0.015^2)]}_{\text{area per fin (both sides), m}^2}\left(50\frac{\text{fins}}{\text{m}}\right)\left(15 \frac{\text{W}}{\text{m}^2\text{K}}\right)[(85 - 22) \text{ K}]$$

so

$$Q_{\text{net}} = 478 \text{ W/m} = 4.02 \, Q_{\text{without fins}} \qquad \blacksquare$$
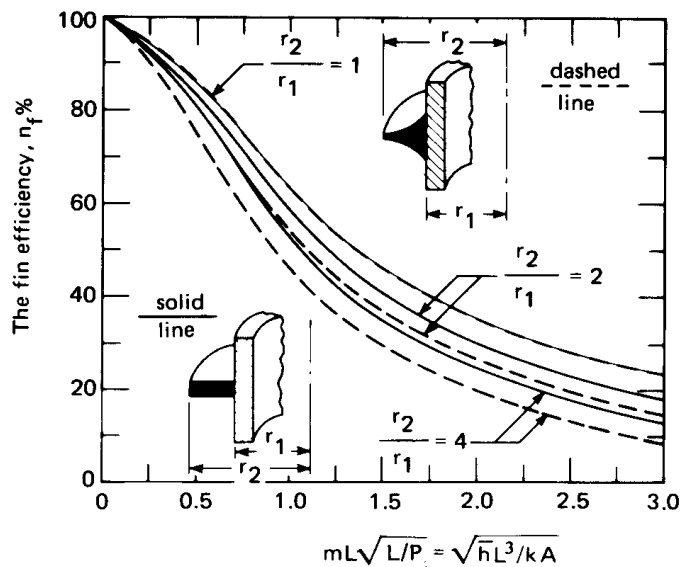
Comparison of a constant thickness circular fin, and a hyperbolic fin with thickness inversely proportional to radius. $(L \equiv r_2 - r_1$ and m is based on the area, A, shown in black.)
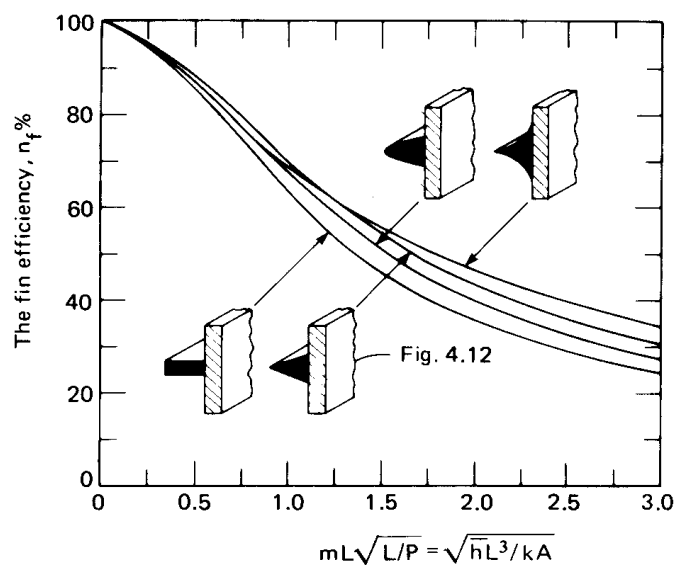
Comparison of four straight fins: constant thickness, triangular, parabolic, and hyperbolic. (m is based on A shown in black.)

Figure 4.13 The efficiency of several fins with variable cross section.

181

Wall thermal resistance and fin root temperature

We have assumed, so far, that we know the root temperature of a fin. That assumption is accurate in many cases. However, for heat to flow into a fin, the material below the root must have a temperature gradient. Think, for example, about hot water flowing in a tube with external fins to remove heat: Heat must flow through the tube wall to each fin's base. Some heat will flow axially along the tube wall to the fin's base, instead of flowing radially, straight to the base. Heat conduction near the base of almost any fin can clearly depend on many factors. In this case, the tube wall thickness, the spacing of fins, the magnitude of the inner and outer heat transfer coefficients, and the thermal conductivity of the metal or metals all affect the actual heat flow pattern.

If the heat flow into the fin is substantial, the temperature at the root will be depressed relative to unfinned portions of the tube. The fin-root depression is generally greater when the fin Biot number is larger, the fin efficiency is lower, the fins are farther apart, and the fin conductivity is much higher than the tube wall conductivity. Fortunately, in many cases of practical interest, the fin's Biot number is very small [eqn. (4.27)], the wall has high conductivity, and the internal heat transfer coefficient is large relative to the external one. The last point—that most of the thermal resistance is external to the metal—makes the thermal resistance of the metal unimportant. For such situations, we can reasonably neglect the axial temperature variation in the tube wall [4.8–4.10], and a simple one-dimensional resistance model will give good accuracy.

The literature provides some numerical estimates of fin root depression. Huang and Shah [4.8] reported that, for typical heat exchanger designs, $\text{Bi}_{\text{fin}} < 10^{-3}$ and $\eta_{\text{f}} > 80\%$ and that root temperature depression alters total heat transfer by less than 4%. For finned-tube heat exchangers typical of air-conditioning systems, $\text{Bi}_{\text{fin}} < 5 \times 10^{-4}$. For such designs, Comini and Savino [4.9] found that one-dimensional models differed from fully three-dimensional numerical simulations by no more than 2%. The one-dimensional model is conservative, in the sense of slightly overestimating the overall thermal resistance [4.8].

Example 4.11

Suppose that the brass pipe in Example 4.10 has a thickness of 1 mm and that the forced convection heat transfer coefficient inside is 600 W/m^{2}K, with water at 85°C. Estimate the heat loss per meter of pipe.

SOLUTION. Neglecting axial gradients in the tube wall, the overall thermal resistance between the water and the air includes the inside convection resistance, a one-dimensional tube wall resistance, and the resistance of the outside surface. The latter accounts for both the finned and unfinned sections, assuming that the unfinned surface and the fin root are at the same temperature. From Example 4.10

$$R_{\text{outside}} = \frac{85 - 22}{478} = 0.1318 \text{ K·m/W}$$

For the thin tube wall, we use a simple slab resistance, so that the overall thermal resistance is

$$\begin{aligned} R_{\text{overall}} &= \frac{1}{\overline{h}_i \pi D_i} + \frac{t_w}{k \pi D_i} + R_{\text{outer}} \\ &= \frac{1}{(600)\pi(0.028)} + \frac{0.001}{(26)\pi(0.028)} + 0.1318 \\ &= 0.01895 + 0.00044 + 0.1318 = 0.1512 \text{ K·m/W} \end{aligned}$$

Observe that the tube wall resistance is completely negligible in this calculation. The total heat loss is

$$Q_{\text{net}} = \frac{85 - 22}{0.1512} = 416.7 \text{ W/m}$$

which is lower than in Example 4.10 as a result of the inside convection resistance. The fins here are relatively far apart (2 cm), and the resistance could be reduced significantly with a tighter spacing. ∎

Problems

4.1 Make a table listing the general solutions of all steady, unidimensional constant-properties heat conduction problems in Cartesian, cylindrical and spherical coordinates, with and without uniform heat generation. This table should prove to be a very useful tool in future problem solving. It should include a total of 18 solutions. State any restrictions on your solutions. Do not include calculations.

4.2 The left side of a slab of thickness L is kept at 0°C. The right side is cooled by air blowing over it at T_∞°C; $\overline{h}_{\text{RHS}}$ is known. An exothermic reaction takes place in the slab such that heat is generated at $\dot{q} = A(T - T_\infty)$ W/m^3, where A is a constant. Find a fully dimensionless expression for the temperature distribution in the slab.

4.3 A long, wide plate of known size, material, and thickness L is connected across the terminals of a power supply and serves as a resistance heater. The plate is insulated on the bottom and transfers heat out the top by convection to a fluid at T_∞. The voltage, current, and T_∞ are known. The temperature, T_{tc}, of the bottom is measured with a thermocouple. Obtain expressions for: (a) temperature distribution in the plate; (b) $\overline{h}$ at the top; and (c) temperature at the top. Note that your answers must depend on *known information* only. [$T_{top} = T_{tc} - EIL^2/(2k \cdot \text{volume})$]

4.4 The heat transfer coefficient, $\overline{h}$, resulting from a forced flow over a flat plate depends on the fluid velocity, viscosity, density, specific heat, and thermal conductivity, as well as on the length of the plate. Develop the dimensionless functional equation for the heat transfer coefficient. [The exact equations, in dimensionless form, are in Sections 6.5 and 6.7.]

4.5 Water vapor condenses on a cold pipe and drips off the bottom in regularly spaced nodes as sketched in Fig. 3.9. The wavelength of these nodes, λ, depends on the liquid-vapor density difference, $\rho_f - \rho_g$, the surface tension, σ, and the gravity, g. Find how λ varies with its dependent variables. Compare your solution to the exact result, eqn. (9.6a).

4.6 A liquid film flows down a vertical wall. The local film velocity at any distance from the wall depends on that distance, gravity, the liquid kinematic viscosity, and the film thickness. Obtain the dimensionless functional equation for the local velocity (cf. Section 8.5).
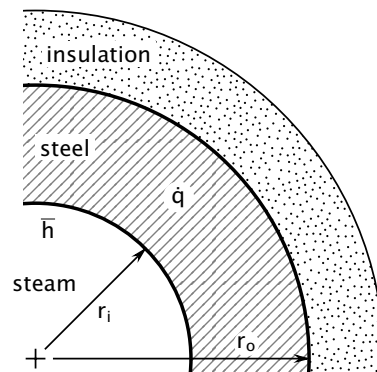

Figure 4.14   Configuration for Problem 4.7.

4.7 A steam preheater consists of a thick, electrically conducting, cylindrical shell insulated on the outside, with wet steam flowing down the middle (Fig. 4.14). The steam's temperature is fixed by the known pressure in the pipe. The preheating is driven by electrical resistance heating of $\dot{q}$ W/m^3 in the cylinder wall. Find the temperature in the cylinder wall as a function of position. Plot Θ against ρ, where Θ is an appropriate dimensionless temperature and $\rho = r/r_o$. Note that Bi will be a parameter in the solution. Use an inside radius of $\rho_i = 2/3$ and several values of Bi. *On the basis of this plot*, recommend criteria (in terms of Bi) for: (a) replacing the convective boundary condition on the inside with a simple constant temperature condition; and (b) neglecting temperature variations within the cylinder wall.

4.8 Steam condenses inside a thick-walled pipe, keeping the inside at a specified temperature, T_i. The pipe is electrically heated at a rate $\dot{q}$ W/m^3. The outside wall is cooled by natural convection with a heat transfer coefficient, $\overline{h}$ to a fluid at T_∞.

    a. Derive the dimensionless expression temperature distribution in the pipe wall, $\Theta = (T - T_\infty)/(T_i - T_\infty)$, as a function of: the radius ratios, $\rho = r/r_o$ and $\rho_i = r_i/r_o$; a heat generation number, $\Gamma = \dot{q}r_o^2/k(T_i - T_\infty)$; and the Biot number.

    b. Plot this result for the case $\rho_i = 2/3$, Bi = 1, and for several values of Γ.

    c. Discuss any interesting aspects of your result.

4.9 Solve Problem 2.5 if you have not already done so, putting it in dimensionless form before you begin. Then let the Biot numbers approach infinity in the solution. You should get the same solution we got in Example 2.4, using b.c.'s of the first kind. Do you?

4.10 Complete the algebra that is missing between eqns. (4.30) and eqn. (4.31b) and eqn. (4.41).

4.11 Complete the algebra that is missing in applying the boundary conditions of eqns. (4.47) to eqn. (4.35) so as to obtain eqn. (4.48). *Hint:* Keep the equations in terms of $e^{\pm mL}$ and $e^{\pm mL\xi}$, rather than cosh and sinh, until the final steps.

4.12 Obtain eqn. (4.50) from the general solution for a fin [eqn. (4.35)], using the b.c.'s $T(x = 0) = T_0$ and $T(x = L) = T_\infty$ and observing how your result simplifies if L becomes very, very long.

4.13 A thermometer well consists of a 304 stainless steel tube reaching into a pipe, with its end closed. The tube has a 2 cm O.D. and a 1.88 cm I.D. The thermometer bulb is in good contact with the end of the well. Steam at 260°C flows through the pipe, and that the heat transfer coefficient between the steam and the tube wall is 300 W/m^{2}K. What is the minimum length, L, for the well to ensure an error less than 0.5% of the difference between the pipe wall temperature and the temperature of the steam? [3.44 cm.]

4.14 Thin fins with a 2 mm by 20 mm rectangular cross section and a thermal conductivity of 50 W/m·K protrude from a wall at $T_0 = 170$°C; outside, $\overline{h} \simeq 600$ W/m^{2}K and $T_\infty = 20$°C. What is the heat flow rate into each fin and what is the effectiveness?

4.15 A thin rod is anchored at a wall at $T = T_0$ on one end. It is insulated at the other end. Plot the dimensionless temperature distribution in the rod as a function of dimensionless length: (a) if the rod is exposed to an environment at T_∞ through a heat transfer coefficient; (b) if the rod's surface is entirely insulated but heat is [somehow] *removed* from the fin material at the uniform rate $\dot{q} = -\overline{h}P(T_0 - T_\infty)/A$ W/m^3. Comment on the implications of this theoretical comparison.

4.16 A tube of outside diameter d_o and inside diameter d_i carries fluid at $T = T_1$ from one wall at temperature T_1 to another wall, a distance L away, at T_r. Outside the tube $\overline{h}_o$ is small enough to neglect, but inside the tube $\overline{h}_i$ is not small. Treat the tube as a fin and plot the dimensionless temperature distribution in it as a function of dimensionless length.

4.17 The shape of the fin in Fig. 4.12 is changed so that $A(x) = 2\delta(x/L)^2 b$ instead of $2\delta(x/L)b$. Calculate the temperature distribution and the heat flux at the base. Plot the temperature distribution and fin thickness against x/L. Derive an expression for the fin efficiency, η_f. *Hint:* From your study of ordinary differential equations, recall a variable coefficient equation called Euler's equation.

4.18 Work Problem 2.21, if you have not already done so, nondimensionalizing the problem before you attempt to solve it. It should now be much simpler.

4.19 One end of a copper rod 30 cm long is held at 200°C, and the other end is held at 93°C. The air and the room surrounding the rod are at $T_\infty = 38$°C. At the rod's circumference, the effective heat transfer coefficient is 17 W/m^{2}K, including both convection and radiation. If the rod's diameter is 1.25 cm, what is the net heat transfer from the rod's circumference? [19.13 W.]

4.20 How much error will the insulated-tip approximation cause in calculating the heat flow into the fin in Example 4.8? [3.67%]

4.21 A straight cylindrical fin 0.6 cm in diameter and 6 cm long protrudes from a magnesium block at 300°C. Air at 35°C is forced past the fin so that $\bar{h}$ is 130 W/m^{2}K. Calculate the heat removed by the fin, the fin efficiency, and the fin effectiveness.

4.22 A 2 cm diameter, horizontal, 1.0% steel rod connects a block of ice with a block of dry ice (CO_2) in a 30°C room. The frozen blocks are otherwise insulated. The rod is embedded in each block with a 20 cm span between them. The heat transfer coefficient to the environment is 10 W/m^{2}K. Determine whether the ice will begin to melt when the rod is at steady state.

4.23 A fin of triangular axial section (Fig. 4.12) 0.1 m in length and 0.02 m wide at its base is used to extend the surface area of a 0.5% carbon steel wall. If the wall is at 40°C and heated gas flows past at 200°C ($\bar{h} = 230$ W/m^{2}K), compute the heat removed by the fin per meter of breadth, b, of the fin.

4.24 Consider the concrete slab in Example 2.1. Suppose that the heat generation were to cease abruptly at time $t = 0$ and the slab were to start cooling back toward T_w. Predict $T - T_w$ as a function of time, noting that the initial parabolic temperature profile can be nicely approximated as a sine function. (Without the sine approximation, this problem would require the Fourier series methods of Chapter 5.)

4.25 A 6061-T6 aluminum steam condenser tube has a 20 mm O.D. with an array of fins on its outer surface. The fins are 0.8 mm thick

with a diameter of 35 mm and a center-to-center spacing of 5 mm. The steam inside is at 10 atm and the air and room outside are at 18°C, with an effective $\bar{h}_{\text{outside}}$ = 6 W/m²K. The heat transfer coefficient for condensation is very large and the tube wall is not thick. What is the mass rate of condensation if the pipe is 1.5 m in length? [$\dot{m}_{\text{cond}}$ = 0.802 kg/hr.]

4.26 How long must a 0.4 cm cylindrical copper fin be if the temperature of its insulated tip is to exceed the surrounding air temperature by 20% of $(T_0 - T_\infty)$? Consider T_{air} = 20°C and $\bar{h}$ = 28 W/m²K. [27.3 cm]

4.27 A 2 cm ice cube sits on a shelf of widely spaced aluminum rods, 3 mm in diameter, in a refrigerator at 10°C. How rapidly, in mm/min, do the rods melt their way through the ice cube if $\bar{h}$ at the surface of the rods is 10 W/m²K (including both convection and radiation). Be sure that you understand the physical mechanism before you make the calculation. h_{sf} = 333 kJ/kg. (You can check your result experimentally, if you have a such a refrigerator shelf.)

4.28 The highest heat flux that can be achieved in nucleate boiling (called q_{max}—see the qualitative discussion in Section 9.1) depends upon ρ_g, the saturated vapor density; h_{fg}, the latent heat vaporization; σ, the surface tension; a characteristic length, l; and the buoyancy force per unit volume, $g(\rho_f - \rho_g)$, where ρ_f is the saturated liquid density. Develop the dimensionless functional equation for q_{max} in terms of dimensionless length.

4.29 You want to rig a handle for a door in the wall of a furnace. The door is at 160°C. You consider bending a 40 cm length of 6.35 mm diam. 0.5% carbon steel rod into a U-shape and welding the ends to the door. Surrounding air at 24°C will cool the handle ($\bar{h}$ = 12 W/m²K including both convection and radiation). What is the coolest temperature of the handle? How close to the door can you grasp the handle without getting burned if T_{burn} = 65°C? How might you improve the design?

4.30 A 14 cm long by 1 cm square brass rod is supplied with 25 W at its base. The other end is insulated. It is cooled by air at 20°C, with $\bar{h}$ = 68 W/m²K. Develop an equation for appropriate dimensionless temperature, Θ, as a function of ξ, mL, and other known information. Calculate the base temperature. [169°C]

4.31 A cylindrical fin has a constant imposed heat flux of q_1 at one end and q_2 at the other end, and it is cooled convectively along its length. Develop an equation for the dimensionless temperature distribution in the fin. Specialize this result for $q_2 = 0$ and $L \longrightarrow \infty$, and compare it to eqn. (4.50).

4.32 A thin annular cylinder of radius r_o serves as an electrical resistance heater. The temperature along an axial line at $\theta_1 = 0$ is kept at T_1. Another line, θ_2 radians away, is kept at T_2. Derive dimensionless expressions for the temperature distributions in the two sections.

4.33 Heat transfer is augmented, in a particular heat exchanger, with a field of 7 mm diameter fins protruding 20 mm into a flow. The fins are arranged in a hexagonal array, with a minimum center-to-center spacing of 1.8 cm. The fins are bronze, and $\overline{h}_f$ around the fins is 168 W/m^{2}K. On the wall itself, $\overline{h}_w$ is only 54 W/m^{2}K. Calculate $\overline{h}_{\text{eff}} \equiv Q_{\text{wall}}/A_{\text{wall}}(T_{\text{wall}} - T_\infty)$ for the wall with its fins. [228 W/m^{2}K]

4.34 An engineer seeks to study the effect of temperature on the curing of concrete by controlling the curing temperature in the following way. A sample slab of thickness L is subjected to a heat flux, q_w, on one side, and it is cooled to temperature T_1 on the other. Derive a dimensionless expression for the steady temperature in the slab. Plot the expression and offer a criterion for neglecting the internal heat generation in the slab.

4.35 Develop the dimensionless temperature distribution in a spherical shell with the inside wall kept at one temperature and the outside wall at a second temperature. Reduce your solution for the two limiting cases in which $r_{\text{outside}} \gg r_{\text{inside}}$ and in which r_{outside} is very close to r_{inside}. Discuss these limits.

4.36 Does the temperature distribution during steady heat transfer in an object with b.c.'s of only the first kind depend on k? Explain. What if you had second-kind boundary conditions? What about third-kind conditions?

4.37 A long, 5 mm diameter duralumin rod is wrapped with an electrical resistor over 30 mm of its length. The resistor imparts a surface flux of 40 kW/m^2. Evaluate the temperature distribution of the rod on either side of the heated section if $\overline{h} = 150$ W/m^{2}K around the unheated rod and $T_{\text{ambient}} = 27°$C. [135°C]

4.38 The heat transfer coefficient between a cool surface and a saturated vapor, when the vapor condenses in a film on the surface, depends on: the liquid density and specific heat; the liquid conductivity and kinematic viscosity; the latent heat; the temperature difference; the buoyant force per unit volume, $g(\rho_f - \rho_g)$; and the position, x, on the cooler surface. Develop the dimensionless functional equation for $\overline{h}$. *Hint:* You can find the conventional form of this equation by looking ahead in this textbook.

4.39 A duralumin pipe passing through a cold room has a 4 cm I.D. and a 5 cm O.D. It carries water that sometimes sits stationary. It is proposed to put electric heating rings around the pipe to protect it against freezing during cold periods as low as $-7°C$. The heat transfer coefficient outside the pipe is 9 W/m²K (including both convection and radiation). Determine how far apart the heaters would have to be if they brought the pipe temperature to 40°C locally. How much power do they require? *Hint:* heat conduction in the water may be neglected (why?). [37.6 W]

4.40 Evaluate $d(\tanh x)/dx$.

4.41 The specific entropy of an ideal gas depends on its specific heat at constant pressure, its temperature and pressure, the ideal gas constant and reference values of the temperature and pressure. Obtain the dimensionless functional equation for the specific entropy and compare it with the known equation for ideal gas entropy.

4.42 A proposed design for a large freezer's door has a 2.5 cm thick layer of insulation (k_{in} = 0.04 W/m·K) covered on the inside, outside, and edges with a continuous aluminum skin 3.2 mm thick (k_{Al} = 165 W/m·K). The door closes against a nonconducting seal 1 cm wide. Heat gain through the door can result from conduction straight through the insulation and skins (normal to the plane of the door) and from conduction in the aluminum skin only, going from the skin outside, around the edge skin, and to the inside skin. The heat transfer coefficients to the inside, $\overline{h}_i$, and outside, $\overline{h}_o$, are each 12 W/m²K, accounting for both convection and radiation. The temperature outside the freezer is 25°C, and the temperature inside is $-15°C$.

   a. If the door is 1 m wide, estimate the one-dimensional heat gain through the door, neglecting any conduction around the

edges of the skin. Your answer will be in watts per meter of door height.

b. Now estimate the heat gain through the aluminum skin that wraps the outside and inside of the door. Heat will be conducted from the outside, around the edge of the door, to the inside. For this calculation, assume that the insulation is perfectly adiabatic and ignore the bottom and the top of the door. Your answer will again be in watts per meter of door height.

c. Suggest a few design changes that might reduce the heat conduction around the edges of the door.

4.43 A thermocouple epoxied onto a high conductivity surface is intended to measure the surface temperature. The thermocouple consists of two bare wires of diameter $D_w = 0.51$ mm. One wire is made of Chromel (Ni-10% Cr with $k_{cr} = 17$ W/m·K) and the other of constantan (Ni-45% Cu with $k_{cn} = 23$ W/m·K). The ends of the wires are welded together to create an approximately rectangular measuring junction, with a width $w \approx D_w$ and a length $l \approx 2D_w$. The wires extend perpendicularly away from the surface and do not touch one another. A layer of an epoxy ($k_{ep} = 0.5$ W/m·K) separates the thermocouple junction from the surface by 0.2 mm. The heat transfer coefficient between the wires and the surroundings at 20°C is $\overline{h} = 28$ W/m²K, including both convection and radiation. If the thermocouple reads $T_{tc} = 40$°C, estimate the actual temperature T_s of the surface and suggest a better arrangement of the wires.

4.44 The resistor leads in Example 4.9 were assumed to be "infinitely long" fins. What is the minimum length they each must have if they are to be modeled this way? What are the effectiveness, ε_f, and efficiency, η_f, of the wires? Discuss the meaning of your calculated effectiveness and efficiency.

4.45 We use the following experiment to measure local heat transfer coefficients, h, inside pipes that carry flowing liquids. We pump liquid with a known bulk temperature through a pipe which serves as an electric resistance heater, and whose outside is perfectly insulated. A thermocouple measures its outside temperature. We know the volumetric heat release in the pipe wall, $\dot{q}$, from resistance and current measurements. We also know the pipe diameter, wall thickness, and thermal conductivity. (*Continued on next page.*)

Derive an equation for h. (Remember that, since h is unknown, a boundary condition of the third kind by itself is not sufficient to find $T(r)$.) Then, nondimensionalize your result.

References

[4.1] V. L. Streeter and E. B. Wylie. *Fluid Mechanics*. McGraw-Hill Book Company, New York, 7th ed., 1979. Chapter 4.

[4.2] E. Buckingham. On physically similar systems; illustrations of the use of dimensional equations. *Phys. Rev.*, **4**:345–376, October 1914. doi: 10.1103/PhysRev.4.345.

[4.3] E. Buckingham. Model experiments and the forms of empirical equations. *Trans. ASME*, **37**:263–296, 1915. Available in GoogleBooks.

[4.4] Lord Rayleigh, John Wm. Strutt. The principle of similitude. *Nature*, **95**: 66–68, March 1915. Open access. doi: 10.1038/095066c0. url: https://www.nature.com/articles/095066c0.pdf.

[4.5] J. O. Farlow, C. V. Thompson, and D. E. Rosner. Plates of the dinosaur stegosaurus: Forced convection heat loss fins? *Science*, **192**(4244): 1123–1125 and cover, June 1976. doi: 10.1126/science.192.4244.1123.

[4.6] A. D. Kraus, A. Aziz, and J.R. Welty. *Extended Surface Heat Transfer*. John Wiley & Sons, Inc., New York, 2001.

[4.7] P. J. Schneider. *Conduction Heat Transfer*. Addison-Wesley Publishing Co., Inc., Reading, Mass., 1955.

[4.8] L. J. Huang and R. K. Shah. Assessment of calculation methods for efficiency of straight fins of rectangular profile. *Int. J. Heat Fluid Flow*, **13**(3):282–293, September 1992. doi: 10.1016/0142-727X(92)90042-8.

[4.9] G. Comini and S. Savino. Accuracy of one-dimensional design procedures for finned-tube heat exchangers. *Applied Thermal Engineering*, **29**:2863–2869, October 2009. doi: 10.1016/j.applthermaleng.2009.02.007.

[4.10] L. C. Thomas. Heat transfer in fin assemblies: Significance of two-dimensional effects—a reexamination of the issue. *J. Heat Transfer*, **121**:748–752, August 1999. doi: 10.1115/1.2826047.

5. Transient and multidimensional heat conduction

When I was a lad, winter was really cold. It would get so cold that if you went outside with a cup of hot coffee it would freeze. I mean it would freeze fast. That cup of hot coffee would freeze so fast that it would still be hot after it froze. Now that's cold!   **Old Northwoods Tall Tale**

5.1   Introduction

James Watt, of course, did not invent the steam engine. What he did do was to eliminate a destructive transient heating and cooling process that wasted a great amount of energy. By 1763, the great puffing engines of Savery and Newcomen had been used for over half a century to pump the water out of Cornish mines and to do other tasks. What has that to do with our subject? Well, consider what happened that same year, when the young instrument maker, Watt, was called upon to renovate the Newcomen engine model at the University of Glasgow. The Glasgow engine was then being used as a demonstration in the course on natural philosophy. Watt did much more than just renovate the machine—he first recognized, and eventually eliminated, its major shortcoming.

The cylinder of Newcomen's engine was cold when steam entered it and nudged the piston outward. A great deal of steam was wastefully condensed on the cylinder walls until they were warm enough to accommodate it. When the cylinder was filled, the steam valve was closed and jets of water were activated inside the cylinder to cool it again and condense the steam. This created a powerful vacuum, which sucked the piston back in on its working stroke. First, Watt tried to eliminate the wasteful initial condensation of steam by insulating the cylinder. But that

simply reduced the vacuum and cut the power of the working stroke. Then he realized that, if he led the steam outside to a *separate condenser*, the cylinder could stay hot while the vacuum was created.

The separate condenser was the main issue in Watt's first patent (1769), and its introduction immediately doubled the thermal efficiency of steam engines from a maximum of 1.1% to 2.2%. By the time Watt died in 1819, his invention had led to efficiencies of 5.7%, and his engine had altered the face of the world by powering the Industrial Revolution. And from 1769 until today, the steam power cycles that engineers study in their thermodynamics courses are accurately represented as steady flow—rather than transient—processes.

The repeated transient heating and cooling in Newcomen's engine was the kind of process that today's design engineer might still carelessly ignore, but the lesson that we learn from history is that transient heat transfer can be of overwhelming importance. Today, for example, designers of walk-in freezers know that such systems need relatively little energy to keep food cold at steady conditions. The real cost of operating them results from the consumption of energy needed to bring the food down to a low temperature and the losses resulting from people entering and leaving the system. These transient heat transfer processes are a dominant concern in the design of food storage units.

We therefore turn our attention to the analysis of unsteady heat transfer. We begin with a more detailed consideration of the lumped-capacity system that we looked at in Section 1.3. And our starting point is the dimensional analysis of such a system.

5.2   Lumped-capacity solutions

Dimensional analysis of transient heat conduction

Consider a fairly representative problem of one-dimensional transient heat conduction: a slab initially at uniform temperature. The temperature of one wall is suddenly changed to a new temperature while the other wall is cooled or heated convectively. The equations are:

$$\frac{\partial^2 T}{\partial x^2} = \frac{1}{\alpha}\frac{\partial T}{\partial t} \quad \text{with} \quad \begin{cases} \text{i.c.:} & T(t=0) = T_i \\ \text{b.c.:} & T(t>0, x=0) = T_1 \\ \text{b.c.:} & -k\left.\frac{\partial T}{\partial x}\right|_{x=L} = \overline{h}\,(T - T_1)_{x=L} \end{cases}$$

The solution of this problem must take the form of the following dimen-
sional functional equation:

$$T - T_1 = \text{fn}\left[(T_i - T_1), x, L, t, \alpha, \overline{h}, k\right]$$

There are eight variables in four dimensions (K, s, m, W), so we look for
$8 - 4 = 4$ pi-groups. We anticipate, from Section 4.3, that they will include

$$\Theta \equiv \frac{(T - T_1)}{(T_i - T_1)}, \quad \xi \equiv \frac{x}{L}, \quad \text{and Bi} \equiv \frac{\overline{h}L}{k},$$

and we write

$$\Theta = \text{fn}(\xi, \text{Bi}, \Pi_4) \tag{5.1}$$

One possible candidate for Π_4, which is independent of the other three,
is

$$\Pi_4 \equiv \text{Fo} = \alpha t / L^2 \tag{5.2}$$

where Fo is the *Fourier number.* Another candidate that we use later is

$$\Pi_4 \equiv \zeta = \frac{x}{\sqrt{\alpha t}} \quad \left(\text{this is exactly } \frac{\xi}{\sqrt{\text{Fo}}}\right) \tag{5.3}$$

If the problem involved b.c.'s of only the first kind, the heat transfer
coefficient, $\overline{h}$—and hence the Biot number—would go out of the problem.
Then the dimensionless function eqn. (5.1) is

$$\Theta = \text{fn}(\xi, \text{Fo}) \tag{5.4}$$

By the same token, if the b.c.'s had introduced different values of $\overline{h}$ at
$x = 0$ and $x = L$, *two* Biot numbers would appear in the solution as they
did in eqn. (4.24).

Dimensional analysis is particularly revealing in the case of the lumped-
capacity problem [see eqns. (1.19)–(1.22)]. Neither k nor x enters the
problem because we do not retain any features of the internal conduction
problem. Therefore, we have ρc rather than α. Furthermore, we do not
have to separate ρ and c because they appear only as a product. Finally,
we use the volume-to-external-area ratio, V/A, as a characteristic length
since no one linear dimension has any significance. Thus, for the transient
lumped-capacity problem, the dimensional equation is

$$T - T_\infty = \text{fn}\left[(T_i - T_\infty), \rho c, V/A, \overline{h}, t\right] \tag{5.5}$$

With six variables in the dimensions J, K, m, and s, only two pi-groups will appear in the dimensionless function equation.

$$\Theta = \mathrm{fn}\left(\frac{\overline{h}At}{\rho cV}\right) = \mathrm{fn}\left(\frac{t}{T}\right) \tag{5.6}$$

This is exactly the form of the simple lumped-capacity solution, eqn. (1.22). Notice, too, that the group t/T can be viewed as

$$\frac{t}{T} = \frac{hk(V/A)t}{\rho c(V/A)^2 k} = \frac{\overline{h}(V/A)}{k} \cdot \frac{\alpha t}{(V/A)^2} = \mathrm{Bi\,Fo} \tag{5.7}$$

Electrical and mechanical analogies to the lumped-thermal-capacity problem

We take the term *capacitance* from electrical circuit theory and can sketch the simple resistance-capacitance circuit, analogous to the preceding problem, in Fig. 5.1. Here, the electrical capacitor is initially charged to a voltage, E_o. When the switch is suddenly opened, the capacitor discharges through the resistor and the capacitor's voltage drops according to the relation

$$\frac{dE}{dt} + \frac{E}{RC} = 0 \tag{5.8}$$

The solution of eqn. (5.8) with the i.c. $E(t = 0) = E_o$ is

$$E = E_o\, e^{-t/RC} \tag{5.9}$$

and the current can be computed from Ohm's law, once $E(t)$ is known:

$$I = \frac{E}{R} \tag{5.10}$$

Normally, in a heat conduction problem the *thermal capacitance*, ρcV, is distributed over a range of temperature that varies in space. But when the Biot number is small, $T(t)$ is uniform in the body and we can *lump* the
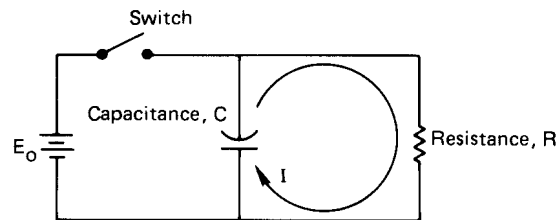

Figure 5.1   A simple resistance-capacitance circuit.

capacitance into a single circuit element. The thermal resistance is $1/\overline{h}A$, and the temperature difference $(T - T_\infty)$ is analogous to $E(t)$. Thus, the thermal response, analogous to eqn. (5.9), is [see eqn. (1.22)]

$$T - T_\infty = (T_i - T_\infty) \exp\left(-\frac{\overline{h}At}{\rho c V}\right)$$

Notice that the electrical time constant, analogous to $\rho c V/\overline{h}A$, is RC.
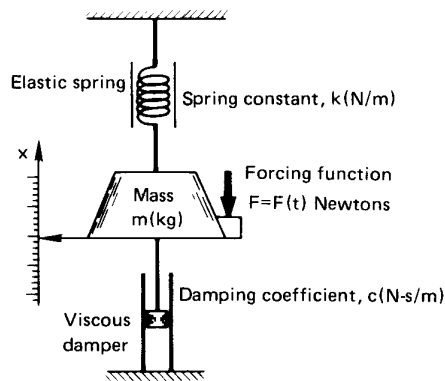

**Figure 5.2** A spring-mass-damper system with a forcing function.

Now consider a slightly more complex system that is also analogous to slightly more complex lumped capacity heat transfer. Figure 5.2 shows a spring-mass-damper system. The well-known response equation (actually, a force balance) for this system is

$$\underbrace{m}\frac{d^2x}{dt^2} + \underbrace{c}\frac{dx}{dt} + \underbrace{k}\,x = F(t) \qquad\qquad (5.11)$$

where k is analogous to $1/C$ or to $\overline{h}A$

the damping coefficient is analogous to R or to $\rho c V$

What is the mass analogous to?

A term analogous to mass would arise from electrical inductance, but we did not include it in the electrical circuit. Mass has the effect of carrying the system beyond its final equilibrium point. Thus, in an underdamped mechanical system, we might obtain the sort of response shown in Fig. 5.3 if we specified the velocity at $x = 0$ and provided no forcing function. Electrical inductance provides a similar effect. But the Second Law of Thermodynamics does not permit temperatures to overshoot their equilibrium values spontaneously. *There are no physical elements analogous to mass or inductance in thermal systems.*

Figure 5.3 Response of an unforced spring-mass-damper system with an initial velocity.
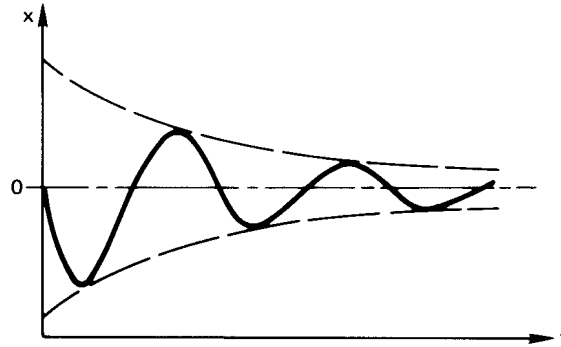
Another mechanical element that we've introduced here does have a thermal analogy, however. It is the forcing function, F. We consider a (massless) spring-damper system with a forcing function F that probably is time-dependent, and we ask: "What might a thermal forcing function look like?"

Lumped-capacity solution with a variable ambient temperature

To answer the preceding question, let us suddenly immerse an object at a temperature $T = T_i$, with Bi $\ll 1$, into a cool bath whose temperature is rising as $T_\infty(t) = T_i + bt$, where T_i and b are constants. Then eqn. (1.20) becomes

$$\frac{d(T - T_i)}{dt} = -\frac{T - T_\infty}{T} = -\frac{T - T_i - bt}{T}$$

where we subtract the constant T_i within the derivative. Then

$$\frac{d(T - T_i)}{dt} + \frac{T - T_i}{T} = \frac{bt}{T} \tag{5.12}$$

so the forcing function is bt/T, the effect of the rising bath temperature.

To solve eqn. (5.12) we must first recall that the general solution of a linear ordinary differential equation with constant coefficients is equal to the sum of any particular solution of the complete equation and the general solution of the homogeneous equation. We know the latter: it is $T - T_i = (\text{constant}) \exp(-t/T)$. A particular solution of the complete equation can often be formed by guessing solutions and trying them in the complete equation. Here we discover that
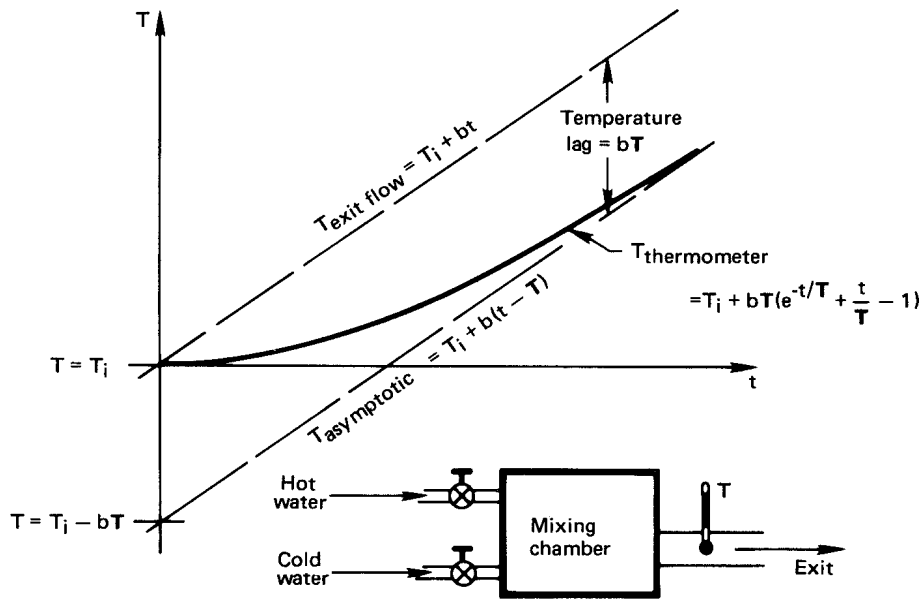
$$T - T_i = bt - bT$$

Figure 5.4 Response of a thermometer to a linearly increasing ambient temperature.

satisfies eqn. (5.12). Thus, the general solution of eqn. (5.12) is the sum of these general and particular solutions:

$$T - T_i = C_1 e^{-t/T} + b(t - T) \tag{5.13}$$

The constant C_1 is found by applying the initial condition, as in the following example.

Example 5.1

The flow rates of hot and cold water are regulated into a mixing chamber. We measure the temperature of the water as it leaves, using a thermometer with a time constant, T. On a particular day, the system started with cold water at $T = T_i$ in the mixing chamber. Then hot water is added in such a way that the outflow temperature rises linearly, as shown in Fig. 5.4, with $T_{\text{exit flow}} = T_i + bt$. How will the thermometer report the temperature variation?

SOLUTION. The initial condition for eqn. (5.13) in this case is $T - T_i = 0$ at $t = 0$. Substituting eqn. (5.13) in the i.c., we get

$$0 = C_1 - bT \quad \text{so} \quad C_1 = bT$$

and the response equation is

$$T - (T_i + bt) = b\boldsymbol{T}\left(e^{-t/\boldsymbol{T}} - 1\right) \tag{5.14}$$

This result is plotted in Fig. 5.4. Notice that the thermometer reading has a transient portion, $b\boldsymbol{T}e^{-t/\boldsymbol{T}}$, which decays for a few time constants and then can be neglected, and a steady portion, $T_i + b(t - \boldsymbol{T})$, which persists thereafter. When the steady response is established, the thermometer follows the bath with a temperature lag of $b\boldsymbol{T}$. This constant error is reduced when either $\boldsymbol{T}$ or the rate the temperature rises, b, is reduced. ∎

The lumped capacity solution for arbitrary variations of $T_\infty(t)$ is given in Problem 5.52 (see also Problems 5.3, 5.53, and 5.54,).

Second-order lumped-capacity systems

Now we look at situations in which two lumped-thermal-capacity systems are connected in series. Such an arrangement is shown in Fig. 5.5. Heat is transferred through two slabs with a contact, or interfacial, resistance h_c^{-1} between them. We shall require that $h_c L_1/k_1$, $h_c L_2/k_2$, and $\overline{h}L_2/k_2$ are all much less than one, so we can lump the thermal capacitance of each slab. Then the differential equations for the temperature response of each slab are

$$\text{slab 1}: \quad -(\rho c V)_1 \frac{dT_1}{dt} = h_c A(T_1 - T_2) \tag{5.15}$$

$$\text{slab 2}: \quad -(\rho c V)_2 \frac{dT_2}{dt} = \overline{h}A(T_2 - T_\infty) - h_c A(T_1 - T_2) \tag{5.16}$$

and the initial conditions on the temperatures T_1 and T_2 are

$$T_1(t = 0) = T_2(t = 0) = T_i \tag{5.17}$$

We next identify two time constants for this problem[1]:

$$\boldsymbol{T}_1 \equiv (\rho c V)_1/h_c A \quad \text{and} \quad \boldsymbol{T}_2 \equiv (\rho c V)_2/\overline{h}A$$

Then eqn. (5.15) becomes

$$T_2 = \boldsymbol{T}_1 \frac{dT_1}{dt} + T_1 \tag{5.18}$$

---

[1]Notice that we could also have used $(\rho c V)_2/h_c A$ for $\boldsymbol{T}_2$ since both h_c and $\overline{h}$ act on slab 2. The choice is arbitrary—although the resulting solutions (while giving the same answers) will not look the same.
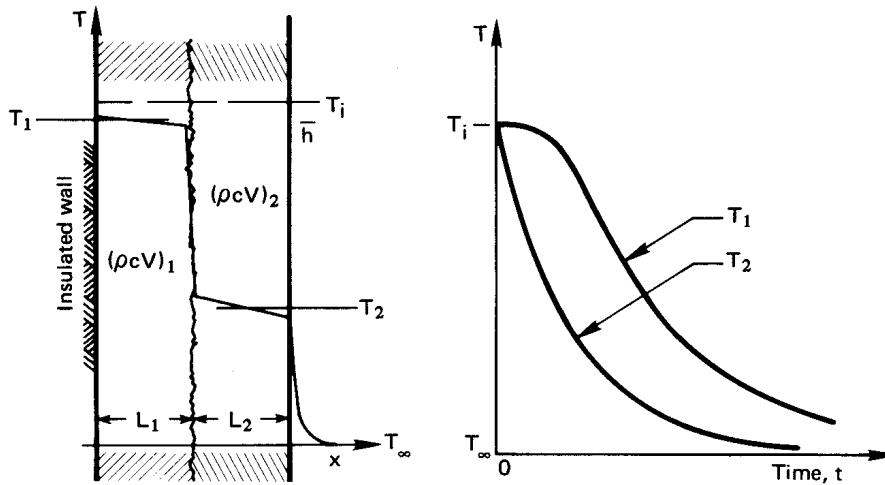
Figure 5.5 Two slabs conducting in series through a contact resistance.

which we substitute in eqn. (5.16) to get

$$T_1 T_2 \frac{d^2 T_1}{dt^2} - T_2 \frac{dT_1}{dt} = \left(T_1 \frac{dT_1}{dt} + T_1 - T_\infty \right) + \frac{h_c}{\overline{h}} T_1 \frac{dT_1}{dt}$$

or

$$\frac{d^2 T_1}{dt^2} + \underbrace{\left[\frac{1}{T_1} + \frac{1}{T_2} + \frac{h_c}{\overline{h} T_2} \right]}_{\equiv b} \frac{dT_1}{dt} + \underbrace{\frac{T_1 - T_\infty}{T_1 T_2}}_{\equiv c(T_1 - T_\infty)} = 0 \qquad (5.19a)$$

If we call $T_1 - T_\infty \equiv \theta$, then eqn. (5.19a) can be written as

$$\frac{d^2 \theta}{dt^2} + b \frac{d\theta}{dt} + c\theta = 0 \qquad (5.19b)$$

Thus we have reduced the pair of first-order equations, eqn. (5.15) and eqn. (5.16), to a single second-order equation, eqn. (5.19b).

The general solution of eqn. (5.19b) is obtained by guessing a solution of the form $\theta = C_1 e^{Dt}$. Substitution of this guess into eqn. (5.19b) gives

$$D^2 + bD + c = 0 \qquad (5.20)$$

from which we find that $D = -(b/2) \pm \sqrt{(b/2)^2 - c}$. This gives us two values of D, from which we can get two exponential solutions. By adding

them together, we form a general solution:

$$\theta = C_1 \exp\left[-\frac{b}{2} + \sqrt{\left(\frac{b}{2}\right)^2 - c}\,\right]t + C_2 \exp\left[-\frac{b}{2} - \sqrt{\left(\frac{b}{2}\right)^2 - c}\,\right]t \quad (5.21)$$

To solve for the two constants we substitute eqn. (5.21) in the first of i.c.'s (5.17) and get

$$T_i - T_\infty = \theta_i = C_1 + C_2 \qquad (5.22)$$

The second i.c. can be put into terms of T_1 with the help of eqn. (5.15):

$$-\frac{dT_1}{dt}\bigg|_{t=0} = \frac{h_c A}{(\rho c V)_1}(T_1 - T_2)_{t=0} = 0$$

We substitute eqn. (5.21) in this and obtain

$$0 = \left[-\frac{b}{2} + \sqrt{\left(\frac{b}{2}\right)^2 - c}\,\right]C_1 + \left[-\frac{b}{2} - \sqrt{\left(\frac{b}{2}\right)^2 - c}\,\right]\underbrace{C_2}_{=\,\theta_i - C_1}$$

so

$$C_1 = -\theta_i\left[\frac{-b/2 - \sqrt{(b/2)^2 - c}}{2\sqrt{(b/2)^2 - c}}\right]$$

and

$$C_2 = +\theta_i\left[\frac{-b/2 + \sqrt{(b/2)^2 - c}}{2\sqrt{(b/2)^2 - c}}\right]$$

So we obtain at last:

$$\boxed{\begin{aligned}\frac{T_1 - T_\infty}{T_i - T_\infty} \equiv \frac{\theta}{\theta_i} &= \frac{b/2 + \sqrt{(b/2)^2 - c}}{2\sqrt{(b/2)^2 - c}} \exp\left[-\frac{b}{2} + \sqrt{\left(\frac{b}{2}\right)^2 - c}\,\right]t \\ &+ \frac{-b/2 + \sqrt{(b/2)^2 - c}}{2\sqrt{(b/2)^2 - c}} \exp\left[-\frac{b}{2} - \sqrt{\left(\frac{b}{2}\right)^2 - c}\,\right]t\end{aligned}} \quad (5.23)$$

This is a pretty complicated result—all the more complicated when we remember that b involves three algebraic terms [recall eqn. (5.19a)]. Yet the equation is not at all sophisticated. A system involving three capacitances in series would similarly yield a third-order equation of correspondingly higher complexity, and so forth.

5.3   Transient conduction in a one-dimensional slab

We next extend consideration to heat flow in bodies whose internal resistance is significant—to situations in which the lumped capacitance assumption is no longer appropriate. When the temperature within, say, a one-dimensional body varies with position as well time, we must solve the heat conduction equation for $T(x, t)$. We shall do this somewhat complicated task for the simplest case and then look at the results of such calculations for other situations.
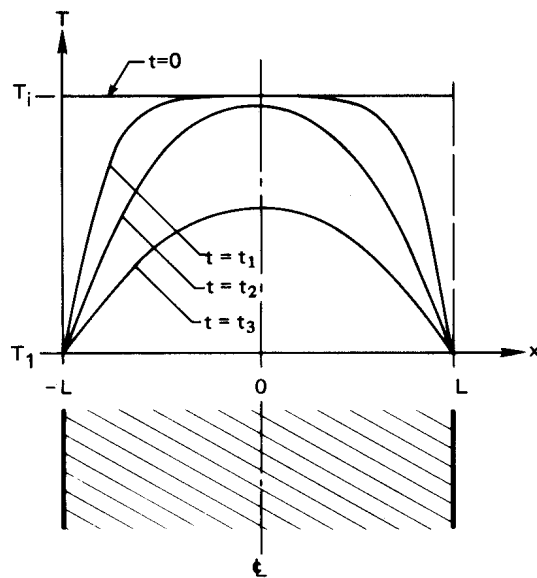
Figure 5.6   The transient cooling of a slab; $\xi = (x/L) + 1$.

A simple slab, shown in Fig. 5.6, is initially at a temperature T_i. The temperature of the surface of the slab is suddenly changed to T_1, and we wish to calculate the interior temperature profile as a function of time. The heat conduction equation is

$$\frac{\partial^2 T}{\partial x^2} = \frac{1}{\alpha} \frac{\partial T}{\partial t} \tag{5.24}$$

with the following b.c.'s and i.c.:

$$T(-L, t > 0) = T(L, t > 0) = T_1 \quad \text{and} \quad T(x, t = 0) = T_i \tag{5.25}$$

In fully dimensionless form, eqn. (5.24) and eqn. (5.25) are

$$\frac{\partial^2 \Theta}{\partial \xi^2} = \frac{\partial \Theta}{\partial \text{Fo}} \tag{5.26}$$

and

$$\Theta(0, \text{Fo}) = \Theta(2, \text{Fo}) = 0 \quad \text{and} \quad \Theta(\xi, 0) = 1 \qquad (5.27)$$

where we have nondimensionalized the problem in accordance with eqn. (5.4), using $\Theta \equiv (T - T_1)/(T_i - T_1)$ and $\text{Fo} \equiv \alpha t / L^2$; but, a more easily usable final result, we have set ξ equal to $(x/L) + 1$ instead of x/L.

The general solution of eqn. (5.26) may be found using the separation of variables technique described in Section 4.2, leading to the dimensionless form of eqn. (4.11):

$$\Theta = e^{-\hat{\lambda}^2 \text{Fo}} \left[G \sin(\hat{\lambda}\xi) + E \cos(\hat{\lambda}\xi) \right] \qquad (5.28)$$

Direct nondimensionalization of eqn. (4.11) would show that $\hat{\lambda} \equiv \lambda L$, since λ had units of (length)$^{-1}$. The solution therefore appears to have introduced a fourth dimensionless group, $\hat{\lambda}$. This needs explanation. The number λ, which was introduced in the separation-of-variables process, is called an *eigenvalue*.[2] In the present problem, $\hat{\lambda} = \lambda L$ will turn out to be a number—or rather a sequence of numbers—that is independent of system parameters.

Substituting the general solution, eqn. (5.28), in the first b.c. gives

$$0 = e^{-\hat{\lambda}^2 \text{Fo}} (0 + E) \quad \text{so} \quad E = 0$$

and substituting it in the second yields

$$0 = e^{-\hat{\lambda}^2 \text{Fo}} [G \sin 2\hat{\lambda}]$$

so either

$$G = 0 \qquad \text{or} \qquad 2\hat{\lambda} = 2\hat{\lambda}_n = n\pi, \text{ for } n = 0, 1, 2, \ldots$$

We then have two choices for the constant G. The first, $G = 0$, would give $\Theta \equiv 0$ in all situations, so that the initial condition could never be accommodated. (This is what mathematicians call a *trivial* solution.) The second choice, $\hat{\lambda}_n = n\pi/2$, actually yields a string of solutions, each of the form

$$\Theta = G_n e^{-n^2 \pi^2 \text{Fo}/4} \sin\left(\frac{n\pi}{2}\xi\right) \qquad (5.29)$$

where G_n is the constant appropriate to the nth one of these solutions.

We still face the problem that none of eqns. (5.29) will fit the initial condition, $\Theta(\xi, 0) = 1$. To get around this, we remember that the sum of

---

[2]The word *eigenvalue* is a curious hybrid of the German term *eigenwert* and its English translation, *characteristic value.*

any number of solutions of a linear differential equation is also a solution. Then we write

$$\Theta = \sum_{n=1}^{\infty} G_n \, e^{-n^2 \pi^2 \text{Fo}/4} \, \sin\left(n\frac{\pi}{2}\xi\right) \tag{5.30}$$

where we drop $n = 0$ since it gives zero contribution to the series. And we arrive, at last, at the problem of choosing the G_n's so that eqn. (5.30) will fit the initial condition:

$$\Theta(\xi, 0) = \sum_{n=1}^{\infty} G_n \sin\left(n\frac{\pi}{2}\xi\right) = 1 \tag{5.31}$$

The problem of picking the values of G_n that will make this equation true is called "making a Fourier series expansion" of the function $f(\xi) = 1$. We shall not pursue strategies for making Fourier series expansions in any general way. Instead, we merely show how to accomplish the task for the particular problem at hand. We begin with a mathematical trick. We multiply eqn. (5.31) by $\sin(m\pi/2)$, where m may or may not equal n, and we integrate the result between $\xi = 0$ and 2.

$$\int_0^2 \sin\left(\frac{m\pi}{2}\xi\right) d\xi = \sum_{n=1}^{\infty} G_n \int_0^2 \sin\left(\frac{m\pi}{2}\xi\right) \sin\left(\frac{n\pi}{2}\xi\right) d\xi \tag{5.32}$$

(The interchange of summation and integration turns out to be legitimate, although we have not proved here that it is.[3]) With the help of a table of integrals, we find that

$$\int_0^2 \sin\left(\frac{m\pi}{2}\xi\right) \sin\left(\frac{n\pi}{2}\xi\right) d\xi = \begin{cases} 0 & \text{for } n \neq m \\ 1 & \text{for } n = m \end{cases}$$

Thus, when we complete the integration of eqn. (5.32), we get

$$-\frac{2}{m\pi} \cos\left(\frac{m\pi}{2}\xi\right)\Big|_0^2 = \sum_{n=1}^{\infty} G_n \times \begin{cases} 0 & \text{for } n \neq m \\ 1 & \text{for } n = m \end{cases}$$

This reduces to

$$-\frac{2}{m\pi}\left[(-1)^n - 1\right] = G_n$$

so

$$G_n = \frac{4}{n\pi} \quad \text{where } n \text{ is an odd number}$$

---

[3]What is normally required is that the series in eqn. (5.31) be *uniformly convergent.*

Table 5.1 Terms of series solutions for slabs, cylinders, and spheres. J_0 and J_1 are Bessel functions of the first kind.

	A_n	f_n	Equation for $\hat{\lambda}_n$
Slab	$\dfrac{2\sin\hat{\lambda}_n}{\hat{\lambda}_n + \sin\hat{\lambda}_n \cos\hat{\lambda}_n}$	$\cos\left(\hat{\lambda}_n \dfrac{x}{L}\right)$	$\cot\hat{\lambda}_n = \dfrac{\hat{\lambda}_n}{\mathrm{Bi}_L}$
Cylinder	$\dfrac{2\,J_1(\hat{\lambda}_n)}{\hat{\lambda}_n\left[J_0^2(\hat{\lambda}_n) + J_1^2(\hat{\lambda}_n)\right]}$	$J_0\left(\hat{\lambda}_n \dfrac{r}{r_o}\right)$	$\hat{\lambda}_n J_1(\hat{\lambda}_n) = \mathrm{Bi}_{r_o} J_0(\hat{\lambda}_n)$
Sphere	$2\,\dfrac{\sin\hat{\lambda}_n - \hat{\lambda}_n \cos\hat{\lambda}_n}{\hat{\lambda}_n - \sin\hat{\lambda}_n \cos\hat{\lambda}_n}$	$\left(\dfrac{r_o}{\hat{\lambda}_n r}\right)\sin\left(\dfrac{\hat{\lambda}_n r}{r_o}\right)$	$\hat{\lambda}_n \cot\hat{\lambda}_n = 1 - \mathrm{Bi}_{r_o}$

Substituting this result into eqn. (5.30), we finally obtain the solution to the problem:

$$\Theta(\xi, \mathrm{Fo}) = \frac{4}{\pi} \sum_{n=\mathrm{odd}}^{\infty} \frac{1}{n}\, e^{-(n\pi/2)^2 \mathrm{Fo}}\, \sin\left(\frac{n\pi}{2}\xi\right) \tag{5.33}$$

Equation (5.33) admits a very nice simplification for large time (or at large Fo). Suppose that we wish to evaluate Θ at the center of the slab—at $x = 0$ or $\xi = 1$. Then

$$\Theta(0, \mathrm{Fo}) = \frac{4}{\pi} \times$$

$$\left\{ \underbrace{\exp\left[-\left(\frac{\pi}{2}\right)^2 \mathrm{Fo}\right]}_{\substack{= 0.085 \text{ at Fo} = 1 \\ = 0.781 \text{ at Fo} = 0.1 \\ = 0.976 \text{ at Fo} = 0.01}} - \frac{1}{3}\underbrace{\exp\left[-\left(\frac{3\pi}{2}\right)^2 \mathrm{Fo}\right]}_{\substack{\simeq 10^{-10} \text{ at Fo} = 1 \\ = 0.036 \text{ at Fo} = 0.1 \\ = 0.267 \text{ at Fo} = 0.01}} + \frac{1}{5}\underbrace{\exp\left[-\left(\frac{5\pi}{2}\right)^2 \mathrm{Fo}\right]}_{\substack{\simeq 10^{-27} \text{ at Fo} = 1 \\ = 0.0004 \text{ at Fo} = 0.1 \\ = 0.108 \text{ at Fo} = 0.01}} + \cdots \right\}$$

Thus, for values of Fo somewhat greater than 0.1, only the first term in the series makes a non-negligible contribution to the solution. We discuss these one-term solutions in Section 5.5. But first, let us see what happens if the slab had been subjected to b.c.'s of the third kind.

Suppose that the walls of the slab had been cooled by symmetrical convection such that the b.c.'s were

$$\overline{h}(T_\infty - T)_{x=-L} = -k\frac{\partial T}{\partial x}\bigg|_{x=-L} \quad \text{and} \quad \overline{h}(T - T_\infty)_{x=L} = -k\frac{\partial T}{\partial x}\bigg|_{x=L}$$

or in dimensionless form, using Θ and ξ as before and setting $\text{Bi} = \overline{h}L/k$,

$$-\Theta\Big|_{\xi=0} = -\frac{1}{\text{Bi}} \frac{\partial \Theta}{\partial \xi}\Big|_{\xi=0} \quad \text{and} \quad \frac{\partial \Theta}{\partial \xi}\Big|_{\xi=1} = 0$$

The solution is somewhat harder to find than eqn. (5.33) was, but the result is[4]

$$\Theta = \sum_{n=1}^{\infty} \exp\left(-\hat{\lambda}_n^2 \, \text{Fo}\right) \left(\frac{2\sin\hat{\lambda}_n \cos[\hat{\lambda}_n(\xi-1)]}{\hat{\lambda}_n + \sin\hat{\lambda}_n \cos\hat{\lambda}_n}\right) \tag{5.34}$$

where the values of $\hat{\lambda}_n$ are given as a function of n and $\text{Bi} = \overline{h}L/k$ by the transcendental equation

$$\cot\hat{\lambda}_n = \frac{\hat{\lambda}_n}{\text{Bi}} \tag{5.35}$$

The successive positive roots of this equation, $\hat{\lambda}_n = \hat{\lambda}_1, \hat{\lambda}_2, \hat{\lambda}_3, \ldots$, depend upon Bi. Thus, $\Theta = \text{fn}(\xi, \text{Fo}, \text{Bi})$, as we would expect. This result, although more complicated than the result for b.c.'s of the first kind, still reduces to a single term for $\text{Fo} \gtrsim 0.2$.

Similar series solutions can be constructed for cylinders and spheres that are convectively cooled at their outer surface, $r = r_o$. The solutions for slab, cylinders, and spheres all have the form

$$\Theta = \frac{T - T_\infty}{T_i - T_\infty} = \sum_{n=1}^{\infty} A_n \exp\left(-\hat{\lambda}_n^2 \, \text{Fo}\right) f_n \tag{5.36}$$

where the coefficients A_n, the functions f_n, and the equations for the dimensionless eigenvalues $\hat{\lambda}_n$ are given in Table 5.1.

5.4 Temperature-response charts

Methods of solution like those in Section 5.3 were once the norm in solving heat conduction problems. Today, direct numerical solution of the differential equations has largely replaced series methods for problems of any complexity. Available software requires little more than inputting the shape, boundary and initial conditions, and material properties. The series solutions, however, lead to certain simplified

---

[4]See, for example, [5.1, §2.3.4] or [5.2, §3.4.3] for details of this calculation.

equations and to graphical representations which are often far easier to use than software. Graphs also reveal much about the behavior of heat conduction in simple configurations.

Such graphs can take many forms. We offer Figs. 5.7, 5.8, and 5.9 as forms we deem most useful. They are for slabs cooled or heated on one side and insulated on the other, for infinitely long cylinders cooled or heated on the outside, and for spheres heated or cooled on the outside. In each chart, the temperature Θ is given as a function of the Biot number at different values of the Fourier number (the dimensionless time). Each set of curves is for four positions within the body.

Notice some features common to all these sets of curves:

- For a given Biot number and position, Θ decreases from the initial value of one, toward a final value of zero as Fo increases. For Bi > 1, the heat transfer process is effectively finished by the time Fo reaches 1 to 2, depending on the shape of the body.

- The rate of cooling or heating increases with increasing Bi since the external thermal resistance is lower.

- When Bi is on the order of 0.1 or less, the internal temperature is nearly the same at all positions within the body: internal temperature gradients are negligible because the external resistance dominates. This is pure *lumped-capacity* behavior, and the simple lumped capacity solution eqn. (1.22) can be used instead of the series solutions.

- As mentioned in Section 5.3, when Fo $\gtrsim$ 0.2, only the first term of either eqn. (5.34) or (5.36) is important. We can then have a very simple equation for Θ, which we will discuss in Section 5.5.

- For small values of Fo (very short times after the transient begins), the center of the body remains close to $\Theta = 1$ (negligible temperature change) especially when Bi is not very large. In fact, for the sphere, $\Theta > 0.965$ for all Bi when Fo $\leq$ 0.05. Cases like this are best analyzed using the semi-infinite body solutions to be discussed in Section 5.6 [especially eqn. (5.53)].

Figures 5.7, 5.8, and 5.9 are of greatest value for doing calculations in the ranges $0.05 \lesssim$ Fo $\lesssim 0.2$ and Bi $\gtrsim 0.1$, where simplifications of the series solutions do not apply. They can also be used to quickly read an approximate value in other ranges.
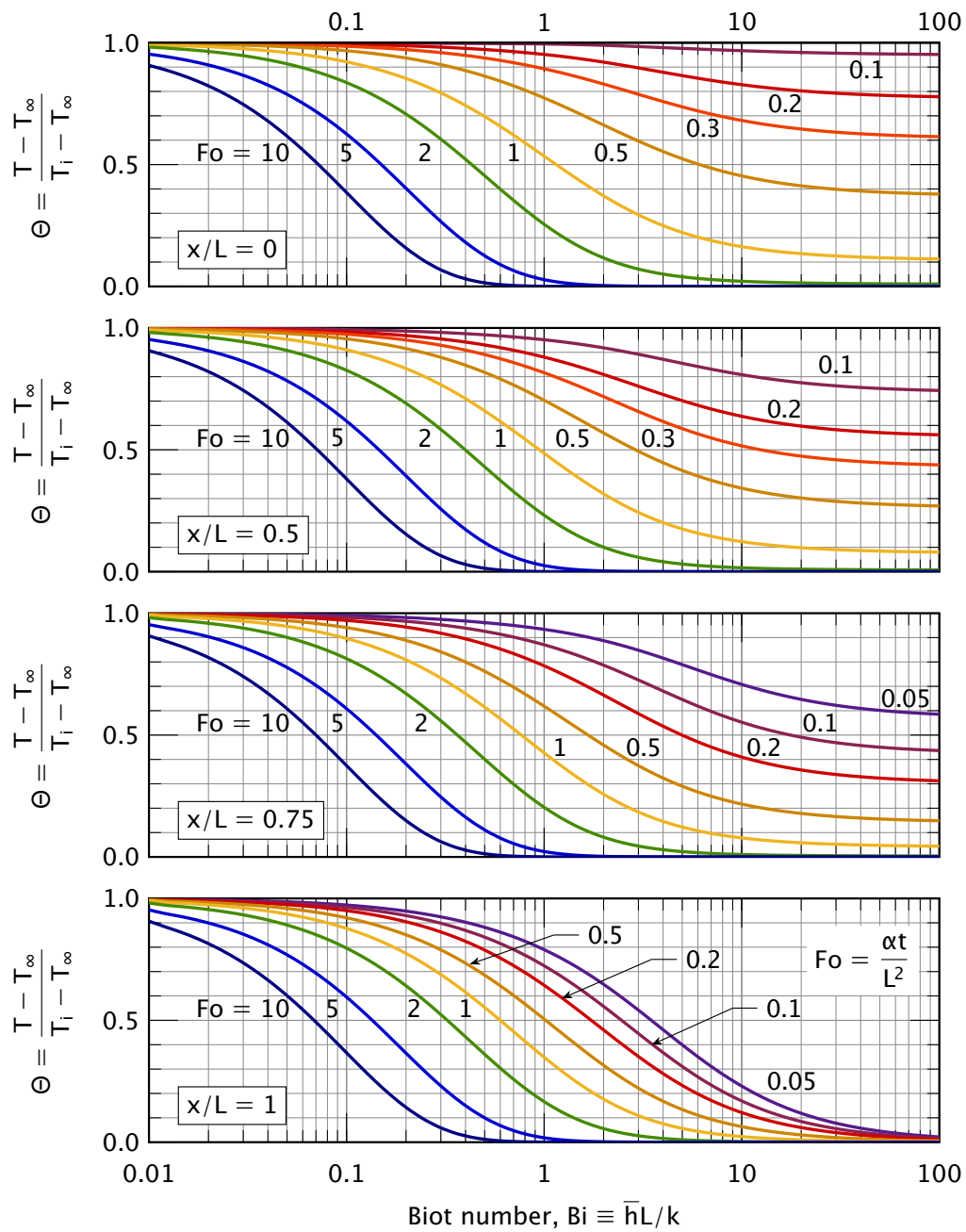
Figure 5.7 The transient temperature distribution in a *slab* at four positions: $x/L = 0$ is the center, $x/L = 1$ is one outside boundary.
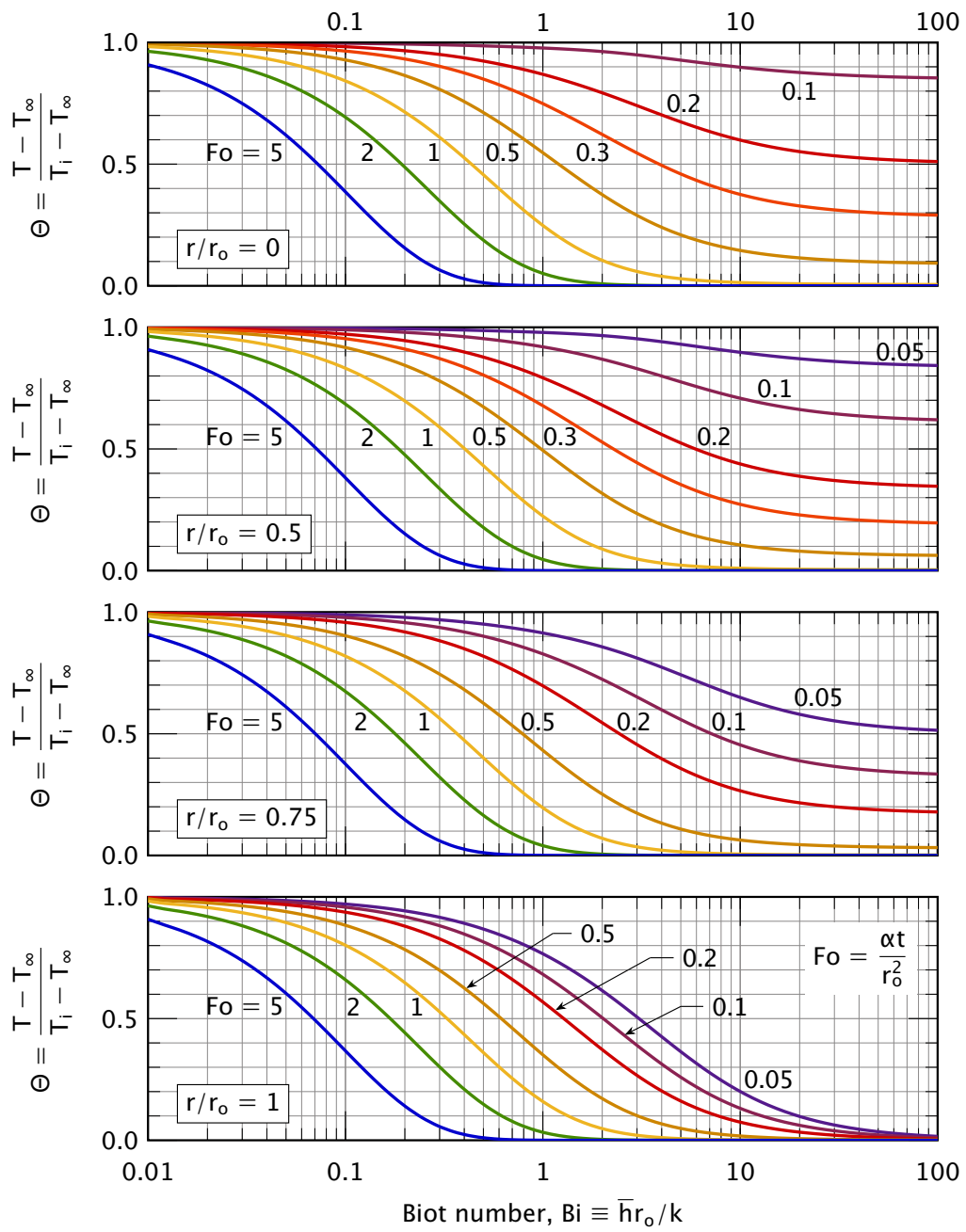
Figure 5.8 The transient temperature distribution in a long *cylinder* of radius r_o at four positions: $r/r_o = 0$ is the centerline; $r/r_o = 1$ is the outside boundary.
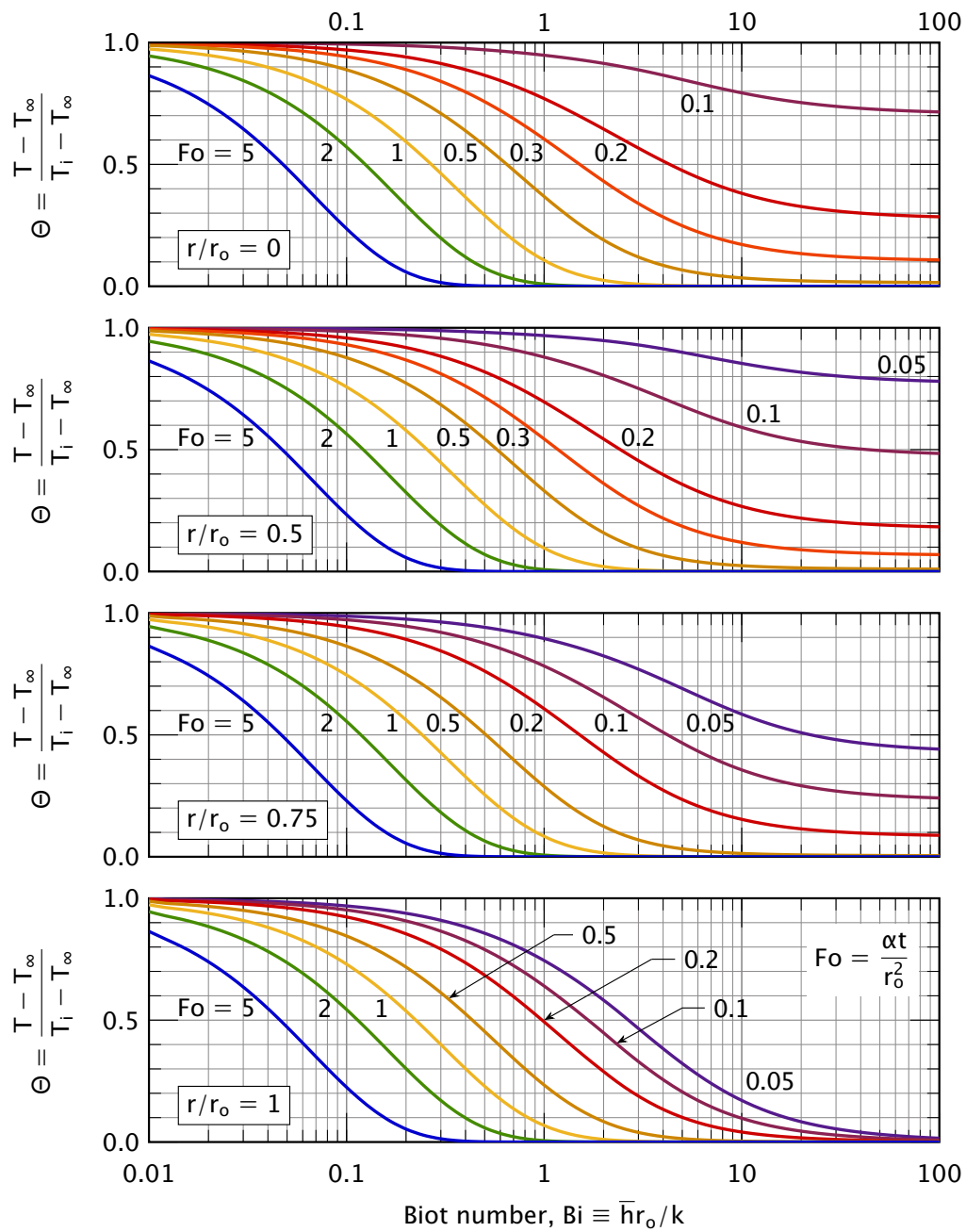
Figure 5.9 The transient temperature distribution in a *sphere* of radius r_o at four positions: $r/r_o = 0$ is the center; $r/r_o = 1$ is the outside boundary.

Figures 5.7, 5.8, and 5.9 are the authors' original work. However, various temperature response charts are often called by the generic name *Heisler charts*, after charts published by Heisler in 1947 [5.3].

Another useful chart derivable from eqn. (5.34) gives the heat removal from a body up to a time of interest:

$$\int_0^t Q \, dt = -\int_0^t kA \left.\frac{\partial T}{\partial x}\right|_{\text{surface}} dt$$

$$= -\int_0^{\text{Fo}} kA \frac{(T_i - T_\infty)}{L} \left.\frac{\partial \Theta}{\partial \xi}\right|_{\text{surface}} \left(\frac{L^2}{\alpha}\right) d\text{Fo}$$

Dividing this integral by the internal energy of the body relative to T_∞, we get a quantity Φ that approaches one as $t \longrightarrow \infty$, when all the energy has been transferred to the surroundings:

$$\Phi \equiv \frac{\int_0^t Q \, dt}{\rho c V (T_i - T_\infty)} = -\int_0^{\text{Fo}} \left.\frac{\partial \Theta}{\partial \xi}\right|_{\text{surface}} d\text{Fo} \tag{5.37}$$

For a slab, the volume is $V = AL$. Substituting the appropriate temperature distribution [e.g., eqn. (5.34) for a slab] into eqn. (5.37), we obtain Φ as an infinite series

$$\Phi(\text{Fo, Bi}) = 1 - \sum_{n=1}^{\infty} D_n \exp\left(-\hat{\lambda}_n^2 \, \text{Fo}\right) \tag{5.38}$$

The coefficients D_n are functions of $\hat{\lambda}_n$—and thus of Bi—for slabs, cylinders, and spheres (e.g., for a slab $D_n = A_n \sin \hat{\lambda}_n / \hat{\lambda}_n$). These functions can be used to plot $\Phi(\text{Fo, Bi})$ once and for all. Such curves are given in Fig. 5.10.

The quantity Φ has a close relationship to the mean temperature of a body at any time, $\overline{T}(t)$. Specifically, the internal energy lost as heat by time t determines the difference between the initial temperature and the mean temperature at time t

$$\int_0^t Q \, dt = [U(0) - U(t)] = \rho c V \left[T_i - \overline{T}(t)\right] \tag{5.39}$$

Thus, we find the relationship of $\overline{T}(t)$ to Φ, defining $\overline{\Theta}$ as shown:

$$\overline{\Theta} \equiv \frac{\overline{T}(t) - T_\infty}{T_i - T_\infty} = 1 - \frac{\int_0^t Q(t) \, dt}{\rho c V (T_i - T_\infty)} = 1 - \Phi \tag{5.40}$$
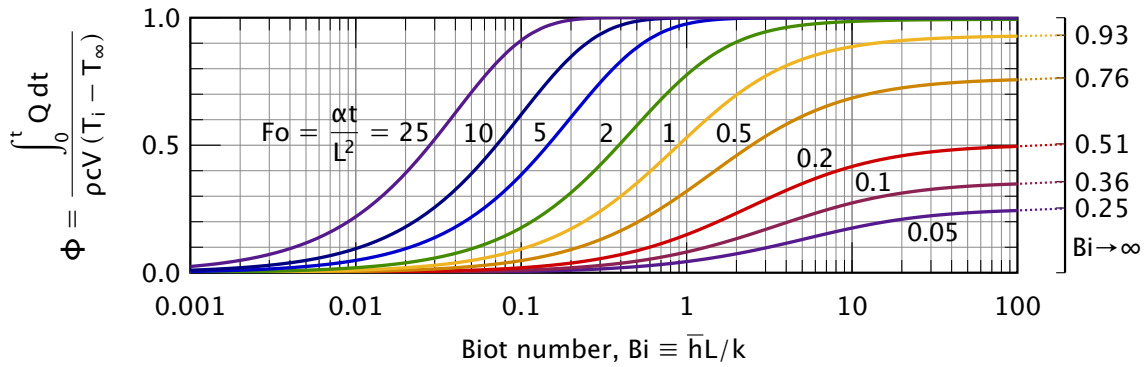
a. *Slab* of thickness L and any area, cooled on one side and insulated on the other
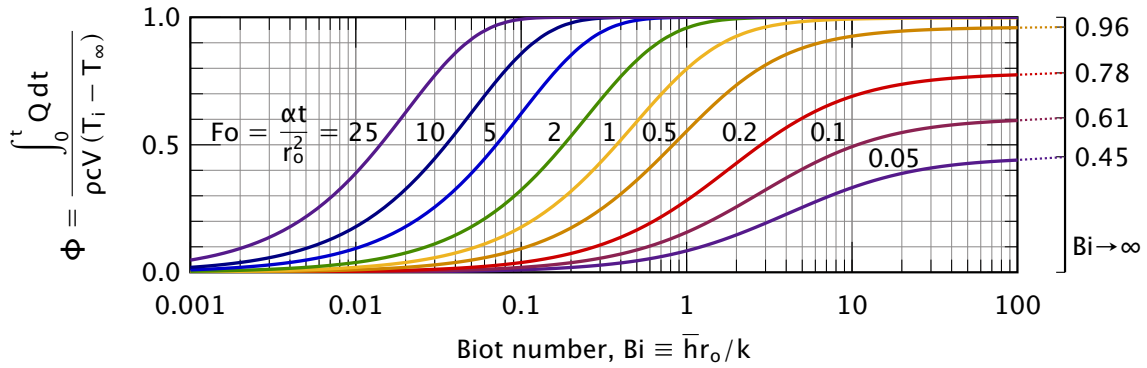
b. *Cylinder* of radius r_o either infinite or insulated on both ends, and cooled on its surface
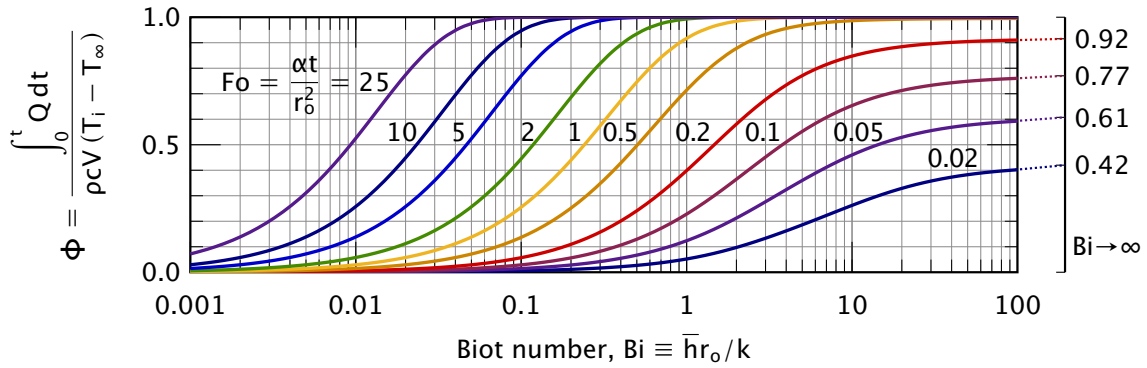
c. *Sphere* of radius r_o

Figure 5.10 The heat removal from suddenly-cooled bodies as a function of $\overline{h}$ and time.

213

Example 5.2

A dozen approximately spherical apples, 10 cm in diameter are taken from a 30°C environment and laid out on a rack in a refrigerator at 5°C. They have approximately the same physical properties as water, and $\overline{h}$ is approximately 6 W/m²K as the result of natural convection. What will be the temperature of the centers of the apples after 1 hr? How long will it take to bring the centers to 10°C? How much heat will the refrigerator have to carry away to get the centers to 10°C?

SOLUTION. After 1 hr, or 3600 s:

$$
\begin{aligned}
\text{Fo} = \frac{\alpha t}{r_o^2} &= \left(\frac{k}{\rho c} \right)_{20°C} \frac{3600 \text{ s}}{(0.05 \text{ m})^2} \\
&= \frac{(0.603 \text{ J/s·m·K})(3600 \text{ s})}{(997.6 \text{ kg/m}^3)(4180 \text{ J/kg·K})(0.0025 \text{ m}^2)} = 0.208
\end{aligned}
$$

Furthermore, $\text{Bi} = (\overline{h}r_o/k) = 6(0.05)/0.603 = 0.498 \approx 0.5$. Therefore, we read from Fig. 5.9 in the upper middle:

$$\Theta \approx 0.84$$

After 1 hr:

$$T_{\text{center}} = 0.84(30 - 5)°C + 5°C = 26.0°C$$

To find the time to bring the center to 10°C, we first calculate

$$\Theta = \frac{10 - 5}{30 - 5} = 0.2$$

and Bi is still 0.5. Then from Fig. 5.9 we read

$$\text{Fo} \approx 1.3 = \frac{\alpha t}{r_o^2}$$

so

$$t = \frac{1.3(997.6)(4180)(0.0025)}{0.603} = 22,475 \text{ s} = 6 \text{ hr } 15 \text{ min}$$

Finally, we look up Φ at $\text{Bi} = 0.5$ and $\text{Fo} = 1.3$ in Fig. 5.10, for spheres:

$$\Phi \approx 0.82 = \frac{\displaystyle\int_0^t Q \, dt}{\rho c \left(\frac{4}{3}\pi r_0^3 \right) (T_i - T_\infty)}$$

so

$$\int_0^t Q\, dt = 997.6(4180)\left(\frac{4}{3}\pi(0.05)^3\right)(25)(0.82) = 44{,}760 \text{ J/apple}$$

Therefore, for the 12 apples,

$$\text{total energy removal} = 12(44.76) = 537 \text{ kJ} \qquad\blacksquare$$

The temperature-response charts in Fig. 5.7 through Fig. 5.10 without a doubt cover the most useful configurations. And they can be adapted to still more physical situations. Beyond these charts, hundreds of additional charts have been drawn for other cases; see, for example, Schneider's [5.4] catalog of such charts. Analytical solutions, including many other series results, are available for thousands more problems, and any reader faced with a complex heat conduction calculation would do well consult the literature before trying to solve it. An excellent starting point is Carslaw and Jaeger's comprehensive treatise on heat conduction [5.5].

Example 5.3

We use a 1 mm diameter Nichrome (20% Ni, 80% Cr) wire, immersed in liquid, both as an electrical resistance heater and as a resistance thermometer. We wish to measure the boiling heat transfer coefficient, $\overline{h}$, by supplying an alternating current and measuring the difference between the liquid temperature, T_∞, and the average heater temperature, T_{av}. We get $\overline{h} = 30{,}000$ W/m^{2}K at a wire temperature of $100°$C and are delighted with such a high value. Then a colleague suggests that $\overline{h}$ is so high because the surface temperature is rapidly oscillating as a result of the alternating current. Is this hypothesis correct?

SOLUTION. Heat is being generated in proportion to the product of voltage and current, or as $\sin^2 \omega t$, where ω is the frequency of the current in rad/s. If the boiling action removes heat rapidly enough in comparison with the heat capacity of the wire, the surface temperature may well vary significantly. This transient conduction problem was first solved by Jeglic in 1962 [5.6]. It was redone in a different form two years later by Switzer and Lienhard (see, e.g. [5.7]), who gave response curves in the form

$$\frac{T_{\max} - T_{av}}{T_{av} - T_\infty} = \text{fn}(\text{Bi}, \psi) \qquad (5.41)$$

where the left-hand side is the dimensionless range of the temperature oscillation, and $\psi = \omega\delta^2/\alpha$, where δ is a characteristic length [see Problem 5.56]. Because this problem is common and the solution is not widely available, we include the curves for flat plates and cylinders in Figs. 5.11 and 5.12, respectively, on pages 217 and 218.

In the present case:

$$\text{Bi} = \frac{\overline{h}\,\text{radius}}{k} = \frac{30,000(0.0005)}{13.8} = 1.09$$

$$\frac{\omega r^2}{\alpha} = \frac{[2\pi(60)](0.0005)^2}{0.00000343} = 27.5$$

and from the chart for cylinders, Fig. 5.12, we find that

$$\frac{T_{\max} - T_{\text{av}}}{T_{\text{av}} - T_\infty} \simeq 0.04$$

A temperature fluctuation of only 4% is probably not serious. The experiment appears to have been valid. ∎

5.5 One-term solutions

We have noted previously that when the Fourier number is greater than 0.2 or so, the series solutions from eqn. (5.36) may be approximated using only the first term:

$$\Theta \approx A_1 \cdot f_1 \cdot \exp\left(-\hat{\lambda}_1^2\,\text{Fo}\right). \tag{5.42}$$

Likewise, the fractional heat loss, Φ, or the mean temperature $\overline{\Theta}$ from eqn. (5.40), can be approximated using just the first term of eqn. (5.38):

$$\overline{\Theta} = 1 - \Phi \approx D_1 \exp\left(-\hat{\lambda}_1^2\,\text{Fo}\right). \tag{5.43}$$

Table 5.2 lists the values of $\hat{\lambda}_1$, A_1, and D_1 for slabs, cylinders, and spheres as a function of the Biot number. The one-term solution's error in Θ is less than 0.1% for a sphere with Fo ≥ 0.28 and for a slab with Fo ≥ 0.43. These errors are largest for Biot numbers near one. If high accuracy is not required, the one-term solutions may be used whenever Fo ≥ 0.2.

Ostrogorsky [5.8] has provided simple correlations for $\hat{\lambda}_1$, A_1, and D_1, as well as two and three term solutions accurate for Fo $\gtrsim 0.05$ [5.9]. These solutions are convenient for numerical work—in fact, we used those results to compute Figs. 5.7–5.10.

To appreciate the greater precision possible with the one-term solutions, the reader should repeat Example 5.2 using them (Problem 5.57).
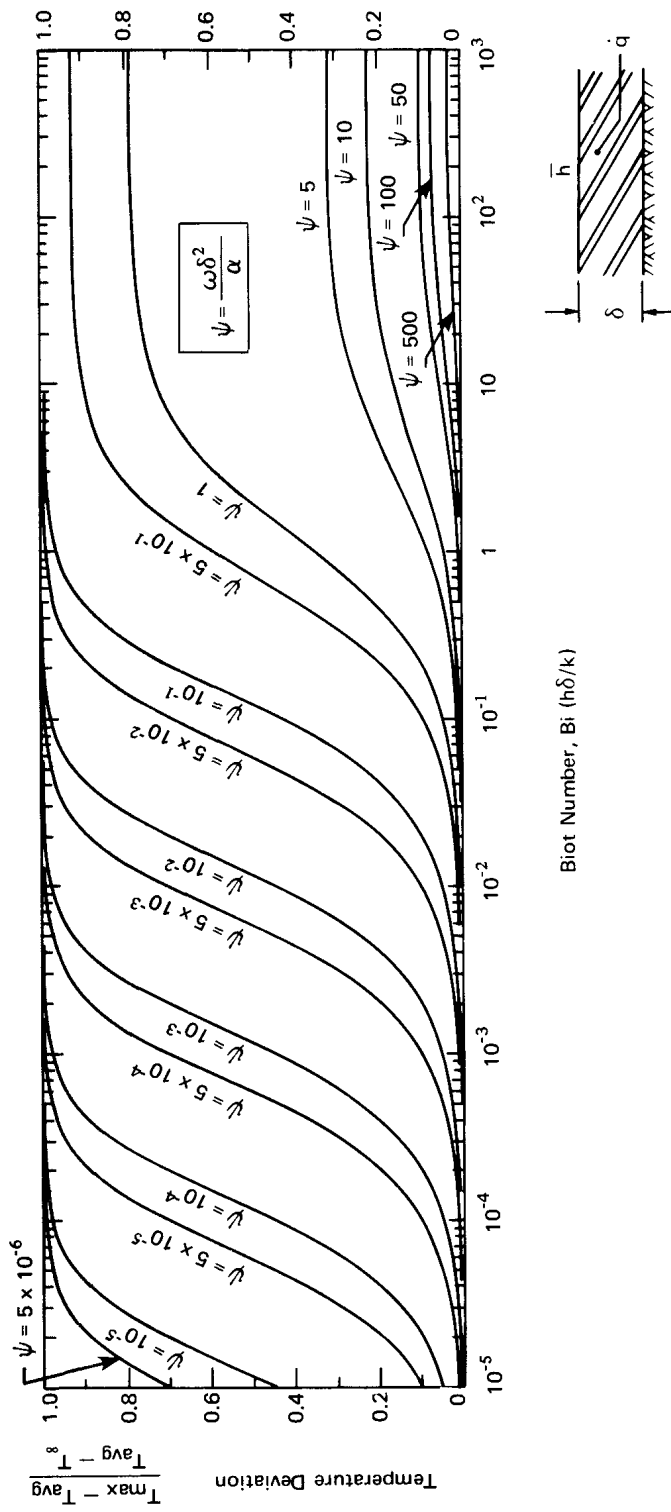
Figure 5.11: Temperature deviation at the surface of a *flat plate* heated with alternating current.
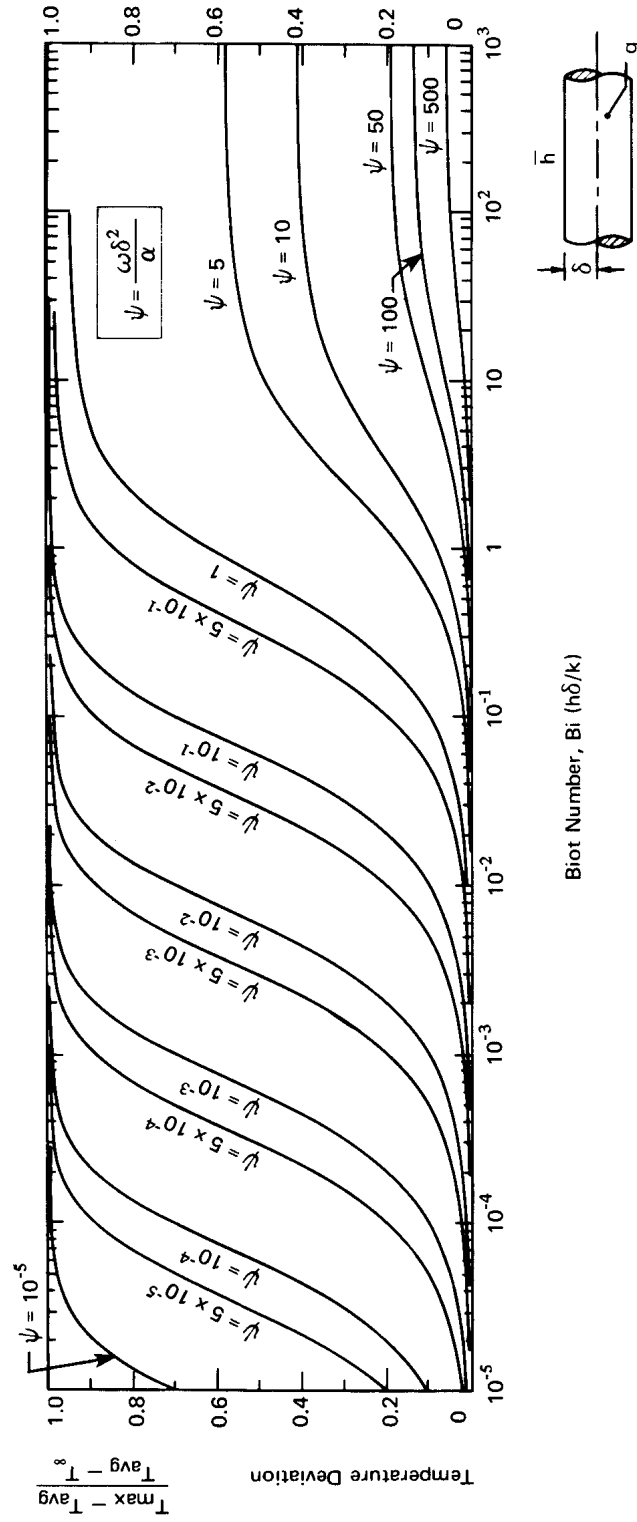
217

Figure 5.12: Temperature deviation at the surface of a *cylinder* heated with alternating current.

218

Table 5.2 One-term coefficients for transient conduction with surface convection [5.1].

Bi	Slab			Cylinder			Sphere		
	$\hat{\lambda}_1$	A_1	D_1	$\hat{\lambda}_1$	A_1	D_1	$\hat{\lambda}_1$	A_1	D_1
0.01	0.09983	1.0017	1.0000	0.14124	1.0025	1.0000	0.17303	1.0030	1.0000
0.02	0.14095	1.0033	1.0000	0.19950	1.0050	1.0000	0.24446	1.0060	1.0000
0.03	0.17234	1.0049	1.0000	0.24403	1.0075	1.0000	0.29910	1.0090	1.0000
0.04	0.19868	1.0066	1.0000	0.28143	1.0099	1.0000	0.34503	1.0120	1.0000
0.05	0.22176	1.0082	0.9999	0.31426	1.0124	0.9999	0.38537	1.0150	1.0000
0.06	0.24253	1.0098	0.9999	0.34383	1.0148	0.9999	0.42173	1.0179	0.9999
0.07	0.26153	1.0114	0.9999	0.37092	1.0173	0.9999	0.45506	1.0209	0.9999
0.08	0.27913	1.0130	0.9999	0.39603	1.0197	0.9999	0.48600	1.0239	0.9999
0.09	0.29557	1.0145	0.9998	0.41954	1.0222	0.9998	0.51497	1.0268	0.9999
0.10	0.31105	1.0161	0.9998	0.44168	1.0246	0.9998	0.54228	1.0298	0.9998
0.15	0.37788	1.0237	0.9995	0.53761	1.0365	0.9995	0.66086	1.0445	0.9996
0.20	0.43284	1.0311	0.9992	0.61697	1.0483	0.9992	0.75931	1.0592	0.9993
0.25	0.48009	1.0382	0.9988	0.68559	1.0598	0.9988	0.84473	1.0737	0.9990
0.30	0.52179	1.0450	0.9983	0.74646	1.0712	0.9983	0.92079	1.0880	0.9985
0.40	0.59324	1.0580	0.9971	0.85158	1.0931	0.9970	1.05279	1.1164	0.9974
0.50	0.65327	1.0701	0.9956	0.94077	1.1143	0.9954	1.16556	1.1441	0.9960
0.60	0.70507	1.0814	0.9940	1.01844	1.1345	0.9936	1.26440	1.1713	0.9944
0.70	0.75056	1.0918	0.9922	1.08725	1.1539	0.9916	1.35252	1.1978	0.9925
0.80	0.79103	1.1016	0.9903	1.14897	1.1724	0.9893	1.43203	1.2236	0.9904
0.90	0.82740	1.1107	0.9882	1.20484	1.1902	0.9869	1.50442	1.2488	0.9880
1.00	0.86033	1.1191	0.9861	1.25578	1.2071	0.9843	1.57080	1.2732	0.9855
1.10	0.89035	1.1270	0.9839	1.30251	1.2232	0.9815	1.63199	1.2970	0.9828
1.20	0.91785	1.1344	0.9817	1.34558	1.2387	0.9787	1.68868	1.3201	0.9800
1.30	0.94316	1.1412	0.9794	1.38543	1.2533	0.9757	1.74140	1.3424	0.9770
1.40	0.96655	1.1477	0.9771	1.42246	1.2673	0.9727	1.79058	1.3640	0.9739
1.50	0.98824	1.1537	0.9748	1.45695	1.2807	0.9696	1.83660	1.3850	0.9707
1.60	1.00842	1.1593	0.9726	1.48917	1.2934	0.9665	1.87976	1.4052	0.9674
1.80	1.04486	1.1695	0.9680	1.54769	1.3170	0.9601	1.95857	1.4436	0.9605
2.00	1.07687	1.1785	0.9635	1.59945	1.3384	0.9537	2.02876	1.4793	0.9534
2.20	1.10524	1.1864	0.9592	1.64557	1.3578	0.9472	2.09166	1.5125	0.9462
2.40	1.13056	1.1934	0.9549	1.68691	1.3754	0.9408	2.14834	1.5433	0.9389
3.00	1.19246	1.2102	0.9431	1.78866	1.4191	0.9224	2.28893	1.6227	0.9171
4.00	1.26459	1.2287	0.9264	1.90808	1.4698	0.8950	2.45564	1.7202	0.8830
5.00	1.31384	1.2402	0.9130	1.98981	1.5029	0.8721	2.57043	1.7870	0.8533
6.00	1.34955	1.2479	0.9021	2.04901	1.5253	0.8532	2.65366	1.8338	0.8281
8.00	1.39782	1.2570	0.8858	2.12864	1.5526	0.8244	2.76536	1.8920	0.7889
10.00	1.42887	1.2620	0.8743	2.17950	1.5677	0.8039	2.83630	1.9249	0.7607
20.00	1.49613	1.2699	0.8464	2.28805	1.5919	0.7542	2.98572	1.9781	0.6922
50.00	1.54001	1.2727	0.8260	2.35724	1.6002	0.7183	3.07884	1.9962	0.6434
100.00	1.55525	1.2731	0.8185	2.38090	1.6015	0.7052	3.11019	1.9990	0.6259
∞	1.57080	1.2732	0.8106	2.40483	1.6020	0.6917	3.14159	2.0000	0.6079

5.6 Transient heat conduction to a semi-infinite region

Introduction

Bronowksi's classic television series, *The Ascent of Man* [5.10], included a brilliant reenactment of the ancient ceremonial procedure by which the Japanese forged Samurai swords (see Fig. 5.13). The metal is heated, folded, beaten, and formed, over and over, to create a blade of remarkable toughness and flexibility. When the blade is formed to its final configuration, a tapered sheath of clay is baked on the outside of it, so the cross section is as shown in Fig. 5.13. The red-hot blade with the clay sheath is then subjected to a rapid quenching, which cools the uninsulated cutting edge quickly and the back part of the blade very slowly. The result is a layer of case-hardening that makes the blade very hard at the edge and more flexible at points farther from the edge.

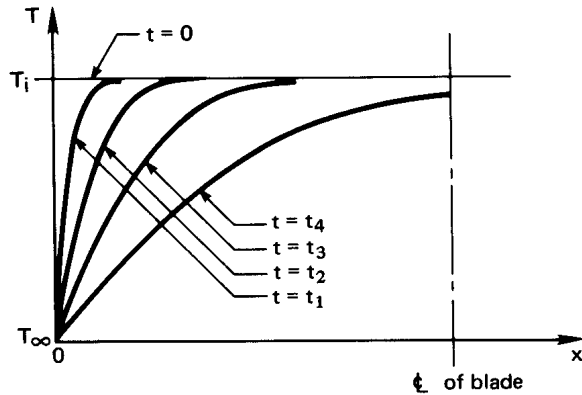Figure 5.13 The ceremonial case-hardening of a Samurai sword.

Figure 5.14   The initial cooling of a thin sword blade. Prior to $t = t_4$, the blade might as well be infinitely thick insofar as cooling is concerned.

The blade is then tough and ductile, so it will not break, but has a fine hard outer shell that can be honed to sharpness. We need only look a little way up the side of the clay sheath to find a cross section that was thick enough to prevent the blade from experiencing the sudden effects of the cooling quench. The success of the process actually relies on the *failure* of the cooling to penetrate the clay very deeply in a short time.

So we need to ask, "Is a particular heating or cooling restricted to the surface of a body?" or, turning the question around, "Under what conditions can we view the depth of a body as *infinite* with respect to the thickness of the region that has felt the heat transfer process?"

First let us answer this question in the case where a finite body is exposed to a sudden temperature change—no clay retardant or even a heat transfer coefficient—just a sudden change of surface temperature. The temperature distribution, in this case, is sketched in Fig. 5.14 for four sequential times. Only the fourth curve—that for which $t = t_4$—is noticeably influenced by the opposite wall. Up to that time, the wall might as well have infinite depth.

Since any body subjected to a sudden change of temperature is infinitely large in comparison with the initial region of temperature change, we must learn how to treat heat transfer during this initial period.

Solution aided by dimensional analysis

The calculation of the temperature distribution in a semi-infinite region poses a difficulty: we can impose a definite b.c. at only one position—the exposed boundary. We get around that difficulty in a nice way with the help of dimensional analysis.

When the one boundary of a semi-infinite region, initially at $T = T_i$, is suddenly cooled (or heated) to a new temperature, T_∞, as in Fig. 5.14, the dimensional function equation is

$$T - T_\infty = \text{fn}[t, x, \alpha, (T_i - T_\infty)]$$

which has *no characteristic length or time.* Since there are five variables in K, m, and s, we should look for two nondimensional groups:

$$\underbrace{\frac{T - T_\infty}{T_i - T_\infty}}_{\equiv \Theta} = \text{fn}\left(\underbrace{\frac{x}{\sqrt{\alpha t}}}_{\equiv \zeta} \right) \tag{5.44}$$

The very important thing that we learn from this exercise in dimensional analysis is that position and time collapse into one independent variable. This means that the heat conduction equation and its b.c.s must transform from a partial differential equation into a simpler ordinary differential equation in the single variable, $\zeta = x/\sqrt{\alpha t}$. Thus, we transform each side of

$$\frac{\partial^2 T}{\partial x^2} = \frac{1}{\alpha} \frac{\partial T}{\partial t}$$

as follows, where we set $\Delta T \equiv T_i - T_\infty$:

$$\frac{\partial T}{\partial t} = (T_i - T_\infty) \frac{\partial \Theta}{\partial t} = \Delta T \frac{\partial \Theta}{\partial \zeta} \frac{\partial \zeta}{\partial t} = \Delta T \left(-\frac{x}{2t\sqrt{\alpha t}} \right) \frac{\partial \Theta}{\partial \zeta};$$

$$\frac{\partial T}{\partial x} = \Delta T \frac{\partial \Theta}{\partial \zeta} \frac{\partial \zeta}{\partial x} = \frac{\Delta T}{\sqrt{\alpha t}} \frac{\partial \Theta}{\partial \zeta};$$

$$\text{and} \quad \frac{\partial^2 T}{\partial x^2} = \frac{\Delta T}{\sqrt{\alpha t}} \frac{\partial^2 \Theta}{\partial \zeta^2} \frac{\partial \zeta}{\partial x} = \frac{\Delta T}{\alpha t} \frac{\partial^2 \Theta}{\partial \zeta^2}.$$

Substituting the first and last of these derivatives in the heat conduction equation, we get the ordinary differential equation

$$\frac{d^2 \Theta}{d\zeta^2} = -\frac{\zeta}{2} \frac{d\Theta}{d\zeta} \tag{5.45}$$

Notice that we changed from partial to total derivative notation since Θ now depends solely on ζ. The i.c. for eqn. (5.45) is

$$T(t = 0) = T_i \quad \text{or} \quad \Theta(\zeta \to \infty) = 1 \tag{5.46}$$

and the one known b.c. is

$$T(x = 0) = T_\infty \quad \text{or} \quad \Theta(\zeta = 0) = 0 \tag{5.47}$$

If we denote $d\Theta/d\zeta$ as χ, then eqn. (5.45) becomes the first-order equation

$$\frac{d\chi}{d\zeta} = -\frac{\zeta}{2}\chi$$

which can be integrated once to get

$$\chi \equiv \frac{d\Theta}{d\zeta} = C_1 e^{-\zeta^2/4} \tag{5.48}$$

We integrate this a second time to get

$$\Theta = C_1 \int_0^\zeta e^{-\zeta^2/4}\, d\zeta + \underbrace{\Theta(0)}_{\substack{= 0 \text{ according} \\ \text{to the b.c.}}} \tag{5.49}$$

The b.c. is now satisfied, and we need only substitute eqn. (5.49) in the i.c., eqn. (5.46), to solve for C_1:

$$1 = C_1 \int_0^\infty e^{-\zeta^2/4}\, d\zeta$$

This particular definite integral is given by integral tables as $\sqrt{\pi}$, so

$$C_1 = \frac{1}{\sqrt{\pi}}$$

Thus the solution to the problem of conduction in a semi-infinite region, subject to a b.c. of the first kind is

$$\boxed{\Theta = \frac{1}{\sqrt{\pi}} \int_0^\zeta e^{-\zeta^2/4}\, d\zeta = \frac{2}{\sqrt{\pi}} \int_0^{\zeta/2} e^{-s^2}\, ds \equiv \operatorname{erf}(\zeta/2)} \tag{5.50}$$

The second integral in eqn. (5.50), obtained by a change of variables, is called the *error function*, $\operatorname{erf}(x)$. Its name arises from its relationship to certain statistical problems related to the Gaussian distribution, which describes random errors. In Table 5.3, we list values of the error function and the *complementary error function*, $\operatorname{erfc}(x) \equiv 1 - \operatorname{erf}(x)$. Equation (5.50) is also plotted in Fig. 5.15.

Table 5.3 Error function and complementary error function.

$\zeta/2$	$\text{erf}(\zeta/2)$	$\text{erfc}(\zeta/2)$	$\zeta/2$	$\text{erf}(\zeta/2)$	$\text{erfc}(\zeta/2)$
0.00	0.00000	1.00000	1.10	0.88021	0.11980
0.05	0.05637	0.94363	1.20	0.91031	0.08969
0.10	0.11246	0.88754	1.30	0.93401	0.06599
0.15	0.16800	0.83200	1.40	0.95229	0.04771
0.20	0.22270	0.77730	1.50	0.96611	0.03389
0.30	0.32863	0.67137	1.60	0.97635	0.02365
0.40	0.42839	0.57161	1.70	0.98379	0.01621
0.50	0.52050	0.47950	1.80	0.98909	0.01091
0.60	0.60386	0.39614	1.8214	*0.99000*	*0.01000*
0.70	0.67780	0.32220	1.90	0.99279	0.00721
0.80	0.74210	0.25790	2.00	0.99532	0.00468
0.90	0.79691	0.20309	2.50	0.99959	0.00041
1.00	0.84270	0.15730	3.00	0.99998	0.00002

In Fig. 5.15 we see that the early-time curves shown in Fig. 5.14 have collapsed into a single curve. We did this using what is known as a *similarity transformation*[5]: $\zeta/2 = x/2\sqrt{\alpha t}$. From the figure or from Table 5.3, we see that $\Theta \geq 0.99$ when

$$\frac{\zeta}{2} = \frac{x}{2\sqrt{\alpha t}} \geq 1.8214 \quad \text{or} \quad x \geq \delta_{99} \equiv 3.64\sqrt{\alpha t} \tag{5.51}$$

In other words, the local value of $(T - T_\infty)$ is more than 99% of $(T_i - T_\infty)$ for positions in the slab farther from the surface than $\delta_{99} = 3.64\sqrt{\alpha t}$.

Example 5.4

For what maximum time can a Samurai sword be analyzed as a semi-infinite region after it is quenched, if it has no clay coating and $\overline{h}_{\text{external}} \cong \infty$?

SOLUTION. First, we must guess the half-thickness of the sword (say, 3 mm) and its material (probably wrought iron with an average α around 1.5×10^{-5} m^2/s). The sword will be semi-infinite until δ_{99} equals the

---

[5]The transformation is based upon the "similarity" of spatial and temporal changes in this problem.

$$\Theta = \frac{T - T_\infty}{T_i - T_\infty}$$
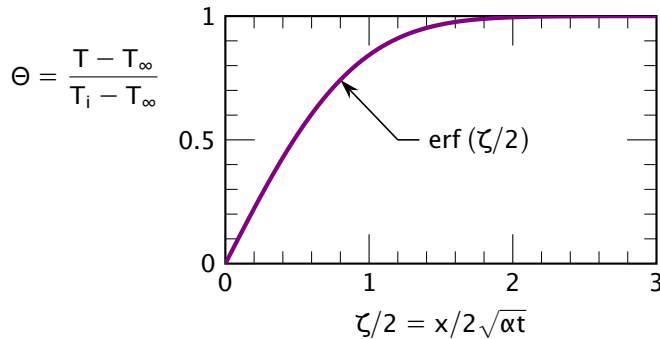
erf $(\zeta/2)$

$\zeta/2 = x/2\sqrt{\alpha t}$

Figure 5.15   Temperature distribution in a semi-infinite region.

half-thickness. Inverting eqn. (5.51), we find

$$t \leqslant \frac{\delta_{99}^2}{3.64^2 \alpha} = \frac{(0.003 \text{ m})^2}{13.3(1.5)(10)^{-5} \text{ m}^2/\text{s}} = 0.045 \text{ s}$$

Thus the quench would be felt at the centerline of the sword within only 1/20 s. The thermal diffusivity of clay is smaller than that of steel by a factor of about 30, so the quenching of the clay-covered steel must continue for over 1 s before the temperature of the steel is affected at all, if the clay and the sword thicknesses are comparable. ∎

Equation (5.51) provides an interesting foretaste of the notion of a fluid boundary layer. In the context of Fig. 1.9 and Fig. 1.10, we observe that free stream flow around an object is disturbed in a thin layer near the object because the fluid adheres to it. It turns out that the thickness, δ_{99}, of this boundary layer of altered flow velocity increases in the downstream direction. For flow over a flat plate, this thickness is approximately $4.92\sqrt{\nu t}$, where t is the time required for an element of the stream fluid to move from the leading edge of the plate to a point of interest. This is quite similar to eqn. (5.51), except that the thermal diffusivity, α, has been replaced by its counterpart, the kinematic viscosity, ν, and the constant is a bit larger. The velocity profile will resemble Fig. 5.15.

If we repeated the problem with a boundary condition of the third kind, we would expect to get $\Theta = \Theta(\text{Bi}, \zeta)$—except that there is no length, L, upon which to build a Biot number. Therefore, we must replace L with $\sqrt{\alpha t}$, which has the dimension of length, so that

$$\Theta = \Theta\left(\zeta, \frac{\overline{h}\sqrt{\alpha t}}{k}\right) \equiv \Theta(\zeta, \beta) \tag{5.52}$$

The term $\beta \equiv \overline{h}\sqrt{\alpha t}/k$ is like the product: $\text{Bi}\sqrt{\text{Fo}}$. The solution of this problem (see, e.g., [5.5], §2.7) can be conveniently written in terms of the complementary error function, $\text{erfc}(x) = 1 - \text{erf}(x)$:

$$\Theta = \text{erf}\frac{\zeta}{2} + \exp\left(\beta\zeta + \beta^2\right)\left[\text{erfc}\left(\frac{\zeta}{2} + \beta\right)\right] \qquad (5.53)$$

We offer our own original graph of this result in Fig. 5.16. This figure effectively shows curves of temperature (Θ) as a function of position ($\beta\zeta$) for various values of time (β).

Equation (5.53) can be used for bodies of any shape as long as Fo is low, that is, as long as heat transfer still occurs only near the surface. When we apply this equation to a cylinder or a sphere, their curvature will give rise to small errors—less than 6% for cylinders and 12% for spheres when Fo ≲ 0.05, decreasing quickly as Fo as Fo decreases [5.9]. For larger Fo, Figs. 5.7–5.9 may be used.

Example 5.5

Many of us have passed our finger through an 800°C candle flame and know that if we limit exposure to about ¼ s we will not be burned. Why not?

SOLUTION. The short exposure to the flame causes only a *very* superficial heating, so we consider the finger to be a semi-infinite region and go to eqn. (5.53) to calculate $(T_{\text{burn}} - T_{\text{flame}})/(T_i - T_{\text{flame}})$. It turns out that the burn threshold of human skin, T_{burn}, is about 65°C. (That is why 140°F or 60°C tap water is considered to be "scalding.") Therefore, we shall calculate how long it will take for the surface temperature of the finger to rise from body temperature (37°C) to 65°C, when it is protected by an assumed $\overline{h} \cong 100$ W/m^{2}K. We shall assume that the thermal conductivity of human flesh equals that of its major component—water—and that the thermal diffusivity is equal to the known value for beef. Then

$$\Theta = \frac{65 - 800}{37 - 800} = 0.963$$

$$\beta\zeta = \frac{\overline{h}x}{k} = 0 \quad \text{since } x = 0 \text{ at the surface}$$

$$\beta^2 = \frac{\overline{h}^2\alpha t}{k^2} = \frac{100^2(0.135 \times 10^{-6})t}{0.63^2} = 0.0034(t \text{ s})$$
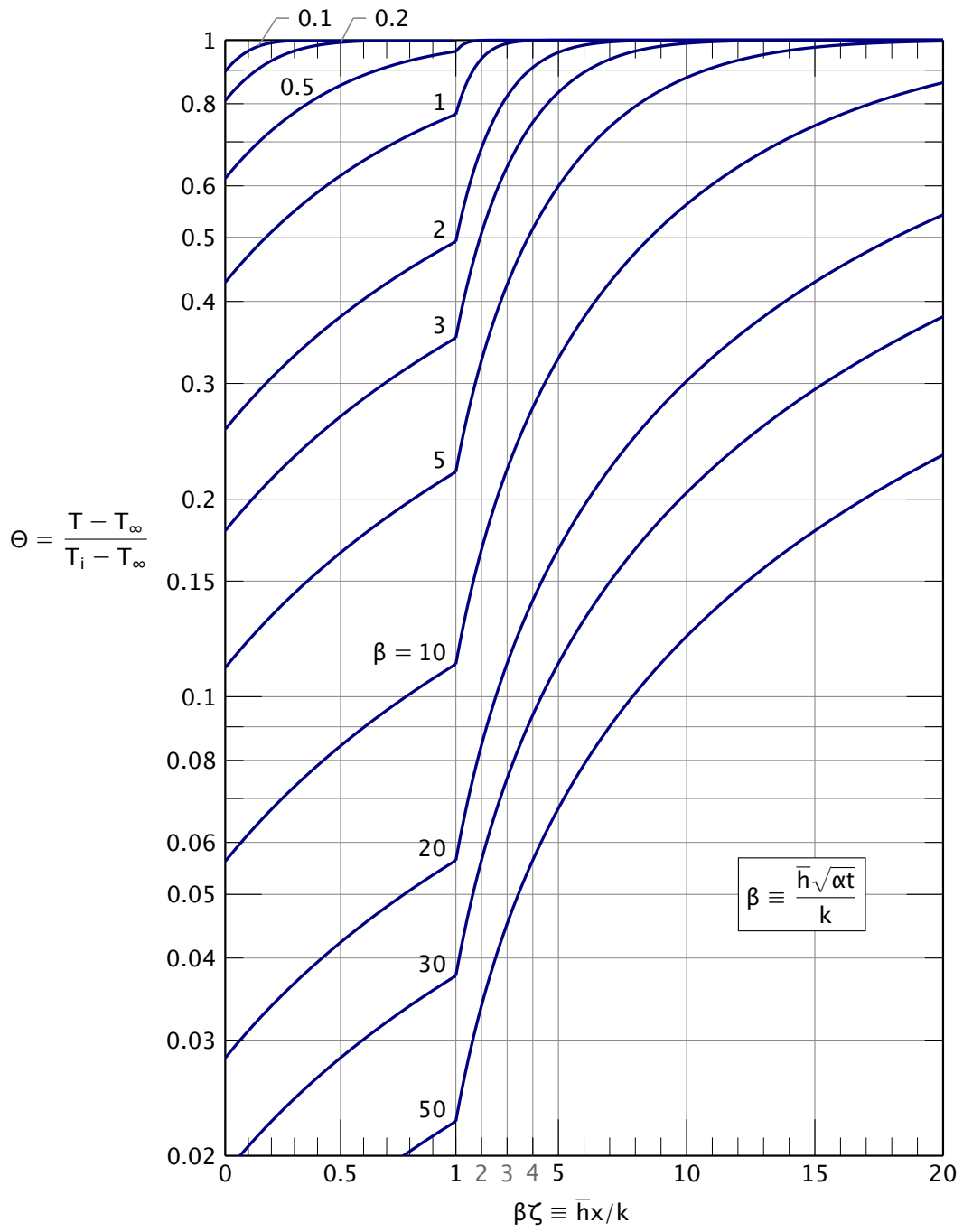
Figure 5.16 The cooling of a semi-infinite region by an environment at T_∞ through a heat transfer coefficient $\overline{h}$.

The situation is quite far into the top-left corner of Fig. 5.16. We can see only that $\beta < 0.1$. Instead, we must go to eqn. (5.53):

$$0.963 = \underbrace{\text{erf } 0}_{=0} + e^{0.0034t} \left[\text{erfc}\left(0 + \sqrt{0.0034\,t}\right) \right]$$

By trial and error, we get $t \cong 0.33$ s. In fact, it can be shown that

$$\Theta(\zeta = 0, \beta) \cong 1 - \frac{2\beta}{\sqrt{\pi}} \qquad \text{for } \beta \ll 1$$

which can be solved directly for $\beta = (1 - 0.963)\sqrt{\pi}/2 = 0.03279$, which is about the same answer.

Thus one's skin comes to the burn point in about ⅓ of a second if we have guessed a reasonable value of $\overline{h}$. ∎

Experiment 5.1

Immerse your hand in the subfreezing air in the freezer compartment of your refrigerator. Next immerse your finger in a mixture of ice cubes and water, but do not move it. Then, immerse your finger in a mixture of ice cubes and water , swirling it around as you do so. Describe your initial sensation in each case, and explain the differences in terms of Fig. 5.16. What variable has changed from one case to another? ♦

Heat transfer

Heat will be removed from the exposed surface of a semi-infinite region, with a b.c. of either the first or the third kind, in accordance with Fourier's law:

$$q = -k \left. \frac{\partial T}{\partial x} \right|_{x=0} = \frac{k(T_\infty - T_i)}{\sqrt{\alpha t}} \left. \frac{d\Theta}{d\zeta} \right|_{\zeta=0}$$

For the b.c. of the first kind, we differentiate Θ as given by eqn. (5.50) to obtain

$$q = \frac{k(T_\infty - T_i)}{\sqrt{\alpha t}} \left(\frac{1}{\sqrt{\pi}} e^{-\zeta^2/4} \right)_{\zeta=0} = \frac{k(T_\infty - T_i)}{\sqrt{\pi \alpha t}} \qquad (5.54)$$

Thus, q decreases with increasing time, as $t^{-1/2}$. When the temperature of the surface is first changed, the heat removal rate is enormous. Then it drops off rapidly.

We also might suddenly apply a specified heat flux, q_w, at the boundary of a semi-infinite region (a second-kind b.c.). In such a case, we can differentiate the heat conduction equation with respect to x, so that

$$\alpha \frac{\partial^3 T}{\partial x^3} = \frac{\partial^2 T}{\partial t\, \partial x}$$

When we substitute $q = -k\, \partial T/\partial x$ in this, we obtain

$$\alpha \frac{\partial^2 q}{\partial x^2} = \frac{\partial q}{\partial t}$$

with the b.c.'s:

$$q(x = 0, t > 0) = q_w \quad \text{or} \quad \left. \frac{q_w - q}{q_w} \right|_{x=0} = 0$$

$$q(x \geqslant 0, t = 0) = 0 \quad \text{or} \quad \left. \frac{q_w - q}{q_w} \right|_{t=0} = 1$$

What we have done here is quite elegant. We have made the problem of predicting the local heat flux q into exactly the same form as that of predicting the local temperature in a semi-infinite region subjected to a step change of wall temperature. Therefore, the solution must be the same:

$$\frac{q_w - q}{q_w} = \operatorname{erf}\left(\frac{x}{2\sqrt{\alpha t}}\right). \tag{5.55}$$

The temperature distribution is obtained by integrating Fourier's law. At the wall, for example

$$\int_{T_i}^{T_w} dT = -\int_{\infty}^{0} \frac{q}{k}\, dx$$

where $T_i = T(x \to \infty)$ and $T_w = T(x = 0)$. Then

$$T_w = T_i + \frac{q_w}{k} \int_0^{\infty} \operatorname{erfc}(x/2\sqrt{\alpha t})\, dx$$

This becomes

$$T_w = T_i + \frac{q_w}{k} \sqrt{\alpha t} \underbrace{\int_0^{\infty} \operatorname{erfc}(\zeta/2)\, d\zeta}_{=2/\sqrt{\pi}}$$

so

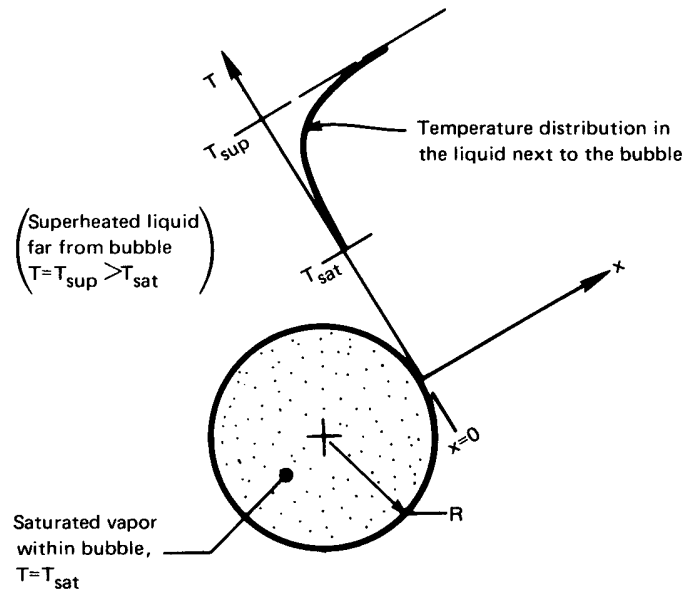$$\boxed{T_w(t) = T_i + 2\frac{q_w}{k} \sqrt{\frac{\alpha t}{\pi}}} \tag{5.56}$$

Figure 5.17   A bubble growing in a superheated liquid.

Example 5.6   Predicting the Growth Rate of a Vapor Bubble in an Infinite Superheated Liquid

This prediction is relevant to a large variety of processes, ranging from nuclear reactor thermohydraulics to direct-contact heat exchangers. It was originally presented by Max Jakob and others in the early 1930s (see, e.g., [5.11, Chap. I]). Jakob (pronounced Yah′-kob) was an important figure in heat transfer during the 1920s and 1930s. He left Nazi Germany in 1936 to come to the United States. We will encounter his name again in Chapter 8.

Figure 5.17 shows how growth occurs. A small gas or vapor cavity in the heated surface below the liquid will grow into the liquid above. The bottom of a tea kettle is such a surface.

This bubble grows into the surrounding liquid because its boundary is kept at the saturation temperature, T_{sat}, by the coexistence of liquid and vapor. Therefore heat must flow from the surrounding liquid, which is slightly hotter, at T_{sup}, to the interface, where evaporation occurs. So long as the layer of cooled liquid is thin, we may not suffer too much error by using the one-dimensional semi-infinite region solution to predict the heat flow.

Thus, we can write the energy balance at the bubble interface, $R(t)$:

$$\underbrace{\left(-q \ \frac{\text{W}}{\text{m}^2}\right)\left(4\pi R^2 \ \text{m}^2\right)}_{\text{heat transfer into bubble}} = \underbrace{\left(\rho_g h_{fg} \ \frac{\text{J}}{\text{m}^3}\right)\left(\frac{dV}{dt} \ \frac{\text{m}^3}{\text{s}}\right)}_{\substack{\text{rate of energy increase} \\ \text{of the bubble}}}$$

where ρ_g and h_{fg} are the vapor density and latent heat of vaporization at the saturation temperature. Substituting eqn. (5.54) for q and $4\pi R^3/3$ for the volume, V, the result is

$$\frac{k(T_{\text{sup}} - T_{\text{sat}})}{\sqrt{\alpha \pi t}} = \rho_g h_{fg} \frac{dR}{dt} \tag{5.57}$$

Integrating eqn. (5.57) from $R = 0$ at $t = 0$ up to R at t, we obtain Jakob's prediction:

$$R = \frac{2}{\sqrt{\pi}} \frac{k \Delta T}{\rho_g h_{fg} \sqrt{\alpha}} \sqrt{t} \tag{5.58}$$

∎

This analysis was done without assuming the curved bubble interface to be plane, 24 years after Jakob's work, by Plesset and Zwick [5.12]. It was verified in a more exact way after another 5 years by Scriven [5.13]. These calculations are more complicated, but they lead to a very similar result:

$$R = \frac{2\sqrt{3}}{\sqrt{\pi}} \frac{k \Delta T}{\rho_g h_{fg} \sqrt{\alpha}} \sqrt{t} = \sqrt{3} \, R_{\text{Jakob}}. \tag{5.59}$$

Both predictions are compared with some of the data of Dergarabedian [5.14] in Fig. 5.18. The data and the exact theory match almost perfectly. The simple theory of Jakob et al. shows the correct dependence of R on all its variables, but has a growth rate that is low by a factor of $\sqrt{3}$. This discrepancy occurs because the expansion of the spherical bubble causes a relative motion of liquid toward the bubble surface, which helps to thin the region of thermal influence in the radial direction [5.15, pg. 89]. Consequently, the temperature gradient and heat transfer rate are higher than in Jakob's model, which neglected the liquid motion. Therefore, the temperature profile flattens out more slowly than Jakob predicted, and the bubble grows more rapidly.
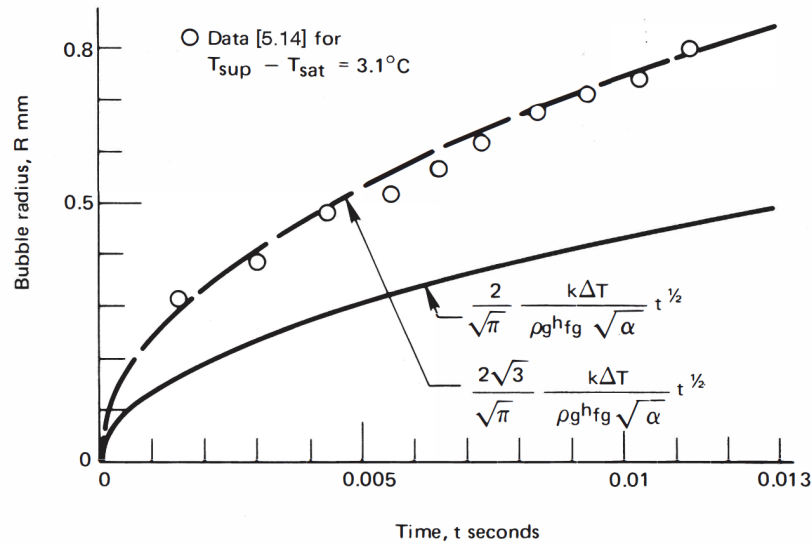
Figure 5.18 The growth of a vapor bubble—predictions and measurements.

Contact temperature between two semi-infinite regions

The more advanced theory of heat conduction (see, e.g., [5.5]) shows that if two semi-infinite regions at uniform temperatures T_1 and T_2 are placed together suddenly, their interface temperature, T_s, is given by

$$\frac{T_s - T_2}{T_1 - T_2} = \frac{\sqrt{(k\rho c_p)_1}}{\sqrt{(k\rho c_p)_1} + \sqrt{(k\rho c_p)_2}} \qquad (5.60)$$

For semi-infinite regions initially at uniform temperatures, T_s does not vary with time. A constant value of T_s means the two bodies each behave as a semi-infinite body whose surface temperature changed to T_s at time zero. Consequently, our previous results—eqns. (5.50), (5.51), and (5.54)—all apply to each of these bodies during the period when they may be treated as semi-infinite.[6] We need only replace T_∞ by T_s in those equations.

Experiment 5.2

Let us touch various objects in the room around us—glass, wood, corkboard, paper, steel—perhaps even gold or diamond. Rank them

---

[6]For any finite body, T_s will *eventually* change.

in order of which feels coldest at the first instant of contact (see Problem 5.29).

We identify one region with our body temperature ($T_1 \simeq 37°$C) and the other with an with an object at, say $T_2 \simeq 20°$C, that we touch. Equation (5.60) will then allow us to calculate the temperature, T_s, that the surface of our finger immediately reaches upon contact. Compare the ranking you obtain experimentally to the ranking given by this equation.

Notice that our bloodstream and capillary systems provide a heat source to our finger, so eqn. (5.60) is valid only for a moment. Then we start replacing the heat we've lost to the objects. If we include a diamond among the objects that we touch, it will first seem quite cold since it has the highest known value of α. Diamonds are sometimes called by the slang term "ice" for that reason. However, most diamonds are also quite small. They thus behave as a semi-infinite region only very briefly before they warm toward our finger's temperature.   ♦

Conduction to a semi-infinite region with a harmonically oscillating temperature at the boundary

Suppose that we approximate the annual variation of the ambient temperature as sinusoidal, $\overline{T} + \Delta T \cos \omega t$, where $\overline{T}$ is the time-average surface temperature. Then we may ask what the influence of this variation will be on the temperature $T(x, t)$ beneath the ground. We want to calculate $T - \overline{T}$ as a function of: depth, x; thermal diffusivity, α; frequency of oscillation, ω; amplitude of oscillation, ΔT; and time, t. There are six variables in K, m, and s, so the problem can be represented in three dimensionless variables:

$$\Theta \equiv \frac{T - \overline{T}}{\Delta T}; \qquad \Omega \equiv \omega t; \qquad \xi \equiv x\sqrt{\frac{\omega}{2\alpha}}.$$

We pose the problem as follows in these variables. The heat conduction equation is

$$\frac{1}{2}\frac{\partial^2 \Theta}{\partial \xi^2} = \frac{\partial \Theta}{\partial \Omega} \tag{5.61}$$

and the b.c.'s are

$$\Theta\Big|_{\xi=0} = \cos \omega t \qquad \text{and} \qquad \Theta\Big|_{\xi>0} = \text{finite}$$

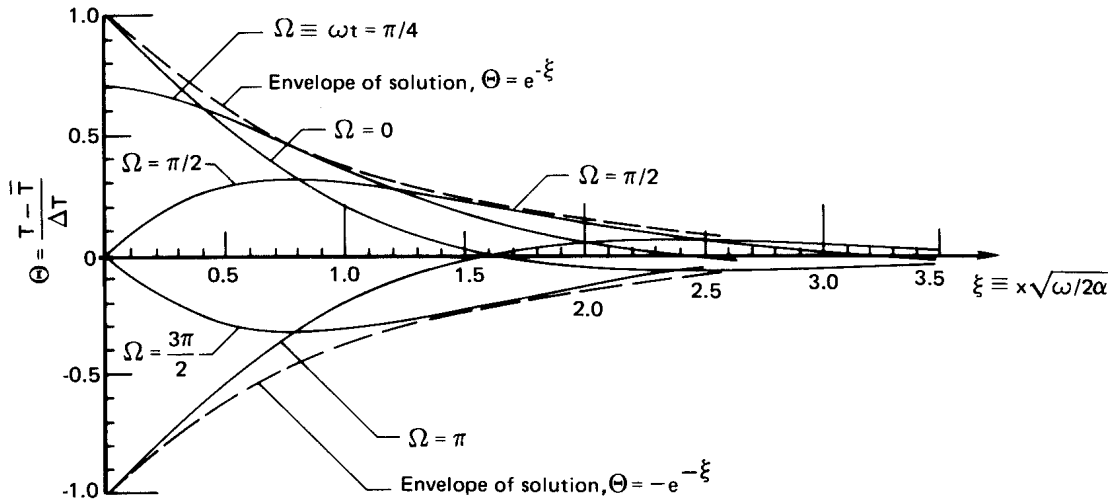No i.c. is needed because, after the initial transient decays, the remaining steady oscillation must be periodic.

Figure 5.19 The temperature variation within a semi-infinite region whose temperature varies harmonically at the boundary.

The solution is given by Carslaw and Jaeger (see [5.5, §2.6] or work Problem 5.16):

$$\Theta(\xi, \Omega) = e^{-\xi} \cos(\Omega - \xi) \qquad (5.62)$$

This result is plotted in Fig. 5.19. The surface temperature variation decays exponentially into the region and suffers a phase shift as it does so.

Example 5.7

How deep in the earth must we dig to find the temperature wave that was launched by the coldest part of the last winter if it is now high summer?

SOLUTION. $\omega = 2\pi$ rad/yr, and $\Omega = \omega t = 0$ at the hottest time in summer. First, we must find the depths at which the $\Omega = 0$ curve reaches its local extrema.

$$\frac{d\Theta}{d\xi}\bigg|_{\Omega=0} = -e^{-\xi} \cos(0 - \xi) + e^{-\xi} \sin(0 - \xi) = 0$$

This gives

$$\tan(0 - \xi) = 1 \quad \text{so} \quad \xi = \frac{3\pi}{4}, \frac{7\pi}{4}, \dots$$

and the first minimum occurs where $\xi = 3\pi/4 = 2.356$, as we can see in Fig. 5.19. Thus,

$$\xi = x\sqrt{\omega/2\alpha} = 2.356$$

or, if we take $\alpha = 0.139 \times 10^{-6}$ m^2/s (for coarse, gravelly earth [5.16]),

$$x = 2.356 \bigg/ \sqrt{\frac{2\pi}{2\,(0.139 \times 10^{-6})}\frac{1}{365(24)(3600)}} = 2.783 \text{ m}$$

If we dug in the earth, we would find it growing colder and colder until it reached a maximum coldness at a depth of about 2.8 m. Farther down, it would begin to warm up again, but not much. In midwinter ($\Omega = \pi$), the reverse would be true. ∎

5.7 Steady multidimensional heat conduction

Introduction

The general equation for $T(\vec{r})$ during steady conduction in a region of constant thermal conductivity, without heat sources, is called Laplace's equation:

$$\nabla^2 T = 0 \tag{5.63}$$

It looks easier to solve than it is, since the Laplacian, $\nabla^2 T$, is a sum of several second partial derivatives [recall eqn. (2.12) and eqn. (2.14)]. We solved one two-dimensional heat conduction problem in Example 4.1, but this was not difficult because the boundary conditions matched the coordinates very nicely. Depending upon one's mathematical background and the specific problem, the analytical solution of multidimensional problems can be anything from a straightforward calculation to a considerable challenge. The reader who wishes to study such analyses in depth should refer to [5.5] or [5.17].

Faced with a steady multidimensional problem, four routes are open to us:

- Check whether the analytical solution is available in a heat conduction text or in other published literature.

- Solve the problem analytically.

- Obtain the solution by numerical analysis.

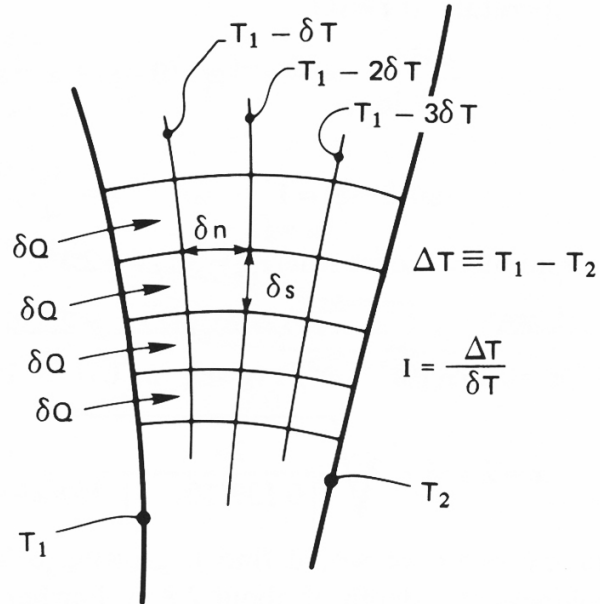- Obtain the solution graphically if the problem is two-dimensional.

Figure 5.20   The two-dimensional flow of heat between two isothermal walls.

The last of these options is out of style as a solution method, yet it is remarkably simple and effective. We turn to it next since anyone who takes the trouble to master it will develop an uncommonly strong intuitive understanding of multidimensional heat transfer along the way.

The flux plot

The method of *flux plotting* will solve all steady planar problems in which all boundaries are held at either of two temperatures or are insulated. With a little skill, it provides accuracies of a few percent—almost always greater than the accuracy with which the b.c.'s and k can be specified. And it reveals the physics of the problem very clearly.

Figure 5.20 shows heat flowing from one isothermal wall to another in a regime that does not conform to any convenient coordinate scheme. We identify a series of channels, each which carries the same heat flow, δQ W/m. We also include a set of equally spaced isotherms, δT apart, between the walls. Since the heat fluxes in all channels are the same,

$$\left| \delta Q \right| = k \frac{\delta T}{\delta n} \delta s \tag{5.64}$$

Notice that if we arrange things so that δQ, δT, and k are the same for flow through each rectangle in the flow field, then $\delta s / \delta n$ must be the

same for each rectangle. We therefore arbitrarily set the ratio equal to one, so all the elements appear as distorted *squares.*

The objective then is to sketch the isothermal lines and the adiabatic,[7] or heat flow, lines that run perpendicular to them. This sketch is to be done subject to two constraints:

1. Isothermal and adiabatic lines must intersect at right angles.

2. They must subdivide the region into elements that are nearly square— "nearly" because they have slightly curved sides.

Once the grid has been sketched, the temperature anywhere in the field can be read directly from the sketch. And the heat flow per unit depth into the paper is

$$Q \text{ (W/m)} = Nk \, \delta T \, \frac{\delta s}{\delta n} = \frac{N}{I} k \Delta T \tag{5.65}$$

where N is the number of heat flow channels and I is the number of temperature increments, $\Delta T / \delta T$.

The first step in constructing a flux plot is to draw the boundaries of the region accurately *in ink*, using drawing software or drafting instruments. The next is to obtain a soft pencil (such as a no. 2 grade) and a soft eraser. We begin with an example that was executed nicely in the influential *Heat Transfer Notes* [5.18] of the mid-twentieth century. This example is shown in Fig. 5.21.

The particular example happens to have an axis of symmetry in it. We immediately interpret this as an adiabatic boundary because heat cannot cross it. The problem therefore reduces to the simpler one of sketching lines in only one half of the area. We illustrate this process in four steps. Notice the following steps and features in this plot:

- Begin by dividing the region, by sketching in either a single isothermal or adiabatic line.

- Fill in the lines perpendicular to the original line so as to make squares. Allow the original line to move in such a way as to accommodate squares. This will *always* require some erasing. Therefore:

- *Never* make the original lines dark and firm.

---

[7]Adiabatic lines are ones *in the direction of heat flow*: Since by definition there can be no component of heat flow normal to them, they *must* be adiabatic.
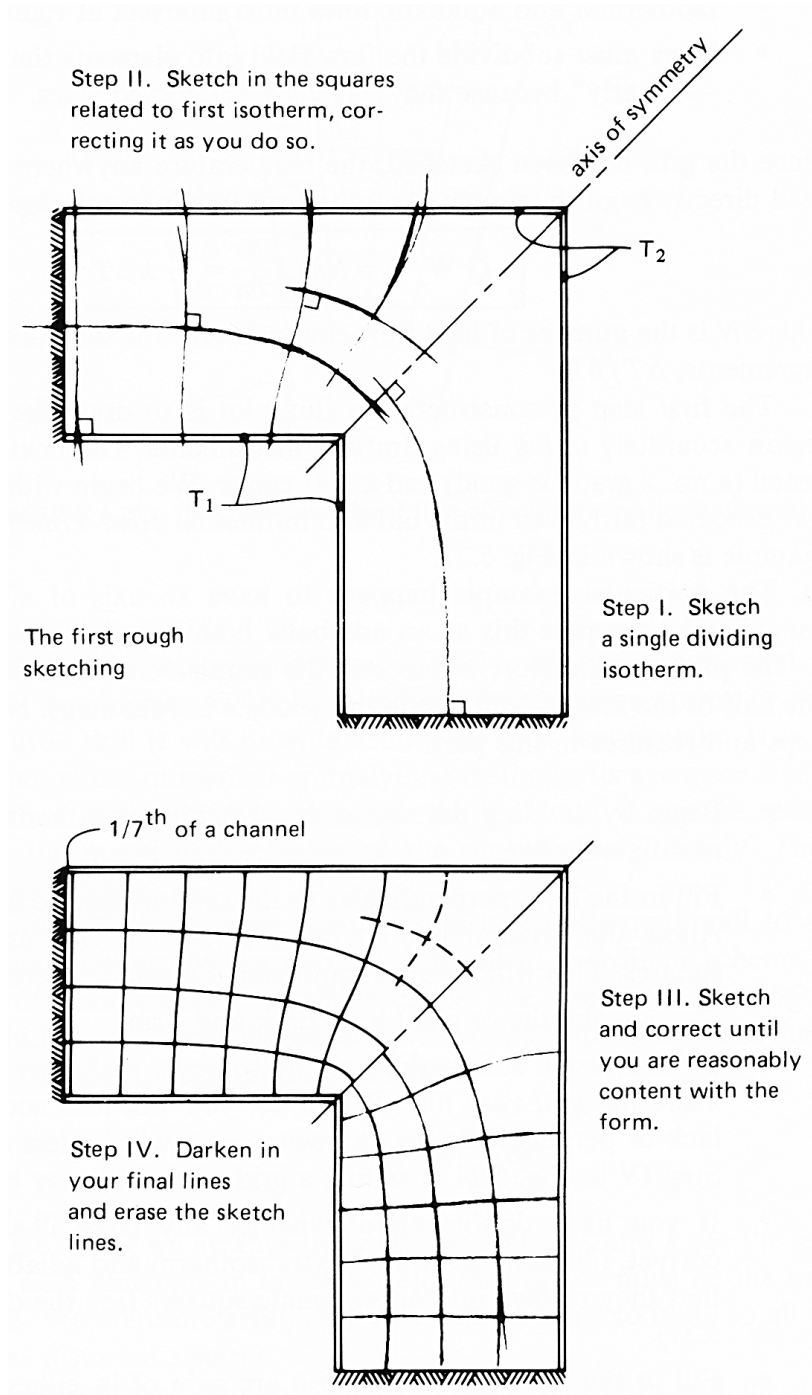
Step II. Sketch in the squares related to first isotherm, correcting it as you do so.

axis of symmetry

T_2

T_1

The first rough sketching

Step I. Sketch a single dividing isotherm.

1/7th of a channel

Step III. Sketch and correct until you are reasonably content with the form.

Step IV. Darken in your final lines and erase the sketch lines.

Figure 5.21 The evolution of a flux plot.

- By successive subdividing of the squares, make the final grid. *Do not make the grid very fine.* If you do, you will lose accuracy because the lack of perpendicularity and squareness will be less evident to the eye. Step IV in Fig. 5.21 is as fine a grid as should ever be made.

- If you have doubts about whether any large, ill-shaped regions are correct, fill them in with an extra isotherm and adiabatic line to be sure that they resolve into appropriate squares (see the dashed lines in Fig. 5.21).

- Fill in the final grid, when you are sure of it, either in hard pencil or pen, and erase any lingering background sketch lines.

- Your flow channels need not come out even. Notice that there is an extra 1/7 of a channel in Fig. 5.21. This is simply counted as 1/7 of a square in eqn. (5.65).

- Never allow isotherms or adiabatic lines to intersect themselves.

When the sketch is complete, we return to eqn. (5.65) to compute the heat flux. In this case

$$Q = \frac{N}{I} k \Delta T = \frac{2(6.14)}{4} k \Delta T = 3.07 \, k \Delta T$$

When the authors of [5.18] drew the flux plot for this problem, they obtained $N/I = 3.00$—a value only 2% below ours. This kind of agreement is typical when flux plotting is done with care.

One must be careful not to grasp at a false axis of symmetry. Figure 5.22 shows a shape similar to the one that we just treated, but with unequal legs. In this case, no lines must enter (or leave) the corners A and B. The reason is that since there *is* no symmetry, we have no guidance as to the direction of the lines at these corners. In particular, we know that a line leaving A will no longer arrive at B.

Example 5.8

A structure consists of metal walls, 8 cm apart, with insulating material ($k = 0.12$ W/m·K) between. Ribs 4 cm long protrude from one wall every 14 cm. They can be assumed to stay at the temperature of that wall. Find the heat flux through the wall if the first wall is at 40°C and the one with ribs is at 0°C. Find the temperature in the middle of the wall, 2 cm from a rib, as well.
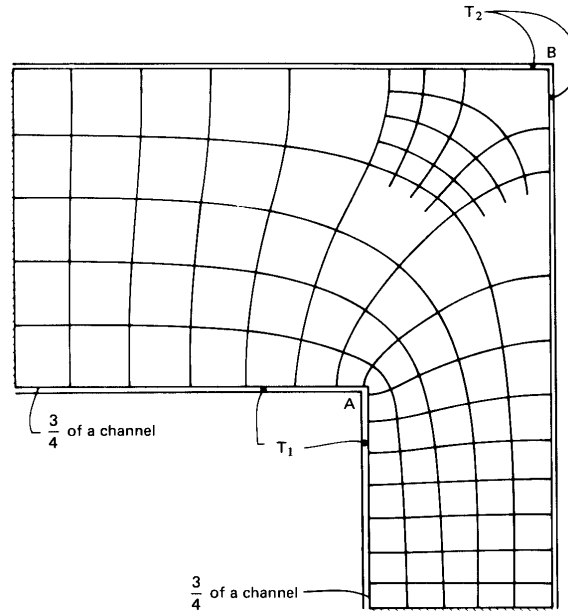
Figure 5.22 A flux plot with no axis of symmetry to guide construction.

SOLUTION. The flux plot for this configuration is shown in Fig. 5.23. For a typical section, there are approximately 5.6 isothermal increments and 6.15 heat flow channels, so

$$Q = \frac{N}{I} k\Delta T = \frac{2(6.15)}{5.6}(0.12)(40 - 0) = 10.54 \text{ W/m}$$

where the factor of 2 accounts for the fact that there are two halves in the section. We deduce the temperature for the point of interest, *A*, by a simple proportionality:

$$T_{\text{point } A} = \frac{2.1}{5.6}(40 - 0) = 15°\text{C} \qquad\qquad \blacksquare$$

The shape factor

A heat conduction *shape factor S* may be defined for steady problems involving two isothermal surfaces as follows:

$$Q \equiv S\, k\Delta T \qquad\qquad (5.66)$$

Thus far, every steady heat conduction problem we have done has taken this form. For these situations, the heat flow always equals a function of the geometric shape of the body multiplied by $k\Delta T$.
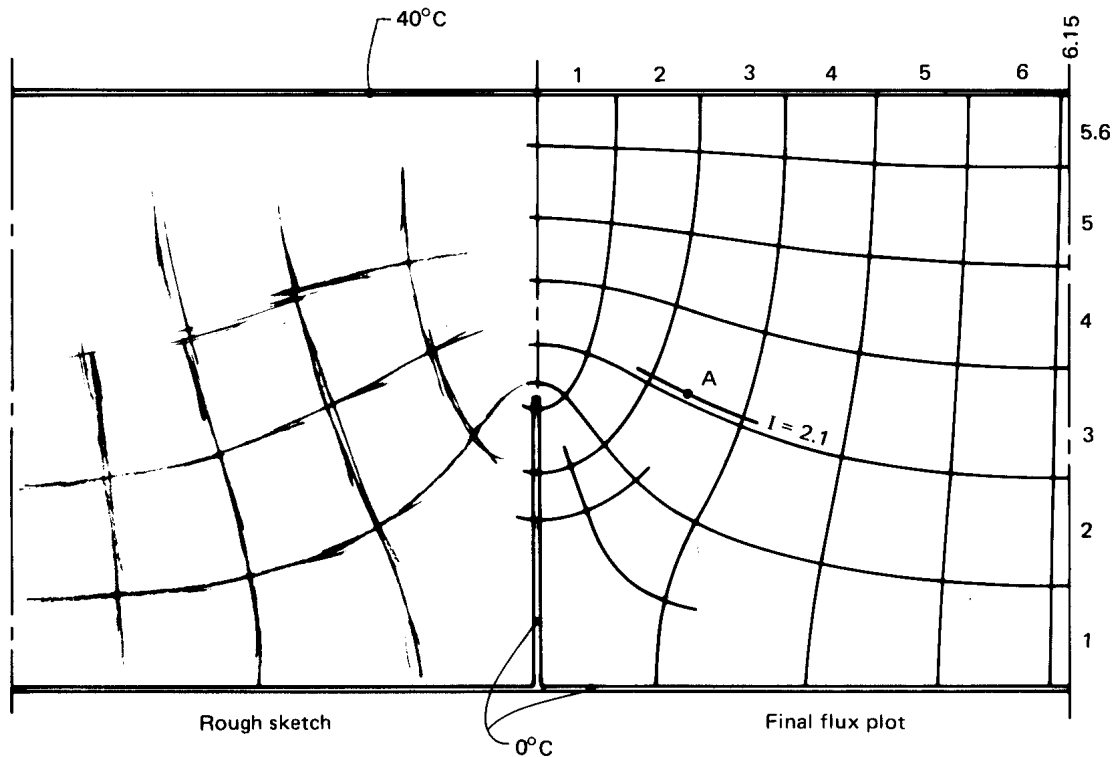
Figure 5.23 Heat transfer through a wall with isothermal ribs.

The shape factor can be obtained analytically, numerically, or through flux plotting. For example, let us compare eqn. (5.65) and eqn. (5.66):

$$Q \text{ (W/m)} = (S \text{ dimensionless})\left(k\Delta T \ \frac{\text{W}}{\text{m}}\right) = \frac{N}{I}\, k\Delta T \qquad (5.67)$$

This shows S to be dimensionless in a two-dimensional problem; but in three dimensions S has units of meters:

$$Q \text{ (W)} = (S \text{ m})\left(k\Delta T \ \frac{\text{W}}{\text{m}}\right) \qquad (5.68)$$

It also follows that the thermal resistance of a two-dimensional body is

$$R_t = \frac{1}{kS} \qquad \text{where} \qquad Q = \frac{\Delta T}{R_t} \qquad (5.69)$$

For a three-dimensional body, eqn. (5.69) is unchanged except that the dimensions of Q and R_t differ.[8]

---

[8]Recall that we noted after eqn. (2.22) that the dimensions of R_t changed, depending on whether or not Q was expressed per unit length.
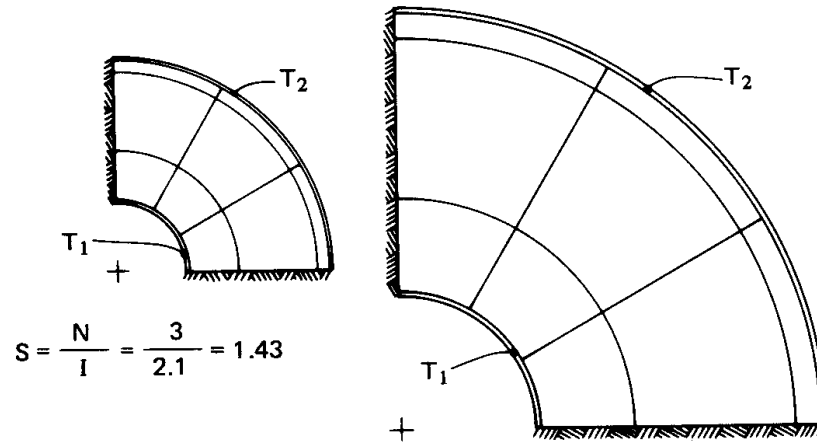
Figure 5.24 The shape factor for two similar bodies of different size.

The virtue of the shape factor is that it summarizes a heat conduction solution in a given configuration. Once S is known, it can be used again and again. That S is nondimensional in two-dimensional configurations means that Q is independent of the size of the body. Thus, in Fig. 5.21, S is always 3.07—regardless of the size of the figure—and in Example 5.8, S is $2(6.15)/5.6 = 2.20$, whether or not the wall is made larger or smaller. When a body's breadth is increased so as to increase Q, its thickness in the direction of heat flow is also increased so as to decrease Q by the same factor.

Example 5.9

Calculate the shape factor for a one-quarter section of a thick cylinder.

SOLUTION. We already know R_t for a thick cylinder. It is given by eqn. (2.22). From it we compute

$$S_{\text{cyl}} = \frac{1}{kR_t} = \frac{2\pi}{\ln(r_o/r_i)}$$

so on the case of a quarter-cylinder,

$$S = \frac{\pi}{2\ln(r_o/r_i)}$$

The quarter-cylinder is pictured in Fig. 5.24 for a radius ratio, $r_o/r_i = 3$, but for two different sizes. In both cases $S = 1.43$. (Note that the same S is also given by the flux plot shown.) ∎
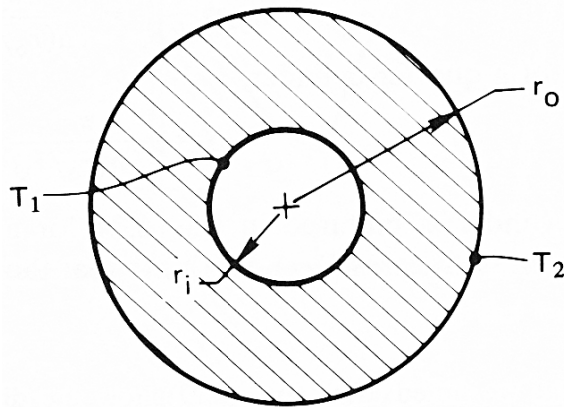
Figure 5.25   Heat transfer through a thick, hollow sphere.

Example 5.10

Calculate S for a three-dimensional object—a thick hollow sphere, as shown in Fig. 5.25. Notice that, in this case, since we expect the shape factor to have the dimension of length, it should increase linearly with the size of the sphere.

SOLUTION. The general solution of the heat conduction equation in spherical coordinates for purely radial heat flow (see Problem 4.1) is:

$$T = \frac{C_1}{r} + C_2$$

when $T = \mathrm{fn}(r$ only). The b.c.'s are

$$T(r_i) = T_i \quad \text{and} \quad T(r_o) = T_o$$

substituting the general solution in the b.c.'s we get

$$\frac{C_1}{r_i} + C_2 = T_i \quad \text{and} \quad \frac{C_1}{r_o} + C_1 = T_o$$

Therefore,

$$C_1 = \frac{T_i - T_o}{r_o - r_i} r_i r_o \quad \text{and} \quad C_2 = T_i - \frac{T_i - T_o}{r_o - r_i} r_o$$

Putting C_1 and C_2 in the general solution, and setting $\Delta T \equiv T_i - T_o$, we get

$$T = T_i + \Delta T \left[\frac{r_i r_o}{r(r_o - r_i)} - \frac{r_o}{r_o - r_i} \right]$$

Then

$$Q = -kA\frac{dT}{dr} = \frac{4\pi(r_i r_o)}{r_o - r_i}\,k\Delta T$$

$$S = \frac{4\pi(r_i r_o)}{r_o - r_i}\,\text{m}$$

where S does indeed have the dimension of meters and is hence size dependent. ∎

Table 5.4 on page 246 includes a number of analytically derived shape factors for use in calculating the heat flux in different configurations. Notice that these results will not give temperature distributions. To obtain that information, one must solve the Laplace equation, $\nabla^2 T = 0$, by one of the methods listed at the beginning of this section. Notice, too, that this table is restricted to bodies with isothermal and insulated boundaries.

The table lists two-dimensional configurations only for situations in which we have two fixed temperatures, so that heat flows from one object to another or from one side of an object to the other. Steady solutions are not possible for a two-dimensional object that transfers heat to an infinite or semi-infinite medium. For the same reason, cases 5, 6, and 7 in the table require that the medium far from the isothermal plane also be at temperature T_2. (Of course, no real medium is truly infinite, so some steady state can eventually be reached.) Three-dimensional configurations are a different story. They can come to equilibrium in infinite or semi-infinite surroundings (see cases 4, 8, 12, and 13.)

Two other useful facts can help in finding shape factors. One is that the shape factor inside a two-dimensional polygon is equal to the shape factor for the infinite region outside it, for any combination of isothermal and adiabatic boundaries, if no heat is transferred to the region at infinity. The other is that objects with inverse symmetry, as in Problem 5.22, cases (g) and (j), have a shape factor of one [5.19].

Example 5.11

A spherical heat source 6 cm in diameter, and kept at 35°C, is buried with its center 30 cm below a soil surface. The surface of the soil is kept at 21°C. If the steady heat transfer rate is 14 W, what is the thermal conductivity of this sample of soil?

SOLUTION. The value is S by situation 7 in Table 5.4:

$$Q = S\,k\Delta T = \left(\frac{4\pi R}{1 - R/2h}\right)k\Delta T$$

Then

$$k = \frac{14 \text{ W}}{(35 - 21)\text{K}} \frac{1 - (0.06/2)/2(0.3)}{4\pi(0.06/2) \text{ m}} = 2.55 \text{ W/m·K} \qquad \blacksquare$$

Readers who desire a broader catalogue of shape factors should refer to [5.20] or [5.21].

The problem of locally vanishing resistance

Suppose that two different temperatures are specified on adjacent sides of a square, as shown in Fig. 5.26. Counting channels beyond $N \simeq 10$ is futile, but it is clear that they multiply without limit in the lower left corner. The shape factor in this case is

$$S = \frac{N}{I} = \frac{\infty}{4} = \infty$$

The problem is that we have violated our rule that isotherms cannot intersect and have created a singularity at the corner. If we actually tried to sustain such a situation, the figure would be correct at some distance from the corner. At the corner itself, heat conduction in the bounding region would force the two temperatures to merge smoothly. And an infinite S could never really occur.
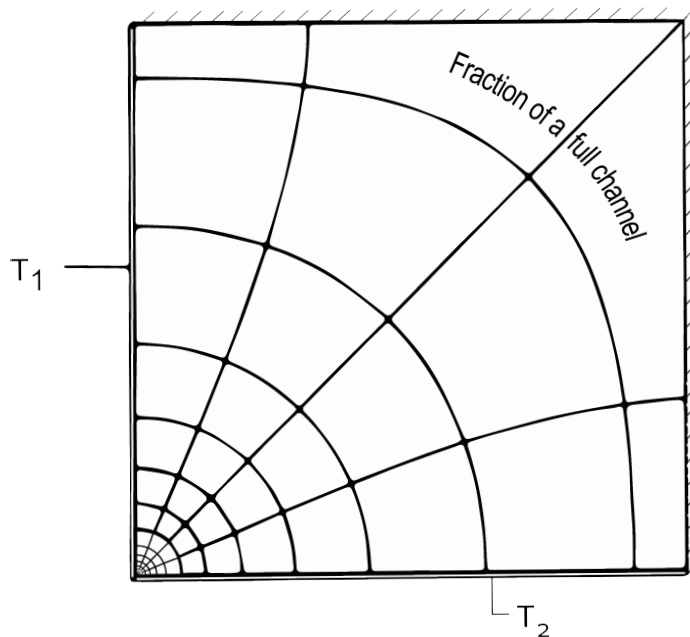
Figure 5.26   Resistance vanishes where two isothermal boundaries intersect.
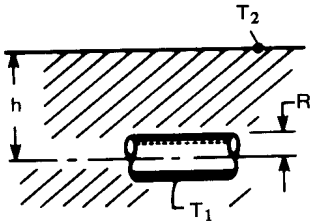
Table 5.4 Conduction shape factors: $Q = S k\Delta T$, $R_t = 1/(kS)$.

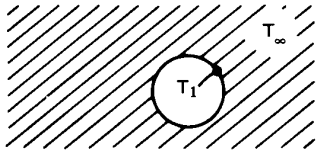| Situation	Shape factor, S	Dimensions	Source
1. Conduction through a slab	A/L	meter	Example 2.2
2. Conduction through wall of a long thick cylinder	$\dfrac{2\pi}{\ln(r_o/r_i)}$	none	Example 5.9
3. Conduction through a thick-walled hollow sphere	$\dfrac{4\pi(r_o r_i)}{r_o - r_i}$	meter	Example 5.10
4. The boundary of a spherical hole of radius R conducting into an infinite medium	$4\pi R$	meter	Problems 5.19 and 2.15
5. Cylinder of radius R and length L, transferring heat to a parallel isothermal plane; $h \ll L$	$\dfrac{2\pi L}{\cosh^{-1}(h/R)}$	meter	[5.20]
6. Same as item 5, but with $L \longrightarrow \infty$ (two-dimensional conduction)	$\dfrac{2\pi}{\cosh^{-1}(h/R)}$	none	[5.20]
7. An isothermal sphere of radius R transfers heat to an isothermal plane; $R/h < 0.8$ (see item 4)	$\dfrac{4\pi R}{1 - R/2h}$	meter	[5.20, 5.22]
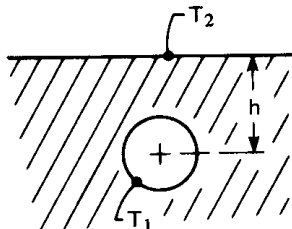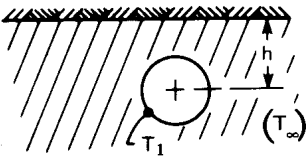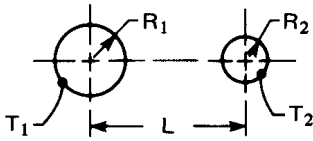
Table 5.4 Conduction shape factors: $Q = S\,k\Delta T$, $R_t = 1/(kS)$ *(con't)*.

Situation	Shape factor, S	Dimensions	Source
8. An isothermal sphere of radius R, near an insulated plane, transfers heat to a semi-infinite medium at T_∞ (see items 4 and 7) 	$\dfrac{4\pi R}{1 + R/2h}$	meter	[5.23]
9. Parallel cylinders exchange heat in an infinite conducting medium 	$\dfrac{2\pi}{\cosh^{-1}\left(\dfrac{L^2 - R_1^2 - R_2^2}{2R_1 R_2}\right)}$	none	[5.5]
10. Same as 9, but with cylinders widely spaced; $L \gg R_1$ and R_2	$\dfrac{2\pi}{\cosh^{-1}\left(\dfrac{L}{2R_1}\right) + \cosh^{-1}\left(\dfrac{L}{2R_2}\right)}$	none	[5.20]
11. Cylinder of radius R_i surrounded by eccentric cylinder of radius $R_o > R_i$; centerlines a distance L apart (see item 2)	$\dfrac{2\pi}{\cosh^{-1}\left(\dfrac{R_o^2 + R_i^2 - L^2}{2R_o R_i}\right)}$	none	[5.5]
12. Isothermal disk of radius R on an otherwise insulated plane conducts heat into a semi-infinite medium at T_∞ below it	$4R$	meter	[5.5]
13. Isothermal ellipsoid of semimajor axis b and semiminor axes a conducts heat into an infinite medium at T_∞ with $b > a$ (see item 4 for $b = a$)	$\dfrac{4\pi b\sqrt{1 - a^2/b^2}}{\tanh^{-1}\left(\sqrt{1 - a^2/b^2}\right)}$	meter	[5.20]

5.8 Transient multidimensional heat conduction— the tactic of superposition

Consider the cooling of a stubby cylinder, such as the one shown in Fig. 5.27a. The cylinder is initially at $T = T_i$, and it is suddenly subjected to a common b.c. on all sides. It has a length $2L$ and a radius r_o. Finding the temperature field in this situation is inherently complicated. It requires solving the heat conduction equation for $T = T(r, z, t)$ with b.c.'s of the first, second, or third kind.

However, Fig. 5.27a suggests that this can somehow be viewed as a combination of an infinite cylinder and an infinite slab. It turns out that the problem *can be analyzed* from that point of view.

If the body is subject to uniform b.c.'s of the first, second, or third kind, and it has a uniform initial temperature, then its temperature response will simply be the product of the infinite slab and infinite cylinder solutions. (Carslaw and Jaeger [5.5, §1.15] provide a proof of this useful fact.) So, when the cylinder in Fig. 5.27a begins convective cooling into surroundings at T_∞ at time $t = 0$, we can write the temperature response as

$$T(r, z, t) - T_\infty = \left[T_{\text{slab}}(z, t) - T_\infty \right] \times \left[T_{\text{cyl}}(r, t) - T_\infty \right] \qquad (5.70a)$$

Observe that the slab has as a characteristic length L, its half thickness, while the cylinder has as its characteristic length R, its radius. In dimensionless form, we may write eqn. (5.70a) as

$$\Theta \equiv \frac{T(r, z, t) - T_\infty}{T_i - T_\infty} = \left[\Theta_{\text{inf slab}}(\xi, \text{Fo}_s, \text{Bi}_s) \right] \times \left[\Theta_{\text{inf cyl}}(\rho, \text{Fo}_c, \text{Bi}_c) \right]$$
$$(5.70b)$$

For the cylindrical component of the solution,

$$\rho = \frac{r}{r_o}, \quad \text{Fo}_c = \frac{\alpha t}{r_o^2}, \quad \text{and} \quad \text{Bi}_c = \frac{\overline{h} r_o}{k},$$

while for the slab component of the solution

$$\xi = \frac{z}{L} + 1, \quad \text{Fo}_s = \frac{\alpha t}{L^2}, \quad \text{and} \quad \text{Bi}_s = \frac{\overline{h} L}{k}.$$

The component solutions are none other than those discussed in Sections 5.3–5.5. Note that the component solutions usually have *different* values of Fo and Bi.
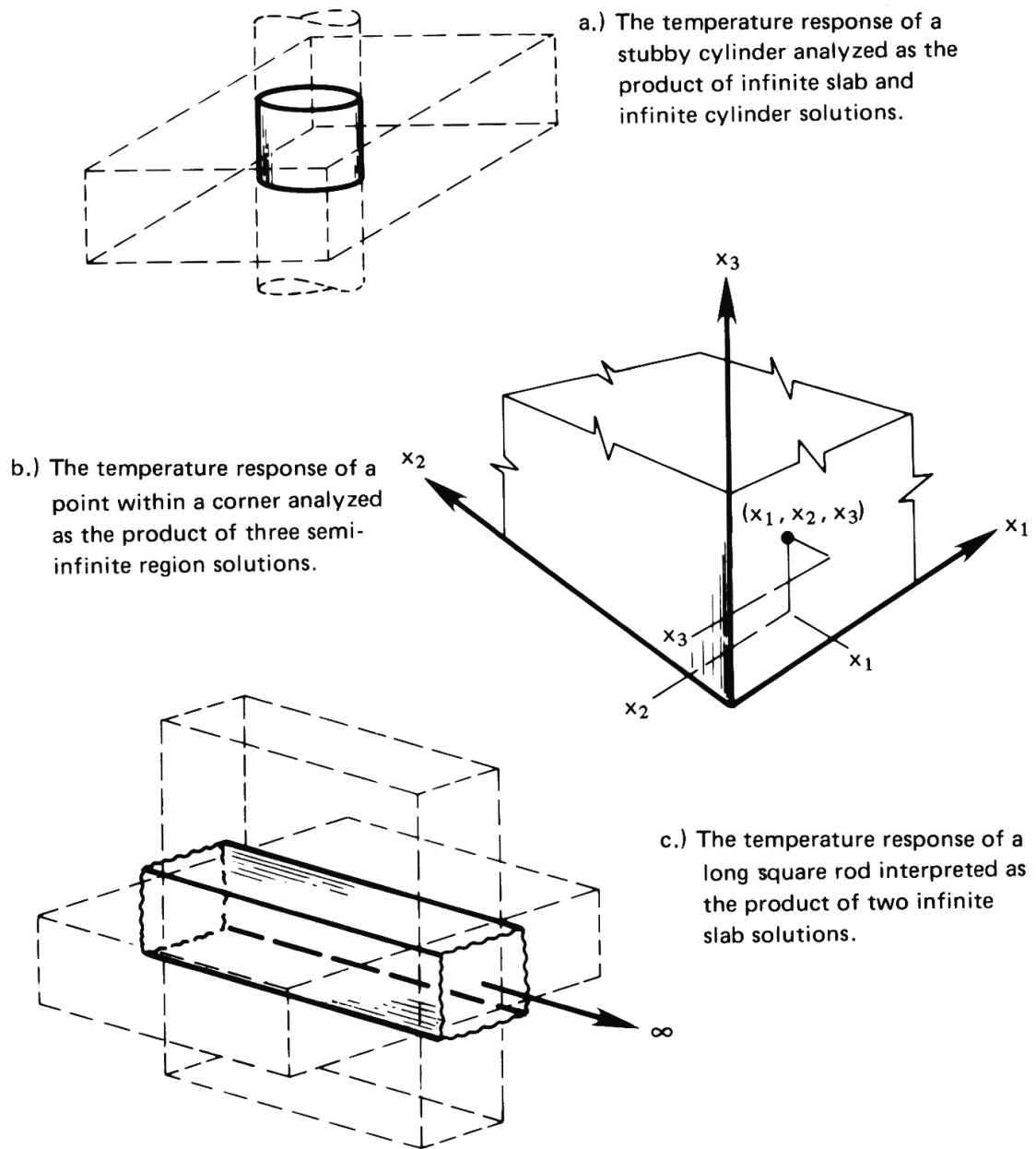
a.) The temperature response of a stubby cylinder analyzed as the product of infinite slab and infinite cylinder solutions.

b.) The temperature response of a point within a corner analyzed as the product of three semi-infinite region solutions.

c.) The temperature response of a long square rod interpreted as the product of two infinite slab solutions.

Figure 5.27 Various solid bodies whose transient cooling can be treated as the product of one-dimensional solutions.

249

Figure 5.27b shows a point inside a one-eighth-infinite region, near the corner. This case may be regarded as the product of three semi-infinite bodies. To find the temperature at this point we write

$$\Theta \equiv \frac{T(x_1, x_2, x_3, t) - T_\infty}{T_i - T_\infty} = \left[\Theta_{\text{semi}}(\zeta_1, \beta)\right]\left[\Theta_{\text{semi}}(\zeta_2, \beta)\right]\left[\Theta_{\text{semi}}(\zeta_3, \beta)\right]$$

(5.71)

in which Θ_{semi} is either the semi-infinite body solution given by eqn. (5.53) when convection is present at the boundary or the solution given by eqn. (5.50) when the boundary temperature itself is changed at time zero.

Several other geometries can also be represented by product solutions. Note that, for each of these solutions, the initial condition must be $\Theta = 1$ for each factor in the product.

Example 5.12

A very long 4 cm square iron rod at $T_i = 100°\text{C}$ is suddenly immersed in a coolant at $T_\infty = 20°\text{C}$ with $\overline{h} = 800 \text{ W/m}^2\text{K}$. What is the temperature on a line 1 cm from one side and 2 cm from the adjoining side, after 10 s?

SOLUTION. With reference to Fig. 5.27c, see that the bar may be treated as the product of two slabs, each 4 cm thick. We first evaluate $\text{Fo}_1 = \text{Fo}_2 = \alpha t / L^2 = (0.0000226 \text{ m}^2/\text{s})(10 \text{ s})/(0.04 \text{ m}/2)^2 = 0.565$, and $\text{Bi}_1 = \text{Bi}_2 = \overline{h}L/k = 800(0.04/2)/76 = 0.2105$, and we then write

$$\Theta\left[\left(\frac{x}{L}\right)_1 = 0, \left(\frac{x}{L}\right)_2 = \frac{1}{2}, \text{Fo}_1, \text{Fo}_2, \text{Bi}_1^{-1}, \text{Bi}_2^{-1}\right]$$

$$= \underbrace{\Theta_1\left[\left(\frac{x}{L}\right)_1 = 0, \text{Fo}_1 = 0.565, \text{Bi}_1^{-1} = 4.75\right]}_{\simeq 0.93 \text{ from interpolation in the upper set of curves in Fig. 5.7}}$$

$$\times \underbrace{\Theta_2\left[\left(\frac{x}{L}\right)_2 = \frac{1}{2}, \text{Fo}_2 = 0.565, \text{Bi}_2^{-1} = 4.75\right]}_{\simeq 0.91 \text{ from interpolation in the second set of curves in Fig. 5.7}}$$

Thus, at the axial line of interest,

$$\Theta = (0.93)(0.91) = 0.846$$

so

$$\frac{T - 20}{100 - 20} = 0.846 \quad \text{or} \quad T = 87.7°\text{C} \qquad \blacksquare$$

Product solutions can also be used to determine the mean tempera-ture, $\overline{\Theta}$, and the total heat removal, Φ, from a multidimensional object. For example, when two or three solutions (Θ_1, Θ_2, and perhaps Θ_3) are multiplied to obtain Θ, the corresponding mean temperature of the multi-dimensional object is simply the product of the one-dimensional mean temperatures from eqn. (5.40):

$$\overline{\Theta} = \overline{\Theta}_1(\text{Fo}_1, \text{Bi}_1) \times \overline{\Theta}_2(\text{Fo}_2, \text{Bi}_2) \qquad \text{for two factors} \qquad (5.72\text{a})$$

$$\overline{\Theta} = \overline{\Theta}_1(\text{Fo}_1, \text{Bi}_1) \times$$
$$\overline{\Theta}_2(\text{Fo}_2, \text{Bi}_2) \times \overline{\Theta}_3(\text{Fo}_3, \text{Bi}_3) \quad \text{for three factors} \qquad (5.72\text{b})$$

Since $\Phi = 1 - \overline{\Theta}$, a simple calculation shows that Φ can found from Φ_1, Φ_2, and Φ_3 as follows:

$$\Phi = \Phi_1 + \Phi_2 (1 - \Phi_1) \qquad \text{for two factors} \qquad (5.72\text{c})$$

$$\Phi = \Phi_1 + \Phi_2 (1 - \Phi_1) +$$
$$\Phi_3 (1 - \Phi_2)(1 - \Phi_1) \qquad \text{for three factors} \qquad (5.72\text{d})$$

Example 5.13

For the bar described in Example 5.12, what is the mean temperature after 10 s and how much heat has been lost at that time?

SOLUTION. For the Biot and Fourier numbers given in Example 5.12, we find from Fig. 5.10a

$$\Phi_1(\text{Fo}_1 = 0.565, \text{Bi}_1 = 0.2105) \simeq 0.10$$
$$\Phi_2(\text{Fo}_2 = 0.565, \text{Bi}_2 = 0.2105) \simeq 0.10$$

and, with eqn. (5.72c),

$$\Phi = \Phi_1 + \Phi_2 (1 - \Phi_1) = 0.19$$

The mean temperature is

$$\overline{\Theta} = \frac{\overline{T} - 20}{100 - 20} = 1 - \Phi = 0.81$$

so

$$\overline{T} = 20 + 80(0.81) = 84.8°C$$

The heat lost, per unit length, is

$$\int_0^t Q \, dt = \rho c_p A \, (T_i - T_\infty) \, \Phi$$

$$= (7,897)(447)(0.04)^2(100 - 20)(0.19) = 85.8 \text{ kJ/m} \quad \blacksquare$$

Problems

5.1 Rework Example 5.1, and replot the solution, with one change. This time, insert the thermometer at time zero with an initial temperature less than $(T_i - b\pmb{T})$.

5.2 A body at an initial temperature T_i is suddenly immersed in a bath whose temperature is rising as $T_{\text{bath}} = T_i + (T_0 - T_i)e^{t/\tau}$. Find the temperature response of the body if: it is immersed at time $t = 0$; the Biot number of the body is small; and the time constant of the bath, τ, is ten times that of the body, $\pmb{T}$. Plot the temperatures of the body and the bath temperature for $0 \le t/\tau \le 2$.

5.3 A body of known volume and surface area is immersed in a bath whose temperature is varying sinusoidally with a frequency ω about an average value. The heat transfer coefficient is known and the Biot number is small. Find the temperature variation of the body after a long time has passed, and plot it along with the bath temperature. Comment on any interesting aspects of the solution.

A suggested program for solving this problem follows.

- Write the differential equation for the body's temperature response.

- To get the particular solution of the complete equation, guess that $T - T_{\text{mean}} = C_1 \cos \omega t + C_2 \sin \omega t$. Substitute this in the differential equation and find C_1 and C_2 values that will make the resulting equation valid.

- Then add the homogeneous solution to the particular solution. The result will have one unknown constant.

- Write any initial condition you wish—the simplest one you can think of—to eliminate the constant.

- Let the time be large and note which terms vanish from the solution. Throw them away.

- Combine the two trigonometric terms in the solution into a term involving $\sin(\omega t - \beta)$, where $\beta = \text{fn}(\omega \boldsymbol{T})$ is the phase lag of the body temperature.

5.4 A block of copper floats on a large pool of liquid mercury in a thin metal container (Fig. 5.28). The system is initially at a uniform temperature, T_i. The heat transfer coefficient between the mercury and external environment is $\overline{h}_m$, and that between the copper and the mercury is $\overline{h}_c$. The external temperature is suddenly reduced from T_i to $T_s < T_i$. Predict the temperature response of the copper block, neglecting the internal resistance of both the copper and the mercury. Check your result by seeing that it fits both initial conditions and that it gives the expected behavior as $t \longrightarrow \infty$.
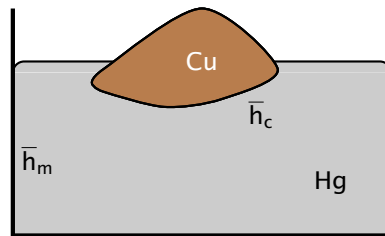
Figure 5.28   Configuration for Problem 5.4.

5.5 Sketch the electrical circuit that is analogous to the second-order lumped capacity system treated in Fig. 5.5 and explain it fully.

5.6 A one-inch diameter copper sphere with a thermocouple in its center is mounted as shown in Fig. 5.29 and immersed in water that is saturated at 211°F. The figure shows an actual thermocouple reading as a function of time during the quenching process. If the Biot number is small, the center temperature can be interpreted as the uniform temperature of the sphere during the quench. First draw tangents to the curve, and graphically differentiate it. Then use the resulting values of dT/dt to construct a graph of the heat transfer coefficient as a function of $(T_{\text{sphere}} - T_{\text{sat}})$. Check to see whether or not the largest value of the Biot number is too great to permit the use of lumped-capacity methods.
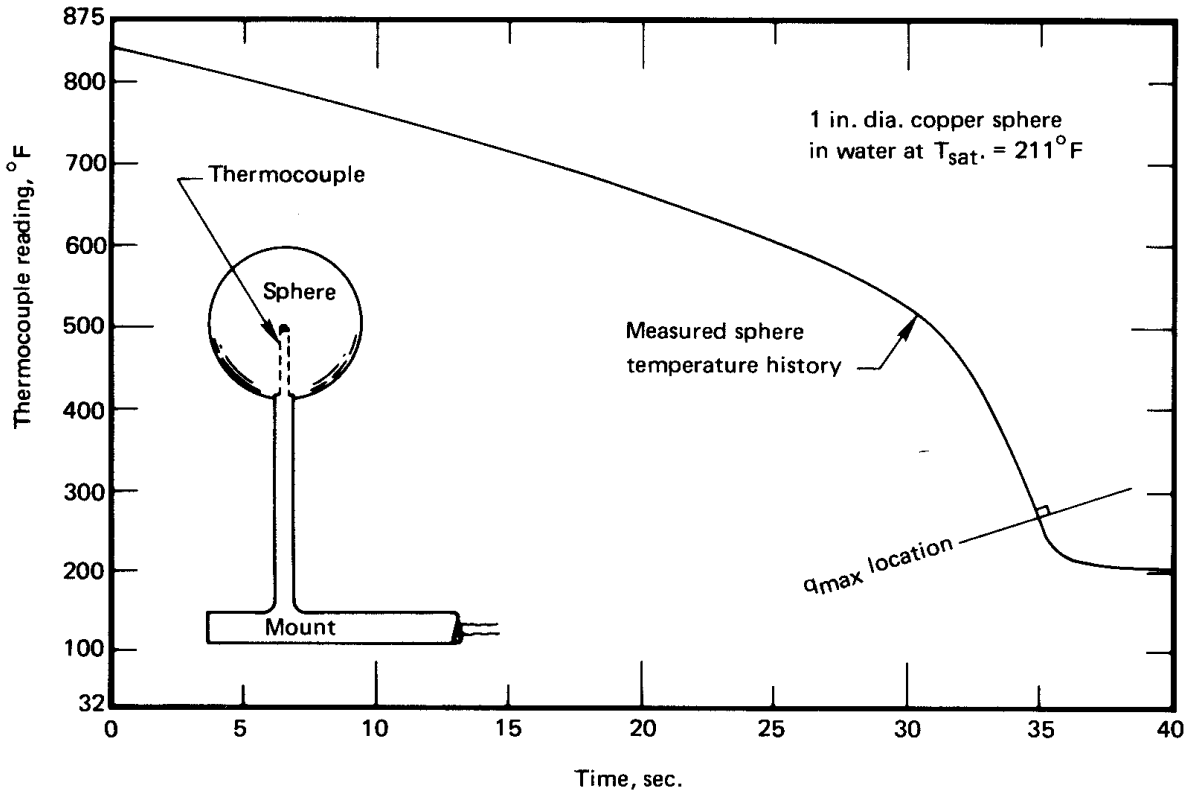
Figure 5.29 Configuration and temperature response for Problem 5.6

5.7 A butt-welded 36-gage thermocouple is placed in a gas flow whose temperature rises at the rate 20°C/s. The thermocouple steadily records a temperature 2.4°C below the known gas flow temperature. If ρc is 3800 kJ/m³K for the thermocouple material, what is $\bar{h}$ on the thermocouple? [$\bar{h} = 1006$ W/m²K]

5.8 Check the point on Fig. 5.7 at Fo = 0.1, Bi = 10, and $x/L = 0$ analytically. How many eigenvalues do you need compute to obtain two-digit accuracy?

5.9 Prove that when Bi is large, eqn. (5.34) reduces to eqn. (5.33).

5.10 For a slab, calculate Φ for Bi = 0.1 and Fo = 2.5 analytically and compare to Fig. 5.10a.

5.11 Sketch the chart for one position in Fig. 5.7, 5.8, or 5.9 and identify:

- The region in which b.c.'s of the third kind can be replaced with b.c.'s of the first kind.
- The region in which a lumped-capacity response can be assumed.
- The region in which the solid can be viewed as a semi-infinite region.

5.12 Water flows over a flat slab of Nichrome, 0.05 mm thick, which serves as a resistance heater using AC power. The apparent value of $\overline{h}$ is 2000 W/m^{2}K. How much surface temperature fluctuation will there be? [1.4% of average ΔT]

5.13 Put Jakob's bubble growth formula, eqn. (5.58), into dimensionless form, identifying a "Jakob number", Ja $\equiv c_p(T_{\text{sup}} - T_{\text{sat}})/h_{fg}$ as one of the groups. (Ja is the ratio of sensible heat to latent heat.) Be certain that your nondimensionalization is consistent with the Buckingham pi-theorem.

5.14 A 7 cm long vertical glass tube is filled with water that is slightly superheated to $T = 102°$C—not enough to trigger boiling. The top is suddenly opened to an ambient pressure of 1 atm. Plot the decrease of the height of water in the tube by evaporation as a function of time until the bottom of the tube has cooled by 0.05°C. [Total time is 29 minutes]

5.15 A slab is cooled convectively on both sides from a known initial temperature. Compare the variation of surface temperature with time as given in Fig. 5.7 with that given by eqn. (5.53) if Bi = 2. Discuss the meaning of your comparisons.

5.16 To obtain eqn. (5.62), assume a complex solution of the form $\Theta = f(\xi)\exp(i\Omega)$, where $i \equiv \sqrt{-1}$. This form assures that the real part of your solution has the required periodicity; and, by substituting into eqn. (5.61), you get an easy-to-solve ordinary d.e. for $f(\xi)$.

5.17 A steel piston cylinder wall is subjected to an oscillating surface temperature which we approximate as $T = 650°$C $+ (300°$C$) \cos \omega t$. The piston cycles eight times per second. To assess the thermal stress, we need to plot the amplitude of the temperature variation in the steel as a function of depth. Make this plot. If the cylinder is 1 cm thick, can we view it as having infinite depth?

5.18 A 40 cm diameter pipe at 75°C is buried in a large block of Portland cement. It runs parallel with a 15°C isothermal surface at a depth of 1 m. Plot the temperature distribution along the line normal to the 15°C surface that passes through the center of the pipe. Compute the heat loss from the pipe analytically. Then obtain the solution using either a flux plot or (if available) numerical software.

5.19 Derive shape factor 4 in Table 5.4.

5.20 Verify shape factor 9 in Table 5.4 with a flux plot. Use $R_1/R_2 = 2$ and $R_1/L = $ ½. (Be sure to start out with enough blank paper surrounding the cylinders.)

5.21 A copper block 1 in. thick and 3 in. square is held at 100°F on one 1 in. by 3 in. surface. The opposing 1 in. by 3 in. surface is adiabatic for 2 in. and 90°F for 1 inch. The remaining surfaces are adiabatic. Find the rate of heat transfer using a flux plot. [$Q \simeq 39$ W]

5.22 Obtain the shape factor for any or all of the situations pictured in Fig. 5.30a through j on pages 257–258. In each case, present a well-drawn flux plot. You may optionally check these results using numerical simulation software. [$S_b \simeq 1.03$, $S_c \simeq 0.29$, $S_g = 1$]

5.23 Two copper slabs, 3 cm thick and insulated on the outside, are suddenly slapped tightly together. The one on the left side is initially at 100°C and the one on the right side at 0°C. Determine the left-hand adiabatic boundary's temperature after 2.3 s have elapsed. [$T_{\text{wall}} \simeq 80.5$°C]

5.24 Eggs cook as their proteins denature and coagulate. An egg is considered to be "hard-boiled" when its yolk is firm, which corresponds to a center temperature of 75°C. Estimate the time required to hard-boil an egg if:

The time to cook depends on whether a soft or hard boiled egg desired. Eggs may be cooked by placing them (cold or warm) into cold water before heating starts or by placing warm eggs directly into simmering water [5.24].
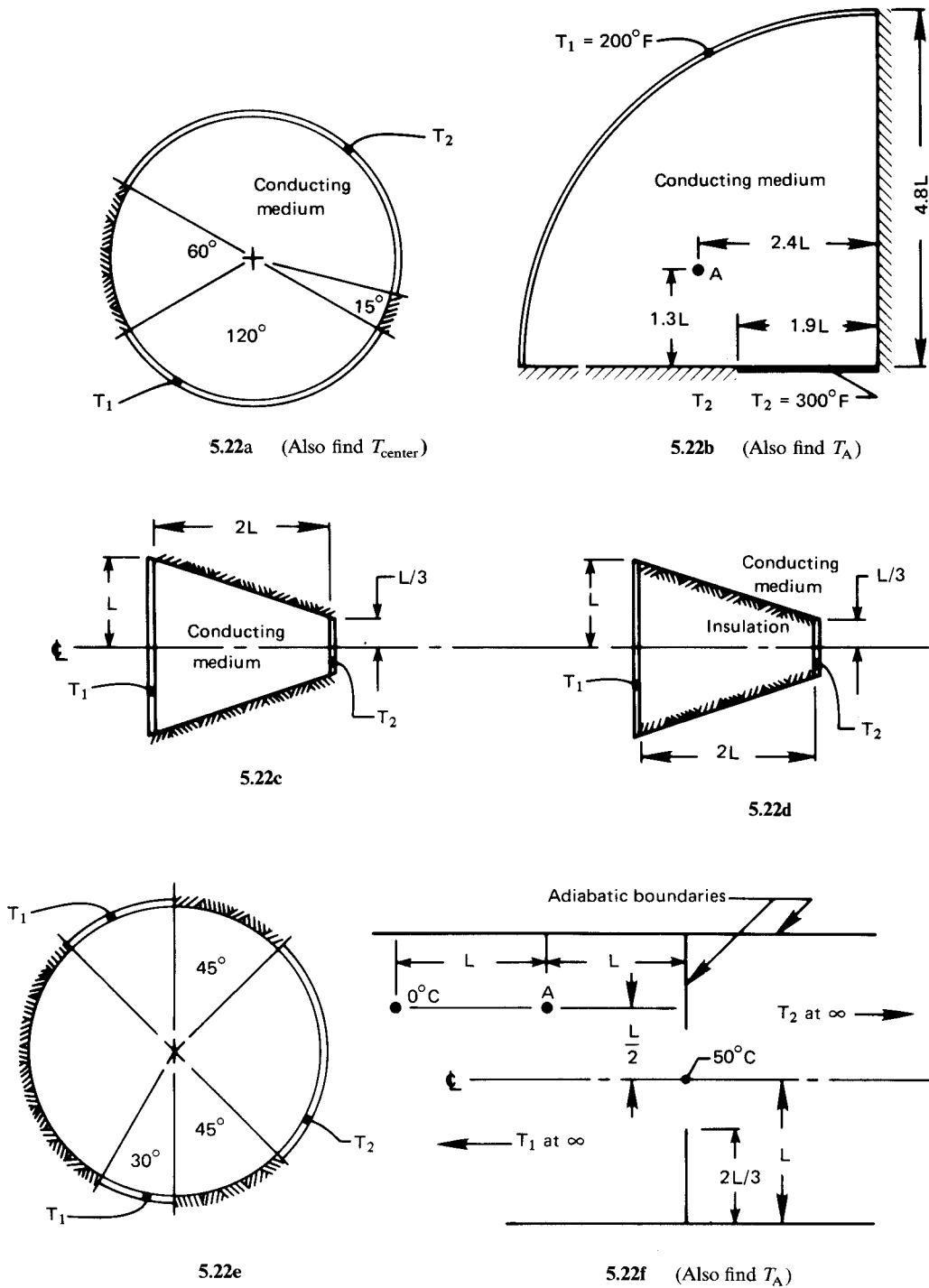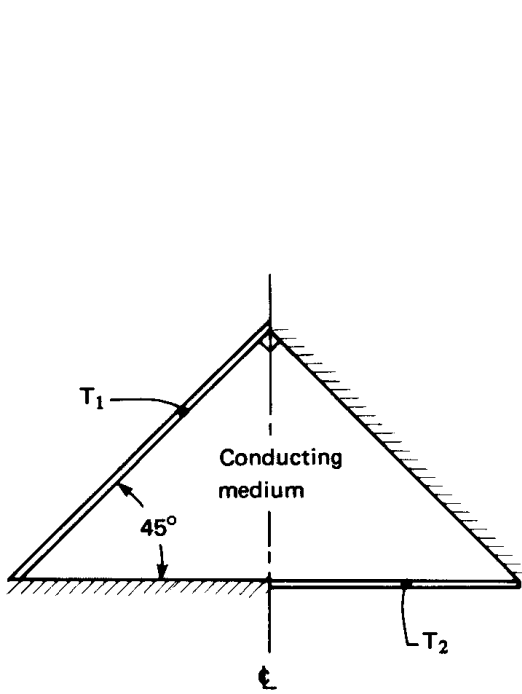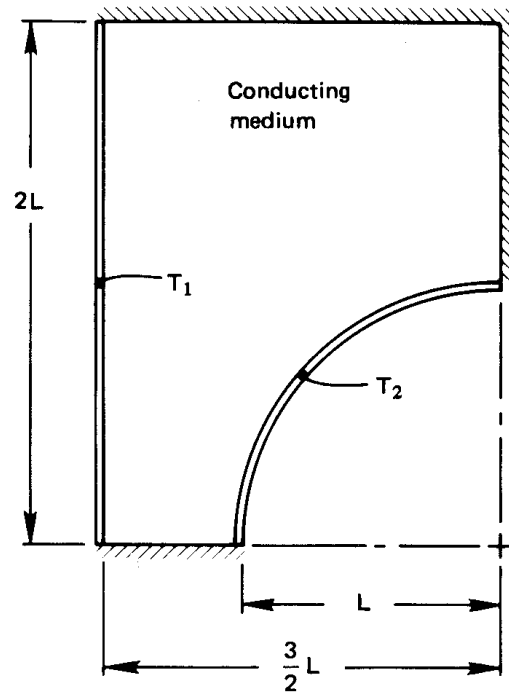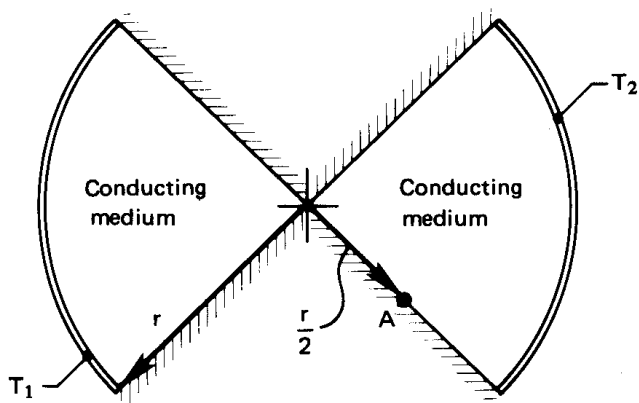
- The minor diameter is 45 mm.
- k for the entire egg is about the same as for egg white. No significant heat release or change of properties occurs during cooking.
- $\overline{h}$ between the egg and the water is 1000 W/m^{2}K.
- The egg has a uniform temperature of 20°C when it is put into simmering water at 85°C.

5.22a　(Also find T_{center})

5.22b　(Also find T_A)

5.22c

5.22d

5.22e

5.22f　(Also find T_A)

Figure 5.30　Configurations for Problem 5.22

257

Figure 5.30 Configurations for Problem 5.22 *(con't)*
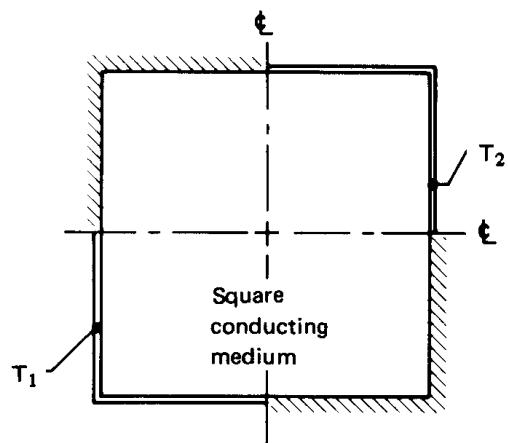
5.25 Prove that T_1 cannot oscillate for the second-order lumped capacity system described by eqn. (5.23).

5.26 Explain the reason that when isothermal and adiabatic lines are interchanged in a two-dimensional body, the new shape factor is the inverse of the original one.

5.27 A 0.5 cm diameter cylinder at 300°C is suddenly immersed in saturated water at 1 atm. The water boils and $\overline{h} = 10,000$ W/m²K. Find the centerline and surface temperatures for the cases that follow. *Hint:* Evaluate Bi in each case before you begin.

  a. After after 0.2 s if the cylinder is copper.

  b. After after 0.2 s if the cylinder is Nichrome V. [$T_{\text{sfc}} \simeq 216$°C]

  c. If the cylinder is Nichrome V, obtain the most accurate value of the temperatures after 0.04 s that you can [$T_{\text{sfc}} \simeq 259$°C]

5.28 A large, flat electrical resistance strip heater is fastened to a firebrick wall, which is uniformly at 15°C. When the heater is suddenly turned on, it releases heat at the uniform rate of 4000 W/m². Plot the temperature of the brick immediately under the heater as a function of time if the other side of the heater is insulated. What is the heat flux at a depth of 1 cm inside the wall when the surface reaches 200°C. [$q = 338$ W/m²K]

5.29 Do Experiment 5.2 and submit a report on the results.

5.30 An approximately spherical container, 2 cm in diameter, containing electronic equipment is placed in wet mineral soil with its center 2 m below the surface. The soil surface is kept at 0°C. If the interior construction of the sphere is such that its temperature stays uniform, determine the rate at which energy can be released by the equipment without driving the sphere surface above 30°C. [$Q = 1.0$ kW]

5.31 A semi-infinite slab of ice at -10°C is exposed to air at 15°C through a heat transfer coefficient of 10 W/m²K. First, describe in words what happens after the ice is exposed. Then determine the initial and asymptotic ($t \rightarrow \infty$) rates of melting in kg/m²s. The latent heat of fusion of ice, h_{sf}, is 333,300 J/kg. [$\dot{m}_{\text{melt}} = 0.45$ g/m²s]

5.32 One side of an insulating firebrick wall, 10 cm thick and initially at 20°C, is exposed to 1000°C flame through a heat transfer coefficient

of 230 W/m^{2}K. How long will it be before the other side is too hot to touch, say, at 65°C? Estimate properties at 500°C, and assume that $\bar{h}$ is low enough that the cool side can be treated as insulated. [A little under 4 hours]

5.33 A particular lead bullet travels for 0.5 s within a shock wave that heats the air near the bullet to 300°C. Approximate the bullet as a cylinder 0.8 cm in diameter. What is its surface temperature at impact if $\bar{h} = 600$ W/m^{2}K and if the bullet was initially at 20°C? What is its center temperature?

5.34 A loaf of bread is removed from an oven at 125°C and set on a counter to cool in a kitchen at 25°C. The loaf is 30 cm long, 15 cm high, and 12 cm wide. Assume, for this problem, that the counter is a very poor heat conductor so that bottom of the loaf loses no heat. If $k = 0.05$ W/m·K and $\alpha = 5 \times 10^{-7}$ m^2/s for bread, and $\bar{h} = 10$ W/m^{2}K, when will the hottest part of the loaf have cooled to 60°C? [About 1 h 5 min.]

5.35 A 1½ ton block of lead, 50 cm on each side, is initially at 20°C. The block is hoisted into a hot air stream at 200°C and $\bar{h}$ around the cube is 272 W/m^{2}K. Plot the cube temperature along a line from the center to the middle of one face after 20 minutes have elapsed.

5.36 A 1.24 mm diameter jet of clean water, superheated to 150°C, issues from a small orifice at 27 m/s, into air at 1 atm. Evaporation at $T = T_{\text{sat}}$ begins immediately on the surface of the jet. Plot the centerline temperature of the jet and $T(r/r_o = 0.6)$ as functions of distance from the orifice up to about 5 m. Neglect any axial conduction and any dynamic interactions between the jet and the air. (See [5.25] for this experiment.)

5.37 A 3 cm thick slab of aluminum (initially at 50°C) is slapped tightly against a 5 cm slab of copper (initially at 20°C). The outsides are both insulated and the contact resistance is negligible. What is the initial interfacial temperature? Which slab will determine how long the interface keeps its initial temperature? Estimate the time until the interface temperature begins to change. [At least 0.7 s]

5.38 A cylindrical underground gasoline tank, 2 m in diameter and 4 m long, is embedded in 10°C soil with $k = 0.8$ W/m·K and $\alpha = 1.3 \times 10^{-6}$ m^2/s. Water at 27°C is injected into the tank to test

it for leaks. It is well-stirred with a submerged ½ kW pump. We observe the water level in a 10 cm I.D. transparent standpipe and measure its rate of rise and fall. What rate of change of height will occur after one hour if there is no leakage? Will the level rise or fall? Neglect thermal expansion and deformation of the tank, which should be complete by the time the tank is filled. *Hint:* You will need to look ahead to eqn. (8.7) to solve this problem. [−18.4 cm/h]

5.39 A 47°C copper cylinder, 3 cm in diameter, is suddenly immersed horizontally in water at 27°C in a reduced gravity environment. Plot T_{cyl} as a function of time if $g = 0.76$ m/s^2 and if $\overline{h} = [2.733 + 10.448(\Delta T°C)^{1/6}]^2$ W/m^{2}K. (If you cannot integrate the resulting equation analytically, do it numerically.)

5.40 The mechanical engineers at the University of Utah end spring semester by roasting a pig and having a picnic. The pig is roughly cylindrical and about 26 cm in diameter. It is roasted over a propane flame, whose products have properties similar to those of air, at 280°C. The hot gas flows across the pig at about 2 m/s. If the meat is cooked when it reaches 95°C, and if it is to be served at 2:00 pm, what time should cooking commence? Assume Bi to be large, but note Problem 7.40. The pig is initially at 25°C. [About 9:30 am]

5.41 People from cold northern climates know not to grasp metal with their bare hands in subzero weather. A very slightly frosted piece of, say, cast iron will stick to your hand like glue in, say, −20°C weather and might tear off patches of skin. Explain this *quantitatively*.

5.42 A 4 cm diameter rod of type 304 stainless steel has a very small hole down its center. The hole is clogged with wax that has a melting point of 60°C. The rod is at 20°C. In an attempt to free the hole, a workman swirls the end of the rod—and about a meter of its length—in a tank of water at 80°C. If $\overline{h}$ is 688 W/m^{2}K on both the end and the sides of the rod, plot the depth of the melt front as a function of time up to, say, 4 cm. *Hint:* Look back at Section 5.8.

5.43 A cylindrical insulator contains a single, very thin electrical resistor wire that runs along a line halfway between the center and the outside. The wire liberates 480 W/m. The thermal conductivity of the insulation is 3 W/m·K, and the outside perimeter is held at 20°C. Develop a flux plot for the cross section, considering carefully how the field should look in the neighborhood of the point through

which the wire passes. Evaluate the temperature at the center of the insulation.

5.44 A long, 10 cm square copper bar is bounded by 260°C gas flows on two opposing sides. These flows impose heat transfer coefficients of 46 W/m²K. The two intervening sides are cooled by natural convection to water at 15°C, with a heat transfer coefficient of 525 W/m²K. What is the heat flow through the block and the temperature at the center of the block? *Hint:* This could be a pretty complicated problem, but take the trouble to calculate the Biot numbers for each side before you begin. What do they tell you? [34.7 °C]

5.45 Lord Kelvin made an interesting estimate of the age of the earth in 1864. He assumed that the earth originated as a mass of molten rock at 4144 K (7000°F) and that it had been cooled by outer space at 0 K ever since. To do this, he assumed that Bi for the earth is very large and that cooling had thus far penetrated through only a relatively thin (one-dimensional) layer. Using $\alpha_{\text{rock}} = 1.18 \times 10^{-6}$ m²/s and the measured surface temperature gradient of the earth, ½₇ K/m, find Kelvin's value of Earth's age. (Kelvin's result turns out to be much less than the accepted value of 4.54 billion years. His calculation fails because Earth is not solid. Rather, the molten core is convectively stirred below the solid lithosphere. Consequently, the surface gradient has little to do with Earth's age.)

5.46 A pure aluminum cylinder, 4 cm diam. by 8 cm long, is initially at 300°C. It is plunged into a liquid bath at 40°C with $\overline{h} = 500$ W/m²K. Calculate the hottest and coldest temperatures in the cylinder after one minute. Compare these results with the lumped capacity calculation, and discuss the comparison.

5.47 When Ivan cleaned his freezer, he accidentally put a large can of frozen juice into the refrigerator. The juice can is 17.8 cm tall and has an 8.9 cm I.D. The can was at −15°C in the freezer, but the refrigerator is at 4°C. The can now lies on a shelf of widely-spaced plastic rods, and air circulates freely over it. Thermal interactions with the rods can be ignored. The effective heat transfer coefficient to the can (for simultaneous convection and thermal radiation) is 8 W/m²K. The can has a 1.0 mm thick cardboard skin with

$k = 0.2$ W/m·K. The frozen juice has approximately the same physical properties as ice.

    a. How important is the cardboard skin to the thermal response of the juice? Justify your answer quantitatively.

    b. If Ivan finds the can in the refrigerator 30 minutes after putting it in, will the juice have begun to melt?

5.48 A cleaning crew accidentally switches off the heating system in a warehouse one Friday night during the winter, just ahead of the holidays. When the staff return two weeks later, the warehouse is quite cold. In some sections, moisture that condensed has formed a layer of ice 1 to 2 mm thick on the concrete floor. The concrete floor is 25 cm thick and sits on compacted earth. Both the slab and the ground below it are now at 20°F. The building operator turns on the heating system, quickly warming the air to 60°F. If the heat transfer coefficient between the air and the floor is 15 W/m²K, how long will it take for the ice to start melting? Take $\alpha_{concr} = 7.0 \times 10^{-7}$ m²/s and $k_{concr} = 1.4$ W/m·K, and make justifiable approximations as appropriate.

5.49 A thick wooden wall, initially at 25°C, is made of fir. It is suddenly exposed to flames at 800°C. If the effective heat transfer coefficient for convection and radiation between the wall and the flames is 80 W/m²K, how long will it take the wooden wall to reach an assumed ignition temperature of 430°C?

5.50 Cold butter does not spread as well as warm butter. A small tub of whipped butter bears a label suggesting that, before use, it be allowed to warm up in room air for 30 minutes after being removed from the refrigerator. The tub has a diameter of 9.1 cm with a height of 5.6 cm, and the properties of whipped butter are: $k = 0.125$ W/m·K, $c_p = 2520$ J/kg·K, and $\rho = 620$ kg/m³. Assume that the tub's plastic walls offer negligible thermal resistance, that $\overline{h} = 10$ W/m²K outside the tub. Ignore heat gained from the countertop below the tub. If the refrigerator temperature was 5°C and the tub has warmed for 30 minutes in a room at 20°C, find: the temperature in the center of the butter tub, the temperature around the edge of the top surface of the butter, and the total energy (in J) absorbed by the butter tub.

5.51 A two-dimensional, 90° annular sector has an adiabatic inner arc, $r = r_i$, and an adiabatic outer arc, $r = r_o$. The flat surface along $\theta = 0$ is isothermal at T_1, and the flat surface along $\theta = \pi/2$ is isothermal at T_2. Show that the shape factor is $S = (2/\pi) \ln(r_o/r_i)$.

5.52 Suppose that $T_\infty(t)$ is the time-dependent temperature of the environment surrounding a convectively-cooled, lumped object.

a. When T_∞ is not constant, show that eqn. (1.19) leads to

$$\frac{d}{dt}(T - T_\infty) + \frac{(T - T_\infty)}{\mathcal{T}} = -\frac{dT_\infty}{dt}$$

where the time constant $\mathcal{T}$ is defined as usual.

b. If the object's initial temperature is T_i, use either an integrating factor or Laplace transforms to show that $T(t)$ is

$$T(t) = T_\infty(t) + \left[T_i - T_\infty(0)\right] e^{-t/\mathcal{T}} - e^{-t/\mathcal{T}} \int_0^t e^{s/\mathcal{T}} \frac{d}{ds} T_\infty(s)\, ds$$

5.53 Use the equation derived in Problem 5.52b to verify eqn. (5.14).

5.54 Suppose that a thermocouple with an initial temperature T_i is placed into an airflow for which its Bi $\ll 1$ and its time constant is $\mathcal{T}$. Suppose also that the temperature of the airflow varies harmonically as $T_\infty(t) = T_i + \Delta T \cos(\omega t)$.

a. Use the equation derived in Problem 5.52b to find the temperature of the thermocouple, $T_{tc}(t)$, for $t > 0$. (If you wish, note that the real part of $e^{i\omega t}$ is Re$\{e^{i\omega t}\} = \cos \omega t$ and use complex variables to do the integration.)

b. Approximate your result for $t \gg \mathcal{T}$. Then determine the value of $T_{tc}(t)$ for $\omega \mathcal{T} \ll 1$ and for $\omega \mathcal{T} \gg 1$. Explain in physical terms the relevance of these limits to the frequency response of the thermocouple—its ability to follow various frequencies.

c. If the thermocouple has a time constant of $\mathcal{T} = 0.1$ sec, estimate the highest frequency temperature variation that it will measure accurately.

5.55 A particular tungsten lamp filament has a diameter of 100 μm and sits inside a glass bulb filled with inert gas. The effective heat transfer coefficient for convection and radiation is 750 W/m·K and

the electrical current is at 60 Hz. How much does the filament's surface temperature fluctuate if the gas temperature is 200°C and the average wire temperature is 2900°C?

5.56 The consider the parameter ψ in eqn. (5.41).

   a. If the timescale for heat to diffuse a distance δ is δ^2/α, explain the physical significance of ψ and the consequence of large or small values of ψ.

   b. Show that the timescale for the thermal response of a wire of radius δ with Bi $\ll 1$ is $\rho c_p \delta/(2\overline{h})$. Then explain the meaning of the new parameter $\phi = \rho c_p \omega \delta/(4\pi \overline{h})$.

   c. When Bi $\ll 1$, is ϕ or ψ a more relevant parameter?

5.57 Repeat the calculations of Example 5.2 using the one-term solutions. Discuss the differences between your solution and the numbers in the example. Which provides greater accuracy?

5.58 The lumped-capacity solution, eqn. (1.22) depends on $t/\mathcal{T}$. (a) Write $t/\mathcal{T}$ in terms of Bi and Fo for a slab, a cylinder, and a sphere [slab: $t/\mathcal{T} = \text{Bi}_L \text{Fo}_l$]. (b) For a sphere with Fo = 1, 2, and 5, plot the lumped-capacity solution as a function of Bi on semilogarithmic coordinates. How do these curves compare to those in Fig. 5.9?

5.59 Use the lumped-capacity solution to derive an equation for the heat removal, Φ, as a function of t. Then put this equation in terms of Fo and Bi for a cylinder. Plot the result on semilogarithmic coordinates as a function of Bi for Fo = 25, 10, 5, and 2. Compare these curves to Fig. 5.10b.

5.60 Write down the one-term solutions for Θ for a slab with Bi = {0.01, 0.05, 0.1, 0.5, 1}. Compare these to the corresponding lumped capacity equation (see Problem 5.58). Ostrogorsky [5.8] has shown that $\hat{\lambda}_1 \simeq \sqrt{m \cdot \text{Bi}}$ for Bi $\leqslant 0.1$, where $m = 1$ for a slab, 2 for a cylinder, and 3 for a sphere. How does that formula compare to your results?

5.61 When the one-term solution, eqn. (5.42), is plotted on semilogarithmic coordinates as log Θ versus Fo for fixed values of Bi and position, what is the shape of the curve obtained? Make such a plot for a sphere with Bi = {0.5, 1, 2, 5, 10} at $r/r_o = 1$ for $0.2 \leqslant \text{Fo} \leqslant 1.5$.

5.62 The solution for a semi-infinite body with convection, eqn. (5.53), contains a parameter β which is like $\text{Bi}\sqrt{\text{Fo}}$. For cylinders with Bi = 1 and Bi = 10, use eqn. (5.53) to find Θ when Fo = 0.05 for each of the four positions shown in Fig. 5.8, noting that r and x coordinates have different origins. How to these values compare to the values in Fig. 5.8?

5.63 Use eqn. (5.53), for a semi-infinite body, to write an equation for Θ at the surface of a body as a function of Bi and Fo. Plot this function on semilogarithmic axes for Fo = 0.05, 0.02, and 0.01 over the domain $0.01 \leqslant \text{Bi} \leqslant 100$. Compare to Figs. 5.7–5.9. (If you encounter numerical problems for large values of Bi, note that $e^{x^2}\text{erfc}\,x \sim 1/\sqrt{\pi}x$ as $x \longrightarrow \infty$.)

5.64 Use the method outlined in [5.19] to find the shape factors for Figs. 5.30g and 5.30j.

5.65 Work Problem 11.56, about an ablating heat shield on a spacecraft.

5.66 The flux plots in Fig. 5.31 are for pentagons with bottom edge at $T = 1$. In (a), the top right edge is at $T = 0$, while in (b), both top edges are at $T = 0$. All other edges are adiabatic. Find the shape factor for each flux plot. What is the product of these two shape factors? Explain why.

a. Top right edge isothermal   **b.** Both top edges isothermal
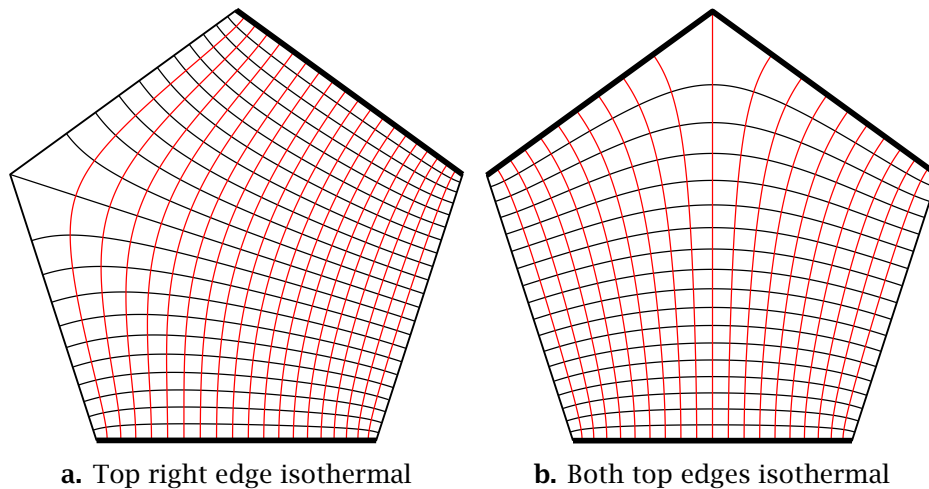
Figure 5.31 Flux plots for regular pentagons with isothermal bottom edges and either one or two top edges isothermal.

References

[5.1] H. D. Baehr and K. Stephan. *Heat and Mass Transfer*. Springer-Verlag, Berlin, 1998.

[5.2] A. F. Mills. *Basic Heat and Mass Transfer*. Prentice-Hall, Inc., Upper Saddle River, NJ, 2nd ed., 1999.

[5.3] M. P. Heisler. Temperature charts for induction and constant temperature heating. *Trans. ASME*, **69**(3):227–236, 1947. doi: 10.1115/1.4017360.

[5.4] P. J. Schneider. *Temperature Response Charts*. John Wiley & Sons, Inc., New York, 1963.

[5.5] H. S. Carslaw and J. C. Jaeger. *Conduction of Heat in Solids*. Oxford University Press, New York, 2nd ed., 1959.

[5.6] F. A. Jeglic. An analytical determination of temperature oscillations in wall heated by alternating current. Technical Note D-1286, NASA, July 1962.

[5.7] F. A. Jeglic, K. A. Switzer, and J. H. Lienhard. Surface temperature oscillations of electric resistance heaters supplied with alternating current. *J. Heat Transfer*, **102**(2):392–393, May 1980. doi: 10.1115/1.3244303.

[5.8] A. G. Ostrogorsky. Simple explicit equations for transient heat conduction in finite solids. *J. Heat Transfer*, **131**(1):011303, January 2009. doi: 10.1115/1.2977540.

[5.9] A. G. Ostrogorsky. Eigenvalues and three-term approximation of Fourier series solution of heat conduction transients, valid for $0.02 <$ Fo $< \infty$ and all Bi. *J. Serbian Society for Computational Mechanics*, **11**(1):110–118, 2017. doi: 10.24874/jsscm.2017.11.01.11.

[5.10] J. Bronowski. *The Ascent of Man*. Chapter 4. Little, Brown and Company, Boston, 1973.

[5.11] N. Zuber. Hydrodynamic aspects of boiling heat transfer. Technical Report AECU-4439, US Atomic Energy Commission, June 1959. doi: 10.2172/4175511. UCLA doctoral dissertation.

[5.12] M. S. Plesset and S. A. Zwick. The growth of vapor bubbles in superheated liquids. *J. Appl. Phys.*, **25**:493–500, April 1954. doi: 10.1063/1.1721668.

[5.13] L. E. Scriven. On the dynamics of phase growth. *Chem. Eng. Sci.*, **10**:1–13, April 1959. doi: 10.1016/0009-2509(59)80019-1.

[5.14] P. Dergarabedian. The rate of growth of bubbles in superheated water. *J. Appl. Mech., Trans. ASME*, **20**(4):537–545, December 1953. doi: 10.1115/1.4010761.

[5.15] L. R. Glicksman and J. H. Lienhard V. *Modeling and Approximation in Heat Transfer*. Cambridge University Press, New York, 2016. Uses basic physical principles to develop simple models of complex processes. Follows the approach of MIT's doctoral qualifying exams in heat transfer.

[5.16] E. R. G. Eckert and R. M. Drake, Jr. *Analysis of Heat and Mass Transfer*. Hemisphere Publishing Corp., Washington, D.C., 1987.

[5.17] V. S. Arpaci. *Conduction Heat Transfer*. Ginn Press/Pearson Custom Publishing, Needham Heights, Mass., 1991.

[5.18] L. M. K. Boelter, V. H. Cherry, H. A. Johnson, and R. C. Martinelli. *Heat Transfer Notes*. McGraw-Hill Book Company, New York, 1965.

[5.19] J. H. Lienhard. Heat conduction through 'Yin-Yang' bodies. *J. Heat Transfer*, **103**(3):600–601, 1981. url: http://www.uh.edu/engines/Yin-YangBodies.jpg.

[5.20] E. Hahne and U. Grigull. Formfaktor und Formwiderstand der stationären mehrdimensionalen Wärmeleitung. *Int. J. Heat Mass Transfer*, **18**(6): 751–767, June 1975. doi: 10.1016/0017-9310(75)90205-7.

[5.21] M. M. Yovanovich. Conduction and thermal contact resistances (conductances). In W. M. Rohsenow, J. P. Hartnett, and Y. I. Cho, editors, *Handbook of Heat Transfer*, Chapter 3. McGraw-Hill, New York, 3rd ed., 1998.

[5.22] P. M. Morse and H. Feshbach. *Methods of Theoretical Physics*. McGraw-Hill Book Company, New York, 1953.

[5.23] R. Rüdenberg. Die ausbreitung der luft—und erdfelder um hochspannungsleitungen besonders bei erd—und kurzschlüssen. *Electrotech. Z.*, **36**:1342–1346, 1925.

[5.24] S. H. Corriher. *Cookwise: the hows and whys of successful cooking*. Wm. Morrow and Company, New York, 1997. Includes excellent descriptions of the physical and chemical processes of cooking. *The* cookbook for those who enjoyed freshman chemistry.

[5.25] J. H. Lienhard and R. B. Day. The breakup of superheated liquid jets. *J. Basic Engineering*, **92**(3):515–521, September 1970. url: http://www.uh.edu/engines/BreakupSuperheatedLiquidJets.pdf.

PART III

CONVECTIVE HEAT TRANSFER

6. Laminar and turbulent boundary layers

In cold weather, if the air is calm, we are not so much chilled as when there is wind along with the cold; for in calm weather, our clothes and the air entangled in them receive heat from our bodies; this heat...brings them nearer than the surrounding air to the temperature of our skin. But in windy weather, this heat is prevented...from accumulating; the cold air, by its impulse...both cools our clothes faster and carries away the warm air that was entangled in them.

notes on "The General Effects of Heat", Joseph Black, c. 1790s

6.1   Some introductory ideas

Joseph Black's centuries-old description of heat convection sounds odd to our ears. Yet it is surprisingly accurate. Cold air really does sweep away warm air that is "entangled" with a warm body. Cold air really does replace warm air. What Black called "entanglement" is a fluid-mechanical process that we must deal with before we can analyze convective heating and cooling.

Our aim in this chapter is to predict h and $\overline{h}$ for various situations. Our first step will be learning how fluids move around the bodies that they heat or cool. Only then can we predict how much heat flow results from those fluid motions.

Flow boundary layer

Fluids stick to bodies as they flow over them. Their velocity drops from that of the flowing fluid stream down to zero at the surface. This change takes place in a layer that builds up around the body, as shown in Fig. 6.1.
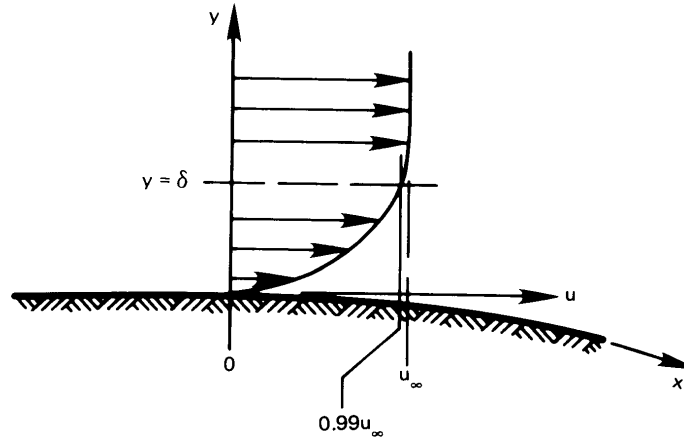
271

Figure 6.1 A boundary layer of thickness δ.

We call this layer the *boundary layer*, or b.l. We define the b.l. thickness, δ, as the distance above the surface at which the fluid has 99% of the outer, "free-stream" velocity, u_∞. A boundary layer is normally very thin compared with the size of the body in the flow.[1]

Ludwig Prandtl[2] (see Fig. 6.2) and his students first predicted boundary layer behavior in 1904. We shall discuss their results and other mathematical analyses in Sections 6.2 and 6.3. Then we shall move on to the analysis of heat transfer in boundary layers.

First, however, let us describe the b.l. more completely. We begin with the dimensional functional equation for the boundary layer thickness on a flat surface

$$\delta = \text{fn}(u_\infty, \rho, \mu, x)$$

where x is the length along the surface and ρ and μ are the fluid density in kg/m³ and dynamic viscosity in kg/m·s. We have five variables in kg, m, and s, so we anticipate two pi-groups:

$$\frac{\delta}{x} = \text{fn}(\text{Re}_x) \qquad \text{Re}_x \equiv \frac{\rho u_\infty x}{\mu} = \frac{u_\infty x}{\nu} \tag{6.1}$$

---

[1]We qualify this remark when we treat the b.l. quantitatively.

[2]Prandtl was educated at the Technical University in Munich and finished his doctorate there in 1900. He was given a chair in a new fluid mechanics institute at Göttingen University in 1904—the same year that he presented his historic paper explaining the boundary layer. His work at Göttingen during the early 20th century set the course of modern fluid mechanics and aerodynamics and laid the foundations for the analysis of heat convection [6.2].
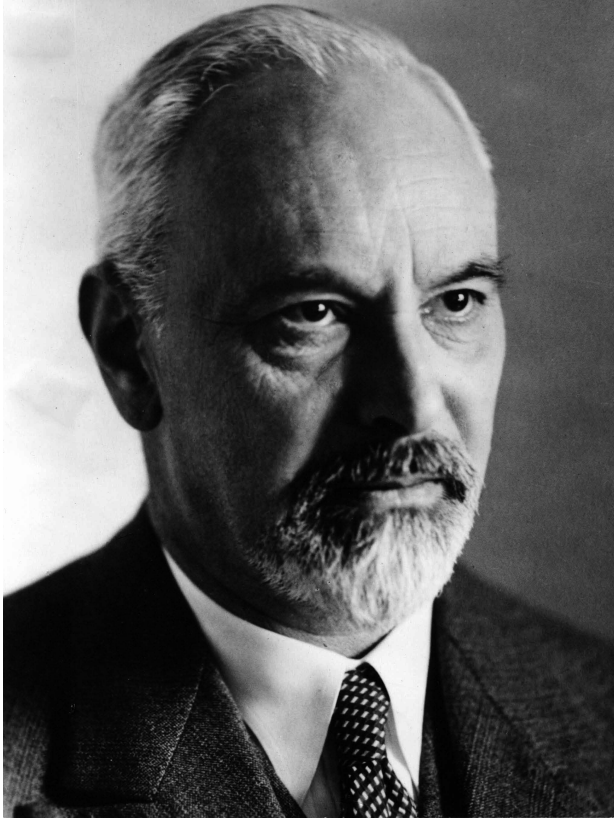
Figure 6.2   Ludwig Prandtl (1875–1953). (Courtesy of *Appl. Mech. Rev.* [6.1])

Here, ν is the kinematic viscosity μ/ρ, and Re_x is called the *Reynolds number*. The Reynolds number characterizes the relative influences of inertial and viscous forces in a fluid flow problem. The subscript on Re—x in this case—tells what length it is based upon.

Prandtl's analysis gave the actual form of eqn. (6.1) for one case: a flat surface where u_∞ is constant:

$$\boxed{\dfrac{\delta}{x} = \dfrac{4.92}{\sqrt{\mathrm{Re}_x}}} \tag{6.2}$$

Thus, if the Reynolds number is large—more than 1000 or so—then δ/x will be small. This condition is often met, except very near the leading edge or when the fluid moves slowly or has high viscosity. Later, we shall find that thinner boundary layers offer less resistance to heat flow. And we now see that the b.l. is the "entangled" fluid that Joseph Black found to carry heat away.

Osborne Reynolds (1842 to 1912)
　　　Reynolds was born in Ireland but he
　　　taught at the University of Manchester.
　　　He was a significant contributor to the
　　　subject of fluid mechanics in the late
　　　19th C. [6.3]. His original laminar-to-
　　　turbulent flow transition experiment,
　　　pictured below, was still being used as
　　　a student experiment at the University
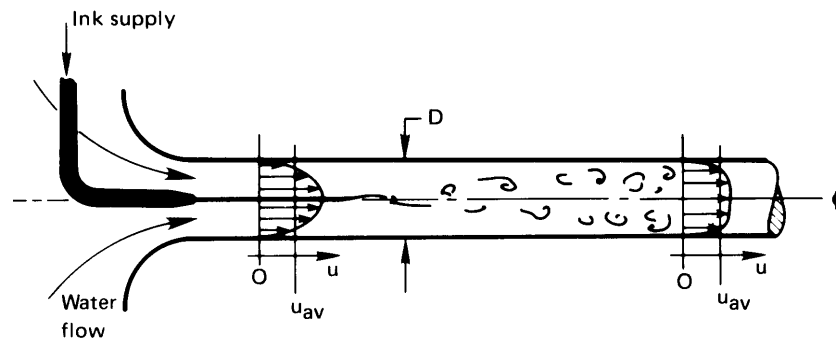　　　of Manchester in the 1970s.

Figure 6.3　Osborne Reynolds and his laminar–turbulent flow
transition experiment. (Detail from a portrait at the University
of Manchester.)

　　　The Reynolds number is named after Osborne Reynolds (see Fig. 6.3),
who discovered the laminar–turbulent transition during fluid flow in a
tube. He injected ink into a steady and undisturbed flow of water and
found that, beyond a certain average velocity, u_{av}, the liquid streamline
marked with ink would become wobbly and then break up into increasingly
disorderly eddies, and it would finally be completely mixed into the water,
as is suggested in the sketch.

　　　To define the transition, we first note that the transitional value of
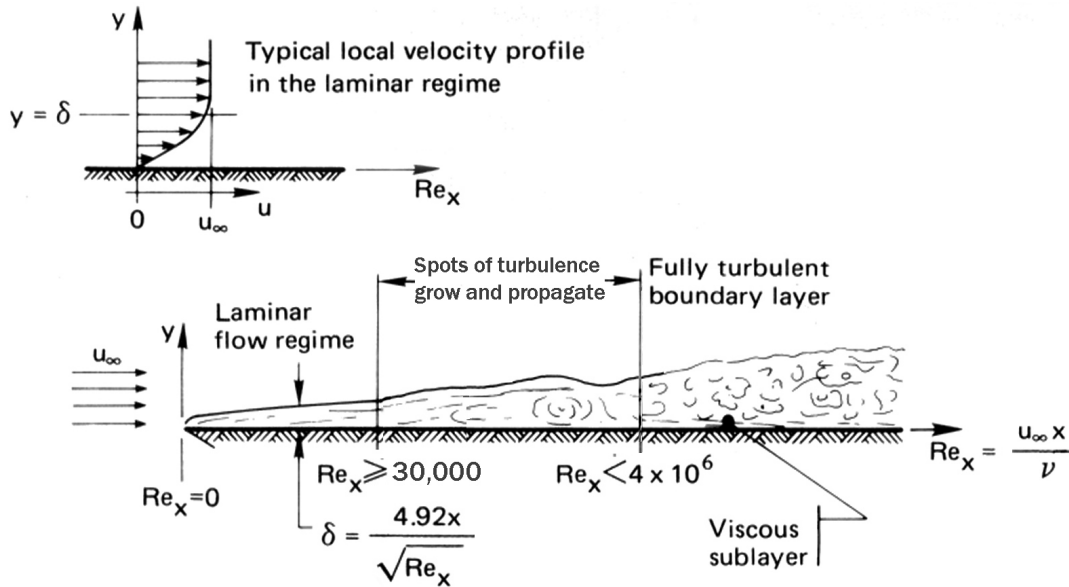the average velocity, $(u_{av})_{crit}$, must depend on the pipe diameter, D, on

Figure 6.4 Boundary layer on a long, flat surface with a sharp leading edge.

μ, and on ρ—four variables in kg, m, and s. Therefore, only one pi-group arises:

$$\mathrm{Re}_{\text{critical}} \equiv \frac{\rho D (u_{\text{av}})_{\text{crit}}}{\mu} \tag{6.3}$$

The maximum Reynolds number for which laminar flow in a pipe will always be stable, regardless of the level of background noise, is 2100. In a reasonably careful experiment, laminar flow can be made to persist up to Re = 10,000. With enormous care it can be increased still another order of magnitude. But the value below which the flow will *always* be laminar—the critical value of Re—is 2100.

Much the same sort of thing happens in a boundary layer. Figure 6.4 shows a b.l. within a fluid flowing over a plate with a sharp leading edge. The flow is laminar up to a location x_l where Re_x has the value

$$\mathrm{Re}_{\text{critical}} = \frac{u_\infty x_l}{\nu} \tag{6.4}$$

At larger values of x the b.l. exhibits sporadic vortex-like instabilities over a fairly long range, and it finally settles into a fully turbulent b.l. at a location x_u, at which $\mathrm{Re}_x = u_\infty x_u / \nu$.

The locations where transition begins and ends depend on a number of factors. These include the level of free-stream turbulence, the shape of the leading edge, the surface roughness, and the presence of acoustic or structural vibrations [6.4, §5.5]. Laminar flow can begin to break down when $Re_x \gtrsim 30,000$. The number 30,000 is practical minimum for a highly disturbed flow. For the conditions of a laboratory wind tunnel, transition often starts for Re_x between 2×10^5 and 5×10^5. However, very careful laboratory experiments have delayed the onset of transition to $Re_x \simeq 2.8 \times 10^6$ and fully turbulent flow to $Re_x \simeq 4 \times 10^6$ [6.5]. The transition region has about same length as the laminar region [6.6].

These numbers are all for flat surfaces. If a surface curves away from the flow (as in Fig. 6.1), turbulence can begin at even lower Reynolds numbers. The fact that the transition to turbulence is subject to so many influences creates much troublesome uncertainty. We deal further with transition in Section 6.9.

Thermal boundary layer

When a wall is at a temperature T_w, different from the temperature of the free stream, T_∞, a *thermal boundary layer* is present. The thermal b.l. has a thickness, δ_t, different from the *flow* b.l. thickness, δ. A thermal b.l. is pictured in Fig. 6.5. Now, with reference to this picture, we equate the heat conducted away from the wall by the fluid to the same heat transfer expressed in terms of a convective heat transfer coefficient

$$\underbrace{-k_f \left. \frac{\partial T}{\partial y} \right|_{y=0}}_{\substack{\text{conduction} \\ \text{into the fluid}}} \equiv h(T_w - T_\infty) \tag{6.5}$$

where k_f is the fluid's thermal conductivity. Notice two things about this result. First, Fourier's law of conduction correctly expresses the heat removal *at the wall* because the fluid touching the wall has zero velocity. Second, although eqn. (6.5) looks like a b.c. of the third kind, is not. This condition *defines h*, whose value we have yet to determine.

Equation (6.5) can be arranged in the form

$$\left. \frac{\partial \left(\dfrac{T_w - T}{T_w - T_\infty} \right)}{\partial (y/L)} \right|_{y/L=0} = \frac{hL}{k_f} \equiv Nu_L, \text{ the Nusselt number} \tag{6.5a}$$
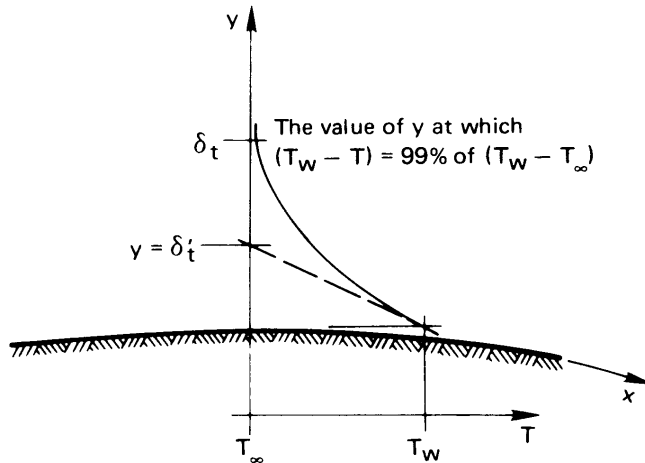
Figure 6.5 The thermal boundary layer during the flow of cool fluid over a warm plate. The b.l. thickness δ_t is a few times greater than the extrapolated thickness δ_t'.

where L is a characteristic dimension of the body—the length of a plate or the diameter of a cylinder, say. If if we write eqn. (6.5) at a point, x, along a flat surface, then we can put $\mathrm{Nu}_x \equiv hx/k_f$. From Fig. 6.5 we see immediately that the physical significance of Nu is

$$\mathrm{Nu}_L = \frac{L}{\delta_t'} \tag{6.6}$$

In other words, the Nusselt number is inversely proportional to the thickness of the thermal b.l.

The Nusselt number is named after Wilhelm Nusselt,[3] whose work on convective heat transfer was as fundamental as Prandtl's was in analyzing the related fluid dynamics (see Fig. 6.6).

We now turn to the detailed evaluation of h. And, as the preceding remarks make very clear, this evaluation will have to start with a description of the flow field in the boundary layer.

---

[3]Nusselt finished his doctorate in mechanical engineering at the Technical University in Munich in 1907 [6.7]. During a teaching appointment at Dresden (1913 to 1917) he made two of his most important contributions. He did the dimensional analysis of heat convection before he had access to Buckingham and Rayleigh's work. In so doing, he showed how to generalize limited data, and he set the pattern of subsequent analysis. He also showed how to predict convective heat transfer during film condensation. After moving about Germany and Switzerland from 1907 until 1925, he was named to the prestigious Chair of Theoretical Mechanics at Munich. During his early years in this post, he made seminal contributions to heat exchanger design methodology. He held this position until 1952. He was succeeded in the chair by another of Germany's heat transfer luminaries, Ernst Schmidt.

Figure 6.6 Ernst Kraft Wilhelm Nusselt (1882–1957). This photograph, provided by his student, G. Lück, shows Nusselt at the Kesselberg waterfall in 1912. He was an avid mountain climber.

6.2   Laminar incompressible boundary layer on a flat surface

We predict the boundary layer flow field by solving the equations that express conservation of mass and momentum in the b.l. Thus, the first order of business is to develop these equations.

Conservation of mass—The continuity equation

A two- or three-dimensional velocity field can be expressed in vectorial form as

$$\vec{u} = u\vec{\imath} + v\vec{\jmath} + w\vec{k}$$

where u, v, and w are the x, y, and z components of velocity. Figure 6.7 shows a two-dimensional velocity flow field. If the flow is steady, the paths of individual particles appear as steady *streamlines*. The streamlines can be expressed in terms of a *stream function, $\psi(x, y)$* = constant, where each value of the constant identifies a separate streamline, as shown in the figure.

Since the streamlines are the paths followed by fluid particles, the velocity vector, $\vec{u}$, is always tangent to them. Therefore, no fluid flows *across* a streamline. This means that the mass flow rate between two
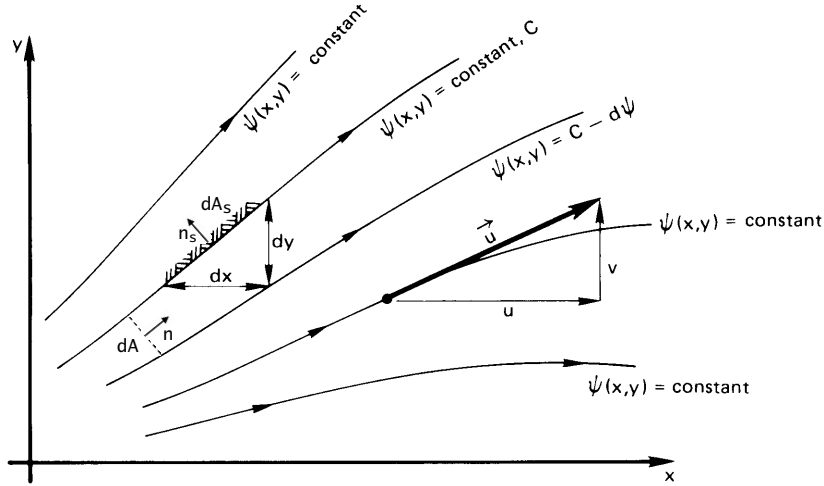
Figure 6.7 A steady, incompressible, two-dimensional flow field represented by streamlines, or lines of constant ψ.

adjacent streamlines is constant, like the difference in ψ between them. If the area per unit depth between two adjacent streamlines is dA and $\vec{n}$ is the unit normal vector to that area, then the mass flow rate between the streamlines is $d\dot{m} = \rho\vec{u} \cdot \vec{n}\,dA$. To obtain a convenient relationship between velocity and the stream function, we may require that the difference in ψ be proportional to the mass flow rate between the streamlines

$$d\dot{m} = \rho\vec{u} \cdot \vec{n}\,dA = \rho\,d\psi \qquad (6.7)$$

(for an incompressible flow with constant ρ along each streamline).

Next we can consider an area dA_s that lies on a streamline—the cross-hatched section in Fig. 6.7. The normal vector $\vec{n}_s$ for this section points toward the upper left of the figure. No mass crosses a streamline, so the mass flow through dA_s is $d\dot{m} = \rho\vec{u} \cdot \vec{n}_s\,dA_s = 0$. With trigonometry, we may show that $\vec{n}_s dA_s = -dy\,\vec{\imath} + dx\,\vec{\jmath}$. Taking the dot product, $d\dot{m}$ becomes

$$d\dot{m} = -\rho v\,dx + \rho u\,dy = 0 \qquad (6.8)$$

To find $d\psi$ in terms of dx and dy, we may differentiate the stream function along any streamline, $\psi(x, y) = $ constant, in Fig. 6.7, with the result:

$$d\psi = \left.\frac{\partial\psi}{\partial x}\right|_y dx + \left.\frac{\partial\psi}{\partial y}\right|_x dy = 0 \qquad (6.9)$$

These relations *define* the stream function in terms of the velocities. By substituting eqns. (6.8) and (6.9) into eqn. (6.7), and dividing through by ρ, we obtain

$$v \equiv -\left.\frac{\partial \psi}{\partial x}\right|_y \quad \text{and} \quad u \equiv \left.\frac{\partial \psi}{\partial y}\right|_x \tag{6.10}$$

Furthermore,

$$\frac{\partial^2 \psi}{\partial y \partial x} = \frac{\partial^2 \psi}{\partial x \partial y}$$

so that

$$\boxed{\frac{\partial u}{\partial x} + \frac{\partial v}{\partial y} = 0} \tag{6.11a}$$

This result is called the two-dimensional *continuity equation* for incompressible flow. The equation states mathematically that the flow is *continuous*, in the sense that whatever mass enters an incompressible volume of fluid must also leave it. In three dimensions, the continuity equation for an incompressible flow is

$$\boxed{\nabla \cdot \vec{u} \equiv \frac{\partial u}{\partial x} + \frac{\partial v}{\partial y} + \frac{\partial w}{\partial z} = 0} \tag{6.11b}$$

Example 6.1

Fluid moves with a uniform velocity, u_∞, in the x-direction. Find the stream function and see if it gives plausible behavior (see Fig. 6.8).

SOLUTION. $u = u_\infty$ and $v = 0$. Therefore, from eqns. (6.10)

$$u_\infty = \left.\frac{\partial \psi}{\partial y}\right|_x \quad \text{and} \quad 0 = -\left.\frac{\partial \psi}{\partial x}\right|_y$$

Integrating these equations, we get

$$\psi = u_\infty y + \text{fn}(x) \quad \text{and} \quad \psi = 0 + \text{fn}(y)$$

Comparing these equations, we see that $\text{fn}(x) = \text{constant}$ and $\text{fn}(y) = u_\infty y + \text{constant}$, so

$$\psi = u_\infty y + \text{constant}$$

The final equation gives a series of equally spaced, horizontal streamlines, as we would expect (see Fig. 6.8). We set the arbitrary constant equal to zero in the figure so that the stream function is zero at the wall. ∎
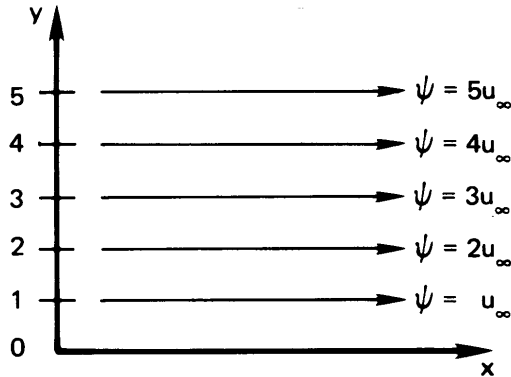
Figure 6.8 Streamlines in a uniform horizontal flow field, $\psi = u_\infty y$.

Conservation of momentum

The momentum equation in a viscous flow is a complicated vectorial expression called the Navier-Stokes equation, which is derived in any advanced fluid mechanics text [6.8, 6.9]. We shall offer a very restrictive derivation of the equation—one that applies only to a two-dimensional incompressible b.l. flow, as shown in Fig. 6.9.

Here we see how shear stresses acting upon an element **A** continuously distort and rotate it. We use heavy arrows in the enlargement of **A** to display pressure forces and horizontal shear stresses.[4] Lighter arrows show the momentum fluxes entering and leaving **A**. Notice that both x- and y-directed momentum enters and leaves element **A**.

To see how momentum flux works, let us imagine a man standing in the open door of a moving railroad boxcar. A child standing on the ground throws him a soccer ball. The man catches the ball, and one component of its momentum pushes him backward. However, the other component pushes him to the side opposite the direction the train is moving. Fluid entering element **A** affects its motion in the same way.

The velocities must adjust to satisfy the conservation of linear momentum. To evaluate momentum conservation, we consider a stationary control volume surrounding the particle **A** at one instant in time, say the instant when it is rectangular as shown in the figure. We require that the sum of the external forces acting on the control volume in the x-direction

---

[4]The stress, τ, is often given two subscripts. The first one identifies the direction normal to the plane on which it acts, and the second one identifies the line along which it acts. Thus, if both subscripts are the same, the stress acts normal to a surface—it must be a pressure or tension instead of a shear stress.
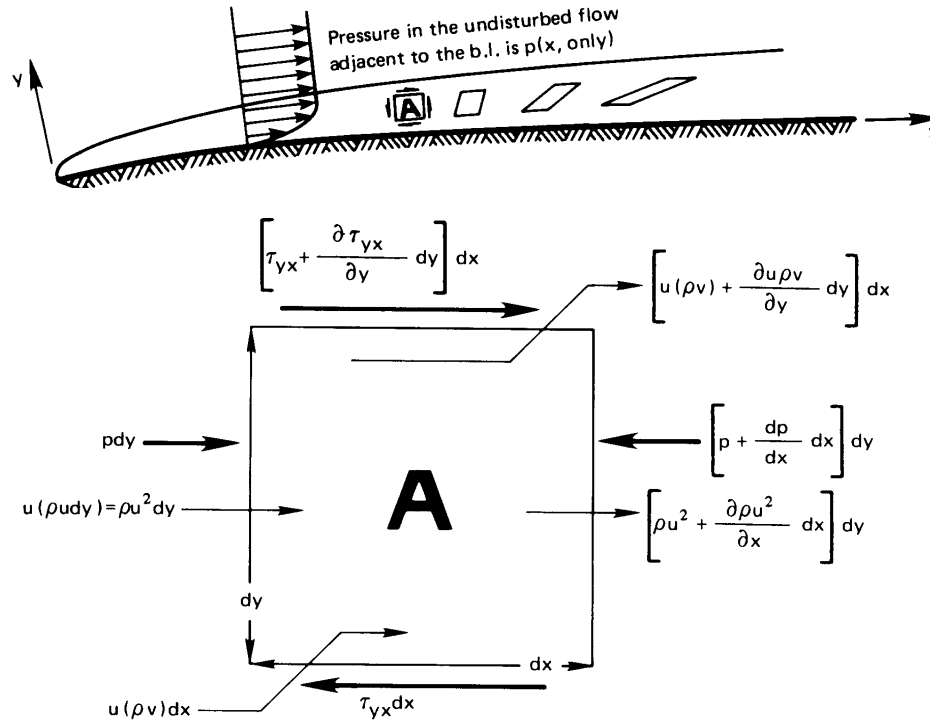
Figure 6.9 Forces acting in a two-dimensional incompressible boundary layer.

must be balanced by the rate at which x-directed momentum flows out of the control volume.

The external forces, shown in Fig. 6.9, are

$$\left(\tau_{yx} + \frac{\partial \tau_{yx}}{\partial y}\, dy\right) dx - \tau_{yx}\, dx + p\, dy - \left(p + \frac{dp}{dx}\, dx\right) dy$$

$$= \left(\frac{\partial \tau_{yx}}{\partial y} - \frac{dp}{dx}\right) dx\, dy$$

The rate at which x-directed momentum flows out of **A** is

$$\left(\rho u^2 + \frac{\partial \rho u^2}{\partial x}\, dx\right) dy - \rho u^2\, dy + \left[u(\rho v) + \frac{\partial u\rho v}{\partial y}\, dy\right] dx$$

$$- u(\rho v)\, dx = \left(\frac{\partial \rho u^2}{\partial x} + \frac{\partial \rho u v}{\partial y}\right) dx\, dy$$

Setting the right-hand sides of these two equations equal, we obtain a

statement of conservation of x-directed momentum for the b.l.:

$$\left(\frac{\partial \tau_{yx}}{\partial y} - \frac{dp}{dx}\right) dx\, dy = \left(\frac{\partial \rho u^2}{\partial x} + \frac{\partial \rho uv}{\partial y}\right) dx\, dy$$

The shear stress in this result can be eliminated with the help of Newton's law of viscous shear stress

$$\tau_{yx} = \mu \frac{\partial u}{\partial y}$$

so that the momentum equation becomes

$$\frac{\partial}{\partial y}\left(\mu \frac{\partial u}{\partial y}\right) - \frac{dp}{dx} = \left(\frac{\partial \rho u^2}{\partial x} + \frac{\partial \rho uv}{\partial y}\right)$$

Finally, we may limit use of the equation to temperature and pressure ranges for which $\rho \cong$ constant and $\mu \cong$ constant. Then

$$\frac{\partial u^2}{\partial x} + \frac{\partial uv}{\partial y} = -\frac{1}{\rho}\frac{dp}{dx} + \nu \frac{\partial^2 u}{\partial y^2} \qquad (6.12)$$

This equation is one form of the steady, two-dimensional, incompressible boundary layer momentum equation.[5]

If we multiply eqn. (6.11a) by u and subtract the result from the left-hand side of eqn. (6.12), we obtain a second form of the momentum equation:

$$\boxed{u\frac{\partial u}{\partial x} + v\frac{\partial u}{\partial y} = -\frac{1}{\rho}\frac{dp}{dx} + \nu \frac{\partial^2 u}{\partial y^2}} \qquad (6.13)$$

Equation (6.13) has a number of so-called *boundary layer approximations* built into it:

- $|\partial u/\partial x| \ll |\partial u/\partial y|$. Shear stress in the x-direction is much greater than in the y-direction ($\tau_{yx} \gg \tau_{xy}$).

- $v \ll u$. The y-component of momentum is negligible.

- $p \neq \mathrm{fn}(y)$. The y pressure gradient is negligible.

We may obtain the streamwise pressure gradient by writing the Bernoulli equation for the free-stream flow just above the boundary layer where there is no viscous shear stress:

$$\frac{p}{\rho} + \frac{u_\infty^2}{2} = \text{ constant}$$

---

[5]A more complete derivation shows this result to remain valid for variable density if μ is constant and gravity is not important. Gravity taken into account in Section 8.2.

By differentiating this equation, we determine the pressure gradient in terms of the free-stream velocity gradient:

$$\frac{1}{\rho}\frac{dp}{dx} = -u_\infty \frac{du_\infty}{dx}$$

Substituting into eqn. (6.13):

$$u\frac{\partial u}{\partial x} + v\frac{\partial u}{\partial y} = u_\infty \frac{du_\infty}{dx} + v\frac{\partial^2 u}{\partial y^2} \tag{6.14}$$

And if there is no pressure gradient in the flow—if u_∞ and p are constant, as they would be for flow past a flat plate—then eqns. (6.13) and (6.14) become

$$\boxed{u\frac{\partial u}{\partial x} + v\frac{\partial u}{\partial y} = v\frac{\partial^2 u}{\partial y^2}} \tag{6.15}$$

Predicting the velocity profile in the laminar boundary layer without a pressure gradient

Exact solution. Two strategies for solving eqn. (6.15) for the velocity profile have long been used. The first was developed by Prandtl's student, H. Blasius,[6] before World War I. This approach gives an exact solution, and we shall sketch it only briefly.

First we introduce the stream function, ψ, into eqn. (6.15), reducing the number of dependent variables from two (u and v) to just one—namely, ψ. By substituting eqns. (6.10) into eqn. (6.15):

$$\frac{\partial \psi}{\partial y}\frac{\partial^2 \psi}{\partial y \partial x} - \frac{\partial \psi}{\partial x}\frac{\partial^2 \psi}{\partial y^2} = v\frac{\partial^3 \psi}{\partial y^3} \tag{6.16}$$

Equation (6.16) can be converted into an ordinary d.e. with the following change of variables

$$\psi(x, y) \equiv \sqrt{u_\infty v x}\, f(\eta) \quad \text{where} \quad \eta \equiv \sqrt{\frac{u_\infty}{v x}}\, y \tag{6.17}$$

where $f(\eta)$ is an as-yet-undetermined function. [This transformation is quite similar to the one that we used to make an ordinary d.e. of the

---

[6]Blasius achieved great fame for many accomplishments in fluid mechanics and then gave it up. Despite how much he had achieved, he was eventually quoted as saying: "I decided that I had no gift for it; all of my ideas came from Prandtl."

Table 6.1 Exact velocity profile in the boundary layer on a flat surface with no pressure gradient

$y\sqrt{u_\infty/\nu x}$		u/u_∞	$v\sqrt{x/\nu u_\infty}$	
η	$f(\eta)$	$f'(\eta)$	$(\eta f' - f)/2$	$f''(\eta)$
0.00	0.00000	0.00000	0.00000	0.33206
0.20	0.00664	0.06641	0.00332	0.33199
0.40	0.02656	0.13277	0.01322	0.33147
0.60	0.05974	0.19894	0.02981	0.33008
0.80	0.10611	0.26471	0.05283	0.32739
1.00	0.16557	0.32979	0.08211	0.32301
2.00	0.65003	0.62977	0.30476	0.26675
3.00	1.39682	0.84605	0.57067	0.16136
4.00	2.30576	0.95552	0.75816	0.06424
4.918	3.20169	*0.99000*	0.83344	0.01837
6.00	4.27964	0.99898	0.85712	0.00240
8.00	6.27923	1.00000^-	0.86039	0.00001

heat conduction equation, between eqns. (5.44) and (5.45).] After some manipulation of partial derivatives, this substitution gives (Problem 6.2)

$$f\,\frac{d^2f}{d\eta^2} + 2\frac{d^3f}{d\eta^3} = 0 \tag{6.18}$$

and

$$\frac{u}{u_\infty} = \frac{df}{d\eta} \qquad \frac{v}{\sqrt{u_\infty \nu/x}} = \frac{1}{2}\left(\eta\frac{df}{d\eta} - f\right) \tag{6.19}$$

The boundary conditions for this flow are

$$\left.\begin{array}{rl}
u(y=0)=0 & \text{or} \quad \dfrac{df}{d\eta}\bigg|_{\eta=0} = 0 \\[2ex]
u(y=\infty)=u_\infty & \text{or} \quad \dfrac{df}{d\eta}\bigg|_{\eta=\infty} = 1 \\[2ex]
v(y=0)=0 & \text{or} \quad f(\eta=0)=0
\end{array}\right\} \tag{6.20}$$

The solution of eqn. (6.18) subject to these b.c.'s must be done numerically (see Problem 6.3).

The solution of the Blasius problem is listed in Table 6.1, and the dimensionless velocity components are plotted in Fig. 6.10. The u component increases from zero at the wall ($\eta = 0$) to 99% of u_∞ at $\eta = 4.92$.
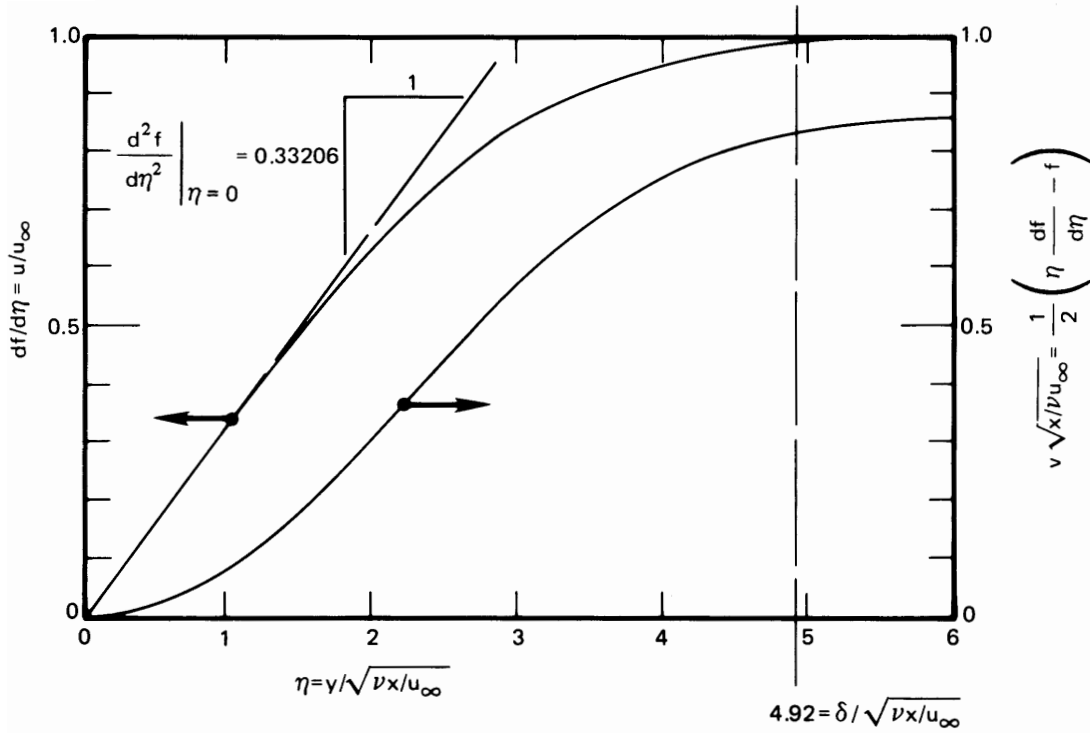
Figure 6.10 The dimensionless velocity components in a laminar boundary layer.

Thus, the b.l. thickness is given by

$$4.92 = \frac{\delta}{\sqrt{\nu x / u_\infty}}$$

or, as we stated earlier, in eqn. (6.2),

$$\frac{\delta}{x} = \frac{4.92}{\sqrt{u_\infty x / \nu}} = \frac{4.92}{\sqrt{Re_x}}$$

Concept of similarity. The exact solution for $u(x, y)$ reveals a most useful fact—namely, that u can be expressed as a function of a single variable, η:

$$\frac{u}{u_\infty} = f'(\eta) = f'\left(y\sqrt{\frac{u_\infty}{\nu x}}\right)$$

We call this a *similarity solution.* To see why, we solve eqn. (6.2) for

$$\sqrt{\frac{u_\infty}{\nu x}} = \frac{4.92}{\delta(x)}$$

and substitute this into $f'(y\sqrt{u_\infty/\nu x})$. The result is

$$f' = \frac{u}{u_\infty} = \text{fn}\left[\frac{y}{\delta(x)}\right] \tag{6.21}$$

The velocity profile thus has the same shape with respect to the b.l. thickness at each x-position. We say, in other words, that the profile is *similar* at each position. We found the same behavior for conduction into a semi-infinite region. In that case [recall eqn. (5.51)], $x/\sqrt{t}$ always had the same value at the outer limit of the thermally disturbed region.

Boundary layer similarity makes it especially easy to use a simple approximate method for solving other b.l. problems. That method, called the *momentum integral method*, is the subject of the next subsection.

Example 6.2

Air at 27°C blows over a flat surface with a sharp leading edge at 1.5 m/s. Find the b.l. thickness 0.5 m from the leading edge. Check the b.l. assumption that $u \gg v$ at that location.

SOLUTION. The kinematic viscosity is $\nu = 1.575 \times 10^{-5}$ m^2/s. Then

$$\text{Re}_x = \frac{u_\infty x}{\nu} = \frac{1.5(0.5)}{1.575 \times 10^{-5}} = 47,619$$

The Reynolds number is low enough that the flow will be laminar (unless the b.l. is subject to large disturbances. See pg. 275). Then

$$\delta = \frac{4.92x}{\sqrt{\text{Re}_x}} = \frac{4.92(0.5)}{\sqrt{47,619}} = 0.01127 = 1.127 \text{ cm}$$

Remember that the b.l. analysis is valid only if $\delta/x \ll 1$. In this case, $\delta/x = 1.127/50 = 0.0225$.

From Fig. 6.10 or Table 6.1, we observe that v/u is greatest beyond the outside edge of the b.l., at large η. Using data from Table 6.1 at $\eta = 8$, v at $x = 0.5$ m is

$$v = \frac{0.8604}{\sqrt{x/\nu u_\infty}} = 0.8604\sqrt{\frac{(1.575 \times 10^{-5})(1.5)}{(0.5)}}$$

$$= 0.00591 \text{ m/s}$$

or, since $u/u_\infty \longrightarrow 1$ at large η

$$\frac{v}{u} = \frac{v}{u_\infty} = \frac{0.00591}{1.5} = 0.00394 \qquad ■$$

Since v grows larger as x grows smaller, the condition $v \ll u$ is not satisfied very near the leading edge. There, the b.l. approximations themselves break down. We say more about this breakdown after eqn. (6.34).

Momentum integral method.[7] A second method for solving the b.l. momentum equation is approximate and much easier to apply to a wide range of problems than is any exact method of solution. The idea is this: We are not really interested in the details of the velocity or temperature profiles in the b.l., beyond learning their slopes at the wall: these slopes give us the shear stress at the wall, $\tau_w = \mu(\partial u/\partial y)_{y=0}$, and the heat flux at the wall, $q_w = -k(\partial T/\partial y)_{y=0}$. Therefore, we integrate the b.l. equations from the wall, $y = 0$, to the b.l. thickness, $y = \delta$, to make ordinary d.e.'s of them. Although these much simpler equations do not reveal anything new about the temperature and velocity profiles, they do give quite accurate explicit equations for τ_w and q_w.

Let us see how this procedure works with the b.l. momentum equation. We consider the case in which the pressure gradient is zero ($dp/dx = 0$), and integrate eqn. (6.12) across the b.l.:

$$\int_0^\delta \frac{\partial u^2}{\partial x}\,dy + \int_0^\delta \frac{\partial(uv)}{\partial y}\,dy = \nu \int_0^\delta \frac{\partial^2 u}{\partial y^2}\,dy$$

At $y = \delta$, u can be approximated as the free-stream value, u_∞, and other quantities can be evaluated as if y lay outside the b.l.:

$$\int_0^\delta \frac{\partial u^2}{\partial x}\,dy + \Big[\underbrace{(uv)_{y=\delta}}_{=u_\infty v_\infty} - \underbrace{(uv)_{y=0}}_{=0}\Big] = \nu\left[\underbrace{\left(\frac{\partial u}{\partial y}\right)_{y=\delta} - \left(\frac{\partial u}{\partial y}\right)_{y=0}}_{\cong 0}\right] \quad (6.22)$$

The continuity equation (6.11a) can be integrated thus:

$$v_\infty - \underbrace{v_{y=0}}_{=0} = -\int_0^\delta \frac{\partial u}{\partial x}\,dy \quad (6.23)$$

Multiplying this equation by u_∞ gives

$$u_\infty v_\infty = -\int_0^\delta \frac{\partial u u_\infty}{\partial x}\,dy$$

Using this result in eqn. (6.22), we obtain

$$\int_0^\delta \frac{\partial}{\partial x}\big[u(u - u_\infty)\big]\,dy = -\nu\,\frac{\partial u}{\partial y}\bigg|_{y=0}$$

---

[7]This method was developed by Pohlhausen, von Kármán, and others. See the discussion in [6.8, Chap. XII].

Finally, since $\mu(\partial u/\partial y)_{y=0} = \tau_w$, the shear stress on the wall at position x, we have[7]

$$\boxed{\frac{d}{dx}\int_0^{\delta(x)} u(u - u_\infty)\,dy = -\frac{\tau_w}{\rho}} \tag{6.24}$$

Equation (6.24) expresses the conservation of linear momentum in integral form. This equation shows that the momentum deficit of the fluid in the b.l. changes at a rate proportional the wall shear stress. When we use eqn. (6.24) in place of eqn. (6.15), we are said to be *using an integral method*.

We may nondimensionalize eqn. (6.24) as follows:

$$\frac{d}{dx}\left[\delta\int_0^1 \frac{u}{u_\infty}\left(\frac{u}{u_\infty} - 1\right)d\left(\frac{y}{\delta}\right)\right] = -\frac{\tau_w(x)}{\rho u_\infty^2} \equiv -\frac{1}{2}C_f(x) \tag{6.25}$$

where $\tau_w/(\rho u_\infty^2/2)$ is the *skin friction coefficient*, C_f (see pg. 291). Equation (6.25) will be satisfied precisely by Blasius's exact solution for u/u_∞ (Problem 6.4). However, the point is to use eqn. (6.25) to determine u/u_∞ when we do not already have an exact solution, by making an approximation to the velocity profile.

To find an approximate velocity profile, we recall that the laminar boundary layer exhibits similarity. So, we can guess that the profile has the form of eqn. (6.21): $u/u_\infty = \mathrm{fn}(y/\delta)$. The approximation should satisfy the following four boundary conditions on the velocity profile:

$$\left.\begin{array}{lll} \text{i)} & u/u_\infty = 0 & \text{at} \quad y/\delta = 0 \\ \text{ii)} & u/u_\infty \cong 1 & \text{at} \quad y/\delta = 1 \\ \text{iii)} & \partial u/\partial y \cong 0 & \text{at} \quad y/\delta = 1 \end{array}\right\} \tag{6.26}$$

and, by evaluating eqn. (6.15) at the wall,

$$\underbrace{u\,\frac{\partial u}{\partial x}}_{=0} + \underbrace{v\,\frac{\partial u}{\partial y}}_{=0} = \nu\left.\frac{\partial^2 u}{\partial y^2}\right|_{y=0}$$

so

$$\text{iv)} \quad \partial^2 u/\partial y^2 = 0 \quad \text{at} \quad y/\delta = 0 \tag{6.27}$$

---

[7]The interchange of integration and differentiation is consistent with Leibnitz's rule for differentiation of an integral (Problem 6.14).

If we now write $\text{fn}(y/\delta)$ as a polynomial with four constant coefficients—a, b, c, and d—

$$\frac{u}{u_\infty} = a + b\frac{y}{\delta} + c\left(\frac{y}{\delta}\right)^2 + d\left(\frac{y}{\delta}\right)^3 \tag{6.28}$$

then the four b.c.s on the velocity profile give

    i) $0 = a$ which eliminates a immediately
    ii) $1 = 0 + b + c + d$
    iii) $0 = b + 2c + 3d$
    iv) $0 = 2c$ which eliminates c as well

Solving the middle two equations for b and d, we obtain $d = -\frac{1}{2}$ and $b = +\frac{3}{2}$, so

$$\frac{u}{u_\infty} = \frac{3}{2}\frac{y}{\delta} - \frac{1}{2}\left(\frac{y}{\delta}\right)^3 \tag{6.29}$$

We compare this approximate velocity profile with the exact Blasius profile in Fig. 6.11, and they agree to within a maximum error of 8%. The only remaining problem is calculating $\delta(x)$. To do this, we substitute eqn. (6.29) into eqn. (6.25) and integrate to get (see Problem 6.5):

$$-\frac{d}{dx}\left[\delta\left(\frac{39}{280}\right)\right] = -\frac{\nu}{u_\infty\delta}\left(\frac{3}{2}\right) \tag{6.30}$$

or

$$-\frac{39}{280}\left(\frac{2}{3}\right)\left(\frac{1}{2}\right)\frac{d\delta^2}{dx} = -\frac{\nu}{u_\infty}$$

We integrate using the b.c. $\delta = 0$ at $x = 0$:

$$\delta^2 = \frac{280}{13}\frac{\nu x}{u_\infty} \tag{6.31a}$$

or

$$\frac{\delta}{x} = \frac{4.64}{\sqrt{\text{Re}_x}} \tag{6.31b}$$

This b.l. thickness is of the correct functional form, and the constant is lower than the exact value by only 5.6%.
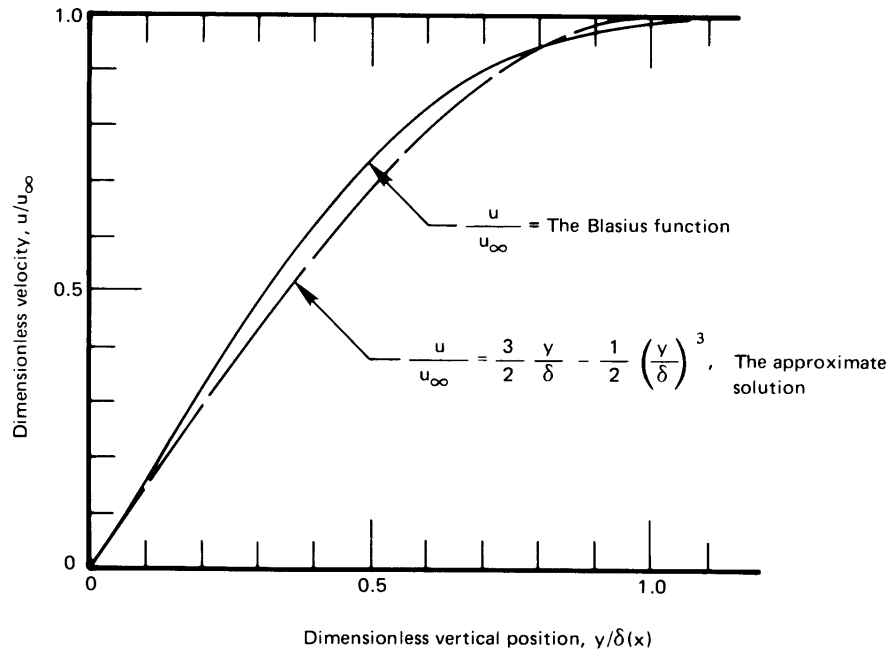
Figure 6.11 Comparison of the third-degree polynomial fit, eqn. (6.29), to the exact b.l. velocity profile. Notice that the approximate result has been forced to $u/u_\infty = 1$ instead of 0.99 at $y = \delta$.

The skin friction coefficient

Since the function $f(\eta)$ gives all information about flow in the b.l., the shear stress at the wall can be obtained from it by using Newton's law of viscous shear:

$$\tau_w = \mu \left. \frac{\partial u}{\partial y} \right|_{y=0} = \mu \left. \frac{\partial}{\partial y} (u_\infty f') \right|_{y=0} = \mu u_\infty \left(\frac{df'}{d\eta} \frac{\partial \eta}{\partial y} \right)_{y=0}$$

$$= \mu u_\infty \frac{\sqrt{u_\infty}}{\sqrt{\nu x}} \left. \frac{d^2 f}{d\eta^2} \right|_{\eta=0}$$

But from Fig. 6.10 and Table 6.1, we see that $d^2 f/d\eta^2 |_{\eta=0} = 0.33206$, so

$$\tau_w = 0.332 \frac{\mu u_\infty}{x} \sqrt{\text{Re}_x} \tag{6.32}$$

The integral method that we just outlined would have given 0.323 for the constant in eqn. (6.32) instead of 0.332 (Problem 6.6).

The *local skin friction coefficient* is defined as

$$C_f \equiv \frac{\tau_w}{\rho u_\infty^2/2} = \frac{0.664}{\sqrt{\text{Re}_x}} \tag{6.33}$$

The *overall skin friction coefficient*, $\overline{C}_f$, is based on the average of the shear stress over the length, L, of the plate

$$\overline{\tau}_w = \frac{1}{L}\int_0^L \tau_w \, dx = \frac{\rho u_\infty^2}{2L}\int_0^L \frac{0.664}{\sqrt{u_\infty x/\nu}} \, dx = 1.328\frac{\rho u_\infty^2}{2}\sqrt{\frac{\nu}{u_\infty L}}$$

so

$$\overline{C}_f \equiv \frac{\overline{\tau}_w}{\rho u_\infty^2/2} = \frac{1.328}{\sqrt{\text{Re}_L}} \tag{6.34}$$

Notice that $C_f(x)$ approaches infinity at the leading edge of the flat surface. This means that to stop the fluid that first touches the front of the plate—dead in its tracks—would require infinite shear stress right at that point. Nature, of course, will not allow such a thing to happen; and it turns out that the boundary layer approximations are not valid near the leading edge.

In fact, the range $x \lesssim 5\delta$ is too close to the leading edge to use this analysis with accuracy because the b.l. is relatively thick and ν is no longer $\ll u$. With eqn. (6.2), this range converts to approximately

$$x \gtrsim 600\,\nu/u_\infty \quad \text{for a boundary layer to exist}$$

or $\text{Re}_x \gtrsim 600$. In Example 6.2, this condition is satisfied for x greater than about 6 mm. The region where b.l. approximations fail is usually very small.

Example 6.3

Calculate the average shear stress and the overall friction coefficient for the surface in Example 6.2 if its total length is $L = 0.5$ m. Compare $\overline{\tau}_w$ with τ_w at the trailing edge. At what point on the surface does $\tau_w = \overline{\tau}_w$? Finally, estimate what fraction of the surface can legitimately be analyzed using boundary layer theory.

SOLUTION.

$$\overline{C}_f = \frac{1.328}{\sqrt{\text{Re}_{0.5}}} = \frac{1.328}{\sqrt{47,619}} = 0.00609$$

and

$$\overline{\tau}_w = \frac{\rho u_\infty^2}{2} \overline{C}_f = \frac{1.177(1.5)^2}{2} 0.00609 = 0.00806 \underbrace{\text{kg/m·s}^2}_{\text{N/m}^2}$$

This is very little drag. (In English units, it amounts only to about $1/5$ ounce/ft^2.) At $x = L$,

$$\left.\frac{\tau_w(x)}{\overline{\tau}_w}\right|_{x=L} = \frac{\rho u_\infty^2/2}{\rho u_\infty^2/2}\left[\frac{0.664/\sqrt{\text{Re}_L}}{1.328/\sqrt{\text{Re}_L}}\right] = \frac{1}{2}$$

and $\tau_w(x) = \overline{\tau}_w$ at the location where

$$\frac{0.664}{\sqrt{x}} = \frac{1.328}{\sqrt{0.5}}$$

Solving, the local shear stress equals the average value at

$$x = \frac{1}{8} \text{ m} \qquad \text{or} \qquad \frac{x}{L} = \frac{1}{4}$$

Thus, the shear stress, which is initially infinite, plummets to $\overline{\tau}_w$ one-fourth of the way from the leading edge and drops to only one-half of $\overline{\tau}_w$ over the remaining 75% of the plate.

The boundary layer approximations fail when

$$x \lesssim 600\,\frac{\nu}{u_\infty} = 600\,\frac{1.575 \times 10^{-5}}{1.5} = 0.0063 \text{ m}$$

Thus, the preceding analysis should be good over almost 99% of the 0.5 m length of the surface. ■

6.3   The energy equation

Derivation

We now know how fluid moves in the b.l. Next, we must extend the heat conduction equation to allow for fluid motion. Then, we can solve it to get the temperature field in the b.l. and then calculate h, using Fourier's law:

$$h = \frac{q}{T_w - T_\infty} = -\frac{k}{T_w - T_\infty} \left.\frac{\partial T}{\partial y}\right|_{y=0} \qquad (6.35)$$
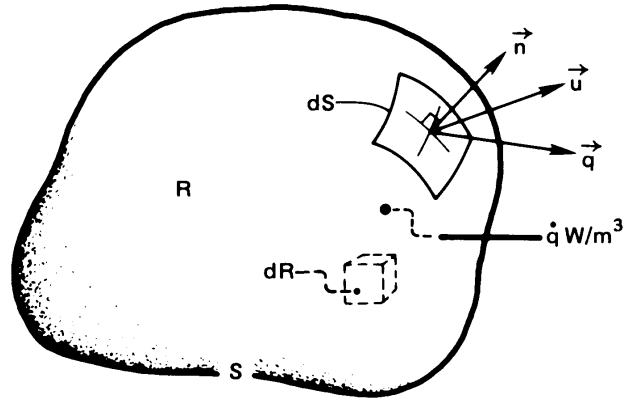
Figure 6.12 Control volume in a heat-flow and fluid-flow field.

To predict T, we extend the analysis of Section 2.1. Figure 2.4 shows a volume containing a solid subjected to a temperature field. We now allow this volume to contain a moving fluid with a velocity field $\vec{u}(x, y, z)$, as shown in Fig. 6.12. We make the following restrictive approximations:

- Pressure variations in the flow are not large enough to affect thermodynamic properties. From thermodynamics, we know that the specific internal energy, $\hat{u}$, is related to the specific enthalpy as $\hat{h} = \hat{u} + p/\rho$, and that $d\hat{h} = c_p \, dT + (\partial \hat{h}/\partial p)_T \, dp$, where $c_p = (\partial h/\partial T)_p$. We shall neglect the effect of dp on enthalpy, internal energy, and density. This approximation is reasonable for most liquid flows and for gases flowing at speeds less than about 1/3 the speed of sound.

- Under these conditions, density changes result only from temperature changes. If temperature-induced changes in density are also small, the flow will behave as if incompressible. In that case, $\nabla \cdot \vec{u} = 0$ (Section 6.2).

- Temperature variations in the flow are not large enough to change k significantly. When we consider the flow field, we will also presume μ to be unaffected by temperature change.

- Potential and kinetic energy changes are negligible in comparison to thermal energy changes. Since the kinetic energy of a fluid can change as a result of pressure gradients, this again means that pressure variations may not be too large.

- The viscous stresses do not dissipate enough energy to warm the fluid significantly.

Just as we wrote eqn. (2.7) for a control volume in Section 2.1, we now write conservation of energy for a moving fluid in the form

$$\underbrace{\frac{d}{dt}\int_R \rho\hat{u}\,dR}_{\substack{\text{rate of internal}\\\text{energy increase}\\\text{in } R}} = -\underbrace{\int_S (\rho\hat{h})\,\vec{u}\cdot\vec{n}\,dS}_{\substack{\text{rate of internal energy and}\\\text{flow work out of } R}}$$

$$-\underbrace{\int_S (-k\nabla T)\cdot\vec{n}\,dS}_{\substack{\text{net heat conduction}\\\text{rate out of } R}} + \underbrace{\int_R \dot{q}\,dR}_{\substack{\text{rate of heat}\\\text{generation in } R}} \qquad (6.36)$$

In the second integral, $\vec{u}\cdot\vec{n}\,dS$ represents the volume flow rate through an element dS of the control surface. The position of R is not changing in time, so we can bring the time derivative inside the first integral. If we then we call in Gauss's theorem [eqn. (2.8)] to make the surface integrals into volume integrals, eqn. (6.36) becomes

$$\int_R \left(\frac{\partial(\rho\hat{u})}{\partial t} + \nabla\cdot(\rho\vec{u}\hat{h}) - \nabla\cdot k\nabla T - \dot{q}\right)dR = 0$$

Because the integrand must vanish identically (recall the footnote on pg. 55 in Chapter 2) and, if k depends only weakly on T,

$$\frac{\partial(\rho\hat{u})}{\partial t} + \underbrace{\nabla\cdot(\rho\vec{u}\hat{h})}_{= \rho\vec{u}\cdot\nabla\hat{h} + \hat{h}\nabla\cdot(\rho\vec{u})} - k\nabla^2 T - \dot{q} = 0$$

Since we are neglecting pressure effects, we may introduce the following approximation:

$$d(\rho\hat{u}) = d(\rho\hat{h}) - dp \approx d(\rho\hat{h}) = \rho d\hat{h} + \hat{h}\,d\rho$$

Thus, collecting and rearranging terms

$$\rho\left(\frac{\partial\hat{h}}{\partial t} + \vec{u}\cdot\nabla\hat{h}\right) + \hat{h}\underbrace{\left(\frac{\partial\rho}{\partial t} + \nabla\cdot(\rho\vec{u})\right)}_{=0} = k\nabla^2 T + \dot{q}$$

The two derivatives involving density are each negligible when density changes are small. However, we can show (Problem 6.36) that the two terms sum to zero for density changes of *any* size.

Upon substituting $d\hat{h} \approx c_p \, dT$, we obtain our final result:

$$\rho c_p \left(\underbrace{\frac{\partial T}{\partial t}}_{\substack{\text{energy} \\ \text{storage}}} + \underbrace{\vec{u} \cdot \nabla T}_{\substack{\text{enthalpy} \\ \text{convection}}} \right) = \underbrace{k \nabla^2 T}_{\substack{\text{heat} \\ \text{conduction}}} + \underbrace{\dot{q}}_{\substack{\text{heat} \\ \text{generation}}} \tag{6.37}$$

This is the *energy equation* for a flow with low pressure gradients. It is the same as the corresponding equation for a solid body, (2.11), except for the enthalpy transport—or convection—term, $\rho c_p \vec{u} \cdot \nabla T$.

Consider the term in parentheses in eqn. (6.37):

$$\frac{\partial T}{\partial t} + \vec{u} \cdot \nabla T = \frac{\partial T}{\partial t} + u \frac{\partial T}{\partial x} + v \frac{\partial T}{\partial y} + w \frac{\partial T}{\partial z} \equiv \frac{DT}{Dt} \tag{6.38}$$

D/Dt is the so-called *material derivative*, which is treated in some detail in every fluid mechanics course. The material derivative of temperature gives the rate of change of the temperature of a fluid particle as it moves in a flow field.

In a steady two-dimensional flow field without heat sources, eqn. (6.37) reduces to

$$u \frac{\partial T}{\partial x} + v \frac{\partial T}{\partial y} = \alpha \left(\frac{\partial^2 T}{\partial x^2} + \frac{\partial^2 T}{\partial y^2} \right) \tag{6.39}$$

Furthermore, in a b.l., $\partial^2 T/\partial x^2 \ll \partial^2 T/\partial y^2$, so our b.l. energy equation for a takes the form

$$u \frac{\partial T}{\partial x} + v \frac{\partial T}{\partial y} = \alpha \frac{\partial^2 T}{\partial y^2} \tag{6.40}$$

Heat and momentum transfer analogy for $\nu = \alpha$

Consider a b.l. in a fluid of temperature T_∞, flowing over a flat surface at temperature T_w. The momentum equation (6.15) and its b.c.'s can be written as

$$u \frac{\partial}{\partial x} \left(\frac{u}{u_\infty} \right) + v \frac{\partial}{\partial y} \left(\frac{u}{u_\infty} \right) = \nu \frac{\partial^2}{\partial y^2} \left(\frac{u}{u_\infty} \right) \quad \begin{cases} \dfrac{u}{u_\infty} \bigg|_{y=0} = 0 \\[2mm] \dfrac{u}{u_\infty} \bigg|_{y=\infty} = 1 \\[2mm] \dfrac{\partial}{\partial y} \left(\dfrac{u}{u_\infty} \right)_{y=\infty} = 0 \end{cases} \tag{6.41}$$

And the energy equation (6.40) can be expressed in terms of a dimension-less temperature, $\Theta = (T - T_w)/(T_\infty - T_w)$, as

$$u\frac{\partial\Theta}{\partial x} + v\frac{\partial\Theta}{\partial y} = \alpha\frac{\partial^2\Theta}{\partial y^2} \qquad \left\{ \begin{array}{l} \Theta(y = 0) = 0 \\[4pt] \Theta(y = \infty) = 1 \\[4pt] \left.\dfrac{\partial\Theta}{\partial y}\right|_{y=\infty} = 0 \end{array} \right. \qquad (6.42)$$

Notice that the problems of predicting u/u_∞ and Θ are *identical*, with one exception: eqn. (6.41) has ν in it whereas eqn. (6.42) has α. If ν and α should happen to be equal, the temperature distribution in the b.l. is

for $\nu = \alpha$: $\dfrac{T - T_w}{T_\infty - T_w} = f'(\eta)$ derivative of the Blasius function

because the two problems must have the same solution.

In this case, we can immediately calculate the heat transfer coefficient using eqn. (6.5):

$$h = \frac{k}{T_\infty - T_w}\left.\frac{\partial(T - T_w)}{\partial y}\right|_{y=0} = k\left(\frac{\partial f'}{\partial\eta}\frac{\partial\eta}{\partial y}\right)_{\eta=0}$$

but $d^2f/d\eta^2\big|_{\eta=0} = 0.33206$ (see Fig. 6.10) and $\partial\eta/\partial y = \sqrt{u_\infty/\nu x}$, so

$$\frac{hx}{k} = \mathrm{Nu}_x = 0.33206\sqrt{\mathrm{Re}_x} \quad \text{for } \nu = \alpha \qquad (6.43)$$

Normally, in using eqn. (6.43) or any other forced convection equation, properties should be evaluated at the *film temperature*, $T_f = (T_w + T_\infty)/2$.

Example 6.4

Water flows over a flat heater, 0.06 m in length, at 15 atm pressure and 440 K. The free-stream velocity is 2 m/s and the heater is held at 460 K. What is the average heat flux?

SOLUTION. At $T_f = (460 + 440)/2 = 450$ K:

$$\nu = 1.725 \times 10^{-7} \text{ m}^2/\text{s}$$
$$\alpha = 1.724 \times 10^{-7} \text{ m}^2/\text{s}$$

Therefore, $\nu \cong \alpha$, and we can use eqn. (6.43). First, we must calculate the average heat flux, $\overline{q}$. To do this, we set $\Delta T \equiv T_w - T_\infty$ and write

$$\overline{q} = \frac{1}{L} \int_0^L (h\Delta T)\, dx = \frac{\Delta T}{L} \int_0^L \frac{k}{x} \mathrm{Nu}_x\, dx = 0.332 \frac{k\Delta T}{L} \underbrace{\int_0^L \sqrt{\frac{u_\infty}{\nu x}}\, dx}_{= \, 2\sqrt{u_\infty L/\nu}}$$

so

$$\overline{q} = 2\left(0.332\frac{k}{L}\sqrt{\mathrm{Re}_L}\right)\Delta T = 2q_{x=L}$$

Note that the average heat flux is twice that at the trailing edge, $x = L$. Using $k = 0.674$ W/m·K for water at the film temperature,

$$\overline{q} = 2(0.332)\frac{0.674}{0.06}\sqrt{\frac{2(0.06)}{1.72 \times 10^{-7}}}(460 - 440)$$
$$= 124{,}604 \text{ W/m}^2 = 125 \text{ kW/m}^2 \qquad \blacksquare$$

Equation (6.43) is clearly a very restrictive heat transfer solution. We must now find how to evaluate q when ν does not equal α.

6.4 The Prandtl number and the boundary layer thicknesses

Dimensional analysis

We now apply dimensional analysis to expose an important link between the velocity and thermal boundary layers. To find the dimensional functional equation, look at the parameters in the b.l. momentum equation, (6.15), the b.l. energy equation, (6.40), the definition of h, eqn. (6.35), and the boundary conditions on u and T. From these,

$$h = \mathrm{fn}(\nu, \alpha, k, x, u_\infty)$$

We have excluded $T_w - T_\infty$ on the basis of Newton's original hypothesis, borne out in eqn. (6.43)—that $h \neq \mathrm{fn}(\Delta T)$ during forced convection.

In this situation, as discussed at the end of Section 4.3, heat and work do not convert into one another. That means we should not regard J as N·m, but rather as a single dimension. Further, J and K appear only together, as J/K, in h and k. Hence, the six variables have only dimensions J/K, m, and s. The $6 - 3 = 3$ dimensionless groups are then:

$$\Pi_1 = \frac{hx}{k} \equiv \mathrm{Nu}_x \qquad \Pi_2 = \frac{\rho u_\infty x}{\mu} \equiv \mathrm{Re}_x$$
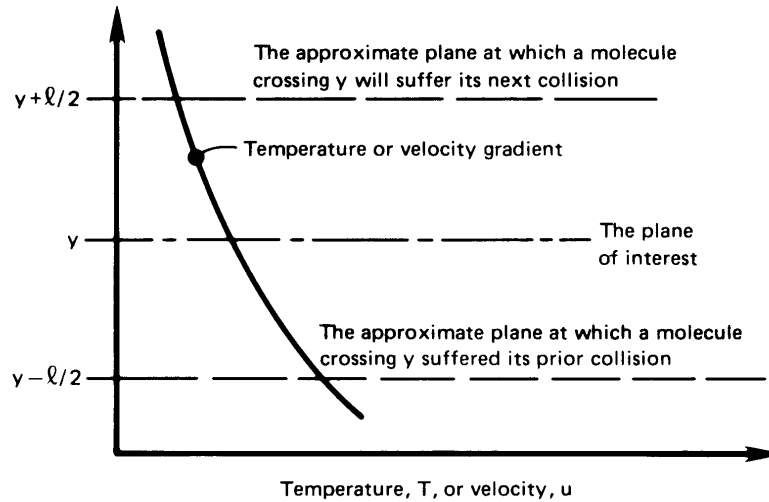
Figure 6.13 Momentum and energy transfer in a gas with a velocity or temperature gradient.

and a new group:

$$\Pi_3 = \frac{\mu c_p}{k} = \frac{\nu}{\alpha} \equiv \mathrm{Pr}, \text{ Prandtl number}$$

Thus,

$$\mathrm{Nu}_x = \mathrm{fn}(\mathrm{Re}_x, \mathrm{Pr}) \tag{6.44}$$

Equation (6.43) was developed for the case in which $\nu = \alpha$ or $\mathrm{Pr} = 1$; therefore, (6.43) is of the same form as eqn. (6.44), although the Pr dependence of Nu_x is not displayed.

We can better understand the physical meaning of the Prandtl number if we briefly consider how to predict its value in a gas.

Kinetic theory of μ and k

Figure 6.13 shows a small neighborhood of a point in a gas where there exists a velocity or temperature gradient. We identify the *mean free path* of molecules between collisions as ℓ. The planes at $y \pm \ell/2$ bracket the average travel of those molecules passing through plane y.[8]

---

[8]Actually, if we consider only those collisions that pass the plane y, the average travel of the colliding molecules is greater than $\ell/2$—a fact that does not affect our discussion here. This and other fine points of kinetic theory are explained in detail in [6.10].

The shear stress, τ_{yx}, can be expressed as the change of x-momentum of molecules that pass through the y-plane of interest, per unit area:

$$\tau_{yx} = \begin{pmatrix} \text{mass flux of molecules} \\ \text{from } y - \ell/2 \text{ to } y + \ell/2 \end{pmatrix} \cdot \begin{pmatrix} \text{change in fluid} \\ \text{velocity} \end{pmatrix}$$

The mass flux from bottom to top is proportional to $\rho\overline{C}$, where $\overline{C}$, the mean molecular speed. The molecular speed $\overline{C}$ is $\gg u$ and v (except for gases flow near the speed of sound). Thus,

$$\tau_{yx} = C_1\left(\rho\overline{C}\right)\left(\ell\frac{du}{dy}\right)\frac{\text{N}}{\text{m}^2} \text{ and this also equals } \mu\frac{du}{dy} \tag{6.45a}$$

where C_1 is a constant on the order of one (see Problem 6.50). By the same token,

$$q_y = C_2\left(\rho c_v\overline{C}\right)\left(\ell\frac{dT}{dy}\right)\frac{\text{W}}{\text{m}^2} \text{ and this also equals } -k\frac{dT}{dy} \tag{6.45b}$$

where c_v is the specific heat at constant volume and C_2 is another constant of order one. It follows immediately that

$$\mu = C_1\left(\rho\overline{C}\ell\right) \qquad \text{so} \qquad \nu = C_1\left(\overline{C}\ell\right) \tag{6.45c}$$

and

$$k = C_2\left(\rho c_v\overline{C}\ell\right) \qquad \text{so} \qquad \alpha = C_2\frac{\overline{C}\ell}{\gamma} \tag{6.45d}$$

where $\gamma \equiv c_p/c_v$ is approximately constant and on the order of one for a given gas. Thus, for a gas,

$$\text{Pr} \equiv \frac{\nu}{\alpha} = \text{ a constant on the order of one}$$

More detailed use of the kinetic theory of gases reveals more specific information as to the value of the Prandtl number, and the following points are borne out reasonably well experimentally, as you can determine from Tables A.5 and A.6:

- For simple monatomic gases, $\text{Pr} = \frac{2}{3}$.

- For diatomic gases in which vibration is unexcited (such as N_2 and O_2 at room temperature), $\text{Pr} = \frac{5}{7}$.

- As the complexity of gas molecules increases, Pr approaches an upper value of one.

- Pr is least sensitive to temperature in gases made up of the simplest molecules because their structure is least responsive to temperature changes.

In a liquid, the physical mechanisms of molecular momentum and energy transport are much more complicated, and Pr can be far from one. For example (cf. Table A.3):

- For liquids composed of fairly simple molecules, excluding metals, Pr is of the order of magnitude of 1 to 10.

- For liquid metals, Pr is of the order of magnitude of 10^{-2} or less.

- If the molecular structure of a liquid is very complex, Pr might reach values on the order of 10^5. This is true of oils made of long-chain hydrocarbons, for example.

- In liquids, Pr is much more sensitive to temperature than in gases. Pr often decreases rapidly as temperature rises, as a result of declining viscosity.

Thus, while Pr can vary over almost eight orders of magnitude in common fluids, it is still the result of molecular mechanisms of heat and momentum transfer.

Boundary layer thicknesses, δ and δ_t, and the Prandtl number

We have seen that, for Pr = 1, the dimensionless velocity and temperature profiles are identical on a flat surface. Thus, $\delta = \delta_t$ for Pr = 1. We also can make the following inferences:

- When Pr > 1, $\delta > \delta_t$, and when Pr < 1, $\delta < \delta_t$. This is true because high viscosity ν leads to a thick velocity b.l., and a high thermal diffusivity α gives a thick thermal b.l.

- Since the exact governing equations (6.41) and (6.42) are identical for either b.l., except for the appearance of α in one and ν in the other, we expect that

$$\frac{\delta_t}{\delta} = \text{fn}\left(\frac{\nu}{\alpha} \text{ only}\right)$$

Combining these observations, and defining $\phi \equiv \delta_t/\delta$, we conclude that

$$\phi = \text{ monotonically decreasing function of Pr only} \qquad (6.46)$$

The fact that ϕ is independent of x will greatly simplify the use of the integral method to find h. We shall establish the correct form of eqn. (6.46) in the next section.

6.5 Heat transfer coefficient for laminar, incompressible flow over a flat surface

The integral method for solving the energy equation

Integrating the b.l. energy equation (6.40) in the same way as the momentum equation gives

$$\int_0^{\delta_t} u \frac{\partial T}{\partial x}\, dy + \int_0^{\delta_t} v \frac{\partial T}{\partial y}\, dy = \alpha \int_0^{\delta_t} \frac{\partial^2 T}{\partial y^2}\, dy$$

And, with the chain rule of differentiation in the form $x\, dy = d(xy) - y\, dx$, we can rearrange this as

$$\int_0^{\delta_t} \frac{\partial uT}{\partial x}\, dy - \int_0^{\delta_t} T\frac{\partial u}{\partial x}\, dy + \int_0^{\delta_t} \frac{\partial vT}{\partial y}\, dy - \int_0^{\delta_t} T\frac{\partial v}{\partial y}\, dy = \alpha\frac{\partial T}{\partial y}\bigg|_0^{\delta_t}$$

or

$$\int_0^{\delta_t} \frac{\partial uT}{\partial x}\, dy + \underbrace{vT\bigg|_0^{\delta_t}}_{= \, T_\infty v|_{y=\delta_t} - 0} - \int_0^{\delta_t} T\underbrace{\left(\frac{\partial u}{\partial x} + \frac{\partial v}{\partial y}\right)}_{= \, 0,\ \text{eqn. (6.11a)}}\, dy$$

$$= \underbrace{\alpha\,\frac{\partial T}{\partial y}\bigg|_{\delta_t}}_{= \, 0} - \alpha\frac{\partial T}{\partial y}\bigg|_0$$

We can evaluate v at $y = \delta_t$ with the continuity equation in the form of eqn. (6.23). Then the preceding expression reduces to:

$$\int_0^{\delta_t} \frac{\partial}{\partial x}u(T - T_\infty)\, dy = \frac{1}{\rho c_p}\left(-k\frac{\partial T}{\partial y}\bigg|_0\right) = \text{fn}(x\text{ only})$$

or

$$\boxed{\frac{d}{dx}\int_0^{\delta_t} u(T - T_\infty)\, dy = \frac{q_w}{\rho c_p}} \tag{6.47}$$

Equation (6.47) expresses the conservation of thermal energy in integrated form. It shows that the rate thermal energy is carried away by the b.l. flow is matched by the rate heat is transferred into the b.l. at the wall.

Predicting the temperature distribution in the laminar thermal boundary layer

Next we shall paraphrase our use of an approximate velocity profile (Section 6.3) to create an approximate temperature profile. We previously guessed the velocity profile in such a way as to make it match what we know to be true. We also know certain things to be true of the temperature profile.

The temperatures at the wall and at the outer edge of the b.l. are known. Furthermore, the temperature distribution should be smooth as it blends into T_∞ for $y > \delta_t$. This condition is imposed by setting $\partial T/\partial y$ equal to zero at $y = \delta_t$. A fourth condition is obtained by writing eqn. (6.40) at the wall, where $u = v = 0$. This gives $\partial^2 T/\partial y^2\big|_{y=0} = 0$. These four conditions take the following dimensionless form:

$$\left.\begin{aligned}
\frac{T - T_\infty}{T_w - T_\infty} &= 1 &&\text{at } y/\delta_t = 0\\[2mm]
\frac{T - T_\infty}{T_w - T_\infty} &= 0 &&\text{at } y/\delta_t = 1\\[2mm]
\frac{\partial[(T - T_\infty)/(T_w - T_\infty)]}{\partial(y/\delta_t)} &= 0 &&\text{at } y/\delta_t = 1\\[2mm]
\frac{\partial^2[(T - T_\infty)/(T_w - T_\infty)]}{\partial(y/\delta_t)^2} &= 0 &&\text{at } y/\delta_t = 0
\end{aligned}\right\} \tag{6.48}$$

Equations (6.48) provide enough information to approximate the temperature profile with a cubic function:

$$\frac{T - T_\infty}{T_w - T_\infty} = a + b\,\frac{y}{\delta_t} + c\left(\frac{y}{\delta_t}\right)^2 + d\left(\frac{y}{\delta_t}\right)^3 \tag{6.49}$$

Substituting eqn. (6.49) into eqns. (6.48), we get

$$a = 1 \qquad -1 = b + c + d \qquad 0 = b + 2c + 3d \qquad 0 = 2c$$

which gives

$$a = 1 \qquad b = -\tfrac{3}{2} \qquad c = 0 \qquad d = \tfrac{1}{2}$$

so the temperature profile is

$$\boxed{\frac{T - T_\infty}{T_w - T_\infty} = 1 - \frac{3}{2}\frac{y}{\delta_t} + \frac{1}{2}\left(\frac{y}{\delta_t}\right)^3} \tag{6.50}$$

Predicting the heat flux in the laminar boundary layer

Equation (6.47) contains an as-yet-unknown quantity—the thermal b.l. thickness, δ_t. To calculate δ_t, we substitute the temperature profile, eqn. (6.50), and the velocity profile, eqn. (6.29), into the integral form of the energy equation, (6.47), which we first express as

$$u_\infty(T_w - T_\infty)\frac{d}{dx}\left[\delta_t \int_0^1 \frac{u}{u_\infty}\left(\frac{T - T_\infty}{T_w - T_\infty}\right) d\left(\frac{y}{\delta_t}\right)\right]$$

$$= -\frac{\alpha(T_w - T_\infty)}{\delta_t}\left.\frac{d\left(\dfrac{T - T_\infty}{T_w - T_\infty}\right)}{d(y/\delta_t)}\right|_{y/\delta_t = 0} \tag{6.51}$$

This form will work fine as long as $\delta_t < \delta$. But if $\delta_t > \delta$, the velocity will be given by $u/u_\infty = 1$, instead of eqn. (6.29), beyond $y = \delta$. Let us proceed for the moment in the hope that the requirement $\delta_t \leqslant \delta$ will be met. Introducing $\phi = \delta_t/\delta$ and defining $\eta \equiv y/\delta_t$, we get

$$\delta_t \frac{d}{dx}\left[\delta_t \underbrace{\int_0^1 \left(\frac{3}{2}\eta\phi - \frac{1}{2}\eta^3\phi^3\right)\left(1 - \frac{3}{2}\eta + \frac{1}{2}\eta^3\right) d\eta}_{= \frac{3}{20}\phi - \frac{3}{280}\phi^3}\right] = \frac{3\alpha}{2u_\infty} \tag{6.52}$$

Since ϕ is a constant for any Pr [recall eqn. (6.46)], we separate variables:

$$2\delta_t \frac{d\delta_t}{dx} = \frac{d\delta_t^2}{dx} = \frac{3\alpha/u_\infty}{\left(\dfrac{3}{20}\phi - \dfrac{3}{280}\phi^3\right)}$$

Integrating this result with respect to x and taking $\delta_t = 0$ at $x = 0$, we get

$$\delta_t = \sqrt{\frac{3\alpha x}{u_\infty}}\bigg/\sqrt{\frac{3}{20}\phi - \frac{3}{280}\phi^3} \tag{6.53}$$

In the integral formulation, $\delta = 4.64x/\sqrt{\mathrm{Re}_x}$ [eqn. (6.31b)]. We use this expression, to be consistent, and divide by δ to obtain

$$\frac{\delta_t}{\delta} \equiv \phi = 0.9638\bigg/\sqrt{\mathrm{Pr}\,\phi(1 - \phi^2/14)}$$

Rearranging this gives

$$\frac{\delta_t}{\delta} = \frac{1}{1.025\,\mathrm{Pr}^{1/3}\left[1 - (\delta_t^2/14\delta^2)\right]^{1/3}} \cong \frac{1}{1.025\,\mathrm{Pr}^{1/3}} \tag{6.54}$$
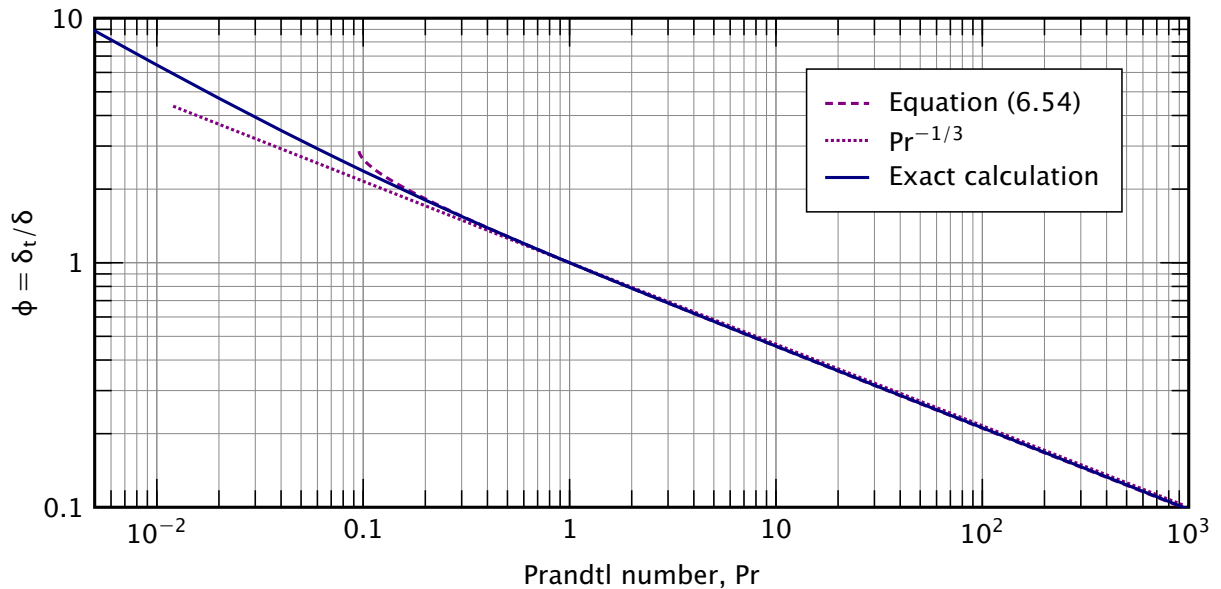
Figure 6.14 The exact and approximate Prandtl number influence on the ratio of b.l. thicknesses for T_w = constant.

The unsimplified form of eqn. (6.54) is shown in Fig. 6.14, along with the exact solution given by Pohlhausen in 1921 [6.8, 6.11]. (Pohlhausen's numerical calculations were extended by Evans [6.12], whose results were used to make this figure.) The results agree to within 0.4% for $Pr \geqslant 0.3$.

It turns out that the exact ratio, δ/δ_t, is represented to within 1–2% by the simple expression

$$\boxed{\frac{\delta_t}{\delta} = Pr^{-1/3}} \qquad Pr \geqslant 0.6 \qquad (6.55)$$

The integral method's simplified result is only slightly more accurate for high Pr: within 0.5–1% for $Pr \geqslant 4$.

In Section 6.4, we noted that the lowest Pr for pure gases is 0.67 and that Pr for nonmetallic liquids ranges from about 1 to 10^5. Thus, Fig. 6.14 shows that the integral method's solution for δ_t/δ is very accurate for gases and nonmetallic liquids. Liquid metals, on the other hand, have Prandtl numbers in the range of 0.005–0.05 for which the figure shows $3 < \delta_t/\delta < 9$. The assumptions of the integral analysis fail completely for liquid metals.

The final step in predicting the heat flux is to write Fourier's law:

$$q = -k \left.\frac{\partial T}{\partial y}\right|_{y=0} = -k \frac{T_w - T_\infty}{\delta_t} \left.\frac{\partial \left(\frac{T - T_\infty}{T_w - T_\infty}\right)}{\partial (y/\delta_t)}\right|_{y/\delta_t=0} \tag{6.56}$$

Using the dimensionless temperature distribution given by eqn. (6.50), we get

$$q = +k \frac{T_w - T_\infty}{\delta_t} \frac{3}{2}$$

or

$$h \equiv \frac{q}{\Delta T} = \frac{3k}{2\delta_t} = \frac{3}{2} \frac{k}{\delta} \frac{\delta}{\delta_t} \tag{6.57}$$

Notice that h is greater when the thermal b.l. is thinner.

Substituting eqns. (6.54) and (6.31b) for δ/δ_t and δ, we obtain

$$\text{Nu}_x \equiv \frac{hx}{k} = \frac{3}{2} \frac{\sqrt{\text{Re}_x}}{4.64} 1.025\,\text{Pr}^{1/3} = 0.3314\,\text{Re}_x^{1/2}\,\text{Pr}^{1/3}$$

Considering the various approximations, this equation is very close to Pohlhausen's exact solution, which he fitted to this power-law:

$$\boxed{\text{Nu}_x = 0.332\,\text{Re}_x^{1/2}\,\text{Pr}^{1/3}} \qquad \text{Pr} \geqslant 0.6 \tag{6.58}$$

Equation (6.58) is within 2% of the exact solution for any $\text{Pr} \geqslant 0.6$, and within 1% for $0.6 \leqslant \text{Pr} \leqslant 2$. It applies to a laminar, two-dimensional b.l. on a flat surface with $T_w = \text{constant}$.

Some other laminar boundary layer heat transfer equations

We have thus far shown how to derive many boundary layer convection equations. We now simply present the final results for additional, constant wall temperature situations.

High Pr. At high Pr, the exact solution approaches this limit [6.8, Chp. XII]:

$$\text{Nu}_x \longrightarrow 0.3387\,\text{Re}_x^{1/2}\,\text{Pr}^{1/3}, \quad \text{Pr} \longrightarrow \infty \tag{6.59}$$

This equation is accurate to better than 1% for $\text{Pr} \geqslant 2$.
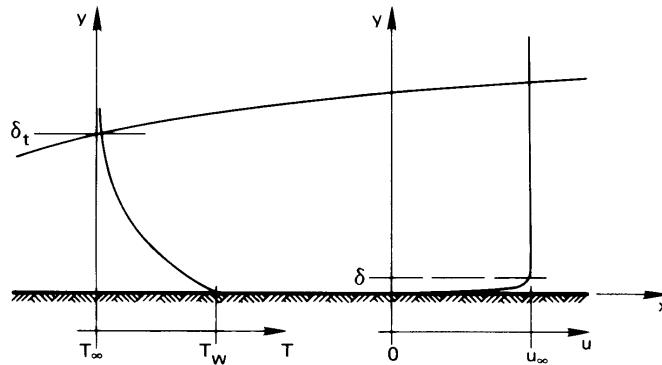
Figure 6.15 A laminar b.l. in a low-Pr liquid. The velocity b.l. is so thin that $u \cong u_\infty$ in almost the entire the thermal b.l.

Low Pr. Figure 6.15 shows a low-Pr liquid flowing over a flat plate. In this case $\delta_t \gg \delta$, and for all practical purposes $u = u_\infty$ everywhere within the thermal b.l. It is as though the no-slip condition $[u(y = 0) = 0]$ and the influence of viscosity were removed from the problem. Thus, by considering the energy equation and the definition of h, we find the following dimensional functional equation:

$$h = \text{fn}(k, x, u_\infty, \rho c_p) \tag{6.60}$$

There are five variables in J/K, m, and s, so there are only two pi-groups:

$$\text{Nu}_x = \frac{hx}{k} \quad \text{and} \quad \Pi_2 \equiv \text{Re}_x \text{Pr} = \frac{u_\infty x}{\alpha}$$

The new group, Π_2, is called the *Péclet* number, Pe_x, where the subscript identifies the length upon which it is based. It can be interpreted as follows:

$$\text{Pe}_x \equiv \frac{u_\infty x}{\alpha} = \frac{\rho c_p u_\infty \Delta T}{k \Delta T} = \frac{\text{heat capacity rate of fluid in the b.l.}}{\text{axial heat conductance of the b.l.}} \tag{6.61}$$

So long as Pe_x is large, the b.l. approximation that $\partial^2 T/\partial x^2 \ll \partial^2 T/\partial y^2$ will be valid; but for small Pe_x (i.e., $\text{Pe}_x \ll 100$), the approximation will be violated and a boundary layer solution cannot be used.

The limit of the exact solution of the b.l. equations for low Pr is:

$$\text{Nu}_x \longrightarrow \sqrt{\frac{\text{Pe}_x}{\pi}} = 0.565 \, \text{Pe}_x^{1/2}, \quad \text{Pr} \longrightarrow 0 \tag{6.62}$$

The exact solution is no more than 20% greater than this expression when $\text{Pr} \leqslant 0.05$ [6.13]. We must also have $\text{Pe}_x \gtrsim 100$.

General correlation for any Pr. Churchill and Ozoe [6.14] recommend the following empirical correlation for laminar flow on a flat, constant-temperature surface for the entire range of Pr:

$$\text{Nu}_x = \frac{0.339 \, \text{Re}_x^{1/2} \, \text{Pr}^{1/3}}{\left[1 + (0.0468/\text{Pr})^{2/3}\right]^{1/4}} \qquad \begin{array}{l} \text{Pe}_x > 100 \\[8pt] T_w = \text{constant} \end{array} \qquad (6.63)$$

This relationship proves to be quite accurate, and it approximates eqns. (6.59) and (6.62), respectively, in the high- and low-Pr limits. The calculations of an average Nusselt number for the general case is left as an exercise (Problem 6.10).

Boundary layer with an unheated starting length. Figure 6.16 shows a b.l. with a heated region that starts at a distance x_0 from the leading edge. The heat transfer in this instance is easily obtained using integral methods (see Problem 6.41):

$$\text{Nu}_x = \frac{0.332 \, \text{Re}_x^{1/2} \, \text{Pr}^{1/3}}{\left[1 - (x_0/x)^{3/4}\right]^{1/3}}, \qquad \begin{cases} x > x_0 \\[4pt] \text{Pr} \geqslant 0.6 \\[4pt] T_w = \text{const. for } x > x_0 \end{cases} \qquad (6.64)$$
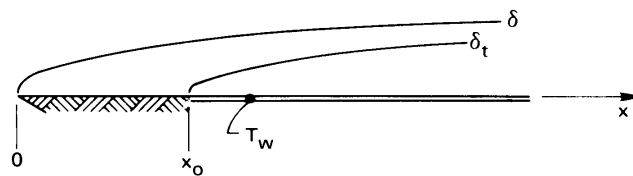
Figure 6.16 A b.l. with an unheated region at the leading edge.

Average heat transfer coefficient, $\overline{h}$. The heat transfer coefficient h, is the ratio of two quantities, q and ΔT, either of which might vary with x. So far, we have only dealt with the *uniform wall temperature problem*. Equations (6.58), (6.59), (6.62), and (6.63), for example, can all be used to calculate $q(x)$ when T_w (and $\Delta T \equiv T_w - T_\infty$) is a specified constant.

At the end of this section (pg. 311), we will see how to predict $T(x) - T_\infty$ when $q = q_w$ is a specified constant. That is called the *uniform wall heat flux problem*.

The term $\overline{h}$ designates either $\overline{q}/\Delta T$ in the uniform wall temperature problem or $q/\overline{\Delta T}$ in the uniform wall heat flux problem. Thus,

uniform wall temp.: $\overline{h} \equiv \dfrac{\overline{q}}{\Delta T} = \dfrac{1}{\Delta T}\left[\dfrac{1}{L}\int_0^L q\,dx\right] = \dfrac{1}{L}\int_0^L h(x)\,dx$

$$\tag{6.65}$$

uniform heat flux: $\overline{h} \equiv \dfrac{q}{\overline{\Delta T}} = \dfrac{q}{\dfrac{1}{L}\displaystyle\int_0^L \Delta T(x)\,dx}$ $\tag{6.66}$

The Nusselt number based on $\overline{h}$ and a characteristic length, L, is designated $\overline{\mathrm{Nu}}_L$. This average Nusselt number is not to be construed as an average of Nu_x, which would be meaningless in either of these cases.

Thus, for a flat surface (with $x_0 = 0$), we use eqn. (6.58) in eqn. (6.65) to get

$$\overline{h} = \frac{1}{L}\int_0^L \underbrace{h(x)}_{=\frac{k}{x}\mathrm{Nu}_x}\,dx = \frac{0.332\,k\,\mathrm{Pr}^{1/3}}{L}\sqrt{\frac{u_\infty}{\nu}}\int_0^L \frac{\sqrt{x}\,dx}{x}$$

$$= 0.664\,\mathrm{Re}_L^{1/2}\,\mathrm{Pr}^{1/3}\left(\frac{k}{L}\right) \quad (6.67)$$

Thus, $\overline{h} = 2h(x = L)$ in a laminar flow, and

$$\boxed{\overline{\mathrm{Nu}}_L = \frac{\overline{h}L}{k} = 0.664\,\mathrm{Re}_L^{1/2}\,\mathrm{Pr}^{1/3}} \quad \begin{array}{l}\mathrm{Pr} \geqslant 0.6 \\[4pt] T_w = \text{constant}\end{array} \quad (6.68)$$

A similar calculation gives $\overline{\mathrm{Nu}}_L$ for liquid metal flows, under the same conditions as eqn. (6.62):

$$\overline{\mathrm{Nu}}_L = 1.13\,\mathrm{Pe}_L^{1/2} \tag{6.69}$$

Some further observations.   The preceding results are restricted to the two-dimensional, incompressible, laminar b.l. on a flat isothermal wall at velocities that are not too high. These conditions are usually met if:

- Re_x or Re_L is not above the turbulent transition value, which is typically over one hundred thousand (see discussion on pg. 275).

- The Mach number of the flow, Ma $\equiv u_\infty/$(sound speed), is less than about 0.3. For low Ma, temperature and density changes caused by the pressure gradients that drive the flow are negligible. (If $p\,dV$ work were significant, we would also need to include N and m separately in the dimensional analysis of this problem, rather than including only J.) A related condition is:

- The Eckert number, Ec $\equiv u_\infty^2/c_p(T_w - T_\infty)$, is substantially less than one. This means that heating by viscous dissipation—which we have neglected—does not play any role in the problem.

And we note how h and Nu depend on their independent variables:

$$h \text{ or } \overline{h} \propto \frac{1}{\sqrt{x}} \text{ or } \frac{1}{\sqrt{L}}, \ k^{2/3}, \ \sqrt{\rho u_\infty}, \ c_p^{1/3}, \ \mu^{-1/6}$$

$$\text{Nu}_x \text{ or } \overline{\text{Nu}}_L \propto \sqrt{x} \text{ or } \sqrt{L}, \ k^{-1/3}, \ \sqrt{\rho u_\infty}, \ c_p^{1/3}, \ \mu^{-1/6} \tag{6.70}$$

Thus, $h \longrightarrow \infty$ and Nu_x vanishes at the leading edge, $x = 0$. Of course, an infinite value of h, like infinite shear stress, will not really occur at the leading edge because the b.l. description will actually break down in a small neighborhood of $x = 0$.

Fluid Properties. In all of the preceding discussion, we have assumed the fluid properties to be constant. Actually, k, ρ, c_p, and especially liquid viscosity μ, might all vary noticeably with T within the b.l. Fortunately, if the properties are all evaluated at the average, or *film*, temperature of the b.l., $T_f = (T_w + T_\infty)/2$, the results will normally be quite accurate.

Appendix A gives liquid and gas properties only at one pressure for each temperature. However, μ, k, and c_p change very little with pressure, especially in liquids. Gas density increases almost linearly with pressure.

Example 6.5

In a wind tunnel experiment, air at 20°C and moving at 15 m/s is warmed by an isothermal steam-heated plate at 110°C, ½ m in length and ½ m in width. Find the average heat transfer coefficient and the total heat transferred. What are h, δ_t, and δ at the trailing edge?

SOLUTION. We evaluate properties at $T_f = (110 + 20)/2 = 65$°C. Then

$$\text{Pr} = 0.703 \quad \text{and} \quad \text{Re}_L = \frac{u_\infty L}{\nu} = \frac{15(0.5)}{0.0000195} = 384,600$$

and if the wind tunnel has low turbulence, the flow ought to be laminar up to the trailing edge. The Nusselt number is then

$$\overline{\mathrm{Nu}}_L = 0.664 \, \mathrm{Re}_L^{1/2} \, \mathrm{Pr}^{1/3} = 366.2$$

and

$$\overline{h} = 366.2 \frac{k}{L} = \frac{366.2(0.0292)}{0.5} = 21.4 \text{ W/m}^2\text{K}$$

The value is quite low because of the low conductivity of air. The total heat flux is then

$$Q = \overline{h}A\,\Delta T = 21.4(0.5)^2(110 - 20) = 482 \text{ W}$$

By comparing eqns. (6.58) and (6.68), we see that $h(x = L) = \frac{1}{2}\overline{h}$, so

$$h(\text{trailing edge}) = \tfrac{1}{2}(21.4) = 10.7 \text{ W/m}^2\text{K}$$

And finally,

$$\delta(x = L) = 4.92L/\sqrt{\mathrm{Re}_L} = \frac{4.92(0.5)}{\sqrt{384,600}} = 3.97 \text{ mm}$$

and

$$\delta_t = \frac{\delta}{\sqrt[3]{\mathrm{Pr}}} = \frac{3.97}{\sqrt[3]{0.703}} = 4.46 \text{ mm}$$

Note that the b.l. is indeed *very* thin: $\delta_t/L = 4.46/500 = 0.0089$. ∎

The problem of uniform wall heat flux

When the heat flux at the heater wall, q_w, is specified instead of the temperature, we need to calculate T_w. We leave as an exercise the problem of estimating Nu_x for $q_w = $ constant by the integral method (Problem 6.11). The exact result is represented to 1% accuracy by [6.6, App. B]

$$\boxed{\mathrm{Nu}_x = 0.4587 \, \mathrm{Re}_x^{1/2} \, \mathrm{Pr}^{1/3}} \qquad \mathrm{Pr} \geqslant 0.7 \qquad (6.71)$$

where $\mathrm{Nu}_x = hx/k = q_w x/k(T_w - T_\infty)$.

We must be very careful in discussing *average* results in the constant heat flux case. The problem now might be that of finding an average temperature difference [cf. eqn. (6.66)]:

$$\overline{T_w - T_\infty} = \frac{1}{L} \int_0^L (T_w - T_\infty)\,dx = \frac{1}{L} \int_0^L \frac{q_w x}{k(0.4587\sqrt{u_\infty/\nu}\,\mathrm{Pr}^{1/3})} \frac{dx}{\sqrt{x}}$$

or

$$\overline{T_w - T_\infty} = \frac{q_w L/k}{0.688 \, \mathrm{Re}_L^{1/2} \, \mathrm{Pr}^{1/3}} \tag{6.72}$$

which can be put into the form $\overline{\mathrm{Nu}}_L = \overline{h}L/k = 0.688 \, \mathrm{Re}_L^{1/2}\mathrm{Pr}^{1/3}$ for $\overline{h} = q_w/(\overline{T_w - T_\infty})$.

Churchill and Ozoe later pointed out that their eqn. (6.63) will describe $(T_w - T_\infty)$ with high accuracy over the full range of Pr if the constants are changed as follows [6.15]:

$$\boxed{\mathrm{Nu}_x = \frac{0.464 \, \mathrm{Re}_x^{1/2} \, \mathrm{Pr}^{1/3}}{\left[1 + (0.0205/\mathrm{Pr})^{2/3}\right]^{1/4}}} \quad \begin{array}{l} \mathrm{Pe}_x > 100 \\[6pt] q_w = \text{constant} \end{array} \tag{6.73}$$

The average Nusselt number for this case is derived in Problem 6.44.

The result for an unheated starting length followed by a uniform heat flux is discussed later [see eqn. (6.116) and Fig. 6.22)].

Example 6.6

Air at 15°C flows at 1.8 m/s over a 0.6 m-long heating panel. The panel is intended to supply 420 W/m^2 to the air, but the surface can sustain only about 110°C without being damaged. What are the maximum and the average temperatures of the plate? Is it safe?

SOLUTION. In accordance with eqn. (6.71),

$$\Delta T_{\max} = \Delta T_{x=L} = \frac{qL}{k \, \mathrm{Nu}_{x=L}} = \frac{qL/k}{0.4587 \, \mathrm{Re}_x^{1/2} \, \mathrm{Pr}^{1/3}}$$

or if we evaluate properties at $(85 + 15)/2 = 50°$C, for the moment,

$$\Delta T_{\max} = \frac{420(0.6)/0.0281}{0.4587\left[0.6(1.8)/1.797 \times 10^{-5}\right]^{1/2}(0.705)^{1/3}} = 89.6°\mathrm{C}$$

This will give $T_{w_{\max}} = 15 + 89.6 = 104.6°$C. This is very close to 110°C. If 110°C is at all conservative, $q = 420$ W/m^2 should be safe—particularly since it only occurs over a very small distance at the end of the plate.

From eqn. (6.72) we find that

$$\overline{\Delta T} = \frac{0.4587}{0.6795} \Delta T_{\max} = 60.5°\mathrm{C}$$

so

$$\overline{T_w} = 15 + 60.5 = 75.5°\mathrm{C} \qquad\qquad \blacksquare$$

6.6   The Reynolds-Colburn analogy

We have seen that the molecular mechanisms of heat and momentum transport are very similar and that the laminar thermal and momentum boundary layers grow in a similar way. The difference between heat and momentum transport in a laminar b.l. on an isothermal wall comes down to a single physical property, the Prandtl number (Fig. 6.4). We might then wonder whether the heat transfer rate and the wall shear stress are also related through Pr.

To see if this is the case, we can compare the skin friction coefficient, eqn. (6.33), to the Nusselt number for an isothermal wall, eqn. (6.58). We rearrange eqn. (6.58) to find

$$\frac{\mathrm{Nu}_x}{\mathrm{Re}_x \mathrm{Pr}^{1/3}} = \frac{0.332}{\sqrt{\mathrm{Re}_x}} \tag{6.74}$$

The right-hand side is *precisely* $C_f/2$. This result is an example of what has come to be called the *Reynolds-Colburn analogy* between heat transfer and momentum transfer.

The analogy is usually expressed in terms of a slightly different ratio of dimensionless groups, called the *Stanton number*:

$$\mathrm{St, \ Stanton \ number} \ \equiv \frac{\mathrm{Nu}_x}{\mathrm{Re}_x \mathrm{Pr}} = \frac{h}{\rho c_p u_\infty} \tag{6.75}$$

The physical significance of the Stanton number is

$$\mathrm{St} \ = \frac{h\Delta T}{\rho c_p u_\infty \Delta T} = \frac{\text{actual heat flux}}{\text{maximum possible enthalpy change}} \tag{6.76}$$

We may write the Reynolds-Colburn analogy in terms of St as

$$\mathrm{St} \, \mathrm{Pr}^{2/3} = \frac{C_f}{2} \tag{6.77}$$

The Reynolds-Colburn analogy can be used directly to infer shear stress from heat transfer measurements, or vice versa. For example, if the skin friction coefficient has been measured in one fluid, the analogy may allow us to estimate heat transfer for another fluid that has a different Prandtl number.

At this point, we may wonder whether this analogy is generally applicable. Suppose that we had used the Nusselt number for a constant heat flux wall, eqn. (6.71), instead:

$$\frac{\mathrm{Nu}_x}{\mathrm{Re}_x \mathrm{Pr}^{1/3}} = \frac{0.4587}{\sqrt{\mathrm{Re}_x}} \neq \frac{C_f}{2} = \frac{0.332}{\sqrt{\mathrm{Re}_x}} \tag{6.78}$$

The previous analogy does not apply here because the laminar thermal boundary layer grows at a different rate on a constant flux wall than on a constant temperature wall. Other changes to the flow, such as having a pressure gradient or using liquid metal (very low Pr), can also invalidate the analogy.

The Reynolds-Colburn analogy is more widely applicable for turbulent flow. The reason is that turbulent motion transports heat and momentum in a way that is much less sensitive to the wall boundary condition. We develop a more general version of the analogy for turbulent flow in Section 6.8.

In fact, Reynolds, who developed the analogy in 1874 [6.16], later used it to study heat transfer in turbulent pipe flow. His approach was followed by many researchers during the 20$^{\text{th}}$ century (see Section 7.3). The chemical engineer A. P. Colburn formalized the Prandtl number dependence of the analogy in 1933 [6.17]. He then successfully correlated data for a number of configurations involving turbulent flow.[9]

6.7 Turbulent boundary layers

Turbulence

> Big whirls have little whirls,
> That feed on their velocity.
> Little whirls have littler whirls,
> And so on, to viscosity.

This bit of doggerel by British fluid mechanician L. F. Richardson, says much about the nature of turbulence. We can view fluid turbulence as a spectrum of vortices (or "whirls"). Kinetic energy dissipates from the larger ones to smaller ones, until viscous shear stresses damp out the very smallest of these vortices.

Notice, for example, the cloud patterns in a weather satellite image. One or two enormous vortices have continental proportions. They in turn feed smaller "weather-making" vortices hundreds of kilometers in diameter. These further dissipate into vortices of cyclone and tornado

---

[9]Colburn also looked at the flat plate boundary layer, and his plot of laminar flow data using eqn. (6.77) seemed to work. But in 1946, he admitted to Max Jakob that a "slide-rule error" had slipped into that plot. In fact, the problem ran deeper than just a calculation: He had plotted data from a *constant heat flux* experiment. When his plot was corrected, the data lay above eqn. (6.77)—as we would expect from eqn. (6.78). Neither Colburn nor Jakob noted the importance of the wall boundary condition [6.6].
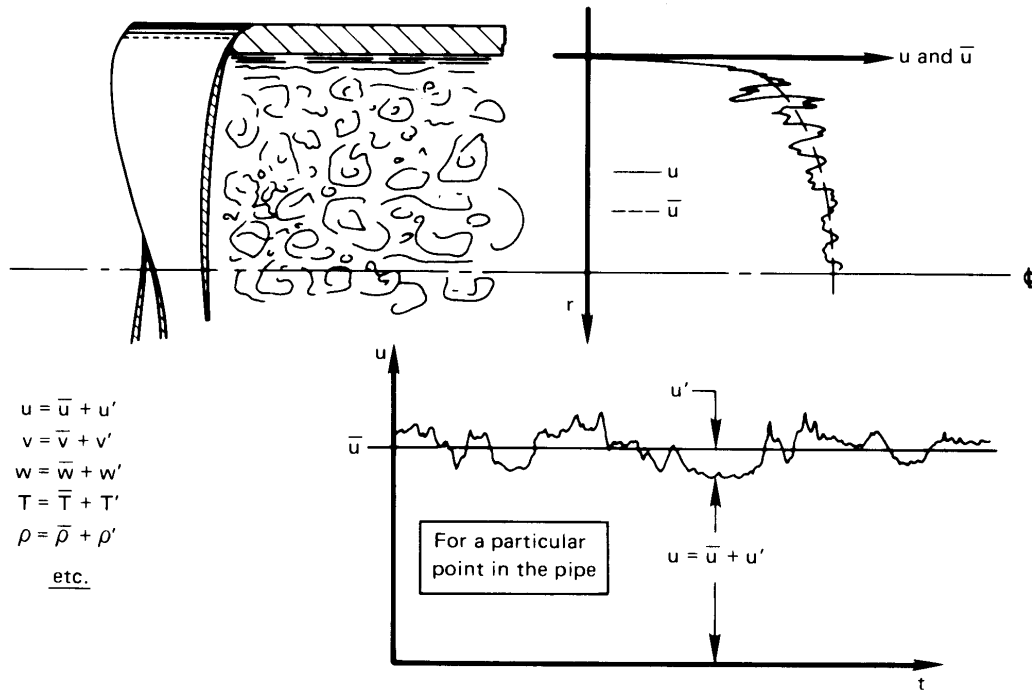
Figure 6.17 Fluctuation of u and other quantities in a turbulent pipe flow.

proportions—sometimes with that level of violence but more often not. These dissipate into still smaller whirls as they interact with the ground and its various protrusions. The next time the wind blows, stand behind any tree and *feel* the vortices. In the Great Plains of North America, where there are few vortex generators (such as trees), one sees small cyclonic eddies called "dust devils." The process continues right on down to millimeter or even micrometer scales. There, momentum exchange is no longer identifiable as turbulence but appears simply as viscous twisting and stretching of the fluid.

The same kind of process exists within, say, a turbulent pipe flow at high Reynolds number. Such a flow is shown in Fig. 6.17. Turbulence in such a case consists of coexisting vortices which vary in size from a substantial fraction of the pipe radius down to micrometer dimensions. The spectrum of sizes varies with location in the pipe. The size and intensity of vortices at the wall must clearly approach zero, since the fluid velocity goes to zero at the wall.

Figure 6.17 shows the fluctuation of a typical flow variable—namely, velocity—both with location in the pipe and with time. This fluctuation arises because of the turbulent motions that are superposed on the average local flow. Other flow variables, such as T or ρ, can vary in the same manner. For any variable, in this case u, we can write a local time-average value as

$$\overline{u} \equiv \frac{1}{\mathbf{T}} \int_0^{\mathbf{T}} u \, dt \tag{6.79}$$

where $\mathbf{T}$ is a time that is much longer than the period of typical fluctuations.[10] Equation (6.79) is most useful for so-called *stationary processes*— ones for which $\overline{u}$ is nearly time-independent.

If we substitute $u = \overline{u} + u'$ in eqn. (6.79), where u is the actual local velocity and u' is the instantaneous magnitude of the fluctuation, we obtain

$$\overline{u} = \underbrace{\frac{1}{\mathbf{T}} \int_0^{\mathbf{T}} \overline{u} \, dt}_{=\overline{u}} + \underbrace{\frac{1}{\mathbf{T}} \int_0^{\mathbf{T}} u' \, dt}_{=\overline{u'}} \tag{6.80}$$

This is consistent with the fact that

$$\overline{u'} \text{ or any other average fluctuation} = 0 \tag{6.81}$$

since the fluctuations are defined as deviations from the average.

We now want to create a measure of the size, or *length scale*, of turbulent vortices. This might be done experimentally by placing two velocity-measuring devices very close to one another in a turbulent flow field. When the probes are close, their measurements will be very highly correlated with one another. Then, suppose that the two velocity probes are moved apart until the measurements first become unrelated to one another. That spacing gives an indication of the average size of the turbulent vortices.

Prandtl invented a slightly different (although related) measure of the length scale of turbulence, called the *mixing length*, ℓ. He saw ℓ as an average distance that a parcel of fluid moves between interactions. It is essentially the size of a typical turbulent eddy. The mixing length is thus similar to the molecular mean free path (although far larger). We can use the idea of ℓ, along with physical reasoning, to examine the behavior of the turbulent shear stress.

---

[10]Take care not to interpret this $\mathbf{T}$ as the thermal time constant that we introduced in Chapter 1; we denote time constants with italics as T.
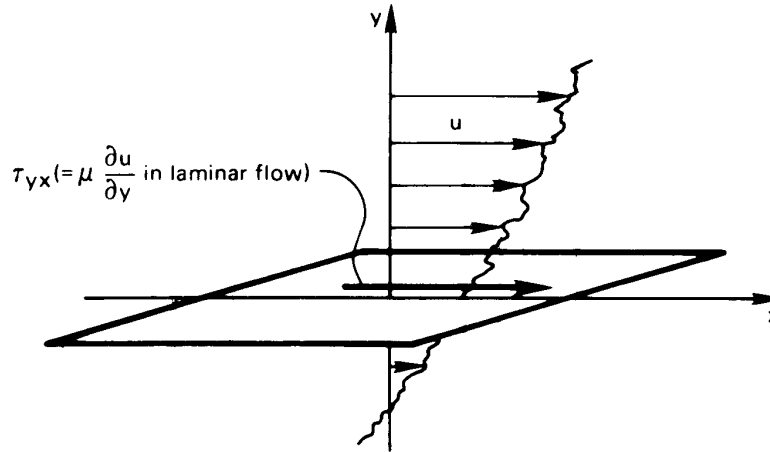
Figure 6.18 The shear stress, τ_{yx}, in a laminar or turbulent flow.

The shear stresses of turbulence arise from the same kind of momentum exchange process that gives rise to the molecular viscosity. Recall that, in the latter case, a kinetic calculation gave eqn. (6.45a) for the laminar shear stress

$$\tau_{yx} = (\text{constant})\left(\rho\overline{C}\right) \underbrace{\left(\ell\frac{\partial u}{\partial y}\right)}_{=u'} \tag{6.45a}$$

where ℓ was the molecular mean free path and u' was the velocity difference for a molecule that had travelled a distance ℓ in the mean velocity gradient. In the turbulent flow case, pictured in Fig. 6.18, we can think of Prandtl's parcels of fluid (rather than individual molecules) as carrying the x-momentum. Let us rewrite eqn. (6.45a) in the following way:

- The shear stress τ_{yx} becomes a fluctuation in shear stress, τ'_{yx}, resulting from the turbulent movement of a parcel of fluid relative to the mean flow

- ℓ changes from the mean free path to the mixing length

- $\overline{C}$ is replaced by $v = \overline{v} + v'$, the instantaneous vertical speed of the fluid parcel

- The velocity fluctuation, u', is for a fluid parcel that moves a distance ℓ through the mean velocity gradient, $\partial\overline{u}/\partial y$, so that $u' = \ell(\partial\overline{u}/\partial y)$

With these changes, we replace eqn. (6.45a) by

$$\tau'_{yx} = (\text{constant}) \left[\rho (\overline{v} + v') \right] u' \tag{6.82}$$

Equation (6.82) can also be derived formally and precisely from the Navier-Stokes equation. When this is done, the constant turns out to equal -1.

The time average of the fluctuating shear stress, eqn. (6.82), is

$$\overline{\tau'_{yx}} = -\frac{\rho}{T} \int_0^T (\overline{v} u' + v' u') \, dt = -\rho \overline{v} \underbrace{\overline{u'}}_{=0} - \rho \overline{v' u'} \tag{6.83}$$

Notice that, while $\overline{u'} = \overline{v'} = 0$, averages of products of fluctuations (such as $\overline{u' v'}$ or $\overline{u'^2}$) do not generally vanish. Thus,

$$\overline{\tau'_{yx}} = -\rho \overline{v' u'} \tag{6.84}$$

In addition to the fluctuating shear stress, the flow will have a mean shear stress associated with the mean velocity gradient, $\partial \overline{u} / \partial y$. That stress is simply $\mu (\partial \overline{u} / \partial y)$, just as in Newton's law of viscous shear.

How to calculate $\overline{v' u'}$ is not obvious (although it can be measured), so we shall not make direct use of eqn. (6.84). Instead, we can try to model $\overline{v' u'}$. From the preceding discussion, we see that $\overline{v' u'}$ should go to zero when the velocity gradient, $\partial \overline{u} / \partial y$, is zero, and that it should increase when the velocity gradient increases. We might therefore assume $\overline{v' u'}$ to be proportional to $\partial \overline{u} / \partial y$. Then the total time-average shear stress, τ_{yx}, can be expressed as the sum of mean flow and turbulent contributions that are each proportional to the mean velocity gradient. Specifically,

$$\tau_{yx} = \mu \frac{\partial \overline{u}}{\partial y} - \rho \overline{v' u'} \tag{6.85a}$$

$$= \mu \frac{\partial \overline{u}}{\partial y} + \underbrace{\left(\begin{matrix} \text{some other factor, which} \\ \text{reflects turbulent mixing} \end{matrix} \right)}_{\equiv \, \rho \, \cdot \, \varepsilon_m} \frac{\partial \overline{u}}{\partial y} \tag{6.85b}$$

or

$$\tau_{yx} = \rho (v + \varepsilon_m) \frac{\partial \overline{u}}{\partial y} \tag{6.85c}$$

where ε_m is called the *eddy diffusivity for momentum*.

The eddy diffusivity itself may be expressed in terms of the mixing length. Suppose that $\overline{u}$ increases in the y-direction, so that $\partial\overline{u}/\partial y > 0$. Then, when a fluid parcel moves downward into slower moving fluid, it has $u' \cong \ell(\partial\overline{u}/\partial y)$. If that parcel moves upward into faster fluid, the sign changes. The vertical velocity fluctuation, v', is instead positive for an upward moving parcel and negative for a downward motion. On average, u' and v' for the eddies should be about the same size. Hence, we expect that

$$\rho\varepsilon_m\frac{\partial\overline{u}}{\partial y} = -\rho\overline{v'u'} = -\rho(\text{constant})\left(\pm\ell\left|\frac{\partial\overline{u}}{\partial y}\right|\right)\left(\mp\ell\frac{\partial\overline{u}}{\partial y}\right) \qquad (6.86\text{a})$$

$$= \rho(\text{constant})\,\ell^2\left|\frac{\partial\overline{u}}{\partial y}\right|\frac{\partial\overline{u}}{\partial y} \qquad (6.86\text{b})$$

where the absolute value is needed to get the right sign for the fluctuating stress when $\partial\overline{u}/\partial y < 0$. Both $\partial\overline{u}/\partial y$ and $\overline{v'u'}$ can be measured, so we may arbitrarily make the constant in eqns. (6.86) equal to one, to obtain a *measurable* definition of the mixing length. We also obtain an expression for the eddy diffusivity in terms of the mixing length:

$$\varepsilon_m = \ell^2\left|\frac{\partial\overline{u}}{\partial y}\right| \qquad (6.87)$$

Turbulence near walls

Convective heat transfer is the cooling or heating of solid surfaces by flowing fluids. Thus, we are principally interested in how turbulence behaves near those surfaces. The gradients in a turbulent boundary layer are very steep near the wall and weaker farther from the wall, where the eddies are larger and turbulent mixing is more efficient. This situation is in contrast to the gradual variation of velocity and temperature in a laminar boundary layer, where heat and momentum are transferred by molecular diffusion rather than the vertical motion of vortices. In fact, the most important transport processes in turbulent convection occur in the steep gradients very close to walls. The outer part of the b.l. is less significant.

Let us consider the turbulent flow close to a wall. When the boundary layer momentum equation, eqn. (6.40), is time-averaged for turbulent

flow, the result is

$$\underbrace{\rho\left(\overline{u}\frac{\partial\overline{u}}{\partial x} + \overline{v}\frac{\partial\overline{u}}{\partial y}\right)}_{\substack{\text{these terms are negligible}\\\text{close to the wall}}} = \frac{\partial}{\partial y}\left(\mu\frac{\partial\overline{u}}{\partial y} - \rho\overline{v'u'}\right) \tag{6.88}$$

$$= \frac{\partial}{\partial y}\tau_{yx} \tag{6.89}$$

$$= \frac{\partial}{\partial y}\left[\rho(\nu + \varepsilon_m)\frac{\partial\overline{u}}{\partial y}\right] \tag{6.90}$$

where the last two steps follow from eqns. (6.85). In the innermost region of a turbulent boundary layer—$y/\delta \lesssim 0.2$, where δ is the b.l. thickness—the mean velocities are small enough that the convective terms in eqn. (6.88) can be neglected. As a result, $\partial\tau_{yx}/\partial y \cong 0$. The total shear stress is thus essentially constant in y and must equal the wall shear stress:

$$\tau_w \cong \tau_{yx} = \rho(\nu + \varepsilon_m)\frac{\partial\overline{u}}{\partial y} \tag{6.91}$$

Equation (6.91) shows that the near-wall velocity profile does not depend directly upon x. In functional form

$$\overline{u} = \text{fn}(\tau_w, \rho, \nu, y) \tag{6.92}$$

Notice that ε_m does not appear as an explicit variable since it is defined by the velocity field. The effect of the streamwise position is likewise carried in τ_w, which varies slowly with x. As a result, *the flow field near the wall is not very sensitive to upstream conditions,* except through their effect on τ_w.

Equation (6.92) involves five variables in three dimensions (kg, m, s), so just two dimensionless groups are needed to describe the velocity profile:

$$\frac{\overline{u}}{u^*} = \text{fn}\left(\frac{u^*y}{\nu}\right) \tag{6.93}$$

The velocity scale $u^* \equiv \sqrt{\tau_w/\rho}$ is called the *friction velocity*. The friction velocity is a speed that is characteristic of the turbulent fluctuations in the boundary layer.

Equation (6.91) can be integrated to find the near wall velocity profile:

$$\underbrace{\int_0^{\overline{u}} d\overline{u}}_{=\overline{u}(y)} = \frac{\tau_w}{\rho}\int_0^y \frac{dy}{\nu + \varepsilon_m} \tag{6.94}$$

To complete the integration, we need an equation for $\varepsilon_m(y)$. Measurements show that the mixing length varies linearly with the distance from the wall for small y

$$\ell = \kappa y \quad \text{for} \quad y/\delta \lesssim 0.2 \tag{6.95}$$

where $\kappa = 0.41$ is called the *von Kármán constant*. Physically, this says that the turbulent eddies at a location y must not be bigger than the distance to the wall. That makes sense, since eddies cannot cross into the wall.

The viscous sublayer. Very near the wall, eqn. (6.95) shows that the eddy size ℓ must become tiny. Since ε_m varies as ℓ^2, ε_m will become much smaller than ν. In other words, very close to the wall turbulent shear stress is negligible compared to viscous shear stress. When we integrate eqn. (6.94) in this region, we find

$$\begin{aligned}\overline{u}(y) &\cong \frac{\tau_w}{\rho} \int_0^y \frac{dy}{\nu} = \frac{\tau_w}{\rho}\frac{y}{\nu} \\ &= \frac{(u^*)^2 y}{\nu}\end{aligned} \tag{6.96}$$

Experimentally, eqn. (6.96) is found to apply for $u^* y/\nu \lesssim 7$. We call this thin region the *viscous sublayer*. The sublayer is on the order of tens to hundreds of micrometers thick, depending upon the fluid and the shear stress. Because turbulent mixing is ineffective in the sublayer, the sublayer is responsible for a major fraction of the thermal resistance of a turbulent boundary layer.

Even a small wall roughness can disrupt the thin thermal sublayer and greatly reduce the thermal resistance. Wall roughness can likewise greatly increase the wall shear stress in turbulent flow. More on these matters in Section 7.3.

The log layer. Farther away from the wall, ℓ is larger and turbulent shear stress is dominant: $\varepsilon_m \gg \nu$. Then, from eqns. (6.91) and (6.87)

$$\tau_w \cong \rho\varepsilon_m\frac{\partial\overline{u}}{\partial y} = \rho\ell^2\left|\frac{\partial\overline{u}}{\partial y}\right|\frac{\partial\overline{u}}{\partial y} \tag{6.97}$$

Assuming the velocity gradient to be positive, we may take the square root of eqn. (6.97), rearrange, and integrate:

$$\int d\overline{u} = \sqrt{\frac{\tau_w}{\rho}} \int \frac{dy}{\ell} \tag{6.98}$$

$$\overline{u}(y) = u^* \int \frac{dy}{\kappa y} + \text{constant} \tag{6.99}$$

$$= \frac{u^*}{\kappa} \ln y + \text{constant} \tag{6.100}$$

Experimental data may be used to fix the constant, with the result that

$$\frac{\overline{u}(y)}{u^*} = \frac{1}{\kappa} \ln\left(\frac{u^* y}{\nu}\right) + B \tag{6.101}$$

where $B \cong 5.5$. Equation (6.101) is sometimes called the *log law*. Experiments show it to apply for $u^* y/\nu \gtrsim 30$ and $y/\delta \lesssim 0.2$.

Other regions of the turbulent b.l. For the range $7 < u^* y/\nu < 30$, the so-called *buffer layer*, more complicated equations for ℓ, ε_m, or $\overline{u}$ are used to connect the viscous sublayer to the log layer [6.18-6.20]. For the outer part of the turbulent boundary layer ($y/\delta \gtrsim 0.2$), the mixing length is approximately constant: $\ell \cong 0.09\delta$. Gradients in the outer part are weak and do not directly affect transport at the wall. This part of the b.l. is nevertheless an important component of the streamwise momentum balance; and that balance determines how τ_w and δ vary along the wall.[11]

Skin friction coefficient. Various expressions have been proposed for the skin friction coefficient for a turbulent boundary layer on a flat plate. White [6.4, 6.21] has derived the following equation, which has 1–2% accuracy for any Re_x:

$$C_f(x) = \frac{0.455}{\left[\ln(0.06\,\text{Re}_x)\right]^2} \tag{6.102}$$

6.8   Heat transfer in turbulent boundary layers

The turbulent thermal boundary layer, like the turbulent momentum boundary layer, has inner and outer regions. Turbulent mixing becomes increasingly weak closer to the wall in the inner region. There, heat transport is controlled by heat conduction in the sublayer. Farther from the wall, the temperature profile is logarithmic. Turbulent mixing is the dominant mode of heat transport outside the viscous sublayer.

---

[11]A momentum integral analysis of the turbulent boundary layer [6.4] leads to these expressions: $\delta(x)/x = 0.16\,\text{Re}_x^{-1/7}$ and $C_f(x) = 0.027\,\text{Re}_x^{-1/7}$. They are reasonably accurate for $10^6 \leqslant \text{Re}_x \leqslant 10^9$.

The thermal and momentum boundary layers end where turbulence dies out and uniform free-stream conditions prevail. As a result, the thermal and momentum boundary layers have the same thickness. At first, this might seem to suggest that Prandtl number does not affect turbulent heat transfer, but in fact it does. The Prandtl number determines behavior in the sublayer near the wall, where molecular viscosity and thermal conductivity still control the transport of heat and momentum.

The Reynolds-Colburn analogy for turbulent flow

Boussinesq introduced the eddy diffusivity for momentum, eqn. (6.85), in 1877 [6.22]. That, in turn, suggested a version of Fourier's law for turbulent flow

$$q = -k\frac{\partial \overline{T}}{\partial y} - \underbrace{\left(\begin{array}{l}\text{another constant, which}\\ \text{reflects turbulent mixing}\end{array}\right)}_{\equiv \rho c_p \cdot \varepsilon_h}\frac{\partial \overline{T}}{\partial y}$$

where $\overline{T}$ is the local time-average temperature and ε_h is the *eddy diffusivity for heat*. Therefore,

$$q = -\rho c_p (\alpha + \varepsilon_h)\frac{\partial \overline{T}}{\partial y} \tag{6.103}$$

This result immediately suggests yet another definition:

$$\text{turbulent Prandtl number, } \mathrm{Pr}_t \equiv \frac{\varepsilon_m}{\varepsilon_h} \tag{6.104}$$

Equation (6.103) can be written in terms of ν and ε_m by introducing Pr and Pr_t:

$$q = -\rho c_p \left(\frac{\nu}{\mathrm{Pr}} + \frac{\varepsilon_m}{\mathrm{Pr}_t}\right)\frac{\partial \overline{T}}{\partial y} \tag{6.105}$$

Before we try to build the Reynolds-Colburn analogy for turbulent flow, we must note the behavior of Pr and Pr_t:

- Pr is a physical property of the fluid. For gases, Pr is near one and is very weakly dependent on temperature. For nonmetallic liquids, Pr may be orders of magnitude greater than one, and it often has a strong temperature dependence.

- Pr_t is a property of the flow field more than the fluid. Pr_t is normally close to one, and well within a factor of two. The value varies with location in the b.l., but for nonmetallic fluids, Pr_t is often near 0.85. (We do not consider liquid metals in this section.)

The time-average boundary-layer energy equation is similar to the time-average momentum equation [eqn. (6.88)]

$$\underbrace{\rho c_p \left(\overline{u} \frac{\partial \overline{T}}{\partial x} + \overline{v} \frac{\partial \overline{T}}{\partial y} \right)}_{\text{negligible close to the wall}} = -\frac{\partial}{\partial y} q = \frac{\partial}{\partial y} \left[\rho c_p \left(\frac{\nu}{\text{Pr}} + \frac{\varepsilon_m}{\text{Pr}_t} \right) \frac{\partial \overline{T}}{\partial y} \right] \qquad (6.106)$$

and, since we can neglect the convective terms, $\partial q / \partial y \cong 0$ near the wall. The heat flux close to the wall thus does not vary with y, and so must equal q_w:

$$q \cong q_w = -\rho c_p \left(\frac{\nu}{\text{Pr}} + \frac{\varepsilon_m}{\text{Pr}_t} \right) \frac{\partial \overline{T}}{\partial y} \qquad (6.107)$$

We may integrate this equation as we did eqn. (6.91), with the result that

$$\frac{T_w - \overline{T}(y)}{q_w / (\rho c_p u^*)} = \begin{cases} \text{Pr} \left(\dfrac{u^* y}{\nu} \right) & \text{thermal sublayer} \\[2mm] \dfrac{1}{\kappa} \ln \left(\dfrac{u^* y}{\nu} \right) + A(\text{Pr}) & \text{thermal log layer} \end{cases} \qquad (6.108)$$

Measurements show that the thermal sublayer extends to $u^* y / \nu \lesssim 7$, followed by a smooth transition to the thermal log layer, which spans $u^* y / \nu \gtrsim 30$ to $y/\delta \lesssim 0.2$.

The term A in eqn. (6.108) depends upon the Prandtl number. It reflects the thermal resistance of the sublayer near the wall. As was done for the constant B in the velocity profile, eqn. (6.101), we may use experimental data or numerical simulations to determine $A(\text{Pr})$ [6.9, 6.23, 6.24]. For $\text{Pr} \geq 0.5$, an approximate fit is

$$A(\text{Pr}) \cong 12.7 \, \text{Pr}^{2/3} - 7.2 \qquad (6.109)$$

To obtain the Reynolds-Colburn analogy, we subtract the dimensionless log-law, eqn. (6.101), from its thermal counterpart, eqn. (6.108):

$$\frac{T_w - \overline{T}(y)}{q_w / (\rho c_p u^*)} - \frac{\overline{u}(y)}{u^*} = A(\text{Pr}) - B \qquad (6.110a)$$

At the outer edge of the log-layer, the temperature and velocity are not far from the free-stream values. So, we may approximate them as $\overline{T}(y) \cong T_\infty$ and $\overline{u}(y) \cong u_\infty$:

$$\frac{T_w - T_\infty}{q_w / (\rho c_p u^*)} - \frac{u_\infty}{u^*} = A(\text{Pr}) - B \qquad (6.110b)$$

We eliminate the friction velocity in favor of the skin friction coefficient by using the definitions of each:

$$\frac{u^*}{u_\infty} = \sqrt{\frac{\tau_w}{\rho u_\infty^2}} = \sqrt{\frac{C_f}{2}} \tag{6.110c}$$

Hence,

$$\frac{T_w - T_\infty}{q_w/(\rho c_p u_\infty)}\sqrt{\frac{C_f}{2}} - \sqrt{\frac{2}{C_f}} = A(\mathrm{Pr}) - B \tag{6.110d}$$

Rearrangement of the last equation gives

$$\frac{q_w}{(\rho c_p u_\infty)(T_w - T_\infty)} = \frac{C_f/2}{1 + [A(\mathrm{Pr}) - B]\sqrt{C_f/2}} \tag{6.110e}$$

The left-hand side is simply the Stanton number, $\mathrm{St} = h/(\rho c_p u_\infty)$, from Section 6.6. Upon substituting $B = 5.5$ and eqn. (6.109) for $A(\mathrm{Pr})$, we obtain the Reynolds-Colburn analogy for turbulent flow:

$$\boxed{\mathrm{St} = \frac{\mathrm{Nu}_x}{\mathrm{Re}_x \mathrm{Pr}} = \frac{C_f/2}{1 + 12.7\left(\mathrm{Pr}^{2/3} - 1\right)\sqrt{C_f/2}}} \qquad \mathrm{Pr} \geqslant 0.5 \tag{6.111}$$

Equation (6.111) can be used with eqn. (6.102) for C_f, or with data for C_f, to calculate the local heat transfer coefficient in a turbulent boundary layer. The result is valid for either uniform T_w or uniform q_w. The reason is that the thin, near-wall part of the boundary layer, which controls most of the thermal resistance, is not strongly dependent on the upstream history of the flow.

Equation (6.111) is valid for smooth walls with zero or mild pressure gradients. The factor $12.7\,(\mathrm{Pr}^{2/3} - 1)$ in the denominator accounts for the thermal resistance of the sublayer. If the walls are rough, the sublayer will be disrupted and that term must be replaced by one that takes account of the roughness (see Section 7.3).

Experimental data for air—from five independent studies—are plotted in Fig. 6.19. Equation (6.111) predicts those data with a standard deviation of $\pm 5.5\%$. The 95% confidence interval—two sample standard deviations—is thus $\pm 11\%$ [6.25]. Figure 6.19 includes 328 data points, of which 326 (99.4%) are within $\pm 15\%$ of eqn. (6.111). This equation also displays excellent agreement with data for water and for high-Pr oils [6.6].
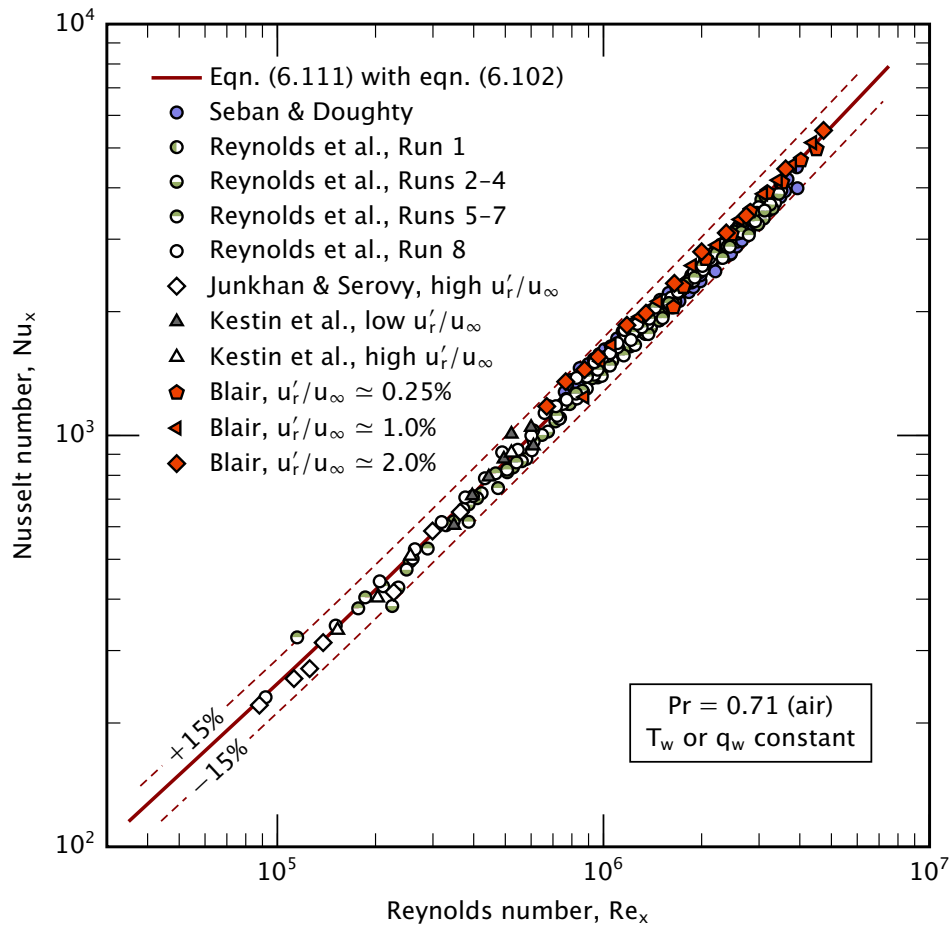
Figure 6.19 Comparison of eqn. (6.111) to air (data from several investigators [6.26–6.30]). Both constant T_w and constant q_w data are shown. u'_r is the root-mean-square turbulent fluctuation in the free-stream flow [6.6].

Power-law correlations for local turbulent heat transfer

Although eqn. (6.111) gives an excellent prediction of the local value of h in a turbulent boundary layer, a number of simpler power-law expressions have been suggested in the literature. For example, Reynolds et al. [6.27] made extensive measurements for air flow over a constant-temperature plate, from which they proposed the following correlation

$$\mathrm{Nu}_x = 0.0296\,\mathrm{Re}_x^{0.8}\,\mathrm{Pr}^{0.6} \quad \text{for gases} \tag{6.112}$$

We can use this equation for gases other than air because Pr for air is close to that of most other gases. However, we cannot use eqn. (6.112) for liquids with higher Prandtl numbers. Equation (6.112) agrees very closely with eqn. (6.111) for air (see Fig. 6.22 in Section 6.9).

Žukauskas and coworkers performed experiments on water and an oil at various free-stream temperatures, with Prandtl numbers up to 85 [6.23]. They suggested the following correlation which fit their data for these liquids to about ±15%:

$$\mathrm{Nu}_x = 0.032 \, \mathrm{Re}_x^{0.8} \, \mathrm{Pr}^{0.43} \quad \text{for nonmetallic liquids} \qquad (6.113)$$

This equation overpredicts the air data of Fig. 6.19 by 15–25% [6.6].

Equations (6.112) and (6.113) both apply for either constant T_w or constant q_w.

Variable properties. For liquids, when the wall temperature and the free-stream temperature are not close, the viscosity may change significantly across the boundary layer. In this case, the Nusselt number may be adjusted by multiplying the right-hand side of eqn. (6.111) or eqn. (6.113) by the factor $(\mathrm{Pr}_\infty/\mathrm{Pr}_w)^{1/4}$, where Pr_∞ is the Prandtl number at the free-stream temperature, T_∞, and Pr_w is that at the wall temperature, T_w, with other physical properties evaluated at T_∞ [6.23, 6.31].

For gases, variable properties may be accommodated by multiplying the right-hand side of eqn. (6.111) or eqn. (6.112) by $(T_\infty/T_w)^{0.4}$ [6.27].

Example 6.7

The prow of a destroyer has a sharp 'V' shape. It sails out of a river port, where the water temperature is 24°C, into 10°C ocean water. If the ship travels at 5 knots, find C_f and h at a distance of 1 m from the forward edge of the hull. Turbulent transition is expected to occur somewhere between $\mathrm{Re}_x = 5 \times 10^4$ and 1.5×10^5. Assume that the local free-stream pressure gradient is mild.

SOLUTION. If we assume that the metal hull's heat capacity holds it at the river temperature for a time, we can take the properties of water at $T_f = (10 + 24)/2 = 17°C$: $\nu = 1.085 \times 10^{-6} \, \mathrm{m^2/s}$, $k = 0.5927 \, \mathrm{W/m \cdot K}$, $\rho = 998.8 \, \mathrm{kg/m^3}$, $c_p = 4187 \, \mathrm{J/kg \cdot K}$, and Pr = 7.66.

One knot is 0.5144 m/s, so $u_\infty = 5(0.5144) = 2.572 \, \mathrm{m/s}$. Then, $\mathrm{Re}_x = (2.572)(1)/(1.085 \times 10^{-6}) = 2.371 \times 10^6$, indicating that the flow is fully turbulent.

From eqn. (6.102):

$$C_f(x) = \frac{0.455}{[\ln(0.06\,\mathrm{Re}_x)]^2}$$

$$= \frac{0.455}{\{\ln[0.06(2.371 \times 10^6)]\}^2} = 0.003232$$

For h, we can use the more accurate eqn. (6.111)

$$h(x) = \rho c_p u_\infty \cdot \frac{C_f/2}{1 + 12.7\left(\mathrm{Pr}^{2/3} - 1\right)\sqrt{C_f/2}}$$

$$= \frac{998.8(4187)(2.572)(0.003232/2)}{1 + 12.7[(7.66)^{2/3} - 1]\sqrt{0.003232/2}}$$

$$= 7,028 \ \mathrm{W/m^2K}$$

or the approximate power law, eqn. (6.113):

$$h(x) = \frac{k}{x} \cdot 0.032\,\mathrm{Re}_x^{0.8}\,\mathrm{Pr}^{0.43}$$

$$= \frac{(0.5927)(0.032)(2.371 \times 10^6)^{0.8}(7.66)^{0.43}}{(1.0)}$$

$$= 5,729 \ \mathrm{W/m^2K}$$

The two values of h differ by about 22%, which is consistent with the uncertainty of the power law, eqn. (6.113). ∎

6.9 Turbulent transition and overall heat transfer

We now know how to calculate h for the laminar region and the fully turbulent region of the b.l. However, these regions are separated by a lengthy transition region (Fig. 6.4). To assess the overall heat transfer, we must deal with transition.

Figures 6.20 and 6.21 show data for water and air boundary layers undergoing turbulent transition. Our equations for laminar and fully turbulent flow are also plotted. The data show that Nu_x rises steeply in the transition region and that it varies approximately as a straight line on log-log coordinates. That means that the Nusselt number in the transition region, $\mathrm{Nu}_{\mathrm{trans}}$, varies as a power of Reynolds number:

$$\mathrm{Nu}_{\mathrm{trans}} \cong a\,\mathrm{Re}_x^c \tag{6.114a}$$
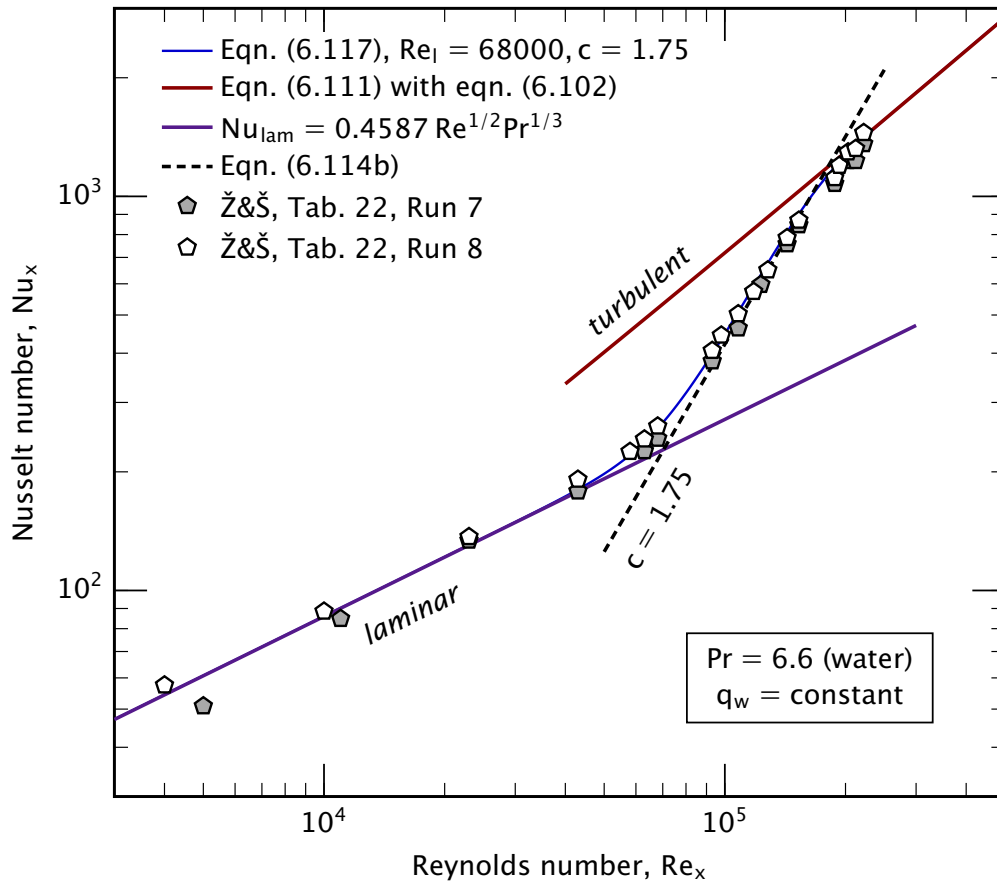
Figure 6.20 Nusselt number across the transition region for water flowing over a constant heat flux plate (data of Žukauskas and Šlančiauskas [6.23]). Adapted from [6.6].

The value of c is simply the slope of eqn. (6.114a) on a log-log plot. That slope is $c = 1.75$ in Fig. 6.20.

Equation (6.114a) intersects the laminar curve at Re_l. For example, in Fig. 6.20, the intersection is at $Re_l \cong 68,000$. Thus, a can be written in terms of the laminar Nusselt number at Re_l:

$$\mathrm{Nu_{trans}} = \mathrm{Nu_{lam}}(\mathrm{Re}_l, \mathrm{Pr}) \left(\frac{\mathrm{Re}_x}{\mathrm{Re}_l}\right)^c \qquad (6.114b)$$

The values of c and Re_l can be estimated for any particular set of data by plotting it. The legends of Figs. 6.20 and 6.21 state the values of c and Re_l that fit each data set.
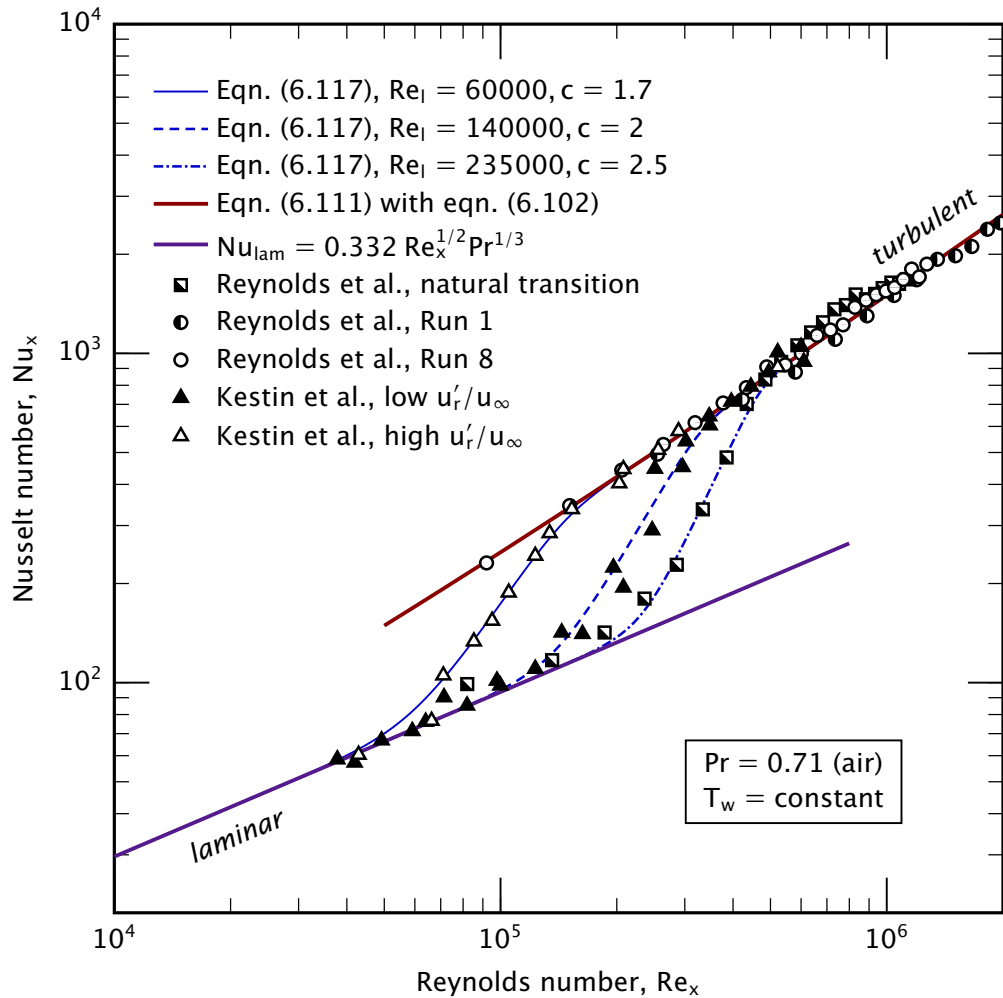
Figure 6.21 Nusselt numbers measured across the transition region for air flowing over constant temperature plates (data from [6.27–6.29, 6.32]). Adapted from [6.6].

The value of Re_l is very much dependent on details of the flow configuration that are often hard to predict. The amount of turbulence in the stream above the plate has a strong effect, as do surface roughness, system vibrations, and similar factors.

Lienhard examined many experimental data sets and found that the slope c gradually increases as the Reynolds number at the start of transi-

tion, Re_l, increases [6.6]. Measured values of c range from 1.4 to 2.6 for $30,000 \leqslant \mathrm{Re}_l \leqslant 500,000$. A correlation for c, to $\pm 8\%$, is:

$$c = 0.9922 \, \log_{10} \mathrm{Re}_l - 3.013 \qquad \mathrm{Re}_l \leqslant 500,000 \qquad (6.115)$$

For higher values of Re_l, fewer data are available, but the values of c are clearly much higher (up to 6 for the right-most curve in Fig. 6.22).

Effect of free-stream turbulence and of unheated starting length

Blair [6.30] measured h for constant wall heat flux in a carefully controlled wind-tunnel experiment. His heater had a short unheated starting length, which raised h in the laminar region relative to the prediction of eqn. (6.71), as seen in Fig. 6.22. He varied the free-stream turbulence by placing different grids upstream of the plate. This allowed him to change the location of transition to turbulence.

The figure shows three different ranges of turbulent transition, with transition occurring at lower Reynolds number for higher levels of free-stream turbulence. The later transition begins, the more rapidly it progresses: notice the steepness of the transition for the lowest turbulence level, 0.25% ($c = 6$). Great care is required to achieve such a low level of turbulence in a laboratory system, and most real systems undergo transition at a *much* lower Reynolds number.

Blair's results are in excellent agreement with both eqns. (6.111) and (6.112) for low turbulence levels. For Blair's highest turbulence level, h just after transition is about 5% above the equations, a difference that is hardly discernible on this log-log plot. (Blair's other experiments showed increases of up to 18% when u'_r/u_∞ rose to 6%.)

The heat transfer for a laminar, constant heat flux boundary with an unheated starting length can be predicted using eqn. (6.64) if the constant 0.332 is replaced by 0.4587 [6.6]:

$$\mathrm{Nu}_x = \frac{0.4587 \, \mathrm{Re}_x^{1/2} \, \mathrm{Pr}^{1/3}}{\left[1 - (x_0/x)^{3/4} \right]^{1/3}} \qquad \begin{cases} q_w = \text{const. for } x > x_0 \\ \text{laminar flow, } \mathrm{Pr} > 0.6 \end{cases} \qquad (6.116)$$

For Blair's experiment, $x_0 = 4.3$ cm. Equation 6.116 is in excellent agreement with Blair's laminar flow data.[12]

---

[12]In reality, many of the experimental reports of turbulent b.l. heat transfer have involved an unheated starting length, but authors have often used laminar theory to remove the effect from the data. Blair presented his data without such adjustments.
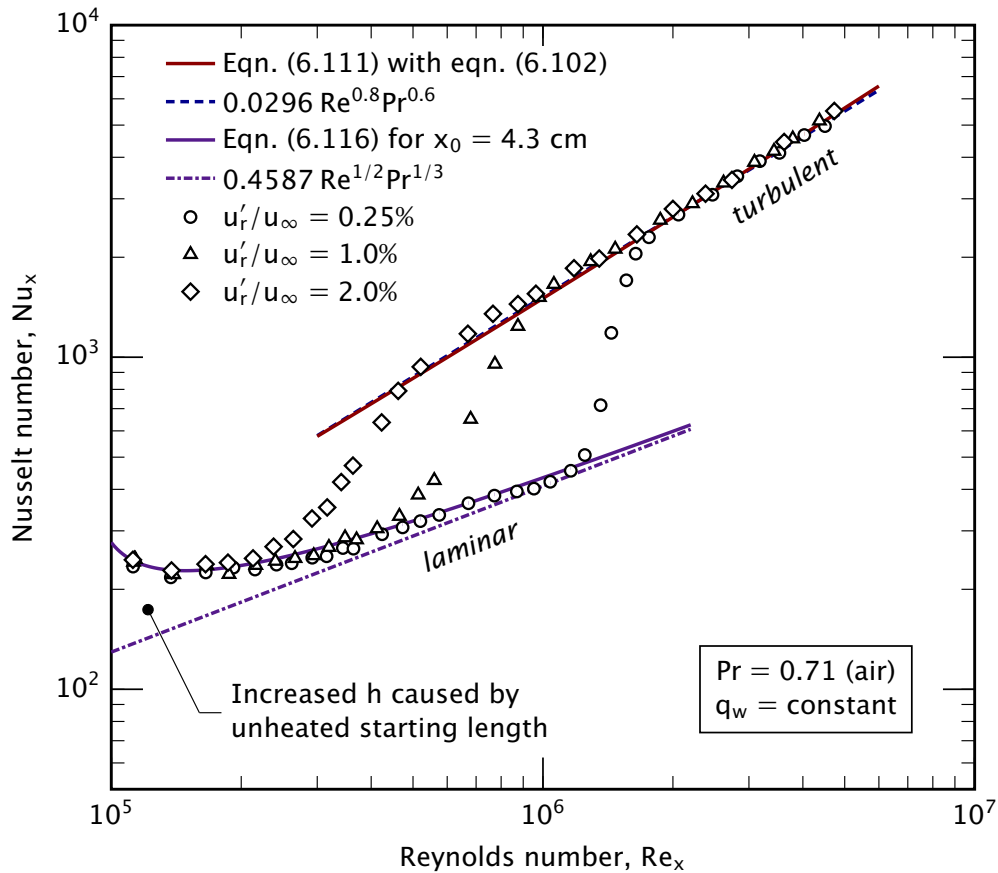
Figure 6.22 Comparison of eqn. (6.111) to the constant wall heat flux data of Blair [6.30] for three nominal levels of free-stream turbulence in air, where u'_r is the root-mean-square velocity fluctuation. The laminar equation, (6.71), and a power-law, eqn. (6.112), are also shown. Blair's unheated starting length raises h in the laminar region, as predicted by eqn. (6.116) [6.6]. $u_\infty = 30.3$ m/s, $T_\infty = 22°$C.

In practical situations with significant disturbances ($u'_r/u_\infty \gtrsim 3\%$), transition is likely to begin in the range $4 \times 10^4 \lesssim \text{Re}_l \lesssim 10^5$. Only with extremely low levels of turbulence ($u'_r/u_\infty \lesssim 0.5\%$) can Re_l exceed 10^6; Schubauer and Skramstad [6.5] reported limiting values of $\text{Re}_l \simeq 2.8 \times 10^6$ for $u'_r/u_\infty < 0.1\%$.[13]

---

[13]Mayle [6.33] and Blair [6.34] discuss estimation of Re_l when u'_r/u_∞ is known. However, u'_r usually decays in the flow direction, so local values are rarely available. Mayle

A correlation for laminar, transitional, and turbulent flow

Churchill [6.15] suggested that a single formula could smoothly blend the expressions for the laminar, transitional, and fully turbulent Nusselt numbers. Lienhard reviewed the available measurements of Nu_x in transitional flow, which led him to simplify Churchill's formula to [6.6]:

$$Nu_x(Re_x, Pr) = \left[Nu_{x,\text{lam}}^5 + \left(Nu_{x,\text{trans}}^{-10} + Nu_{x,\text{turb}}^{-10} \right)^{-1/2} \right]^{1/5} \quad (6.117)$$

This equation is continuous over the three regions, as seen in Fig. 6.20 where it follows the data between the laminar and transitional regions.

In eqn. (6.117), the laminar Nusselt number is calculated with eqn. (6.58) if the wall temperature is uniform or eqn. (6.71) if the wall heat flux is uniform. The transitional Nusselt number is calculated with eqn. (6.114b). The turbulent Nusselt number may be evaluated using eqn. (6.111) or an appropriate power law. All three terms should be used at each Reynolds number because the exponents in the formula diminish the influence of each term outside its proper region.

Example 6.8

How well does eqn. (6.117) fit the transitional data in Fig. 6.21?

SOLUTION. These data are for uniform wall temperature, so the laminar Nusselt number can be calculated using eqn. (6.58):

$$Nu_{\text{lam}} = 0.332 \, Re_x^{1/2} Pr^{1/3} \quad (6.58)$$

The turbulent Nusselt number, Nu_{turb} can be calculated from eqn. (6.111) (or, because these are air data, eqn. (6.112) could be used).

The values of c and Re_l must be estimated for each data set. This is easy to do by trial and error if the curves are being created numerically. If working by hand, printing Fig. 6.21 and using a straight-edge to draw a line through the transition range allows the values to be read from the plot. For instance, a line through the transitional data shown as open triangles has a slope of about 1.75; and that line intersects the laminar curve at a Reynolds number of about 61,000, where the laminar Nusselt number is about 73. Thus, with eqn. (6.114b),

$$Nu_{\text{trans}} = 73 \left(\frac{Re_x}{61,000} \right)^{1.75} \quad (6.118)$$

suggested an empirical equation, which we can write as $Re_l = (3.6 \times 10^5)(100 u_r'/u_\infty)^{-5/4}$ for a laminar b.l. starting at the leading edge. This equation has fairly limited accuracy in most cases (e.g., it predicts Blair's Re_l to within only a factor of two or so).

A similar process generates Nu_{trans} for the other three data sets.

For each data set, we substitute Nu_{lam}, Nu_{trans}, and Nu_{turb} into eqn. (6.117). The curves calculated are shown in Fig. 6.21, with the corresponding values of c and Re_l. Equation (6.117) fits the data well.■

Average Nusselt number for the entire plate

The average heat transfer coefficient—including the laminar, transitional, and turbulent regions—may be found by integrating h with eqn. (6.117). Depending on the wall boundary condition, either eqn. (6.65) or eqn. (6.66) applies. The computation can be done with common software packages.

An algebraic formula can be obtained by noticing that the transition region starts and ends rather sharply. We may approximate the integral in three distinct pieces, without using eqn. (6.117). For uniform T_w,

$$\overline{h} = \frac{1}{L\Delta T} \int_0^L q_w \, dx$$

$$= \frac{1}{L} \left[\int_0^{x_l} h_{\text{laminar}} \, dx + \int_{x_l}^{x_u} h_{\text{trans}} \, dx + \int_{x_u}^{L} h_{\text{turbulent}} \, dx \right] \qquad (6.119)$$

where $x_l = (\nu/u_\infty)\text{Re}_l$ is the start of transition and $x_u = (\nu/u_\infty)\text{Re}_u$ is the end. The first two integrals can be evaluated by hand. The third integral is less simple analytically, unless a power law is adopted for the turbulent region. For gas flows, we may use eqn. (6.112) for the turbulent region. After integration, we have:

$$\overline{\text{Nu}}_L \equiv \frac{\overline{h}L}{k} = 0.037 \, \text{Pr}^{0.6} \left(\text{Re}_L^{0.8} - \text{Re}_u^{0.8} \right) + 0.664 \, \text{Re}_l^{1/2} \text{Pr}^{1/3}$$

$$+ \underbrace{\frac{1}{c} \left(0.0296 \, \text{Re}_u^{0.8} \text{Pr}^{0.6} - 0.332 \, \text{Re}_l^{1/2} \text{Pr}^{1/3} \right)}_{\text{contribution of transition region}} \quad \text{for gases} \quad (6.120)$$

A similar equation may be developed for liquids by using eqn. (6.113) for the turbulent region.

Example 6.9

In a wind tunnel experiment, an aluminum plate 2.0 m in length and 1.0 m wide is held at a temperature of 310 K and is cooled on one surface by air flowing at 10 m/s. The air in the wind tunnel has a temperature of 290 K and is at 1 atm pressure. The Reynolds

numbers at the beginning and end of the turbulent transition regime are observed to be 400,000 and 870,000. What is the heat loss from the plate?

SOLUTION. We evaluate properties at the film temperature of 300 K: $\nu = 1.575 \times 10^{-5}$ m^2/s, $k = 0.0264$ W/m·K, and Pr $= 0.708$. At 10 m/s, the plate Reynolds number is $\text{Re}_L = (10)(2)/(1.575 \times 10^{-5}) = 1.270 \times 10^6$.

First, we must compute c from eqn. (6.115):

$$c = 0.9922 \log_{10}(400,000) - 3.013 = 2.55$$

Now we may use eqn. (6.120):

$$\overline{\text{Nu}}_L = 0.037(0.708)^{0.6}\left[(1.270 \times 10^6)^{0.8} - (8.70 \times 10^5)^{0.8}\right]$$
$$+ 0.664\,(4.00 \times 10^5)^{1/2}(0.708)^{1/3}$$
$$+ \frac{1}{2.55}\left[0.0296(8.70 \times 10^5)^{0.8}(0.708)^{0.6}\right.$$
$$\left. - 0.332\,(4.00 \times 10^5)^{1/2}(0.708)^{1/3}\right]$$

Evaluating, we see that the contributions of the turbulent, laminar, and transition regions are of similar size:

$$\overline{\text{Nu}}_L = \underbrace{599.9}_{\text{turb.}} + \underbrace{374.3}_{\text{lam.}} + \underbrace{459.2}_{\text{trans.}} = 1,433$$

In fact, the transition region contributes 35% of the total. The average heat transfer coefficient is

$$\overline{h} = \frac{1433(0.0264)}{2.0} = 18.92 \text{ W/m}^2\text{K}$$

and the convective heat loss from the plate is

$$Q = (2.0)(1.0)(18.92)(310 - 290) = 756.0 \text{ W}$$

If thermal radiation were included using eqn. (2.31) with $\varepsilon_{\text{Al}} = 0.09$, then $h_{\text{rad}} = 0.55$ W/m^{2}K and the additional heat removal is 22 W. ∎

Example 6.10

Suppose that Re_u had not been given in Example 6.9. How could we find its value?

SOLUTION. The transition curve, eqn. (6.114b), intersects the turbulent curve for gases, eqn. (6.112), at Re_u. We may set them equal at Re_u:

$$\left(0.332\,\text{Re}_l^{1/2}\text{Pr}^{1/3}\right)\left(\frac{\text{Re}_u}{\text{Re}_l}\right)^c = 0.0296\,\text{Re}_u^{0.8}\,\text{Pr}^{0.6}$$

Substituting Re_l, Pr, and c from Example 6.9 and rearranging:

$$\text{Re}_u^{2.55-0.8} = \frac{0.0296(0.708)^{0.6}(400{,}000)^{2.55}}{0.332(400{,}000)^{1/2}(0.708)^{1/3}}$$

Solving gives us $\text{Re}_u = 870{,}300$.   ∎

Example 6.11

Suppose that the transition region were omitted in Example 6.9, as if the flow abruptly changed from laminar to turbulent at some value Re_{trans}. How much error would result from that calculation?

SOLUTION. Without the transition region, eqn. (6.120) reduces to

$$\overline{\text{Nu}}_L \equiv \frac{\overline{h}L}{k} = 0.037\,\text{Pr}^{0.6}\left(\text{Re}_L^{0.8} - \text{Re}_{\text{trans}}^{0.8}\right) + 0.664\,\text{Re}_{\text{trans}}^{1/2}\text{Pr}^{1/3}$$

If we take $\text{Re}_{\text{trans}} = \text{Re}_l = 400{,}000$, we find $\overline{\text{Nu}}_L = 1760$ (high by $+23\%$). If instead $\text{Re}_{\text{trans}} = \text{Re}_u = 870{,}000$, then $\overline{\text{Nu}}_L = 1152$ (low by -20%). Neither value is very accurate.   ∎

A word about the analysis of turbulent boundary layers

The preceding discussion has avoided in-depth theoretical analysis of heat transfer in turbulent boundary layers. During the first part of the twentieth century, sophisticated integral methods were used to analyze boundary layer heat transfer in many flows, both with and without pressure gradients (dp/dx). In subsequent decades, computational methods largely replaced integral analyses, particularly methods based on turbulent kinetic energy and viscous dissipation (so-called k-ε models). These methods are described in the technical literature and in monographs on turbulence [6.35, 6.36], and they have been widely implemented in commercial and industrial fluid-dynamics codes.

We have found our way around detailed analysis by presenting some correlations for the simple plane surface. In the next chapter, we deal with more complicated configurations. A few of these configurations will be amenable to elementary analyses, but for others we shall only be able to present the best data correlations available.

Problems

6.1 Verify that eqn. (6.13) follows from eqns. (6.11a) and (6.12).

6.2 The student with some analytical ability (or some assistance from the instructor) should complete the algebra between eqns. (6.16) and (6.20).

6.3 Use a computer to solve eqn. (6.18) subject to b.c.'s (6.20). To do this you need all three b.c.'s at $\eta = 0$, but one is presently at $\eta = \infty$. There are three ways to get around this:

- Start out by guessing a value of $df'/d\eta$ at $\eta = 0$—say, $df'/d\eta = 1$. When η is large—say, 6 or 10—$df'/d\eta$ will asymptotically approach a constant. If the constant > 1, go back and guess a lower value of $df'/d\eta$, or vice versa, until the constant converges on one. (One might invent a number of means to automate the successive guesses.)

- The correct value of $df'/d\eta$ is approximately 0.33206 at $\eta = 0$. You might cheat and begin with it, but where is the fun in that?

- There exists a clever way to map $df/d\eta = 1$ at $\eta = \infty$ back into the origin. (Consult your instructor.)

6.4 Verify that the Blasius solution (Table 6.1) satisfies eqn. (6.25). To do this, carry out the required numerical and/or graphical integration. *Hint:* At any given x, $y/\delta = \eta/4.92$.

6.5 Verify eqn. (6.30).

6.6 Use the velocity profile given by the integral method to calculate τ_w and compare the result to eqn. (6.32).

6.7 Approximate the laminar b.l. velocity profile with the very simple equation $u/u_\infty = y/\delta$ and calculate δ and C_f, using the momentum integral method. How accurate is each? [C_f is about 13% low.]

6.8 In a certain flow of water at 40°C over a flat plate, $\delta = 0.005\sqrt{x}$ for δ and x measured in meters. Plot *to scale* on a single graph (with an appropriately expanded y-scale):

- δ and δ_t for the water flow
- δ and δ_t for an air flow at the same temperature and velocity

6.9 A thin film of liquid with a constant thickness, δ_0, falls down a vertical plate. The liquid has reached its terminal velocity so that the flow is steady with viscous shear stress and weight in balance. The b.l. equation for such a flow is the same as eqn. (6.13), except that the gravity force must also be included. Thus,

$$u\frac{\partial u}{\partial x} + v\frac{\partial u}{\partial y} = -\frac{1}{\rho}\frac{dp}{dx} + g + \nu\frac{\partial^2 u}{\partial y^2}$$

where x increases in the downward direction and y is normal to the wall. Assume that the hydrostatic pressure gradient in the surrounding air is negligible. Then:

- Simplify the equation to describe this situation.
- Write the b.c.'s for the equation, neglecting any air drag on the film.
- Solve for the velocity distribution in the film, assuming that you know δ_0 (cf. Chapter 8).

This solution is the starting point in the study of many heat and mass transfer processes.

6.10 Beginning with eqn. (6.63), show that $\overline{\mathrm{Nu}}_L$ for a laminar b.l. over a flat, isothermal surface is given over the entire range of Pr by this equation:

$$\overline{\mathrm{Nu}}_L = \frac{0.677\,\mathrm{Re}_L^{1/2}\,\mathrm{Pr}^{1/3}}{\left[1 + (0.0468/\mathrm{Pr})^{2/3}\right]^{1/4}} \qquad (6.121)$$

6.11 Use an integral method to predict Nu_x for a laminar b.l. over a uniform heat flux plate that will be valid for all fluids other than liquid metals. Compare your result to eqn. (6.71). What temperature difference does your result give at the leading edge of the plate?

6.12 (a) Verify that eqn. (6.120) follows from eqn. (6.119). (b) Derive an equation for liquids that is analogous to eqn. (6.120).

6.13 Fluid at a uniform speed U flows into a channel between two parallel plates a distance d apart. A laminar boundary layer grows on each plate. (a) At approximately what distance from the inlet will the two boundary layers first touch? (b) If the flow remains laminar, qualitatively sketch the velocity distribution between the plates a long distance after the boundary layers meet, noting that the mass flow rate is constant along the channel. [(a) $x/d \cong 0.01(Ud/\nu)$.]

6.14 Execute the differentiation in eqn. (6.24) with the help of Leibnitz's rule for the differentiation of an integral and show that the equation before it is the result.

6.15 Liquid at 23°C flows at 2 m/s over a smooth, sharp-edged, flat surface 12 cm in length which is kept at 57°C. Calculate h at the trailing edge: (a) if the fluid is water; and (b) if the fluid is glycerin. (c) Compare the drag forces in the two cases. [(b) $h = 346$ W/m²K. (c) The glycerin produces 23.4 times as much drag.]

6.16 Air at -10°C flows over a smooth, sharp-edged, almost-flat, aerodynamic surface at 240 km/hr. The surface is at 10°C. Turbulent transition begins at $Re_l = 140,000$ and ends at $Re_u = 315,000$. Find: (a) the x-coordinates within which laminar-to-turbulent transition occurs; (b) $\overline{h}$ for a 2 m long surface; (c) h at the trailing edge for a 2 m surface; and (d) δ and h at x_l. [$\delta_{x_l} \simeq 0.4$ mm]

6.17 Find $\overline{h}$ in Example 6.9 using eqn. (6.120) with $Re_l = 80,000$. Compare with the value in the example and discuss the implication of your result. *Hint:* See Example 6.10

6.18 For system described in Example 6.9, plot the local value of h over the whole length of the plate using eqn. (6.117). On the same graph, plot h from eqn. (6.58) for $Re_x < 800,000$ and from eqn. (6.112) for $Re_x > 400,000$. Discuss the results.

6.19 Mercury at 25°C flows at 0.7 m/s over a 4 cm-long flat heater at 60°C. The flow is laminar. Find $\overline{h}$, $\overline{\tau}_w$, $h(x = 0.04$ m), and $\delta(x = 0.04$ m).

6.20 A large plate is at rest in water at 15°C. The plate suddenly begins moving parallel to itself, at 1.5 m/s. The resulting fluid movement is not exactly like that in the b.l. that we have studied in this chapter because the velocity profile builds up uniformly, all along the plate, instead of beginning at an edge. The transient momentum equation takes the form

$$\frac{1}{\nu}\frac{\partial u}{\partial t} = \frac{\partial^2 u}{\partial y^2}$$

Determine u at 0.015 m above the plate for $t = 1, 10$, and 1000 s. Do this by first posing the problem with boundary and initial conditions and then comparing to the semi-infinite body heat conduction solution in Section 5.6. [$u \cong 0.003$ m/s after 10 s.]

6.21 When Pr is large, the velocity b.l. thickness on an isothermal, flat heater is much larger than δ_t. The velocity profile inside the thermal b.l. is approximately $u/u_\infty \cong \frac{3}{2}y/\delta = \frac{3}{2}\phi(y/\delta_t)$. Use the integral energy equation to derive Nu_x for this case based on this velocity profile.

6.22 For air flowing above an isothermal plate, plot the ratio of $h(x)_{\mathrm{laminar}}$ to $h(x)_{\mathrm{turbulent}}$ as a function of Re_x in the range of Re_x that might be either laminar or turbulent. What does the plot suggest about designing for effective heat transfer?

6.23 Water at 7°C flows at 0.38 m/s across the top of a 0.207 m-long, thin copper plate. Methanol at 87°C flows across the bottom of the same plate, at the same speed but in the opposite direction. Make the obvious first guess as to the plate temperature to use when evaluating physical properties. Then plot the plate temperature as a function of position. (Do not bother to make additional corrections to the physical properties. That is done in Problem 6.24.) With everything that varies along the plate, determine where the local heat flux would be least.

6.24 Work Problem 6.23 taking full account of property variations.

6.25 Example 6.6 had a uniform wall heat flux of $q_w = 420$ W/m². If instead the wall temperature were fixed at its average value of 76°C, what would be the *average* wall heat flux?

6.26 In Sect. 6.4, we noted that the kinetic theory of gases predicts values of Pr ranging from 2/3 for monatomic ideal gases and 1 for complex molecules. Show how this is borne out for gases at 400 K, using Table A.6 in Appendix A.

6.27 A 2 ft-square slab of mild steel leaves a forging operation with a thickness of 0.25 in. at 1000°C. It is laid flat on an insulating bed and 27°C air is blown over the top side at 30 m/s. How long will it take to cool to 200°C? Assume that the flow is laminar and state your assumptions about property evaluation. [25.3 min.]

6.28 Solve Problem 6.27 numerically, recalculating properties at successive times. If you worked Problem 6.27, compare the results.

6.29 Plot q_w against x for the situation described in Example 6.9. (If you have already worked Problem 6.18, this calculation will be short.)

6.30 Consider the plate in Example 6.9. Suppose that instead of specifying $T_w = 310$ K, we specified $q_w = 500$ W/m². Plot T_w against x for this case.

6.31 A thin metal sheet separates air at 44°C, flowing at 48 m/s, from water at 4°C, flowing at 0.2 m/s. Both fluids start at a leading edge and move in the same direction. Plot q_w as a function of x up to $x = 0.1$ m. How does T_{plate} vary?

6.32 A mixture of 60% glycerin and 40% water flows over a 1-m-long flat plate. The glycerin is at 20°C and the plate is at 40°C. A small temperature sensor 1 mm above the trailing edge records 35°C. What is u_∞, and what is u at the sensor position?

6.33 Approximately what maximum value of $\overline{h}$ can be achieved in a laminar flow over a 5 m plate, based on data from Table A.3? What sort of physical circumstances would be required to achieve such a value?

6.34 A 17°C sheet of water, initially Δ_1 m, thick flows next to a horizontal plate starting at the leading edge. The sheet has a uniform initial speed of u_∞ m/s. Develop a dimensionless equation for the thickness Δ_2 at a distance L from the leading edge. Assume that $\delta \ll \Delta_2$. Evaluate the result for $u_\infty = 1$ m/s, $\Delta_1 = 0.01$ m, and $L = 0.1$ m, in water at 27°C.

6.35 A good approximation to the temperature dependence of μ in gases is given by the Sutherland formula:

$$\frac{\mu}{\mu_{\text{ref}}} = \left(\frac{T}{T_{\text{ref}}}\right)^{1.5}\left(\frac{T_{\text{ref}} + S}{T + S}\right) \tag{6.122}$$

The reference state can be chosen anywhere, and T and T_{ref} are expressed in kelvin. Use data for air at two points to evaluate S for air. Use this value to predict a third point and compare to data.

6.36 We derived a steady-state continuity equation in Section 6.2. Now derive the time-dependent, compressible, three-dimensional version of the equation:

$$\frac{\partial \rho}{\partial t} + \nabla \cdot (\rho \vec{u}) = 0 \tag{6.123}$$

To do this, paraphrase the development of equation (2.10), requiring that mass be conserved instead of energy. Show that this equation reduces to eqn. (6.11b) for steady, constant density flow.

6.37 The very smallest-scale motions in a fully turbulent flow are responsible for most of the viscous dissipation of kinetic energy. The dissipation rate, ε (W/kg), is imposed on the small eddies by the larger-scale motion of the flow. Further, the small eddies have no preferred spatial orientation. Thus, ε and ν are the independent variables that define the small-scale motion.

   a. Use dimensional analysis to find the characteristic length and velocity scales of the small-scale motion, η and u_η. These are called the *Kolmogorov* scales of the flow.

   b. Compute the Reynolds number for the *small-scale motion* and interpret the result.

   c. The Kolmogorov length scale characterizes the smallest motions found in a turbulent flow. If ε is 10 W/kg and the mean free path of an air molecule at 1 bar and 20°C is 67 nm, show that turbulent motion is a continuum phenomenon and thus is properly governed by the equations of this chapter.

6.38 The temperature outside is 35°F, but with the wind chill it's 24°F. And you forgot your hat. If you go outdoors for long, are you in danger of freezing your ears? Why or why not?

6.39 To heat the airflow in a wind tunnel, an experimenter uses an array of electrically heated, Nichrome V strips. Each strip is 20 cm by 2.5 cm and very thin. They are stretched across the flow with the thin edge facing into the wind. The air flows along both sides. The strips are spaced vertically, each 1 cm above the next. Air at 1 atm and 20°C enters the array of strips at 10 m/s.

   a. How much power must each strip deliver to raise the mean temperature of the airstream to 30°C?

   b. What is the heat flux if the electrical dissipation in the strips is uniform?

   c. What are the average and maximum temperatures of the strips?

6.40 An airflow sensor consists of a 5 cm long, heated copper slug that is smoothly embedded 10 cm from the leading edge of a flat plate. The overall length of the plate is 15 cm, and the width of the plate and the slug are both 10 cm. The slug is electrically heated by an internal heating element, but, owing to its high thermal conductivity, the slug has a nearly uniform temperature along its

airside surface. The heater's controller adjusts its power to keep the slug surface at a fixed temperature. The air velocity is calculated from measurements of the slug temperature, the air temperature, and the heating power.

a. If the air is at 280 K, the slug is at 300 K, and the heater power is 5.0 W, find the airspeed assuming the flow is laminar. *Hint:* For $x_1/x_0 = 1.5$, integration shows that

$$\int_{x_0}^{x_1} x^{-1/2}\left[1 - (x_0/x)^{3/4}\right]^{-1/3} dx = 1.0035\sqrt{x_0}$$

b. Suppose that a disturbance trips the boundary layer near the leading edge, causing it to become turbulent over the whole plate. The air speed, air temperature, and the slug's set-point temperature remain the same. Make a very rough estimate of the heater power that the controller now delivers, without doing a lot of analysis.

6.41 Equation (6.64) gives Nu_x for a flat plate with an unheated starting length. This equation may be derived using the integral energy equation (6.47), the velocity and temperature profiles from eqns. (6.29) and (6.50), and $\delta(x)$ from eqn. (6.31a). Equation (6.52) is again obtained; however, in this case, $\phi = \delta_t/\delta$ is a function of x for $x > x_0$. Derive eqn. (6.64) by starting with eqn. (6.52), neglecting the term $3\phi^3/280$, and replacing δ_t by $\phi\delta$. After some manipulation, you will obtain

$$x\frac{4}{3}\frac{d}{dx}\phi^3 + \phi^3 = \frac{13}{14\,\text{Pr}}$$

Show that the solution of this o.d.e. is

$$\phi^3 = Cx^{-3/4} + \frac{13}{14\,\text{Pr}}$$

for an unknown constant C. Then apply an appropriate initial condition and the definition of q_w and Nu_x to obtain eqn. (6.64).

6.42 Make a spreadsheet to compare eqn. (6.111) to eqn. (6.112) and eqn. (6.113) for Prandtl numbers of 0.7, 6, 50, and 80 over the range $2 \times 10^5 \leqslant \text{Re}_x \leqslant 10^7$, keeping in mind the ranges of validity of the various equations. What conclusions do you draw?

6.43 Liquid metal flows past a flat plate. Axial heat conduction is negligible, and the momentum b.l. has negligible thickness. (a) If the plate is isothermal, use eqn. (5.54) to derive eqn. (6.62). (b) Derive the corresponding expression for the local Nusselt number if the plate has a constant wall heat flux. (c) Find the average Nusselt number in both cases.

6.44 Beginning with eqn. (6.73) show that $\overline{\mathrm{Nu}}_L$ is given over the entire range of Pr for a laminar b.l. on a flat, constant flux surface by:

$$\overline{\mathrm{Nu}}_L = \frac{0.696\,\mathrm{Re}_L^{1/2}\,\mathrm{Pr}^{1/3}}{\left[1 + (0.0205/\mathrm{Pr})^{2/3}\right]^{1/4}} \qquad (6.124)$$

6.45 For laminar flow over a flat plate flow with Pr > 0.6, how does $\bar{h}$ for T_w constant compare to $\bar{h}$ for q_w constant? At what location on a plate with q_w constant is the local plate temperature the same as the average plate temperature? At what location on a plate with T_w constant is the local heat flux the same as the average heat flux?

6.46 Two power laws are available for the skin friction coefficient in turbulent flow: $C_f(x) = 0.027\,\mathrm{Re}_x^{-1/7}$ and $C_f(x) = 0.059\,\mathrm{Re}_x^{-1/5}$. The former is due to White and the latter to Prandtl [6.4]. Equation (6.102) is more accurate and wide ranging than either. Plot all three expressions on semi-log coordinates for $10^5 \leqslant \mathrm{Re}_x \leqslant 10^9$. Over what range are the power laws in reasonable agreement with eqn. (6.102)? Also plot the laminar equation (6.33) on same graph for $\mathrm{Re}_x \leqslant 10^6$. Comment on all your results.

6.47 Reynolds et al. [6.27] provide the following measurements for air flowing over a flat plate at 127 ft/s with $T_\infty = 86°\mathrm{F}$ and $T_w = 63°\mathrm{F}$. Plot these data on log-log coordinates as Nu_x vs. Re_x, and fit a power law to them. How does your fit compare to eqn. (6.112)?

$\mathrm{Re}_x \times 10^{-6}$	$\mathrm{St} \times 10^3$	$\mathrm{Re}_x \times 10^{-6}$	$\mathrm{St} \times 10^3$	$\mathrm{Re}_x \times 10^{-6}$	$\mathrm{St} \times 10^3$
0.255	2.73	1.353	2.01	2.44	1.74
0.423	2.41	1.507	1.85	2.60	1.75
0.580	2.13	1.661	1.79	2.75	1.72
0.736	2.11	1.823	1.84	2.90	1.68
0.889	2.06	1.970	1.78	3.05	1.73
1.045	2.02	2.13	1.79	3.18	1.67
1.196	1.97	2.28	1.73	3.36	1.54

6.48 Blair and Werle [6.37] reported the b.l. data below. Their experiment had a uniform wall heat flux with a 4.29 cm unheated starting length, $u_\infty = 30.2$ m/s, and $T_\infty = 20.5°$C.

    a. Plot these data as Nu_x versus Re_x on log-log coordinates. Identify the regions likely to be laminar, transitional, and turbulent flow.

    b. Plot the appropriate theoretical equation for Nu_x in laminar flow on this graph. Does the equation agree with the data?

    c. Plot eqn. (6.112) for Nu_x in turbulent flow on this graph. How well do the data and the equation agree?

    d. At what Re_x does transition begin? Find values of c and Re_l that fit eqn. (6.114b) to these data, and plot the fit on this graph.

    e. Plot eqn. (6.117) through the entire range of Re_x.

$Re_x \times 10^{-6}$	$St \times 10^3$	$Re_x \times 10^{-6}$	$St \times 10^3$	$Re_x \times 10^{-6}$	$St \times 10^3$
0.112	2.94	0.362	1.07	1.27	2.09
0.137	2.23	0.411	1.05	1.46	2.02
0.162	1.96	0.460	1.01	1.67	1.96
0.183	1.68	0.505	1.05	2.06	1.84
0.212	1.56	0.561	1.07	2.32	1.86
0.237	1.45	0.665	1.34	2.97	1.74
0.262	1.33	0.767	1.74	3.54	1.66
0.289	1.23	0.865	1.99	4.23	1.65
0.312	1.17	0.961	2.15	4.60	1.62
0.338	1.14	1.06	2.24	4.83	1.62

6.49 Figure 6.21 shows a fit to the following air data from Kestin et al. [6.29] using eqn. (6.117). The plate temperature was 100°C (over its entire length) and the free-stream temperature varied between 20 and 30°C. Follow the steps used in Problem 6.48 to reproduce that fit and plot it with these data.

$Re_x \times 10^{-3}$	Nu_x	$Re_x \times 10^{-3}$	Nu_x	$Re_x \times 10^{-3}$	Nu_x
60.4	42.9	445.3	208.0	336.5	153.0
76.6	66.3	580.7	289.0	403.2	203.0
133.4	85.3	105.2	71.1	509.4	256.0
187.8	105.0	154.2	95.1	907.5	522.0
284.5	134.0	242.9	123.0		

6.50 A study of the kinetic theory of gases shows that the mean free path of a molecule in air at one atmosphere and 20°C is 67 nm and that its mean speed is 467 m/s. Use eqns. (6.45) obtain C_1 and C_2 from the known physical properties of air. We have asserted that these constants should be on the order of 1. Are they?

6.51 The two most important fluids for thermal engineering are air and water. Using data from Appendix A, plot the Prandtl number of air and of saturated liquid water from 280 K to 650 K (for water, stop plotting at 644 K, which is very close to the critical point temperature of 647.1 K). Comment on the trends in this chart.

References

[6.1] S. Juhasz. Notes on Applied Mechanics Reviews – Referativnyi Zhurnal Mekhanika exhibit at XIII IUTAM, Moscow 1972. *Appl. Mech. Rev.*, **26**(2): 145–160, 1973.

[6.2] J. H. Lienhard. Prandtl, Ludwig. In *Complete Dictionary of Scientific Biography*. 2018. Retrieved on 13 July 2018 from www.encyclopedia.com.

[6.3] R. H. Kargon. Reynolds, Osborne. In *Complete Dictionary of Scientific Biography*. 2018. Retrieved on 13 July 2018 from www.encyclopedia.com.

[6.4] F. M. White. *Viscous Fluid Flow*. McGraw-Hill, Inc., New York, 2nd ed., 1991.

[6.5] G. B. Schubauer and H. K. Skramstad. Laminar-boundary-layer oscillations and transition on a flat plate. Report 909, NACA, Washington, DC, 1948. url: http://hdl.handle.net/2060/19930091976.

[6.6] J. H. Lienhard V. Heat transfer in flat-plate boundary layers: a correlation for laminar, transitional, and turbulent flow. *J. Heat Transfer*, **142**(6): 061805, June 2020. doi: 10.1115/1.4046795.

[6.7] J. H. Lienhard. Nusselt, Ernst Kraft Wilhelm. In *Complete Dictionary of Scientific Biography*. 2018. Retrieved on 13 July 2018 from www.encyclopedia.com.

[6.8] H. Schlichting. *Boundary-Layer Theory*. (trans. J. Kestin). McGraw-Hill Book Company, New York, 7th ed., 1979.

[6.9] F. M. White. *Viscous Fluid Flow*. McGraw-Hill Book Company, New York, 1974.

[6.10] C. L. Tien and J. H. Lienhard. *Statistical Thermodynamics*. Hemisphere Publishing Corp., Washington, D.C., revised ed., 1978. url: https://www.uh.edu/engines/StatisticalThermodynamics.pdf.

[6.11] E. Pohlhausen. Der wärmeaustausch zwischen festen Körpern und Flüssigkeiten mit kleiner reibung und kleiner Wärmeleitung. *Zeitschrift für Angewandte Mathematik und Mechanik (ZAMM) / J. Applied Mathematics and Mechanics*, **1**(2):115–121, 1921. doi: 10.1002/zamm.19210010205.

[6.12] H. L. Evans. Mass transfer through laminar boundary layers—7. Further similar solutions to the *b*-equation for the case *B* = 0. *Int. J. Heat Mass Transfer*, **5**(1):35–57, 1962. doi: 10.1016/0017-9310(62)90100-X.

[6.13] Y.-M. Chen. Heat transfer of a laminar flow passing a wedge at small Prandtl number: a new approach. *Int. J. Heat Mass Transfer*, **28**(8): 1517–1523, August 1985. doi: 10.1016/0017-9310(85)90254-6.

[6.14] S. W. Churchill and H. Ozoe. Correlations for laminar forced convection in flow over an isothermal flat plate and in developing and fully developed flow in an isothermal tube. *J. Heat Transfer*, **95**(3):416–419, February 1973. doi: 10.1115/1.3450078.

[6.15] S. W. Churchill. A comprehensive correlating equation for forced convection from flat plates. *AIChE J.*, **22**(2):264–268, March 1976. doi: 10.1002/aic.690220207.

[6.16] O. Reynolds. On the extent and action of the heating surface for steam boilers. *Proc. Manchester Lit. Phil. Soc.*, **14**:7–12, 1874. The doi is for a 1961 reprint in *IJHMT*. doi: 10.1016/0017-9310(61)90087-4.

[6.17] A. P. Colburn. A method of correlating forced convection heat transfer data and a comparison with fluid friction. *Trans. Amer. Inst. Chem. Engrs.*, **29**:174–206, 1933. The doi is for a 1964 reprint in *IJHMT*. doi: 10.1016/0017-9310(64)90125-5.

[6.18] J. A. Schetz. *Foundations of Boundary Layer Theory for Momentum, Heat, and Mass Transfer.* Prentice-Hall, Inc., Englewood Cliffs, NJ, 1984.

[6.19] P. S. Granville. A modified Van Driest formula for the mixing length of turbulent boundary layers in pressure gradients. *J. Fluids Engr.*, **111**(1): 94–97, March 1989. doi: 10.1115/1.3243606.

[6.20] P. S. Granville. A near-wall eddy viscosity formula for turbulent boundary layers in pressure gradients suitable for momentum, heat, or mass transfer. *J. Fluids Engr.*, **112**(2):240–243, June 1990. doi: 10.1115/1.2909395.

[6.21] F. M. White. A new integral method for analyzing the turbulent boundary layer with arbitrary pressure gradient. *J. Basic Engr.*, **91**:371–378, September 1969. doi: 10.1115/1.3571122.

[6.22] J. Boussinesq. Essai sur la théorie des eaux courante. *Mem. Pres. Acad. Sci.,*, **XXIII**(1):1–680, 1877. url: https://www.irphe.fr/~clanet/otherpaperfile/articles/Boussinesq/N0003328_PDF_1_770.pdf.

[6.23] A. Žukauskas and A. Šlančiauskas. *Heat Transfer in Turbulent Fluid Flows.* Hemisphere Publishing Corp., Washington, D.C., 1987.

[6.24] B. S. Petukhov. Heat transfer and friction in turbulent pipe flow with variable physical properties. In T.F. Irvine, Jr. and J. P. Hartnett, editors, *Advances in Heat Transfer*, Vol. 6, pp. 504–564. Academic Press, Inc., New York, 1970. doi: 10.1016/S0065-2717(08)70153-9.

[6.25] T. G. Beckwith, R. D. Marangoni, and J. H. Lienhard. *Mechanical Measurements*. Pearson/Prentice Hall, Upper Saddle River, NJ, 6th ed., 2007.

[6.26] R. A. Seban and D. L. Doughty. Heat transfer to turbulent boundary layers with variable free-stream velocity. *Trans. ASME*, **78**(1):217–223, January 1956. doi: 10.1115/1.4013621.

[6.27] W. C. Reynolds, W. M. Kays, and S. J. Kline. Heat transfer in the incompressible turbulent boundary layer. I–constant wall temperature. Memorandum 12-1-58W, NASA, Washington, D.C., December 1958. url: http://hdl.handle.net/2060/19980228020.

[6.28] G. H. Junkhan and G. K. Serovy. Effects of free-stream turbulence and pressure gradient on flat-plate boundary-layer velocity profiles and on heat transfer. *J. Heat Transfer*, **89**(2):169–175, May 1967. doi: 10.1115/1.3614346.

[6.29] J. Kestin, P. F. Maeder, and H. E. Wang. The influence of turbulence on the transfer of heat from plates with and without a pressure gradient. *Int. J. Heat Mass Transfer*, **3**:133–154, September 1961. doi: 10.1016/0017-9310(61)90076-X.

[6.30] M. F. Blair. Influence of free-stream turbulence on turbulent boundary layer heat transfer and mean profile development, Part I–experimental data. *J. Heat Transfer*, **105**(1):33–40, February 1983. doi: 10.1115/1.3245555.

[6.31] A. A. Žukauskas and A. B. Ambrazyavichyus. Heat transfer from a plate in a liquid flow. *Int. J. Heat Mass Transfer*, **3**(4):305–309, December 1961. doi: 10.1016/0017-9310(61)90045-X.

[6.32] W. C. Reynolds, W. M. Kays, and S. J. Kline. Heat transfer in the incompressible turbulent boundary layer. IV–Effect of location of transition and prediction of heat transfer in a known transition region. Memorandum 12-4-58W, NASA, Washington, D.C., December 1958. url: http://hdl.handle.net/2060/20050158659.

[6.33] R. E. Mayle. The role of laminar-turbulent transition in gas turbine engines. In *Intl. Gas Turbine Aeroengine Congress & Exposition, Orlando, FL*. American Society of Mechanical Engineers, June 1991. doi: 10.1115/91-GT-261. Paper No. 91-GT-261.

[6.34] M. F. Blair. Influence of free-stream turbulence on boundary layer transition in favorable pressure gradients. *J. Engineering for Power*, **104**(4): 743–750, October 1982. doi: 10.1115/1.3227340.

[6.35] S. B. Pope. *Turbulent Flows.* Cambridge University Press, Cambridge, 2000.

[6.36] P. A. Libby. *Introduction to Turbulence.* Taylor & Francis, Washington, D.C., 1996.

[6.37] M. F. Blair and M. J. Werle. The influence of freestream turbulence on the zero pressure and gradient fully turbulent boundary layer. UTRC Report R80-915388-12, United Technologies Research Center, East Hartford, CT, September 1980. url: https://apps.dtic.mil/sti/pdfs/ADA101094.pdf.

7. Forced convection in a variety of configurations

The bed was soft enough to suit me...But I soon found that there came such a draught of cold air over me from the sill of the window that this plan would never do at all, especially as another current from the rickety door met the one from the window and both together formed a series of small whirlwinds in the immediate vicinity of the spot where I had thought to spend the night.　　**Moby Dick,** H. Melville, 1851

7.1　Introduction

Consider for a moment the fluid flow pattern within a shell-and-tube heat exchanger, such as shown in Fig. 3.5. The shell-pass flow moves up and down across the tube bundle from one baffle to the next. The flow around each pipe is determined by the complexities of the one before it, and the direction of the mean flow relative to each pipe can vary. Yet the problem of determining the heat transfer in this situation, however difficult it appears to be, is a task that must be undertaken.

The flow within the tubes of the exchanger is somewhat more tractable, but it, too, brings with it several problems that do not arise in the flow of fluids over a flat surface. Heat exchangers thus present a kind of microcosm of internal and external forced convection problems. Other such problems arise everywhere that energy is delivered, controlled, utilized, or produced. They arise in the complex flow of water through nuclear heating elements or in the liquid heating tubes of a solar collector—in the flow of a cryogenic liquid coolant in certain digital computers or in the circulation of refrigerant in the spacesuit of a lunar astronaut.

We dealt with the simple configuration of flow over a flat surface in Chapter 6. This situation has considerable importance in its own right, and it also reveals a number of analytical methods that apply to other configurations. Now we wish to undertake several of these more complex flow configurations.

Incompressible forced convection heat transfer problems normally admit an extremely important simplification: the fluid flow problem can be solved without reference to the temperature distribution in the fluid. Thus, we can find the velocity distribution first. Then, we can put the velocity into the energy equation as known information and solve for the temperature distribution. Two complications can impede this procedure, however:

- If the fluid properties (especially μ and ρ) vary significantly with temperature, we cannot predict the velocity without knowing the temperature, and vice versa. The problems of predicting velocity and temperature become intertwined and harder to solve. We encounter such a situation later in the study of natural convection, where the fluid is driven by thermally induced density changes.

- Either the fluid flow solution or the temperature solution itself can become prohibitively hard to find. When that happens, we resort to the correlation of experimental data with the help of dimensional analysis.

Our aim in this chapter is to present the analysis of a few simple problems and to show the progression toward increasingly empirical solutions as the problems become progressively more unwieldy. We begin this undertaking with one of the simplest problems: that of predicting laminar heat convection in a pipe.

7.2   Heat transfer to or from laminar flows in pipes

Not many industrial pipe flows are laminar, but laminar heating and cooling does occur in an increasing variety of modern instruments and equipment: micro-electro-mechanical systems (MEMS), laser coolant lines, and many compact heat exchangers, for example. As in any forced convection problem, we first describe the flow field. This description will include a number of ideas that apply to turbulent as well as laminar flow.
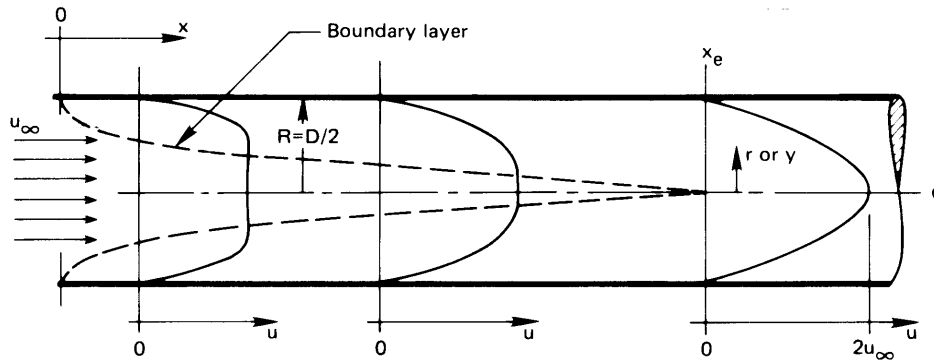
Figure 7.1 The development of a laminar velocity profile in a pipe.

Development of a laminar flow

Figure 7.1 shows the evolution of a steady laminar velocity profile begin-ning at the entrance to a pipe. Throughout the length of the pipe, the mass flow rate, $\dot{m}$ (kg/s), is constant, of course, and the *average* (or *bulk*) velocity u_{av} over the cross-sectional area A_c of the pipe is also constant:

$$\dot{m} = \int_{A_c} \rho u \, dA_c = \rho u_{av} A_c \tag{7.1}$$

The velocity profile, on the other hand, changes greatly near the inlet to the pipe. A b.l. builds up from the front, generally accelerating the otherwise undisturbed core. The b.l. eventually occupies the entire flow area and defines a velocity profile that changes very little thereafter. We call such a flow *fully developed*. A flow is fully developed from the hydrodynamic standpoint when

$$\frac{\partial u}{\partial x} = 0 \quad \text{or} \quad v = 0 \tag{7.2}$$

at each radial location in the cross section (see Problem 7.25). An attribute of a hydrodynamically fully developed flow is that the streamlines are all parallel to one another.

The concept of a fully developed flow, from the thermal standpoint, is a little more complicated. We must first understand the notion of the *mixing-cup*, or *bulk*, enthalpy and temperature, $\hat{h}_b$ and T_b. The enthalpy is of interest because we use it in writing the First Law of Thermodynamics. This requires specifying both the net flow of thermal energy, and of flow

work, into open control volumes. The bulk enthalpy is an average enthalpy for the fluid flowing through a cross section of the pipe:

$$\dot{m}\,\hat{h}_b \equiv \int_{A_c} \rho u \hat{h}\,dA_c \tag{7.3}$$

If we assume that fluid pressure variations in the pipe are too small to affect the thermodynamic state much (see Section 6.3). We can assume a constant value of c_p if the temperature variations are not too great. Then $\hat{h} = c_p(T - T_{\text{ref}})$, and

$$\dot{m}\,c_p(T_b - T_{\text{ref}}) = \int_{A_c} \rho c_p u (T - T_{\text{ref}})\,dA_c \tag{7.4}$$

from which we obtain the mixing-cup temperature

$$T_b = \frac{\int_{A_c} \rho c_p u T\,dA_c}{\dot{m}c_p} \tag{7.5}$$

In words, then,

$$T_b \equiv \frac{\text{rate of flow of enthalpy through a cross section}}{\text{rate of flow of heat capacity through a cross section}}$$

Thus, if the pipe were broken at any x-station and allowed to discharge into a cup, the enthalpy of the mixed fluid in the cup would equal the average enthalpy of the fluid flowing through the cross section, and the temperature of the fluid in the mixing cup would be T_b. This definition of T_b is perfectly general and applies to either laminar or turbulent flow. For a circular pipe, with $dA_c = 2\pi r\,dr$, eqn. (7.5) becomes

$$T_b = \frac{\int_0^R \rho c_p u T\,2\pi r\,dr}{\int_0^R \rho c_p u\,2\pi r\,dr} \tag{7.6}$$

A fully developed flow, from the thermal standpoint, is one for which the relative shape of the temperature profile does not change with x. We state this mathematically as

$$\frac{\partial}{\partial x}\left(\frac{T_w - T}{T_w - T_b}\right) = 0 \tag{7.7}$$

where T generally depends on x and r. This equation means that the profile is scaled up or down with the temperature difference $T_w - T_b$, which might vary. Of course, a flow must be hydrodynamically developed if it is to be thermally developed.
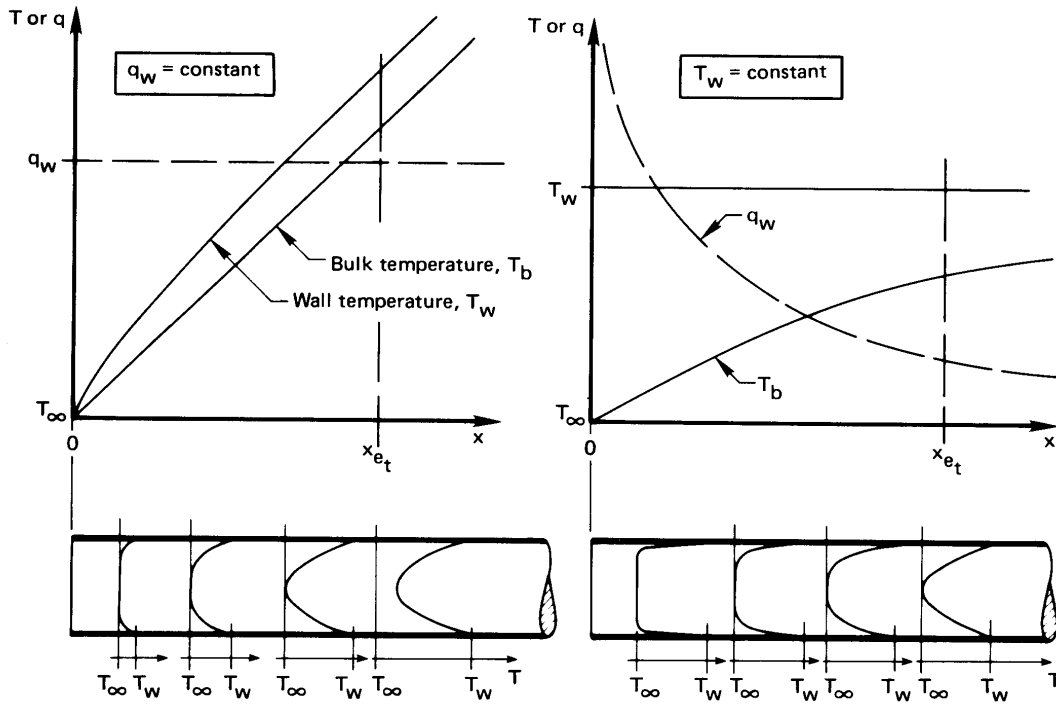
Figure 7.2 The thermal development of flows in tubes with a uniform wall heat flux and with a uniform wall temperature (the *entrance region*).

Figure 7.2 shows the response of a fully developed hydrodynamic profile to the imposition of a uniform heat flux or to an altered wall temperature. Figure 7.3 shows the same situations, but further downstream—after the entrance behavior has fully evolved. Figure 7.2 extends to the where the shape of the temperature profile remains the same except or being further displaced or stretched. Figure 7.3 shows the subsequent temperature profile being shifted but otherwise unchanged in the constant q_w case. In the constant T_w case, the temperature profile is stretched uniformly.

If we consider a small section of pipe, dx long with perimeter P, then its surface area is $P\,dx$ (e.g., $2\pi R\,dx$ for a circular pipe) and an energy balance on the section is[1]

$$dQ = q_w\,P dx = \dot{m}d\hat{h}_b \tag{7.8}$$

$$= \dot{m}c_p\,dT_b \tag{7.9}$$

---

[1]Here we make the same approximations as were made in deriving the energy equation in Section 6.3.
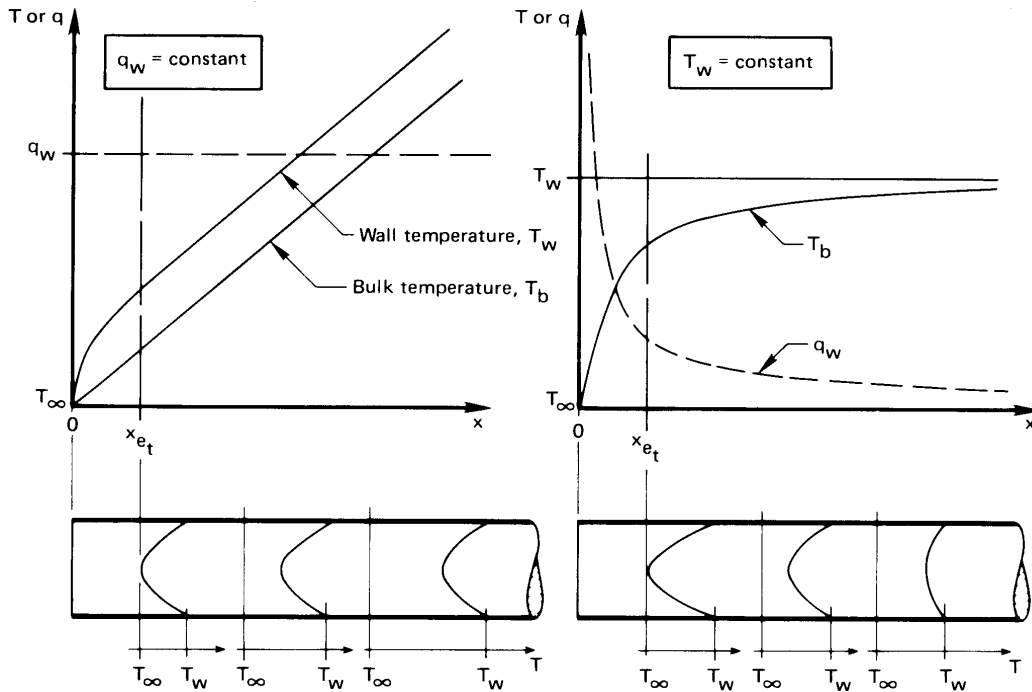
Figure 7.3 The thermal behavior of flows in tubes with a uniform wall heat flux and with a uniform temperature (the *thermally developed region*).

so that

$$\frac{dT_b}{dx} = \frac{q_w P}{\dot{m} c_p} \tag{7.10}$$

This result is valid whether or not q_w is constant, and it is also valid for the bulk temperature in a turbulent flow.

Once the flow is fully developed (Fig. 7.3), the boundary layers stop changing, so h becomes constant. When q_w is constant, $T_w - T_b$ will also be constant in fully developed flow, so that the temperature profile will retain the same shape while the temperature rises at a constant rate at all values of r. Thus, at any radial position,

$$\frac{\partial T}{\partial x} = \frac{dT_b}{dx} = \frac{q_w P}{\dot{m} c_p} = \text{constant} \tag{7.11}$$

In the uniform wall temperature case, the temperature profile keeps the same shape, but its amplitude decreases with x, as does q_w. The lower

right-hand corner of Fig. 7.3 is drawn to conform with this requirement, as expressed in eqn. (7.7).

The velocity profile in laminar tube flows

The *hydrodynamic entry length*, x_e, within which the velocity profile becomes fully developed, depends on u_{av}, μ, ρ, and D—five variables in the three dimensions kg, m and s. Thus, we can express their interdependency in two pi-groups:

$$\frac{x_e}{D} = \text{fn}\,(\text{Re}_D)$$

where $\text{Re}_D \equiv \rho u_{av} D / \mu$. The matter of entry length is discussed by White [7.1, Chap. 4], who quotes

$$\frac{x_e}{D} \simeq 0.03\,\text{Re}_D \tag{7.12}$$

The constant, 0.03, guarantees that the local shear stress (drag) on the pipe wall will be within 5% of the value for fully developed flow when $x > x_e$. The number 0.05 can be used, instead, if a deviation of just 1.4% is desired. The thermal entry length, x_{e_t}, turns out to be different from x_e. We deal with it shortly.

The hydrodynamic entry length for a pipe carrying fluid at speeds near the minimum transitional Reynolds number (2100) will extend beyond 100 diameters. Since heat transfer in pipes shorter than this is very often important, we will eventually have to address the hydrodynamic entry region, as well.

The velocity profile for a fully developed laminar incompressible pipe flow can be derived from the momentum equation for an axisymmetric flow. It turns out that the b.l. approximations all happen to be valid for a fully developed pipe flow:

- The pressure is constant across any section.

- $\partial^2 u / \partial x^2$ is exactly zero.

- The radial velocity v is not just small, it is zero.

- The term $\partial u / \partial x$ is not just small, it is zero.

The boundary layer equation for cylindrically symmetrical flows is quite similar to that for a flat surface, eqn. (6.13):

$$u\frac{\partial u}{\partial x} + v\frac{\partial u}{\partial r} = -\frac{1}{\rho}\frac{dp}{dx} + \frac{\nu}{r}\frac{\partial}{\partial r}\left(r\frac{\partial u}{\partial r}\right) \tag{7.13}$$

For fully developed flows, we may go beyond the b.l. assumptions and set v and $\partial u/\partial x$ equal to zero, so eqn. (7.13) becomes

$$\frac{1}{r}\frac{d}{dr}\left(r\frac{du}{dr}\right) = \frac{1}{\mu}\frac{dp}{dx}$$

We integrate this twice and get

$$u(r) = \left(\frac{1}{4\mu}\frac{dp}{dx}\right)r^2 + C_1 \ln r + C_2$$

The velocity should be finite as $r \to 0$ (where $\ln r \to -\infty$), so C_1 must be zero. The no-slip b.c. at the tube wall, $u(R) = 0$, gives $C_2 = (-dp/dx)R^2/4\mu$, so

$$u(r) = \frac{R^2}{4\mu}\left(-\frac{dp}{dx}\right)\left[1 - \left(\frac{r}{R}\right)^2\right] \tag{7.14}$$

Equation (7.14) is the famous Hagen-Poiseuille[2] parabolic velocity profile. We can identify the lead constant $(-dp/dx)R^2/4\mu$ as the maximum centerline velocity, $u_{\max}$, found at $r = 0$. In accordance with the conservation of mass (see Problem 7.1), $u_{\max} = 2u_{\mathrm{av}}$, so

$$\frac{u}{u_{\mathrm{av}}} = 2\left[1 - \left(\frac{r}{R}\right)^2\right] \tag{7.15}$$

Thermal behavior of a flow with a uniform heat flux at the wall

The b.l. energy equation for a fully developed laminar incompressible flow, eqn. (6.40), takes the following simple form in a pipe flow where the radial velocity is equal to zero:

$$u\frac{\partial T}{\partial x} = \alpha\frac{1}{r}\frac{\partial}{\partial r}\left(r\frac{\partial T}{\partial r}\right) \tag{7.16}$$

For a fully developed flow with $q_w = $ constant, T_w and T_b increase linearly with x. In particular, by integrating eqn. (7.10), we find

$$T_b(x) - T_{b_{\mathrm{in}}} = \int_0^x \frac{q_w P}{\dot{m}c_p}\,dx = \frac{q_w P x}{\dot{m}c_p} \tag{7.17}$$

---

[2]The German scientist G. Hagen showed experimentally how u varied with r, dp/dx, μ, and R, in 1839. J. Poiseuille (pronounced pwah-ZAY, or, somewhat more accurately, pwah-ZAY-uh) did the same thing, almost simultaneously (1840), in France. Poiseuille was a physician interested in blood flow, and we find, today, that any medical student is familiar with "Poiseuille's law."

Then, from eqns. (7.11) and (7.1), we get

$$\frac{\partial T}{\partial x} = \frac{dT_b}{dx} = \frac{q_w P}{\dot{m} c_p} = \frac{q_w (2\pi R)}{\rho c_p u_{av} (\pi R^2)} = \frac{2 q_w \alpha}{u_{av} R k}$$

Using this result and eqn. (7.15) in eqn. (7.16), we obtain

$$4\left[1 - \left(\frac{r}{R}\right)^2\right]\frac{q_w}{Rk} = \frac{1}{r}\frac{d}{dr}\left(r\frac{dT}{dr}\right) \tag{7.18}$$

This ordinary d.e. in r can be integrated twice to obtain

$$T = \frac{4 q_w}{Rk}\left(\frac{r^2}{4} - \frac{r^4}{16R^2}\right) + C_1 \ln r + C_2 \tag{7.19}$$

The temperature must be finite[3] as $r \rightarrow 0$, so $C_1 = 0$. The second constraint on the temperature profile is that it should yield the local value of the bulk temperature, eqn. (7.6). Substituting eqn. (7.19) with $C_1 = 0$ into eqn. (7.6) and carrying out the indicated integrations, we get

$$C_2 = T_b - \frac{7}{24}\frac{q_w R}{k}$$

so

$$T - T_b = \frac{q_w R}{k}\left[\left(\frac{r}{R}\right)^2 - \frac{1}{4}\left(\frac{r}{R}\right)^4 - \frac{7}{24}\right] \tag{7.20}$$

and at $r = R$, eqn. (7.20) gives

$$T_w - T_b = \frac{11}{24}\frac{q_w R}{k} = \frac{11}{48}\frac{q_w D}{k} \tag{7.21}$$

so the local Nu_D for fully developed flow, based on $h(x) = q_w/[T_w(x) - T_b(x)]$, is

$$Nu_D \equiv \frac{q_w D}{(T_w - T_b)k} = \frac{48}{11} = 4.364 \quad (q_w = \text{constant}) \tag{7.22}$$

Equation (7.22) is surprisingly simple. Indeed, the fact that there is only one dimensionless group is predictable by dimensional analysis. In this case, the dimensional functional equation is merely

$$h = \text{fn}(D, k)$$

---

[3]With $C_1 = 0$ in our equations for the velocity or temperature profiles, $\partial u/\partial r = 0$ or $\partial T/\partial r = 0$ at $r = 0$. That is consistent with zero shear stress or zero heat flux across the centerline—the result of having a symmetrical velocity or temperature profile.

We exclude ΔT, because h should be independent of ΔT in forced convection; μ, because the flow is parallel regardless of the viscosity; and ρu_{av}^2, because there is no influence of momentum in a fully developed, laminar incompressible flow that never changes direction. The three remaining variables effectively have only two dimensions, W/K and m, resulting in just one dimensionless group, Nu_D, which must therefore be a constant.

Example 7.1

Water at 20°C flows through a small-bore tube 1 mm in diameter at a uniform speed of 0.2 m/s. The flow is fully developed at a point beyond which a constant heat flux of 6000 W/m² is imposed. How much farther down the tube will the water reach 74°C at its hottest point?

SOLUTION. We shall evaluate properties at $(74 + 20)/2 = 47$°C: $k = 0.6396$ W/m·K, $\alpha = 1.546 \times 10^{-7}$, and $\nu = 5.832 \times 10^{-7}$ m²/s. Therefore, $Re_D = (0.001 \text{ m})(0.2 \text{ m/s})/5.832 \times 10^{-7}$ m²/s $= 343$, and the flow is laminar. We note that T is greatest at the wall and we call $x = L$ the point where $T_{wall} = 74$°C. Then eqn. (7.17) gives:

$$T_b(x = L) = 20 + \frac{q_w P}{\dot{m} c_p} L = 20 + \frac{4 q_w \alpha}{u_{av} D k} L$$

And eqn. (7.21) gives

$$74 = T_b(x = L) + \frac{11}{48} \frac{q_w D}{k} = 20 + \frac{4 q_w \alpha}{u_{av} D k} L + \frac{11}{48} \frac{q_w D}{k}$$

so

$$\frac{L}{D} = \left(54 - \frac{11}{48} \frac{q_w D}{k}\right) \frac{u_{av} k}{4 q_w \alpha}$$

or

$$\frac{L}{D} = \left[54 - \frac{11}{48} \frac{6000(0.001)}{0.6396}\right] \frac{0.2(0.6396)}{4(6000)1.546(10)^{-7}} = 1788$$

so the wall temperature reaches the limiting temperature of 74°C at

$$L = 1788(0.001 \text{ m}) = 1.788 \text{ m}$$

While we did not evaluate the thermal entry length, it may be shown to be much, much less than 1788 diameters. ∎

We can calculate the heat transfer coefficient in the preceding example with the help of eqn. (7.22). The result turns out to be rather large:

$$h = \text{Nu}_D \, \frac{k}{D} = 4.364 \, \frac{0.6396}{0.001} = 2,791 \text{ W/m}^2\text{K}$$

The high h is a direct result of the small tube diameter, which keeps the thermal boundary layer thin and the thermal resistance low. The effect of small size leads directly to the notion of a *microchannel heat exchanger*. Small scale fabrication technologies, such as have been developed in the semiconductor industry, allow us to create channels whose characteristic diameter is in the range of 100 μm. These tiny channels yield heat transfer coefficients in the range of 10^4 W/m^{2}K for water [7.2]. If, instead, we could use liquid sodium ($k \approx 80$ W/m·K) as the working fluid, the laminar flow heat transfer coefficient would be on the order of 10^6 W/m^{2}K—a range usually associated with boiling processes!

Thermal behavior of the flow in an isothermal pipe

The dimensional analysis that showed Nu_D = constant for flow with a uniform heat flux at the wall is unchanged when the pipe wall is isothermal. Thus, Nu_D should still be constant. But for this b.c. (see, e.g., [7.3, Chap. 8]) the constant changes to

$$\text{Nu}_D = 3.657 \quad \text{for} \quad T_w = \text{constant} \tag{7.23}$$

for fully developed flow. We show how the bulk temperature, T_b, varies in Section 7.4.

The thermal entrance region

The thermal entrance region is of great importance in laminar flow because the thermally undeveloped region becomes extremely long for higher-Pr fluids. The entry-length equation, (7.12), takes the following form for the thermal entry region, where the velocity profile is assumed to be fully developed before heat transfer starts at $x = 0$ [7.4, 7.5][4]:

$$\frac{x_{e_t}}{D} \simeq \begin{cases} 0.034 \, \text{Re}_D\text{Pr} & \text{for } T_w = \text{constant} \\ 0.043 \, \text{Re}_D\text{Pr} & \text{for } q_w = \text{constant} \end{cases} \tag{7.24}$$

---

[4]The Nusselt number will be within 5% of the fully developed value beyond x_{e_t}. When the velocity and temperature profiles develop simultaneously, the coefficient next to Re_DPr ranges between about 0.028 and 0.053 depending upon the Prandtl number and the wall boundary condition.

Entry lengths can become very long in certain cases. For the flow of cold water ($\text{Pr} \simeq 10$), the entry length can reach more than 600 diameters as we approach the transition Reynolds number. For Pr on the order of 10^4 (oil flows, for example), a fully developed profile is virtually unobtainable.

A complete analysis of the heat transfer rate in the thermal entry region becomes quite complicated. The reader interested in details should look at [7.3, Chap. 8]. Dimensional analysis of the entry problem shows that the local value of h depends on u_{av}, μ, ρ, D, c_p, k, and x—eight variables in m, s, kg, and J/K. This means that we should anticipate four pi-groups:

$$\text{Nu}_D = \text{fn}\,(\text{Re}_D, \text{Pr}, x/D) \tag{7.25}$$

In other words, we add to the already familiar Nu_D, Re_D, and Pr a new length parameter, x/D. The solution of the constant wall temperature problem, originally formulated by Graetz in 1885 [7.6] and solved in a convenient form by Sellars, Tribus, and Klein in 1956 [7.7], includes an arrangement of the dimensionless groups Re_D, Pr, and x/D. Their analysis showed that, in this instance, these groups combine into a simple product, which we call the *Graetz number*:

$$\text{Graetz number, } \text{Gz} \equiv \frac{\text{Re}_D \text{Pr}\, D}{x} \tag{7.26}$$

Figure 7.4 shows values of $\text{Nu}_D \equiv hD/k$ for both the uniform wall temperature and uniform wall heat flux cases. The independent variable in the figure is a dimensionless length equal to $2/\text{Gz} = x/(R\,\text{Re}_D\text{Pr})$. The figure also presents an average Nusselt number, $\overline{\text{Nu}}_D$, for the isothermal wall case:

$$\overline{\text{Nu}}_D \equiv \frac{\overline{h}D}{k} = \frac{D}{k}\left(\frac{1}{L}\int_0^L h\,dx\right) = \frac{1}{L}\int_0^L \text{Nu}_D\,dx \tag{7.27}$$

Here, since $h = q(x)/[T_w - T_b(x)]$, we cannot simply average only q or ΔT. We show how to find the change in T_b using $\overline{h}$ for an isothermal wall in Section 7.4. For a fixed heat flux, the change in T_b is given by eqn. (7.17), and a value of $\overline{h}$ is not needed.

For an isothermal wall, the exact solutions for the Nusselt number in thermally developing flow have been curve-fitted to the following expressions [7.4, 7.8][5] with errors of less than 1%:

$$\text{Nu}_D = \begin{cases} 3.657 + 0.2362\,\text{Gz}^{0.488}\,e^{-57.2/\text{Gz}} & \text{for Gz} \leqslant 1000 \\ 1.077\,\text{Gz}^{1/3} - 0.7 & \text{for Gz} > 1000 \end{cases} \tag{7.28}$$

$$\overline{\text{Nu}}_D = \frac{3.657}{\tanh(2.264\text{Gz}^{-1/3} + 1.7\text{Gz}^{-2/3})} + 0.0499\,\text{Gz}\tanh(\text{Gz}^{-1}) \tag{7.29}$$

---

[5]The value 1000 after eqn. (7.28) corrects an apparent misprint in [7.4] and [7.5].
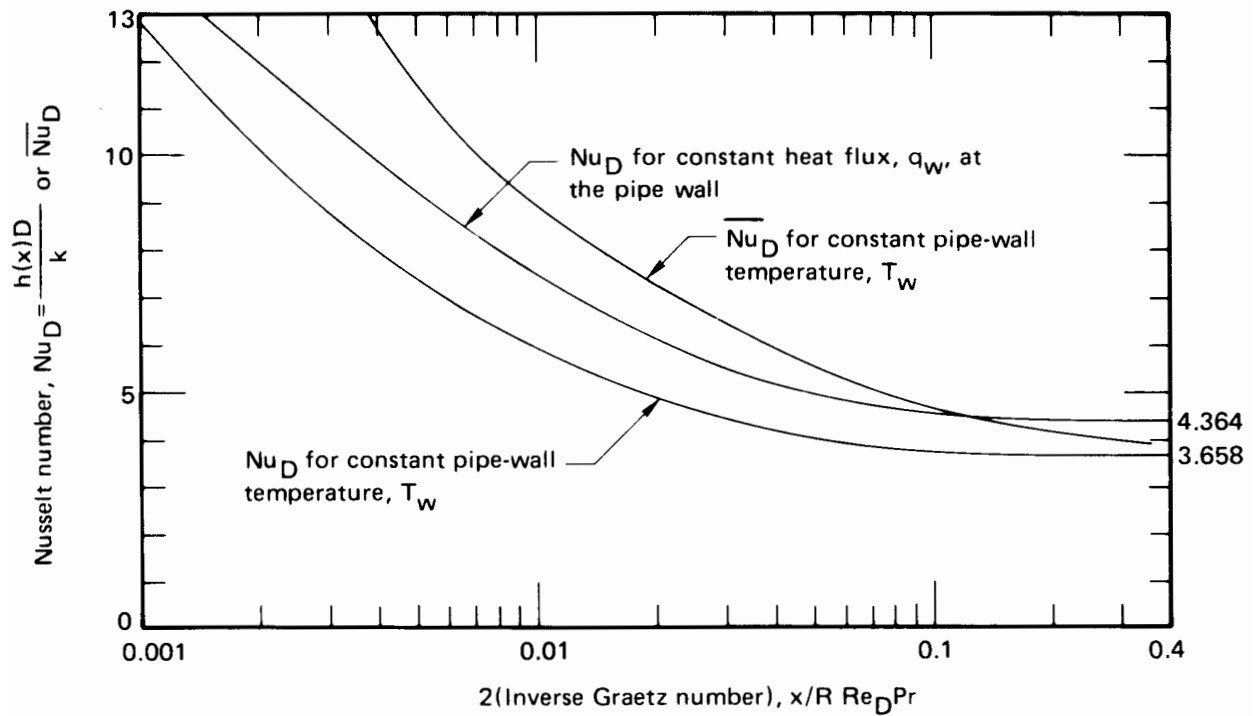
Figure 7.4 Local and average Nusselt numbers for the thermal entry region in a hydrodynamically developed laminar pipe flow.

For fixed q_w, a slightly more complicated formula reproduces the exact result for the local Nusselt number to within 1%:

$$\text{Nu}_D = \begin{cases} 4.364 + 0.263 \, \text{Gz}^{0.506} \, e^{-41/\text{Gz}} & \text{for Gz} \leqslant 667 \\ 1.302 \, \text{Gz}^{1/3} - 0.5 & \text{for } 667 \leqslant \text{Gz} \leqslant 2 \times 10^4 \quad (7.30) \\ 1.302 \, \text{Gz}^{1/3} - 1 & \text{for } 2 \times 10^4 \leqslant \text{Gz} \end{cases}$$

Example 7.2

A fully developed flow of air at 27°C moves at 2 m/s in a 1 cm I.D. pipe. An electric resistance heater surrounds the last 20 cm of the pipe and supplies a constant heat flux to bring the air out at $T_b = 40$°C. What power input is needed to do this? What will be the wall temperature at the exit?

SOLUTION. This is a case in which the wall heat flux is uniform along the pipe. We first must compute $\text{Gz}_{20 \text{ cm}}$, evaluating properties at

$(27 + 40)/2 \simeq 34°C$:

$$\text{Gz}_{20 \text{ cm}} = \frac{\text{Re}_D \text{Pr}\, D}{x}$$

$$= \frac{\dfrac{(2 \text{ m/s})(0.01 \text{ m})}{(1.63 \times 10^{-5} \text{ m}^2/\text{s})}(0.710)(0.01 \text{ m})}{0.2 \text{ m}} = 43.56$$

From eqn. (7.30), we compute $\text{Nu}_D = 5.06$, so

$$T_{w_\text{exit}} - T_b = \frac{q_w D}{5.06\, k}$$

Notice that we still have two unknowns, q_w and T_w. The bulk temperature is specified as 40°C, and q_w is obtained from this number by a simple energy balance:

$$q_w (2\pi R x) = \rho c_p u_\text{av} (T_b - T_\text{entry}) \pi R^2$$

so

$$q_w = 1.150 \frac{\text{kg}}{\text{m}^3} \cdot 1007 \frac{\text{J}}{\text{kg·K}} \cdot 2 \frac{\text{m}}{\text{s}} \cdot (40 - 27)°\text{C} \cdot \underbrace{\frac{R}{2x}}_{1/80} = 376 \text{ W/m}^2$$

Then

$$T_{w_\text{exit}} = 40°\text{C} + \frac{(376 \text{ W/m}^2)(0.01 \text{ m})}{5.06(0.0267 \text{ W/m·K})} = 67.9°\text{C} \qquad \blacksquare$$

7.3 Turbulent pipe flow

Turbulent entry length

The entry lengths x_e and x_{e_t} are generally shorter in turbulent flow than in laminar flow. Table 7.1 gives the thermal entry length for various values of Pr and Re_D. Positions farther down the pipe than these will have Nu_D within 5% of the fully developed values. These results are for a uniform wall heat flux imposed on a hydrodynamically fully developed flow. Very similar results are obtained for a uniform wall temperature.

For Prandtl numbers typical of gases and nonmetallic liquids, the entry length is not strongly sensitive to the Reynolds number. For $\text{Pr} > 1$ in particular, the entry length is just a few diameters. This rapid response is

Table 7.1 Thermal entry lengths, x_{et}/D, for turbulent pipe flow, beyond which Nu_D will be no more than 5% above its fully developed value [7.9]

Pr	Re_D		
	20,000	100,000	500,000
0.01	7	22	32
0.7	10	12	14
3.0	4	3	3

because the heat transfer rate is controlled by the thin thermal sublayer on the wall, and it develops very quickly.

Only liquid metals give fairly long thermal entrance lengths, and, for these fluids, x_{e_t} depends on both Re and Pr in a complicated way. Since liquid metals have very high thermal conductivities, the heat transfer rate is also more strongly affected by the temperature distribution away from the wall, toward the center of the pipe. We discuss liquid metals in more detail at the end of this section.

When heat transfer begins at the pipe inlet, the velocity and temperature profiles develop simultaneously. The entry length is then very strongly affected by the shape of the inlet. For example, an inlet that induces vortices in the pipe—a sharp bend or contraction—can create a much longer entry length than occurs for a thermally developing flow. These vortices may require 20 to 40 diameters to die out. For various types of inlets, Bhatti and Shah [7.9] provide the following correlation for $\overline{\mathrm{Nu}}_D$ with $L/D > 3$ for air (or other fluids with Pr ≈ 0.7)

$$\frac{\overline{\mathrm{Nu}}_D}{\mathrm{Nu}_\infty} = 1 + \frac{C}{(L/D)^n} \qquad \text{for Pr} = 0.7 \qquad (7.31)$$

where Nu_∞ is the fully developed value of the Nusselt number, and C and n depend on the inlet configuration as shown in Table 7.2.

Whereas the entry effect on the local Nusselt number is confined to a few ten's of diameters, the effect on the average Nusselt number may persist for a hundred diameters. This is because much additional length is needed to average out the higher heat transfer rates near the entry.

Table 7.2 Constants for the gas-flow simultaneous entry length correlation, eqn. (7.31), for various inlet configurations

Inlet configuration	C	n
Long, straight pipe	0.9756	0.760
Square-edged inlet	2.4254	0.676
180° circular bend	0.9759	0.700
90° circular bend	1.0517	0.629
90° sharp elbow	2.0152	0.614

Illustrative experiment

Figure 7.5 shows average heat transfer data given by Kreith [7.10, Chap. 8] for air flowing in a 1 in. I.D. isothermal pipe 60 in. in length (2.54 cm I.D., 152 cm long). Let us see how these data compare with what we know about pipe flows thus far.

The data are plotted for a single Prandtl number on $\overline{\mathrm{Nu}}_D$ vs. Re_D coordinates. This format is consistent with eqn. (7.25) in the fully developed range, but the actual pipe includes a significant entry region. Therefore, the data in the lower left portion of the graph reflect entry behavior.

For laminar flow at $\mathrm{Re}_D = 750$, the data show $\overline{\mathrm{Nu}}_D \simeq 3.66$. This value is as expected for fully developed flow in an isothermal pipe. However, the pipe is too short for the flow to be fully developed over much, if any, of its length. As a result, $\overline{\mathrm{Nu}}_D$ is not constant for the data in the laminar range. The rate of rise of $\overline{\mathrm{Nu}}_D$ with Re_D becomes very great in the transitional range, which lies between $\mathrm{Re}_D = 2100$ and about 5000 in this case. Above $\mathrm{Re}_D \simeq 5000$, the flow is turbulent and it turns out that $\overline{\mathrm{Nu}}_D \simeq \mathrm{Re}_D^{0.8}$.

The Reynolds-Colburn analogy and heat transfer

As we saw in Section 6.8, heat transfer in a turbulent b.l. is closely related to shear stress on the wall through the Reynolds-Colburn analogy eqn. (6.111):

$$\mathrm{St}_x = \frac{h}{\rho c_p u_\infty} = \frac{C_f(x)/2}{1 + 12.7\left(\mathrm{Pr}^{2/3} - 1\right)\sqrt{C_f(x)/2}} \qquad (6.111)$$

For a pipe flow, h is defined as $q_w/(T_w - T_b)$, and we can merely replace u_∞ with u_{av} and $C_f(x)$ with the friction coefficient for fully developed
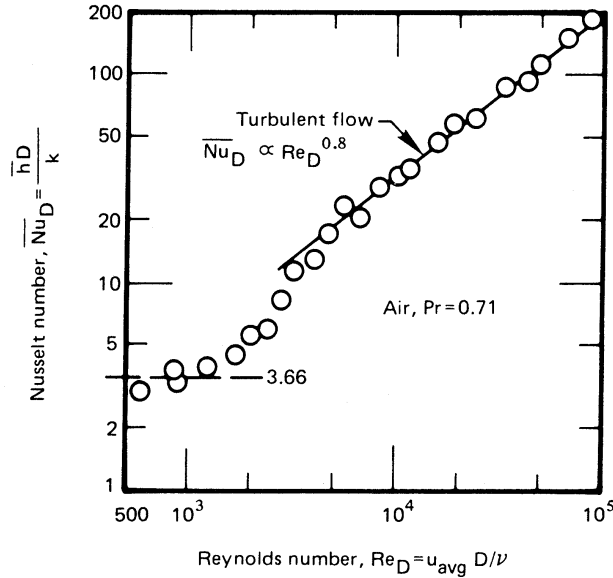
Figure 7.5 Heat transfer to air flowing in a 1 in. I.D., 60 in. long pipe, after Kreith [7.10].

pipe flow, C_f (which is constant) to get

$$\text{St} = \frac{h}{\rho c_p u_{\text{av}}} = \frac{C_f/2}{1 + 12.7\left(\text{Pr}^{2/3} - 1\right)\sqrt{C_f/2}} \tag{7.32}$$

This equation applies for $\text{Pr} \gtrsim 0.7$ and for either uniform q_w or uniform T_w situations. This form, however, is limited to smooth walls.

The frictional resistance to flow in a pipe is normally expressed in terms of the Darcy-Weisbach friction factor, f:

$$f \equiv \frac{\text{head loss}}{\left(\dfrac{\text{pipe length}}{D} \dfrac{u_{\text{av}}^2}{2}\right)} = \frac{\Delta p}{\left(\dfrac{L}{D} \dfrac{\rho u_{\text{av}}^2}{2}\right)} \tag{7.33}$$

where Δp is the pressure drop in a pipe of length L. However, the pressure drop is determined by the wall shear stress

$$\tau_w = \frac{\text{frictional force on liquid}}{\text{surface area of pipe}} = \frac{\Delta p\left[(\pi/4)D^2\right]}{\pi D L} = \frac{\Delta p D}{4L}$$

which leads to the relationship between τ_w and C_f:

$$f = \frac{\tau_w}{\rho u_{\text{av}}^2/8} = 4C_f \tag{7.34}$$

Substituting eqn. (7.34) in eqn. (7.32) and rearranging the result, we obtain, for fully developed flow in a smooth pipe,

$$\text{Nu}_D = \frac{(f/8)\text{Re}_D \, \text{Pr}}{1 + 12.7\left(\text{Pr}^{2/3} - 1\right)\sqrt{f/8}} \tag{7.35}$$

The friction factor is given graphically in Fig. 7.6 on pg. 370 as a function of Re_D and the relative roughness, ε/D, where ε is the surface roughness of the pipe wall. Equation (7.35) can be used directly along with Fig. 7.6 to calculate the Nusselt number for smooth-walled pipes ($\varepsilon/D = 0$).

Historical formulations based on power laws. A number of the earliest correlations for the Nusselt number in turbulent pipe flow, although still widely quoted, have been largely superseded. These power-law correlations were based on other forms of Reynolds-Colburn analogy. In particular, in 1933 Colburn himself suggested [7.11]

$$\mathrm{St} = \frac{C_f}{2}\,\mathrm{Pr}^{-2/3} = \frac{f}{8}\,\mathrm{Pr}^{-2/3} \tag{7.36}$$

or

$$\mathrm{Nu}_D = \mathrm{Re}_D\,\mathrm{Pr}^{1/3}(f/8) \tag{7.37}$$

For smooth pipes, the curve $\varepsilon/D = 0$ in Fig. 7.6 is approximately given by

$$\frac{f}{4} = C_f = \frac{0.046}{\mathrm{Re}_D^{0.2}} \tag{7.38}$$

for $\mathrm{Re}_D \geqslant 10,000$ [7.12], so eqn. (7.37) becomes

$$\mathrm{Nu}_D = 0.023\,\mathrm{Re}_D^{0.8}\,\mathrm{Pr}^{1/3} \tag{7.39a}$$

This equation is called the *Colburn equation*. Actually, Colburn's equation is quite similar to an earlier result developed by Dittus and Boelter in 1930 for heating pipes (see [7.13, pg. 552]):

$$\mathrm{Nu}_D = 0.0243\,\mathrm{Re}_D^{0.8}\,\mathrm{Pr}^{0.4} \tag{7.39b}$$

And, Colburn noted that his result was similar to a contemporaneous correlation from McAdams [7.14]:

$$\mathrm{Nu}_D = 0.0225\,\mathrm{Re}_D^{0.8}\,\mathrm{Pr}^{0.4} \tag{7.39c}$$

These equations are intended for smooth pipes at reasonably low temperature differences for which properties do not vary much over the cross-section of the pipe.

In 1936, a study by Sieder and Tate [7.15] showed that when $|T_w - T_b|$ is large enough to cause significant changes of μ, the Colburn equation can be modified in the following way for liquids:

$$\mathrm{Nu}_D = 0.023\,\mathrm{Re}_D^{0.8}\,\mathrm{Pr}^{1/3}\left(\frac{\mu_b}{\mu_w}\right)^{0.14} \tag{7.40}$$

where all properties are evaluated at the local bulk temperature except μ_w, which is the viscosity evaluated at the wall temperature.

These early relations proved to be fair approximations. They gave maximum errors of $+25\%$ and -40% in the range $0.67 \leqslant \text{Pr} \leqslant 100$ and usually were considerably more accurate than this.

The Colburn, Dittus-Boelter, and McAdams equations together had a profound impact on 20th century work in heat transfer. However, subsequent research provided far more data and a much improved theoretical understanding of how to represent the data accurately. A key problem with power law correlations is that the exponents on Re_D and Pr are not truly independent of the value of Pr [7.16].

Modern formulations.   Research on turbulent pipe flow was continued for many decades after the studies of the 1930's, notably by B. S. Petukhov and his co-workers at the Moscow Institute for High Temperature during the 1950's and 1960's. This later work combined experimental data with the theoretical description of boundary layer structure summarized in Section 6.7. Much of this research is described in a 1970 survey article by Petukhov [7.17].

Petukhov recommended several variations on eqn. (7.35), and the most precise of these could represent the data of several careful studies of fully turbulent flow to an accuracy of $\pm 6\%$ to $\pm 10\%$. Gnielinski [7.16] extended Petukhov's approach to a far larger set of experimental data and to a wider range of Prandtl and Reynolds number, right down to turbulent transition. Gnielinski proposed the following modification of eqn. (7.35)

$$\text{Nu}_D = \frac{(f/8)\,(\text{Re}_D - 1000)\,\text{Pr}}{1 + 12.7\sqrt{f/8}\left(\text{Pr}^{2/3} - 1\right)} \tag{7.41}$$

for $2300 \leqslant \text{Re}_D \leqslant 5 \times 10^6$ and for $0.6 \leqslant \text{Pr} \leqslant 10^5$. In using this equation, the friction factor for smooth pipes may be computed from Filonenko's equation [7.18]:

$$f = \frac{1}{\left(1.82\log_{10}\text{Re}_D - 1.64\right)^2} \tag{7.42}$$

Gnielinski's result reproduces more than 90% of the liquid data examined to within $\pm 20\%$ and is even more accurate for gases. The equation may be used for either uniform wall temperature or uniform heat flux.
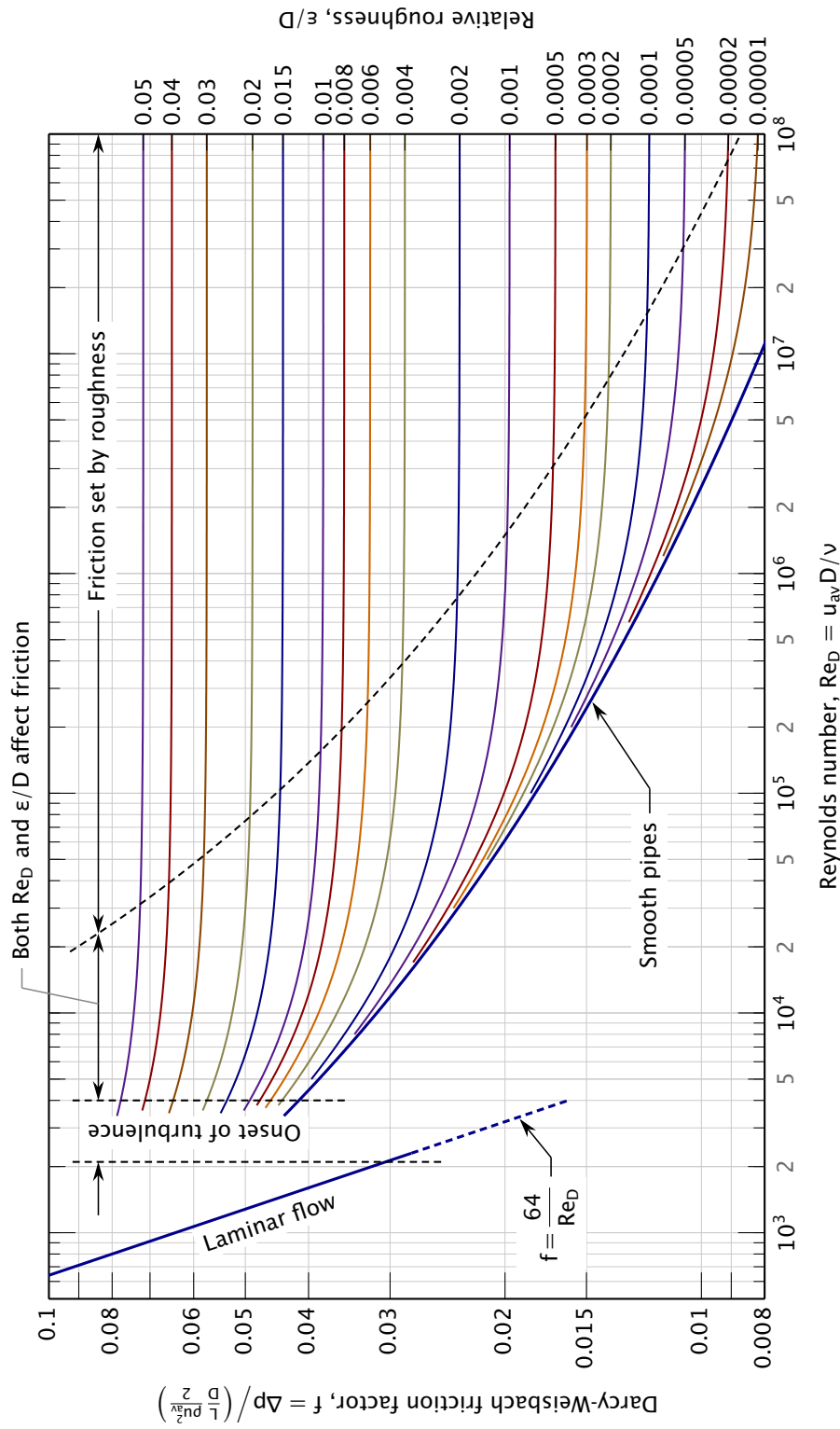
Figure 7.6: Pipe friction factors. Rough wall curves follow eqn. (7.50), and the smooth pipe curve follows eqn. (7.42). The dashed curve through the rough walled regime marks friction factors within 1% of the limiting value [7.19]. For higher Re_D, the friction factor depends only on ε/D. This graph is called a *Moody diagram*, after L. F. Moody's original version from 1944 [7.20].

In the spirit earlier researchers, Gnielinski also proposed two power-law approximations for smooth pipes each valid within only a limited range of Pr:

$$\text{Nu}_D = 0.0214(\text{Re}_d^{0.8} - 100)\text{Pr}^{0.4} \qquad 0.6 \leqslant \text{Pr} \leqslant 1.5 \qquad (7.43a)$$

$$\text{Nu}_D = 0.012(\text{Re}_d^{0.87} - 280)\text{Pr}^{0.4} \qquad 1.5 \leqslant \text{Pr} \leqslant 500 \qquad (7.43b)$$

Both fits are in good agreement with eqn. (7.41) for $2300 \leqslant \text{Re}_D \leqslant 5 \times 10^6$.

Variations in physical properties.   Sieder and Tate's work on property variations was also refined in later years [7.17]. The effect of variable physical properties is dealt with differently for liquids and gases. In both cases, the Nusselt number is first calculated with all properties evaluated at T_b using eqn. (7.41). For liquids, one then corrects by multiplying with a viscosity ratio. Over the interval $0.025 \leqslant (\mu_b/\mu_w) \leqslant 12.5$,

$$\text{Nu}_D = \text{Nu}_D\Big|_{T_b}\left(\frac{\mu_b}{\mu_w}\right)^n \qquad \text{where } n = \begin{cases} 0.11 & \text{for } T_w > T_b \\ 0.25 & \text{for } T_w < T_b \end{cases} \qquad (7.44)$$

For gases and a temperatures ratio *in kelvin* within $0.27 \leqslant (T_b/T_w) \leqslant 2.7$,

$$\text{Nu}_D = \text{Nu}_D\Big|_{T_b}\left(\frac{T_b}{T_w}\right)^n \qquad \text{where } n = \begin{cases} 0.47 & \text{for } T_w > T_b \\ 0 & \text{for } T_w < T_b \end{cases} \qquad (7.45)$$

After eqn. (7.42) is used in calculating Nu_D, f should also be corrected for the effect of variable properties. For liquids, with $0.5 \leqslant (\mu_b/\mu_w) \leqslant 3$

$$f = f\Big|_{T_b} \times K \qquad \text{where } K = \begin{cases} (7 - \mu_b/\mu_w)/6 & \text{for } T_w > T_b \\ (\mu_b/\mu_w)^{-0.24} & \text{for } T_w < T_b \end{cases} \qquad (7.46)$$

For gases, the data are much weaker [7.21, 7.22]. For $0.14 \leqslant (T_b/T_w) \leqslant 3.3$ the exponents are about the same for both heating and cooling

$$f = f\Big|_{T_b}\left(\frac{T_b}{T_w}\right)^m \qquad \text{where } m \approx \begin{cases} 0.23 & \text{for } T_w > T_b \\ 0.23 & \text{for } T_w < T_b \end{cases} \qquad (7.47)$$

Example 7.3

A 21.5 kg/s flow of water is dynamically and thermally developed in a 12 cm I.D. pipe. The pipe is held at 90°C and $\varepsilon/D = 0$. Find h and f where the bulk temperature of the fluid has reached 50°C.

SOLUTION. We evaluate the bulk properties at 50°C

$$u_{av} = \frac{\dot{m}}{\rho A_c} = \frac{21.5}{988\pi(0.06)^2} = 1.924 \text{ m/s}$$

so

$$Re_D = \frac{u_{av}D}{\nu} = \frac{1.924(0.12)}{5.60 \times 10^{-7}} = 412,300$$

and

$$Pr = 3.61, \qquad \frac{\mu_b}{\mu_w} = \frac{5.54 \times 10^{-4}}{3.16 \times 10^{-4}} = 1.75$$

From eqn. (7.42), $f = 0.0136$ at T_b, and since $T_w > T_b$, $n = 0.11$ in eqn. (7.44). Thus, with eqn. (7.41) we have

$$Nu_D = \frac{(0.0136/8)(4.12 \times 10^5 - 1000)(3.61)}{1 + 12.7\sqrt{0.0136/8}\,(3.61^{2/3} - 1)}(1.75)^{0.11} = 1,570$$

or

$$h = Nu_D \frac{k}{D} = 1570\frac{0.642}{0.12} = 8,400 \text{ W/m}^2\text{K}$$

This result is based upon correcting a correlation for the Nusselt number that uses the friction factor at the bulk temperature. To calculate the pressure drop, one must use f corrected according to eqn. (7.46):

$$f = (0.0136)(7 - 1.74)/6 = 0.0119 \qquad\blacksquare$$

Rough-walled pipes

Sufficiently large roughness on a pipe wall will disrupt the viscous and thermal sublayers at the base of the boundary layer (see Section 6.7). Figure 7.6 shows the effect of roughness height ε on the friction factor, f. As the Reynolds number increases, the viscous sublayer becomes thinner and smaller levels of roughness influence f. Once the Reynolds number is high enough, roughness completely overwhelms the viscous sublayer, and ε/D alone determines the friction factor. Some typical pipe roughnesses are given in Table 7.3.

We can determine whether roughness will affect friction and heat transfer by comparing ε to the viscous sublayer thickness. We saw in Section 6.7 that the thickness of the sublayer is around 30 times ν/u^*,

Table 7.3 Representative wall roughness of commercially available pipes when new.

Pipe	ε (μm)	Pipe	ε (μm)
Glass	0.31	Asphalted cast iron	120.
Drawn tubing	1.5	Galvanized iron	150.
Steel or wrought iron	46.	Cast iron	260.

where $u^* = \sqrt{\tau_w/\rho}$ is the friction velocity. We define the ratio of ε and ν/u^* as the *roughness Reynolds number*, Re_ε

$$\text{Re}_\varepsilon \equiv \frac{u^*\varepsilon}{\nu} = \text{Re}_D \frac{\varepsilon}{D}\sqrt{\frac{f}{8}} \qquad (7.48\text{a})$$

where the second equality follows from the definitions of u^* and f (and a little algebra). Experimental data show that the smooth and rough regions of friction factor seen in Fig. 7.6 correspond approximately to the following ranges of Re_ε:

$$\text{Re}_\varepsilon < 5 \qquad \text{hydraulically smooth} \qquad (7.48\text{b})$$
$$5 \leqslant \text{Re}_\varepsilon \leqslant 70 \qquad \text{transitionally rough} \qquad (7.48\text{c})$$
$$70 < \text{Re}_\varepsilon \qquad \text{fully rough} \qquad (7.48\text{d})$$

(We note that the dashed curve through the rough walled regime in Fig. 7.6 marks friction factors within 1% of the limiting value [7.19] and lies a bit farther right than eqn. (7.48d) would, had it been plotted.)

In the fully rough regime, Bhatti and Shah [7.9] provide the following correlation for the local Nusselt number

$$\text{Nu}_D = \frac{(f/8)\,\text{Re}_D\,\text{Pr}}{1 + \sqrt{f/8}\left(4.5\,\text{Re}_\varepsilon^{0.2}\text{Pr}^{0.5} - 8.48\right)} \qquad (7.49)$$

which applies for the ranges

$$10^4 \leqslant \text{Re}_D, \quad 0.5 \leqslant \text{Pr} \leqslant 10, \quad \text{and } 0.002 \leqslant \frac{\varepsilon}{D} \leqslant 0.05$$

The friction factor may be read from Fig. 7.6 or computed from Haaland's equation [7.23], valid for $0 \leqslant \varepsilon/D \leqslant 0.05$ and $4000 \leqslant \text{Re}_D \leqslant 10^8$:

$$f = \frac{1}{\left\{1.8\,\log_{10}\left[\dfrac{6.9}{\text{Re}_D} + \left(\dfrac{\varepsilon/D}{3.7}\right)^{1.11}\right]\right\}^2} \qquad (7.50)$$

The heat transfer coefficient on a rough wall can be several times that for a smooth wall at the same Reynolds number. The friction factor, and thus the pressure drop and pumping power, will also be higher. Nevertheless, designers sometimes deliberately roughen tube walls so as to raise h and reduce the surface area needed for heat transfer. Several manufacturers offer tubing that has had some pattern of roughness impressed upon its interior surface. Periodic ribs are one common configuration. Specialized correlations have been developed for a number these "enhanced tubes" [7.24, 7.25].

Example 7.4

Repeat Example 7.3, now assuming the pipe to have a wall roughness of $\varepsilon = 360$ μm.

SOLUTION. The Reynolds number and physical properties are unchanged. From eqn. (7.50)

$$f = \left\{ 1.8 \, \log_{10} \left[\frac{6.9}{412,300} + \left(\frac{360 \times 10^{-6}/0.12}{3.7} \right)^{1.11} \right] \right\}^{-2}$$

$$= 0.02651$$

The roughness Reynolds number is then

$$\mathrm{Re}_{\varepsilon} = (412,300) \frac{360 \times 10^{-6}}{0.12} \sqrt{\frac{0.02651}{8}} = 71.2$$

This corresponds to fully rough flow. With eqn. (7.49) we have

$$\mathrm{Nu}_D = \frac{(0.02651/8)(4.123 \times 10^5)(3.61)}{1 + \sqrt{0.02651/8} \left[4.5(71.2)^{0.2}(3.61)^{0.5} - 8.48 \right]}$$

$$= 2,959$$

so

$$h = 2959 \, \frac{0.642}{0.12} = 15.8 \text{ kW/m}^2\text{K}$$

In this case, wall roughness causes a factor of 1.9 increase in h and a factor of 2.2 increase in f and the pumping power. We have omitted the variable properties corrections used in Example 7.3 because they apply only to smooth-walled pipes. ∎

Heat transfer to fully developed liquid-metal flows in tubes

All our convection equations have, so far, been for Prandtl numbers of 2/3 (monatomic gases) or higher. The exception is eqn. (6.62) which applies to the uncommon situation of liquid metal flow over a flat plate. Now we turn our attention to tubular convection by liquid metals, which is far more widely used but also more complex.

Liquid metal thermal conductivities are much higher than for other liquids, and their Pr's are generally on the order of 10^{-2} to 10^{-3}. Their high thermal conductivity yields much greater heat transfer coefficients. Liquid metal coolants thus need less surface area for a given heat load. That is why they have sometimes been used to cool the nuclear reactors that power ships, where space and weight must be limited.

Liquid metals may also have low vapor pressures. That means they can used be at high temperatures with less, or no, pressurization. Higher temperature operation generally improves a power plant's energy efficiency.

The liquid metal coolants that have been widely used, and widely studied, include mercury, sodium, lead, sodium-potassium eutectic alloy, or NaK, and lead-bismuth eutectic. NaK is of particular interest because it stays liquid at room temperature; and it can be used up to 785°C with no pressurization.

Materials with very low Pr's continue to emerge as useful: liquid tin has been studied for use in concentrating solar power [7.26]; liquid silicon is a potential medium of energy storage [7.27]; and so on. These low Pr materials offer a high payoff in effective heat transfer and thermodynamic efficiency, but at the cost of serious engineering challenges. They can be toxic, corrosive, and sometimes flammable; and containing them involves significant material selection and design problems.

Theory and experiments.   We have already done the dimensional analysis of forced convention by liquid metal heat flowing over a flat plate, in Section 6.5. There we found that

$$\mathrm{Nu}_x = \mathrm{fn}(\mathrm{Pe}_x) \qquad \text{for } \mathrm{Pe}_x = u_\infty x / \alpha \tag{7.51}$$

(recall eqn. 6.60 et seq.). For low Pr liquids, viscous effects are confined to a region very close to the wall. Thus, the thermal b.l. extends far beyond δ, and it is hardly influenced by the momentum b.l. or by viscosity.

Heat transfer to liquid metals in pipes shows similar behavior (see Fig. 7.7). When $\mathrm{Pr} \ll 1$, the region of thermal influence extends far beyond
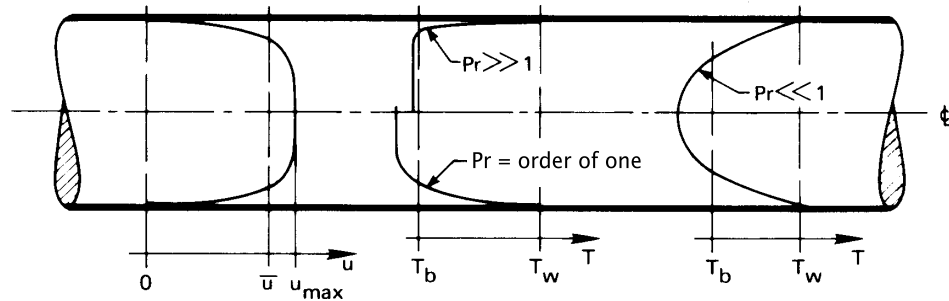
Figure 7.7 Velocity and temperature profiles during fully developed turbulent flow in a pipe.

the momentum b.l., and the temperature profile is not much influenced by the slow fluid close to the wall. (Conversely, if $Pr \gg 1$, the temperature profile is largely shaped within the viscous sublayer. At high or even moderate Pr, ν is therefore very important; but at low Pr, ν should drop out of the functional equation.) Thus, we expect Nu_D for liquid metals in pipes also to depend primarily on the Péclet number, $Pe_D = u_{av}D/\alpha$.

In 1956, Lubarsky and Kaufman [7.28] collected measured values of Nu_D for liquid metals flowing in pipes with a constant wall heat flux, q_w, as shown in Fig. 7.8. Fourteen separate data sets are included, for Prandtl numbers in the approximate range 0.005 to 0.04. Although most of the data correlate fairly well on Nu_D vs. Pe_D coordinates, certain sets of data are badly scattered.

The scatter occurs in part because liquid metal experiments are hard to carry out. Because the heat transfer coefficients are very high, temperature differences are small, and they must often be measured at high absolute temperatures for which heat losses are significant. Some of the very low data may result from added thermal resistance caused by a failure of the metals to wet the inner surface of the pipe. Or they might result from corrosion of the pipe. It is also hard to keep liquid metals pure. Impurities can also lead to lower values of h, for example, by forming poorly conducting oxide deposits on the pipe wall. In addition to these thermophysical issues, some the data shown in Fig. 7.8 are for lower Reynolds number conditions that are not fully turbulent, particularly those with $Pe_d < 200$. And for the very dense liquid metals, buoyancy-driven circulation, from temperature gradients in the liquid, might have contributed to convection.

Lubarsky and Kaufman discussed each of the data sets in detail and flagged cases for which problems seemed apparent. The data they ques-
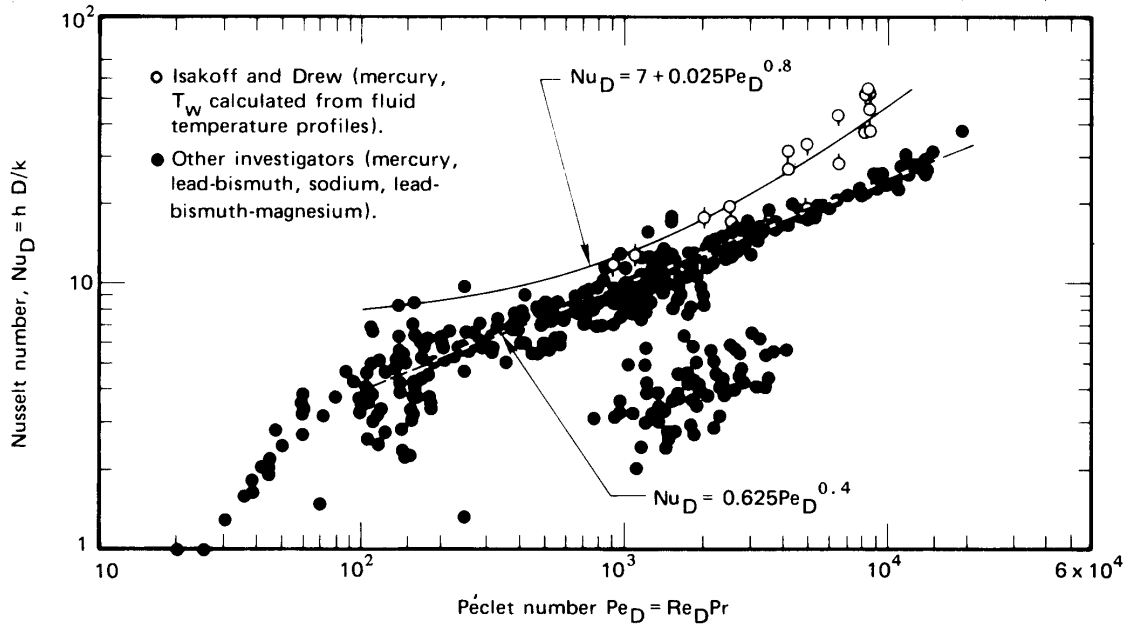
Figure 7.8 Historical comparison of measured and predicted
Nusselt numbers for liquid metals heated in long tubes with
uniform wall heat flux, q_w. (See Lubarsky and Kaufman [7.28]
for details and data source references.)

tioned included the entire cloud of points in the lower middle of the
figure, which are almost entirely from a single study. After excluding
problematic data sets, they put the following empirical curve through the
bulk of the remaining data, as shown in Fig. 7.8:

$$\text{Nu}_D = 0.625 \, \text{Pe}_D^{0.4} \tag{7.52}$$

for $\text{Pe}_D = u_{\text{av}}D/\alpha > 200$.

A body of theory for turbulent liquid metal heat transfer, however,
yields a prediction of the form

$$\text{Nu}_D = C_1 + C_2 \, \text{Pe}_D^{n} \tag{7.53}$$

for $\text{Pe}_D = u_{\text{av}}D/\alpha$. The original suggestion of this type, due to Lyon [7.29]
and shown in Fig. 7.8, does not track the data very well. Seban and
Shimazaki [7.30] suggested different theoretical values for a uniform wall
temperature, based on a simplified turbulence model:

$$\text{Nu}_D = 5.0 + 0.025 \, \text{Pe}_D^{0.8} \tag{7.54}$$
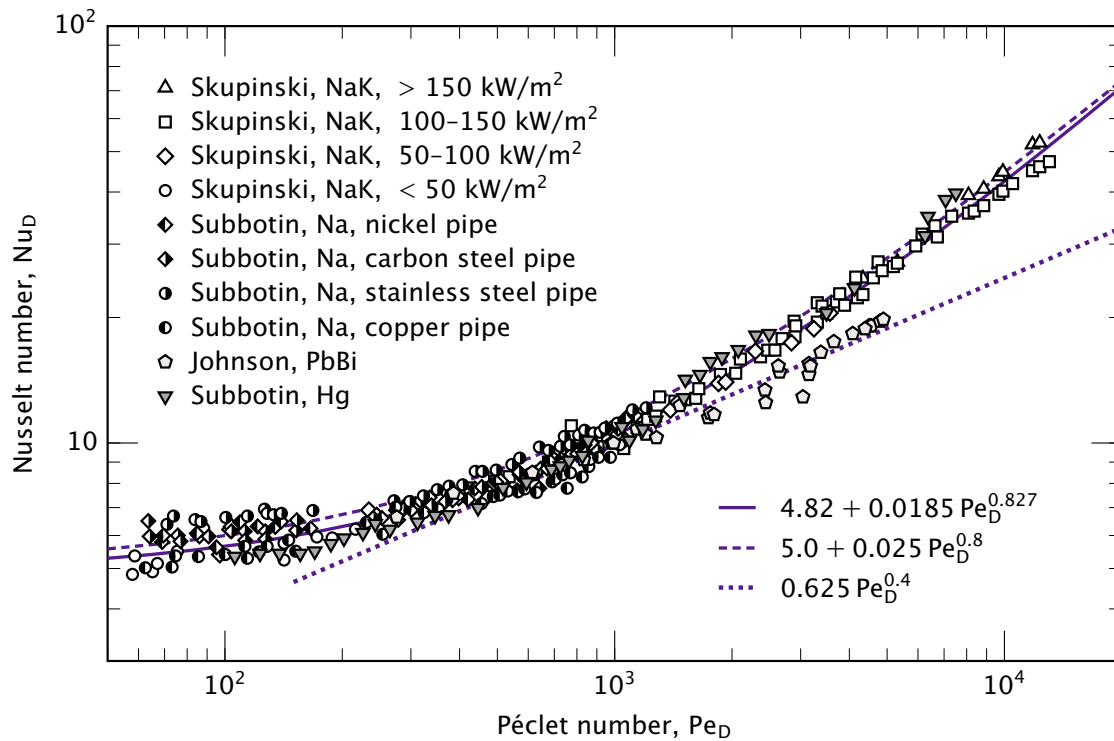
Figure 7.9 Liquid metal data from several investigators for uniform wall heat flux: Skupinski et al., NaK, Pr = 0.0153 [7.31]; Subbotin et al., Na, Pr = 0.0065 [7.32]; Johnson et al., PbBi, Pr ≃ 0.042 [7.33]; Subbotin et al., Hg, Pr ≃ 0.025 [7.34].

During the 1960's additional measurements were published, showing greater consistency and lower scatter. Some of those data are shown in Fig. 7.9, together with eqns. (7.52) and (7.54) and one data set from Fig. 7.8 [7.33]. Skupinski et al. [7.31], in one of these later studies, correlated their data as follows:

$$\boxed{\mathrm{Nu}_D = 4.82 + 0.0185\,\mathrm{Pe}_D^{0.827}} \tag{7.55}$$

This correlation is also shown in Fig. 7.9, and it lies in middle of most of the measurements. In this equation, properties may be evaluated at the average of the inlet and outlet bulk temperatures, and the flow should be fully developed ($L/D \gtrsim 30$).

Pacio et al. comprehensively reviewed existing measurements and correlations in 2015 [7.35]. Equation (7.55) provided the best prediction, with

68% of all accepted data lying within ±20% of the equation. Taler [7.36], using modern numerical turbulence models and considering many data sets, reached similar conclusions for $Pe_D > 100$. These findings are all for uniform wall heat flux. The data for uniform wall temperature are sparse.

In the thermally developing region, Lee [7.37] showed numerically that the Reynolds and Prandtl numbers must be treated as independent variables. Lee also found that heat conduction in the liquid metal along the axis of the pipe could become significant in the thermally developing region, but that it is negligible in the fully developed turbulent region for all values of Pe_D.

Example 7.5

Johnson et al. [7.33] measured heat transfer coefficients for lead-bismuth eutectic flowing in a 16.6 mm ID pipe at 1.75 m/s with a heat flux of 50.4 kW/m² and a bulk temperature of 441.5 K. What was the temperature of the pipe wall?

SOLUTION. The thermal diffusivity is approximately 6.5×10^{-6} m²/s at this temperature [7.38], so:

$$Pe_D = \frac{(1.75)(16.6 \times 10^{-3})}{6.5 \times 10^{-6}} = 4470$$

With eqn. (7.55), we compute

$$Nu_D = 4.82 + 0.0185(4470)^{0.827} = 24.2$$

With $k = 10.9$ W/m·K,

$$h = \frac{(24.2)(10.9)}{16.6 \times 10^{-3}} = 15.9 \times 10^3 \text{ W/m}^2\text{K}$$

which is a value comparable to the very high values we would expect in nucleate boiling of water (see Chapter 9). The wall temperature is

$$T_w = T_b + \frac{q_w}{h} = 441.5 + \frac{50.4 \times 10^3}{15.9 \times 10^3} = 441.5 + 3.2 = 444.7 \text{ K}$$

The experimental value reported by Johnson et al. was 446.0 K with $h = 11.1 \times 10^3$ W/m²K, about 30% below subsequent experiments. The temperature discrepancy, however, is very small—4.5 K measured versus 3.2 K calculated. This highlights one of the great difficulties of high heat flux experimentation: accurately measuring a small ΔT. ∎

7.4   Heat transfer surface viewed as a heat exchanger

Let us reconsider the problem of a fluid flowing through a pipe with a uniform wall temperature, T_w. By now we can predict $\bar{h}$ for a pretty wide range of conditions. Suppose that we need to know the net heat transfer to a pipe of known length once $\bar{h}$ is known. This problem is complicated by the fact that the bulk temperature, T_b, is varying along its length.

However, we need only recognize that this section of pipe is a heat exchanger whose overall heat transfer coefficient, U, is just $\bar{h}$, between T_w and T_b. Thus, if we wish to know how much pipe surface area is needed to raise the bulk temperature from T_{b_in} to T_{b_out}, we can calculate it using eqns. (3.12) and (3.13):

$$Q = (\dot{m}c_p)_b \left(T_{b_\text{out}} - T_{b_\text{in}}\right) = \bar{h}A(\text{LMTD})$$

or

$$A = \frac{(\dot{m}c_p)_b \left(T_{b_\text{out}} - T_{b_\text{in}}\right)}{\bar{h}} \frac{\ln\left(\dfrac{T_{b_\text{out}} - T_w}{T_{b_\text{in}} - T_w}\right)}{(T_{b_\text{out}} - T_w) - (T_{b_\text{in}} - T_w)} \tag{7.56}$$

By the same token, heat transfer in a duct can be analyzed with the effectiveness method (Section 3.3) if the exiting fluid temperature is unknown. Suppose that we do not know T_{b_out} in the example above. Then we can write an energy balance at any cross section, as we did in eqn. (7.9):

$$dQ = q_w P \, dx = hP(T_w - T_b) \, dx = \dot{m}c_p \, dT_b$$

Integration can be done from $T_b(0) = T_{b_\text{in}}$ to $T_b(L) = T_{b_\text{out}}$:

$$\int_0^L \frac{hP}{\dot{m}c_p} \, dx = -\int_{T_{b_\text{in}}}^{T_{b_\text{out}}} \frac{d(T_w - T_b)}{(T_w - T_b)}$$

$$\frac{P}{\dot{m}c_p} \int_0^L h \, dx = -\ln\left(\frac{T_w - T_{b_\text{out}}}{T_w - T_{b_\text{in}}}\right)$$

We recognize in this the definition of $\bar{h}$ from eqn. (7.27). Hence,

$$\frac{\bar{h}PL}{\dot{m}c_p} = -\ln\left(\frac{T_w - T_{b_\text{out}}}{T_w - T_{b_\text{in}}}\right)$$

which can be rearranged as

$$\frac{T_{b_\text{out}} - T_{b_\text{in}}}{T_w - T_{b_\text{in}}} = 1 - \exp\left(-\frac{\bar{h}PL}{\dot{m}c_p}\right) \tag{7.57}$$

This equation applies to either laminar or turbulent flow. The same equation will give the variation of bulk temperature if $T_{b_{\text{out}}}$ is replaced by $T_b(x)$, L is replaced by x, and $\overline{h}$ is calculated as the average value over the length 0 to x.

When the heat capacity rate of one stream in a heat exchanger is much higher than the other ($C_{\max} \gg C_{\min}$), the high capacity stream's temperature will hardly change. A heat exchanger for which one stream is isothermal is called a *single-stream* heat exchanger (recall Section 3.3). In the present case, a wall with a uniform temperature, T_w, can be regarded as a stream with a very large heat capacity rate. Thus, the left-hand side of eqn. (7.57) is the heat exchanger effectiveness. And we can form the NTU on the right-hand side with a few substitutions: write $C_{\min} = \dot{m}c_p$; replace U with $\overline{h}$; and note that $PL = A$, the heat exchanger surface area. Under these substitutions, $\overline{h}PL/\dot{m}c_p = UA/C_{\min} = $ NTU, and eqn. (7.57) becomes

$$\varepsilon = 1 - \exp\left(-\text{NTU}\right) \tag{7.58}$$

which is the same as eqn. (3.22).

Equation (7.57) applies to ducts of any cross-sectional shape. We may cast it in terms of the *hydraulic diameter*, $D_h \equiv 4A_c/P$, by substituting $\dot{m} = \rho u_{\text{av}} A_c$:

$$\frac{T_{b_{\text{out}}} - T_{b_{\text{in}}}}{T_w - T_{b_{\text{in}}}} = 1 - \exp\left(-\frac{\overline{h}PL}{\rho c_p u_{\text{av}} A_c}\right) \tag{7.59a}$$

$$= 1 - \exp\left(-\frac{\overline{h}}{\rho c_p u_{\text{av}}} \frac{4L}{D_h}\right) \tag{7.59b}$$

For a circular tube, with $A_c = \pi D^2/4$ and $P = \pi D$, $D_h = 4(\pi D^2/4)/(\pi D) = D$. To use eqn. (7.59b) for a noncircular duct, of course, we will need the value of $\overline{h}$ for the that duct's shape. We discuss noncircular ducts the next section (Section 7.5).

Example 7.6

Air at 20°C is hydrodynamically fully developed as it flows in a 1 cm I.D. pipe. The average velocity is 0.7 m/s. If the flow enters a section where the pipe wall is at 60°C, what is the bulk temperature 0.25 m farther downstream?

SOLUTION. We evaluate properties at (20+60)/2 = 40°C:

$$\text{Re}_D = \frac{u_{\text{av}}D}{\nu} = \frac{(0.7)(0.01)}{1.69 \times 10^{-5}} = 417$$

The flow is therefore laminar. To account for the thermal entry region, we compute the Graetz number from eqn. (7.26)

$$\text{Gz} = \frac{\text{Re}_D \text{Pr}\, D}{x} = \frac{(421)(0.709)(0.01)}{0.25} = 11.8$$

Substituting this value into eqn. (7.29), we find $\overline{\text{Nu}}_D = 4.27$. Thus,

$$\overline{h} = \frac{4.27(0.0270)}{0.01} = 11.5 \text{ W/m}^2\text{K}$$

Then, using eqn. (7.59b),

$$\frac{T_{b_{\text{out}}} - T_{b_{\text{in}}}}{T_w - T_{b_{\text{in}}}} = 1 - \exp\left[-\frac{11.5}{1.13(1007)(0.7)}\frac{4(0.25)}{0.01}\right]$$

so that

$$\frac{T_b - 20}{60 - 20} = 0.764 \qquad \text{or} \qquad T_b = 50.6°\text{C} \qquad \blacksquare$$

7.5   Heat transfer coefficients for noncircular ducts

So far, we have focused on flows within circular tubes, which are by far the most common configuration. Nevertheless, other cross-sectional shapes often occur. For example, the fins of a heat exchanger may form a rectangular passage through which air flows. Sometimes, the passage cross-section is very irregular, as might happen when fluid passes through a clearance between other objects. In situations like these, all the qualitative ideas that we developed in Sections 7.1–7.3 still apply, but the Nusselt numbers for circular tubes cannot be used in calculating heat transfer rates.

The hydraulic diameter, which was introduced in connection with eqn. (7.59b), provides a basis for approximating heat transfer coefficients in noncircular ducts. Recall that the hydraulic diameter is defined as

$$D_h \equiv \frac{4\,A_c}{P} \tag{7.60}$$

where A_c is the cross-sectional area and P is the passage's wetted perimeter (Fig. 7.10). The hydraulic diameter measures the fluid cross-sectional area per unit length of wall perimeter. In turbulent flow, where most of the convection resistance is in the sublayer on the wall, this ratio determines the heat transfer coefficient to within about ±20% across a broad range

$$D_h = \frac{4A_c}{P}$$
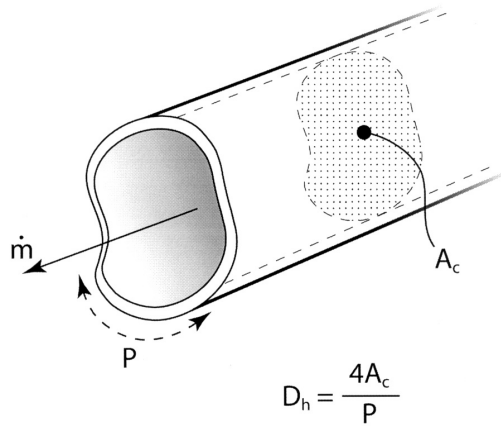
Figure 7.10 Flow in a noncircular duct.

of duct shapes, by using a simple replacement of D by D_h in circular tube equations. In contrast, for fully-developed laminar flow, where the thermal resistance extends into the core of the duct, the heat transfer coefficient depends on the details of the duct shape, and D_h alone cannot define the heat transfer coefficient. Nevertheless, the hydraulic diameter provides an appropriate characteristic length for cataloging laminar Nusselt numbers.

The factor of four in the definition of D_h ensures that it gives the actual diameter of a circular tube, D, as noted in the preceding section. Some other important cases include:

$$\begin{array}{cc} \text{a rectangular duct of} \\ \text{width } a \text{ and height } b \end{array} \quad D_h = \frac{4\,ab}{2a + 2b} = \frac{2ab}{a + b} \qquad (7.61a)$$

$$\begin{array}{c} \text{an annular duct of} \\ \text{inner diameter } D_i \text{ and} \\ \text{outer diameter } D_o \end{array} \quad \begin{aligned} D_h &= \frac{4\left(\pi D_o^2/4 - \pi D_i^2/4\right)}{\pi\left(D_o + D_i\right)} \\ &= (D_o - D_i) \end{aligned} \qquad (7.61b)$$

and, for very wide parallel plates, eqn. (7.61a) with $a \gg b$ gives

$$\begin{array}{c} \text{two parallel plates} \\ \text{a distance } b \text{ apart} \end{array} \quad D_h = 2b \qquad (7.61c)$$

Turbulent flow in noncircular ducts

With some caution, we may use D_h directly in place of the circular tube diameter when calculating turbulent heat transfer coefficients and bulk temperature changes. Specifically, D_h replaces D in the Reynolds number,

which is then used to calculate f and Nu_{D_h} from the circular tube formulæ. The mass flow rate and the bulk velocity must be based on the true cross-sectional area, which does *not* usually equal $\pi D_h^2/4$ (see Problem 7.48). The following example illustrates the procedure.

Example 7.7

An air duct carries chilled air at an inlet bulk temperature of $T_{b_\mathrm{in}} = 17°C$ and $u_\mathrm{av} = 1$ m/s. The duct is made of very smooth and thin galvanized steel, has a square cross-section of 0.3 m by 0.3 m, and is not insulated. A 15 m length of the duct runs outdoors through warm, dry air at $T_\infty = 37°C$. The heat transfer coefficient on the outside surface, due to natural convection and thermal radiation, is 5 W/m^{2}K. Find the bulk temperature change of the air over this length.

SOLUTION. From eqn. (7.61a) with $a = b$

$$D_h = a = 0.3 \text{ m}$$

Using properties of air at the inlet temperature (290 K)

$$\mathrm{Re}_{D_h} = \frac{u_\mathrm{av}D_h}{\nu} = \frac{(1)(0.3)}{(1.578 \times 10^{-5})} = 19{,}011$$

The Reynolds number for turbulent transition in a noncircular duct is typically approximated by the circular tube value of about 2300, so this flow is turbulent. The friction factor is obtained from eqn. (7.42)

$$f = \left[1.82\log_{10}(19{,}011) - 1.64\right]^{-2} = 0.02646$$

and the Nusselt number is found with Gnielinski's equation, (7.41)

$$\mathrm{Nu}_{D_h} = \frac{(0.02646/8)(19{,}011 - 1{,}000)(0.713)}{1 + 12.7\sqrt{0.02646/8}\left[(0.713)^{2/3} - 1\right]} = 49.82$$

The heat transfer coefficient is

$$h = \mathrm{Nu}_{D_h}\frac{k}{D_h} = \frac{(49.82)(0.02623)}{0.3} = 4.371 \text{ W/m}^2\text{K}$$

The remaining problem is to find the bulk temperature change. The thin metal duct wall offers little thermal resistance, but convection resistance outside the duct must be considered. Heat travels first from the air at T_∞ through the outside heat transfer coefficient to the duct

wall, through the duct wall, and then through the inside heat transfer coefficient to the flowing air—effectively through three resistances in series from the fixed temperature T_∞ to the rising temperature T_b. We have seen in Section 2.4 that an overall heat transfer coefficient may be used to describe such series resistances. Here, with $A_{\text{inside}} \simeq A_{\text{outside}}$, we find U based on inside area to be

$$U = \frac{1}{A_{\text{inside}}} \left[\frac{1}{(hA)_{\text{inside}}} + \underbrace{R_{t\,\text{wall}}}_{\text{neglect}} + \frac{1}{(hA)_{\text{outside}}} \right]^{-1}$$

$$= \left(\frac{1}{4.371} + \frac{1}{5} \right)^{-1} = 2.332 \text{ W/m}^2\text{K}$$

We then adapt eqn. (7.59b) by replacing $\overline{h}$ by U and T_w by T_∞:

$$\frac{T_{b_{\text{out}}} - T_{b_{\text{in}}}}{T_\infty - T_{b_{\text{in}}}} = 1 - \exp\left(-\frac{U}{\rho u_{\text{av}} c_p} \frac{4L}{D_h} \right)$$

$$= 1 - \exp\left[-\frac{2.332}{(1.217)(1)(1007)} \frac{4(15)}{0.3} \right] = 0.3165$$

The outlet bulk temperature is therefore

$$T_{b_{\text{out}}} = [17 + (37 - 17)(0.3165)] \text{ °C} = 23.3 \text{ °C} \qquad \blacksquare$$

The results obtained by substituting D_h for D in turbulent circular tube equations are generally accurate to within $\pm 20\%$ and are often within $\pm 10\%$. Worse results are obtained for duct cross-sections having sharp corners, such as an acute triangle. Specialized equations for "effective" hydraulic diameters have been developed for specific geometries and can improve the accuracy to 5 or 10% [7.9].

When only a portion of the duct cross-section is heated—one wall of a rectangle, for example—the procedure for finding h is the same. The hydraulic diameter is based upon the entire *wetted* perimeter, not simply the heated part. However, in eqn. (7.59a), P is the *heated* perimeter: eqn. (7.59b) does *not* apply for nonuniform heating.

One situation in which one-sided or unequal heating often occurs is an annular duct, with the inner tube serving as a heating element. The hydraulic diameter procedure will typically predict the heat transfer coefficient on the outer tube to within $\pm 10\%$, irrespective of the heating configuration. The heat transfer coefficient on the inner surface, however, is sensitive to both the diameter ratio and the heating configuration.

For that surface, the hydraulic diameter approach is not very accurate, especially if $D_i \ll D_o$; other methods have been developed to accurately predict heat transfer in annular ducts (see [7.3] or [7.9]).

Laminar flow in noncircular ducts

Laminar velocity profiles in noncircular ducts develop in essentially the same way as for circular tubes, and the fully developed velocity profiles are generally paraboloidal in shape. For example, for fully developed flow between parallel plates located at $y = b/2$ and $y = -b/2$,

$$\frac{u}{u_{\text{av}}} = \frac{3}{2}\left[1 - 4\left(\frac{y}{b}\right)^2\right] \tag{7.62}$$

for u_{av} the bulk velocity. This should be compared to eqn. (7.15) for a circular tube. The constants and coordinates differ, but the equations are otherwise identical. Likewise, analysis of the temperature profiles between parallel plates leads to constant Nusselt numbers, which may be expressed in terms of the hydraulic diameter for various boundary conditions:

$$\text{Nu}_{D_h} = \frac{hD_h}{k} = \begin{cases} 7.541 & \text{for fixed plate temperatures} \\ 8.235 & \text{for fixed flux at both plates} \\ 5.385 & \text{one plate fixed flux, one adiabatic} \end{cases} \tag{7.63}$$

Some other cases are summarized in Table 7.4, and many more have been considered in the literature (see, especially, Shah and London [7.5]). The latter have covered different wall boundary conditions and a wide variety cross-sectional shapes, both practical and ridiculous: triangles, circular sectors, trapezoids, rhomboids, hexagons, limaçons, and even crescent moons!

The boundary conditions should be considered carefully when the duct is small because h can become large: If the conduction resistance of the tube wall is comparable to the convective resistance within the duct, then temperature or heat flux variations around the tube perimeter must be expected. Such variations can significantly affect the laminar Nusselt number. The rectangular duct values in Table 7.4 for fixed wall flux, for example, are based on a uniform temperature around the perimeter of the tube, as if the wall has no conduction resistance around its perimeter. That might be the case for a copper duct heated at a fixed rate in watts per meter of duct length.

Table 7.4 Additional, laminar, fully developed Nusselt numbers based on the hydraulic diameters given in eqn. (7.61)

Cross-section	T_w fixed	q_w fixed
Circular	3.657	4.364
Square	2.976	3.608
Rectangular		
$a = 2b$	3.391	4.123
$a = 4b$	4.439	5.331
$a = 8b$	5.597	6.490
Parallel plates	7.541	8.235

Laminar entry length equations for noncircular ducts are also given by Shah and London [7.5].

7.6 Heat transfer during cross flow over cylinders

Fluid flow pattern

Predicting the heat transfer from any object in a cross flow can be very difficult. Let us consider one of the more common cross-flow cases, fluid flow perpendicular to a simple cylinder. Figure 7.11 shows how the flow develops as $\mathrm{Re}_D \equiv u_\infty D/\nu$ is increased from below 5 to nearly 10^7. An interesting feature of this evolving flow pattern is the fairly continuous way in which one flow transition follows another. The flow field degenerates into greater and greater degrees of disorder with each successive transition until, rather strangely, it regains order at the highest values of Re_D.

The flow field behind a cylinder goes through a large variety of changing forms as Re_D increases. Most of these forms are accompanied by a vortex shedding frequency, f_v, so let us first look at that. Dimensional analysis shows that a dimensionless frequency called the *Strouhal number*, Str, depends on the Reynolds number of the flow:

$$\mathrm{Str} \equiv \frac{f_v D}{u_\infty} = \mathrm{fn}(\mathrm{Re}_D) \tag{7.64}$$

Figure 7.12 defines this relationship experimentally on the basis of about 550 data points [7.39]. The Strouhal numbers stay a little over 0.2 over
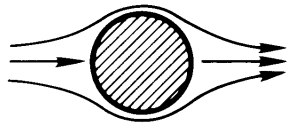
$Re_D < 5$ Regime of unseparated flow.
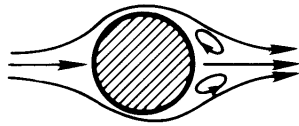
$5 \text{ to } 15 \leqslant Re_D < 40$ A fixed pair of Föppl vortices in the wake
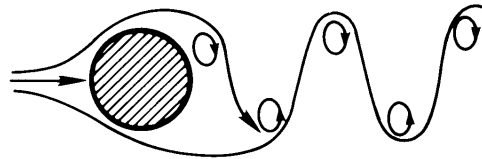
$40 \leqslant Re_D < 90 \text{ and } 90 \leqslant Re_D < 150$

Two regimes in which vortex street is laminar:
    Periodicity governed in low Re_D range by wake instability

    Periodicity governed in high Re_D range by vortex shedding.
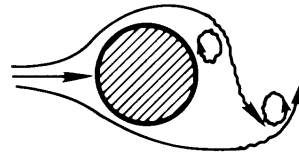
$150 \leqslant Re_D < 300$ Transition range to turbulence in vortex.

$300 \leqslant Re_D \gtrsim 3 \times 10^5$ Vortex street is fully turbulent, and the flow field is increasingly 3-dimensional.
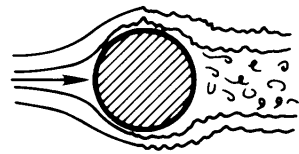
$3 \times 10^5 \gtrsim Re_D < 3.5 \times 10^6$

Laminar boundary layer has undergone turbulent transition. The wake is narrower and disorganized. No vortex street is apparent.
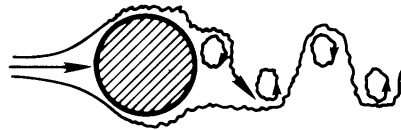
$3.5 \times 10^6 \leqslant Re_D < \infty \text{ (?)}$

Re-establishment of the turbulent vortex street that was evident in $300 \leqslant Re_D \gtrsim 3 \times 10^5$. This time the boundary layer is turbulent and the wake is thinner.

Figure 7.11 Regimes of fluid flow across circular cylinders [7.39].

388
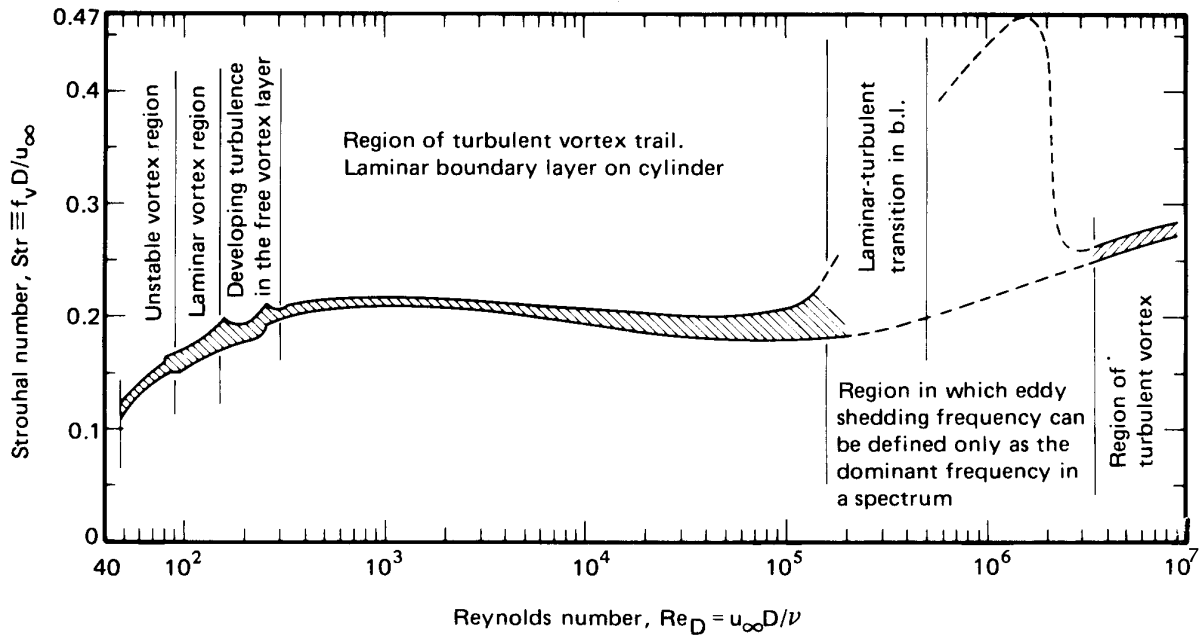
Figure 7.12 The Strouhal–Reynolds number relationship for circular cylinders, as defined by the data [7.39].

most of the range of Re_D. This means that behind a given object, the vortex-shedding frequency rises almost linearly with velocity.

Experiment 7.1

When there is a gentle breeze blowing outdoors, go out and locate a large tree with a straight trunk or, say, a telephone pole. Wet your finger and place it in the wake a couple of diameters downstream and about one radius off center. Estimate the vortex-shedding frequency and use Str $\simeq 0.21$ to estimate u_∞. Is your value of u_∞ reasonable?♦

Heat transfer

The action of vortex shedding greatly complicates the heat removal process. Giedt's data [7.40] in Fig. 7.13 show how the heat removal changes as the constantly fluctuating fluid motion to the rear of the cylinder changes with Re_D. Direct prediction by the sort of b.l. methods that we discussed in Chapter 6 is out of the question. However, a great deal can be done
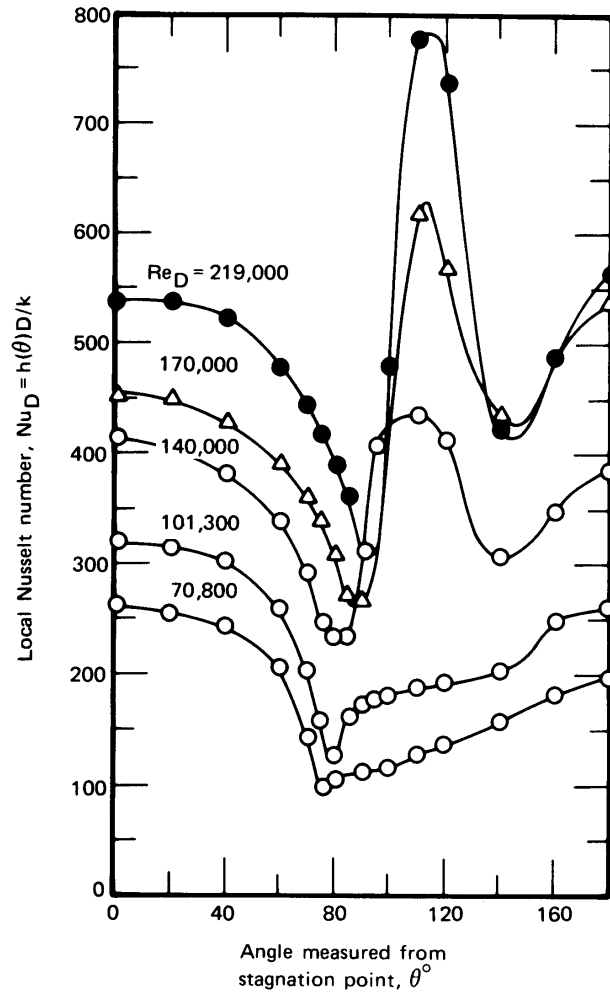
Figure 7.13　Giedt's local measurements of heat transfer around a cylinder in a normal cross flow of air.

with the data using relations of the form

$$\overline{\mathrm{Nu}}_D = \mathrm{fn}(\mathrm{Re}_D, \mathrm{Pr})$$

The broad study of Churchill and Bernstein [7.41] probably brings the correlation of heat transfer data from cylinders about as far as it is possible. For the entire range of the available data, they offer

$$\overline{\mathrm{Nu}}_D = 0.3 + \frac{0.62\,\mathrm{Re}_D^{1/2}\,\mathrm{Pr}^{1/3}}{\left[1 + (0.4/\mathrm{Pr})^{2/3}\right]^{1/4}}\left[1 + \left(\frac{\mathrm{Re}_D}{282{,}000}\right)^{5/8}\right]^{4/5} \qquad (7.65)$$

This expression underpredicts most of the data by about 20% in the range $40,000 < \mathrm{Re}_D < 400,000$ but is quite good at other Reynolds numbers above $\mathrm{Pe}_D \equiv \mathrm{Re}_D\mathrm{Pr} = 0.2$. This agreement is evident in Fig. 7.14, where eqn. (7.65) is compared with data.

Greater accuracy and, in most cases, greater convenience results from breaking the correlation into component equations:

- Below $\mathrm{Re}_D = 4000$, the bracketed term $\left[1 + (\mathrm{Re}_D/282,000)^{5/8}\right]^{4/5}$ is $\simeq 1$, so

$$\overline{\mathrm{Nu}}_D = 0.3 + \frac{0.62\,\mathrm{Re}_D^{1/2}\mathrm{Pr}^{1/3}}{\left[1 + (0.4/\mathrm{Pr})^{2/3}\right]^{1/4}} \qquad (7.66)$$

- For $\mathrm{Pe} \leqslant 0.2$, the Nakai-Okazaki [7.42] relation should be used

$$\overline{\mathrm{Nu}}_D = \frac{1}{0.8237 - \ln(\mathrm{Pe}^{1/2})} \qquad (7.67)$$

- In the range $40,000 < \mathrm{Re}_D < 400,000$, somewhat better results are given by

$$\overline{\mathrm{Nu}}_D = 0.3 + \frac{0.62\,\mathrm{Re}_D^{1/2}\,\mathrm{Pr}^{1/3}}{\left[1 + (0.4/\mathrm{Pr})^{2/3}\right]^{1/4}}\left[1 + \left(\frac{\mathrm{Re}_D}{282,000}\right)^{1/2}\right] \qquad (7.68)$$

than by eqn. (7.65).

All properties in eqns. (7.65) to (7.68) are to be evaluated at a film temperature $T_f = (T_w + T_\infty)/2$.

Example 7.8

An electric resistance wire heater 0.1 mm in diameter is placed perpendicular to an air flow. It holds a temperature of 40°C in a 20°C air flow while it dissipates 17.8 W/m to the flow. How fast is the air flowing?

SOLUTION. $\overline{h} = (17.8 \text{ W/m})/[\pi(0.0001 \text{ m})(40 - 20)\,K] = 2833$ W/m²K. Therefore, $\overline{\mathrm{Nu}}_D = 2833(0.0001)/0.0265 = 10.69$, where we have evaluated $k = 0.0265$ W/m·K at $T = 30°$C.

We now want to find the value of Re_D for which $\overline{\mathrm{Nu}}_D$ is 10.69. From Fig. 7.14 we see that Re_D is around 300 when the ordinate is on the order of 10. This means that we can solve eqn. (7.66) to get an accurate value of Re_D

$$\mathrm{Re}_D = \left\{(\overline{\mathrm{Nu}}_D - 0.3)\left[1 + \left(\frac{0.4}{\mathrm{Pr}}\right)^{2/3}\right]^{1/4}\bigg/ 0.62\,\mathrm{Pr}^{1/3}\right\}^2$$
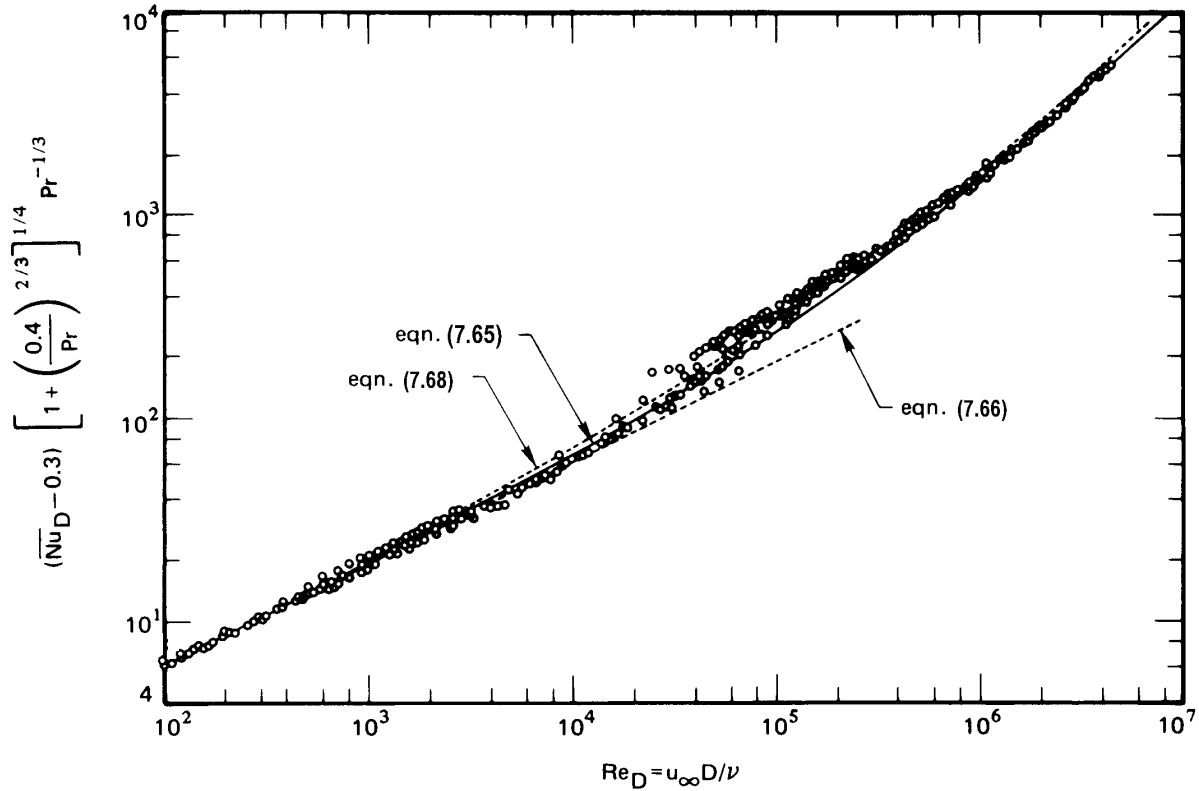
Figure 7.14 Comparison of Churchill and Bernstein's correlation with data by many workers from several countries for heat transfer during cross flow over a cylinder. (See [7.41] for data sources.) Fluids include air, water, and sodium, with both q_w and T_w constant.

and Pr = 0.712, so

$$\text{Re}_D = \left\{ (10.69 - 0.3)\left[1 + \left(\frac{0.40}{0.712}\right)^{2/3}\right]^{1/4} \middle/ 0.62(0.712)^{1/3} \right\}^2 = 457$$

Then

$$u_\infty = \frac{\nu}{D}\text{Re}_D = \left(\frac{1.602 \times 10^{-5}}{10^{-4}}\right)457 = 73.2 \text{ m/s}$$

The scatter of the data in this range is quite small—less than 10%, it would appear—in Fig. 7.14. Therefore, this method can be used to measure local velocities with good accuracy. If the device is calibrated,

its accuracy is improved further. Such an air speed indicator is called a *hot-wire anemometer*, as discussed further in Problem 7.45. ■

Heat transfer during flow across tube bundles

A rod or tube bundle is an arrangement of parallel cylinders that heat, or are being heated by, a fluid that might flow normal to them, parallel with them, or at some other angle to them. The flow through conventional water-cooled nuclear reactors, for example, is parallel to the fuel rods. However, the flow on the shell side of most shell-and-tube heat exchangers is essentially normal to the tube bundles.

Figure 7.15 shows the two basic configurations of a tube bundle in a cross flow. In one, the tubes are in a line with the flow; in the other, the tubes are staggered in alternating rows. For either of these configurations, heat transfer data can be correlated reasonably well with power-law relations of the form

$$\overline{\mathrm{Nu}}_D = C \, \mathrm{Re}_D^n \, \mathrm{Pr}^{1/3} \tag{7.69}$$

but with the Reynolds number based on the maximum mean velocity, which occurs in the minimum transverse area of the passages between the tubes. With reference to Fig. 7.15, if u_∞ is the bulk velocity approaching the tube bundle

$$u_{\max} = u_\infty \frac{S_T}{S_T - D} = \frac{u_\infty}{1 - D/S_T} \tag{7.70}$$

Thus, the Nusselt number based on the average heat transfer coefficient over any particular isothermal tube is

$$\overline{\mathrm{Nu}}_D = \frac{\overline{h}D}{k} \quad \text{and} \quad \mathrm{Re}_D = \frac{u_{\max}D}{\nu} \tag{7.71}$$

Žukauskas at the Lithuanian Academy of Sciences Institute in Vilnius wrote two comprehensive review articles on tube-bundle heat transfer [7.43, 7.44]. In these he summarized his work and that of other then-Soviet workers, together with earlier work from the West. He was able to correlate data over very large ranges of Pr, Re_D, S_T/D, and S_L/D (see Fig. 7.15) with an expression of the form

$$\overline{\mathrm{Nu}}_D = \mathrm{Pr}^{0.36}(\mathrm{Pr}/\mathrm{Pr}_w)^n \, \mathrm{fn}(\mathrm{Re}_D) \quad \text{with } n = \begin{cases} 0 & \text{for gases} \\ \frac{1}{4} & \text{for liquids} \end{cases} \tag{7.72}$$

where properties are to be evaluated at the local fluid bulk temperature, except for Pr_w, which is evaluated at the uniform tube wall temperature, T_w.
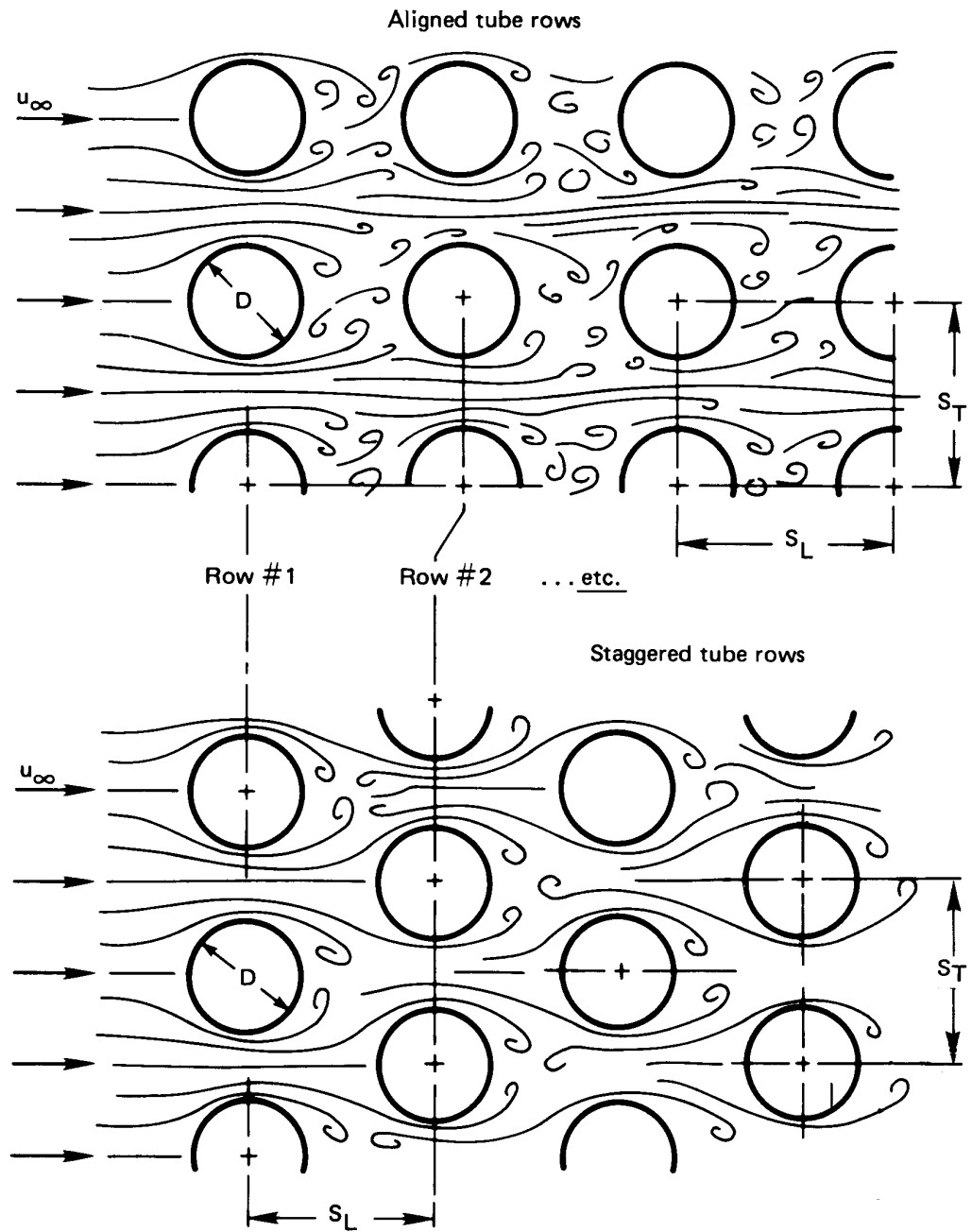
Figure 7.15 Aligned and staggered tube rows in tube bundles.

The function $\mathrm{fn}(\mathrm{Re}_D)$ takes the following form for the various circumstances of flow and tube configuration:

$100 \leqslant \mathrm{Re}_D \leqslant 10^3$:

aligned rows:	$\mathrm{fn}(\mathrm{Re}_D) = 0.52\,\mathrm{Re}_D^{0.5}$	(7.73a)
staggered rows:	$\mathrm{fn}(\mathrm{Re}_D) = 0.71\,\mathrm{Re}_D^{0.5}$	(7.73b)

$10^3 \leqslant \mathrm{Re}_D \leqslant 2 \times 10^5$:

aligned rows: $\quad \mathrm{fn}(\mathrm{Re}_D) = 0.27\,\mathrm{Re}_D^{0.63},\ \ S_T/S_L \geqslant 0.7$ (7.73c)

For $S_T/S_L < 0.7$, heat exchange is much less effective. Therefore, aligned tube bundles are not designed in this range and no correlation is given.

staggered rows: $\quad \mathrm{fn}(\mathrm{Re}_D) = 0.35(S_T/S_L)^{0.2}\,\mathrm{Re}_D^{0.6},$
$$S_T/S_L \leqslant 2 \qquad (7.73\mathrm{d})$$
$$\mathrm{fn}(\mathrm{Re}_D) = 0.40\,\mathrm{Re}_D^{0.6},\ \ S_T/S_L > 2 \qquad (7.73\mathrm{e})$$

$\mathrm{Re}_D > 2 \times 10^5$:

aligned rows: $\quad \mathrm{fn}(\mathrm{Re}_D) = 0.033\,\mathrm{Re}_D^{0.8}$ (7.73f)

staggered rows: $\quad \mathrm{fn}(\mathrm{Re}_D) = 0.031(S_T/S_L)^{0.2}\,\mathrm{Re}_D^{0.8},$
$$\mathrm{Pr} > 1 \qquad (7.73\mathrm{g})$$
$$\overline{\mathrm{Nu}}_D = 0.027(S_T/S_L)^{0.2}\,\mathrm{Re}_D^{0.8},$$
$$\mathrm{Pr} = 0.7 \qquad (7.73\mathrm{h})$$

All of the preceding relations apply to the inner rows of tube bundles. The heat transfer coefficient is smaller in the rows at the front of a bundle, facing the oncoming flow. The heat transfer coefficient can be corrected so that it will apply to any of the front rows using Fig. 7.16.

Early in this chapter we alluded to the problem of predicting the heat transfer coefficient during the flow of a fluid at an angle other than 90° to the axes of the tubes in a bundle. Žukauskas provides empirical corrections in Fig. 7.17 to account for this problem.

The work of Žukauskas does not extend to liquid metals. However, Kalish and Dwyer [7.45] present the results of an experimental study of heat transfer to sodium-potassium eutectic (NaK), which sometimes used as a nuclear reactor coolant. For tubes all at a uniform heat flux in an
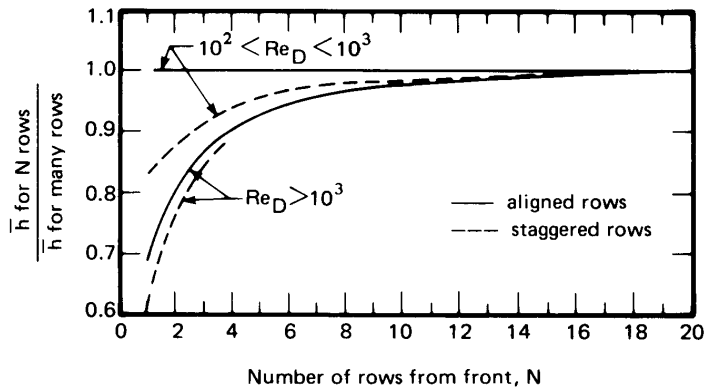
Figure 7.16 Correction for the heat transfer coefficients in the front rows of a tube bundle [7.43].

equilateral triangular array, as shown in Fig. 7.18, Kalish and Dwyer give

$$\mathrm{Nu}_D = \left(4.60 + 0.193\,\mathrm{Pe}_D^{0.614}\right)\sqrt{C\,\frac{P-D}{P}\left(\frac{\sin\phi + \sin^2\phi}{1 + \sin^2\phi}\right)} \qquad (7.74)$$

where

- Pe_D is the Péclet number based on the mean flow velocity through the narrowest opening between the tubes.

- C is the constant given in Fig. 7.18.

- P is the "pitch" of the tube array, as shown in Fig. 7.18, and D is the tube diameter.

- the angle between the flow and the rod axis is $30° \leqslant \phi \leqslant 90°$

For nuclear reactors, flow of liquid metals parallel to the fuel rods is more common than cross flow over the rods. Data and correlations
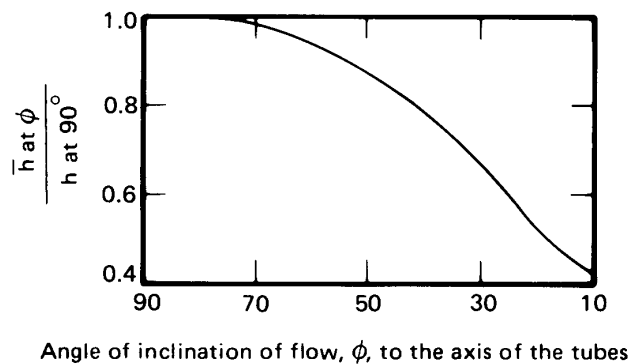
Figure 7.17 Correction for the heat transfer coefficient in flows that are not perfectly perpendicular to heat exchanger tubes [7.43].
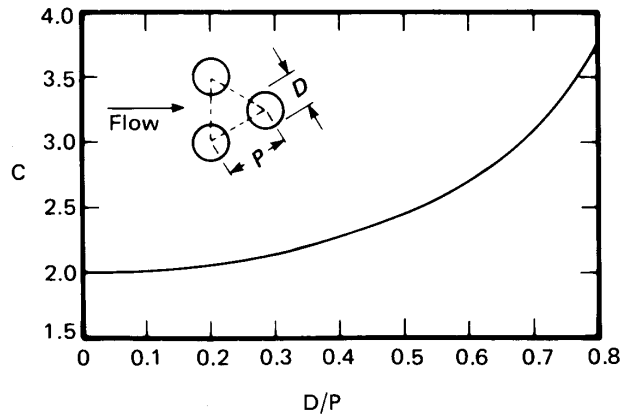
Figure 7.18 Geometric correction for the Kalish-Dwyer equation (7.74).

for parallel flow have been reviewed by El-Genk and Schriener [7.46]. Further information on designing tube-bundle heat exchangers, including pressure drop calculations, can be found the comprehensive handbook by Hewitt [7.47].

7.7 Finding and assessing correlations for other configurations

We said at the outset that this chapter would progressively treat heat convection problems that lie further and further beyond the reach of analysis. However, we must not forget that even the most completely empirical relations in Section 7.6 were devised by people who were keenly aware of the theoretical framework into which these relations had to fit. Notice, for example, that eqn. (7.66) reduces to $\mathrm{Nu}_D \propto \sqrt{\mathrm{Pe}_D}$ as Pr becomes small. That sort of theoretical requirement did not just pop out of a data plot. Instead, it was a consideration that led the authors to design an empirical equation that agreed with theory at low Pr. In other words, theoretical considerations such discussed in Chapter 6 guide the correlation of limited data for situations that cannot be analyzed fully.

We often need to know the behavior of an unfamiliar convection situation. The first thing we should do is look for an existing correlation. Information already exists for many known configurations. Some examples include: axial flow through tube or rod bundles; flow over such bluff bodies as spheres, cubes, or cones; the flow through heat sinks used to cool electronics (Fig. 4.10); or the flow inside such enhanced channels as we saw in Fig. 4.6b.

Places where we might begin our search for such correlations include: the *Handbook of Single-Phase Convective Heat Transfer* [7.48], specialized

textbooks on the topics of interest (e.g., for enhanced tubes, the book by Webb and Kim [7.49]), or review articles on the subject from either heat transfer journals or the series *Advances in Heat Transfer*. For a more wide ranging search, various high-quality scientific databases, such as *Scopus*, *Web of Science*, and *Compendex* allow one to search for peer-reviewed papers using keywords, to find more recent papers that have cited an older paper or review, or to find the papers that were the source of the data that became the basis of a correlation. If you have access to a university library, asking the reference librarian for advice is an excellent first step. In addition, the manufacturers of heat transfer components will sometimes provide simple correlations for their equipment within its range of use.

It is very important that we think critically once we have found a correlation. Questions you should ask yourself include:

- Does my case fall within the range of dimensionless parameters upon which the correlation is based, or must I extrapolate to reach my case? It is generally never safe to make such extrapolations.

- What geometric differences exist between the situation represented in the correlation and the one with which I am dealing? Such elements include inlet flow conditions, bends or bumps in channels, aspect ratios that do not match, and hardware that interferes with the flow. One must be alert to all kinds of deviations from the intended situation, many of which might be unexpected.

- Are the boundary conditions of the correlation the same as my boundary conditions? Laminar flows are especially sensitive to b.c.'s, while turbulent flows are less sensitive.

- To what extent do the data scatter around the correlating equation? Is the correlation accompanied by discussion of uncertainty, either in terms of the data used to create it or in terms of the ability of the correlation to predict the measured data?

- Does the correlating equation have any basis in theory? If it is only, say, a least-squares fit to the existing data in dimensional form, one might be unjustified in using it for more than interpolation of those data.

- Is the correlation based on a single lab's work, or did it aggregate data from multiple, independent studies? Was it based on an examination of hundreds of data points or only a handful?

- Are the ranges of physical variables large enough to guarantee that I can rely on the correlation for the full range of the dimensionless groups that it claims to embrace? For example, if the data were based on measurements with a single fluid (only, say, for air), how was the Prandtl number dependence assigned? Even a correlation with a strong footing in theory should not be extrapolated into very different ranges of Pr (e.g., from air to a liquid metal or an oil) because the Prandtl number dependence (and Reynolds number dependence) can change with the range considered.

- Can I actually see the data points? In this regard, you must notice whether you are looking at a correlation on linear or logarithmic coordinates. Errors usually appear smaller than they really are on logarithmic coordinates. Compare, for example, the data of Figs. 8.3 and 8.10.

- Am I looking at a primary or secondary source (i.e., is this the author's original presentation or someone's report of the original)? If it is a secondary source, have I been given enough information to question the result given? This matter is particularly important when using the Internet for information.

- Has the correlation been signed *by the persons who formulated it*? Has it been subjected to critical review by independent experts in the field?

- What nuisance variables might make our systems different? Consider, for example, surface roughness, fluid purity, problems of surface wetting, or strong vibrations and pressure fluctuations.

Problems

7.1 Prove that in fully developed laminar flow in a circular pipe, the quantity $(-dp/dx)R^2/4\mu$ is twice the average velocity. To do this, set the mass flow rate through the pipe equal to (ρu_{av})(area).

7.2 A flow of air at $27°C$ and 1 atm is hydrodynamically fully developed in a 1 cm I.D. pipe with $u_{av} = 2$ m/s. Plot (to scale) T_w, q_w, and T_b as a function of the distance x after the point where: (a) T_w is changed to $68.4°C$; or (b) q_w is set to 378 W/m^2. Indicate x_{e_t} on your graphs.

7.3 Prove that $C_f = 16/\text{Re}_D$ in fully developed laminar flow in a circular pipe.

7.4 Air at 200°C flows at 4 m/s perpendicular to a 3 cm O.D. pipe that is kept at 240°C. (a) Find $\overline{h}$. (b) If the air were replaced with pressurized water at 200°C, what velocities would give the same $\overline{\text{Nu}}_D$ or the same Re_D? (c) If someone wanted to model the water flow with an air experiment, would you see any problem in doing so? [$u_\infty = 0.0156$ m/s for same $\overline{\text{Nu}}_D$.]

7.5 Compare the h value calculated in Example 7.3 with those calculated from the Dittus-Boelter, Colburn, McAdams, and Sieder-Tate equations. Comment on the comparison.

7.6 Water at $T_{b_{\text{local}}} = 10$°C flows in a 3 cm I.D. pipe at 10 m/s. The pipe walls are kept at 70°C and the flow is fully developed. Evaluate h and the local value of dT_b/dx at the point of interest. The relative roughness, ε/D, is 0.006.

7.7 Water at 10°C flows perpendicular to a 3 cm O.D. cylinder at 70°C. The velocity is 1 m/s. Evaluate $\overline{h}$. [6 kW/m²K]

7.8 Consider the hot wire anemometer in Example 7.8. Suppose that the heat input is constant at 17.8 W/m and plot u_∞ vs. T_{wire} for flow speeds that can be considered incompressible (Mach number below 0.3).

7.9 Water at 20°C flows at 2 m/s over a 2 m length of 35 mm O.D. pipe. Water at 60°C flows inside the pipe at the same speed. Compare $\overline{h}$ for flow normal to the pipe with that for flow inside the pipe, assuming fully developed flow. If the pipe is copper with a wall thickness of 1.4 mm, what is the overall heat transfer coefficient? Which is the largest of the three thermal resistances?

7.10 A thermally fully developed flow of NaK in a 5 cm I.D. pipe moves at $u_{\text{av}} = 8$ m/s. Is the flow laminar or turbulent? At a location where $T_b = 395$°C and $T_w = 403$°C, what are the local heat transfer coefficient and heat flux?

7.11 Water enters a smooth walled, 7 cm I.D. pipe at 5°C at a bulk velocity of 0.86 m/s. The pipe wall is kept at 73°C by low pressure steam condensing outside. Plot T_b against the position in the pipe

until $(T_w - T_b)/68 = 0.01$. Neglect the entry length, but consider property variations. *Hint:* Use a spreadsheet.

7.12 Air at 20°C flows over a very large bank of 2 cm O.D. tubes that are kept at 100°C. The air approaches at an angle 15° off normal to the tubes. The tube array is staggered, with $S_L = 3.5$ cm and $S_T = 2.8$ cm. Find $\bar{h}$ on the first tubes and on the tubes deep in the array if the air velocity is 4.3 m/s before it enters the array. $[\bar{h}_{\text{deep}} = 136 \text{ W/m}^2\text{K}]$

7.13 Rework Problem 7.11 using a single value of $\bar{h}$ evaluated at $5 + \frac{3}{4}(73 - 5) = 56°C$ and treating the pipe as a heat exchanger. At what length would you judge that the pipe is no longer efficient as an exchanger? Explain.

7.14 Find a heat transfer journal and look up any correlation of heat transfer data. Evaluate the applicability of that correlation according to the criteria outlined in Section 7.7.

7.15 Water at 24°C flows at 0.8 m/s in a smooth, 1.5 cm I.D. tube that is kept at 30°C. The system is extremely clean and quiet, and the flow stays laminar until a noisy air compressor is turned on in the laboratory. Vibrations cause the flow to abruptly go turbulent. Calculate the ratio of the turbulent h to the laminar h. $[h_{\text{turb}} = 4430 \text{ W/m}^2\text{K}]$

7.16 In a laboratory experiment, air flows at 27°C over a bluff body, 12 cm wide, held at 77°C. The measured heat flux is 646 W/m^2 when the air moves at 2 m/s and 3590 W/m^2 at 18 m/s. In a second test, everything else is the same, but now 17°C water at 0.4 m/s is used, giving $q_w = 131,000$ W/m^2. The correlations in Chapter 7 suggest that, with such limited data, we can probably create a correlation in the form: $\overline{\text{Nu}}_L = C\text{Re}^a\text{Pr}^b$. Estimate the constants C, a, and b. One easy way to do this is by cross-plotting the data on log-log coordinates.

7.17 Air at 1.38 MPa (200 psia) flows at 12 m/s in an 11 cm I.D. duct. At one location, the bulk temperature is 40°C and the pipe wall is at 268°C. Evaluate h if $\varepsilon/D = 0.002$. $[h = 397 \text{ W/m}^2\text{K}]$

7.18 How does $\bar{h}$ during cross flow over a cylindrical heater vary with the diameter when Re_D is very large?

7.19 Air enters a 0.8 cm I.D. tube at 20°C with an average velocity of 0.8 m/s. The tube wall is kept at 40°C. Plot $T_b(x)$ until it reaches 39°C. Use properties evaluated at $[(20 + 40)/2]$°C for the whole problem, but report the local error in h at the end to get a sense of the error incurred using constant properties.

7.20 Write Re_D in terms of $\dot{m}$ in pipe flow and explain why this representation could be particularly useful in dealing with compressible pipe flows. How will Re_D vary in an isothermal gas flow as the pressure drops?

7.21 NaK at 394°C flows at 0.57 m/s normal to a 1.82 m length of 0.036 m O.D. tube. The tube is kept at 404°C. Find $\overline{h}$ and the heat removal rate from the tube. [25.3 kW]

7.22 Verify the value of h specified in Problem 3.22.

7.23 Compare the value of h given in Example 7.3 the value obtained using the Reynolds-Colburn analogy in the form of eqn. (7.37). By what percentage do these values differ?

7.24 A homemade heat exchanger consists of a copper plate, 0.5 m square, with twenty 1.5 cm I.D. copper tubes soldered to it. The ten tubes on top are evenly spaced across the top and parallel with two sides. The ten on the bottom are also evenly spaced, but they run at 90° to the top tubes. The exchanger is used to cool methanol flowing through the top tubes at 0.48 m/s from an initial temperature of 73°C, using water in the bottom tubes flowing at 0.91 m/s and entering at 7°C. What is the temperature of the methanol when it is mixed in a header on the outlet side? Do you think that this heat exchanger is designed well? [$T_{\mathrm{meth,out}} \simeq 65$°C]

7.25 Use the continuity equation to show that $\partial u/\partial x = 0$ in a circular pipe implies that the radial velocity $v = 0$. Also show that $v = 0$ implies that $\partial u/\partial x = 0$. *Hint*: You will need to look up the divergence operator in cylindrical coordinates.

7.26 Report the maximum percentage scatter of the data in Fig. 7.14. What is happening in the fluid flow in the range for which the scatter is worst?

7.27 Water at 27°C flows at 2.2 m/s in a 0.04 m I.D. thin-walled copper pipe. Air at 227°C flows across it at 7.6 m/s. Find the pipe wall temperature. [$T_{\mathrm{pipe}} = 28$°C]

7.28 Freshly painted aluminum rods, 0.02 m in diameter, are withdrawn from a drying oven at 150°C and cooled in a 3 m/s cross flow of air at 23°C. How long will it take to cool them to 40°C so they can be handled? [10.4 min.]

7.29 At what speed, u_∞, must 20°C air flow across the following insulated tube before the insulation on it will do any good? The tube is at 60°C and is 6 mm in diameter. The insulation is 12 mm in diameter, with $k = 0.08$ W/m·K. (Notice that we do *not* ask for the u_∞ for which the insulation will do the most harm, as discussed in Example 2.6) [5 cm/s]

7.30 Water at 37°C flows at 3 m/s across at 6 cm O.D. tube that is held at 97°C. In a second configuration, 37°C water flows at an average velocity of 3 m/s through a bundle of 6 cm O.D. tubes that are held at 97°C. The bundle is staggered, with $S_T/S_L = 2$. Compare the heat transfer coefficients for the two situations.

7.31 A very old air cooler was designed to chill 64°C air flowing at $u_{av} = 30$ m/s, fully developed, in a 1 m length of 8 cm I.D. smooth, highly conducting tubing. The refrigerant was the now-banned Freon 12 flowing in the opposite direction at $u_{av} = 0.5$ m/s, within eight smooth 1 cm I.D. tubes equally spaced around the outside of the large tube. The Freon entered at -15°C and was fully developed over almost the entire length. Determine the exiting air temperature, assuming that solder provides perfect thermal contact between the small tubes and the large tube and ignoring conduction resistance in the tube walls. Criticize the heat exchanger and propose a better design.

7.32 Calculate $\overline{Nu}_D$ directly from Giedt's data in Fig. 7.13 for air flowing over a cylinder at $Re_D = 140,000$. Compare your result with the appropriate correlation and with Fig. 7.14.

7.33 A 25 mph wind blows across a 0.25 in. (6.35 mm) telephone wire. What is the musical note for the pitch of the hum that it emits? *Hint:* The note could comfortably be sung by many adult men.

7.34 A large Nichrome V slab, 0.2 m thick, has two parallel 1 cm I.D. holes drilled through it. Their centers are 8 cm apart. One carries liquid CO_2 at 1.2 m/s from a -13°C reservoir below. The other carries methanol at 1.9 m/s from a 47°C reservoir above. Take

account of the intervening Nichrome and compute the heat transfer rate. Will the CO_2 be significantly warmed by the methanol? *Hint:* Recall Table 5.4.

7.35 Consider the situation described in Problem 4.37 but suppose that we do not know $\overline{h}$. Suppose, instead, that we know there is a 10 m/s cross flow of 27°C air over the rod. Rework the problem under these conditions. [The temperature is about 11°C lower]

7.36 A liquid whose properties are not known flows across a 40 cm O.D. tube at 20 m/s. The measured heat transfer coefficient is 8000 W/m^{2}K. We can be confident that Re$_D$ is very large indeed. What would $\overline{h}$ be if D were 53 cm? What would $\overline{h}$ be if u_∞ were 28 m/s? *Hint:* Work Problem 7.18. [11.2 kW/m^2]

7.37 Water flows at 4 m/s, at a temperature of 100°C, in a 6 cm I.D. thin-walled tube with a 2 cm layer of 85% magnesia insulation on it. The outside heat transfer coefficient is 6 W/m^{2}K, and the outside temperature is 20°C. Find: (a) U based on the inside area; (b) Q W/m; and (c) the temperature on either side of the insulation. How significant is the thermal resistance of forced convection? [$Q = 47.3$ W/m]

7.38 Glycerin is added to water in a mixing tank at 20°C. The mixture discharges through a 4 m length of 0.04 m I.D. tubing under a constant 3 m head. Plot the discharge rate in m^3/hr as a function of the percentage of glycerin in the mixture (see Table A.3). *Hint:* Remember to include the velocity head of the jet leaving the tube.

7.39 Plot $\overline{h}$ as a function of the percentage of glycerin for the discharge pipe in Problem 7.38. Assume a small temperature difference.

7.40 Rework Problem 5.40 without assuming Bi to be very large.

7.41 Water enters a 0.5 cm I.D. pipe at 24°C. The pipe walls are held at 30°C. Plot T_b against distance from entry if u_{av} is 0.27 m/s, neglecting entry behavior in your calculation. Indicate the entry region on your graph, however.

7.42 Devise a numerical method to find the velocity distribution and friction factor for laminar flow in a square duct of side length a. Set up a square grid of size N by N and solve the finite difference

equations by hand for $N = 2$, 3, and 4. *Hint*: First show that the velocity distribution is given by the solution to the equation

$$\frac{\partial^2 \overline{u}}{\partial \overline{x}^2} + \frac{\partial^2 \overline{u}}{\partial \overline{y}^2} = 1$$

where $u = 0$ on the sides of the square and we define $\overline{x} = (x/a)$, $\overline{y} = (y/a)$, and $\overline{u} = u/[(a^2/\mu)(dp/dz)]$. Then show that the friction factor, f [eqn. (7.34)], is given by

$$f = \frac{-2}{\dfrac{\rho u_{av} a}{\mu} \displaystyle\iint \overline{u}\, d\overline{x} d\overline{y}}$$

Note that the double integral can be evaluated as $\sum_{i,j=1}^{N}(\overline{u}_{i,j}/N^2)$.

7.43 Chilled air at $15°C$ and 1 m/s enters a horizontal duct. The duct is made of thin galvanized steel and is not insulated. A 30 m section of the duct runs outdoors through humid air at $30°C$. Condensation on the outside of the duct is undesirable, but will occur if the duct wall is at or below the dew point temperature of $20°C$.

   a. Suppose that the duct's square cross-section is 0.3 m by 0.3 m and the effective outside heat transfer coefficient is 5 W/m^2K in still air. Determine whether condensation occurs.

   b. The single duct is replaced by four circular horizontal ducts, each 0.17 m in diameter. The ducts are parallel to one another in a vertical plane with a center-to-center separation of 0.5 m. Each duct is wrapped with a layer of fiberglass insulation 6 cm thick ($k_i = 0.04$ W/m·K) and carries air at the same inlet temperature and speed as before. If a 15 m/s wind blows perpendicular to the plane of the circular ducts, find the bulk temperature of the air exiting the ducts.

7.44 An x-ray *monochrometer* is a mirror that reflects only a single wavelength from a broadband beam of x-rays. Over 99% of the beam's energy arrives on other wavelengths and is absorbed, creating a high heat flux on the monochrometer's surface. Consider a monochrometer made from a silicon block 10 mm long and 3 mm by 3 mm in cross-section which absorbs 12.5 W/mm^2 over an elongated elliptical area of 6 mm^2 (a heat load of 75 W). To control the temperature, it is proposed to pump liquid nitrogen through

a circular channel bored down the center of the silicon block. The channel is 10 mm long and 1 mm in diameter. LN_2 enters the channel at 80 K and a pressure of 1.6 MPa ($T_{sat} = 111.5$ K). The entry to this channel is a long, straight passage of the same diameter.

    a. For what range of mass flow rates will the LN_2 have a bulk temperature rise of less than 1.5 K over the length of the channel?

    b. At your minimum flow rate, estimate the maximum wall temperature in the channel. As a first approximation, assume that the silicon conducts heat well enough to distribute the 75 W heat load uniformly over the channel surface. Could boiling occur in the channel? Discuss the influence of entry length and variable property effects.

7.45 Fluctuating turbulent fluid velocities can be measured with a *constant temperature hot-wire anemometer*, in which a long, fine wire (typically platinum, 4 μm in diameter and 1.25 mm long) supported between two much larger needles. The needles are connected to an electronic bridge circuit which electrically heats the wire while rapidly adjusting the heating voltage, V_w, so that the wire's electrical resistance R_w—and thus its temperature—stays constant. The electrical power dissipated in the wire, V_w^2/R_w, is convected away at the surface of the wire. Analyze the heat loss from the wire to show

$$V_w^2 = (T_{wire} - T_{flow})\left(A + Bu^{1/2}\right)$$

where u is the instantaneous flow speed perpendicular to the wire. Assume that u is between 2 and 100 m/s and that the fluid is an isothermal gas. The constants A and B depend on properties, dimensions, and resistance; they are usually found through an experimental calibration. This result is called *King's law*.

7.46 Olive oil is pumped into a helical coil at 20°C and 0.3 kg/s. The coil is made of 1 cm I.D. copper tubing with a 1 mm wall thickness, and consists of ten turns with a diameter of 50 cm. The total length of tubing is 17 m. The coil is surrounded by a bath of water at 50°C, stirred so as to give an external heat transfer coefficient of 3000 W/m²K. (a) Determine the bulk temperature of the oil leaving the coil. (b) An engineer suggests raising the outlet temperature by adding fins to the coil. Is his suggestion a good one? Explain.

7.47 A film manufacturing process involves spraying an emulsion onto the surface of a polymer film and then curing the coating by raising its temperature. A proposed design will pass a continuous strip of coated film through an air tunnel. The film enters the right-hand side of the tunnel at 20°C and warm air enters the left-hand side at 60°C. The film surface needs to reach 40°C to cure properly, but must not exceed 55°C.

The film is 70 mm wide. The film has a thickness of 150 μm and moves at a speed of 40 mm/s. The coating may be taken to have the same properties as the film. The 0.5 m long air tunnel has the same width as the film and a height of 10 mm both above and below the film, for a total height of 20 mm. The tunnel walls are adiabatic and have a surface of bright aluminum ($\varepsilon \approx 0.15$). The coated film has the following properties: $k = 0.2$ W/m·K, $c_p = 1300$ J/kg·K, $\rho = 1380$ kg/m^3, and $\varepsilon \approx 0.9$.

   a. Suppose that the air enters at a bulk velocity of 0.5 m/s. Calculate the heat capacity rates of the air flow and of the film. Use this information to help you make a qualitative sketch of the bulk temperature distributions of the air and the film from one end of the tunnel to the other.

   b. Compare the speed of the film to the bulk velocity of the air. Does this suggest a reasonable simplification to use in estimating the heat transfer coefficient between the film and the air?

   c. What is the Biot number of the film based on its thickness? What does this tell you?

   d. Now calculate the outlet temperature of the film.

   e. How will raising the air speed to 4 m/s affect the performance? Estimate the resulting outlet temperature of the film.

7.48 (a) Show that the Reynolds number for a circular tube may be written in terms of the mass flow rate as $\mathrm{Re}_D = 4\dot{m}/\pi\mu D$. (b) Show that this result does not apply to a noncircular tube, specifically $\mathrm{Re}_{D_h} \neq 4\dot{m}/\pi\mu D_h$.

7.49 Go to Figs. 7.14, 8.3, 8.6, 9.7, and 9.13. In each case, pick out what seems to be the data point that differs most from the corresponding correlation. Scale the distances between the point and the curve and report the percentage by which the correlation differs from each of your selected data points.

7.50 Air flows in a 10 mm I.D. tube at 2 m/s and 57°C. At a location where the flow is fully developed, the wall temperature drops to 27°C. (a) What is the bulk temperature 200 mm downstream of the drop? (b) Plot the heat transfer coefficient along the 200 mm tube length. On the same graph, plot the h for the same velocity and temperatures over a 200 mm long flat plate. $[T_b = 44.3°C]$

7.51 Consider the water-cooled annular resistor of Problem 2.49 (Fig. 2.24). The resistor is 1 m long and dissipates 9.4 kW. Water enters the inner pipe at 47 °C with a mass flow rate of 0.39 kg/s. The water passes through the inner pipe, then reverses direction and flows through the outer annular passage, counter to the inside stream.

  a. Determine the bulk temperature of water leaving the outer passage. [52.8°C]

  b. Solve Problem 2.49 if you have not already done so. Compare the thermal resistances between the resistor and each water stream, R_i and R_o.

  c. Use the thermal resistances to form differential equations for the streamwise (x-direction) variation of the inside and outside bulk temperatures ($T_{b,o}$ and $T_{b,i}$) and an equation the local resistor temperature. Use your equations to obtain an equation for $T_{b,o} - T_{b,i}$ as a function of x.

  d. Sketch qualitatively the distributions of bulk temperature for both passages and for the resistor. Discuss the size of: the difference between the resistor and the bulk temperatures; and overall temperature rise of each stream. Does the resistor temperature change much from one end to the other?

  e. Your boss suggests roughening the inside surface of the pipe to an equivalent sand-grain roughness of 500 μm. Would this change lower the resistor temperature significantly?

  f. If the outlet water pressure is 1 bar, will the water boil? *Hint:* See Problem 2.48.

  g. Solve your equations from part (c) to find $T_{b,i}(x)$ and $T_r(x)$. Arrange your results in terms of $NTU_o \equiv 1/(\dot{m}c_p R_o)$ and $NTU_i \equiv 1/(\dot{m}c_p R_i)$. Considering the size of these parameters, assess the approximation that T_r is constant in x.

References

[7.1] F. M. White. *Viscous Fluid Flow*. McGraw-Hill Book Company, New York, 1974.

[7.2] S. S. Mehendale, A. M. Jacobi, and R. K. Shah. Fluid flow and heat transfer at micro- and meso-scales with application to heat exchanger design. *Appl. Mech. Revs.*, **53**(7):175–193, 2000. doi: 10.1115/1.3097347.

[7.3] W. M. Kays, M. E. Crawford, and B. Weigand. *Convective Heat and Mass Transfer*. McGraw-Hill Book Company, New York, 4th ed., 2005.

[7.4] R. K. Shah and M. S. Bhatti. Laminar convective heat transfer in ducts. In S. Kakaç, R. K. Shah, and W. Aung, editors, *Handbook of Single-Phase Convective Heat Transfer*, Chapter 3. Wiley-Interscience, New York, 1987.

[7.5] R. K. Shah and A. L. London. *Laminar Flow Forced Convection in Ducts*. Academic Press, Inc., New York, 1978. doi: 10.1016/C2013-0-06152-X. Supplement 1 to the series *Advances in Heat Transfer*.

[7.6] L. Graetz. Über die wärmeleitungfähigkeit von flüssigkeiten. *Ann. Phys.*, **261**(7):337–357, 1885. doi: 10.1002/andp.18852610702. url: https://archive.org/details/bub_gb_qwcAAAAAMAAJ/page/n347.

[7.7] S. R. Sellars, M. Tribus, and J. S. Klein. Heat transfer to laminar flow in a round tube or a flat plate—the Graetz problem extended. *Trans. ASME*, **78**(2):441–448, February 1956. doi: 10.1115/1.4013701.

[7.8] H. D. Baehr and K. Stephan. *Heat and Mass Transfer*. Springer-Verlag, Berlin, 1998.

[7.9] M. S. Bhatti and R. K. Shah. Turbulent and transition flow convective heat transfer in ducts. In S. Kakaç, R. K. Shah, and W. Aung, editors, *Handbook of Single-Phase Convective Heat Transfer*, Chapter 4. Wiley-Interscience, New York, 1987.

[7.10] F. Kreith. *Principles of Heat Transfer*. Intext Press, Inc., New York, 3rd ed., 1973.

[7.11] A. P. Colburn. A method of correlating forced convection heat transfer data and a comparison with fluid friction. *Trans. Amer. Inst. Chem. Engrs.*, **29**:174–206, 1933. The doi is for a 1964 reprint in *IJHMT*. doi: 10.1016/0017-9310(64)90125-5.

[7.12] E. C. Koo. *Mechanisms of isothermal and non-isothermal flow of fluids in pipes*. Sc.D. thesis, Massachusetts Institute of Technology, Cambridge, 1932. url: http://hdl.handle.net/1721.1/61824.

[7.13] L. M. K. Boelter, V. H. Cherry, H. A. Johnson, and R. C. Martinelli. *Heat Transfer Notes*. McGraw-Hill Book Company, New York, 1965.

[7.14] W. H. McAdams. *Heat Transmission*. McGraw-Hill, New York, 1933.

[7.15] E. N. Sieder and G. E. Tate. Heat transfer and pressure drop of liquids in tubes. *Ind. Eng. Chem.*, **28**(12):1429–1435, December 1936. doi: doi.org/10.1021/ie50324a027.

[7.16] V. Gnielinski. New equations for heat and mass transfer in turbulent pipe and channel flow. *Int. Chemical Engineering*, **16**:359–368, 1976. The doi is for the German language version. doi: 10.1007/BF02559682.

[7.17] B. S. Petukhov. Heat transfer and friction in turbulent pipe flow with variable physical properties. In T.F. Irvine, Jr. and J. P. Hartnett, editors, *Advances in Heat Transfer*, Vol. 6, pp. 504–564. Academic Press, Inc., New York, 1970. doi: 10.1016/S0065-2717(08)70153-9.

[7.18] G. K. Filonenko. Hydraulic resistance in pipes. *Teploenergetika*, **1**(4): 40–44, 1954.

[7.19] J. McGovern. Friction factor diagrams for pipe flow. Technical note, Dublin Institute of Technology, October 2011. url: https://arrow.dit.ie/engschmecart/28/.

[7.20] L. F. Moody. Friction factors for pipe flow. *Trans. ASME*, **66**(8):671–684, November 1944. doi: https://doi.org/10.1115/1.4018140.

[7.21] D. M. McEligot. Convective heat transfer in internal gas flows with temperature-dependent properties. In A. S. Majumdar and R. A. Mashelkar, editors, *Advances in Transport Processes*, Vol. IV, pp. 113–200. Wiley, New York, 1986.

[7.22] M. F. Taylor. Prediction of friction and heat-transfer coefficients with large variations in fluid properties. Technical Memorandum X-2145, NASA, Washington, D.C., December 1970. url: http://hdl.handle.net/2060/19710004556.

[7.23] S. E. Haaland. Simple and explicit formulas for the friction factor in turbulent pipe flow. *J. Fluids Engr.*, **105**(1):89–90, March 1983. doi: 10.1115/1.3240948.

[7.24] T. S. Ravigururajan and A. E. Bergles. Development and verification of general correlations for pressure drop and heat transfer in single-phase turbulent flow in enhanced tubes. *Exptl. Thermal Fluid Sci.*, **13**:55–70, July 1996. doi: 10.1016/0894-1777(96)00014-3.

[7.25] R. L. Webb. Enhancement of single-phase heat transfer. In S. Kakaç, R. K. Shah, and W. Aung, editors, *Handbook of Single-Phase Convective Heat Transfer*, Chapter 17. Wiley-Interscience, New York, 1987.

[7.26] C. Amy, D. Budenstein, M. Bagepalli, D. England, F. DeAngelis, G. Wilk, C. Jarrett, C. Kelsall, J. Hirschey, H. Wen, A. Chavan, B. Gilleland, C. Yuan, W. C. Chueh, K. H. Sandhage, Y. Kawajiri, and A. Henry. Pumping liquid metal at high temperatures up to 1,673 kelvin. *Nature*, **550**:199–203, October 2017. url: https://doi.org/10.1038/nature24054.

[7.27] C. Amy, H. R. Seyf, M. A. Steiner, D. J. Friedman, and A. Henry. Thermal energy grid storage using multi-junction photovoltaics. *Energy Environ. Sci.*, **12**:334–343, 2019. doi: 10.1039/C8EE02341G. url: http://doi.org/10.1039/C8EE02341G.

[7.28] B. Lubarsky and S. J. Kaufman. Review of experimental investigations of liquid-metal heat transfer. Report NACA-TR-1270, NACA Lewis Flight Propulsion Lab., Cleveland, OH, January 1956. url: http://hdl.handle.net/2060/19930091001.

[7.29] R. N. Lyon, editor. *Liquid Metals Handbook.* A.E.C. and Dept. of the Navy, Washington, D.C., 1952. url: https://babel.hathitrust.org/cgi/pt?id=umn.31951t002544483.

[7.30] R. A. Seban and T. T. Shimazaki. Heat transfer to a fluid flowing turbulently in a smooth pipe with walls at a constant temperature. *Trans. ASME*, **73** (6):803–907, August 1951. doi: 10.1115/1.4016437.

[7.31] E. Skupinski, J. Tortel, and L. Vautrey. Determination des coefficients de convection d'un alliage sodium-potassium dans un tube circulaire. *Int. J. Heat Mass Transfer*, **8**(6):937–951, June 1965. doi: 10.1016/0017-9310(65)90077-3.

[7.32] V. I. Subbotin, A. K. Papovyants, P. L. Kirillov, and N. N. Ivanovskii. A study of heat transfer to molten sodium in tubes. *Soviet J. Atomic Energy*, **13**(4):991–994, June 1963. doi: 10.1007/BF01480861.

[7.33] H. A. Johnson, J. P. Hartnett, and W. J. Clabaugh. Heat transfer to molten lead-bismuth eutectic in turbulent pipe flow. *Trans. ASME*, **75**(6):1191–1198, August 1953. doi: 10.1115/1.4015579.

[7.34] V. I. Subbotin, P.A. Ushakov, B. N. Gabrianovich, V. D. Taranov, and I. P. Sviridenko. Heat transfer to liquid metals in round tubes. *J. Engineering Physics*, **6**(4):19–27, 1963.

[7.35] J. Pacio, L. Marocco, and T. Wetzel. Review of data and correlations for turbulent forced convective heat transfer of liquid metals in pipes. *Heat Mass Transfer*, **51**:153–164, 2015. doi: 10.1007/s00231-014-1392-3.

[7.36] D. Taler. Semi-empirical heat transfer correlations for turbulent tube flow of liquid metals. *Int. J. Numerical Methods for Heat & Fluid Flow*, **28** (1):151–172, 2018. doi: 10.1108/HFF-09-2017-0367.

[7.37] S.-L. Lee. Liquid metal heat transfer in turbulent pipe flow with uniform wall heat flux. *Int. J. Heat Mass Transfer*, **26**(3):349–356, March 1983. doi: 10.1016/0017-9310(83)90039-X.

[7.38] Nuclear Energy Agency. Handbook on lead-bismuth eutectic alloy and lead properties, materials compatibility, thermal-hydraulics and technologies. NEA No. 7268, Organisation for Economic Co-operation and Development, Paris, August 2015. url: https://www.oecd-nea.org/science/pubs/2015/7268-lead-bismuth-2015.pdf.

[7.39] J. H. Lienhard. Synopsis of lift, drag, and vortex frequency data for rigid circular cylinders. Bulletin 300, Wash. State Univ., Pullman, WA, 1966. url: http://www.uh.edu/engines/vortexcylinders.pdf.

[7.40] W. H. Giedt. Investigation of variation of point unit-heat-transfer coefficient around a cylinder normal to an air stream. *Trans. ASME*, **71**(4): 375–381, May 1949. doi: 10.1115/1.4017081.

[7.41] S. W. Churchill and M. Bernstein. A correlating equation for forced convection from gases and liquids to a circular cylinder in crossflow. *J. Heat Transfer*, **99**(2):300–306, May 1977. doi: 10.1115/1.3450685.

[7.42] S. Nakai and T. Okazaki. Heat transfer from a horizontal circular wire at small Reynolds and Grashof numbers—1 pure convection. *Int. J. Heat Mass Transfer*, **18**(3):387–396, March 1975. doi: 10.1016/0017-9310(75)90028-9.

[7.43] A. Žukauskas. Heat transfer from tubes in crossflow. In T.F. Irvine, Jr. and J. P. Hartnett, editors, *Advances in Heat Transfer*, Vol. 8, pp. 93–160. Academic Press, Inc., New York, 1972. doi: 10.1016/S0065-2717(08)70038-8.

[7.44] A. Žukauskas. Heat transfer from tubes in crossflow. In T. F. Irvine, Jr. and J. P. Hartnett, editors, *Advances in Heat Transfer*, Vol. 18, pp. 87–159. Academic Press, Inc., New York, 1987. doi: 10.1016/S0065-2717(08)70118-7.

[7.45] S. Kalish and O. E. Dwyer. Heat transfer to NaK flowing through unbaffled rod bundles. *Int. J. Heat Mass Transfer*, **10**(11):1533–1558, November 1967. doi: 10.1016/0017-9310(67)90006-3.

[7.46] M. S. El-Genk and T. M. Schriener. A review of experimental data and heat transfer correlations for parallel flow of alkali liquid metals and lead-bismuth eutectic in bundles. *Nucl. Eng. Des.*, **317**:199–219, June 2017. doi: 10.1016/j.nucengdes.2017.03.028.

[7.47] G. F. Hewitt, editor. *Heat Exchanger Design Handbook 2008*. Begell House, New York, 2008.

[7.48] S. Kakaç, R. K. Shah, and W. Aung, editors. *Handbook of Single-Phase Convective Heat Transfer*. Wiley-Interscience, New York, 1987.

[7.49] R. L. Webb and N.-H. Kim. *Principles of Enhanced Heat Transfer*. Taylor & Francis, New York, 2nd ed., 2005.

8. Natural convection in single-phase fluids and during film condensation

There is a natural place for everything to seek, as:
Heavy things go downward, fire upward, and rivers to the sea.

adapted from ***The Anatomy of Melancholy,*** **R. Burton, 1621**

8.1 Scope

The remaining convection processes that we deal with are largely gravity-driven. Unlike forced convection, in which the driving force is external to the fluid, these so-called natural convection processes are driven by body forces exerted directly within the fluid as the result of heating or cooling. Two such mechanisms are remarkably similar. They are *single-phase natural convection* and *film condensation.* Because these processes have so much in common, we deal with both mechanisms in this chapter. We develop the governing equations side by side in two brief opening sections. Then we treat each mechanism independently: convection in Sections 8.3 and 8.4, and condensation in Section 8.5.

Chapter 9 deals with other natural and forced convection heat transfer processes that involve phase change (beyond that which occurs in film condensation.) These include:

- *Nucleate boiling.* This heat transfer process is highly disordered as opposed to the processes described in this chapter.

- *Film boiling.* This process is so similar to film condensation that we can often just modify film condensation predictions.

- *Dropwise condensation.* This mode is analogous to nucleate boiling.
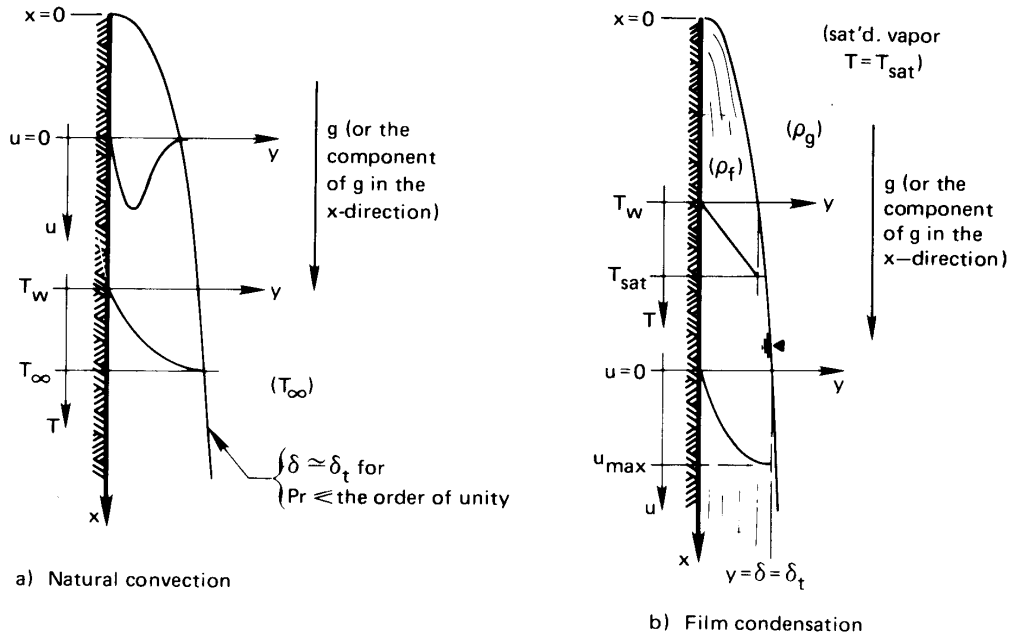
Figure 8.1 The convective boundary layers for natural convection and film condensation. In both sketches, but particularly in that for film condensation, the y-coordinate has been stretched making each layer look thicker than it really is.

8.2   The nature of film condensation and of natural convection

Description

The natural convection problem is sketched in its simplest form on the left-hand side of Fig. 8.1. Here a vertical isothermal plate cools the fluid adjacent to it. The cooled fluid becomes denser and sinks downward to form a b.l. The figure would be inverted if the plate were warmer than the fluid next to it. Then the fluid would buoy upward.

The corresponding film condensation problem is shown in its simplest form in Fig. 8.1b. An isothermal vertical plate cools an adjacent vapor, which condenses and forms a liquid film on the wall.[1] The film is normally

---

[1]Under certain circumstances, the condensate might instead form individual droplets, which roll off without forming into a film. This process is *dropwise condensation*. See Section 9.10.

very thin and flows rather like a b.l. as the figure suggests. While natural convection can carry fluid either upward or downward, condensate can move only downward. The temperature in the liquid film rises from T_w at the cool wall to the saturation temperature, T_{sat}, at the outer edge.

In both problems, but particularly in film condensation, the b.l. and the film are normally thin enough to accommodate the b.l. assumptions [recall the discussion following eqn. (6.13)]. A second feature of both problems is that δ and δ_t are closely related. In the condensing film they are equal, since the edge of the condensate film forms the edge of both b.l.'s. In natural convection, δ and δ_t are approximately equal when Pr is on the order of one or less, because all cooled (or heated) fluid must buoy downward (or upward). When Pr is large, not just the cooled (or heated) fluid will fall (or rise). Owing to its high viscosity, the buoyant fluid will also drag unheated fluid with it. In this case, δ can exceed δ_t. The analysis that follows below is for cases in which $\delta \cong \delta_t$.

Governing equations

To describe laminar film condensation and laminar natural convection, we must add a gravity term to the momentum equation. First we examine the dimensions of the terms in the momentum equation (6.13):

$$\left(u\frac{\partial u}{\partial x} + v\frac{\partial u}{\partial y} \right) \underbrace{\frac{m}{s^2}}_{= \frac{kg \cdot m}{kg \cdot s^2} = \frac{N}{kg}} = -\frac{1}{\rho}\frac{dp}{dx} \underbrace{\frac{m^3}{kg}\frac{N}{m^2 \cdot m}}_{= \frac{N}{kg}} + \nu\frac{\partial^2 u}{\partial y^2} \underbrace{\frac{m^2}{s}\frac{m}{s \cdot m^2}}_{= \frac{m}{s^2} = \frac{N}{kg}}$$

(8.1)

where $\partial p/\partial x \simeq dp/dx$ in the b.l. since the pressure does not vary with y, and where $\mu \simeq$ constant. Thus, every term in the equation has units of acceleration or (equivalently) force per unit mass. The component of gravity in the x-direction therefore enters the momentum balance as $+g$: both x and g point downward in Fig. 8.1. Gravity would enter as $-g$ if it acted opposite the x-direction.

$$u\frac{\partial u}{\partial x} + v\frac{\partial u}{\partial y} = -\frac{1}{\rho}\frac{dp}{dx} + g + \nu\frac{\partial^2 u}{\partial y^2}$$

(8.2)

The pressure gradient for both problems is the hydrostatic gradient outside the b.l. Thus,

$$\underbrace{\frac{dp}{dx} = \rho_\infty g}_{\substack{\text{natural} \\ \text{convection}}} \qquad \underbrace{\frac{dp}{dx} = \rho_g g}_{\substack{\text{film} \\ \text{condensation}}}$$

(8.3)

where ρ_∞ is the density of the undisturbed fluid and ρ_g (and ρ_f below) are the saturated vapor and liquid densities. Equation (8.2) then becomes

$$u\frac{\partial u}{\partial x} + v\frac{\partial u}{\partial y} = \left(1 - \frac{\rho_\infty}{\rho}\right)g + v\frac{\partial^2 u}{\partial y^2} \qquad \text{for natural convection} \qquad (8.4)$$

$$u\frac{\partial u}{\partial x} + v\frac{\partial u}{\partial y} = \left(1 - \frac{\rho_g}{\rho_f}\right)g + v\frac{\partial^2 u}{\partial y^2} \qquad \text{for film condensation} \qquad (8.5)$$

Two boundary conditions that apply to *both* problems are

$$\begin{aligned} u(y = 0) &= 0 & \text{the no-slip condition} \\ v(y = 0) &= 0 & \text{no flow into the wall} \end{aligned} \Big\} \qquad (8.6a)$$

The third b.c. is different for the film condensation and natural convection problems:

$$\left.\frac{\partial u}{\partial y}\right|_{y=\delta} = 0 \qquad \begin{array}{l}\text{condensation:} \\ \text{negligible shear at edge of film}\end{array}$$

$$u(y = \delta) = 0 \qquad \begin{array}{l}\text{natural convection:} \\ \text{undisturbed fluid outside the b.l.}\end{array} \left.\begin{array}{c} \\ \\ \\ \\ \end{array}\right\} \qquad (8.6b)$$

The energy equation for either of the two cases is eqn. (6.40):

$$u\frac{\partial T}{\partial x} + v\frac{\partial T}{\partial y} = \alpha\frac{\partial^2 T}{\partial y^2} \qquad (6.40)$$

We leave the identification of the b.c.'s for temperature until later.

The crucial fact to recognize is that the momentum equation is now linked to the energy equation. Let us consider how that occurs:

In natural convection: The velocity, u, is driven by buoyancy, which is reflected in the term $(1 - \rho_\infty/\rho)g$ in the momentum equation. The density, $\rho = \rho(T)$, varies with T, so it is impossible to solve the momentum and energy equations independently of one another.

In film condensation: The third boundary condition (8.6b) for the momentum equation involves the film thickness, δ. But to calculate δ we must make an energy balance on the film to find out how much latent heat—and thus how much condensate—it has absorbed. This will bring $(T_{\text{sat}} - T_w)$ into the solution of the momentum equation.

The boundary layer on a flat surface in forced convection was easy to analyze because the momentum equation could be solved completely before the energy equation was approached. We do not have that advantage in predicting either natural convection or film condensation.

8.3   Laminar natural convection on a vertical isothermal surface

Dimensional analysis and experimental data

Before we apply dimensional analysis to the natural convection problem, let us simplify the buoyancy term, $(1 - \rho_\infty/\rho)g$, in eqn. (8.4). We derived the equation for incompressible flow, but we modified it by admitting a small variation of density with temperature in this term only[2]. Now we will eliminate $(\rho - \rho_\infty)$ in favor of $(T - T_\infty)$ using the thermal expansion coefficient, β, where $\hat{v}$ is the specific volume:

$$\beta \equiv \frac{1}{\hat{v}} \left.\frac{\partial \hat{v}}{\partial T}\right|_p = -\frac{1}{\rho} \left.\frac{\partial \rho}{\partial T}\right|_p \simeq -\frac{1}{\rho} \frac{\rho - \rho_\infty}{T - T_\infty} = -\frac{(1 - \rho_\infty/\rho)}{T - T_\infty} \tag{8.7}$$

For liquids and saturated vapors, β should be evaluated with data from Appendix A. If the fluid is an ideal gas, β takes a very simple form

$$\beta = \frac{1}{\hat{v}} \frac{\partial}{\partial T} \left(\frac{RT}{p}\right)_p = \frac{1}{T} \qquad \text{for an ideal gas}$$

where R is the gas constant and T is the absolute temperature in K.

Figure 8.2 shows natural convection from a vertical surface, hotter than its surroundings. In this case, or the cold plate shown in Fig. 8.1a, we replace $(1 - \rho_\infty/\rho)g$ with $-g\beta(T - T_\infty)$. The sign of the substitution is the same in either case (see Fig. 8.2). However, the direction in which buoyancy acts will depend upon whether T is greater or less than T_∞ and on whether g acts in the $+x$ direction ($g > 0$) or the $-x$ direction ($g < 0$). Then the momentum equation, (8.4), becomes

$$u\frac{\partial u}{\partial x} + v\frac{\partial u}{\partial y} = -g\beta(T - T_\infty) + \nu\frac{\partial^2 u}{\partial y^2} \tag{8.8}$$

for the plate orientation in Fig. 8.1a, with g in the $+x$ direction. The density, ρ, has been eliminated, and the coupling of the momentum and energy equations is now very clear.

Dimensional analysis.   The functional equation for the heat transfer coefficient in natural convection is now (cf. Section 6.4)

$$h \text{ or } \overline{h} = \text{fn}(k, |T_w - T_\infty|, g\beta, \nu, \alpha, x \text{ or } L)$$

---

[2]The use of constant properties except for density in the buoyancy term is called the *Boussinesq approximation*, after Joseph Valentin Boussinesq (1842–1929).

$$-\frac{1}{\rho}\frac{dp}{dx} = \frac{1}{\rho}\rho_\infty g$$

$$-\frac{1}{\rho}\frac{dp}{dx} - g = -\left(1 - \frac{\rho_\infty}{\rho}\right)g$$

$$\simeq \beta g\,(T - T_\infty)$$

Gravity, g. When g is
directed against the
x-axis (downward in
this case), we take it
to be negative.
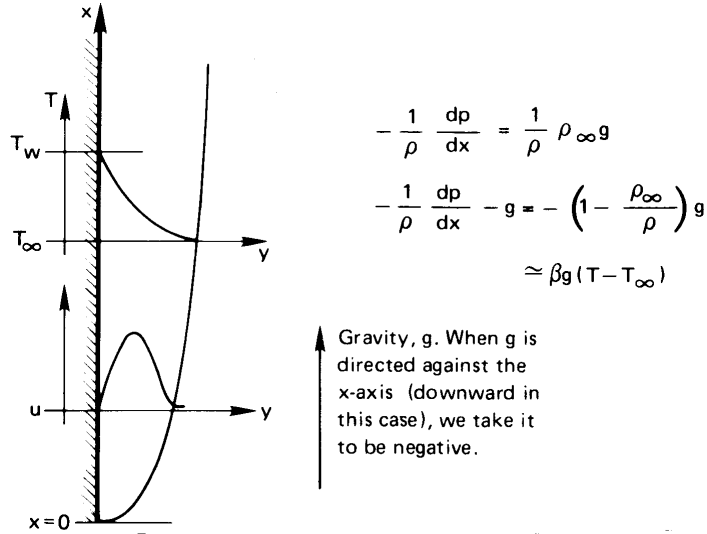
Figure 8.2 Natural convection from
a vertical heated plate.

where $g\beta$ only appears as a product in eqn. (8.8), and L is a length that must be specified for a given problem. Notice that, while we could take h to be independent of ΔT in the forced convection problem (Section 6.4), the explicit appearance of $(T - T_\infty)$ in eqn. (8.8) shows that we cannot do so here. The sign of $T_w - T_\infty$ should not matter to h or $\overline{h}$.

The functional equation has seven variables in W, m, s, and K (where we again regard J as a unit independent of N and m, since no conversion between heat and work takes place). We therefore seek $7 - 4 = 3$ pi-groups. Considering $\overline{h}$, with L a characteristic length and $\Delta T \equiv |T_w - T_\infty|$, the groups may be chosen as

$$\overline{\mathrm{Nu}}_L \equiv \frac{\overline{h}L}{k}, \qquad \mathrm{Pr} \equiv \frac{\nu}{\alpha}, \qquad \mathrm{Gr}_L \equiv \frac{g\beta\Delta T L^3}{\nu^2} \tag{8.9}$$

The third group is new to us: the Grashof (pronounced Gráhs-hoff) number, Gr_L, where the subscript denotes the length on which it is based.[3] We therefore expect to correlate natural convection data with functional equations of the form

$$\mathrm{Nu}_L = \mathrm{fn}(\mathrm{Gr}_L, \mathrm{Pr}) \tag{8.10}$$

The Grashof number can be interpreted by noticing that $g\beta\Delta T$ is the buoyancy force per unit mass on a parcel of fluid. Neglecting drag, if the

---

[3]Nu, Pr, and Gr were all suggested by Nusselt in his pioneering paper on convective heat transfer [8.1]. Grashof was a notable nineteenth-century mechanical engineering professor who was simply given the honor of having a dimensionless group named after him posthumously (see, e.g., [8.2]). He did not work on natural convection.

parcel accelerates under that force for a distance L, elementary dynamics shows that it will reach a speed $u = \sqrt{2g\beta\Delta TL}$. Thus, the Grashof number is proportional to $(uL/\nu)^2$, the square of a Reynolds number. In a laminar forced convection b.l., $Nu_L \propto Re_L^{1/2}$; so here, we might anticipate that $Nu_L \propto Gr_L^{1/4}$.

Another attribute of the dimensionless functional equation is that the most influential independent variable is usually the product of Gr_L and Pr. This product is called the Rayleigh number, Ra_L:

$$Ra_L \equiv Gr_L Pr = \frac{g\beta\Delta TL^3}{\alpha\nu} \tag{8.11}$$

Thus, most (but not all) analyses and correlations of natural convection take the form:

$$Nu = fn\big(\underbrace{Ra}, \underbrace{Pr}\big) \tag{8.12}$$

<div style="text-align:center">secondary parameter
most important
independent variable</div>

Comparison to data.   Figure 8.3 is a careful selection of high quality data for natural convection from vertical isothermal surfaces. These data were organized by Churchill and Chu [8.3], and they span 13 orders of magnitude of the Rayleigh number. The correlation of these data in the coordinates of Fig. 8.2 is exactly in the form of eqn. (8.12), and it shows the dominant influence of Ra_L, while the influence of Pr is smaller.

The data correlate on these coordinates within a few percent up to $Ra_L/[1 + (0.492/Pr^{9/16})]^{16/9} \simeq 10^8$. That is about where the b.l. starts exhibiting turbulent behavior. Beyond that point, measured values of the overall Nusselt number, $\overline{Nu}_L$, exhibit substantial scatter.

Churchill and Chu offered several equations for various circumstances. The one that best characterizes laminar natural convection from a vertical plate for $Ra_L \lesssim 10^9$ is:

$$\overline{Nu}_L = 0.68 + 0.670\, Ra_L^{1/4} \left[1 + \left(\frac{0.492}{Pr}\right)^{9/16}\right]^{-4/9} \tag{8.13a}$$

The form of this correlation is not at all accidental. Not only is it consistent with dimensional analysis, eqn. (8.12), but it also has the basic form of a classical theoretical prediction done independently by Squire [8.4] and by Eckert [8.5]. Churchill and Chu fitted the coefficients and Pr dependence
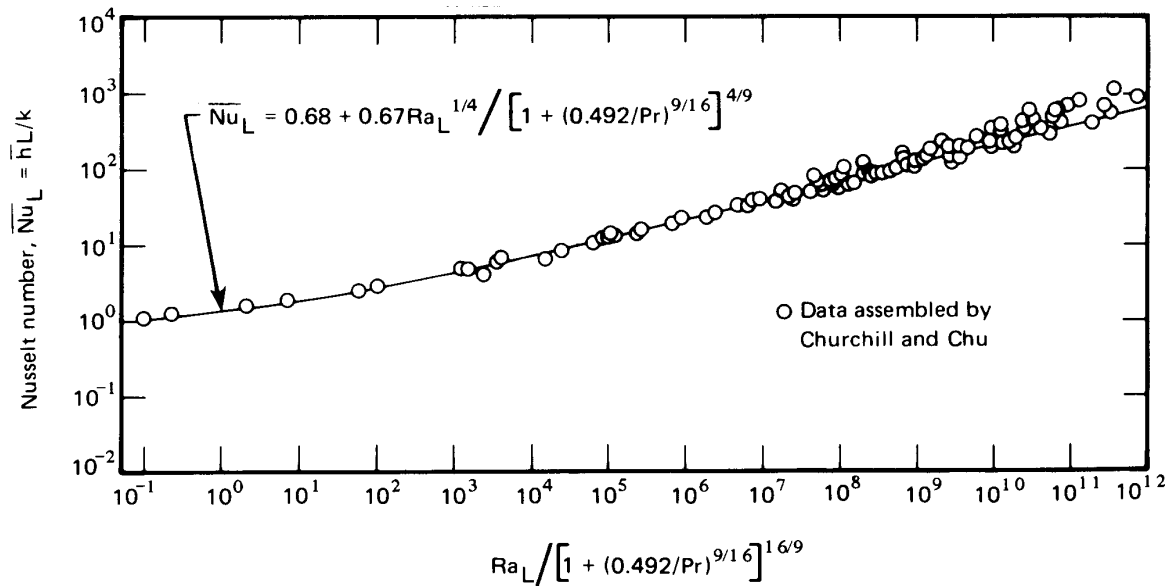
Figure 8.3 The correlation of $\overline{h}$ data for vertical isothermal surfaces by Churchill and Chu [8.3], using $Nu_L = fn(Ra_L, Pr)$. (Applies to full range of Pr.)

of the theory to experimental data from 13 independent studies with many different fluids. The added constant 0.68 accounts for very low values of Ra_L at which boundary layer behavior begins to break down.

Equation (8.13a) lies on the low side of the data after the boundary layer becomes turbulent at Rayleigh numbers[4] above 10^9. Churchill and Chu recommend the following equation to account for turbulence:

$$\overline{Nu}_L = \left\{ 0.825 + \frac{0.387 \ Ra_L^{1/6}}{\left[1 + (0.492/Pr)^{9/16}\right]^{8/27}} \right\}^2 \tag{8.13b}$$

This result can be used for all Ra_L and Pr, although eqn. (8.13a) is more accurate for laminar conditions.

Both eqns. (8.13a) and (8.13b) may be used for either uniform wall temperature or uniform heat flux. The properties should be evaluated at an average film temperature, $T_f = (T_\infty + T_w)/2$.

---

[4]Bejan and Lage [8.6] suggest that turbulent flow is more accurately assumed to occur for $Gr_L \gtrsim 10^9$.

Example 8.1

Verify the first heat transfer coefficient in Table 1.1. It is for air at 20°C next to a 0.30 m high wall at 50°C.

SOLUTION. At $T_f = 35°C = 308$ K, we find Pr = 0.710, $\nu = 1.643 \times 10^{-5}$ m^2/s, $\alpha = 2.315 \times 10^{-5}$ m^2/s, $k = 0.02672$ W/m·K, and $\beta = 1/(273 + 35) = 0.00325$ K^{-1}. Then

$$\mathrm{Ra}_L = \frac{g\beta\Delta TL^3}{\alpha\nu} = \frac{9.8(0.00325)(30)(0.30)^3}{(1.643)(2.315)10^{-10}} = 6.78 \times 10^7$$

The Churchill-Chu laminar correlation, eqn. (8.13a), gives

$$\overline{\mathrm{Nu}}_L = 0.68 + 0.67 \frac{(6.78 \times 10^7)^{1/4}}{\left[1 + (0.492/0.710)^{9/16}\right]^{4/9}} = 47.33$$

so

$$\overline{h} = 47.33 \left(\frac{0.02672}{0.30}\right) = 4.22 \text{ W/m}^2\text{K}$$

This value matches Table 1.1.   ∎

Example 8.2

Thin metal sheets of length L are dipped in an electroplating bath in the vertical position. Their initial average temperature, T_i, is cooler than the liquid in the bath. How rapidly will they come up to bath temperature, T_b?

SOLUTION. Because the metal is thin and conductive, we can probably take Bi $\ll 1$ and use the lumped-capacity response equation (1.20). We obtain $\overline{h}$ from eqn. (8.13a), assuming that $\overline{\mathrm{Nu}}_L$ is large enough to neglect the small added constant 0.68:

$$\overline{h} = \underbrace{0.67 \frac{k}{L}\left[1 + \left(\frac{0.492}{\mathrm{Pr}}\right)^{9/16}\right]^{-4/9}\left(\frac{g\beta L^3}{\alpha\nu}\right)^{1/4}}_{\text{call this } B} \Delta T^{1/4}$$

Since $\overline{h} \propto \Delta T^{1/4}$, with $\Delta T = T_b - T$, eqn. (1.20) becomes

$$\frac{d(T_b - T)}{dt} = -\frac{BA}{\rho cV}(T_b - T)^{5/4}$$

where V/A = the half-thickness of the plate, w. Integrating from time 0 to t, we get

$$\int_{T_i}^{T} \frac{d(T_b - T)}{(T_b - T)^{5/4}} = -\int_{0}^{t} \frac{B}{\rho c w} \, dt$$

so

$$T_b - T = \left[\frac{1}{(T_b - T_i)^{1/4}} + \frac{B}{4\rho c w} t \right]^{-4}$$

(Before we use this result, we should check Bi $= Bw\Delta T^{1/4}/k$ to be certain that it is, in fact, less than one.) The temperature can be put in dimensionless form as

$$\frac{T_b - T}{T_b - T_i} = \left[1 + \frac{B\,(T_b - T_i)^{1/4}}{4\rho c w} t \right]^{-4}$$

where the coefficient of t is a kind of inverse time constant of the response. Thus, the temperature dependence of $\overline{h}$ in natural convection leads to a solution quite different from the exponential response that resulted from a constant $\overline{h}$, eqn. (1.22).   ∎

Classical Squire-Eckert prediction of *h* in laminar natural convection on a vertical wall

The Squire-Eckert formulation, done in the 1930s, begins with the integrated momentum and energy equations. We will consider the case of a warm, vertical wall (Fig. 8.2) with gravity downward. We assume $\delta = \delta_t$ and integrate eqns. (8.8) and (6.40) to the same value of δ, yielding

$$\frac{d}{dx} \int_0^{\delta} \left(u^2 - \underbrace{u u_\infty}_{\substack{= 0, \text{ since} \\ u_\infty = 0}} \right) dy = -\nu \left. \frac{\partial u}{\partial y} \right|_{y=0} + g\beta \int_0^{\delta} (T - T_\infty) \, dy \quad (8.14)$$

for momentum, and, for energy,

$$\frac{d}{dx} \int_0^{\delta} u(T - T_\infty) \, dy = \frac{q_w}{\rho c_p} = -\alpha \left. \frac{\partial T}{\partial y} \right|_{y=0} \quad (6.47)$$

The integrated momentum equation is the same as eqn. (6.24) except that it includes the buoyancy term; and the sign of buoyancy term is opposite that in eqn. (8.8) because gravity acts in the $-x$ direction.

The approximation that the thermal b.l. thickness, δ_t, should be roughly equal to the momentum b.l. thickness, δ, would seemingly limit

the results to Prandtl numbers not too much larger than one. In fact, the analysis also proves to be accurate for large Pr because the velocity profile exerts diminishing influence on the temperature profile as Pr increases.

Velocity and temperature profiles.   To estimate the temperature and velocity profiles for use in eqns. (8.14) and (6.47), we proceed as we did in Sections 6.2 and 6.3 for forced convection. We write a set of known facts about the profiles, then use these facts to evaluate the constants in polynomial expressions for u and T.

Since the temperature profile has a fairly simple shape, we choose a simple quadratic expression:

$$\frac{T - T_\infty}{T_w - T_\infty} = a + b\left(\frac{y}{\delta}\right) + c\left(\frac{y}{\delta}\right)^2 \tag{8.15}$$

We require this profile to meet three boundary conditions:

- $T(y = 0) = T_w$ from which $1 = a$

- $T(y = \delta) = T_\infty$ from which $0 = 1 + b + c$

- $\left.\dfrac{\partial T}{\partial y}\right|_{y=\delta} = 0$ from which $0 = b + 2c$

Thus, $a = 1$, $b = -2$, and $c = 1$, giving following temperature profile:

$$\frac{T - T_\infty}{T_w - T_\infty} = 1 - 2\left(\frac{y}{\delta}\right) + \left(\frac{y}{\delta}\right)^2 = \left(1 - \frac{y}{\delta}\right)^2 \tag{8.16}$$

The velocity profile has a peak between 0 and δ (Fig. 8.1), so we will represent it with a cubic function:

$$u = u_c(x)\left[\left(\frac{y}{\delta}\right) + c\left(\frac{y}{\delta}\right)^2 + d\left(\frac{y}{\delta}\right)^3\right] \tag{8.17}$$

Since we do not know the peak velocity, we write u_c as an as-yet-unknown function of x: u_c will have to increase with x, since the flow accelerates as it rises. We know three boundary conditions for u:

- $u(y = 0) = 0$ $\begin{cases} \text{we have already satisfied this condition by} \\ \text{writing eqn. (8.17) with no lead constant} \end{cases}$

- $u(y = \delta) = 0$ or $0 = (1 + c + d)$

- $\left.\dfrac{\partial u}{\partial y}\right|_{y=\delta} = 0$ or $0 = u_c(1 + 2c + 3d)$

These conditions give $c = -2$ and $d = 1$, so

$$\frac{u}{u_c(x)} = \frac{y}{\delta}\left(1 - \frac{y}{\delta}\right)^2 \tag{8.18}$$

We could also have written the momentum equation (8.8) at the wall, where $u = v = 0$, and created a fourth condition:

$$\left.\frac{\partial^2 u}{\partial y^2}\right|_{y=0} = -\frac{g\beta(T_w - T_\infty)}{\nu}$$

Then we could have evaluated $u_c(x)$ as $g\beta(T_w - T_\infty)\delta^2/4\nu$. A correct expression for u_c will eventually depend upon these variables, but we will not attempt to make u_c fit this particular condition. Doing so would yield two equations, (8.14) and (6.47), in a single unknown, $\delta(x)$. It would be impossible to satisfy both of them. Instead, we allow the velocity profile to violate this condition slightly by writing

$$u_c(x) = C_1 \frac{g\beta(T_w - T_\infty)}{\nu} \delta^2(x) \tag{8.19}$$

Then we solve the *two* integrated conservation equations for the *two* unknowns, C_1 (which we expect will be close to ¼) and $\delta(x)$.

The dimensionless temperature and velocity profiles are plotted in Fig. 8.4. With them are included Schmidt and Beckmann's exact calculation for air (Pr = 0.7) from [8.4]. Notice that the approximation to the temperature profile is better than the approximation to the velocity profile. That is fortunate, since the temperature profile ultimately determines the heat transfer rate.

Solution of momentum and energy equations. When we substitute eqns. (8.16) and (8.18) in the momentum equation (8.14), using eqn. (8.19) for $u_c(x)$, we get

$$C_1^2\left(\frac{g\beta(T_w - T_\infty)}{\nu}\right)^2 \frac{d}{dx}\left[\delta^5 \underbrace{\int_0^1 \left(\frac{y}{\delta}\right)^2\left(1 - \frac{y}{\delta}\right)^4 d\left(\frac{y}{\delta}\right)}_{=1/105}\right]$$

$$= -C_1 g\beta(T_w - T_\infty)\delta \underbrace{\frac{\partial}{\partial(y/\delta)}\left[\frac{y}{\delta}\left(1 - \frac{y}{\delta}\right)^2\right]_{y/\delta=0}}_{=1}$$

$$+ g\beta(T_w - T_\infty)\delta \underbrace{\int_0^1 \left(1 - \frac{y}{\delta}\right)^2 d\left(\frac{y}{\delta}\right)}_{=1/3} \tag{8.20}$$
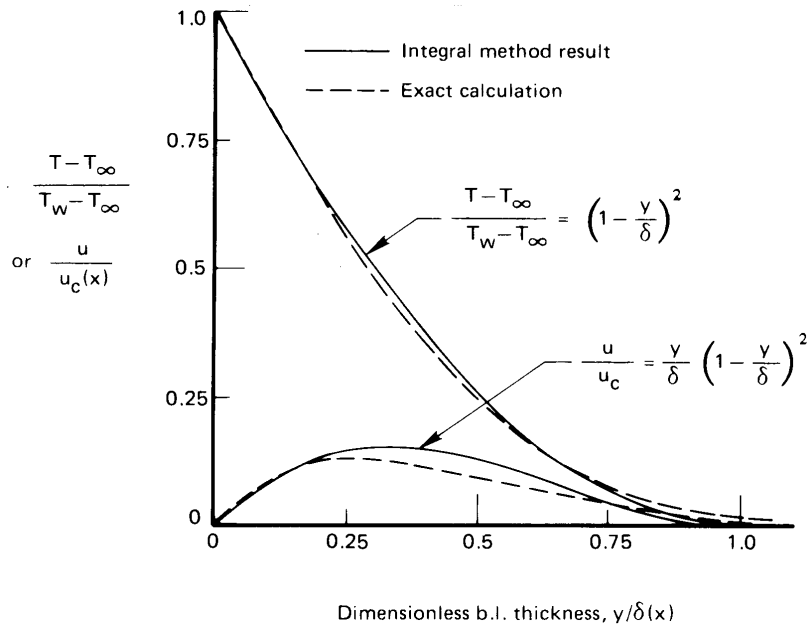
Figure 8.4 The temperature and velocity profiles for air in a laminar convection b.l. (Pr = 0.7)

Equation (8.20) then becomes

$$\left(\frac{1}{21} C_1^2 \frac{g\beta(T_w - T_\infty)}{\nu^2}\right) \delta^3 \frac{d\delta}{dx} = \frac{1}{3} - C_1$$

or

$$\frac{d\delta^4}{dx} = 84\left(\frac{1}{3} - C_1\right)\left(C_1^2 \frac{g\beta(T_w - T_\infty)}{\nu^2}\right)^{-1}$$

Integrating this with the b.c. $\delta(0) = 0$, gives

$$\delta^4 = 84\left(\frac{1}{3} - C_1\right)\left(C_1^2 \frac{g\beta(T_w - T_\infty)}{\nu^2}\right)^{-1} x \qquad (8.21)$$

Substituting eqns. (8.16), (8.18), and (8.19) in eqn. (6.47) likewise gives

$$(T_w - T_\infty)C_1 \frac{g\beta(T_w - T_\infty)}{\nu} \frac{d}{dx}\left[\delta^3 \underbrace{\int_0^1 \frac{y}{\delta}\left(1 - \frac{y}{\delta}\right)^4 d\left(\frac{y}{\delta}\right)}_{=1/30}\right]$$

$$= -\alpha \frac{T_w - T_\infty}{\delta} \underbrace{\frac{d}{d(y/\delta)}\left[\left(1 - \frac{y}{\delta}\right)^2\right]}_{=-2}{}_{y/\delta=0}$$

or

$$3 \frac{C_1}{30} \delta^3 \frac{d\delta}{dx} = \frac{C_1}{40} \frac{d\delta^4}{dx} = 2 \left(\mathrm{Pr} \frac{g\beta(T_w - T_\infty)}{\nu^2} \right)^{-1}$$

Integrating this with the b.c. $\delta(0) = 0$, we get

$$\delta^4 = 80 \left(C_1 \mathrm{Pr} \frac{g\beta(T_w - T_\infty)}{\nu^2} \right)^{-1} x \qquad (8.22)$$

By equating eqns. (8.21) and (8.22) for δ^4, we may solve for C_1:

$$C_1 = \frac{\mathrm{Pr}}{3 \left(\dfrac{20}{21} + \mathrm{Pr} \right)} \qquad (8.23)$$

Then, from eqn. (8.22):

$$\delta^4 = 240 \left(\frac{20}{21} + \mathrm{Pr} \right) \left(\mathrm{Pr}^2 \frac{g\beta(T_w - T_\infty)}{\nu^2} \right)^{-1} x$$

or

$$\frac{\delta}{x} = 3.936 \left(\frac{0.952 + \mathrm{Pr}}{\mathrm{Pr}^2} \right)^{1/4} \frac{1}{\mathrm{Gr}_x^{1/4}} \qquad (8.24)$$

Equation (8.24) can be combined with the known temperature profile, eqn. (8.16), and substituted in Fourier's law to find q:

$$q = -k \left. \frac{\partial T}{\partial y} \right|_{y=0} = -\frac{k(T_w - T_\infty)}{\delta} \underbrace{\left. \frac{d \left(\dfrac{T - T_\infty}{T_w - T_\infty} \right)}{d \left(\dfrac{y}{\delta} \right)} \right|_{y/\delta=0}}_{=-2} = 2 \frac{k\Delta T}{\delta} \quad (8.25)$$

so, writing $h = q/(T_w - T_\infty) \equiv q/\Delta T$, we obtain[5]

$$\mathrm{Nu}_x \equiv \frac{qx}{\Delta T k} = 2 \frac{x}{\delta} = \frac{2}{3.936} (\mathrm{PrGr}_x)^{1/4} \left(\frac{\mathrm{Pr}}{0.952 + \mathrm{Pr}} \right)^{1/4}$$

or

$$\mathrm{Nu}_x = 0.508 \, \mathrm{Ra}_x^{1/4} \left(\frac{\mathrm{Pr}}{0.952 + \mathrm{Pr}} \right)^{1/4} \qquad (8.26)$$

This result is the Squire-Eckert equation for the local heat transfer from a vertical isothermal wall during laminar natural convection. The result holds true for either $T_w > T_\infty$ or $T_w < T_\infty$.

---

[5]Recall that, on page 419, we speculated that Nu would vary as $\mathrm{Gr}^{1/4}$. Indeed, it does!

The average heat transfer coefficient can be obtained from

$$\overline{h} = \frac{\int_0^L q(x)\,dx}{L\Delta T} = \frac{\int_0^L h(x)\,dx}{L}$$

Thus,

$$\overline{\text{Nu}}_L = \frac{\overline{h}L}{k} = \frac{1}{k}\int_0^L \frac{k}{x}\,\text{Nu}_x\,dx = \frac{4}{3}\left.\text{Nu}_x\right|_{x=L}$$

or

$$\overline{\text{Nu}}_L = 0.678\,\text{Ra}_L^{1/4}\left(\frac{\text{Pr}}{0.952 + \text{Pr}}\right)^{1/4} \tag{8.27}$$

The Squire-Eckert equation lies within 1.2% of the Churchill-Chu correlation for large Ra_L and Pr, and it differs by only 5.5% if the fluid is a gas with $\text{Ra}_L > 10^5$. Typical Ra_L values are much higher than this, so the Squire-Eckert prediction is actually quite accurate in most cases of interest. The prediction fails at low Pr; and it is limited to laminar conditions, $\text{Ra}_L \lesssim 10^9$. Properties should be evaluated as described on page 420.

Example 8.3

A thin-walled metal tank containing fluid at 40°C cools in air at 14°C; $\overline{h}$ is very large inside the tank. If the sides are 0.40 m high, compute $\overline{h}$, $\overline{q}$, and δ at the top. Use the Squire-Eckert analysis to determine whether the b.l. assumptions are reasonable. Omit thermal radiation.

SOLUTION. All properties are evaluated at $T_f = 27°C$. Thus,

$$\beta_{\text{air}} = 1/T_f = 1/(273 + 27) = 0.00333 \text{ K}^{-1}$$
$$\text{Ra}_L = \frac{g\beta\Delta T L^3}{\nu\alpha} = \frac{9.8(0.00333)(40 - 14)(0.4)^3}{(1.578 \times 10^{-5})\,(2.213 \times 10^{-5})} = 1.555 \times 10^8$$

This corresponds to laminar flow. We may use eqn. (8.27), or eqn. (8.13a), with Pr = 0.713

$$\overline{\text{Nu}}_L = 0.678\left(1.555 \times 10^8\right)^{1/4}\left(\frac{0.713}{0.952 + 0.713}\right)^{1/4} = 61.25$$

so

$$\overline{h} = \frac{61.25(0.02623)}{0.40} = 4.02 \text{ W/m}^2\text{K}$$

and

$$\overline{q} = \overline{h}\,\Delta T = 4.02(40 - 14) = 104 \text{ W/m}^2$$

The b.l. thickness at the top of the tank is given by eqn. (8.24) at $x = L$:

$$\frac{\delta}{L} = 3.936 \left(\frac{0.952 + 0.713}{0.713^2}\right)^{1/4} \frac{1}{(\text{Ra}_L/\text{Pr})^{1/4}} = 0.0431$$

Thus, the b.l. thickness at the end of the plate is only 4% of the height, or 1.7 cm thick. This thickness exceeds typical forced convection b.l.'s, but it is still quite thin. ∎

Note on the validity of the boundary layer approximations

The boundary layer approximations are sometimes put to a rather severe test in natural convection problems. Thermal b.l. thicknesses are often fairly large, and the usual analyses that take the b.l. to be thin can be significantly in error. This is particularly true as Gr becomes small. Figure 8.5 includes three pictures that illustrate this. These pictures are interferograms (or in the case of Fig. 8.5c, data deduced from an interferogram). An interferogram is a photograph made in a kind of lighting that causes regions of uniform density to appear as alternating light and dark bands.

Figure 8.5a was made at the University of Kentucky by G.S. Wang and R. Eichhorn. The Grashof number based on the radius of the leading edge is 2250 in this case. This is low enough to result in a b.l. that is larger than the radius near the leading edge. Figure 8.5b and c are from Kraus's classic study of natural convection visualization methods [8.7]. Figure 8.5c shows that, at Gr = 585, the b.l. assumptions are quite unreasonable since the cylinder is small in comparison with the large region of thermal disturbance.

The analysis of free convection becomes a far more complicated problem at low Gr's, since the b.l. equations can no longer be used. We shall not discuss any of the numerical solutions of the full Navier-Stokes equations that have been carried out in this regime. We shall instead note that correlations of data using functional equations of the form

$$\text{Nu} = \text{fn}(\text{Ra}, \text{Pr})$$

will be the first thing that we resort to in such cases. Indeed, Fig. 8.3 reveals that Churchill and Chu's equation (8.13a) already serves this purpose in the case of the vertical isothermal plate, at low values of $\text{Ra} \equiv \text{Gr}\,\text{Pr}$.
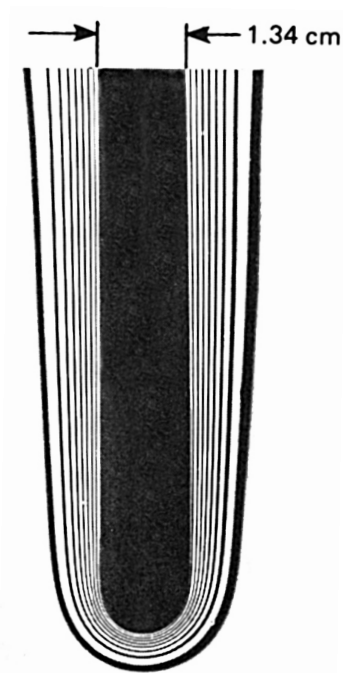
a. A 1.34 cm wide flat plate with a rounded leading edge in air. $T_w = 46.5°C$, $\Delta T = 17.0°C$, $Gr_{radius} \simeq 2250$
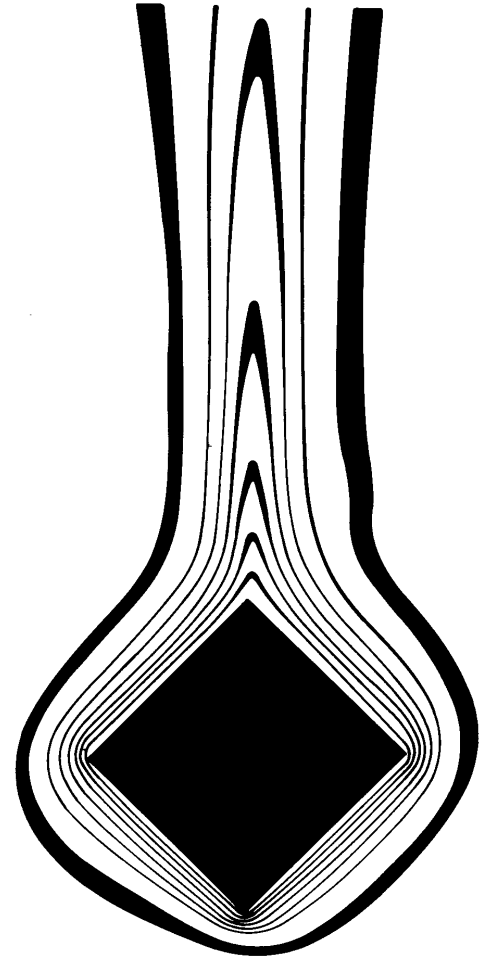
b. A square cylinder with a fairly low value of Gr. (Rendering of an interferogram shown in [8.7].)
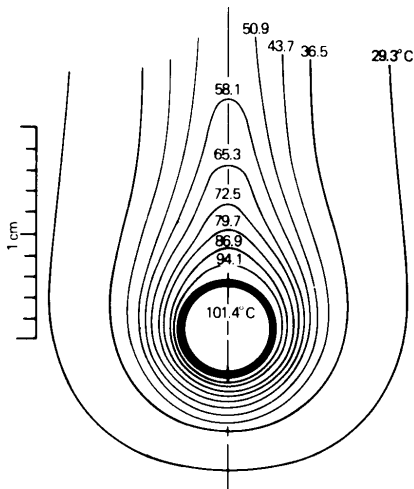
c. Measured isotherms around a cylinder in air when $Gr_D \approx 585$ (from [8.7]).

Figure 8.5 The thickening of the b.l. during natural convection at low Gr, as illustrated by interferograms made on two-dimensional bodies. (The dark lines in the pictures are isotherms.)

429
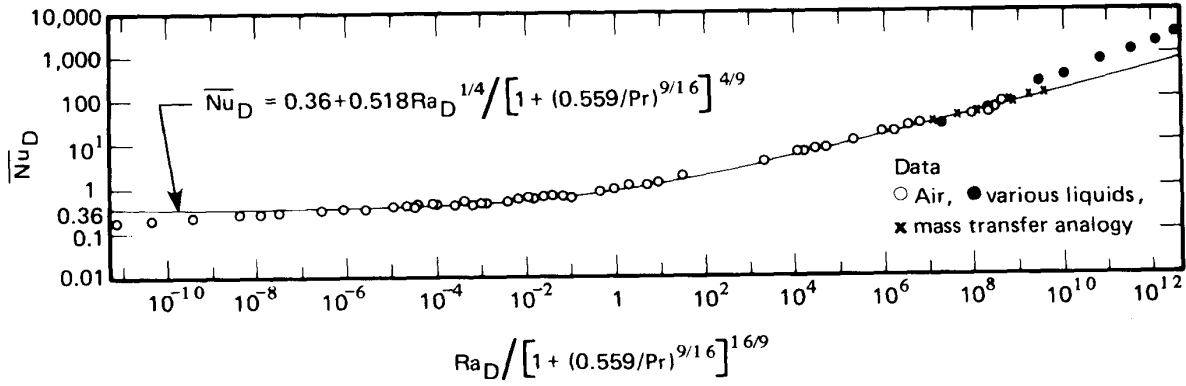
Figure 8.6 The data of many investigators for heat transfer from isothermal horizontal cylinders during natural convection, as correlated by Churchill and Chu [8.8].

8.4   Natural convection in other situations

Natural convection from horizontal isothermal cylinders

Churchill and Chu [8.8] provide yet another comprehensive correlation of existing data for the case of natural convection from horizontal isothermal cylinders. An equation with the same form as eqn. (8.13a) applies. Data from a variety of sources, over about 24 orders of magnitude of the Rayleigh number based on the diameter, Ra_D, are shown in Fig. 8.6, together with the fitted result:

$$\overline{Nu}_D = 0.36 + \frac{0.518\, Ra_D^{1/4}}{\left[1 + (0.559/Pr)^{9/16}\right]^{4/9}} \tag{8.28}$$

Churchill and Chu recommend that eqn. (8.28) be used in the range $10^{-6} \leqslant Ra_D \leqslant 10^9$.

When Ra_D is greater than 10^9, the flow becomes turbulent. The following equation is a little more complex, but it gives comparable accuracy over a larger range:

$$\overline{Nu}_D = \left\{ 0.60 + 0.387\left[\frac{Ra_D}{\left[1 + (0.559/Pr)^{9/16}\right]^{16/9}} \right]^{1/6} \right\}^2 \tag{8.29}$$

The recommended range of applicability of eqn. (8.29) is

$$10^{-6} \leqslant \text{Ra}_D$$

Example 8.4

Space vehicles are subject to a "g-jitter," or background variation of acceleration, on the order of 10^{-6} or 10^{-5} earth gravities. Brief periods of gravity up to 10^{-4} or 10^{-2} earth gravities can be exerted by accelerating the whole vehicle. A certain line carrying hot oil through air is 5 mm in diameter and at 127°C. How does the heat loss by natural convection vary with g-level if $T_\infty = 27$°C in the air around the tube?

Solution. The film temperature is 350 K. We evaluate properties at this temperature and write g as $g_e \times$ (g-level), where g_e is g at the earth's surface and the g-level is the fraction of g_e in the space vehicle. With $\beta = 1/T_f$ for an ideal gas

$$\text{Ra}_D = \frac{g\beta\Delta T\, D^3}{\nu\alpha} = \frac{9.8\left(\dfrac{127-27}{350}\right)(0.005)^3}{(2.073\times 10^{-5})(2.93\times 10^{-5})}\,(g\text{-level})$$

$$= (576.2)\,(g\text{-level})$$

From eqn. (8.29), with $\text{Pr} = 0.707$, we compute

$$\overline{\text{Nu}}_D = \left\{0.6 + 0.387\underbrace{\left[\frac{576.2}{\left[1 + (0.559/0.707)^{9/16}\right]^{16/9}}\right]^{1/6}}_{=0.926}(g\text{-level})^{1/6}\right\}^2$$

(8.30)

so

g-level	$\overline{\text{Nu}}_D$	$\overline{h} = \overline{\text{Nu}}_D\left(\dfrac{0.0297}{0.005}\right)$	$Q = \pi D\overline{h}\Delta T$
10^{-6}	0.480	2.85 W/m²K	4.47 W/m of tube
10^{-5}	0.542	3.22 W/m²K	5.06 W/m of tube
10^{-4}	0.639	3.80 W/m²K	5.97 W/m of tube
10^{-2}	1.061	6.30 W/m²K	9.90 W/m of tube

The numbers in the rightmost column are quite low. Convective cooling is extremely inefficient at these low gravities. ∎
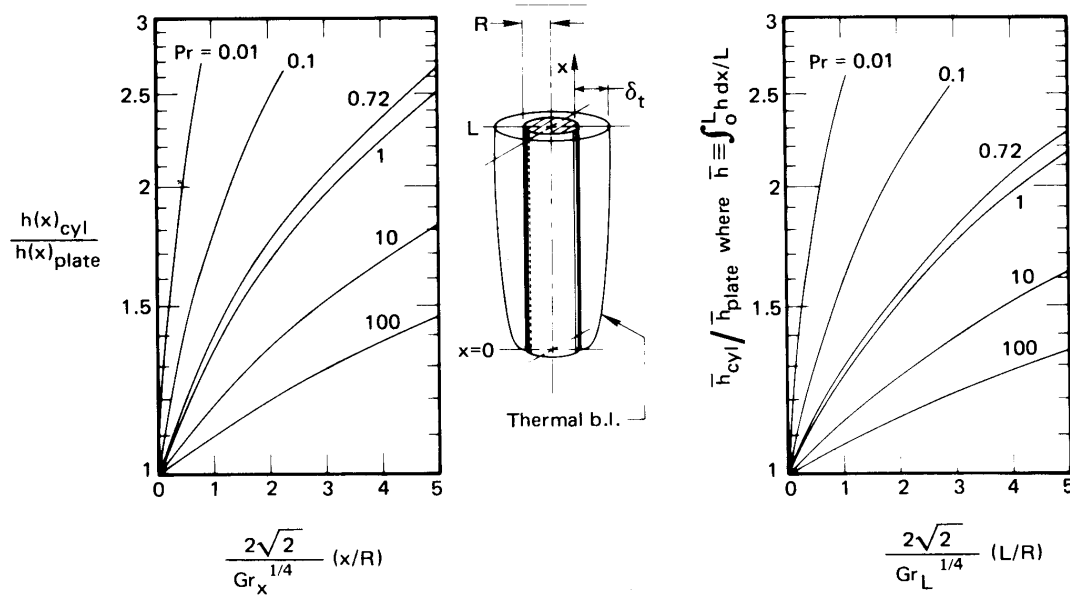
Figure 8.7   Corrections for h and $\overline{h}$ on vertical isothermal plates to adapt them to vertical isothermal cylinders [8.9].

Natural convection from vertical cylinders

The heat transfer from the wall of a cylinder with its axis running vertically is the same as that from a vertical plate, as long as the thermal b.l. is thin. However, if the b.l. is thick, as is indicated in Fig. 8.7, heat transfer will be enhanced by the curvature of the thermal b.l. This correction was first considered some years ago by Sparrow and Gregg, and the analysis was subsequently extended with the help of more powerful numerical methods by Cebeci [8.9].

Figure 8.7 includes the corrections to the vertical plate results that were calculated for many Pr's by Cebeci. The left-hand graph gives a correction that must be multiplied by the local flat-plate Nusselt number to get the vertical cylinder result. Notice that the correction increases when the Grashof number decreases. The right-hand curve gives a similar correction for the overall Nusselt number on a cylinder of height L. Notice that in either situation, the correction for all but liquid metals is less than 10% if $(x$ or $L)/R < 0.08\ \mathrm{Gr}_{x\ \mathrm{or}\ L}^{1/4}$.

Heat transfer from general submerged bodies

Spheres.   The sphere is interesting because the value of Nu_D as $Ra_D \rightarrow 0$ is clearly defined. We look first at this limit.

Buoyancy forces may approach zero by virtue of small diameter, low gravity, very high viscosity, or a very low thermal expansion coefficient. In this situation, heated fluid will no longer be convected away: only conduction will serve to remove heat. Using shape factor number 4 in Table 5.4 ($S = 4\pi R$), we may compute

$$\lim_{Ra_D \rightarrow 0} Nu_D = \frac{Q}{A\Delta T} \frac{D}{k} = \frac{S\,k\Delta T\,D}{\pi D^2\,k\Delta T} = \frac{4\pi(D/2)}{\pi D} = 2 \tag{8.31}$$

Every proper correlation of data for heat transfer from spheres therefore has a lead constant of 2.[6] A typical example is that of Yuge [8.10] for spheres immersed in gases:

$$\overline{Nu}_D = 2 + 0.43\,Ra_D^{1/4}, \quad Ra_D < 10^5 \tag{8.32}$$

A more complex expression [8.11] encompasses other Prandtl numbers:

$$\boxed{\overline{Nu}_D = 2 + \frac{0.589\,Ra_D^{1/4}}{\left[1 + (0.492/Pr)^{9/16}\right]^{4/9}}} \quad Ra_D < 10^{12} \tag{8.33}$$

This result has an estimated uncertainty of 5% in air and an rms error of about 10% at higher Prandtl numbers.

Rough estimate of Nu for other bodies.   In 1973 Lienhard [8.12] noted that, for laminar convection in which the b.l. does not separate, the expression

$$\boxed{\overline{Nu}_\tau \simeq 0.52\,Ra_\tau^{1/4}} \tag{8.34}$$

would predict heat transfer from any submerged body within about 10% if Pr is not $\ll 1$. The characteristic dimension in eqn. (8.34) is the length that fluid travels in the unseparated b.l., τ.

---

[6]Although Nu_D for spheres approaches a limiting value at small Ra_D, *no* such limit exists for cylinders or vertical surfaces because steady state conduction is not possible for infinite cylinders or planes in an infinite medium. The constants in eqns. (8.13a) and (8.28) are not valid at extremely low values of Ra_D.

In the case of spheres without separation, for example, $\tau = \pi D/2$, the distance from the bottom to the top around the circumference. Thus, for spheres, eqn. (8.34) becomes

$$\frac{\overline{h}\pi D}{2k} = 0.52\left[\frac{g\beta\Delta T(\pi D/2)^3}{\nu\alpha}\right]^{1/4}$$

or

$$\frac{\overline{h}D}{k} = 0.52\left(\frac{2}{\pi}\right)\left(\frac{\pi}{2}\right)^{3/4}\left[\frac{g\beta\Delta T D^3}{\nu\alpha}\right]^{1/4}$$

or

$$\overline{\mathrm{Nu}}_D = 0.464\,\mathrm{Ra}_D^{1/4}$$

This is within 8% of Yuge's correlation if Ra_D remains fairly large.

Laminar heat transfer from inclined and horizontal plates

In 1953, Rich [8.13] showed that heat transfer from inclined plates could be predicted by vertical plate formulas if the component of the gravity vector along the surface of the plate was used in the calculation of the Grashof number. Thus, g is replaced by $g\cos\theta$, where θ is the angle of inclination measured from the vertical, as shown in Fig. 8.8. The heat transfer rate therefore decreases as $(\cos\theta)^{1/4}$.

Subsequent studies have shown that Rich's result is substantially correct for the lower surface of a heated plate or the upper surface of a cooled plate. For the upper surface of a heated plate or the lower surface of a cooled plate, the boundary layer becomes unstable and separates at a relatively low value of Gr. Experimental observations of such instability have been reported by many authors [8.14–8.17].

In the limit $\theta = 90°$—a horizontal plate—the fluid flow above a hot plate or below a cold plate must form one or more plumes, as shown in Figs. 8.8c and d. In such cases, the b.l. is unstable for all but small Rayleigh numbers, and even then a plume must leave the center of the plate. The unstable cases can only be represented by empirical correlations.

Theoretical considerations, and experiments, show that the Nusselt number for stable laminar b.l.s on horizontal and slightly inclined plates varies as $\mathrm{Ra}^{1/5}$ [8.18, 8.19]. For the unstable cases, when the Rayleigh number exceeds 10^4 or so, the experimental variation is as $\mathrm{Ra}^{1/4}$ until the flow becomes fully turbulent for Rayleigh numbers above about 10^7. Beyond this range, experiments show a $\mathrm{Ra}^{1/3}$ variation of the Nusselt number [8.20, 8.21]. In the latter case, both Nu_L and $\mathrm{Ra}_L^{1/3}$ are proportional to L, so the heat transfer coefficient is *independent* of L. Moreover, the flow field in these situations is driven mainly by the component of gravity normal to the plate.
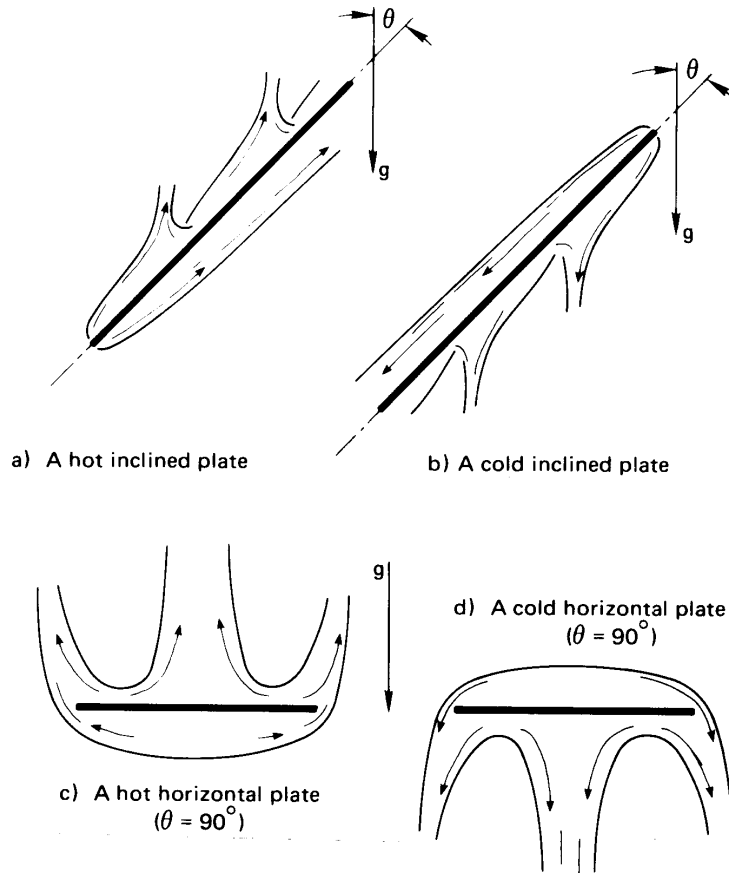
Figure 8.8 Natural convection b.l.'s on some inclined and horizontal surfaces. The b.l. separation, shown here for the unstable cases in (a) and (b), occurs only at sufficiently large values of Gr.

Unstable Cases: For the lower side of cold plates and the upper side of hot plates, the boundary layer becomes increasingly unstable as Ra is increased. The prediction of Nu depends on the specific case.

- For plate inclinations $\theta \lesssim 45°$ and $10^5 \leqslant \mathrm{Ra}_L \leqslant 10^9$, replace g with $g \cos\theta$ in eqn. (8.13a).

- For horizontal plates with $\mathrm{Ra}_L \geqslant 10^7$, nearly identical results have been obtained by many investigators. From these results, Raithby and Hollands propose [8.11]:

$$\overline{\mathrm{Nu}}_L = 0.14\,\mathrm{Ra}_L^{1/3}\left(\frac{1 + 0.0107\,\mathrm{Pr}}{1 + 0.01\,\mathrm{Pr}}\right), \quad 0.024 \leqslant \mathrm{Pr} \leqslant 2000 \quad (8.35)$$

This formula is consistent with available data up to $Ra_L = 2 \times 10^{11}$, and probably goes higher. As noted before, the choice of length scale L is immaterial. Fujii and Imura's results support using eqn. (8.35) for $60° \leq \theta \leq 90°$ with g in the Rayleigh number.

For high Ra in gases, temperature differences and variable properties effects can be large. From experiments on upward facing plates, Clausing and Berton [8.21] suggest evaluating all gas properties at a reference temperature, in kelvin, of

$$T_{\text{ref}} = T_w - 0.83\,(T_w - T_\infty) \quad \text{for} \quad 1 \leq T_w/T_\infty \leq 3. \tag{8.36}$$

- For horizontal plates of area A and perimeter P at lower Rayleigh numbers, Raithby and Hollands suggest [8.11]

$$\overline{Nu}_{L*} = \frac{0.560\,Ra_{L*}^{1/4}}{\left[1 + (0.492/Pr)^{9/16}\right]^{4/9}} \tag{8.37a}$$

where, following Lloyd and Moran [8.20], a characteristic length scale $L^* = A/P$, is used in the Rayleigh and Nusselt numbers. If $\overline{Nu}_{L*} \lesssim 10$, the b.l.s will be thick, and the result should be corrected as follows:

$$\overline{Nu}_{\text{corrected}} = \frac{1.4}{\ln(1 + 1.4/\overline{Nu}_{L*})} \tag{8.37b}$$

These equations are recommended for $1 < Ra_{L*} < 10^7$.

- In general, for inclined plates in the unstable cases, Raithby and Hollands [8.11] recommend that the heat flow be computed first using the formula for a vertical plate with $g\cos\theta$, then computed using the formula for a horizontal plate with $g\sin\theta$ (i.e., for the component of gravity normal to the plate), and that the larger value of the heat flow be taken.

Stable Cases: For the upper side of cold plates and the lower side of hot plates, the flow is generally stable. The following results assume that the flow is not obstructed at the edges of the plate. If edge circulation is blocked by an adiabatic wall, for example, $\overline{h}$ will be lower [8.22, 8.23].

- For $\theta < 88°$ and $10^5 \leq Ra_L \leq 10^{11}$, eqn. (8.13a) is still valid for the upper side of cold plates and the lower side of hot plates when g is replaced with $g\cos\theta$ in the Rayleigh number [8.14].

- For downward-facing hot plates and upward-facing cold plates of width L with very slight inclinations, Fujii and Imura give:

$$\overline{\mathrm{Nu}}_L = 0.58\,\mathrm{Ra}_L^{1/5} \tag{8.38}$$

This equation is valid for $10^6 \leqslant \mathrm{Ra}_L < 10^9$ if $87° \leqslant \theta \leqslant 90°$ and continues for $10^9 \leqslant \mathrm{Ra}_L < 10^{11}$ if $89° \leqslant \theta \leqslant 90°$. Here, Ra_L is based on g (*not* $g\cos\theta$). Fujii and Imura's results are for two-dimensional plates—ones in which infinite breadth has been approximated by suppression of end effects.

For circular plates of diameter D in the stable horizontal configurations, the data of Kadambi and Drake [8.24] suggest that

$$\overline{\mathrm{Nu}}_D = 0.82\,\mathrm{Ra}_D^{1/5}\,\mathrm{Pr}^{0.034} \tag{8.39}$$

Natural convection with uniform heat flux

When q_w is specified instead of $\Delta T \equiv (T_w - T_\infty)$, ΔT becomes the unknown dependent variable. Because $h \equiv q_w/\Delta T$, the dependent variable appears in the Nusselt number; however, for natural convection, it also appears in the Rayleigh number. Thus, the situation is more complicated than in forced convection.

Since Nu often varies as $\mathrm{Ra}^{1/4}$, we may write

$$\mathrm{Nu}_x = \frac{q_w}{\Delta T}\frac{x}{k} \propto \mathrm{Ra}_x^{1/4} \propto \Delta T^{1/4}x^{3/4}$$

The relationship between x and ΔT is then

$$\Delta T = C\,x^{1/5} \tag{8.40}$$

where the constant of proportionality C involves q_w and the relevant physical properties. The average of ΔT over a heater of length L is

$$\overline{\Delta T} = \frac{1}{L}\int_0^L C\,x^{1/5}\,dx = \frac{5}{6}\,C \tag{8.41}$$

We plot $\Delta T/C$ against x/L in Fig. 8.9. Here, $\overline{\Delta T}$ and $\Delta T(x/L = 0.5)$ are within 4% of each other. This observation suggests that, if we are interested in *average* values of ΔT, we can use ΔT evaluated at the midpoint of the plate in Ra_L and in $\overline{\mathrm{Nu}}_L = q_wL/k\overline{\Delta T}$. Churchill and Chu, for example, show that their vertical plate correlation, eqn. (8.13a), represents data for constant q_w exceptionally well in the range $\mathrm{Ra}_L > 1$ when Ra_L is based
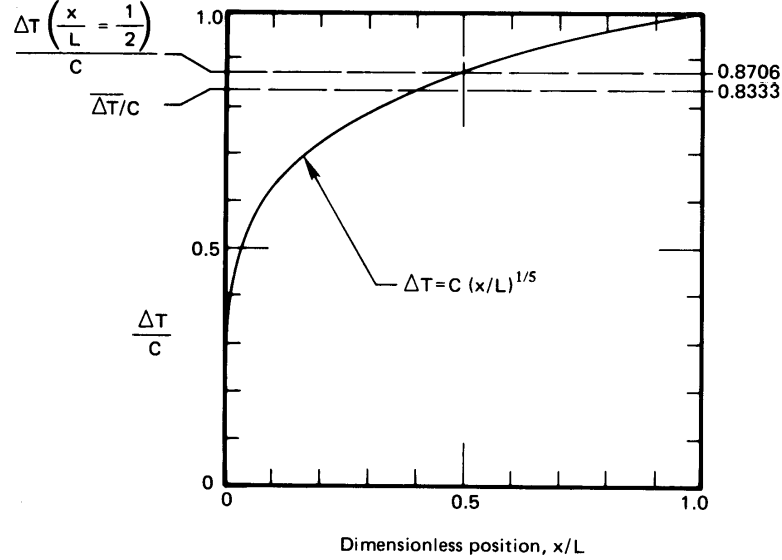
Figure 8.9 The mean value of $\Delta T \equiv T_w - T_\infty$ during natural convection.

on ΔT at the middle of the plate. This approach eliminates the variation of ΔT with x from the calculation, but the temperature difference at the middle of the plate must still be found by iteration.

To avoid iterating, we need to eliminate ΔT from the Rayleigh number. We can do this by introducing a modified Rayleigh number, Ra_x^*, defined as

$$\mathrm{Ra}_x^* \equiv \mathrm{Ra}_x \mathrm{Nu}_x \equiv \frac{g\beta\Delta T x^3}{\nu\alpha}\frac{q_w x}{\Delta T k} = \frac{g\beta q_w x^4}{k\nu\alpha} \tag{8.42}$$

For example, in eqn. (8.13a), we replace Ra_L with $\mathrm{Ra}_L^*/\overline{\mathrm{Nu}}_L$. The result is

$$\overline{\mathrm{Nu}}_L = 0.68 + \frac{0.67\left(\mathrm{Ra}_L^*\right)^{1/4}}{\overline{\mathrm{Nu}}_L^{1/4}\left[1 + (0.492/\mathrm{Pr})^{9/16}\right]^{4/9}}$$

which may be rearranged as

$$\overline{\mathrm{Nu}}_L^{1/4}\left(\overline{\mathrm{Nu}}_L - 0.68\right) = \frac{0.67\left(\mathrm{Ra}_L^*\right)^{1/4}}{\left[1 + (0.492/\mathrm{Pr})^{9/16}\right]^{4/9}} \tag{8.43a}$$

When $\overline{\mathrm{Nu}}_L \gtrsim 5$, the term 0.68 may be neglected, with the result

$$\overline{\mathrm{Nu}}_L = \frac{0.73\left(\mathrm{Ra}_L^*\right)^{1/5}}{\left[1 + (0.492/\mathrm{Pr})^{9/16}\right]^{16/45}} \tag{8.43b}$$

Raithby and Hollands [8.11] give the following, somewhat simpler corre-
lations for laminar natural convection from vertical plates with a uniform
wall heat flux:

$$\text{Nu}_x = 0.630 \left(\frac{\text{Ra}_x^* \, \text{Pr}}{4 + 9\sqrt{\text{Pr}} + 10\,\text{Pr}} \right)^{1/5} \tag{8.44a}$$

$$\overline{\text{Nu}}_L = \frac{6}{5} \left(\frac{\text{Ra}_L^* \, \text{Pr}}{4 + 9\sqrt{\text{Pr}} + 10\,\text{Pr}} \right)^{1/5} \tag{8.44b}$$

These equations apply for all Pr and for Nu $\gtrsim$ 5. Equations for lower Nu
or Ra* are given in [8.11].

Example 8.5

A horizontal circular disk heater of diameter 0.17 m faces downward
in air at 27°C. The disk is polished aluminum with $\varepsilon = 0.05$. If it
delivers 15 W, estimate its average surface temperature.

SOLUTION. We have no formula for this specific situation, but we may
improvise by following the lead of Churchill and Chu—we replace Ra$_D$
with Ra$_D^*/\overline{\text{Nu}}_D$ in eqn. (8.39) for downward facing isothermal disks:

$$(\overline{\text{Nu}}_D)^{6/5} = \left(\frac{q_w D}{\Delta T k} \right)^{6/5} = 0.82 \, (\text{Ra}_D^*)^{1/5} \, \text{Pr}^{0.034}$$

We start by neglecting radiation, so $q_w = 15/(\pi R^2) = 661$ W/m^2, and
evaluating all properties at T_∞. Then

$$\overline{\Delta T} = \frac{1.18(q_w D/k)}{\left(\dfrac{g\beta q_w D^4}{k\nu\alpha} \right)^{1/6} \text{Pr}^{0.028}}$$

$$= \frac{\left(\dfrac{(1.18)(661)(0.17)}{0.02623} \right)}{\left[\dfrac{9.8(661)(0.17)^4}{300(0.02623)(1.578)(2.213)10^{-10}} \right]^{1/6} (0.713)^{0.028}} = 144 \text{ K}$$

The radiation heat transfer coefficient may be calculated at $T_m =$
$(27 + 144/2 + 273) = 372$ K, so $h_{\text{rad}} = 4(0.05)(5.67 \times 10^{-8})(372)^3 =$
0.584 W/m^{2}K. The radiation heat flux is $0.584(144) = 84$ W/m^2.

Now we must return the calculation, reevaluating all properties at $T_f = 27 + (144/2) = 99°C$, and reducing q_w to $661 - 84 = 577$ W/m^2:

$$\overline{\Delta T}_{\text{corrected}} = \frac{\left(\dfrac{(1.18)(577)(0.17)}{0.03136}\right)}{\left[\dfrac{9.8(577)(0.17)^4}{(372)(0.03136)(2.315)(3.281)10^{-10}}\right]^{1/6}(0.706)^{0.028}}$$

$$= 131 \text{ K}$$

The surface temperature is $27 + 126 = 158°C$. An additional iteration changes $\overline{\Delta T}$ by only about 2%.

The disk is rather hot. While we are uncertain as to the exact temperature, since our formula was improvised, the cooling process is clearly ineffective in this case. ■

Some other natural convection problems

We have clearly moved into the realm of handbook information at this point. And it would be beyond the scope of this book to go much further. Still, two matters deserve at least qualitative mention. They are:

Natural convection in enclosures. When a natural convection process occurs within a confined space, the heated fluid buoys up and then follows the contours of the container, releasing heat and in some way returning to the hotter surface. This recirculating convection process normally increases heat transfer above that which would occur by conduction through the stationary fluid. Natural convection like this is common in buildings (as in rooms, attics, multiply glazed windows, and uninsulated walls), in hot or cold liquid storage systems, and in crystal growth and solidification processes. Survey articles on natural convection in enclosures have been written by Yang [8.25], Raithby and Hollands [8.11], and Catton [8.26].

Combined natural and forced convection. When forced convection along, say, a vertical wall occurs at a relatively low velocity but at a relatively high heating rate, the resulting density changes can give rise to a superimposed natural convection process. We saw on page 419 that $Gr_L^{1/2}$ plays the role of a natural convection Reynolds number. It follows that we can estimate the relative importance of natural and forced convection by considering the ratio

$$\frac{Gr_L}{Re_L^2} = \frac{\text{strength of natural convection flow}}{\text{strength of forced convection flow}} \tag{8.45}$$

where Re_L is for the forced flow parallel to the wall. If this ratio is small compared to one, the flow is essentially driven by forced convection, whereas if it is much larger than one, we have natural convection. When Gr_L/Re_L^2 is on the order of one, we have a *mixed convection* process. Both buoyant and forced flow contribute to heat transfer.

Of course, the relative orientation of the forced flow and the natural convection flow matters. For example, compare cool air flowing downward past a hot wall to cool air flowing upward along a hot wall. The former situation is called *opposing flow* and the latter is called *assisting flow*. Opposing flow may lead to boundary layer separation and degraded heat transfer. For further information, see [8.27–8.29].

8.5 Film condensation

Dimensional analysis and experimental data

We now return to the problem of film condensation, recalling our discussion in Section 8.2. The dimensional functional equation for h (or $\overline{h}$) in film condensation can be written as[7]

$$h \text{ or } \overline{h} = \text{fn}[g(\rho_f - \rho_g), \nu, k, (T_{\text{sat}} - T_w), h_{fg}, \rho_f, c_p, L \text{ or } x] \qquad (8.46)$$

Many of these variables appear in the differential equations (8.5) and (6.40), but others arise through the boundary conditions. The b.c.s carry the thermal conductivity, k, and the temperature difference. The latent heat of vaporization, h_{fg}, and liquid density, ρ_f, strongly affect δ, which appears in the b.c.'s, eqn. (8.6b). The film thickness, δ, also depends slightly on the sensible heat, $c_p\Delta T$, since the liquid film must be cooler than T_{sat}. Notice, too, that $g(\rho_f - \rho_g)$ is included as a product because gravity enters the problem only as it acts upon the density difference.

The problem is therefore expressed in nine variables which have the units J, kg, m, s, and K, since no heat is converted into work, or work into heat, in this situation. So, we look for $9 - 5 = 4$ pi-groups. The ones we choose are

$$\Pi_1 = \overline{Nu}_L \equiv \frac{\overline{h}L}{k} \qquad\qquad \Pi_2 = Pr \equiv \frac{\nu}{\alpha} \qquad\qquad (8.47)$$

$$\Pi_3 = Ja \equiv \frac{c_p(T_{\text{sat}} - T_w)}{h_{fg}} \qquad \Pi_4 \equiv \frac{g(\rho_f - \rho_g)h_{fg}L^3}{\nu k(T_{\text{sat}} - T_w)} \qquad (8.48)$$

---

[7]Note that, throughout this section, k, μ, c_p, and Pr refer to properties of the liquid, rather than the vapor.

Two of these groups are new to us. The group Π_3 is called the *Jakob number*, Ja, to honor Max Jakob's pioneering work on problems of phase change during the 1930s. The Jakob number compares the maximum sensible heat absorbed by the liquid to the latent heat absorbed. The group Π_4 does not normally bear anyone's name, but, if it were multiplied by Ja, it could be regarded as a Rayleigh number for the condensate film.

Notice that if we condensed water at 1 atm on a wall 10°C below T_{sat}, then Ja would equal $4.21(10/2257) = 0.0183$. Although 10°C is a fairly large temperature difference in a condensation process, it gives a maximum sensible heat that is less than 2% of the latent heat. The Jakob number is accordingly small in most cases of practical interest and sensible heat can often be neglected. The same is true of the role of the Prandtl number. Therefore, during film condensation

$$\overline{\text{Nu}}_L = \text{fn}\left(\underbrace{\frac{g(\rho_f - \rho_g)h_{fg}L^3}{\nu k(T_{\text{sat}} - T_w)}}, \underbrace{\text{Pr}, \text{Ja}} \right) \tag{8.49}$$

secondary independent
variables

primary independent variable, Π_4

Equation (8.49) is not restricted to any geometrical configuration, since the same variables govern h during film condensation on any body. Figure 8.10, for example, shows laminar film condensation data given for spheres by Dhir[8] [8.30]. They have been correlated according to eqn. (8.49). The data are for only one value of Pr but for a range of Π_4 and Ja. They generally correlate well within ±10%, despite a broad variation of the not-very-influential variable, Ja. The predictive curve shown in Fig. 8.10 is discussed later in this section.

Laminar film condensation on a vertical plate

Consider the following feature of film condensation. The latent heat of a liquid is normally a very large number. Therefore, even a high rate of heat transfer will typically result in only very thin films. These films move relatively slowly, so it is safe to neglect the inertia terms in the

---

[8]Vijay K. Dhir very kindly recalculated his data into the form shown in Fig. 8.10 for use here.
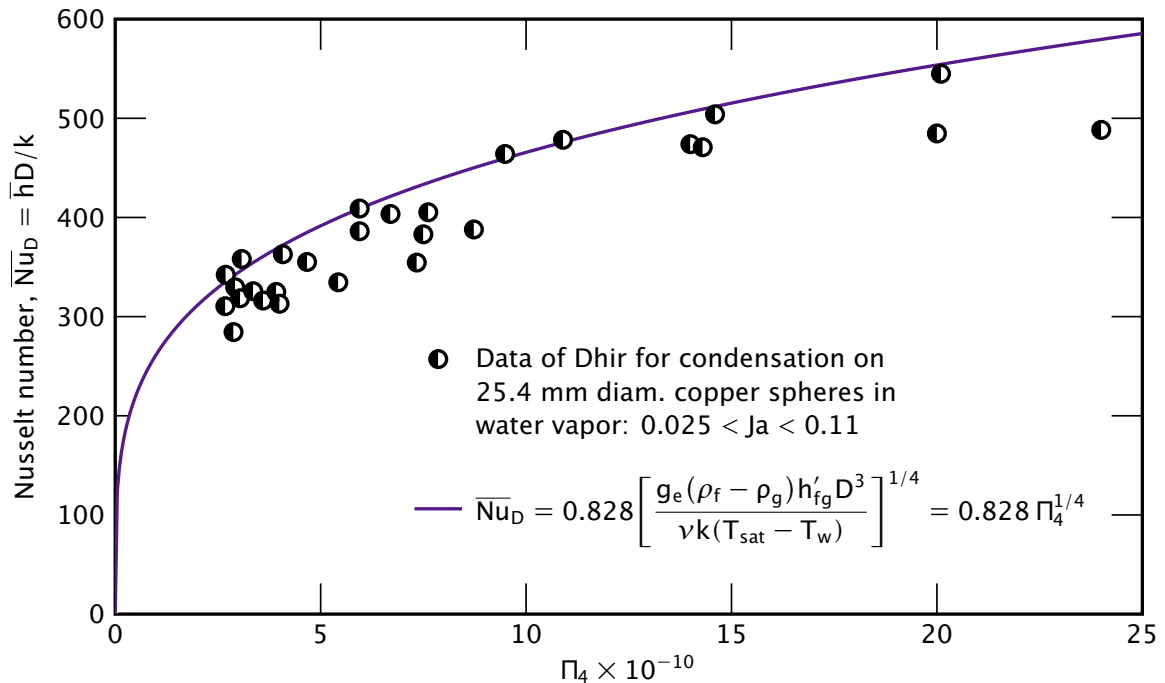
Figure 8.10 Correlation of Dhir's data [8.30] for laminar film condensation on spheres at one value of Pr and a range of Π_4 and Ja, with properties evaluated at $(T_{sat} + T_w)/2$. Analytical prediction is from [8.31].

momentum equation (8.5):

$$\underbrace{u\frac{\partial u}{\partial x} + v\frac{\partial u}{\partial y}}_{\simeq 0} = \left(1 - \frac{\rho_g}{\rho_f}\right)g + \underbrace{v\frac{\partial^2 u}{\partial y^2}}_{\simeq v\,d^2u/dy^2}$$

This result will give $u = u(y, \delta)$ when it is integrated, where δ is the local b.l. thickness. We recognize that $\delta = \delta(x)$, so that u is not strictly dependent on y alone. However, the y-dependence is predominant, so that the momentum equation can be approximated as an o.d.e.

$$\frac{d^2u}{dy^2} = -\frac{\rho_f - \rho_g}{\rho_f}\frac{g}{v} \tag{8.50}$$

This simplification was made by Nusselt in 1916 when he set down the original analysis of film condensation [8.32]. On the same basis, he

also eliminated the convective terms from the energy equation (6.40):

$$\underbrace{u\frac{\partial T}{\partial x} + v\frac{\partial T}{\partial y}}_{\simeq 0} = \alpha \frac{\partial^2 T}{\partial y^2}$$

The integration of eqn. (8.50) subject to the b.c.'s

$$u(y = 0) = 0 \quad \text{and} \quad \left.\frac{\partial u}{\partial y}\right|_{y=\delta} = 0$$

gives the parabolic velocity profile:

$$u = \frac{(\rho_f - \rho_g)g\delta^2}{2\rho_f \nu}\left[2\left(\frac{y}{\delta}\right) - \left(\frac{y}{\delta}\right)^2\right] \tag{8.51}$$

And integration of the energy equation subject to the b.c.'s

$$T(y = 0) = T_w \quad \text{and} \quad T(y = \delta) = T_{\text{sat}}$$

gives the linear temperature profile:

$$T = T_w + (T_{\text{sat}} - T_w)\frac{y}{\delta} \tag{8.52}$$

To complete the analysis, we must calculate δ. We can do this in two steps. First, we express the mass flow rate per unit width of film, $\dot{m}$, in terms of δ, with the help of eqn. (8.51):

$$\dot{m} = \int_0^\delta \rho_f u\, dy = \frac{g(\rho_f - \rho_g)}{3\nu}\delta^3 \tag{8.53}$$

Second, we neglect the sensible heat absorbed in cooling the interior of the film below T_{sat} and express the local heat flux in terms of the rate of change of $\dot{m}$ (see Fig. 8.11):

$$|q| = k\left.\frac{\partial T}{\partial y}\right|_{y=0} = k\frac{T_{\text{sat}} - T_w}{\delta} = h_{fg}\frac{d\dot{m}}{dx} \tag{8.54}$$

Substituting eqn. (8.53) into eqn. (8.54), we obtain a first-order differential equation for δ:

$$k\frac{T_{\text{sat}} - T_w}{\delta} = \frac{h_{fg}g(\rho_f - \rho_g)}{\nu}\delta^2\frac{d\delta}{dx} \tag{8.55}$$

a) Mass balance   b) Energy balance
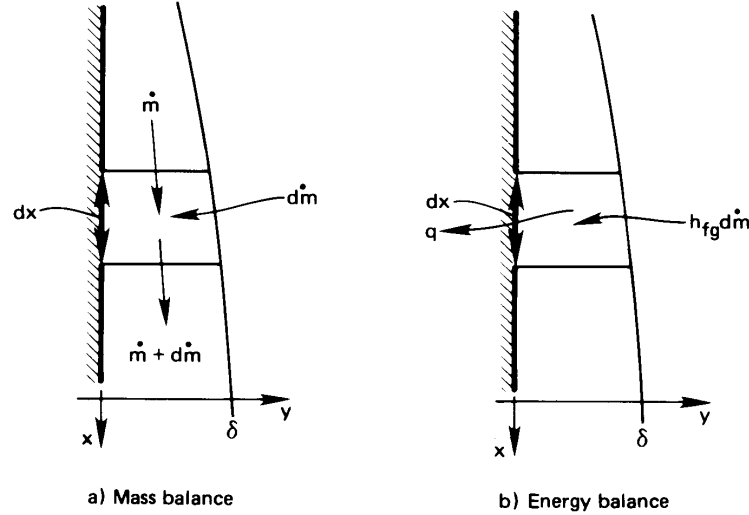
Figure 8.11 Heat and mass flow in an element of a condensing film.

This o.d.e. can be integrated directly, subject to the b.c. $\delta(0) = 0$:

$$\delta = \left[\frac{4\nu k(T_{\text{sat}} - T_w)x}{g(\rho_f - \rho_g)h_{fg}} \right]^{1/4} \tag{8.56}$$

Both Nusselt and, subsequently, Rohsenow [8.33] suggested replacing h_{fg} with a corrected value, h'_{fg}, which would account for subcooling of the liquid film through a dependence on Ja. We will give an expression for this correction below. For the moment, we simply write this yet-to-be-provided h'_{fg} in place of h_{fg} in the equations that follow.

Finally, we calculate the heat transfer coefficient

$$h \equiv \frac{q}{T_{\text{sat}} - T_w} = \frac{1}{T_{\text{sat}} - T_w} \left[\frac{k(T_{\text{sat}} - T_w)}{\delta} \right] = \frac{k}{\delta} \tag{8.57}$$

so

$$\text{Nu}_x = \frac{hx}{k} = \frac{x}{\delta} \tag{8.58}$$

Thus, we substitute eqn. (8.56) into eqn. (8.58) and get

$$\text{Nu}_x = 0.707 \left[\frac{g(\rho_f - \rho_g)h'_{fg}x^3}{\nu k(T_{\text{sat}} - T_w)} \right]^{1/4} \tag{8.59}$$

This equation carries the functional dependence that we anticipated in eqn. (8.49):

$$\mathrm{Nu}_x = \mathrm{fn}\Big(\underbrace{\Pi_4}, \underbrace{\mathrm{Ja}}, \underbrace{\mathrm{Pr}} \Big)$$

> eliminated in so far as we neglected convective terms in the energy equation

> this is carried implicitly in h'_{fg}

> this is clearly the dominant variable

The liquid properties in Π_4, Ja, and Pr (with the exception of h_{fg}) are to be evaluated at the mean film temperature. However, if $T_{\mathrm{sat}} - T_w$ is small—and it often is—one might approximate them at T_{sat}.

At this point we should ask how great are the missing influences of Pr and Ja and what degree of approximation is involved in representing the influence of Ja through h'_{fg}. Sparrow and Gregg [8.34] answered these questions with a complete b.l. analysis of film condensation. They did not introduce Ja in a corrected latent heat but instead showed its effect directly.

Figure 8.12 displays two figures from the Sparrow and Gregg paper. The first shows heat transfer results plotted in the form

$$\frac{\mathrm{Nu}_x}{\sqrt[4]{\Pi_4}} = \mathrm{fn}(\mathrm{Ja}, \mathrm{Pr}) \longrightarrow 1 \text{ as Ja} \longrightarrow 0 \tag{8.60}$$

Notice that the calculation approaches Nusselt's simple result for all Pr as Ja $\rightarrow$ 0. It also approaches Nusselt's result, even for fairly large values of Ja, if Pr is not much smaller than one. The second figure shows how the temperature deviates from the linear profile that we assumed to exist in the film in developing eqn. (8.52). Since a Jakob number of 0.02 is about as large as normally occurs in laminar condensation, the linear temperature profile is a very sound assumption for nonmetallic liquids.

Sadasivan and Lienhard [8.35] have shown that the Sparrow-Gregg formulation can be expressed with high accuracy, for Pr $\geqslant$ 0.6, by including Pr in the latent heat correction:

$$h'_{fg} = h_{fg}\big[1 + (0.683 - 0.228/\mathrm{Pr})\mathrm{Ja}\big] \tag{8.61}$$

This equation may be used in eqn. (8.59) and in the relevant equations below. (For Pr $\rightarrow \infty$, eqn. (8.61) matches Rohsenow's result [8.33].) In many cases, the difference between h_{fg} and h'_{fg} is quite small.
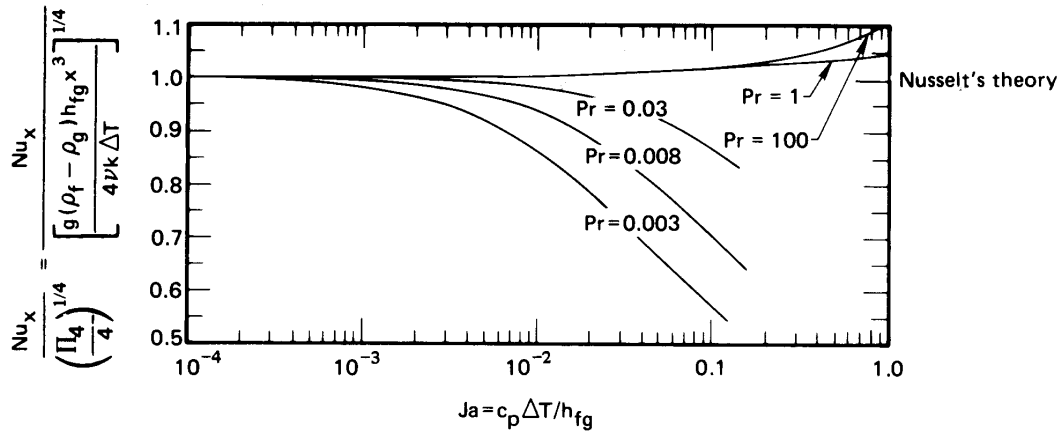
Predicted heat transfer results
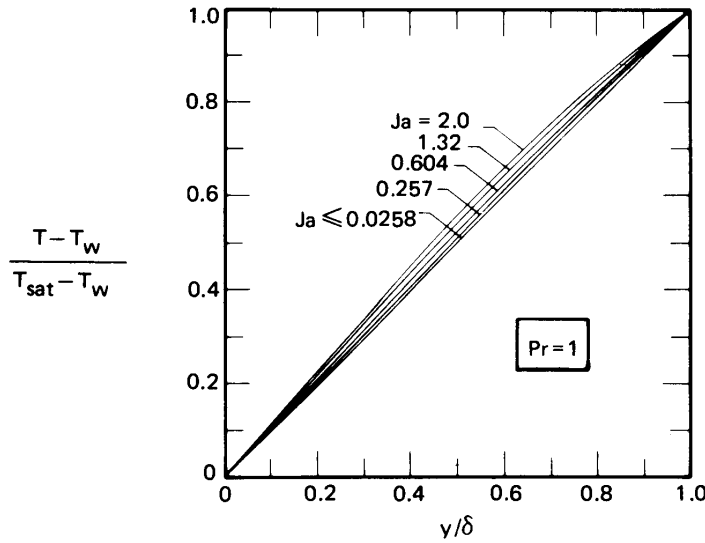
Predicted temperature profiles in condensing films

Figure 8.12 Results of the exact b.l. analysis of laminar film condensation on a vertical plate [8.34].

The Sparrow and Gregg analysis proves that Nusselt's analysis is quite accurate for all Prandtl numbers above the liquid-metal range. High Jakob numbers, for which Nusselt's analysis requires some correction, generally involve relatively thick films. And thick films are likely to

become turbulent. Therefore the exact analysis is seldom applicable when Ja is large.

The average heat transfer coefficient is calculated in the usual way for $T_{\text{wall}} = \text{constant}$:

$$\overline{h} = \frac{1}{L} \int_0^L h(x)\, dx = \tfrac{4}{3} h(L) \tag{8.62a}$$

so

$$\boxed{\overline{\mathrm{Nu}_L} = 0.9428 \left[\frac{g(\rho_f - \rho_g)h'_{fg}L^3}{\nu k(T_{\text{sat}} - T_w)} \right]^{1/4}} \tag{8.62b}$$

Example 8.6

Water at atmospheric pressure condenses on a strip 30 cm high that is held at 90°C. Calculate the overall heat transfer per meter, the film thickness at the bottom, and the condensate mass flow rate per meter.

Solution. Take liquid properties at 95°C, but ρ_g and h_{fg} at 100°C.

$$\delta = \left[\frac{4\nu k(T_{\text{sat}} - T_w)x}{g(\rho_f - \rho_g)h'_{fg}} \right]^{1/4}$$

where we have replaced h_{fg} with h'_{fg}:

$$h'_{fg} = 2257 \left[1 + \left(0.683 - \frac{0.228}{1.85} \right) \frac{4.210(10)}{2257} \right] = 2281 \text{ kJ/kg}$$

The small latent heat correction, raised to the ¼ power in calculating δ, is clearly negligible.

$$\delta = \left[\frac{4(3.091 \times 10^{-7})(0.6773)(10)\, x}{(9.806)(961.9 - 0.60)(2281 \times 10^3)} \right]^{1/4} = 0.000140\, x^{1/4}$$

Then

$$\delta(L) = 0.000104 \text{ m} = 0.104 \text{ mm}$$

Notice how thin the film is. Finally, we use eqns. (8.58) and (8.62a) to compute

$$\overline{\mathrm{Nu}_L} = \frac{4}{3} \frac{L}{\delta} = \frac{4(0.3)}{3(0.000104)} = 3846$$

so

$$q = \frac{\mathrm{Nu}_L\, k\Delta T}{L} = \frac{3846(0.6773)(10)}{0.3} = 8.68 \times 10^4 \text{ W/m}^2$$

(This flux would correspond to a heat flow of 86.8 kW on an area about half the size of a desk top. Such a high heat removal with such a small temperature difference is typical of film condensation. It is a very efficient heat removal process.) Then

$$Q = (8.68 \times 10^4)(0.3) = 26,050 \text{ W/m} = 26.1 \text{ kW/m}$$

The rate of condensate flow, $\dot{m}$ is

$$\dot{m} = \frac{Q}{h'_{fg}} = \frac{26.1}{2281} = 0.0114 \text{ kg/m·s} \qquad \blacksquare$$

Condensation on other bodies

Nusselt also applied his prediction to bodies other than vertical plates. However, without modern computers such predictions were limited to only a few cases. In 1971 Dhir and Lienhard [8.31] showed how Nusselt's method could be readily extended to a large class of problems. They showed that one need only to replace the gravity, g, with an effective gravity, g_{eff}

$$g_{\text{eff}} \equiv \frac{x(gR)^{4/3}}{\int_0^x g^{1/3} R^{4/3} \, dx} \qquad (8.63)$$

in eqns. (8.56) and (8.59), to predict δ and Nu_x for a variety of bodies. The terms in eqn. (8.63) are as follows (see Fig. 8.13).

- x is the distance along the film measured from the uppermost point.

- $g = g(x)$ is the component of gravity (or other body force) along x; g can vary from point to point, as it does in Fig. 8.13b and c.

- $R(x)$ is a radius of curvature about the vertical axis. In Fig. 8.13a, R is a constant that factors out of eqn. (8.63). In Fig. 8.13c, R is infinite. Since R appears to the same power in both the numerator and the denominator, it again can be factored out of eqn. (8.63). Only in axisymmetric bodies, where R varies with x, need R be included. When R can be factored out,

$$g_{\text{eff}} \text{ reduces to } \frac{xg^{4/3}}{\int_0^x g^{1/3} \, dx} \qquad (8.64)$$
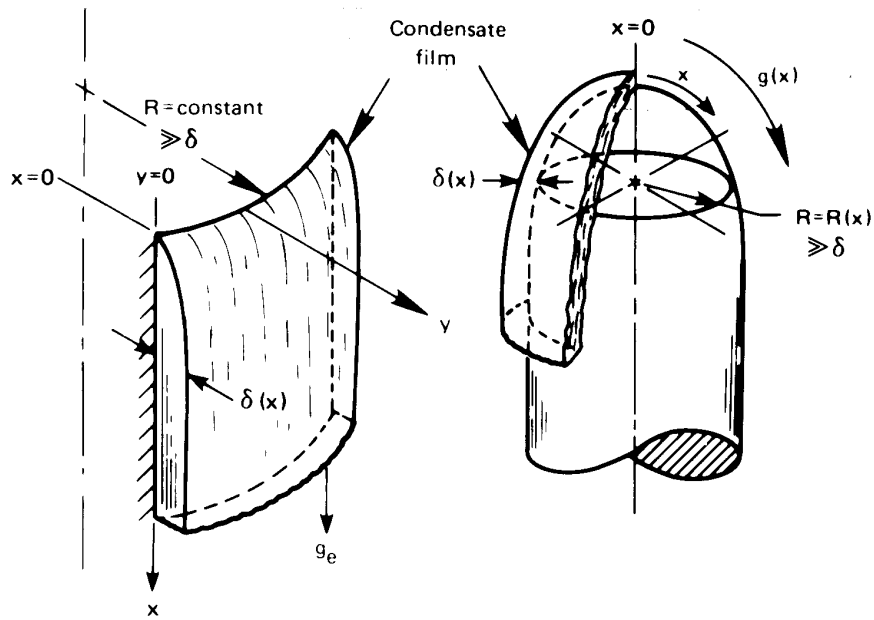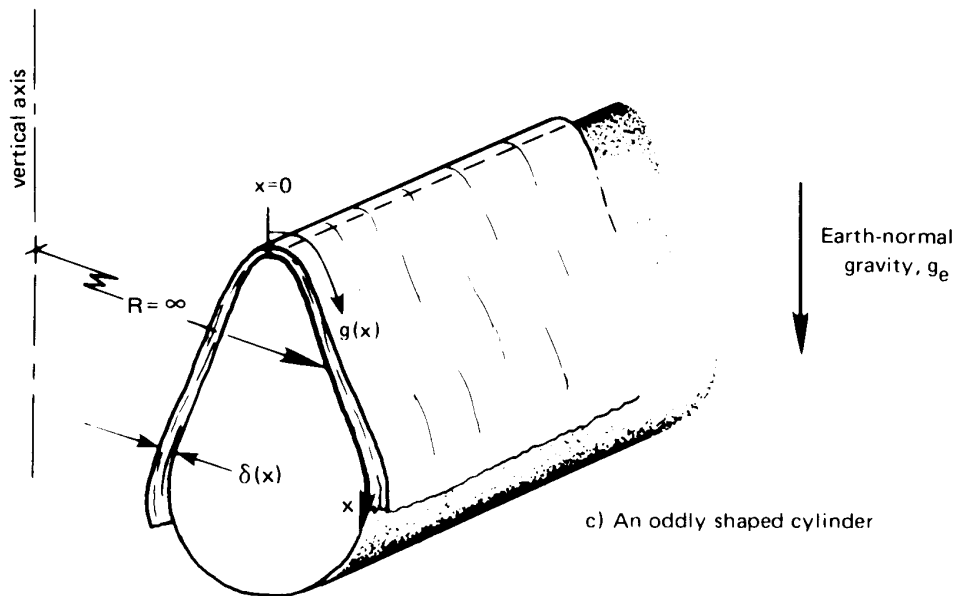
Figure 8.13 Condensation on various bodies. $g(x)$ is the component of gravity or other body force in the x-direction.

In subsequent equations, g_e is the actual gravity away from the body. On Earth's surface, g_e is earth-normal gravity. We introduce g_e at this point to distinguish it from $g(x)$.

Example 8.7   Condensation on an inclined plate

Find Nu_x for laminar film condensation on the top of a flat surface sloping at angle θ from vertical.

SOLUTION. In this case $g = g_e \cos \theta$ and $R = \infty$. Therefore, eqn. (8.63) or (8.64) reduces to

$$g_{\text{eff}} = \frac{xg_e^{4/3}(\cos \theta)^{4/3}}{g_e^{1/3}(\cos \theta)^{1/3} \int_0^x dx} = g_e \cos \theta \tag{8.65}$$

as we might expect. Then, for a slanting plate,

$$Nu_x = 0.707 \left[\frac{(g_e \cos \theta)(\rho_f - \rho_g)h'_{fg}x^3}{\nu k(T_{\text{sat}} - T_w)} \right]^{1/4} \tag{8.66}$$

$\blacksquare$

Example 8.8   Condensation on a horizontal cylinder

Find the overall Nusselt number for a horizontal cylinder.

SOLUTION. There is an important conceptual hurdle here. The radius $R(x)$ is infinity, as shown in Fig. 8.13c—it is not the radius of the cylinder. Using plane geometry, $g(x)$ is easily shown to equal $g_e \sin(2x/D)$, where D is the diameter of the cylinder. Then

$$g_{\text{eff}} = \frac{xg_e^{4/3}(\sin 2x/D)^{4/3}}{g_e^{1/3} \int_0^x (\sin 2x/D)^{1/3} dx}$$

and, with $h(x)$ from eqn. (8.59),

$$\overline{h} = \frac{2}{\pi D} \int_0^{\pi D/2} \frac{1}{\sqrt{2}} \frac{k}{x} \left[\frac{(\rho_f - \rho_g)h'_{fg}x^3}{\nu k(T_{\text{sat}} - T_w)} \frac{xg_e(\sin 2x/D)^{4/3}}{\int_0^x (\sin 2x/D)^{1/3} dx} \right]^{1/4} dx$$

This integral can be evaluated in terms of Gamma functions (see Problem 8.57). The result, when it is put back in the form of a Nusselt number, is

$$\overline{\mathrm{Nu}}_D = 0.728 \left[\frac{g_e (\rho_f - \rho_g) h'_{fg} D^3}{\nu k (T_{\mathrm{sat}} - T_w)} \right]^{1/4} \tag{8.67}$$

for a horizontal cylinder. (Nusselt got 0.725 for the lead constant, but he approximated the integral using a hand calculation.) ∎

This calculation has been applied to a number of additional cases.

Sphere of diameter D:

$$\overline{\mathrm{Nu}}_D = 0.828 \left[\frac{g_e (\rho_f - \rho_g) h'_{fg} D^3}{\nu k (T_{\mathrm{sat}} - T_w)} \right]^{1/4} \tag{8.68}$$

This result[9] is the one compared to experimental data in Fig. 8.10.

Vertical cone with the apex on top, the bottom insulated, and a cone angle of $\alpha°$:

$$\mathrm{Nu}_x = 0.874 \left[\cos(\alpha/2) \right]^{1/4} \left[\frac{g_e (\rho_f - \rho_g) h'_{fg} x^3}{\nu k (T_{\mathrm{sat}} - T_w)} \right]^{1/4} \tag{8.69}$$

Rotating horizontal disk[10]: In this case, $g = \omega^2 x$, where x is the distance from the center and ω is the speed of rotation. The Nusselt number, based on $L = (\mu/\rho_f \omega)^{1/2}$, is

$$\overline{\mathrm{Nu}} = 0.9034 \left[\frac{\nu (\rho_f - \rho_g) h'_{fg}}{k (T_{\mathrm{sat}} - T_w)} \right]^{1/4} = \text{constant} \tag{8.70}$$

This result might seem strange at first glance. It says that $\mathrm{Nu} \neq \mathrm{fn}(x \text{ or } \omega)$. The reason is that δ just happens to be independent of x in this configuration.

The Nusselt solution can thus be bent to fit many complicated geometric figures. One of the most complicated ones to have been dealt with is the reflux condenser shown in Fig. 8.14. In such a configuration,

---

[9]There is an error in [8.31]: the constant given there is 0.785. The value of 0.828 given here is correct.

[10]This problem was originally solved by Sparrow and Gregg [8.36].
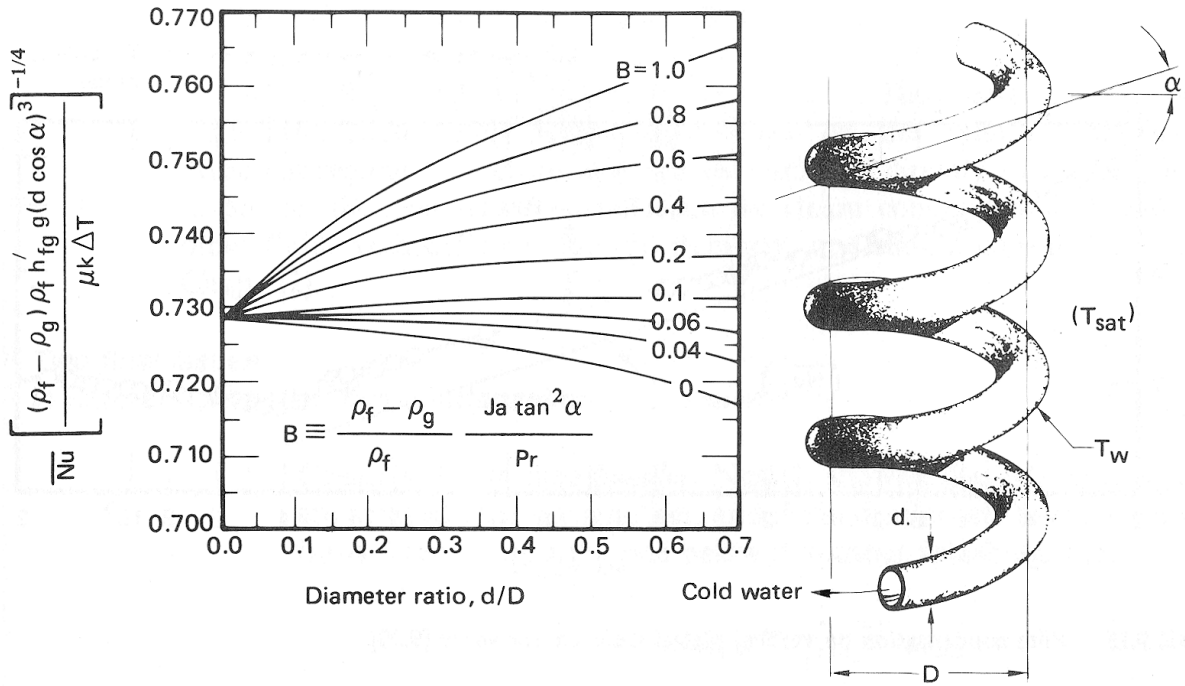
Figure 8.14 Fully developed film condensation heat transfer on a helical reflux condenser [8.37].

cooling water flows through a helically wound tube and vapor condenses on the outside, running downward along the tube. As the condensate flows, centripetal forces sling the liquid outward at a downward angle. This complicated flow was analyzed by Karimi [8.37], who found that

$$\overline{\mathrm{Nu}} \equiv \frac{\overline{h}d\cos\alpha}{k} = \left[\frac{(\rho_f - \rho_g)\rho_f h'_{fg} g (d\cos\alpha)^3}{\mu k \Delta T} \right]^{1/4} \mathrm{fn}\!\left(\frac{d}{D}, B\right) \quad (8.71)$$

where B is a centripetal parameter:

$$B \equiv \frac{\rho_f - \rho_g}{\rho_f} \frac{c_p \Delta T}{h'_{fg}} \frac{\tan^2\alpha}{\mathrm{Pr}}$$

and α is the helix angle (see Fig. 8.14). The function on the righthand side of eqn. (8.71) is a complicated one that must be evaluated numerically. Karimi's result is plotted in Fig. 8.14.

Laminar–turbulent transition

The mass flow rate of condensate per unit width of film, $\dot{m}$, is more commonly designated as Γ_c (kg/m · s). Its calculation in eqn. (8.53) involved substituting eqn. (8.51) into

$$\dot{m} \text{ or } \Gamma_c = \rho_f \int_0^\delta u \, dy$$

Equation (8.51) gives $u(y)$ independently of any geometric features. The geometry determines the local values of $\delta(x)$. Thus, the resulting equation for the mass flow rate is still given by eqn. (8.53)

$$\Gamma_c = \frac{(\rho_f - \rho_g)g\delta^3}{3\nu} \tag{8.53a}$$

This expression is valid for any location along any film, regardless of the shape of the body. The specific configuration will lead to variations of $g(x)$ and $\delta(x)$, but eqn. (8.53a) still applies.

A useful Reynolds number may be defined in terms of Γ_c. This definition is easily set because Γ_c is equal to $\rho u_{\text{av}}\delta$:

$$\text{Re}_c = \frac{\rho u_{\text{av}}\delta}{\mu} = \frac{\Gamma_c}{\mu} = \frac{\rho_f(\rho_f - \rho_g)g\delta^3}{3\mu^2} \tag{8.72}$$

This Reynolds number dictates the onset of film instability, just as Re dictates the instability of a b.l. or of a pipe flow.[11] When $\text{Re}_c \cong 7$, scallop-shaped ripples become visible on the condensate film. When Re_c reaches about 400, a full-scale laminar-to-turbulent transition occurs.

Gregorig, Kern, and Turek [8.38] reviewed many data for the film condensation of water and added their own measurements. Figure 8.15 shows these data in comparison with Nusselt's theory, eqn. (8.62b). The comparison is almost perfect up to $\text{Re}_c \cong 7$. The heat transfer rates then begin to exceed the prediction. That increase is caused by ripples. The effect is minor at first. But it increases to about 20% just before the full laminar-to-turbulent transition occurs at $\text{Re}_c \simeq 400$.

Above $\text{Re}_c = 400$, $\overline{\text{Nu}}_L$ begins to rise with Re_c. The Nusselt number becomes dependent on the Prandtl number in the turbulent regime. Therefore, one can use Fig. 8.15 directly, as a data correlation, to predict the heat transfer coefficient for steam condensing at 1 atm. But for other fluids with different Prandtl numbers, one should consult [8.39] or [8.40].

---

[11]Two Reynolds numbers are in use for film condensation: Γ_c/μ and $4\Gamma_c/\mu$. The latter one, which is simply four times as large as the one we use, is more common in the American literature and is based on the hydraulic diameter of the film (see Problem 8.54).
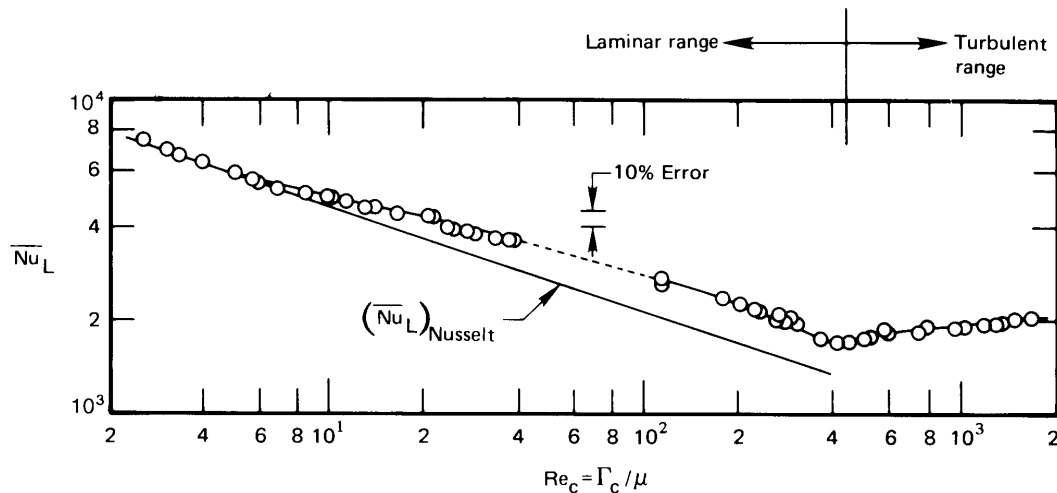
Figure 8.15 Film condensation on vertical plates. Data are for water with Pr = 2.2 ± 20% [8.38].

Two final issues in natural convection film condensation

- *Condensation in tube bundles.* Nusselt showed that if n horizontal tubes are arrayed over one another, and if the condensate leaves each one and flows directly onto the one below it without splashing, then

$$\text{Nu}_{D\text{for } n \text{ tubes}} = \frac{\text{Nu}_{D\,1\,\text{tube}}}{n^a} \tag{8.73}$$

Nusselt's value was $a = 1/4$. However, a more detailed analysis and later measurements suggest $a = 1/6$ [8.40]. (These analyses envision the films flowing smoothly from one tube to another, which is rather optimistic.) In addition, the effects of vapor shear stress on the condensate and of pressure losses on the saturation temperature are often important in tube bundles. These effects are discussed by Rose et al. [8.40] and Marto [8.39].

- *Condensation in the presence of noncondensable gases.* When the condensing vapor is mixed with noncondensable air, uncondensed air must constantly diffuse away from the condensing film and vapor must diffuse inward toward the film. This coupled diffusion process can considerably slow condensation. The resulting h can easily be cut by a factor of two if there is as little as 1% by mass of air mixed into the steam [8.41]. For this reason, flow within condensers is

designed to help sweep out noncondensable gases. The analysis of noncondensable gases in condensation is a problem in mass transfer (see Problem 11.42). The literature is discussed in [8.39, 8.40].

Problems

8.1   Show that Π_4 in the film condensation problem can properly be interpreted as $\Pr \mathrm{Re}^2/\mathrm{Ja}$. *Hint*: A characteristic velocity is needed— use the speed that the liquid would reach in free fall over a distance L.

8.2   A 20 cm high vertical plate is kept at 34°C in a 20°C room. Plot (*to scale*) δ and h vs. height and the temperature and velocity vs. y at the top. What are the maximum values of δ and u? *Hint*: Use the Squire-Eckert results.

8.3   Redo the Squire-Eckert analysis, neglecting inertia, to get a high-Pr approximation to Nu_x. Compare your result to the Squire-Eckert formula. Explain the difference.

8.4   Assume a linear temperature profile and a simple triangular velocity profile, as shown in Fig. 8.16, for natural convection on a vertical isothermal plate. Derive $\mathrm{Nu}_x = \mathrm{fn}(\Pr, \mathrm{Gr}_x)$, compare your result with the Squire-Eckert result, and discuss the comparison. *Hint*: This very crude approximation yields results that are in error by only 15% or so.
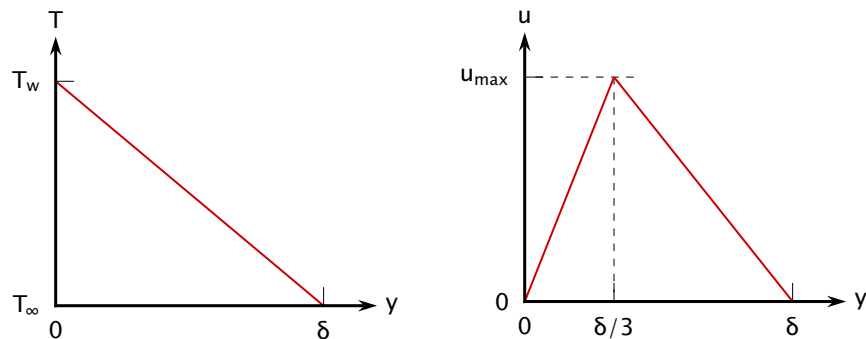
Figure 8.16   Profiles for Problem 8.4.

8.5   An uninsulated horizontal cylindrical duct of diamond-shaped cross section (Fig. 8.17) carries air at 35°C. Since almost all thermal resistance is in the natural convection b.l. on the outside, take T_w to be approximately 35°C. $T_\infty = 25$°C. Estimate the natural convection

heat loss per meter of duct. By how much might the result change if the b.l. were to separate at the corners? [$Q = 24.0$ W/m.]
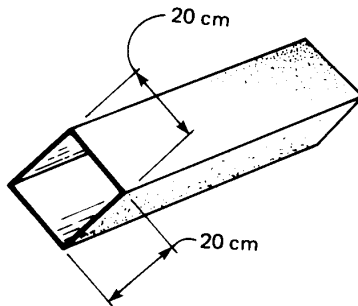
Figure 8.17   Configuration for Problem 8.5.

8.6 A 3 m high, electrically heated panel in a wall delivers 175 W/m^2 to still air an 18°C room. Radiation from the panel can be approximated as uniform at 100 W/m^2. What is the average temperature of the panel? What is the temperature at the top? At the bottom? *Hint*: The temperature at the bottom of the panel is 18°C.

8.7 Find pipe diameters and wall temperatures for which the film condensation heat transfer coefficients given in Table 1.1 are valid. Assume the vapor to be at 1 atm. Note that you will need to locate data for benzene, which is not covered in App. A; this kind of hurdle is common in engineering.

8.8 Consider Example 8.6. What value of wall temperature (if any), or what height of the plate, would result in a laminar-to-turbulent transition at the bottom in this example?

8.9 A plate spins, as shown in Fig. 8.18, in a vapor that rotates synchronously with it. Neglect earth-normal gravity and calculate Nu$_L$ as a result of film condensation. *Hint*: Note the aspects of this problem that are similar to the rotating horizontal disk discussed on page 452.

8.10 A laminar liquid film at T_{sat} flows down a vertical wall that is also at T_{sat}. Flow is fully developed and the film thickness is δ_o. Along a particular horizontal line, the wall temperature drops to a lower value, T_w, and it is kept at that temperature everywhere below. Call the line where the wall temperature changes $x = 0$. If the region adjacent to the film is saturated vapor of the flowing liquid, calculate $\delta(x)$, Nu$_x$, and Nu$_L$, where $x = L$ is the bottom edge of the wall. (Neglect any transition behavior in the neighborhood of $x = 0$.) *Hint*: Begin with eqn. (8.55).
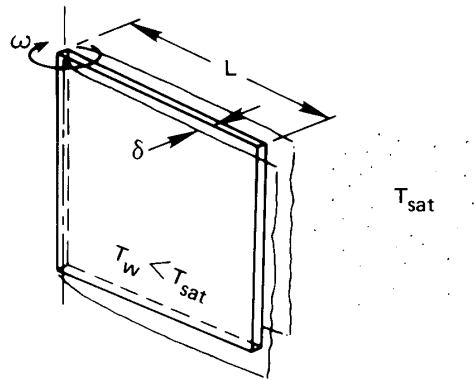
Figure 8.18 Configuration for
Problem 8.9.

8.11 Prepare a table of formulas of the form

$$\overline{h}\,(\text{W/m}^2\text{K}) = C[\Delta T/L\ \text{K/m}]^{1/4}$$

for natural convection at normal gravity in air and in water at $T_\infty = 27°\text{C}$. Assume that T_w is close to $27°\text{C}$. Your table should include results for vertical plates, horizontal cylinders, spheres, and possibly additional geometries. Do not include your calculations.

8.12 For what value of Pr is the condition

$$\left.\frac{\partial^2 u}{\partial y^2}\right|_{y=0} = \frac{g\beta(T_w - T_\infty)}{\nu}$$

satisfied exactly in the Squire-Eckert b.l. solution? [Pr = 2.86.]

8.13 The side wall of a house is 10 m in height. The overall heat transfer coefficient between the interior air and the exterior surface is 2.5 W/m²K. On a cold, still winter night $T_{\text{outside}} = -30°\text{C}$ and $T_{\text{inside air}} = 25°\text{C}$. What is $\overline{h}_{\text{conv}}$ on the exterior wall of the house if $\varepsilon = 0.9$? Is the external convection laminar or turbulent? $[\overline{h} = 4.59\ \text{W/m}^2\text{K}]$

8.14 Consider Example 8.2. The sheets are mild steel, 2 m long and 6 mm thick. The bath is basically water at $60°\text{C}$, and the sheets are put in it at $18°\text{C}$. (a) Plot the sheet temperature as a function of time. (b) By approximating $\overline{h}$ at $\Delta T = [(60 + 18)/2 - 18]°\text{C}$, plot the conventional exponential response on the same graph.

8.15 In eqn. 8.7, we linearized the temperature dependence of the density difference. Suppose that a wall at temperature T_w sits in water

at $T_\infty = 7°C$. Use the data in Table A.3 to plot $|\rho_w - \rho_\infty|$ and $|-\rho_f \beta_f (T_w - T_\infty)|$ for $7°C \leqslant T_w \leqslant 100°C$, where $(..)_f$ is a value at the film temperature. How well does the linearization work?

8.16 A 77°C vertical wall heats 27°C air. Evaluate $\delta_{top}/L, \text{Ra}_L$, and L where the line in Fig. 8.3 ceases to be straight. Comment on the implications of your results. [$\delta_{top}/L \simeq 0.6$.]

8.17 A horizontal 8 cm O.D. pipe carries steam at 150°C through a room at 17°C. The pipe is covered by a 1.5 cm layer of 85% magnesia insulation. Evaluate the heat loss by natural convection per meter of pipe. [$Q = 97.3$ W/m.]

8.18 What heat rate (in W/m) must be supplied to a 0.01 mm horizontal wire to keep it 30°C above the 10°C water around it?

8.19 A vertical run of copper tubing, 5 mm in diameter and 20 cm long, carries condensing vapor at 60°C through 27°C air. What is the total heat loss? *Hint*: Are any of the thermal resistances negligible? [$Q = 0.94$ W]

8.20 A body consists of two cones joined at their bases. The diameter is 10 cm and the overall length of the joined cones is 25 cm. The axis of the body is vertical, and the body is kept at 27°C in 7°C air. What is the rate of heat removal from the body by natural convection? [$Q = 3.38$ W.]

8.21 Consider the plate dealt with in Example 8.1. Plot $\overline{h}$ as a function of the angle of inclination of the plate as the hot side is tilted both upward and downward over the range $\pm 90°$. Note that you must make do with discontinuous formulæ in different ranges of θ.

8.22 You are asked to design a vertical wall panel heater, 1.5 m high, for a dwelling. What should the heat flux be if no part of the wall should exceed 33°C? How much heat goes to the room if the panel is 7 m wide with $\varepsilon = 0.7$? *Hint*: Natural convection removes only about 200 W depending on what room temperature you assume.

8.23 A 14 cm high vertical surface is heated by condensing steam at 1 atm. Provide an expression for the fractional change of heat removal if H_2O is replaced with a different condensing fluid to heat the wall. Choose an organic fluid and evaluate the percentage change in $\overline{h}$ if the wall is at 30°C for both fluids.

8.24 A 1 cm O.D. tube extends 27 cm horizontally through a region of saturated steam at 1 atm. The outside of the tube can be maintained at any temperature between 50°C and 150°C. Plot the heat transfer as a function of tube temperature, omitting thermal radiation.

8.25 A 2 m high vertical plate condenses steam at 1 atm. Below what wall temperature will Nusselt's prediction of $\bar{h}$ begin to lose accuracy? Below what temperature will the condensing film be turbulent?

8.26 A helical reflux condenser is made of 0.8 cm O.D. copper tubing with a wall temperature of 30°C. It condenses steam at 1 atm. Find $\bar{h}$ if $\alpha = 18°$ and the coil diameter is 7 cm. [$\bar{h} = 9.5$ kW/m^{2}K]

8.27 The coil diameter of a helical condenser is 5 cm and the tube diameter is 5 mm. The condenser carries water at 15°C and is in a bath of saturated steam at 1 atm. Specify the number of coils and a reasonable helix angle if 6 kg/hr of steam is to be condensed. $h_{inside} = 600$ W/m^{2}K. [4.4 coils]

8.28 A schedule 40, 304 stainless steel steam pipe with a 4 in. nominal diameter carries saturated steam at 150 psia in a processing plant. Calculate the heat loss per unit length of pipe if it is bare and the surrounding air is still at 68°F. How much would this heat loss be reduced if the pipe were insulated with a 1 in. layer of jacketed glass-fiber pipe insulation? Assume $\varepsilon_{ss} = 0.55$ and $\varepsilon_{gf} = 0.9$.

8.29 What is the maximum speed of air in the natural convection b.l. in Example 8.3? [$u_{max} = 0.35$ m/s]

8.30 Several of the uniform-T_w, natural convection correlations in this chapter include a small additive constant and a complicated Pr factor: eqns. (8.13a), (8.28), and (8.33). Suppose that Pr is large and that Ra is large enough to neglect that additive constant. What form do these correlations take? What if you write them in terms of Gr instead of Ra? In the same limits, what is the form of the turbulent flow correlations, eqns. (8.13b) and (8.29)?

8.31 An industrial process includes a very large horizontal cylinder immersed in a pool of water. The water is at 27°C. The diameter of the cylinder is 5 m, and it is kept at 67°C. First, find $\bar{h}$. Then suppose that the diameter is increased to 10 m. What is the new $\bar{h}$? Explain the similarity of these answers in the turbulent natural convection regime. [$\bar{h} \simeq 1000$ W/m^{2}K]

8.32 A vertical jet of liquid of diameter d and moving at velocity u_∞ impinges on a horizontal disk rotating ω rad/s. There is no heat transfer in the system. Develop an expression for $\delta(r)$, where r is the radial coordinate on the disk. Contrast the r dependence of δ with that of a condensing film on a rotating disk and explain the difference qualitatively. *Hint*: δ will vary as $r^{-2/3}$.

8.33 We have seen that if properties are constant, $h \propto \Delta T^{1/4}$ in natural convection. If we consider the variation of properties as T_w is increased over T_∞, will h depend more or less strongly on ΔT in air? in water?

8.34 A film of liquid falls along a vertical plate. It is initially saturated, and it is surrounded by saturated vapor. The film thickness is δ_o. If the wall temperature below a certain point on the wall (call it $x = 0$) is raised to a value of T_w, slightly above T_{sat}, derive expressions for $\delta(x)$, Nu_x, and x_f—the distance at which the plate becomes dry. Calculate x_f if the fluid is water at 1 atm, if $T_w = 105°C$, and $\delta_o = 0.1$ mm. *Hint*: The plate will dry out in just over 0.5 m.

8.35 In a particular solar steam generator, water containing high absorptance dye runs down a vertical plate in a laminar film. The film's initial thickness is δ_o. The sun's rays pass through parallel glass plates (see Section 10.6) a short distance away from the liquid surface, depositing q_s W/m^2 at the surface of the film. Assume the water to be saturated at the inlet and the plate behind it to be insulated. Develop an expression for $\delta(x)$ as the water evaporates. Develop an expression for the maximum length of wetted plate, and determine an expression for the maximum value of δ_o for laminar solution to be valid.

8.36 What heat flux can be achieved at the surface of a horizontal 0.01 mm diameter electrical resistance wire in still 27°C air if its melting point is 927°C? Neglect radiation. *Hint*: Your answer will be remarkably large.

8.37 A 0.03 m O.D. vertical pipe, 3 m in length with $\varepsilon = 0.7$, carries refrigerant through a 24°C room at low humidity. How much heat does it absorb from the room if the pipe wall is at 10°C? [$Q = 25.8$ W]

8.38　A 1 cm O.D. tube at 50°C runs horizontally in 20°C air. What is the critical radius of 85% magnesia insulation on the tube? The insulation has been coated to have a very low emissivity. *Hint*: An iterative solution is required.

8.39　A 25.4 mm (1 in.) ice cube is suspended in 20°C air. Estimate the drip rate in gm/min. Neglect ΔT through the departing water film, and assume poor convection on the top surface. $h_{sf} = 333.3$ kJ/kg.

8.40　A horizontal electrical resistance heater, 1 mm in diameter, releases 100 W/m in water at 17°C. What is the wire temperature? [$T_w \approx$ 47°C]

8.41　Solve Problem 5.39 using the correct formula for the heat transfer coefficient.

8.42　A vertical rod, 20 mm long and 5 mm in diameter, becomes red hot when it is used to shunt an electrical current in air at room temperature. How much power can it dissipate if its melting point is 1000°C? Note all assumptions and corrections. Include radiation using $\mathcal{F}_{\text{rod-room}} = 0.15$. *Hint*: More than half the heat transfer is by radiation.

8.43　A 0.25 mm diameter platinum wire, 0.2 m long, is to be held horizontally at 1035°C. It is black. How much electric power is needed? Is it legitimate to treat it as a constant-wall-temperature heater in calculating the convective part of the heat transfer? The surroundings are at 20°C and the surrounding room is effectively black.

8.44　A vertical plate, 11.6 m long, condenses saturated steam at 1 atm. We want to be sure that the film stays laminar. What is the lowest allowable plate temperature, and what is $\bar{q}$ at this temperature? [$\bar{q} = 25$ kW/m^2]

8.45　A straight horizontal fin exchanges heat by laminar natural convection with the surrounding air.

　　a. Show that

$$\frac{d^2\theta}{d\xi^2} = m^2 L^2 \theta^{5/4}$$

　　where m is based on $\overline{h}_o \equiv \overline{h}(T = T_o)$.

　　b. If you have access to appropriate software for integrating an o.d.e., solve the equation for $m^2 L^2$ values ranging from 10^{-3} to 10^3. Express the results as η/η_o, where η is the fin

efficiency and η_o is the efficiency that would result if $\overline{h}_o$ were the uniform heat transfer coefficient over the entire fin.

8.46 A 2.5 cm black sphere ($\mathcal{F} = 1$) is in radiation-convection equilibrium with air at 20°C. The surroundings are at 1000 K. What is the temperature of the sphere? *Hint*: An iterative solution is required.

8.47 Develop expressions for $\overline{h}(D)$ and $\overline{Nu}_D$ during condensation on a vertical circular plate.

8.48 A 5 mm rim surrounds a horizontal metal disk, 300 mm in diameter, to form a shallow container. The disk is at 95°C and is surrounded by saturated water vapor at 100°C.

   a. Estimate the steady heat flux to the disk and rate of condensation.

   b. If the container is initially empty, estimate the time to fill it.

8.49 A proposed design for a nuclear power plant uses molten lead to remove heat from the reactor core. The heated lead is then used to boil water to drive a steam turbine. Water at 60°C and 70 bar ($T_{sat} = 286$°C) flows at $\dot{m} = 2$ kg/s through a section of pipe heated by the lead. The pipe is stainless steel ($k_s = 15$ W/m·K) with a wall thickness of 12 mm and a 62 mm O.D. The lead outside the pipe is almost-stationary and at 477°C.

   a. At a point where the liquid water has a bulk temperature $T_b = 80$°C, estimate the inside and outside wall temperatures of the pipe, T_{w_i} and T_{w_o}, to within about 5°C. Neglect the entry length and variable properties effects and take $\beta_{lead} \approx 0.000118$ K^{-1}. *Hint:* Guess an outside wall temperature above 370°C when computing $\overline{h}$ for the lead.

   b. At what distance from the inlet will the inside wall of the pipe reach T_{sat}? What changes to the design may be needed?

8.50 A flat plate, 10 cm long and 40 cm wide, is inclined at 30° from vertical. It is held at a uniform temperature of 250 K. Saturated HCFC-22 vapor at 260 K condenses onto the plate. Determine:

   a. The ratio h'_{fg}/h_{fg}.

   b. The average heat transfer coefficient and the rate in watts at which the plate must be cooled.

   c. The film thickness at the bottom of the plate, and the plate's rate of condensation in g/s.

8.51 One component in a particular automotive air-conditioning system is a "receiver", a small vertical cylindrical tank that contains a pool of liquid refrigerant, HFC-134a, with vapor above it. The receiver stores extra refrigerant for the system and helps to regulate the pressure. The receiver is at equilibrium with surroundings at 330 K. A 5 mm diameter, spherical thermistor inside the receiver monitors the liquid level. The thermistor is a temperature-sensing resistor driven by a small electric current; it dissipates a power of 0.1 W. When the system is full y charged with refrigerant, the thermistor sits below the liquid surface. When refrigerant leaks from the system, the liquid level drops and the thermistor eventually sits in vapor. The thermistor is small compared to the receiver, and its power is too low to affect the bulk temperature in the receiver.

   a. Find the thermistor's temperature when the system is fully charged. *Hint:* $\overline{\mathrm{Nu}}_D \gg 2$.

   b. Find the thermistor's temperature when enough refrigerant has leaked that the thermistor sits in vapor. Neglect radiation.

8.52 Ammonia vapor at 300 K and 1.062 MPa pressure condenses onto the outside of a horizontal tube. The tube has an O.D. of 19.1 mm.

   a. Suppose that the outside of the tube has a uniform temperature of 290 K. Determine the average condensation heat transfer coefficient.

   b. The tube is cooled by cold water flowing through it, and the thermal resistance of the thin copper tube is negligible. If the bulk temperature of the water is 275 K at a location where the outside surface of the tube is at 290 K, what is the heat transfer coefficient inside the tube?

   c. Using the heat transfer coefficients you just found, estimate the largest wall thickness for which the thermal resistance of the tube could be neglected. Describe the variation the tube wall temperature around the circumference and along the length of the tube.

8.53 An inclined plate in a piece of process equipment is tilted 30° above horizontal. The plate is 20 cm long in the inclined plane and 25 cm wide. The plate is held at 280 K by a liquid flowing past its underside. The liquid is cooled by a refrigeration system

capable of removing 12 W, but if the heat load exceeds 12 W, the temperature of both the liquid and the plate will begin to rise. The upper surface of the plate is in contact with ammonia vapor at 300 K and a varying pressure. An engineer suggests that an increase of the bulk temperature of the liquid will signal that the pressure has exceeded a level of about $p_{crit} = 551$ kPa.

a. Explain why the gas's pressure will affect the heat transfer to the coolant. What is the significance $p_{crit} = 551$ kPa?

b. Suppose that the pressure is 255.3 kPa. What is the heat transfer rate (W) from the gas to the plate, if the plate temperature is $T_w = 280$ K? Will the coolant temperature rise?

c. Suppose that the pressure rises to 1062 kPa. What is the heat transfer rate if the plate is still at $T_w = 280$ K? Will the coolant temperature rise?

For gaseous ammonia at 255.3 kPa and 290 K: $\beta = 0.0040$ K^{-1}, $\rho = 1.86$ kg/m^3, $c_p = 2314$ J/kgK, $\mu = 9.75 \times 10^{-6}$ kg/m^3, and $k = 0.0247$ W/m·K. Take other data from Appendix A.

8.54 The film Reynolds number Re$_c$ in eqn. (8.72) was based on the thickness, δ. Show that the Reynolds number would be four times larger if it were based on the hydraulic diameter of the film.

8.55 A characteristic length scale for a falling liquid film is $\ell = (v^2/g)^{1/3}$. If the Nusselt number for a laminar film condensing on plane wall is written as Nu$_\ell \equiv h\ell/k$, derive an expression for Nu$_\ell$ in terms of Re$_c$. Show that, when $\rho_f \gg \rho_g$, Nu$_\ell = (3\text{Re}_c)^{-1/3}$.

8.56 Plot eqns. (8.13a) and (8.13b) on the coordinates matching Fig. 8.3. (Since each has a slightly different Pr dependence, use Pr = 0.7.) Over what range are these equations in good agreement? Copy data points from Fig. 8.3 for abscissa values of 10^9, 10^{10}, 10^{11}, and 10^{12} and add them to your graph. How do the data compare to the correlations?

8.57 Perform the integration for $\overline{h}$ in Example 8.8 and obtain eqn. (8.67). *Hint*: Recall that the gamma function, $\Gamma(z)$, is a tabulated special function. It may be shown that [8.42, §12.41]:

$$\int_0^{\pi/2} \cos^{2m-1}\theta \sin^{2n-1}\theta \, d\theta = \frac{\Gamma(m)\Gamma(n)}{2\,\Gamma(m+n)} \quad \text{for } m, n > 0$$

8.58 If the oil line in Example 8.4 is polished stainless steel with $\varepsilon = 0.17$, how does the total heat loss vary with g-level?

8.59 Using data from Tables A.4 and A.5, plot β for saturated ammonia vapor over 200 K $\leqslant T \leqslant$ 380 K, together with the ideal gas expression, $\beta_{IG} = 1/T$. Also calculate $Z = P/\rho RT$. Is ammonia vapor more like an ideal gas near the triple point or critical point temperature?

References

[8.1] W. Nusselt. Das grundgesetz des wärmeüberganges. *Gesund. Ing.*, **38**: 872, 1915.

[8.2] C. J. Sanders and J. P. Holman. Franz Grashof and the Grashof Number. *Int. J. Heat Mass Transfer*, **15**(3):562–563, March 1972. doi: 10.1016/0017-9310(72)90220-7.

[8.3] S. W. Churchill and H. H. S. Chu. Correlating equations for laminar and turbulent free convection from a vertical plate. *Int. J. Heat Mass Transfer*, **18**(11):1323–1329, November 1975. doi: 10.1016/0017-9310(75)90243-4.

[8.4] S. Goldstein, editor. *Modern Developments in Fluid Mechanics*, Vol. 2, Chapter 14. Oxford University Press, New York, 1938.

[8.5] E. R. G. Eckert and R. M. Drake, Jr. *Analysis of Heat and Mass Transfer*. Hemisphere Publishing Corp., Washington, D.C., 1987.

[8.6] A. Bejan and J. L. Lage. The Prandtl number effect on the transition in natural convection along a vertical surface. *J. Heat Transfer*, **112**(3): 787–790, August 1990. doi: 10.1115/1.2910457.

[8.7] W. Kraus. *Messungen des Temperatur- und Geschwindigkeitsfeldes bei freier Konvektion*. Verlag G. Braun, Karlsruhe, 1955. Chapter F.

[8.8] S. W. Churchill and H. H. S. Chu. Correlating equations for laminar and turbulent free convection from a horizontal cylinder. *Int. J. Heat Mass Transfer*, **18**(9):1049–1053, September 1975. doi: 10.1016/0017-9310(75)90222-7.

[8.9] T. Cebeci. Laminar-free-convective-heat transfer from the outer surface of a vertical slender circular cylinder. In *Proc. Fifth Int. Heat Transfer Conf.*, Vol. 3, pp. 15–19. Tokyo, September 3–7, 1974.

[8.10] T. Yuge. Experiments on heat transfer from spheres including combined forced and natural convection. *J. Heat Transfer*, **82**(3):214, August 1960. doi: 10.1115/1.3679912.

[8.11] G. D. Raithby and K. G. T. Hollands. Natural convection. In W. M. Rohsenow, J. P. Hartnett, and Y. I. Cho, editors, *Handbook of Heat Transfer*, Chapter 4. McGraw-Hill, New York, 3rd ed., 1998.

[8.12] J. H. Lienhard. On the commonality of equations for natural convection from immersed bodies. *Int. J. Heat Mass Transfer*, **16**(11):2121–2123, November 1973. doi: 10.1016/0017-9310(73)90116-6.

[8.13] B. R. Rich. An investigation of heat transfer from an inclined flat plate in free convection. *Trans. ASME*, **75**(4):489–499, May 1953. doi: 10.1115/1.4015329.

[8.14] T. Fujii and H. Imura. Natural convection heat transfer from a plate with arbitrary inclination. *Int. J. Heat Mass Transfer*, **15**(4):755–767, April 1972. doi: 10.1016/0017-9310(72)90118-4.

[8.15] G. C. Vliet. Natural convection local heat transfer on constant heat transfer inclined surface. *J. Heat Transfer*, **91**(4):511–516, November 1969. doi: 10.1115/1.3580235.

[8.16] L. Pera and B. Gebhart. On the stability of natural convection boundary layer flow over horizontal and slightly inclined surfaces. *Int. J. Heat Mass Transfer*, **16**(6):1147–1163, June 1973. doi: 10.1016/0017-9310(73)90127-0.

[8.17] M. Al-Arabi and M. K. El-Riedy. Natural convection heat transfer from isothermal horizontal plates of different shapes. *Int. J. Heat Mass Transfer*, **19**:1399–1404, December 1976. doi: 10.1016/0017-9310(76)90069-7.

[8.18] L. Pera and B. Gebhart. Natural convection boundary layer flow over horizontal and slightly inclined surfaces. *Int. J. Heat Mass Transfer*, **16**(6):1131–1147, June 1973. doi: 10.1016/0017-9310(73)90126-9.

[8.19] B. Gebhart, Y. Jaluria, R. L. Mahajan, and B. Sammakia. *Buoyancy-Induced Flows and Transport*. Hemisphere Publishing Corp., Washington, D.C., 1988.

[8.20] J. R. Lloyd and W. R. Moran. Natural convection adjacent to horizontal surface of various planforms. *J. Heat Transfer*, **96**(4):443–447, November 1974. doi: 10.1115/1.3450224.

[8.21] A. M. Clausing and J. J. Berton. An experimental investigation of natural convection from an isothermal horizontal plate. *J. Heat Transfer*, **111**(4): 904–908, November 1989. doi: 10.1115/1.3250804.

[8.22] F. Restrepo and L. R. Glicksman. The effect of edge conditions on natural convection heat transfer from a horizontal plates. *Int. J. Heat Mass Transfer*, **17**(1):135–142, January 1974. doi: 10.1016/0017-9310(74)90046-5.

[8.23] D. W. Hatfield and D. K. Edwards. Edge and aspect ratio effects on natural convection from the horizontal heated plate facing downwards. *Int. J. Heat Mass Transfer*, **24**(6):1019–1024, June 1981. doi: 10.1016/0017-9310(81)90132-0.

[8.24] V. Kadambi and R. M. Drake, Jr. Free convection heat transfer from horizontal surfaces for prescribed variations in surface temperature and mass flow through the surface. Tech. Rept. Mech. Eng. HT-1, Princeton Univ., June 1959.

[8.25] K. T. Yang. Natural convection in enclosures. In S. Kakaç, R. K. Shah, and W. Aung, editors, *Handbook of Single-Phase Convective Heat Transfer*, Chapter 13. Wiley-Interscience, New York, 1987.

[8.26] I. Catton. Natural convection in enclosures. In *Proc. Sixth Int. Heat Transfer Conf.*, Vol. 6, pp. 13–31, Toronto, August 7–11, 1978.

[8.27] S. W. Churchill. A comprehensive correlating equation for laminar, assisting, forced and free convection. *AIChE J.*, **23**(1):10–16, January 1977. doi: 10.1002/aic.690230103.

[8.28] T. S. Chen and B. F. Armaly. Mixed convection in external flow. In S. Kakaç, R. K. Shah, and W. Aung, editors, *Handbook of Single-Phase Convective Heat Transfer*, Chapter 14. Wiley-Interscience, New York, 1987.

[8.29] W. Aung. Mixed convection in internal flow. In S. Kakaç, R. K. Shah, and W. Aung, editors, *Handbook of Single-Phase Convective Heat Transfer*, Chapter 15. Wiley-Interscience, New York, 1987.

[8.30] V. K. Dhir. Quasi-steady laminar film condensation of steam on copper spheres. *J. Heat Transfer*, **97**(3):347–351, August 1975. doi: 10.1115/1.3450377.

[8.31] V. K. Dhir and J. H. Lienhard. Laminar film condensation on plane and axisymmetric bodies in non-uniform gravity. *J. Heat Transfer*, **93**(1): 97–100, February 1971. doi: 10.1115/1.3449773.

[8.32] W. Nusselt. Die oberflächenkondensation des wasserdampfes. *Z. Ver. Dtsch. Ing.*, **60**:541 and 569, 1916.

[8.33] W. M. Rohsenow. Heat transfer and temperature distribution in laminar-film condensation. *Trans. ASME*, **78**(8):1645–1648, November 1956. doi: 10.1115/1.4014125.

[8.34] E. M. Sparrow and J. L. Gregg. A boundary-layer treatment of laminar-film condensation. *J. Heat Transfer*, **81**(1):13–18, February 1959. doi: 10.1115/1.4008118.

[8.35] P. Sadasivan and J. H. Lienhard. Sensible heat correction in laminar film boiling and condensation. *J. Heat Transfer*, **109**(2):545–547, May 1987. doi: 10.1115/1.3248122.

[8.36] E. M. Sparrow and J. L. Gregg. A theory of rotating condensation. *J. Heat Transfer*, **81**(2):113–120, May 1959. doi: 10.1115/1.4008150.

[8.37] A. Karimi. Laminar film condensation on helical reflux condensers and related configurations. *Int. J. Heat Mass Transfer*, **20**(11):1137–1144, November 1977. doi: 10.1016/0017-9310(77)90122-3.

[8.38] R. Gregorig, J. Kern, and K. Turek. Improved correlation of film condensation data based on a more rigorous application of similarity parameters. *Wärme- und Stoffübertragung*, **7**:1–13, March 1974. doi: 10.1007/BF01438315.

[8.39] P. J. Marto. Condensation. In W. M. Rohsenow, J. P. Hartnett, and Y. I. Cho, editors, *Handbook of Heat Transfer*, Chapter 14. McGraw-Hill, New York, 3rd ed., 1998.

[8.40] J. Rose, H. Uehara, S. Koyama, and T. Fujii. Film condensation. In S. G. Kandlikar, M. Shoji, and V. K. Dhir, editors, *Handbook of Phase Change: Boiling and Condensation*, Chapter 19. Taylor & Francis, Philadelphia, 1999.

[8.41] V. E. Denny, A. F. Mills, and V. J. Jusionis. Laminar film condensation from a steam-air mixture undergoing forced flow down a vertical surface. *J. Heat Transfer*, **93**(3):297–304, August 1971. doi: 10.1115/1.3449814.

[8.42] E. T. Whittaker and E. N. Watson. *A Course of Modern Analysis*. Cambridge University Press, Cambridge, UK, 4th ed., 1927.

9. Heat transfer in boiling and other phase-change configurations

*For a charm of powerful trouble,
like a Hell-broth boil and bubble.. . .
. . .Cool it with a baboon's blood,
then the charm is firm and good.*

Macbeth, **Wm. Shakespeare**

"A watched pot never boils"—the water in a teakettle takes a long time to get hot enough to boil because natural convection initially warms it rather slowly. Once boiling begins, the water is heated the rest of the way to the saturation point very quickly. Boiling is of interest to us because it is remarkably effective in carrying heat from a heater into a liquid. The heater in question might be a red-hot horseshoe quenched in a bucket or the core of a nuclear reactor with coolant flowing through it. Our aim is to learn enough about the boiling process to deal with systems that use boiling for cooling. We begin by considering pool boiling—the boiling that occurs when a stationary heater transfers heat to an otherwise stationary liquid.

9.1 Nukiyama's experiment and the pool boiling curve

Hysteresis in the q vs. ΔT relation for pool boiling

In 1934, Shiro Nukiyama [9.1] did the experiment pictured in Fig. 9.1. He boiled saturated water on a horizontal wire that functioned both as an electric resistance heater and as a resistance thermometer. By calibrating the resistance of a Nichrome wire as a function of temperature before

Nukiyama's experiment
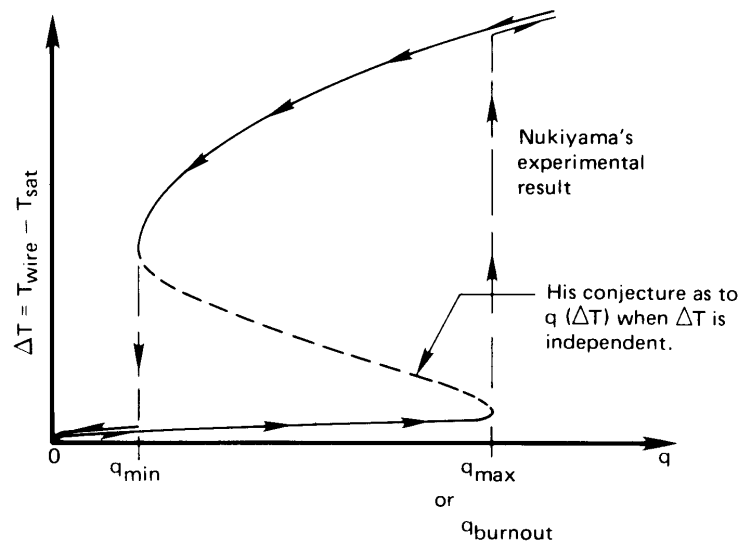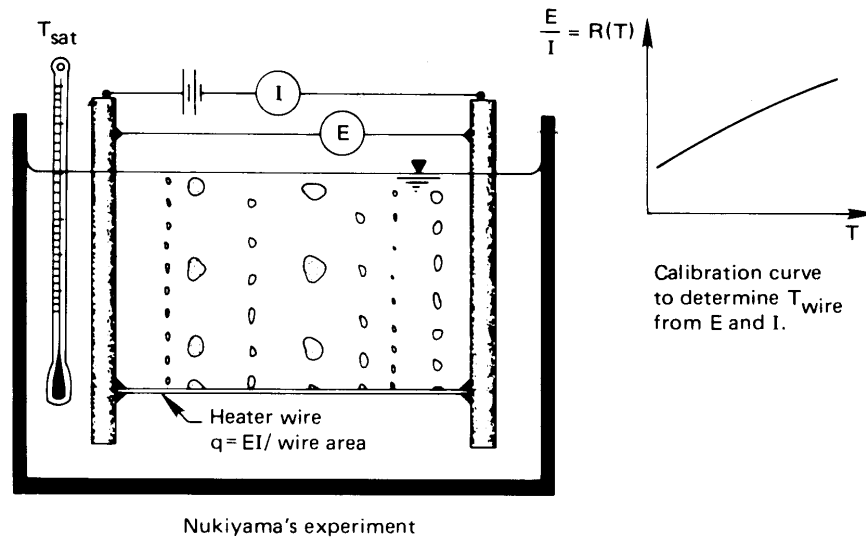
Figure 9.1 Nukiyama's boiling hysteresis loop.

he did the experiment, he was able to obtain both the heat flux and the temperature from the observed current and voltage. He found that, as he increased the power input to the wire,the heat flux rose sharply but the temperature of the wire increased relatively little. Suddenly, at a particular high value of the heat flux, the wire abruptly melted. Nukiyama then

obtained a platinum wire and tried again. This time the wire reached the same limiting heat flux, but then turned almost white-hot without melting.

As he reduced the power input to the white-hot wire, the temperature dropped in a continuous way, as shown in Fig. 9.1, until the heat flux was far below the value where the first temperature jump occurred. Then the temperature dropped abruptly to the original q vs. $\Delta T = (T_{wire} - T_{sat})$ curve, as shown. Nukiyama suspected that the hysteresis would not occur if ΔT could be specified as the independently controlled variable. He conjectured that such an experiment would result in the connecting line shown between the points where the temperatures jumped.

In 1937, Drew and Mueller [9.2] succeeded in making ΔT the independent variable by boiling organic liquids outside a tube. They allowed steam to condense inside the tube at an elevated pressure. The steam's saturation temperature—and hence the tube-wall temperature—was varied by controlling the steam's pressure. This permitted them to obtain a few scattered data points that seemed to bear out Nukiyama's conjecture.

Measurements of this kind proved inherently hard to make accurately. Therefore, the relatively few data that researchers obtained were, for many years, interpreted as verifying Nukiyama's suggestion that the boiling curve is continuous.

Figure 9.2 is a completed boiling curve for saturated water at atmospheric pressure on a particular flat horizontal heater. It displays the behavior shown in Fig. 9.1, but it has been rotated to place the independent variable, ΔT, on the abscissa. Nukiyama guessed that the behavior he measured on the left and on the right would be connected by a continuous curve. We show the regions as unconnected for reasons that we explain subsequently.

Modes of pool boiling

The boiling curve in Fig. 9.2 is divided into several regimes of behavior. We consider these regimes, and the transitions that divide them, next.

Natural convection.   Water that is not in contact with its own vapor does not boil at the so-called normal boiling point,[1] T_{sat}. Instead, it continues to rise in temperature until bubbles finally begin to form. On conventional machined metal surfaces, boiling occurs when the surface is a few degrees above T_{sat}. Below the bubble inception point, heat is removed by natural convection, as can be predicted by the methods laid out in Chapter 8.

---

[1]This notion might be new to some readers. It is explained in Section 9.2.
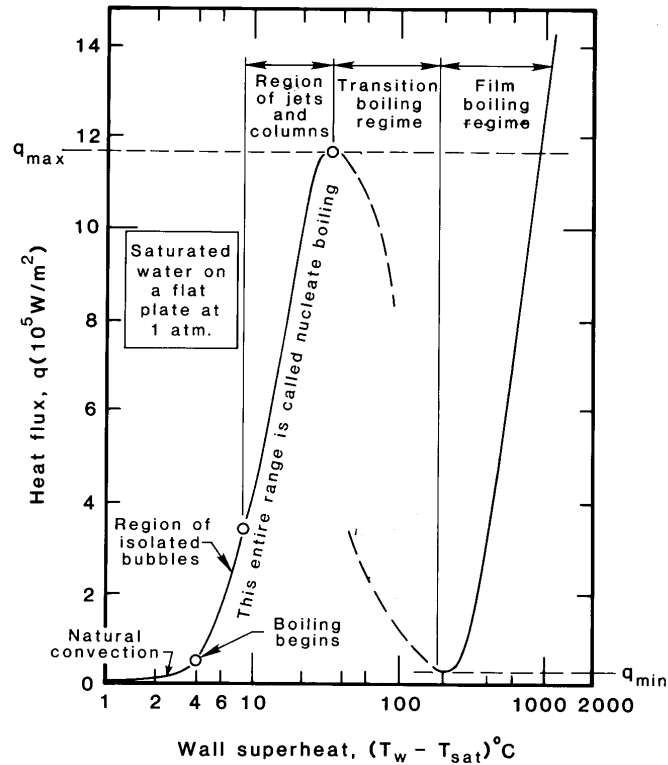
Figure 9.2   Typical boiling curve and regimes of boiling for an unspecified heater surface.

Nucleate boiling.   The nucleate boiling regime embraces two distinct regions that lie between bubble inception and Nukiyama's first transition point:

1. *The region of isolated bubbles.* In this range, bubbles rise from isolated nucleation sites, more or less as they are sketched in Fig. 9.1. As q and ΔT increase, more and more sites are activated. Figure 9.3a is a photograph of this regime as it appears on a horizontal plate.

2. *The region of slugs and columns.* When the active sites become very numerous, the bubbles start to merge into one another, and an entirely different kind of vapor escape path comes into play. Vapor formed at the surface merges immediately into jets that feed into large overhead bubbles or "slugs" of vapor. This process is shown as it occurs on a horizontal cylinder in Fig. 9.3b.

c. Two views of transitional boiling in acetone on a 3.2 mm diam. tube.
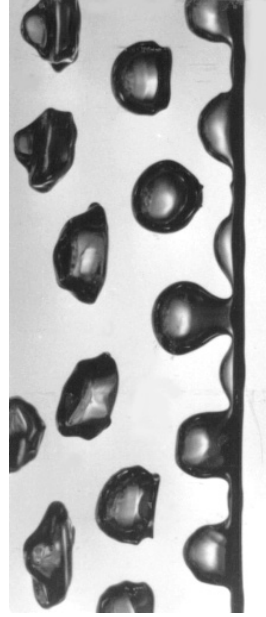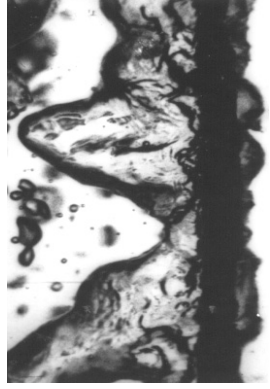
d. Film boiling of acetone on a 0.645 mm wire at earth-normal gravity. The true width of this image is 3.48 cm.

a. Isolated bubble regime—water.

3.45 cm length of 0.645 mm diam. wire in methanol at 10 earth-normal gravities. $q = 1.04 \times 10^6$ W/m^2

3.75 cm length of 1.64 mm diam. wire in benzene at earth-normal gravity. $q = 0.35 \times 10^6$ W/m^2

b. Two views of the regime of slugs and columns.

Figure 9.3: Typical photographs of boiling in the four regimes identified in Fig. 9.2 (All photos by JHL IV).

475

Peak heat flux, q_{max}.   We would clearly like to operate heat exchange equipment at the upper end of the region of slugs and columns. Here the temperature difference is low while the heat flux is very high. Heat transfer coefficients in this range are enormous. However, it is very dangerous to run equipment near q_{max} in systems for which q is the independent variable (as in nuclear reactors). If q is raised beyond the upper limit of the nucleate boiling regime, such a system will suffer the sudden and damaging increase of temperature that we indicate in Fig. 9.1. This transition[2] is known by a variety of names: the *burnout* point (although a complete burning up or melting away does not always accompany it); the *peak heat flux* (a modest descriptive term); the *boiling crisis* (a Russian term); and the *DNB*, or *departure from nucleate boiling*, and the *CHF*, or *critical heat flux* (terms more often used in flow boiling). We shall refer to it as the peak heat flux and designate it q_{max}.

Transitional boiling regime.   It might seem odd that the heat flux actually diminishes with ΔT after q_{max} is reached. However, the effectiveness of the vapor escape process in this regime becomes worse and worse. As ΔT is further increased, the hot surface becomes completely blanketed in vapor and q reaches a minimum heat flux which we call q_{min}. Figure 9.3c shows two typical instances of transitional boiling just beyond the peak heat flux.

Film boiling.   Once a stable vapor blanket is established, q again increases with increasing ΔT. The mechanics of the heat removal process during film boiling, and the regular removal of bubbles, has a great deal in common with film condensation, but the heat transfer coefficients are much lower because heat must be conducted through a vapor film instead of through a liquid film. We see an instance of film boiling in Fig. 9.3d.

Experiment 9.1

Set an open pan of cold tap water on your stove to boil. Observe the following stages as you watch:

- At first nothing appears to happen; then you notice that numerous small, stationary bubbles have formed over the bottom of the pan. These bubbles have nothing to do with boiling. Water

---

[2]We defer a proper physical explanation of the transition to Section 9.3.

normally contains a small amount of air in solution. The first bubbles that appear as the water warms up, are just air driven out of solution.

- Suddenly the pan will begin to "sing" with a somewhat high-pitched buzzing-humming sound as the first vapor bubbles are triggered. They grow at the heated surface and condense very suddenly when their tops encounter the still-cold water above them. This so-called *cavitation* collapse is accompanied by a small "ping" or "click," over and over, as the process is repeated at a fairly high frequency.

- As the temperature of the liquid bulk rises, the singing is increasingly muted. You may then look in the pan and see a number of points on the bottom where a feathery blur appears to be affixed. These columns are actually strings of many small bubbles emerging too rapidly to be seen individually. The bubbles in these columns condense completely at some distance above the heater surface. Notice that the air bubbles are all gradually being swept away.

- The "singing" finally gives way to a full rolling boil, accompanied by a gentle burbling sound. Bubbles no longer condense but now reach the liquid surface, where they spill their vapor into the air.

- A full rolling-boil process, in which the liquid bulk is saturated, is a kind of isolated-bubble process, as plotted in Fig. 9.2. No kitchen stove supplies energy fast enough to boil water in the slugs-and-columns regime. In fact, that gives us some sense of the relative intensity of the slugs-and-columns process.   ♦

Experiment 9.2

Repeat Experiment 9.1 with a glass beaker instead of a kitchen pan. Place a strobe light, blinking about 6 to 10 times per second, behind the beaker with a piece of frosted glass or tissue paper between it and the beaker. You can now see the evolution of bubble columns from the first singing mode up to the rolling boil. You will also be able to see natural convection in the refraction of the light before boiling begins. The view will be best if the backlight enters at about 15 degrees off of a line straight into the frosted glass.   ♦
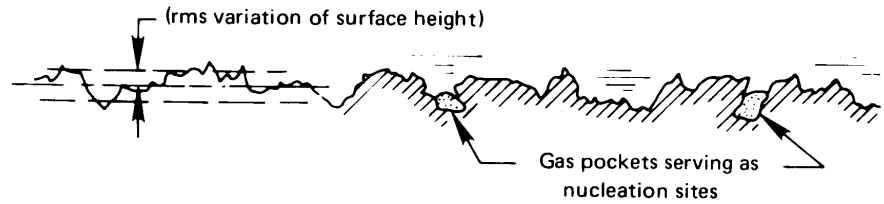
Figure 9.4 Enlarged sketch of a typical metal surface.

9.2 Nucleate boiling

Inception of boiling

Figure 9.4 shows a highly enlarged sketch of a heater surface. Most metal-finishing operations score tiny grooves on the surface, but they also typically involve some *chattering* or bouncing action, which hammers small holes into the surface. When a surface is wetted, liquid is prevented by surface tension from entering these holes, so small gas or vapor pockets remain when liquid fills the container above them. These little pockets are the sites at which bubble nucleation occurs.

To see why vapor pockets serve as nucleation sites, consider Fig. 9.5. Here we see the problem in highly idealized form. Suppose that a spherical bubble of pure saturated steam is at equilibrium with an infinite super-heated liquid. The size of this equilibrium bubble will then be determined by the requirements of *thermal* and *mechanical* equilibrium.

Thermal equilibrium requires that the temperature is uniformly T_{sup} throughout. Mechanical equilibrium requires that the saturated vapor pressure inside the bubble is slightly higher than the ambient pressure. That is because surface tension imposes an added pressure, as the cutaway sketch in Fig. 9.5 explains. And, this internal pressure must correspond to the saturation pressure at T_{sup}. The equilibrium bubble will thus be one in which the bubble radius is

$$R_b = \frac{2\sigma}{p_{\text{sat}}(T_{\text{sup}}) - p_{\text{ambient}}} \tag{9.1}$$

Two states of a bubble in equilibrium are designated with black dots in the p-v diagram, Fig. 9.5. These are the liquid just outside the bubble, and the vapor within it. Notice that the external liquid is superheated by $(T_{\text{sup}} - T_{\text{sat}})$ above its boiling point at the ambient pressure; but the vapor inside, being held at just the right elevated pressure by surface tension, is saturated.
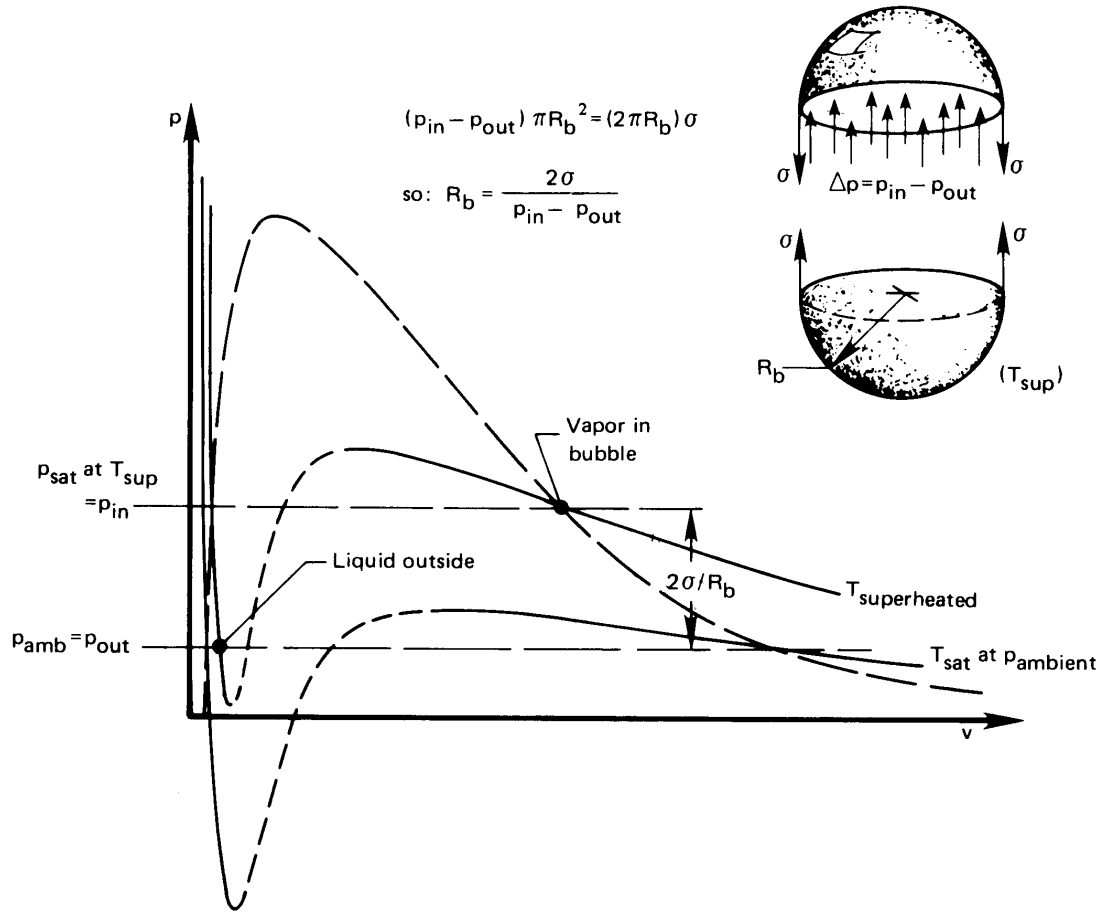
Figure 9.5 The conditions required for simultaneous mechanical and thermal equilibrium of a vapor bubble. The scale of this p-v diagram is exaggerated for clarity.

Physical digression: Surface tension

The surface tension of water in contact with its vapor is given with great accuracy by [9.3]:

$$\sigma_{\text{water}} = 235.8 \left(1 - \frac{T_{\text{sat}}}{T_c}\right)^{1.256} \left[1 - 0.625\left(1 - \frac{T_{\text{sat}}}{T_c}\right)\right] \frac{\text{mN}}{\text{m}} \qquad (9.2\text{a})$$

where both T_{sat} and the critical-point temperature, $T_c = 647.096$ K, are expressed in K. The units of σ are millinewtons (mN) per meter. Table 9.1 gives additional values of σ for several pure substances.

Table 9.1 Surface tension of various substances from the collection of Jasper [9.4][a] and other sources.

Substance	Temperature Range (°C)	σ (mN/m)	$\sigma = a - bT$ (°C)	
			a (mN/m)	b (mN/m°C)
Acetone	25 to 50		26.26	0.112
Ammonia	−70	42.39		
	−60	40.25		
	−50	37.91		
	−40	35.38		
Aniline	15 to 90		44.83	0.1085
Benzene	10	30.21		
	30	27.56		
	50	24.96		
	70	22.40		
Butyl alcohol	10 to 100		27.18	0.08983
Carbon tetrachloride	15 to 105		29.49	0.1224
Cyclohexanol	20 to 100		35.33	0.0966
Ethyl alcohol	10 to 100		24.05	0.0832
Ethylene glycol	20 to 140		50.21	0.089
Hydrogen	−258	2.80		
	−255	2.29		
	−253	1.95		
Isopropyl alcohol	10 to 100		22.90	0.0789
Mercury	5 to 200		490.6	0.2049
Methane	90	18.877		
	100	16.328		
	115	12.371		
Methyl alcohol	10 to 60		24.00	0.0773
Naphthalene	100 to 200		42.84	0.1107
Nicotine	−40 to 90		41.07	0.1112
Nitrogen	−195 to −183		26.42	0.2265
Octane	10 to 120		23.52	0.09509
Oxygen	−202 to −184		−33.72	−0.2561
Pentane	10 to 30		18.25	0.11021
Toluene	10 to 100		30.90	0.1189
Water	10 to 100		75.83	0.1477

Substance	Temperature Range (°C)	$\sigma = \sigma_o \left[1 - T\ (\text{K})/T_c\right]^n$		
		σ_o (mN/m)	T_c (K)	n
Carbon dioxide	−56 to 31	75.00	304.26	1.25
CFC-12 (R12) [9.5]	−148 to 112	56.52	385.01	1.27
HCFC-22 (R22) [9.5]	−158 to 96	61.23	369.32	1.23
HFC-134a (R134a) [9.6]	−30 to 101	59.69	374.18	1.266
Propane (R290) [9.7]	−173 to 96	53.13	369.85	1.242

[a] The overall function $\sigma = \sigma(T)$ is not really linear, but Jasper linearized it accurately over modest ranges of temperature.

Most of the expressions in Table 9.1 are linear curve fits that apply to small ranges of surface tension. However, eqn. (9.2a) is a specialized refinement of the following simple, but quite accurate and widely-used, semi-empirical equation for correlating surface tension:

$$\sigma = \sigma_o(1 - T_{\text{sat}}/T_c)^{11/9} \tag{9.2b}$$

We include similar correlations for CO_2, propane, and some refrigerants at the bottom of Table 9.1. Equations of this type are discussed in [9.8].

It is easy to see that the equilibrium bubble, whose radius is described by eqn. (9.1), is unstable. If its radius is less than this value, surface tension will overbalance $(p_{\text{sat}}(T_{\text{sup}}) - p_{\text{ambient}})$. When that happens, vapor inside will condense at this higher pressure and the bubble will collapse. If the bubble radius is slightly larger than the equation specifies, liquid at the interface will evaporate and the bubble will begin to grow.

Thus, as the heater surface temperature is increased, higher and higher values of $(p_{\text{sat}}(T_{\text{sup}}) - p_{\text{ambient}})$ will result and the equilibrium radius, R_b, will decrease in accordance with eqn. (9.1). It follows that smaller and smaller vapor pockets become unstable, and active bubble growth will be triggered as the temperature is increased. As an approximation, we can use eqn. (9.1) to specify the radius of those vapor pockets that become active nucleation sites. More accurate estimates can be made using Hsu's bubble inception theory [9.9] or the more recent technical literature [9.10, 9.11].

Example 9.1

Estimate the approximate size of active nucleation sites in water at 1 atm on a wall superheated by 8 K and by 16 K. These temperatures are roughly in the regime of isolated bubbles indicated in Fig. 9.2.

SOLUTION. $p_{\text{sat}} = 1.340 \times 10^5$ N/m^2 at 108°C and 1.769×10^5 N/m^2 at 116°C, and σ is given as 57.36 mN/m at $T_{\text{sat}} = 108$°C and as 55.77 mN/m at $T_{\text{sat}} = 116$°C by eqn. (9.2a). Then, at 108°C, R_b from eqn. (9.1) is

$$R_b = \frac{2(57.36 \times 10^{-3}) \text{ N/m}}{(1.340 \times 10^5 - 1.013 \times 10^5) \text{ N/m}^2}$$

and similarly for 116°C, so the radius of active nucleation sites is on the order of

$$R_b = 0.0035 \text{ mm at } T = 108°C \quad \text{or} \quad 0.0016 \text{ mm at } 116°C$$

This means that active nucleation sites would be holes with diameters very roughly on the order of a few micrometers—at least on the heater represented by Fig. 9.2. That is within the range of roughness of commercially finished metal surfaces. ∎

Region of isolated bubbles

The mechanism of heat transfer enhancement in the isolated bubble regime was hotly argued in the years following World War II. A few conclusions emerged from that debate, and we shall attempt to identify them. These bubbles act as small pumps that keep replacing liquid heated at the wall with cool liquid. The question is that of specifying the correct mechanism. Figure 9.6 shows the way bubbles probably act to remove hot liquid from the wall and introduce cold liquid to be heated.

The number of active nucleation sites generating bubbles will clearly exert a strong influence on q. On the basis of his experiments, Yamagata showed in 1955 [9.12] that

$$q \propto \Delta T^a n^b \tag{9.3}$$

where $\Delta T \equiv T_w - T_{\text{sat}}$ and n is the site density or number of active sites per square meter. A great deal of subsequent work was done to fix the constant of proportionality and the constant exponents, a and b. The exponents turn out to be approximately $a = 1.2$ and $b = 1/3$.

The problem with eqn. (9.3) is that it introduces what engineers call a *nuisance variable*. A nuisance variable is one that varies from system to system and cannot easily be evaluated—the site density, n, in this case. Normally, n increases with ΔT in some way, but how? If all sites were identical in size, all sites would be activated simultaneously, and q would be a discontinuous function of ΔT. When the sites have a typical distribution of sizes, n (and hence q) can increase very strongly with ΔT.

Fortunately, n varies approximately as $\Delta T^{5 \text{ or } 6}$ for a large class of factory-finished materials, so q varies roughly as ΔT^3. This has made it possible for various researchers to create very rough correlations that work for a large variety of materials. Dhir [9.11] summarizes several.

Warren Rohsenow [9.13] made one of the earliest, and most durable, of those nucleate boiling correlations in 1952:

$$\frac{c_p (T_w - T_{\text{sat}})}{h_{fg} \, \text{Pr}^s} = C_{\text{sf}} \left[\frac{q}{\mu h_{fg}} \sqrt{\frac{\sigma}{g(\rho_f - \rho_g)}} \right]^{0.33} \tag{9.4}$$
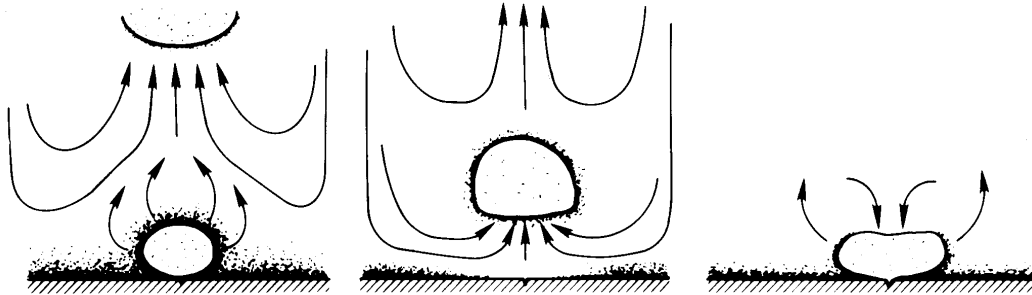
A bubble growing and departing in saturated liquid.
The bubble grows, absorbing heat from the
superheated liquid on its periphery. As it leaves, it
entrains cold liquid onto the plate which then warms
up until nucleation occurs and the cycle repeats.

A bubble growing in subcooled liquid.
When the bubble protrudes into cold liquid,
steam can condense on the top while
evaporation continues on the bottom. This
action provides a short-circuit to cool the
wall. Then, when the bubble caves in, cold
liquid is brought to the wall.

Figure 9.6 Heat removal by bubble action during boiling. Dark
regions denote locally superheated liquid.

where all properties, unless otherwise noted, are for liquid at T_{sat}. The
constant C_{sf} is an empirical correction for typical surface conditions.
Table 9.2 includes a set of values of C_{sf} for common surfaces as well as
the Prandtl number exponent, s. A more extensive compilation of these
constants was published by Pioro in 1999 [9.14].

The Yamagata equation (9.3) applies only to the first of the two nucleate
boiling regimes, whereas Rohsenow's is for both. Rohsenow's equation is
frankly empirical, however, and does not depend on the rational analysis of
either nucleate boiling process. While it represents $q(\Delta T)$ in both regimes,
it is not terribly accurate in either one. Figure 9.7 shows Rohsenow's
original comparison of eqn. (9.4) with data for water over a large range of
conditions. The correlation shows typical errors in heat flux of 100% and
typical errors in ΔT of about 25%.

Thus, our ability to predict the nucleate pool boiling heat flux is poor.
Our ability to predict ΔT is better because, with $q \propto \Delta T^3$, a large error
in q gives a much smaller error in ΔT. The nuisance variable n is a
formidable barrier to predicting $q(\Delta T)$. However, we are in luck because
we do not often have to calculate q, given ΔT, in the nucleate boiling
regime. More often, the major problem is to avoid exceeding q_{max}. We
turn our attention to predicting this limit in the next section.

Table 9.2 Selected values of the surface correction factor for use with eqn. (9.4) [9.13].

Surface–Fluid Combination	C_{sf}	s
Water–nickel	0.006	1.0
Water–platinum	0.013	1.0
Water–copper	0.013	1.0
Water–brass	0.006	1.0
CCl_4–copper	0.013	1.7
Benzene–chromium	0.010	1.7
n-Pentane–chromium	0.015	1.7
Ethyl alcohol–chromium	0.0027	1.7
Isopropyl alcohol–copper	0.0025	1.7
35% K_2CO_3–copper	0.0054	1.7
50% K_2CO_3–copper	0.0027	1.7
n-Butyl alcohol–copper	0.0030	1.7

Example 9.2

What is C_{sf} for the heater surface in Fig. 9.2?

SOLUTION. From eqn. (9.4) we obtain

$$\frac{q}{\Delta T^3}\, C_{sf}^3 = \frac{\mu c_p^3}{h_{fg}{}^2 \mathrm{Pr}^3} \sqrt{\frac{g(\rho_f - \rho_g)}{\sigma}}$$

where, since the liquid is water, we take s to be 1.0. Then, for water at $T_{sat} = 100°C$: $c_p = 4.22$ kJ/kg·K, Pr = 1.75, $(\rho_f - \rho_g) = 958$ kg/m^3, $\sigma = 0.0589$ N/m or kg/s^2, $h_{fg} = 2257$ kJ/kg, $\mu = 0.000282$ kg/m·s. Thus,

$$\frac{q}{\Delta T^3}\, C_{sf}^3 = 3.10 \times 10^{-7} \frac{\mathrm{kW}}{\mathrm{m^2 K^3}}$$

At $q = 800$ kW/m^2, we read $\Delta T = 22$ K from Fig. 9.2. This gives

$$C_{sf} = \left[\frac{3.10 \times 10^{-7}(22)^3}{800}\right]^{1/3} = 0.016$$

This value is comparable to the table's value of C_{sf} for a platinum surface under water. ∎
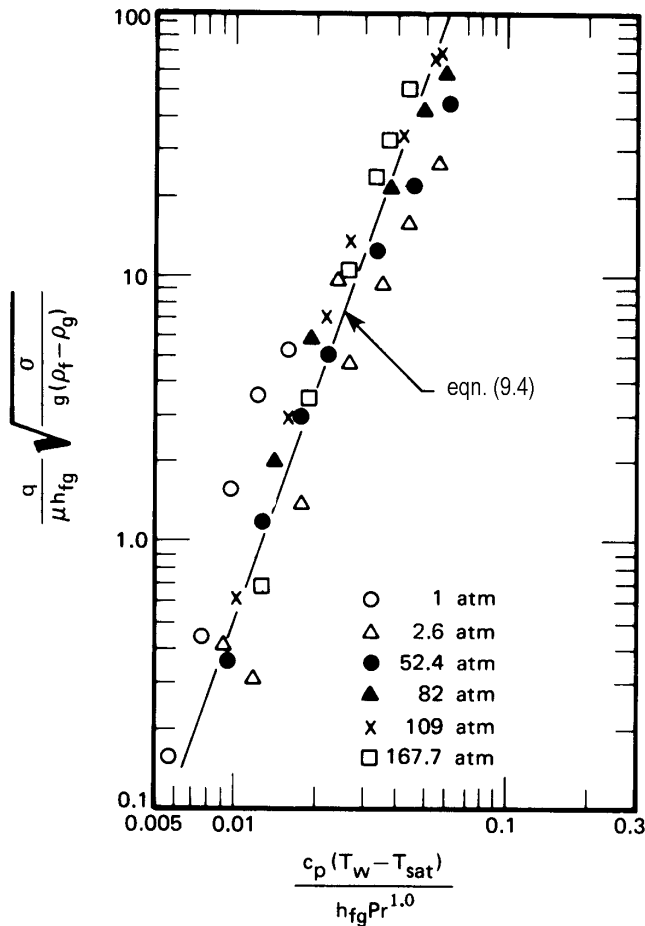
Figure 9.7 Illustration of Rohsenow's [9.13] correlation applied to data for water boiling on 0.61 mm diameter platinum wire.

9.3 Peak pool boiling heat flux

Transitional boiling regime and Taylor instability

We can better understand the peak heat flux if we first consider the process that connects the peak and the minimum heat fluxes. During high heat flux transitional boiling, a large amount of vapor is glutted about the heater. It wants to buoy upward, but it has no clearly defined escape route. The columns that carry vapor away from the heater in the region of slugs and columns are unstable in this regime, and they can no longer serve as an escape route. Therefore, vapor buoys up in big slugs—then liquid falls in, touches the surface briefly, and a new slug begins to form. Figure 9.3c shows part of this process.

The high and low heat flux transitional boiling regimes are different in character. The low heat flux region does not look like Fig. 9.2c. Rather, it is almost indistinguishable from the film boiling shown in Fig. 9.2d. However, the two processes display common conceptual keys: In each, the heater is almost completely blanketed with vapor. In each, we must contend with the unstable configuration of a liquid on top of a vapor.

Figure 9.8 shows two commonplace examples of such behavior. In either an inverted honey jar or the water condensing from a cold water pipe, we have seen how a heavy fluid falls into a light one (water or honey, in this case, collapses into air). The heavy phase falls down at one node of a wave and the light fluid rises into the other node. This process is inverted during film boiling as we see in Fig. 9.3d. Here, a light gas rises into a heavy liquid.

This collapse process, whether the wave collapses from above or below, is called *Taylor instability*. The process is named in honor of G. I. Taylor, who first predicted it. The so-called Taylor wavelength, λ_d, is the length of the wave that grows fastest and therefore predominates during the collapse of an infinite plane horizontal interface.[3] The form of λ_d can be found by writing the dimensional functional equation

$$\lambda_d = \text{fn}\left[\sigma, g(\rho_f - \rho_g)\right] \tag{9.5}$$

These variables appear because the wave is formed by the balancing forces of surface tension against inertia and gravity. The three variables involve m and kg/s^2, so we look for just one dimensionless group:

$$\lambda_d \sqrt{\frac{g(\rho_f - \rho_g)}{\sigma}} = \text{ constant}$$

This relationship was derived analytically by Bellman and Pennington [9.15] for one-dimensional waves and by Sernas [9.16] for the two-dimensional waves that actually occur in a plane horizontal interface. The results were

$$\lambda_d \sqrt{\frac{g(\rho_f - \rho_g)}{\sigma}} = \begin{cases} 2\pi\sqrt{3} & \text{for one-dimensional waves} \\ 2\pi\sqrt{6} & \text{for two-dimensional waves} \end{cases} \tag{9.6a}$$

We shall make use of these most rapidly collapsing waves. However, the

---

[3]The subscript d is taken from the idea that the wavelength most susceptible to collapse is the most "dangerous" one.
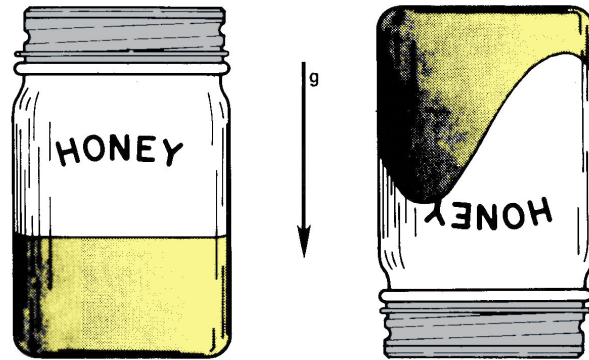
a. Taylor instability in the surface of the honey in an inverted honey jar
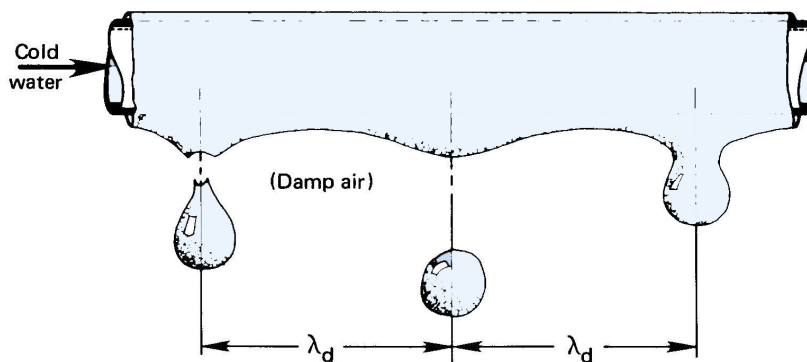
b. Taylor instability in the interface of the water condensing on the underside of a small cold water pipe.

Figure 9.8 Two examples of Taylor instabilities that one might commonly observe.

shortest waves that will collapse are shorter than λ_d, e.g.:

$$\lambda_{\min} \sqrt{\frac{g(\rho_f - \rho_g)}{\sigma}} = 2\pi \quad \text{for one-dimensional waves} \tag{9.6b}$$

Experiment 9.3

Hang a metal rod horizontally by threads at both ends. The rod should be about 30 cm in length and perhaps 1 to 2 cm in diameter. Pour molasses, motor oil, or glycerin in a narrow cake pan and lift the

pan up under the rod until it is submerged. Then lower the pan and watch the liquid drain into it. Take note of the wave action on the underside of the rod. The same experiment can be done in an even more satisfactory way by running cold water through a horizontal copper tube above a beaker of boiling water. The condensing liquid will also come off in a Taylor wave such as is shown in Fig. 9.8. In either case, the waves will approximate λ_{d_1} (the length of a one-dimensional wave, since they are arrayed on a line.) The wavelength will not exactly match eqn. (9.6a) since the rod or pipe curvature will alter it somewhat; but it will be close, as long as the tube diameter is not a great deal less than the wavelength.   ♦

Throughout the transitional and film boiling regimes, vapor rises into liquid on the nodes of Taylor waves; and at q_{max} this rising vapor has taken the form of jets. These jets arrange themselves on a staggered square grid, as shown in Fig. 9.9. The basic spacing of the grid is λ_{d_2} (the two-dimensional Taylor wavelength). In accordance with eqn. (9.6a)

$$\lambda_{d_2} = \sqrt{2}\,\lambda_{d_1} \tag{9.7}$$

Thus, the spacing of the most basic module of jets is actually λ_{d_1}, as shown in Fig. 9.9. For water at 1 atm, using eqn. (9.6a) with the properties in Example 9.2, we find λ_{d_1} = 2.72 cm.

Next we see how the jets become unstable at the peak heat flux and bring about burnout.

Helmholtz instability of vapor jets

Figure 9.10 shows a commonplace example of what is called *Helmholtz instability*. This is the phenomenon that causes the vapor jets to cave in when the vapor velocity in them reaches a critical value. Any flag in a breeze will constantly be in a state of collapse as the result of relatively high pressures where the velocity is low and relatively low pressures where the velocity is high, as is indicated in the top view.

This same instability is shown as it occurs in a vapor jet wall in Fig. 9.11. This situation differs from the flag in one important particular. Surface tension in the jet walls tends to balance the flow-induced pressure forces that bring about collapse. Thus, while the flag is unstable in *any* breeze, the vapor velocity in the jet must reach a limiting value, u_g, before the jet becomes unstable.
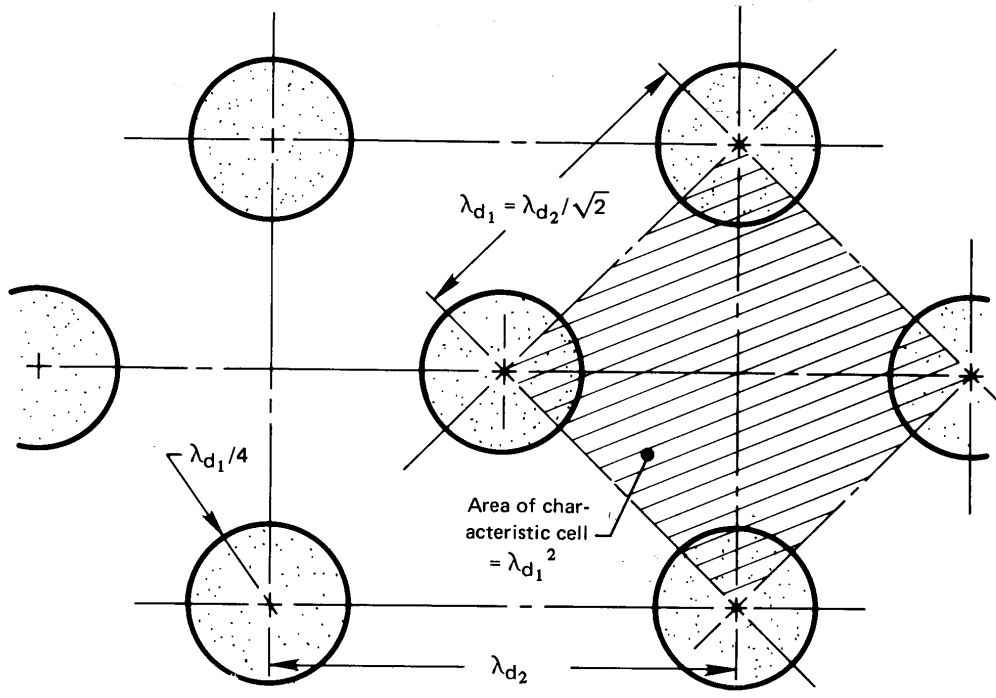
a. Plan view of bubbles rising from surface
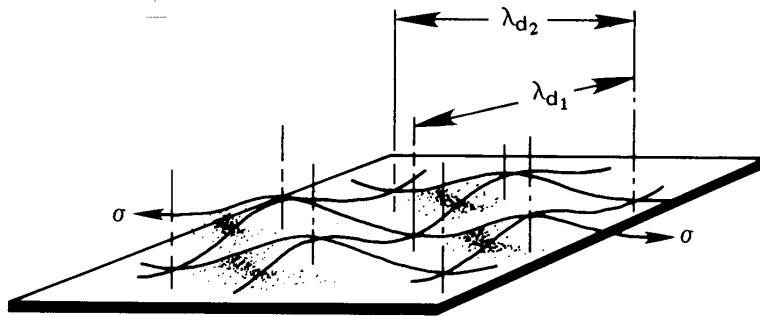
b. Waveform underneath the bubbles shown in **a.**

Figure 9.9 The array of vapor jets as seen on an infinite
horizontal heater surface.
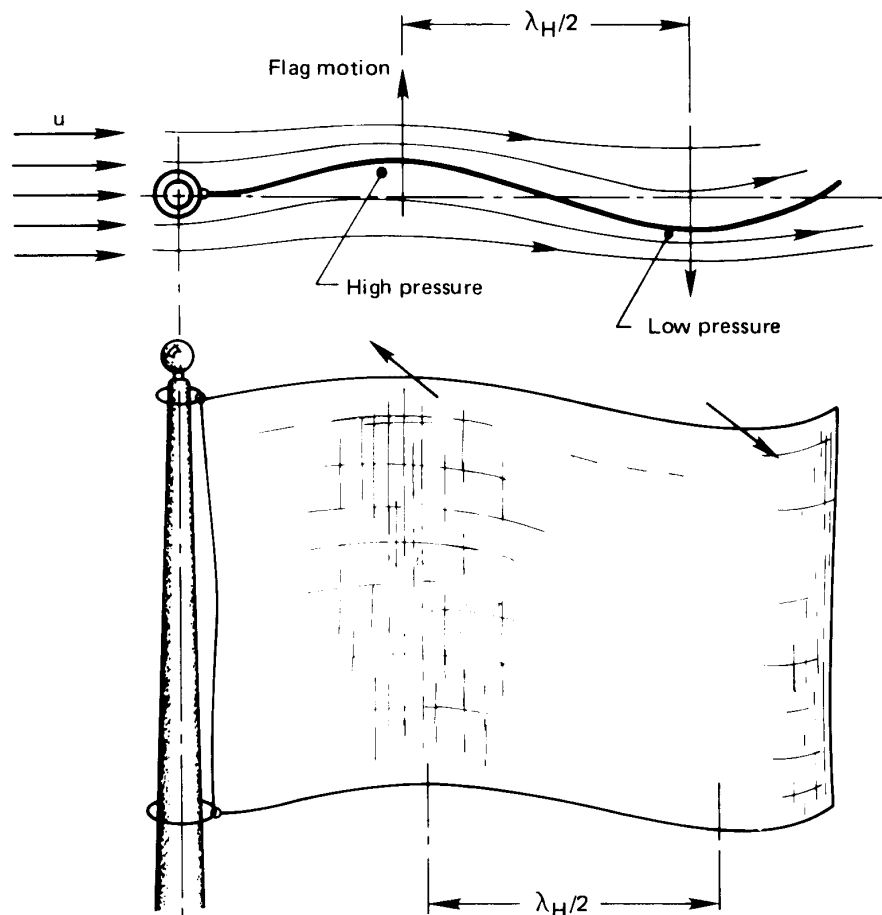
Figure 9.10 The flapping of a flag due to Helmholtz instability.

Lamb [9.17] gives the following relation between the vapor flow u_g, shown in Fig. 9.11, and the wavelength of a disturbance in the jet wall, λ_H:

$$u_g = \sqrt{\frac{2\pi\sigma}{\rho_g \lambda_H}} \tag{9.8}$$

This result, like eqn. (9.6a), can be predicted to within a constant using dimensional analysis (see Problem 9.19).

A real liquid–vapor interface will usually be irregular, and therefore it can be viewed as containing all possible sinusoidal wavelengths super-posed on one another. One problem we face is that of guessing whether
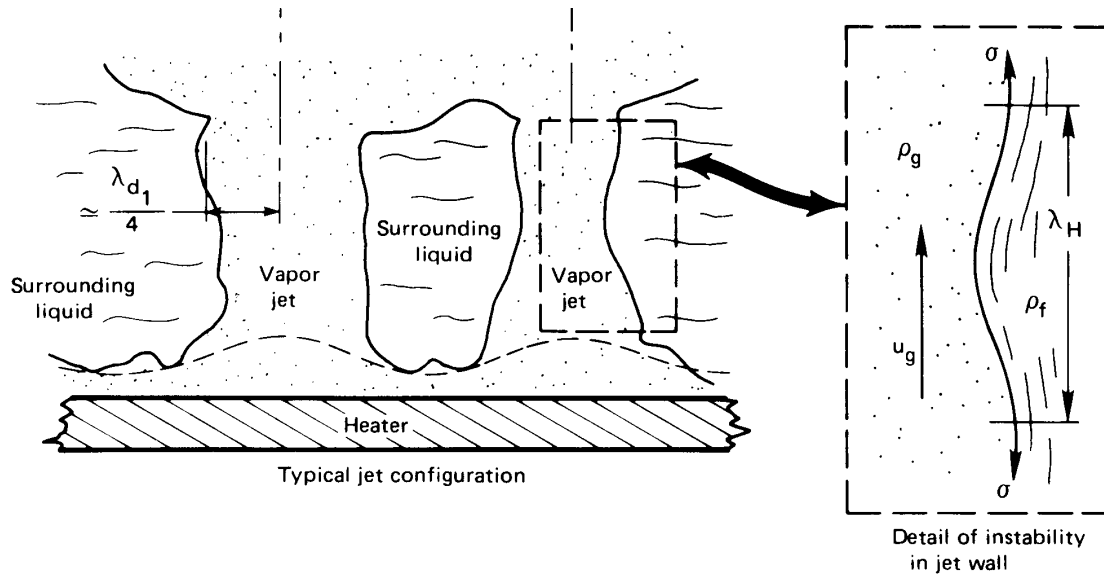
Figure 9.11 Helmholtz instability of vapor jets.

or not one of those wavelengths will be better developed than the others
and therefore more liable to collapse during the brief life of the jet.

Example 9.3

Saturated water at 1 atm flows slowly down the inside wall of a
10 cm I.D. vertical tube. Steam flows rapidly upward in the center.
The wall of the pipe has circumferential corrugations in it, with a 4 cm
wavelength in the axial direction. Neglect problems raised by radial
curvature and the finite thickness of the liquid, and estimate the steam
velocity required to destabilize the liquid flow.

SOLUTION. If we can neglect the liquid velocity, the flow will be
Helmholtz-stable until the steam velocity reaches the value given by
eqn. (9.8):

$$u_g = \sqrt{\frac{2\pi(0.0589)}{0.598(0.04)}}$$

Thus, the maximum stable steam velocity would be $u_g = 3.93$ m/s.
Beyond that, the liquid would form whitecaps and be blown back
upward. ∎

Example 9.4

A long narrow rectangular container holds mercury at 300 K. It is abruptly turned upside down. What is the minimum width for which capillary forces will hold the mercury in place without it collapsing and falling out?

SOLUTION. The mercury will collapse by Taylor instability when the spacing reaches the wavelength given by eqn. (9.6b):

$$\lambda_{min} = 2\pi\sqrt{\frac{\sigma}{g(\rho_f - \rho_g)}} = 2\pi\sqrt{\frac{0.485}{9.8(13530)}} = 0.012 \text{ m} = 1.2 \text{ cm} \quad \blacksquare$$

Prediction of q_{max}

General expression for q_{max}. The heat flux must be balanced by the latent heat carried away in the jets when the liquid is saturated. Thus, we can write immediately

$$q_{max} = \rho_g h_{fg} u_g \left(\frac{A_j}{A_h}\right) \tag{9.9}$$

where A_j is the cross-sectional area of a jet and A_h is the heater area that supplies each jet.

For any heater configuration, two things must be determined. One is the length of the particular disturbance in the jet wall, λ_H, which will trigger Helmholtz instability and fix u_g in eqn. (9.8) for use in eqn. (9.9). The other is the ratio A_j/A_h. The prediction of q_{max} in conventional pool boiling configurations always comes down to these two problems.

q_{max} on an infinite horizontal plate. The original analysis of this type was done by Zuber in his doctoral dissertation at UCLA in 1958 (see [9.18]). He first guessed that the jet radius was $\lambda_{d_1}/4$. This guess has been corroborated as we shall see in a moment, and (with reference to Fig. 9.9) it gives

$$\frac{A_j}{A_h} = \frac{\text{cross-sectional area of circular jet}}{\text{area of the square portion of the heater that feeds the jet}}$$

$$= \frac{\pi(\lambda_{d_1}/4)^2}{(\lambda_{d_1})^2} = \frac{\pi}{16} \tag{9.10}$$

Lienhard and Dhir [9.19–9.21] guessed that the Helmholtz-unstable wavelength might be equal to λ_{d_1}, so eqn. (9.9) became

$$q_{max} = \rho_g h_{fg} \sqrt{\frac{2\pi\sigma}{\rho_g} \frac{1}{2\pi\sqrt{3}} \sqrt{\frac{g(\rho_f - \rho_g)}{\sigma}} \times \frac{\pi}{16}}$$

or[4]

$$\boxed{q_{max} = 0.149 \, \rho_g^{1/2} h_{fg} \sqrt[4]{g(\rho_f - \rho_g)\sigma}} \tag{9.11}$$

We now move to the matter of verifying eqn. (9.11) experimentally. The configurations to which it applies must exhibit the following features:

- They must be horizontal flat plates

- No side flow can be entrained. The heaters must have side walls (if they are not infinite). Entrained flow can greatly alter q_{max}.

- The surface must be well-wetted (have high contact angle). Fortunately, water wets most off-the-shelf metals.

- The heaters must be large enough to accommodate a few wavelengths.

She and Dhir [9.22] revisited these factors using heaters below cylindrical side-walls in 2021, showing in detail how small size raises q_{max}. They also showed that q_{max} increases when the surface is only partially wetted by the liquid (i.e., has a high contact angle), and that q_{max} increases as a result of induced convection for small heaters without sidewalls.

Let us look more closely at the last item above. We compare eqn. (9.11) to data for square flat plates with vertical sidewalls in Fig. 9.12. These data from four data sources, for eight fluids, and a range of gravity from earth-normal up to 17.5 times earth-normal. As long as the width or diameter of the heater is more than about $3\lambda_{d_1}$, the prediction is quite accurate. When the width or diameter is less than $3\lambda_{d_1}$, a small integral number of jets sit on the plate, and the plate may be larger or smaller in area than $16/\pi$ per jet. The actual q_{max} falls below that predicted by eqn. (9.11) as the heater size is further reduced. But it then becomes greater as a single vapor column serves an increasingly small heater area [see eqn. (9.17)].

---

[4]Readers are reminded that $\sqrt[n]{x} \equiv x^{1/n}$.
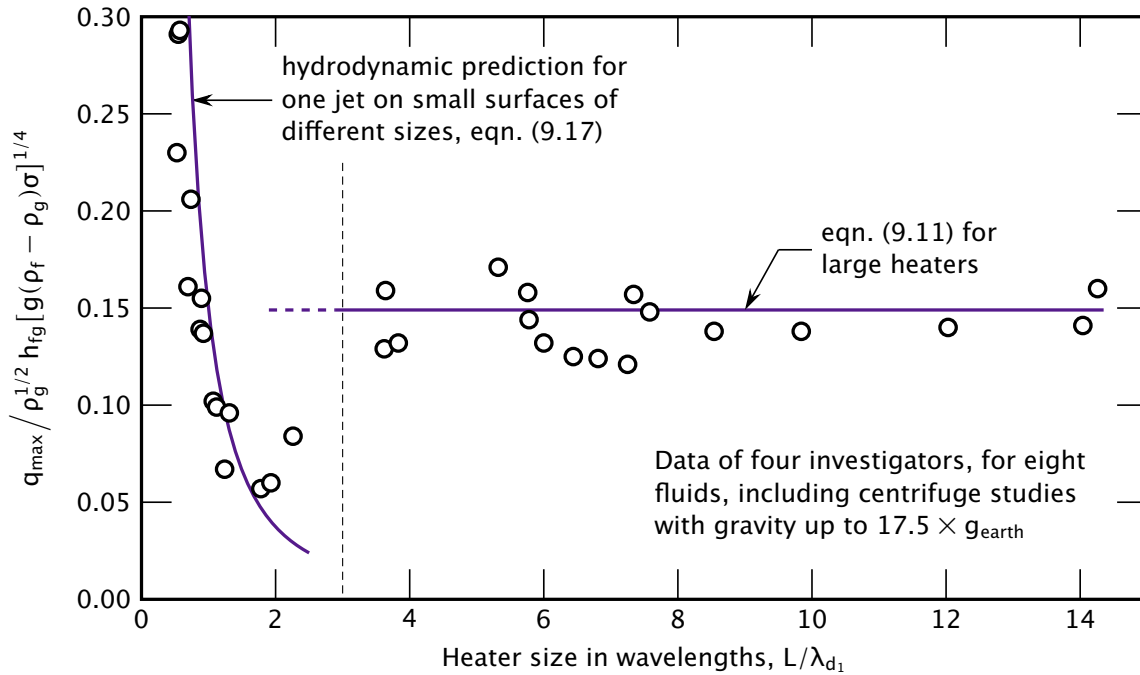
Figure 9.12 The q_{max} prediction for infinite horizontal heaters compared to data for 8 fluids and gravity between 1 to 17.5 times earth-normal gravity, from 4 investigators, as reported in [9.19].

In fact, C. F. Bonilla, in 1941, was the first to propose that CHF is an instability where rising vapor velocity trips liquid to collapse into the vapor column. He suggested that q_{max} is like the flooding of a distillation column[5] [9.23, 9.24]. We include his experiments in Fig. 9.12.

S. S. Kutateladze (then working in Leningrad and later director of the Heat Transfer Laboratory near Novosibirsk, Siberia) also recognized the similarity of burnout to column flooding [9.25]. V. M. Borishansky, working with Kutateladze [9.24], did the dimensional analysis of q_{max} based on the flooding mechanism, and got the following relationship, which, lacking a characteristic length and being of the same form as eqn.

---

[5]As a matter of interest, A. P. Colburn wrote to Bonilla about this suggestion: "A correlation [of the flooding velocity plots with] boiling data would not serve any great purpose and would perhaps be very misleading." And T. H. Chilton—another eminent chemical engineer of that period—wrote to him: "I venture to suggest that you delete from the manuscript…the relationship between boiling rates and loading velocities in packed towers." Thus, the technical conservatism of the period prevented Bonilla's idea from gaining acceptance for another decade.

(9.11), could have meaning only for an infinite horizontal plate:

$$q_{max} = C\,\rho_g^{1/2}h_{fg}\sqrt[4]{g(\rho_f - \rho_g)\sigma}$$

He compared this equation with data for burnout for many fluids, and in many configurations (*none of which was a large flat plate*), and he got $C = 0.131$ [9.25].

Zuber read the Russian literature and considered the character of flooding: At any level in a distillation column, vapor rises while liquid flows downward in counterflow. He realized that, when one drives the process too far, the flows become Helmholtz-unstable and collapse. The liquid then cannot move downward and the column "floods."

The assumptions in his hydrodynamic analysis yielded $C = \pi/24 = 0.1309$. That matched the Borishansky/Kutateladze value, but it was lower by 14% than eqn. (9.11). The Russian value was low because it was based on the wrong data. Zuber's was low because he forced certain of his assumptions to match the Russian result.

We therefore designate the Zuber-Kutateladze equation for the peak heat flux on a flat plate as q_{max_z}. However, we cannot apply it directly to any actual physical configuration.

$$q_{max_z} \equiv 0.131\,\rho_g^{1/2}h_{fg}\sqrt[4]{g(\rho_f - \rho_g)\sigma} \tag{9.12}$$

Example 9.5

Predict the peak heat flux for Fig. 9.2.

SOLUTION. We use eqn. (9.11) to evaluate q_{max} for water at 100°C on an infinite flat plate:

$$
\begin{aligned}
q_{max} &= 0.149\,\rho_g^{1/2}h_{fg}\sqrt[4]{g(\rho_f - \rho_g)\sigma} \\
&= 0.149(0.597)^{1/2}(2,257,000)\sqrt[4]{9.8(958.2 - 0.6)(0.0589)} \\
&= 1.260 \times 10^6 \ \text{W/m}^2 \\
&= 1.260 \ \text{MW/m}^2
\end{aligned}
$$

Figure 9.2 shows $q_{max} \simeq 1.16$ MW/m^2, which is less by only 8%.   ■

Example 9.6

What is q_{max} in mercury on a large flat plate at 1 atm?

SOLUTION. The normal boiling point of mercury is 355°C. At this temperature, $h_{fg} = 294,900$ J/kg, $\rho_f = 12,740$ kg/m³, $\rho_g = 4.0$ kg/m³, and $\sigma \simeq 0.418$ kg/s², so

$$q_{max} = 0.149(4.0)^{1/2}(294,900)\sqrt[4]{9.8(12740 - 4)(0.418)}$$
$$= 1.328 \text{ MW/m}^2$$

The result is very close to that for water. The increases in density and surface tension have been offset by a much lower latent heat. ∎

Peak heat flux in other pool boiling configurations

The prediction of q_{max} in configurations other than an infinite flat heater will involve a characteristic length, L. Thus, the dimensional functional equation for q_{max} becomes

$$q_{max} = \text{fn}\Big[\rho_g, h_{fg}, \sigma, g(\rho_f - \rho_g), L\Big]$$

This equation involves six variables and four dimensions: J, m, s, and kg, where, once more in accordance with Section 4.3, we note that no significant conversion from work to heat is occurring and J must be retained as a separate unit. There are thus two pi-groups.

The first group can arbitrarily be multiplied by $24/\pi$ to give

$$\Pi_1 = \frac{q_{max}}{(\pi/24)\rho_g^{1/2}h_{fg}\sqrt[4]{\sigma g(\rho_f - \rho_g)}} = \frac{q_{max}}{q_{max_z}} \tag{9.13}$$

Notice that the factor of $24/\pi$ has served to make the denominator equal to q_{max_z} (Zuber's expression for q_{max}). Thus, for q_{max} on a flat plate, Π_1 equals 0.149/0.131, or 1.14. The second pi-group is

$$\Pi_2 = \frac{L}{\sqrt{\sigma/g(\rho_f - \rho_g)}} = 2\pi\sqrt{3}\frac{L}{\lambda_{d_1}} \equiv L' \tag{9.14}$$

The latter group, Π_2, is the square root of the *Bond number*, Bo—a group that has often been used to compare buoyant force with capillary forces.

Predictions and correlations of q_{max} have been made for several *finite* geometries in the form

$$\frac{q_{max}}{q_{max_z}} = \text{fn}(L') \tag{9.15}$$

The dimensionless characteristic length in eqn. (9.15) might be a dimensionless radius (R'), a dimensionless diameter (D'), or a dimensionless

height (H'). The graphs in Fig. 9.13 are comparisons of several of the existing predictions and correlations with experimental data. These predictions and others are listed in Table 9.3. Notice that the last three items in Table 9.3 (10, 11, and 12) are general expressions from which several of the preceding expressions in the table can be obtained.

The equations in Table 9.3 are all valid within ±15% or 20%, which is very close to the inherent scatter of q_{max} data. However, they are subject to the following conditions:

- The bulk liquid is saturated.

- There are no extreme or artificial surface textures.

- There is no forced convection.

Very small Bond number.   Another limitation on all the equations in Table 9.3 is that neither the size of the heater nor the relative force of gravity can be too small. When $L' \lesssim 0.15$ in most configurations, the Bond number is

$$\text{Bo} \equiv L'^2 = \frac{g(\rho_f - \rho_g)L^3}{\sigma L} = \frac{\text{buoyant force}}{\text{capillary force}} \lesssim 0.02$$

In such cases, the process becomes completely dominated by surface tension and the Taylor-Helmholtz wave mechanisms no longer operate. As L' is reduced, the peak and minimum heat fluxes cease to occur and the boiling curve becomes monotonic. Bakhru and Lienhard [9.26] showed that, when nucleation occurs on a sufficiently small wire, the wire is immediately enveloped in vapor in that region. The system passes directly from natural convection into film boiling, and no nucleate boiling can occur.

Example 9.7

A metal body, only roughly spherical in shape, has a surface area of 400 cm^2 and a volume of 600 cm^3. It is quenched in saturated water at 1 atm. What is the most rapid rate of heat removal during the quench?

Solution. The cooling process progresses along the boiling curve from film boiling, through q_{min}, up the transitional boiling regime, through q_{max}, and down the nucleate boiling curve. Cooling is finally completed by natural convection. If you have ever seen a red-hot horseshoe quenched, you might recall the great gush of bubbling that
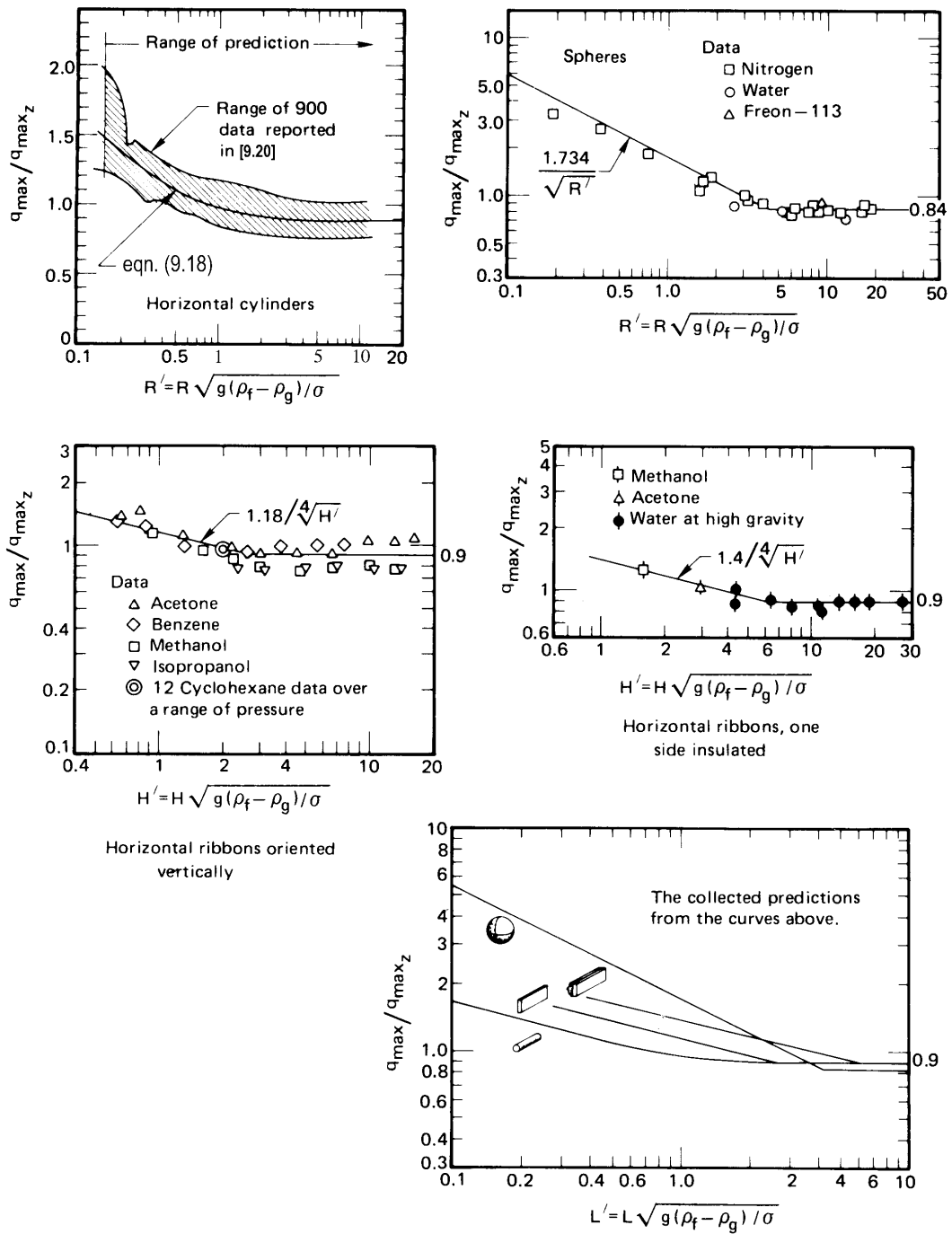
Figure 9.13 The peak pool boiling heat flux on several heaters. Note how q_{max} increases in all cases, as the heater size is reduced below λ_{d_1}.

Table 9.3: Predictions of the peak pool boiling heat flux

Situation	q_{max}/q_{max_z}	Basis for L'	Range of L'	Source	Eqn. No.
1. Infinite flat heater	1.14	Heater width or diameter	$L' \geqslant 30$	[9.20]	(9.16)
2. Small flat heater[†]	$1.14(\lambda_{d_1}^2 N_j/A_{heater})$	Heater width or diameter	$10 < L' < 20$	[9.20]	(9.17)
3. Horizontal cylinder	$0.89 + 2.27 e^{-3.44\sqrt{R'}}$	Cylinder radius, R	$R' \geqslant 0.15$	[9.27]	(9.18)
4. Large horizontal cylinder	0.90	Cylinder radius, R	$R' \geqslant 1.2$	[9.21]	(9.19)
5. Small horizontal cylinder	$0.94/(R')^{1/4}$	Cylinder radius, R	$0.15 \leqslant R' \leqslant 1.2$	[9.21]	(9.20)
6. Large sphere	0.84	Sphere radius, R	$R' \geqslant 4.26$	[9.28]	(9.21)
7. Small sphere	$1.734/(R')^{1/2}$	Sphere radius, R	$0.15 \leqslant R' \leqslant 4.26$	[9.28]	(9.22)
Small horizontal ribbon oriented vertically					
8. plain	$1.18/(H')^{1/4}$	Height of side, H	$0.15 \leqslant H' \leqslant 2.96$	[9.21]	(9.23)
9. one side insulated	$1.4/(H')^{1/4}$	Height of side, H	$0.15 \leqslant H' \leqslant 5.86$	[9.21]	(9.24)
10. Any large finite body	~ 0.90	Characteristic length, L	cannot specify generally; $L' \gtrsim 4$	[9.21]	(9.25)
11. Small slender cylinder of any cross section	$1.4/(P')^{1/4}$	Transverse perimeter, P	$0.15 \leqslant P' \leqslant 5.86$	[9.21]	(9.26)
12. Small bluff body	Constant$/(L')^{1/2}$	Characteristic length, L	cannot specify generally; $L' \lesssim 4$	[9.21]	(9.27)

[†]N_j is the number of vapor jets on a heater, which may either be estimated on the basis of λ_{d_1} and heater dimensions or be observed experimentally.

occurs as q_{max} is reached. We therefore calculate the most rapid heat flow as $Q = q_{max}A_{spheroid}$, where q_{max} is given for large bodies by eqn. (9.25) in Table 9.3:

$$q_{max} = 0.9\,q_{max_z} = 0.9(0.131)\rho_g^{1/2}h_{fg}\sqrt[4]{g\sigma(\rho_f - \rho_g)}$$

so

$$Q = \left[0.9(0.131)(0.597)^{1/2}(2,257,000)\sqrt[4]{9.8(0.0589)(958)}\ \text{W/m}^2\right]$$
$$\times\,(400\times 10^{-4}\ \text{m}^2)$$

or

$$Q = 39,900\ \text{W}\ \ \text{or}\ \ 39.9\ \text{kW}$$

This rate of energy removal is a startlingly large for such a small object.

To complete the calculation, we must check whether or not L' is large enough to justify the use of eqn. (9.25):

$$L' = \frac{V/A}{\sqrt{\sigma/g(\rho_f - \rho_g)}} = \frac{0.0006}{0.04}\sqrt{\frac{9.8(958)}{0.0589}} = 6.0$$

This is larger than the value of about 4 for which a body must be considered "large." ∎

9.4 Film boiling

Film boiling bears an uncanny similarity to film condensation. The similarity is so great that, in 1950, Bromley [9.29] was able to predict film boiling from cylinders by using eqn. (8.67) for condensation on cylinders almost directly. He observed that the boundary condition $(\partial u/\partial y)_{y=\delta} = 0$ at the liquid–vapor interface in film condensation would have to change to something in between $(\partial u/\partial y)_{y=\delta} = 0$ and $u(y = \delta) = 0$ during film boiling. The reason is that the external liquid is not so easily set into motion.

Bromley then redid the film condensation analysis, merely changing k and ν from liquid to vapor properties. The change of boundary conditions gave eqn. (8.67) with the constant changed from 0.729 to 0.512. He also changed k and ν to vapor values. By comparing the equation with experimental data, he fixed the constant at the intermediate value of 0.62.

Thus, $\overline{\mathrm{Nu}}_D \equiv \overline{h}D/k_g$ became

$$\overline{\mathrm{Nu}}_D = 0.62 \left[\frac{(\rho_f - \rho_g)gh'_{fg}D^3}{\nu_g k_g (T_w - T_{\text{sat}})} \right]^{1/4} \tag{9.28}$$

where vapor and liquid properties should be evaluated at $T_{\text{sat}} + \Delta T/2$ and at T_{sat}, respectively.

The latent heat correction in this case is similar in form to that for film condensation, but with different constants in it. Sadasivan and Lienhard [9.30] have shown it to be

$$h'_{fg} = h_{fg} \left[1 + (0.968 - 0.163/\mathrm{Pr}_g)\mathrm{Ja}_g \right] \tag{9.29}$$

for $\mathrm{Pr}_g \geqslant 0.6$, where $\mathrm{Ja}_g = c_{p_g}(T_w - T_{\text{sat}})/h_{fg}$.

Twenty years after Bromley, Dhir and Lienhard [9.31] did the same thing for *spheres*, as Bromley had done for *cylinders*. Their result [cf. eqn. (8.68)] was

$$\overline{\mathrm{Nu}}_D = 0.67 \left[\frac{(\rho_f - \rho_g)gh'_{fg}D^3}{\nu_g k_g (T_w - T_{\text{sat}})} \right]^{1/4} \tag{9.30}$$

The preceding expressions are based on heat transfer by convection through the vapor film alone. However, when film boiling occurs much beyond q_{min} in water, the heater glows dull cherry-red to white-hot. Radiation in such cases can be enormous. One's first temptation might be simply to add a radiation heat transfer coefficient, $\overline{h}_{\text{rad}}$ to $\overline{h}_{\text{boiling}}$ as obtained from eqn. (9.28) or (9.30), where

$$\overline{h}_{\text{rad}} = \frac{q_{\text{rad}}}{T_w - T_{\text{sat}}} = \frac{\varepsilon\sigma(T_w^4 - T_{\text{sat}}^4)}{T_w - T_{\text{sat}}}$$

and where ε is a surface radiation property of the heater called the emittance (see Section 10.1).

Unfortunately, such addition would not be correct, because the additional radiative heat transfer will increase the vapor blanket thickness, reducing $\overline{h}_{\text{boiling}}$. Bromley [9.29] suggested for cylinders the approximate relation

$$\overline{h}_{\text{total}} = \overline{h}_{\text{boiling}} + \tfrac{3}{4}\overline{h}_{\text{rad}}, \qquad \overline{h}_{\text{rad}} < \overline{h}_{\text{boiling}} \tag{9.31}$$

More accurate corrections that have subsequently been offered are considerably more complex than this [9.10]. One of the most comprehensive is that of Pitschmann and Grigull [9.32]. Their correlation, which is fairly intricate, brings together an enormous range of heat transfer data for cylinders, within 20%. Radiation is seldom important when the heater temperature is less than 300°C.

The use of the analogy between film condensation and film boiling is somewhat questionable during film boiling on a vertical surface. In this case, the liquid–vapor interface becomes Helmholtz-unstable at a short distance from the leading edge. However, Leonard, Sun, and Dix [9.33] have shown that by using $\lambda_{d_1}/\sqrt{3}$ in place of D in eqn. (9.28), one obtains a very satisfactory prediction of $\overline{h}$ for rather tall vertical plates.

The analogy between film condensation and film boiling also deteriorates when it is applied to small curved bodies. The reason is that the thickness of the vapor film in boiling is far greater than the liquid film during condensation. Consequently, a curvature correction, which could be ignored in film condensation, must be included during film boiling from small cylinders, spheres, and other curved bodies. The first curvature correction to be made was an empirical one given by Westwater and Breen [9.34] in 1962. They showed, for cylinders, that the equation

$$\overline{\mathrm{Nu}}_D = \left[\left(0.715 + \frac{0.263}{R'} \right) (R')^{1/4} \right] \overline{\mathrm{Nu}}_{D_{\mathrm{Bromley}}} \tag{9.32}$$

applies when $R' < 1.86$. Otherwise, Bromley's equation should be used directly.

9.5 Minimum heat flux

Zuber [9.18] also provided a prediction of the minimum heat flux, $q_{\min}$, along with his prediction of $q_{\max}$. He assumed that, as $T_w - T_{\mathrm{sat}}$ is reduced in the film boiling regime, the rate of vapor generation eventually becomes too small to sustain the Taylor wave action that characterizes film boiling. Zuber's $q_{\min}$ prediction, based on this assumption, has to include an arbitrary constant. The result for flat horizontal heaters is

$$q_{\min} = C \, \rho_g h_{fg} \sqrt[4]{\frac{\sigma g (\rho_f - \rho_g)}{(\rho_f + \rho_g)^2}} \tag{9.33}$$

Zuber guessed a value of C which Berenson [9.35] subsequently corrected on the basis of experimental data. Berenson used measured values of $q_{\min}$

on large flat heaters to get

$$q_{\min \text{ Berenson}} = 0.09 \, \rho_g h_{fg} \sqrt[4]{\frac{\sigma g (\rho_f - \rho_g)}{(\rho_f + \rho_g)^2}} \qquad (9.34)$$

Lienhard and Wong [9.36] did the parallel prediction for horizontal wires and found that

$$q_{\min} = 0.515 \left[\frac{18}{R'^2 (2R'^2 + 1)} \right]^{1/4} q_{\min \text{ Berenson}} \qquad (9.35)$$

The problem with all of these expressions is that some contact frequently occurs between the liquid and the heater wall at film boiling heat fluxes higher than the minimum. When this happens, the boiling curve deviates above the film boiling curve and finds a higher minimum than those reported above. The values of the constants shown above should therefore be viewed as practical lower limits of $q_{\min}$. We return to this matter in the next section.

Example 9.8

Check the value of $q_{\min}$ shown in Fig. 9.2.

SOLUTION. The heater is a flat surface, so we use eqn. (9.34) and the physical properties given in Example 9.5.

$$q_{\min} = 0.09(0.597)(2,257,000) \sqrt[4]{\frac{9.8(0.0589)(958)}{(959)^2}}$$

or

$$q_{\min} = 19.0 \text{ kW/m}^2$$

From Fig. 9.2 we read 20.0 kW/m^2, which is the same, to within the accuracy of the graph. ■

9.6   Transition boiling

The transition boiling regime of pool boiling has received less attention than nucleate or film boiling. That is because when the heat flux decreases with temperature, the situation is inherently unstable—it can be sustained only when the wall temperature can be fixed absolutely. The studies of

transition boiling that have been done reveal that it is highly sensitive to the heater surface condition, particularly to wettability. Hence by understanding transition boiling, we also come to understand much about the influence of surface condition on boiling.

The first systematic and accurate measurements of transition boiling were provided by Berenson [9.35] in 1960. Figure 9.14 shows two sets of his data—the upper set is for different surface condition and the lower one is for different surface roughnesses.

The upper set makes it clear that a change of surface condition has a great influence upon transition boiling and the onset of film boiling. The oxidation of the surface has the effect of dramatically changing the *contact angle*[6]—making it far easier for the liquid to wet the surface when it touches it. Transition boiling is more susceptible than any other mode to variations in the contact angle.

The bottom set of curves shows that roughness has a very strong influence upon nucleate boiling. In this case, nucleate boiling is far more susceptible to roughness than any other mode of boiling except, perhaps, the very lowest end of the film boiling range. That is because as roughness increases the number of active nucleation sites, the heat transfer rises in accordance with the Yamagata relation, eqn. (9.3).

It is important to recognize that neither roughness nor surface condition affects film boiling, because the liquid does not touch the heater. The fact that both affect the beginning of the lower film boiling means that they actually cause film boiling to break down by initiating liquid–solid contact at low heat fluxes.

Figure 9.15 shows what an actual boiling curve looks like under the influence of a wetting contact angle. This figure is based on the work of Witte and Lienhard [9.24, 9.39]. On it are identified a *nucleate-transition* and a *film-transition* boiling region. These are continuations of nucleate boiling

---

[6]The contact angle is measured in the liquid, from the surface to the liquid-vapor interface. A contact angle of 0° means that the liquid completely wets a surface. A spherical droplet standing on a non-wetting surface has a 180° contact angle. In the case of water, hydrophilic surfaces have low contact angles, whereas hydrophobic surfaces have high contact angles. Wetting is affected by surface texture, particularly when substantial pockets of air within the texture prevent full contact of the liquid with the surface.

As an example, both lotus leaves and rose petals have high contact angles with water (160° and 152°, respectively), making droplets on them bead into a nearly spherical shape. The lotus leaf's surface structure prevents droplets from making full contact, so that they can roll right off [9.37]. But the structures on a rose petal hold droplets in place—even if the petal is turned upside down [9.38].
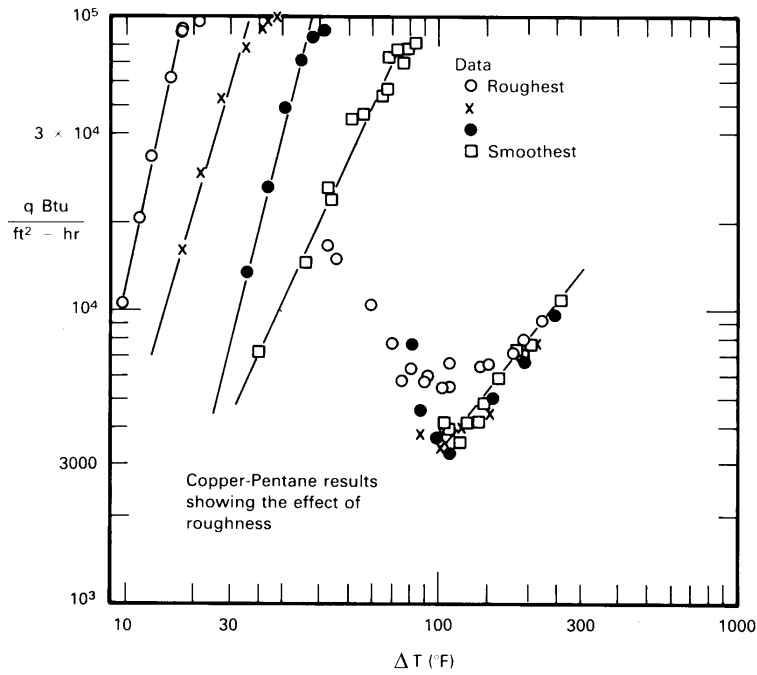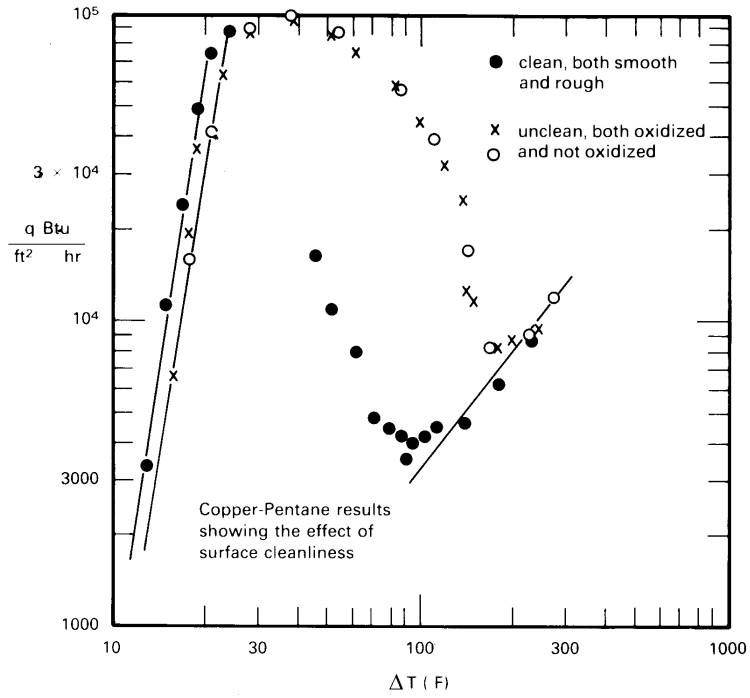
Figure 9.14 Typical data from Berenson's [9.35] study of the effect of surface condition on the boiling curve of a copper plate.
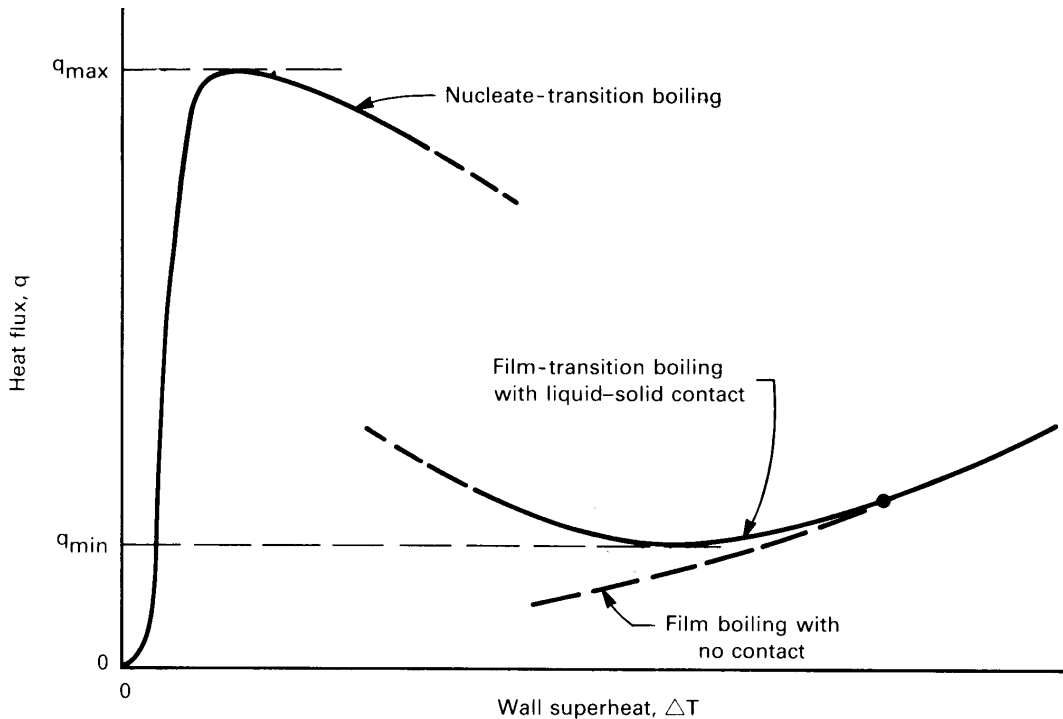
Figure 9.15 The transition boiling regime.

behavior with decreasing liquid–solid contact (as shown in Fig. 9.3c) and of film boiling behavior with increasing liquid–solid contact, respectively. A correlation for the transition-film boiling heat flux was developed by Ramilison and Lienhard [9.40].

These two regions of transition boiling are often connected by abrupt jumps, which may occur in different locations depending upon whether the surface temperature is rising or falling, leading to hysteresis of the boiling curve. More recent work on transition boiling has been reviewed by Ghiaasiaan [9.41].

9.7 Other system influences

Surface effects in pool boiling

Figure 9.14 provides a useful picture of the influence of roughness and surface condition on q_{max}—influences that are not predicted by the hydrodynamic theory. Ramilison et al. [9.42] correlated these effects for

large flat-plate heaters using the rms surface roughness, r in μm, and the receding contact angle for the liquid on the heater material, β, in degrees:

$$\frac{q_{\max}}{q_{\max_Z}} = 1.042(1 - \beta/180)^{3.0} r^{0.125} \qquad (9.36)$$

where $2 \leqslant r \leqslant 12$ μm and $0 \leqslant \beta \leqslant 40°$. This correlation collapses Berenson's data to ±6%. Variations from the predictions of hydrodynamic theory reached 40% as a result of roughness and wettability. Liaw and Dhir [9.43] showed that increasing the contact angle lowered $q_{\max}$ on a vertical wall, although well-wetted surfaces remained within the predictions of hydrodynamic theory [9.44].

A great deal of more recent work on boiling has focused on cooling very small systems where it is practical to use microfabrication techniques to create "structured surfaces"—surfaces with complex built-up microtextures. These surfaces have proved to be useful for achieving higher boiling heat fluxes at lower temperature differences while maintaining high values of $q_{\max}$. Among the most promising surface structures are those that use subsurface porosity to pump additional liquid into the heated area.

It is important that we note that these studies reflect a great variety of small scale configurations. We refer the reader to an excellent summary of this work by Reed and Dhir [9.44], as well as the review by Shoji and Mori [9.45]. Those authors conclude that, while structured surfaces have great potential, they often include data that reflect the hydrodynamic influence of small sizes (Figs. 9.12 and 9.13) and which may not isolate the independent effects of surface texture, contact angle, and size.

Experiments on small heaters are also susceptible to induced convection when sidewalls are not present [9.46]. Induced convection from the side generally reduces $q_{\max}$ on large flat heaters and increases $q_{\max}$ on very small heaters. Such experiments may fall within the left-hand region of Fig. 9.12 as well. Further research is required to fully understand how induced flow together with heater sizes below λ_{d_1} affect $q_{\max}$ on common surfaces.

Subcooling

A stationary pool will normally not remain below its saturation temperature over an extended period of time. When heat is transferred to the pool, the liquid soon becomes saturated—as it does in a teakettle (recall Experiment 9.1). However, before a liquid comes up to temperature, or if
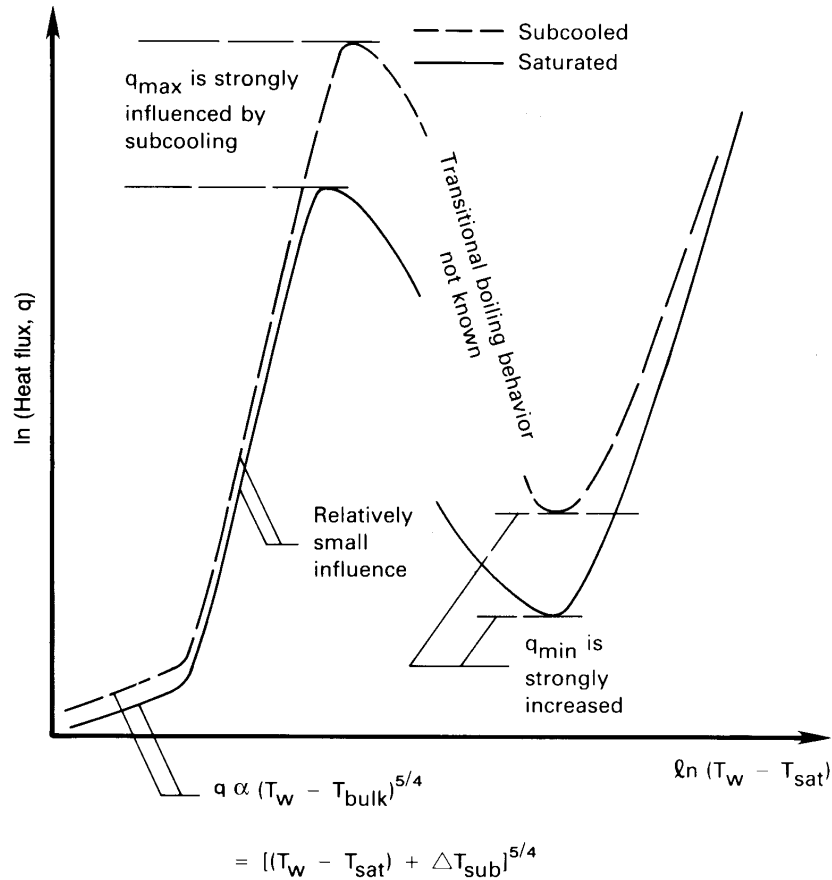
Figure 9.16 The influence of subcooling on the boiling curve.

a very small rate of forced convection continuously replaces warm liquid with cool liquid, we can justly ask what the effect of a cool liquid bulk might be.

Figure 9.16 shows how a typical boiling curve would be shifted if $T_{bulk} < T_{sat}$: We know, for example (recall Section 8.3), that in laminar natural convection, q will increase as $(T_w - T_{bulk})^{5/4}$ or as $[(T_w - T_{sat}) + \Delta T_{sub}]^{5/4}$, where $\Delta T_{sub} \equiv T_{sat} - T_{bulk}$. During *nucleate boiling*, the influence of subcooling on q is known to be small. The *peak and minimum heat fluxes* are known to increase linearly with ΔT_{sub}. These increases are quite significant. The *film boiling* heat flux increases rather strongly, especially at lower heat fluxes. The influence of ΔT_{sub} on transitional boiling is not well documented.

Gravity

The influence of elevated gravity (or any other such body force) is of concern when boiling processes take place in rotating or accelerating systems. The reduction of gravity has a significant impact on boiling processes aboard space vehicles. Since g appears explicitly in the equations for q_{max}, q_{min}, and $q_{\text{film boiling}}$, we know what its influence is. Both q_{max} and q_{min} increase directly as $g^{1/4}$ in finite bodies, and there is an additional gravitational influence through the parameter L'. However, we noted in the previous section that hydrodynamic transitions deteriorate and vanish entirely as R' is reduced below about 0.15. These equations have been validated with experiments that varied gravity.

Although gravity is crucial to bubble removal in the nucleate boiling regime, data suggest that the heat transfer rate is only weakly affected by gravity, perhaps as $g^{1/8}$ [9.41]. (The presence of $g^{1/2}$ in Rohsenow's empirical correlation for nucleate boiling is a weakness that serves as a warning not to apply it for anything but earth-normal gravity.) The onset of nucleate boiling, however, will be affected by the role that gravity plays in displacing the low-ΔT region of natural convection.

Forced convection

A superposed flow over a given heater generally improves heat transfer in all regimes of the boiling curve. But flow is particularly effective in raising q_{max}. Let us look at the influence of forced flow on the different regimes of boiling.

Influences of forced convection on nucleate boiling. Figure 9.17 shows nucleate boiling during the forced convection of water over a flat plate. Bergles and Rohsenow [9.47] offered an empirical strategy for predicting the heat flux during nucleate flow boiling when the net vapor generation is still relatively small. (The photograph in Fig. 9.17 shows how a more substantial buildup of vapor can radically alter flow boiling behavior.) They suggested that

$$q = q_{\text{FC}} \sqrt{1 + \left[\frac{q_B}{q_{\text{FC}}} \left(1 - \frac{q_i}{q_B} \right) \right]^2} \tag{9.37}$$

where

- q_{FC} is the single-phase forced convection heat transfer for the heater, as one might calculate using the methods of Chapters 6 and 7.

- q_B is the *pool* boiling heat flux for that liquid and that heater from eqn. (9.4).

- q_i is the heat flux from the pool boiling curve evaluated at the value of $(T_w - T_{sat})$ where boiling begins during flow boiling (see Fig. 9.17). An estimate of $(T_w - T_{sat})_{onset}$ can be made by intersecting the forced convection equation $q = h_{FC}(T_w - T_b)$ with the following equation [9.48]:

$$(T_w - T_{sat})_{onset} = \left(\frac{8\sigma T_{sat} q}{\rho_g h_{fg} k_f} \right)^{1/2} \tag{9.38}$$

Equation (9.37) will provide a first approximation in most boiling configurations, but it is restricted to subcooled flows or other situations in which vapor generation is not too great.

Peak heat flux in flow over submerged bodies.   The peak heat flux on a submerged body is strongly augmented by an external flow around it. We know from dimensional analysis that

$$\frac{q_{max}}{\rho_g h_{fg} u_\infty} = \text{fn}\left(\text{We}_D, \rho_f/\rho_g \right) \tag{9.39}$$

where the Weber number, We, is

$$\text{We}_L \equiv \frac{\rho_g u_\infty^2 L}{\sigma} = \frac{\text{inertia force}/L}{\text{surface force}/L}$$

and where L is any characteristic length.

Kheyrandish and Lienhard [9.49] suggest fairly complex expressions of this form for q_{max} on horizontal cylinders in cross flows. For a cylindrical liquid jet impinging on a heated disk of diameter D, Sharan and Lienhard [9.50] obtained

$$\frac{q_{max}}{\rho_g h_{fg} u_{jet}} = \left(0.21 + 0.0017 \rho_f/\rho_g \right) \left(\frac{d_{jet}}{D} \right)^{1/3} \left(\frac{1000 \rho_g/\rho_f}{\text{We}_D} \right)^A \tag{9.40}$$

where, if we call $\rho_f/\rho_g \equiv r$,

$$A = 0.486 + 0.06052 \ln r - 0.0378 (\ln r)^2 + 0.00362 (\ln r)^3 \tag{9.41}$$

This correlation represents all the existing data within $\pm 20\%$ over the full range of the data.

Flow boiling over a flat plate
$q = 480{,}000 \text{ W/m}^2$, $u_\infty = 0.52 \text{ m/s}$
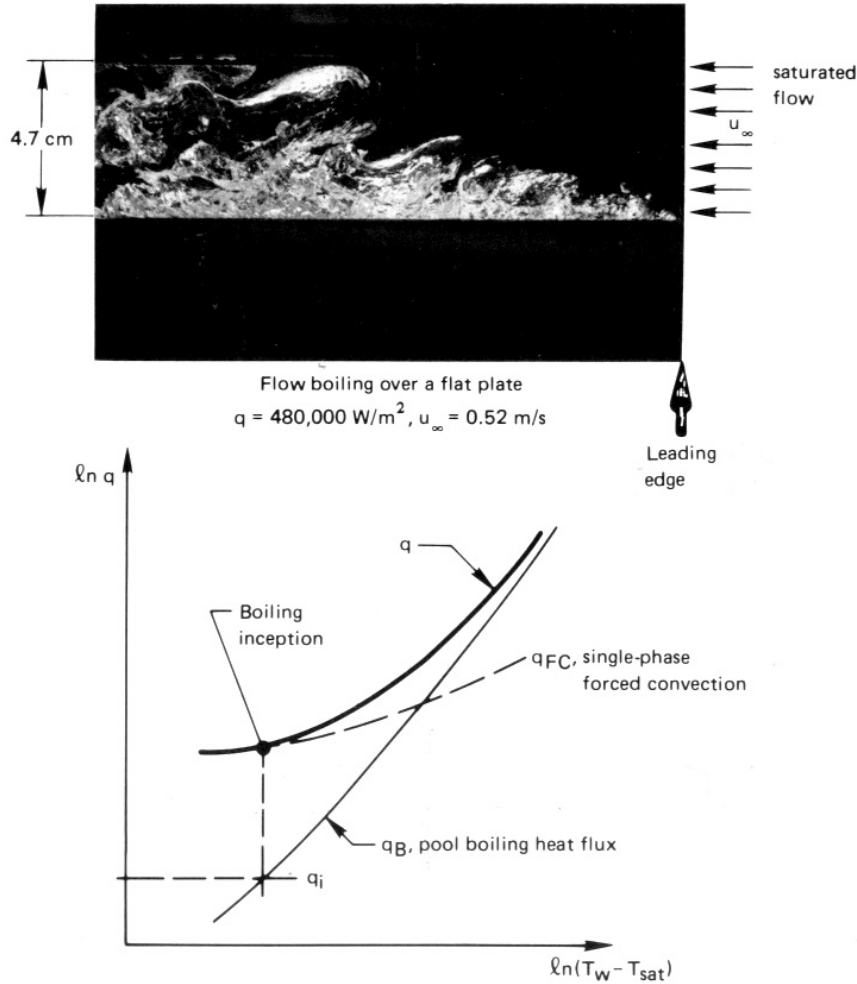
Figure 9.17 Forced convection boiling on an external surface.

The influence of fluid flow on film boiling.   Bromley et al. [9.51] showed that the film boiling heat flux during forced flow normal to a cylinder should take the form

$$q = \text{constant} \left(\frac{k_g \rho_g h'_{fg} \Delta T u_\infty}{D} \right)^{1/2} \tag{9.42}$$

for $u_\infty^2/(gD) \geqslant 4$ with h'_{fg} from eqn. (9.29). Their data fixed the constant at 2.70. Witte [9.52] obtained the same relationship for flow over a sphere and recommended a value of 2.98 for the constant.

Additional work in the literature deals with forced film boiling on plane surfaces and combined forced and subcooled film boiling in a variety of geometries [9.53]. Although these studies are beyond our present scope, it is worth noting that one may attain very high cooling rates in film boiling by combining forced convection and subcooling.

9.8   Forced convection boiling in tubes

Flowing fluids often undergo boiling or condensation heat transfer to fluids moving through tubes. For example, such phase change occurs in all vapor-compression power cycles and refrigerators. Boilers, condensers, steam generators, or evaporators involve heat transfer within tubes. The prediction of heat transfer coefficients in these systems is often essential to determining U and sizing the equipment. So let us consider the problem of predicting boiling heat transfer to liquids flowing through tubes.

Relationship between heat transfer and temperature difference

Forced convection boiling in a tube or duct becomes very hard to delineate because it takes so many forms. In addition to the usual system variables considered in pool boiling, convective boiling exhibit many regimes of behavior. Thus, we need to several boiling mechanisms and the transitions between them, as well.

Collier and Thome's excellent book, *Convective Boiling and Condensation* [9.54], provides a comprehensive discussion of the issues involved in forced convection boiling. Figure 9.18 is their representation of the fairly simple case of flow of liquid in a *uniform wall heat flux* tube, in which body forces can be neglected. This situation is representative of a fairly low heat flux at the wall. The vapor fraction, or *quality*, x, of the flow increases steadily until the wall "dries out." Then the wall temperature rises rapidly. With a very high wall heat flux, the pipe could burn out before dryout occurs.

Figure 9.19, also from Collier and Thome, shows how the regimes shown in Fig. 9.18 are distributed in heat flux and in position along the tube. Notice that high enough heat fluxes can cause burnout at any station in the pipe. In the subcooled nucleate boiling regime (*B* in Fig. 9.18) and the low quality saturated regime (*C*), the heat transfer can be predicted using eqn. (9.37) in Section 9.6. But in the subsequent regimes of slug flow and annular flow (*D*, *E*, and *F*) the heat transfer mechanism changes substantially. Nucleation is increasingly suppressed, and vaporization
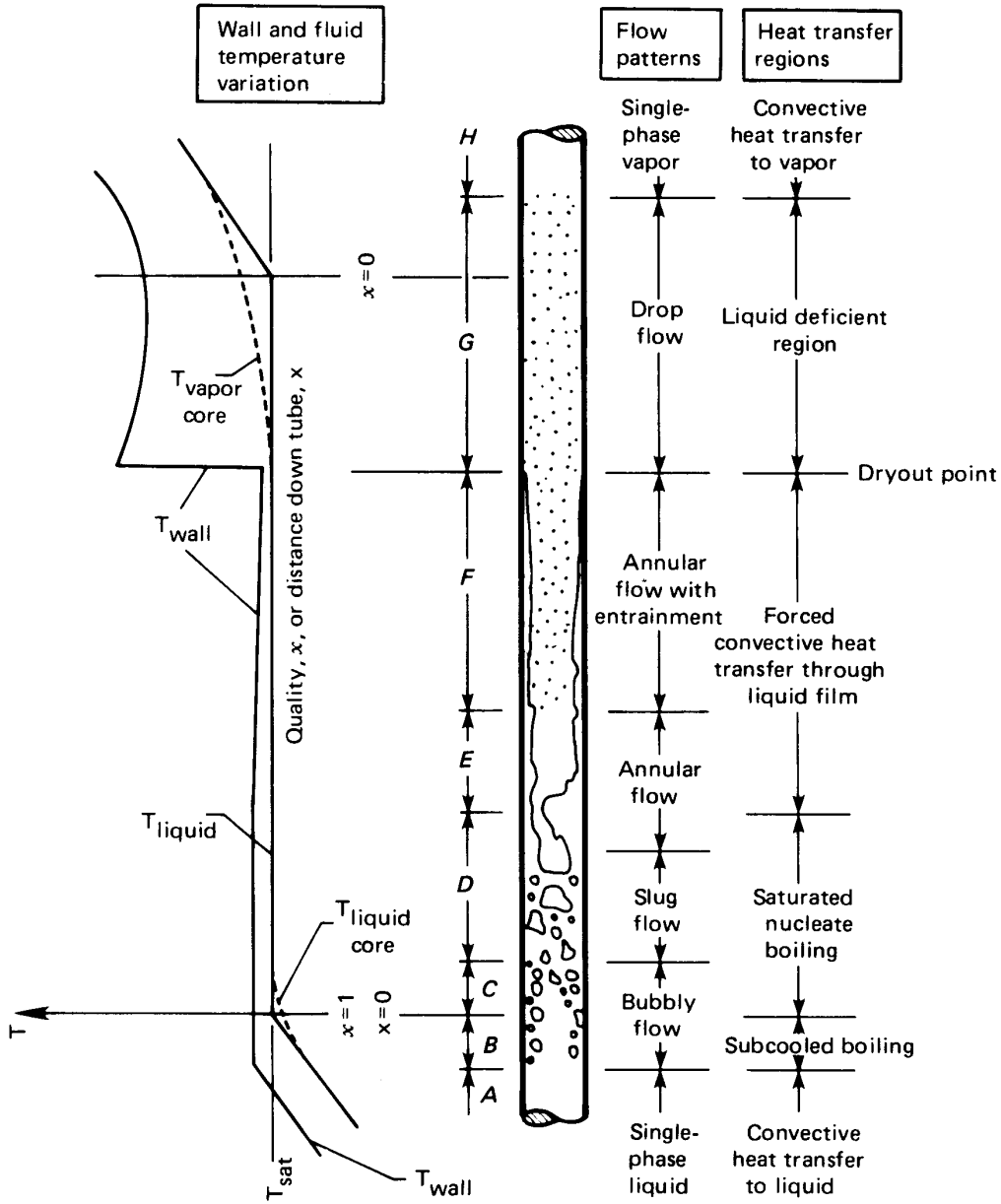
Figure 9.18 The development of a two-phase flow in a vertical tube with a uniform wall heat flux (not to scale).

513
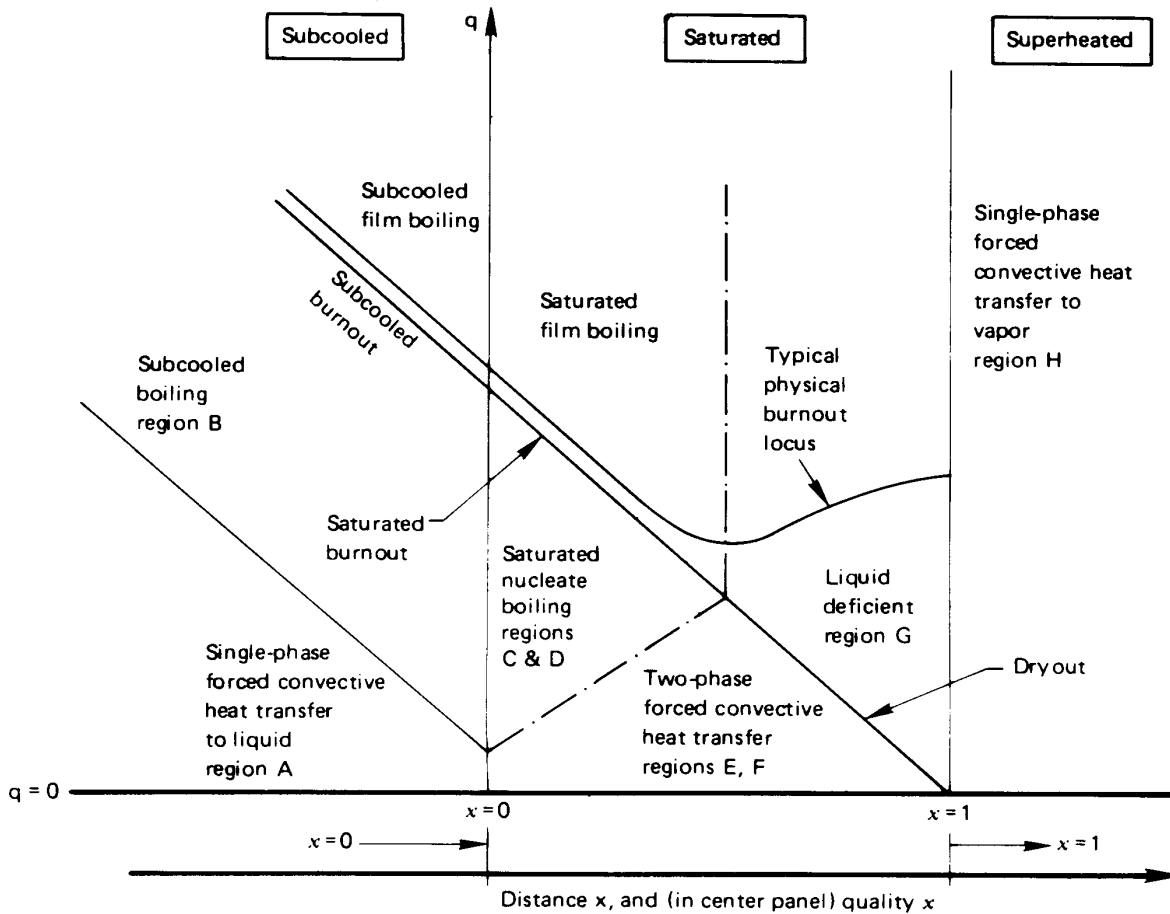
Figure 9.19 The influence of heat flux on two-phase flow behavior.

takes place mainly at the free surface of the liquid film on the tube wall—the flow regime that we call *convective boiling.*

Most efforts to model flow boiling differentiate between nucleate-boiling-controlled heat transfer and convective boiling heat transfer. In those regimes where fully developed nucleate boiling occurs (the later parts of *C*), the heat transfer coefficient is essentially unaffected by the mass flow rate and the flow quality. Locally, conditions are similar to pool boiling.

In convective boiling, on the other hand, vaporization occurs away from the wall, with a liquid-phase convection process dominating at the wall. For example, in the annular regions *E* and *F*, heat is convected from

the wall by the liquid film, and vaporization occurs at the interface of the film with the vapor in the core of the tube. Convective boiling can also dominate at low heat fluxes or high mass flow rates, where wall nucleation is again suppressed. Vaporization then occurs mainly on entrained bubbles in the core of the tube. The heat transfer coefficient in convective boiling is essentially independent of the heat flux; but it is strongly affected by the mass flow rate and quality.

Building a model to capture these complicated and competing trends has presented a challenge to researchers for several decades. One early effort by Chen [9.55] used a weighted sum of a nucleate boiling heat transfer coefficient and a convective boiling coefficient, where the weighting depended on local flow conditions. This model represented water data to an accuracy of about ±30% [9.56], but did not work well with most other fluids. Steiner and Taborek [9.57] substantially improved Chen's mechanistic prediction. Many other investigators have instead pursued correlations built from dimensional analysis and physical reasoning.

Correlation through dimensional analysis

To do a dimensional analysis, we first note that the liquid and vapor phases may have different velocities. Thus, we avoid introducing a flow speed and instead rely on the superficial mass flux, G, through the pipe:

$$G \equiv \frac{\dot{m}}{A_{\text{pipe}}} \ \text{kg/m}^2\text{s} \tag{9.43}$$

This mass flow per unit area is constant along the duct if the flow is steady. From this, we can define a "liquid only" Reynolds number

$$\text{Re}_{\text{lo}} \equiv \frac{GD}{\mu_f} \tag{9.44}$$

which would be the Reynolds number if all the flowing mass were in the liquid state. Then we may use Re_{lo} to compute a liquid-only heat transfer coefficient, h_{lo} from Gnielinski's equation, eqn. (7.41), using liquid properties at T_{sat}.

We then write the flow boiling heat transfer coefficient, h_{fb} for saturated flow in *vertical* tubes as:

$$h_{\text{fb}} = \text{fn}\Big(h_{\text{lo}}, G, x, h_{fg}, q_w, \rho_f, \rho_g\Big) \tag{9.45}$$

Note that tube diameter and other liquid properties, such as viscosity and conductivity, are represented indirectly through h_{lo}. This functional

equation has eight variables in four dimensions (m, kg, s, K). We thus obtain four dimensionless groups, specifically

$$\frac{h_{\text{fb}}}{h_{\text{lo}}} = \text{fn}\left(x, \frac{q_w}{Gh_{fg}}, \frac{\rho_g}{\rho_f}\right) \tag{9.46}$$

In fact, the situation is even a bit simpler than this, since arguments related to the pressure gradient show that the quality and the density ratio can be combined into a single group, called the *convection number*:

$$\text{Co} \equiv \left(\frac{1-x}{x}\right)^{0.8}\left(\frac{\rho_g}{\rho_f}\right)^{0.5} \tag{9.47}$$

The other dimensionless group in eqn. (9.46) is called the *boiling number*:

$$\text{Boi} \equiv \frac{q_w}{Gh_{fg}} \tag{9.48}$$

so that

$$\frac{h_{\text{fb}}}{h_{\text{lo}}} = \text{fn}\,(\text{Boi}, \text{Co}) \tag{9.49}$$

When the convection number is large (Co $\gtrsim$ 1), as for low quality, nucleate boiling dominates. In this range, $h_{\text{fb}}/h_{\text{lo}}$ rises with increasing Boi and is approximately independent of Co. When the convection number is smaller, as at higher quality, the effect of the boiling number declines and $h_{\text{fb}}/h_{\text{lo}}$ increases with decreasing Co.

Correlations having the general form of eqn. (9.49) were developed by Schrock and Grossman [9.58], Shah [9.59], and Gungor and Winterton [9.60]. Kandlikar [9.56, 9.61, 9.62] refined this approach further, obtaining good accuracy and better capturing the parametric trends. His method is to calculate $h_{\text{fb}}/h_{\text{lo}}$ from each of the following two correlations and to choose the larger value:

$$\left.\frac{h_{\text{fb}}}{h_{\text{lo}}}\right|_{\text{nbd}} = (1-x)^{0.8}\left[0.6683\,\text{Co}^{-0.2}f_o + 1058\,\text{Boi}^{0.7}F\right] \tag{9.50a}$$

$$\left.\frac{h_{\text{fb}}}{h_{\text{lo}}}\right|_{\text{cbd}} = (1-x)^{0.8}\left[1.136\,\text{Co}^{-0.9}f_o + 667.2\,\text{Boi}^{0.7}F\right] \tag{9.50b}$$

where "nbd" means "nucleate boiling dominant," "cbd" means "convective boiling dominant," and f_o is a factor that characterizes the orientation of the tube.

Table 9.4 Fluid-dependent parameter *F* in the Kandlikar correlation for copper tubing. Additional values are given in [9.61].

Fluid	F	Fluid	F
Water	1.0	R-124	1.90
Propane	2.15	R-125	1.10
R-12	1.50	R-134a	1.63
R-22	2.20	R-152a	1.10
R-32	1.20	R-410a	1.72

In these equations, f_o is set to one for vertical tubes[7] and *F* is a fluid-dependent parameter whose value is given in Table 9.4. The parameter *F* arises here for the same reason that fluid-dependent parameters appear in nucleate boiling correlations: surface tension, contact angles, and other fluid-dependent variables influence nucleation and bubble growth. The values in Table 9.4 are for commercial grades of copper tubing. For stainless steel tubing, Kandlikar recommends $F = 1$ for all fluids. Equations (9.50) are applicable for the saturated boiling regimes (*C* through *F*) with quality in the range $0 < x \leqslant 0.8$. For subcooled conditions, see Problem 9.21.

Example 9.9

0.6 kg/s of saturated H_2O at $T_b = 207°C$ flows in a 5 cm diameter vertical tube heated at a rate of 184,000 W/m^2. Find the wall temperature at a point where the quality x is 20%.

SOLUTION. Data for water are taken from Tables A.3–A.5. We first compute h_{lo}.

$$G = \frac{\dot{m}}{A_{\text{pipe}}} = \frac{0.6}{0.001964} = 305.6 \text{ kg/m}^2\text{s}$$

and

$$\text{Re}_{lo} = \frac{GD}{\mu_f} = \frac{(305.6)(0.05)}{1.297 \times 10^{-4}} = 1.178 \times 10^5$$

---

[7]The value for horizontal tubes is given in eqn. (9.52).

From eqns. (7.42) and (7.41):

$$f = \frac{1}{[1.82 \log_{10}(1.178 \times 10^5) - 1.64]^2} = 0.01736$$

$$\mathrm{Nu}_D = \frac{(0.01736/8)(1.178 \times 10^5 - 1000)(0.892)}{1 + 12.7\sqrt{0.01736/8}\,[(0.892)^{2/3} - 1]} = 236.3$$

Hence,

$$h_{\mathrm{lo}} = \frac{k_f}{D}\,\mathrm{Nu}_D = \frac{0.6590}{0.05}\,236.3 = 3,115 \ \mathrm{W/m^2K}$$

Next, we find the parameters for eqns. (9.50). From Table 9.4, $F = 1$ for water, and for a vertical tube, $f_o = 1$. Also,

$$\mathrm{Co} = \left(\frac{1-x}{x}\right)^{0.8}\left(\frac{\rho_g}{\rho_f}\right)^{0.5} = \left(\frac{1-0.20}{0.2}\right)^{0.8}\left(\frac{9.014}{856.5}\right)^{0.5} = 0.3110$$

$$\mathrm{Boi} = \frac{q_w}{G h_{fg}} = \frac{184,000}{(305.6)(1,913,000)} = 3.147 \times 10^{-4}$$

Substituting into eqns. (9.50):

$$h_{\mathrm{fb}}\Big|_{\mathrm{nbd}} = (3,115)(1-0.2)^{0.8}\Big[0.6683\,(0.3110)^{-0.2}(1)$$
$$+ 1058\,(3.147 \times 10^{-4})^{0.7}(1)\Big] = 11,950 \ \mathrm{W/m^2K}$$

$$h_{\mathrm{fb}}\Big|_{\mathrm{cbd}} = (3,115)(1-0.2)^{0.8}\Big[1.136\,(0.3110)^{-0.9}(1)$$
$$+ 667.2\,(3.147 \times 10^{-4})^{0.7}(1)\Big] = 14,620 \ \mathrm{W/m^2K}$$

Since the second value is larger, we use it: $h_{\mathrm{fb}} = 14,620 \ \mathrm{W/m^2K}$. Then,

$$T_w = T_b + \frac{q_w}{h_{\mathrm{fb}}} = 207 + \frac{184,000}{14,620} = 220°\mathrm{C} \qquad \blacksquare$$

The Kandlikar correlation leads to mean deviations of 16% for water and 19% for the various refrigerants. The Gungor and Winterton correlation [9.60], which is popular for its simplicity, does not contain fluid-specific coefficients, but it is somewhat less accurate than either the Kandlikar equations or the more complex Steiner and Taborek method [9.56, 9.57].
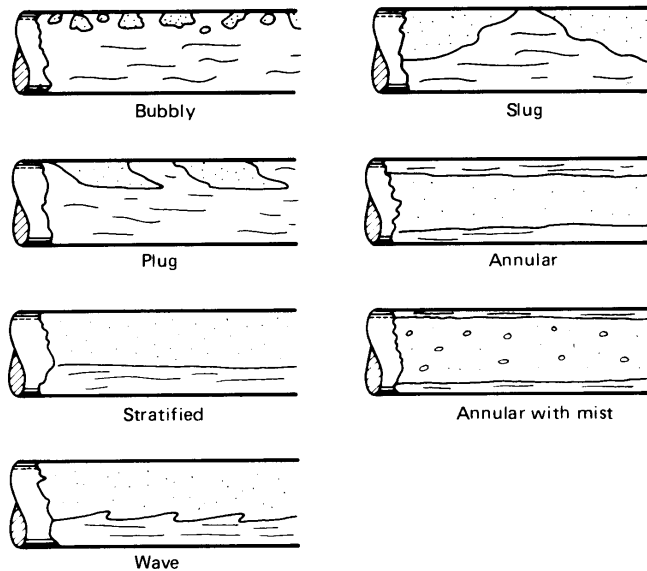
Figure 9.20   The discernible flow regimes during boiling, condensation, or adiabatic flow from left to right in horizontal tubes.

Two-phase flow and heat transfer in horizontal tubes

The preceding discussion of flow boiling in tubes is largely restricted to vertical tubes. Several of the flow regimes in Fig. 9.18 will be altered as shown in Fig. 9.20 if the tube is oriented horizontally. The reason is that, especially at low quality, liquid will tend to flow along the bottom of the pipe and vapor along the top. The patterns shown in Fig. 9.20, by the way, will also be observed during the reverse process—condensation—or during adiabatic two-phase flow.

Which flow pattern actually occurs depends on several parameters in a fairly complex way. Many means have been suggested for predicting what flow pattern will result for a given set of conditions in a pipe. We suggest the work of Dukler, Taitel, and their coworkers. They summarized their two-phase flow-regime maps in [9.63] and [9.64].

For the prediction of heat transfer, the most important additional parameter is the Froude number, Fr_{lo}, which characterizes the strength of the flow's inertia (or momentum) relative to the gravitational forces that drive the separation of the liquid and vapor phases:

$$Fr_{lo} \equiv \frac{G^2}{\rho_f^2 \, gD} \tag{9.51}$$

When $Fr_{lo} < 0.04$, the top of the tube becomes relatively dry and h_{fb}/h_{lo} begins to decline as the Froude number decreases further.

Kandlikar found that he could modify his correlation to account for gravitational effects in horizontal tubes by changing the value of f_o in eqns. (9.50):

$$f_o = \begin{cases} 1 & \text{for } \mathrm{Fr_{lo}} \geq 0.04 \\ (25\,\mathrm{Fr_{lo}})^{0.3} & \text{for } \mathrm{Fr_{lo}} < 0.04 \end{cases} \tag{9.52}$$

Peak heat flux

We have seen that there are two limiting heat fluxes in flow boiling in a tube: dryout and burnout. The latter is the more dangerous of the two since it occurs at higher heat fluxes and gives rise to more catastrophic temperature rises. Collier and Thome provide an extensive discussion of the subject [9.54].

One effective set of empirical formulas was developed by Katto [9.65]. He used dimensional analysis to show that

$$\frac{q_{\max}}{G h_{fg}} = \mathrm{fn}\!\left(\frac{\rho_g}{\rho_f}, \frac{\sigma \rho_f}{G^2 L}, \frac{L}{D} \right)$$

where L is the length of the tube and D its diameter. Since $G^2 L / \sigma \rho_f$ is a Weber number, we can see that this equation is of the same form as eqn. (9.39). Katto identifies several regimes of flow boiling with both saturated and subcooled liquid entering the pipe. For each of these regions, he and Ohne [9.66] later fit a successful correlation of this form to existing data.

Pressure gradients in flow boiling

Pressure gradients in flow boiling interact with the flow pattern and the void fraction, and they can change the local saturation temperature of the fluid. Gravity, flow acceleration, and friction all contribute to pressure change, and friction can be particularly hard to predict. In particular, the frictional pressure gradient can increase greatly as the flow quality rises from the pure liquid state to the pure vapor state; the change can amount to more than two orders of magnitude at low pressures.

Data correlations are usually used to estimate the frictional pressure loss, but they are, at best, accurate to within about ±30%. Whalley [9.67] provides a nice introduction such methods. Certain complex models, designed for use in computer codes, can be used to make more accurate predictions [9.68].

9.9 Forced convective condensation heat transfer

When vapor is blown or forced past a cool wall, it exerts a shear stress on the condensate film. If the direction of forced flow is downward, it will drag the condensate film along, thinning it out and enhancing heat transfer. It is not hard to show (see Problem 9.22) that

$$\frac{4\mu k(T_{\text{sat}} - T_w)x}{gh'_{fg}\rho_f(\rho_f - \rho_g)} = \delta^4 + \frac{4}{3}\left[\frac{\tau_\delta \delta^3}{(\rho_f - \rho_g)g}\right] \tag{9.53}$$

where τ_δ is the shear stress exerted by the vapor flow on the condensate film.

Equation (9.53) is the starting point for any analysis of forced convection condensation on an external surface. Notice that if τ_δ is negative—if the shear opposes the direction of gravity—then it will have the effect of thickening δ and reducing heat transfer. Indeed, if for any value of δ,

$$\tau_\delta = -\frac{3g(\rho_f - \rho_g)}{4}\delta, \tag{9.54}$$

the shear stress will have the effect of halting the flow of condensate completely for a moment until δ grows to a larger value.

Heat transfer solutions based on eqn. (9.53) are complex because they require that one solve the boundary layer problem in the vapor in order to evaluate τ_δ; and this solution must be matched with the velocity at the outside surface of the condensate film. Collier and Thome [9.54] discuss such solutions in some detail. One explicit result has been obtained in this way for condensation on the outside of a horizontal cylinder by Shekriladze and Gomelauri [9.69]:

$$\overline{\text{Nu}}_D = 0.64\left\{\frac{\rho_f u_\infty D}{\mu_f}\left[1 + \left(1 + 1.69\frac{gh'_{fg}\mu_f D}{u_\infty^2 k_f(T_{\text{sat}} - T_w)}\right)^{1/2}\right]\right\}^{1/2} \tag{9.55}$$

where u_∞ is the free stream velocity and $\overline{\text{Nu}}_D$ is based on the liquid conductivity. Equation (9.55) is valid up to $\text{Re}_D \equiv \rho_f u_\infty D/\mu_f = 10^6$. Notice, too, that under appropriate flow conditions (large values of u_∞, for example), gravity becomes unimportant and

$$\overline{\text{Nu}}_D \longrightarrow 0.64\sqrt{2\text{Re}_D} \tag{9.56}$$

The prediction of heat transfer during forced convective condensation in tubes becomes a different problem for each of the many possible flow regimes. See [9.54, §10.5] or [9.70] for details.

9.10   Dropwise condensation

An automobile windshield normally is covered with droplets during a light rainfall. They are hard to see through, and one must keep the windshield wiper moving constantly to achieve any kind of visibility. Water has a high surface tension, and, unless it is very pure, it forms a significant contact angle with glass. Water normally beads up into droplets on car windshields. Visibility can be improved by mixing a surfactant chemical into the windshield-washing water to reduce the surface tension, so that the droplets will spread into a film. Visibility can also be improved by preparing a surface with a "wetting agent" to reduce the contact angle.[8]

Such behavior can also occur on a metallic condensing surface, but there is an important difference: metal surfaces are usually wetting. When vapor condenses, a continuous film is formed. It is regrettable that this is the case, because what is called *dropwise* condensation is an extremely effective heat removal mechanism.

Figure 9.21 shows how dropwise condensation works. Droplets grow from active nucleation sites on the surface, and in this sense there is a great similarity between nucleate boiling and dropwise condensation. The similarity persists as the droplets grow, touch, and merge with one another until one is large enough to be pulled away from its position by gravity. It then slides off, wiping away the smaller droplets in its path and leaving a dry swath in its wake. New droplets immediately begin to grow at the nucleation sites in the path.

The repeated re-creation of the early droplet growth cycle creates a very efficient heat removal mechanism. It is typically ten times more effective than film condensation under the same temperature difference. Indeed, condensing heat transfer coefficients of 200,000 W/m^{2}K can be obtained with water at 1 atm [9.71]. Were it possible to sustain dropwise condensation, we would certainly design equipment in such a way as to make use of it because condenser sizes and costs could be significantly reduced.

Wetting can be temporarily suppressed, and dropwise condensation can be encouraged, by treating an otherwise clean surface (or the vapor) with oil, kerosene, a fatty acid, or a silane compound. Ion beam implantation of nitrogen into metals can also produce dropwise condensation [9.72]. But these treatments either wash away or break down fairly quickly, especially in steam atmospheres. More permanent solutions have

---

[8]A way in which one can accomplish these ends is by wiping the wet window with a cigarette. It is hard to tell which of the two effects the many nasty chemicals in the cigarette achieve.
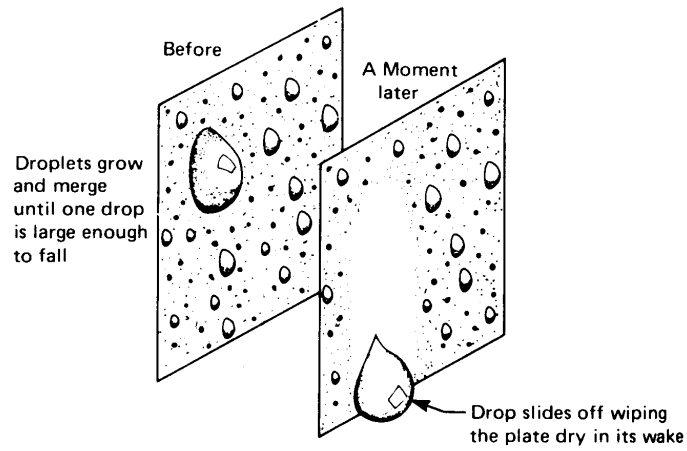
a. The process of liquid removal during dropwise condensation.
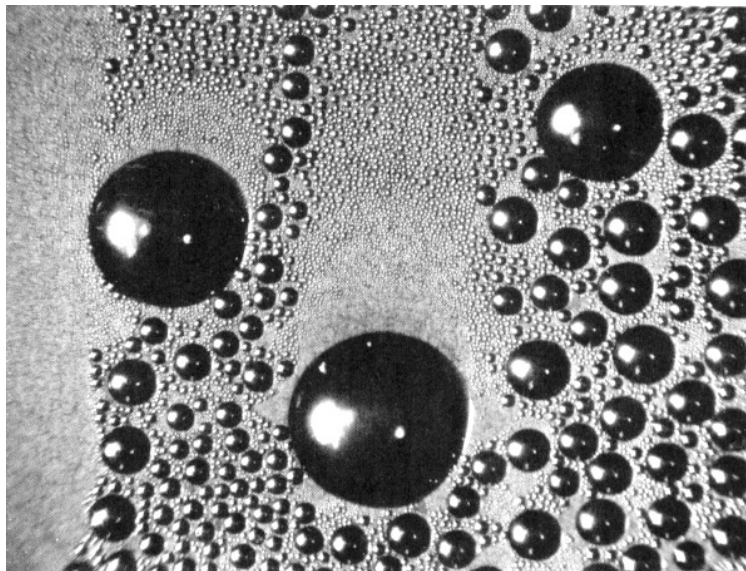
b. Typical photograph of dropwise condensation provided by Professor Borivoje B. Mikić. Notice the dry paths on the left and in the wake of the middle droplet.

Figure 9.21 Dropwise condensation.

proven very elusive, with the result that the liquid condensed in heat exchangers almost always forms a film.

Laboratory experiments on dropwise condensation have typically been done on surfaces that have been pretreated with oleic, stearic, or other fatty acids, or with dioctadecyl disulphide or one of the silanes. See [9.73] for discussion of these nonwetting agents or *promoters* as they are called. Such promoters, lacking durability, are normally impractical for industrial use.[9]

The obvious tactic of coating the surface with a thin, nonwetting, polymer film (such as PTFE, or Teflon) has also proven challenging. Historically, such films have required thicknesses in the range of 20 to 30 μm, which add just enough conduction resistance to reduce the overall heat transfer coefficient to a value similar to film condensation [9.73], fully defeating the purpose! More recently, techniques for grafting polymer films to metals have appeared, allowing an apparently durable film of only about 40 nm thickness [9.74]. For steam condensation, these films have contact angles of $130°$ with reported heat transfer coefficients above 35 kW/m^{2}K. Similarly, coatings of graphene have produced contact angles of $90°$ with heat transfer coefficients around 60 kW/m^{2}K [9.75]. These recent approaches show great promise for resolving a long-standing problem.

Most refrigerants and hydrocarbons have lower surface tension than water, and these liquids spread into films very readily. The challenge of promoting dropwise condensation is accordingly greater [9.76].

Noble metals, such as gold, platinum, and palladium, can also be used as nonwetting coatings, and they have sufficiently high thermal conductivity to avoid the problem encountered with polymeric coatings. For gold, however, the minimum effective coating thickness is about 0.2 μm, or about ⅛ troy ounce per square meter [9.77]—far too expensive for the vast majority of technical applications.

Just as for film condensation, the presence of a small amount of a noncondensable gas, such as air, can greatly reduce the heat transfer rates of dropwise condensation (see discussion on page 455). Because heat transfer coefficients are much higher for dropwise condensation, the sensitivity to noncondensable gases is correspondingly greater. This fact has challenged many experimental studies of dropwise condensation.

Rose [9.73] offers the following expression for the dropwise condensation of steam on short vertical walls, with no noncondensable gases

---

[9]Experienced plant engineers were once known to have added rancid butter through the cup valves of commercial condensers to get at least a temporary improvement of performance through dropwise condensation.
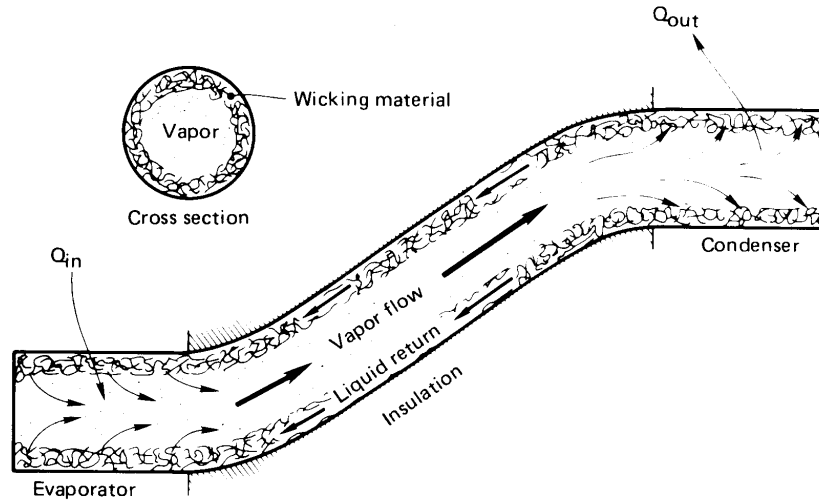
Figure 9.22 A typical heat pipe configuration.

present. It applies for pressures from near atmospheric down to 1 kPa, for contact angles near 90°:

$$q = T^{0.8}\left(5\Delta T + 0.3\,\Delta T^2\right) \text{ kW/m}^2 \qquad (9.57)$$

Here, T is in °C and ΔT is the difference between the bulk vapor and surface temperatures. Temperature differences in the supporting data sets are generally below 8 K.

9.11 The heat pipe

A *heat pipe* is a device that combines the high efficiencies of boiling and condensation. It is aptly named because it literally pipes heat from a hot region to a cold one.

The operation of a heat pipe is shown in Fig. 9.22. The pipe is a tube that can be bent or turned in any way that is convenient. The inside of the tube is lined with a layer of wicking material. The wick is wetted with an appropriate liquid. One end of the tube is exposed to a heat source that evaporates the liquid from the wick. The vapor then flows from the hot end of the tube to the cold end, where it is condensed. Capillary action moves the condensed liquid axially along the wick, back to the evaporator where it is again vaporized.

Placing a heat pipe between a hot region and a cold one is thus similar to connecting the regions with a material of extremely high thermal conductivity—potentially orders of magnitude higher than any solid material. Such devices are used not only for achieving high heat transfer rates between a source and a sink but for a variety of less obvious purposes. They are used, for example, to level out temperatures in systems, since they function almost isothermally and offer very little thermal resistance.

Design considerations in matching a heat pipe to a given application center on the following issues.

- *Selection of the right fluid.* The intended operating temperature of the heat pipe can be met only with a fluid whose saturation temperatures cover the design temperature range. Depending on the temperature range needed, the fluid can be a cryogen, an organic substance, water, a liquid metal, or, in principle, almost any fluid. However, the following characteristics will serve to limit the vapor mass flow per watt, provide good capillary action in the wick, and control the temperature rise between the wall and the wick:

  i) High latent heat

  ii) High surface tension

  iii) Low liquid viscosities

  iv) High thermal conductivity

  Two fluids that meet these four criteria admirably are water and mercury, although toxicity and wetting problems discourage the use of the latter. Ammonia is useful at temperatures that are a bit too low for water. At high temperatures, sodium and lithium have good characteristics, while nitrogen is good for cryogenic temperatures.

  Fluids can be compared using the *merit number*, $M = h_{fg}\sigma/\nu_f$. M generally rises to a maximum as the temperature increases, then falls off again. We should select fluids that operate near their maximum M. Good fluid selections usually result in values of M that range from about 10^{10} to 10^{12} kg/s^3 (see Problem 9.36).

- *Selection of the tube material.* The tube material must be compatible with the working fluid. Gas generation and corrosion are particular considerations. Copper tubes are widely used with water, methanol, and acetone, but they cannot be used with ammonia. Stainless steel tubes can be used with ammonia and many liquid metals, but are

not suitable for long term service with water. In some aerospace applications, aluminum is used for its low weight, typically with ammonia as the working fluid.

- *Selection and installation of the wick.* Like the tube material, the wick material must be compatible with the working fluid. In addition, the working fluid must be able to wet the wick. Wicks can be fabricated from a metallic mesh, from a layer of sintered beads, or simply by scoring grooves along the inside surface of the tube. Many ingenious schemes have been created for bonding the wick to the inside of the pipe and keeping it at optimum porosity.

- *Operating limits of the heat pipe.* The heat transfer through a heat pipe is restricted by

    i) Viscous drag in the wick at low temperature
    ii) The sonic, or choking, speed of the vapor
    iii) Drag of the vapor on the counterflowing liquid in the wick
    iv) Ability of capillary forces in the wick to pump the liquid through the pressure rise between evaporator and condenser
    v) The boiling burnout heat flux in the evaporator section.

    These items must each be dealt with in detail during the design of a new heat pipe [9.78].

- *Control of the pipe performance.* Often a given heat pipe will be called upon to function over a range of conditions—under varying evaporator heat loads, for example. One way to vary its performance is through the introduction of a noncondensable gas in the pipe. This gas will collect at the condenser, limiting the area of the condenser that vapor can reach. By varying the amount of gas, the thermal resistance of the heat pipe can be controlled. In the absence of active control of the gas, an increase in the heat load at the evaporator will raise the pressure in the pipe, compressing the noncondensable gas and lowering the thermal resistance of the pipe. The result is that the temperature at the evaporator remains essentially constant even as the heat load rises as falls.

Heat pipes have proven useful in cooling high power-density electronic devices. The evaporator is located on a small electronic component to be cooled, perhaps a microprocessor, and the condenser is finned and

cooled by a forced air flow (in a desktop or mainframe computer) or is unfinned and cooled by conduction into the exterior casing or structural frame (in a laptop computer). These applications rely on having a heat pipe with much larger condenser area than evaporator area. Thus, the heat fluxes on the condenser are kept relatively low, and the ultimate heat disposal can be as simple as a small fan blowing air over the condenser. Typical heat pipe cooling systems for personal computer equipment are shown in Fig. 9.23.

The reader interested in designing or selecting a heat pipe will find a broad discussion in the book by Dunn and Reay [9.78].

Problems

9.1 A large square tank with insulated sides has a copper base 1.27 cm thick. The base is heated to $650°C$ and saturated water is suddenly poured in the tank. Plot the temperature of the base as a function of time on the basis of Fig. 9.2 if the bottom of the base is insulated. In your graph, indicate the regimes of boiling and note the temperature at which cooling is most rapid. Note that the base is being *quenched* (recall discussion in Example 9.7).

9.2 Predict q_{max} for the two heaters in Fig. 9.3b. At what percentage of q_{max} is each one operating? *Hint:* Both are operating close to burnout.

9.3 A very clean glass container of water at $70°C$ is depressurized until it is subcooled $30°C$. Then it suddenly and explosively "flashes" (or boils). What is the pressure at which this happens? Approximately what diameter of gas bubble, or other disturbance in the liquid, caused it to flash?

9.4 Plot the unstable bubble radius as a function of liquid superheat for water at 1 atm. How far is it reasonable to draw your curve and why?

9.5 In chemistry class you have probably witnessed the phenomenon of "bumping" in a test tube (the explosive boiling that blows the contents of the tube all over the ceiling). Yet you have never seen this happen in a kitchen pot. Explain why not.

9.6 Use van der Waals equation of state (recall your thermodynamics course) to approximate the highest reduced temperature to which
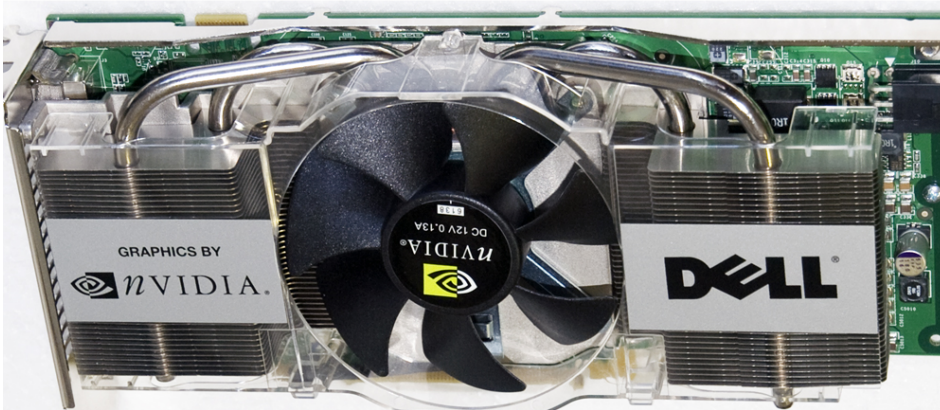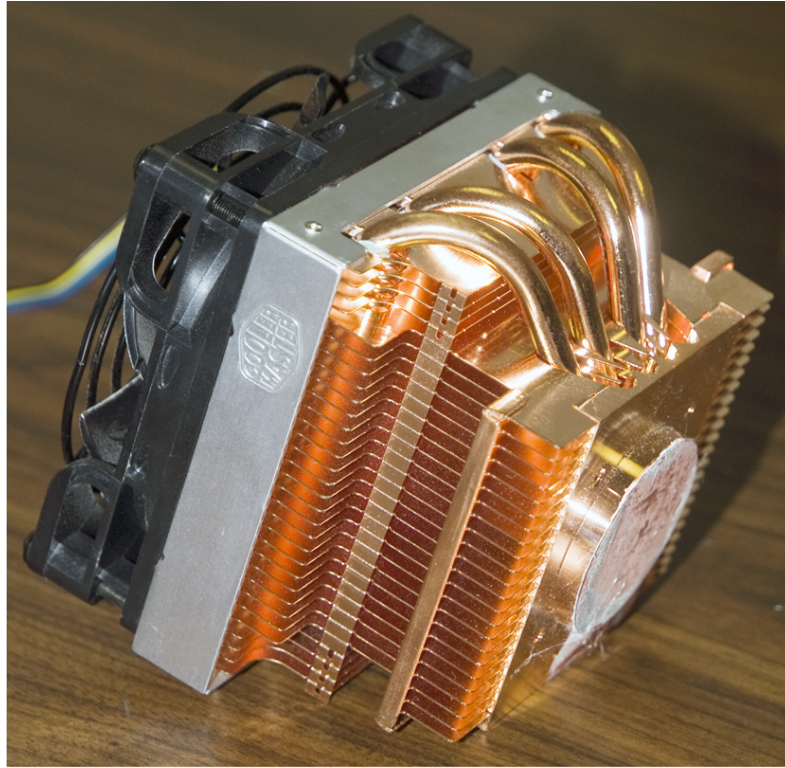
Figure 9.23 Two heat-pipe-cooled computer heat sinks. Top: A Cooler Master unit for cooling a CPU. The copper disk on the right affixes to the CPU. The visible heat pipes carry heat to the fin array which is cooled by the fan on the left. Bottom: A Dell *n*Vidia graphics card cooled by a copper block beneath the fan in the center. The block feeds four heat pipes which carry heat to the fin arrays on either side of the fan in the center. Courtesy of Gene Quach, PC&C Computers, Houston, TX.

water can be superheated at low pressure. How many degrees of superheat does this suggest that water can sustain at the low pressure of 1 atm? (It turns out that this calculation is accurate within about 10%.) What would R_b be at this superheat?

9.7 Use Yamagata's equation, (9.3), to determine how nucleation site density increases with ΔT for Berenson's curves in Fig. 9.14. In other words, find c in the relation $n = \text{constant } \Delta T^c$. *Hint*: In all cases, the site density is very strongly dependent on ΔT.

9.8 Suppose that C_{sf} for a given surface is high by 50%. Estimate the percentage error in q calculated for a given value of ΔT. [Low by 70%.]

9.9 Water at 100 atm boils on a nickel heater whose temperature is 6°C above T_{sat}. Estimate h and q.

9.10 Water boils on a large flat plate at 1 atm. Calculate q_{max} if the plate is operated on the surface of the moon (at ⅙ of $g_{\text{earth−normal}}$). What would q_{max} be in a space vehicle experiencing 10^{-4} of $g_{\text{earth−normal}}$?

9.11 Water at 1 atm and at its boiling point is electrically heated by a 2 mm diameter horizontal copper wire. Plot q vs. ΔT from $\Delta T = 0$ up to the copper's melting point. Note that parts of this curve would be inaccessible.

9.12 Redo Problem 9.11 for a 30 mm diameter sphere in water at 10 atm.

9.13 Verify eqn. (9.17).

9.14 Make a sketch of the q vs. $(T_w − T_{\text{sat}})$ relation for a pool boiling process, and describe a graphical method for locating the points where h is maximum and minimum. What numerical values do you get for these two h's from Fig. 9.2? [$\overline{h} = 48,000$ and 680 W/m²K]

9.15 A 2 mm diameter jet of methanol is directed normal to the center of a 1.5 cm diameter disk heater at 1 m/s. How many watts can safely be supplied by the heater? [$Q_{\text{max}} = 6,450$ W]

9.16 Saturated water at 1 atm boils on a ½ cm diameter platinum rod. Estimate the temperature of the rod at burnout. [$T_{\text{rod}} = 119$°C]

9.17 Plot $(T_w − T_{\text{sat}})$ and the quality x as a function of position z for the conditions in Example 9.9. Set $z = 0$ where $x = 0$ and end the

plot where the quality reaches 80%. *Hint*: The solution will require trial and error.

9.18 Plot $(T_w - T_{sat})$ and the quality x as a function of position in an 8 cm I.D. pipe if 0.3 kg/s of water at 100°C passes through it and $q_w = 200,000 \text{ W/m}^2$. *Hint*: The solution will require trial and error.

9.19 Use dimensional analysis to verify the form of eqn. (9.8).

9.20 Compare the peak heat flux calculated from the data given in Problem 5.6 with the appropriate prediction. [The prediction is within 11%.]

9.21 The Kandlikar correlation, eqn. (9.50a), can be adapted subcooled flow boiling, with $x = 0$ (region B in Fig. 9.19). Noting that $q_w = h_{fb}(T_w - T_{sat})$, show that

$$q_w = \left[1058 \, h_{lo} F (Gh_{fg})^{-0.7} (T_w - T_{sat}) \right]^{10/3}$$

in subcooled flow boiling [9.61].

9.22 Verify eqn. (9.53) by repeating the analysis following eqn. (8.50) but using the b.c. $(\partial u / \partial y)_{y=\delta} = \tau_\delta / \mu$ in place of $(\partial u / \partial y)_{y=\delta} = 0$. Verify the statement that includes eqn. (9.54).

9.23 A 7 cm O.D. pipe carrying cool water has an outside temperature of 40°C. Saturated steam at 80°C flows across it. Plot $\bar{h}_{condensation}$ over the range of Reynolds numbers $0 \leqslant \text{Re}_D \leqslant 10^6$. Do you get the value at $\text{Re}_D = 0$ that you would anticipate from Chapter 8?

9.24 (a) Suppose that you have pits of roughly 2 μm diameter in a metallic heater surface. At about what temperature might you expect water to boil on that surface if the pressure is 20 atm? (b) Measurements have shown that water at atmospheric pressure can be superheated about 200°C above its normal boiling point. Roughly how large an embryonic bubble would be needed to trigger nucleation in water in such a state? *Hint for (b)*: Your result should be ten times the atomic lattice spacing of copper.

9.25 Use dimensional analysis to obtain the dimensionless functional form of the q_{max} equation for pool boiling and of the q_{max} equation for flow boiling on external surfaces. Compare your results to equations in the text.

9.26 An imaginary chemist produces a nondegradable additive that will increase σ by a factor of ten for water at 1 atm. By what factor will the additive improve q_{max} during pool boiling on: (a) infinite flat plates, and (b) small horizontal cylinders? By what factor will it improve burnout in the flow of jet on a disk? [q_{max} will approximately double]

9.27 Steam at 1 atm is blown at 26 m/s over a 1 cm O.D. cylinder at 90°C. What is $\bar{h}$? Can you suggest any physical process within the cylinder that could sustain this temperature in this flow?

9.28 The water shown in the photo in Fig. 9.17 is at 1 atm, and the Nichrome heater can be approximated as nickel. What is $T_w - T_{sat}$? *Hint*: You will need to read a missing dimension from the figure.

9.29 For film boiling on horizontal cylinders, eqn. (9.6a) must take the form

$$\lambda_d = 2\pi\sqrt{3}\left[\frac{g(\rho_f - \rho_g)}{\sigma} + \frac{2}{(\text{diam.})^2}\right]^{-1/2}$$

If ρ_f is 748 kg/m^3 for saturated acetone, compare this λ_d, and the infinite flat plate value, to Fig. 9.3d. *Hint*: Note that one can extract a range of wavelengths from the photos, owing to a disturbance which, we can see, is moving horizontally across the wave pattern. Your calculation should show this formula to be far better than the flat plate value; but the comparison will certainly not be perfect.

9.30 Water at 47°C flows through a 13 cm diameter thin-walled tube at 8 m/s. Saturated water vapor, at 1 atm, flows across the tube at 50 m/s. Evaluate T_{tube}, U, and q. [$T_{tube} = 69$°C]

9.31 A 1 cm diameter thin-walled tube carries liquid metal through saturated water at 1 atm. The throughflow of metal is increased until burnout occurs. At that point the metal temperature is 250°C and h inside the tube is 9600 W/m^{2}K. What is the wall temperature at burnout? [$T_{wall} = 132$°C]

9.32 At about what velocity of liquid metal flow does burnout occur in Problem 9.31 if the metal is mercury?

9.33 Explain, in physical terms, why eqns. (9.23) and (9.24), instead of differing by a factor of two, are almost equal. How do these equations change when H' is large? *Hint*: In thinking this through, remember that burnout depends on the amount of vapor produced.

9.34 A liquid enters the heated section of a pipe at a location $z = 0$ with a specific enthalpy $\hat{h}_{\text{in}}$. If the wall heat flux is $q_w(z)$ and the pipe diameter is D, show that the enthalpy a distance $z = L$ downstream is

$$\hat{h} = \hat{h}_{\text{in}} + \frac{\pi D}{\dot{m}} \int_0^L q_w(z)\, dz$$

Since the quality may be defined as $x \equiv (\hat{h} - \hat{h}_{f,\text{sat}})/h_{fg}$, show that for constant q_w, when $x \geqslant 0$

$$x = \frac{\hat{h}_{\text{in}} - \hat{h}_{f,\text{sat}}}{h_{fg}} + \frac{4 q_w L}{G D h_{fg}}$$

9.35 Consider again the x-ray monochrometer described in Problem 7.44. Suppose now that the mass flow rate of liquid nitrogen is 0.023 kg/s, that the nitrogen is saturated at 110 K when it enters the heated section, and that the passage horizontal. Estimate the quality and the wall temperature at end of the heated section if $F = 4.70$ for nitrogen in eqns. (9.50). As before, assume the silicon to conduct well enough that the heat load is distributed uniformly over the surface of the passage.

9.36 Use data from Appendix A and Table 9.1 to calculate the merit number, M, for the following potential heat-pipe working fluids over the range 200 K to 600 K in 100 K increments: water, mercury, methanol, ammonia, and HCFC-22. Indicate when data are unavailable for a fluid at some temperature. What fluids are best suited for particular temperature ranges?

9.37 Use Rose's dropwise condensation correlation, eqn. (9.57), to plot q vs. ΔT for steam pressures of 1 kPa, 10 kPa, and 100 kPa, with $\Delta T \leqslant 8$ K. Calculate the range of h for each pressure. Comment on the magnitudes of the numbers you obtain.

9.38 Cercignani [9.79] used nonequilibrium gas kinetics to derive the following expression for the evaporation rate ($\text{kg/m}^2\text{s}$) from a superheated liquid surface at T_0 into vapor at a lower temperature:

$$\dot{m}'' = \rho_{g,0} \sqrt{\frac{R T_0}{2\pi}} \left(\frac{\alpha \sigma}{\sigma + \alpha(1 - \sigma)} \right) \left(\frac{\Delta p_g}{p_{g,0}} \right) \qquad (9.58)$$

Here: $\alpha = 32\pi/(32 + 9\pi)$; R is the gas constant of the vapor in J/kg·K; $p_{g,0}$ is the saturation vapor pressure at T_0; Δp_g is the

difference between the saturation vapor pressure and pressure of the vapor far from the surface; and $0 < \sigma \leq 1$, the accommodation coefficient, characterizes the likelihood that a vapor molecule will not bounce off of the liquid surface after hitting it. Lu et al. [9.80] measured water evaporation rates for $\Delta p_g / p_{g,0} \lesssim 0.4$, reporting that $\sigma = 0.31$ for interfaces at 22–50°C. Equation (9.58) matches these data very well. Assuming that σ stays near 0.31 at higher temperatures, plot the evaporative heat flux into saturated vapor at 100°C from a water surface between 100 and 110°C.

References

[9.1] S. Nukiyama. The maximum and minimum values of the heat q transmitted from metal to boiling water under atmospheric pressure. *J. Jap. Soc. Mech. Eng.*, **37**:367–374, 1934. Translation: *Int. J. Heat Mass Transfer*, **9**:1419–1433, 1966. doi: 10.1016/0017-9310(66)90138-4.

[9.2] T. B. Drew and C. Mueller. Boiling. *Trans. AIChE*, **33**:449, 1937.

[9.3] International Association for the Properties of Water and Steam. Revised release on surface tension of ordinary water substance. Technical Report IAPWS R1-76, June 2014. url: http://www.iapws.org/.

[9.4] J. J. Jasper. The surface tension of pure liquid compounds. *J. Phys. Chem. Ref. Data*, **1**(4):841–1010, 1972. doi: 10.1063/1.3253106.

[9.5] M. Okado and K. Watanabe. Surface tension correlations for several fluorocarbon refrigerants. *Heat Transfer: Japanese Research*, **17**(1): 35–52, 1988.

[9.6] A. P. Fröba, S. Will, and A. Leipertz. Saturated liquid viscosity and surface tension of alternative refrigerants. *Int. J. Thermophys.*, **21**(6):1225–1253, November 2000. doi: 10.1023/A:1006689724974.

[9.7] V.G. Baidakov and I.I. Sulla. Surface tension of propane and isobutane at near-critical temperatures. *Russ. J. Phys. Chem.*, **59**(4):551–554, 1985.

[9.8] P.O. Binney, W.-G. Dong, and J. H. Lienhard. Use of a cubic equation to predict surface tension and spinodal limits. *J. Heat Transfer*, **108**(2):405–410, 1986. url: http://www.uh.edu/engines/cubicequationsurfacetension.pdf.

[9.9] Y. Y. Hsu. On the size range of active nucleation cavities on a heating surface. *J. Heat Transfer*, **84**(3):207–216, August 1962. doi: 10.1115/1.3684339.

[9.10] G. F. Hewitt. Boiling. In W. M. Rohsenow, J. P. Hartnett, and Y. I. Cho, editors, *Handbook of Heat Transfer*, Chapter 15. McGraw-Hill, New York, 3rd ed., 1998.

[9.11] V. K. Dhir. Nucleate pool boiling. In F. A. Kulacki, editor, *Handbook of Thermal Science and Engineering*, Chapter 41, pp. 1645–1694. Springer, Cham, Switzerland, 2018. doi: 10.1007/978-3-319-26695-4_41.

[9.12] K. Yamagata, F. Hirano, K. Nishiwaka, and H. Matsuoka. Nucleate boiling of water on the horizontal heating surface. *Mem. Fac. Eng. Kyushu*, **15**: 98, 1955.

[9.13] W. M. Rohsenow. A method of correlating heat transfer data for surface boiling of liquids. *Trans. ASME*, **74**(6):969, August 1952. doi: 10.1115/1.4015984.

[9.14] I. L. Pioro. Experimental evaluation of constants for the Rohsenow pool boiling correlation. *Int. J. Heat. Mass Transfer*, **42**(11):2003–2013, June 1999. doi: 10.1016/S0017-9310(98)00294-4.

[9.15] R. Bellman and R. H. Pennington. Effects of surface tension and viscosity on Taylor instability. *Quart. Appl. Math.*, **12**:151–162, 1954. doi: 10.1090/qam/63198.

[9.16] V. Sernas. Minimum heat flux in film boiling—a three dimensional model. In *Proc. 2nd Can. Cong. Appl. Mech.*, pp. 425–426, Canada, 1969. Univ. of Waterloo.

[9.17] H. Lamb. *Hydrodynamics*. Dover Publications, Inc., New York, 6th ed., 1945.

[9.18] N. Zuber. Hydrodynamic aspects of boiling heat transfer. Report AECU-4439, US Atomic Energy Commission, June 1959. doi: 10.2172/4175511. UCLA doctoral dissertation.

[9.19] J. H. Lienhard and V. K. Dhir. Extended hydrodynamic theory of the peak and minimum pool boiling heat fluxes. Contractor Report NASA-CR-2270, NASA, Washington, D.C., July 1973. url: http://hdl.handle.net/2060/19730019076.

[9.20] J. H. Lienhard, V. K. Dhir, and D. M. Riherd. Peak pool boiling heat-flux measurements on finite horizontal flat plates. *J. Heat Transfer*, **95**(4):477–482, November 1973. doi: 10.1115/1.3450092. url: https://engines.egr.uh.edu/sites/engines/files/talks/PeakPoolBoiling.pdf.

[9.21] J. H. Lienhard and V. K. Dhir. Hydrodynamic prediction of peak pool-boiling heat fluxes from finite bodies. *J. Heat Transfer*, **95**(2):152–158, May 1973. doi: 10.1115/1.3450013.

[9.22] Z. She and V. K. Dhir. Parametric effects of heater size, contact angle, and surrounding vessel size on pool boiling critical heat flux from horizontal surfaces. *Journal of Electronic Packaging*, **143**(4):041113, December 2021. doi: 10.1115/1.4052716.

[9.23] C. F. Bonilla and C. W. Perry. Heat transmission to boiling binary liquid mixtures. *Trans. AIChE*, **37**:269–290, 1941.

[9.24] J. H. Lienhard and L. C. Witte. An historical review of the hydrodynamic theory of boiling. *Rev. Chem. Engr.*, **3**(3):187–280, 1985. Available online at http://www.uh.edu/engines/HydrodynamicHistory.pdf.

[9.25] S. S. Kutateladze. On the transition to film boiling under natural convection. *Kotloturbostroenie*, **3**:10, 1948.

[9.26] N. Bakhru and J. H. Lienhard. Boiling from small cylinders. *Int. J. Heat Mass Transfer*, **15**:2011–2025, 1972. url: http://www.uh.edu/engines/BoilingFromSmallCylinders.pdf.

[9.27] K. H. Sun and J. H. Lienhard. The peak pool boiling heat flux on horizontal cylinders. *Int. J. Heat Mass Transfer*, **13**(9):1425–1439, September 1970. doi: 10.1016/0017-9310(70)90178-X.

[9.28] J. S. Ded and J. H. Lienhard. The peak pool boiling heat flux from a sphere. *AIChE J.*, **18**(2):337–342, March 1972. doi: 10.1002/aic.690180215.

[9.29] A. L. Bromley. Heat transfer in stable film boiling. *Chem. Eng. Progr.*, **46**:221–227, 1950.

[9.30] P. Sadasivan and J. H. Lienhard. Sensible heat correction in laminar film boiling and condensation. *J. Heat Transfer*, **109**(2):545–547, May 1987. doi: 10.1115/1.3248122.

[9.31] V. K. Dhir and J. H. Lienhard. Laminar film condensation on plane and axisymmetric bodies in non-uniform gravity. *J. Heat Transfer*, **93**(1):97–100, February 1971. doi: 10.1115/1.3449773.

[9.32] P. Pitschmann and U. Grigull. Filmverdampfung an waagerechten Zylindern. *Wärme- und Stoffübertragung*, **3**:75–84, June 1970. doi: 10.1007/BF01108028.

[9.33] J. E. Leonard, K. H. Sun, and G. E. Dix. Low flow film boiling heat transfer on vertical surfaces: Part II: Empirical formulations and application to BWR-LOCA analysis. In *Proc. ASME-AIChE Nat. Heat Transfer Conf.*, St. Louis, August 1976. American Society of Mechanical Engineers.

[9.34] J. W. Westwater and B. P. Breen. Effect of diameter of horizontal tubes on film boiling heat transfer. *Chem. Eng. Progr.*, **58**:67–72, 1962.

[9.35] P. J. Berenson. Transition boiling heat transfer from a horizontal surface. Heat Transfer Lab. Tech. Rep. 17, Massachusetts Institute of Technology, Cambridge, MA, 1960. url: http://hdl.handle.net/1721.1/61478.

[9.36] J. H. Lienhard and P. T. Y. Wong. The dominant unstable wavelength and minimum heat flux during film boiling on a horizontal cylinder. *J. Heat Transfer*, **86**(2):220–226, May 1964. doi: 10.1115/1.3687103. url: https://engines.egr.uh.edu/sites/engines/files/talks/FilmBoilingWavelength.pdf.

[9.37] L. Feng, Y. Zhang, J. Xi, Y. Zhu, N. Wang, F. Xia, and L. Jiang. Petal effect: A superhydrophobic state with high adhesive force. *Langmuir*, **24**(8): 4114–4119, March 2008. Open access. doi: 10.1021/la703821h.

[9.38] W. Barthlott and C. Neinhuis. Purity of the sacred lotus, or escape from contamination in biological surfaces. *Planta*, **202**(1):1–8, Apr 1997. doi: 10.1007/s004250050096.

[9.39] L. C. Witte and J. H. Lienhard. On the existence of two transition boiling curves. *Int. J. Heat Mass Transfer*, **25**(6):771–779, June 1982. doi: 10.1016/0017-9310(82)90089-8. url: https://engines.egr.uh.edu/sites/engines/files/talks/TwoTransitionBoilingRegimes.pdf.

[9.40] J. R. Ramilison and J. H. Lienhard. Transition boiling heat transfer and the film transition region. *J. Heat Transfer*, **109**(3):746–752, August 1987. doi: 10.1115/1.3248153. url: https://engines.egr.uh.edu/sites/engines/files/talks/Ramilison1987.pdf.

[9.41] S. M. Ghiaasiaan. Transition and film boiling. In F. A. Kulacki, editor, *Handbook of Thermal Science and Engineering*, Chapter 42, pp. 1695–1746. Springer, Cham, Switzerland, 2018.

[9.42] J. M. Ramilison, P. Sadasivan, and J. H. Lienhard. Surface factors influencing burnout on flat heaters. *J. Heat Transfer*, **114**(1):287–290, February 1992. doi: 10.1115/1.2911261.

[9.43] S. P. Liaw and V. K. Dhir. Void fraction measurements during saturated pool boiling of water on partially wetted vertical surfaces. *J. Heat Transfer*, **111**(3):731–738, August 1989. doi: 10.1115/1.3250744.

[9.44] J. Reed and V. K. Dhir. Assessment of critical heat flux on finite size surfaces under pool boiling. In *2019 35th Thermal Measurement, Modeling Management Symposium (SEMI-THERM)*, San Jose, CA, March 2019. Paper no. 978-0578-43862-7/19.

[9.45] S. Mori and Y. Utaka. Critical heat flux enhancement by surface modification in a saturated pool boiling: A review. *Int. J. Heat Mass Transfer*, **108**: 2534–2557, May 2017. doi: 10.1016/j.ijheatmasstransfer.2017.01.090.

[9.46] J. H. Lienhard and J. B. Keeling. An induced-convection effect upon the peak-boiling heat flux. *J. Heat Transfer*, **92**(1):1–5, February 1970. doi: 10.1115/1.3449633.

[9.47] A. E. Bergles and W. M. Rohsenow. The determination of forced-convection surface-boiling heat transfer. *J. Heat Transfer*, **86**(3):365–372, August 1964. doi: 10.1115/1.3688697.

[9.48] E. J. Davis and G. H. Anderson. The incipience of nucleate boiling in forced convection flow. *AIChE J.*, **12**:774–780, July 1966. doi: 10.1002/aic.690120426.

[9.49] K. Kheyrandish and J. H. Lienhard. Mechanisms of burnout in saturated and subcooled flow boiling over a horizontal cylinder. In *Proc. ASME-AIChE Nat. Heat Transfer Conf.*, Denver, August 4–7, 1985.

[9.50] A. Sharan and J. H. Lienhard. On predicting burnout in the jet-disk configuration. *J. Heat Transfer*, **107**(2):398–401, May 1985. doi: 10.1115/1.3247428.

[9.51] L. A. Bromley, N. R. LeRoy, and J. A. Robbers. Heat transfer in forced convection film boiling. *Ind. Eng. Chem.*, **45**(12):2639–2646, December 1953. doi: 10.1021/ie50528a027.

[9.52] L. C. Witte. Film boiling from a sphere. *Ind. Eng. Chem. Fund.*, **7**(3):517–518, August 1968. doi: 10.1021/i160027a026.

[9.53] L. C. Witte. External flow film boiling. In S. G. Kandlikar, M. Shoji, and V. K. Dhir, editors, *Handbook of Phase Change: Boiling and Condensation*, Chapter 13, pp. 311–330. Taylor & Francis, Philadelphia, 1999. doi: 10.1201/9780203752654.

[9.54] J. G. Collier and J. R. Thome. *Convective Boiling and Condensation*. Oxford University Press, Oxford, 3rd ed., 1996.

[9.55] J. C. Chen. Correlation for boiling heat transfer to saturated fluids in convective flow. *Industrial & Engineering Chemistry Process Design and Development*, **5**(3):322–329, 1966. doi: 10.1021/i260019a023.

[9.56] S. G. Kandlikar. A general correlation for saturated two-phase flow boiling heat transfer inside horizontal and vertical tubes. *J. Heat Transfer*, **112**(1):219–228, February 1990. doi: 10.1115/1.2910348.

[9.57] D. Steiner and J. Taborek. Flow boiling heat transfer in vertical tubes correlated by an asymptotic model. *Heat Transfer Engr.*, **13**(2):43–69, 1992. doi: 10.1080/01457639208939774.

[9.58] V. E. Schrock and L. M. Grossman. Forced convection boiling in tubes. *Nucl. Sci. Engr.*, **12**:474–481, 1962. doi: 10.13182/NSE62-A26094.

[9.59] M. M. Shah. Chart correlation for saturated boiling heat transfer: equations and further study. *ASHRAE Trans.*, **88**:182–196, 1982.

[9.60] A. E. Gungor and R. S. H. Winterton. Simplified general correlation for flow boiling heat transfer inside horizontal and vertical tubes. *Chem. Engr. Res. Des.*, **65**:148–156, 1987.

[9.61] S. G. Kandlikar and H. Nariai. Flow boiling in circular tubes. In S. G. Kandlikar, M. Shoji, and V. K. Dhir, editors, *Handbook of Phase Change: Boiling and Condensation*, Chapter 15, pp. 367–402. Taylor & Francis, Philadelphia, 1999. doi: 10.1201/9780203752654.

[9.62] S. G. Kandlikar, S. T. Tian, J. Yu, and S. Koyama. Further assessment of pool and flow boiling heat transfer with binary mixtures. In G. P. Celata, P. Di Marco, and R. K. Shah, editors, *Two-Phase Flow Modeling and Experimentation*. Edizioni ETS, Pisa, 1999.

[9.63] Y. Taitel and A. E. Dukler. A model for predicting flow regime transitions in horizontal and near horizontal gas-liquid flows. *AIChE J.*, **22**(1):47–55, January 1976. doi: 10.1002/aic.690220105.

[9.64] A. E. Dukler and Y. Taitel. Flow pattern transitions in gas–liquid systems measurement and modelling. In J. M. Delhaye, N. Zuber, and G. F. Hewitt, editors, *Advances in Multi-Phase Flow*, Vol. II. Hemisphere/McGraw-Hill, New York, 1985.

[9.65] Y. Katto. A generalized correlation of critical heat flux for the forced convection boiling in vertical uniformly heated round tubes. *Int. J. Heat Mass Transfer*, **21**(12):1527–1542, December 1978. doi: 10.1016/0017-9310(78)90009-1.

[9.66] Y. Katto and H. Ohno. An improved version of the generalized correlation of critical heat flux for convective boiling in uniformly heated vertical tubes. *Int. J. Heat. Mass Transfer*, **27**(9):1641–1648, September 1984. doi: 10.1016/0017-9310(84)90276-X.

[9.67] P. B. Whalley. *Boiling, Condensation, and Gas-Liquid Flow*. Oxford University Press, Oxford, 1987.

[9.68] B. Chexal, J. Horowitz, G. McCarthy, M. Merilo, J.-P. Sursock, J. Harrison, C. Peterson, J. Shatford, D. Hughes, M. Ghiaasiaan, V.K. Dhir, W. Kastner, and W. Köhler. Two-phase pressure drop technology for design and analysis. Technical Report 113189, Electric Power Research Institute, Palo Alto, CA, August 1999.

[9.69] I. G. Shekriladze and V. I. Gomelauri. Theoretical study of laminar film condensation of flowing vapour. *Int. J. Heat. Mass Transfer*, **9**(6):581–591, June 1966. doi: 10.1016/0017-9310(66)90092-5.

[9.70] P. J. Marto. Condensation. In W. M. Rohsenow, J. P. Hartnett, and Y. I. Cho, editors, *Handbook of Heat Transfer*, Chapter 14. McGraw-Hill, New York, 3rd ed., 1998.

[9.71] J. W. Rose. Film and dropwise condensation. In F. A. Kulacki, editor, *Handbook of Thermal Science and Engineering*, Chapter 50, pp. 2031–2074. Springer, Cham, Switzerland, 2018. doi: 10.1007/978-3-319-26695-4_50.

[9.72] M. H. Rausch, A. Leipertz, and A. P. Fröba. Dropwise condensation of steam on ion implanted titanium surfaces. *Int. J. Heat and Mass Transfer*, **53**(1):423–430, 2010. doi: 10.1016/j.ijheatmasstransfer.2009.09.014.

[9.73] J. W. Rose. Dropwise condensation theory and experiment: A review. *Proc. Instn. Mech. Engrs., Part A: J. Power and Energy*, **216**(2):115–128, 2002. doi: 10.1243/09576500260049034.

[9.74] A. T. Paxson, J. L. Yagüe, K. K. Gleason, and K. K. Varanasi. Stable dropwise condensation for enhancing heat transfer via the initiated chemical vapor deposition (iCVD) of grafted polymer films. *Advanced Materials*, **26**(3): 418–423, 2014. doi: 10.1002/adma.201303065.

[9.75] D. J. Preston, D. L. Mafra, N. Miljkovic, J. Kong, and E. N. Wang. Scalable graphene coatings for enhanced condensation heat transfer. *Nano Letters*, **15**(5):2902–2909, March 2015. doi: 10.1021/nl504628s.

[9.76] K. Khalil, D. Soto, T. Farnham, A. Paxson, A. U. Katmis, K. K. Gleason, and K. K. Varanasi. Grafted nanofilms promote dropwise condensation of low-surface-tension fluids for high-performance heat exchangers. *Joule*, **3**(5):1377–1388, June 2019. doi: 10.1016/j.joule.2019.04.009.

[9.77] D. W. Woodruff and J. W. Westwater. Steam condensation on electroplated gold: effect of plating thickness. *Int. J. Heat. Mass Transfer*, **22**(4):629–632, April 1979. doi: 10.1016/0017-9310(79)90066-8.

[9.78] P. D. Dunn and D. A. Reay. *Heat Pipes*. Pergamon Press Ltd., Oxford, UK, 4th ed., 1994.

[9.79] C. Cercignani. *Rarefied Gas Dynamics*. Cambridge University Press, Cambridge, 2000.

[9.80] Z. Lu, I. Kinefuchi, K. L. Wilke, G. Vaartstra, and E. N. Wang. A unified relationship for evaporation kinetics at low Mach numbers. *Nature Comm.*, **10**:2368, May 2019. doi: 10.1038/s41467-019-10209-w.

PART IV

THERMAL RADIATION HEAT TRANSFER

10. Radiative heat transfer

The sun that shines from Heaven shines but warm,
And, lo, I lie between that sun and thee:
The heat I have from thence doth little harm,
Thine eye darts forth the fire that burneth me:
And were I not immortal, life were done
Between this heavenly and earthly sun.
Venus and Adonis, **Wm. Shakespeare, 1593**

10.1   The problem of radiative exchange

Chapter 1 included an introduction to heat radiation. We shall now assume
that the following concepts from Chapter 1 are understood:

- Electromagnetic wave spectrum
- Heat radiation & infrared radiation
- Black body
- Absorptance, α
- Reflectance, ρ
- Transmittance, τ
- $\alpha + \rho + \tau = 1$
- $e(T)$ and $e_\lambda(T)$ for black bodies

- Stefan-Boltzmann law
- Wien's law
- Planck's law
- Radiant heat exchange
- Configuration factor, $F_{1\text{-}2}$
- Emittance, ε
- Transfer factor, $\mathcal{F}_{1\text{-}2}$
- Radiation shielding

We shall also make use of the concept of a radiation heat transfer co-
efficient, which we introduced in Section 2.3. Please review these ideas
before proceeding further (pp. 26–34).
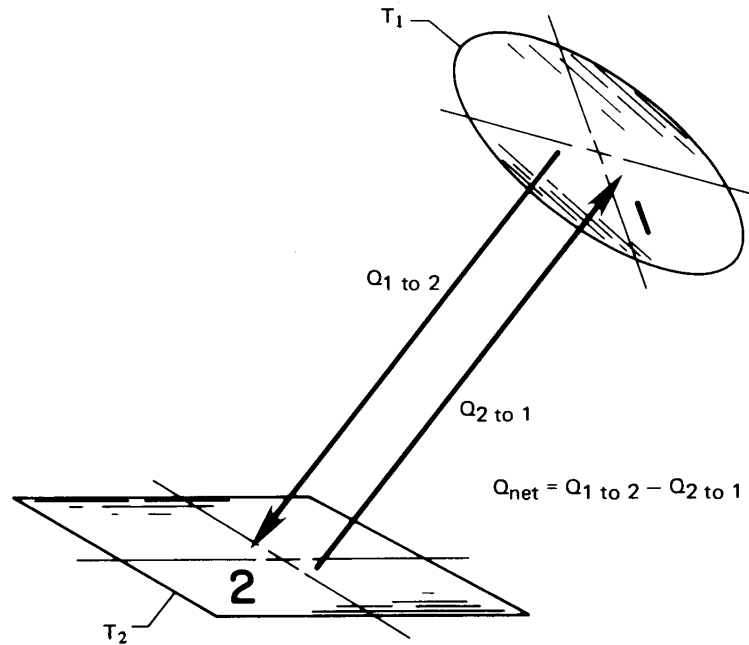
Figure 10.1 Thermal radiation between two arbitrary surfaces.

The heat exchange problem

Figure 10.1 shows two arbitrary surfaces radiating energy to one another. The net heat exchange, Q_{net}, from the hotter surface (1) to the cooler surface (2) depends on the following influences:

- T_1 and T_2

- The areas of surfaces 1 and 2, A_1 and A_2

- The shape, orientation, and spacing of surfaces 1 and 2

- The radiative properties of the surfaces

- Additional surfaces in the environment, which may reflect radiation from surface 1 to surface 2 and vice versa

- The medium between surfaces 1 and 2 if it absorbs, emits, or "reflects" radiation. (When the medium is air, we can usually neglect these effects.)

If surfaces 1 and 2 are black, if they are surrounded by air, and if no heat flows between them by conduction or convection, then only the first three considerations are involved in determining Q_{net}. We saw some elementary examples of how this could be done in Chapter 1, leading to

$$Q_{\text{net}} = A_1 F_{1\text{-}2}\, \sigma \left(T_1^4 - T_2^4 \right) \tag{10.1}$$

The last three considerations complicate the problem considerably. In Chapter 1, we saw that these nonideal factors are sometimes included in a *transfer factor* $\mathcal{F}_{1\text{-}2}$, such that

$$Q_{\text{net}} = A_1 \mathcal{F}_{1\text{-}2}\, \sigma \left(T_1^4 - T_2^4 \right) \tag{10.2}$$

Before we undertake the problem of evaluating heat exchange among real bodies, we need several definitions.

Some definitions

Emittance. A real body at temperature T does not emit with the black body emissive power $e_b = \sigma T^4$ but rather with some fraction, ε, of e_b. The same is true of the *monochromatic* (or single wavelength) emissive power, $e_\lambda(T)$, which is always lower for a real body than the black body value given by Planck's law, eqn. (1.30). Thus, we define either the monochromatic emittance, ε_λ

$$\varepsilon_\lambda \equiv \frac{e_\lambda(\lambda, T)}{e_{\lambda_b}(\lambda, T)} \tag{10.3}$$

or the total emittance, ε

$$\varepsilon \equiv \frac{e(T)}{e_b(T)} = \frac{\displaystyle\int_0^\infty e_\lambda(\lambda, T)\, d\lambda}{\sigma T^4} = \frac{\displaystyle\int_0^\infty \varepsilon_\lambda\, e_{\lambda_b}(\lambda, T)\, d\lambda}{\sigma T^4} \tag{10.4}$$

For real bodies, both ε and ε_λ are greater than zero and less than one; for black bodies, $\varepsilon = \varepsilon_\lambda = 1$. The emittance is determined entirely by the properties of the surface of the particular body and its temperature. It is independent of the environment of the body.

Table 10.1 lists typical values of the total emittance for a variety of substances. Notice that most metals have quite low emittances, unless they are oxidized. Most nonmetals have emittances that are quite high—approaching the black body limit of one.

One particular kind of surface behavior is that for which ε_λ is independent of λ. We call such a surface a *gray body*. The monochromatic

Table 10.1 Total emittances for a variety of surfaces [10.1]

Metals			Nonmetals		
Surface	*Temp. (°C)*	ε	*Surface*	*Temp. (°C)*	ε
Aluminum			Asbestos	40	0.93-0.97
Polished, 98% pure	200–600	0.04-0.06	Brick		
Commercial sheet	90	0.09	Red, rough	40	0.93
Heavily oxidized	90–540	0.20-0.33	Silica	980	0.80-0.85
Brass			Fireclay	980	0.75
Highly polished	260	0.03	Ordinary refractory	1090	0.59
Dull plate	40–260	0.22	Magnesite refractory	980	0.38
Oxidized	40–260	0.46-0.56	White refractory	1090	0.29
Copper			Carbon		
Highly polished electrolytic	90	0.02	Filament	1040–1430	0.53
Slightly polished to dull	40	0.12-0.15	Lampsoot	40	0.95
Black oxidized	40	0.76	Concrete, rough	40	0.94
Gold: pure, polished	90–600	0.02-0.035	Glass		
Iron and steel			Smooth	40	0.94
Mild steel, polished	150–480	0.14-0.32	Quartz glass (2 mm)	260–540	0.96-0.66
Steel, polished	40–260	0.07-0.10	Pyrex	260–540	0.94-0.74
Sheet steel, rolled	40	0.66	Gypsum	40	0.80-0.90
Sheet steel, strong rough oxide	40	0.80	Ice	0	0.97-0.98
Cast iron, oxidized	40–260	0.57-0.66	Limestone	400–260	0.95-0.83
Iron, rusted	40	0.61-0.85	Marble	40	0.93-0.95
Stainless, polished	40	0.07-0.17	Black gloss	40	0.90
Stainless, after repeated heating	230–900	0.50-0.70	White paint	40	0.89-0.97
			Lacquer	40	0.80-0.95
Wrought iron, smooth	40	0.35	Mica	40	0.75
Wrought iron, dull oxidized	20–360	0.94	Paints		
Lead			Various oil paints	40	0.92-0.96
Polished	40–260	0.05-0.08	Red lead	90	0.93
Oxidized	40–200	0.63	Paper		
Mercury: pure, clean	40–90	0.10-0.12	White	40	0.95-0.98
Platinum			Other colors	40	0.92-0.94
Pure, polished plate	200–590	0.05-0.10	Roofing	40	0.91
Oxidized at 590°C	260–590	0.07-0.11	Plaster, rough lime	40–260	0.92
Drawn wire and strips	40–1370	0.04-0.19	Quartz	100–1000	0.89-0.58
Silver	200	0.01-0.04	Rubber	40	0.86-0.94
Tin	40–90	0.05	Snow	10–20	0.82
Tungsten			Water, thickness ≥0.1 mm	40	0.96
Filament	540–1090	0.11-0.16	Wood	40	0.80-0.90
Filament	2760	0.39	Oak, planed	20	0.90
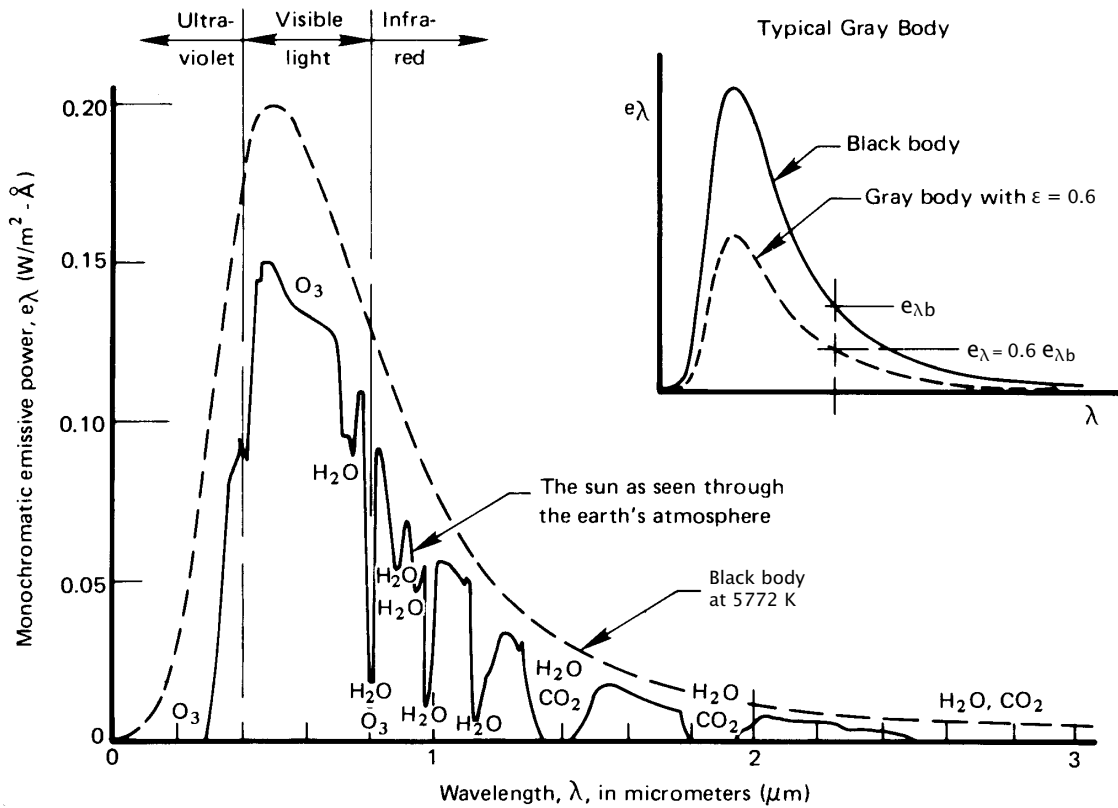
Figure 10.2 Comparison of the sun's energy as typically seen through the earth's atmosphere with that of a black body having the same mean temperature, size, and distance from the earth. (Notice that e_λ, just outside the earth's atmosphere, is far less than near the surface of the sun because the radiation has spread out over a vastly greater area.)

emissive power, $e_\lambda(T)$, for a gray body is a constant fraction, ε, of $e_{b_\lambda}(T)$, as indicated in the inset of Fig. 10.2. In other words, for a gray body, $\varepsilon_\lambda = \varepsilon$. No real body is gray, but many exhibit approximately gray behavior. We see in Fig. 10.2, for example, that the sun appears to us on earth as an approximately gray body with an emittance of approximately 0.6. Some materials—for example, copper, aluminum oxide, and certain paints—are actually pretty close to being gray surfaces at normal temperatures.

Yet, the emittance of most common materials and coatings varies with wavelength in the thermal range. The total emittance ε accounts for this behavior at a particular temperature. By using it, we can write

Specular or mirror-like reflection of incoming ray.

Reflection which is between diffuse and specular (a real surface).

Diffuse radiation in which directions of departure are uninfluenced by incoming ray angle, θ.
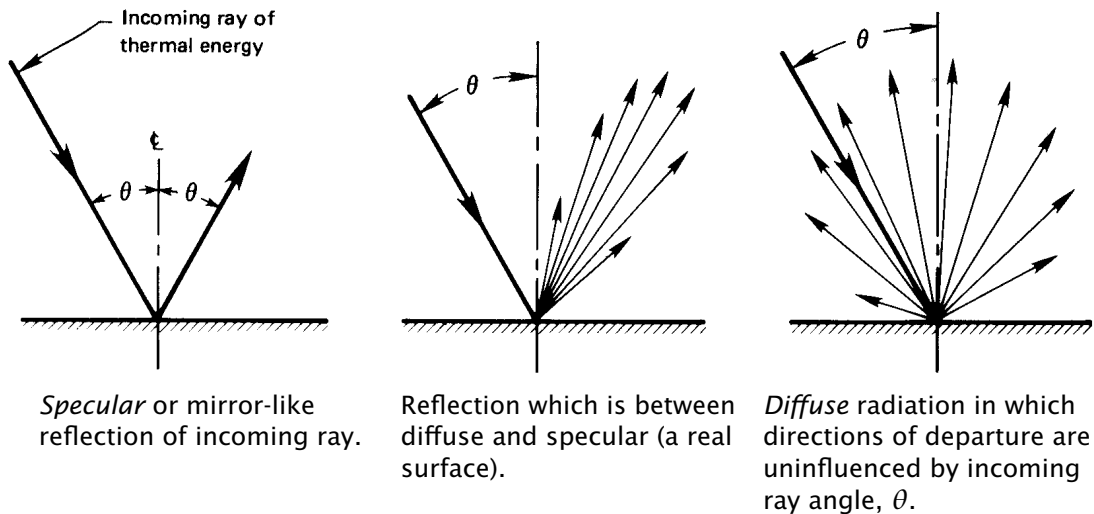
Figure 10.3 Specular and diffuse reflection of radiation. Arrows indicate the magnitude of the heat flux in the directions indicated.

the emissive power as if the body were gray, without integrating over wavelength:

$$e(T) = \varepsilon \sigma T^4 \tag{10.5}$$

We shall use this type of "gray body approximation" often in this chapter.

In situations where surfaces at very different temperatures are involved, the wavelength dependence of ε_λ must be dealt with explicitly. This occurs, for example, when sunlight heats objects here on earth. Solar radiation (from a high temperature source) is on visible wavelengths, whereas radiation from low temperature objects on earth is mainly in the infrared range. We look at this issue further in the next section.

Diffuse and directional emission and reflection. The energy emitted by a non-black surface, together with that portion of an incoming ray of energy that is reflected by the surface, may leave the body *diffusely* or *directionally*, as shown in Fig. 10.3. That energy may also be emitted or reflected in a way that lies between these limits. A mirror reflects visible radiation in an almost perfectly *specular* fashion. (The "reflection" of a billiard ball as it rebounds from the side of a pool table is also specular.) When reflection or emission is diffuse, there is no preferred direction for outgoing rays. Black body emission is always diffuse.

The character of the emittance or reflectance of a surface will normally change with the wavelength of the radiation. If we take account of both directional and spectral characteristics, then properties like emittance and reflectance depend on wavelength, temperature, and angles of incidence and/or departure. In this chapter, we shall assume diffuse behavior for most surfaces. This approximation works well for many problems in engineering, in part because most tabulated spectral and total emittances have been averaged over all angles (in which case they are properly called *hemispherical* properties).

Experiment 10.1

Obtain a flashlight with as narrow a spot focus as you can find. Direct it at an angle onto a mirror, onto the surface of a bowl filled with sugar, and onto a variety of other surfaces, all in a darkened room. In each case, move the palm of your hand around the surface of an imaginary hemisphere centered on the point where the spot touches the surface. Notice how your palm is illuminated, and categorize the kind of reflectance of each surface—at least in the range of visible wavelengths. ♦

Intensity of radiation. To account for the effects of geometry on radiant exchange, we must think about how angles of orientation affect the radiation between surfaces. Consider radiation from a circular surface element, dA, as shown at the top of Fig. 10.4. If the element is black, the radiation that it emits is indistinguishable from that which would be emitted from a black cavity at the same temperature, and that radiation is diffuse — the same in all directions. If it were non-black but diffuse, the heat flux leaving the surface would again be independent of direction. Thus, the rate at which energy is emitted in any direction from this diffuse element is proportional to the projected area of dA normal to the direction of view, as shown in the upper right side of Fig. 10.4.

If an aperture of area dA_a is placed at a radius r and angle θ from dA and is normal to the radius, it will see dA as having an area $\cos\theta\,dA$. The energy dA_a receives will depend on the solid angle,[1] $d\omega$, it subtends. Radiation that leaves dA within the solid angle $d\omega$ stays within $d\omega$ as it travels to dA_a. Hence, we define a quantity called the *intensity of radiation*,

---

[1]The unit of solid angle is the *steradian*. One steradian is the solid angle subtended by a spherical segment whose area equals the square of its radius. A full sphere therefore subtends $4\pi r^2/r^2 = 4\pi$ steradians. The aperture dA_a subtends $d\omega = dA_a/r^2$.
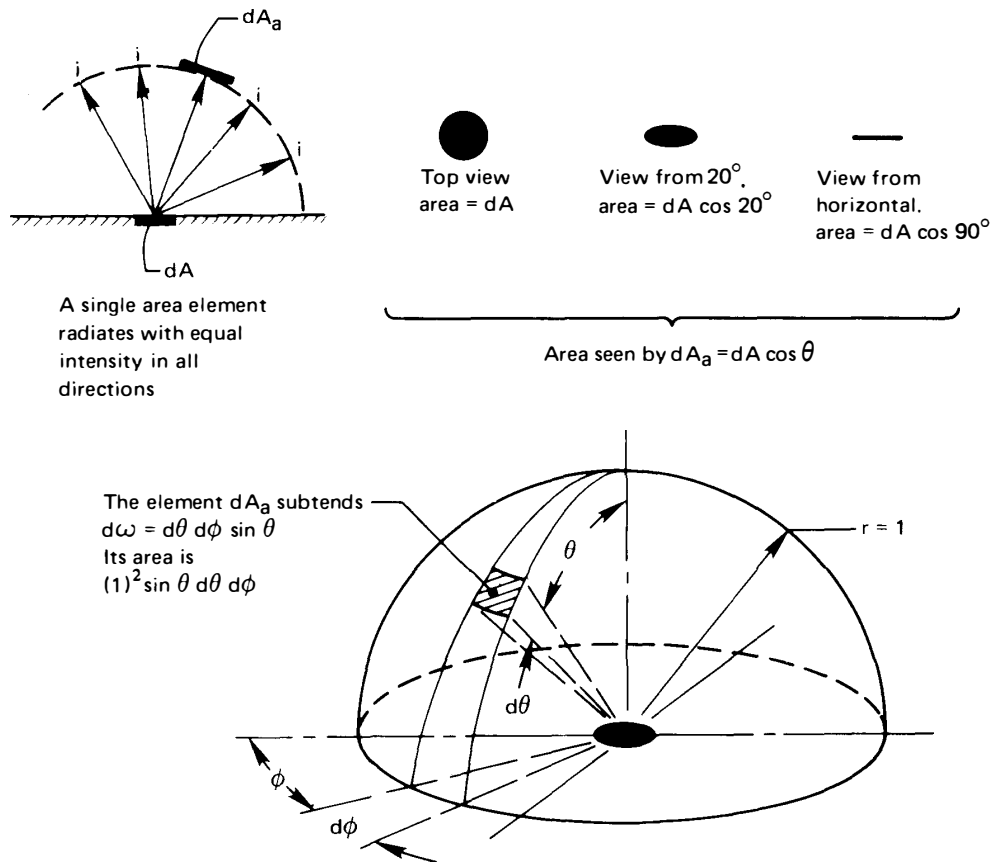
Figure 10.4 Radiation intensity through a unit sphere.

i (W/m^2·steradian) using an energy conservation statement:

$$dQ_{\text{outgoing}} = (i\,d\omega)(\cos\theta\,dA) = \begin{cases} \text{radiant energy from } dA \\ \text{that is intercepted by } dA_a \end{cases} \quad (10.6)$$

Notice that while the heat flux from dA decreases with θ (as indicated on the right side of Fig. 10.4), the intensity of radiation from a diffuse surface is uniform in all directions.

Finally, we use our definition of i to express it in terms of the heat flux from dA. We do this by dividing eqn. (10.6) by dA and integrating over the entire hemisphere. For convenience we set $r = 1$, and we note (see Fig. 10.4) that $d\omega = \sin\theta\,d\theta d\phi$.

$$q_{\text{outgoing}} = \int_{\phi=0}^{2\pi} \int_{\theta=0}^{\pi/2} i\cos\theta\,(\sin\theta\,d\theta d\phi) = \pi i \quad (10.7\text{a})$$

In the particular case of a black body,

$$i_b = \frac{e_b}{\pi} = \frac{\sigma T^4}{\pi} = \text{fn}(T \text{ only}) \tag{10.7b}$$

For a given wavelength, we likewise define the monochromatic intensity

$$i_\lambda = \frac{e_\lambda}{\pi} = \text{fn}(T, \lambda) \tag{10.7c}$$

10.2 Kirchhoff's law

The problem of predicting α

The total emittance, ε, of a surface is determined only by the physical properties and temperature of that surface, as can be seen from eqn. (10.4). The total absorptance, α, on the other hand, depends on the *source* from which the surface absorbs radiation, as well as the surface's own characteristics. This happens because the surface may absorb some wavelengths better than others. Thus, the total absorptance will depend on the way that incoming radiation is distributed in wavelength. And that distribution, in turn, depends on the temperature and physical properties of the surface or surfaces from which radiation is absorbed.

The total absorptance α thus depends on the physical properties and temperatures of *all* bodies involved in the heat exchange process. Kirchhoff's law[2] is an expression that allows us to determine α under certain restrictions.

Kirchhoff's law

Kirchhoff's law is a relationship between the monochromatic, directional emittance and the monochromatic, directional absorptance of a surface that is in thermodynamic equilibrium with its surroundings

$$\boxed{\varepsilon_\lambda(T, \theta, \phi) = \alpha_\lambda(T, \theta, \phi)} \quad \begin{array}{l} \text{exact form of} \\ \text{Kirchhoff's law} \end{array} \tag{10.8a}$$

Kirchhoff's law states that a body in thermodynamic equilibrium emits as much energy as it absorbs in each direction and at each wavelength. If this

---

[2]Gustav Robert Kirchhoff (1824–1887) developed important new ideas in electrical circuit theory, thermal physics, spectroscopy, and astronomy. He formulated this particular "Kirchhoff's Law" when he was only 25. He and Robert Bunsen (inventor of the Bunsen burner) subsequently went on to do significant work on radiation from gases.

were not so, for example, a body might absorb more energy than it emits in one direction, θ_1, and might also emit more than it absorbs in another direction, θ_2. The body would thus pump heat out of its surroundings from the first direction, θ_1, and into its surroundings in the second direction, θ_2. Since whatever matter lies in the first direction would be refrigerated without any work input, the Second Law of Thermodynamics would be violated. Similar arguments can be built for the wavelength dependence. In essence, then, Kirchhoff's law is a consequence of the laws of thermodynamics.

For a diffuse body, the emittance and absorptance do not depend on the angles, and Kirchhoff's law becomes

$$\boxed{\varepsilon_\lambda(T) = \alpha_\lambda(T)} \qquad \begin{array}{l}\text{diffuse form of} \\ \text{Kirchhoff's law}\end{array} \qquad (10.8\text{b})$$

If, in addition, the body is gray, Kirchhoff's law is further simplified

$$\boxed{\varepsilon(T) = \alpha(T)} \qquad \begin{array}{l}\text{diffuse, gray form} \\ \text{of Kirchhoff's law}\end{array} \qquad (10.8\text{c})$$

Equation (10.8c) is the most widely used form of Kirchhoff's law. Yet, it is a somewhat dangerous result, since many surfaces are not even approximately gray. If radiation is emitted on wavelengths much different from those that are absorbed, then a non-gray surface's variation of ε_λ and α_λ with wavelength will matter, as we discuss next.

Total absorptance during radiant exchange

Let us restrict our attention to diffuse surfaces, so that eqn. (10.8b) is the appropriate form of Kirchhoff's law. Consider two plates, as shown in Fig. 10.5. Let the plate at T_1 be non-black and that at T_2 be black. Then net heat transfer from plate 1 to plate 2 is the difference between what plate 1 emits and what it absorbs. Since all the radiation reaching plate 1 comes from a black source at T_2, we may write

$$q_{\text{net}} = \underbrace{\int_0^\infty \varepsilon_{\lambda_1}(T_1)\, e_{\lambda_b}(T_1)\, d\lambda}_{\text{emitted by plate 1}} - \underbrace{\int_0^\infty \alpha_{\lambda_1}(T_1)\, e_{\lambda_b}(T_2)\, d\lambda}_{\substack{\text{radiation from plate 2} \\ \text{absorbed by plate 1}}} \qquad (10.9)$$
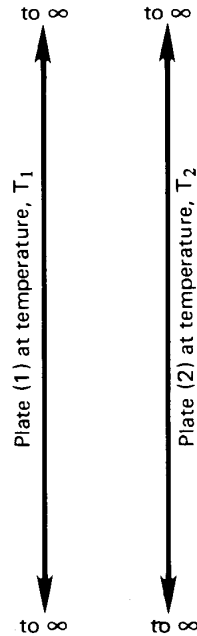
Figure 10.5 Heat transfer between two infinite parallel plates.

From eqn. (10.4), we may write the first integral in terms of total emittance, as $\varepsilon_1 \sigma T_1^4$. We *define* the total absorptance, $\alpha_1(T_1, T_2)$, as the second integral divided by σT_2^4. Hence,

$$q_{\text{net}} = \underbrace{\varepsilon_1(T_1)\,\sigma T_1^4}_{\text{emitted by plate 1}} - \underbrace{\alpha_1(T_1, T_2)\,\sigma T_2^4}_{\text{absorbed by plate 1}} \qquad (10.10)$$

We see that the total absorptance depends on T_2 as well as T_1.

Why does total absorptance depend on both temperatures? It depends on T_1 simply because α_{λ_1} is a property of plate 1 that may be temperature dependent. It depends on T_2 because the spectrum of radiation from plate 2 depends on the temperature of plate 2 according to Planck's law, as we saw in Fig. 1.15.

As a typical example, consider solar radiation incident on a warm roof, painted black. From Table 10.1, we see that ε is on the order of 0.94. It turns out that α is just about the same. If we repaint the roof white, ε will not change noticeably. However, much of the energy arriving from the sun is carried in visible wavelengths, owing to the sun's very high

surface temperature (about 5772 K).[3] Our eyes tell us that white paint reflects sunlight very strongly in these wavelengths, and indeed this is the case—80 to 90% of the sunlight is reflected. The absorptance of white paint to energy from the sun is only 0.1 to 0.2—much less than ε for the energy it emits, which is mainly at infrared wavelengths. For both paints, eqn. (10.8b) applies. However, in this situation, eqn. (10.8c) is only accurate for the black paint.

The gray body approximation

The simplest first estimate for total absorptance is the diffuse, gray body approximation, eqn. (10.8c). It is accurate if the monochromatic emittance does not vary strongly with wavelength and if the bodies exchanging radiation are at sufficiently similar absolute temperature. The more strongly the emittance varies with wavelength, the closer these temperatures must be. Several examples are studied in [10.2], showing that some common materials may be modeled as gray for up to 30% difference in absolute temperature, whereas highly selective materials in worst-case scenarios may have large errors at only a 10% temperature difference.

With eqn. (10.8c), the net heat flux between diffuse, gray, facing plates can be expressed very simply:

$$
\begin{aligned}
q_{\text{net}} &= \varepsilon_1(T_1)\,\sigma\,T_1^4 - \alpha_1(T_1, T_2)\,\sigma\,T_2^4 \\
&\cong \varepsilon_1(T_1)\,\sigma\,T_1^4 - \varepsilon_1(T_1)\,\sigma\,T_2^4 \\
&= \varepsilon_1\sigma\left(T_1^4 - T_2^4\right)
\end{aligned} \tag{10.11}
$$

More advanced texts describe techniques for calculating total absorptance (by integration) in other situations [10.3, 10.4].

We should always mistrust eqn. (10.8c) when solar radiation is absorbed by a low temperature object—a space vehicle or something on earth's surface, say. Because the temperatures of the sun and the absorbing object are very far apart, the solar energy's wavelengths are well separated from the object's emitted wavelengths. In this case, the best first approximation is to set total absorptance to a value for visible wavelengths of radiation (near 0.5 μm, like sunlight). Total emittance may be taken at the object's actual temperature, typically for infrared wavelengths. We return to solar absorptance in Section 10.6.

---

[3]Ninety percent of the sun's energy is on wavelengths between 0.33 and 2.2 μm (see Figure 10.2). For a black object at 300 K, 90% of the radiant energy is between 6.3 and 42 μm, in the infrared. This fact is at the heart of the "greenhouse effect" (see pp. 599–602).
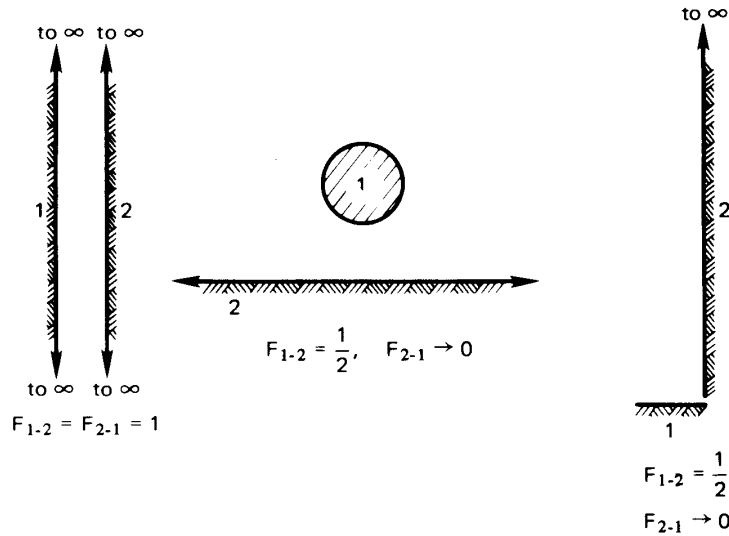
Figure 10.6 Some configurations for which the value of the view factor is immediately apparent.

10.3   Radiant heat exchange between two finite black bodies

Let us now return to the purely geometric problem of evaluating the view factor, F_{1-2}. Although the evaluation of F_{1-2} is also used in the calculation of heat exchange among diffuse, nonblack bodies, it is the *only* correction of the Stefan-Boltzmann law that we need for black bodies.

Some evident results.   Figure 10.6 shows three elementary situations in which the value of F_{1-2} is evident using just the definition:

$$F_{1-2} \equiv \text{fraction of field of view of (1) occupied by (2).}$$

When the surfaces are each isothermal and diffuse, this corresponds to

$$F_{1-2} = \text{fraction of energy leaving (1) that reaches (2)}$$

A second apparent result in regard to the view factor is that all the radiant energy leaving a body (1) reaches something else. Thus, conservation of energy requires

$$1 = F_{1-1} + F_{1-2} + F_{1-3} + \cdots + F_{1-n} \qquad (10.12)$$

$$1 = F_{1\text{-}1} + F_{1\text{-}2} + F_{1\text{-}3} + F_{1\text{-}4}$$
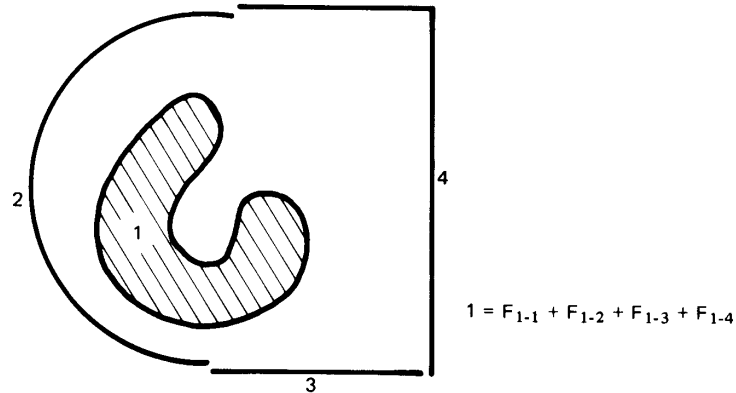
Figure 10.7 A body (1) that views three other bodies and itself as well.

where (2), (3),…,(n) are all of the bodies in the neighborhood of (1). Figure 10.7 shows a representative situation in which a body (1) is surrounded by three other bodies. It sees all three bodies, but it also views itself, in part. This accounts for the inclusion of the view factor, $F_{1\text{-}1}$ in eqn. (10.12).

By the same token, it should also be apparent from Fig. 10.7 that the kind of sum expressed by eqn. (10.12) would also be true for any subset of the bodies seen by body (1). Thus,

$$F_{1\text{-}(2+3)} = F_{1\text{-}2} + F_{1\text{-}3}$$

Of course, such a sum makes sense only when all the view factors are based on the same viewing surface (body 1 in this case). One might be tempted to write this sort of sum in the opposite direction, but it would clearly be untrue,

$$F_{(2+3)\text{-}1} \neq F_{2\text{-}1} + F_{3\text{-}1},$$

since each view factor is for a different viewing surface—$(2 + 3)$, 2, and 3, in this case.

View factor reciprocity. So far, we have referred to the net radiation from black surface (1) to black surface (2) as Q_{net}. Let us refine our notation a bit, and call this $Q_{\text{net}_{1\text{-}2}}$:

$$Q_{\text{net}_{1\text{-}2}} = A_1 F_{1\text{-}2} \, \sigma \left(T_1^4 - T_2^4 \right) \tag{10.13}$$

Likewise, the net radiation from (2) to (1) is

$$Q_{\text{net}_{2\text{-}1}} = A_2 F_{2\text{-}1} \, \sigma \left(T_2^4 - T_1^4 \right) \tag{10.14}$$

Of course, $Q_{\text{net}_{1\text{-}2}} = -Q_{\text{net}_{2\text{-}1}}$. It follows that

$$A_1 F_{1\text{-}2}\, \sigma \left(T_1^4 - T_2^4\right) = -A_2 F_{2\text{-}1}\, \sigma \left(T_2^4 - T_1^4\right)$$

or

$$\boxed{A_1 F_{1\text{-}2} = A_2 F_{2\text{-}1}} \qquad\qquad (10.15)$$

This result, called *view factor reciprocity*, is very useful in calculations.

Example 10.1

A jet of liquid metal at 2000°C pours from a crucible. It is 3 mm in diameter. A long cylindrical radiation shield, 5 cm diameter, surrounds the jet through an angle of 330°, but there is a 30° slit in it. The jet and the shield radiate as black bodies. They sit in a room at 30°C, and the shield has a temperature of 700°C. Calculate the net heat transfer: from the jet to the room through the slit; from the jet to the shield; and from the inside of the shield to the room.

SOLUTION. By inspection, we see that $F_{\text{jet-room}} = 30/360 = 0.08333$ and $F_{\text{jet-shield}} = 330/360 = 0.9167$. The area of the jet per unit length is $A_{\text{jet}} = \pi(0.003)$ m^2/m length. Thus,

$$
\begin{aligned}
Q_{\text{net}_{\text{jet-room}}} &= A_{\text{jet}} F_{\text{jet-room}}\, \sigma \left(T_{\text{jet}}^4 - T_{\text{room}}^4\right) \\
&= \pi(0.003)(0.08333)(5.67 \times 10^{-8})(2273^4 - 303^4) \\
&= 1.19 \text{ kW/m}
\end{aligned}
$$

Likewise,

$$
\begin{aligned}
Q_{\text{net}_{\text{jet-shield}}} &= A_{\text{jet}} F_{\text{jet-shield}}\, \sigma \left(T_{\text{jet}}^4 - T_{\text{shield}}^4\right) \\
&= \pi(0.003)(0.9167)(5.67 \times 10^{-8})(2273^4 - 973^4) \\
&= 12.64 \text{ kW/m}
\end{aligned}
$$

The heat absorbed by the shield leaves it by radiation and convection to the room. (The 700°C shield temperature would, in reality, have to have been determined by a calculation that balanced these two effects with the radiation absorbed from the jet.)

To find the radiation from the *inside* of the shield to the room, we need $F_{\text{shield-room}}$. Since any radiation passing out of the slit goes to the room, we can find this view factor equating view factors of the shield and the jet to the room with their view factors to the slit. We treat the

slit as a plane surface extending between the edges of the shield. The slit's area is $A_{\text{slit}} = (0.05)\sin(30°/2) = 0.01294 \text{ m}^2/\text{m}$ length. Hence, using our reciprocity and summation rules, eqns. (10.12) and (10.15),

$$F_{\text{slit-jet}} = \frac{A_{\text{jet}}}{A_{\text{slit}}} F_{\text{jet-room}} = \frac{\pi(0.003)}{0.01294}(0.0833) = 0.06067$$

$$F_{\text{slit-shield}} = 1 - F_{\text{slit-jet}} = 1 - 0.06067 = 0.9393$$

$$F_{\text{shield-room}} = \frac{A_{\text{slit}}}{A_{\text{shield}}} F_{\text{slit-shield}}$$
$$= \frac{0.01294}{\pi(0.05)(330/360)}(0.9393) = 0.08441$$

Hence, for heat transfer from the inside of the shield only,

$$Q_{\text{net}_{\text{shield-room}}} = A_{\text{shield}} F_{\text{shield-room}}\, \sigma\,(T_{\text{shield}}^4 - T_{\text{room}}^4)$$
$$= \left[\frac{\pi(0.05)330}{360}\right](0.08441)(5.67 \times 10^{-8})(973^4 - 303^4)$$
$$= 611 \text{ W/m}$$

Both the jet and the inside of the shield have relatively small view factors to the room, so that comparatively little heat is lost through the slit. ∎

Calculation of the black-body view factor, $F_{1\text{-}2}$. When a view factor is not obvious, as those in Fig. 10.6 were, or when it cannot be obtained from other view factors using equations such as (10.12) or (10.15), one must resort to direct integration. Let us see how to do that.

Consider two elements, dA_1 and dA_2, of larger black bodies 1 and 2, as shown in Fig. 10.8. Body 1 and body 2 are each isothermal. Since element dA_2 subtends a solid angle $d\omega_1$, we use eqn. (10.6) to write

$$dQ_{1\text{ to }2} = (i_1 d\omega_1)(\cos\beta_1\, dA_1)$$

But from eqn. (10.7b),

$$i_1 = \frac{\sigma T_1^4}{\pi}$$

Note that because black bodies radiate diffusely, i_1 does not vary with angle; and because these bodies are isothermal, it does not vary with position. The element of solid angle is given by

$$d\omega_1 = \frac{\cos\beta_2\, dA_2}{s^2}$$
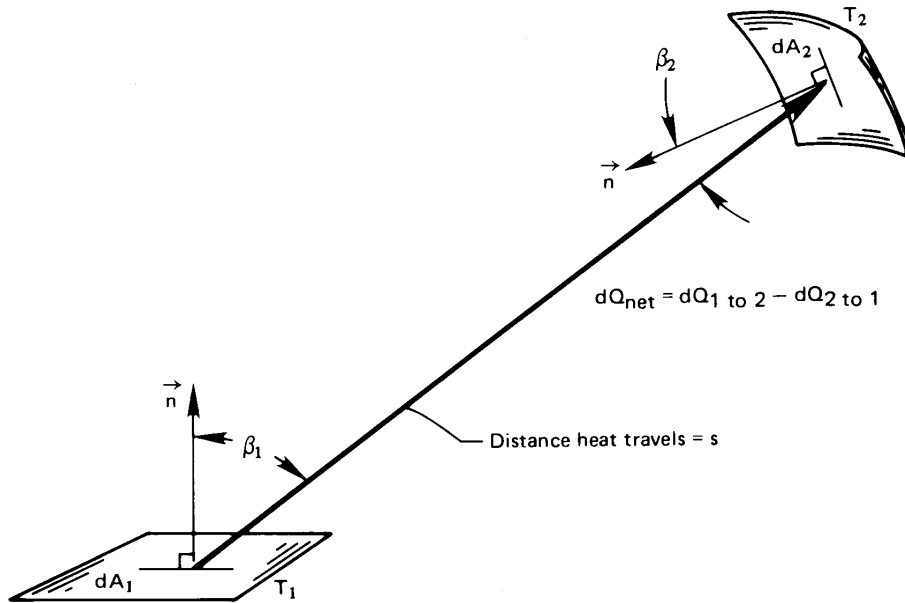
Figure 10.8 Radiant exchange between two black elements that are part of the bodies 1 and 2.

where s is the distance from element 1 to element 2 and $\cos \beta_2$ enters because dA_2 is not necessarily normal to s. Thus,

$$dQ_{1 \text{ to } 2} = \frac{\sigma T_1^4}{\pi} \left(\frac{\cos \beta_1 \cos \beta_2 \, dA_1 dA_2}{s^2} \right)$$

By the same token,

$$dQ_{2 \text{ to } 1} = \frac{\sigma T_2^4}{\pi} \left(\frac{\cos \beta_2 \cos \beta_1 \, dA_2 dA_1}{s^2} \right)$$

Then

$$Q_{\text{net}_{1-2}} = \sigma (T_1^4 - T_2^4) \int_{A_1} \int_{A_2} \frac{\cos \beta_1 \cos \beta_2}{\pi s^2} \, dA_1 dA_2 \qquad (10.16)$$

The view factors F_{1-2} and F_{2-1} are immediately obtainable from eqn. (10.16). If we compare this result with $Q_{\text{net}_{1-2}} = A_1 F_{1-2} \sigma (T_1^4 - T_2^4)$, we get

$$\boxed{F_{1-2} = \frac{1}{A_1} \int_{A_1} \int_{A_2} \frac{\cos \beta_1 \cos \beta_2}{\pi s^2} \, dA_1 dA_2} \qquad (10.17a)$$

From the inherent symmetry of the problem, we can also write

$$F_{2\text{-}1} = \frac{1}{A_2} \int_{A_2} \int_{A_1} \frac{\cos\beta_2 \cos\beta_1}{\pi s^2} \, dA_2 dA_1 \qquad (10.17\text{b})$$

We can easily see that eqns. (10.17a) and (10.17b) are consistent with the reciprocity relation, eqn. (10.15).

The direct evaluation of $F_{1\text{-}2}$ from eqn. (10.17a) becomes fairly involved, even for the simplest configurations. Howell, Mengüç, and Siegel [10.5] provide a comprehensive discussion of such calculations and a large catalog of results. Howell [10.6] gives an even more extensive tabulation of view factor equations, which is available on the World Wide Web.

We list some typical expressions for view factors in Tables 10.2 and 10.3. Table 10.2 gives equations for $F_{1\text{-}2}$ for two-dimensional bodies—various configurations of cylinders and strips that approach infinite length. Table 10.3 gives $F_{1\text{-}2}$ for some three-dimensional configurations.

Many view factors have been evaluated numerically and presented in graphical form for easy reference. Figure 10.9, for example, includes graphs for configurations 1, 2, and 3 from Table 10.3. The reader should study these results and be sure that the trends they show make sense. Is it clear, for example, that as the abscissa becomes large, $F_{1\text{-}2} \longrightarrow$ constant, which is < 1, in each case? Can you locate the configuration on the right-hand side of Fig. 10.6 in Fig. 10.9? And so forth.

Figure 10.10 shows view factors for another kind of configuration—one in which one area is very small in comparison with the other one. Many solutions like this exist because they are a bit less difficult to calculate, and they can often be very useful in practice.

To find shape factors for configurations that lack charts or tabulated equations, we may often combine known shape factors for components of the configuration, using eqns. (10.12) and (10.15). Examples 10.2, 10.3, and 10.4 illustrate this very useful technique.

Example 10.2

Find $F_{1\text{-}2}$ for the configuration of two offset squares of area A, as shown in Fig. 10.11.

SOLUTION. In this case we see how to obtain a view factor by the creative use of the various equations relating view factors to one

Table 10.2   View factors for a variety of two-dimensional configurations (infinite in extent normal to the paper)
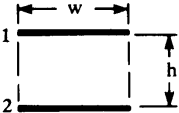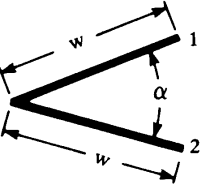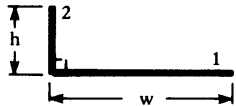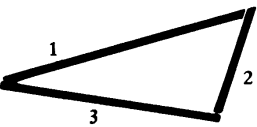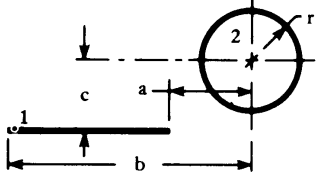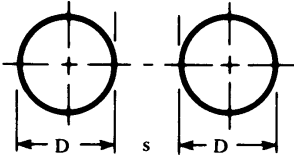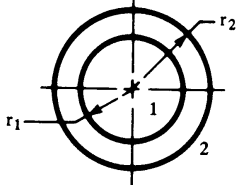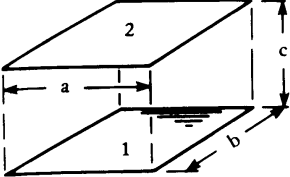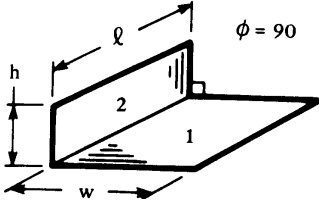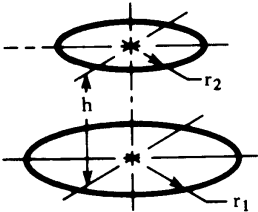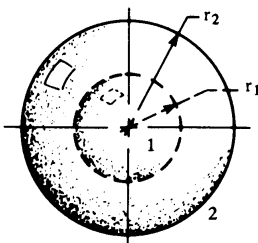
Configuration	Equation
1.	$$F_{1\text{-}2} = F_{2\text{-}1} = \sqrt{1 + \left(\frac{h}{w}\right)^2} - \left(\frac{h}{w}\right)$$
2.	$$F_{1\text{-}2} = F_{2\text{-}1} = 1 - \sin(\alpha/2)$$
3.	$$F_{1\text{-}2} = \frac{1}{2}\left[1 + \frac{h}{w} - \sqrt{1 + \left(\frac{h}{w}\right)^2}\,\right]$$
4.	$$F_{1\text{-}2} = (A_1 + A_2 - A_3)/2A_1$$
5.	$$F_{1\text{-}2} = \frac{r}{b-a}\left[\tan^{-1}\frac{b}{c} - \tan^{-1}\frac{a}{c}\right]$$
6.	Let $X = 1 + s/D$. Then: $$F_{1\text{-}2} = F_{2\text{-}1} = \frac{1}{\pi}\left[\sqrt{X^2 - 1} + \sin^{-1}\frac{1}{X} - X\right]$$
7.	$$F_{1\text{-}2} = 1, \quad F_{2\text{-}1} = \frac{r_1}{r_2}, \text{ and}$$ $$F_{2\text{-}2} = 1 - F_{2\text{-}1} = 1 - \frac{r_1}{r_2}$$

Table 10.3 View factors for some three-dimensional configurations

Configuration	Equation
1.	Let $X = a/c$ and $Y = b/c$. Then: $$F_{1\text{-}2} = \frac{2}{\pi XY} \left\{ \ln\left[\frac{(1 + X^2)(1 + Y^2)}{1 + X^2 + Y^2} \right]^{1/2} \right. - X\tan^{-1}X - Y\tan^{-1}Y \left. + X\sqrt{1 + Y^2}\,\tan^{-1}\frac{X}{\sqrt{1 + Y^2}} + Y\sqrt{1 + X^2}\,\tan^{-1}\frac{Y}{\sqrt{1 + X^2}} \right\}$$
2.	Let $H = h/\ell$ and $W = w/\ell$. Then: $$F_{1\text{-}2} = \frac{1}{\pi W}\left\{ W\tan^{-1}\frac{1}{W} - \sqrt{H^2 + W^2}\,\tan^{-1}(H^2 + W^2)^{-1/2} \right. \\ + H\tan^{-1}\frac{1}{H} + \frac{1}{4}\ln\left\{ \left[\frac{(1 + W^2)(1 + H^2)}{1 + W^2 + H^2} \right] \right. \\ \left. \left. \times \left[\frac{W^2(1 + W^2 + H^2)}{(1 + W^2)(W^2 + H^2)} \right]^{W^2} \left[\frac{H^2(1 + H^2 + W^2)}{(1 + H^2)(H^2 + W^2)} \right]^{H^2} \right\} \right\}$$
3.	Let $R_1 = r_1/h$, $R_2 = r_2/h$, and $X = 1 + (1 + R_2^2)/R_1^2$. Then: $$F_{1\text{-}2} = \frac{1}{2}\left[X - \sqrt{X^2 - 4(R_2/R_1)^2} \right]$$
4.	Concentric spheres: $$F_{1\text{-}2} = 1, \qquad F_{2\text{-}1} = (r_1/r_2)^2, \qquad F_{2\text{-}2} = 1 - (r_1/r_2)^2$$
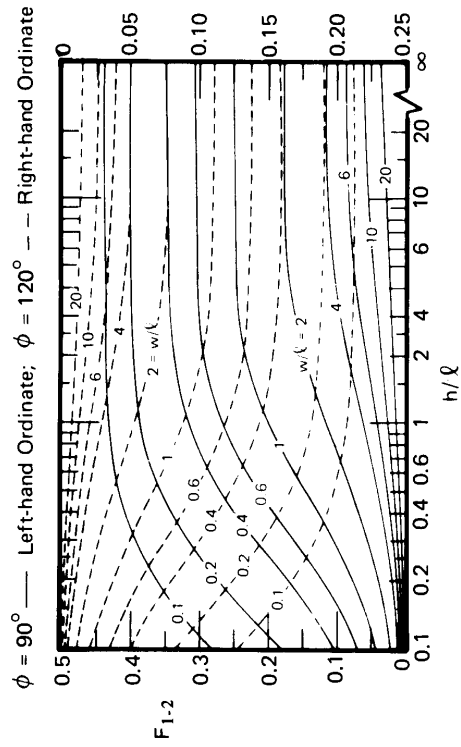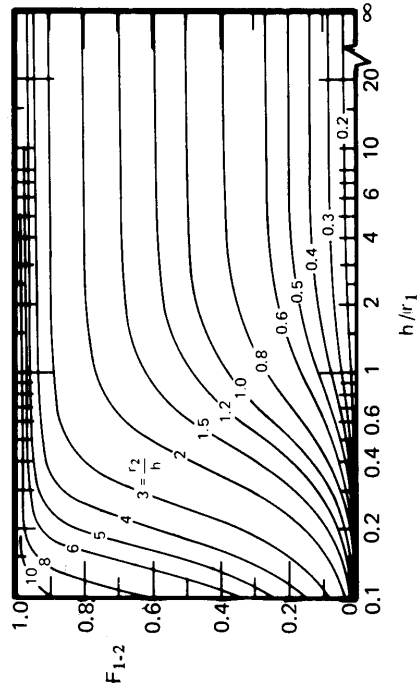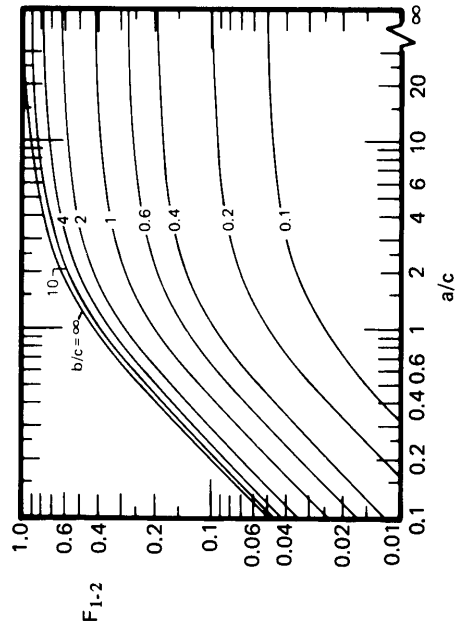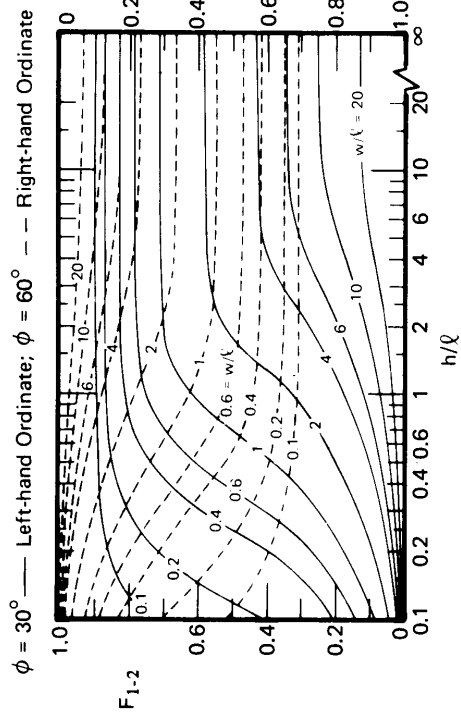
Figure 10.9: The view factor for three very small surfaces "looking at" three large surfaces ($A_1 \ll A_2$).

563
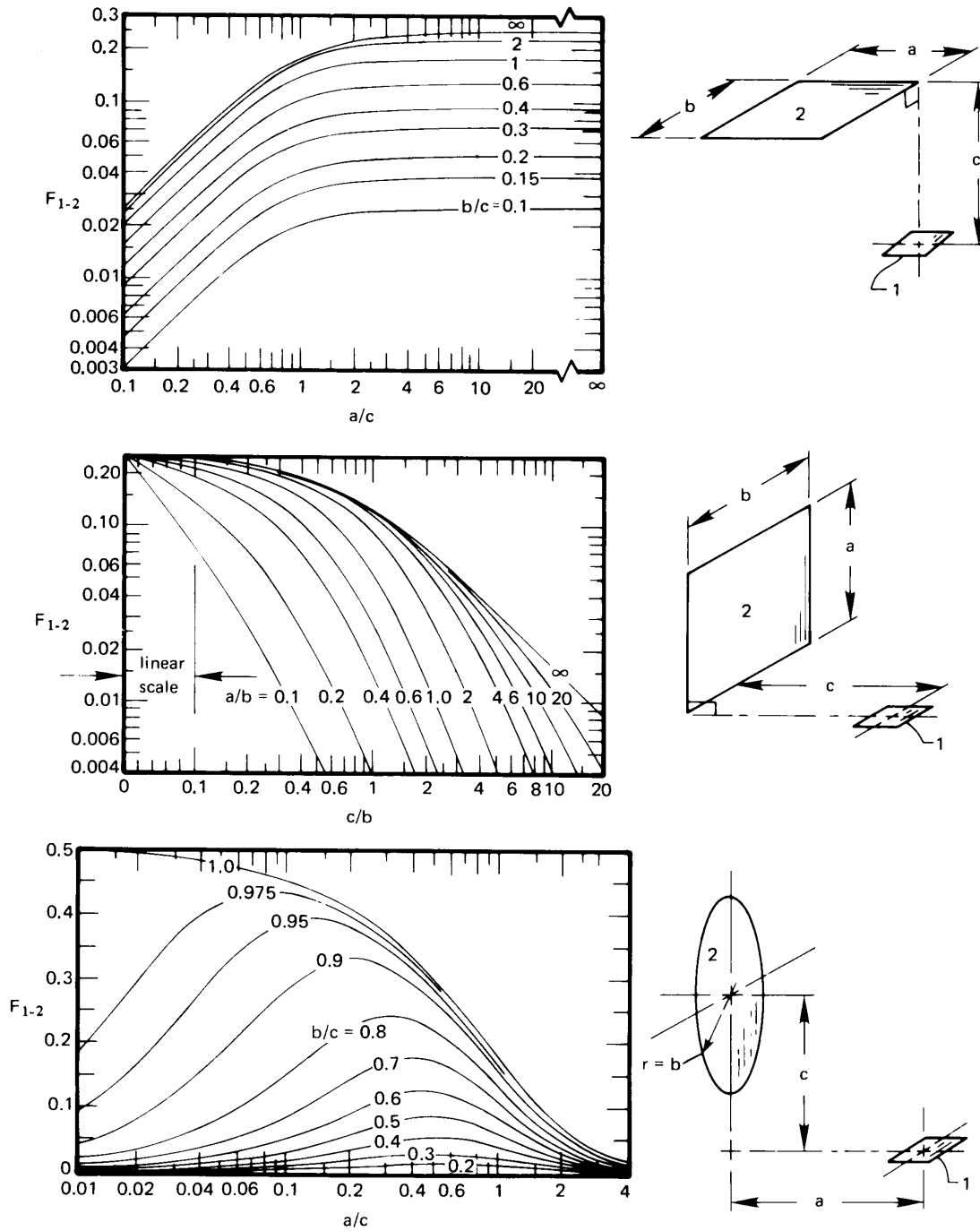
Figure 10.10 The view factor for three very small surfaces "looking at" three large surfaces ($A_1 \ll A_2$).
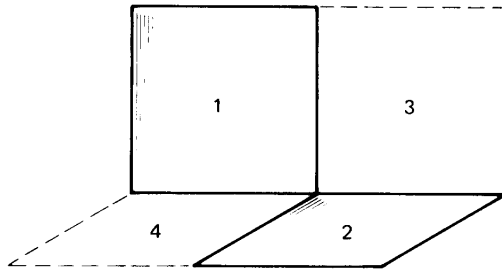
Figure 10.11   Radiation between two offset perpendicular squares.

another. Consider two fictitious areas 3 and 4 as indicated by the dotted lines. The view factor between the combined areas, (1+3) and (2+4), can be obtained from Fig. 10.9. In addition, we can write that view factor in terms of the unknown $F_{1\text{-}2}$ and other known view factors:

$$(2A)F_{(1+3)\text{-}(4+2)} = AF_{1\text{-}4} + AF_{1\text{-}2} + AF_{3\text{-}4} + AF_{3\text{-}2}$$
$$2F_{(1+3)\text{-}(4+2)} = 2F_{1\text{-}4} + 2F_{1\text{-}2}$$
$$F_{1\text{-}2} = F_{(1+3)\text{-}(4+2)} - F_{1\text{-}4}$$

And $F_{(1+3)\text{-}(4+2)}$ can be read from Fig. 10.9 (at $\phi = 90$, $w/\ell = 1/2$, and $h/\ell = 1/2$) as 0.245 and $F_{1\text{-}4}$ as 0.20. Thus,

$$F_{1\text{-}2} = (0.245 - 0.20) = 0.045 \qquad\qquad \blacksquare$$

Example 10.3

A heater (h) as shown in Fig. 10.12 radiates to the partially conical shield (s) that surrounds it. If the heater and shield are black, calculate the net heat transfer from the heater to the shield.

SOLUTION. First imagine a plane (i) laid across the open top of the shield:

$$F_{h-s} + F_{h-i} = 1$$

F_{h-i} can be obtained from Fig. 10.9 or case 3 of Table 10.3, for $R_1 = r_1/h = 5/20 = 0.25$ and $R_2 = r_2/h = 10/20 = 0.5$. The result is $F_{h-i} = 0.192$. Then

$$F_{h-s} = 1 - 0.192 = 0.808$$
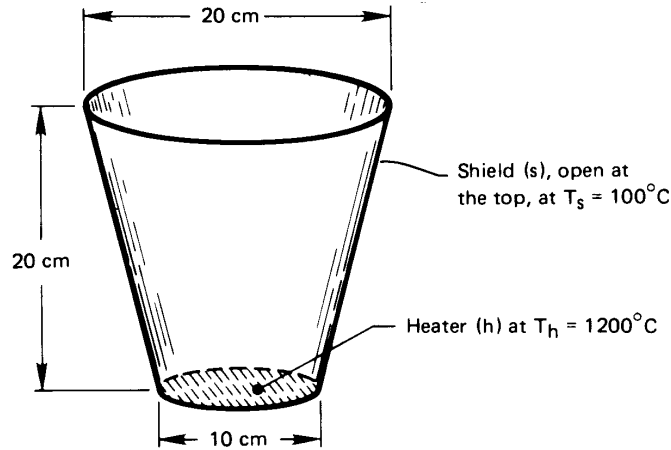
Figure 10.12 Heat transfer from a disk heater to its radiation shield.

Thus,

$$
\begin{aligned}
Q_{\text{net}_{h-s}} &= A_h F_{h-s} \, \sigma \left(T_h^4 - T_s^4 \right) \\
&= \frac{\pi}{4}(0.1)^2(0.808)(5.67 \times 10^{-8}) \left[(1200 + 273)^4 - 373^4 \right] \\
&= 1687 \text{ W} \qquad\qquad\qquad\qquad\qquad\qquad\qquad \blacksquare
\end{aligned}
$$

Example 10.4

Suppose that the shield in Example 10.3 were heating the region where the heater is presently located. What would F_{s-h} be?

SOLUTION. From eqn. (10.15) we have

$$
A_s F_{s-h} = A_h F_{h-s}
$$

But the frustum-shaped shield has an area of

$$
\begin{aligned}
A_s &= \pi (r_1 + r_2)\sqrt{h^2 + (r_2 - r_1)^2} \\
&= \pi (0.05 + 0.1)\sqrt{0.2^2 + 0.05^2} = 0.09715 \text{ m}^2
\end{aligned}
$$

and

$$
A_h = \frac{\pi}{4}(0.1)^2 = 0.007854 \text{ m}^2
$$

so

$$F_{s-h} = \frac{0.007854}{0.09715} (0.808) = 0.0653 \qquad \blacksquare$$

10.4 Heat transfer among gray bodies

Electrical analogy for gray body heat exchange

An electric circuit analogy for heat exchange among diffuse gray bodies was developed by Oppenheim [10.7] in 1956. He began with the definition of two new quantities:

$$H \ (\text{W/m}^2) \equiv \textit{irradiance} = \begin{cases} \text{flux of energy that irradiates} \\ \text{the surface} \end{cases}$$

and

$$B \ (\text{W/m}^2) \equiv \textit{radiosity} \ = \begin{cases} \text{total flux of radiative energy} \\ \text{away from the surface} \end{cases}$$

The radiosity can be expressed as the sum of the irradiated energy that is reflected by the surface and the radiation emitted by it. Thus,

$$B = \rho H + \varepsilon e_b \qquad (10.18)$$

We can immediately write the net heat flux leaving any particular surface as the difference between B and H for that surface. Then, with the help of eqn. (10.18), we get

$$q_{\text{net}} = B - H = B - \frac{B - \varepsilon e_b}{\rho} \qquad (10.19)$$

This equation can be rearranged as

$$q_{\text{net}} = \frac{\varepsilon}{\rho} e_b - \frac{1 - \rho}{\rho} B \qquad (10.20)$$

If the surface is opaque, so that $\tau = 0$, then $1 - \rho = \alpha$; and if it is gray, $\alpha = \varepsilon$. Then, eqn. (10.20) gives

$$q_{\text{net}} A = Q_{\text{net}} = \frac{e_b - B}{\rho / \varepsilon A} = \frac{e_b - B}{(1 - \varepsilon) / \varepsilon A} \qquad (10.21)$$

Equation (10.21) may be viewed as a form of Ohm's law. It tells us that $(e_b - B)$ can be seen as a driving potential for transferring heat away from a surface through an effective surface resistance, $(1 - \varepsilon) / \varepsilon A$.
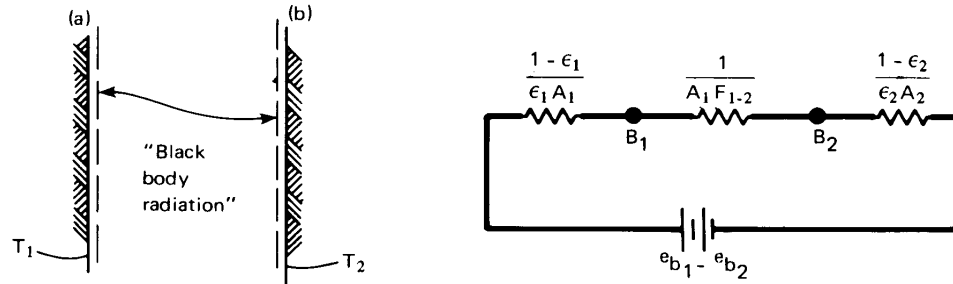
Figure 10.13 The electrical circuit analogy for radiation between two gray infinite plates.

Now consider heat transfer from one infinite gray plate to another parallel to it. Radiant energy flows past an imaginary surface, parallel to the first infinite plate and quite close to it, as shown as a dotted line in Fig. 10.13. If the gray plate is diffuse, its radiation has the same geometrical distribution as that from a black body, and it will travel to other objects in the same way that black body radiation would. Therefore, we can treat the radiation leaving the imaginary surface—the radiosity, that is—as though it were black body radiation travelling to an imaginary surface above the other plate. Thus, by analogy to eqn. (10.13),

$$Q_{\text{net}_{1\text{-}2}} = A_1 F_{1\text{-}2}(B_1 - B_2) = \frac{B_1 - B_2}{\left(\dfrac{1}{A_1 F_{1\text{-}2}}\right)} \tag{10.22}$$

where the final fraction is also a form of Ohm's law: the radiosity difference $(B_1 - B_2)$, can be said to drive heat through the geometrical resistance, $1/A_1 F_{1\text{-}2}$, that describes the field of view between the two surfaces.

When two gray surfaces exchange radiation only with each other, the net radiation flows through a surface resistance for each surface and a geometric resistance for the configuration. The electrical circuit shown in Fig. 10.13 expresses the analogy and gives us means for calculating $Q_{\text{net}_{1\text{-}2}}$ using Ohm's law. Recalling that $e_b = \sigma T^4$, we obtain

$$Q_{\text{net}_{1\text{-}2}} = \frac{e_{b_1} - e_{b_2}}{\sum \text{resistances}} = \frac{\sigma(T_1^4 - T_2^4)}{\left(\dfrac{1 - \varepsilon}{\varepsilon A}\right)_1 + \dfrac{1}{A_1 F_{1\text{-}2}} + \left(\dfrac{1 - \varepsilon}{\varepsilon A}\right)_2} \tag{10.23}$$

For the particular case of infinite parallel plates, $F_{1\text{-}2} = 1$ and $A_1 = A_2$

(Fig. 10.6); and, with $q_{\mathrm{net_{1-2}}} = Q_{\mathrm{net_{1-2}}}/A_1$, we find

$$\boxed{q_{\mathrm{net_{1-2}}} = \frac{\sigma\left(T_1^4 - T_2^4\right)}{\left(\dfrac{1}{\varepsilon_1} + \dfrac{1}{\varepsilon_2} - 1\right)}} \qquad (10.24)$$

Comparing eqn. (10.24) with eqn. (10.2), we may identify

$$\mathcal{F}_{1\text{-}2} = \frac{1}{\left(\dfrac{1}{\varepsilon_1} + \dfrac{1}{\varepsilon_2} - 1\right)} \qquad (10.25)$$

for infinite, gray, parallel plates. Notice, too, that if the plates are both black ($\varepsilon_1 = \varepsilon_2 = 1$), then both surface resistances are zero and

$$\mathcal{F}_{1\text{-}2} = 1 = F_{1\text{-}2}$$

which, of course, is what we would have expected.

Example 10.5   One gray body enclosed by another

Evaluate the heat transfer and the transfer factor for one gray body enclosed by another, as shown in Fig. 10.14.

SOLUTION. The electrical circuit analogy is exactly the same as that shown in Fig. 10.13, and $F_{1\text{-}2}$ is still one. Therefore, with eqn. (10.23),

$$Q_{\mathrm{net_{1-2}}} = \frac{\sigma\left(T_1^4 - T_2^4\right)}{\left(\dfrac{1 - \varepsilon_1}{\varepsilon_1 A_1} + \dfrac{1}{A_1} + \dfrac{1 - \varepsilon_2}{\varepsilon_2 A_2}\right)} \qquad (10.26)$$
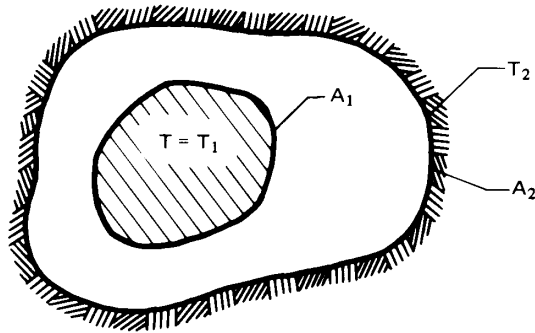
Figure 10.14   Heat transfer between an enclosed body and the body surrounding it.

The transfer factor may again be identified by comparison to eqn. (10.2):

$$Q_{\text{net}_{1\text{-}2}} = A_1 \underbrace{\frac{1}{\dfrac{1}{\varepsilon_1} + \dfrac{A_1}{A_2}\left(\dfrac{1}{\varepsilon_2} - 1\right)}}_{=\,\mathcal{F}_{1\text{-}2}} \sigma\left(T_1^4 - T_2^4\right) \qquad (10.27)$$

This calculation is valid only when body 1 does not view itself. ∎

Example 10.6   Transfer factor reciprocity

Derive $\mathcal{F}_{2\text{-}1}$ for the enclosed bodies shown in Fig. 10.14.

SOLUTION. The net radiation from each body is equal and opposite:

$$Q_{\text{net}_{1\text{-}2}} = -Q_{\text{net}_{2\text{-}1}}$$

$$A_1 \mathcal{F}_{1\text{-}2}\, \sigma\left(T_1^4 - T_2^4\right) = -A_2 \mathcal{F}_{2\text{-}1}\, \sigma\left(T_1^4 - T_2^4\right)$$

from which we obtain the reciprocity relationship for transfer factors:

$$\boxed{A_1 \mathcal{F}_{1\text{-}2} = A_2 \mathcal{F}_{2\text{-}1}} \qquad (10.28)$$

Hence, with the result of Example 10.5, we have

$$\mathcal{F}_{2\text{-}1} = \frac{A_1}{A_2}\, \mathcal{F}_{1\text{-}2} = \frac{1}{\dfrac{1}{\varepsilon_1}\dfrac{A_2}{A_1} + \left(\dfrac{1}{\varepsilon_2} - 1\right)} \qquad (10.29)$$

∎

Example 10.7   Small gray object in a large environment

Derive $\mathcal{F}_{1\text{-}2}$ for a small gray object (1) in a large isothermal environment (2), the result that was given as eqn. (1.35).

SOLUTION. We may use eqn. (10.27) with $A_1/A_2 \ll 1$:

$$\mathcal{F}_{1\text{-}2} = \frac{1}{\dfrac{1}{\varepsilon_1} + \underbrace{\dfrac{A_1}{A_2}}_{\ll 1}\left(\dfrac{1}{\varepsilon_2} - 1\right)} \cong \varepsilon_1 \qquad (10.30)$$

A large enclosure does not reflect much radiation back to the small object, and therefore acts as a perfect absorber of the small object's radiation—a black body. Note that the same result is obtained for *any* value of A_1/A_2 if the enclosure is black ($\varepsilon_2 = 1$). ∎

Additional two-body exchange problems

Radiation shields.   A radiation shield is a surface, usually of high re-
flectance, that is placed between a high-temperature source and its cooler
environment. Earlier examples in this chapter and in Chapter 1 show how
such a surface can reduce heat exchange. Let us now examine the role
of reflectance (or emittance, $\varepsilon = 1 - \rho$) in the performance of a radiation
shield.

Consider a gray body 1 surrounded by another gray body 2, as dis-
cussed in Example 10.5. Suppose now that a thin sheet of reflective
material is placed between bodies 1 and 2 as a radiation shield. The sheet
will reflect radiation arriving from body 1 back toward body 1; likewise,
owing to its low emittance, it will radiate little energy to body 2.

The radiation from body 1 to the inside of the shield and from the
outside of the shield to body 2 are each two-body exchange problems,
coupled by the shield temperature. We may put the various radiation
resistances in series to find (see Problem 10.46)

$$Q_{\mathrm{net}_{1\text{-}2}} = \frac{\sigma\left(T_1^4 - T_2^4\right)}{\left(\dfrac{1-\varepsilon_1}{\varepsilon_1 A_1} + \dfrac{1}{A_1} + \dfrac{1-\varepsilon_2}{\varepsilon_2 A_2}\right) + \underbrace{2\left(\dfrac{1-\varepsilon_s}{\varepsilon_s A_s}\right) + \dfrac{1}{A_s}}_{\text{added by shield}}} \tag{10.31}$$

assuming $F_{1\text{-s}} = F_{\text{s-}2} = 1$. Note that the radiation shield reduces $Q_{\mathrm{net}_{1\text{-}2}}$
more if its emittance is smaller, i.e., if it is highly reflective.

Specular surfaces.   The electrical circuit analogy that we have developed
is for diffuse surfaces. If the surface reflection or emission has directional
characteristics, different methods of analysis must be used [10.4].

One important special case deserves to be mentioned. If the two
gray surfaces in Fig. 10.14 are diffuse emitters but are perfectly specular
reflectors—that is, if they each have only mirror-like reflections—then an
energy balance shows that the transfer factor is [10.8, §4.3.1]

$$\mathcal{F}_{1\text{-}2} = \frac{1}{\left(\dfrac{1}{\varepsilon_1} + \dfrac{1}{\varepsilon_2} - 1\right)} \qquad \begin{array}{l}\text{for specularly}\\ \text{reflecting bodies}\end{array} \tag{10.32}$$

Remarkably, this result is identical to eqn. (10.25) for parallel plates. Since
parallel plates are a special case of the situation in Fig. 10.14, it follows in
that case that eqn. (10.25) is true for either specular or diffuse reflection.

Example 10.8

A physics experiment uses liquid nitrogen as a coolant. Saturated liquid nitrogen at 80 K flows through a 6.35 mm O.D. stainless steel line ($\varepsilon_l = 0.2$) inside a vacuum chamber. The chamber walls are at $T_c = 230$ K and are at some distance from the line. Determine the heat gain of the line per unit length. If a second thin stainless steel tube, 12.7 mm in diameter, is placed around the line to act as radiation shield, to what rate is the heat gain reduced? Find the temperature of the shield.

SOLUTION. The nitrogen coolant will hold the surface of the line at essentially 80 K, since the thermal resistances of the tube wall and the internal convection or boiling process are small. Without the shield, we can model the line as a small object in a large enclosure, as in Example 10.7:

$$Q_{\text{gain}} = (\pi D_l)\varepsilon_l\sigma(T_c^4 - T_l^4)$$
$$= \pi(0.00635)(0.2)(5.67 \times 10^{-8})(230^4 - 80^4) = 0.624 \text{ W/m}$$

With the shield, eqn. (10.31) applies. Assuming that the chamber area is large compared to the shielded line ($A_c \gg A_s$),

$$Q_{\text{gain}} = \frac{\sigma(T_c^4 - T_l^4)}{\left(\dfrac{1-\varepsilon_l}{\varepsilon_l A_l} + \dfrac{1}{A_l} + \underbrace{\dfrac{1-\varepsilon_c}{\varepsilon_2 A_c}}_{\text{neglect}}\right) + 2\left(\dfrac{1-\varepsilon_s}{\varepsilon_s A_s}\right) + \dfrac{1}{A_s}}$$

$$= \frac{\pi(0.00635)(5.67 \times 10^{-8})(230^4 - 80^4)}{\left(\dfrac{1-0.2}{0.2} + 1\right) + \dfrac{0.00635}{0.0127}\left[2\left(\dfrac{1-0.2}{0.2}\right) + 1\right]}$$

$$= 0.328 \text{ W/m}$$

The radiation shield would cut the heat gain by 47%.

The temperature of the shield, T_s, may be found using the heat loss and considering the heat flow from the chamber to the shield, with the shield now acting as a small object in a large enclosure:

$$Q_{\text{gain}} = (\pi D_s)\varepsilon_s\sigma(T_c^4 - T_s^4)$$
$$0.328 \text{ W/m} = \pi(0.0127)(0.2)(5.67 \times 10^{-8})(230^4 - T_s^4)$$

Solving, we find $T_s = 213$ K. ∎

The electrical circuit analogy when more than two gray bodies are involved in heat exchange

Let us first consider a three-body interaction, as pictured in at the bottom and left-hand sides of Fig. 10.15. The triangular circuit for three bodies is not so easy to analyze as the in-line circuits obtained in two-body problems. The idea is to apply energy conservation at each radiosity node in the circuit. We equate the net heat transfer from any one of the bodies (which we designate as i)

$$Q_{\text{net}_i} = \frac{e_{b_i} - B_i}{\dfrac{1 - \varepsilon_i}{\varepsilon_i A_i}} \tag{10.33a}$$

to the sum of the net radiation to each of the other bodies (call them j)

$$Q_{\text{net}_i} = \sum_j \left(\frac{B_i - B_j}{1 \big/ A_i F_{i\text{-}j}} \right) \tag{10.33b}$$

For the three bodies shown in Fig. 10.15, this procedure leads to three equations

$$Q_{\text{net}_1}, \text{ at node } B_1: \quad \frac{e_{b_1} - B_1}{\dfrac{1 - \varepsilon_1}{\varepsilon_1 A_1}} = \frac{B_1 - B_2}{\dfrac{1}{A_1 F_{1\text{-}2}}} + \frac{B_1 - B_3}{\dfrac{1}{A_1 F_{1\text{-}3}}} \tag{10.34a}$$

$$Q_{\text{net}_2}, \text{ at node } B_2: \quad \frac{e_{b_2} - B_2}{\dfrac{1 - \varepsilon_2}{\varepsilon_2 A_2}} = \frac{B_2 - B_1}{\dfrac{1}{A_1 F_{1\text{-}2}}} + \frac{B_2 - B_3}{\dfrac{1}{A_2 F_{2\text{-}3}}} \tag{10.34b}$$

$$Q_{\text{net}_3}, \text{ at node } B_3: \quad \frac{e_{b_3} - B_3}{\dfrac{1 - \varepsilon_3}{\varepsilon_3 A_3}} = \frac{B_3 - B_1}{\dfrac{1}{A_1 F_{1\text{-}3}}} + \frac{B_3 - B_2}{\dfrac{1}{A_2 F_{2\text{-}3}}} \tag{10.34c}$$

If the temperatures T_1, T_2, and T_3 are known (so that e_{b_1}, e_{b_2}, e_{b_3} are known), these equations can be solved simultaneously for the three unknowns, B_1, B_2, and B_3. After solving, one can compute the net heat transfer to or from any body i from either of eqns. (10.33).

Thus far, we have considered only cases in which the surface temperature is known for each body involved in the heat exchange process. Let us consider two other possibilities.
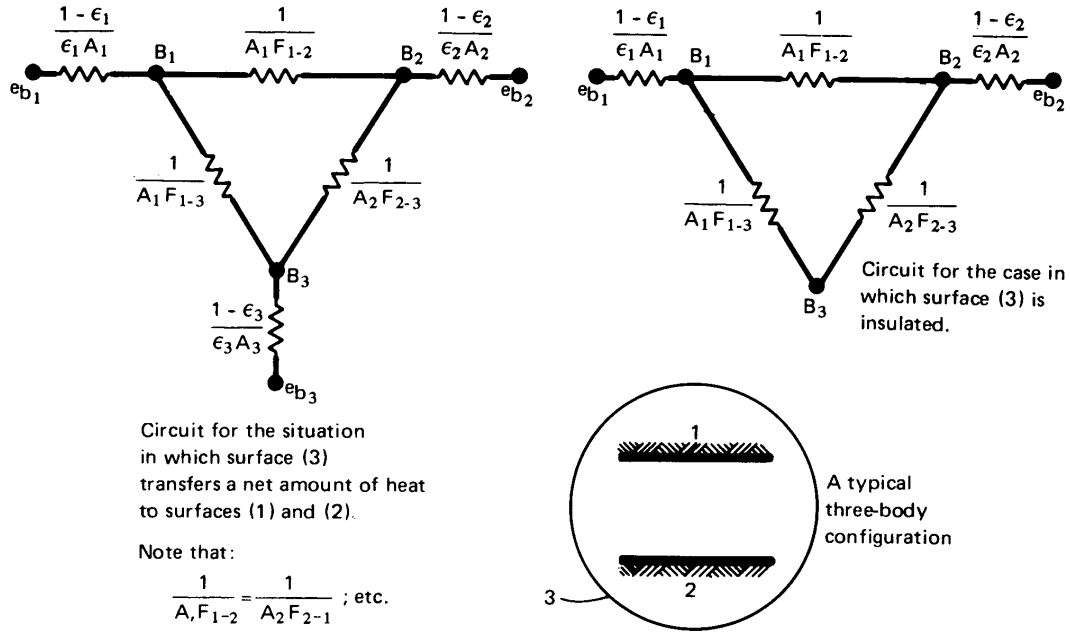
Figure 10.15 The electrical circuit analogy for radiation among three gray surfaces.

An insulated wall. If a wall is adiabatic, $Q_{net} = 0$ at that wall. For example, if wall 3 in Fig. 10.15 is insulated, then eqn. (10.33b) shows that $e_{b_3} = B_3$. We can eliminate one leg of the circuit, as shown on the right-hand side of Fig. 10.15; likewise, the left-hand side of eqn. (10.34c) equals zero. This means that all radiation absorbed by an adiabatic wall is immediately reemitted. Such walls are sometimes called "refractory surfaces" in discussing thermal radiation.

The circuit for an insulated wall can be treated as a series-parallel circuit, since all the heat from body 1 flows to body 2, even if it does so by travelling first to body 3. Then

$$Q_{net_1} = \cfrac{e_{b_1} - e_{b_2}}{\cfrac{1 - \varepsilon_1}{\varepsilon_1 A_1} + \cfrac{1}{\cfrac{1}{1/(A_1 F_{1-3}) + 1/(A_2 F_{2-3})} + \cfrac{1}{1/(A_1 F_{1-2})}} + \cfrac{1 - \varepsilon_2}{\varepsilon_2 A_2}}$$

(10.35)

A specified wall heat flux. The heat flux leaving a surface may be known, for example, if it is an electrically powered radiant heater. In this case, the left-hand side of one of eqns. (10.34) can be replaced with the surface's known Q_{net}, via eqn. (10.33b).

For the adiabatic wall case just considered, if surface 1 had a specified heat flux, then eqn. (10.35) could be solved for e_{b_1} and the unknown temperature T_1.

Example 10.9

Two very long strips, 1 m wide and 2.40 m apart, face each other as shown in Fig. 10.16. (a) Find $Q_{net_{1-2}}$ (W/m) if the surroundings are black and at 250 K. (b) Find $Q_{net_{1-2}}$ (W/m) if they are connected by an insulated and isothermal diffuse reflector between the edges on both sides. Also evaluate the temperature of the reflector in part (b).

SOLUTION. From Table 10.2, case 1, we find $F_{1-2} = 0.2 = F_{2-1}$. In addition, $F_{2-3} = 1 - F_{2-1} = 0.8$, irrespective of whether surface 3 represents the surroundings or the insulated shield.

In case (a), surface 3 is the surroundings at $T_3 = 250$ K. Evaluating $e_{b_1} = \sigma T_1^4$ and $e_{b_2} = \sigma T_2^4$, the nodal equations (10.34a) and (10.34b) become

$$\frac{1451 - B_1}{(1 - 0.3)/0.3} = \frac{B_1 - B_2}{1/0.2} + \frac{B_1 - B_3}{1/0.8}$$

$$\frac{459.3 - B_2}{(1 - 0.5)/0.5} = \frac{B_2 - B_1}{1/0.2} + \frac{B_2 - B_3}{1/0.8}$$

Equation (10.34c) cannot be used directly for black surroundings, since $\varepsilon_3 = 1$ and the surface resistance in the left-hand side denominator would be zero. But the numerator is also zero in this case, since
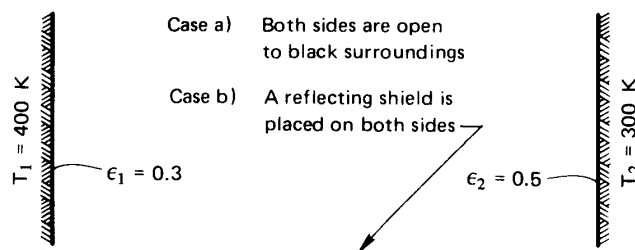
Figure 10.16 Illustration for Example 10.9.

$e_{b_3} = B_3$ for black surroundings. And since we now know $B_3 = \sigma T_3^4 = 221.5 \text{ W/m}^2\text{K}$, we can use it directly in the two equations above. Thus,

$$B_1 - \ 0.14\,B_2 - 0.56(221.5) = \ 435.6$$
$$-B_1 + 10.00\,B_2 - 4.00(221.5) = 2296.5$$

or

$$\left. \begin{array}{r} B_1 - \ 0.14\,B_2 = \ 559.6 \\ -B_1 + 10.00\,B_2 = 3182.5 \end{array} \right\} \quad \text{so} \quad \left\{ \begin{array}{l} B_1 = 612.1 \text{ W/m}^2 \\ B_2 = 379.5 \text{ W/m}^2 \end{array} \right.$$

The net flow from surface 1 to surface 2 is quite small:

$$Q_{\text{net}_{1\text{-}2}} = \frac{B_1 - B_2}{1/(A_1 F_{1\text{-}2})} = 46.53 \text{ W/m}$$

Since each strip also loses heat to the surroundings, $Q_{\text{net}_1} \neq Q_{\text{net}_2} \neq Q_{\text{net}_{1\text{-}2}}$.

For case (b), with the adiabatic shield in place, eqn. (10.34c) can be combined with the other two nodal equations:

$$0 = \frac{B_3 - B_1}{1/0.8} + \frac{B_3 - B_2}{1/0.8}$$

The three equations can be solved manually, by the use of determinants, or with matrix algebra software. The result is

$$B_1 = 987.7 \text{ W/m}^2 \qquad B_2 = 657.4 \text{ W/m}^2 \qquad B_3 = 822.6 \text{ W/m}^2 \quad (10.36)$$

In this case, because surface 3 is adiabatic, all net heat transfer from surface 1 is to surface 2: $Q_{\text{net}_1} = Q_{\text{net}_{1\text{-}2}}$. Then, from eqn. (10.33b), we get

$$Q_{\text{net}_{1\text{-}2}} = \left[\frac{987.7 - 657.4}{1/(1)(0.2)} + \frac{987.7 - 822.6}{1/(1)(0.8)} \right] = 198 \text{ W/m} \quad (10.37)$$

Of course, because surface 3 is insulated, $Q_{\text{net}_{1\text{-}2}}$ may be calculated much more directly using eqn. (10.35):

$$Q_{\text{net}_{1\text{-}2}} = \frac{5.67 \times 10^{-8}(400^4 - 300^4)}{\dfrac{0.7}{0.3} + \dfrac{1}{\dfrac{1}{1/0.8 + 1/0.8} + 0.2} + \dfrac{0.5}{0.5}} = 198 \text{ W/m} \quad (10.38)$$

The result, of course, is the same. We note that the presence of the reflector significantly increases the net heat flow from surface 1 to surface 2.

The temperature of the reflector (3) is obtained from eqn. (10.33a) with $Q_{\text{net}_3} = 0$:

$$0 = e_{b_3} - B_3 = 5.67 \times 10^{-8} T_3^4 - 822.6$$

so

$$T_3 = 347 \text{ K} \qquad \blacksquare$$

Algebraic solution of multisurface enclosure problems

An *enclosure* can consist of any number of surfaces that exchange radiation with one another. The evaluation of radiant heat transfer amongst these surfaces proceeds in essentially the same way as for three surfaces. For multisurface problems, however, the electrical circuit approach is less convenient than a formulation based on matrices. The matrix equations are usually solved on a computer.

An enclosure formed by n surfaces is shown in Fig. 10.17. As before, we will assume that:

- Each surface is diffuse, gray, and opaque, so that $\varepsilon = \alpha$ and $\rho = 1 - \varepsilon$.

- The temperature and net heat flux are uniform over each surface (more precisely, the radiosity must be uniform and the other properties are averages for each surface). Either the temperature or the flux must be specified on every surface.

- The view factor, $F_{i\text{-}j}$, between any two surfaces i and j is known.

- Conduction and convection within the enclosure can be neglected, and any fluid in the enclosure is transparent and nonradiating.

We are interested in determining the heat fluxes at the surfaces where temperatures are specified, and vice versa.

The rate of heat loss from the ith surface of the enclosure can conveniently be written in terms of the radiosity, B_i, and the irradiation, H_i, from eqns. (10.19) and (10.21)

$$q_{\text{net}_i} = B_i - H_i = \frac{\varepsilon_i}{1 - \varepsilon_i}\left(\sigma T_i^4 - B_i\right) \qquad (10.39)$$
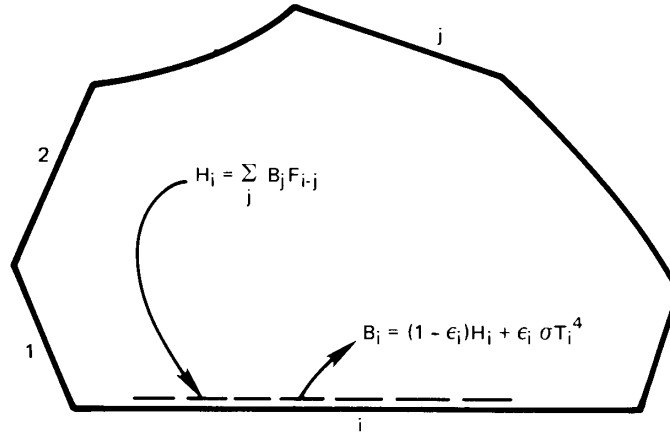
Figure 10.17 An enclosure composed of n diffuse, gray surfaces.

where

$$B_i = \rho_i H_i + \varepsilon_i e_{b_i} = (1 - \varepsilon_i)H_i + \varepsilon_i \sigma T_i^4 \qquad (10.40)$$

However, $A_i H_i$, the irradiating heat transfer incident on surface i, is the sum of the energies reaching i from all other surfaces, including itself

$$A_i H_i = \sum_{j=1}^{n} A_j B_j F_{j\text{-}i} = \sum_{j=1}^{n} B_j A_i F_{i\text{-}j}$$

where we have used the reciprocity rule, $A_j F_{j\text{-}i} = A_i F_{i\text{-}j}$. Thus

$$H_i = \sum_{j=1}^{n} B_j F_{i\text{-}j} \qquad (10.41)$$

It follows from eqns. (10.40) and (10.41) that

$$B_i = (1 - \varepsilon_i) \sum_{j=1}^{n} B_j F_{i\text{-}j} + \varepsilon_i \sigma T_i^4 \qquad (10.42)$$

This equation applies to every surface, $i = 1, \ldots, n$. When all the surface temperatures are specified, the result is a system of n linear equations for the n unknown radiosities.

For numerical purposes, it is convenient to introduce the Kronecker delta,

$$\delta_{ij} = \begin{cases} 1 & \text{for } i = j \\ 0 & \text{for } i \neq j \end{cases} \qquad (10.43)$$

and to rearrange eqn. (10.42) as a system of linear equations

$$\sum_{j=1}^{n} \underbrace{\left[\delta_{ij} - (1 - \varepsilon_i)F_{i\text{-}j} \right]}_{\equiv C_{ij}} B_j = \varepsilon_i \, \sigma T_i^4 \quad \text{for } i = 1, \ldots, n \qquad (10.44)$$

The radiosities are then found by inverting the matrix C_{ij}. The rate of heat loss from the ith surface, $Q_{\text{net}_i} = A_i q_{\text{net}_i}$, can be obtained from eqn. (10.39).

For those surfaces where heat fluxes are prescribed, we can eliminate the $\varepsilon_i \sigma T_i^4$ term in eqn. (10.42) or (10.44) using eqn. (10.39). We again obtain a matrix equation that can be solved for the B_i's. Finally, eqn. (10.39) is solved for the unknown temperature of surface in question.

In many cases, the radiosities themselves are of no particular interest. The heat flows are what is really desired. With a bit more algebra (see Problem 10.45), one can formulate a matrix equation for the n unknown values of q_{net_i}, for $i = 1, \ldots, n$:

$$\sum_{j=1}^{n} \left[\frac{\delta_{ij}}{\varepsilon_i} - \frac{(1 - \varepsilon_j)}{\varepsilon_j} F_{i\text{-}j} \right] q_{\text{net}_j} = \sum_{j=1}^{n} \left(\delta_{ij} - F_{i\text{-}j} \right) \sigma T_j^4 \qquad (10.45)$$

Example 10.10

Two sides of a long triangular duct, as shown in Fig. 10.18, are made of stainless steel ($\varepsilon = 0.5$) and are maintained at $500°C$. The third side is of copper ($\varepsilon = 0.15$) and has a uniform temperature of $100°C$. Calculate the rate of heat transfer to the copper base per meter of length of the duct.

Solution. Assume the duct walls to be gray and diffuse and that convection is negligible. The view factors can be calculated from configuration 4 of Table 10.2:

$$F_{1\text{-}2} = \frac{A_1 + A_2 - A_3}{2A_1} = \frac{0.5 + 0.3 - 0.4}{1.0} = 0.4 \qquad (10.46)$$

Similarly, $F_{2\text{-}1} = 0.67$, $F_{1\text{-}3} = 0.6$, $F_{3\text{-}1} = 0.75$, $F_{2\text{-}3} = 0.33$, and $F_{3\text{-}2} = 0.25$. The surfaces cannot "see" themselves, so $F_{1\text{-}1} = F_{2\text{-}2} = F_{3\text{-}3} = 0$. Equation (10.42) leads to three algebraic equations for the
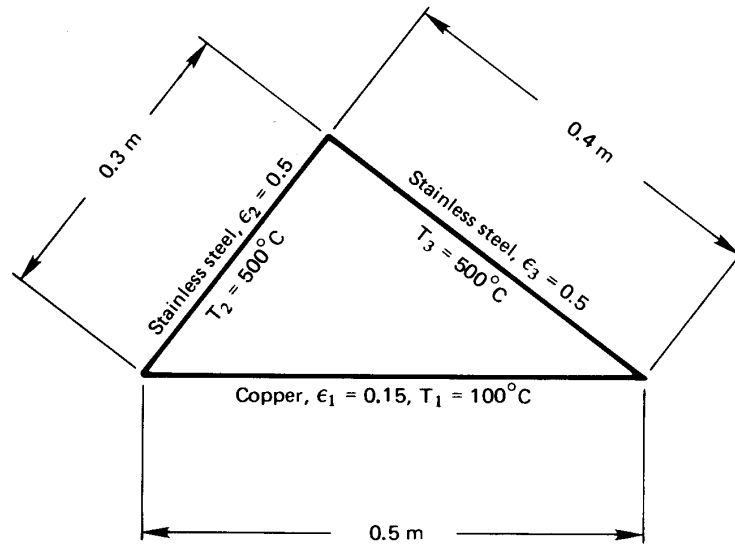
Figure 10.18 Illustration for Example 10.10.

three unknowns, B_1, B_2, and B_3.

$$B_1 = \underbrace{(1 - \varepsilon_1)}_{0.85} \, (\underbrace{F_{1\text{-}1}}_{0} B_1 + \underbrace{F_{1\text{-}2}}_{0.4} B_2 + \underbrace{F_{1\text{-}3}}_{0.6} B_3) + \underbrace{\varepsilon_1}_{0.15} \, \sigma T_1^4$$

$$B_2 = \underbrace{(1 - \varepsilon_2)}_{0.5} \, (\underbrace{F_{2\text{-}1}}_{0.67} B_1 + \underbrace{F_{2\text{-}2}}_{0} B_2 + \underbrace{F_{2\text{-}3}}_{0.33} B_3) + \underbrace{\varepsilon_2}_{0.5} \, \sigma T_2^4$$

$$B_3 = \underbrace{(1 - \varepsilon_3)}_{0.5} \, (\underbrace{F_{3\text{-}1}}_{0.75} B_1 + \underbrace{F_{3\text{-}2}}_{0.25} B_2 + \underbrace{F_{3\text{-}3}}_{0} B_3) + \underbrace{\varepsilon_3}_{0.5} \, \sigma T_3^4$$

This system can easily be solved numerically using matrix methods. Alternatively, we can substitute the third equation into the first two to eliminate B_3, and then use the second equation to eliminate B_2 from the first. The result is

$$B_1 = 0.232 \, \sigma T_1^4 + 0.319 \, \sigma T_2^4 + 0.447 \, \sigma T_3^4$$

Equation (10.39) gives the rate of heat loss by surface 1 as

$$Q_{\text{net}_1} = A_1 \frac{\varepsilon_1}{1 - \varepsilon_1} \, (\sigma T_1^4 - B_1)$$

$$= A_1 \frac{\varepsilon_1}{1 - \varepsilon_1} \, \sigma \left(T_1^4 - 0.232 \, T_1^4 - 0.319 \, T_2^4 - 0.447 \, T_3^4 \right)$$

$$= (0.5)\left(\frac{0.15}{0.85}\right)(5.67 \times 10^{-8})$$
$$\times \left[(373)^4 - 0.232(373)^4 - 0.319(773)^4 - 0.447(773)^4\right] \text{ W/m}$$
$$= -1294 \text{ W/m}$$

The negative sign indicates that the copper base is gaining heat.　■

Enclosures with nonisothermal, nongray, or nondiffuse surfaces

The representation of enclosure heat exchange by eqn. (10.44) or (10.45) is actually quite powerful. For example, if the primary surfaces in an enclosure are not isothermal, they may be subdivided into a larger number of smaller surfaces, each of which is approximately isothermal. Then either equation may be used to calculate the heat exchange among the set of smaller surfaces.

For those cases in which the gray surface approximation, eqn. (10.8c), cannot be applied (owing to very different temperatures or strong wavelength dependence in ε_λ), eqns. (10.44) and (10.45) may be applied on a monochromatic basis, since the monochromatic form of Kirchhoff's law, eqn. (10.8b), remains valid. The results must, of course, be integrated over wavelength to get the heat exchange. The calculation is usually simplified by breaking the wavelength spectrum into a few discrete bands within which radiative properties are approximately constant [10.4, Chpt. 6].

When the surfaces are not diffuse—when emission or reflection vary with angle—a variety of other methods can be applied. Among them, the Monte Carlo technique is probably the most widely used. The Monte Carlo technique tracks emissions and reflections through various angles among the surfaces and estimates the probability of absorption or re-reflection [10.5, 10.9]. This method allows complex situations to be numerically computed with relative ease, provided that one is careful to obtain statistical convergence.

10.5 Gaseous radiation

We have treated every radiation problem thus far as though radiation between the surfaces of interest is unobstructed by any fluid or particles between them. This is clearly true if a vacuum separates the surfaces. Liquids, on the other hand, simply absorb infrared radiation over a very short distance, ending any radiant heat flow to other surfaces. Thus, we do not consider radiation when heat is transferred across a liquid layer.

Air normally allows most radiation to pass right through, and so far we have treated all gases as if they are fully transparent. This approximation is reasonable for air and other symmetrical molecules when the gases do not contain many suspended particles or droplets. However, all gases interact with photons to some extent. Gas molecules can absorb or deflect photons, and can even emit additional photons. These interactions can be especially important when more complex molecules, such as water vapor or carbon dioxide, have a significant concentration, at high temperatures, as in furnaces, or when long distances are involved, as in the earth's atmosphere. In those cases, gases may play a leading role in the heat exchange process.

How gases interact with photons

The photons of radiant energy passing through a gaseous region can be impeded in two ways. Some can be "scattered," or deflected in various directions, and some can be absorbed by the molecules. Scattering is a fairly minor influence in most gases unless they contain foreign particles, such as dust or fog. In cloudless air, for example, we are aware of the scattering of sunlight only when it passes through many miles of the atmosphere. The short, bluish wavelengths of sun light are scattered most strongly by gas molecules, through a process known as *Rayleigh scattering*. That scattered light gives the sky its blue hues.

At sunset, sunlight passes through the atmosphere at a shallow angle for hundreds of miles. Radiation in the blue wavelengths has all been scattered out before the sun's light reaches us. Thus, we see only the unscattered reddish hues that remain.

When particles suspended in a gas have diameters near the wavelength of light, a more complex type of scattering can occur, known as *Mie scattering*. Such scattering occurs from the water droplets in clouds (often making them a brilliant white color). It also occurs in gases that contain soot or in pulverized coal combustion. Mie scattering has a strong angular variation that changes with both wavelength and particle size [10.10].

The absorption or emission of radiation by molecules, rather than by particles, will be our principal focus. The interaction of molecules with radiation—photons, that is—is governed by quantum mechanics. At this point, it's helpful to recall a few facts from molecular physics. Each photon has an energy hc_o/λ, where h is Planck's constant, c_o is the speed of light, and λ is the wavelength of light. Thus, photons of shorter
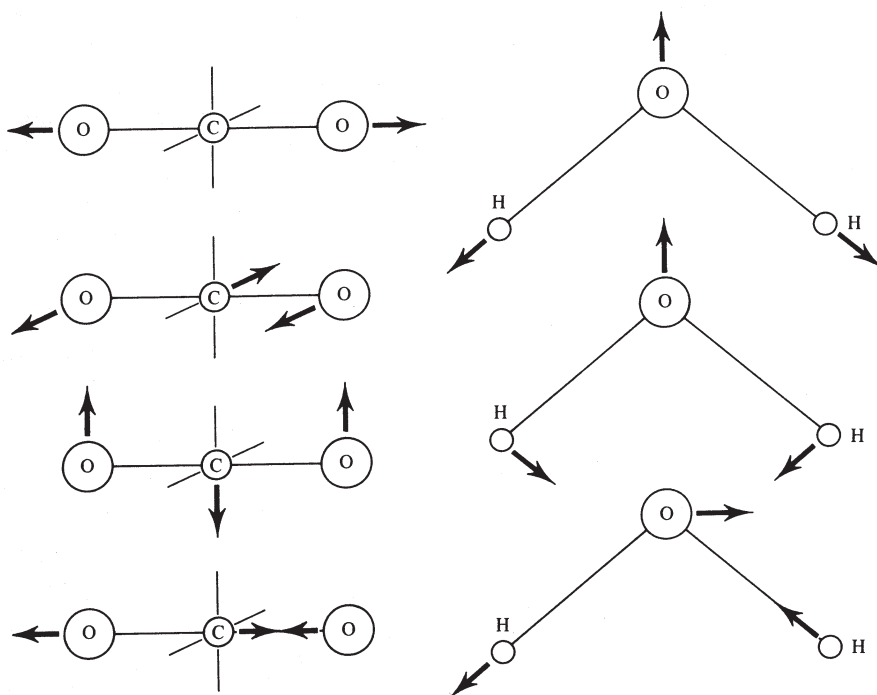
Figure 10.19 Vibrational modes of carbon dioxide and of water.

wavelengths have higher energies: ultraviolet photons are more energetic than visible photons, which are in turn more energetic than infrared photons. At low temperature, objects emit mostly infrared photons; but as they become hotter, objects emit more and more visible photons.

Molecules can store energy by rotation, by vibration (Fig. 10.19), or in their electrons. Whereas the possible energy of a photon varies smoothly with wavelength, the energies of molecules are constrained by quantum mechanics to change only in discrete steps between the molecule's allowable "energy levels." The available energy levels depend on the molecule's chemical structure.

When a molecule emits a photon, its energy drops in a discrete step (a *quantum*) from a higher energy level to a lower one. The energy given up is carried away by the photon. As a result, the wavelength of that photon is determined by the specific change in molecular energy level that caused it to be emitted. Just the opposite happens when a photon is absorbed: the photon's wavelength must match a specific energy level change available to that particular molecule. As a result, each molecular species can absorb

only photons at, or very close to, particular wavelengths! Often, these wavelengths are tightly grouped into so-called *absorption bands*, outside of which the gas is essentially transparent to photons.

The fact that a molecule's structure determines how it absorbs and emits light has been used extensively by chemists as a tool for deducing molecular structure. A knowledge of the energy levels in a molecule, in conjunction with quantum theory, allows specific atoms and bonds to be identified. This kind of measurement is called *spectroscopy* (see [10.11, Chpt. 13 & 14] for an introduction; see [10.12] to go overboard).

At the wavelengths that correspond to thermal radiation at typical temperatures, transitions in the vibrational and rotation modes of molecules have the greatest influence on radiative absorptance. Such transitions can be driven by photons only when the molecule has some asymmetry.[4] Thus, for all practical purposes, monatomic and symmetrical diatomic molecules are transparent to thermal radiation. The major components of air—N_2 and O_2—are therefore nonabsorbing; so, too, are H_2 and such monatomic gases as argon.

Asymmetrical molecules like CO_2, H_2O, CH_4, O_3, NH_3, N_2O, and SO_2, on the other hand, each absorb thermal radiation of certain wavelengths. The first two of these, CO_2 and H_2O, are always present in air. To understand how the interaction works, consider the possible vibrations of CO_2 and H_2O shown in Fig. 10.19. For CO_2, the topmost mode of vibration is symmetrical and has no interaction with thermal radiation at normal pressures. The other three modes produce asymmetries in the molecule when they occur; each is important to thermal radiation.

The primary absorption wavelength for the two middle modes of CO_2 is 15 μm, which lies in the thermal infrared. The wavelength for the bottommost mode is 4.3 μm. For H_2O, middle mode of vibration interacts strongly with thermal radiation at 6.3 μm. The other two both affect 2.7 μm radiation, although the bottom one does so more strongly. In addition, H_2O has a rotational mode that absorbs thermal radiation having wavelengths of 14 μm or more. Both of these molecules show additional absorption lines at shorter wavelengths, which result from the superposition of two or more vibrations and their harmonics (e.g., at 2.7 μm for CO_2 and at 1.38 and 1.87 μm for H_2O, as seen in Fig. 10.2). Additional absorption bands can appear at high temperature or high pressure.

---

[4]The asymmetry required is in the distribution of electric charge—the dipole moment. A vibration of the molecule must create a fluctuating dipole moment in order to interact with photons. A rotation interacts with photons only if the molecule has a permanent dipole moment, as do CO_2 and H_2O.
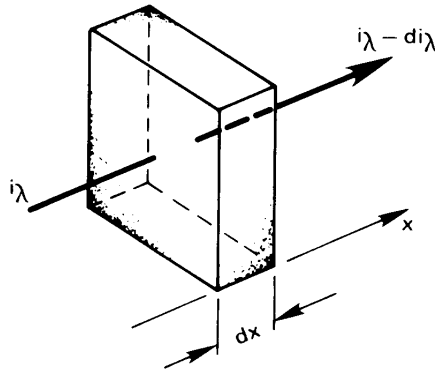
Figure 10.20 The attenuation of radiation through an absorbing and/or scattering gas.

Absorptance, transmittance, and emittance

Figure 10.20 shows radiant energy passing through an absorbing gas with a monochromatic intensity i_λ. As it passes through an element of thickness dx, the intensity will be reduced by an amount di_λ

$$di_\lambda = -\rho \kappa_\lambda i_\lambda \, dx \qquad (10.47)$$

where ρ is the gas density and κ_λ is called the *monochromatic absorption coefficient*. If the gas scatters radiation out of the x-direction and into another direction, we replace κ_λ with γ_λ, the *monochromatic scattering coefficient*. If it both absorbs and scatters radiation, we replace κ_λ with $\beta_\lambda \equiv \kappa_\lambda + \gamma_\lambda$, the *monochromatic extinction coefficient*.[5] The dimensions of κ_λ, β_λ, and γ_λ are all m^2/kg.

Limiting our attention to gases that absorb and taking $\rho \kappa_\lambda$ to be constant through the gas, we can integrate eqn. (10.47) from an initial intensity i_{λ_0} at $x = 0$

$$i_\lambda(x) = i_{\lambda_0} \, e^{-\rho \kappa_\lambda x} \qquad (10.48)$$

This result is called *Beer's law* (pronounced "Bayr's" law). For a gas layer of a given depth $x = L$, the ratio of final to initial intensity defines that layer's *monochromatic transmittance*, τ_λ:

$$\tau_\lambda \equiv \frac{i_\lambda(L)}{i_{\lambda_0}} = e^{-\rho \kappa_\lambda L} \qquad (10.49)$$

Further, since nonscattering gases do not reflect radiant energy, $\tau_\lambda + \alpha_\lambda = 1$. Thus, the monochromatic absorptance, α_λ, is

$$\alpha_\lambda = 1 - e^{-\rho \kappa_\lambda L} \qquad (10.50)$$

---

[5]All three coefficients, κ_λ, γ_λ, and β_λ, are expressed on a mass basis. They could, alternatively, have been expressed in terms of the volumetric concentration of various molecules within the gas.
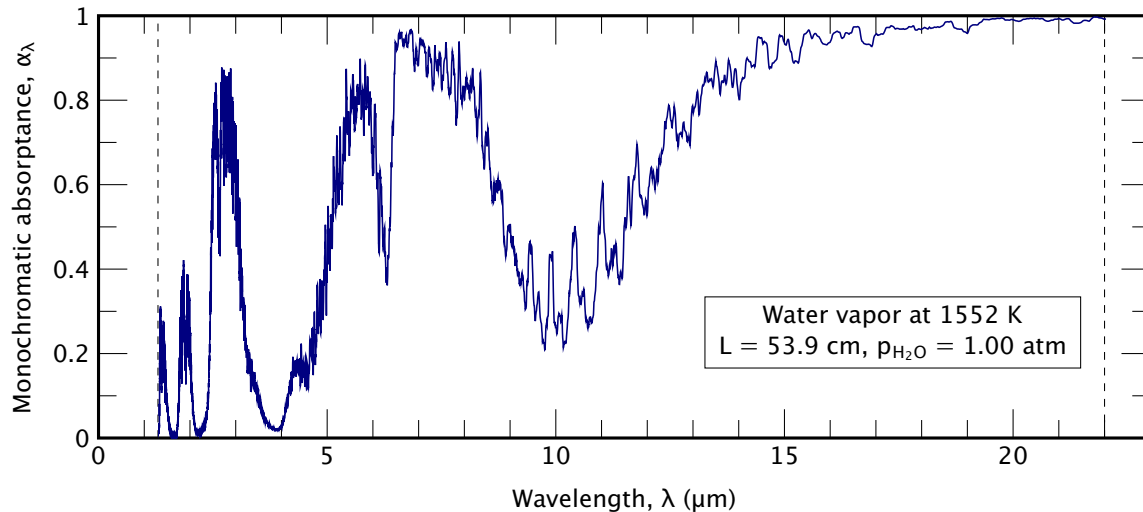
Figure 10.21 Monochromatic absorptance of a 53.9 cm thick layer of steam at 1552 K, from 1.3 to 22 μm. (From the data of Mancini et al. [10.13].)

Both τ_λ and α_λ depend on the density and thickness of the gas layer. The product $\rho\kappa_\lambda L$ is sometimes called the *optical depth* of the gas. For very small values of $\rho\kappa_\lambda L$, the gas is transparent to the wavelength λ.

The dependence of α_λ on λ is normally very strong. As we have seen, a given molecule will absorb radiation in certain wavelength bands, while allowing radiation with somewhat higher or lower wavelengths to pass almost unhindered. Figure 10.21 shows the absorptance of water vapor as a function of wavelength for a fixed depth. We can see the absorption bands at wavelengths surrounding 1.38, 1.87, 2.7, and 6.3 μm that we mentioned before.

A comparison of Fig. 10.21 with Fig. 10.2 readily shows why radiation from the sun, as viewed from the earth's surface, shows a number of spiky indentations at certain wavelengths. Several of those indentations occur in bands where atmospheric water vapor absorbs incoming solar radiation, in accordance with Fig. 10.21. The other indentations in Fig. 10.2 occur where ozone and CO_2 absorb radiation. The sun itself does not have these regions of low emittance; instead, much of the radiation in these bands is absorbed by gases in the atmosphere before it can reach the ground.

Just as α_λ and ε_λ are equal to one another for a diffuse solid surface, they are equal for a gas. We may demonstrate this by considering an isothermal gas that is in thermal equilibrium with a black enclosure that contains it. The radiant intensity within the enclosure is that of a black

body, i_{λ_b}, at the temperature of the gas and enclosure. Equation (10.47) shows that a small section of gas absorbs radiation, reducing the intensity by an amount $\rho \kappa_\lambda i_{\lambda_b} \, dx$. To maintain equilibrium, the gas must therefore emit an equal amount of radiation:

$$di_\lambda = \rho \kappa_\lambda i_{\lambda_b} \, dx \qquad (10.51)$$

Now, if radiation from some other source is transmitted through a nonscattering isothermal gas, we can combine the absorption from eqn. (10.47) with the emission from eqn. (10.51) to form an energy balance called the *equation of transfer*

$$\frac{di_\lambda}{dx} = -\rho \kappa_\lambda i_\lambda + \rho \kappa_\lambda i_{\lambda_b} \qquad (10.52)$$

Integration of this equation yields a result similar to eqn. (10.48):

$$i_\lambda(L) = i_{\lambda_0} \underbrace{e^{-\rho \kappa_\lambda L}}_{=\tau_\lambda} + i_{\lambda_b} \underbrace{\left(1 - e^{-\rho \kappa_\lambda L}\right)}_{\equiv \varepsilon_\lambda} \qquad (10.53)$$

The first righthand term represents the transmission of the incoming intensity, as in eqn. (10.48), and the second is the radiation emitted by the gas itself. The coefficient of the second righthand term defines the monochromatic emittance, ε_λ, of the gas layer. Finally, comparison to eqn. (10.50) shows that

$$\varepsilon_\lambda = \alpha_\lambda = 1 - e^{-\rho \kappa_\lambda L} \qquad (10.54)$$

Again, we see that for very small optical depth ($\rho \kappa_\lambda L \ll 1$), the gas will neither absorb nor emit radiation of wavelength λ.

Heat transfer from gases to walls

We now see that predicting the total emittance, ε_g, of a gas layer will be complex. We have to account for the gases' absorption bands as well as the layer's thickness and density. Such predictions can be done, but the calculations are complicated. For making simpler (but less accurate) estimates, correlations of ε_g have been developed.

Such correlations are based on the following model: An isothermal gas of temperature T_g and thickness L is bounded by walls at the single temperature T_w. The gas consists of a small fraction of an absorbing species (say CO_2) mixed into a nonabsorbing species (say N_2). If the absorbing gas has a partial pressure p_a and the mixture has a total pressure p, the correlation takes this form:

$$\varepsilon_g = \text{fn}(p_a L, T_g, p) \qquad (10.55)$$

The parameter $p_a L$ is a measure of the layer's optical depth. The parameters T_g and p account for changes in the absorption bands with temperature and pressure.

Hottel and Sarofim [10.14] provided correlations for CO_2 and H_2O, built from research done by Hottel and others before 1960. Later, additional data were obtained by many other investigators; and, in 2015 and 2016, Alberti et al. [10.15, 10.16] published more accurate correlations. Those correlations follow Hottel's framework and take the form

$$\varepsilon_g(p_a L, T_g, p) = \varepsilon^0(p_a L, T_g) \times C(p, p_a L, T_g) \qquad (10.56)$$

The function ε^0 is the *standard emissivity* for a total pressure of $p = 1$ atm with a very small partial pressure, p_a, of the absorbing species. This function is plotted in Figs. 10.22 and 10.23 for CO_2 and H_2O, respectively.

The second function, C, is the *pressure correction factor*, which accounts for different values of p_a or p (see Figs. 10.24 and 10.25 on pages 591 and 592). The pressure correction factor is greatest at low temperatures and has a value closer to one at high temperatures.

When both CO_2 and H_2O are present in the same mixture, we can add their emissivities. However, the absorption bands of the two gases overlap. For example, both gases absorb strongly around 2.7 μm. As a result, the emissivity is a bit less than obtained by addition, and a correction must be subtracted (see [10.17] for details). When the optical depth is $\lesssim 10$ bar-cm and the total pressure is $\lesssim 10$ atm, the correction is $\lesssim 0.01$

To find the net heat transfer between the gas and the walls, we must also find the total absorptance, α_g, of the gas for radiation from the walls. Despite the equality of the monochromatic emittance and absorptance, ε_λ and α_λ, the total values, ε_g and α_g, will not generally be equal because the absorbed radiation may come from a wall at a different temperature than the gas and with a different wavelength distribution. Hottel and Sarofim show that α_g may be estimated from the correlation for ε_g as follows:[6]

$$\alpha_g = \varepsilon_g\left(p_a L \frac{T_w}{T_g}, p, T_w\right) \times \left(\frac{T_g}{T_w}\right)^{1/2} \qquad (10.57)$$

Finally, we need an appropriate value of L for a given enclosure. The preceding correlations for ε_g and α_g are based a one-dimensional path of length L through the gas. Even for a pair of flat plates a distance ℓ apart, the choice of length is not obvious since radiation can travel much farther than ℓ if it follows a path that is not perpendicular to the plates.

For enclosures that have black walls at a uniform temperature, we can use an effective path length, L_0, called the *geometrical mean beam length*,

---

[6]Hottel originally recommended replacing the exponent ½ by 0.65 for CO_2 and 0.45 for H_2O. Both theory, and later work on scaling rules, suggest keeping the value ½ [10.18].
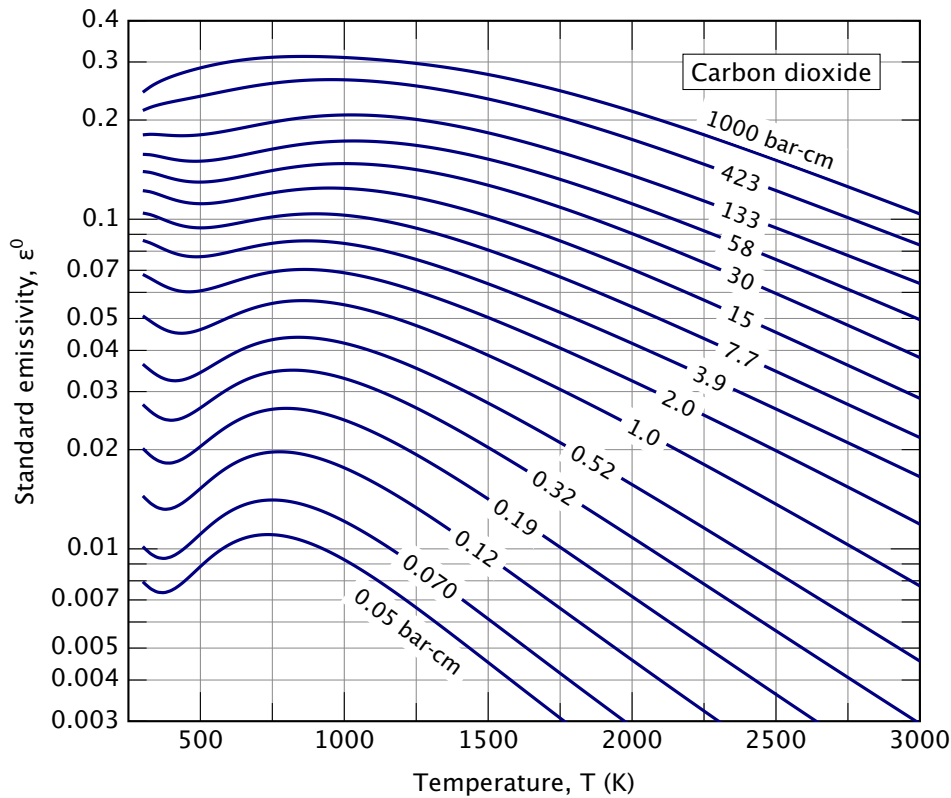
Figure 10.22 Standard emissivity, ε^0, of CO_2 in N_2 or air at
1 atm [10.15].

to represent both the volume and shape of a gaseous region.

$$L_0 \equiv \frac{4\,(\text{volume of gas})}{\text{boundary area that is irradiated}} \tag{10.58}$$

Thus, for two infinite parallel plates a distance ℓ apart, $L_0 = 4A\ell/2A = 2\ell$.
Some other values of L_0 for gas volumes exchanging heat with all points
on their boundaries are in Table 10.4.

   These values of L_0 are appropriate when the gas has a small optical
depth. For cases where the gas is more strongly absorbing, better accuracy
can be obtained by replacing the constant 4 in eqn. (10.58) by 3.6, which
lowers the mean beam length by 10% [10.5].
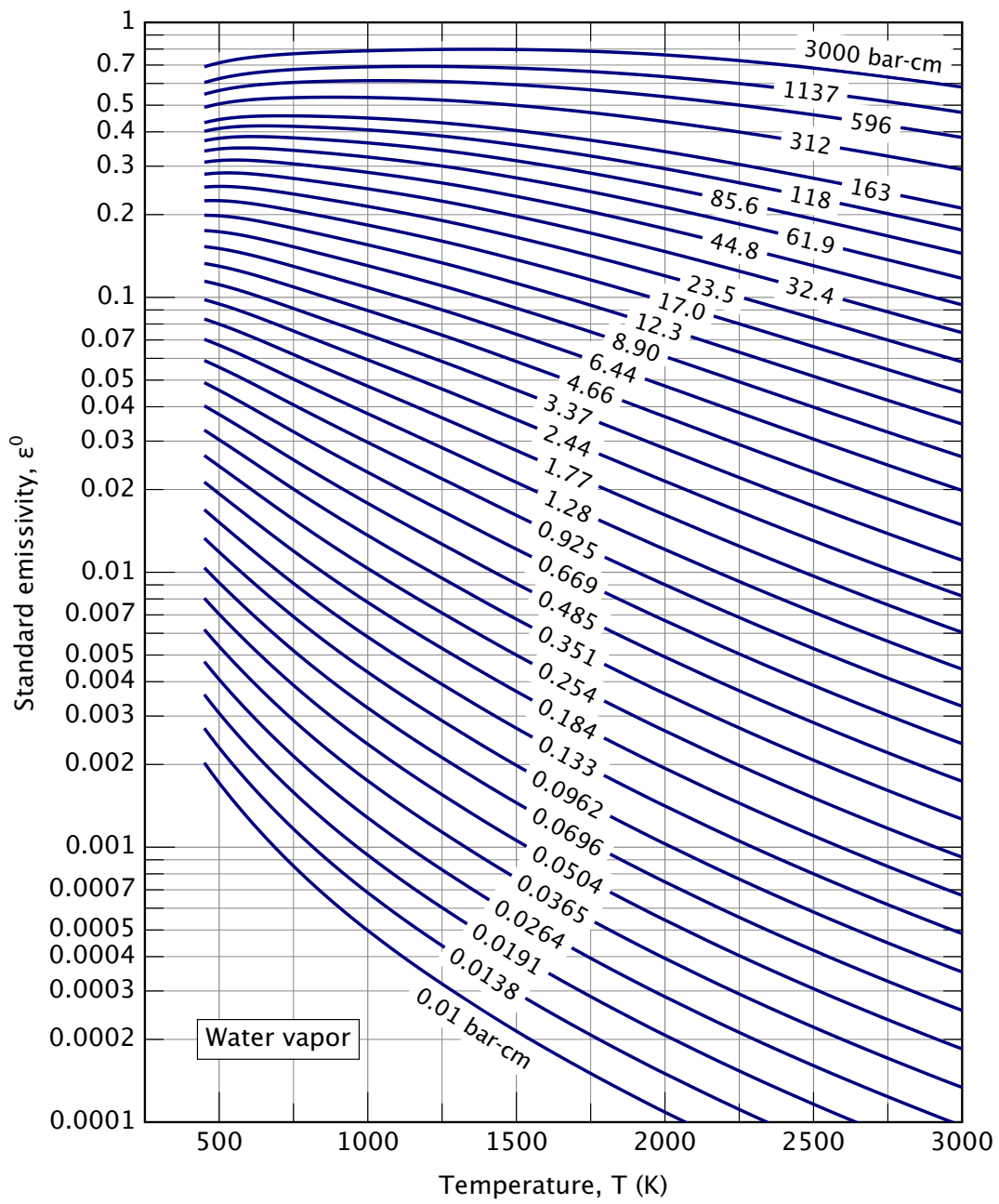
Figure 10.23 Standard emissivity, ε^0, of H_2O in N_2 or air at 1 atm [10.16].

(a) $T = 500\,\mathrm{K}$

(b) $T = 800\,\mathrm{K}$

(c) $T = 1000\,\mathrm{K}$

(d) $T = 1500\,\mathrm{K}$
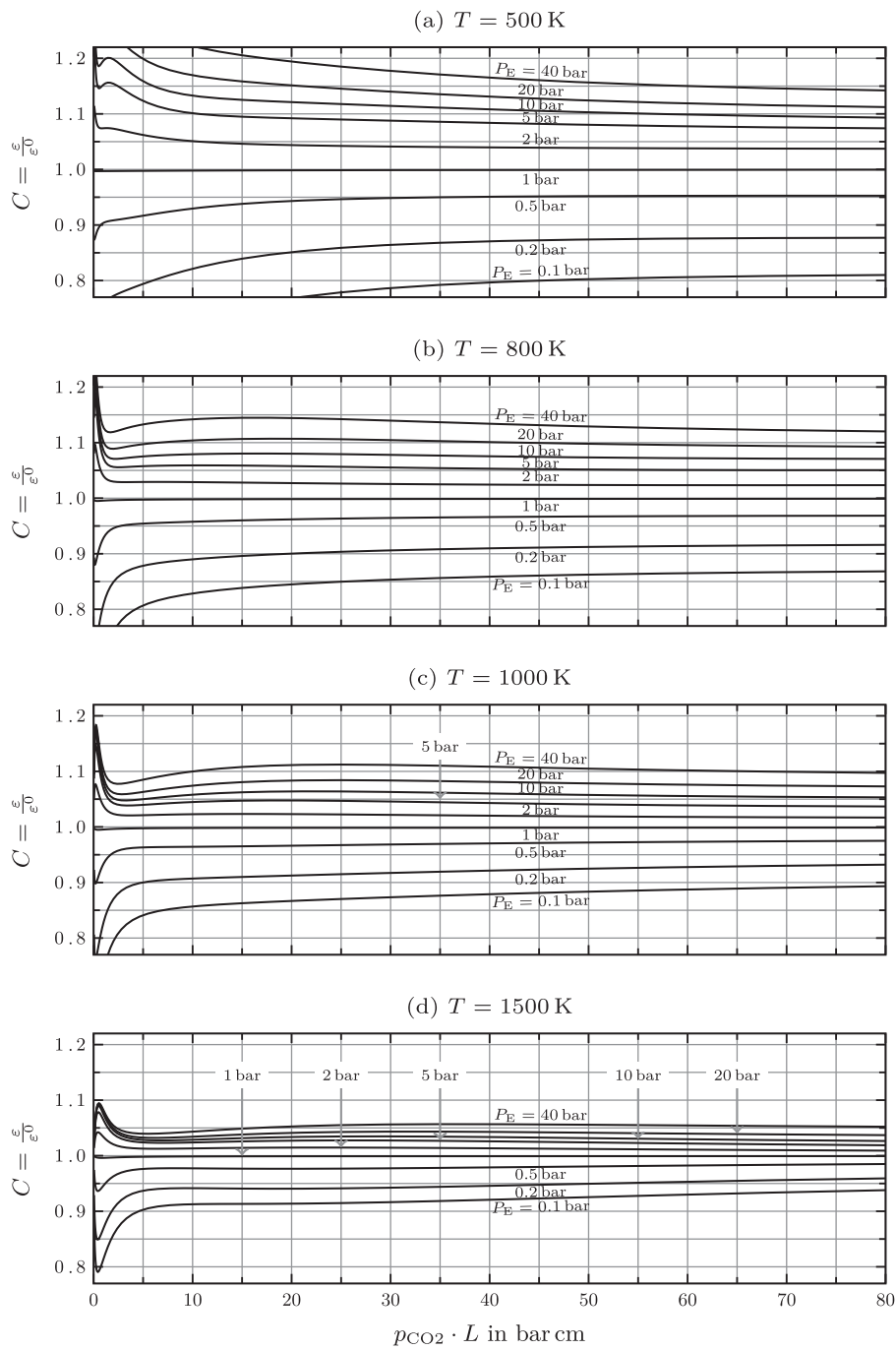
Figure 10.24 Pressure correction factor C for CO_2 as a function of $p_{CO_2}L$ for various pressures [10.15]. The effective pressure for CO_2 is calculated as: $P_E = p + 0.28\,p_{CO_2}$. (Reprinted with permission of Elsevier.)
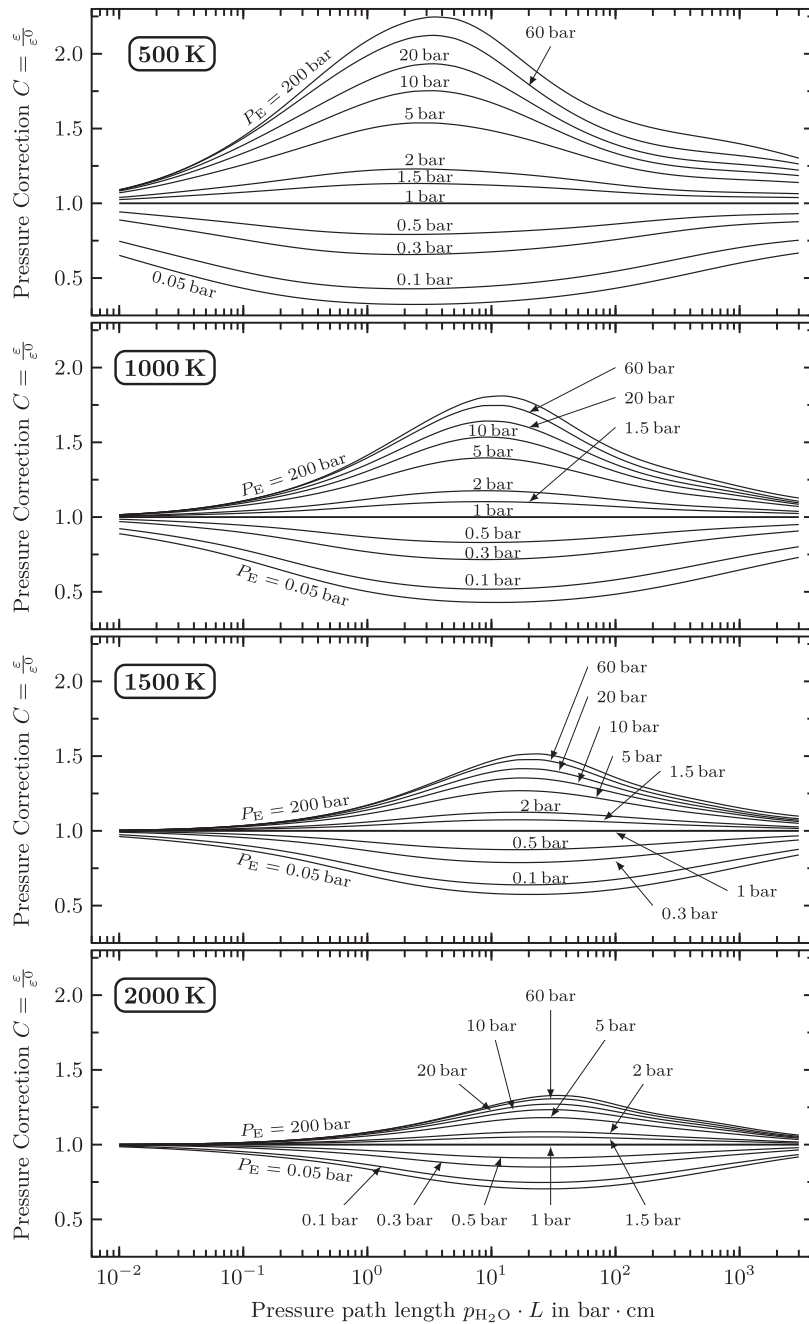
Figure 10.25 Pressure correction factor C for H_2O as a function of $p_{H_2O}L$ for various pressures [10.16]. The effective pressure for H_2O is calculated as: $P_E = p(1 + 5x_{H_2O})$ where x_{H_2O} is the mole fraction of water vapor. (Reprinted with permission of Elsevier.)

Table 10.4 Mean beam length, L_0, for several geometries

Configuration	L_0
Cube of side ℓ	$2\ell/3$
Sphere of diameter D	$2D/3$
Infinite cylinder of diameter D	D
Cylinder with length equal to diameter D	$2D/3$

We are now in position to treat a problem in which hot gases (say the products of combustion) radiate to a black container. Consider the following example.

Example 10.11

A long cylindrical combustor 40 cm in diameter contains a gas at 1200°C consisting of 0.8 atm N_2 and 0.2 atm CO_2. The combustor walls are black. What is the net heat radiated to the walls if they are at 300°C?

SOLUTION. Let us first obtain ε_g. From Table 10.4, $L_0 = D = 40$ cm. We have a total pressure of $p = 1.0$ atm, $p_a = p_{CO_2} = 0.2$ atm $= 0.203$ bar, and $T_g = 1473$ K. With $p_a L = (0.203)(40) = 8.11$ bar-cm, Fig. 10.22a gives ε^0 as 0.084 and Fig. 10.24 gives $C \cong 1$, so $\varepsilon_g = 0.085$.

Next, we use eqn. (10.57) to obtain α_g. With $T_w = 573$, and $p_a L(T_w/T_g) = 3.16$ bar-cm, the appropriate value of ε_g is 0.073:

$$\alpha_g = (0.073)\left(\frac{1200 + 273}{300 + 273}\right)^{0.5} = 0.12$$

The optical depth of the gas is low, so α_g and ε_g are small.

Now we can calculate $Q_{\text{net}_{g\text{-}w}}$. For problems in which one wall surrounds one gas, the mean beam length accounts for all geometrical effects, and no separate view factor is required. The net heat transfer to the wall is calculated using the surface area of the wall:

$$
\begin{aligned}
Q_{\text{net}_{g\text{-}w}} &= A_w\left(\varepsilon_g \sigma T_g^4 - \alpha_g \sigma T_w^4\right) \\
&= \pi(0.4)(5.67 \times 10^{-8})\left[(0.084)(1473)^4 - (0.12)(573)^4\right] \\
&= 27 \text{ kW/m} \qquad \blacksquare
\end{aligned}
$$

Total the mean beam length and the scaling rule for α_g, eqn. (10.57), are simple but crude tools for dealing with gas radiation. They were introduced in the mid-twentieth century to facilitate engineering calculations without using numerical methods. They oversimplify both the geometry and the wavelength dependence of radiation in molecular gases.

Much more accurate tools are available [10.4, 10.5, 10.19]. Band models of radiation efficiently account for wavelength dependence by considering only discrete "bands" of wavelength. The zonal method for gas-filled enclosures is similar to the approach of Sect. 10.4: the enclosure is divided into isothermal volumes and surfaces, and pairwise energy balances formed among the zones. The most versatile technique is the previously-mentioned Monte Carlo method, which tracks a statistical ensemble of photons as they travel from point-to-point. The Monte Carlo method can tackle nongray, nondiffuse, and nonisothermal walls that contain nongray, scattering, and nonisothermal gases.

And finally, gaseous radiation can be less important than we might first think. Consider a bright orange candle flame and a "cold-blue" hydrogen flame. Both have a lot of water vapor in them, as a result of burning oxygen. But the candle warms our hands while the hydrogen flame does not, even though the temperature in the hydrogen flame is higher. It turns out that what radiates both heat and light from the candle is not gas, but soot—small solid particles of almost black-body carbon. The CO_2 and H_2O in the candle flame actually radiate relatively little heat.

10.6   Solar energy

The sun

The sun continually irradiates the earth at a rate of about 1.74×10^{14} kW. If we imagine this energy to be distributed over a circular disk with the earth's diameter, the solar irradiation is about 1361 W/m^2, as measured by satellites above the atmosphere [10.20]. Much of this energy reaches the ground, where it sustains the processes of life.

The temperature of the sun varies from tens of millions of kelvin in its core to between 4000 and 6000 K at its surface, where most of the sun's thermal radiation originates. The wavelength distribution of the sun's energy is not quite that of a black body, but it may be approximated as such. A straightforward calculation (see Problem 10.49) shows that a black body of the sun's size and distance from the earth would produce the same irradiation as the sun if its temperature were 5772 K.

The solar radiation reaching the earth's surface is always less than that above the atmosphere owing to atmospheric absorption and the earth's curvature. Solar radiation usually arrives at an angle of less than 90° to the surface because the sun is rarely directly overhead. We have seen that a radiant heat flux arriving at an angle less than 90° is reduced by the cosine of that angle (Fig. 10.4). The sun's angle varies with latitude, time of day, and day of year. Trigonometry and data for the earth's rotation can be used to find the appropriate angle.

Figure 10.2 shows the reduction of solar radiation by atmospheric absorption for one particular set of atmospheric conditions. In fact, when the sun's rays pass through the atmosphere at a low angle (near the horizon), the path of radiation through the atmosphere is longer, providing relatively more opportunity for atmospheric absorption and scattering. Additional moisture in the air can increase the absorption by H_2O, and, of course, clouds can dramatically reduce the solar radiation reaching the ground.

The consequence of these various effects is that the solar radiation received on the ground is almost never more than 1200 W/m^2 and is often only a few hundred W/m^2. Extensive data are available for estimating the ground level solar irradiation at a given location, time, and date [10.21].

The distribution of the Sun's energy and atmospheric irradiation

Figure 10.26 shows what becomes of the solar energy that impinges on the earth if we average it over the year and the globe, taking account of all kinds of weather. Only 45% of the sun's energy actually reaches the earth's surface. The mean energy received is about 235 W/m^2 if averaged over the surface and the year. The lower left-hand portion of the figure shows how this energy is, in turn, all returned to the atmosphere and to space.

The solar radiation reaching the earth's surface includes direct radiation that has passed through the atmosphere and diffuse radiation that has been scattered, but not absorbed, by the atmosphere. Atmospheric gases also irradiate the surface. This gas irradiation is quite important to maintaining the temperature of objects on the surface.

In Section 10.5, we saw that the energy radiated by a gas depends upon the depth of the gas, its temperature, and the molecules present in it. The emittance of the atmosphere has been characterized in detail [10.22–10.24]. For practical calculations, however, the sky may conveniently be

47% reaches the earth's surface

47% is transmitted to the earth directly and by diffuse radiation

30% is reflected back to space

23% is absorbed in the atmosphere

Radiation that reaches the outer atmosphere from the sun

Sensible heat transfer to atmosphere

Net radiation from surface

Evaporation
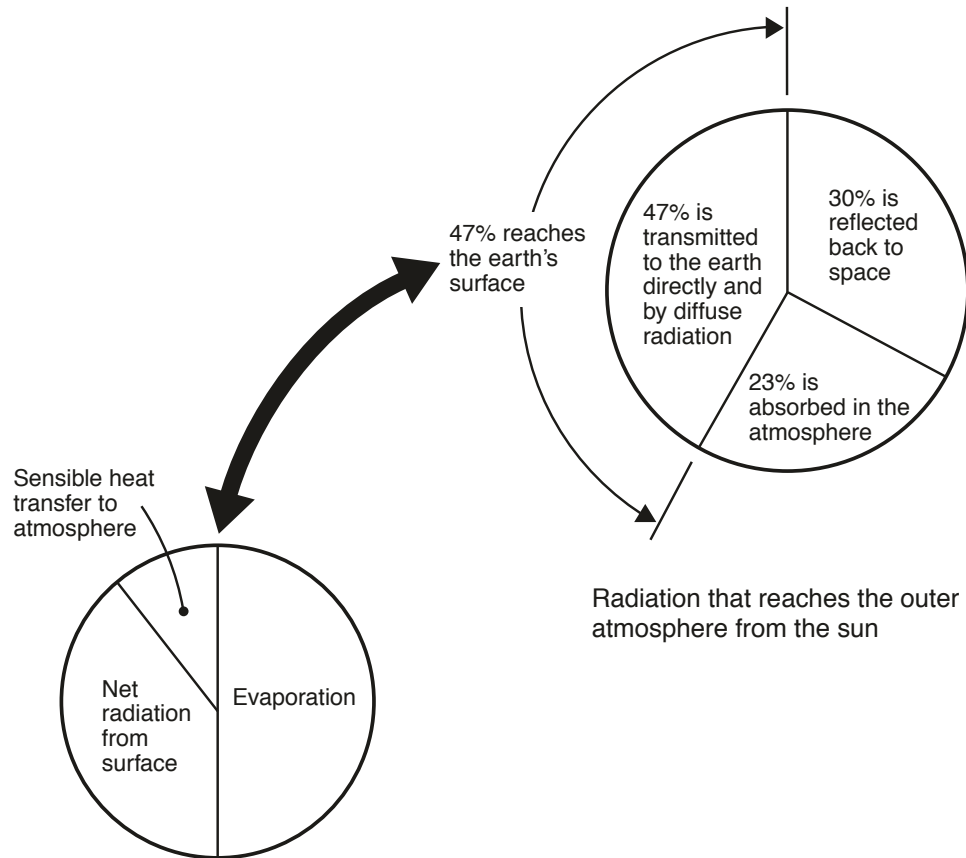
The flow of energy from the earth's surface back to - and through - the earth's atmosphere

Figure 10.26 The approximate distribution of the flow of the sun's energy to and from the earth's surface [10.22].

treated as a black radiator having some appropriate temperature. This effective *sky temperature* usually lies between 5 and 30 K below the ground level air temperature.

The sky temperature decreases as the amount of water vapor in the air goes down. For cloudless skies, the sky temperature may be estimated

using the dew-point temperature, T_{dp}, and the hour past midnight, t:

$$T_{sky} = T_{air} \Big[0.711 + 0.0056 \, T_{dp}$$
$$+ \, 7.3 \times 10^{-5} \, T_{dp}^2 + 0.013 \cos(2\pi t/24) \Big]^{1/4} \quad (10.59)$$

where T_{sky} and T_{air} are in kelvin and T_{dp} is in °C. This equation applies for dew points between -20°C and $+30$°C [10.25].

It is fortunate that sky temperatures are relatively warm. In the absence of an atmosphere, not only would more of the sun's radiation reach the ground during the day, but at night heat would radiate directly into the bitter cold of outer space. Such conditions prevail on the Moon, where average daytime surface temperatures are about 110°C while average nighttime temperatures plunge to about -150°C.

Selective emitters, absorbers, and transmitters

We have noted that most of the sun's energy lies at wavelengths near the visible region of the electromagnetic spectrum and that most of the radiation from objects at temperatures typical of the earth's surface is on much longer, infrared wavelengths (see pg. 554). One result is that materials may be chosen or designed to be selectively good emitters or reflectors of both solar and infrared radiation.

Table 10.5 shows the infrared emittance and solar absorptance for several materials. Among these, we identify several particularly selective solar absorbers and solar reflectors. The selective absorbers have a high absorptance for solar radiation and a low emittance for infrared radiation. Consequently, they do not strongly reradiate the solar energy that they absorb. The selective solar reflectors, on the other hand, reflect solar energy strongly and also radiate heat efficiently in the infrared. Solar reflectors stay much cooler than solar absorbers in bright sunlight.

A comprehensive review of selective absorber materials has been given by Kennedy [10.26]. Coatings with solar absorptance above 90% and infrared emittance below 10% are commercially available. Materials that radiate strongly between 8 and 13 μm take advantage of the higher atmospheric transmissivity in that band to further cool surfaces [10.27]. In fact, certain aerogel coatings with high solar reflectivity, high infrared transmittance, and low thermal conductivity can radiately cool surfaces to *below* ambient temperature [10.28].

Table 10.5 Solar absorptance and infrared emittance for several surfaces near 300 K [10.5, 10.21].

Surface	α_{solar}	ε_{IR}
Aluminum, pure	0.09	0.1
Carbon black in acrylic binder	0.94	0.83
Copper, polished	0.3	0.04
Selective Solar absorbers		
Black Cr on Ni plate	0.95	0.09
CuO on Cu (Ebanol C)	0.90	0.16
Nickel black on steel	0.81	0.17
Sputtered cermet on steel	0.96	0.16
Selective Solar Reflectors		
Magnesium oxide	0.14	0.7
Snow	0.2–0.35	0.82
White paint		
Acrylic	0.26	0.90
Zinc Oxide	0.12–0.18	0.93

Example 10.12

In Section 10.2, we discussed white paint on a roof as a selective solar absorber. Consider now a barn roof under a sunlit sky. The solar radiation on the plane of the roof is 600 W/m^2, the air temperature is 35°C, and a light breeze produces a convective heat transfer coefficient of $\overline{h} = 8$ W/m^{2}K. The sky temperature is 18°C. Find the temperature of the roof if it is painted with a non-selective black paint having $\varepsilon = 0.9$. By how much would the roof temperature be lowered if it were repainted with white acrylic paint?

SOLUTION. Heat loss from the roof to the inside of the barn will lower the roof temperature. Since we don't have enough information to evaluate that loss, we can make an upper bound on the roof temperature by assuming that no heat is transferred to the interior. Then, an energy balance on the roof must account for radiation absorbed from the sun and the sky and for heat lost by convection and reradiation:

$$\alpha_{solar}q_{solar} + \varepsilon_{IR}\sigma T_{sky}^4 = \overline{h}\left(T_{roof} - T_{air}\right) + \varepsilon_{IR}\sigma T_{roof}^4$$

Rearranging and substituting the given numbers,

$$8\left[T_{\text{roof}} - (273 + 35)\right] + \varepsilon_{\text{IR}}\left(5.67 \times 10^{-8}\right)\left[T_{\text{roof}}^4 - (273 + 18)^4\right]$$
$$= \alpha_{\text{solar}}(600)$$

For the non-selective black paint, $\alpha_{\text{solar}} = \varepsilon_{\text{IR}} = 0.90$. Solving by iteration, we find

$$T_{\text{roof}} = 338 \text{ K} = 65°\text{C}$$

For white acrylic paint, from Table 10.5, $\alpha_{\text{solar}} = 0.26$ and $\varepsilon_{\text{IR}} = 0.90$. We find

$$T_{\text{roof}} = 312 \text{ K} = 39°\text{C}$$

The white painted roof is only a few degrees warmer than the air. The roof temperature would be lowered by 24°C if it were repainted. ∎

Ordinary window glass is a very selective transmitter of solar radiation. Glass is nearly transparent to wavelengths below 2.7 μm or so. More than 90% of the incident solar energy passes through. At longer wavelengths, in the infrared, glass is virtually opaque to radiation. Thus, solar energy passing through a window cannot pass back out as infrared reradiation. This is precisely why we make greenhouses out of glass.

A *greenhouse* is a structure in which we use glass to capture solar energy in the interior of a lower temperature space. The glass lets sunlight enter the space, it stops cool air from flowing into the space, and it absorbs infrared reradiation from the interior rather than letting it pass directly back to the sky. All these factors help make the interior warmer than the outside.

The atmospheric greenhouse effect and global warming

The atmosphere creates a *greenhouse effect* on the earth's surface that is very similar to that caused by a pane of glass. Solar energy passes through the atmosphere, and most of it arrives on wavelengths between 0.3 and 3 μm. The earth's surface, having a mean temperature of 15°C or so, radiates mainly on infrared wavelengths between 4 and 40 μm.

Certain atmospheric gases have strong absorption bands at these longer wavelengths. Those gases absorb energy radiated from the surface, then reemit it toward both the surface and outer space. That reduces the net rate of radiative heat loss from the surface to outer space. The result is that the surface stays some 30 K warmer than the atmosphere.

In effect, the atmosphere functions as a radiation shield against infrared heat loss to space.

The gases mainly responsible for this atmospheric greenhouse effect are CO_2, H_2O, CH_4, N_2O, O_3, and some chlorofluorocarbons and hydrofluorocarbons that are used as refrigerants [10.29]. If the concentration of these gases rises or falls, the strength of the greenhouse effect will change and the surface temperature will also rise or fall. All but the fluorocarbons are partly generated by natural processes: H_2O by evaporation, CO_2 by animal and microbial respiration, CH_4 through decay processes, and so on.

Human activities, however, have significantly increased the concentrations of all of these gases. Fossil fuel combustion increased the CO_2 concentration by more than 30% during the twentieth century. Methane concentrations have risen through leakage of hydrocarbon fuels, rice agriculture, and livestock production. In fact, CO_2 levels for the 800,000 years prior to the industrial age fluctuated between 160 and 300 ppm; but, as of May 2019, the CO_2 level had reached 415 ppm and was still rising steadily [10.30].

Earth's surface temperature has risen along with the concentrations of these gases. An increase of about 0.8 K occurred during the twentieth century, with 0.5 K of that change coming between 1950 and 2000 (see Fig. 10.27). This trend has continued to accelerate. Data showing this rise are extensive. They are derived from multiple sources. And they have been the subject of very detailed scrutiny [10.31–10.33].

The question of how much of the rise is the result of anthropogenic greenhouse gases was, for a long time, the focus of an important, although often heated, public debate. And indeed, many factors must be considered in examining the causes of Earth's temperature rise because of the complex coupling between the atmosphere, the oceans, and the land. Some illustrations follow.

The concentration of water vapor in the atmosphere rises with increasing surface temperature, amplifying any warming trend by blocking more infrared radiation. Increased cloud cover has both warming and cooling effects. Atmospheric aerosols (two-thirds of which result from sulfate and carbon pollution from fossil fuels) significantly offset the warming effect of greenhouse gases [10.34]. The melting of polar ice caps as temperatures rise reduces the planet's reflectance, or *albedo*, allowing more solar energy to be absorbed. And the melting of arctic permafrost is likely to release vast amounts of CO_2, CH_4, and N_2O into the atmosphere, accelerating warming. The oceans have absorbed both energy and CO_2, slowing the rates of change up to now. All of these factors must be built
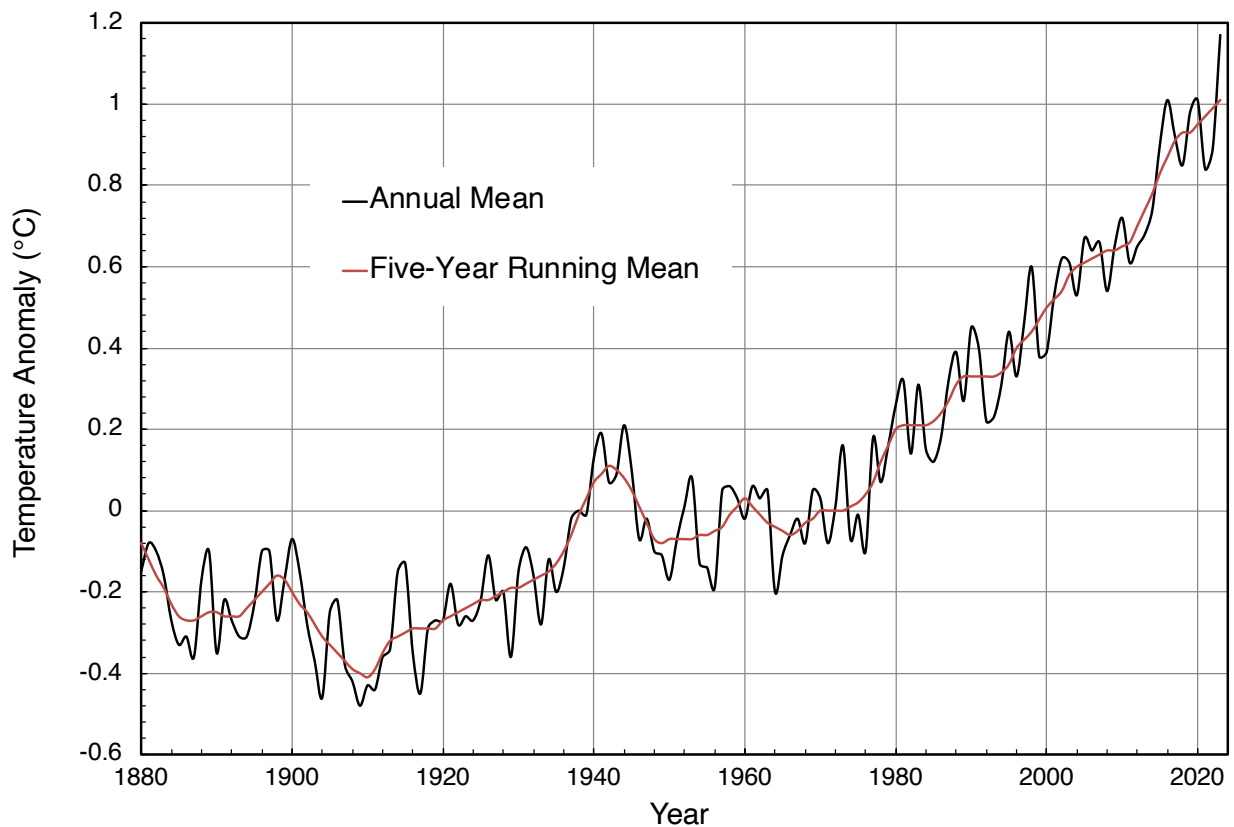
Figure 10.27 Global surface temperature change relative to the mean temperature from 1951–1980 (Courtesy of the NASA Goddard Institute for Space Studies [10.31, 10.32]).

into an accurate assessment of gas emission and climate change (see, for example, [10.35]).

Notice that many of these effects are examples of *positive feedback*—processes that result in their own amplification. Melting polar ice reduces solar reflectance and thawing tundra releases more greenhouse gases, both then increasing the rates of warming and accelerating melting...

The data and the associated scientific research overwhelmingly show that the temperature rise in Fig. 10.27 is caused by human activity, mainly through burning fossil fuels [10.33]. And, despite claims by some that we cannot pin down the reason for this global change, the mechanism of cause and effect is simple: the earth's infrared cooling is impeded by greenhouse gases, so earth's temperature rises to keep radiative equilibrium with the sun and deep space.

Computer simulations project a continuing temperature rise in the present century, based on various scenarios for future fossil fuel use and future government policies to reduce greenhouse gas emissions. The outlook is not very positive, with best estimates of twenty-first century warming ranging from roughly 1.8–4.0 K. The likely impacts vary around the planet, but they include: impaired food crop production; rising sea levels; more frequent droughts, storms, fires, and floods; and less reliable water supply, especially for densely populated areas [10.36–10.38].

The use of solar power

Solar energy offers a clean alternative to fossil fuels, available in all parts of the world. Since the middle of the 20th century, intensive research and development has greatly increased the efficiency, and lowered the costs, of solar technology.

Large-scale solar electricity production is challenging. Suppose that we aim to replace an 800 MW fossil power plant with photovoltaic electricity. If the average intensity of sunlight over an 8 hr day is 615 W/m² and a representative photovoltaic panel has 15% efficiency, we need roughly 26 square kilometers (10 square miles) of collector area to match the steady, 24-hour output of the power plant. Yet, plants of this scale have been built in sunny parts of the world.

To provide steady power—day and night, rain or shine—we would also need to store energy, perhaps with an array of batteries or a system that pumps water to a higher elevation during the day and then releases it through a turbine at night. But even without storage, solar electricity can help meet daytime needs, with other power sources kicking in at night.

Apart from electricity generation, solar energy is used directly to heat water or air. The energy efficiency increases to as much as 60–70% for direct thermal collection, versus 10–20% for the photovoltaic panels widely deployed for electrical power. Solar water heating, to moderate temperatures (50 to 90°C), is most often used in houses or buildings.

Figure 10.28 shows a representative water-heating solar collector. Solar radiation passes through one or more glass plates and impinges on a metal plate that absorbs the solar wavelengths. The absorber plate is usually a selective solar absorber, perhaps blackened copper. The glass plates might be treated with anti-reflective coatings, raising their solar transmissivity to 98% or more. The absorber plate reemits some heat as long-wavelength infrared radiation, but the glass, which is nearly opaque to these wavelengths, traps the reradiated heat in the collector. Multiple
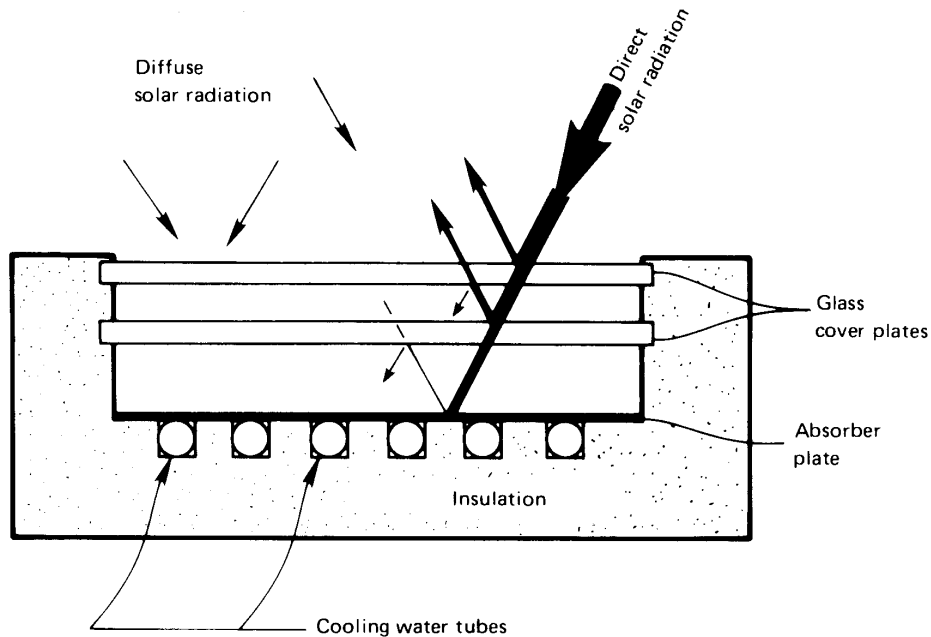
Figure 10.28 A flat-plate solar collector.

layers of glass reduce both convective and reradiative and losses from the absorber plate to the surrounding environment.

Water flowing through tubes brazed to the absorber plate carries the energy away for use. The flow rate is chosen to give a temperature rise appropriate to the end use.

In another configuration, a narrow absorber plate sits inside an evacuated cylindrical tube. The vacuum eliminates convective loss from the absorber, raising thermal efficiency. A row of tubes form a single collector. Due to the space between the tubes, part of the frontal area of the collector does not absorb sunlight, offsetting the advantage of the vacuum.

If the working fluid is to be brought to a fairly high temperature, the direct radiation from the sun must be focused from a large area down to a much smaller one, using reflecting mirrors. Collectors equipped with a small parabolic or Fresnel reflector, focused on a water pipe, can heat the water to between 100 and 200°C. Large arrays of mirrors focused onto a central receiving tower can achieve temperatures of 500°C or more, suitable for driving a Rankine cycle to generate electricity. In any scheme intended to produce electrical power with a conventional thermal cycle, energy must be concentrated with an area ratio on the order of 1000 : 1 to

achieve a practical cycle efficiency. Solar energy systems, and their design and deployment, are discussed in detail in Refs. [10.21] and [10.39].

A question of overriding concern for the 21st century is "How much of the renewable energy that reaches Earth can we safely utilize?" Of the 1.74×10^{14} kW arriving from the sun, 33% is simply reflected back into outer space. If we were able to collect and use the remainder, 1.16×10^{14} kW, before it too was reradiated to space, each of the 7.7 billion or so people on the planet would have 15 MW at his or her disposal. The vast majority of that power must obviously be used to sustain the natural world around us, but some comparisons can provide a perspective.

Total power consumption in the USA averaged roughly 3.2×10^9 kW in 2015. Dividing by that year's population of 320 million people gives a per capita consumption of roughly 10 kW. Worldwide, energy was consumed at a rate about 1.7×10^9 kW. That means that world energy consumption was near 0.01% of the renewable energy passing into and out of Earth's ecosystem. This consumption has increased steadily for many years, at an average annual rate of 2%, because many countries that once used very little energy are rapidly developing to use far more.

We must also bear in mind two aspects of this 0.01% figure. First, it is low enough that we could conceivably aim to get all of our energy from renewable sources. Second, while 0.01% seems small, the absolute amount of power it represents is enormous. Just how much renewable energy we can claim without creating new ecological problems is unknown.

Fossil fuels account for most of the world's energy consumption. But gas emissions from the production and use of those fuels are a major contributor to climate change. Our long-term hope for a sustainable energy supply will depend, in considerable measure, on increasing our use of solar power, wind power, and other low carbon energy sources. Nuclear fission remains an important option, if we are willing to adopt some means of nuclear waste disposal. Nuclear fusion—the process by which we might create mini-suns upon the earth—is also a hope for the future. And under any scenario, we serve our best interests by raising the efficiency of all our energy consuming technologies.

Problems

10.1 What will ε_λ of the sun appear to be to an observer on the earth's surface for $\lambda = 0.2$ μm and 0.65 μm? Refer to Fig. 10.2. [$\varepsilon_{0.65 \text{ μm}} \simeq 0.77$]

10.2 Plot e_{λ_b} against λ for $T = 300$ K and $10,000$ K with the help of eqn. (1.30). About what fraction of the energy from each black body is visible? [41% at $10,000$ K]

10.3 A 0.6 mm diameter wire, with $\varepsilon = 0.85$, is drawn out through a mandril at $950°$C. The wire then passes through a long cylindrical shield of commercial aluminum sheet, 7 cm in diameter. The shield is horizontal in still air at $25°$C. What is the temperature of the shield? Is it reasonable to neglect natural convection inside or radiation outside the shield? [$T_{\text{shield}} = 153°$C]

10.4 A 1 ft^2 shallow pan with adiabatic sides is filled to the brim with water at $32°$F. It radiates to a night sky whose temperature is $-18°$F, while a $50°$F breeze blows over it at 1.5 ft/s. Will the water freeze or warm up?

10.5 An alcohol-in-glass thermometer is held vertically, with bulb down, in a room with air at $10°$C and walls at $27°$C. What temperature will the thermometer read if everything can be considered black? State your assumptions.

10.6 Rework Problem 10.5, taking the room to be wallpapered and considering the thermometer to be nonblack. [Not much change]

10.7 Two thin aluminum plates, the first polished and the second painted black, are placed horizontally outdoors, where they are cooled by air at $10°$C. The heat transfer coefficient is 5 W/m^{2}K on both the top and the bottom. The sun irradiates the top with 750 W/m^2, and the top radiates to the sky at 250 K. The earth below the plates is black and at $10°$C. Find the equilibrium temperature of each plate. [One plate is at $12°$C]

10.8 An instrument holder of 98% pure aluminum, 1 cm in diameter and 16 cm in length, protrudes from a small housing on an orbital space vehicle. The holder "sees" almost nothing but outer space at an effective temperature of 30 K. The base of the holder is $0°$C and you must find the temperature of the sample at its tip. It will help if you note that aluminum is used, so that the temperature of the tip stays quite close to that of the root. *Hint*: Recall Section 4.5. [$T_{\text{tip}} = -0.7°$C]

10.9 The bottom of the box shown in Fig. 10.29 is a radiant heater. The top of the box is open to the surroundings. What percentage of

Figure 10.29 Configuration for Problem 10.9.
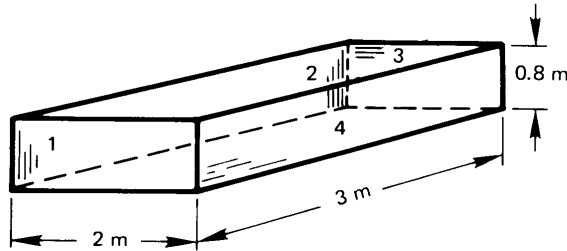
the heat goes out the top? What fraction impinges on each of the four sides? *Hint*: The percentages must add up to 100.

Figure 10.30 Configuration for Problem 10.11.
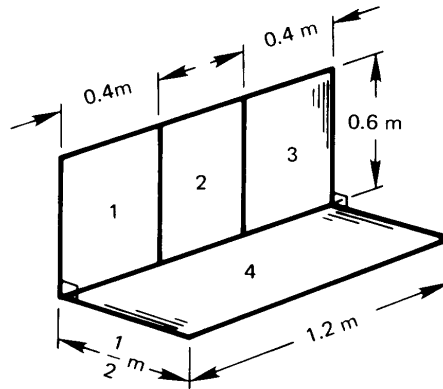
10.10 Consider Fig. 10.11. Find $F_{1-(2+4)}$ and $F_{(2+4)-1}$. [$F_{(2+4)-1} = 0.087$]

10.11 Find F_{2-4} for the surfaces shown in Fig. 10.30. [0.255]

10.12 What is F_{1-2} for the squares shown in Fig. 10.31?

10.13 A particular internal combustion engine has an exhaust manifold at 600°C running parallel to a coolant line at 20°C. If both the manifold and the coolant line are 4 cm in diameter, their centers are 7 cm apart, and if both are approximately black, how much heat will be transferred to the coolant line by radiation? [383 W/m]

Figure 10.31 Configuration for Problem 10.12.
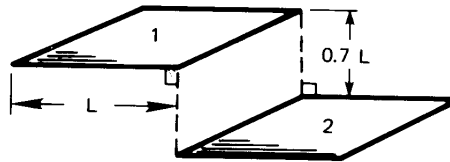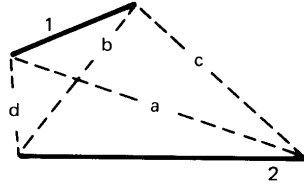
Figure 10.32 Configuration for Problem 10.14.
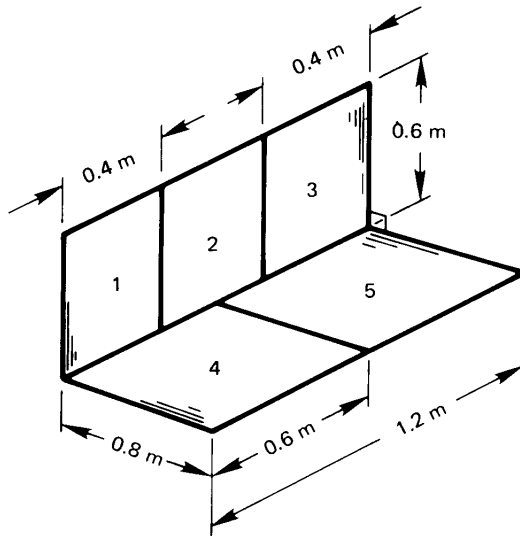
Figure 10.33 Configuration for Problem 10.15.

10.14 Prove that F_{1-2} for any pair of two-dimensional plane surfaces, as shown in Fig. 10.32, is equal to $[(a + b) - (c + d)]/2L_1$. This is called the *string rule* because we can imagine that the numerator equals the difference between the lengths of a set of crossed strings (*a* and *b*) and a set of uncrossed strings (*c* and *d*).

10.15 Find F_{1-5} for the surfaces shown in Fig. 10.33. [0.035]

10.16 Find $F_{1-(2+3+4)}$ for the surfaces shown in Fig. 10.34.

10.17 A cubic box, 1 m on each edge, is black except for one side, which has an emittance of 0.2 and is kept at 300°C. An adjacent side is kept at 500°C. The other sides are insulated. Find Q_{net} inside the box. [2.5 kW]

10.18 Rework Problem 10.17, but this time set the emittance of the insulated walls equal to 0.6. Compare the temperature of the
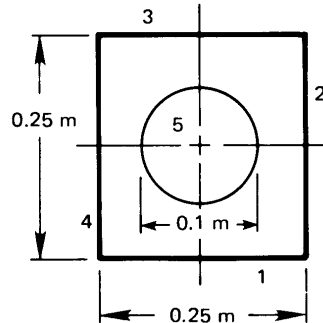
Figure 10.34 Configuration for Problem 10.16.

insulated walls to the value you would get if the walls were black. [479°C]

10.19 An insulated black cylinder, 10 cm in length and with an inside diameter of 5 cm, has a black cap on one end and a cap with an emittance of 0.1 on the other. The black end is kept at 100°C and the reflecting end is kept at 0°C. Find Q_{net} inside the cylinder and the temperature of the insulated wall.

10.20 Rework Example 10.3 if the shield has an inside emittance of 0.34 and the room is at 20°C. How much cooling must be provided to keep the shield at 100°C? [551 W]

10.21 A smooth gray object of emittance ε_1 and area A_1 and does not view itself and sits in a much larger isothermal environment, A_2. Suppose that the object is roughened by making many small cavities covering its entire surface, without changing the radiative properties of the material. The rough surface now has an area $A_r > A_1$. The projected area of the rough surface is a smooth surface that just touches the peaks of the cavities, and it has the same area, A_1, as the original smooth surface. Starting with eqn. (10.26), show that the roughened surface emits radiation to the surroundings as if the original smooth surface had become "blacker". Further show that the effective emittance after roughening is bounded between ε_1 and 1. *Hint:* Because the surroundings are effectively black, the value of A_2 does not affect the heat transfer: shrink A_2 until it reaches the projected surface.

10.22 A 30 ft by 40 ft house has a conventional sloping roof with a 30.3° pitch and the peak running in the 40 ft direction. Calculate the

temperature of the roof in 20℃ still air when the sun is overhead: (a) if the roof is made of wooden shingles; and (b) if it is commercial aluminum sheet. The incident solar energy is 670 W/m², the effective sky temperature is 22℃, the roofing materials are gray radiators, and the roof is very well insulated.

10.23 Use the electrical circuit analogy to calculate the radiant heat transfer from a 0.2 m diameter stainless steel hemisphere ($\varepsilon_{ss} = 0.4$) to a copper floor ($\varepsilon_{Cu} = 0.15$) that forms its base. The hemisphere is kept at 300°C and the base at 100°C. [21.24 W]

10.24 A hemispherical indentation in a smooth wrought-iron plate has an 8 mm radius. How much heat radiates from the 40°C dent to the -20°C surroundings? [48% increase relative to a flat surface]

10.25 A conical hole in a block of metal for which $\varepsilon = 0.5$ is 5 cm in diameter at the surface and 5 cm deep. By what factor will the radiation from the area of the hole be changed by the presence of the hole? (This problem can be done to a close approximation using the methods in this chapter if the cone is not very deep and slender. If it is, then the fact that the apex is receiving far less radiation makes it incorrect to use the network analogy.)

10.26 A single-pane window in a large room is 4 ft wide and 6 ft high. The room is kept at 70°F, but the pane is at 67°F owing to heat loss to the colder outdoor air. Find: (a) the heat transfer by radiation to the window; (b) the heat transfer by natural convection to the window; and (c) the fraction of heat transferred to the window by radiation. [(c) 80%]

10.27 Suppose that the window pane temperature is unknown in Problem 10.26. The outdoor air is at 40°F and $\overline{h}$ is 62 W/m²K on the outside of the window. It is nighttime and the effective temperature of the sky is 15°F. Assume $F_{window-sky} = 0.5$. Take the rest of the surroundings to be at 40°F. Find T_{window} and draw the analogous electrical circuit, giving numerical values for all thermal resistances. Discuss the circuit. *Hint:* Your calculation may be simplified by noting that the window is opaque to infrared radiation but offers very little resistance to conduction. Thus, the window temperature is almost the same on the inside and outside.

10.28 A very effective low-temperature insulation is made by evacuating the space between parallel metal sheets. Convection is eliminated,

conduction occurs only at spacers, and radiation is responsible for what little heat transfer occurs. Calculate q between 150 K and 100 K for three cases: (a) two sheets of *highly* polished aluminum; (b) three sheets of highly polished aluminum; and (c) three sheets of rolled sheet steel. Assume that the design minimizes heat conduction.

10.29 Three identical, long black walls, 1 m wide, form an equilateral triangular tube. One wall is held at 400 K, one is at 300 K, and the third is insulated. Find Q W/m and the temperature of the third wall. [$T_{3rd} = 360$ K]

10.30 Two 1 cm diameter rods run parallel, with centers 4 cm apart. One is held at 1500 K and is black. The other is unheated, and $\varepsilon = 0.66$. They are both encircled by a cylindrical black radiation shield at 400 K. Evaluate the heat loss from the rod, and find the temperature of the unheated rod. [281 W/m]

10.31 A small-diameter heater is centered in a large cylindrical radiation shield. Discuss the relative importance of the emittance of the shield during specular and diffuse radiation.

10.32 Two 1 m wide commercial aluminum sheets are joined at a 120° angle along one edge. The back (or 240° angle) sides are insulated. The plates are both held at 120°C. The 20°C surroundings are distant. What is the net radiant heat transfer from the left-hand plate to the right-hand side and to the surroundings? [83 W/m]

10.33 Two parallel disks of 0.5 m diameter are separated by an infinite parallel plate, midway between them, with a 0.2 m diameter hole in it. The disks and the hole are on the same centerline. What is the view factor between the two disks if they are 0.6 m apart?

10.34 An evacuated spherical cavity, 0.3 m in diameter in a zero-gravity environment, is kept at 300°C. Saturated steam at 1 atm is then placed in the cavity. (a) What is the initial radiant heat flux to the steam? (b) Determine how long it will take for $q_{conduction}$ to become less than $q_{radiation}$. Correct for the rising steam temperature if it is necessary to do so. [(b) 0.35 s]

10.35 Verify cases (1), (2), and (3) in Table 10.2 using the string method described in Problem 10.14.

10.36 Two long parallel heaters consist of 120° segments of 10 cm diameter parallel cylinders whose centers are 20 cm apart. The

convex surfaces face each other, symmetrically placed on the plane connecting their centers. Find F_{1-2} using the string method described in Problem 10.14. [F_{1-2} = 0.2216]

10.37 Two long parallel strips of rolled sheet steel lie along sides of an imaginary 1 m equilateral triangular cylinder. One piece is 1 m wide and kept at 20°C. The other is 1/2 m wide, centered in an adjacent leg, and kept at 400°C. The surroundings are distant and they are insulated. Find Q_{net}. *Hint*: You will need a shape factor; it can be found using the method described in Problem 10.14. [2930 W]

10.38 Find the shape factor from the hot to the cold strip in Problem 10.37 using Table 10.2, not the string method. If your instructor asks you to do so, complete Problem 10.37 after you have F_{1-2}.

10.39 Prove that the view factor for the second case in Table 10.3 reduces to that given for the third case in Table 10.2 when the figure becomes very long.

10.40 Show that F_{1-2} for the first case in Table 10.3 reduces to the expected result when plates 1 and 2 are extended to infinity.

10.41 In Problem 2.26 you were asked to neglect radiation in showing that q was equal to 8227 W/m^2 as the result of conduction alone. Discuss the validity of the assumption quantitatively.

10.42 A 100°C sphere with ε = 0.86 is centered within a second sphere at 300°C with ε = 0.47. The outer diameter is 0.3 m and the inner diameter is 0.1 m. What is the radiant heat flux? [433 W/m^2]

10.43 Verify F_{1-2} for case 4 in Table 10.2. *Hint:* This can be done without integration.

10.44 Consider the approximation made in eqn. (10.30) for a small gray object in a large isothermal enclosure. How small must A_1/A_2 be in order to introduce less than 10% error in $\mathcal{F}_{1-2}$ if the small object has an emittance of ε_1 = 0.5 and the enclosure is: a) commercial aluminum sheet; b) rolled sheet steel; c) rough red brick; d) oxidized cast iron; or e) polished electrolytic copper. Assume that both the object and its environment have temperatures in the range of 40 to 90°C.

10.45 Derive eqn. (10.45), starting with eqns. (10.39–10.41).

Table 10.6 Monochromatic absorption coefficient for water

λ (μm)	$\rho\kappa_\lambda$ (cm^{-1})	Color
0.3	0.0067	
0.4	0.00058	violet
0.5	0.00025	green
0.6	0.0023	orange
0.8	0.0196	
1.0	0.363	
2.0	69.1	
2.6–10.0	> 100.	

10.46 (a) Derive eqn. (10.31), which is for a single radiation shield between two bodies. Include a sketch of the radiation network. (b) Repeat the calculation in the case when two radiation shields lie between body 1 and body 2, the second just outside the first.

10.47 Use eqn. (10.32) to find the net heat transfer from between two specularly reflecting bodies that are separated by a specularly reflecting radiation shield. Compare the result to eqn. (10.31). Does specular reflection reduce the heat transfer?

10.48 Some values of the monochromatic absorption coefficient for liquid water, as $\rho\kappa_\lambda$ (cm^{-1}), are listed in Table 10.6 [10.5]. For each wavelength, find the thickness of a layer of water for which the monochromatic transmittance is 10%. On this basis, discuss the colors one might see underwater and water's infrared emittance.

10.49 The sun has a diameter of 1.3914×10^6 km. The earth has a mean diameter of 12,742 km and lies at a mean distance of 1.496×10^8 km from the center of the sun. (a) If the earth is treated as a flat disk normal to the radius from sun to earth, determine the view factor $F_{\text{sun–earth}}$. (b) Use this view factor and the measured solar irradiation of 1361 ± 0.5 W/m^2 to show that the effective black body temperature of the sun is 5772 K [10.20].

10.50 A long, section of cylindrical shell has a radius R, but it does not form a complete circle. Instead, the cylindrical shell forms an arc spanning an angle θ less than 180°. Because the shell is curved, the inside surface of the shell (surface 1) views itself. Derive an expression for the view factor $F_{1\text{-}1}$, and evaluate $F_{1\text{-}1}$ for $\theta = 30°$.

10.51 Solve Problem 1.46, finding the Stefan-Boltzmann constant in terms of other fundamental physical constants.

Table 10.7 λT in μm·K as a function of f

f	λT	f	λT	f	λT
0.0500	1884	0.4000	3583	0.8000	6864
0.1000	2195	0.5000	4107	0.9000	9376
0.2000	2676	0.6000	4745	0.9500	12461
0.3000	3119	0.7000	5590		

10.52 The fraction of blackbody radiation between wavelengths of 0 and λ is given by the *radiation fractional function*, f:

$$f = \frac{1}{\sigma T^4} \int_0^\lambda e_{\lambda,b}\, d\lambda \qquad (10.60)$$

  a. Work Problem 1.46.

  b. Show that

$$f(\lambda T) = 1 - \frac{15}{\pi^4} \int_0^{c_2/\lambda T} \frac{t^3}{e^t - 1}\, dt \qquad (10.61)$$

  where c_2 is the second radiation constant, hc/k_B, equal to 14387.8 μm·K.

  c. Use the software of your choice to plot $f(\lambda T)$ and check that your results match Table 10.7.

10.53 Read Problem 10.52. Then find the central range of wavelengths that includes 80% of the energy emitted by blackbodies at room temperature (300 K) and at the solar temperature (5772 K).

10.54 Read Problem 10.52. A crystalline silicon solar cell can convert photons to conducting electrons if the photons have a wavelength less than $\lambda_{band} = 1.11$ μm, the *bandgap* wavelength. Longer wavelengths do not produce an electric current, but simply get absorbed and heat the silicon. For a solar cell at 320 K, make a rough estimate of the fraction of solar radiation on wavelengths below the bandgap? Why is this important?

10.55 Two stainless steel blocks have surface roughness of about 10 μm and $\varepsilon \approx 0.5$. They are brought into contact, and their interface is near 300 K. Ignore the points of direct contact and make a rough estimate of the conductance across the air-filled gaps, approximating them as two flat plates. Is radiation important? Considering Table 2.2, what is the relative importance of direct contact?

10.56 A 0.8 m long cylindrical combustion chamber is 0.2 m in diameter. The hot gases within it are at a temperature of 1200°C and a pressure of 1 atm, and the absorbing components consist of 12% by volume of CO_2 and 18% CO_2. Determine how much cooling is needed to hold the walls at 730°C if they are black. *Hints*: For this small optical depth, the emissivities of CO_2 and CO_2 may be added without correction. The gas mixture is approximately ideal, with vol% of a = mole fraction, $x_a = p_a/p$.

References

[10.1] E. M. Sparrow and R. D. Cess. *Radiation Heat Transfer*. Hemisphere Publishing Corp., Washington, D.C., 1978.

[10.2] J. H. Lienhard V. Linearization of nongray radiation exchange: The internal fractional function reconsidered. *J. Heat Transfer*, **141**:052701, May 2019. url: https://doi.org/10.1115/1.4042158.

[10.3] D. K. Edwards. *Radiation Heat Transfer Notes*. Hemisphere Publishing Corp., Washington, D.C., 1981.

[10.4] M. F. Modest and S. Mazumder. *Radiative Heat Transfer*. Academic Press, London, UK, 4th ed., 2021.

[10.5] J. R. Howell, M. P. Mengüç, and R. Siegel. *Thermal Radiation Heat Transfer*. CRC Press (Taylor and Francis), Boca Raton, FL, 6th ed., 2015.

[10.6] J. R. Howell. *A Catalog of Radiation Heat Transfer Configuration Factors*. University of Texas, Austin, 2nd ed., 2001. url: http://www.thermalradiation.net/indexCat.html.

[10.7] A. K. Oppenheim. Radiation analysis by the network method. *Trans. ASME*, **78**(4):725–735, May 1956. doi: 10.1115/1.4013795.

[10.8] R. Siegel and J. R. Howell. Thermal radiation heat transfer, Volume 2: Thermal radiation exchange between surfaces and enclosures. Special Publication SP-164, NASA, Washington, D.C., January 1969. url: http://hdl.handle.net/2060/19690020939.

[10.9] W.-J. Yang, H. Taniguchi, and K. Kudo. Radiative heat transfer by the Monte Carlo method. In T.F. Irvine, Jr., J. P. Hartnett, Y. I. Cho, and G. A. Greene, editors, *Advances in Heat Transfer*, Vol. 27. Academic Press, Inc., San Diego, 1995.

[10.10] H. C. van de Hulst. *Light Scattering by Small Particles*. Dover Publications Inc., New York, 1981.

[10.11] P. Atkins and J. de Paula. *Atkins' Physical Chemistry*. W. H. Freeman and Co., New York, 8th ed., 2006.

[10.12] G. Herzberg. *Molecular Spectra and Molecular Structure.* Kreiger Publishing, Malabar, Florida, 1989. In three volumes.

[10.13] M. Alberti, R. Weber, M. Mancini, A. Fateev, and S. Clausen. Validation of HITEMP-2010 for carbon dioxide and water vapour at high temperatures and atmospheric pressures in 450–7600 cm^{-1} spectral range. *J. Quant. Spectroscopy and Radiative Transfer*, **157**:14–33, 2015. doi: 10.1016/j.jqsrt.2015.01.016.

[10.14] H. C. Hottel and A. F. Sarofim. *Radiative Transfer.* McGraw-Hill Book Company, New York, 1967.

[10.15] M. Alberti, R. Weber, and M. Mancini. Re-creating Hottel's emissivity charts for carbon dioxide and extending them to 40 bar pressure using HITEMP-2010 data base. *Combustion and Flame*, **162**(3):597–612, 2015. The authors provide a spreadsheet to facilitate calculations. doi: 10.1016/j.combustflame.2014.09.005.

[10.16] M. Alberti, R. Weber, and M. Mancini. Re-creating Hottel's emissivity charts for water vapor and extending them to 40 bar pressure using HITEMP-2010 data base. *Combustion and Flame*, **169**:141–153, 2016. The authors provide a spreadsheet to facilitate calculations. doi: 10.1016/j.combustflame.2016.04.013.

[10.17] M. Alberti, R. Weber, and M. Mancini. Overlap corrections for emissivity calculations of H_2O-CO_2-CO-N_2 mixtures. *J. Quant. Spectroscopy and Radiative Transfer*, **205**:230–240, 2018. doi: 10.1016/j.jqsrt.2017.10.005.

[10.18] D. K. Edwards and R. Matavosian. Scaling rules for total absorptivity and emissivity of gases. *J. Heat Transfer*, **106**(4):684–689, 1984. doi: 10.1115/1.3246739.

[10.19] M. F. Modest. Radiative heat transfer in turbulent combustion. *J. Heat Mass Transfer*, **145**(7):073101, February 2023. doi: 10.1115/1.4056402.

[10.20] A. Prša et al. Nominal values for selected solar and planetary quantities: IUA 2015 Resolution B3. *The Astronomical Journal*, **152**(2):41, August 2016. doi: 10.3847/0004-6256/152/2/41.

[10.21] J. A. Duffie and W. A. Beckman. *Solar Engineering of Thermal Processes.* John Wiley & Sons, Inc., Hoboken, N.J., 4th ed., 2013.

[10.22] K. E. Trenberth, J. T. Fasullo, and J. Kiehl. Earth's global energy budget. *Bull. Amer. Meteor. Soc.*, **90**(3):311–324, March 2009. doi: 10.1175/2008BAMS2634.1.

[10.23] P. Berdahl and R. Fromberg. The thermal radiance of clear skies. *Solar Energy*, **29**(4):299–314, 1982. doi: 10.1016/0038-092X(82)90245-6.

[10.24] A. Skartveit, J. A. Olseth, G. Czeplak, and M. Rommel. On the estimation of atmospheric radiation from surface meteorological data. *Solar Energy*, **56**:349–359, April 1996. doi: 10.1016/0038-092X(95)00117-A.

[10.25] P. Berdahl and M. Martin. Emissivity of clear skies. *Solar Energy*, **32**(5): 663–664, 1984. doi: 10.1016/0038-092X(84)90144-0.

[10.26] C. E. Kennedy. Review of mid- to high-temperature solar selective materials. Technical Report NREL/TP-520-31267, National Renewable Energy Laboratory, Golden, Colorado, July 2002. doi: 10.2172/15000706.

[10.27] D. Zhao, A. Aili, Y. Zhai, S. Xu, G. Tan, X. Yin, and R. Yang. Radiative sky cooling: Fundamental principles, materials, and applications. *Applied Physics Reviews*, **6**(2):021306, 2019. doi: 10.1063/1.5087281.

[10.28] A. Leroy, B. Bhatia, C. C. Kelsall, A. Castillejo-Cuberos, M. Di Capua H., L. Zhao, L. Zhang, A. M. Guzman, and E. N. Wang. High-performance subambient radiative cooling enabled by optically selective and thermally insulating polyethylene aerogel. *Sci. Advances*, **5**(10), 2019. doi: 10.1126/sciadv.aat9480.

[10.29] J. A. Fay and D. S. Gollub. *Energy and Environment.* Oxford University Press, New York, 2002.

[10.30] D. Lüthi, M. Le Floch, B. Bereiter, T. Blunier, J.-M. Barnola, U. Siegenthaler, D. Raynaud, J. Jouzel, H. Fischer, K. Kawamura, and T. F. Stocker. High-resolution carbon dioxide concentration record 650,000-800,000 years before present. *Nature*, May 2008. doi: 10.1038/nature06949.

[10.31] J. Hansen, R. Ruedy, M. Sato, and K. Lo. Global surface temperature change. *Rev. Geophys.*, **48**:RG4004, 2010. Additional data and updates are at http://data.giss.nasa.gov/gistemp/.

[10.32] GISTEMP Team. *GISS Surface Temperature Analysis (GISTEMP v4)*, 2024. url: https://data.giss.nasa.gov/gistemp/. Dataset accessed 13 Feb. 2024.

[10.33] IPCC Core Writing Team, R. K. Pachauri, and L. A. Meyer, editors. *Climate Change 2014: Synthesis Report. Contribution of Working Groups I, II and III to the Fifth Assessment Report of the Intergovernmental Panel on Climate Change.* IPCC, Geneva, 2014. url: http://www.ipcc.ch.

[10.34] D. M. Murphy, S. Solomon, R. W. Portmann, K. H. Rosenlof, P. M. Forster, and T. Wong. An observationally based energy balance for the earth since 1950. *J. Geophysical Research: Atmospheres*, **114**:D17107, 2009. doi: 10.1029/2009JD012105.

[10.35] P. A. Stott, S. F. B. Tett, G. S. Jones, M. R. Allen, J. F. B. Mitchell, and G. J. Jenkins. External control of 20th century temperature by natural and anthropogenic forcings. *Science*, **290**:2133–2137, December 2000. doi: 10.1126/science.290.5499.2133.

[10.36] D. S. Battisti and R. L. Naylor. Historical warnings of future food insecurity with unprecedented seasonal heat. *Science*, **323**:240–244, January 2009. doi: 10.1126/science.1164363.

[10.37] J. Schewe et al. Multimodel assessment of water scarcity under climate change. *Proc. Nat. Acad. Sci.*, **111**:3245–3250, 2014. doi: 10.1073/pnas.1222460110.

[10.38] AAAS Climate Science Panel. What we know: The reality, risks, and response to climate change. Technical report, American Association for the Advancement of Science, Washington, D.C., July 2014. url: http://whatweknow.aaas.org/.

[10.39] MIT Energy Initiative. The future of solar energy. Technical report, Massachusetts Institute of Technology, Cambridge, MA, 2015. url: http://energy.mit.edu/publication/future-solar-energy/.

PART V

MASS TRANSFER

11. An introduction to mass transfer

The edge of a colossal jungle, so dark-green as to be almost black, fringed with white surf, ran straight, like a ruled line, far, far away along a blue sea whose glitter was blurred by a creeping mist. The sun was fierce, the land seemed to glisten and drip with steam.

Heart of Darkness, Joseph Conrad, 1902

11.1 Introduction

We have, so far, dealt with heat transfer by convection, radiation, and conduction. Conduction is the diffusion of heat by random molecular action. Heat is transported as hotter molecules mix with or agitate colder ones. A similar process occurs in mixtures of different molecules: mass diffuses as molecules of one kind randomly penetrate regions occupied by molecules of another kind. Up to this point, we have limited our attention to media of unvarying composition in which mass diffusion is meaningless. Many heat transfer processes, however, occur in mixtures where composition differences can drive heat transport, thereby coupling heat diffusion to mass diffusion.

When water vapor condenses out of moist air onto a cold drinking glass, the latent heat of condensation is transferred from the vapor to the glass, warming it. When water evaporates from our skin, as sweat, the latent heat is transferred from our bodies to the vapor, which then carries it away. In both of these examples heat and vapor diffuse simultaneously. A small amount of diffusing water vapor can transport a large amount of energy because water's latent heat is quite large.

During mass transfer processes, an individual chemical species travels from points of high concentration to points of low concentration. Warm water on sweating skin has a higher vapor pressure than surrounding, drier air. This concentration difference drives the diffusion of vapor away from the skin, leading to evaporation and a welcome cooling effect.
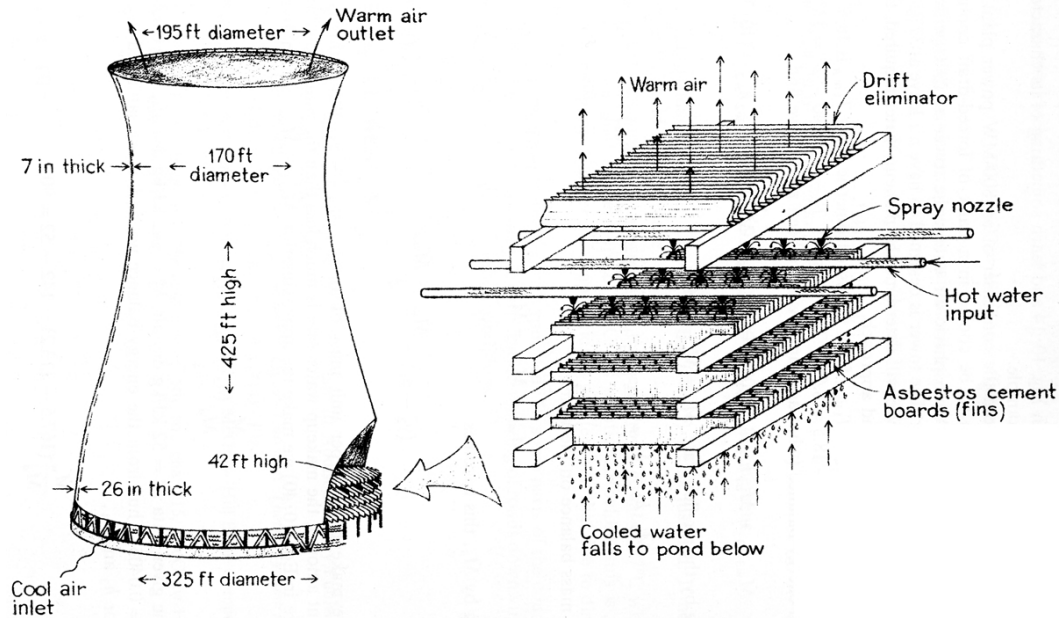
Figure 11.1 Schematic diagram of a natural-draft cooling tower
at the Rancho Seco nuclear power plant. (From [11.1], courtesy
of W. C. Reynolds.)

We have harnessed evaporative cooling in large-scale industrial equip-
ment. Figure 11.1 shows a huge cooling tower used to cool the water leav-
ing a power plant's condensers. The tower is essentially an empty shell, the
bottom of which is packed with plates or plastic louvres. The hot water to
be cooled is sprayed onto the packing and showers downward as droplets
that provide a large surface area for evaporation. A small portion of the
water vaporizes into the cool, dry air that enters the tower from below. The
remaining water, having been cooled by evaporation, falls to the bottom,
where it is collected and recirculated. Moist air flows out of the top, and
white plumes of water droplets may form as it mixes with cool air outside.

The temperature of the air rises as it absorbs the warm vapor and, in
the *natural-draft* form of cooling tower shown above, the upper portion
of the tower acts as an enormous chimney through which the warm,
moist air buoys, pulling in cool air at the base. In a *mechanical-draft*
cooling tower (Fig. 11.2), fans are used to draw air through the packing.
Mechanical-draft towers are much shorter and can sometimes be seen on
the roofs of buildings.

Figure 11.2 A mechanical-draft cooling tower. The fans are located within the cylindrical housings at the top. Air is drawn in through the louvres on the side.

A dilute species diffusing through another species, such as water vapor in air, behaves very much like heat diffusing from high temperature to low temperature. The rate at which a species moves from high concentration to low concentration is given by Fick's law, eqn. (2.19), which is analogous to Fourier's law, eqn. (2.2). Like energy, the mass of a species is conserved. The equation that describes species conservation is analogous to the energy equation, eqn. (6.37). When a moving fluid transfers mass, a mass transfer coefficient, like a heat transfer coefficient, serves to simplify the analysis of convection. And, if the mass flow rates are low enough that they do not change the velocity field, our previous results for heat transfer coefficients provide mass transfer coefficients in the same configuration, through a simple change of variables. With these tools, we can solve many important mass transfer problems, such as calculating rates of evaporative cooling.

In later sections of this chapter, 11.8–11.10, we introduce more complex aspects of mass transfer. We will see that, when mass transfer rates are high, boundary layers can thicken or thin depending on the direction of mass flow. This phenomenon changes both the mass and heat transfer coefficients. Such behavior is critical in steam condensers with air leaks and outside spacecraft reentering the atmosphere. Further, because the physical properties of mixtures are often unknown, we will study elementary means of estimating their values.

Most of this chapter deals with two-component, or *binary*, mixtures. In the last section, 11.11, we introduce multicomponent mass transfer theory. We also introduce the chemical potential, whose gradient is the true thermodynamic driving force for mass diffusion. The chemical potential gradient can be replaced by the concentration gradient in ideal gas mixtures and in dilute liquid solutions. In other kinds of mixtures, the chemical potential itself must be considered.

We begin our study of mass transfer by learning to describe concentration and mass flux in mixtures.

11.2 Mixture compositions and species fluxes

The composition of mixtures

A mixture of chemical species has definite physical properties, such as a density, as if the mixture were a single substance. Air is a familiar example. The properties of a mixture depend on the relative amount of each component, as well as the temperature and pressure. To determine the properties of a mixture, we must identify the proportion of each species present.

The amount of species i in a mixture might be described by its mass per unit volume, the *partial density* in kg of i per m^3, ρ_i. The composition of the entire mixture may be described by stating the partial density of each of its components. The mass density of the mixture itself, ρ, is simply the total mass of all species per unit volume:

$$\rho = \sum_i \rho_i \tag{11.1}$$

The *proportion* of species i in the mixture can be described by the mass of i per unit mass of the mixture, which is simply ρ_i/ρ. This ratio is called the *mass fraction*, m_i:

$$m_i \equiv \frac{\rho_i}{\rho} = \frac{\text{mass of species } i}{\text{mass of mixture}} \tag{11.2}$$

The mass fraction is obviously equivalent to the percent-by-weight of i. From eqn. (11.1), we see that

$$\sum_i m_i = \sum_i \rho_i/\rho = 1 \quad \text{and} \quad 0 \leqslant m_i \leqslant 1 \tag{11.3}$$

If M_i is the molar mass of species i in kg/kmol, the *molar concentration* of species i, c_i in kmol/m^3, is just

$$c_i \equiv \frac{\rho_i}{M_i} = \frac{\text{moles of } i}{\text{volume}} \tag{11.4}$$

Molar concentration is often stated in units of mol/L, in which case it is called *molarity*.

The molar concentration of the entire mixture, c, is the total number of moles for all species per unit volume. Thus,

$$c = \sum_i c_i. \tag{11.5}$$

The *mole fraction* of species i, x_i, is the number of moles of i per mole of mixture:

$$x_i \equiv \frac{c_i}{c} = \frac{\text{moles of } i}{\text{mole of mixture}} \tag{11.6}$$

Like a mixture's mass fractions, a mixture's mole fractions sum to one:

$$\sum_i x_i = \sum_i c_i/c = 1 \quad \text{and} \quad 0 \leqslant x_i \leqslant 1 \tag{11.7}$$

The effective molar mass of a mixture is the number of kg of mixture per kmol of mixture: $M \equiv \rho/c$. Expressions for M in terms of mole or mass fraction follow from eqns. (11.1), (11.4), and (11.6) or from eqns. (11.5), (11.4), and (11.2):

$$M = \sum_i x_i M_i \quad \text{or} \quad \frac{1}{M} = \sum_i \frac{m_i}{M_i} \tag{11.8}$$

We can easily derive the following relations to convert mole fraction to mass fraction (Problem 11.1) :

$$m_i = \frac{x_i M_i}{M} = \frac{x_i M_i}{\sum_k x_k M_k} \quad \text{and} \quad x_i = \frac{M m_i}{M_i} = \frac{m_i/M_i}{\sum_k m_k/M_k} \tag{11.9}$$

Ideal gases

The definitions above apply to any substance, but they say nothing about temperature or pressure dependence. For an ideal gas mixture, however, we can relate the concentrations to T and p.

For each component i of an ideal gas mixture, the *partial pressure*, p_i, exerted by species i is:

$$p_i = \rho_i R_i T \tag{11.10}$$

In eqn. (11.10), R_i is the ideal gas constant for species i

$$R_i \equiv \frac{R^\circ}{M_i} \tag{11.11}$$

where R° is the universal gas constant, 8314.46 J/kmol· K. The partial pressure is directly related to the partial molar concentration c_i:

$$p_i = \rho_i R_i T = (M_i c_i)\left(\frac{R^\circ}{M_i}\right) T$$

$$= c_i R^\circ T \tag{11.12}$$

Remarkably, c is a function of p and T only

$$c = \sum_i c_i = \sum_i \frac{p_i}{R^\circ T} = \frac{p}{R^\circ T} \tag{11.13}$$

The last two terms of eqn. (11.13) reveal Dalton's law of partial pressures[1]:

$$p = \sum_i p_i \tag{11.14}$$

Finally, we combine eqns. (11.6), (11.12), and (11.13) to obtain a very useful relationship between x_i and p_i:

$$x_i = \frac{c_i}{c} = \frac{p_i}{c R^\circ T} = \frac{p_i}{p} \tag{11.15}$$

The last two equalities are restricted to ideal gases.

Example 11.1 Composition of air

The mixture that we deal with most often is air. The composition of dry air by mass and mole fraction is listed below. Determine x_{O_2}, p_{O_2}, c_{O_2}, and ρ_{O_2} for air at 1 atm.

Species	Mass Fraction	Mole Fraction
N_2	0.7552	0.7808
O_2	0.2314	find this
Ar	0.01288	0.00934
trace gases	< 0.001	< 0.001

---

[1] John Dalton offered his "law" as an empirical principle in 1801. But we can deduce it for ideal gases using molecular principles. We obtain it here from eqn. (11.10), which is true for ideal gas molecules because they occupy mixtures without influencing one another. While Dalton's law is strictly true only for ideal gases, it happens to be quite accurate even when gases deviate greatly from ideality. This fact lets us simplify many calculations.

SOLUTION. To make these calculations, we need the molar mass of each species, which are given in Table 11.3 on page 689. We can start by checking the value of M_{air}, using the second of eqns. (11.8):

$$
M_{\text{air}} = \left(\frac{m_{\text{N}_2}}{M_{\text{N}_2}} + \frac{m_{\text{O}_2}}{M_{\text{O}_2}} + \frac{m_{\text{Ar}}}{M_{\text{Ar}}} \right)^{-1}
$$

$$
= \left(\frac{0.7552}{28.01 \text{ kg/kmol}} + \frac{0.2314}{32.00 \text{ kg/kmol}} + \frac{0.0128}{39.95 \text{ kg/kmol}} \right)^{-1}
$$

$$
= 28.97 \text{ kg/kmol}
$$

We may calculate the mole fraction of oxygen using the second of eqns. (11.9)

$$
x_{\text{O}_2} = \frac{m_{\text{O}_2} M}{M_{\text{O}_2}} = \frac{(0.2314)(28.97 \text{ kg/kmol})}{32.00 \text{ kg/kmol}} = 0.2095
$$

The partial pressure of oxygen in 1 atm air is, by eqn. (11.15),

$$
p_{\text{O}_2} = x_{\text{O}_2}\, p = (0.2095)(101,325 \text{ Pa}) = 2.123 \times 10^4 \text{ Pa}
$$

We may now obtain c_{O_2} from eqn. (11.12):

$$
c_{\text{O}_2} = \frac{p_{\text{O}_2}}{R^\circ T}
$$

$$
= (2.123 \times 10^4 \text{ Pa})/(300 \text{ K})(8314.5 \text{ J/kmol·K})
$$

$$
= 0.008510 \text{ kmol/m}^3 = 8.510 \text{ mol/m}^3
$$

Finally, eqn. (11.4) gives the partial density of oxygen

$$
\rho_{\text{O}_2} = c_{\text{O}_2} M_{\text{O}_2} = (0.008510 \text{ kmol/m}^3)(32.00 \text{ kg/kmol})
$$

$$
= 0.2723 \text{ kg/m}^3 \qquad \blacksquare
$$

Velocities and fluxes

Molecules in a gas or liquid constantly collide with other molecules, causing them to bounce randomly from place to place. If species A is concentrated in one region of a fluid, with species B concentrated in an adjacent region, this random molecular motion will cause species A to diffuse into the region of species B, and vice versa. On average, then, molecules of species A will have a velocity $\vec{v}_A$ toward the region of species B, with

Figure 11.3 Species *A* diffuses into the region occupied by species *B*, and vice versa. Each species has a different average velocity.
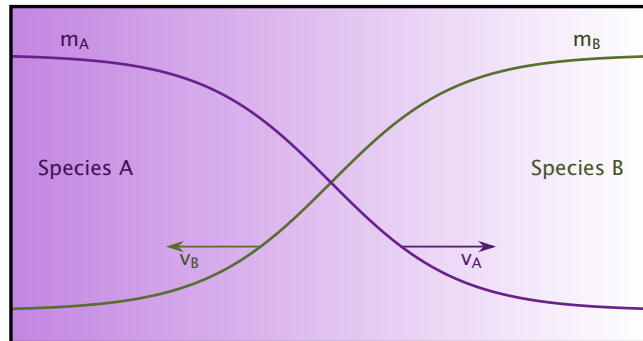
Figure 11.4 The mixture composed of species *A* and *B* moves rightward at velocity $\vec{V}$. The convective velocity $\vec{V}$ adds to the diffusive velocites $\vec{v}_A$ and $\vec{v}_B$.
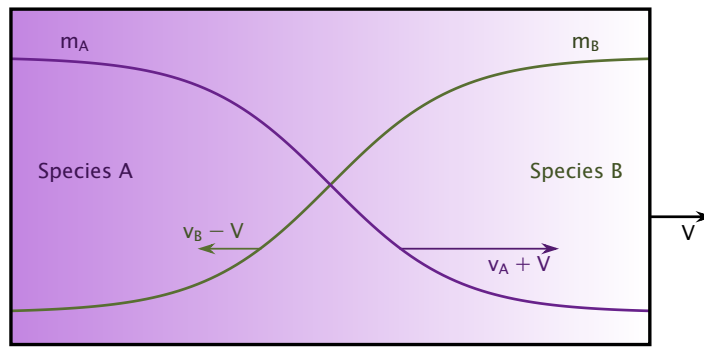
species *B* having an average velocity $\vec{v}_B$ toward the region of species *A* (Fig. 11.3). We see that each species in a mixture can have a different *species average velocity*, $\vec{v}_i$.

The entire mixture might also be flowing. The mixture's velocity would add to the velocity of every individual species in the mixture, even while individual species might diffuse past one another (Fig. 11.4). The movement of an individual species is then a sum of convection by the moving mixture and diffusion along its own concentration gradient.

To connect the mixture's *mass average velocity*, $\vec{v}$, to the average velocity of each species in the mixture, we write the mixture's momentum per unit volume as a sum over the species that compose the mixture:

$$\rho\vec{v} = \sum_i \rho_i \vec{v}_i \tag{11.16}$$

The vector $\rho\vec{v}$ is also the mixture's *mass flux*, $\vec{n}$, in units of kg/m^{2}s.[2]

---

[2]The mass average velocity, $\vec{v}$, given by eqn. (11.16) is identical to the fluid velocity, $\vec{u}$, used in previous chapters—imagine applying eqn. (11.16) to a "mixture" composed of only one species. We use the symbol $\vec{v}$ here simply because $\vec{v}$ is the more common notation in the mass transfer literature.

Likewise, the mass flux of a single species i is

$$\vec{n}_i = \rho_i \vec{v}_i \tag{11.17}$$

and, from eqn. (11.16), we see that the mixture's mass flux equals the sum of all species' mass fluxes

$$\vec{n} = \sum_i \vec{n}_i = \rho \vec{v} \tag{11.18}$$

The average velocity difference between a species and the mixture, $\vec{v}_i - \vec{v}$, is a result of diffusion. Thus, we identify the *diffusional mass flux,* $\vec{j}_i$, of a species relative to the mixture as:

$$\vec{j}_i \equiv \rho_i(\vec{v}_i - \vec{v}) \tag{11.19}$$

The species' total mass flux, $\vec{n}_i$, includes both this diffusional mass flux and bulk convection by the mean flow, as is easily shown:

$$
\begin{array}{c}
\boxed{
\begin{aligned}
\vec{n}_i = \rho_i \vec{v}_i = \quad & \rho_i \vec{v} \quad + \rho_i(\vec{v}_i - \vec{v}) \\
= \quad & \underbrace{m_i \vec{n}}_{\text{convection}} + \underbrace{\vec{j}_i}_{\text{diffusion}}
\end{aligned}
}
\end{array}
\tag{11.20}
$$

The relative contributions of convection and diffusion are fixed as soon as we know the velocity field and the partial densities. But the *causes* of diffusion need further discussion, which we defer to Section 11.3.

Combining eqns. (11.18) and (11.20), we find that

$$\vec{n} = \sum_i \vec{n}_i = \sum_i \rho_i \vec{v} + \sum_i \vec{j}_i = \rho \vec{v} + \sum_i \vec{j}_i = \vec{n} + \sum_i \vec{j}_i$$

Hence

$$\sum_i \vec{j}_i = 0 \tag{11.21}$$

Diffusional mass fluxes must sum to zero because they are each defined relative to the mean mass flux.

Fluxes and velocities may also be stated in molar terms. The *mole flux* of species i is $\vec{N}_i = c_i \vec{v}_i$, in kmol/m²s. The *mixture's mole flux, $\vec{N}$,* is the sum over all species

$$\vec{N} = \sum_i \vec{N}_i = \sum_i c_i \vec{v}_i = c \vec{v}^* \tag{11.22}$$

where we define the *mole-average velocity*, $\vec{v}^*$, as shown. The last flux we define is the *diffusional mole flux*, $\vec{J}_i$:

$$\vec{J}_i = c_i(\vec{v}_i - \vec{v}^*) \tag{11.23}$$

By putting the definitions of $\vec{N}$ and $\vec{N}_i$ into eqn. (11.23), we find that

$$\boxed{\vec{N}_i = x_i\vec{N} + \vec{J}_i} \tag{11.24}$$

Finally, substituting eqn. (11.24) into eqn. (11.22) gives

$$\vec{N} = \sum_i \vec{N}_i = \vec{N}\sum_i x_i + \sum_i \vec{J}_i = \vec{N} + \sum_i \vec{J}_i$$

so that

$$\sum_i \vec{J}_i = 0 \tag{11.25}$$

Thus, the diffusional mole fluxes also sum to zero.

Example 11.2

A small carbon particle oxidizes in air at 1300 K through a surface reaction that produces carbon monoxide gas: $C + \frac{1}{2}O_2 \longrightarrow CO$. Figure 11.5 shows the carbon-air interface in coordinates that move with the interface. In these coordinates, the solid carbon appears to flow toward the surface, rather than the surface slowly moving into the carbon, as it actually does. Oxygen flows toward the carbon surface and carbon monoxide flows away.

If carbon is consumed at a rate of 20 g/m²s, find the mass fluxes and mass-average velocity through an imaginary surface, s, that stays close to the gas side of the interface. The estimated CO concentration near the surface is $m_{CO,s} \cong 0.05$, and the gas density is $\rho_s = 0.27$ kg/m³. Under these conditions, oxygen is consumed as fast as it diffuses to the surface, so that $m_{O_2,s}$ remains very low.

SOLUTION. The mass balance for the reaction is

$$12.0 \text{ kg C} + \frac{32.0}{2} \text{ kg O}_2 \longrightarrow 28.0 \text{ kg CO}$$
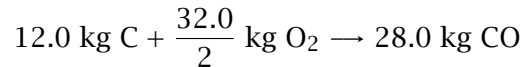
The carbon flows through a second imaginary surface, u, just below the interface, and the mass fluxes are related by

$$n_{C,u} = -\frac{12}{16}\, n_{O_2,s} = \frac{12}{28}\, n_{CO,s}$$
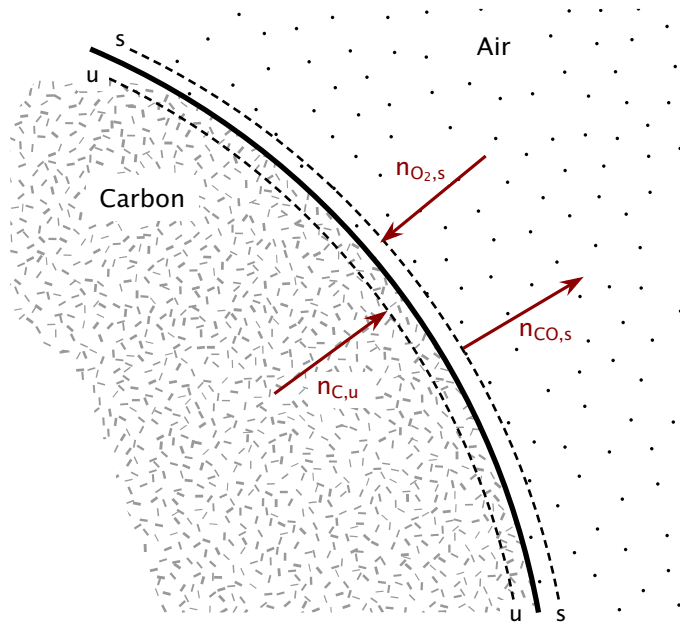
Figure 11.5 Carbon oxidation in air.

The minus sign arises because the O_2 flow is opposite the C and CO flows. With the given value, $n_{C,u} = 20$ g/m²s, we find

$$n_{O_2,s} = -\frac{16}{12}(20 \text{ g/m}^2\text{s}) = -26.7 \text{ g/m}^2\text{s}$$

$$n_{CO,s} = \frac{28}{12}(20 \text{ g/m}^2\text{s}) = 46.7 \text{ g/m}^2\text{s}$$

The total mass flux at the s-surface, from eqn. (11.18), is

$$n_s = n_{CO,s} + n_{O_2,s} = 46.7 - 26.7 = 20.0 \text{ g/m}^2\text{s}$$

as was expected since mass conservation requires that $n_s = n_u = n_{C,u}$. Note the nitrogen and other gases in air have no mass flux at the surface because they do not react.

The net mass flux away from the surface causes a convective velocity in the gas near the surface. From eqn. (11.20), the mass-average velocity is

$$v_s = \frac{n_s}{\rho_s} = \frac{0.020 \text{ kg/m}^2\text{s}}{0.27 \text{ kg/m}^3} = 0.0741 \text{ m/s}$$

The speed at which the carbon interface recedes is approximately $-n_{C,u}/\rho_C \cong -10$ μm/s, where the density of solid carbon is $\rho_C \cong$

2200 kg/m^3. This speed is utterly negligible relative to the gas velocity, as if the interface were in fact at rest.

To find the diffusional mass fluxes, we can again use eqn. (11.20)

$$n_{CO,s} = m_{CO,s} n_s + j_{CO,s}$$
$$n_{O_2,s} = m_{O_2,s} n_s + j_{O_2,s}$$

which gives us

$$j_{CO,s} = n_{CO,s} - m_{CO,s} n_s = \quad 46.7 - (0.05)(20.0) = \quad 45.7 \text{ g/m}^2\text{s}$$
$$j_{O_2,s} = n_{O_2,s} - \underbrace{m_{O_2,s}}_{\cong 0} n_s \cong -26.7 - 0 \qquad\qquad = -26.7 \text{ g/m}^2\text{s}$$

Note that $j_{O_2,s}$ and $j_{CO,s}$ do *not* sum to zero because the nonreacting species in air, particularly nitrogen, diffuse against the convective velocity, v_s. We discuss this very important phenomenon in Section 11.5.

To find the mass fluxes and concentration of nitrogen at the *s*-surface, work Problem 11.4. For more information on the oxidation and combustion of carbon particles, see Refs. [11.2, 11.3]. ■

11.3 Fick's law of diffusion in binary mixtures

A *binary mixture* contains only two species. Each species will diffuse from regions where its concentration is high toward regions where its concentration is low—just as heat diffuses from a region of high temperature toward a region of low temperature. We have already noted in Section 2.1 that mass diffusion obeys Fick's law

$$\boxed{\vec{j_1} = -\rho \mathcal{D}_{12} \nabla m_1}$$ (11.26)

and that Fick's law is analogous to Fourier's law.

The constant of proportionality, $\rho\mathcal{D}_{12}$, includes a physical property called the *diffusion coefficient*, $\mathcal{D}_{12}$, for species 1 diffusing through species 2. Like the thermal diffusivity, α, or the kinematic viscosity, ν (which is a momentum diffusivity), the mass diffusivity $\mathcal{D}_{12}$ has units of m^2/s. These three diffusivities form three dimensionless groups:

$$\begin{aligned} &\text{The Prandtl number} &&\text{Pr} \equiv \nu/\alpha \\ &\text{The Schmidt number}[3] &&\text{Sc} \equiv \nu/\mathcal{D}_{12} \\ &\text{The Lewis number}[4] &&\text{Le} \equiv \alpha/\mathcal{D}_{12} = \text{Sc}/\text{Pr} \end{aligned}$$ (11.27)

Each group compares the strength of two diffusive processes. We make considerable use of the Schmidt number later in this chapter.

We can write Fick's law for the flux of species 2 as well

$$\vec{j_2} = -\rho \mathcal{D}_{21} \nabla m_2 \qquad (11.28)$$

A simple calculation shows that species 2 has the same diffusivity through species 1 as species 1 has through species 2, if the mixture is binary (Problem 11.7):

$$\mathcal{D}_{21} = \mathcal{D}_{12} \qquad (11.29)$$

Fick's law may alternatively be written in terms of the molar diffusion flux, $\vec{J_1}$, and the mole fraction, x_1:

$$\vec{J_1} = -c\mathcal{D}_{12} \nabla x_1 \qquad (11.30)$$

The mole-based and mass-based forms of Fick's law are identical: one form can be derived from the other form using the definitions of concentration and flux (Problem 11.8).

In some cases, the binary form of Fick's law can be adapted to multi-component mixtures to find the diffusion flux of one species, i, relative to the rest of the mixture, m:

$$\vec{j_i} = -\rho \mathcal{D}_{im} \nabla m_i \qquad (11.31)$$

A mixture of air and water vapor is a very important example. Air itself is mixture, but it is mostly composed of the very similar molecules N_2 and O_2 (Example 11.1). As a result, air can be treated as if it were a single species, and we can write Fick's law using a binary diffusion coefficient for water and air, $\mathcal{D}_{H_2O,air}$. More generally, suppose that a mixture is dominated by one species with very low concentrations of several other

---

[3]Ernst Schmidt (1892–1975) served successively as the professor of thermodynamics at the Technical Universities of Danzig, Braunschweig, and Munich (see Chapter 6, footnote 3). His many contributions to heat and mass transfer include the introduction of aluminum foil as radiation shielding, the first measurements of velocity and temperature fields in a natural convection boundary layer, and a once widely-used graphical procedure for solving unsteady heat conduction problems. He was among the first to develop the analogy between heat and mass transfer.

[4]Warren K. Lewis (1882–1975) was a professor of chemical engineering at M.I.T. from 1910 to 1975. He defined the original paradigm of chemical engineering, that of "unit operations"; and, through his textbook with Walker and McAdams, *Principles of Chemical Engineering*, he laid the foundations of the discipline. He was a prolific inventor in the area of industrial chemistry. He also did important early work on simultaneous heat and mass transfer in connection with evaporation problems.
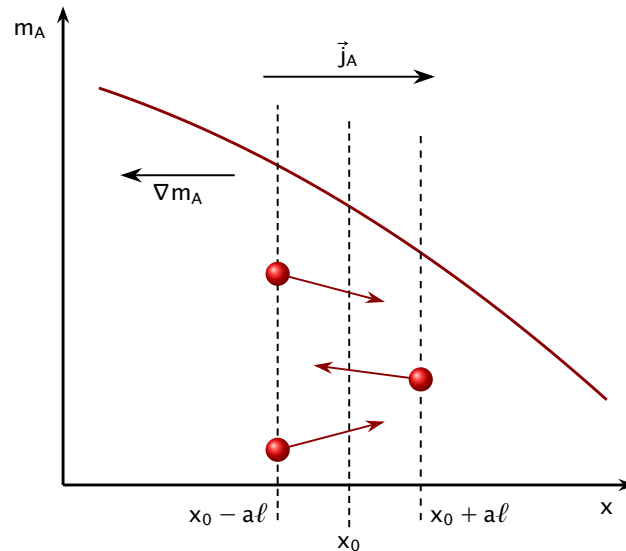
Figure 11.6   One-dimensional diffusion.

species. Then the other species primarily interact with the dominant species and not with each other, and eqn (11.31) is applicable to each of those other species. Section 11.10 provides a formula to calculate $\mathcal{D}_{im}$ in that situation.

A kinetic model of diffusion

The diffusion coefficient depends on composition, temperature, and pressure. Equations that predict $\mathcal{D}_{12}$ and $\mathcal{D}_{im}$ are given in Section 11.10. For now, let us see how Fick's law arises from the same elementary molecular kinetics that led to Fourier's and Newton's laws in Section 6.4.

Consider diffusion in a gas composed of two species, A and A', where A' is very similar to A as if some of the molecules in a pure gas had merely been labeled without changing their properties. The resulting diffusion process is called *self-diffusion*. Assume that the temperature and pressure of the mixture are uniform and that the mass-average velocity is zero.

Figure 11.6 shows a one-dimensional concentration distribution, in which molecules of A diffuse down their concentration gradient in the x-direction. This process is entirely analogous to the transport of energy and momentum shown in Fig. 6.13.

Individual molecules move at a speed C, which varies randomly from molecule to molecule as they travel between collisions with one another. The average speed of the molecules is $\overline{C}$. The average mass flux of A

molecules crossing the plane $x = x_0$, in either direction, is proportional to $(\rho m_A)\overline{C}$. Call this flux $\eta(\rho m_A)\overline{C}$, where η is a constant of proportionality. The molecules travel a distance of about one mean free path, ℓ, prior to crossing the x_0-plane. Call this distance $a\ell$, where a is a number close to one.

We can now calculate the net mass flux across the x_0-plane:

$$j_A\big|_{x_0} = \underbrace{\left(\eta\rho\overline{C}m_A\right)_{x_0-a\ell}}_{\text{flux traveling left}} - \underbrace{\left(\eta\rho\overline{C}m_A\right)_{x_0+a\ell}}_{\text{flux traveling right}}$$

$$= \eta\rho\overline{C}\left(m_A\big|_{x_0-a\ell} - m_A\big|_{x_0+a\ell}\right) \tag{11.32}$$

where $\rho\overline{C}$ is independent of x because the mixture temperature and pressure are uniform. We can approximate the difference using the derivative at x_0 (Problem 11.9):

$$j_A\big|_{x_0} = \eta\rho\overline{C}\left(-2a\ell\,\frac{dm_A}{dx}\bigg|_{x_0}\right)$$

$$= -\rho(2\eta a\overline{C}\ell)\,\frac{dm_A}{dx}\bigg|_{x_0} \tag{11.33}$$

Thus, we identify the self-diffusion coefficient as

$$\mathcal{D}_{AA'} = (2\eta a)\overline{C}\ell \tag{11.34}$$

and obtain Fick's law

$$j_A = -\rho\mathcal{D}_{AA'}\frac{dm_A}{dx} \tag{11.35}$$

The constant, $2\eta a$, in eqn. (11.34) can be found with a more detailed kinetic theory calculation, the result of which is given in Section 11.10.

Typical values of the binary diffusion coefficient

Table 11.1 lists some experimental values of the diffusion coefficient in binary gas mixtures and dilute liquid solutions. For gases, the diffusion coefficient is typically on the order of 10^{-5} m^2/s near room temperature. For liquids, the diffusion coefficient is much smaller, on the order of 10^{-9} m^2/s near room temperature. For both liquids and gases, the diffusion coefficient rises with increasing temperature. In solids, typical diffusion coefficients range from about 10^{-20} to about 10^{-9} m^2/s, depending upon what substances are involved and the temperature [11.4].

Table 11.1 Typical diffusion coefficients for binary gas mixtures at 1 atm and dilute liquid solutions [11.5, 11.6].

Gas mixture	*T* (K)	$\mathcal{D}_{12}$ (m^2/s)
air-carbon dioxide	276	1.42×10^{-5}
air-ethanol	313	1.45
air-helium	276	6.24
air-naphthalene	303	0.86
air-water	313	2.88
argon-helium	295	8.3
	628	32.1
	1068	81.0
(dilute solute, 1)-(liquid solvent, 2)	*T* (K)	$\mathcal{D}_{12}$ (m^2/s)
ethanol-benzene	288	2.25×10^{-9}
benzene-ethanol	298	1.81
water-ethanol	298	1.24
carbon dioxide-water	298	2.00
ethanol-water	298	1.05
methane-water	275	0.85
	333	3.55

The diffusion of water vapor through air is of particular technical importance. An empirical correlation for that mixture is

$$\mathcal{D}_{H_2O,air} = 1.87 \times 10^{-10} \left(\frac{T^{2.072}}{p} \right) \quad \text{for} \quad 282 \text{ K} \leqslant T \leqslant 450 \text{ K} \qquad (11.36)$$

where $\mathcal{D}_{H_2O,air}$ is in m^2/s, T is in kelvin, and p is in atm [11.7]. This correlation fits measured data to about $\pm 10\%$.

Applicability of Fick's Law

Fick's law works well for binary gases at low density and for dilute solutes in liquid or solid solutions. When the solute is not dilute, but instead concentrated, the diffusion coefficient can vary with the solute's concentration. This variation occurs because the solute molecules interact with

each other when they are not dilute. In chemical terms, we no longer have an *ideal* solution. These complex intermolecular forces affect the flux, making it dependent on both the concentration and the concentration gradient (see Sections 11.10 and 11.11).

Fick's law employs just one species' concentration gradient. That's appropriate for a binary mixture in which the two species' gradients are equal and opposite: $\nabla m_1 = \nabla(1 - m_2) = -\nabla m_2$. However, when three species diffuse, *two* gradients must be independently known. The flux of any one species will depend on both those gradients through a pair of diffusion coefficients. As a result, the binary forms of Fick's law, eqns. (11.26) and (11.31), are insufficient. In fact, multicomponent diffusion can be counter-intuitive. For example, a strong gradient in one species' concentration may cause another species to move in *opposition* to its own gradient. We discuss such phenomena in Section 11.11.

Coupled diffusion phenomena

Mass diffusion can be driven by factors other than concentration gradients, although the latter are of primary importance. For example, temperature gradients can induce mass diffusion in a process known as *thermal diffusion* or the *Soret effect*. The diffusional mass flux resulting from combined temperature and concentration gradients is [11.8]

$$\vec{j_i} = -\rho \mathcal{D}_{12} \left[\nabla m_1 + \frac{M_1 M_2}{M^2} k_T \nabla \ln(T) \right] \qquad (11.37)$$

where k_T is called the *thermal diffusion ratio* and is generally quite small. Thermal diffusion is occasionally used in chemical separation processes.

A pressure gradient that acts unequally on different species can also cause diffusion. This effect is normally small, but it can be harnessed for centrifuge separations. Electric fields can force the diffusional separation of species that have different charges, an effect used to desalinate brackish water by electrodialysis.

A related phenomenon is the generation of a heat flux by a concentration gradient (as distinct from heat convected by diffusing mass), called the *diffusion-thermo* or *Dufour effect*.

In this chapter, we deal only with mass transfer produced by concentration gradients. Transport problems involving coupled phenomena are explored in the book by Kjelstrup et al. [11.9].

11.4   The equation of species conservation

Conservation of species

Just as we formed an equation of energy conservation in Chapter 6, we now form an equation of *species conservation*—one that applies to each substance in a mixture. This equation should account not only for the convection and diffusion of each species: it should also allow the possibility that a species is created or destroyed by chemical reactions within mixture.[5]

We again begin withan arbitrary control volume, R, with boundary, S, as shown in Fig. 11.7. The control volume is fixed in space, and fluid might move through it. Species i may accumulate in R, it may travel in and out of R by bulk convection and diffusion through S, and it may be created within R by chemical reactions. The rate of creation of species i is $\dot{r}_i$ (kg/m^{3}s); and, because the total mass is conserved during a chemical reaction, $\sum \dot{r}_i = 0$. The rate of change of the mass of species i in R is then described by the following balance:

$$\underbrace{\frac{d}{dt} \int_R \rho_i \, dR}_{\substack{\text{rate of increase} \\ \text{of } i \text{ in } R}} = - \int_S \vec{n}_i \cdot d\vec{S} + \int_R \dot{r}_i \, dR$$

$$= - \underbrace{\int_S \rho_i \vec{v} \cdot d\vec{S}}_{\substack{\text{rate of convection} \\ \text{of } i \text{ out of } R}} - \underbrace{\int_S \vec{j}_i \cdot d\vec{S}}_{\substack{\text{diffusion of } i \\ \text{out of } R}} + \underbrace{\int_R \dot{r}_i \, dR}_{\substack{\text{rate of creation} \\ \text{of } i \text{ in } R}} \qquad (11.38)$$

This species balance is identical to our energy balance, eqn. (6.36), except that the partial density of i has taken the place of energy and diffusional mass flux has taken the place of heat flux.

We convert the surface integrals to volume integrals using Gauss's theorem, eqn. (2.8), and rearrange the result:

$$\int_R \left[\frac{\partial \rho_i}{\partial t} + \nabla \cdot (\rho_i \vec{v}) + \nabla \cdot \vec{j}_i - \dot{r}_i \right] dR = 0 \qquad (11.39)$$

The control volume R was chosen arbitrarily, so the integral can only equal zero if the integrand itself is identically zero. Thus, we obtain the

---

[5]Reactions within the mixture are called *homogeneous reactions*. Reactions on surfaces surrounding the mixture are called *heterogeneous reactions*. Heterogeneous reactions will appear in the boundary conditions of the species equation, but not in the equation itself.
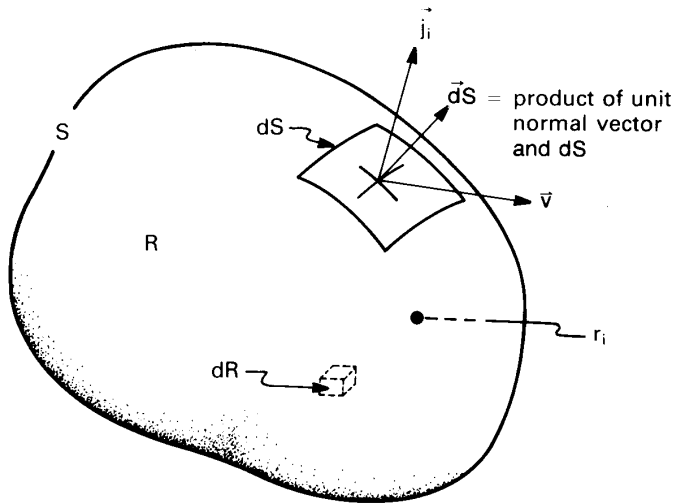
Figure 11.7 Control volume in a fluid-flow and mass-diffusion field.

general form of the species conservation equation:

$$\boxed{\frac{\partial \rho_i}{\partial t} + \nabla \cdot (\rho_i \vec{v}) = -\nabla \cdot \vec{j}_i + \dot{r}_i} \tag{11.40}$$

We can obtain a mass conservation equation for the entire mixture by summing eqn. (11.40) over all species, applying eqns. (11.1), (11.16), and (11.21) and requiring that there be no net creation of mass:

$$\sum_i \left[\frac{\partial \rho_i}{\partial t} + \nabla \cdot (\rho_i \vec{v}) \right] = \sum_i \left(-\nabla \cdot \vec{j}_i + \dot{r}_i \right) = -\nabla \cdot \sum_i \vec{j}_i + \sum_i \dot{r}_i = 0$$

so that

$$\frac{\partial \rho}{\partial t} + \nabla \cdot (\rho \vec{v}) = 0 \tag{11.41}$$

This equation applies to any mixture, including those with varying density (see Problem 6.36).

Incompressible mixtures. For an incompressible mixture, $\nabla \cdot \vec{v} = 0$ (see Section 6.2 or Problem 11.12). The convective term in eqn. (11.40) may therefore be rewritten as

$$\nabla \cdot (\rho_i \vec{v}) = \vec{v} \cdot \nabla \rho_i + \rho_i \underbrace{\nabla \cdot \vec{v}}_{=0} = \vec{v} \cdot \nabla \rho_i \tag{11.42}$$

The resulting, incompressible species equation is very similar to the incompressible energy equation, eqn. (6.37)

$$\frac{\partial \rho_i}{\partial t} + \vec{v} \cdot \nabla \rho_i = -\nabla \cdot \vec{j}_i + \dot{r}_i \tag{11.43}$$

$$\rho c_p \left(\frac{\partial T}{\partial t} + \vec{v} \cdot \nabla T \right) = -\nabla \cdot \vec{q} + \dot{q} \tag{6.37}$$

The reaction term, $\dot{r}_i$, is analogous to the heat generation term, $\dot{q}$; the diffusional mass flux, $\vec{j}_i$, is analogous to the heat flux, $\vec{q}$; and $d\rho_i$ is analogous to $\rho c_p dT$. We exploit this analogy in Section 11.6.

We can further simplify eqn. (11.43) if the product $\rho \mathcal{D}_{im}$ is spatially uniform, by eliminating $\vec{j}_i$ using Fick's law, eqn. (11.31), for effectively binary diffusion (Problem 11.13):

$$\frac{\partial m_i}{\partial t} + \vec{v} \cdot \nabla m_i = \mathcal{D}_{im} \nabla^2 m_i + \dot{r}_i / \rho \tag{11.44}$$

The equation of species conservation may also be stated in molar variables, using c_i or x_i, N_i, and J_i (Problem 11.14.) Molar analysis sometimes has advantages over mass-based analysis (see pg. 653).

Interfacial boundary conditions

To solve the heat conduction equation for a temperature distribution, the temperature or heat flux must be specified at each boundary of the domain of interest (Section 4.1). Likewise, to solve the species conservation equation for a concentration distribution, the concentration or mass flux must be given at the boundaries.

Temperature and concentration behave differently at the interface between two regions. The temperature changes continuously across an interface, so that the media on either side have the same temperature where they meet. Concentration, on the other hand, need *not* be continuous across an interface, even in a state of thermodynamic equilibrium. Water in a cup, for example, has a discontinuous change in the concentration of water at the air-water interface, going from nearly 100% water in the liquid phase to only a few percent in the gas phase. The concentration of oxygen in the air above the water is 23% by mass while the concentration of oxygen in the water is only about 10 ppm.

Ammonia, unlike oxygen, is highly soluble in water. The liquid can contain more than 40% ammonia by mass at 10°C and a pressure slightly above 1 atm. The solubility decreases rapidly with temperature. In fact,
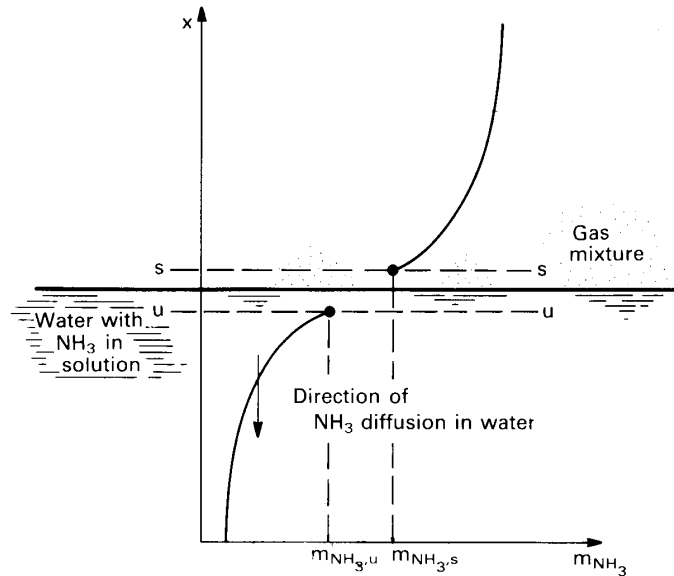
Figure 11.8 Absorption of ammonia into water.

the absorption of ammonia into water is exothermic, so that an ammonia absorber must be actively cooled to stabilize the temperature and maintain solubility. Conversely, heating can be used to drive ammonia vapor out of water. An absorption refrigeration cycle applies both processes.

Absorption refrigeration pulls heat from a cooled space by vaporizing liquid ammonia. The vapor is then absorbed into water in a direct contact exchanger (Fig. 3.2), after which the liquid mixture is pumped to higher pressure and separated in a distillation column. Absorption eliminates the vapor compressor needed by other refrigeration systems.[6]

Figure 11.8 illustrates a liquid-vapor surface in the absorber. The absorbed ammonia diffuses from the surface into the bulk liquid. Suppose that surfaces s and u are very close to either side of the interface. The mass fraction of ammonia on the vapor side of the interface, $m_{NH_3,s}$, is quite different from that on the liquid side, $m_{NH_3,u}$.

The value of $m_{NH_3,u}$ is a boundary condition for mass transfer into the water. Data for *phase equilibrium* set $m_{NH_3,u}$ as a function of $m_{NH_3,s}$

---

[6]Ammonia absorption refrigeration was invented and patented by Ferdinand Carré in France in 1859. Ammonia refrigeration cycles, both absorption and vapor-compression, have seen wide use ever since. Unlike many synthetic refrigerants, ammonia neither damages the ozone layer nor contributes to climate change.
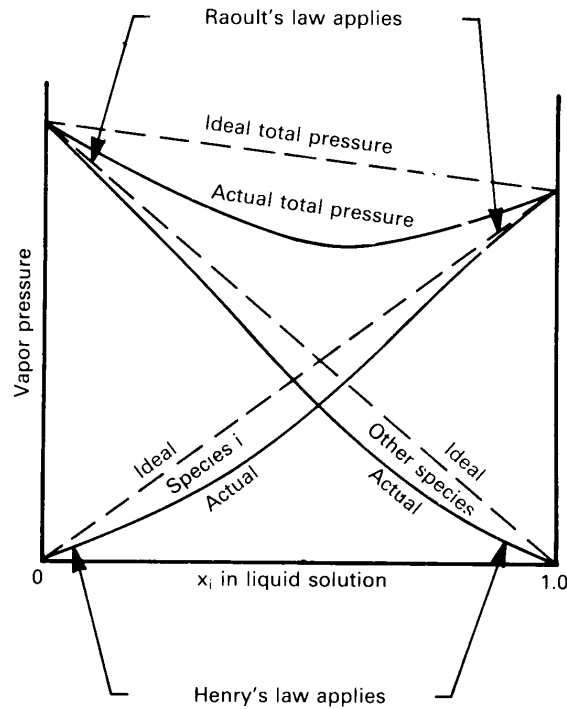
Figure 11.9 Partial and total vapor-pressure above a binary liquid solution, showing the regimes of Raoult's and Henry's laws for species i or the other species.

for a given temperature and pressure. Phase equilibrium is immensely important in chemical engineering, but the topic is complex [11.10, 11.11]. Here, we introduce only the very simplest equilibrium relationships.

Gas-liquid interfaces. For a gas mixture in contact with a liquid mixture, two simplified rules set the vapor composition (Fig. 11.9). When the liquid is *rich* in species i, the partial pressure of species i in the gas phase, p_i, can be characterized approximately with *Raoult's law*, which says that

$$p_i = p_{\text{sat},i}\, x_i \qquad \text{for } x_i \approx 1 \qquad (11.45)$$

where $p_{\text{sat},i}$ is the saturation pressure of pure i at the interface temperature and x_i is the mole fraction of i in the liquid. When the species i is *dilute* in the liquid, *Henry's law* applies. It says that

$$p_i = H\, x_i \qquad \text{for } x_i \ll 1 \qquad (11.46)$$

where H is a temperature-dependent constant available in data tabulations (see [11.12]). The literature reports H in a regrettable variety of units!

Figure 11.9 shows how the vapor pressure varies over a liquid mixture of species i and another species, and it indicates the regions of validity of Raoult's and Henry's laws. For example, when x_i is near one, Raoult's law applies to species i; when x_i is near zero, Raoult's law applies to the other species.

If the vapor pressure were to obey Raoult's law over the entire range of liquid composition, the solution is called an *ideal solution*, shown with dashed lines in Fig. 11.9. Most solutions approach ideality only when x_i is near one. In this case, the other species is a *dilute solute*.

Example 11.3   Mass fraction of vapor above liquid water

A pot of water at 100°C sits in air at 1 atm total pressure and cools toward room temperature. What is the mass fraction of water vapor above the surface of the water as a function of the surface temperature?

SOLUTION. Raoult's law applies almost exactly in this situation, since the concentration of air in water is very small: < 25 ppm at room temperature and less as temperature rises. Thus, $x_{H_2O} \cong 1$, and by eqn. (11.45), the vapor pressure is $p_{H_2O,s} \cong p_{sat,H_2O}(T)$. Data for the saturation pressure as a function of temperature can be taken from a steam table or from Table A.5 on pg. 754. (Table A.5 also includes an equation for $p_{sat,H_2O}(T)$.) With $p_{H_2O,s}$ and eqn. (11.15), the mole fraction is

$$x_{H_2O,s} = p_{H_2O,s}/p_{atm} = p_{sat,H_2O}(T)/(101,325 \text{ Pa}) \qquad (11.47)$$

The mass fraction can be calculated from eqn. (11.9), noting that $x_{air} = 1 - x_{H_2O}$ and substituting $M_{H_2O} = 18.02$ kg/kmol and $M_{air} = 28.96$ kg/kmol

$$m_{H_2O,s} = \frac{(x_{H_2O,s})(18.02)}{\left[(x_{H_2O,s})(18.02) + (1 - x_{H_2O,s})(28.96)\right]} \qquad (11.48)$$

The result is plotted in Fig. 11.10. Note that the mass fraction is less than 10% if the surface temperature is below about 54°C.   ∎

Example 11.4   Boiling point elevation of seawater

Bromley et al. [11.13] analyzed a sample of Pacific Ocean seawater. They found that it contained 3.45% by weight of dissolved salts, amounting to 1.137 mole of salts per kg of H_2O. Determine the boiling point of this seawater.
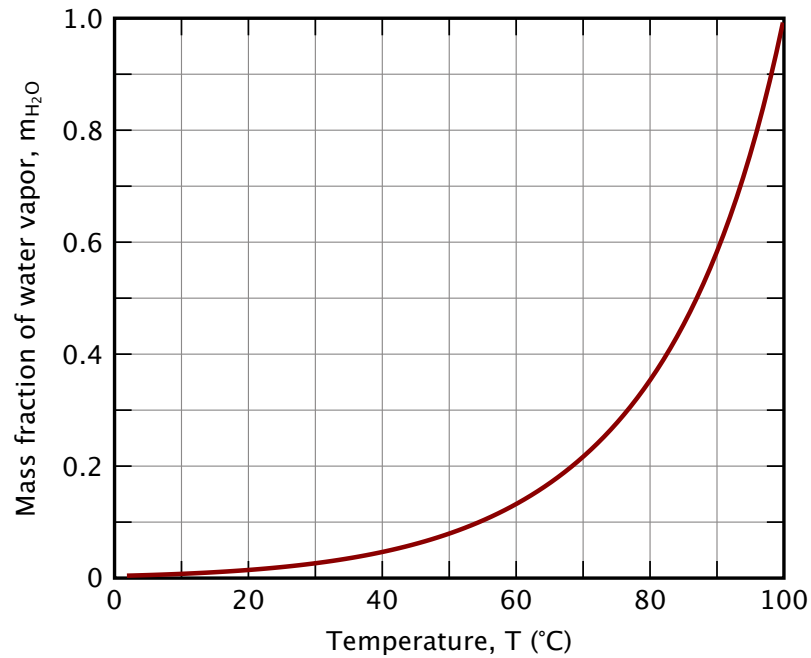
Figure 11.10 Mass fraction of water vapor in air adjacent to a liquid water surface as a function of surface temperature (1 atm total pressure).

SOLUTION. 1 kg of H_2O contains $(1/18.02) \times 10^3 = 55.49$ mol H_2O. The mole fraction of salt in the seawater is then

$$x_{salts} = \frac{1.137}{1.137 + 55.49} = 0.0201$$

From Raoult's law, the vapor pressure of water over seawater will be 1 atm when the saturation pressure of water is

$$p_{sat,\, H_2O}(T_{BP}) = \frac{p_{H_2O}}{x_{H_2O}} = \frac{101,325}{1 - 0.0201} = 103,403 \text{ Pa}$$

A steam table (or software) gives $T_{BP} = 100.54°C$. In other words, the dissolved salts produce a *boiling point elevation* of 0.54 K. Although this value seems small, seawater distillation systems use a cascade of vaporization stages, with stage-to-stage temperature differences of about 4 K and progressively rising salinity. Boiling point elevation cannot be neglected in the stage-to-stage design. ■

Example 11.5   Carbonated drink

Carbonated drinks contain about 7 g of CO_2 per liter of water. If a drink is in an unopened can at 25°C, what is the partial pressure of CO_2 in the space above the liquid in the can? What happens to the CO_2 when the can is opened?

SOLUTION. The Henry's law constant for CO_2 in water is $H = 1.63 \times 10^8$ Pa [11.12]. With $M_{CO_2} = 44.01$ g/mol, $M_{H_2O} = 18.02$ g/mol, and $\rho_{H_2O} = 997$ g/L, eqn. (11.9) gives

$$x_{CO_2} = \frac{7/44.01}{7/44.01 + 997/18.02} = 0.00287$$

Henry's law, eqn. (11.46), then provides

$$p_{CO_2} = Hx_{CO_2} = (1.63 \times 10^8)(0.00287) = 468 \text{ kPa}$$

The partial pressure of CO_2 accounts for almost all of the total pressure in the can.[7]

When the can is opened, the pressure drops to 1 atm, and the drink is supersaturated with CO_2. The CO_2 bubbles out until equilibrium is reached. At that point, the drink is "flat". ∎

Gas-solid interfaces.   When a solid is exposed to a gas, some of it will vaporize. Camphor, for example, produces an aromatic vapor that has been used for centuries in medicine and religious rites. Naphthalene produces a toxic vapor once used to keep moths away from wool clothing. Dry ice (solid CO_2), which vaporizes rapidly in room temperature air, often appears in science experiments for children. For most solid materials, however, vaporization is undetectably tiny.

We call a direct solid-to-vapor phase transition *sublimation*. The concentration of sublimed solid material in an adjacent gas is usually stated as a vapor pressure, p_v, which may be correlated from data as [11.14]

$$\ln p_v = A - \frac{B}{C + T} \tag{11.49}$$

---

[7]The drink contains dissolved sugar and favorings, so Raoult's law shows that $p_{H_2O} < p_{sat,H_2O}(25°C) = 3.17$ kPa, which is negligible. If some air is also present in the can, the pressure will be slightly higher. The gauge pressure in an unopened can be measured by attaching a strain gauge to the can and opening it, as is done in some undergraduate classes. The calculated p_{CO_2} is quite consistent with such experiments.

where T is the solid's surface temperature, and A, B, and C are constants.[8]

A gas can also be absorbed into an adjacent solid. Only very small amounts of gas are absorbed into most inorganic solids, but the consequences may sometimes be significant. For example, gas absorption is used to case-harden steel in a process called *carburization*. A low-carbon steel is exposed to a hot carbon-rich gas mixture, typically containing CO and a hydrocarbon. That causes carbon to be absorbed into the surface of the metal. Carbon diffuses inward from the surface. A typical goal is to raise the carbon mass fraction to 0.8% over a depth of about 2 mm (see Problem 11.18). Carburization increases the surface hardness and wear resistance of the steel.

Similarly, hydrogen gas stored in a steel-walled pressure vessel can leak when it is absorbed into the wall. Upon absorption, molecular hydrogen dissociates into hydrogen atoms, which readily diffuse through the steel. The hydrogen atoms recombine on the opposite surface of the wall where they are desorbed [11.16]. Hydrogen absorption can lead to embrittlement of steel containers and to leakage from a wide range of container vessels. The light-weight composite storage tanks used in hydrogen fuel-cell vehicles, for example, are protected from leakage with polymer liners.

Example 11.6

Ice at $-10°C$ is exposed to 1 atm air. What is the mass fraction of water vapor above the surface of the ice?

SOLUTION. To begin, we need the vapor pressure, p_v, of water above ice. A typical curve-fit of vapor pressure data is

$$\ln p_v(\text{kPa}) = 21.99 - 6141/(T \text{ K}) \qquad \text{for } 243 \text{ K} \leqslant T \leqslant 273 \text{ K}$$

At $T = -10°C = 263.15$ K this yields $p_v = 0.260$ kPa. The remainder of the calculation follows exactly the approach of Example 11.3.

$$x_{H_2O,s} = 0.260/101.325 = 0.00257$$

$$m_{H_2O,s} = \frac{(0.00257)(18.02)}{[(0.00257)(18.02) + (1 - 0.00257)(28.96)]}$$

$$= 0.00160$$

---

[8]The *Antoine equation*, eqn. (11.49), was proposed in 1888 by the French naval engineer Louis Charles Antoine (1825–1898). The case $C = 0$ follows directly from the Clausius-Clapeyron equation, $dp/dT = p h_{sf}/(R°T^2)$, if h_{sf} varies negligibly with T. The Antoine equation also applies to the vapor pressure of liquids [11.15].

While this amount is small, it leads to a steady loss of mass. An ice cube left in the freezer will sublime away over a period of months (Problem 11.33). ∎

11.5 Mass transfer through a stationary medium

When a species dissolves into a solid layer, or a stagnant layer of a different fluid, the concentration gradient formed will cause the species to diffuse from one side of the layer to the other. The resulting mass transfer process resembles a heat conduction process when the concentration of the dissolved species is not too high. Let us first examine this process in the steady state.

Steady mass diffusion in a stationary medium

The species conservation equation, (11.40), simplifies greatly for steady mass transfer without reactions

$$\boxed{\nabla \cdot (\rho_i \vec{v}) + \nabla \cdot \vec{j_i} = \nabla \cdot \vec{n_i} = 0} \tag{11.50}$$

In one dimension, this is just

$$\frac{dn_i}{dx} = \frac{d}{dx}(\rho_i v + j_i) = \frac{d}{dx}(m_i n + j_i) = 0 \tag{11.51}$$

In other words, the mass flux of species i, n_i, is independent of x.

When the convective mass flux of i, $\rho_i v = m_i n$, is small, the transport of i is mainly by the diffusional flux, j_i. The following pair of examples show how this situation might arise.

Example 11.7

A slab, made of species 1, separates two volumes of gas. On one side, the pressure of species 2 is high, and on the other it is low. Species 2 two is soluble in the slab material and thus has different concentrations at each inside face of the slab, as shown in Fig. 11.11. What is the mass transfer rate of species 2 through the slab if the concentration of species 2 is low?

SOLUTION. The mass transfer rate in the slab satisfies eqn. (11.51)

$$\frac{dn_2}{dx} = 0$$
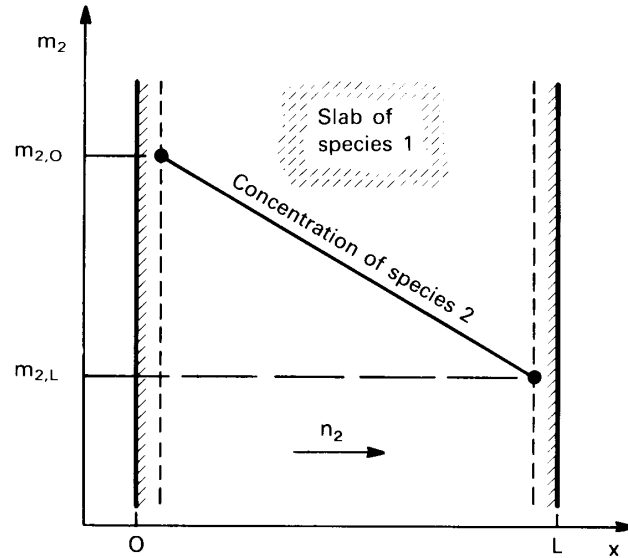
Figure 11.11 One-dimensional, steady diffusion of a dilute species through a stationary slab.

If species 2 is dilute, with $m_2 \ll 1$, the convective transport will be small

$$n_2 = m_2 n + j_2 \cong j_2$$

With Fick's law, we have

$$\frac{dn_2}{dx} \cong \frac{dj_2}{dx} = \frac{d}{dx}\left(-\rho \mathcal{D}_{21}\frac{dm_2}{dx}\right) = 0$$

If $\rho \mathcal{D}_{21} \cong$ constant, the mass fraction satisfies

$$\frac{d^2 m_2}{dx^2} = 0$$

Integrating and applying the boundary conditions, $m_2(x = 0) = m_{2,0}$ and $m_2(x = L) = m_{2,L}$, we obtain the concentration distribution:

$$m_2(x) = m_{2,0} + (m_{2,L} - m_{2,0})\left(\frac{x}{L}\right)$$

The mass flux is then

$$n_2 \cong j_2 = -\rho \mathcal{D}_{21}\frac{dm_2}{dx} = \frac{\rho \mathcal{D}_{21}}{L}(m_{2,0} - m_{2,L}) \qquad (11.52)$$

This, in essence, is the same calculation as made in Example 2.2 in Chapter 2. ∎

An interesting subtlety underlies this calculation. The diffuisional fluxes sum to zero, $j_1 + j_2 = 0$, so the slab itself must have a nonzero diffusional flux, j_1. However, because the slab is at rest, its total mass flux, n_1, is zero. Both conditions are met because the net mass flow through the slab ($n = n_2$) creates a non-zero mass average velocity, v. Thus

$$n_1 = 0 = \rho_1 v + j_1 \qquad (11.53)$$

The velocity v is sometimes called the *counterdiffusion velocity*; however, v is simply the mass-average speed at which the mixture flows when the net mass flux is not zero.

Example 11.8

Suppose that the concentration of species 2 in the slab were not small in the preceding example. How would the total mass flux of species 2 differ from the diffusional flux?

SOLUTION. The counterdiffusion velocity in the slab, by eqn. (11.53), is

$$v = -\frac{j_1}{\rho_1} = \frac{j_2}{\rho_1}$$

The mass flux for species 2 is

$$n_2 = \rho_2 v + j_2 = j_2 \left(\frac{\rho_2}{\rho_1} + 1 \right)$$
$$= j_2 \left(\frac{m_2}{m_1} + 1 \right)$$
$$= j_2 \left(\frac{1}{1 - m_2} \right) \qquad (11.54)$$

When $m_2 \ll 1$, $j_2 \cong n_2$ and convection is negligible. On the other hand, if $m_2 = 0.5$ at some point, then $n_2 = 2 j_2$! In that case, the convective transport $\rho_2 v$ is *equal* to the diffusive transport j_2. ∎

From these two examples, we see that steady mass diffusion is directly analogous to heat conduction *only* if the convective transport is negligible. That condition is met when the transferred species is dilute, with the other medium at rest. When the transferred species has a high concentration, significant convective transport can occur, even in a solid medium.

As a practical example, many desalination plants separate fresh water from salt water using polymeric reverse-osmosis membranes. These membranes absorb a considerable volume fraction of water—7 to 35% in one study [11.17]. The membranes are often modeled as nonporous, but with the water transported through by *both* diffusion and convection [11.18].

Unsteady mass diffusion in a stationary medium

Similar conclusions apply to unsteady mass diffusion. Consider a medium at rest through which a dilute species i diffuses. From the species conservation equation, (11.40) with $\dot{r}_i = 0$,

$$\frac{\partial \rho_i}{\partial t} = -\nabla \cdot \left(\rho_i \vec{v} + \vec{j}_i \right)$$
$$= -\nabla \cdot \left(m_i \vec{n} + \vec{j}_i \right) \tag{11.55}$$

If $m_i \ll 1$, $m_i n$ is negligible so that only diffusion contributes significantly to the mass flux of i. With Fick's law, eqn. (11.31),

$$\frac{\partial \rho_i}{\partial t} \approx -\nabla \cdot \vec{j}_i = \nabla \cdot (\rho \mathcal{D}_{im} \nabla m_i)$$

For small m_i, the density ρ and the diffusion coefficient $\mathcal{D}_{im}$ will not vary much, and we can factor both through the derivatives. The result is

$$\frac{\partial m_i}{\partial t} = \mathcal{D}_{im} \nabla^2 m_i \tag{11.56}$$

which is called the *mass diffusion equation*. The equation has the same form as the heat conduction equation. Solutions for the unsteady diffusion of a *dilute* species in a stationary medium are thus analogous to those for heat conduction when the boundary conditions are the same.

Example 11.9

A semi-infinite stationary medium (1) has an initially uniform concentration, $m_{i,0}$ of species i. At time $t = 0$, the end plane at $x = 0$ is placed in contact with a second medium (2) that has a concentration $m_{i,s}$. What is the distribution of species i in medium 1 for $t > 0$ if species i remains dilute?

SOLUTION. The mass fraction just inside the solid surface, $m_{i,u}$, can be calculated from $m_{i,s}$ and solubility data (see Fig. 11.12). This concentration is the boundary condition at $x = 0$ for $t > 0$. We have

$$\frac{\partial m_i}{\partial t} = \mathcal{D}_{im_1} \frac{\partial^2 m_i}{\partial x^2} \tag{11.57}$$

with

$$m_i = m_{i,0} \quad \text{for} \quad t = 0 \quad (\text{all } x)$$
$$m_i = m_{i,u} \quad \text{for} \quad x = 0 \quad (t > 0)$$
$$m_i \to m_{i,0} \quad \text{for} \quad x \to \infty \quad (t > 0)$$
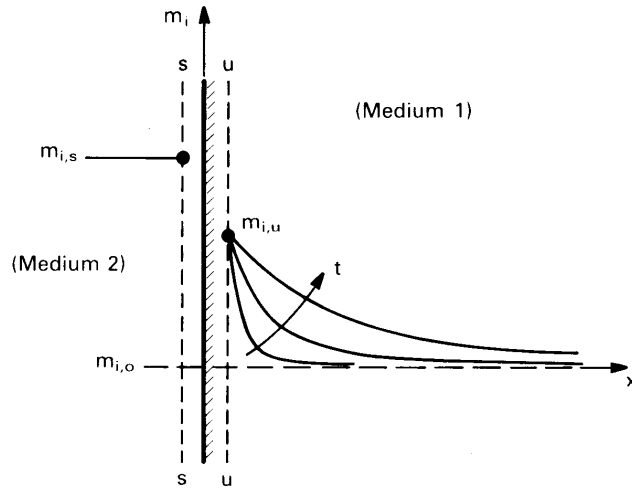
Figure 11.12 Mass diffusion into a semi-infinite stationary medium.

This problem is mathematically identical to that for transient heat conduction into a semi-infinite region (Section 5.6), and its solution is analogous to eqn. (5.50):

$$\frac{m_i - m_{i,u}}{m_{i,0} - m_{i,u}} = \text{erf}\left(\frac{x}{2\sqrt{\mathcal{D}_{im_1}t}}\right) \qquad \blacksquare$$

The reader can solve all sorts of unsteady mass diffusion problems by direct analogy to the methods of Chapters 4 and 5 when the concentration of the diffusing species is low.

At high concentrations of the diffusing species, counterdiffusion velocities can be induced as in Example 11.8. Counterdiffusion may be significant in concentrated metallic alloys, as for example, during annealing of a butt-welded junction between dissimilar metals. In those situations, eqn. (11.56) is sometimes modified to use a concentration-dependent, spatially varying *interdiffusion coefficient* [11.4].

Steady diffusion of a non-dilute species

Let us now find the mass flux when the diffusing species is not dilute, as in Example 11.8. We substitute Fick's law for j_2 in to eqn. (11.54)

$$n_2 = \left(-\rho \mathcal{D}_{12}\frac{dm_2}{dx}\right)\left(\frac{1}{1 - m_2}\right) = \text{constant in } x \qquad (11.58a)$$
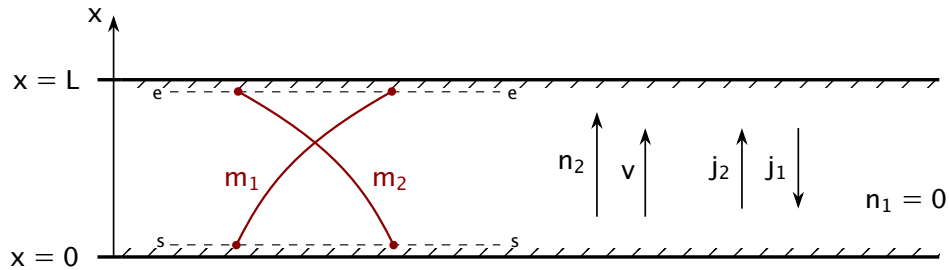
Figure 11.13 Steady mass transfer through a stagnant layer. Species 2 enters at $x = 0$ and leaves at $x = L$. Species 1 is at rest. The mass flux n_2 and the counterdiffusion (mass average) velocity v are constant, but the concentrations, m_1 and m_2, and the diffusive fluxes, j_1 and j_2, are functions of x.

then rearrange and integrate from one side to the other (Fig. 11.13), assuming that $\rho \mathcal{D}_{12}$ does not vary much and that $m_2 < 1$:

$$\frac{n_2}{\rho \mathcal{D}_{12}} \int_0^L dx = - \int_{m_{2,0}}^{m_{2,L}} \frac{dm_2}{1 - m_2}$$

Upon performing the integration

$$n_2 = \frac{\rho \mathcal{D}_{12}}{L} \ln\left(\frac{1 - m_{2,L}}{1 - m_{2,0}}\right)$$

With the two mass fractions, we may calculate the mass flux.

We can write eqn. (11.58) as

$$n_2 = \frac{\rho \mathcal{D}_{12}}{L} \ln\left(1 + \frac{m_{2,0} - m_{2,L}}{1 - m_{2,0}}\right) = \frac{\rho \mathcal{D}_{12}}{L} \ln(1 + B_{m,2}) \qquad (11.59)$$

where we define $B_{m,2}$, the *mass transfer driving force*, as shown. The driving force can be either positive or negative.

When $B_{m,2}$ is small, the mass flow is purely diffusive with negligible counterdiffusion. For instance, m_2 was small in Example 11.7, and so the mass flow was purely diffusive, with $n_2 \approx j_2$. In terms of the mass transfer driving force, when m_2 is small, $1 - m_{2,0} \approx 1$ so $B_{m,2} \approx m_{2,L} - m_{2,0}$. Further, the concentration difference itself is small when m_2 is small. Therefore, $|B_{m,2}| \ll 1$ and $\ln(1 + B_{m,2}) \approx B_{m,2} \approx m_{2,L} - m_{2,0}$. Hence, eqn. (11.59) reduces to eqn. (11.52), the pure mass diffusion case that is analogous to the heat conduction problem of Example 2.2.

The counterdiffusion velocity corresponding to eqn. (11.59) is

$$v = \frac{n}{\rho} = \frac{n_2}{\rho} = \frac{\mathcal{D}_{12}}{L} \ln(1 + B_{m,2}) \qquad (11.60)$$

When $B_{m,2}$ is small, $v \to 0$, so that counterdiffusion will not be important if species 2 is dilute.

Additional calculations show that the concentration profile generally is not a straight line (except when $B_{m,2} \ll 1$ as in Example 11.7):

$$\frac{1 - m_2(x)}{1 - m_{2,0}} = \left(\frac{1 - m_{2,L}}{1 - m_{2,0}}\right)^{x/L} = \left(1 + B_{m,2}\right)^{x/L} \qquad (11.61)$$

Molar formulation. Equation (11.58) could have been obtained in molar form by starting with the mole flux, eqn. (11.24), and using the molar form of Fick's law, eqn. (11.30), with the assumption that $c\mathcal{D}_{12}$ is constant:

$$N_2 = \frac{c\mathcal{D}_{12}}{L} \ln\left(\frac{1 - x_{2,L}}{1 - x_{2,0}}\right) \qquad (11.62)$$

For an ideal gas, $c = p/R^\circ T$, according to eqn. (11.13). Thus, the product $c\mathcal{D}_{12}$ does not depend on the local mole fractions. In contrast, $\rho\mathcal{D}_{12}$ varies with the local composition. As a result the molar formulation is more broadly accurate than the mass formulation (see Problems 11.19 and 11.47).

Example 11.10   Stefan tube measurement of $\mathcal{D}_{12}$

In 1873, Josef Stefan[9] derived a form of eqn. (11.62), which he applied for measuring diffusion coefficients in binary gas mixtures [11.21]. A long slender tube contained a pool of volatile liquid below a column of a different gas which was insoluble in the liquid. As the volatile liquid evaporated, its vapor would diffuse through the gas to the open top of the tube, where it would be swept away by the flowing gas above (Fig. 11.14). By observing the fall of the liquid level, Stefan could determine $\mathcal{D}_{12}$. How was he able to do this?

---

[9] Josef Stefan (1835–1893) was an Austrian physicist and a professor at the University of Vienna. He made seminal contributions to several areas of heat and mass transfer, including the Stefan-Boltzmann law of radiation, the Maxwell-Stefan equations of diffusion, the discovery of counterdiffusion in mass transfer, and the theory of moving boundaries during phase change [11.19]. Ludwig Boltzmann was his student. Stefan also analyzed the transient behavior of the Stefan tube in 1889 (see Mitrović [11.20]).
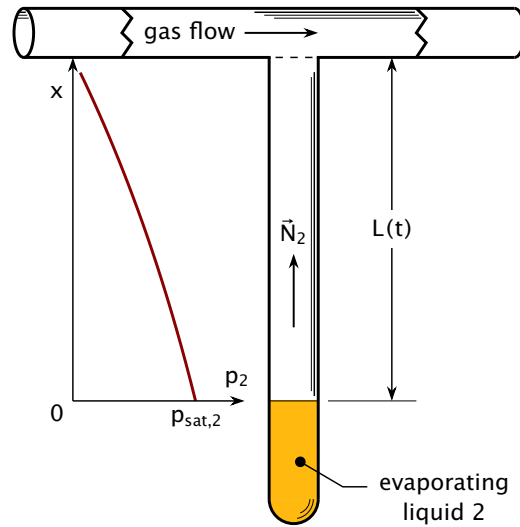
Figure 11.14 Schematic drawing of Stefan's evaporation tube. The molar flow rate of vapor is N_2.

SOLUTION. Let the gas be species 1 and the vapor species 2. The mole fraction of vapor above the liquid, $x_{2,0}$ is the liquid's vapor pressure, $p_{\text{sat},2}$, divided by the total pressure, p (Example 11.3). The mole fraction drops to $x_{2,L} = 0$ at the top of the tube. If the liquid evaporates slowly, the length of gas-filled tube above the liquid, $L(t)$, increases only slowly, and we may assume that the evaporation rate is quasi-steady and given by eqn (11.62) at any time. Then, if $\rho_{\text{liq},2}$ is the liquid's density and M_2 the liquid's molar mass,

$$
\underbrace{\rho_{\text{liq},2}\frac{dL}{dt}}_{\substack{\text{liquid evaporation} \\ \text{rate per unit area}}} = M_2 N_2 = \underbrace{\frac{M_2 c \mathcal{D}_{12}}{L} \ln\left(\frac{p}{p - p_{\text{sat},2}}\right)}_{\substack{\text{mass flux of vapor} \\ \text{per unit area}}}
\tag{11.63}
$$

By integrating from the initial length, L_0, and initial time, t_0,

$$
\int_{L_0}^{L(t)} L\,dL = \frac{M_2 c \mathcal{D}_{12}}{\rho_{\text{liq},2}} \ln\left(\frac{p}{p - p_{\text{sat},2}}\right) \int_{t_0}^{t} dt
$$

$$
\frac{L^2(t) - L_0^2}{2} = \frac{M_2 c \mathcal{D}_{12}}{\rho_{\text{liq},2}} \ln\left(\frac{p}{p - p_{\text{sat},2}}\right)(t - t_0)
$$

Finally, we solve for $\mathcal{D}_{12}$ and substitute for c using eqn. (11.13)

$$
\mathcal{D}_{12} = \frac{[L^2(t) - L_0^2]}{2(t - t_0)}\left(\frac{\rho_{\text{liq},2}}{M_2}\right)\left(\frac{R^\circ T}{p}\right)\left[\ln\left(\frac{p}{p - p_{\text{sat},2}}\right)\right]^{-1}
\tag{11.64}
$$
∎

Stefan tube measurements have provided diffusion coefficients for hundreds of gas pairs. A typical laboratory tube is 5–10 mm in diameter and 10–20 cm long. The evaporation rates are low, and a single measurement can take half a day. Measurements are possible only over fairly narrow temperature intervals within which the vapor pressure is suitable. Note that a volatile solid can be used in place of a liquid. Marrero and Mason discuss Stefan tube measurements in detail [11.7].

11.6   Convective mass transfer at low rates

Figure 11.15 shows a flat-plate boundary layer in which species i is transferred from the wall to the free stream. Free stream values, at the edge of the b.l., are labeled with the subscript e, and values just above the wall are labeled with the subscript s. The mass fraction of species i varies from $m_{i,s}$ to $m_{i,e}$ across a *concentration boundary layer*.
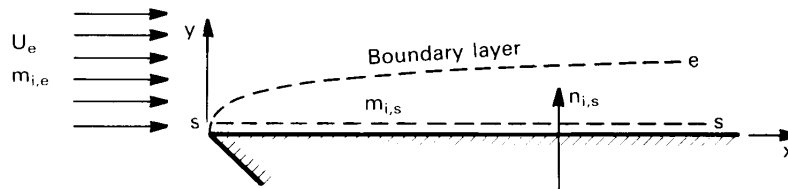
Figure 11.15   Concentration boundary layer on a flat plate.

In the previous section, we saw that mass diffusion is analogous to heat conduction if the mass fraction of the diffusing species is low. Under what conditions is mass convection analogous to heat convection? Put differently, heat convection is the process of heat conduction through a moving fluid. When is mass convection simply mass *diffusing* through a moving fluid, without changing the velocity profile?

Two questions must be answered. First, is the concentration of the transferred species low enough that mass transfer normal to the wall is purely diffusive? And second, is the mass transfer rate through the wall low enough that the velocity profile in the boundary layer is the same as for the analogous heat convection problem?

The answer to the first question follows Section 11.5. If the diffusing species has a low concentration, so that m_i is small, its mass flux in the

y-direction is mainly by diffusion:[10]

$$n_i = m_i n + j_i \simeq j_i$$

For the second question, we note that when the mass transfer driving force $B_{m,i}$ is small, the counterdiffusion velocity normal to the wall is small, as suggested by eqn. (11.60). Thus, the velocity profile is negligibly affected by mass transfer.[11] In fact, a sufficiently small value of $B_{m,i}$ ensures that both the first and the second conditions are met (see Section 11.8):

$$\left| B_{m,i} \right| = \left| \frac{m_{i,s} - m_{i,e}}{1 - m_{i,s}} \right| \lesssim 0.2 \qquad \begin{array}{l} \text{condition for low-rate} \\ \text{mass convection} \end{array} \qquad (11.65)$$

This criterion applies when only one species, species i, is transferred through the s-surface. The evaporation of water into air is typical example of single-species transfer: only water vapor crosses the s-surface. For water surface temperatures below about 65℃ (149°F), Fig. 11.10 and simple calculations show that $B_{m,\mathrm{H_2O}} \leqslant 0.2$.

The mass transfer coefficient. In the notation of Fig. 11.15, the wall heat flux is

$$q_s = h \left(T_s - T_e \right) \qquad (1.17)$$

where h is the convective heat transfer coefficient. At the wall, where the fluid is at rest by virtue of the no-slip condition, the heat flux is carried entirely by conduction. The flow field controls the steepness of the fluid's temperature gradient at the wall, and thereby sets the value of h (eqn. (6.35)).

Similarly, in convective mass transfer, the diffusional mass flux from a surface, $j_{i,s}$, is the product of a mass transfer coefficient and the concentration difference

$$j_{i,s} \equiv g_{m,i} \left(m_{i,s} - m_{i,e} \right) \qquad (11.66)$$

where $g_{m,i}$ (kg/m^2·s) is the *mass transfer coefficient* for species i. Like h, $g_{m,i}$ depends on the velocity, the fluid, and the configuration.

---

[10]In situations like catalysis, where no net mass flows through the wall, mass transfer near the wall is purely diffusive at any concentration (Problem 11.6.)

[11]Advanced boundary layer theory, taking account of the velocity of the transferred species through the wall, provides a fuller description of this flow [11.22].

The analogy to convective heat transfer. The species conservation equation and the energy equation are very similar for incompressible flow, as seen in Section 11.4. With no chemical reactions or heat generation, those equations are

$$\frac{\partial \rho_i}{\partial t} + \vec{v} \cdot \nabla \rho_i = -\nabla \cdot \vec{j}_i \tag{11.43}$$

$$\rho c_p \left(\frac{\partial T}{\partial t} + \vec{v} \cdot \nabla T \right) = -\nabla \cdot \vec{q} \tag{6.37}$$

The equations state that changes in mass or energy per unit volume result from convection by a velocity field $\vec{v}$ and from diffusion under either Fick's or Fourier's law.

What are the quantities are analogous in these equations? For the mass or energy change per unit volume

$$d\rho_i \quad \text{is analogous to} \quad \rho c_p dT \tag{11.67a}$$

or, since density is nearly constant when species i is dilute

$$\rho \, dm_i \quad \text{is analogous to} \quad \rho c_p dT \tag{11.67b}$$

Fourier's law and Fick's law (for effectively binary diffusion) may be rewritten to display the mass and energy per unit volume

$$\vec{j}_i = -\rho \mathcal{D}_{im} \nabla m_i = -\mathcal{D}_{im} (\rho \nabla m_i)$$

$$\vec{q} = -k \nabla T \qquad = -\frac{k}{\rho c_p} \left(\rho c_p \nabla T \right)$$

Hence, the analogy for the diffusivities is:

$$\mathcal{D}_{im} \quad \text{is analogous to} \quad \frac{k}{\rho c_p} = \alpha \tag{11.67c}$$

It follows that the Schmidt number and the Prandtl number are analogous:

$$Sc = \frac{\nu}{\mathcal{D}_{im}} \quad \text{is analogous to} \quad Pr = \frac{\nu}{\alpha} \tag{11.67d}$$

Thus, for example, a high Schmidt number signals a thin concentration boundary layer, just as a high Prandtl number signals a thin thermal boundary layer.

Table 11.2 Analogous quantities in convective heat and mass transfer. For incompressible flow with $|B_{m,i}| \lesssim 0.2$.

Analogous quantity	Heat convection	Mass convection
diffusivity	α	$\mathcal{D}_{i,m}$
	$\Pr = \dfrac{\nu}{\alpha}$	$\mathrm{Sc} = \dfrac{\nu}{\mathcal{D}_{i,m}}$
transfer coefficient	$\dfrac{h}{c_p}$	$g_{m,i}$
	$\mathrm{Nu}_x = \dfrac{hx}{k}$	$\mathrm{Nu}_{m,x} = \dfrac{g_{m,i}x}{\rho \mathcal{D}_{i,m}}$
functional relationship	$\mathrm{Nu}_x = \mathrm{fn}(\mathrm{Re}_x, \Pr)$	$\mathrm{Nu}_{m,x} = \mathrm{fn}(\mathrm{Re}_x, \mathrm{Sc})$

Finally, the transfer coefficients written in terms of the amounts per unit volume are

$$j_{i,s} = g_{m,i}\left(m_{i,s} - m_{i,e}\right) = \left(\frac{g_{m,i}}{\rho}\right)\rho\left(m_{i,s} - m_{i,e}\right)$$

$$q_s = h\left(T_s - T_e\right) \qquad = \left(\frac{h}{\rho c_p}\right)\rho c_p\left(T_s - T_e\right)$$

from which we see that

$$g_{m,i} \quad \text{is analogous to} \quad \frac{h}{c_p} \tag{11.67e}$$

Thus, the solution of a heat convection problem becomes the solution of a low-rate mass convection problem upon replacing the heat transfer variables by the analogous mass transfer variables, using eqns. (11.67).

The Nusselt number for heat transfer is a function of the Reynolds and Prandtl numbers

$$\mathrm{Nu}_x = \frac{hx}{k} = \frac{(h/c_p)x}{\rho(k/\rho c_p)} = \mathrm{fn}(\mathrm{Re}_x, \Pr) \tag{11.68}$$

The Nusselt number for mass transfer follows by making the substitutions of the analogy. Specifically, by replacing h/c_p by $g_{m,i}$, $k/\rho c_p$ by $\mathcal{D}_{i,m}$, and Pr by Sc, we obtain

$$\boxed{\mathrm{Nu}_{m,x} \equiv \frac{g_{m,i}x}{\rho \mathcal{D}_{im}} = \mathrm{fn}(\mathrm{Re}_x, \mathrm{Sc})} \tag{11.69}$$

where $Nu_{m,x}$ is the *Nusselt number for mass transfer*. Nu_m is often called the *Sherwood number*[12], Sh.

Table 11.2 summarizes analogy between convective heat transfer and low-rate mass transfer.

Example 11.11   Naphthalene sublimation

A naphthalene model of a printed circuit board (PCB) is placed in a wind tunnel. The naphthalene slowly sublimes as a result of forced convection mass transfer. If the first 5 cm of the naphthalene model is a flat plate, calculate the average rate of loss of naphthalene from that part of the model. The conditions are isothermal at 303 K, and the air speed is 5 m/s.

SOLUTION. Let us first find the mass fraction of naphthalene just above the model surface. A relationship for the vapor pressure of naphthalene (in mmHg) is $\log_{10} p_v = 11.450 - 3729.3/(T \text{ K})$. At 303 K, this gives $p_v = 0.1387$ mmHg $= 18.49$ Pa. The mole fraction of naphthalene is thus $x_{\text{nap},s} = 18.49/101325 = 1.825 \times 10^{-4}$, and with eqn. (11.9) and $M_{\text{nap}} = 128.2$ kg/kmol, the mass fraction is

$$m_{\text{nap},s} = \frac{(1.825 \times 10^{-4})(128.2)}{(1.825 \times 10^{-4})(128.2) + (1 - 1.825 \times 10^{-4})(28.96)}$$

$$= 8.074 \times 10^{-4}$$

The mass fraction of naphthalene in the free stream, $m_{\text{nap},s}$, is zero. Is the mass transfer rate is low enough to use the analogy of heat and mass transfer? From eqn. (11.65):

$$B_{m,\text{nap}} = \left(\frac{8.074 \times 10^{-4} - 0}{1 - 8.074 \times 10^{-4}} \right) = 8.081 \times 10^{-4} \ll 0.2$$

The analogy therefore applies.

For forced convection in a flat plate boundary layer, the Reynolds number is

$$Re_L = \frac{u_\infty L}{\nu} = \frac{(5)(0.05)}{1.867 \times 10^{-5}} = 1.339 \times 10^4 \quad \text{(laminar)}$$

[12]Thomas K. Sherwood (1903–1976) obtained his doctoral degree at MIT in 1929 under the supervision Warren K. Lewis, and he served as a professor of Chemical Engineering at MIT from 1930 to 1969. His research dealt with mass transfer and related industrial processes. Sherwood wrote the first significant textbook on mass transfer, *Absorption and Extraction*, published in 1937.

Here, we used the viscosity of pure air because the concentration of naphthalene is very low. For laminar flow, eqn. (6.68) is appropriate:

$$\overline{\mathrm{Nu}}_L = \frac{\overline{h}L}{k} = 0.664 \, \mathrm{Re}_L^{1/2} \, \mathrm{Pr}^{1/3} \tag{6.68}$$

Under the analogy, the Nusselt number for mass transfer is

$$\overline{\mathrm{Nu}}_{m,L} = \frac{\overline{g_{m,i}}\,L}{\rho \mathcal{D}_{im}} = 0.664 \, \mathrm{Re}_L^{1/2} \, \mathrm{Sc}^{1/3}$$

The diffusion coefficient for naphthalene in air, from Table 11.1, is $\mathcal{D}_{\mathrm{nap,air}} = 0.86 \times 10^{-5}$ m/s, and thus $\mathrm{Sc} = 1.867 \times 10^{-5}/0.86 \times 10^{-5} = 2.17$. Hence,

$$\overline{\mathrm{Nu}}_{m,L} = 0.664 \, (1.339 \times 10^4)^{1/2} \, (2.17)^{1/3} = 99.5$$

Using the density of pure air,

$$\begin{aligned}
\overline{g_{m,\mathrm{nap}}} &= \frac{\rho \mathcal{D}_{\mathrm{nap,air}}}{L} \, \overline{\mathrm{Nu}}_{m,L} \\
&= \frac{(1.166)(0.86 \times 10^{-5})}{0.05}(99.5) = 0.0200 \, \mathrm{kg/m^2 s}
\end{aligned}$$

The average mass flux from this part of the model is

$$\begin{aligned}
\overline{n_{\mathrm{nap},s}} &= \overline{g_{m,\mathrm{nap}}} \, (m_{\mathrm{nap},s} - m_{\mathrm{nap},e}) \\
&= (0.0200)(8.074 \times 10^{-4} - 0) \\
&= 1.61 \times 10^{-5} \, \mathrm{kg/m^2 s} = 58.0 \, \mathrm{g/m^2 h} \qquad \blacksquare
\end{aligned}$$

Naphthalene sublimation is an experimental technique for inferring heat transfer coefficients. The mass of naphthalene lost from an object over a length of time defines the sublimation rate and, thus, the mass transfer coefficient. The analogy to heat transfer then yields the heat transfer coefficient. Experiments at several air speeds numbers will reveal the dependence on Reynold number. However, the Schmidt number of naphthalene in air is not equal to the Prandtl number of air. To correct for this difference, an educated guess for the Prandtl number dependence of the Nusselt number is needed, e.g., $\mathrm{Nu} \propto \mathrm{Pr}^n$ for $1/3 \leqslant n \leqslant 0.4$ [11.23].

Boundary conditions. Two wall conditions are common in convective heat transfer: uniform temperature and uniform heat flux. The analogous mass transfer wall conditions are uniform concentration and, infrequently, uniform mass flux. Example 11.11 used the mass transfer analog of

the uniform wall temperature solution because the mass fraction of naphthalene was uniform over the surface of the model. Had the mass flux been uniform, we would have used the analog of the uniform heat flux solution (see Problem 11.29).

Natural convection in mass transfer.   A density difference caused by a temperature difference can create flow and convection, as discussed in Chapter 8. Density differences can also be caused by composition differences, resulting in natural convection mass transfer. Equation (8.4) still governs the buoyancy-driven flow

$$u\frac{\partial u}{\partial x} + v\frac{\partial u}{\partial y} = (1 - \rho_\infty/\rho)g + v\frac{\partial^2 u}{\partial y^2} \qquad (8.4)$$

but now the species equation, not the energy equation, governs the density variation. To avoid solving these equations, we may apply the analogy between heat and mass transfer.

For natural convection heat transfer, the buoyancy term in eqn. (8.4) is $(1 - \rho_\infty/\rho) = \beta(T - T_\infty)$. The Grashof and Rayleigh numbers depend on $\beta\Delta T$, but that factor simply equals $\Delta\rho/\rho$. So, in terms of density

$$\mathrm{Gr}_L = \frac{g\Delta\rho L^3}{\rho v^2} \quad \text{and} \quad \mathrm{Ra}_L = \frac{g\Delta\rho L^3}{\rho\alpha v} = \frac{g\Delta\rho L^3}{\mu\alpha} \qquad (11.70)$$

The analogy between heat transfer and mass transfer is straightforward when Gr or Ra use the density difference. As before, Nu_m and Sc replace Nu and Pr. Equation (11.70) gives Gr_L and

$$\mathrm{Ra}_L = \mathrm{Gr}_L\mathrm{Sc} = \frac{g\Delta\rho L^3}{\mu\mathcal{D}_{12}} \qquad (11.71)$$

We compute the density difference using the concentration difference.

If *both* temperature and concentration vary, the density difference depends on both m_i and T. The Grashof or Rayleigh number based on density is still correct for the analogy, provided that the Prandtl and Schmidt numbers are approximately equal (that is, for Lewis numbers near one).[13] This condition is usually met by gas mixtures. We look at an example like that in the next section.

---

[13]When the Lewis number is far from one, the concentration and thermal boundary layers may have very different thicknesses, which complicates their relationship to the buoyancy-driven velocity field.

11.7 Simultaneous heat and mass transfer at low rates

Cooling towers, dehumidifiers, and combustors are just three important examples of equipment in which heat and mass transfer occur simultaneously. A common situation involves evaporation, as when warm water vaporizes into cool, dry air. The enthalpy of water vapor is much higher than that of liquid water at the same temperature. As a result, water evaporated from the surface has a powerful cooling effect, equal to the product of the latent heat of vaporization and the evaporation rate. The cooling effect becomes stronger as the water surface temperature rises because the vapor pressure of water increases rapidly with temperature (see Example 11.3).

In the carbon oxidation problem of Example 11.2, heat is released as carbon is oxidized, and the rate of oxidation increases with surface temperature. The rate at which the surface is cooled by convection and radiation also increases with temperature. The steady temperature of the burning carbon is set by a balance between the rate of cooling and the rate of heat release.

As an example of simultaneous heat and mass transfer, let's think about coffee.

Example 11.12   Heat loss from a coffee cup

Many engineering students have come to appreciate the value of hot coffee. But coffee is never hot for long! Evaporation is the main source of heat loss. Let's estimate the rate of cooling from the top of a 9 cm diameter cup of coffee at 60℃ (140°F), if the cup is in a room at 25℃, 50% RH, and 1 atm. The diffusion coefficient of water vapor in air at the film temperature is $\mathcal{D}_{H_2O,air} = 2.82 \times 10^{-5}$ m^2/s.

Solution. Heat is removed by evaporative cooling, natural convection, and thermal radiation. We'll first find the partial density of water vapor and the density of the mixture, so that we can compute the mass fraction of water vapor and the Grashof number. If we treat the coffee as nearly pure water, eqn. (11.45) shows that the vapor partial of water is

$$p_{H_2O,s} = p_{sat}(T_s) = p_{sat}(333 \text{ K}) = 19,940 \text{ Pa}$$

with the saturation pressure taken from a steam table and the s-surface located just above the coffee. Relative humidity is defined as

$\text{RH} = p_{\text{H}_2\text{O},e}/p_{\text{sat}}(T_e)$ so

$$p_{\text{H}_2\text{O},e} = (0.50)p_{\text{sat}}(298 \text{ K}) = (0.50)(3,169 \text{ Pa}) = 1,585 \text{ Pa}$$

The densities can be found with eqns. (11.1), (11.10), and (11.11)

$$\rho_{\text{mixture}} = \rho_{\text{H}_2\text{O}} + \rho_{\text{air}} = \frac{p_{\text{H}_2\text{O}}M_{\text{H}_2\text{O}}}{R^\circ T} + \frac{p_{\text{air}}M_{\text{air}}}{R^\circ T}$$

with $p_{\text{air}} = (101325 \text{ Pa} - p_{\text{H}_2\text{O}})$ by Dalton's law, eqn. (11.14). At the s-surface,

$$\begin{aligned}
\rho_{\text{mix},s} &= \frac{(19940)(18.02)}{(8314.5)(333)} + \frac{(101325 - 19940)(28.96)}{(8314.5)(333)} \\
&= \underbrace{0.1298}_{=\rho_{\text{H2O},s}} + 0.8513 = 0.9810 \text{ kg/m}^3
\end{aligned}$$

and in the environment,

$$\begin{aligned}
\rho_{\text{mix},e} &= \frac{(1585)(18.02)}{(8314.5)(298)} + \frac{(101325 - 1585)(28.96)}{(8314.5)(298)} \\
&= \underbrace{0.01153}_{=\rho_{\text{H2O},e}} + 1.166 = 1.177 \text{ kg/m}^3
\end{aligned}$$

The mass fractions of water vapor, with eqn. (11.2), are

$$m_{\text{H}_2\text{O},s} = \rho_{\text{H}_2\text{O},s}/\rho_{\text{mix},s} = (0.1298)/(0.9810) = 0.1323$$
$$m_{\text{H}_2\text{O},e} = \rho_{\text{H}_2\text{O},e}/\rho_{\text{mix},e} = (0.01153)/(1.177) = 0.00980$$

Checking $B_{m,\text{H}_2\text{O}}$ shows that low mass transfer rates prevail:

$$B_{m,\text{H}_2\text{O}} = \left(\frac{m_{\text{H}_2\text{O},s} - m_{\text{H}_2\text{O},e}}{1 - m_{\text{H}_2\text{O},s}}\right) = \frac{0.1323 - 0.00980}{1 - 0.1323} = 0.1412 < 0.2$$

To find the natural convection heat and mass transfer coefficients, we need the Grashof number. With eqn. (11.70),

$$\text{Gr}_D = \frac{g\Delta\rho D^3}{\rho_f \nu_{\text{air},f}^2} = \frac{(9.806)(0.1323 - 0.00980)(0.09)^3}{(1.079)(1.716 \times 10^{-5})^2} = 2.756 \times 10^6$$

using the film density $\rho_f = (\rho_s + \rho_e)/2$ and the viscosity of pure air at the film temperature, $T_f = 316 \text{ K}$. The Schmidt number is

$$\text{Sc} = \frac{\nu}{\mathcal{D}_{\text{H}_2\text{O,air}}} = \frac{1.716 \times 10^{-5}}{2.82 \times 10^{-5}} = 0.609$$

The Nusselt number is approximated by eqn. (8.37a), where $L^* = A/P = D/4$. Written terms of D and Gr_D, that correlation is

$$\overline{Nu}_D = \frac{0.560\sqrt{2}\ Gr_D^{1/4}Pr^{1/4}}{\left[1 + (0.492/Pr)^{9/16}\right]^{4/9}}$$

and with $Pr = 0.708$, $\overline{Nu}_D = 22.7$. Analogously, for mass transfer

$$\overline{Nu}_{m,D} = \frac{0.560\sqrt{2}\ Gr_D^{1/4}Sc^{1/4}}{\left[1 + (0.492/Sc)^{9/16}\right]^{4/9}} = 21.5$$

The heat and mass transfer coefficients are then

$$\overline{h} = \frac{k\overline{Nu}_D}{D} = \frac{(0.0273)(22.7)}{0.09} = 6.89 \text{ W/m}^2\text{K}$$

$$\begin{aligned}\overline{g}_{m,H_2O} &= \frac{\rho_f \mathcal{D}_{H_2O,air}\overline{Nu}_{m,D}}{D} \\ &= \frac{(1.079)(2.82 \times 10^{-5})(21.5)}{0.09} = 7.27 \times 10^{-3} \text{ kg/m}^2\text{s}\end{aligned}$$

We now calculate the heat losses. For natural convection,

$$Q_{nc} = \left(\frac{\pi D^2}{4}\right)\overline{h}(T_s - T_e) = \cdots = 1.53 \text{ W}$$

For radiation, with $\varepsilon_{H_2O} = 0.9$,

$$Q_{rad} = \left(\frac{\pi D^2}{4}\right)\varepsilon_{H_2O}\sigma\left(T_s^4 - T_e^4\right) = \cdots = 1.43 \text{ W}$$

The evaporative loss, with $h_{fg} = 2.359$ MJ/kg, is

$$Q_{evap} = \left(\frac{\pi D^2}{4}\right)h_{fg}\overline{g}_{m,H_2O}(m_{H_2O,s} - m_{H_2O,e}) = \cdots = 13.4 \text{ W}$$

The evaporative loss is largest by an order of magnitude. Putting a lid on your coffee cup will ensure that it stays warm much longer! ∎

The wet bulb temperature

A sling psychrometer is used to measure the humidity of air. As shown in Fig. 11.16, the device consists of two thermometers mounted side-by-side on a swivel handle. A wet cloth is wrapped about the bulb of one while the other remains dry. The pair are "slung" in a rotary motion until they reach steady state.
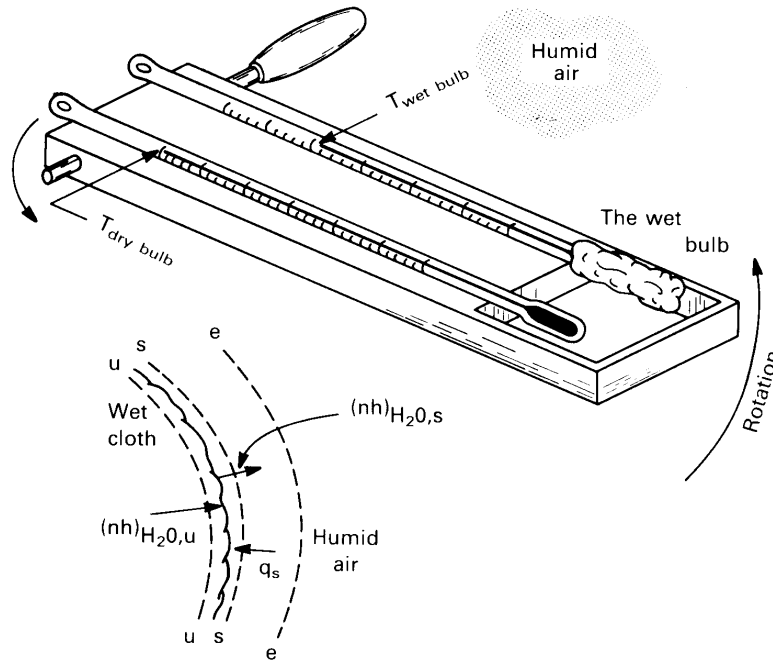
Figure 11.16 The wet bulb of a sling psychrometer.

The wet-bulb thermometer cools as the latent heat of evaporating water is given up, until its temperature drops enough that the rate of evaporative cooling just balances the rate of convective heating by the warmer air. This final temperature, called the *wet-bulb temperature*, is directly related to the concentration of water in the surrounding air.

The highest ambient air temperatures normally encountered are low enough that the mass transfer rate remains modest. We can show this by computing an upper bound on $B_{m,\text{H}_2\text{O}}$, using conditions that maximize the evaporation rate: the highest likely air temperature and the lowest humidity. Let us set those values, say, at 130°F (54°C) and zero humidity $(m_{\text{H}_2\text{O},e} = 0)$.[14] The vapor pressure on the wet bulb will be less than the saturation pressure at 130°F because evaporation will keep the bulb at a lower temperature. So, with eqn. (11.15)

$$x_{\text{H}_2\text{O,s}} < p_{\text{sat}}(130°\text{F})/p_{\text{atm}} = (15{,}347 \text{ Pa})/(101{,}325 \text{ Pa}) = 0.152$$

and, with eqn. (11.48),

$$m_{\text{H}_2\text{O},s} < 0.100$$

[14]In July 2023, Death Valley, California had temperatures above 125°F (51.7°C) with relative humidities around 5%.

Thus, the criterion for low-rate mass transfer, eqn. (11.65), is met:

$$B_{m,H_2O} = \left(\frac{m_{H_2O,s} - m_{H_2O,e}}{1 - m_{H_2O,s}} \right) < 0.111 < 0.2$$

To form an energy balance on the wick, consider the u, s, and e surfaces shown in Fig. 11.16. At the steady temperature, no heat is conducted past the u-surface (into the wet bulb), but liquid water flows through it to the surface of the wick where it evaporates. An energy balance on the region between the u and s surfaces gives

$$\underbrace{n_{H_2O,s}\hat{h}_{H_2O,s}}_{\substack{\text{enthalpy of water} \\ \text{vapor leaving}}} - \underbrace{q_s}_{\substack{\text{heat convected} \\ \text{to the wet bulb}}} = \underbrace{n_{H_2O,u}\hat{h}_{H_2O,u}}_{\substack{\text{enthalpy of liquid} \\ \text{water entering}}} \qquad (11.72a)$$

Since mass is conserved, $n_{H_2O,s} = n_{H_2O,u}$; and $\hat{h}_{H_2O,s} - \hat{h}_{H_2O,u} = h_{fg}$. Hence,

$$n_{H_2O,s}\, h_{fg}\big|_{T_{\text{wet-bulb}}} = \overline{h}(T_e - T_{\text{wet-bulb}})$$

The mass fraction of water vapor is low, so that $n_{H_2O,s} \cong j_{H_2O,s}$, and $j_{H_2O,s}$ can be written in terms of the mass transfer coefficient

$$\overline{g}_{m,H_2O}\,(m_{H_2O,s} - m_{H_2O,e})\, h_{fg}\big|_{T_{\text{wet-bulb}}} = \overline{h}(T_e - T_{\text{wet-bulb}}) \qquad (11.72b)$$

The heat and mass transfer coefficients depend on the shape and flow rates of the psychrometer, so it would appear that $T_{\text{wet-bulb}}$ depends on the device used to measure it. The two coefficients are not independent, however, owing to the analogy between heat and mass transfer.

For forced convection in cross flow (Section 7.6), the heat transfer coefficient follows the approximate form

$$\frac{\overline{h}D}{k} = C\,\text{Re}^a\text{Pr}^b$$

where C is a constant and typical values of a and b are $a \cong 1/2$ and $b \cong 1/3$. From the analogy,

$$\frac{\overline{g}_{m,i}D}{\rho \mathcal{D}_{H_2O,\text{air}}} = C\,\text{Re}^a\text{Sc}^b$$

and, by dividing the second expression into the first,

$$\frac{\overline{h}}{\overline{g}_{m,i}\,c_p}\frac{\mathcal{D}_{H_2O,\text{air}}}{\alpha} = \left(\frac{\text{Pr}}{\text{Sc}} \right)^b$$

Both $\alpha/\mathcal{D}_{m,i}$ and Sc/Pr are equal to the Lewis number, Le. Hence,

$$\frac{\overline{h}}{\overline{g}_{m,i}\,c_p} = \text{Le}^{1-b} \cong \text{Le}^{2/3} \tag{11.73}$$

Equation (11.73) shows that the ratio of $\overline{h}$ to $\overline{g}_{m,i}$ depends only on two physical properties of the gas mixture, Le and c_p, and not the shape or flow rate. The Lewis number for air–water systems is about 0.847, and, because the concentration of water vapor is usually very low, c_p can often be approximated by $c_{p_{\text{air}}}$.

The relationship between h and $g_{m,i}$ was identified by Warren K. Lewis in 1922 for the case Le $= 1$ [11.24]. (Lewis approximated Le as one for the air–water system he studied.) The more general form, eqn. (11.73), was proposed by Chilton and Colburn in 1934 [11.25]. That form is another Reynolds-Colburn style analogy, like eqn. (6.77).

Substituting eqn. (11.73) into eqn. (11.72b) gives our final result:

$$\boxed{T_e - T_{\text{wet-bulb}} = \left(\frac{h_{fg}\big|_{T_{\text{wet-bulb}}}}{c_{p_{\text{air}}}\,\text{Le}^{2/3}}\right)\left(m_{\text{H}_2\text{O},s} - m_{\text{H}_2\text{O},e}\right)} \tag{11.74}$$

In this equation, $m_{\text{H}_2\text{O},s}$ depends on the vapor pressure at $T_s = T_{\text{wet-bulb}}$. Consequently, we need data (or an equation) for the vapor pressure to calculate $m_{\text{H}_2\text{O},e}$ function of the wet and dry bulb temperatures. Such calculations closely approximate the psychrometric charts found in thermodynamics textbooks (see Problem 11.31).[15]

The wet-bulb temperature is a helpful concept in many phase-change processes. When a small body without internal heat sources evaporates or sublimes, it cools to a steady "wet-bulb" temperature at which convective heating is balanced by latent heat removal. The body will stay at that temperature until the phase-change process is complete. Consequently, the wet-bulb temperature appears in the evaporation of water droplets, the sublimation of dry ice, and the combustion of fuel sprays.

Example 11.13

What is the dry-bulb temperature if the wet-bulb temperature is 15℃ (59°F) and the relative humidity is: a) 0%; b) 100%? Take $p = 1$ atm.

---

[15]The wet-bulb temperature for air–water systems is very close to the *adiabatic saturation temperature* of the air–water mixture—the temperature reached by a mixture if it is brought to saturation with water by adding water vapor without adding heat. The adiabatic saturation temperature is a thermodynamic property of an air–water mixture, and its value is shown on psychrometric charts as the "wet-bulb" temperature.

SOLUTION. At 15°C, $c_{p,\text{air}} = 1006$ J/kg·K, $h_{fg} = 2.466$ MJ/kg, and $x_{\text{H}_2\text{O},s} = p_{\text{sat,H}_2\text{O}}/p_{\text{atm}} = (1,705)/(101,325) = 0.01683$. With eqn. (11.48), $m_{\text{H}_2\text{O},s} = 0.01054$. (a) Substituting into eqn. (11.74) with $m_{\text{H}_2\text{O},e} = 0$,

$$T_e - 15 = \left(\frac{(2.466 \times 10^6)}{(1006)(0.847)^{2/3}} \right)(0.01054 - 0) = 28.86$$

so $T_e = 43.9$°C (111°F). (b) When the relative humidity is 100%, the air is saturated with water vapor. The air can absorb no additional moisture, so evaporation cannot occur. The wet and dry bulb temperatures are equal, at 15°C. ∎

Evaporative cooling (sweating!) helps our bodies avoid overheating in hot weather. If the humidity is high, however, sweating is produces less evaporation, and we are at greater risk of heat stroke (see Problem 11.34).

Sweating is very effective for heat removal, and the process has been adapted industrially. For example, a porous wall exposed to hot gases can be cooled by bleeding liquid water through its surface, where the water evaporates and offsets convective heating by the hot gas. Unsurprisingly, this technique is called *sweat cooling*. See Section 11.9 for more details.

Example 11.14   D² law of droplet evaporation

A very small water droplet sprayed into a gas comes to its wet-bulb temperature quickly, and then evaporates until it is gone. How does the droplet diameter change in time?

SOLUTION. The mass balance for an evaporating droplet of diameter $D(t)$ and density ρ_l is

$$\underbrace{\frac{d}{dt}\left(\frac{\rho_l \pi D^3}{6} \right)}_{\text{rate of mass increase}} = -\underbrace{(\pi D^2)\overline{g}_{m,\text{H}_2\text{O}}(m_{\text{H}_2\text{O},s} - m_{\text{H}_2\text{O},e})}_{\text{rate of evaporation}}$$

Because the droplet is very small, the Grashof (or Reynolds) number will be small, and from eqn. (8.31), $\overline{\text{Nu}}_{m,D} = \overline{g}_{m,\text{H}_2\text{O}}D/\rho\mathcal{D}_{\text{H}_2\text{O,gas}} = 2$. Substituting and rearranging

$$\frac{\pi D^2 \rho_l}{2}\frac{dD}{dt} = -2\pi D\rho\mathcal{D}_{\text{H}_2\text{O,gas}}(m_{\text{H}_2\text{O},s} - m_{\text{H}_2\text{O},e})$$

$$D\frac{dD}{dt} = -\frac{4\rho\mathcal{D}_{H_2O,gas}}{\rho_l}(m_{H_2O,s} - m_{H_2O,e})$$

Integration from an initial diameter D_0 gives

$$D_0^2 - D^2(t) = \left[\frac{8\rho\mathcal{D}_{H_2O,gas}}{\rho_l}(m_{H_2O,s} - m_{H_2O,e})\right]t \qquad (11.75)$$

The droplet diameter squared drops as a straight line in time and reaches zero after a finite evaporation time. This result is called the D^2 *law*. The law has been studied extensively in the combustion and aerosol literatures [11.26–11.28]. ∎

Dew-point temperature and dehumidification

A cool surface in warm, moist air will condense water vapor if the saturation pressure of water at the surface's temperature is below the partial pressure of water in the air. Such *dew formation* is familiar: for instance, it causes droplets to form on a glass of ice water. The temperature at which saturation is reached is called the *dew-point temperature.*

Engineers harness dew formation to remove moisture from humid air, often to make living spaces more comfortable. In a typical dehumidifier design, a fin-tube heat exchanger with refrigerant in the tubes is cooled below the dew point temperature, causing water to condense on the fins and drying the air. The mass fraction of water vapor decreases near the liquid surface, and the concentration of air rises (Fig. 11.17).

The net mass flux toward the liquid is only the mass flux of condensing water vapor: the air, which does not condense, is stationary. The bulk velocity (counterdiffusion velocity) toward the surface opposes the diffusion of air away from the surface. As a result, the concentration gradient of air at the surface is not zero even though the mass flux of air is zero. The presence of air greatly impedes condensation, and mass transfer process is low rate.

The heat released by condensation at the liquid surface and the heat convected to the surface are removed by heat transfer into the liquid film:

$$n_{H_2O,s}h_{fg} + h(T_e - T_s) = h_{cond}(T_s - T_c) \qquad (11.76a)$$

Here

$$n_{H_2O,s} = g_{m,H_2O}(m_{H_2O,e} - m_{H_2O,s}) \qquad (11.76b)$$

where $m_{H_2O,s}$ must be calculated from vapor pressure at T_s, as in Example 11.3. The local film condensation heat transfer coefficient, h_{cond}, may be calculated using the methods of Section 8.5.
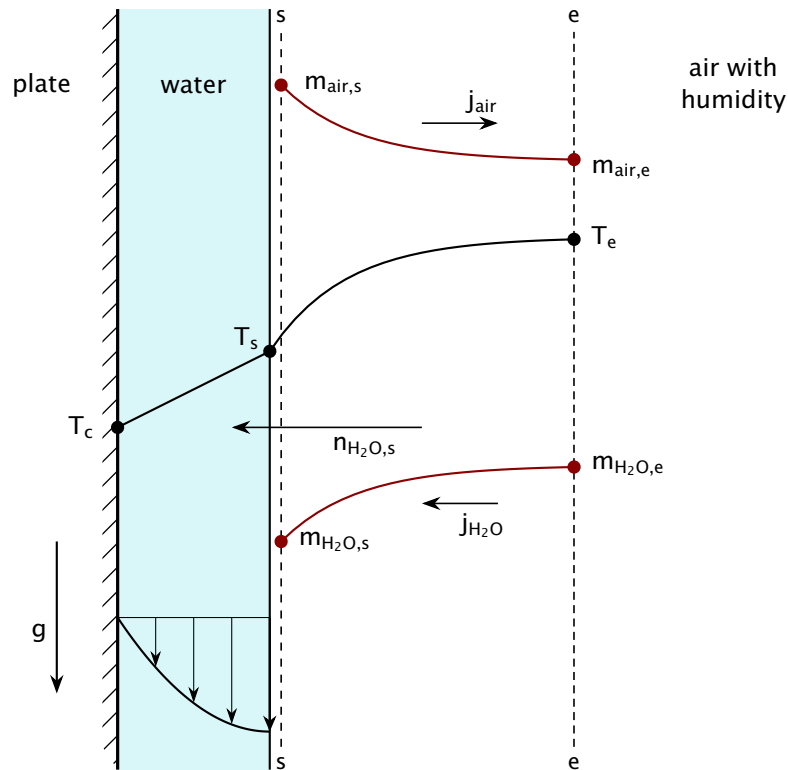
Figure 11.17 Air and water concentration profiles adjacent to a dehumidifier plate.

11.8 The Couette flow, or stagnant film, model

A Couette flow occurs when a plane layer of fluid is subjected to a uniform shear stress, without streamwise gradients. Such a flow occurs in a fluid between two parallel plates if one moves relative to the other.[16] If the plates align with the x-direction, the velocity changes only in the the y-direction, perpendicular to the plates. Similarly, if one plate were hot and the other cold, temperature gradients would occur only in the y-direction (Problem 11.37).

Couette flow is the simplest model for a boundary layer. As we saw in Chapter 6, the gradients in a boundary layer are strong in the y-direction and weak in the x-direction. This behavior is especially pronounced in the

---

[16]Named for the French physicist Maurice Marie Alfred Couette (1858–1943). He developed the rotating cylinder viscometer, in which a fluid layer between concentric cylinders experiences a uniform shear stress when one cylinder rotates.
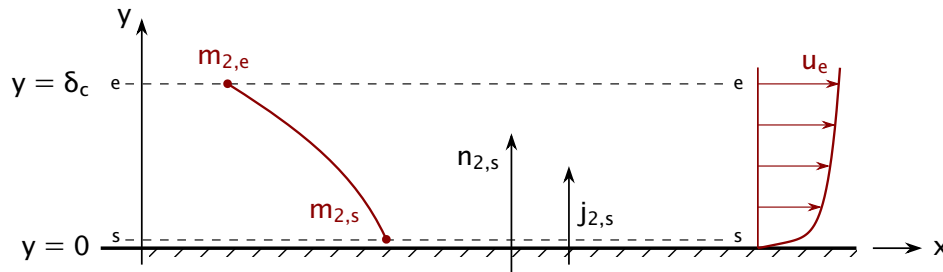
Figure 11.18 Couette flow b.l. model with one species transferred, showing turbulent mean velocity and concnetration profiles with negligible mean gradients in the x-direction.

near-wall part of a turbulent boundary layer, and we exploited that fact to neglect x derivatives when modeling turbulent friction and heat transfer. In eqns. (6.88) and (6.106), shear stress and heat flux were presumed be independent of x, which rendered them constant in the y-direction as well. In effect, we treated the near-wall turbulent boundary layer as a Couette flow, subject to a uniform shear stress and uniform heat flux.

Heat transfer in a Couette flow behaves much like heat transfer across a stagnant layer: the heat flux, from Fourier's law in laminar flow or eqn. (6.107) in turbulent flow, is constant in the y-direction. The temperature changes only in the y-direction. For that reason, Couette flow models of boundary layers are sometimes called *stagnant film* models.[17]

The Couette flow model also applies to the mass transfer boundary layer. Suppose that species 2 is transferred from the s-surface above a wall, through a boundary layer containing species 1, to the e-surface at the b.l.'s outside edge (Fig. 11.18). Species 1 does not move in the direction perpendicular to the wall, and the boundary may be approximated to have negligible gradients in the x-direction. We studied this problem in Section 11.5. If the effective thickness of this concentration boundary is δ_c, the mass flux of species 2 is given by eqn. (11.59):

$$n_2 = \frac{\rho \mathcal{D}_{12}}{\delta_c} \ln\left(1 + \frac{m_{2,s} - m_{2,e}}{1 - m_{2,s}}\right) = \frac{\rho \mathcal{D}_{12}}{\delta_c} \ln(1 + B_{m,2}) \qquad (11.77)$$

We can make this model equation more broadly useful with three modifications. First, we can write $n_{2,s}$ in terms of the mass transfer coefficient, without assuming that m_2 is small. Starting with eqn. (11.20)

---

[17]Here, "film" refers to the b.l. as if it were a film of fluid stuck to the wall.

at the s-surface,

$$n_{2,s} = m_{2,s}n_s + j_{2,s} \qquad (11.78\text{a})$$

we note that $n_s = n_{2,s}$ and rearrange, substituting eqn. (11.66) for $j_{2,s}$:

$$n_{2,s}(1 - m_{2,s}) = j_{2,s} = g_{m,2}(m_{2,s} - m_{2,e})$$

Thus,

$$n_{2,s} = g_{m,2}\left(\frac{m_{2,s} - m_{2,e}}{1 - m_{2,s}}\right) = g_{m,2}B_{m,2} \qquad (11.78\text{b})$$

Second, we extend analysis leading to eqn. (11.77) to allow for turbulent flow. In eqn. (11.58a), we used Fick's law for pure diffusion. If the boundary layer is turbulent, we can proceed by analogy to eqn. (6.103), assuming an eddy diffusivity for species 2, ε_2, and calling the time-average mass fraction $\overline{m}_2$

$$j_2 = -\rho(\mathcal{D}_{12} + \varepsilon_2)\frac{\partial\overline{m}_2}{\partial y} \qquad (11.79\text{a})$$

With $\overline{n}_2 = \overline{m}_2\overline{n} + j_2$ and $\overline{n} = \overline{n}_2 = n_{2,s}$

$$n_{2,s}(1 - \overline{m}_2) = -\rho(\mathcal{D}_{12} + \varepsilon_2)\frac{\partial\overline{m}_2}{\partial y} \qquad (11.79\text{b})$$

Rearranging and integrating, as in Section 11.5,

$$\ln\left(1 + \frac{m_{2,s} - m_{2,e}}{1 - m_{2,s}}\right) = n_{2,s}\int_0^{\delta_c} \frac{dy}{\rho(\mathcal{D}_{12} + \varepsilon_2)}$$

Then, with eqn. (11.78b) the definition of $B_{m,2}$:

$$\ln(1 + B_{m,2}) = g_{m,2}B_{m,2}\int_0^{\delta_c} \frac{dy}{\rho(\mathcal{D}_{12} + \varepsilon_2)}$$

$$g_{m,2} = \frac{\ln(1 + B_{m,2})}{B_{m,2}}\left[\int_0^{\delta_c} \frac{dy}{\rho(\mathcal{D}_{12} + \varepsilon_2)}\right]^{-1} \qquad (11.79\text{c})$$

The third and final modification connects eqn. (11.79c), which depends on $B_{m,2}$ and therefore on the rate of mass transfer, to the low-rate mass transfer coefficient discussed in Section 11.6. In the limit of small $B_{m,2}$

$$g_{m,2}^* \equiv \lim_{B_{m,2}\to 0} g_{m,2}$$

$$= \left[\int_0^{\delta_c} \frac{dy}{\rho(\mathcal{D}_{12} + \varepsilon_2)}\right]^{-1} \lim_{B_{m,2}\to 0}\frac{\ln(1 + B_{m,2})}{B_{m,2}} = \left[\int_0^{\delta_c} \frac{dy}{\rho(\mathcal{D}_{12} + \varepsilon_2)}\right]^{-1}$$
$$(11.80)$$

where we define $g_{m,i}^*$ as the mass transfer coefficient *at a low rate* of mass transfer. We have assumed that the integral is approximately independent of $B_{m,2}$, following [11.22].

Equations (11.79c) and (11.78b) now reduce to

$$g_{m,2} = g_{m,2}^* \frac{\ln(1 + B_{m,2})}{B_{m,2}} \tag{11.81}$$

and

$$n_{2,s} = g_{m,2}^* \left[\frac{\ln(1 + B_{m,2})}{B_{m,2}} \right] B_{m,2} \tag{11.82}$$

These equations apply when species 2 is transferred while other components are stationary. Note that the result is the same for laminar flow, as seen simply by setting $\varepsilon_2 = 0$. Because the Couette flow model neglects streamwise gradients, we expect better accuracy for turbulent flows than for laminar flows.

The blowing factor. The group $\ln(1 + B_{m,2})/B_{m,2}$ is called the *blowing factor*. When $B_{m,2} > 0$, mass flows away from the wall (that's called *blowing*.) For positive $B_{m,2}$, the blowing factor is a positive number less than one, so $g_{m,2} < g_{m,2}^*$. In physical terms, blowing adds species 2 near the wall, reducing the near wall concentration gradient and lowering the mass flux. When $B_{m,2} < 0$, mass flows toward the wall (which is called *suction*). The blowing factor is greater than one, and $g_{m,2} > g_{m,2}^*$. Suction removes species 2 at the wall, making the concentration gradient steeper and increasing the mass flux.

The blowing factor has experimental and numerical validation for turbulent b.l.s when the flowing and transferred fluids have similar properties. Other correction factors should be used when properties differ widely, or with strong streamwise gradients, or for high transfer rates in laminar flow [11.29, 11.30].

When $|B_{m,2}| \lesssim 0.2$, the blowing factor is within about 10% of one. For that range, mass transfer is low rate—meaning $g_{m,2} \cong g_{m,2}^*$—as claimed in eqn. (11.65).

Concentration polarization in reverse osmosis

In reverse osmosis desalination, pressurized salty water flows through a planar channel between semipermeable membranes. The membranes allow water to pass through, but not salts. The water flow convects salts
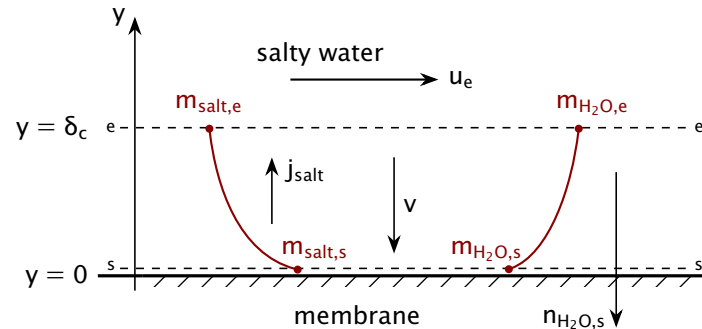
Figure 11.19 Concentration profiles of salt and water during reverse osmosis desalination. The salt is at rest: $n_{salt} = \rho_{salt} v + j_{salt} = 0$.

toward the membrane, where their concentration builds up until salt diffusion away from the membrane balances its convection toward the membrane. The steady-state salt concentration is higher at the membrane surface than in the bulk liquid (Fig 11.19).

The difference between salt concentration at the membrane and in the bulk liquid is called *concentration polarization*. The increased concentration at the membrane surface raises the osmotic pressure, which reduces the water flux through the membrane. High concentration polarization also increases the risk that low-solubility salts will precipitate onto the membrane, reducing the passage of water.[18]

Desalination membranes are rolled into cylindrical modules, typically 20 cm in diameter and 1 m in length for seawater systems. A set of modules are inserted end-to-end in a pressure vessel 6 to 8 m long. The membranes are held apart by mesh spacers, which cause heavy mixing of the flow in the channels between them. Over the length of the membrane pressure vessel, about 50% of the water is withdrawn through the membranes, leaving increasing salty and slow-moving brine in the channels. As a result of these complications, membrane mass transfer coefficient is known only empirically. The coefficient will change with the local flow speed, the spacer design, and the channel cross-section.

Example 11.15   Seawater reverse osmosis desalination

In one seawater reverse-osmosis membrane module, the low-rate mass transfer coefficient is $g^*_{m,H_2O} = 4 \times 10^{-2}$ kg/m^{2}s with a seawater salt

---

[18]Seawater, and most groundwater, contain a mixture of salts. Typical seawater includes Cl^-, Na^+, $SO_4{}^{2-}$, Mg^{2+}, Ca^{2+}, K^+, $HCO_3{}^-$, Br^-, and smaller amounts of other ions. These ions precipitate in various forms, such as $CaCO_3$ (calcite) and $CaSO_4 \cdot 2\,H_2O$ (gypsum).

concentration of 3.5 wt% [11.31]. Find the concentration polarization for both a typical water flux of 15 L/m²h and a high water flux of 35 L/m²h.

SOLUTION. From eqn. (11.82)

$$n_{H_2O,s} = g^*_{m,H_2O} \left[\frac{\ln(1 + B_{m,H_2O})}{B_{m,H_2O}} \right] B_{m,H_2O} = g^*_{m,H_2O} \ln(1 + B_{m,H_2O})$$

Rearranging

$$B_{m,H_2O} = \frac{m_{H_2O,s} - m_{H_2O,e}}{1 - m_{H_2O,s}} = \exp(n_{H_2O,s}/g^*_{m,H_2O}) - 1$$

and solving for $m_{H_2O,s}$

$$m_{H_2O,s} = 1 - (1 - m_{H_2O,e}) \exp(-n_{H_2O,s}/g^*_{m,H_2O})$$

Since $m_{salts} = 1 - m_{H_2O}$,

$$m_{salts,s} = m_{salts,e} \exp(-n_{H_2O,s}/g^*_{m,H_2O})$$

so that the concentration polarization, CP, is

$$CP \equiv \frac{m_{salts,s} - m_{salts,e}}{m_{salts,e}} = \exp\left(\frac{-n_{H_2O,s}}{g^*_{m,H_2O}} \right) - 1 = \exp\left(\frac{|n_{H_2O,s}|}{g^*_{m,H_2O}} \right) - 1$$

where $n_{H_2O,s} < 0$, since water flows toward the membrane. Concentration polarization is greater for lower mass transfer coefficients.

The water mass flux is the product of the volume flux and the density. At 15 L/m²h

$$n_{H_2O,s} = -\frac{(998 \text{ kg/m}^3)(15 \text{ L/m}^2\text{h})(10^{-3} \text{ m}^3\text{/L})}{3600 \text{ s/h}}$$

$$= -4.16 \times 10^{-3} \text{ kg/m}^2\text{s}$$

and at 35 L/m²h, $n_{H_2O,s} = -9.71 \times 10^{-3}$ kg/m²s. With the mass transfer coefficient, CP at each flux is

$$CP = \exp\left(\frac{|n_{H_2O,s}|}{g^*_{m,H_2O}} \right) - 1 = \begin{cases} 10.9\% & \text{at 15 L/m}^2\text{h} \\ 27.5\% & \text{at 35 L/m}^2\text{h} \end{cases}$$

Designers would avoid the high flux condition to limit the crystallization of low-solubility salts on the membrane. Further calculations show $B_{m,H_2O} = -0.217$ at the higher flux, slightly exceeding the criterion for low-rate mass transfer, eqn. (11.65). ■

11.9 Heat transfer at high mass transfer rates

The heat transfer coefficient, like the mass transfer coefficient, can be increased or decreased by mass transfer at the wall. In this section, we provide a highly simplified model for the effect of mass transfer on the heat transfer coefficient, and we explore several typically high-rate scenarios.

The multicomponent energy equation. Each species in a mixture carries its own enthalpy, $\hat{h}_i$. In a flow with mass transfer, different species have different velocities, and so the enthalpy transport of each species must be summed when writing the energy equation. For steady, low-speed flow without internal heat generation or chemical reactions, the energy balance on the surface S of a region R, eqn. (6.36), becomes

$$-\underbrace{\int_S (-k\nabla T) \cdot \vec{n}\, dS}_{\substack{\text{net heat conduction} \\ \text{rate out of } R}} - \underbrace{\int_S \left(\sum_i \rho_i \hat{h}_i \vec{v}_i\right) \cdot \vec{n}\, dS}_{\substack{\text{rate of all species'} \\ \text{enthalpy flow out of } R}} = 0$$

Applying Gauss's theorem to the volume R and requiring the resulting integrand to vanish gives

$$\nabla \cdot \left(-k\nabla T + \sum_i \rho_i \hat{h}_i \vec{v}_i\right) = 0 \tag{11.83}$$

This equation shows that the total energy flux—the sum of heat conduction and enthalpy transport—is conserved in steady flow.[19]

A Couette flow model for heat transfer. Suppose that a single species i is transported across a boundary layer that has a temperature difference. Both the temperature and the concentration have gradients in the y-direction, which complicates a turbulent flow analysis. Consequently, we limit this discussion to a laminar Couette flow model.

---

[19]The multicomponent energy equation becomes much more complicated when kinetic energy, body forces, and thermal and pressure diffusion are taken into account. The complexities are such that many published derivations of the multicomponent energy equation are incorrect, as discussed by Mills [11.32]. A key problem has been the assignment of an independent kinetic energy to the ordinary diffusion velocity. Such an assignment is wrong because diffusion results from the ordinary thermal motion of the fluid: the kinetic energy of diffusing molecules is merely part of the thermodynamic internal energy of the gas.
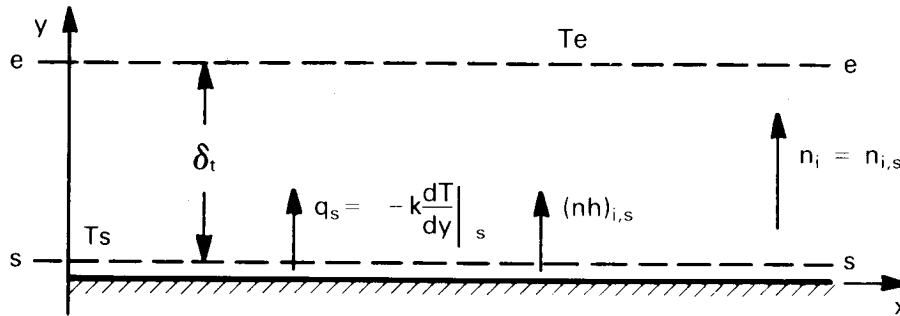
Figure 11.20 Energy and mass transport in a thermal boundary layer. Species i flows from the wall (s) to the freestream (e).

Mass and energy transport across the thermal boundary layer are shown in Fig. 11.20. For Couette flow, eqn. (11.83) simplifies to

$$\frac{d}{dy}\left(-k\frac{dT}{dy} + \rho_i \hat{h}_i v_i\right) = 0 \tag{11.84}$$

For a constant specific heat capacity and negligible pressure dependence (as in Section 6.3), the enthalpy of species i may be written as $\hat{h}_i = c_{p,i}(T - T_{\text{ref}})$. In a Couette flow, as in Section 11.8, n_i is constant in y and equals $n_{i,s}$. Equation (11.84) becomes

$$\frac{d}{dy}\left(-k\frac{dT}{dy} + n_{i,s}c_{p,i}T\right) = 0$$

Integrating twice and applying the boundary conditions

$$T(y = 0) = T_s \quad \text{and} \quad T(y = \delta_t) = T_e$$

we obtain the temperature profile:

$$\frac{T - T_s}{T_e - T_s} = \frac{\exp\left(\dfrac{n_{i,s}c_{p,i}}{k}y\right) - 1}{\exp\left(\dfrac{n_{i,s}c_{p,i}}{k}\delta_t\right) - 1} \tag{11.85}$$

The heat transfer coefficient, by its definition, eqn. (6.5), is:

$$h \equiv \frac{-k\dfrac{dT}{dy}\bigg|_s}{T_s - T_e} = \frac{n_{i,s}c_{p,i}}{\exp\left(\dfrac{n_{i,s}c_{p,i}}{k}\delta_t\right) - 1} \tag{11.86}$$

Defining h^* as the value of h in the limit of zero mass transfer

$$h^* \equiv \lim_{n_{i,s} \to 0} h = \frac{k}{\delta_t} \qquad (11.87)$$

Substitution of eqn. (11.87) into eqn. (11.86) yields

$$\boxed{\frac{h}{h^*} = \frac{(n_{i,s} c_{p,i}/h^*)}{\exp(n_{i,s} c_{p,i}/h^*) - 1}} \qquad (11.88)$$

We can calculate h^* as if there were *no* mass transfer, using the methods of Chapters 6 through 8.[20]

Equation (11.88) shows that when $n_{i,s}$ is large and positive—the blowing case (recall pg. 673)—h is smaller than h^*: blowing decreases the heat transfer coefficient, just as it decreases the mass transfer coefficient. Likewise, when $n_{i,s}$ is large and negative—the suction case—h is larger than h^*: suction increases the heat transfer coefficient. If $n_{i,s} c_{p,i}/h^* \lesssim 0.2$, then h is within about 10% of h^*, which is less than the uncertainty of most correlations for h^*. In gases, if $B_{m,i}$ is small, $n_{i,s} c_{p,i}/h^*$ is also small.

Properties can be evaluated at the film temperature and film composition. If the composition does not vary much, it's fine to use the freestream composition. For large variations in density or specific heat capacity, more sophisticated corrections to h and $g_{m,i}$ should be used, as described by Mills [11.29].

Further examples of simultaneous heat and mass transfer

Transpiration cooling. *Transpiration cooling* is illustrated in Fig. 11.21. A wall exposed to a high temperature gas flow is kept cool by injecting a gas into the flow through a porous section of the surface. Some of the heat transfer to the wall is absorbed when by raising the temperature of the gas as it flows from the coolant reservoir to the surface. The gas blowing of the wall thickens the boundary layer and reduces h, as well.

Transpiration is applied in high heat flux aerospace systems, such as hypersonic wings or scramjet combustion chambers [11.33]. In a similar process, *film cooling*, gas is injected through small holes in the surface. Film cooling is commonly used to protect gas turbine blades [11.34] and the throats of liquid-fueled rocket engines [11.35].

---

[20]With eqn. (11.87), the calculated value of h^* *defines* the effective film thickness δ_t.
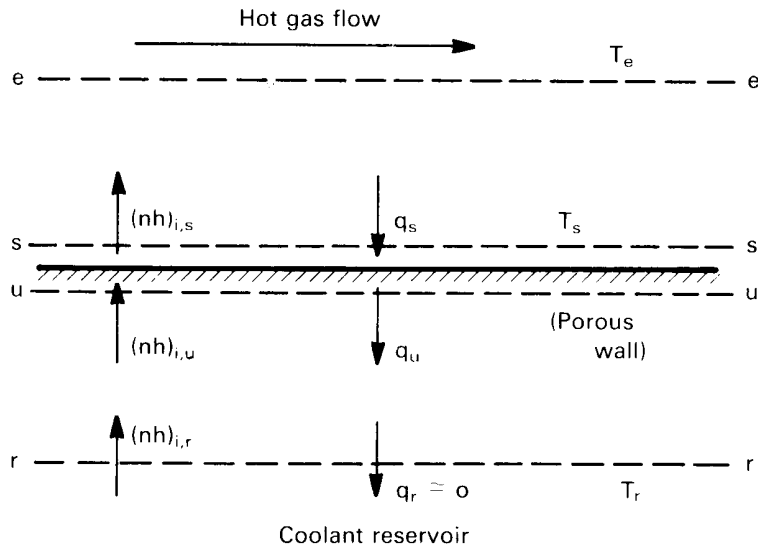
Figure 11.21 Transpiration cooling. The coolant, species i, flows from the reservoir, through the porous wall, and into the hot gas.

Let us construct a steady-state energy balance for a porous wall. The temperatures and the enthalpy and heat fluxes are as shown in Fig. 11.21. The coolant reservoir is far enough behind the surface that temperature gradients at its edge (the r-surface) are negligible with a conductive heat flux, q_r, of zero. An energy balance between the r- and u-surfaces gives

$$n_{i,r}\hat{h}_{i.r} = n_{i,u}\hat{h}_{i,u} - q_u \tag{11.89}$$

Between the u- and s-surfaces

$$n_{i,u}\hat{h}_{i,u} - q_u = n_{i,s}\hat{h}_{i,s} - q_s \tag{11.90}$$

Since the enthalpy of the transpired species does not change when it passes out of the wall,

$$\hat{h}_{i,u} = \hat{h}_{i,s} \tag{11.91}$$

and steady-state mass conservation gives

$$n_{i,r} = n_{i,u} = n_{i,s} \tag{11.92}$$

Thus, eqn. (11.90) reduces to

$$q_s = q_u \tag{11.93}$$

The flux q_u is the conductive heat flux into the wall, while q_s is the convective heat transfer from the gas stream:

$$q_s = h(T_e - T_s) \tag{11.94}$$

Combining eqns. (11.89) through (11.94), we obtain

$$n_{i,s}\left(\hat{h}_{i,s} - \hat{h}_{i,r}\right) = h(T_e - T_s) \tag{11.95}$$

This equation shows that heat convected to the wall is absorbed by the enthalpy rise of the transpired gas. To find the wall temperature, we write the enthalpy as $\hat{h}_i = c_{p,i}(T_s - T_{\text{ref}})$

$$n_{i,s}c_{p,i}(T_s - T_r) = h(T_e - T_s) \tag{11.96}$$

and rearrange

$$T_s = \frac{hT_e + n_{i,s}c_{p,i}T_r}{h + n_{i,s}c_{p,i}} \tag{11.97}$$

Further calculation (Problem 11.40) shows that

$$T_s = T_r + (T_e - T_r)\exp(-n_{i,s}c_{p,i}/h^*) \tag{11.98}$$

The wall temperature decreases exponentially toward T_r as the mass flux of the transpired gas increases. Transpiration cooling is most effective when injecting a gas with a high specific heat capacity (Problem 11.40).

Sweat Cooling.   Sweat cooling, mentioned in Section 11.7, is a variant of transpiration cooling in which a *liquid* is bled through a porous wall. The liquid is vaporized by convective heat flow to the wall, and the latent heat of vaporization acts as a powerful heat sink. Figure 11.21 also represents this process. The energy balances, eqns. (11.89) and (11.90), and mass conservation, eqn. (11.92), are unchanged, but the enthalpies at the s- and u-surfaces are now differ by the latent heat of vaporization:

$$\hat{h}_{i,u} + h_{fg} = \hat{h}_{i,s} \tag{11.99}$$

Thus, eqn. (11.93) becomes

$$q_s = q_u + h_{fg}n_{i,s}$$

and eqn. (11.95) takes the form

$$n_{i,s}\left[h_{fg} + c_{p,i_f}(T_s - T_r)\right] = h(T_e - T_s) \tag{11.100}$$

where c_{p,i_f} is the specific heat of *liquid i*. Since the latent heat is generally much larger than the sensible heat, a comparison of eqn. (11.100) to eqn. (11.96) shows that sweat cooling has a much greater efficiency per unit mass of coolant. As discussed in Section 11.7, sweat cooling has substantial importance at low mass transfer rates, as well.

Combustion and catalysis. When chemical reactions occur, both the mass and energy balances must be changed. If the reactions occur in the bulk (*homogeneous* reactions), the mass flux of a reactant will vary across the boundary layer. Similarly, the energy equation will need to incorporate the enthalpy change caused by the reaction. A burning fuel droplet is an example. Liquid fuel vaporizes and diffuses into the gas phase, where it reacts with oxygen that is supplied by diffusion toward the droplet. The reaction products diffuse away. The flame sits in a reaction zone surrounding the droplet, and if enough soot forms, the flame will glow yellow-orange as the soot radiates heat [11.26, 11.27].

When reactions occur only on a boundary (*heterogeneous* reactions), the reaction stoichiometry relates the mole fluxes to and from the surface. The heat of reaction appears in the energy balance at the surface, and eqn. (11.88) for high-rate *h* must be modified to account for the transfer of more than one species. For example, in a gasoline engine's catalytic converter, oxygen, nitrogen oxides, and carbon compounds diffuse to the catalyst surface where a combination of reactions produce water, carbon dioxide, and nitrogen that diffuse away and are carried out the tail pipe. No mass is transferred through the catalyst surface.

Mills [11.29] discusses mass transfer with chemical reactions.

Ablating heat shield for spacecraft reentry. In lunar exploration missions, the crew returns to Earth in a small crew module. The module encounters the atmosphere about 100 km above Earth at a speed of about 11 km/s (25,000 mph). The module slows to 0.13 km/s (300 mph) in only a few minutes. During deceleration, the module's immense kinetic energy is dissipated by friction and drag, heating the gases around the module.

Air approaches the blunt end of the capsule with a Mach number greater than 30 (Fig. 11.22a). A strong shock wave forms upstream of the capsule, called a *bow shock*. Air passing through the bow shock is heated by compression and friction to temperatures on the order of 11,000 K [11.36]. The high temperature causes gas molecules to dissociate and ionize, and the ionized gas blacks-out radio communication during
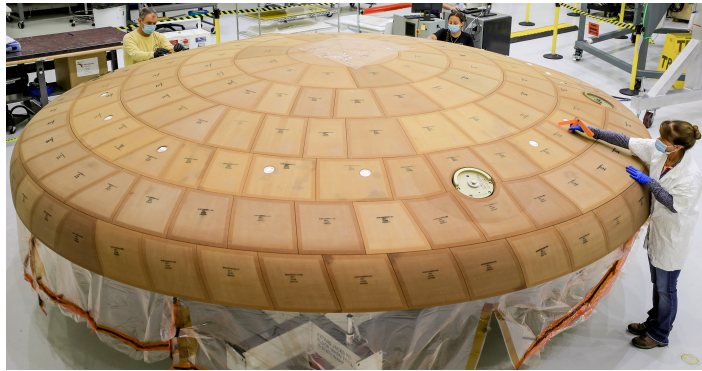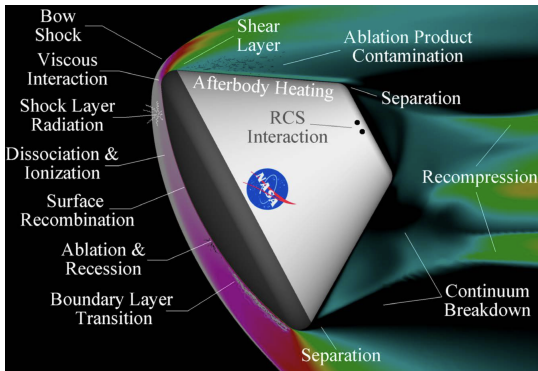
a. Thermofluid conditions during reentry

b. NASA's heat shield for the Orion crew module

Figure 11.22 (a) Flow field around crew module during reentry (NASA image); (b) Technicians at the NASA Kennedy Space Center preparing the heat shield of the Orion crew module for Artemis II lunar mission (NASA: Isaac Watson, July 2020).

part of the reentry. At these hypersonic conditions, the shock wave and the heated gases are very close to the module's surface.

The gases heat the surface of the crew module by convection, gas radiation, and catalytic recombination reactions between the gas molecules and the surface. This aerodynamic heating creates convective heat fluxes that can reach 400 W/cm^2. The radiative heat fluxes are similarly large in the earliest part of reentry, when the shock wave is strongest and the gases behind it are hottest. To protect the crew, a heat shield is placed on the bottom of the capsule, where heating is most intense (Fig. 11.22b). In NASA's Apollo and Artemis missions, the heat shield has been made from AVCOAT, an epoxy novolac resin with silica fibers filled into a fiberglass matrix [11.37, 11.38].

The heat shield is designed to burn away, or *ablate*, during reentry. The ablation process involves sublimation, melting, and charring of the surface and pyrolysis of the material deeper within the shield. Numerical models are necessary to analyze these complex conditions [11.39]. Pyrolysis within the heat shield generates gases that blow outward through the surface, reducing the convective and catalytic heat fluxes. The overall cooling process is similar to transpiration cooling and sweat cooling.

In NASA's Artemis missions, ablation limits surface temperature of the heat shield to around 2800°C. Detailed analysis of the similar aerodynamic heating during Mars landings can be found in the open literature [11.40].

Noncondensable gases in steam or vapor condensers.   Condensers, which cool vapors until they liquefy, are essential components of steam power plants. Condensers are also widely used in chemical processing and chemical separations. Many vapors will contain small amounts of a noncondensable gas. For example, water that is boiled to make steam for a power turbine may contain a bit of dissolved air, which is released into the steam. A desalination plant that evaporates water vapor from seawater may release carbon dioxide as a result of bicarbonate present in seawater. Even a very small amount of a noncondensable gas can sharply reduce the heat transfer rate, as noted in Section 8.5 (pg. 455).

When vapor containing a gas is condensed, the gas is swept toward the condenser surface. Then it remains behind as the vapor liquefies. The accumulation of gas lowers the vapor concentration at the condenser surface, so the vapor's partial pressure is less than that of the nearly pure vapor away from the surface. Vapor at a lower partial pressure has a lower saturation temperature, so that greater subcooling is needed to liquefy it.

The gas by the condenser surface is stationary in the direction perpendicular to the wall, since the gas has no mass flux into the condensate film. The concentration of gas, however, is higher near the wall, similar to the salts by the reverse osmosis membrane described in Section 11.8. Thus, the gas diffuses away from the wall, down the concentration gradient. This diffusion flux acts in opposition to the convective flow of the gas-vapor mixture toward the wall (Fig. 11.23). Similarly, the vapor must diffuse through the gas to reach the wall and condense. The blowing factor is clearly negative, and strong suction is likely.

Industrial condensers are heat exchangers with a coolant as one stream and a vapor as the other. Vapor enters at one end and flows toward the other end as it condenses. The mass flow rate of vapor decreases along the length of the condenser. Noncondensable gases are swept with the vapor toward the outlet, where they accumulate. Temperatures tend to be lower at the outlet end of the condenser. If the vapor condenses completely, the outlet end of the condenser will contain mostly gas, so that removal of the gas, or "venting," is relatively straightforward.

As an example, in a vertical downflow in-tube condenser, vapor flows downward inside a tube bundle, while a liquid coolant (perhaps cold water) flows through the shell side (Fig. 11.24). The condensate forms a film that runs down the inside of the tubes. Noncondensable gases are swept to the bottom, where a gas-vapor interface forms. The position of the interface can fluctuate as the load on the condenser fluctuates. In
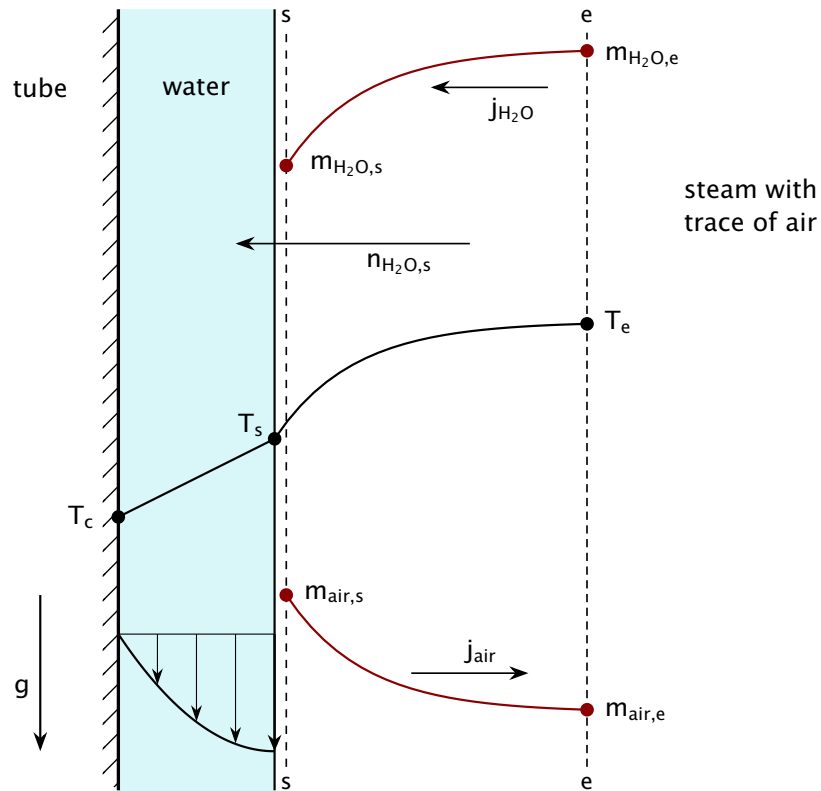
Figure 11.23   Concentration and temperature at surface of a condenser tube with a noncondensable gas present.

fact, control of the condenser pressure may be gained by controlling the rate of venting of the gas at the bottom [11.42].

Venting is less convenient if vapor is on the shell side of a condenser, especially in crossflow configurations, because the vapor flow path is not tightly defined [11.43]. Steam power plant condensers, for instance, are often horizontal shell-and-tube heat exchangers with water inside the tubes and steam on the shell side. These condensers almost always operate at subatmospheric pressure to minimize the bottom temperature, which maximizes power generation. In this case, a *steam ejector* can remove noncondensable gas from the shell side. The gas is entrained into a jet of medium pressure steam that flows into a Venturi nozzle and out the condenser. In a pressurized condenser, a thermally regulated valve does the same job. The valve opens if the temperature drops below a set point that signals an elevated concentration of gas.
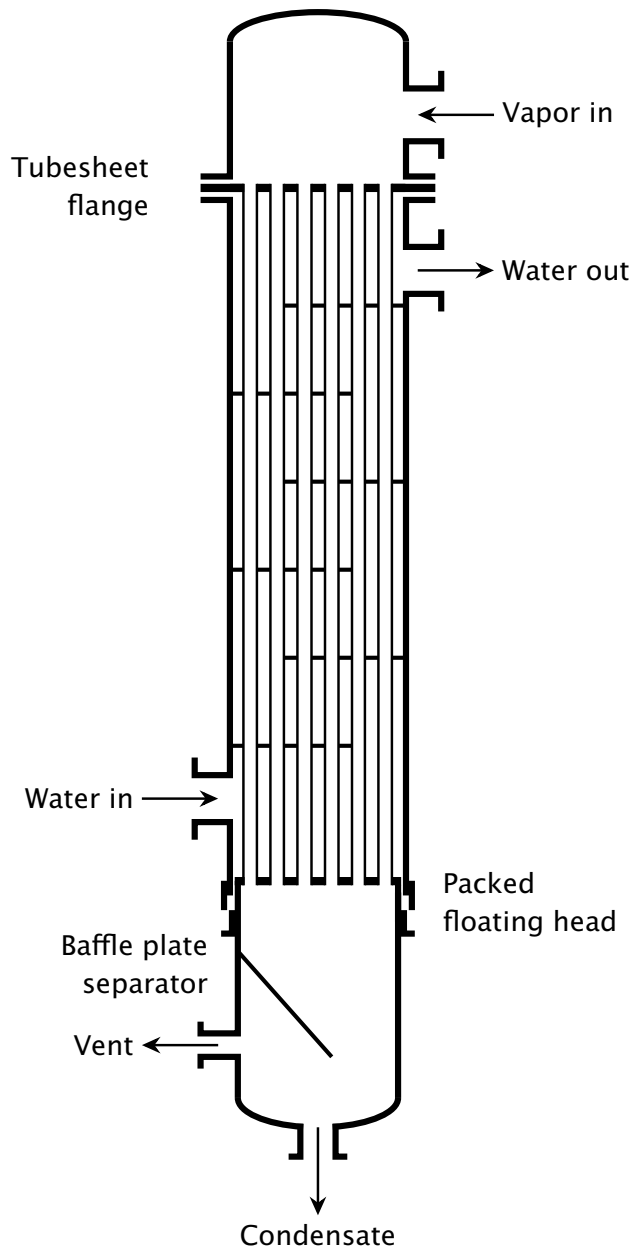
Figure 11.24 Vertical in-tube downflow condenser. The floating head at the bottom allows for thermal expansion and maintenance (assembly details not shown; see Mueller [11.41]). A second vent may be included at the tubesheet flange to remove air from the shell side.

11.10   Transport properties of mixtures

When we lack data for the transport properties of mixtures, we may estimate them using theoretical predictions or empirical models. Here, we give a few basic procedures for evaluating $\mathcal{D}_{12}$, $\mathcal{D}_{im}$, k, and μ in gas mixtures, using results from kinetic theory—particularly the Chapman-Enskog theory [11.8, 11.44, 11.45]. We also consider how to estimate $\mathcal{D}_{12}$ in dilute liquid solutions using the Sutherland-Einstein framework.

The diffusion coefficient for binary gas mixtures

As a starting point, we return to our simple model for the self-diffusion co-efficient of a gas, eqn. (11.34). We can approximate the average molecular speed, $\overline{C}$, by Maxwell's equilibrium formula [11.45]

$$\overline{C} = \left(\frac{8k_\mathrm{B}N_A T}{\pi M}\right)^{1/2} \tag{11.101}$$

where k_B is Boltzmann's constant and N_A is Avogadro's number.

If the molecules are rigid spheres, kinetic theory shows the mean free path to be

$$\ell = \frac{k_\mathrm{B}T}{\sqrt{2}\pi d^2 p} \tag{11.102}$$

where d is the effective molecular diameter. Substituting these values of $\overline{C}$ and ℓ into eqn. (11.34) and noting that more detailed kinetic theory gives $2\eta a = 1/2$, we find

$$\begin{aligned}
\mathcal{D}_{AA'} &= (2\eta a)\overline{C}\ell \\
&= \frac{(k_\mathrm{B}/\pi)^{3/2}}{d^2}\left(\frac{N_A}{M}\right)^{1/2}\frac{T^{3/2}}{p}
\end{aligned} \tag{11.103}$$

The diffusion coefficient varies as p^{-1} and $T^{3/2}$, based on the simple model for self-diffusion.

Of course, molecules are not really hard spheres, and different species will have different sizes. The Chapman-Enskog kinetic theory takes those factors into account, leading to

$$\mathcal{D}_{AB} = \frac{(1.8583 \times 10^{-7})T^{3/2}}{p\,\Omega_D^{AB}(T)}\sqrt{\frac{1}{M_A} + \frac{1}{M_B}} \tag{11.104}$$

where the units of p, T, and $\mathcal{D}_{AB}$ are atm, K, and m²/s, respectively. The function $\Omega_D^{AB}(T)$, called a *collision integral*, accounts for scattering during
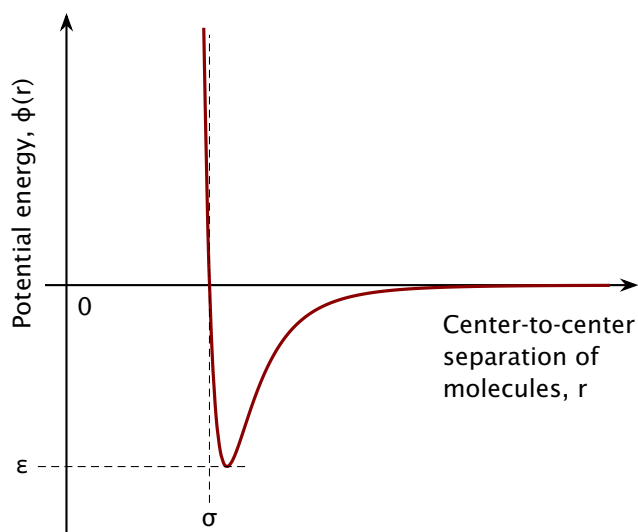
Figure 11.25   Lennard-Jones intermolecular potential: $\phi(r) = 4\varepsilon[(\sigma/r)^{12} - (\sigma/r)^{6}]$

the collisions between molecules of A and B. It depends, in general, on which molecular species collide and the temperature.

The specific type of molecules matter owing to the intermolecular forces of attraction and repulsion that act during collisions, which are used to compute Ω_D^{AB}. A good approximation to those forces is given by the Lennard-Jones potential energy function (Fig. 11.25).[21] This potential is based on two parameters, σ and ε. The zero potential distance, σ, resembles a molecular diameter, and the potential well depth, ε, is the energy required to completely separate two molecules from one another. Values of σ and ε are given for a few molecules in Table 11.3.[22]

The calculations can be simplified using effective values of σ and ε and proceeding as if this effective type of molecule were colliding with itself. Then the collision integral $\Omega_D^{AB}(T)$ can be can be approximated by a collision integral Ω_D for this effective molecule:

$$\Omega_D^{AB}(T) \cong \sigma_{AB}^2 \, \Omega_D\left(k_{\mathrm{B}} T / \varepsilon_{AB}\right) \qquad (11.105)$$

---

[21]John Edward Jones was born in 1894 and educated in theoretical physics at Bristol University. He served as a flyer in the First World War, then proposed his attraction formula in his doctorate at Manchester. Stated as a potential, he had $\phi(r) = 4\varepsilon[(\sigma/r)^n - (\sigma/r)^m)]$ for r the molecular separation. The next year he married Katherine Lennard and attached her maiden name to his own. He arrived at the famous $(n, m) = (12, 6)$ in 1931, under the name Lennard-Jones [11.46]. Tables 11.3 and 11.4 are for that potential.

[22]Each pair of constants was determined by fitting to viscosity data. Different fits can achieve similar accuracy, and so different authors have reported different pairs of values for the same gas [11.47]. A value of σ from one pair should *never* be combined with a value of ε from another pair.

where σ_{AB}, for the collision of molecules of A and B, is

$$\sigma_{AB} = (\sigma_A + \sigma_B)/2 \qquad (11.106)$$

and the effective potential well depth for that collision is

$$\varepsilon_{AB} = \sqrt{\varepsilon_A \varepsilon_B} \qquad (11.107)$$

The calculation of the collision integral Ω_D from the Lennard-Jones potential is laborious. Some values are tabulated in Table 11.4.

Substitution of eqn. (11.104) into (11.105) results in a working formula for the binary diffusion coefficient

$$\boxed{\mathcal{D}_{AB} = \frac{(1.8583 \times 10^{-7})T^{3/2}}{p\,\sigma_{AB}^2 \Omega_D}\sqrt{\frac{1}{M_A} + \frac{1}{M_B}}} \qquad (11.108)$$

where, again, the units of p, T, and $\mathcal{D}_{AB}$ are atm, K, and m^2/s, respectively, and σ_{AB} is in Å (1 Å= 0.1 nm) [11.44].

Equation (11.108) indicates that the diffusivity varies as p^{-1} and is independent of species concentrations, just as the simple model indicated that it should. The temperature dependence of Ω_D adds to the temperature dependence of $\mathcal{D}_{AB}$: at low temperatures, $\mathcal{D}_{AB} \propto T^{11/6}$, but as temperature rises the dependence ranges up to T^2 and then back down to $T^{3/2}$ [11.7, 11.17].

Air, by the way, can be treated as a single substance in Table 11.3 as a result of the similarity of its two main constituents, N$_2$ and O$_2$.

Example 11.16

Compute $\mathcal{D}_{AB}$ for the diffusion of hydrogen in air at 282 K and 1 atm.

SOLUTION. Let air be species A and H$_2$ be species B. Then we read from Table 11.3

$$\sigma_A = 3.711 \text{ Å}, \quad \sigma_B = 2.899 \text{ Å}, \quad \frac{\varepsilon_A}{k_\text{B}} = 78.6 \text{ K}, \quad \frac{\varepsilon_B}{k_\text{B}} = 40.0 \text{ K}$$

and calculate these values

$$\sigma_{AB} = (3.711 + 2.899)/2 = 3.305 \text{ Å}$$

$$\varepsilon_{AB}/k_\text{B} = \sqrt{(78.6)(40.0)} = 56.1 \text{ K}$$

Table 11.3 Lennard-Jones constants of selected species, with molar masses. From viscosity data [11.48] except as noted.

Species	σ (Å)	ε/k_B (K)	$M\left(\frac{\text{kg}}{\text{kmol}}\right)$	Species	σ (Å)	ε/k_B (K)	$M\left(\frac{\text{kg}}{\text{kmol}}\right)$
Air	3.711	78.6	28.96	H_2	2.899	40.0	2.016[b]
Ar	3.327	143.8	39.95[a]	H_2O	2.641	809.1	18.02
Br_2	4.296	507.9	159.81	H_2O_2	4.196	289.3	34.01
CCl_4	5.947	322.7	153.82	H_2S	3.623	301.1	34.08
CH_3OH	3.626	481.8	32.04	He	2.524	9.87	4.003[a]
CH_4	3.758	148.6	16.04	Hg	2.969	750	200.59
CO	3.702	91.0	28.01[b]	I_2	5.160	474.2	253.81
CO_2	3.859	213.0	44.01[b]	Kr	3.510	207.4	83.80[a]
C_2H_6	4.443	215.7	30.07	NH_3	2.900	558.3	17.03
C_2H_5OH	4.530	362.6	46.07	N_2	3.705	84.94	28.01[a]
CH_3COCH_3	4.600	560.2	58.08	N_2O	3.828	232.4	44.01
C_3H_8	5.021	254.0	44.10[b]	Ne	2.801	33.92	20.18[c]
$n\text{-}C_5H_{12}$	5.740	337.0	72.15[b]	O_2	3.392	121.7	32.00[a]
C_6H_6	5.349	412.3	78.11	SF_6	5.128	222.1	146.06
Cl_2	4.217	316.0	70.91	SO_2	4.112	335.4	64.06
F_2	3.357	112.6	38.00	Xe	3.903	262.7	131.29[a]

[a]From [11.49]. [b]From [11.50]. [c]From [11.51], using vapor pressure data.

Hence, $k_B T/\varepsilon_{AB} = 5.027$, and $\Omega_D = 0.8410$ from Table 11.4. Then

$$\mathcal{D}_{AB} = \frac{(1.8583 \times 10^{-7})(282)^{3/2}}{(1)(3.305)^2(0.8410)}\sqrt{\frac{1}{2.016} + \frac{1}{28.96}} \text{ m}^2/\text{s}$$
$$= 6.98 \times 10^{-5} \text{ m}^2/\text{s}$$

An experimental value [11.7] is 6.58×10^{-5} m^2/s, so the prediction is higher by 6%. ∎

Limitations. Equation (11.108) was derived for low density gases with molecules that are nonpolar and spherically symmetric. Poling et al. [11.5] compared eqn. (11.108) to data for binary mixtures of monatomic, polyatomic, nonpolar, and polar gases like those in Table 11.3. They reported an average absolute error of 7.9%. Better accuracy can be obtained using a mixture-specific equation for $\Omega_D^{AB}(T)$ [11.54, Chap. 11] or using values of σ_{AB} and ε_{AB} that have been fit to the pair of gases considered [11.53], rather than estimated with eqns. (11.106) and (11.107).

Table 11.4 Lennard-Jones collision integrals for diffusivity and for viscosity and thermal conductivity [11.52].

k_BT/ε	Ω_D	Ω_μ	k_BT/ε	Ω_D	Ω_μ	k_BT/ε	Ω_D	Ω_μ	k_BT/ε	Ω_D	Ω_μ
0.10	4.0127	4.1039	1.20	1.3218	1.4542	5.00	0.8427	0.9266	30.00	0.6234	0.7005
0.15	3.4833	3.5879	1.30	1.2744	1.4010	5.50	0.8266	0.9102	32.00	0.6172	0.6939
0.20	3.1328	3.2686	1.40	1.2335	1.3550	6.00	0.8127	0.8961	34.00	0.6114	0.6878
0.25	2.8677	3.0336	1.50	1.1983	1.3151	6.50	0.8005	0.8837	36.00	0.6060	0.6820
0.30	2.6509	2.8456	1.60	1.1678	1.2801	7.00	0.7897	0.8726	38.00	0.6010	0.6766
0.35	2.4695	2.6777	1.70	1.1414	1.2491	7.50	0.7800	0.8627	40.00	0.5962	0.6715
0.40	2.3171	2.5327	1.80	1.1175	1.2215	8.00	0.7711	0.8537	45.00	0.5854	0.6599
0.45	2.1823	2.4003	1.90	1.0956	1.1971	8.50	0.7631	0.8454	50.00	0.5759	0.6496
0.50	2.0662	2.2867	2.00	1.0760	1.1753	9.00	0.7556	0.8378	55.00	0.5674	0.6405
0.55	1.9681	2.1774	2.20	1.0418	1.1379	9.50	0.7487	0.8308	60.00	0.5598	0.6322
0.60	1.8779	2.0828	2.40	1.0131	1.1069	10.00	0.7422	0.8242	65.00	0.5528	0.6246
0.65	1.7979	1.9994	2.60	0.9888	1.0807	12.00	0.7202	0.8017	70.00	0.5465	0.6177
0.70	1.7298	1.9230	2.80	0.9679	1.0581	14.00	0.7025	0.7834	75.00	0.5406	0.6113
0.75	1.6699	1.8521	3.00	0.9499	1.0386	16.00	0.6877	0.7681	80.00	0.5352	0.6053
0.80	1.6139	1.7885	3.20	0.9342	1.0215	18.00	0.6750	0.7549	90.00	0.5254	0.5946
0.85	1.5633	1.7327	3.40	0.9200	1.0064	20.00	0.6640	0.7433	100.00	0.5167	0.5851
0.90	1.5175	1.6821	3.60	0.9071	0.9929	22.00	0.6542	0.7330	125.00	0.4989	0.5654
0.95	1.4763	1.6360	3.80	0.8954	0.9807	24.00	0.6453	0.7238	150.00	0.4847	0.5497
1.00	1.4394	1.5933	4.00	0.8847	0.9697	26.00	0.6374	0.7153	175.00	0.4729	0.5366
1.10	1.3767	1.5175	4.50	0.8617	0.9461	28.00	0.6301	0.7076	200.00	0.4630	0.5256

When the density is high enough that the gas is not ideal, $\mathcal{D}_{12}$ will decrease more rapidly with p or ρ than suggested by eqn. (11.108). At these higher densities, molecular interactions are not limited to infrequent two molecule collisions. Three molecules may collide, or a single molecule might collide with a joined pair of molecules (a *dimer*). At even higher density, the motions of nearby molecules may become coordinated. The transport properties of dense gases can be estimated using corresponding states theory, absolute reaction-rate theory, or modified Enskog theory, amongst other approaches [11.5, 11.54].

Conversely, when the gas density is so low that the mean free path is near the dimensions of the system—as in some microscale devices—or when it is near the length scale of gradients in the gas—as in a shock wave at high Mach number—we enter the realm of *rarefied gas dynamics*. Kinetic theory must be modified to account for system boundaries or for spatially rapid changes in gas properties [11.55, 11.56].

Diffusion coefficients for multicomponent gases

An effective binary diffusivity $\mathcal{D}_{im}$ may sometimes be used to represent the diffusion of species i into a mixture m. For example, if a low concentration of species i diffuses into a homogeneous mixture of n species, then $\vec{J}_j \cong 0$ for $j \neq i$, and one may show that

$$\mathcal{D}_{im}^{-1} = \sum_{\substack{j=1 \\ j \neq i}}^{n} \frac{x_j}{\mathcal{D}_{ij}} \tag{11.109}$$

where $\mathcal{D}_{ij}$ is the binary diffusion coefficient for species i and j alone (see Problem 11.53). This rule is called *Blanc's law*.

If a mixture is dominantly composed of one species, A, and includes only small traces of several other species, then the diffusion coefficient of each trace gas is approximately the same as if the other trace gases were not present, so that

$$\mathcal{D}_{im} \cong \mathcal{D}_{iA} \tag{11.110}$$

Finally, if the binary diffusion coefficient has the same value for each pair of species in a mixture, then one may show that $\mathcal{D}_{im} = \mathcal{D}_{ij}$, as intuition might suggest (Problem 11.53).

Diffusion coefficients for binary liquid mixtures

The kinetic theory of gases is based on a detailed description of infrequent collisions between pairs of molecules. In a liquid, each molecule is always in contact with many neighboring molecules, and a simple kinetic model is infeasible. Instead, a less precise approach can be used to correlate experimental measurements.

For a dilute solution of species A in liquid B, the *hydrodynamic model* has met some success. Suppose that, when a force per molecule F_A is applied, the molecules of A reach an average steady speed $\hat{v}_A$ relative to the liquid B. The ratio $\hat{v}_A/F_A$ is called the *mobility* of A. If no force is applied, molecules of A can instead diffuse as a result of concentration gradients or even random molecular motions, called *Brownian motion*[23].

---

[23]Robert Brown (1773–1858) was a Scottish botanist. In 1827, he was examining pollen grains suspended in water, and noted that they continuously jerked about. Were they alive? No, he found the same behavior in dust motes. Without a full atomic theory, he could not tell that the particles were small enough to be knocked about by molecules. Mathematical descriptions of the process had to wait for late 19th and early 20th century.

Thermodynamic and kinetic arguments, such as those given by Sutherland [11.57] and Einstein [11.58], lead to the following expression for the diffusion coefficient of A in B:

$$\mathcal{D}_{AB} = k_B T (\hat{v}_A / F_A) \tag{11.111}$$

Equation (11.111) is usually called the *Einstein relation*.

To evaluate the mobility of a solute, we may make the bold approximation that viscous drag applies on a molecular scale, using a variant of Stokes' law for a sphere at low Reynolds number ($\text{Re}_D < 1$). Specifically, we follow Sutherland in using an expression due to Basset [11.59]:

$$F_A = 6\pi\mu_B\hat{v}_A R_A\left(\frac{1 + 2\mu_B/\beta R_A}{1 + 3\mu_B/\beta R_A}\right) \tag{11.112}$$

Here, R_A is the radius of sphere A and β is a coefficient of "sliding" friction, for a friction force proportional to the velocity differential. Substituting eqn. (11.112) in eqn. (11.111), we get

$$\frac{\mathcal{D}_{AB}\mu_B}{T} = \frac{k_B}{6\pi R_A}\left(\frac{1 + 3\mu_B/\beta R_A}{1 + 2\mu_B/\beta R_A}\right) \tag{11.113}$$

This model is valid if the concentration of A is so low that the molecules of A do not interact with one another.[24]

We usually assume that no slip occurs between a liquid and a solid surface that it touches. For solutes much larger than the solvent molecules, this behavior continues; and so $\beta \longrightarrow \infty$ and eqn. (11.113) simplifies to[25]

$$\frac{\mathcal{D}_{AB}\mu_B}{T} = \frac{k_B}{6\pi R_A} \tag{11.114a}$$

In contrast, for small solute molecules—close in size to the solvent molecules—the solute might slip relative to the solvent, and so β will be

---

[24]Stokes, in his 1856 paper [11.60], argued for the no-slip condition and derived the result known today as *Stokes' law*, $F_A = 6\pi\mu_B v_A R_A$. Even so, fluid drag was not well understood in the 19th century, and some evidence seemed to suggest that frictional slip could occur between a fluid and solid. Basset discussed slip in his 1888 hydrodynamics book, and he developed eqn. (11.112) to account for it. Sutherland, in his 1905 paper, adopted Basset's equation without comment, simply calling it "Stokes' law".

[25]Equation (11.114a) was given by Einstein in a paper submitted May 1905. The more general form, eqn. (11.113), was reported independently by Sutherland in a paper submitted March 1905. Equations (11.113) and (11.114a) are commonly called the *Stokes-Einstein* equation, although Stokes had no hand in applying eqn. (11.112) to diffusion. Equation (11.113) might better be called the *Sutherland-Einstein* equation.

smaller. In the limit $\beta \rightarrow 0$, eqn. (11.113) becomes

$$\frac{\mathcal{D}_{AB}\mu_B}{T} = \frac{k_B}{4\pi R_A} \qquad (11.114b)$$

Experimental data for a diversity of solutes and solvents show a similar trend of $\mathcal{D}_{AB}\mu_B/T$ increasing as solute size decreases [11.61].

Equations (11.113), (11.114a), and (11.114b) each show that $\mathcal{D}\mu/T$ is primarily a function of the size of the diffusing species, with a secondary dependence on intermolecular forces (i.e., on β). Experiments on dilute solutions confirm that $\mathcal{D}\mu/T$ is essentially temperature-independent for a given solute-solvent pair, with the only exception occurring in very high viscosity solutions. Thus, most correlations of experimental data start with some form of eqn. (11.113).

Many such correlations have been developed. One such correlation was given by King et al. [11.62]. They expressed the molecular size in terms of molal volumes at the normal boiling point, $V_{m,A}$ and $V_{m,B}$, and accounted for intermolecular association forces using the latent heats of vaporization at the normal boiling point, $h_{fg,A}$ and $h_{fg,B}$. They obtained

$$\frac{\mathcal{D}_{AB}\mu_B}{T} = \left(4.4 \times 10^{-15} \text{ kg·m/K·s}^2\right)\left(\frac{V_{m,B}}{V_{m,A}}\right)^{1/6}\left(\frac{h_{fg,B}}{h_{fg,A}}\right)^{1/2} \qquad (11.115)$$

which fit their data to a standard deviation of 19.5%. Values of h_{fg} and V_m are given for various substances in Table 11.5.

Equation (11.115) applies for the diffusion of a very dilute solute A through solvent B. The equation is valid for nonelectrolytes, and it appears to be satisfactory for both polar and nonpolar substances. Difficulty fitting polar solvents of high viscosity led King et al. to limit eqn. (11.115) to $\mathcal{D}\mu/T < 1.5 \times 10^{-14}$ kg·m/K·s^2. The predictions of eqn. (11.115) are compared with experimental data in Fig. 11.26. Poling et al. [11.5] discuss more complex models that provide better accuracy.

Data for the diffusion coefficient of hundreds of dilute solutions have been compiled by Großmann et al. [11.63]. They also evaluated several predictive models and used matrix completion methods to estimate values for more than 10,000 solvent-solute pairs at 298 K.

Concentrated liquid solutions. In concentrated solutions—for which one species is not dilute—the diffusion coefficient can vary substantially with concentration. Figure 11.27, for example, shows data for two mixtures in which this variation is strong. The dilute solution limits in this figure,

Table 11.5 Molal specific volumes and latent heats of vaporization for selected liquids at their normal boiling points [11.62].

Substance	V_m (m^3/kmol)	h_{fg} (MJ/kmol)
Alcohols		
Methanol	0.042	35.53
Ethanol	0.064	39.33
n-Propanol	0.081	41.97
Isopropanol	0.072	40.71
n-Butanol	0.103	43.76
tert-Butanol	0.103	40.63
Alkanes and cycloalkanes		
n-Pentane	0.118	25.61
Cyclopentane	0.100	27.32
Isopentane	0.118	24.73
Neopentane	0.118	22.72
n-Hexane	0.141	28.85
Cyclohexane	0.117	33.03
n-Heptane	0.163	31.69
n-Octane	0.185	34.14
n-Nonane	0.207	36.53
n-Decane	0.229	39.33
Miscellaneous		
Acetone	0.074	28.90
Benzene	0.096	30.76
Carbon tetrachloride	0.102	29.93
Ethyl bromide	0.075	27.41
Nitromethane	0.056	25.44
Water	0.0187	40.62

for ethanol in water ($x_1 \rightarrow 0$) and for water in ethanol ($x_1 \rightarrow 1$), align with the values in Table 11.1 at 25℃. Between these limits, the diffusivity varies somewhat erratically.

The strong variation of $\mathcal{D}_{12}$ with concentration arises because the diffusional flux is not linearly proportional to the concentration gradient. In fact, chemical thermodynamics shows that the true driving force for mass diffusion is the *chemical potential* and that the driving force for diffusion is only proportional to concentration if the solution is dilute
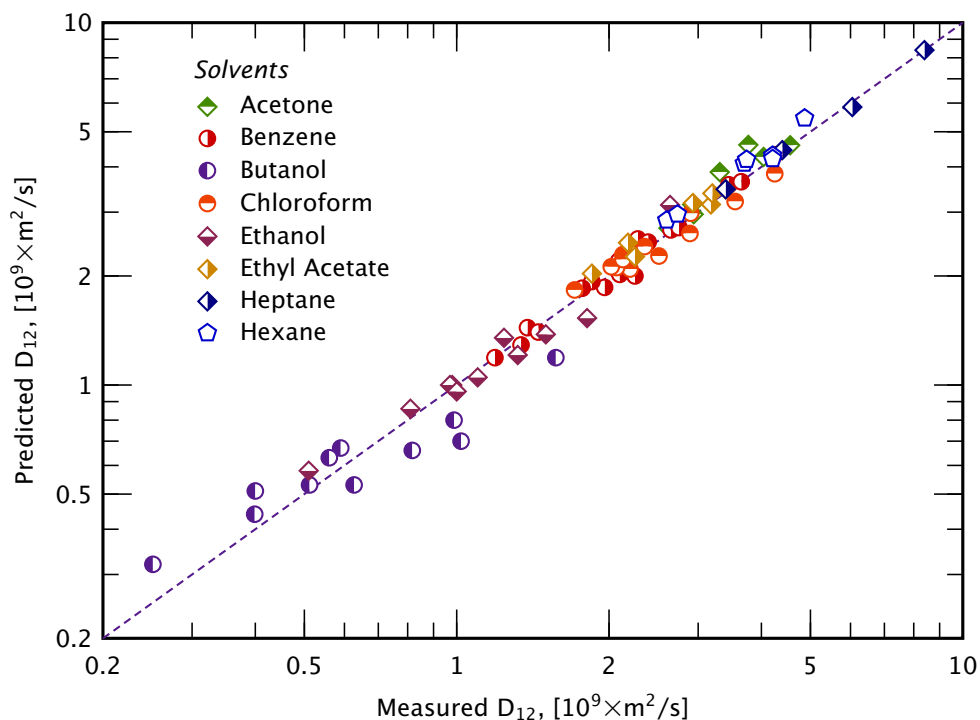
Figure 11.26 Comparison of liquid diffusion coefficients predicted by eqn. (11.115) to measured values for assorted solutes in several organic solvents, from [11.64].

or ideal (see Section 11.11). Nevertheless, experimental studies of the diffusion coefficient usually report the concentration, rather than the chemical potential, because the concentration is easily measurable.

Figure 11.27 also shows that $\mathcal{D}_{\text{eth-H}_2\text{O}}$ increases by more than a factor of two when the temperature increases from just 25℃ to 65℃. At first glance, the rapid change may seem surprising, since eqn. (11.113) predicts a linear increase with *absolute* temperature. Equation (11.113), however, also predicts that diffusivity increases as the dynamic viscosity $\mu_{\text{H}_2\text{O}}$ falls; and, over this temperature range, water's viscosity drops by a factor of two. Together, these two variations account for the increase in $\mathcal{D}_{\text{eth-H}_2\text{O}}$ with T for $x_1 \rightarrow 0$.

The literature contains several predictive models for the concentration dependence of the diffusion coefficient [11.5]. For the particular case of electrolyte solutions, in which electrostatic fields force ions to migrate, a significant body of theory describes solute mobility and diffusivity [11.66].
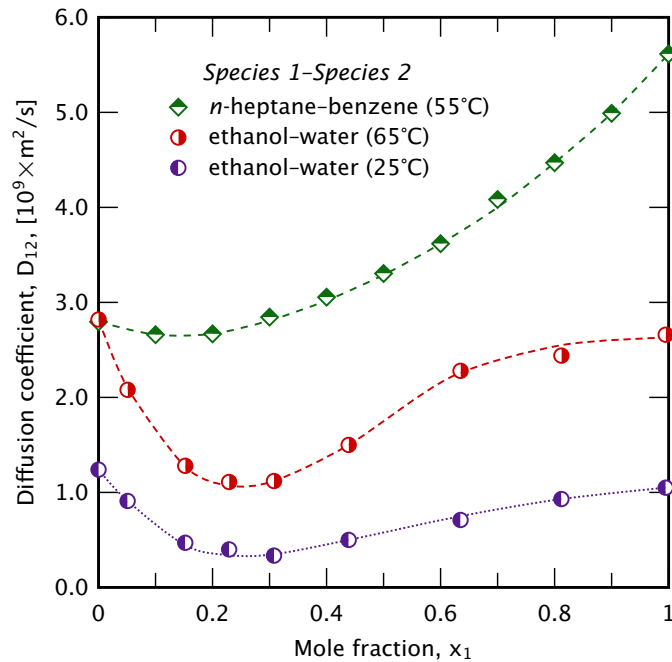
Figure 11.27 Variation of the diffusion coefficient in two concentrated liquid solutions [11.6, 11.65].

The thermal conductivity and viscosity of gases

The viscosity and thermal conductivity of a mixture must sometimes be estimated in convective mass transfer problems. Here, we consider only μ and k for gases.

Two of the most important results from the kinetic theory of gases are the predictions of μ and k for a pure, monatomic gas of species A [11.44]:

$$\mu_A = (2.6693 \times 10^{-6}) \frac{\sqrt{M_A T}}{\sigma_A^2 \Omega_\mu} \tag{11.116}$$

and

$$k_A = \frac{0.083228}{\sigma_A^2 \Omega_\mu} \sqrt{\frac{T}{M_A}} \tag{11.117}$$

Here, Ω_μ is a collision integral for the viscosity and thermal conductivity (see Table 11.4). In these equations μ is in kg/m·s, k is in W/m·K, T is in kelvin, and σ_A again has units of Å.

The equation for μ_A applies equally well to polyatomic gases, but k_A must be corrected to account for internal modes of energy storage—chiefly molecular rotation and vibration. In 1913, Eucken [11.67] gave a

simple analysis showing that this correction was

$$k = \left(\frac{9\gamma - 5}{4\gamma} \right) \mu c_p \qquad (11.118)$$

for an ideal gas, where $\gamma \equiv c_p / c_v$ (see Problem 11.52). You may recall from your thermodynamics courses that γ is 5/3 for monatomic gases, 7/5 for diatomic gases at modest temperatures, and approaches one for very complex molecules. Equation (11.118) should be used with tabulated data for c_p; on average, it will underpredict k by perhaps 10 to 20% [11.5].

An approximate formula for μ in multicomponent gas mixtures was developed by Wilke [11.68], based on the kinetic theory of gases:

$$\mu_m = \sum_{i=1}^{n} \frac{x_i \mu_i}{\sum_{j=1}^{n} x_j \phi_{ij}} \qquad (11.119a)$$

where

$$\phi_{ij} = \frac{\left[1 + (\mu_i / \mu_j)^{1/2} (M_j / M_i)^{1/4} \right]^2}{2\sqrt{2} \left[1 + (M_i / M_j) \right]^{1/2}} \qquad (11.119b)$$

An analogous expression for the thermal conductivity of gas mixtures was derived by Mason and Saxena [11.69]:[26]

$$k_m = \sum_{i=1}^{n} \frac{x_i k_i}{\sum_{j=1}^{n} x_j \phi_{ij}} \qquad (11.119c)$$

Equation (11.119a) is accurate to about 2% and eqn. (11.119c) to about 4% for mixtures of nonpolar gases. For higher accuracy or for mixtures with polar components, refer to [11.5] and [11.54].

Example 11.17   Kinetic prediction of μ and k for air

Compute the transport properties of air at 300 K, and compare your results to data from Table A.6.

---

[26]We have followed [11.5] in omitting an empirical correction factor proposed by Mason and Saxena, $(1.065 \times \phi_{ij})$.

SOLUTION. The mass composition of air was given in Example 11.1. Using the methods of Example 11.1, we obtain the mole fractions as $x_{N_2} = 0.7808$, $x_{O_2} = 0.2095$, and $x_{Ar} = 0.0093$.

We first compute μ and k for the three species to illustrate the use of eqns. (11.116) to (11.118), although we could simply use tabled data in eqns. (11.119a) and (11.119c). From Tables 11.3 and 11.4:

Species	σ (Å)	ε/k_B (K)	M (kg/kmol)	Ω_μ
N_2	3.705	84.94	28.01	0.9975
O_2	3.392	121.7	32.00	1.0984
Ar	3.324	143.8	39.95	1.0848

Substitution of these values into eqn. (11.116) yields

Species	μ_{calc} (kg/m·s)	μ_{data} (kg/m·s)
N_2	1.787×10^{-5}	1.789×10^{-5}
O_2	2.069×10^{-5}	2.065×10^{-5}
Ar	2.282×10^{-5}	2.29×10^{-5}

where the data are from Appendix A (Table A.6). With c_p data from Appendix A, eqns. (11.117) and (11.118) yield the thermal conductivities of the components:

Species	c_p (J/kg·K)	k_{calc} (W/m·K)	k_{data} (W/m·K)
N_2	1041.	0.02525	0.0260
O_2	919.9	0.02583	0.0265
Ar	521.5	0.01785	0.0179

The predictions agree with the data to better than 0.4% for μ and to within 3% for k.

To compute μ_m and k_m, we use eqns. (11.119a) and (11.119c) and the tabulated values of μ and k. Choosing N_2, O_2, and Ar as species 1, 2, and 3, we get

$$\phi_{12} = 0.9925, \quad \phi_{21} = 1.006$$
$$\phi_{13} = 1.049, \quad \phi_{31} = 0.9393$$
$$\phi_{23} = 1.061, \quad \phi_{32} = 0.9371$$

and $\phi_{ii} = 1$. The sums appearing in the denominators are

$$\sum_{j=1}^{3} x_j \phi_{ij} = \begin{cases} 0.9985 & \text{for} \quad i = 1 \\ 1.005 & \text{for} \quad i = 2 \\ 0.9390 & \text{for} \quad i = 3 \end{cases}$$

Finally, eqns. (11.119a) and (11.119c) yield these calculated values:

$$\mu_{m,\text{calc}} = 1.851 \times 10^{-5} \text{ kg/m·s}, \quad \mu_{m,\text{data}} = 1.854 \times 10^{-5} \text{ kg/m·s}$$
$$k_{m,\text{calc}} = 0.02531 \text{ W/m·K}, \quad\quad\quad k_{m,\text{data}} = 0.0264 \text{ W/m·K}$$

The predicted mixture values are within 0.2 and about 4%, respectively, of the air data from Table A.6.

Finally, we need c_{p_m} to compute the Prandtl number of the mixture. For ideal gases, mixture specific heat capacity is merely the mass weighted average, $c_{p_m} = \sum_i m_i c_{p_i}$, equal to 1006 J/kg·K. Then

$$\text{Pr} = (\mu c_p / k)_m = (1.861 \times 10^{-5})(1006)/0.02596 = 0.721$$

This value is 2% above the tabled value of 0.707. The reader may wish to compare these results with those obtained much more directly using the values for air in Table 11.3 or to explore the effects of neglecting argon in the preceding calculations.   ■

11.11   Diffusion in multicomponent and nonideal mixtures

So far, we have considered only binary diffusion in ideal solutions. When three or more species are present, more than one concentration gradient can vary independently. Further, when a mixture is not ideal, the intermolecular forces of diffusion change with the concentration. In this section, we briefly introduce the theory of diffusion in multicomponent and nonideal mixtures.

Fick's law in multicomponent mixtures

In a mixture of three species, two concentration gradients and two diffusional fluxes are independent. Thus,

$$\vec{j_1} = -\rho \mathcal{D}_{11} \nabla m_1 - \rho \mathcal{D}_{12} \nabla m_2 \quad\quad\quad (11.120\text{a})$$
$$\vec{j_2} = -\rho \mathcal{D}_{21} \nabla m_1 - \rho \mathcal{D}_{22} \nabla m_2 \quad\quad\quad (11.120\text{b})$$

with $\vec{j}_3 = -\vec{j}_1 - \vec{j}_2$ and $\nabla m_3 = -\nabla m_1 - \nabla m_2$. These diffusion coefficients are *not* the same as the binary diffusion coefficients previously studied: they can take negative values, and $\mathcal{D}_{ij}$ need not equal $\mathcal{D}_{ji}$ [11.70].

Equation (11.120a) reveals several paradoxical facts about multicomponent diffusion. For example, the flux of species 1 can be non-zero when its concentration gradient *is* zero—provided that species 2 has a non-zero concentration gradient. Similarly, the cross-coupling of gradients can cause a species to diffuse into a region where its concentration is higher; or, if terms on the right-hand side of eqn. (11.120a) sum to zero, species i may have zero flux when its concentration gradient is not zero.

Duncan and Toor produced all these phenomena in a simple experiment in 1962 [11.71]. They connected a tube between two bulbs, one containing equal mole fractions of CO_2 and N_2, the other containing equal mole fractions of H_2 and N_2. Then they allowed the gases to diffuse until equilibrium was reached. Nitrogen was successively observed to diffuse when it did not have a gradient, to diffuse up its concentration gradient, and not to diffuse when it had a gradient. Upon exchanging the initial concentrations of CO_2 and N_2, they caused CO_2 to display the same behavior.

An n-component mixture has $n - 1$ independent gradients:

$$\vec{j}_i = -\rho \sum_{j=1}^{n-1} \mathcal{D}_{ij} \nabla m_j \quad \text{for } 1 \leqslant i \leqslant n - 1 \tag{11.121}$$

Mutoru and Firoozabadi [11.72] have compiled values of $\mathcal{D}_{ij}$ for ternary and quaternary mixtures.

Maxwell-Stefan equations for ideal mixtures

James Clerk Maxwell studied binary diffusion in his 1867 paper on the kinetic theory of gases. Josef Stefan, in 1871, considered the same problem using physical arguments and force balance. Stefan's physical arguments are also applicable to liquids. The equations they obtained are now called the Maxwell-Stefan equations [11.73, 11.74]. The theory states that the drag forces between diffusing species balance the partial pressure gradients that move the species in opposite directions.

Interspecies drag in binary diffusion. When two particles have an elastic collision, the momentum change of particle 2, $\Delta \vec{P}_2$, is proportional the

velocity difference before the collision, $(\vec{v}_1 - \vec{v}_2)$

$$\Delta\vec{P}_2 \propto \frac{m_1 m_2}{m_1 + m_2}(\vec{v}_1 - \vec{v}_2) \tag{11.122}$$

where m_1 and m_2 are the particles' masses [11.75]. In binary diffusion, the rate of momentum transfer depends on the rate of collisions between the two kinds of molecules. In turn, the collision frequency per unit volume, Z_{12}, depends on the number of molecules of each type per unit volume, $\mathcal{N}_i$.[27] Further, $\mathcal{N}_i = N_A c x_i$, where N_A is Avogadro's number.[28] Thus:

$$Z_{12} \propto \mathcal{N}_1 \mathcal{N}_2 \propto x_1 x_2 \tag{11.123}$$

Now, for one-dimensional diffusion in a slab of area A and thickness dz, the average rate of momentum transfer from species 1 to species 2, $d\dot{P}_{1\rightarrow2}$, is proportional to the product of the momentum transfer per collision and the rate of collisions within the volume

$$d\dot{P}_{1\rightarrow2} = a x_1 x_2 (v_1 - v_2) A\, dz \tag{11.124}$$

where v_1 and v_2 are the species average speeds in the z-direction, and a is a constant of proportionality. This transfer represents a *loss* of momentum from species 1, in other words, a drag force on species 1 by species 2. The drag per unit volume of mixture is therefore

$$f_{12} = a x_1 x_2 (v_1 - v_2) \tag{11.125}$$

We define the *Maxwell-Stefan diffusion coefficient* to be $Ð_{12} \equiv (cR°T)/a$:

$$f_{12} = (cR°T)\frac{x_1 x_2 (v_1 - v_2)}{Ð_{12}} \tag{11.126}$$

This definition applies to either a gas or a liquid. In fact, Problem 11.55 shows that this definition leads directly to the Sutherland-Einstein relation, eqn. (11.111), for a dilute liquid solution.

---

[27]In a low density gas composed of hard-sphere molecules, $Z_{12} = \mathcal{N}_1 \mathcal{N}_2 \sigma_{12}\overline{C}$ where $\sigma_{12} = \pi(d_1 + d_2)^2/4$ and $\overline{C}$ is the average molecular speed from eqn. (11.101) [11.56].
[28]$N_A = 6.0221 \times 10^{23}$ molecules/mol.
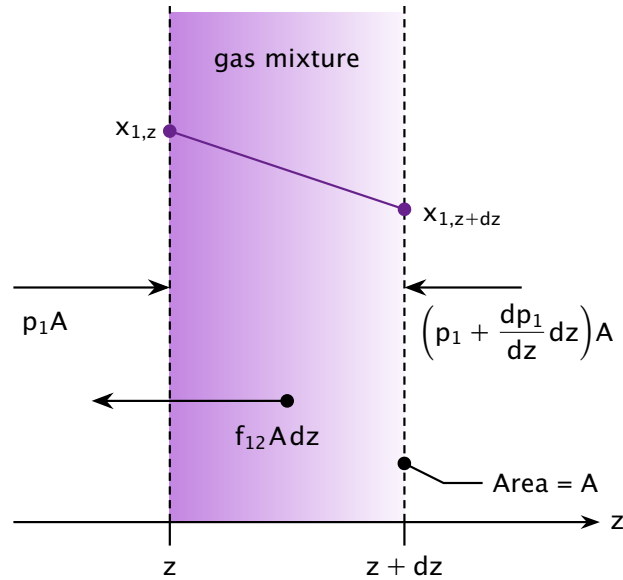
Figure 11.28 Partial pressure and interspecies drag force on species 1 in a thin slab of gas mixture.

Ideal gas mixtures.   For an ideal gas, the drag force opposes the partial pressure difference on species 1 across the slab of gas mixture. With reference to Fig. 11.28, the force balance is

$$p_1 A = f_{12} A dz + \left(p_1 + \frac{dp_1}{dz} dz \right) A$$

Canceling terms, and setting $cR°T = p$ for an ideal gas, we have[29]

$$-\frac{dp_1}{dz} = f_{12} = p \left(\frac{x_1 x_2 (v_1 - v_2)}{Đ_{12}} \right) \qquad (11.127a)$$

The left-hand side is the force driving the diffusion of species 1, per unit volume of gas mixture. Likewise, for species 2, the balance is

$$-\frac{dp_2}{dz} = f_{21} = p \left(\frac{x_1 x_2 (v_2 - v_1)}{Đ_{12}} \right) \qquad (11.127b)$$

Clearly, $f_{12} = -f_{21}$, since diffusion creates no net force on the mixture. Only one of eqns. (11.127) is independent.

For a multicomponent gas mixture, and in three dimensions, the generalization of eqns. (11.127) is

$$-\nabla p_i = p \sum_{j=1}^{n} \frac{x_i x_j (\vec{v}_i - \vec{v}_j)}{Đ_{ij}} \qquad (11.128)$$

---

[29]If species 1 moves in the $+z$-direction, $dp_1/dz < 0$.

Upon putting $x_i \vec{v}_i = \vec{N}_i / c$, $x_i = p_i / p$, and setting the total pressure p constant, eqn. (11.128) can take either of the following forms:

$$\nabla x_i = \sum_{j=1}^{n} \frac{x_i \vec{N}_j - x_j \vec{N}_i}{c Đ_{ij}} \tag{11.129a}$$

$$= \sum_{j=1}^{n} \frac{x_i \vec{J}_j - x_j \vec{J}_i}{c Đ_{ij}} \tag{11.129b}$$

Equations (11.129) are two forms of the *Maxwell-Stefan equations* for an ideal gas. Only $n - 1$ equations are independent. Terms with $i = j$ are zero, so that $Đ_{ii}$ is not used. Additional analysis shows that $Đ_{ij} = Đ_{ji}$.

The values of $Đ_{ij}$ for an ideal gas mixture may be calculated using eqn. (11.108). In contrast, the values of $\mathcal{D}_{ij}$ for multicomponent mixtures, in eqn. (11.121), must be computed from $Đ_{ij}$ using matrix methods [11.70].

Equations (11.129) are a system of first-order o.d.e.s. If the fluxes are known, the equations can be integrated to find the concentration profiles. If the fluxes are unknown, values that meet the concentration boundary conditions can be determined iteratively (Problem 11.57).

Fick's Law for binary diffusion in ideal gas. The Maxwell-Stefan equations for a binary ideal gas mixture are equivalent to Fick's law. From eqn. (11.129b) in the z-direction, with $J_1 + J_2 = 0$,

$$-\frac{dx_1}{dz} = \frac{x_2 J_1 - x_1 J_2}{c Đ_{12}}$$

$$-c Đ_{12} \frac{dx_1}{dz} = \frac{c_2 J_1 + c_1 J_1}{c} = J_1$$

so that

$$J_1 = -c Đ_{12} \frac{dx_1}{dz} \tag{11.130}$$

which is the same as eqn. (11.30). For the special case of binary diffusion in an ideal gas, the Maxwell-Stefan diffusion coefficient is the same as the Fick diffusion coefficient, $Đ_{12} = \mathcal{D}_{12}$.

Effective binary Fick diffusion coefficients, $\mathcal{D}_{im}$, were described in Section 11.10. Problem 11.53 shows how those approximations are derived from the Maxwell-Stefan equations.

Chemical potential in nonideal mixtures

For mixtures that are nonideal, such as concentrated liquid solutions, the driving force for diffusion of a species i is the gradient of the chemical potential of i, denoted as μ_i. The chemical potential is a thermodynamic property that characterizes the potential energy of a species in a mixture. A species will diffuse from a region of high chemical potential to a region of low chemical potential, just as a ball rolls downhill from high gravitational potential to low potential. Unlike the ball, however, a diffusing species develops no kinetic energy because the released potential energy is transferred to the other species by intermolecular friction. The chemical potential is measured in joules per mole of species i (J/mol).

The condition of chemical equilibrium is that the chemical potential is uniform for each species in the mixture, with no gradients and no differences across phase boundaries. If the chemical potential in one state is lower than in another state, the substance will move spontaneously toward the state with lower potential. For example, if a substance's chemical potential is lower in the vapor state than the liquid state, it will evaporate.

For a substance that is dilute, or ideal, the chemical potential has the simple form

$$\mu_i(x) = \mu_i^{\circ}(p, T) + R^{\circ} T \ln(x_i) \quad \text{ideal solution} \qquad (11.131)$$

where $\mu_i^{\circ}(p, T)$ is the potential in a reference state, or *standard state*. The standard state is often chosen to be pure species i, $x_i^{\circ} = 1$.[30] Although R° appears, this equation is not limited to gases.[31]

For nonideal solutions, such as concentrated liquids, the expression for μ_i is more complicated:

$$\mu_i = \mu^{\circ}(p, T) + R^{\circ} T \ln(\gamma_i x_i) \quad \text{nonideal solution} \qquad (11.132)$$

Here, γ_i is the *activity coefficient*, another thermodynamic property. It depends on the concentrations of all species in the solution, as well as p and T. In an ideal solution, such as a low density gas or a dilute liquid, $\gamma_i = 1$.

---

[30]The reference state, or standard state, is an arbitrary datum. For ionic solutes in electrochemistry, the standard state is often chosen as a hypothetical ideal solute at a concentration of 1 mol/kg [11.76].

[31]The gas constant is present because $R^{\circ} = k_B N_A$, where k_B is Boltzmann's constant and N_A is Avogadro's number, the number of molecules per mole.

The chemical potential accounts for many interesting phenomena, including all the solubility relations described in Section 11.4. A full discussion occupies entire chapters of textbooks on physical chemistry and chemical engineering [11.10, 11.11]. In this textbook, however, we shall dig no deeper.

Chemical potential driving force. A gradient in any potential energy produces a force, as a gradient in gravitational potential energy produces the gravitational force. Thus, a gradient in the chemical potential creates the force that drives mass diffusion:

$$-\nabla\mu_i = \text{driving force for diffusion of species } i, \text{ per mole} \qquad (11.133)$$

In one dimension, using eqn. (11.131), the driving force per mole is

$$-\frac{d\mu_i}{dz} = -\frac{R^\circ T}{x_i}\frac{dx_i}{dz} \qquad (11.134)$$

To convert this driving force to a driving force per unit volume, we multiply through by c_i (moles i/m^3):

$$-c_i\frac{d\mu_i}{dz} = -cR^\circ T\frac{dx_i}{dz} \qquad (11.135)$$

For an ideal gas, $p = cR^\circ T$, and if the pressure is uniform then

$$-c_i\frac{d\mu_i}{dz} = -p\frac{dx_i}{dz} = -\frac{dp_i}{dz} \quad \text{ideal gas} \qquad (11.136)$$

The last term is the same driving force as in eqn. (11.127a).

For a nonideal mixture, using eqn. (11.132) and shifting to vector form, the chemical potential driving force is

$$-c_i\nabla_{T,p}\mu_i = -cR^\circ T \,\nabla_{T,p}\ln(x_i\gamma_i) \qquad (11.137\text{a})$$

$$= -cR^\circ T \sum_{j=1}^{n-1}\underbrace{\left(\delta_{ij} + x_i\frac{\partial\ln\gamma_i}{\partial x_j}\right)}_{\equiv\Gamma_{ij}}\nabla_{T,p}x_j \qquad (11.137\text{b})$$

$$= -cR^\circ T \sum_{j=1}^{n-1}\Gamma_{ij}\nabla_{T,p}x_j \qquad (11.137\text{c})$$

Here, we define the thermodynamic factor Γ_{ij} as shown, and the gradients $\nabla_{T,p}$ are taken at constant T and p. As before, only $n-1$ gradients are independent.

Intermolecular forces have a complex concentration dependence in nonideal solutions. This variation is largely carried in the activity coefficient, γ_i, and the thermodynamic factor, Γ_{ij}.

Maxwell-Stefan equations in nonideal mixtures

For a nonideal solution, the Maxwell-Stefan equations are again a balance between the chemical potential driving force and the interspecies drag force, similar to the ideal gas equations, (11.128) and (11.129):

$$-c_i \nabla_{T,p} \mu_i = -(cR°T) \sum_{j=1}^{n} \frac{x_i \vec{J}_j - x_j \vec{J}_i}{c Ð_{ij}} \tag{11.138}$$

The chemical potential driving force must now be represented by eqn. (11.137c). Substituting that relationship and dividing by $-cR°T$, we obtain the Maxwell-Stefan equations for a nonideal mixture:

$$\boxed{\sum_{j=1}^{n-1} \Gamma_{ij} \nabla_{T,p} x_j = \sum_{j=1}^{n} \frac{x_i \vec{J}_j - x_j \vec{J}_i}{c Ð_{ij}}} \tag{11.139}$$

This system of equations, like the generalized Fick's law, eqn. (11.121), may be solved using matrix methods with appropriate estimates for Γ_i and $Ð_{ij}$. Many interesting examples are given in [11.70] and [11.77].

The Maxwell-Stefan equations may be extended to electrochemical systems by adding electrostatic forces to eqn. (11.138). For dilute solutions, the result is the *Nernst-Planck equation* (Problem 11.56), which describes the transport of ions in electrolyte solutions.

Binary diffusion in concentrated liquid solutions. If only two species are present, eqn. (11.139) can be simplified as before

$$\Gamma \nabla_{T,p} x_1 = \frac{x_1 \vec{J}_2 - x_2 \vec{J}_1}{c Ð_{12}} = -\frac{c_1 \vec{J}_1 + c_2 \vec{J}_1}{c^2 Ð_{12}} = -\frac{\vec{J}_1}{c Ð_{12}}$$

with $\Gamma = \Gamma_{11}$ from eqn. (11.137b). Then

$$\vec{J}_1 = -c\Gamma Ð_{12} \nabla_{T,p} x_1 \tag{11.140}$$

We immediately see that the Fick coefficient for binary diffusion is related to the Maxwell-Stefan coefficient by

$$\mathcal{D}_{12} = \Gamma Ð_{12} \tag{11.141}$$

The thermodynamic factor, Γ, accounts for most of the concentration dependence of the Fick diffusivity. The Maxwell-Stefan diffusivity is much less sensitive to concentration [11.70]. When $x_1 \to 0$, so that the solution is ideal, $\Gamma \to 1$ and $\mathcal{D}_{12} = Ð_{12}$. For example, in a dilute liquid solution, the Fick and Maxwell-Stefan diffusivities are the same, and the Sutherland-Einstein formula, eqn. (11.113), predicts both.

Problems

11.1 Derive eqns. (11.9).

11.2 A 1000 liter cylinder at 300 K contains a gaseous mixture composed of 0.10 kmol of NH_3, 0.04 kmol of CO_2, and 0.06 kmol of He. (a) Find the mass fraction for each species and the pressure in the cylinder. (b) After the cylinder is heated to 600 K, what are the new mole fractions, mass fractions, and molar concentrations? (c) The cylinder is now compressed isothermally to a volume of 600 liters. What are the molar concentrations, mass fractions, and partial densities? (d) If 0.40 kg of N_2 is injected into the cylinder while the temperature remains at 600 K, find the mole fractions, mass fractions, and molar concentrations. [(a) $m_{CO_2} = 0.475$; (c) $c_{CO_2} = 0.0667$ kmol/m^3; (d) $x_{CO_2} = 0.187$.]

11.3 The pressure of Jupiter's atmosphere increases with depth. The famous clouds of Jupiter are in a layer called the troposphere, in which the pressure rises from 0.1 bar to 10 bar. The top of the troposphere, called the tropopause, is about 50 km above the clouds and is at 0.1 bar and 110 K. The atmospheric mole fractions of hydrogen, helium, and methane are $x_{H_2} = 0.86$, $x_{He} = 0.136$, and $x_{CH_4} = 0.0018$. Other species have small but localized concentrations, e.g., in the troposphere's clouds of ammonia ice. (a) Calculate the molar concentrations and the partial densities of H_2, He, and CH_4 at the tropopause. (b) Find the number of hydrogen atoms per unit volume (number density), $\mathcal{N}_{H_2}$ at the tropopause. (c) Estimate $\mathcal{N}_{H_2}$ at the base of the Jovian troposphere, where the pressure is 10 bar and the temperature is 340 K.

11.4 In Example 11.2, suppose that the only gases at the s-surface are CO, O_2, and N_2. As before, assume that $m_{O_2,s}$ is very small. Find $j_{N_2,s}$, $n_{N_2,s}$, and $m_{N_2,s}$.

11.5 Small automobile batteries commonly contain an aqueous solution of sulfuric acid (H_2SO_4) with lead and lead oxide plates as electrodes. Current is generated by the reaction of the electrolyte with the electrode material. The reaction at the lead electrode (the anode) is

$$Pb(s) + HSO_4^- \longrightarrow PbSO_4(s) + H^+ + 2e^-$$

where the (s) denotes a solid phase component. If the current density at such an electrode is $i = 5$ mA/cm^2, what is the mole flux of HSO$_4$$^-$ (bisulfate) to the electrode? Recall that the charge of an electron is -1.609×10^{-19} C and that 1 A = 1 C/s. What is the mass flux of HSO$_4$$^-$? At what mass rate is PbSO$_4$ produced? A what rate does H$^+$ flow away from the electrode? [$\dot{r}''_{\text{PbSO}_4} = 7.83 \times 10^{-5}$ kg/m^2·s.]

11.6 In *catalysis*, one gaseous species reacts with another on the surface of a catalyst to form a gaseous product. For example, butane (C$_4$H$_{10}$) reacts with hydrogen on the surface of a nickel catalyst to form propane (C$_3$H$_8$) and methane (CH$_4$). This heterogeneous reaction, referred to as *hydrogenolysis*, is

$$\text{C}_4\text{H}_{10} + \text{H}_2 \xrightarrow{\text{Ni}} \text{C}_3\text{H}_8 + \text{CH}_4$$
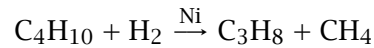
The molar rate of consumption of C$_4$H$_{10}$ per unit area in the reaction is $\dot{R}_{\text{C}_4\text{H}_{10}} = A(e^{-\Delta E/R^\circ T})p_{\text{C}_4\text{H}_{10}}p_{\text{H}_2}^{-2.4}$, where $A = 2.9 \times 10^9$ kmol/m^{2}s, $\Delta E = 1.9 \times 10^8$ J/kmol, and p is in atm [11.78].

  a. If $p_{\text{C}_4\text{H}_{10},s} = p_{\text{C}_3\text{H}_8,s} = 0.2$ atm, $p_{\text{CH}_4,s} = 0.17$ atm, and $p_{\text{H}_2,s} = 0.3$ atm at a nickel surface with conditions of 440°C and 0.87 atm total pressure, what is the rate of consumption of butane?

  b. What are the mole fluxes of butane and hydrogen to the surface? What are the mass fluxes of propane and methane away from the surface?

  c. What is $v_{\text{C}_4\text{H}_{10},s}$? What are v_s and v_s^*?

  d. What is the diffusional mole flux of butane? What is the diffusional mass flux of propane? What is the flux of Ni?

  [(b) $n_{\text{CH}_4,s} = 2.03$ g/m^{2}s; (d) $j_{\text{C}_3\text{H}_8} = 5.58$ g/m^{2}s]

11.7 Show that $\mathcal{D}_{12} = \mathcal{D}_{21}$ in a binary mixture.

11.8 Using the definitions of the fluxes, velocities, and concentrations, derive eqn. (11.30) from eqn. (11.26) for binary diffusion.

11.9 Fill in the details involved in obtaining eqn. (11.33) from eqn. (11.32).

11.10 The salt concentration in the ocean increases with increasing depth, z, because saltier water has greater density and tends to sink. A model equation for the concentration distribution in the upper ocean is

$$S = 33.25 + 0.75 \tanh(0.026z - 3.7)$$

where S is the salinity in grams of salt per kilogram of ocean water and z is the distance below the surface in meters. (a) Plot the mass fraction of salt as a function of z. (The region of rapid transition of $m_{salt}(z)$ is called the *halocline*.) (b) Ignoring the effects of waves or currents, compute $j_{salt}(z)$. Use a value of $\mathcal{D}_{salt,water} = 1.5 \times 10^{-9}$ m^2/s. Indicate the position of maximum diffusion on your plot of the salt concentration. (c) The upper region of the ocean is well mixed by wind-driven waves and turbulence, while the lower region and halocline tend to be calmer. Using $j_{salt}(z)$ from part (b), make a simple estimate of the amount of salt diffused upward in one week in a 5 km^2 horizontal area of the sea. Ignore rainfall and other inflow of fresh water.

11.11 Consider two chambers held at temperatures T_1 and T_2, respectively, and joined by a small insulated tube. The chambers are filled with a binary gas mixture, with the tube open, and allowed to come to steady state. If the Soret effect is taken into account, what is the concentration difference between the two chambers? Assume that an effective mean value of the thermal diffusion ratio is known.

11.12 (a) Work Problem 6.36. (b) In general, a fluid is said to be "incompressible" if the density of a fluid particle does not change as it moves about in the flow (i.e., if $D\rho/Dt = 0$). Show that an incompressible flow satisfies $\nabla \cdot \vec{u} = 0$. (c) How does the condition of incompressibility differ from that of "constant density"? Describe a flow that is incompressible but that does not have "constant density."

11.13 (a) Carefully derive eqn. (11.44). Note that ρ is not assumed constant in eqn. (11.44). (b) If ρ is spatially uniform, show that

$$\frac{D\rho_i}{Dt} = \mathcal{D}_{im}\nabla^2\rho_i + \dot{r}_i \qquad (11.142)$$

where the material derivative, D/Dt, is defined in eqn. (6.38).

11.14 Derive the equation of species conservation on a molar basis, using c_i rather than ρ_i. Also obtain an equation in c_i alone, similar to eqn. (11.44) but without the assumption of incompressibility. What assumptions must be made to obtain the latter result?

11.15 Find the following concentrations: (a) the mole fraction of air in solution with water at 5°C and 1 atm, exposed to air at the same conditions, $H = 4.88 \times 10^4$ atm; (b) the mole fraction of ammonia in air above an aqueous solution, with $x_{NH_3} = 0.05$ at 0.9 atm and 40°C and $H = 1522$ mm Hg; (c) the mole fraction of SO_2 in an aqueous solution at 15°C and 1 atm, if $p_{SO_2} = 28.0$ mm Hg and $H = 1.42 \times 10^4$ mm Hg; and (d) the partial pressure of ethylene over an aqueous solution at 25°C and 1 atm, with $x_{C_2H_4} = 1.75 \times 10^{-5}$ and $H = 11.4 \times 10^3$ atm.

11.16 Use steam table data to calculate: (a) the partial pressure of water over a 3 percent-by-weight aqueous solution of HCl at 50°C; (b) the boiling point at 1 atm of salt water with a mass fraction $m_{NaCl} = 0.18$. [(b) $T_{B.P.} = 101.8°C$.]

11.17 Consider one-dimensional, binary diffusion in which isothermal ideal gases 1 and 2 travel in opposite directions along the z-axis of a tube. Assume that the flow has a zero mass-average velocity, so that mass transfer purely diffusive.

    a. Show that the conservation equations for mass, species, and momentum are satisfied by $v = 0$, $j_1 = -j_2 = $ constant, and $p = $ constant.

    b. With Fick's law, solve for $m_1(z)$ if $m_1(0) = 0$ and $m_1(L) = 1$.

    c. Find j_1 in terms of the molar masses of the gases. (*Hint: ρ is not constant; use $\rho = Mc$ and write M in terms of m_1 before integrating*).

    d. Write the mole fluxes in terms of the mass fluxes and solve for the mole-average velocity, v^*. Under what condition is $v^* = 0$?

    e. Suppose that gas 1 is helium and gas 2 is air at $T = 276$ K and $p = 1$ atm, with $L = 1$ m. Calculate v^*, and j_i and N_i for both gases. Are the molar diffusion rates equal and opposite?

11.18 Suppose that a steel fitting with a carbon mass fraction of 0.2% is put into contact with carburizing gases at $910°C$, and that these gases produce a steady mass fraction, $m_{C,u}$, of 1.0% carbon just within the surface of the metal. The diffusion coefficient of carbon in this steel is [11.79]

$$\mathcal{D}_{C,Fe} = (1.20 \times 10^{-5} \text{ m}^2/\text{s}) \exp[-(1.34 \times 10^8 \text{ J/kmol})/(R°T)]$$

for T in kelvin. How long does it take to produce a carbon concentration of 0.6% by mass at a depth of 0.5 mm? How much less time would it take if the temperature were $950°C$?

11.19 (a) Derive eqn. (11.62) for the mole flux across a stagnant layer, working by analogy to the mass-based analysis of Section 11.5 that led to eqn. (11.58). Assume that $c\mathcal{D}_{12}$ is constant, and use z as the coordinate across the layer. (b) Show that the molar concentration profile, analogous to eqn. (11.61), is

$$\frac{1 - x_2(z)}{1 - x_{2,0}} = \left(\frac{1 - x_{2,L}}{1 - x_{2,0}}\right)^{z/L}$$

11.20 A Stefan tube 1 cm in diameter initially has a pool of liquid carbon tetrachloride 200.0 mm below the top. Pure argon flows over the tube. The system is held at $60°C$ and 8.0×10^4 Pa. During a 12 hr experiment, the pool level drops by 6.1 mm. What is the diffusivity of CCl_4 in Ar? The vapor pressure of CCl_4 is $\log_{10} p_v = 4.023 - 1222/(T - 45.74)$, where p_v is in bar and T in K. The specific gravity of liquid CCl_4 is 1.59.

11.21 A Stefan tube at $60°C$ contains a pool of liquid ethanol 15 cm below the top. Pure nitrogen gas flows across the top. The total pressure is 1.2 bar. Plot the concentration profiles of ethanol and nitrogen in the tube, in terms of both mass fraction and mole fraction (see Problem prob:12.33). The vapor pressure of ethanol (C_2H_5OH) is given by $\log_{10} p_v = 5.247 - 1599/(T - 46.42)$ for p_v is in bar and T in K.

11.22 Consider mass convection in a binary mixture, in which only species 1 is transferred through the s-surface. Show that $g_{m,1} = g_{m,2}$. How does $j_{2,s}$ relate to $n_{1,s}$?

11.23 A small sphere in a gas at rest has a low vapor pressure of species 1, so that species 1 is dilute in the gas phase. When natural convection around the sphere is negligible, the steady mass flux of species 1 in the radial direction is $n_{1,r} \cong j_{1,r} = -\rho \mathcal{D}_{12} dm_1/dr$. Use a mass balance to obtain the s-surface mass flux in terms of the difference between the concentration far from the sphere, $m_{1,\infty}$, and near the surface, $m_{1,s}$. Approximate $\rho \mathcal{D}_{12}$ as constant, which is accurate if species 1 is dilute. Then use eqns. (11.66) and (11.69) to show that $\mathrm{Nu}_{m,D} = 2$. What condition must apply for convection to be negligible?

11.24 *Film absorption* is a process whereby gases are absorbed into a falling liquid film. Typically, a thin film of liquid runs down the inside of a vertical tube through which the gas flows. Analyze this process making assumptions as follows. The film flow is laminar and of constant thickness, δ_0, with a velocity profile given by eqn. (8.51); the gas is only slightly soluble in the liquid, so that it does not penetrate far beyond the liquid surface and so that liquid properties are unaffected by it; and, the gas concentration at the s- and u-surfaces (above and below the liquid-vapor interface, respectively) does not vary along the length of the tube. The inlet concentration of gas in the liquid is $m_{1,0}$. Show that the mass transfer Nusselt number is given by

$$\mathrm{Nu}_{m,x} = \left(\frac{u_0 x}{\pi \mathcal{D}_{12}} \right)^{1/2} \quad \text{with} \quad u_0 = \frac{(\rho_f - \rho_g) g \delta_0^2}{2 \mu_f}$$

The mass transfer coefficient here is based on the concentration difference between the u-surface and the bulk liquid at $m_{1,0}$. *Hint*: The small penetration assumption can be used to reduce the species equation for the film to the diffusion equation, (11.56).

11.25 Benzene vapor flows through a 3 cm I.D. vertical tube. A thin film of initially pure water runs down the inside wall of the tube at a flow rate of 0.3 liter/s. If the tube is 0.5 m long and 40°C, estimate the rate (in kg/s) at which benzene is absorbed into water over the entire length of the tube. The mass fraction of benzene at the u-surface is 0.206. *Hint*: Use the result stated in Problem 11.24. Obtain δ_0 from the results in Chapter 8.

11.26 (a) Write eqn. (11.44) in its boundary layer form. (b) Write this concentration boundary layer equation and its b.c.'s in terms of a

nondimensional mass fraction, ψ, analogous to the dimensionless temperature in eqn. (6.42). (c) For $\nu = \mathcal{D}_{im}$, relate ψ to the Blasius function, f, for flow over a flat plate. (d) Note the similar roles of Pr and Sc in the two boundary layer transport processes. Infer the mass concentration analog of eqn. (6.55) and sketch the concentration and momentum b.l. profiles for Sc $= 1$ and Sc $\gg 1$.

11.27 When Sc is large, momentum diffuses more easily than mass, and the concentration b.l. thickness, δ_c, is much less than the momentum b.l. thickness, δ. On a flat plate, the small part of the velocity profile within the concentration b.l. is approximately $u/U_e = 3y/2\delta$. Compute $\mathrm{Nu}_{m,x}$ based on this velocity profile, assuming a constant wall concentration. *Hint*: Use the mass transfer analogs of eqn. (6.47) and (6.50) and note that $q_w/\rho c_p$ is analogous to $j_{i,s}/\rho$.

11.28 Nitrous oxide is bled through the surface of a porous $3/8$ in. O.D. tube at 0.025 liter/s per meter of tube length. Air flows perpendicular to the tube at 25 ft/s. Both the air and the tube are at $18°$C, and the ambient pressure is 1 atm. Estimate the mean concentration of N_2O at the tube surface. $\mathcal{D}_{\mathrm{air,N_2O}} = 1.48 \times 10^{-5}\ \mathrm{m^2/s}$. *Hint*: First estimate the concentration using properties of pure air; then correct the properties if necessary.

11.29 Helium is bled through a porous vertical wall, 40 cm high, into surrounding air at a rate of 87.0 mg/m^{2}s. Both the helium and the air are at 300 K, the environment is at 1 atm, and $\mathcal{D}_{\mathrm{He,air}} = 7.12 \times 10^{-5}\ \mathrm{m^2/s}$. What is the average concentration of helium in the air along the wall, $\overline{m_{\mathrm{He},s}}$?

11.30 We're off on a drive across West Texas. It's going to be hot today—$40°$C—but we're unsure of the humidity. We attach a "desert water bag" to the shaded side of our pickup truck. It's made of canvas, and it holds a liter and a half of drinking water. When we fill it, we make sure to saturate the canvas inside and out. Water will continue to permeate the fabric, but the weave is tight enough that no water drips from it. Plot the temperature of the water inside the bag as a function of the outdoor humidity. *Hint:* These bags were once widely used in the Western US, but they never found much use along the US Gulf coast.

11.31 The following data were taken at a weather station over a period of several months:

Date	$T_{\text{dry-bulb}}$	$T_{\text{wet-bulb}}$
3/15	15.5°C	11.0°C
4/21	22.0	16.8
5/13	27.3	25.8
5/31	32.7	20.0
7/4	39.0	31.2

Use eqn. (11.74) to find the mass fraction of water in the air at each date. Compare to values from a psychrometric chart.

11.32 During a coating process, a thin film of ethanol is wiped onto a thick flat plate, 0.1 m by 0.1 m. The initial thickness of the liquid film is 0.1 mm, and the initial temperature of both the plate and the film is 303 K. The air above the film is at 303 K, flows at 10 m/s, and contains no ethanol. (a) Assume that the plate is a poor conductor, so that heat transfer from it is negligible. After a short initial transient, the liquid film reaches a steady temperature. Find this temperature and calculate the time required for the film to evaporate. (b) Discuss what happens when the plate is a very good conductor of heat, and calculate a lower bound on the time to evaporate. Properties of ethanol are as follow: $\log_{10}(p_v \text{ mmHg}) = 9.4432 - 2287.8/(T \text{ K})$; $h_{fg} = 9.3 \times 10^5$ J/kg; liquid density, $\rho_{\text{eth}} = 789$ kg/m^3; Sc = 1.30 for ethanol vapor in air; vapor specific heat capacity, $c_{p_{\text{eth}}} = 1420$ J/kg·K.

11.33 Ice cubes left in a freezer will slowly sublime into the air. Suppose that a tray of ice cubes is left in a freezer with air at $-10°$C and a relative humidity of 50%. The air in the freezer is circulated by a small fan, creating a heat transfer coefficient from the top of the ice cube tray of 5 W/m^{2}K. If a 20 g ice cube is rectangular and has an exposed top surface area of 8 cm^2, find the temperature of the ice cube and estimate the time required for it to sublime completely. Assume that no heat is transferred through the ice cube tray. For ice, take $h_{\text{sg}} = 2.837$ MJ/kg, and for water vapor in air, take Sc = 0.63. The vapor pressure of ice is given in Example 11.6.

11.34 Bikram Yoga was a strenuous style of yoga done in a room at 38 to 41°C with relative humidity from 20 to 50%. People doing this

yoga will generate body heat $\dot{Q}_b$ of 300 to 600 W, which must be removed to avoid heat stroke. Calculate the rate at which one's body can cool under these conditions and compare it to the rate of heat generation.

The body sweats more as its need to cool increases, but the amount of sweat evaporated on the skin depends on air temperature and humidity. Sweating cannot exceed about 2 liters per hour, of which only about half evaporates (the rest will simply drip).

Assume that sweating skin has a temperature of 36°C and an emittance of 0.95, and that an average body surface area is $A_b = 1.8$ m². Assume that the walls in the yoga studio are at the air temperature. Assume that the lightweight yoga clothing has no thermal effect. Water's vapor pressure can be taken from a steam table or other database. Convection to a person active in still air can be estimated from the following equation [11.80]:

$$\overline{h} = (5.7 \text{ W/m}^2\text{K})\left(\frac{\dot{Q}_b}{(58.1 \text{ W/m}^2)\, A_b} - 0.8\right)^{0.39}$$

Note that at high humidity and temperature, some people become overheated and must stop exercising.

11.35 Biff Harwell has taken Deb sailing. Deb, and Biff's towel, fall into the harbor. Biff rescues them both from a passing dolphin and then spreads his wet towel out to dry on the fiberglass foredeck of the boat. The incident solar radiation is 1050 W/m²; the ambient air is at 31°C, with $m_{\text{H}_2\text{O}} = 0.017$; the wind speed is 8 knots relative to the boat (1 knot = 1.151 mph); $\varepsilon_{\text{towel}} \cong \alpha_{\text{towel}} \cong 1$; and the sky has the properties of a black body at 280 K. The towel is 3 ft long in the windward direction and 2 ft wide. Help Biff figure out how rapidly (in kg/s) water evaporates from the towel.

11.36 Small water droplets evaporate rapidly dry air. Suppose that a droplet is placed in a room at 30°C, 40% RH, and 1 atm. Calculate the lifetime of the droplet if its initial diameter is 0.2, 0.5, 1, 2, and 5 µm.

11.37 A Couette flow (or stagnant film) model of a laminar boundary layer neglects streamwise derivatives locally, so that the velocity varies in y, but not x, from $u = 0$ at the wall to u_∞ at the edge of the b.l., $y = \delta$. The b.l. thickness δ is assumed increase only

slowly with x. (a) Show that $u/u_\infty = y/\delta$ in laminar flow. (b) Calculate skin friction coefficient, C_f, the temperature profile, $T(y)$, and the Nusselt number, Nu_x, in terms of δ and δ_t. (c) Using eqns. (6.31b) and (6.55), show that the laminar Couette flow model results in estimates of $C_f(x)$ and Nu_x that differ from eqns. (6.33) and (6.58) by a constant on the order of one.

11.38 (a) What are the largest and smallest values of the mass transfer driving force, $B_{m,2}$? (b) Plot the blowing factor as a function of $B_{m,2}$. Indicate on your graph the regions of blowing, suction, and low-rate mass transfer.

11.39 Perform the integration to obtain eqn. (11.85). Then take the derivative and the limit needed to get eqns. (11.86) and (11.87).

11.40 (a) Derive eqn. (11.98) from eqn. (11.97). (b) In a test of a scramjet combustor, gas is injected through a porous section of the combustor wall [11.81]. The gas velocity is 980 m/s. As a result of viscous friction and gas compression, the temperature of an adiabatic section of the wall would be 1048 K: use this temperature as if it were the freestream temperature. The heat transfer coefficient without injection is $h^* = 720$ W/m^{2}K. The injected gas is drawn from a reservoir at 350 K at a mass flux of $n_{i,s} = 0.3$ kg/m^{2}s. What is the wall temperature T_s if the gas is He, Ar, or N$_2$? (c) Plot T_s for each gas if $0 \leqslant n_{i,s} \leqslant 1.5$ kg/m^{2}s.

11.41 Dry ice (solid CO$_2$) is used to cool medical supplies transported by a small plane to a remote village in Alaska. A roughly spherical chunk of dry ice, 5 cm in diameter, falls from the plane through air at 5°C. It reaches a terminal velocity of 40 m/s. What are the temperature and sublimation rate of the dry ice, assuming steady conditions? The latent heat of sublimation is about 590 kJ/kg and $\log_{10}(p_v$ bar$) = 6.81228 - 1301.679/(T$ K $- 3.494)$. The surface temperature will be well below the solid-vapor equilibrium temperature of CO$_2$ at 1 atm, which is -78.5°C. Use this correlation for forced convection over a sphere in air at room temperature

$$\overline{\text{Nu}}_D = 2 + 0.493\,\text{Re}_D^{1/2} + 0.0011\,\text{Re}_D$$

for $7800 \leqslant \text{Re}_D \leqslant 2.9 \times 10^5$ [11.82] and approximate the Prandtl number dependence. Neglect heat conduction into the ice. *Hint*: First use the properties of pure air, and then correct the properties if necessary.

11.42 Steam condenses on a 25 cm high, cold vertical wall in a low-pressure condenser unit. The wall is isothermal at 25°C, and the ambient pressure is 8000 Pa. Air has leaked into the unit and has reached a mass fraction of 0.04. The steam–air mixture is at 45°C and is blown downward past the wall at 8 m/s. (a) Estimate the rate of condensation on the wall. *Hint*: The surface of the condensate film is *not* at the mixture or wall temperature. (b) Compare the result of part (a) to condensation without air in the steam. What do you conclude?

11.43 (a) Compute the binary diffusivity of each of the noble gases when they are individually mixed with nitrogen gas at 1 atm and 300 K. Plot the results as a function of the molar mass of the noble gas. What do you conclude? (b) Consider the addition of a small amount of helium, $x_{He} = 0.04$, to a mixture of nitrogen, $x_{N_2} = 0.48$, and argon, $x_{Ar} = 0.48$. Compute $\mathcal{D}_{He,m}$ and compare it with $\mathcal{D}_{Ar,m}$. Note that the increased concentration of argon does not raise its diffusivity in the mixture.

11.44 A mothball consists of a 2.5 cm diameter sphere of naphthalene ($C_{10}H_8$) that is hung by a wire in a closet. The solid naphthalene slowly sublimes to vapor, which drives off the moths. Estimate the lifetime of this mothball in a closet with a mean temperature of 20°C. Use the following data for naphthalene

$$\sigma = 6.18 \text{ Å}, \qquad \varepsilon/k_B = 561.5 \text{ K},$$

and, for the solid, $\rho_{C_{10}H_8} = 1145 \text{ kg/m}^3$ at 20°C. The vapor pressure of naphthalene near room temperature is approximated by

$$\log_{10}(p_v \text{ mmHg}) = 11.450 - 3729.3/(T \text{ K})$$

The integral you will obtain can be evaluated numerically. The latent heat of sublimation and evaporation rate are low enough that the wet-bulb temperature is essentially the ambient temperature.

11.45 In contrast to the naphthalene mothball described in Problem 11.44, other mothballs are made from paradichlorobenzene (PDB). Estimate the lifetime of a 2.5 cm diameter PDB mothball using the following room temperature property data:

$$\rho_{PDB} = 1248 \text{ kg/m}^3$$
$$\sigma = 5.76 \text{ Å} \qquad \varepsilon/k_B = 578.9 \text{ K} \qquad M_{PDB} = 147.0 \text{ kg/kmol}$$
$$\log_{10}(p_v \text{ mmHg}) = 11.985 - 3570/(T \text{ K})$$

11.46 Compute the diffusivity of methane in air using (a) eqn. (11.108) and (b) Blanc's law, eqn. (11.109). For part (b), treat air as a mixture of oxygen and nitrogen, ignoring argon. Let $x_{\text{methane}} = 0.05$, $T = 420°F$, and $p = 10$ psia. [(a) $\mathcal{D}_{\text{CH}_4,\text{air}} = 7.66 \times 10^{-5}$ m^2/s; (b) $\mathcal{D}_{\text{CH}_4,\text{air}} = 8.02 \times 10^{-5}$ m^2/s.]

11.47 In Section 11.5, $\rho\mathcal{D}_{12}$ or $c\mathcal{D}_{12}$ were at times assumed to be independent of position. Consider this approximation for gases. (a) Do these two groups depend on pressure, temperature, or the proportions of species 1 and 2? Are isobaric conditions necessary to hold either group constant? (b) For what type of mixture is $\rho\mathcal{D}_{12}$ most sensitive to composition? What does this indicate about mole versus mass-based analysis? (c) Do Pr or Sc depend on composition, temperature, or pressure?

11.48 A dilute aqueous solution containing potassium ions is subjected to a 1 V/cm electric field. A measurement suggests that the K$^+$ ions move at 4×10^{-4} cm/s in response to the field. Estimate the effective radius of K$^+$ ions if the solution is at 300 K. The charge of an electron is -1.609×10^{-19} C and 1 V/m = 1 N/C.

11.49 (a) Use eqn. (11.115) to obtain diffusion coefficients for: i) dilute CCl$_4$ diffusing through liquid methanol at 340 K; ii) dilute benzene diffusing through water at 290 K; iii) dilute ethyl alcohol diffusing through water at 350 K; and iv) dilute acetone diffusing through methanol at 370 K. (b) Estimate the effective radius of a methanol molecule in a dilute aqueous solution. [(a) $\mathcal{D}_{\text{acetone,methanol}} = 6.8 \times 10^{-9}$ m^2/s.]

11.50 Use eqn. (11.116) to calculate the dynamic viscosity, μ, of gaseous methane, hydrogen sulfide, and nitrous oxide, under the following conditions: 250 K and 1 atm, 500 K and 1 atm, 250 K and 2 atm, 250 K and 12 atm, 500 K and 12 atm. Is the calculation possible in every case?

11.51 A student is studying the combustion of a premixed gaseous fuel with the following molar composition: 10.3% methane, 15.4% ethane, and 74.3% oxygen. She passes 0.006 ft^3/s of the mixture (at 70°F and 18 psia) through a smooth 3/8 inch I.D. tube, 47 inches long. (a) What is the pressure drop? (b) The student's advisor recommends preheating the fuel mixture, using a Nichrome strip

heater wrapped around the last 5 inches of the duct. If the heater produces 0.8 W/inch, what is the wall temperature at the outlet of the duct? Let $c_{p,\text{CH}_4} = 2280$ J/kg·K, $\gamma_{\text{CH}_4} = 1.3$, $c_{p,\text{C}_2\text{H}_6} = 1730$ J/kg·K, and $\gamma_{\text{C}_2\text{H}_6} = 1.2$, and evaluate the properties at the inlet conditions. *Hint*: Refer to Chapter 7 for pressure drop equations.

11.52 (a) Show that $k = (5/2)\mu c_v$ for a monatomic gas. (b) Obtain Eucken's equation, (11.118), for the Prandtl number of a low density gas:

$$\text{Pr} = 4\gamma/(9\gamma - 5)$$

(c) Recall that for an ideal gas, $\gamma \cong (D + 2)/D$, where D is the number of modes of energy storage of its molecules. Obtain an expression for Pr as a function of D. (d) Use Eucken's formula to compute Pr for gaseous Ar, N_2, and H_2O, accounting for translational and rotational energy storage. Compare the result to 1 atm data from Appendix A over a range of temperatures. Discuss the results obtained for steam as opposed to Ar and N_2.

11.53 Three simplifications of the Maxwell-Stefan equations, (11.139), lead to an effective, binary Fick diffusion coefficient, $\mathcal{D}_{im}$. (a) Show that Blanc's law, eqn. (11.109), applies when species i at low concentration diffuses into an otherwise uniform mixture. (b) Show that if $\mathcal{D}_{ij}$ has the same value for each pair of species and the mixture is ideal, then $\mathcal{D}_{im} = \mathcal{D}_{ij}$. (c) Show that if species $i = 1, 2, 3, \ldots, n - 1$ all have low concentrations, then $\mathcal{D}_{im} = \mathcal{D}_{i,n}$, where species n is the dominant species (or solvent), as stated in eqn. (11.110).

11.54 A dilute solute A in a liquid solution diffuses down the gradient of the chemical potential, μ_A, because a gradient in potential energy causes a force per mole of A, as discussed in Section 11.11. Compute this force and combine the result with the molar form of Fick's law to derive the Einstein relation, eqn. (11.111). Note that the Einstein relation considers the force per molecule and that $R^\circ = k_B N_A$, where N_A is Avogadro's number.

11.55 In Section 11.11, we evaluated the drag on one species as it diffuses past another. Show that this force also leads to the Einstein relation, eqn. (11.111). (Compare to Problem 11.54.)

11.56 Consider a solvent n that contains $n - 1$ dilute solutes with $x_i \ll x_n \cong 1$. (a) Work Problem 11.53c. (b) Show that $\vec{v}^* \cong \vec{v}_n \cong \vec{v}$ if the solutes are dilute. (c) Suppose the solutes are charged ions, such as Na^+ and Cl^- for table salt dissolved in water. An electric potential gradient, $-\nabla \phi$, applied to the solution will create a force per mole of ion, $-z_i \mathcal{F} \nabla \phi$, where z_i is the ion's valence (± 1 for Na^+ and Cl^-) and $\mathcal{F} = 9.6485 \times 10^4$ C/mol is Faraday's constant. Starting with the Maxwell-Stefan equations, derive the *Nernst-Planck equation*:

$$\vec{N}_i = -c \mathcal{D}_{i,n} \nabla x_i + c_i \vec{v}_n - c_i \mathcal{D}_{i,n} z_i \frac{\mathcal{F}}{R^\circ T} \nabla \phi$$

11.57 A liquid mixture of acetone and methanol sits at the bottom of a Stefan tube that is 23.8 cm tall. The top is swept by a flow of pure air. Let species 1 be acetone, species 2 be methanol, and species 3 be air. The temperature is 328.5 K, and the pressure is 745.2 mmHg. The mole fractions just above the liquid are $x_{1,s} = 0.319$ and $x_{2,s} = 0.528$. For these gases, $\mathcal{D}_{12} = 0.0848$ cm^2/s, $\mathcal{D}_{13} = 0.1372$ cm^2/s, and $\mathcal{D}_{23} = 0.1991$ cm^2/s [11.83].

  a. Write the Maxwell-Stefan equations as a matrix o.d.e. for the vector $\mathbf{X}(z) = \{x_1(z), x_2(z)\}$. What is the mole flux of air, N_3? What are the boundary conditions at the liquid surface ($z = 0$) and at the top of the tube ($z = 23.8$ cm)?

  b. Use the software of your choice to solve your equation from part (a) and plot the three concentrations as a function of z. Note that the mole fluxes N_1 and N_2 are not known, so that the equations must be solved iteratively to determine value correspond to the boundary condition at the top of the tube. [*Ans:* $N_1 = 1.782 \times 10^{-7}$ mol/cm^{2}s, $N_2 = 3.126 \times 10^{-7}$ mol/cm^{2}s.]

  c. If part (b) seems too complex, instead use the answers given for part (b) to solve the equations as if the fluxes were known. Does your solution meet the boundary conditions at the top of the tube? (It should.)

  d. Does $J_{air} = 0$ at $z = 0$? Explain.

11.58 A simple model of an ablating heat shield assumes that ablated material is rapidly removed without effecting the flow and that the aerodynamic heat flux, q_{aero}, is constant (Fig. 11.29).
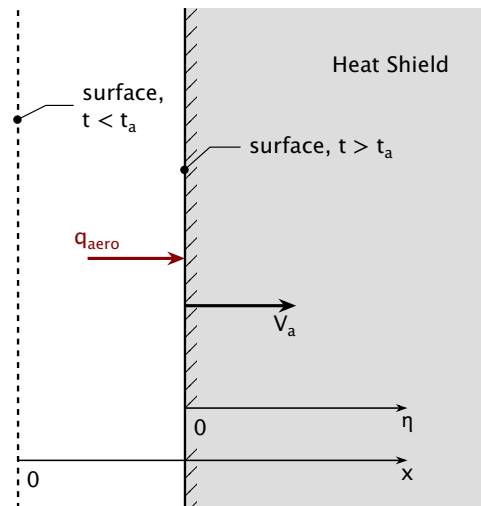
Figure 11.29 Ablating heat shield (Problem 11.58).

a. If the shield is at T_0 when heating starts at $t = 0$, how long until the surface reaches the ablation temperature, T_a, for either melting or sublimation?

b. Once ablation starts, assume the surface recedes at a constant speed, V_a. Find the temperature distribution in the material below the surface for $t > t_a$. *Hint:* Change to a coordinate $\eta = x - V_a(t - t_a)$ attached to the receding surface, and ignore the initial distribution of T.

c. Use an energy balance to determine V_a in terms of material properties and q_{aero}.

d. What combination of material properties best reduces the heat conducted into the heat shield?

References

[11.1] W. C. Reynolds. *Energy, from Nature to Man.* McGraw-Hill Book Company, New York, 1974.

[11.2] A. Makino and C. K. Law. An analysis of the transient combustion and burnout time of carbon particles. *Proc. Combustion Institute,* **32**(2): 2067–2074, 2009. doi: 10.1016/j.proci.2008.07.036.

[11.3] R. H. Hurt and R. E. Mitchell. Unified high-temperature char combustion kinetics for a suite of coals of various rank. *Symposium (International) on Combustion,* **24**(1):1243–1250, 1992. Twenty-Fourth Symposium on Combustion. doi: 10.1016/S0082-0784(06)80146-3.

[11.4] D. R. Poirier and G. H. Geiger. *Transport Phenomena in Materials Processing.* The Minerals, Metals & Materials Society, Warrendale, Pennsylvania, 1994.

[11.5] B. E. Poling, J. M. Prausnitz, and J. P. O'Connell. *The Properties of Gases and Liquids.* McGraw-Hill Book Company, New York, 5th ed., 2000.

[11.6] K. C. Pratt and W. A. Wakeham. The mutual diffusion coefficient of ethanol–water mixtures: determination by a rapid, new method. *Proc. R. Soc. Lond. A*, **336**(1606):393–406, February 1974. doi: 10.1098/rspa.1974.0026.

[11.7] T. R. Marrero and E. A. Mason. Gaseous diffusion coefficients. *J. Phys. Chem. Ref. Data*, **1**(1):3–118, January 1972. doi: 10.1063/1.3253094.

[11.8] S. Chapman and T. G. Cowling. *The Mathematical Theory of Nonuniform Gases.* Cambridge University Press, New York, 2nd ed., 1964.

[11.9] S. Kjelstrup, D. Bedeaux, E. Johannessen, and J. Gross. *Non-equilibrium thermodynamics for engineers.* World Scientific Publishing Co., Singapore, 2nd ed., 2017.

[11.10] P. W. Atkins, J. de Paula, and J. Keeler. *Atkins' Physical Chemistry: Molecular thermodynamics and kinetics.* Oxford University Press, Oxford, 12th ed., 2023.

[11.11] J. M. Prausnitz, R. N. Lichtenthaler, and E. G. de Azevedo. *Molecular Thermodynamics of Fluid-Phase Equilibria.* Prentice-Hall, Englewood Cliffs, N.J., 3rd ed., 1999.

[11.12] R. Sander. Compilation of Henry's law constants (version 5.0.0) for water as solvent. *Atmospheric Chem. Phys.*, **23**(19):10901–12440, 2023. doi: 10.5194/acp-23-10901-2023.

[11.13] L. A. Bromley, D. Singh, P. Ray, S. Sridhar, and S. M. Read. Thermodynamic properties of sea salt solutions. *AIChE J.*, **20**(2):326–335, March 1974. doi: 10.1002/aic.690200218.

[11.14] R. C. Weast, editor. *Handbook of Chemistry and Physics.* Chemical Rubber Co., Cleveland, Ohio, 56th ed., 1976.

[11.15] C. L. Yaws, editor. *The Yaws Handbook of Vapor Pressure.* Gulf Professional Publishing, 2nd ed., 2015. doi: 10.1016/C2014-0-03590-3.

[11.16] D. S. Wilkinson. *Mass Transfer in Solids and Fluids.* Cambridge University Press, Cambridge, 2000.

[11.17] E. Dražević, K. Kovŭutić, and V. Freger. Permeability and selectivity of reverse osmosis membranes: Correlation to swelling revisited. *Water Research*, **49**:444–452, 2014. doi: 10.1016/j.watres.2013.10.029.

[11.18] D. R. Paul. Reformulation of the solution-diffusion theory of reverse osmosis. *J. Membrane Sci.*, **241**(2):371–386, 2004. doi: 10.1016/j.memsci.2004.05.026.

[11.19] J. Crepeau. Josef Stefan and his contributions to heat transfer. In *Proc. ASME 2008 Heat Transfer Conf.*, Jacksonville, FL, August 2008. doi: 10.1115/HT2008-56073. Paper No. HT2008-56073.

[11.20] J. Mitrović. Josef Stefan and his evaporation-diffusion tube—the Stefan diffusion problem. *Chem. Eng. Sci.*, **75**:279–281, 2012. doi: 10.1016/j.ces.2012.03.034.

[11.21] J. Stefan. Versuche über die Verdampfung. *Sitzungsberichte der Mathematisch-Naturwissenschaftlichen Classe der Kaiserlichen Akademie der Wissenschaften*, **68**(1–2):385–423, 1873. url: https://www.digitale-sammlungen.de/en/view/bsb11036802?page=407.

[11.22] W. M. Kays, M. E. Crawford, and B. Weigand. *Convective Heat and Mass Transfer.* McGraw-Hill Book Company, New York, 4th ed., 2005.

[11.23] R.J. Goldstein and H.H. Cho. A review of mass transfer measurements using naphthalene sublimation. *Exptl. Thermal and Fluid Sci.*, **10**(4): 416–434, 1995. doi: 10.1016/0894-1777(94)00071-F.

[11.24] W. K. Lewis. The evaporation of a liquid into a gas. *Mech. Engr.*, **44**(7): 445–446, 1922.

[11.25] T. H. Chilton and A. P. Colburn. Mass transfer (absorption) coefficients: Prediction from data on heat transfer and fluid friction. *Ind. Eng. Chem.*, **26**(11):1183–1187, November 1934. doi: 10.1021/ie50299a012.

[11.26] G. M. Faeth. Current status of droplet and liquid combustion. *Prog. Energy Combust. Sci.*, **3**(4):191–224, 1977. doi: 10.1016/0360-1285(77)90012-0.

[11.27] C. K. Law. Recent advances in droplet vaporization and combustion. *Prog. Energy Combust. Sci.*, **8**(3):171–201, 1982. doi: 10.1016/0360-1285(82)90011-9.

[11.28] J. Finneran, C. P. Garner, and F. Nadal. Deviations from classical droplet evaporation theory. *Proc. Royal Soc. A.*, **477**:20210078, 2021. doi: 10.1098/rspa.2021.0078.

[11.29] A. F. Mills. *Mass Transfer.* Prentice-Hall, Inc., Upper Saddle River, 2001.

[11.30] R. B. Bird, W. E. Stewart, and E. N. Lightfoot. *Transport Phenomena.* John Wiley & Sons, Inc., New York, 2nd ed., 2002.

[11.31] Y. Okamoto and J. H. Lienhard. How RO membrane permeability and other performance factors affect process cost and energy use: A review. *Desalination*, **470**:114064, 2019. doi: 10.1016/j.desal.2019.07.004.

[11.32] A. F. Mills. The use of the diffusion velocity in conservation equations for multicomponent gas mixtures. *Int. J. Heat. Mass Transfer*, **41**(13): 1955–1968, 1998. doi: 10.1016/S0017-9310(97)00306-2.

[11.33] T. Langener, J. von Wolfersdorf, and J. Steelant. Experimental investigations on transpiration cooling for scramjet applications using different coolants. *AIAA J.*, **49**(7):1409–1419, 2011. doi: 10.2514/1.J050698.

[11.34] J. C. Han. Advanced cooling in gas turbines. *J. Heat Transfer*, **140**(11): 113001, July 2018. doi: 10.1115/1.4039644.

[11.35] S. R. Shine and S. Shri Nidhi. Review on film cooling of liquid rocket engines. *Propul. Power Res.*, **7**(1):1–18, 2018. doi: 10.1016/j.jppr.2018.01.004.

[11.36] M. Barzegar Gerdroodbary. Introduction. In M. Barzegar Gerdroodbary, editor, *Aerodynamic Heating in Supersonic and Hypersonic Flows*, Chapter 1, pp. 1–16. Elsevier, Amsterdam, 2023. doi: 10.1016/B978-0-323-91770-4.00001-X.

[11.37] J. Vander Kam and A. Amar. Orion aerosciences and thermal protection system overview. In *Entry, Descent, and Landing Summer Seminar*, July 2021. url: https://www.colorado.edu/irt/hypersonic-vehicles/sites/default/files/attached-files/orion_correct.pdf. Approved for public release NF-1676 20210018325. Video.

[11.38] P. M. Sforza. Thermal protection systems. In P. M. Sforza, editor, *Manned Spacecraft Design Principles*, Chapter 9, pp. 391–452. Butterworth-Heinemann, Boston, 2016. doi: 10.1016/B978-0-12-804425-4.00009-X.

[11.39] A. J. Amar, N. D. Calvert, and B. S. Kirk. Development and verification of the charring ablating thermal protection implicit system solver. In *Proc. 49th AIAA Aerospace Sciences Meeting*, Orlando, FL, January 2011. doi: 10.2514/6.2011-144. AIAA Paper No. 2011-144.

[11.40] H. S. Alpert, D. A. Saunders, M. Mahzari, J. D. Monk, T. R. White, and T. K. West. Inverse estimation and sensitivity analysis of Mars 2020 entry aeroheating environments. *J. Spacecraft and Rockets*, **60**(3):899–911, 2023. doi: 10.2514/1.A35571.

[11.41] A. C. Mueller. Process heat exchangers. In W. M. Rohsenow, J. P. Hartnett, and E. N. Ganić, editors, *Handbook of Heat Transfer Applications*. McGraw-Hill Book Company, New York, 2nd ed., 1985.

[11.42] A. C. Mueller. Discussion of condenser types. In G. F. Hewitt, editor, *Heat Exchanger Design Handbook*. Begell House, New York, 1998. Sect. 3.4.3.

[11.43] A. C. Mueller. Operational problems. In G. F. Hewitt, editor, *Heat Exchanger Design Handbook*. Begell House, New York, 1998. Sect. 3.4.5.

[11.44] J. O. Hirschfelder, C. F. Curtiss, and R. B. Bird. *Molecular Theory of Gases and Liquids*. John Wiley & Sons, Inc., New York, 1954.

[11.45] C. L. Tien and J. H. Lienhard. *Statistical Thermodynamics*. Hemisphere Publishing Corp., Washington, D.C., revised ed., 1978. url: https://www.uh.edu/engines/StatisticalThermodynamics.pdf.

[11.46] J. E. Lennard-Jones. Cohesion. *Proc. Physical Society*, **43**(5):461, September 1931. doi: 10.1088/0959-5309/43/5/301.

[11.47] D. Reichenberg. The indeterminacy of the values of potential parameters as derived from transport and virial coefficients. *AIChE J.*, **19**(4):854–856, 1973. doi: 10.1002/aic.690190429.

[11.48] R. A. Svehla. Estimated viscosities and thermal conductivities of gases at high temperatures. Technical Report NASA-TR-R-132, NASA Lewis Research Center, Cleveland, OH, January 1962. url: http://hdl.handle.net/2060/19630012982.

[11.49] A. B. Weaver and A. A. Alexeenko. Revised variable soft sphere and Lennard-Jones model parameters for eight common gases up to 2200 K. *J. Phys. Chem. Ref. Data*, **44**(2):023103, June 2015. doi: 10.1063/1.4921245.

[11.50] S. T. Lin and H. W. Hsu. Transport collision integral for gases using the Lennard-Jones $(6, n)$ potentials. *J. Chem. Eng. Data*, **14**(3):328–332, July 1969. doi: 10.1021/je60042a010.

[11.51] G. Rutkai, M. Thol, R. Span, and J. Vrabec. How well does the Lennard-Jones potential represent the thermodynamic properties of noble gases? *Molecular Physics*, **115**(9–12):1104–1121, 2017. doi: 10.1080/00268976.2016.1246760.

[11.52] M. Klein and F. J. Smith. Tables of collision integrals for the $(m, 6)$ potential function for 10 values of m. *J. Res. Natl. Bur. Stand. A Phys. Chem.*, **72**(4):359–424, July 1968. doi: 10.6028/jres.072A.033.

[11.53] W. Hogervorst. Diffusion coefficients of noble-gas mixtures between 300 K and 1400 K. *Physica*, **51**(1):59–76, 1971. doi: 10.1016/0031-8914(71)90137-6.

[11.54] J. Millat, J. H. Dymond, and C. A. Nieto de Castro. *Transport Properties of Fluids: Their Correlation, Prediction and Estimation*. Cambridge University Press, Cambridge, UK, 1996.

[11.55] C. Cercignani. *Rarefied Gas Dynamics*. Cambridge University Press, Cambridge, UK, 2000.

[11.56] W. G. Vincenti and C. H. Kruger. *Introduction to Physical Gas Dynamics*. Wiley, New York, NY, 1965. url: https://archive.org/details/introductiontoph00vinc/.

[11.57] W. Sutherland. A dynamical theory of diffusion for non-electrolytes and the molecular mass of albumin. *Phil. Mag., Ser. 6*, **9**(54):781–785, June 1905. doi: 10.1080/14786440509463331.

[11.58] A. Einstein. Über die von der molekularkinetischen Theorie der Wärme geforderte Bewegung von in ruhenden Flüssigkeiten suspendierten Teilchen. *Annalen der Physik*, **322**(8):549–560, 1905. doi: 10.1002/andp.19053220806.

[11.59] A. B. Basset. *A Treatise on Hydrodynamics, with numerous examples*, Vol. II. Deighton, Bell and Co., Cambridge, UK, 1888. url: https://books.google.com/books?id=uMA3AAAAMAAJ.

[11.60] G. G. Stokes. On the effect of internal friction of fluids on the motion of pendulums. *Trans. Cambridge Philosophical Soc.*, **9**(II):8–106, 1856. url: https://hdl.handle.net/2027/mdp.39015012112531.

[11.61] J. C. M. Li and P. Chang. Self-diffusion coefficient and viscosity in liquids. *J. Chem. Phys.*, **23**(3):518–520, March 1955. doi: 10.1063/1.1742022.

[11.62] C. J. King, L. Hsueh, and K.-W. Mao. Liquid phase diffusion of nonelectrolytes at high dilution. *J. Chem. Engr. Data*, **10**(4):348–350, 1965. doi: 10.1021/je60027a014.

[11.63] O. Großmann, D. Bellaire, N. Hayer, F. Jirasek, and H. Hasse. Database for liquid phase diffusion coefficients at infinite dilution at 298 K and matrix completion methods for their prediction. *Digital Discovery*, **1**: 886–897, 2022. doi: 10.1039/D2DD00073C.

[11.64] R. C. Reid, J. M. Prausnitz, and T. K. Sherwood. *The Properties of Gases and Liquids*. McGraw-Hill Book Company, New York, 3rd ed., 1977.

[11.65] S. A. Sanni, C. J. D. Fell, and H. P. Hutchison. Diffusion coefficients and densities for binary organic liquid mixtures. *J. Chem. Eng. Data*, **16**(4): 424–427, 1971. doi: 10.1021/je60051a009.

[11.66] R. A. Robinson and R. H. Stokes. *Electrolyte Solutions*. Dover Publications, Inc., Mineola, NY, 2nd revised ed., 2002.

[11.67] A. Eucken. Über das Wärmeleitvermögen, die spezifische Wärme und die innere Reibung der Gase. *Physikalische Zeitschrift*, **14**:324–332, 1913. url: https://hdl.handle.net/2027/mdp.39015021268936.

[11.68] C. R. Wilke. A viscosity equation for gas mixtures. *J. Chem. Phys.*, **18**(4): 517–519, April 1950. doi: 10.1063/1.1747673.

[11.69] E. A. Mason and S. C. Saxena. Approximate formula for the thermal conductivity of gas mixtures. *Phys. Fluids*, **1**(5):361–369, September 1958. doi: 10.1063/1.1724352.

[11.70] R. Taylor and R. Krishna. *Multicomponent Mass Transfer*. John Wiley & Sons, Inc., New York, 1993.

[11.71] J. B. Duncan and H. L. Toor. An experimental study of three component gas diffusion. *AIChE Journal*, **8**(1):38–41, March 1962. doi: 10.1002/aic.690080112.

[11.72] J. Wambui Mutoru and Abbas Firoozabadi. Form of multicomponent Fickian diffusion coefficients matrix. *J. Chemical Thermodynamics*, **43**(8):1192–1203, 2011. The supplementary data include 888 experimental data sets. doi: 10.1016/j.jct.2011.03.003.

[11.73] J. C. Maxwell. On the dynamical theory of gases. *Philosophical Transactions of the Royal Society of London*, **157**:49–88, 1867. doi: 10.1098/rstl.1867.0004.

[11.74] J. Stefan. Über das Gleichgewicht und die Bewegung, insbesondere die Diffusion von Gasgemengen. *Sitzungsberichte der Mathematisch-Naturwissenschaftlichen Classe der Kaiserlichen Akademie der Wissenschaften*, **63**(1–5):63–124, 1871. url: https://www.digitale-sammlungen.de/view/bsb10812588?page=81.

[11.75] L. D. Landau and E. M. Lifshitz. *Mechanics*. Pergamon Press, Oxford, 1960. Chapter 4.

[11.76] S. I. Sandler. *Chemical, Biochemical, and Engineering Thermodynamics*. Wiley, Hoboken, NJ, 5th ed., 2017.

[11.77] R. Krishna and J. A. Wesselingh. The Maxwell-Stefan approach to mass transfer. *Chemical Engineering Science*, **52**(6):861–911, 1997. doi: 10.1016/S0009-2509(96)00458-7.

[11.78] G. Leclercq, L. Leclercq, L.M. Bouleau, S. Pietrzyk, and R. Maurel. Hydrogenolysis of saturated hydrocarbons: IV. Kinetics of the hydrogenolysis of ethane, propane, butane, and isobutane over nickel. *J. Catalysis*, **88**(1):8–17, 1984. doi: 10.1016/0021-9517(84)90044-7.

[11.79] J. I. Goldstein and A. E. Moren. Diffusion modeling of the carburization process. *Metallurgical Trans. A*, **9**:1515–1525, 1978. doi: 10.1007/BF02661934.

[11.80] American Society of Heating, Refrigerating, and Air-Conditioning Engineers. *2017 ASHRAE Handbook—Fundamentals (SI Edition)*. Atlanta, 2017. Chapter 9. See Table 6.

[11.81] T. Langener, J. von Wolfersdorf, and J. Steelant. Experimental investigations on transpiration cooling for scramjet applications using different coolants. *AIAA Journal*, **49**(7):1409–1419, April 2011. doi: 10.2514/1.J050698.

[11.82] J. B. Will, N. P. Kruyt, and C. H. Venner. An experimental study of forced convective heat transfer from smooth, solid spheres. *Int. J. Heat Mass Transfer*, **109**:1059–1067, June 2017. doi: 10.1016/j.ijheatmasstransfer.2017.02.018.

[11.83] R. Carty and T. Schrodt. Concentration profiles in ternary gaseous diffusion. *Ind. Eng. Chem. Fund.*, **14**(3):276–278, August 1975. doi: 10.1021/i160055a025.

PART VI

APPENDICES

A. Some thermophysical properties of selected materials

A property is that which, once disjoined
And severed from a thing, undoes its nature:
As Weight to a rock,
Heat to a fire,
Flow to the wide waters,
Touch to corporeal things,
Intangibility to the viewless void.

de Rerum Natura, **Lucretius, 50 BCE**

This appendix includes eight tables of thermophysical property data and other physical constants, as listed below.

A *primary source* of thermophysical properties is a document in original measurements of data are first reported. A *secondary source* generally means a document, based on primary sources, that presents other peoples' data and does so critically. The data presented in these tables are neither

primary or even secondary sources, since we have created these tables from a variety of secondary (and even tertiary) sources.

We have, however, arrived at these numbers with great care. We attempted to cross-check other data against different sources, which occasionally led to contradictory values. Such contradictions are usually the result of differences among the experimental samples that are reported or of differences in the accuracy of experiments themselves. We resolved such differences by judging the source, by reducing the number of significant figures to accommodate the conflict, or by omitting those data from the tables. We attempt to report no more decimal places than are accurate. The resulting numbers will suffice for most calculations. However, the reader who needs high accuracy should be sure of the physical constitution of the material and should then consult the most recent secondary or primary sources.

The format of these tables is quite close to that established a half-century ago by R. M. Drake, Jr., in his excellent appendix on thermophysical data [A.1]. Today, most of Drake's values have been superseded by more accurate measurements. One secondary source from which many of the data for solids were obtained is the Purdue University series *Thermophysical Properties of Matter* [A.2]. The Purdue series is the result of an enormous property-gathering effort carried out under the direction of Y. S. Touloukian and several coworkers. Volumes in the series are dated from 1970 onward, and addenda were issued throughout the following decade. NIST, IUPAC, and other agencies have since developed standard reference data and correlations for many fluid substances, some of which are contained in [A.3–A.11]. These correlations are based on critical evaluation of multiple experiments, and they are structured to maintain consistency amongst thermodynamic properties. We have taken most of our data for fluids from those publications. A third secondary source that we used is the G. E. *Heat Transfer Data Book* [A.12].

Numbers for solids that did not come directly from standard reference correlations, [A.2], or [A.3] were obtained from a variety of manufacturers' tables, handbooks, and other technical literature. While we have not documented all these diverse sources and the various compromises that were made in quoting them, the specific citations that follow account for the bulk of the data in these tables.

Table A.1 gives the density, specific heat, thermal conductivity, and thermal diffusivity for various metallic solids. These values were obtained from volumes 1 and 4 of [A.2] or from [A.3] whenever it was possible to find them there. Most thermal conductivity values in the table have been

rounded off to two significant figures. The reason is that k is sensitive to very minor variations in physical structure that cannot be detailed fully here. Notice, for example, the significant differences between pure aluminum and 99% pure aluminum, and the still larger differences for alloyed aluminum. Additional information on the characteristics and use of these metals can be found in the ASM *Metals Handbook* [A.13].

The effect of temperature on thermal conductivity is shown for most of the metals in Table A.1. The specific heat capacity is shown only at 20°C. For most materials, the heat capacity is much lower at cryogenic temperatures. For example, c_p for aluminum, iron, molybdenum, and titanium decreases by two orders of magnitude as temperature decreases from 200 K to 20 K. On the other hand, for most of these metals, c_p changes more gradually for temperatures between 300 K and 800 K, varying by tens of percent to a factor of two. At still higher temperatures, some of these metals (iron and titanium) show substantial spikes in c_p. These are associated with solid-to-solid phase transitions.

Table A.2 gives the same properties as Table A.1 (where they are available) but for nonmetallic substances. Volumes 2 and 5 of [A.2] and also [A.3] provided many of the data here, and they revealed even greater variations in k than the metallic data did. For the various sands reported, k varied by a factor of 500, and for the various graphites by a factor of 50, for example. The sensitivity of k to small variations in the packing of fibrous materials or to the water content of hygroscopic materials forced us to restrict some of the k values to a single significant figure. The effect of water content is illustrated by the data for wet and dry soils. Some data for building materials are from the large compilation in [A.14].

The data for polymers come mainly from their manufacturers' data and are substantially less reliable than, say, those given in Table A.1 for metals. The values quoted are mainly those for room temperature. In processing operations, however, most of these materials are taken to temperatures of several hundred degrees Celsius at which they flow more easily. The specific heat capacity may double from room temperature to such temperatures. These polymers are also produced in a variety of modified forms; and in many applications they may be loaded with significant portions of reinforcing fillers (e.g., 10 to 40% by weight glass fiber). The fillers, in particular, can have a significant effect on thermal properties.

Table A.3 gives ρ, c_p, k, α, ν, Pr, and β for several liquids. Data for water are from [A.15] and [A.16]; they are in agreement with IAPWS recommendations through 2007. Data for ammonia are from [A.4, A.5, A.17], data for carbon dioxide are from [A.6–A.8], data for and methanol

are from [A.9, A.10, A.18], data for nitrogen are from [A.19, A.20], and data for oxygen are from [A.20, A.21]. Data for HFC-134a and HCFC-22 are from [A.22] and [A.23]. Data for CFC-12 and D_2O are from [A.11]. For these liquids, ρ has uncertainties less than 0.2%, c_p has uncertainties of 1–2%, while μ and k have typical uncertainties of 2–5%. Uncertainties may be higher near the critical point. Data for lead follow [A.24], with uncertainty in ρ of 1%, in c_p and μ of 5%, and in k of about 10%. Data for mercury follow [A.3] and [A.25]. Data for NaK follow [A.26]; uncertainties are similar to those for lead. Olive oil data are from [A.27–A.29]. Data for other substances came from [A.2], [A.25], or other sources.

The latent heats of vaporization in Table A.4 are primarily from NIST reference data. Table A.5 provides thermophysical data for saturated vapors. The sources are those already listed for saturated liquids. The uncertainties are as described for gases in the next paragraph.

Table A.6 gives thermophysical properties for gases at 1 atmosphere pressure: air data are from [A.20, A.30]; argon data are from [A.31–A.33]; ammonia data were taken from [A.4, A.5, A.17]; carbon dioxide properties are from [A.6–A.8]; carbon monoxide properties are from [A.23]; helium data are from [A.34–A.36]; hydrogen data are from [A.37–A.39]; nitrogen data came from [A.19, A.20]; oxygen data are from [A.20, A.21]; and water data were taken from [A.15] and [A.16] (in agreement with IAPWS recommendations through 2007). Uncertainties in these data vary among the gases; typically, ρ has uncertainties of 0.02–0.2%, c_p has uncertainties of 0.2–2%, μ has uncertainties of 0.3–3%, and k has uncertainties of 2–5%. The uncertainties are generally lower in the dilute gas region and higher near the saturation line or the critical point. The values for low temperature helium have somewhat larger uncertainties.

Table A.7 lists values for some fundamental physical constants, as given in [A.40] and its successors. Table A.8 points out physical data that are listed in other parts of this book.

References

[A.1] E. R. G. Eckert and R. M. Drake, Jr. *Analysis of Heat and Mass Transfer.* McGraw-Hill Book Company, New York, 1972.

[A.2] Y. S. Touloukian. *Thermophysical Properties of Matter.* vols. 1–6, 10, and 11. Purdue University, West Lafayette, IN, 1970 to 1975.

[A.3] C. Y. Ho, R. W. Powell, and P. E. Liley. Thermal conductivity of the elements: A comprehensive review. *J. Phys. Chem. Ref. Data*, **3**, 1974. Published in book format as Supplement No. 1 to the cited volume.

[A.4] S. A. Monogenidou, M. J. Assael, and M. L. Huber. Reference correlation for the viscosity of ammonia from the triple point to 725 K and up to 50 MPa. *J. Phys. Chem. Ref. Data*, **47**(2):023102, June 2018. doi: 10.1063/1.5036724.

[A.5] S. A. Monogenidou, M. J. Assael, and M. L. Huber. Reference correlations for thermal conductivity of ammonia from the triple point to 680 K and up to 80 MPa. *J. Phys. Chem. Ref. Data*, **47**(4):043101, October 2018. doi: 10.1063/1.5053087.

[A.6] R. Span and W. Wagner. A new equation of state for carbon dioxide covering the fluid region from the triple-point temperature to 1100 K at pressures up to 800 MPa. *J. Phys. Chem. Ref. Data*, **25**(6):1509–1596, November 1996. doi: 10.1063/1.555991.

[A.7] A. Laesecke and C. D. Muzny. Reference correlation for the viscosity of carbon dioxide. *J. Phys. Chem. Ref. Data*, **46**(1):013107, March 2017. doi: 10.1063/1.4977429.

[A.8] M. L. Huber, E. A. Sykioti, M. J. Assael, and R. A. Perkins. Reference correlation of the thermal conductivity of carbon dioxide from the triple point to 1100 K and up to 200 MPa. *J. Phys. Chem. Ref. Data*, **45**(1): 013102, February 2016. doi: 10.1063/1.4940892.

[A.9] E. A. Sykioti, M. J. Assael, M. L. Huber, and R. A. Perkins. Reference correlation of the thermal conductivity of methanol from the triple point to 660 K and up to 245 MPa. *J. Phys. Chem. Ref. Data*, **42**(4):043101, November 2013. doi: 10.1063/1.4829449.

[A.10] H. W. Xiang, A. Laesecke, and M. L. Huber. A new reference correlation for the viscosity of methanol. *J. Phys. Chem. Ref. Data*, **35**(4):1597–1620, November 2006. doi: 10.1063/1.2360605.

[A.11] E. W. Lemmon, I. H. Bell, M. L. Huber, and M. O. McLinden. *NIST Standard Reference Database 23: Reference Fluid Thermodynamic and Transport Properties-REFPROP, Version 10.0*. National Institute of Standards and Technology, Gaithersburg, MD, 2018. doi: 10.18434/T4JS3C. url: https://www.nist.gov/srd/refprop. Properties based upon the most accurate standard reference formulations then available.

[A.12] R. H. Norris, F. F. Buckland, N. D. Fitzroy, R. H. Roecker, and D. A. Kaminski, editors. *Heat Transfer Data Book*. General Electric Co., Schenectady, NY, 1977.

[A.13] ASM Handbook Committee. *Metals Handbook*. ASM, International, Materials Park, OH, 10th ed., 1990.

[A.14] American Society of Heating, Refrigerating, and Air-Conditioning Engineers. *2017 ASHRAE Handbook—Fundamentals (SI Edition)*. Atlanta, 2017. Chapter 26.

[A.15] C.A. Meyer, R. B. McClintock, G. J. Silvestri, and R.C. Spencer. *ASME Steam Tables*. American Society of Mechanical Engineers, New York, NY, 6th ed., 1993.

[A.16] A. H. Harvey, A. P. Peskin, and S. A. Klein. *NIST/ASME Steam Properties*. National Institute of Standards and Technology, Gaithersburg, MD, March 2000. NIST Standard Reference Database 10, Version 2.2.

[A.17] K. Gao, J. Wu, I. H. Bell, A. H. Harvey, and E. W. Lemmon. A reference equation of state with an associating term for the thermodynamic properties of ammonia. *J. Phys. Chem. Ref. Data*, **52**(1):013102, February 2023. Tables based on 2020 prepublication version of this EoS. doi: 10.1063/5.0128269.

[A.18] K. M. deReuck and R. J. B. Craven. *Methanol: International Thermodynamic Tables of the Fluid State-12*. Blackwell Scientific Publications, Oxford, 1993. Sponsored by the International Union of Pure and Applied Chemistry (IUPAC).

[A.19] R. Span, E. W. Lemmon, R. T. Jacobsen, W. Wagner, and A. Yokozeki. A reference equation of state for the thermodynamic properties of nitrogen for temperatures from 63.151 to 1000 K and pressures to 2200 MPa. *J. Phys. Chem. Ref. Data*, **29**(6):1361–1433, November 2000. doi: 10.1063/1.1349047.

[A.20] E. W. Lemmon and R. T. Jacobsen. Viscosity and thermal conductivity equations for nitrogen, oxygen, argon, and air. *Int. J. Thermophys.*, **25**(6):21–69, January 2004. doi: 10.1023/B:IJOT.0000022327.04529.f37.

[A.21] R. B. Stewart, R. T. Jacobsen, and W. Wagner. Thermodynamic properties of oxygen from the triple point to 300 K with pressures to 80 MPa. *J. Phys. Chem. Ref. Data*, **20**(5):917–1021, September 1991. doi: 10.1063/1.555897.

[A.22] R. Tillner-Roth and H. D. Baehr. An international standard formulation of the thermodynamic properties of 1,1,1,2-tetrafluoroethane (HFC-134a) covering temperatures from 170 K to 455 K at pressures up to 70 MPa. *J. Phys. Chem. Ref. Data*, **23**:657–729, September 1994. doi: 10.1063/1.555958.

[A.23] E. W. Lemmon, A. P. Peskin, M. O. McLinden, and D. G. Friend. *Thermodynamic and Transport Properties of Pure Fluids — NIST Pure Fluids*. National Institute of Standards and Technology, Gaithersburg, MD, September 2000. NIST Standard Reference Database No. 12, Version 5.

[A.24] V. Sobolev. Database of thermophysical properties of liquid metal coolants for GEN-IV: sodium, lead, lead-bismuth eutectic. Technical Report CEN-BLG-1069, Belgian Nuclear Research Centre, Mol, Belgium, December 2011.

[A.25] N. B. Vargaftik, Y. K. Vinogradov, and V. S. Yargin. *Handbook of Physical Properties of Liquids and Gases.* Begell House, New York, 3rd ed., 1996.

[A.26] H. J. Bomelburg and C. R. F. Smith. Physical properties. In O. J. Foust, editor, *Sodium-NaK Engineering Handbook*, Vol. 1, Chapter 1. Gordon and Breach, New York, 1972.

[A.27] D. S. Viswanath and G. Natarajan. *Data Book on the Viscosity of Liquids.* Hemisphere Publishing Corp., New York, 1989.

[A.28] D. Dadarlat, J. Gibkes, D. Bicanic, and A. Pasca. Photopyroelectric (PPE) measurement of thermal parameters in food products. *J. Food Engr.*, **30**: 155–162, 1996. doi: 10.1016/S0260-8774(96)00017-9.

[A.29] H. Abramovic and C. Klofutar. The temperature dependence of dynamic viscosity for some vegetable oils. *Acta Chim. Slov.*, **45**(1):69–77, 1998.

[A.30] E. W. Lemmon, R. T. Jacobsen, S. G. Penoncello, and D. G. Friend. Thermodynamic properties of air and mixtures of nitrogen, argon, and oxygen from 60 to 2000 K at pressures to 2000 MPa. *J. Phys. Chem. Ref. Data*, **29**(3):331–385, May 2000. doi: 10.1063/1.1285884.

[A.31] Ch. Tegeler, R. Span, and W. Wagner. A new equation of state for argon covering the fluid region for temperatures from the melting line to 700 K at pressures up to 1000 MPa. *J. Phys. Chem. Ref. Data*, **28**(3):779–850, May 1999. doi: 10.1063/1.556037.

[A.32] B. A. Younglove and H. J. M. Hanley. The viscosity and thermal conductivity coefficients of gaseous and liquid argon. *J. Phys. Chem. Ref. Data*, **15**(4):1323–1337, October 1986. doi: 10.1063/1.555765.

[A.33] R. A. Perkins, D. G. Friend, H. M. Roder, and C. A. Nieto de Castro. Thermal conductivity surface of argon: A fresh analysis. *Int. J. Thermophys.*, **12** (6):965–984, November 1991. doi: 10.1007/BF00503513.

[A.34] R. D. McCarty and V. D. Arp. A new wide range equation of state for helium. In R. W. Fast, editor, *Adv. Cryo. Eng.*, Vol. 35, pp. 1465–1475. 1990. doi: 10.1007/978-1-4613-0639-9_174.

[A.35] E. Bich, J. Millat, and E. Vogel. The viscosity and thermal conductivity of pure monatomic gases from their normal boiling point up to 5000 K in the limit of zero density and at 0.101325 MPa. *J. Phys. Chem. Ref. Data*, **19**(6):1289–1305, November 1990. doi: 10.1063/1.555846.

[A.36] V. D. Arp, R. D. McCarty, and D. G. Friend. Thermophysical properties of helium-4 from 0.8 to 1500 K with pressures to 2000 MPa. Technical Note 1334, National Institute of Standards and Technology, Boulder, CO, 1998.

[A.37] J. W. Leachman, R. T. Jacobsen, S. G. Penoncello, and E. W. Lemmon. Fundamental equations of state for parahydrogen, normal hydrogen, and orthohydrogen. *J. Phys. Chem. Ref. Data*, **38**(3):721–748, September 2009. doi: 10.1063/1.3160306.

[A.38] C. D. Muzny, M. L. Huber, and A. F. Kazakov. Correlation for the viscosity of normal hydrogen obtained from symbolic regression. *J. Chem. Eng. Data*, **58**(4):969–979, March 2013. doi: 10.1021/je301273j.

[A.39] M. J. Assael, J.-A. M. Assael, M. L. Huber, R. A. Perkins, and Y. Takata. Correlation of the thermal conductivity of normal and parahydrogen from the triple point to 1000 K and up to 100 MPa. *J. Phys. Chem. Ref. Data*, **40**(3):033101, July 2011. doi: 10.1063/1.3606499.

[A.40] P. J. Mohr, D. B. Newell, and B. N. Taylor. CODATA recommended values of the fundamental physical constants: 2014. *J. Phys. Chem. Ref. Data*, **45**(4):043102, 2016. doi: 10.1063/1.4954402. url: https://physics.nist.gov/cuu/Constants/.

[A.41] W. Wagner and A. Pruß. The iapws formulation 1995 for the thermodynamic properties of ordinary water substance for general and scientific use. *J. Phys. Chem. Ref. Data*, **31**(2):387–535, June 2002. doi: 10.1063/1.1461829.

Table A.1 Properties of metallic solids

Metal	Properties at 20°C — ρ (kg/m³)	c_p (J/kg·K)	k (W/m·K)	α $(10^{-5}\,\mathrm{m^2/s})$	Thermal Conductivity, k (W/m·K) −170°C	−100°C	0°C	100°C	200°C	300°C	400°C	600°C	800°C	1000°C
Aluminums														
Pure	2,707	905	237	9.61	302	242	236	240	238	234	228	215	≈95 (liq.)	
99% pure			211		220	206	209							
Duralumin (≈4% Cu, 0.5% Mg)	2,787	883	164	6.66		126	164	182	194					
Alloy 6061-T6	2,700	896	167	6.90			166	172	177	180				
Alloy 7075-T6	2,800	841	130	5.52	76	100	121	137	172	177				
Chromium	7,190	453	90	2.77	158	120	95	88	85	82	77	69	64	62
Cupreous metals														
Pure Copper	8,954	384	398	11.57	483	420	401	391	389	384	378	366	352	336
DS-C15715*	8,900	≈384	365	≈10.7			367	355	345	335	320			
Beryllium copper (2.2% Be)	8,250	420	103	2.97				117						
Brass (30% Zn)	8,522	385	109	3.32	73	89	106	133	143	146	147			
Bronze (25% Sn)§	8,666	343	26	0.86										
Constantan (40% Ni)	8,922	410	22	0.61	17	19	22	26	35					
German silver (15% Ni, 22% Zn)	8,618	394	25	0.73	18	19	24	31	40	45	48			
Gold	19,320	129	318	12.76	327	324	319	313	306	299	293	279	264	249
Ferrous metals														
Pure iron	7,897	447	80	2.26	132	98	84	72	63	56	50	39	30	29.5
Cast iron (4% C)	7,272	420	52	1.70										
Steels (C ≤ 1.5%)‖														
AISI 1010††	7,830	434	64	1.88	70		65	61	55	50	45	36	29	
0.5% carbon	7,833	465	54	1.47			55	52	48	45	42	35	31	29
1.0% carbon	7,801	473	43	1.17			43	43	42	40	36	33	29	28
1.5% carbon	7,753	486	36	0.97			36	36	36	35	33	31	28	28

* Dispersion-strengthened copper (0.3% Al₂O₃ by weight); strength comparable to stainless steel.
§ Conductivity data for this and other bronzes vary by a factor of about two.
‖ k and α for carbon steels can vary greatly, owing to trace elements.
†† 0.1% C, 0.42% Mn, 0.28% Si; hot-rolled.

Table A.1 Properties of metallic solids...*continued.*

Metal	Properties at 20°C ρ (kg/m³)	c_p (J/kg·K)	k (W/m·K)	α (10⁻⁵ m²/s)	Thermal Conductivity, k (W/m·K) −170°C	−100°C	0°C	100°C	200°C	300°C	400°C	600°C	800°C	1000°C
Stainless steels:														
AISI 304	8,000	400	13.8	0.4				15	17⁺	19⁻	21	25		
AISI 316	8,000	460	13.5	0.37		12		15	16	17⁺	19⁻	21⁺	24	26⁺
AISI 347	8,000	420	15	0.44		13		16⁺	18⁻	19	20	23	26	28
AISI 410	7,700	460	25	0.7				25⁺	26	27	27⁺	28⁺		
AISI 446	7,500	460						18	19⁻	19	20	21	22	
Lead	11,373	130	35	2.34	40	37	36	34	33	32	17 (liq.)	20 (liq.)		
Magnesium	1,746	1023	156	8.76	169	160	157	154	152	150	148	145	89 (liq.)	
Mercury†					32	30	7.8 (liq.)							
Molybdenum	10,220	251	138	5.38	175	146	139	135	131	127	123	116	109	103
Nickels														
Pure	8,906	445	91	2.30	156	114	94	83	74	67	64	69	73	78
Alumel§§	8,600	532						30	32	35	38			
Chromel P (10% Cr)	8,730	428						19	21	23	25			
Inconel X-750¶	8,510	442	11.6	0.23	8.8	10.6	11.3	13.0	14.7	16.0	18.3	21.8	25.3	29
Nichromeᵖ	8,250	448		0.34				13	15	16	18⁻			
Nichrome V**	8,410	466	10	0.26				11	13	15	17	20	24	
Platinum	21,450	133	71	2.50	78	73	72	72	72	73	74	77	80	84
Silicon‡	2,330	705.5	153	9.31	856	342	168	112	82	66	54	38	29	25
Silver														
99.99⁺% pure	10,524	236	427	17.19	449	431	428	422	417	409	401	386	370	176
99.9% pure	10,524	236	411	16.55		422	405		373	367	364			(liq.)
Tin†	7,304	228	67	4.17	85	76	68	63	60	32 (liq.)	34 (liq.)	38 (liq.)		
Titanium														
Pure†	4,540	523	22	0.93	31	26	22	21	20	20	19	21	21	22
Ti-6%Al-4%V	4,430	580	7.1	0.28				7.8	8.8	10	12⁻			
Tungsten	19,350	133	178	6.92	235	223	182	166	153	141	134	125	122	114
Uranium	18,700	116	28	1.29	22	24	27	29	31	33	36	41	46	
Zinc	7,144	388	121	4.37	124	122	122	117	110	106	100	60 (liq.)		

† Polycrystalline form. §§ 2% Al, 2% Mn, 1% Si ¶ 73% Ni, 15% Cr, 6.75% Fe, 2.5% Ti, 0.85% Nb, 0.8% Al, 0.7% Mn, 0.3% Si. ᵖ 23% Fe, 16% Cr ** 20% Cr, 1.4% Si
‡ Single crystal form.

Table A.2 Properties of nonmetallic solids

Material	Temperature Range (°C)	Density ρ (kg/m^3)	Specific Heat c_p (J/kg·K)	Thermal Conductivity k (W/m·K)	Thermal Diffusivity α (m^2/s)
Aluminum oxide (Al$_2$O$_3$)					
plasma sprayed coating	20			≈4	
HVOF sprayed coating	20			≈14	
polycrystalline (98% dense)	0		725	40	
	27	3900	779	36	1.19×10^{-5}
	127		940	26	
	577		1200	10	
	1077		1270	6.1	
	1577		1350	5.6	
single crystal (sapphire)	0		725	52	
	27	3980	779	46	1.48×10^{-5}
	127		940	32	
	577		1180	13	
Asbestos					
Cement board	20	1920	1000	0.6	
Fiber, densely packed	20	1930		0.8	
Fiber, loosely packed	20	980		0.14	
Asphalt	20–25			0.75	
Beef (lean, fresh)	25	1070	3400	0.48	1.35×10^{-7}
Brick					
B & W, K-28 insulating	300			0.3	
	1000			0.4	
Cement	10	720		0.34	
Common	0–1000			0.7	
Chrome	100			1.9	
Facing	20			1.3	
Fired clay	24	1920	800	0.81–0.98	
Firebrick, insulating	300	2000	960	0.1	5.4×10^{-8}
	1000			0.2	
Butter	20	920	2520	0.22	9.5×10^{-6}
Carbon					
Diamond (type IIb)	20	≈3250	510	1350.0	8.1×10^{-4}
Graphites	20	≈1730	≈710	k varies with structure	
AGOT graphite					
⊥ to extrusion axis	0			141	
	27	1700	800	138	
	500		1600	59.1	
∥ to extrusion axis	0			230	
	27	1700	800	220	
	500		1600	93.6	

Table A.2...*continued.*

Material	Temperature Range (°C)	Density ρ (kg/m^3)	Specific Heat c_p (J/kg·K)	Thermal Conductivity k (W/m·K)	Thermal Diffusivity α (m^2/s)
Pyrolytic graphite					
$\perp$ to layer planes	0			10.6	
	27	2200	710	9.5	
	227			5.4	
	1027			1.9	
$\parallel$ to layer planes	0			2230	
	27	2200	710	2000	
	227			1130	
	1027			400	
Cardboard	0–20	790		0.14	
Cement, Portland	34	2010		0.7	
Clay					
Fireclay	500–750			1.0	
Sandy clay	20	1780		0.9	
Coal					
Anthracite	900	≈1500		≈0.2	
Brown coal	900			≈0.1	
Bituminous in situ		≈1300		0.5–0.7	3 to 4 × 10^{-7}
Concrete					
Limestone gravel	20	1850		0.6	
Sand : cement (3 : 1)	230			0.1	
Sand and gravel	24	2400		1.4–2.9	
	24	2240	900	1.3–2.6	
	24	2080		1.0–1.9	
Corkboard (medium ρ)	30	170		0.04	
Egg white	20		3400	0.56	1.37 × 10^{-7}
Glass					
Lead	44	3040		1.2	
Pyrex (borosilicate)	60–100	2210	753	1.3	7.8 × 10^{-7}
Soda-lime	−73		610	0.9	
	20	2480	750	1.1	
	93		866	1.3	
Glass-fiber insulation batt	24	7.5–8.2	800	0.046–0.048	
	24	13–14	800	0.037–0.039	
Glass-fiber pipe insulation	24	56–88		0.034	
	93			0.040–0.047	
	204			0.063–0.068	
Gypsum wall board	24	640	1150	0.16	
Ice	0	917	2100	2.215	1.15 × 10^{-6}
Ivory	80			0.5	
Lunar surface dust (high vacuum)	250	1500±300	≈600	≈0.0006	≈7 × 10^{-10}

Table A.2...*continued.*

Material	Temperature Range (°C)	Density ρ (kg/m^3)	Specific Heat c_p (J/kg·K)	Thermal Conductivity k (W/m·K)	Thermal Diffusivity α (m^2/s)
Magnesia, 85% (insulation)	38	≈ 200		0.067	
	93			0.071	
	150			0.074	
	204			0.08	
Magnesium oxide					
polycrystalline (98% dense)	27	3500	900	48	1.5×10^{-5}
single crystal	27	3580	900	60	1.9×10^{-5}
Polymers					
acetyl (POM, Delrin)	−18-100	1420	1470	0.30-0.37	
acrylic (PMMA, Plexiglas)	25	1180		0.17	
acrylonitrile butadiene styrene (ABS)		1060		0.14-0.31	
epoxy, bisphenol A (EP), cast	24-55	1200		≈ 0.22	
epoxy/glass-cloth laminate (G-10, FR4)		1800	≈ 1600	0.29	$\approx 1.0 \times 10^{-7}$
polyamide (PA)					
nylon 6,6	0-49	1120	1470	0.25	1.5×10^{-7}
nylon 6,12	0-49	1060	1680	0.22	1.2×10^{-7}
polycarbonate (PC, Lexan)	23	1200	1250	0.29	1.9×10^{-7}
polyethylene (PE)					
HDPE		960	2260	0.33	1.5×10^{-7}
LDPE		920	≈ 2100	0.33	$\approx 1.7 \times 10^{-7}$
polyimide (PI)		1430	1130	0.35	2.2×10^{-7}
polypropylene (PP)		905	1900	0.17-0.20	
polystyrene (PS)		1040	≈ 1350	0.10-0.16	
expanded (EPS)	4-55	13-30	1500	0.035	
extruded board	24	22-58	1500	0.026-0.030	
polytetrafluoroethylene (PTFE, Teflon)	20	2200	1050	0.25	$\approx 1.1 \times 10^{-7}$
polyvinylchloride (PVC)	25	1600		0.16	
Rock wool	24	32-37	800	0.036-0.037	
	24	45	800	0.033-0.035	
Rubber (hard)	0	1200	2010	0.15	6.2×10^{-8}
Silica aerogel	0	140		0.024	
	120	136		0.022	
Silo-cel (diatomaceous earth)	0	320		0.061	

Table A.2...*continued.*

Material	Temperature Range (°C)	Density ρ (kg/m³)	Specific Heat c_p (J/kg·K)	Thermal Conductivity k (W/m·K)	Thermal Diffusivity α (m²/s)
Silicon dioxide					
Fused silica glass	0		703	1.33	
	27	2200	745	1.38	8.4×10^{-7}
	227		988	1.62	
Single crystal (quartz)					
$\perp$ to c-axis	0		709	6.84	
	27	2640	743	6.21	
	227		989	3.88	
$\parallel$ to c-axis	0		709	11.6	
	27	2640	743	10.8	
	227		989	6.00	
Soil (mineral)					
Dry	15	1500	1840	1.	4×10^{-7}
Wet	15	1930		2.	
Soil (k dry to wet, by type)					
Clays				1.1–1.6	
Loams				0.95–2.2	
Sands				0.78–2.2	
Silts				1.6–2.2	
Stone					
Granite (NTS)	20	≈2640	≈820	1.6	≈7.4×10^{-7}
Limestone (Indiana)	100	2300	≈900	1.1	≈5.3×10^{-7}
Sandstone (Berea)	25			≈3	
Slate	100			1.5	
Wood (perpendicular to grain)					
Ash	15	740		0.15–0.3	
Balsa	15	100		0.05	
Cedar	15	480		0.11	
Fir	15	600	2720	0.12	7.4×10^{-8}
Mahogany	20	700		0.16	
Oak	20	600	2390	0.1–0.4	
Particle board (medium ρ)	24	800	1300	0.14	1.3×10^{-7}
Pitch pine	20	450		0.14	
Plywood, Douglas fir	24	550	1200	0.12	1.8×10^{-7}
Sawdust (dry)	17	128		0.05	
Sawdust (dry)	17	224		0.07	
Spruce	20	410		0.11	
Wool (sheep)	20	145		0.05	

Table A.3 Thermophysical properties of saturated liquids

Temperature								
K	°C	ρ (kg/m^3)	c_p (J/kg·K)	k (W/m·K)	α (m^2/s)	ν (m^2/s)	Pr	β (K^{-1})
				Ammonia (R717)				
200	−73	728.7	4318	0.610	1.94×10^{-7}	7.082×10^{-7}	3.65	0.00158
220	−53	705.5	4390	0.600	1.94	4.923	2.54	0.00167
240	−33	681.4	4466	0.578	1.90	3.684	1.94	0.00181
260	−13	656.1	4546	0.547	1.83	2.927	1.60	0.00200
280	7	629.2	4649	0.509	1.74	2.432	1.40	0.00224
300	27	600.2	4796	0.466	1.62	2.083	1.29	0.00258
320	47	568.3	5023	0.420	1.47	1.816	1.23	0.00307
340	67	532.5	5392	0.374	1.30	1.597	1.23	0.00387
360	87	490.3	6082	0.327	1.10	1.407	1.28	0.00540
380	107	436.3	7838	0.280	0.818	1.237	1.51	0.00951
400	127	344.0	22389	0.238	0.309	1.085	3.51	0.0481
				Carbon dioxide (R744)				
220	−53	1166	1962	0.173	7.56×10^{-8}	2.052×10^{-7}	2.72	0.00317
230	−43	1129	1997	0.161	7.12	1.797	2.52	0.00350
240	−33	1089	2051	0.148	6.65	1.584	2.38	0.00392
250	−23	1046	2132	0.137	6.12	1.405	2.29	0.00451
260	−13	999	2255	0.125	5.54	1.252	2.26	0.00538
270	−3	946	2453	0.113	4.86	1.121	2.30	0.00677
280	7	884	2814	0.101	4.06	1.005	2.47	0.00934
290	17	805	3676	0.0889	3.01	0.8972	2.98	0.0157
300	27	679	8698	0.0808	1.37	0.7831	5.72	0.0570
302	29	634	15786	0.0851	0.851	0.7536	8.86	0.119
				CFC-12 (dichlorodifluoromethane, R12, or Freon 12)				
180	−93	1661	822	0.114	8.31×10^{-8}	5.42×10^{-7}	6.52	0.00159
200	−73	1608	837	0.104	7.76	3.87	4.99	0.00167
220	−53	1554	857	0.0960	7.21	2.96	4.11	0.00179
240	−33	1497	882	0.0881	6.67	2.38	3.57	0.00194
260	−13	1437	911	0.0806	6.15	1.97	3.20	0.00215
280	7	1374	947	0.0734	5.64	1.66	2.94	0.00245
300	27	1304	993	0.0665	5.13	1.42	2.76	0.00289
320	47	1226	1059	0.0596	4.59	1.22	2.65	0.00362
340	67	1135	1168	0.0528	3.98	1.04	2.62	0.00501

Table A.3: saturated liquids…*continued*

Temperature		ρ (kg/m^3)	c_p (J/kg·K)	k (W/m·K)	α (m^2/s)	ν (m^2/s)	Pr	β (K^{-1})
K	°C							
Glycerin (glycerol; 1 atm, not saturated)								
273	0	1276	2200	0.282	1.00×10^{-7}	0.0083	83,000	
293	20	1261	2350	0.285	0.962	0.001120	11,630	0.00048
303	30	1255	2400	0.285	0.946	0.000488	5,161	0.00049
313	40	1249	2460	0.285	0.928	0.000227	2,451	0.00049
323	50	1243	2520	0.285	0.910	0.000114	1,254	0.00050
80% glycerin, 20% water								
293	20	1209	2730	0.327	0.99×10^{-7}	4.97×10^{-5}	502	0.00051
303	30	1203	2750	0.327	0.99	2.82	282	0.00052
313	40	1197	2800	0.327	0.98	1.74	178	0.00053
323	50	1191	2860	0.331	0.97	1.14	118	0.00053
60% glycerin, 40% water								
293	20	1154	3180	0.381	1.04×10^{-7}	9.36×10^{-6}	90.0	0.00048
303	30	1148	3180	0.381	1.04	6.89	66.3	0.00050
313	40	1143	3240	0.385	1.04	4.44	42.7	0.00052
323	50	1137	3300	0.389	1.04	3.31	31.8	0.00053
40% glycerin, 60% water								
293	20	1099	3480	0.448	1.20×10^{-7}	3.385×10^{-6}	28.9	0.00041
303	30	1095	3480	0.452	1.22	2.484	20.4	0.00045
313	40	1090	3570	0.461	1.18	1.900	16.1	0.00048
323	50	1085	3620	0.469	1.19	1.493	12.5	0.00051
20% glycerin, 80% water								
293	20	1047	3860	0.519	1.28×10^{-7}	1.681×10^{-6}	13.1	0.00031
303	30	1043	3860	0.532	1.32	1.294	9.8	0.00036
313	40	1039	3915	0.540	1.33	1.030	7.7	0.00041
323	50	1035	3970	0.553	1.35	0.849	6.3	0.00046
Helium I and Helium II								

• k for He I is about 0.020 W/m·K near the λ-transition ($\approx$ 2.17 K).

• k for He II below the λ-transition is hard to measure. It appears to be about 80,000 W/m·K between 1.4 and 1.75 K and it might go as high as 340,000 W/m·K at 1.92 K. These are the highest conductivities known (cf. copper, silver, and diamond).

Table A.3: saturated liquids…*continued*

Temperature		ρ (kg/m^3)	c_p (J/kg·K)	k (W/m·K)	α (m^2/s)	ν (m^2/s)	Pr	β (K^{-1})
K	°C							
HCFC-22 (difluoromonochloromethane, R22)								
160	−113	1605	1061	0.1504	8.82×10^{-8}	7.10×10^{-7}	8.05	0.00163
180	−93	1553	1061	0.1395	8.46	4.77	5.63	0.00170
200	−73	1499	1064	0.1291	8.09	3.55	4.38	0.00181
220	−53	1444	1076	0.1193	7.67	2.79	3.64	0.00196
240	−33	1386	1100	0.1099	7.21	2.28	3.16	0.00216
260	−13	1324	1136	0.1008	6.69	1.90	2.84	0.00245
280	7	1257	1189	0.0918	6.14	1.61	2.62	0.00286
300	27	1183	1265	0.0828	5.53	1.37	2.48	0.00351
320	47	1097	1390	0.0737	4.83	1.17	2.42	0.00469
340	67	990.1	1665	0.0644	3.91	0.981	2.51	0.00756
360	87	823.4	3001	0.0575	2.33	0.786	3.38	0.02388
Heavy water (D$_2$O)								
300	27	1104	4190	0.5969	1.29×10^{-7}	9.48×10^{-7}	7.44	0.003362
400	127	1040	4174	0.6331	1.46	2.44	1.67	0.002846
500	227	920.5	4464	0.5669	1.38	1.43	1.04	0.003806
600	327	712.2	66659	0.4302	0.907	1.14	1.26	0.01231
HFC-134a (1,1,1,2-Tetrafluoroethane, R134a)								
180	−93	1564	1187	0.1391	7.49×10^{-8}	9.45×10^{-7}	12.62	0.00170
200	−73	1510	1205	0.1277	7.01	5.74	8.18	0.00180
220	−53	1455	1233	0.1172	6.53	4.03	6.17	0.00193
240	−33	1397	1266	0.1073	6.06	3.05	5.03	0.00211
260	−13	1337	1308	0.0979	5.60	2.41	4.30	0.00236
280	7	1271	1360	0.0890	5.14	1.95	3.80	0.00273
300	27	1199	1432	0.0803	4.67	1.61	3.45	0.00330
320	47	1116	1542	0.0718	4.17	1.34	3.21	0.00433
340	67	1015	1750	0.0631	3.55	1.10	3.11	0.00657
360	87	870.1	2436	0.0541	2.55	0.883	3.46	0.0154
Lead (1 atm, not saturated)								
601	328	10672	148	16	1.0×10^{-5}	2.52×10^{-7}	0.025	0.000120
800	527	10417	144	18	1.2	1.66	0.014	0.000123
1000	727	10162	141	20	1.4	1.30	0.0092	0.000126
1200	927	9906	138	22	1.6	1.12	0.0068	0.000129

Table A.3: saturated liquids...*continued*

Temperature		ρ (kg/m³)	c_p (J/kg·K)	k (W/m·K)	α (m²/s)	ν (m²/s)	Pr	β (K⁻¹)
K	°C							
				Mercury				
234	−39		141.5	6.97	3.62×10^{-6}	1.5×10^{-7}	0.041	
250	−23		140.5	7.32	3.83	1.4	0.037	
300	27	13,529	139.3	8.34	4.43	1.12	0.0253	0.000181
350	77	13,407	137.7	9.15	4.96	0.974	0.0196	0.000181
400	127	13,286	136.6	9.84	5.42	0.88	0.016	0.000181
500	227	13,048	135.3	11.0	6.23	0.73	0.012	0.000183
600	327	12,809	135.5	12.0	6.91	0.71	0.010	0.000187
700	427	12,567	136.9	12.7	7.38	0.67	0.0091	0.000195
800	527	12,318	139.8	12.8	7.43	0.64	0.0086	0.000207
				Methyl alcohol (methanol)				
240	−33	841.1	2283	0.211	1.10×10^{-7}	1.81×10^{-6}	16.5	0.00114
260	−13	822.0	2347	0.207	1.08	1.24	11.5	0.00115
280	7	803.2	2434	0.204	1.04	0.895	8.59	0.00117
300	27	784.5	2546	0.200	1.00	0.675	6.74	0.00120
320	47	765.6	2684	0.196	0.954	0.528	5.53	0.00126
360	87	725.4	3032	0.188	0.856	0.352	4.11	0.00149
400	127	678.6	3491	0.181	0.762	0.253	3.32	0.00198
440	167	618.8	4165	0.173	0.672	0.189	2.81	0.00309
480	207	530.4	5725	0.166	0.548	0.144	2.63	0.00711
			NaK (eutectic mixture of sodium and potassium)					
473	200	833	908	24.7	3.27×10^{-5}	4.40×10^{-7}	0.013	0.000277
673	400	786	878	26.2	3.80	3.04	0.0080	0.000277
873	600	737	876	25.9	4.01	2.30	0.0057	0.000277
1073	800	688	893	23.9	3.89	1.97	0.0051	0.000277
				Nitrogen				
70	−203	838.5	2015	0.160	9.44×10^{-8}	2.63×10^{-7}	2.78	0.00513
77.2	−195.9	806.6	2041	0.145	8.81	2.00	2.27	0.00566
80	−193	793.9	2056	0.140	8.55	1.83	2.14	0.00591
90	−183	745.0	2141	0.120	7.51	1.38	1.84	0.00711
100	−173	689.4	2318	0.100	6.27	1.10	1.75	0.00927
110	−163	621.5	2743	0.0804	4.72	0.901	1.91	0.0142
120	−153	523.4	4508	0.0610	2.59	0.734	2.84	0.0359

Table A.3: saturated liquids...*continued*

Temperature		ρ (kg/m^3)	c_p (J/kg·K)	k (W/m·K)	α (m^2/s)	ν (m^2/s)	Pr	β (K^{-1})
K	°C							
Oils (some approximate viscosities; 1 atm, not saturated)								
273	0			MS-20		0.0076	100,000	
339	66		California crude (heavy)			0.00008		
289	16		California crude (light)			0.00005		
339	66		California crude (light)			0.000010		
289	16		Light machine oil (ρ = 907)			0.00016		
339	66		Light machine oil (ρ = 907)			0.000013		
289	16			SAE 30		0.00044	≈ 5,000	
339	66			SAE 30		0.00003		
289	16		SAE 30 (Eastern)			0.00011		
339	66		SAE 30 (Eastern)			0.00001		
289	16		Spindle oil (ρ = 885)			0.00005		
339	66		Spindle oil (ρ = 885)			0.000007		
Olive Oil (1 atm, not saturated)								
283	10	920				14.9 $\times 10^{-5}$		
293	20	913	1800	0.24	1.46×10^{-7}	9.02	620	0.000728
303	30	906				5.76		
313	40	900				3.84		
323	50	893				2.67		
333	60	886				1.91		
343	70	880				1.41		
Oxygen								
60	−213	1282	1673	0.194	9.04×10^{-8}	4.51×10^{-7}	4.99	0.00343
70	−203	1237	1678	0.180	8.66	2.01	3.47	0.00370
80	−193	1190	1682	0.166	8.27	2.19	2.65	0.00398
90	−183	1142	1699	0.151	7.79	1.71	2.20	0.00436
100	−173	1091	1738	0.137	7.21	1.40	1.94	0.00492
110	−163	1036	1807	0.122	6.52	1.12	1.80	0.00575
120	−153	973.9	1927	0.107	5.71	1.00	1.75	0.00708
130	−143	902.5	2153	0.0926	4.77	0.856	1.80	0.00953
140	−133	813.2	2691	0.0782	3.56	0.741	2.07	0.0155
150	−123	675.5	5464	0.0642	1.74	0.635	3.65	0.0495

Table A.3: saturated liquids...*continued*

Temperature		ρ (kg/m^3)	c_p (J/kg·K)	k (W/m·K)	α (m^2/s)	ν (m^2/s)	Pr	β (K^{-1})
K	°C							
				Water				
273.16	0.01	999.8	4220	0.5610	1.330×10^{-7}	17.91×10^{-7}	13.47	-6.80×10^{-5}
275	2	999.9	4214	0.5645	1.340	16.82	12.55	-3.55×10^{-5}
280	7	999.9	4201	0.5740	1.366	14.34	10.63	4.36×10^{-5}
285	12	999.5	4193	0.5835	1.392	12.40	8.91	0.000112
290	17	998.8	4187	0.5927	1.417	10.85	7.66	0.000172
295	22	997.8	4183	0.6017	1.442	9.600	6.66	0.000226
300	27	996.5	4181	0.6103	1.465	8.568	5.85	0.000275
305	32	995.0	4180	0.6184	1.487	7.708	5.18	0.000319
310	37	993.3	4179	0.6260	1.508	6.982	4.63	0.000361
320	47	989.3	4181	0.6396	1.546	5.832	3.77	0.000436
340	67	979.5	4189	0.6605	1.610	4.308	2.68	0.000565
360	87	967.4	4202	0.6737	1.657	3.371	2.03	0.000679
373.15	100.0	958.3	4216	0.6791	1.681	2.940	1.75	0.000751
400	127	937.5	4256	0.6836	1.713	2.332	1.36	0.000895
420	147	919.9	4299	0.6825	1.726	2.030	1.18	0.001008
440	167	900.5	4357	0.6780	1.728	1.808	1.05	0.001132
460	187	879.5	4433	0.6702	1.719	1.641	0.955	0.001273
480	207	856.5	4533	0.6590	1.697	1.514	0.892	0.001440
500	227	831.3	4664	0.6439	1.660	1.416	0.853	0.001645
520	247	803.6	4838	0.6246	1.607	1.339	0.833	0.001909
540	267	772.8	5077	0.6001	1.530	1.278	0.835	0.002266
560	287	738.0	5423	0.5701	1.425	1.231	0.864	0.002783
580	307	697.6	5969	0.5346	1.284	1.195	0.931	0.003607
600	327	649.4	6953	0.4953	1.097	1.166	1.06	0.005141
620	347	586.9	9354	0.4541	0.8272	1.146	1.39	0.009092
640	367	481.5	25,940	0.4149	0.3322	1.148	3.46	0.03971
642	369	463.7	34,930	0.4180	0.2581	1.151	4.46	0.05679
644	371	440.7	58,910	0.4357	0.1678	1.156	6.89	0.1030
646	373	403.0	204,600	0.5280	0.06404	1.192	18.6	0.3952
647.0	374	357.3	3,905,000	1.323	0.00948	1.313	138.	7.735

Table A.4   Some latent heats of vaporization, h_{fg} (kJ/kg), with temperatures at triple point, T_{tp} (K), and critical point, T_c (K).

T(K)	Water	Ammonia	CO_2	HCFC-22	HFC-134a	Mercury	Methanol	Nitrogen	Oxygen
60									238.4
70								208.1	230.5
80								195.7	222.3
90								180.5	213.2
100								161.0	202.6
110								134.3	189.7
120				300.4				92.0	173.7
130				294.0					153.1
140				287.9					125.2
150				281.8					79.2
160				275.9					
180				264.3	257.4		1310		
200		1478		252.9	245.7		1290		
220		1426	344.9	241.3	233.9		1269		
230		1398	328.0	235.2	227.8		1258		
240		1369	309.6	228.9	221.5		1247		
250		1339	289.3	222.2	215.0		1235		
260		1307	266.5	215.1	208.2		1222		
270		1273	240.1	207.5	201.0		1209		
273	2501	1263	230.9	205.0	198.6	306.8	1205		
280	2485	1237	208.6	199.4	193.3	306.6	1196		
290	2462	1199	168.1	190.5	185.0	306.2	1181		
300	2438	1158	103.7	180.9	176.1	305.8	1166		
310	2414	1114		170.2	166.3	305.5	1150		
320	2390	1067		158.3	155.5	305.1	1133		
330	2365	1015		144.7	143.3	304.8	1116		
340	2341	958.4		128.7	129.3	304.4	1096		
350	2315	895.5		109.0	112.5	304.1	1076		
360	2290	824.9		81.8	91.0	303.8	1054		
373	2257	717.0			36.1	303.3	1022		
400	2183	346.2				302.4	945		
500	1828					299.2	391		
600	1173					295.9			
700						292.3			
T_{tp}	273.16	195.5	216.6	115.7	169.9	234.2	175.6	63.2	54.3
T_c	647.096	405.6	304.1	369.3	374.2	1746	512.6	126.2	154.6

Table A.5   Thermophysical properties of saturated vapors ($p \neq 1$ atm).

T (K)	p (MPa)	ρ (kg/m³)	c_p (J/kg·K)	k (W/m·K)	μ (kg/m·s)	Pr	β (K⁻¹)
			Ammonia (R717)				
200	0.008610	0.08867	2039	0.0160	6.95×10^{-6}	0.884	0.005146
220	0.03373	0.3184	2137	0.0176	7.49	0.908	0.004862
240	0.1022	0.8969	2293	0.0195	8.07	0.947	0.004746
260	0.2553	2.116	2513	0.0218	8.67	0.998	0.004800
280	0.5507	4.380	2805	0.0246	9.28	1.06	0.005048
300	1.061	8.244	3189	0.0281	9.92	1.12	0.005553
320	1.872	14.50	3723	0.0326	10.6	1.21	0.006453
340	3.079	24.39	4537	0.0387	11.4	1.33	0.008063
360	4.793	40.20	5978	0.0480	12.4	1.55	0.01125
380	7.140	67.33	9403	0.0664	14.0	1.99	0.01955
400	10.30	130.9	37953	0.142	18.0	4.78	0.09262
			Carbon dioxide (R744)				
220	0.5991	15.82	930.3	0.0114	1.106×10^{-5}	0.901	0.006223
230	0.8929	23.27	1005	0.0124	1.158	0.938	0.006615
240	1.283	33.30	1103	0.0136	1.212	0.986	0.007223
250	1.785	46.64	1237	0.0150	1.273	1.05	0.008154
260	2.419	64.42	1430	0.0168	1.342	1.14	0.009611
270	3.203	88.37	1731	0.0194	1.425	1.27	0.01203
280	4.161	121.7	2277	0.0234	1.536	1.50	0.01662
290	5.318	172.0	3614	0.0310	1.705	1.98	0.02811
300	6.713	268.6	11921	0.0557	2.081	4.45	0.09949
302	7.027	308.2	23800	0.0735	2.264	7.33	0.2010
			HCFC-22 (R22)				
160	0.0005236	0.03406	479.2	0.00398	6.69×10^{-6}	0.807	0.006266
180	0.003701	0.2145	507.1	0.00472	7.54	0.810	0.005622
200	0.01667	0.8752	539.1	0.00554	8.39	0.816	0.005185
220	0.05473	2.649	577.8	0.00644	9.23	0.828	0.004947
240	0.1432	6.501	626.2	0.00744	10.1	0.847	0.004919
260	0.3169	13.76	688.0	0.00858	10.9	0.877	0.005131
280	0.6186	26.23	769.8	0.00990	11.8	0.918	0.005661
300	1.097	46.54	885.1	0.0116	12.8	0.977	0.006704
320	1.806	79.19	1071.	0.0140	14.0	1.07	0.008801
340	2.808	133.9	1470.	0.0181	15.7	1.27	0.01402
360	4.184	246.7	3469.	0.0298	19.3	2.24	0.04233

Table A.5: saturated vapors ($p \neq 1$ atm)...*continued.*

T (K)	p (MPa)	ρ (kg/m^3)	c_p (J/kg·K)	k (W/m·K)	μ (kg/m·s)	Pr	β (K^{-1})
HFC-134a (R134a)							
180	0.001128	0.07702	609.7	0.00389	6.90×10^{-6}	1.08	0.005617
200	0.006313	0.3898	658.6	0.00550	7.75	0.929	0.005150
220	0.02443	1.385	710.9	0.00711	8.59	0.859	0.004870
240	0.07248	3.837	770.5	0.00873	9.40	0.829	0.004796
260	0.1768	8.905	841.8	0.0104	10.2	0.826	0.004959
280	0.3727	18.23	929.6	0.0121	11.0	0.845	0.005421
300	0.7028	34.19	1044.	0.0140	11.9	0.886	0.006335
320	1.217	60.71	1211.	0.0163	12.9	0.961	0.008126
340	1.972	105.7	1524.	0.0197	14.4	1.11	0.01227
360	3.040	193.6	2606.	0.0274	17.0	1.62	0.02863
Methyl alcohol (methanol)							
280	0.006177	0.08640	3168	0.0136	9.05×10^{-6}	2.11	
320	0.04849	0.6071	4096	0.0172	10.3	2.46	
360	0.2299	2.668	4856	0.0216	11.5	2.58	
400	0.7737	8.734	5937	0.0275	12.5	2.70	
440	2.051	24.28	7965	0.0369	13.6	2.92	
Nitrogen							
70	0.03855	1.896	1082	0.00635	4.88×10^{-6}	0.831	0.01525
77.24	0.1000	4.557	1123	0.00717	5.44	0.851	0.01475
80	0.1369	6.089	1145	0.00751	5.65	0.862	0.01472
90	0.3605	15.08	1266	0.00887	6.48	0.925	0.01553
100	0.7783	31.96	1503	0.0107	7.43	1.04	0.01842
110	1.466	62.58	2062	0.0138	8.63	1.29	0.02647
120	2.511	125.1	4631	0.0217	10.6	2.27	0.06454
Oxygen							
70	0.006262	0.3457	978.0	0.00599	5.36×10^{-6}	0.874	0.01471
80	0.03012	1.468	974.3	0.00703	6.15	0.852	0.01314
90	0.09935	4.387	970.5	0.00812	6.94	0.829	0.01223
100	0.2540	10.42	1006.	0.00934	7.73	0.833	0.01207
110	0.5434	21.28	1101.	0.0107	8.55	0.876	0.01277
120	1.022	39.31	1276.	0.0125	9.43	0.962	0.01462
130	1.749	68.37	1600.	0.0149	10.5	1.12	0.01868
140	2.788	116.8	2370.	0.0190	11.8	1.48	0.02919
150	4.219	214.9	6625.	0.0297	14.7	3.29	0.08865

Table A.5: saturated vapors ($p \neq 1$ atm)...*continued.*

T (K)	p (MPa)	ρ (kg/m^3)	c_p (J/kg·K)	k (W/m·K)	μ (kg/m·s)	Pr	β (K^{-1})
			Water vapor				
273.16	0.0006177	0.004855	1884	0.01707	0.9216×10^{-5}	1.02	0.003681
275.0	0.0006985	0.005507	1886	0.01717	0.9260	1.02	0.003657
280.0	0.0009918	0.007681	1891	0.01744	0.9382	1.02	0.003596
285.0	0.001389	0.01057	1897	0.01773	0.9509	1.02	0.003538
290.0	0.001920	0.01436	1902	0.01803	0.9641	1.02	0.003481
295.0	0.002621	0.01928	1908	0.01835	0.9778	1.02	0.003428
300.0	0.003537	0.02559	1914	0.01867	0.9920	1.02	0.003376
305.0	0.004719	0.03360	1920	0.01901	1.006	1.02	0.003328
310.0	0.006231	0.04366	1927	0.01937	1.021	1.02	0.003281
320.0	0.01055	0.07166	1942	0.02012	1.052	1.02	0.003195
340.0	0.02719	0.1744	1979	0.02178	1.116	1.01	0.003052
360.0	0.06219	0.3786	2033	0.02369	1.182	1.01	0.002948
373.15	0.1014	0.5982	2080	0.02510	1.227	1.02	0.002902
380.0	0.1289	0.7483	2110	0.02587	1.250	1.02	0.002887
400.0	0.2458	1.369	2218	0.02835	1.319	1.03	0.002874
420.0	0.4373	2.352	2367	0.03113	1.388	1.06	0.002914
440.0	0.7337	3.833	2560	0.03423	1.457	1.09	0.003014
460.0	1.171	5.983	2801	0.03766	1.526	1.13	0.003181
480.0	1.790	9.014	3098	0.04145	1.595	1.19	0.003428
500.0	2.639	13.20	3463	0.04567	1.665	1.26	0.003778
520.0	3.769	18.90	3926	0.05044	1.738	1.35	0.004274
540.0	5.237	26.63	4540	0.05610	1.815	1.47	0.004994
560.0	7.106	37.15	5410	0.06334	1.901	1.62	0.006091
580.0	9.448	51.74	6760	0.07372	2.002	1.84	0.007904
600.0	12.34	72.84	9181	0.09105	2.135	2.15	0.01135
620.0	15.90	106.3	14,940	0.1267	2.337	2.76	0.02000
640.0	20.27	177.1	52,590	0.2500	2.794	5.88	0.07995
642.0	20.76	191.5	737,900	0.2897	2.894	7.37	0.1144
644.0	21.26	211.0	1,253,000	0.3596	3.034	10.6	0.1988
646.0	21.77	243.5	3,852,000	0.5561	3.325	23.0	0.6329
647.0	22.04	286.5	53,340,000	1.573	3.972	135.	9.274

$p_{\text{sat,H}_2\text{O}}$ in MPa for T in kelvin with $p_c = 22.064$ MPa, $T_c = 647.096$ K, and $\theta = 1 - T/T_c$ [A.41]:

$\ln(p_{\text{sat}}/p_c) = (T_c/T)(a\theta + b\theta^{1.5} + c\theta^3 + d\theta^{3.5} + e\theta^4 + f\theta^{7.5})$ where $a = -7.85951783$, $b = 1.84408259$, $c = 11.7866497$, $d = 22.6807411$, $e = -15.9618719$, $f = 1.80122502$.

Table A.6 Thermophysical properties of gases at atmospheric
pressure (101325 Pa)

T (K)	ρ (kg/m^3)	c_p (J/kg·K)	μ (kg/m·s)	ν (m^2/s)	k (W/m·K)	α (m^2/s)	Pr
			Air				
100	3.606	1040	0.7107×10^{-5}	0.1971×10^{-5}	0.00947	0.252×10^{-5}	0.781
150	2.368	1012	1.038	0.4382	0.0142	0.590	0.742
200	1.769	1007	1.333	0.7537	0.0185	1.04	0.726
250	1.413	1006	1.604	1.135	0.0226	1.59	0.715
260	1.359	1006	1.655	1.218	0.0233	1.71	0.713
270	1.308	1006	1.706	1.304	0.0241	1.83	0.711
280	1.261	1006	1.756	1.392	0.0249	1.96	0.710
290	1.218	1006	1.805	1.482	0.0256	2.09	0.708
300	1.177	1006	1.854	1.575	0.0264	2.23	0.707
310	1.139	1007	1.902	1.670	0.0271	2.37	0.706
320	1.103	1007	1.949	1.766	0.0279	2.51	0.705
330	1.070	1008	1.995	1.865	0.0286	2.65	0.704
340	1.038	1009	2.041	1.966	0.0293	2.80	0.703
350	1.009	1009	2.087	2.069	0.0300	2.95	0.702
400	0.8823	1014	2.306	2.613	0.0335	3.74	0.699
450	0.7842	1021	2.512	3.204	0.0368	4.59	0.698
500	0.7058	1030	2.709	3.839	0.0399	5.50	0.698
550	0.6416	1040	2.897	4.515	0.0430	6.45	0.700
600	0.5881	1051	3.077	5.232	0.0460	7.44	0.703
650	0.5429	1063	3.250	5.987	0.0489	8.48	0.706
700	0.5041	1075	3.418	6.780	0.0518	9.55	0.710
750	0.4705	1087	3.580	7.608	0.0545	10.7	0.714
800	0.4411	1099	3.737	8.472	0.0572	11.8	0.717
850	0.4151	1110	3.890	9.371	0.0599	13.0	0.721
900	0.3921	1121	4.039	10.30	0.0625	14.2	0.724
950	0.3715	1131	4.185	11.27	0.0651	15.5	0.727
1000	0.3529	1141	4.328	12.27	0.0677	16.8	0.730
1100	0.3208	1159	4.605	14.36	0.0727	19.6	0.734
1200	0.2941	1174	4.873	16.57	0.0776	22.5	0.738
1300	0.2715	1188	5.133	18.91	0.0824	25.5	0.740
1400	0.2521	1200	5.385	21.36	0.0871	28.8	0.742
1500	0.2353	1210	5.633	23.94	0.0918	32.2	0.743

Table A.6: gases at 1 atm...*continued.*

T (K)	ρ (kg/m³)	c_p (J/kg·K)	μ (kg/m·s)	ν (m²/s)	k (W/m·K)	α (m²/s)	Pr
			Argon				
100	4.982	547.4	0.799×10^{-5}	0.160×10^{-5}	0.00632	0.232×10^{-5}	0.692
150	3.269	527.7	1.20	0.366	0.00939	0.544	0.673
200	2.441	523.7	1.59	0.652	0.01245	0.974	0.669
250	1.950	522.2	1.95	1.00	0.01527	1.50	0.668
300	1.624	521.5	2.29	1.41	0.01787	2.11	0.667
350	1.391	521.2	2.59	1.86	0.02029	2.80	0.666
400	1.217	520.9	2.88	2.37	0.02256	3.56	0.666
450	1.082	520.8	3.16	2.92	0.02470	4.39	0.666
500	0.9735	520.7	3.42	3.51	0.02675	5.28	0.666
550	0.8850	520.6	3.67	4.14	0.02870	6.23	0.665
600	0.8112	520.6	3.91	4.82	0.03057	7.24	0.665
650	0.7488	520.5	4.14	5.52	0.03238	8.31	0.665
700	0.6953	520.5	4.36	6.27	0.03412	9.43	0.665
			Ammonia				
239.83	0.8900	2292	0.8067×10^{-5}	0.9064×10^{-5}	0.0195	0.957×10^{-5}	0.947
300	0.6990	2163	1.016	1.453	0.0254	1.68	0.866
400	0.5207	2287	1.391	2.672	0.0375	3.15	0.849
500	0.4157	2466	1.774	4.266	0.0520	5.07	0.841
600	0.3462	2648	2.143	6.191	0.0686	7.48	0.827
700	0.2966	2827	2.492	8.400	0.0871	10.4	0.809
			Carbon dioxide				
220	2.472	781	1.111×10^{-5}	0.4493×10^{-5}	0.0110	0.568×10^{-5}	0.791
250	2.165	805	1.258	0.5812	0.0130	0.749	0.776
300	1.797	853	1.500	0.8351	0.0168	1.10	0.763
350	1.537	899	1.736	1.130	0.0207	1.50	0.754
400	1.343	942	1.964	1.462	0.0247	1.95	0.748
450	1.193	980	2.182	1.829	0.0288	2.46	0.743
500	1.074	1016	2.392	2.229	0.0329	3.02	0.739
550	0.9756	1047	2.594	2.659	0.0369	3.62	0.735
600	0.8942	1076	2.788	3.118	0.0410	4.26	0.732

Table A.6: gases at 1 atm...*continued.*

T(K)	ρ (kg/m^3)	c_p (J/kg·K)	μ (kg/m·s)	ν (m^2/s)	k (W/m·K)	α (m^2/s)	Pr
			Carbon monoxide				
250	1.367	1042	1.54×10^{-5}	1.13×10^{-5}	0.02306	1.62×10^{-5}	0.697
300	1.138	1040	1.77	1.56	0.02656	2.24	0.694
350	0.975	1040	1.99	2.04	0.02981	2.94	0.693
400	0.853	1039	2.19	2.56	0.03285	3.70	0.692
450	0.758	1039	2.38	3.13	0.03571	4.53	0.691
500	0.682	1040	2.55	3.74	0.03844	5.42	0.691
600	0.5687	1041	2.89	5.08	0.04357	7.36	0.690
700	0.4874	1043	3.20	6.56	0.04838	9.52	0.689
800	0.4265	1046	3.49	8.18	0.05297	11.9	0.689
900	0.3791	1049	3.77	9.94	0.05738	14.4	0.689
1000	0.3412	1052	4.04	11.8	0.06164	17.2	0.689
			Helium				
50	0.9732	5201	0.607×10^{-5}	0.0624×10^{-4}	0.0476	0.0940×10^{-4}	0.663
100	0.4871	5194	0.953	0.196	0.0746	0.295	0.664
150	0.3249	5193	1.25	0.385	0.0976	0.578	0.665
200	0.2437	5193	1.51	0.621	0.118	0.932	0.667
250	0.1950	5193	1.76	0.903	0.138	1.36	0.665
300	0.1625	5193	1.99	1.23	0.156	1.85	0.664
350	0.1393	5193	2.22	1.59	0.174	2.40	0.663
400	0.1219	5193	2.43	1.99	0.190	3.01	0.663
450	0.1084	5193	2.64	2.43	0.207	3.67	0.663
500	0.09753	5193	2.84	2.91	0.222	4.39	0.663
600	0.08128	5193	3.22	3.96	0.252	5.98	0.663
700	0.06967	5193	3.59	5.15	0.281	7.77	0.663
800	0.06096	5193	3.94	6.47	0.309	9.75	0.664
900	0.05419	5193	4.28	7.91	0.335	11.9	0.664
1000	0.04877	5193	4.62	9.46	0.361	14.2	0.665
1100	0.04434	5193	4.95	11.2	0.387	16.8	0.664
1200	0.04065	5193	5.27	13.0	0.412	19.5	0.664
1300	0.03752	5193	5.59	14.9	0.437	22.4	0.664
1400	0.03484	5193	5.90	16.9	0.461	25.5	0.665
1500	0.03252	5193	6.21	19.1	0.485	28.7	0.665

Table A.6: gases at 1 atm...*continued.*

T (K)	ρ (kg/m^3)	c_p (J/kg·K)	μ (kg/m·s)	ν (m^2/s)	k (W/m·K)	α (m^2/s)	Pr
Hydrogen							
50	0.4953	10484	0.2406×10^{-5}	0.4857×10^{-5}	0.0378	0.727×10^{-5}	0.668
100	0.2457	11229	0.4120	1.677	0.0684	2.48	0.677
150	0.1637	12605	0.5515	3.369	0.101	4.90	0.687
200	0.1228	13538	0.6748	5.497	0.133	8.00	0.687
250	0.09821	14054	0.7879	8.023	0.161	11.7	0.686
300	0.08185	14313	0.8938	10.92	0.187	15.9	0.685
350	0.07016	14431	0.9945	14.18	0.210	20.7	0.684
400	0.06139	14479	1.091	17.77	0.231	26.0	0.683
450	0.05457	14500	1.184	21.69	0.251	31.8	0.683
500	0.04912	14513	1.274	25.94	0.271	38.0	0.682
550	0.04465	14528	1.361	30.49	0.290	44.7	0.682
600	0.04093	14549	1.447	35.34	0.309	51.9	0.681
650	0.03779	14578	1.530	40.50	0.328	59.5	0.681
700	0.03509	14614	1.612	45.94	0.346	67.6	0.680
750	0.03275	14658	1.692	51.66	0.365	76.1	0.679
800	0.03070	14710	1.770	57.67	0.384	85.0	0.678
850	0.02890	14769	1.848	63.95	0.403	94.4	0.678
900	0.02729	14836	1.924	70.49	0.422	104	0.677
1000	0.02456	14992	2.073	84.38	0.460	125	0.675
Nitrogen							
100	3.483	1072	0.6959×10^{-5}	0.1998×10^{-5}	0.00938	0.251×10^{-5}	0.795
200	1.711	1044	1.291	0.7547	0.0183	1.02	0.737
300	1.138	1041	1.789	1.572	0.0260	2.19	0.717
400	0.8532	1045	2.221	2.603	0.0328	3.68	0.707
500	0.6825	1056	2.606	3.819	0.0390	5.42	0.705
600	0.5687	1075	2.958	5.201	0.0448	7.33	0.709
700	0.4875	1098	3.283	6.735	0.0503	9.40	0.717
800	0.4266	1122	3.589	8.413	0.0555	11.6	0.725
900	0.3792	1146	3.878	10.23	0.0605	13.9	0.734
1000	0.3413	1167	4.154	12.17	0.0654	16.4	0.742
1100	0.3103	1187	4.420	14.25	0.0701	19.0	0.749
1200	0.2844	1204	4.677	16.44	0.0747	21.8	0.754
1400	0.2438	1232	5.169	21.20	0.0836	27.8	0.762
1600	0.2133	1254	5.640	26.44	0.0923	34.5	0.766

Table A.6: gases at 1 atm…*continued.*

T(K)	ρ (kg/m^3)	c_p (J/kg·K)	μ (kg/m·s)	ν (m^2/s)	k (W/m·K)	α (m^2/s)	Pr
			Oxygen				
100	3.995	935.6	$0.7712{\times}10^{-5}$	$0.1931{\times}10^{-5}$	0.00909	0.243×10^{-5}	0.794
150	2.619	919.8	1.138	0.4343	0.0138	0.572	0.759
200	1.956	914.6	1.472	0.7525	0.0182	1.02	0.738
250	1.562	915.0	1.780	1.139	0.0225	1.57	0.725
300	1.301	919.9	2.065	1.588	0.0265	2.21	0.717
350	1.114	929.1	2.332	2.093	0.0303	2.93	0.714
400	0.9749	941.7	2.584	2.650	0.0340	3.71	0.715
450	0.8665	956.4	2.822	3.257	0.0376	4.54	0.718
500	0.7798	972.2	3.049	3.910	0.0410	5.41	0.722
550	0.7089	988.0	3.265	4.606	0.0444	6.34	0.727
600	0.6498	1003	3.473	5.345	0.0477	7.31	0.731
700	0.5569	1031	3.865	6.940	0.0540	9.40	0.738
800	0.4873	1055	4.233	8.687	0.0600	11.7	0.744
900	0.4332	1074	4.581	10.58	0.0659	14.2	0.747
1000	0.3899	1090	4.912	12.60	0.0715	16.8	0.748
			Steam (H$_2$O vapor)				
373.15	0.5976	2080	12.28×10^{-6}	20.55×10^{-6}	0.02509	2.019×10^{-5}	1.018
393.15	0.5652	2021	13.04	23.07	0.02650	2.320	0.994
413.15	0.5365	1994	13.81	25.74	0.02805	2.622	0.982
433.15	0.5108	1980	14.59	28.56	0.02970	2.937	0.973
453.15	0.4875	1976	15.38	31.55	0.03145	3.265	0.966
473.15	0.4665	1976	16.18	34.68	0.03328	3.610	0.961
493.15	0.4472	1980	17.00	38.01	0.03519	3.974	0.956
513.15	0.4295	1986	17.81	41.47	0.03716	4.357	0.952
533.15	0.4131	1994	18.63	45.10	0.03919	4.758	0.948
553.15	0.3980	2003	19.46	48.89	0.04128	5.178	0.944
573.15	0.3840	2013	20.29	52.84	0.04341	5.616	0.941
593.15	0.3709	2023	21.12	56.94	0.04560	6.077	0.937
613.15	0.3587	2034	21.95	61.19	0.04784	6.554	0.934
673.15	0.3266	2070	24.45	74.86	0.05476	8.100	0.924
773.15	0.2842	2134	28.57	100.5	0.06698	11.04	0.910
873.15	0.2516	2203	32.62	129.7	0.07990	14.42	0.899
973.15	0.2257	2273	36.55	161.9	0.09338	18.20	0.890
1073.15	0.2046	2343	40.38	197.4	0.1073	22.38	0.882

Table A.7 Physical constants from 2018 CODATA. As of the 2018 adjustment, all values listed here are defined exactly.

Avogadro's number, N_A	$6.022\ 140\ 76 \times 10^{26}$	molecules/kmol
Boltzmann's constant, k_B	$1.380\ 649 \times 10^{-23}$	J/K
Universal gas constant, $R° = N_A k_B$	$8314.462\ 618...$	J/kmol·K
Speed of light in vacuum, c_o	$299\ 792\ 458$	m/s
Standard acceleration of gravity, g	$9.806\ 65$	m/s^2
Stefan-Boltzmann constant, σ	$5.670\ 374\ 419...\times 10^{-8}$	W/m^{2}K^4
Wien displacement law constant, $(\lambda T)_{e_{\lambda=\max}}$	$2897.771\ 955...$	μm·K

Table A.8 Additional physical property data given in the text

Location	*Data*	*Page*
Table 1.2	Electromagnetic wave spectrum	28
Figs. 2.2, 2.3	Thermal conductivities of metals, liquids, and gases	52, 53
Eqn. (9.2a), Table 9.1	Surface tension	479, 480
Table 10.1	Total emittances	546
Table 11.3	Lennard-Jones constants and molecular weights	689
Table 11.4	Collision integrals	690
Table 11.5	Molal specific volumes and latent heats	694

B. Units and conversion factors

The underlying standard for all our units is ultimately the *Système International d' Unités* (the "S.I. System"). But the need to deal with English units, and the remnants of earlier metric systems, will remain with us for many years to come. We therefore list some conversion factors to S.I. units from English units and other units in this appendix. Many more conversion factors and an extensive discussion of the S.I. system and may be found in [B.1].

The dimensions that are used consistently in the subject of heat transfer are length, mass, force, energy, temperature, and time. We generally avoid using both force and mass dimensions in the same equation, since force is always expressible in dimensions of mass, length, and time, and vice versa. We do not make a practice of eliminating energy in terms of force times length because work and heat must often be accounted separately in heat transfer problems. The text makes occasional reference to electrical units; however, these are conventional and do not have counterparts in the English system, so no electrical units are discussed here.

We present conversion factors in the form of multipliers that may be applied to English units so as to obtain S.I units. For example, the relationship between Btu and J is

$$1 \text{ Btu} = 1055.05 \text{ J} \tag{B.1}$$

We may rearrange eqn. (B.1) to display a conversion factor whose numerical worth is one:

$$1 = 1055.05 \ \frac{\text{J}}{\text{Btu}} \tag{B.2}$$

761

Table B.1 SI Multiplying Factors

Multiple	Prefix	Symbol	Multiple	Prefix	Symbol
10^{30}	quetta	Q	10^{-30}	quecto	q
10^{27}	ronna	R	10^{-27}	ronto	r
10^{24}	yotta	Y	10^{-24}	yocto	y
10^{21}	zetta	Z	10^{-21}	zepto	z
10^{18}	exa	E	10^{-18}	atto	a
10^{15}	peta	P	10^{-15}	femto	f
10^{12}	tera	T	10^{-12}	pico	p
10^{9}	giga	G	10^{-9}	nano	n
10^{6}	mega	M	10^{-6}	micro	μ
10^{3}	kilo	k	10^{-3}	milli	m
10^{2}	hecto	h	10^{-2}	centi	c
10^{1}	deka	da	10^{-1}	deci	d

Thus, if we were to multiply a given number of Btus by this factor, we would obtain the corresponding number of joules. The latter form is quite useful in changing units within more complex equations. For example, the conversion factor

$$1 = 0.0001663 \; \frac{\text{m/s}}{\text{furlong/fortnight}}$$

could be multiplied by a velocity in furlongs per fortnight[1], on just one side of an equation, to convert it to meters per second.

Note that the S.I. units may have prefixes placed in front of them to indicate multiplication by various powers of ten. For example, the prefix "k" denotes multiplication by 1000 (e.g., 1 km = 1000 m). The complete set of S.I. prefixes is given in Table B.1.

Table B.2 provides multipliers for a selection of common units. As an example of their use, consider the first entry in the table which shows a conversion factor (in column "multiply no.") of 16.018 for changing lbm/ft^3 to kg/m^3. If we consider a liquid with a density of 62.40 lbm/ft^3, we may convert to density in kg/m^3 as follows:

$$62.40 \; \text{lb/ft}^3 \times \left(16.018 \; \frac{\text{kg/m}^3}{\text{lbm/ft}^3} \right) = 999.5 \; \text{kg/m}^3 \qquad \text{(B.3)}$$

---

[1] Shortly after World War II, a group of staff physicists at Boeing Airplane Co. answered angry demands by engineers that calculations be presented in English units with a report translated entirely into such dimensions as these.

Table B.2   Selected Conversion Factors

Dimension	*To get SI*	*=*	*multiply no.*	*×*	*other unit*
Density	kg/m^3	=	16.018	×	lbm/ft^3
	kg/m^3	=	10^3	×	g/cm^3
Diffusivity (α, ν, $\mathcal{D}$)	m^2/s	=	0.092903	×	ft^2/s
	m^2/s	=	10^{-6}	×	centistokes
Energy	J	=	1055.05	×	Btu[a]
	J	=	4.1868	×	cal[b]
	J	=	10^{-7}	×	erg
	J	=	3.6×10^6	×	kW·hr
Energy per unit mass	J/kg	=	2326.0	×	Btu/lbm
	J/kg	=	4186.8	×	cal/g
Flow rate	m^3/s	=	6.3090×10^{-5}	×	gal/min (gpm)
	m^3/s	=	4.7195×10^{-4}	×	ft^3/min (cfm)
	m^3/s	=	10^{-3}	×	L/s
Force	N	=	10^{-5}	×	dyne
	N	=	4.4482	×	lbf
Heat flux	W/m^2	=	3.154	×	Btu/hr·ft^2
	W/m^2	=	10^4	×	W/cm^2
Heat transfer coefficient	W/m^{2}K	=	5.6786	×	Btu/hr·ft^2°F
Length	m	=	10^{-10}	×	ångströms (Å)
	m	=	0.0254	×	inches
	m	=	0.3048	×	feet
	m	=	201.168	×	furlongs
	m	=	1609.34	×	miles
	m	=	3.0857 × 10^{16}	×	parsecs
Mass	kg	=	0.45359	×	lbm
	kg	=	14.594	×	slug

Table B.2…*continued.*

Dimension	To get SI	=	multiply no.	×	other unit
Power	W	=	0.022597	×	ft·lbf/min
	W	=	0.29307	×	Btu/hr
	W	=	745.700	×	hp
Pressure	Pa	=	133.32	×	mmHg (@0°C)
	Pa	=	248.84	×	inH$_2$O (@60°F)
	Pa	=	3376.9	×	inHg (@60°F)
	Pa	=	6894.8	×	psi
	Pa	=	10^5	×	bar
	Pa	=	101325	×	atm
Specific heat capacity	J/kg·K	=	4186.8	×	Btu/lbm·°F
	J/kg·K	=	4186.8	×	cal/g·°C
Temperature	K	=	5/9	×	°R
	K	=	(°C + 273.15)		
	K	=	(°F + 459.67)/1.8		
Thermal conductivity	W/m·K	=	0.14413	×	Btu·in/hr·ft^2°F
	W/m·K	=	1.7307	×	Btu/hr·ft°F
	W/m·K	=	418.68	×	cal/s·cm°C
Viscosity (dynamic)	Pa·s	=	10^{-3}	×	centipoise
	Pa·s	=	1.4881	×	lbm/ft·s
	Pa·s	=	47.880	×	lbf·s/ft^2
Volume	m^3	=	10^{-3}	×	L
	m^3	=	3.7854×10^{-3}	×	gallons
	m^3	=	0.028317	×	ft^3

[a] The British thermal unit, originally defined as the heat that raises 1 lbm of water 1°F, has several values that depend mainly on the initial temperature of the water being warmed. The above is the International Table (*i.e.*, steam table) Btu. A "mean" Btu of 1055.87 J is also common. Related quantities are: 1 therm = 10^5 Btu; 1 quad = 10^{15} Btu ≈ 1 EJ; 1 ton of refrigeration = 12,000 Btu/hr absorbed.

[b] The calorie represents the heat that raises 1 g of water 1°C. Like the Btu, the calorie has several values that depend on the initial temperature of the water. The above is the International Table calorie, or IT calorie. A "thermochemical" calorie of 4.184 J has also been in common use. The dietitian's "Calorie" is actually 1 kilocalorie.

References

[B.1] A. Thompson and B. N. Taylor. *Guide for the Use of the International System of Units (SI)*. National Institute of Standards and Technology, Gaithersburg, MD, 2008. url: http://physics.nist.gov/SP811. NIST Special Pub. 811.

C. Nomenclature

Count every day one letter of my name;
Before you reach the end, dear,
Will come to lead you to my palace halls
A guide whom I shall send, dear.

Abhijñāna Śakuntalạ, Kạlidạsa, 5th C

Arbitrary constants, coefficients, and functions introduced in context are not included here; neither are most geometrical dimensions. Dimensions of symbols are given in S.I. units in parenthesis after the definition. Symbols without dimensions are noted by (–).

A, A_c, A_h, A_j
area (m^2) or function defined in eqn. (9.41); cross-sectional area (m^2); area of heater (m^2); jet cross-sectional area (m^2)

B
radiosity (W/m^2) or the function defined in Fig. 8.14.

$B_{m,i}$
mass transfer driving force, $(m_{i,s} - m_{i,e})/(1 - m_{i,s})$, eqn. (11.59) (–)

b.c.
boundary condition

b.l.
boundary layer

C
heat capacity rate (W/K) or electrical capacitance (s/ohm) or correction factor in Fig. 7.18 or pressure correction factor for gaseous emittance (–)

$\overline{C}$
average thermal molecular speed, eqn. (11.101)

C_c, C_h
heat capacity rate for hot and cold fluids (W/K)

C_{sf}
surface roughness factor (–). (see Table 9.2)

c, c_p, c_v
specific heat, specific heat at constant pressure, specific heat at constant volume (J/kg·K)

c
molar concentration of a mixture (kmol/m^3) or damping coefficient (N·s/m) or exponent in eqn. (6.114a)

c_i
partial molar concentration of species i (kmol/m^3)

c_o
speed of light in vacuum, 2.99792458×10^8 m/s

D or d
diameter (m)

D_h
hydraulic diameter, $4A_c/P$ (m)

$\mathcal{D}_{12}, \mathcal{D}_{im}$
binary diffusion coefficient for species 1 diffusing in species 2, effective binary diffusion coefficient for species i diffusing in mixture m (m^2/s)

$Đ_{ij}$	Maxwell-Stefan diffusion coefficient (m^2/s)
E, E_0	voltage, initial voltage (V)
$e, e_b, e_\lambda, e_{\lambda b}$	
	emissive power (W/m^2) or energy equivalent of mass (J); black body emissive power(W/m^2); monochromatic emissive power (W/m$^2 \cdot$µm); black body monochromatic emissive power (W/m$^2 \cdot$µm)
F	LMTD correction factor (–) or fluid parameter from Table 9.4 (–)
$F(t)$	time-dependent driving force (N)
$F_{1\text{-}2}$	radiation view factor for surface (1) seeing surface (2)
$\mathcal{F}_{1\text{-}2}$	gray-body transfer factor from surface (1) to surface (2)
f	Darcy-Weisbach friction factor(–) [eqn. (7.33) and Fig. 7.6] or Blasius function of η (–)
f_o	orientation factor for eqns. (9.50)
f_v	frequency of vibration (Hz)
G	superficial mass flux $= \dot{m}/A_{\text{pipe}}$
g, g_{eff}	gravitational body force (m/s^2); effective g defined in eqn. (8.63) (m/s^2)
$g_{m,i}$	mass transfer coefficient for species i, (kg/m$^2 \cdot$s)
H	height of ribbon (m), head (m), irradiance (W/m^2), or Henry's law constant (N/m^2)
$h, \overline{h}, h_{\text{rad}}$	local heat transfer coefficient (W/m^{2}K), or enthalpy (J/kg), or height (m), or Planck's constant $(6.626070 \times 10^{-34}$ J·s); average heat transfer coefficient (W/m^{2}K); radiation heat transfer coefficient (W/m^{2}K)

$\hat{h}$	specific enthalpy (J/kg)
h_c	interfacial conductance (W/m^{2}K)
h_{fg}, h_{sf}, h_{sg}	
	latent heat of vaporization; latent heat of fusion; latent heat of sublimation (J/kg)
h'_{fg}	latent heat corrected for sensible heat
$\hat{h}_i$	specific enthalpy of species i (J/kg)
h^*	heat transfer coefficient at zero mass transfer, in Chpt. 11 only (W/m^{2}K)
I	electric current (amperes) or number of isothermal increments (–)
$\vec{i}, \vec{j}, \vec{k}$	unit vectors in the x, y, z directions
i	intensity of radiation (W/m$^2 \cdot$ steradian)
$\vec{i}$	electric current density (amperes/m^2)
$I_0(x)$	modified Bessel function of the first kind of order zero
i.c.	initial condition
$J_0(x), J_1(x)$	
	Bessel function of the first kind of order zero, of order one
$\vec{j}_i$	diffusional mass flux of species i (kg/m$^2 \cdot$s)
$\vec{J}_i$	diffusional mole flux of species i (kmol/m$^2 \cdot$s)
k	thermal conductivity (W/m·K)
k_B	Boltzmann's constant, 1.38065×10^{-23} J/K
k_T	thermal diffusion ratio (–)
L	any characteristic length (m)
L_0	geometrical mean beam length (m)

LMTD	logarithmic mean temperature difference	q_b, q_{FC}, q_i	defined in context of eqn. (9.37)
ℓ	an axial length or length into the paper or mean free molecular path (m or Å) or mixing length (m)	q_{max} or $q_{burnout}$	peak boiling heat flux (W/m^2)
M	molecular weight (of mixture if not subscripted) (kg/kmol) or merit number of heat pipe working fluid, $h_{fg}\sigma/\nu_f$.	q_{min}	minimum boiling heat flux (W/m^2)
		$\dot{q}$	volumetric heat generation (W/m^3)
m	fin parameter, $\sqrt{\overline{h}P/kA}$ (m^{-1})	R	factor defined in eqn. (3.14) (–), C_{min}/C_{max}, radius (m), electrical resistance (ohm), or region (m^3)
m_0	rest mass (kg)		
$\dot{m}$	mass flow rate (kg/s) or mass flux per unit width (kg/m · s)	R	ideal gas constant per unit mass, $R°/M$ (for mixture if not subscripted) (J/kg·K)
m_i	mass fraction of species i (–)		
N	number of adiabatic channels (–) or number of rows in a rod bundle (–)	$R°$	universal gas constant, 8314.46 (J/kmol·K)
		R_t, R_f	thermal resistance (K/W or m^2·K/W), fouling resistance (m^2·K/W)
$\vec{N}$	mole flux (of mixture if not subscripted) (kmol/m^2·s)		
N_A	Avogadro's number, $6.02214076 \times 10^{26}$ molecules/kmol	$r, \vec{r}$	radial coordinate (m), position vector (m)
		r_{crit}	critical radius of insulation (m)
$\mathcal{N}, \mathcal{N}_i$	number density of mixture, number density of species i (molecules/m^3)	$\dot{r}_i$	volume rate of creation of mass of species i (kg/m^3·s)
		S	entropy (J/K), or surface (m^2), or shape factor (N/I)
$\vec{n}$	mass flux (of mixture if not subscripted) (kg/m^2·s), unit normal vector (–)	S_L, S_T	rod bundle spacings (m). See Fig. 7.15
n	summation index (–) or nucleation site density (sites/m^2)	s	specific entropy (J/kg·K)
		T, T_b, T_c, T_f, T_m	temperature (°C, K); bulk temperature (°C, K); thermodynamic critical temperature (K); film temperature (°C, K); mean temperature for radiation exchange (K)
P	factor (–) defined in eqn. (3.14) or pitch of a tube bundle (m) or perimeter (m)		
p	pressure (N/m^2)		
p_i, p_v	partial pressure of species i, vapor pressure (N/m^2)	$\boldsymbol{T}$	time constant, $\rho c V/\overline{h}A$ (s)
		$\mathbf{T}$	a long time over which properties are averaged (s)
Q	rate of heat transfer (W)		
$q, \vec{q}$	heat flux (W/m^2)	t	time (s)

U	overall heat transfer coefficient (W/m^{2}K); internal thermodynamic energy (J); characteristic velocity (m/s)
$u, \vec{u}$	local x-direction fluid velocity (m/s) or specific energy (J/kg); vectorial velocity (m/s)
$u_{\text{av}}, \overline{u}, u_c, u_g$	
	average velocity over an area (m/s); local time-averaged velocity (m/s); characteristic velocity (m/s) [eqn. (8.19)]; Helmholtz-unstable velocity (m/s)
u', v', u'_r, u^*	
	turbulent fluctuations in x or y velocity (m/s); rms turbulent fluctuation (m/s); friction velocity, $\sqrt{\tau_w/\rho}$ (m/s)
$\hat{u}$	specific internal energy (J/kg)
V	volume (m^3); voltage (V)
V_m	molal specific volume (m^3/kmol)
v	local y-direction velocity (m/s)
$\vec{v}$	mass-average velocity, in Chapter 11 only (m/s)
$\vec{v}_i$	average velocity of species i (m/s)
$\vec{v}^*$	mole average velocity (m/s)
$\hat{v}$	specific volume (m^3/kg)
Wk	rate of doing work (W)
w	z-direction velocity (m/s) or width (m)
x, y, z	Cartesian coordinates (m); x is also used to denote any unknown quantity
x_i	mole fraction of species i (–)
x	quality of two-phase flow
Z_{ij}	frequency of collisions between molecules of species i and j (s^{-1})

Greek symbols

α	thermal diffusivity, $k/\rho c_p$ (m^2/s), or helix angle (rad.)
α, α_g	absorptance (–); gaseous absorptance (–)
β	coefficient of thermal expansion (K^{-1}), or relaxation factor (–), or $h\sqrt{\alpha t}/k$, or contact angle (deg), or coefficient of sliding friction (–),
β_λ	monochromatic extinction coefficient (m^2/kg)
$\Gamma, \Gamma(z)$	$\dot{g}L^2/k\Delta T$, gamma function
Γ_c	mass flow rate in film (kg/m·s)
Γ_{ij}	thermodynamic factor, eqn. (11.137b) (–)
γ	c_p/c_v; electrical conductivity ($\Omega\cdot$m)$^{-1}$
γ_i	activity coefficient, eqn. (11.132) (–)
γ_λ	monochromatic scattering coefficient (m^2/kg)
ΔE	activation energy of reaction (J/kmol)
Δp	pressure drop in any system (N/m^2)
ΔT	any temperature difference; various values are defined in context.
$\delta, \delta_c, \delta_t, \delta'_t$	
	flow boundary layer thickness (m) or condensate film thickness (m); concentration boundary layer thickness (m); thermal boundary layer thickness (m); h/k (m).
ε	emittance (–); heat exchanger effectiveness (–); roughness (m)
$\varepsilon_A, \varepsilon_{AB}$	potential well depth for molecules of A, for collisions of A and B (J)

ε_f	fin effectiveness (–)		τ	transmittance (–) or dimensionless time ($T/\mathbf{T}$) or shear stress (N/m^2) or length of travel in b.l. (m)
$\varepsilon_g, \varepsilon^0$	gaseous emittance (–), standard emissivity (–)			
$\varepsilon_m, \varepsilon_h$	eddy diffusivity of mass (–), of heat (–)		τ_w, τ_{yx}	shear stress on a wall (N/m^2), shear stress in the x-direction on the plane normal to the y-direction (N/m^2)
η	independent variable of Blasius function, $y\sqrt{u_\infty/\nu x}$ (–)			
η_f	fin efficiency		τ_δ	shear stress exerted by liquid film (N/m^2)
Θ	a ratio of two temperature differences (–)		Φ	$\Delta T/(\dot{q}L^2/k)$ or fraction of total heat removed (see Fig. 5.10) (–)
θ	$(T - T_\infty)$ (K) or angular coordinate (rad)			
ζ	$x/\sqrt{\alpha t}$		ϕ	angular coordinate (rad), or δ_t/δ (–)
κ_λ	monochromatic absorption coefficient (m^2/kg)		ϕ_{ij}	weighting functions for mixture viscosity or thermal conductivity (–)
$\lambda, \lambda_c, \lambda_H$	wavelength (m) or eigenvalue (m^{-1}); critical Taylor wavelength (m); Helmholtz-unstable wavelength (m)		χ	$d\Theta/d\zeta$
			ψ	$\omega L^2/\alpha$
			Ω	ωt
$\lambda_d, \lambda_{d_1}, \lambda_{d_2}$			$\Omega_D, \Omega_k, \Omega_\mu$	
	most dangerous Taylor-unstable wavelength (m); subscripts denote one- and two-dimensional values			collision integral for diffusivity, thermal conductivity, or dynamic viscosity (–)
$\hat{\lambda}$	dimensionless eigenvalue (–)		ω	frequency of a wave or of rotation (rad/s) or solid angle (sr)
μ	dynamic viscosity (kg/m·s)			
μ_i	chemical potential of species i (J/mol)		$\nabla_{T,p}$	gradient computed while holding T and p constant (m^{-1})
ν	kinematic viscosity, μ/ρ (m^2/s)			
ξ	x/L or $x\sqrt{\omega/2\alpha}$; also $(x/L + 1)$ or x/L (–)		*General subscripts*	
ρ	mass density (kg/m^3) or reflectance (–)		av, avg	denoting bulk or average values
ρ_i	partial density of ith species (kg/m^3)		b, body	denoting any body
σ	surface tension (N/m) or Stefan-Boltzmann constant 5.67037×10^{-8} ($W/m^2 \cdot K^4$)		b	denoting a black body
			c	denoting the critical state
			cbd	denoting a convective boiling dominated value
σ_A, σ_{AB}	collision diameter of molecules of A, for collisions of A with B (Å)		D	denoting a value based on D

e, e_t	denoting a dynamical entry length or a free stream variable; denoting a thermal entry length
f, g	denoting saturated liquid and saturated vapor states
fb	denoting a value for flow boiling
i	denoting initial or inside value, or a value that changes with the index i, or values for the ith species in a mixture
in	denoting a value at the inlet
L	denoting a value based on L or at the left-hand side
lo	denoting a value computed as if all fluid were in liquid state
m	denoting values for mixtures
max, min	denoting maximum or minimum values
n	denoting a value that changes with the index n
nbd	denoting a nucleate boiling dominated value
o	denoting outside, in most cases
out	denoting a value at the outlet
R	denoting a value based on R or at the right-hand side
s	denoting values above an interface
sfc	denoting conditions at a surface
sup, sat, sub	denoting superheated, saturated, or subcooled states
u	denoting values below an interface
w	denoting conditions at a wall
x	denoting a local value at a given value of x

∞	denoting conditions in a fluid far from a surface
λ	denoting radiative properties evaluated at a particular wavelength

General superscripts

*	denoting a value for zero net mass transfer (in Chpt. 11 only)
⊖	denoting a thermodynamic property in the standard state

Dimensionless parameters

Bi	Biot number, hL/k_{body}
Bo	Bond number, $L^2 g(\rho_f - \rho_g)/\sigma$
Boi	Boiling number, q_w/Gh_{fg}
$C_f, \overline{C}_f$	skin friction coefficient, $\tau_w/(\rho u_\infty^2/2)$; overall skin friction coefficient $\overline{\tau_w}/(\rho u_\infty^2/2)$
Co	Convection number, $[(1-x)/x]^{0.8}(\rho_g/\rho_f)^{0.5}$
Da	Damköhler number, $\rho A' \exp(-\Delta E/R^\circ T)/g_m^*$
Ec	Eckert number, $u^2/(c_p \Delta T)$
Fo	Fourier number, $\alpha t/L^2$
Fr	Froude number, $U^2/(gL)$
Gr_L	Grashof number, $g\beta \Delta T L^3/\nu^2$ (for heat transfer), or $g(\Delta\rho/\rho)L^3/\nu^2$
Gz	Graetz number, $\text{RePr}D/x$
H'	L' based on $L \equiv H$
Ja	Jakob number, $c_p \Delta T/h_{fg}$
j	Colburn j-factor, $\text{St}\,\text{Pr}^{2/3}$
L'	$L\sqrt{g(\rho_f - \rho_g)/\sigma}$
Le	Lewis number, $\text{Sc}/\text{Pr} = \alpha/\mathcal{D}_{im}$
M	Merit number, $h_{fg}\sigma/\nu_f$
Ma	Mach number, $u/(\text{sound speed})$

NTU   number of transfer units, $UA/C_{\min}$

$\mathrm{Nu}_x, \overline{\mathrm{Nu}}_L$ local Nusselt number, hx/k_{fluid}; average Nusselt number, $\bar{h}L/k_{\mathrm{fluid}}$

$\mathrm{Nu}_{m,x}, \overline{\mathrm{Nu}}_{m,L}$
   local Nusselt number for mass transfer (or Sherwood number) $g_{m,i}^* x/(\rho \mathcal{D}_{im})$; average Nusselt number for mass transfer, $\overline{g_{m,i}}^* L/(\rho \mathcal{D}_{im})$

Pe_L Péclet number, $UL/\alpha = \mathrm{Re}_L\, \mathrm{Pr}$

$\mathrm{Pr}, \mathrm{Pr}_t$ Prandtl number, $\mu c_p/k = \nu/\alpha$; turbulent Prandtl number, $\varepsilon_m/\varepsilon_h$

Ra_L Rayleigh number, $\mathrm{Gr}\,\mathrm{Pr} = g\beta\Delta T L^3/(\nu\alpha)$ for heat transfer; $g(\Delta\rho/\rho)L^3/(\nu\mathcal{D}_{12})$ for mass transfer

Ra_L^* $\mathrm{Ra}_L\mathrm{Nu}_L = g\beta q_w L^4/(k\nu\alpha)$

$\mathrm{Re}_L, \mathrm{Re}_c, \mathrm{Re}_f, \mathrm{Re}_{\mathrm{lo}}, \mathrm{Re}_l, \mathrm{Re}_u$
   Reynolds number, UL/ν; condensation Re equal to Γ_c/μ; Re for liquid; liquid-only Reynolds number, GD/μ_f; Re at start or end of transition

Sc   Schmidt number for species i in mixture m, $\nu/\mathcal{D}_{im}$

Sh_L Sherwood number, $g_{m,i}^* L/(\rho\mathcal{D}_{im})$

St   Stanton number, $\mathrm{Nu}/(\mathrm{Re}\,\mathrm{Pr}) = h/(\rho c_p u)$

Str   Strouhal number, $f_v D/u_\infty$

We_L Weber number, $\rho_g U_\infty^2 L/\sigma$

Π any dimensionless group

PART VII

INDICES

Citation Index

Subject Index